

Gianfranco Cariolaro

Unified Signal Theory

 Springer

Unified Signal Theory

Gianfranco Cariolaro

Unified Signal Theory

 Springer

Gianfranco Cariolaro
University of Padova
Padova, Italy
cariolar@dei.unipd.it

ISBN 978-0-85729-463-0

e-ISBN 978-0-85729-464-7

DOI 10.1007/978-0-85729-464-7

Springer London Dordrecht Heidelberg New York

British Library Cataloguing in Publication Data

A catalogue record for this book is available from the British Library

Mathematics Subject Classification (2010): 94A12, 22D35, 28C10, 43A25, 47A20, 46C15

© Springer-Verlag London Limited 2011

Matlab[®] and Simulink[®] are registered trademarks of The MathWorks, Inc., 3 Apple Hill Drive, Natick, MA 01760-2098, USA. <http://www.mathworks.com>

Mathematica[®] is a registered trademark of Wolfram Research, Inc., 100 Trade Center Drive, Champaign, IL 61820-7237, USA. <http://www.wolfram.com>

Apart from any fair dealing for the purposes of research or private study, or criticism or review, as permitted under the Copyright, Designs and Patents Act 1988, this publication may only be reproduced, stored or transmitted, in any form or by any means, with the prior permission in writing of the publishers, or in the case of reprographic reproduction in accordance with the terms of licenses issued by the Copyright Licensing Agency. Enquiries concerning reproduction outside those terms should be sent to the publishers.

The use of registered names, trademarks, etc., in this publication does not imply, even in the absence of a specific statement, that such names are exempt from the relevant laws and regulations and therefore free for general use.

The publisher makes no representation, express or implied, with regard to the accuracy of the information contained in this book and cannot accept any legal responsibility or liability for any errors or omissions that may be made.

Cover design: eStudio Calamar S.L.

Printed on acid-free paper

Springer is part of Springer Science+Business Media (www.springer.com)

e pluribus unum

To my son David

Foreword

Methodological reductionism is a driving force of scientific thinking. Unlike the more controversial, and philosophically dubious, connotations of the term, methodological reductionism embodies a general principle of intellectual parsimony. It does not establish debatable hierarchies among pedagogically distinct scientific areas, it does not seek to identify equally controversial ultimate constituents of reality. Instead, it attempts the consolidation of a collection of more or less intuitively connected items into a more general item, of which they become refinements or specializations. This trend towards simplicity (the parsimony of explanation) is the underlying fabric of scientific endeavor. Simplicity is the hallmark of that undefinable quality of science called “elegance”: a simpler proof of a theorem is unmistakably referred to as “more elegant” than a previous more cumbersome proof of the same statement. The incorporation of the descriptive results of Kepler and Galileo into the mechanics of Newton is a major example. Equally spectacular is the unification of a number of relations concerning electromagnetism into the remarkable architecture of Maxwell’s equations. In the same mindset falls the axiomatic minimalism in mathematics (for example, the reduction of the rules of boolean algebras to the five postulates of Huntington) or the current unsatisfied quest for the unification of forces in physics.

Elegance defies an operational definition, but you recognize it when you see it. The present work of Gianfranco Cariolaro falls within the described optics and represents a life-time accomplishment in bringing under a common umbrella a collection of diverse, but obviously interconnected topics of central importance in the current technological landscape. The focus is on the signal, the embodiment of diversification which is the essence of information. Diversification, or choice, may be expressed in an unlimited repertory, some of a static nature, as alphabetic characters, pictographs, etc. But in the present era, characterized by a spectacular flow of information through communication lines, our intuition immediately refers to some physical quantity whose variations in time specify the information one wishes to convey. This is certainly the most spontaneous instantiation of a signal, and this representation is the starting point of the traditional pedagogy of communication theory.

Traditionally, the domain of the signal (time) is paralleled by the less intuitive domain of frequency, and, although (signal, spectrum) form a conceptually indissoluble dual pair, the frequency domain is frequently presented as a formally useful ancilla of the time domain, where ultimately the signal is to be acquired by its users. In addition, different characterizations of time (discrete/continuous) engender different analytical environments for the treatment of the signal.

The present work takes the bold step of going beyond the traditional pedagogy, fitting into a single elegant and original framework the diverse specialties of signal representation and transmission. The signal–spectrum asymmetry fades away in the new treatment, which the author appropriately dubs the “unified theory”. A signal is an entity of either of the two domains, which are linked through the powerful device of the Fourier Transform and its inverse. A signal becomes a function from some domain to the complex field. The only characterization of the function domain is its being an Abelian group, i.e., an abstract semigroup with a commutative and invertible operation: this removes any distinction between continuous and discrete time, as well as the distinction between periodic and aperiodic signals (referring to their spectra). A necessary companion of this novel viewpoint is the adoption of the Haar integral as the operational device, because it subsumes the functions of the standard Lebesgue integral for the continuous case and of the summation operator for the discrete case. Upon this abstract background, the elegant construction developed by the author is the framework from which the traditional topics of communication theory can be rediscovered as specializations, in the best tradition of methodological reductionism. A keen reader willing to explore this tightly framed architecture will certainly emerge with a mature and intellectually rewarding view of this relevant body of knowledge.

Providence, RI, USA

Franco P. Preparata

Preface

The increasing application of information technology in a variety of fields has led to a high degree of diversification, to the extent that it is difficult to clearly delimit the scope of this discipline and to establish its distinctive characteristics. Nevertheless, it is well recognized that *signals* are salient features of this discipline and have a paramount influence on all the related fields, such as physics, astronomy, biology, medicine, oceanography and meteorology, among others, that take advantage of the electronic and the digital revolutions. The fact that signals are the greatest protagonists of this evolution was clear from the beginning of the electronic era. In fact, recalling the definition of electronics as the production, transmission and use of *information* (Everett, 1948) and considering that signals are the physical carriers of information, we arrive at the conclusion that signals play a fundamental role in every field related to information technology. As a natural consequence, it follows that the enormous growth of information technology, and its diversification, are regularly transferred to the discipline that specifically deals with signals, that is, Signal Theory.

The idea of a Unified Signal Theory (UST) stems from the requirement that the large variety of signals (continuous-time, discrete-time, aperiodic, periodic, one-dimensional, two-dimensional, etc.) proposed over the last few decades can be treated efficiently and with conceptual economy. The target of the UST is a unified introduction and development of signal operations, such as convolution, filtering, Fourier transformation, as well as system formulation and analysis. This approach is rather atypical, with respect to standard signal theories, where different definitions and separate developments are provided for each specific class of signals.

Philosophy of the UST The key to this unification was my decision to treat the signal domains as *Abelian groups*, which have an appropriate mathematical structure that permits a unified introduction of the fundamental operations. I used the notation $s(t)$, $t \in I$, to emphasize that function s (the signal) is defined on the Abelian group I and realized, by inspection of all the signal classes of interest in applications, that every signal can be modeled in this unique and unified form. This remark may appear to be trivial, but it is essential for the unification and permits realizing

the leitmotif *e pluribus unum* for signals. Note the fortunate circumstance that the domains of the Fourier transforms are Abelian groups, too, so that we can write every Fourier transform as $S(f)$, $f \in \widehat{T}$, where \widehat{T} is the frequency domain, again an Abelian group.

A further requirement for this unification is a linear functional that permits the development of a coherent Signal Theory architecture. This is given by an *integral* introduced in 1933 by the Hungarian mathematician Alfred Haar, a student of Hilbert, which provides the second fortunate circumstance, because the Haar integral, applied to each specific case, produces all the integrals and the summations usually encountered in the standard signal theories.

In conclusion, the UST is built on two mathematical notions, Abelian groups and the Haar integral, which again is atypical for signal theory.

Using these notions, it is possible to treat the unified signal $s(t)$, $t \in I$, as a single abstract object and to introduce it in the basic definitions and developments. Once the unified architecture is completed, specific results for any given class of signals are simply obtained by particularizing the signal domain, as one-dimensional continuous, one-dimensional discrete, two-dimensional continuous, and so forth.

Originality This atypical formulation leads unavoidably to originality in the development of specific topics within the framework of the unified approach. The idea of unification itself is original, but so are several topics within the UST. The most important ones include: representation of Abelian groups by base–signature pairs; cells (as a generalization of the unit cells used for lattices); general definition of periodicity, formulation of signal symmetries; impulses (as a generalization of the concept of the Dirac delta function); multirate systems defined over structured groups without domain normalizations; ideal and elementary transformations; duality theorem for ideal transformations; band and bandwidth generalizations; unified sampling theorem; multidimensional polyphase decomposition in the signal domain (usually formulated in the z -domain). In my own opinion, the most profound result of the UST is the Duality Theorem on ideal transformations, which collects and unifies a dozen known results. I have published only very few of these original results, the reason being that their formulation would have required several pages of UST preliminaries, which would be far too long and not suitable for a paper.

Mathematical Level The mathematical level is perhaps a little high for engineers (and certainly too low for mathematicians), but it is appropriate for a graduate level in the area of information engineering. The main problem is concerned with the treatment of topological groups, the Abelian groups on which the Haar integral is introduced. Considering that the field of topology is very abstract and difficult for a fully mathematical development, I adopted the compromise of *using the results of Topology, without introducing topological details*. This is a typical “engineering compromise”, as is usually made in engineering oriented books on probability and random processes, whose theoretical background is fully anchored on Measure Theory, but leaving out the mathematical details of this discipline.

Organization of the Book The book is (conceptually) subdivided into three parts.

Part I: *Classical Theory*. Since the UST may appear to be a difficult topic to anyone who is not already familiar with signals, I have introduced a preliminary chapter where the fundamentals of continuous-time and discrete-time signals are developed according to the traditional (not unified) approach, including several illustrations and examples. I hope that with these preliminaries, the book can profitably be read even by readers who do not possess elementary notions on signals.

Part II: *Unified Theory*. The UST itself is developed in six chapters, in *no more than 130 pages*, where sections are explicitly marked **UT** for clarity.¹ The first two chapters deal with UST fundamentals, that is, with Abelian groups and the Haar integral. Then, the unified approach is developed in both the signal domain and the frequency domain (Fourier transform). Finally, systems (conventionally called *transformations*) are developed, concluding with the formulation of the unified sampling theorem. Throughout its development the UST is illustrated in some detail with examples of one-dimensional and two-dimensional applications.

Part III: *Specific Classes of Signals and Applications*. The UST is general and not specific to any particular application. However, in the final nine chapters, we have some real-world applications, namely implementation of the fast Fourier transform (FFT), both one- and multidimensional, sampling and reconstruction of signals, multicarrier modulation system (OFDM), wavelets, image scanning, in particular, television scanning, image compression and tomography (Radon and Hankel transforms).

The last two chapters develop some advanced topics of the UST, with applications to spatio-temporal systems.

Suggested Paths The book could be used by both undergraduate and graduate students, and also by researchers, following three distinct paths.

Undergraduate students should begin with the Classical Theory, presented in Chap. 2. When studying the UST part, they should take in the statements and conclusions, without dwelling on finer mathematical proofs and justifications, and concentrate on one-dimensional signals in Part III.

Graduate students can avoid a detailed study of the Classical Theory, limiting themselves to a fast reading. But they should pay great attention to the mathematical formulation (both one-dimensional and multidimensional) in order to develop the attitude that problems related to signal theory can be approached from a general viewpoint, not merely confined to a specific problem. For graduate students, parts of the book will also be useful for future studies. I suggest that graduate students omit, at first reading, some mathematical details, explicitly indicated with the “jump” symbol \Downarrow .

Researchers could follow the path of graduate students, early concentrating their attention on the mathematical fundamentals and on the advanced applications they are considering in their professional activity.

¹Some sparse contributions of UST are introduced also in Part III.

In this regard, I wish to add some personal considerations derived from my experience (and also from that of my colleagues). I have taught the UST for more than 20 years and realized that students never had conceptual difficulties in understanding the general fundamentals, they rather showed their enthusiasm for the compactness and generality of the formulation (saving their memory). At a first glance, the mathematical fundamentals might discourage a reader, but, depending on the teacher's sensibilities, mathematical details can be adjusted and adapted. In fact, Abelian groups (not so topological groups) represent a very elementary concept. Also, the Haar integral may simply be viewed as a formalism that has exactly the same properties as the ordinary integral on the real line. In conclusion, this book is intended for people who may never have studied signal theory before, as well as for experienced people. It is proposed as a panacea that satisfies everybody, even if it carries the risk of satisfying nobody.

Examples and Problems. Solutions to All Problems I have introduced several examples to illustrate the UST during its development. The final chapters, dedicated to specific classes of signals, may be viewed as extended illustration examples. I have also suggested several problems at the end of each chapter; problems are marked by one to three asterisks indicating the degree of difficulty. The examples and problems were tested on graduate students over the course of several years.

The solutions to all the problems proposed in the book are available on the Springer website www.springer.com/978-0-85729-463-0.

Manuscript Preparation To prepare the manuscript, I have used \LaTeX , supplemented with a personal library of macros. The illustrations too are composed with \LaTeX , sometimes with the help of *Mathematica*[®].

Acknowledgements I wish to thank the hundreds of people, colleagues and students who helped me to formulate this “definitive edition” of the UST. I confine myself to mentioning, with gratitude, the ones who helped me in the final stage: Antonio Assalini, Paolo Baracca, Matteo Canale, Giancarlo Calvagno, Valentina Cellini, Antonio M. Cipriano, Guido Cortelazzo, Francesco de Pellegrini, Michele Elia, Tomaso Erseghe, Lorenzo Finesso, Nicola Laurenti, Umberto Mengali, Lorenzo Novella, Gianfranco Pierobon, Roberto Rinaldo, Edi Ruffa, Beatrice Tomasi, Giuseppe Tronca, Alberto Vigato, and Davide Zennaro.

Particular thanks are due to my colleague and friend Peter Kraniuskas, who first encouraged me to publish this book, and to my son David, who was able to persuade me to do so, by directly contacting Springer.

I am also indebted to Nino Trainito (perhaps the only one to actually read the whole manuscript!), who made several comments and considerably improved the language.

Contents

1	Introduction	1
1.1	“Physical” Signals	1
1.2	“Mathematical” Signals	2
1.3	Historical Note	7
1.4	The Unified Signal Theory	9
1.5	Content of the Book	12
1.6	Conventions on Notation	13
	References	13
Part I	Classic Theory	
2	Classical Signal Theory	17
2.1	Continuous Signal Definitions	17
2.2	Continuous Periodic Signals	21
2.3	Examples of Continuous Signals	23
2.4	Convolution for Continuous Signals	31
2.5	The Fourier Series	37
2.6	The Fourier Transform	42
2.7	Examples of Fourier Transforms	47
2.8	Signal Filtering	50
2.9	Discrete Time Signals	53
2.10	Examples of Discrete Signals	58
2.11	Convolution of Discrete Signals	62
2.12	The Fourier Transform of Discrete Signals	63
2.13	The Discrete Fourier Transform (DFT)	69
2.14	Filtering of Discrete Signals	69
2.15	Sampling Theorem	70
2.16	Final Comments on Classical Theory	72
2.17	Problems	73
	Appendix Fourier Transform of the Signum Signal $\text{sgn}(t)$	78
	References	79

Part II Unified Signal Theory

3	Unified Theory: Fundamentals	83
3.1	The Philosophy of Unified Signal Theory	83
3.2	Abelian Groups	86
3.3	Overview of LCA Groups	89
3.4	The LCA Groups According to Topology	100
3.5	Cells and Group Partitions	101
3.6	Signal Periodicity and Quotient Groups	110
3.7	LCA Quotient Groups and Signal Classes	114
3.8	Multiplicative Groups	119
3.9	Sum and Intersection of Groups	124
3.10	Problems	130
	Appendix A Proof of Theorem 3.1	131
	Appendix B The “True” Quotient Group	132
	Appendix C On the Sum $\mathbb{Z}(T_1) + \mathbb{Z}(T_2)$	133
	References	133
4	Unified Theory: Signal Domain Analysis	135
4.1	The Haar Integral	135
4.2	Haar Integral on the Groups of \mathbb{R}	140
4.3	Haar Integral on the Groups of \mathbb{R}^m	141
4.4	Haar Integral Over Multiplicative Groups	146
4.5	Class of Signals and Vector Spaces	148
4.6	Signal Expansions into Orthogonal Functions	157
4.7	Fundamental Symmetries	163
4.8	Signal Extension and Duration	165
4.9	Convolution	169
4.10	Impulses	172
4.11	One-Dimensional Convolution and Impulses	175
4.12	Multidimensional Convolution and Impulses	178
4.13	Symmetry Theory	183
4.14	Problems	193
	Appendix A Haar Integral Induced by an Isomorphism	196
	Appendix B Integral Independence of a Group Representation	196
	Appendix C Proof of Theorem 4.2 on Coordinate Change in \mathbb{R}^m	197
	Appendix D Proof that $L_p(I)$ Is a Vector Space	198
	Appendix E Proof of Theorem 4.6 on Periodic Convolution	198
	Appendix F Proof of the Noble Identity on Impulse (Theorem 4.8)	199
	References	203
5	Unified Theory: Frequency Domain Analysis	205
5.1	Introduction	205
5.2	First Considerations on the Unified Fourier Transform	207
5.3	The Frequency Domain	211
5.4	Symmetry Between Signals and Fourier Transforms	215
5.5	Rules of the Fourier Transform	217

5.6	Symmetries in the Frequency Domain	222
5.7	Energy and Correlation	227
5.8	Explicit Forms of One-Dimensional Fourier Transforms	229
5.9	Explicit Forms of Multidimensional Fourier Transforms	240
5.10	Examples of Multidimensional Fourier Transforms	246
5.11	Fourier Transform on Multiplicative Groups	254
5.12	The Fractional Fourier Transform	255
5.13	Problems	263
Appendix A	Fourier Kernel from Characters	268
Appendix B	Invertibility of the Fourier Transform	269
Appendix C	Proof of Theorem 5.1 on the Dual Group	269
Appendix D	Proof of Theorem 5.2 on the Representation of the Dual Group	270
Appendix E	Proof of Poisson’s Summation Formula	270
	References	271
6	Unified Theory: Signal Transformations	273
6.1	Definition of Signal Transformation	273
6.2	Fundamental Definitions	276
6.3	Linear Transformations	280
6.4	Variety of Linear Transformations	284
6.5	Other General Topics on Transformations	289
6.6	Nonlinear Transformations	293
6.7	Shift-Invariance in Linear Transformations	296
6.8	Quasi-Invariant Linear Transformations	299
6.9	Impulse and Elementary Transformations	303
6.10	Analysis of Elementary Transformations	306
6.11	Decomposition of QIL Transformations	315
6.12	Transformations in the Frequency Domain (Dual tfs)	321
6.13	Duality Theorem	323
6.14	Duals of QIL Transformations	326
6.15	Filters	329
6.16	Multi-Input Multi-Output QIL Transformations	335
6.17	Problems	338
Appendix A	Proof of Theorem 6.1 on PIL tfs	341
Appendix B	Proof of Theorem 6.2 on SI and of Theorem 6.3 on QI	341
Appendix C	On the Identification of PIL and QIL tfs	342
	References	342
7	Unified Theory: Multirate Transformations	345
7.1	The Class of Multirate Transformations	345
7.2	Cascade of QIL Transformations	349
7.3	Standard Noble Identities	353
7.4	Noble Identities with Modulators	359
7.5	The Polyphase Decomposition	362
7.6	Parallel Architectures	370

7.7	Parallel Architectures of QIL Transformations	374
7.8	Parallel Architectures of PIL Transformations	377
7.9	Parallel Architectures with Modulators	380
7.10	Multirate Application to OFDM (Transmultiplexer)	384
7.11	Problems	395
	Appendix Deduction of Parallel Architecture with EMs	396
	References	397
8	Unified Theory: Sampling and Interpolation	399
8.1	Equalization Conditions	399
8.2	Interpolation Theory	405
8.3	Signal Recovery After a Down-Sampling	409
8.4	The Fundamental Sampling Theorem	409
8.5	The Unified Sampling Theorem	415
8.6	Further Considerations on the Unified Sampling Theorem	419
8.7	$\mathbb{R} \rightarrow \mathbb{Z}(T)$ Sampling	423
8.8	$\mathbb{Z}(T_0) \rightarrow \mathbb{Z}(T)$ Sampling	427
8.9	$\mathbb{R}/\mathbb{Z}(T_p) \rightarrow \mathbb{Z}(T)/\mathbb{Z}(T_p)$ Sampling	431
8.10	Multidimensional Sampling	432
8.11	Errors in Sampling/Interpolation	435
8.12	The “Real” Sampling	440
8.13	Problems	444
	References	447
 Part III Specific Classes of Signals and Applications		
9	Signals Defined on \mathbb{R}	451
9.1	The Time Domain	451
9.2	The Frequency Domain	455
9.3	Remarkable Examples	459
9.4	Gallery of Fourier Pairs	463
9.5	Duration and Bandwidth	471
9.6	Asymptotic Behavior of Signals and Fourier Transforms	474
9.7	The Laplace Transform	480
9.8	Properties of the Laplace Transform	487
9.9	Continuous-Time Filters	489
9.10	Analytic Signal and Hilbert Transform	494
9.11	Problems	499
	Appendix A Proof of the Theorem 9.1 on Band-Duration Incompatibility	501
	Appendix B Proof of Theorems on Asymptotic Behavior	502
	Appendix C Proof of Uncertainty Principle Inequality	503
	Appendix D Inverse Fourier Transform of Raised Cosine	505
	References	506

- 10 Signals on $\mathbb{R}/\mathbb{Z}(T_p)$ 509**
 - 10.1 The Time Domain 509
 - 10.2 The Frequency Domain 510
 - 10.3 Gallery of Fourier Pairs 514
 - 10.4 Filtering of Periodic Signals 519
 - 10.5 Problems 520
 - References 520
- 11 Signals on $\mathbb{Z}(T)$ 521**
 - 11.1 The Time Domain 521
 - 11.2 The Frequency Domain 522
 - 11.3 Remarkable Examples 527
 - 11.4 Gallery of Fourier Pairs 531
 - 11.5 The z -Transform 535
 - 11.6 Properties of the z -Transform 542
 - 11.7 Filters on $\mathbb{Z}(T)$ 546
 - 11.8 Interpolators and Decimators 552
 - 11.9 Signal Multiplexing 558
 - 11.10 Polyphase Decomposition in z -Domain 562
 - 11.11 Problems 566
 - References 567
- 12 Signals on $\mathbb{Z}(T)/\mathbb{Z}(T_p)$ 569**
 - 12.1 The Time Domain 569
 - 12.2 The Frequency Domain 570
 - 12.3 Gallery of Signals and Fourier Transforms on $\mathbb{Z}(T)/\mathbb{Z}(T_p)$ 574
 - 12.4 Symmetries 579
 - 12.5 The Discrete Cosine Transform (DCT) 583
 - 12.6 Matrix Form of the DFT and of Other Transforms 592
 - 12.7 Fractional DFT and DCT 593
 - 12.8 Problems 594
 - References 594
- 13 Signal Analysis via Digital Signal Processing 597**
 - 13.1 Introduction 597
 - 13.2 Computational Complexity of the DFT 598
 - 13.3 Introduction to the FFT 598
 - 13.4 The FFT as a Parallel Computation 602
 - 13.5 Computation of the Multidimensional DFT 610
 - 13.6 The FFT on Separable Lattices 614
 - 13.7 The FFT on Nonseparable Lattices 617
 - 13.8 DFT Computation via FFT 621
 - 13.9 FFT Computation of a Fourier Transform on \mathbb{R} 622
 - 13.10 Other FFT Utilizations 629
 - 13.11 Conventional Durations and Bandwidths 633
 - 13.12 Use of Windows 637
 - 13.13 Problems 640
 - References 641

14 Signal Expansions, Filter Banks, and Subband Decomposition 643

14.1 Generalized Transforms 643

14.2 Signal Expansions as Generalized Transforms 649

14.3 Interpretation of Expansions: The Matrix Viewpoint 652

14.4 Expansions with Periodic Invariance (PI) 657

14.5 Symmetry Theory Interpretation of Signal Expansions 662

14.6 Subband Decomposition from Generalized Transforms 667

14.7 Transmultiplexer from Generalized Transforms 672

14.8 General Formulation of Subband Decomposition 674

14.9 Fundamental Relations of Subband Decomposition 677

14.10 Polyphase Decomposition in Subband Decomposition 683

14.11 Perfect Reconstruction Conditions and Biorthogonality 687

14.12 Two-Channel Filter Banks 691

14.13 One-Dimensional Multichannel Subband Decomposition 699

14.14 Multidimensional Filter Banks 701

14.15 Tree-Structured Filter Banks 703

14.16 The Block Transform 707

14.17 Problems 709

Appendix A Proof of Theorem 14.1 on Projections 711

Appendix B Alias-Free Condition in Subband Decomposition 712

Appendix C z -Domain Analysis of 1D Subband Decomposition 715

References 718

15 Multiresolution and Wavelets 719

15.1 Introduction 719

15.2 The Short-Time Fourier Transform 720

15.3 From the CSTFT to Wavelets 725

15.4 The Continuous Wavelet Transform (CWT) 728

15.5 The Axioms of Multiresolution Analysis 731

15.6 Axiom Interpretation with Symmetry Theory 734

15.7 Projectors from the Axioms 740

15.8 Evaluation of Wavelets from Scaling Function 743

15.9 Evaluation of Decimators and Interpolators 747

15.10 Combination of Interpolators and Decimators 748

15.11 Fourier Analysis in the Wavelet Decomposition 752

15.12 Wavelets from Iterated Filter Banks 757

15.13 The Wavelet Series Expansion 762

15.14 Generalizations on Wavelets 765

15.15 An Example of the Application of Wavelets 769

15.16 Problems 773

Appendix A Proof of Proposition 15.7 on Coefficients at Steps m
and $m + 1$ 774

Appendix B Interpretation of the Expansion of $\varphi(t)$ and $\psi(t)$ 776

References 777

16	Advanced Topics on Multidimensional Signals	779
16.1	Set and Group Transformations	779
16.2	Representation of Gratings	783
16.3	Signals on a Grating	787
16.4	Generation of Subgroups	790
16.5	Lattices and Sublattices	794
16.6	Triangularization and Diagonalization of Integer Matrices	797
16.7	Classes of Lattices	803
16.8	Sum and Intersection of Lattices	808
16.9	Aperiodic Cells	810
16.10	Change of Signal Dimensionality	820
16.11	Composite Dimensionality Changes: Reading and Writing	825
16.12	Discrete Reading	829
16.13	Fourier Analysis of Reading	837
16.14	Problems	838
	Appendix Condition for Getting a Subgroup (Theorem 16.1)	839
	References	841
17	Study of Images	843
17.1	Introduction to Still Images	843
17.2	Scanning of Still Images	846
17.3	Sampling and Reproduction of 2D Images	855
17.4	Scanning of Time-Varying Images	859
17.5	Scanning of Time-Varying Images Revisited	869
17.6	Fourier Analysis of Television Scanning	871
17.7	The Three-Dimensional Television	875
17.8	Numerical Conversion of Images	877
17.9	Projections (Radon Transform)	880
17.10	Cartesian, Polar, and Grating Functions	886
17.11	Properties of the Radon Transform	893
17.12	Image Reconstruction from Projections	894
17.13	The Hankel Connection to Projections	898
17.14	Gallery of Operators Related to Projections	903
17.15	Sampling and Interpolation of Projections	904
17.16	Applications of Radon Transform	911
17.17	Problems	913
	References	914
	Glossary	917
	Index	919

Part I
Classic Theory

Chapter 1

Introduction

1.1 “Physical” Signals

We begin with a clear distinction between “physical” signals, regarded as physical quantities in which an information is conveyed, and “mathematical” signals, the models of “physical” signals. To fix the ideas in a real world environment, these concepts are now introduced with reference to telecommunication systems.

A telecommunication system has the task of transmitting *messages* from one place to another place at some distance, as depicted in Fig. 1.1. The *source* produces a message m to be sent to the *user* through a *transmitting medium* that covers the distance between the transmitter and the receiver. The medium is a physical channel such as a line, a coaxial cable, an optical fiber or a radio link in the free space. The transmitter function is to vary a physical quantity, e.g., an electromagnetic field, in accordance to the message. Finally, the time-varying physical quantity is replicated at the destination point where the receiver extracts the message. The physical carrier that conveys the message is usually called *signal*.

As a specific example, let us consider a transmission of a text document (telex service, an early precursor of today’s email) in which a message consists of a sequence of letters, numbers or signs, usually called *symbols*. Each symbol is expressed as a binary number, and the message becomes a sequence of binary symbols (bits). At this point, the message can be converted, e.g., into a sequence of optical pulses that are obtained by rhythmically switching a laser on and off according to the rule that symbol 1 corresponds to the pulse *presence* and symbol 0 to the pulse *absence* (Fig. 1.2). This optical signal can be applied to an optical fiber that covers the required distance, supplying the receiver with a signal in which pulses are attenuated, delayed and also “distorted”, that is, with a different shape with respect to the original one. The receiver task is to recognize the presence or the absence of the pulses, to restore the binary sequence and, finally, to reproduce the original printed document.

As a second example we consider the transmission (faxing) of a black-and-white still image (photography), where the message has a two-dimensional structure (see Fig. 1.6). The corresponding “physical” signal is given by a luminous intensity (lu-

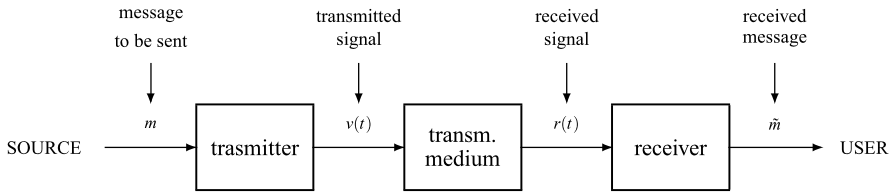


Fig. 1.1 A typical signal environment: a telecommunication system

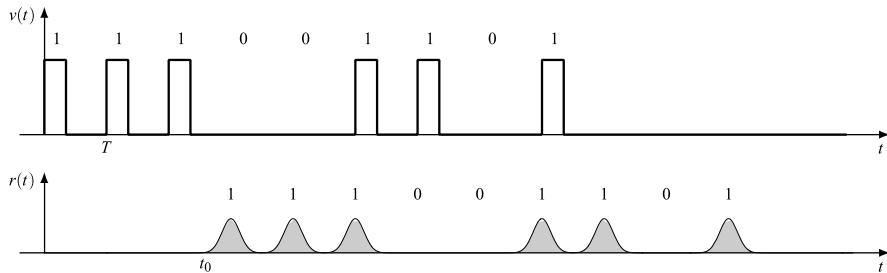


Fig. 1.2 Transmission of a binary digital signal: $s(t)$ transmitted signal and $r(t)$ received signal; T represents the *symbol period* and t_0 a delay

minance) varying along two spatial coordinates. In this case, the transmitter’s task is to perform a *scanning* of the image. In the simplest procedure, the image is subdivided into a sufficiently large number of pixels (picture elements), which pick up a value proportional to the luminance. In such a way, a signal is set up that evolves in time and that can be transmitted. The image can be reproduced from the received signal by restoring the luminance of each pixel.

The example may be complicated by passing to a color image and further complicated for a time varying image (television), in which the message has a *three-dimensional* structure with variations along two spatial coordinates and one time coordinate.

1.2 “Mathematical” Signals

Signal Theory deals with mathematical models rather than with physical models which are considered, e.g., in the field of Electromagnetic Propagation. Roughly speaking, a signal is called *deterministic* when the observer knows perfectly the whole time evolution. Conversely, a signal is called *random* when the evolution is only known in statistical terms. This distinction is not concerned with the signal nature, but only with the observer point of view, and in fact, the same “physical” signal may be regarded as random a priori, before its observation, and as deterministic a posteriori, after its observation.

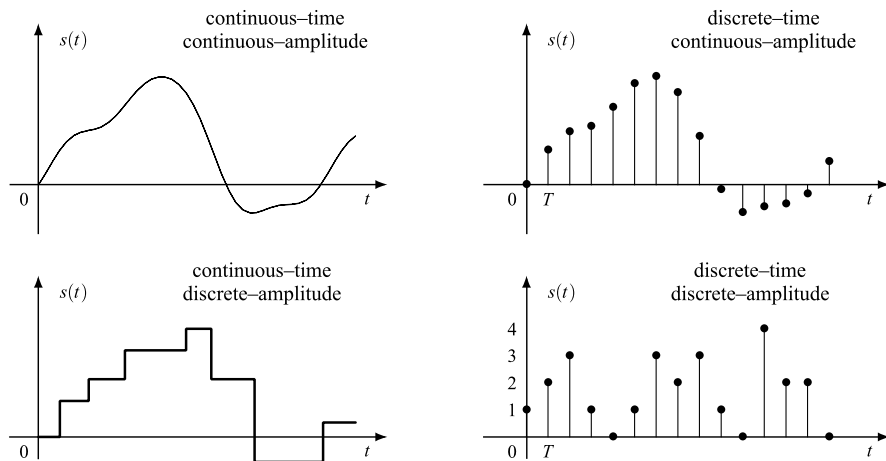


Fig. 1.3 Classification of one-dimensional signals based on domain and amplitude

It is clear that the models require different definitions and approaches. Deterministic signals are studied with the tools of Mathematical Analysis, while random signals are studied with the tools of Probability Theory.

The present book is completely devoted to deterministic signals.

1.2.1 Deterministic Signals

For what above, a deterministic signal (regarded as a model) is simply defined as a function

$$s : I \rightarrow C, \tag{1.1}$$

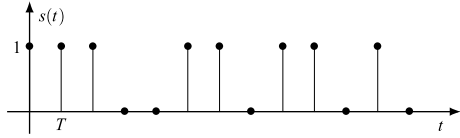
where I is the domain and C is the codomain. Of course, the choice of the function is strictly related to the “physical” signal we are considering, but it is also made on the basis of convenience considerations, as we shall see in the following. By an appropriate choice of the domain I and of the codomain C , we can obtain all the classes of signals of practical interest.

The statement that deterministic signals are simply functions would lead to the conclusion that their study belongs to standard mathematics, particularly to Analysis, so that there would be no need for a specific theory. However, the methodology and even the mentality that are required to study signals widely justify a specific discipline.

The fundamental classes of (one-dimensional) deterministic signals are illustrated in Fig. 1.3:

1. Real functions of a real variable,
2. Real functions of a discrete (countable) variable.

Fig. 1.4 Example of a binary digital signal



The independent variable is commonly, but not necessarily, interpreted as the *time*. Then, we shall denote the signal by $s(t)$, $t \in I$, whenever the codomain will be clear from the context.

Signals of class 1 have a *continuum* as domain and are called *continuous-time signals* or, briefly, *continuous signals*. The domain may be an interval, or a half-line, or more commonly, the real line \mathbb{R} . In the last case, the signal notation becomes

$$s(t), \quad -\infty < t < +\infty \quad \text{or} \quad s(t), \quad t \in \mathbb{R}.$$

Signals of class 2 have a *discrete* set as domain and are called *discrete-time signals* or, briefly, *discrete signals*. In principle, the instants of the domain may be arbitrary, but commonly they are chosen equally spaced with a unitary spacing. Consequently, the signal notation becomes s_n , $-\infty < n < +\infty$ or s_n , $n \in \mathbb{Z}$, where \mathbb{Z} is the set of integers. With an arbitrary spacing T , the notation is

$$s(nT), \quad nT \in \mathbb{Z}(T) \quad \text{or} \quad s(t), \quad t \in \mathbb{Z}(T),$$

where $\mathbb{Z}(T) \triangleq \{nT \mid n \in \mathbb{Z}\}$ is the set of the multiples of T .

Classes 1 and 2 consist of real functions that typically take on values from a continuum. Then, we get *continuous-time continuous-amplitude signals* and *discrete-time continuous-amplitude signals*. However, classes 1 and 2 include functions that take on countably many amplitudes, which are called *quantized* signals. Figure 1.3 shows two examples of quantized signals, for the continuous-time, and the discrete-time case, respectively.

As a further particularization, we find *digital* signals, which are discrete-time and *finite-amplitude* (binary, ternary, etc.). Figure 1.4 shows the binary digital signal that corresponds to the message of Fig. 1.2.

However, Deterministic Signal Theory does not consider specific methodologies for digital and quantized signals, since they are included in the class of continuous-amplitude signals. Methodologies differ in dependence on the continuous or discrete nature of the domain.

We now examine the basic ideas for the choice of the model of a given “physical” signal. To be concrete, we refer to signals that evolve in time as the signal considered in the first example. In principle, a “physical” signal evolving in time assumes a precise value at each instant and hence it determines a function of class 1, i.e., a continuous-time signal. Moreover, such a signal is always: (a) defined on an interval, (b) continuous, and (c) bounded. These properties are justified by physical reasons, since the evolution of a physical quantity has always a finite duration, with no jump variations, and with a finite energy content. From these considerations, it would seem that a single mathematical model would be adequate to represent all

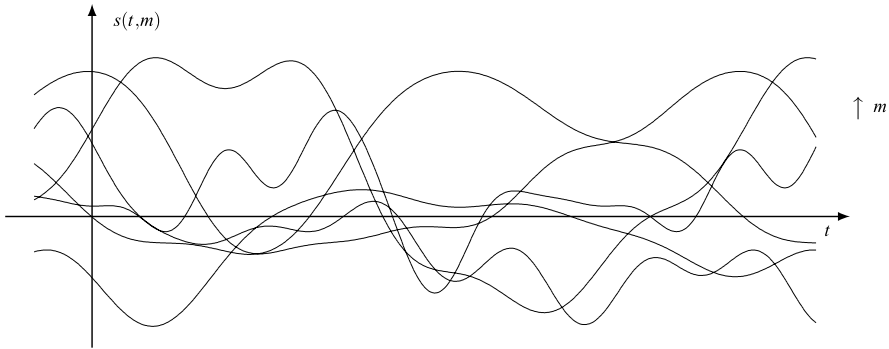


Fig. 1.5 The *random process* regarded as a family of realizations: $s(t, m)$ $m \in \mathcal{M}$; to every m there corresponds a deterministic signal $s(t, m)$

“physical” signals. However, for mathematical convenience, usually, it may be more useful to consider other models, though less linked to the real world. Consider, for instance, the periodic signals, which intrinsically have an infinite-duration, the step signals, and the rectangular impulses which are discontinuous functions. In conclusion, the above physical constraints are not necessarily transferred to mathematical signals.

The introduction of discrete-time signals requires a deeper effort of abstraction which is done whenever the “physical” signal consists of a train of pulses that are equally spaced by T seconds, and we are not interested in modeling the pulse shape, but a single pulse parameter as the amplitude. In this case, to each discrete instant nT we associate the corresponding parameter value thus defining a discrete-time signal $s(nT)$, $n \in \mathbb{Z}$. For instance, the signal illustrated in Fig. 1.2 as a continuous-time signal can be replaced by a binary discrete-time signal, as shown in Fig. 1.4.

1.2.2 Random Signals

According to the formulation of Wiener and Shannon [6] in the 1940s, messages must be unpredictable to have effectively an information content. As a matter of fact, the transmission of a message would not be useful if the receiver could completely predict the message. As a consequence, a theoretical formulation in which messages and signals are known is not sufficient, and the model becomes a *random process*.

To introduce this model in a suggestive way, we still make the reference to a system of Fig. 1.1 where the source chooses a message m from the class of the possible messages \mathcal{M} . The transmitter converts the message $m \in \mathcal{M}$ into a signal

$$s(t, m), \quad t \in I, \quad m \in \mathcal{M}.$$

Thus, we get a family of time-functions (Fig. 1.5) which are called *realizations* or *trajectories* of the random process.

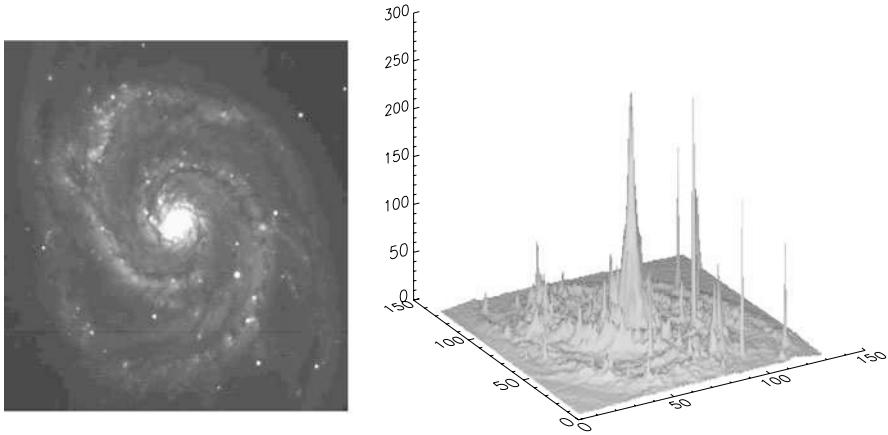


Fig. 1.6 Example of a still image (the galaxy M61) and the corresponding two-dimensional signal representing the image luminance

The theory of Random Processes is not concerned with the single realizations, rather it performs a *statistical characterization* of the whole family by means of the probability tools (distributions and densities, characteristic functions, etc.). In this context, Deterministic Signals are confined to single realizations of a random process.

1.2.3 Multidimensional Signals

Signals considered above and illustrated in Fig. 1.3 are *one-dimensional* since they are functions of one independent variable. They are used to represent “physical” signals whose evolution is along a single coordinate (usually the time).

To represent “physical” signals that evolve along two or more coordinates, we need to introduce functions of so many independent variables. Then, we get *two-dimensional*, *three-dimensional*, and, in general, *multidimensional* signals. The general deterministic signal definition (1.1) includes this variety of signals as soon as we choose a suitable multidimensional domain and we interpret the symbol t as a pair or as a triplet of variables (and, in general, as an n -tuple). For instance, a still image is modeled by a two-dimensional signal of the form

$$s(x, y), \quad (x, y) \in \mathbb{R}^2$$

which represents the luminance value of the point (x, y) (Fig. 1.6). Analogously, a time varying image must be modeled by a three-dimensional signal

$$s(x, y, t), \quad (x, y, t) \in \mathbb{R}^3$$

which represents the luminance of point (x, y) at time t . In these examples, we make reference to a *continuous domain*, but multidimensional signals that are discrete

with respect to one or more coordinates are often considered. The decomposition of an image into pixels is a remarkable example.

1.2.4 Complex Signals

Modern Signal Theory deals with *complex* signals in place of real signals. Therefore, in the general definition (1.1), the codomain C becomes the set \mathbb{C} of complex numbers, and real signals become a particularization.

The introduction of complex signals would not be required to represent “physical” signals, but it stems from reasons of mathematical convenience. The most elementary example is provided by the complex representation of sinusoidal signals, which, as well known, greatly simplifies the circuit analysis in sinusoidal regime. This idea is generalized by Modulation Theory where complex signals are widely used. In general, the extension to complex signals does not lead to any complication, but provides more symmetrical results, particularly in connection with the Fourier transform.

1.3 Historical Note

The study of signals may be dated back at the period of Galileo [8–18] who realized that the pendulum motion can be studied by means of the trigonometric functions, previously used only in geometry. The first example of *frequency analysis* of a (mechanical) system may be ascribed to Euler who, with the discovery of the phenomenon of the mechanical resonance (1739), came up with a very important idea. Specifically, he established that the model, which today is called a linear system, can be identified by iso-frequency oscillations of the form

$$V_0 \cos(2\pi f_0 t + \varphi_0). \quad (1.2)$$

With reference to mechanical systems (pendulum, vibrating strings), Euler realized that the motion solution can be often expressed as iso-frequency oscillations of the form (1.2). However, he did not arrive at the conclusion that this result is the general solution. Some years later, in 1822, Fourier proved that Euler’s solution is really the general one by showing that *every periodic function can be expressed as the sum of sines and cosines*. This is the basic idea in the frequency analysis of signals and systems.

The analysis techniques of mechanical systems were later transferred to electrical circuits. However, it was the study of the transmission media for the telegraph and the telephone that refined the mathematical tools to the today form. In 1855, William Thomson (later appointed Lord Kelvin) published a theory on the electrical telegraph in which he evaluated the impulse response of a coaxial cable. In this analysis, Thomson, continuing Euler’s idea on the sufficiency of the iso-frequency

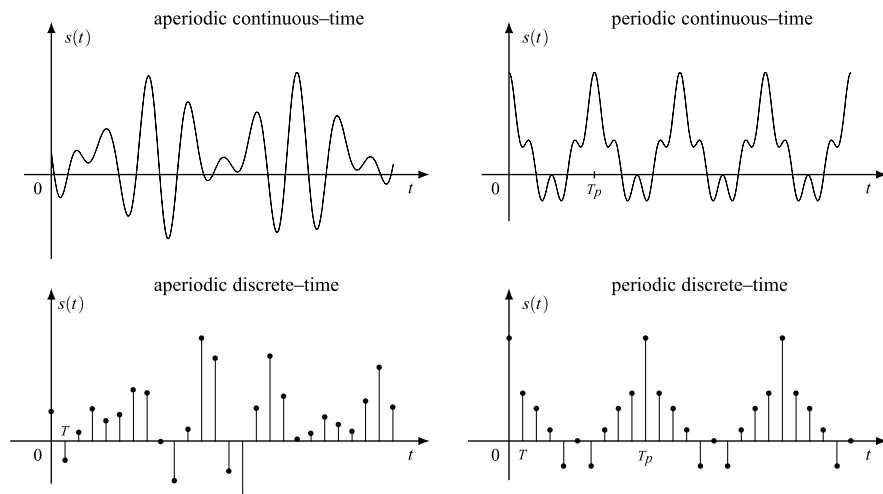


Fig. 1.7 Illustration of the four classes of one-dimensional signals

oscillations analysis, found it convenient to replace the sinusoidal form (1.2) with the exponential form

$$V_0 e^{i(\omega_0 t + \varphi_0)}.$$

The same idea was reconsidered by Heaviside and led to the today's form of the Fourier and Laplace transforms.

In all this long historical evolution, signals were regarded as functions of a real variable, i.e., *continuous-time* signals. The introduction of *discrete-time* signals is more recent and may be dated back to the end of the 1940s, and precisely to Shannon [6, 7], who first used the idea that a band-limited continuous-time signal can be replaced, without loss of information, by a sufficiently dense discrete-time signal (Sampling Theorem). Shannon, moreover, proved that every signal can be converted into a digital form [5].

We now briefly mention the development of signal teaching in the last decades. The first class of signals considered systematically (in the area of information engineering) was the class of periodic signals, and more specifically of *continuous-time periodic signals* (Fig. 1.7). Their study was based on the Fourier series which performs an adequate analysis in the frequency domain. Later on *aperiodic continuous-time signals* were introduced by regarding them as a limiting case of periodic signals with an infinite period, thus getting the passage from the Fourier series to the Fourier integral.

Aperiodic discrete-time signals were introduced more recently in connection with the Sampling Theorem and the Shannon's works. Then, the appearance of computer initiated the digital signal processing and imposed a computational tool improvement with the discovery of the Fast Fourier Transform (FFT) [2].

So, we arrive at *periodic discrete-time signals* which are the only ones that can be handled directly on a digital computer. The availability of powerful computers

together with the possibility of a real time processing led to a systematic study of two- and three-dimensional signals, even if we may encounter earlier outstanding applications. We recall that commercial television was introduced several years earlier than digital computers. However, it was the availability of computer power that developed the study of multidimensional signals.

The last two decades were characterized by a tremendous interest in *wavelets*, a new way to represent and decompose a signal. Wavelets may be seen as a generalization of the frequency domain representation, but are superior in multiresolution analysis.

Coming back to one-dimensional signals, in the previous considerations we have outlined the following four classes of signals (Fig. 1.7): aperiodic continuous-time, periodic continuous-time, aperiodic discrete-time and periodic discrete-time.

These classes of signals are dealt with in a good deal of textbooks (see the biography at the end of Chap. 2), some of which pay much more attention to continuous-time signals, others to discrete-time signals. In particular, by the end of the 1960s the author published a *synoptic* theory [1] where each of the four classes were separately developed, meaning that definitions and developments were carried out independently.¹ Stimulated by the apparent symmetries between definitions and final results, the author envisioned the idea of a unified approach.

Gallery of Signals: E Pluribus Unum In Fig. 1.8, we sketch a gallery of signals: one dimensional continuous-time, one-dimensional discrete-time, real and complex, periodic and aperiodic, two-dimensional continuous-argument, two-dimensional continuous-argument, two-dimensional discrete-argument, two-dimensional mixed-argument. The goal of the UST is realizing the leitmotif *e pluribus unum*.

1.4 The Unified Signal Theory

We have seen that *deterministic signal* is a function $s : I \rightarrow C$, where I is the domain and C is the codomain. Then, the unification possibility stems from the choice of a domain I with a mathematical structure, articulated enough to enable the introduction of fundamental operations, and from the choice of codomain C , broad enough to include the amplitudes of interest. So, we arrive to reformulate a deterministic signal as

$$s : I \rightarrow \mathbb{C}, \quad (1.3)$$

where the domain I is an *Abelian group*² (see Chap. 3) and the codomain is the *set* \mathbb{C} of complex numbers. Signal (1.3) will be denoted in the form

$$s(t), \quad t \in I,$$

¹A similar synoptic theory may be found in [4].

²In the Unified Theory, I is a pair of Abelian groups which represent both the domain and the periodicity of the signals. But, in these preliminaries it is sufficient to consider only the domain.

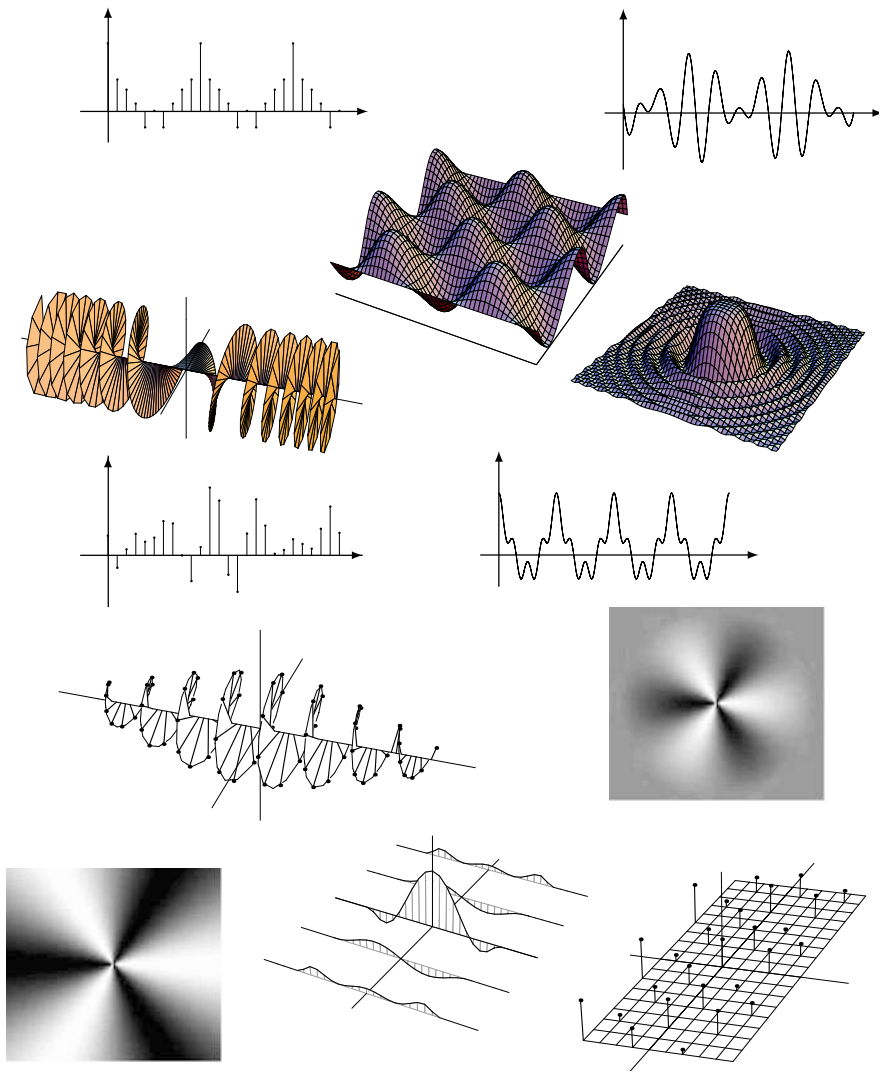


Fig. 1.8 e pluribus unum

which recalls explicitly the domain I , while the codomain is implicit (since it is always \mathbb{C}).

To explain why I must be an Abelian group, consider the convolution of two continuous-time signal $x(t)$ and $y(t)$ which is defined by

$$s(t) = \int_{-\infty}^{+\infty} x(u)y(t - u) du, \quad t \in \mathbb{R}, \tag{1.4}$$

where $s(t)$ is the result of the convolution. In this operation, the arguments t and u are arbitrary points of \mathbb{R} , the set of real numbers, but also $t - u$ must be a point of \mathbb{R} . This is assured by the fact that \mathbb{R} is an Abelian group, the additive group of real numbers.

Now, we show that, with a slight effort of generalization, the convolution for continuous-time signals can be extended to all the signal classes. To this end, we rewrite (1.4) in the form

$$s(t) = \int_{\mathbb{R}} du x(u)y(t - u), \quad t \in \mathbb{R},$$

which emphasizes that the integral must be *extended over the whole signal domain* \mathbb{R} . To arrive at the unified convolution of two signals $x(t)$, $t \in I$, and $y(t)$, $t \in I$, we simply write

$$\boxed{s(t) = \int_I du x(u)y(t - u), \quad t \in I.} \quad (1.5)$$

Then, we have to define the integral over the domain I , which is an Abelian group, where $t, u \in I$ assure that also $t - u \in I$. Now, the most familiar integral, i.e., the Lebesgue integral, can be considered on Abelian groups. This integral works well for *continuous-time* signals, as stated by (1.4), but it has the drawback of inducing a zero measure for all *discrete* groups. In other words, if the integral (1.5) is interpreted as a Lebesgue integral and I is a discrete group, the result is identically zero, and consequently not useful. The appropriate choice is given by the Haar integral [3], which is developed in the field of Topology. This integral provides the Lebesgue integral when $I = \mathbb{R}$ and in this case (1.5) yields (1.4), as we want. When I is a discrete group, the Haar integral turns out to be proportional to the sum of the integrand values, again as we want to have. Moreover, it is defined for multidimensional groups as well and, in this case, (1.5) lets us define the convolution also for multidimensional signals. As we shall see, the rules for the Haar integral are essentially the same as for the Lebesgue integral on \mathbb{R} . This permits us to obtain all the rules for convolution in a unified manner, otherwise each rule should be obtained separately for the different classes of signals.

What has been seen for the convolution holds also for the Fourier transform and for the other operations of Signal Theory. Therefore, the fundamental operations of Signal Theory can be carried out with a unified approach using the Haar integral.

It remains to clarify one point: the Haar integral is defined on *topological* Abelian groups and its learning would require very abstract notions of Topology. In this book, however, these notions will not be developed and only the expression of the Haar integral, in the cases of interest, will be provided. The author's opinion is that this compromise is well adequate for a theory whose final goal is represented by applications.

1.5 Content of the Book

As said in the Preface, the UST can be conceptually subdivided in three parts.

Part I: Classic Theory In Chap. 2, we introduce the fundamental definitions on continuous-time signals, arriving at the frequency analysis given by the Fourier series (for periodic signals) and by the Fourier transform (for aperiodic signals). The same topics are developed for discrete-time signals. Finally, we examine the possibility to represent a continuous-time signal by a discrete-time signal (Sampling Theorem).

This part is formulated with the classical (not unified) approach and is introduced for the reader who is not familiar with the elementary notions on signals.

Part II: Unified Signal Theory It is organized in seven chapters. Chapter 3 deals with the notions on Abelian groups. In Chap. 4, the Haar integral is introduced and the convolution is developed. Chapter 5 develops the Fourier transform, where the preliminary step is to establish the frequency domain \widehat{I} (the dual group) that corresponds to the signal domain I . Then, the Fourier transform and its inverse can be introduced in a complete general form using the Haar integral.

Chapter 6 deals with transformations of signals and particularly *linear transformations* (here transformation is synonymous to a *system*). By means of the Haar integral, we define the linear transformations in a completely general way, in which the output signal domain may be different, even for the dimensionality, from the input signal domain. Then, transformations are developed in the frequency domain. In Chap. 7, the important class of multirate transformations are developed in detail.

Chapter 8 deals with the sampling operation and with the possibility of signal recovery from its sample values (Unified Samplings Theorem). Chapter 16 deals with advance topic on groups and is carried out before the final applications of Part III.

Part III: Specific Classes of Signals and Applications This part is devoted to the study and probing of specific signal classes, to which we can apply all the results of the Unified Theory and also some specific results that do not hold in the unified approach. For instance, for continuous-time signals (Chap. 9) derivative and integral operations can be considered both in the time and in the frequency domain, and specific results can be established. For continuous-time signals, in addition to the Fourier transform, the *Laplace transform* is introduced and related to the Fourier transform. Analogously, for discrete-time signals the *z-transform* is introduced and then related to the corresponding Fourier transform.

Chapter 13 is devoted to digital signal processing, which is essentially based on the Fast Fourier Transform (FFT) algorithm. In Chap. 14, filter banks and sub-band coding are developed, after the formulation of signal expansion as *generalized transforms*. In Chap. 15, wavelets and multiresolution analysis is carried out with illustrations and examples of application.

The final two chapters are devoted to advanced topics of multidimensional signals and to image theory with application to television scanning and tomography.

1.6 Conventions on Notation

The sections where the UST is developed are marked with UT. Sections of advanced topics that can be omitted at the first reading are marked by \Downarrow . Problems are marked by asterisks whose number stands for the increasing difficulty. Sections and problems marked with the symbol ∇ require notions that are developed later on.

Throughout the book, notations are explicitly specified at the first use and are frequently recalled. Signals are denoted in lower-case and Fourier transforms by the corresponding upper-case letters. Hence, if $x(t)$, $t \in I$, denotes a signal, then $X(f)$, $f \in \widehat{I}$, denotes the corresponding Fourier transform. In these notations, the domains are always explicitly indicated, while the codomain is understood as the set of complex numbers. In block diagrams, signal labels are indicated above the connections and domain labels are indicated below.

The Haar integral is denoted in the form

$$\int_I dt x(t)$$

with the “differential” before the integrand, leaving the standard form with the “differential” after the integrand to the ordinary integral.

The UST formulation has led to the introduction of several new terms, not usual in the literature. This has been done with reluctance, but it was necessary to proceed with a more synthetic language. These new terms are marked by an asterisk in the index.

References

1. G. Cariolaro, *Teoria dei Segnali* (Cleup, Padova, 1970)
2. J.W. Cooley, J.W. Tukey, An algorithm for the machine computation of complex Fourier series. *Math. Comput.* **19**, 297–301 (1965)
3. A. Haar, Der Massbegriff in der Theorie der kontinuierlichen Gruppen. *Ann. Math.* **34**, 147–169 (1933)
4. P. Kraniuskas, *Transforms in Signals and Systems* (Addison–Wesley, Wokingham, 1992)
5. B.M. Oliver, J.R. Pierce, C.E. Shannon, The philosophy of PCM. *Proc. IRE* **36**, 1324–1332 (1948)
6. C.E. Shannon, A mathematical theory of communication. *Bell Syst. Tech. J.* **XXVII** (July 1948)
7. C.E. Shannon, Communication in the presence of noise. *Proc. IRE* **37**, 10–21 (1949)

References on the History of Signal Theory

8. A.L. Cauchy, Mémoire sur diverses formulaes dé analyse. *Comptes Rendus* **12**, 283–298 (1841)
9. J.W. Cooley, P.A.W. Lewis, P.D. Welch, Historical notes on the fast Fourier transform. *IEEE Trans. Audio Electroacoust.* **AU–15**, 76–79 (1967)

10. W.C. Dampier, *A History of Science* (Macmillan & Co., New York, 1943)
11. C.F. Gauss, Nachlass: Theoria interpolationis methodo nova tractata, in *Carl Friedrich Gauss, Werke*, vol. 3 (Königlichen Gesellschaft der Wissenschaften, Göttingen, 1866), pp. 265–303
12. O. Heaviside, *Electromagnetic Theory*, vol. I (Chelsea, Manchester, 1971)
13. J.M. Manley, The concept of frequency in linear system analysis. *IEEE Commun. Mag.* **20**, 26–35 (1982)
14. H. Nyquist, Certain factors affecting telegraph speed. *Bell Syst. Tech. J.* **3**, 324–346 (1924)
15. J.W.S. Rayleigh, *Theory of Sound*, 1st edn. (Macmillan & Co., London, 1894)
16. W. Thomson, Theory of electric telegraph. *Proc. R. Soc.* **VII**, 382 (1855)
17. S.P. Thompson, *Life of Lord Kelvin* (Macmillan & Co., London, 1910)
18. W. Thomson, On transient electric currents. *Philos. Mag.* (June 1927)

Part I
Classic Theory

Chapter 2

Classical Signal Theory

2.1 Continuous Signal Definitions

We begin with a formal definition:

Definition 2.1 A continuous-time signal is a complex function of a real variable $s : \mathbb{R} \rightarrow \mathbb{C}$, where the domain \mathbb{R} is the set of real numbers and the codomain \mathbb{C} is the set of complex numbers.

The signal will be denoted by $s(t)$, $t \in \mathbb{R}$, or simply by $s(t)$. The independent variable t is typically interpreted as *time*. From the historical viewpoint, *continuous-time* signals (more briefly, *continuous* signals) represent the most important class, and are the subject of several textbooks [1, 6, 8–25].

An important subclass of continuous signals is given by *real* signals, which can be defined by the relationship

$$s(t) = s^*(t), \tag{2.1}$$

where the asterisk denotes “complex conjugation”.

Another important subclass is given by *periodic* signals, characterized by the relationship

$$s(t + T_p) = s(t), \tag{2.2}$$

where the constant time $T_p > 0$ represents the *period*. Signals that do not satisfy Condition (2.2) are called *aperiodic*.

2.1.1 Signal Symmetries

A signal $s(t)$ is *even* (Fig. 2.1) if for any t

$$s(-t) = s(t), \tag{2.3a}$$

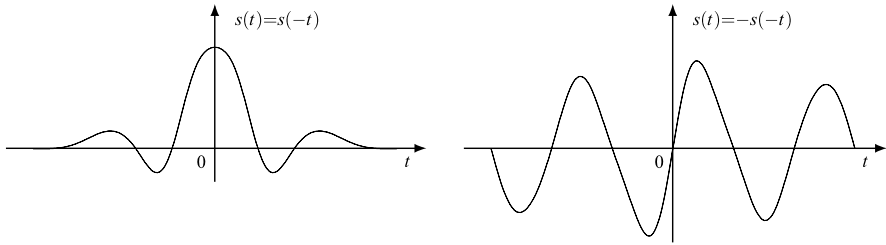


Fig. 2.1 Examples of even and odd signals

it is *odd* (Fig. 2.1) if

$$s(-t) = -s(t). \quad (2.3b)$$

An arbitrary signal can be always decomposed into the sum of an *even* component $s_e(t)$ and an *odd* component $s_o(t)$

$$s(t) = s_e(t) + s_o(t), \quad (2.4)$$

where

$$s_e(t) = \frac{1}{2}[s(t) + s(-t)], \quad s_o(t) = \frac{1}{2}[s(t) - s(-t)]. \quad (2.4a)$$

A signal is *causal* (Fig. 2.2) if it is zero for negative t ,

$$s(t) = 0 \quad \text{for } t < 0. \quad (2.5)$$

A causal signal is neither even nor odd, but can be decomposed into an even and an odd component, according to (2.4) to give $s_e(t) = s_o(t) = \frac{1}{2}s(t)$ for $t > 0$ and $s_e(t) = -s_o(t) = \frac{1}{2}s(-t)$ for $t < 0$.¹ We can link the even and odd components of a causal signal by the relationships

$$s_o(t) = \text{sgn}(t)s_e(t), \quad s_e(t) = \text{sgn}(t)s_o(t), \quad (2.6)$$

where $\text{sgn}(x)$ is the “signum” function

$$\text{sgn}(x) = \begin{cases} -1, & \text{for } x < 0; \\ 0, & \text{for } x = 0; \\ +1, & \text{for } x > 0. \end{cases} \quad (2.7)$$

¹The above relations hold for $t \neq 0$. For $t = 0$ we may have a discontinuity, as shown in Fig. 2.2. The problem of the signal value at discontinuities will be discussed below (see (2.19)).

Fig. 2.2 Decomposition of a causal signal $s(t)$ into the even part $s_e(t)$ and odd part $s_o(t)$

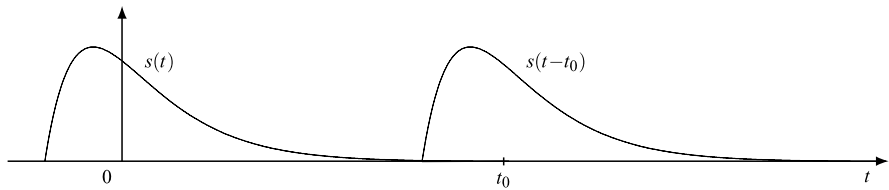
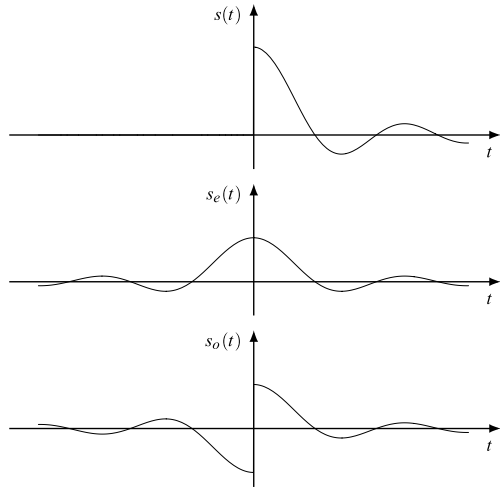


Fig. 2.3 Illustration of a t_0 -shift of a signal

2.1.2 Time-Shift

Given a signal $s(t)$ and a time value t_0 , the signal

$$s_{t_0}(t) = s(t - t_0) \tag{2.8}$$

represents a shifted version of $s(t)$, by the amount t_0 . If $t_0 > 0$ the time-shift is called a *delay* (Fig. 2.3), if $t_0 < 0$ it is called an *advance*, that is, a negative delay.

It is worth noting that to introduce a delay, e.g., of 5 units, we have to write $s(t - 5)$ and not $s(t + 5)$.

2.1.3 Area and Mean Value

The integral of a signal $s(t)$, $t \in \mathbb{R}$, extended over the whole domain \mathbb{R} is called the *area* of the signal

$$\text{area}(s) = \int_{-\infty}^{+\infty} s(t) dt. \tag{2.9}$$

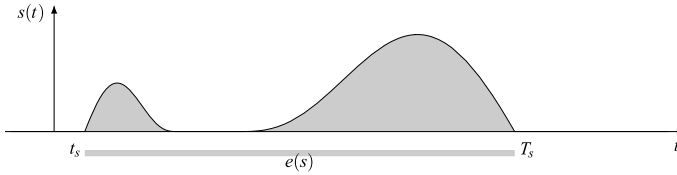


Fig. 2.4 Signal with an extension limited to the interval $[t_s, T_s]$

The limit

$$m_s = \lim_{T \rightarrow \infty} \frac{1}{2T} \int_{-T}^T s(t) dt \quad (2.10)$$

is called the *mean value*. In the context of electrical circuits, m_s is called *direct current* component.

2.1.4 Energy and Power

The *specific energy*, or simply *energy*, is defined by

$$E_s = \int_{-\infty}^{+\infty} |s(t)|^2 dt, \quad (2.11)$$

and the (specific) *power* by the limit

$$P_s = \lim_{T \rightarrow \infty} \frac{1}{2T} \int_{-T}^T |s(t)|^2 dt. \quad (2.12)$$

This terminology derives from the fact that, if $s(t)$ represents a voltage or a current applied to a unitary resistance, E_s equals the physical energy (in joules), while P_s equals the physical power (in watts) dissipated by the resistance.

If $0 < E_s < \infty$, then $s(t)$ is a *finite-energy* signal, and if $0 < P_s < \infty$ then $s(t)$ is a *finite-power* signal. Note that a finite-energy signal has $P_s = 0$ and a finite-power signal has $E_s = \infty$.

Typically, periodic signals have finite power and aperiodic signals have finite energy. However, some aperiodic signals, such as the step function, turn out to be finite-power signals.

2.1.5 Duration and Extension

A signal $s(t)$ that is zero-valued outside of a finite interval $[t_s, T_s]$ is called of *limited duration* and the measure of the interval is the *duration* of the signal. The interval $[t_s, T_s]$ is the *extension* of the signal and gives more information than the duration, because it indicates *where* the signal is significant (Fig. 2.4).

Definition 2.2 A set $e(s)$ such that

$$s(t) = 0, \quad t \notin e(s) \quad (2.13)$$

is the *extension* of $s(t)$ and its measure $D(s)$ is the *duration* of $s(t)$.

The above definition provides a basis for an obvious signal classification. If $e(s) = [t_s, T_s]$ is a finite interval, the signal has a *strictly-limited extension* or is *strictly time-limited*; if $e(s) = (-\infty, T_s]$ with T_s finite, the signal is *upper time-limited*, etc. In particular, the extension of *periodic* signals is always unlimited, $e(s) = (-\infty, +\infty) = \mathbb{R}$, and the extension of *causal* signals is lower time-limited with $e(s) = [0, +\infty)$.

Note that the above definitions are not stringent in the sense that duration and extension are not unique; in general, it is convenient to refer to as the smallest extension and duration (see Chap. 4).

2.1.6 Discontinuous Signals

The class of continuous-time signals includes discontinuous functions. The unit step function is a first example. In function theory, a function may be undefined at points of discontinuity, but in Signal Theory it is customary to assign a precise value at such a point. Specifically, if $s(t)$ has a discontinuity point at $t = t_0$, we assign the average value (*semi-value*)

$$s(t_0) = \frac{1}{2} [s(t_{0-}) + s(t_{0+})], \quad (2.14)$$

where $s(t_{0-})$ and $s(t_{0+})$ are the limits of $s(t)$ when t_0 is approached from the left and the right, respectively.

The reason of this convention is that, at discontinuities, the inverse Fourier transform converges to the semi-value.

2.2 Continuous Periodic Signals

Some of the general definitions given above for continuous-time signals hold for the subclass of periodic signals. This is the case for even and odd symmetries. Other definitions must be suitably modified.

It is worth stressing that in the *condition for periodicity*

$$s(t + T_p) = s(t), \quad t \in \mathbb{R}, \quad (2.15)$$

the period T_p is not unique. In fact, if T_p satisfies the condition (2.15), then also kT_p with k integer, satisfies the same condition. The smallest positive value of T_p

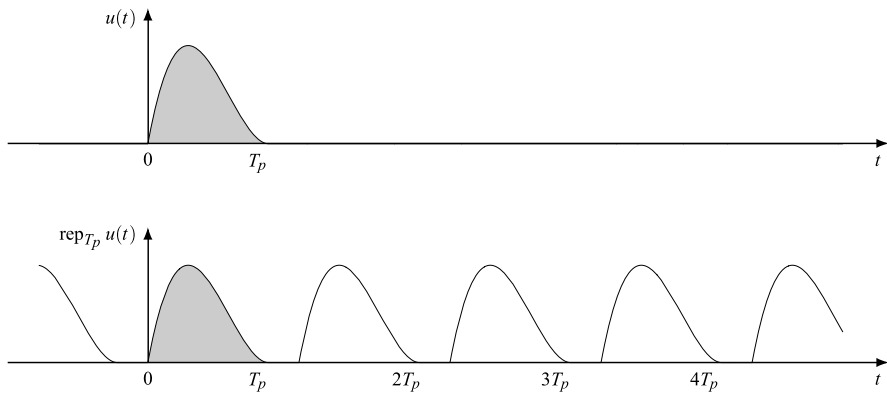


Fig. 2.5 Periodic repetition of an aperiodic signal with period T_p

will be called the *minimum period*, and a general positive value of T_p is a *period* of the signal. We also note that a periodic signal is fully identified by its behavior in a single period $[t_0, t_0 + T_p)$, where t_0 is arbitrary, since outside the period its behavior can be derived from the periodicity condition.

Note that “period” is used in two senses, as the positive real quantity T_p as well as an interval $[t_0, t_0 + T_p)$.

Periodic Repetition Sometimes a periodic signal is expressed as the *periodic repetition* of an aperiodic signal $u(t)$, $t \in \mathbb{R}$, namely (Fig. 2.5)

$$s(t) = \sum_{n=-\infty}^{+\infty} u(t - nT_p) \triangleq \text{rep}_{T_p} u(t), \quad (2.16)$$

where T_p is the *repetition period*.

Periodic repetition does not require that the signal $u(t)$ be of limited-duration as in Fig. 2.5. In general, for every $t \in \mathbb{R}$, a periodic repetition is given as a sum of a bilateral series (see Problem 2.8 for a periodic repetition in which the terms overlap, and see also Sect. 6.10).

2.2.1 Area, Mean Value, Energy and Power Over a Period

For periodic signals, the area definition given in (2.9) is not useful and is replaced by the *area over a period*

$$\text{area}(s) = \int_{t_0}^{t_0+T_p} s(t) dt. \quad (2.17a)$$

The *mean value over a period* is defined by

$$m_s(T_p) = \frac{1}{T_p} \int_{t_0}^{t_0+T_p} s(t) dt. \quad (2.17b)$$

It can be shown that the mean value over a period equals the mean value defined as a limit by (2.10). Moreover, the periodicity property assures that both definitions (2.17a) and (2.17b) are independent of t_0 .

The definition of energy (2.11) is replaced by that of *energy over a period*

$$E_s(T_p) = \int_{t_0}^{t_0+T_p} |s(t)|^2 dt. \quad (2.18a)$$

The *mean power over a period* is defined by

$$P_s(T_p) = \frac{1}{T_p} E_s(T_p) = \frac{1}{T_p} \int_{t_0}^{t_0+T_p} |s(t)|^2 dt. \quad (2.18b)$$

Note that the square root of $P_s(T_p)$ is known as the *root mean square* (rms) value.

2.3 Examples of Continuous Signals

We introduce the first examples of continuous signals, mainly to illustrate the usage of some functions, such as the step function and the Delta function.

2.3.1 Constant Signals

A *constant signal* has the form

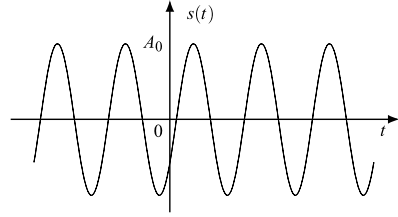
$$s(t) = A,$$

where A is a complex constant. It is even, with finite power, $P_s = |A|^2$, and with mean value A . Constant signals may be regarded as a limit case of periodic signals with an arbitrary period.

2.3.2 Sinusoidal and Exponential Signals

A *sinusoidal signal* (Fig. 2.6)

$$s(t) = A_0 \cos(\omega_0 t + \phi_0) = A_0 \cos(2\pi f_0 t + \phi_0) = A_0 \cos\left(2\pi \frac{t}{T_0} + \phi_0\right) \quad (2.19)$$

Fig. 2.6 Sinusoidal signal

is characterized by its amplitude A_0 , angular frequency ω_0 and phase ϕ_0 . Without loss of generality, we can always assume A_0 and ω_0 positive. The *angular* frequency ω_0 is related to the frequency f_0 by the relation $\omega_0 = 2\pi f_0$. Sinusoidal signals are periodic, with (minimum) period $T_0 = 1/f_0$, finite power, $P_s = \frac{1}{2}A_0^2$, and zero mean value. The signal (2.19) can be expressed as

$$s(t) = A_0 \cos \phi_0 \cos \omega_0 t - A_0 \sin \phi_0 \sin \omega_0 t,$$

which represents the decomposition into even and odd parts. By means of the very important Euler's formulas,

$$\boxed{\cos x = \frac{e^{ix} + e^{-ix}}{2}, \quad \sin x = \frac{e^{ix} - e^{-ix}}{2i}}, \quad (2.20)$$

a sinusoidal signal can also be decomposed into a sum of two *exponential signals*

$$s(t) = A_0 \cos(\omega_0 t + \phi_0) = \frac{1}{2}A_0 e^{i(\omega_0 t + \phi_0)} + \frac{1}{2}A_0 e^{-i(\omega_0 t + \phi_0)}. \quad (2.21)$$

Furthermore, it can be written as the real part of an exponential signal

$$s(t) = \Re A e^{i\omega_0 t}, \quad A = A_0 e^{i\phi_0}.$$

The *exponential signal* has the general form Ae^{pt} , where p is a complex constant. A particular relevance has the exponential signal with p imaginary, that is,

$$s(t) = Ae^{i\omega_0 t} = Ae^{i2\pi f_0 t}.$$

This signal is illustrated in Fig. 2.7. It has finite power $P_s = |A|^2$ and (minimum) period $1/|f_0|$. While for sinusoidal signals the frequency is commonly assumed to be positive, for exponential signals the frequencies may be negative, as well as positive.

Notation As a rule, a *real* amplitude will be denoted by A_0 , and a *complex* amplitude by A . In general, we suppose $A_0 > 0$.

Fig. 2.7 The exponential signal and its sine and cosine projections

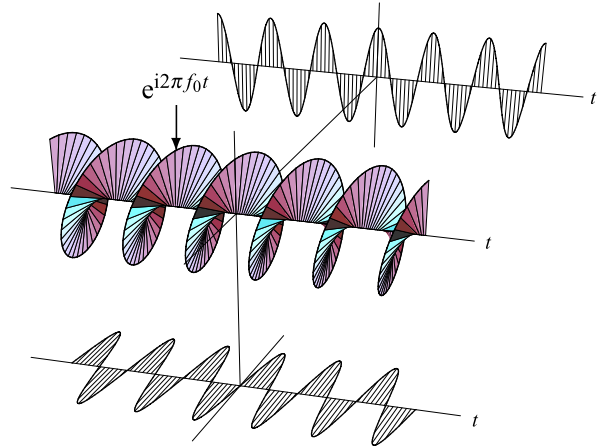
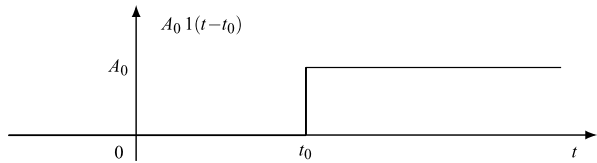


Fig. 2.8 Step signal of amplitude A_0 applied at the instant t_0



2.3.3 Step Signals

A *step signal* has the form (Fig. 2.8)

$$s(t) = A_0 1(t - t_0),$$

where $1(x)$ denotes the *unit step function*

$$1(x) = \begin{cases} 0, & \text{for } x < 0, \\ 1, & \text{for } x > 0. \end{cases} \quad (2.22)$$

It is aperiodic, with finite power $\frac{1}{2}A_0^2$ and mean value $\frac{1}{2}A_0$. Note that, by the conventions on discontinuities, $1(0) = \frac{1}{2}$ and $s(t_0) = \frac{1}{2}A_0$.

The following decomposition

$$A_0 1(t - t_0) = \frac{1}{2}A_0 + \frac{1}{2}A_0 \operatorname{sgn}(t - t_0), \quad (2.23)$$

is worth noticing, where $\operatorname{sgn}(x)$ is the *signum function*, $\frac{1}{2}A_0$ is the mean value and the last term has zero mean value.

The *unit step function* allows writing the *causal version* of a given signal $s(t)$ as

$$s_c(t) = 1(t)s(t),$$

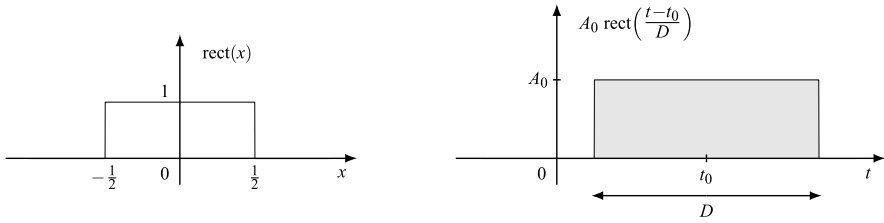


Fig. 2.9 The $\text{rect}(x)$ function and the rectangular impulse of duration D , amplitude A_0 and central instant t_0

which coincides with $s(t)$ for $t > 0$ and is zero for $t < 0$. For instance, the causal version of the linear signal $s(t) = \beta t$, with slope β , is the *ramp* signal $s_c(t) = 1(t)\beta t$.

A notable example of a causal signal is the *causal exponential*

$$s_c(t) = 1(t)e^{p_0 t} \quad (2.24)$$

where $p_0 = \sigma_0 + i\omega_0$ is a complex constant. If $\Re p_0 = \sigma_0 < 0$, this signal approaches zero as $t \rightarrow +\infty$, and has energy $1/|2\sigma_0|$; if $\sigma_0 > 0$ the signal diverges and has infinite energy.

2.3.4 Rectangular and Triangular Pulses

Using the definition

$$\text{rect}(x) = \begin{cases} 1, & \text{for } |x| < \frac{1}{2}, \\ 0, & \text{for } |x| > \frac{1}{2}, \end{cases} \quad (2.25)$$

the pulse² centered at t_0 with duration D and amplitude A_0 (Fig. 2.9) can be written in the form

$$r(t) = A_0 \text{rect}\left(\frac{t - t_0}{D}\right). \quad (2.26)$$

Alternatively, we can express the pulse (2.26) as the difference between two step signals, namely

$$A_0 \text{rect}\left(\frac{t - t_0}{D}\right) = A_0 1(t - t_1) - A_0 1(t - t_2), \quad (2.27)$$

where $t_1 = t_0 - \frac{1}{2}D$ and $t_2 = t_0 + \frac{1}{2}D$. The pulse (2.26) has finite extension, $e(r) = [t_1, t_2]$, finite energy, $E_r = A_0^2 D$, and finite area, $\text{area}(r) = A_0 D$.

²Strictly speaking, a *pulse* denotes a signal of “short” duration, but more generally this term is synonymous with *aperiodic signal*.

Sometimes we shall use the *causal rect function*

$$\text{rect}_+(x) = \text{rect}\left(x - \frac{1}{2}\right) = \begin{cases} 1, & \text{for } 0 < x < 1; \\ 0, & \text{otherwise.} \end{cases} \quad (2.28)$$

The rect functions are useful for writing concisely the *truncated versions* of a given signal $s(t)$ as $s(t) \text{rect}[(t - t_0)D]$ or $s(t) \text{rect}_+[(t - t_0)/D]$, which have extensions $(t_0 - \frac{1}{2}D, t_0 + \frac{1}{2}D)$ and $(t_0, t_0 + D)$, respectively.

A *triangular pulse* is introduced by the function

$$\text{triang}(x) = \begin{cases} 1 - |x| & \text{for } |x| < 1; \\ 0 & \text{for } |x| > 1. \end{cases} \quad (2.29)$$

Note that $\text{triang}(x) = \text{rect}(x/2)(1 - |x|)$. The pulse $A_0 \text{triang}(t/D)$ has extension $(-D, D)$ and amplitude A_0 .

2.3.5 Impulses

Among the continuous signals, a fundamental role is played by the *delta function* or *Dirac function* $\delta(t)$. From a rigorously mathematical point of view, $\delta(t)$ is not an *ordinary function* and should be introduced as a *generalized function* in the framework of *distribution theory* [4] or of the *measure theory* [3].

On the other hand, for all practical purposes, a simple heuristic definition is adequate. Namely, $\delta(t)$ is assumed to vanish for $t \neq 0$ and satisfy the *sifting property*

$$\int_{-\infty}^{\infty} \delta(t)s(t) dt = s(0).$$

In particular, since

$$\int_{-\infty}^{\infty} \delta(t) dt = 1,$$

$\delta(t)$ may be interpreted as a signal with zero duration and unit area.

Intuitively, the Dirac function may be interpreted as a limit of a sequence of suitably chosen ordinary functions. For instance,

$$r_D(t) = \frac{1}{D} \text{rect}\left(\frac{t}{D}\right), \quad (2.30)$$

with $D > 0$, is a signal having unit area and duration D . As D tends to 0, the duration of r_D vanishes while the area maintains the unit value. Even though the limit diverges for $t = 0$, we find it useful to set

$$\delta(t) = \lim_{D \rightarrow 0} r_D(t).$$

Note that

$$\lim_{D \rightarrow 0} \int_{-\infty}^{\infty} r_D(t) s(t) dt = \lim_{D \rightarrow 0} \frac{1}{D} \int_{-D/2}^{D/2} s(t) dt = s(0),$$

so that the value of $s(t)$ at the origin is *sifted*. In conclusion, the sifting property applied to a signal $s(t)$ may be interpreted as a convenient shorthand for the following operations: (i) integrating the signal multiplied by $r_D(t)$, and (ii) evaluating the limit of the integral as $D \rightarrow 0$. Note that these limit considerations imply that

$$\delta(t) = 0 \quad \text{for } t \neq 0. \quad (2.31)$$

The choice of a rectangular pulse in the heuristic derivation is a mere mathematical convenience. Alternatively [1], we could choose a unitary area pulse $r(t)$, e.g., a triangular pulse or a Gaussian pulse, define $r_D(t) = (1/D)r(t/D)$ and apply the above operations.

In practice, we handle the delta function as an ordinary function, and indeed, it is called the *delta function* or *Dirac function*. For instance, we get

$$\boxed{\int_{-\infty}^{\infty} s(t) \delta(t - t_0) dt = \int_{-\infty}^{\infty} s(t + t_0) \delta(t) dt = s(t_0).} \quad (2.32)$$

Moreover,

$$\int_{-\infty}^{\infty} \delta(-t) s(t) dt = \int_{-\infty}^{\infty} \delta(t) s(-t) dt = s(0) = \int_{-\infty}^{\infty} \delta(t) s(t) dt,$$

and $\delta(t)$ is considered an even function. Then, (2.32) can be written in the alternative form

$$\boxed{s(t) = \int_{-\infty}^{+\infty} s(u) \delta(t - u) du.} \quad (2.33)$$

Of course, the delta function has singular properties. For instance, it allows writing a signal of zero duration and with finite area α as

$$\alpha \delta(t - t_0),$$

where t_0 is the *application instant*. In fact, from (2.31) it follows that

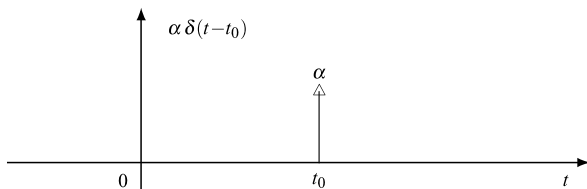
$$\alpha \delta(t - t_0) = 0 \quad \text{for } t \neq t_0,$$

so that the duration is zero and the area is

$$\int_{-\infty}^{+\infty} \alpha \delta(t - t_0) dt = \alpha \int_{-\infty}^{+\infty} \delta(t - t_0) dt = \alpha.$$

We shall use the graphical convention to represent $\alpha \delta(t - t_0)$ by a vertical arrow of length α applied at $t = t_0$ (Fig. 2.10), where the length of the arrow *does not*

Fig. 2.10 Graphical representation of the impulse of area α applied at the instant t_0



represent the amplitude of the impulse but its area. In the Unified Theory, the delta function will be called an *impulse*.

We note that the square of the delta function is undefined (even in distribution theory), so that it makes no sense to talk of energy and power of the delta function. Finally, we note that the formalism of the delta function allows writing the derivative of a discontinuous signal, for example,

$$\frac{dl(t)}{dt} = \delta(t). \quad (2.34)$$

More generally, for a discontinuity at t_0 the derivative of a signal has an impulse of area $s(t_{0+}) - s(t_{0-})$ at t_0 .

In the framework of distribution theory, also derivatives of any order of the delta function are defined, with useful applications in Signal and Control Theory. We confine us to the first derivative, in symbols

$$\delta'(t) = \frac{d\delta(t)}{dt}.$$

Formally, applying the integration by parts, we obtain the *derivative sifting property*

$$\int_{-\infty}^{\infty} \delta'(t)s(t) dt = \delta(t)s(t)|_{-\infty}^{\infty} - \int_{-\infty}^{\infty} \delta(t)s'(t) dt = -s'(0).$$

We may give a heuristic interpretation also to $\delta'(t)$ as

$$\delta'(t) = \lim_{D \rightarrow 0} u_D(t)$$

with

$$u_D(t) = \frac{1}{D^2} \left[\text{rect}\left(\frac{t + D/2}{D}\right) - \text{rect}\left(\frac{t - D/2}{D}\right) \right].$$

Indeed, it can be shown that, under mild conditions, $\lim_{D \rightarrow 0} \int_{-\infty}^{\infty} u_D(t)s(t) dt = s'(0)$.

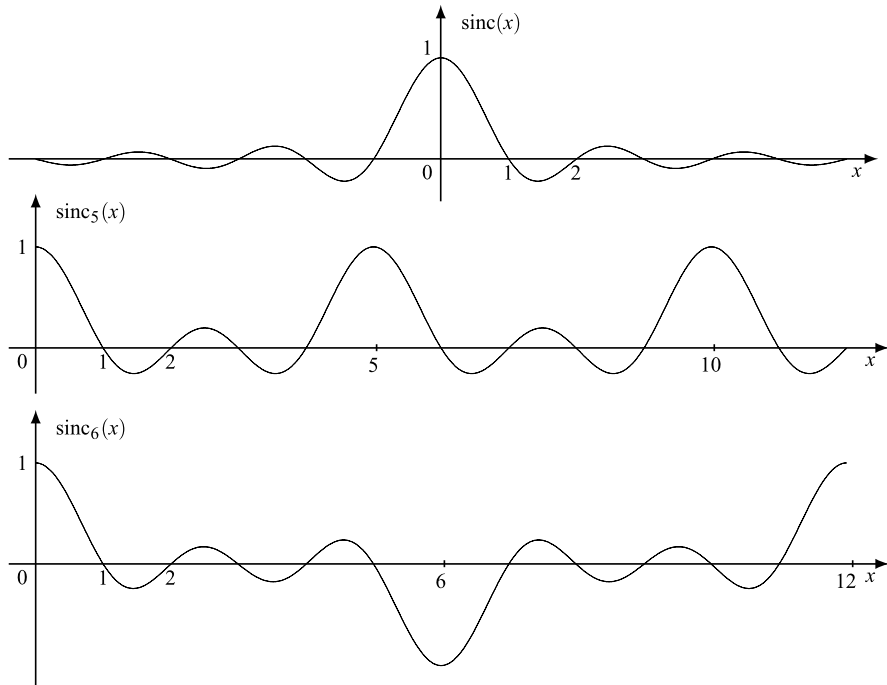


Fig. 2.11 The $\text{sinc}(x)$ function and its periodic version $\text{sinc}_N(x)$ shown for $N = 5$ and $N = 6$

2.3.6 Sinc Pulses

Sinc pulses have the form

$$A_0 \text{sinc}\left(\frac{t - t_0}{T}\right), \quad (2.35)$$

where (Fig. 2.11)

$$\text{sinc}(x) = \frac{\sin \pi x}{\pi x} \quad (2.36)$$

and the value at $x = 0$ is $\text{sinc}(0) = 1$. The pulse (2.35) has a maximum value A_0 at $t = t_0$, it is zero at $t_0 + nT$, with $n = \pm 1, \pm 2, \dots$. It is even-symmetric about t_0 with finite energy $A_0^2 T$ and finite area $A_0 T$.

The sinc function has the *periodic* version (Fig. 2.11)

$$\text{sinc}_N(x) = \frac{1}{N} \frac{\sin \pi x}{\sin \frac{\pi}{N} x}, \quad (2.37)$$

where N is a natural number. This function has period N for N odd and period $2N$ for N even. Hence, the signal

$$s(t) = A_0 \operatorname{sinc}_N\left(\frac{t-t_0}{T}\right) \quad (2.37a)$$

has period NT for N odd and $2NT$ for N even, and similarly to the aperiodic sinc pulse (2.35) has equally spaced zeros, at intervals of length T .

Historical Note The functions sinc and rect were introduced by Woodward [7], who also introduced the symbol rep for periodic repetition. The definition (2.37) of the periodic sinc is new.

2.4 Convolution for Continuous Signals

Convolution is one of the most important operations of Signal and System Theory. It is now introduced for continuous aperiodic signals, and later for periodic signals.

2.4.1 Definition and Interpretation

Given two continuous signals $x(t)$ and $y(t)$, their convolution defines a new signal $s(t)$ according to

$$s(t) = \int_{-\infty}^{+\infty} x(u)y(t-u) du. \quad (2.38)$$

This is concisely denoted by $s = x * y$ or, more explicitly, by $s(t) = x * y(t)$ to indicate the convolution evaluated at time t . The signals $x(t)$ and $y(t)$ are called the *factors* of the convolution.

The interpretation of convolution is depicted in Fig. 2.12. We start with the two signals $x(u)$ and $y(u)$, expressed as functions of the time u . The second signal is then reversed to become $z(u) = y(-u)$, and finally shifted by a *chosen* time t to yield

$$z_t(u) = z(u-t) = y(-(u-t)) = y(t-u),$$

so that (2.38) becomes

$$s(t) = \int_{-\infty}^{+\infty} x(u)z_t(u) du. \quad (2.38a)$$

In conclusion, to evaluate the convolution *at the chosen time* t , we multiply $x(u)$ by $z_t(u)$ and integrate the product.

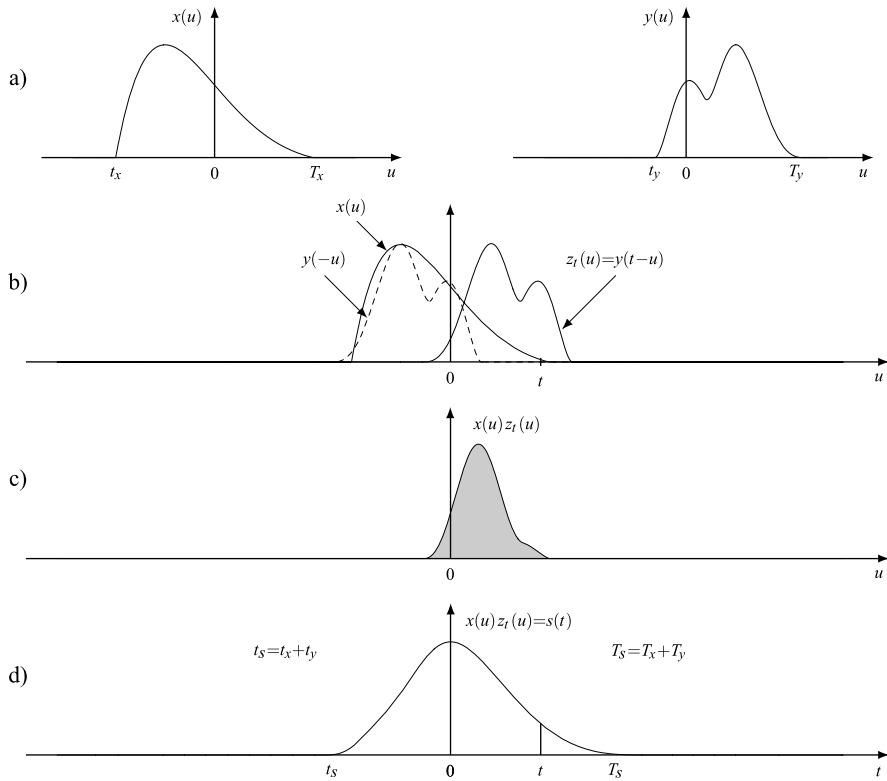


Fig. 2.12 Convolution interpretation: **(a)** signals to be convolved, **(b)** signals $x(u)$ and $z_t(u) = y(t - u)$, **(c)** product $x(u)z_t(u)$ for t fixed, **(d)** result of convolution

In this interpretation, based on (2.38), we hold the first signal while inverting and shifting the second. However, with a change of variable $v = t - u$, we obtain the alternative form

$$s(t) = \int_{-\infty}^{+\infty} x(t - u)y(u) du, \quad (2.38b)$$

in which we hold the second signal and manipulate the first to reach the same result.

Notation In the notation $x * y(t)$, the argument t represents the instant at which the convolution is evaluated; it does not represent the argument of the original signals. The notation $[x * y](t)$, used by some authors [5], is clearer, though a little clumsy, while the notation $x(t) * y(t)$ used by other authors [2] may be misleading, since it suggests interpreting the result of convolution at t as depending only on the values of the two signals at t .

Extension and Duration of the Convolution From the preceding interpretations, it follows that if both convolution *factors* are time-limited, also the convolution it-

self is time-limited. In fact, assuming that the factors have as extensions the finite intervals

$$e(x) = [t_x, T_x], \quad e(y) = [t_y, T_y],$$

then, the extension of $z(u) = y(-u)$ is $e(z) = [-T_y, -t_y]$ and after the t -shifting

$$e(z_t) = [t - T_y, t - t_y].$$

The extension of the integrand is given by the intersection of $e(x)$ and $e(z_t)$, so that (2.38a) can be rewritten in the more specific form

$$s(t) = \int_{e(x) \cap e(z_t)} x(u) z_t(u) du \quad (2.38c)$$

where the t -dependence also appears in the integration interval. If the intersection is empty, the integral is zero and $s(t) = 0$. This occurs whenever the intervals $e(x) = [t_x, T_x]$ and $e(z_t) = [t - T_y, t - t_y]$ are disjoint, and it happens for $t - t_y < t_x$ or $t - T_y > T_x$, i.e., for $t < t_x + t_y$, or $t > T_x + T_y$. Then, the convolution extension is given by the interval

$$e(x * y) = [t_x + t_y, T_x + T_y]. \quad (2.39)$$

In words, the infimum (supremum) of the convolution extension is the sum of the infima (suprema) of the factor extensions. The above rule yields for the durations

$$D(x * y) = D(x) + D(y) \quad (2.39a)$$

so that the convolution duration is given by the sum of the durations of the two factors.

Rule (2.39) is very useful in the convolution evaluation since it allows the knowledge of the extension in advance. It holds even in the limit cases; for instance, if $t_x = -\infty$, it establishes that the convolution is lower time-unlimited.

2.4.2 Convolution Properties

Commutativity We have seen that convolution operation is commutative

$$x * y(t) = y * x(t). \quad (2.40a)$$

Area If we integrate with respect to t in definition (2.38), we find

$$\int_{-\infty}^{+\infty} s(t) dt = \int_{-\infty}^{+\infty} x(t) dt \int_{-\infty}^{+\infty} y(t) dt. \quad (2.40b)$$

Recalling that the integral from $-\infty$ to $+\infty$ is the *area*, we get

$$\text{area}(x * y) = \text{area}(x) \text{area}(y). \quad (2.40c)$$

Time-Shifting By an appropriate variable changes, we can find that the convolution of the shifted signals $x(t - t_{0x})$ and $y(t - t_{0y})$ is given by

$$s(t - t_{0s}) \quad \text{with } t_{0s} = t_{0x} + t_{0y}, \quad (2.40d)$$

that is, the convolution is shifted by the sum of shifts on the factors.

Impulse The impulse has a central role in convolution. In fact, reconsidering (2.33)

$$s(t) = \int_{-\infty}^{+\infty} s(u)\delta(t - u) du \quad (2.41a)$$

and comparing it with definition (2.38), we find that the convolution of an arbitrary signal with the impulse $\delta(t)$ yields the signal itself

$$s(t) = s * \delta(t) = \delta * s(t). \quad (2.41b)$$

As we shall see better in Chap. 4, this result states that the impulse is the *unitary element* of the algebra of convolution.

2.4.3 Evaluation of Convolution and Examples

The explicit evaluation of a convolution may not be easy and must be appropriately organized. The first step is a choice between the two alternatives

$$s(t) = \int_{-\infty}^{+\infty} x(u)y(t - u) du = \int_{-\infty}^{+\infty} y(u)x(t - u) du$$

and, whenever convenient, we can use the rules stated above. In particular, the rule on the extension can be written more specifically in the forms (see (2.38c))

$$s(t) = \int_{e_t} x(u)y(t - u) du, \quad e_t = [t_x, T_x] \cap [t - T_y, t - t_y], \quad (2.42a)$$

$$s(t) = \int_{e_t} x(t - u)y(u) du, \quad e_t = [t - T_x, t - t_x] \cap [t_y, T_y]. \quad (2.42b)$$

Example 2.1 We want to evaluate the convolution of the rectangular pulses (Fig. 2.13)

$$x(t) = A_1 \operatorname{rect}\left(\frac{t}{4D}\right), \quad y(t) = A_2 \operatorname{rect}\left(\frac{t}{2D}\right).$$

Since $e(x) = (-2D, 2D)$ and $e(y) = (-D, D)$ we know in advance that

$$e(s) = (-3D, 3D)$$

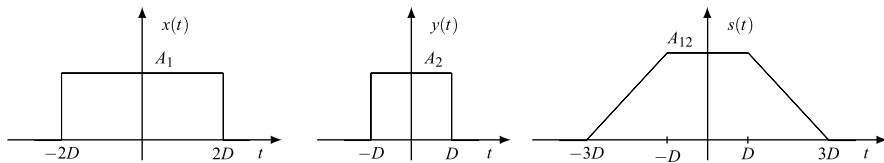


Fig. 2.13 Convolution $s(t) = x * y(t)$ of two rectangular pulses of duration $4D$ and $2D$; the trapezium amplitude is $A_{12} = 2DA_1A_2$

so we limit the evaluation to this interval.

Since the duration of the second pulse is less than the duration of the first one, it is convenient to hold the first while operating on the second. Using (2.42a) and considering that both the pulses are constant within their extensions, we find

$$s(t) = \int_{e_t} A_1 A_2 du = A_1 A_2 \text{meas } e_t$$

where $e_t = (-2D, 2D) \cap (t - D, t + D)$. Then, we have to find the intersection e_t for any t and the corresponding measure. The result is

$$e_t = \begin{cases} \emptyset, & \text{if } t < -3D \text{ or } t > 3D; \\ (-3D, t), & \text{if } -3D < t < -D; \\ (t - D, t + D), & \text{if } -D < t < D; \\ (t, 3D), & \text{if } D < t < 3D; \end{cases}$$

and then

$$s(t) = \begin{cases} 0, & \text{if } t < -3D \text{ or } t > 3D; \\ A_1 A_2 (t + 3D), & \text{if } -3D < t < -D; \\ A_1 A_2 2D, & \text{if } -D < t < D; \\ A_1 A_2 (3D - t), & \text{if } D < t < 3D. \end{cases} \quad (2.43)$$

In conclusion, the convolution of the rectangular pulses has an isosceles trapezoidal form, as illustrated in Fig. 2.13.

In (2.43), we have not specified the convolution values at the connection instants $t = \pm D$ and $t = \pm 3D$. Reconsidering the evaluation details, we find that in the four lines of (2.43) the open intervals can be replaced by closed intervals. Hence, the convolution $s(t)$ turns out to be a continuous function.

Example 2.2 We evaluate the convolution of the signals (Fig. 2.14)

$$x(t) = A_0 \text{rect}\left(\frac{t}{2D}\right), \quad y(t) = 1(t).$$

Since $e(x) = (-D, D)$ and $e(y) = (0, +\infty)$, it follows that $e(x * y) = (-D, +\infty)$. We note that in general the convolution of an arbitrary signal $x(t)$

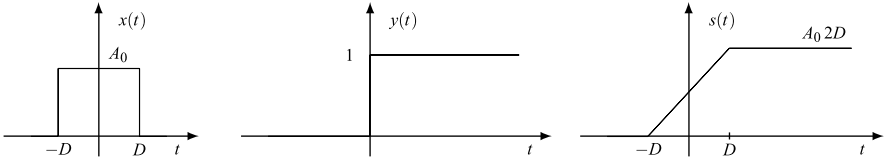


Fig. 2.14 Convolution $s(t) = x * y(t)$ of a rectangular pulse with the step signal

with the unit step signal $1(t)$ is given by the integral of $x(t)$ from $-\infty$ to t ,

$$s(t) = \int_{-\infty}^{+\infty} x(u)1(t-u) du = \int_{-\infty}^t x(u) du,$$

as soon as we take into account that $1(t-u) = 0$ for $u < t$.

In our specific case, we find

$$s(t) = \begin{cases} 0, & \text{if } t < -D; \\ A_0(t+D), & \text{if } -D < t < D; \\ A_0 2D, & \text{if } t > D, \end{cases}$$

which is similar to the step signal, but with a linear roll-off from $-D$ to D .

Example 2.3 We evaluate the convolution of the signals

$$x(t) = A_1 \operatorname{rect}\left(\frac{t}{2D}\right), \quad y(t) = A_2 \cos \omega_0 t.$$

Since $e(y) = (-\infty, +\infty)$, from the rule on extension it follows that also the convolution has the infinite extension $(-\infty, +\infty)$. Holding the second signal, we find

$$\begin{aligned} s(t) &= \int_{-\infty}^{+\infty} y(u)x(t-u) du = \int_{t-D}^{t+D} A_1 A_2 \cos \omega_0 u du \\ &= \frac{A_1 A_2}{\omega_0} [\sin \omega_0(t+D) - \sin \omega_0(t-D)] \\ &= 2 \frac{A_1 A_2}{\omega_0} \sin \omega_0 D \cos \omega_0 t. \end{aligned}$$

Hence, the convolution is a sinusoidal signal with the same frequency as $y(t)$.

2.4.4 Convolution for Periodic Signals

The convolution defined by (2.38) is typically used for *aperiodic* signals, but one of the signals to be convolved may be periodic. If this is the case, the convolution turns

out to be periodic with the same period as the periodic factor. When both signals are periodic, the integral in (2.38) may not exist and a specific definition must be issued.

The convolution of two periodic signals $x(t)$ and $y(t)$ with the same period T_p is then defined as

$$x * y(t) \triangleq \int_{t_0}^{t_0+T_p} x(u)y(t-u) du. \quad (2.44)$$

where the integral is over an arbitrary period $(t_0, t_0 + T_p)$. This form is sometimes called the *cyclic convolution* and then the previous form the *acyclic convolution*.

We can easily check that the periodic signal $s(t) = x * y(t)$ is independent of t_0 and has the same period T_p as the two factors. Moreover, the cyclic convolution has the same properties as the acyclic convolution, *provided that the results are interpreted within the class of periodic signals*. For instance, the area rule (2.40c) still holds provided that areas are interpreted as the integrals over a period (see (2.17a), (2.17b)).

2.5 The Fourier Series

In this section, continuous-time signals are examined in the *frequency domain*. The tool is given by the *Fourier series* for periodic signals and the *Fourier integral* for aperiodic signals.

We recall that in 1822 Joseph Fourier proved that an arbitrary (real) function of a real variable $s(t)$, $t \in \mathbb{R}$, having period T_p , can be expressed as the sum of a series of sine and cosine functions with frequencies multiple of the *fundamental frequency* $F = 1/T_p$, namely

$$s(t) = A_0 + \sum_{k=1}^{\infty} [A_k \cos 2\pi k F t + B_k \sin 2\pi k F t]. \quad (2.45)$$

This is the *Fourier series expansion*, which represents a periodic function by means of the coefficients A_k and B_k . In modern Signal Theory, the popular form of the Fourier series is the expansion into *exponentials*, equivalent to the sine–cosine expansion, but more compact and tractable.

2.5.1 The Exponential Form of Fourier Series

A continuous signal $s(t)$, $t \in \mathbb{R}$, with period T_p , can be represented by the *Fourier series*

$$s(t) = \sum_{n=-\infty}^{\infty} S_n e^{i2\pi n F t}, \quad F = \frac{1}{T_p}, \quad (2.46a)$$

where the *Fourier coefficients* S_n are given by

$$S_n = \frac{1}{T_p} \int_{t_0}^{t_0+T_p} s(t) e^{-i2\pi n F t} dt, \quad n \in \mathbb{Z}. \quad (2.46b)$$

These relationships follow from the orthogonality of exponential functions, namely

$$\frac{1}{T_p} \int_{t_0}^{t_0+T_p} e^{i2\pi n F t} e^{-i2\pi m F t} dt = \delta_{mn} \quad (2.47)$$

where δ_{mn} is the Kronecker symbol ($\delta_{mn} = 1$ for $m = n$ and $\delta_{mn} = 0$ for $m \neq n$). Hence, (2.46a) is an orthogonal function expansion of the given signal in an arbitrary period $(t_0, t_0 + T_p)$. It represents the signal $s(t)$ as a sum of exponential components with frequencies being multiples of the fundamental frequency

$$f_n = nF, \quad n = 0, \pm 1, \pm 2, \dots$$

In the general case of a complex signal $s(t)$, the coefficients S_n have no symmetries. When the signal $s(t)$ is *real*, the coefficients have the *Hermitian symmetry*, namely

$$S_{-n} = S_n^* \quad (2.48)$$

and the signal identification can be limited to the Fourier coefficients S_n with $n \geq 0$.

If we let $S_n = R_n + iX_n$, the Hermitian symmetry (2.48) yields the two conditions

$$R_{-n} = R_n, \quad X_{-n} = -X_n,$$

which state that the real part is an even function (of the integer variable n) and the imaginary part is an odd function. These symmetries are illustrated in Fig. 2.15. The same symmetries hold respectively for the modulus and for the argument of the Fourier coefficients of a real signal.

Continuing with real signals, from the exponential form (2.48) the Hermitian symmetry allows obtaining the sine–cosine form (2.45) (where a real signal is tacitly assumed)

$$s(t) = R_0 + 2 \sum_{n=1}^{\infty} [R_n \cos 2\pi n F t - X_n \sin 2\pi n F t]. \quad (2.49a)$$

We can also obtain a form with only cosine terms but with appropriate phases in their arguments, namely

$$s(t) = S_0 + 2 \sum_{n=1}^{\infty} |S_n| \cos(2\pi n F t + \arg S_n). \quad (2.49b)$$

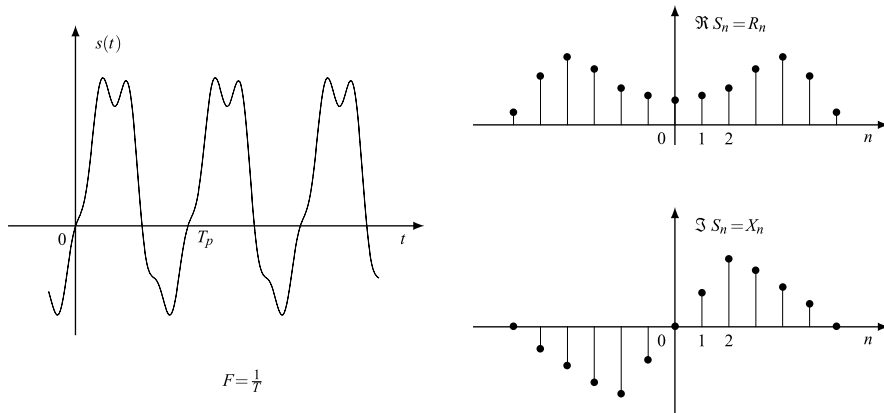


Fig. 2.15 Representation of Fourier coefficients of a *real* periodic signal illustrated by real and imaginary parts

Presence of Negative Frequencies In the exponential form, we find terms with *negative frequencies*. It is worth explaining this assertion clearly. To be concrete, let us assume that the periodic signal under consideration be the model of an electrical voltage $v(t)$. Since this signal is real, we can apply series expansion (2.49b), i.e.,

$$v(t) = V_0 + \sum_{n=1}^{\infty} V_n \cos(2\pi n F t + \varphi_n)$$

where all terms have *positive frequencies* (the constant V_0 can be regarded as a term with zero frequency). These terms, with positive frequencies nF , have a direct connection with the physical world and, indeed, they can be separated and measured by a filter-bank.

The presence of negative frequencies, related to exponentials, is merely a mathematical artifact provided by Euler’s formulas (2.19), which yields

$$V_n \cos(2\pi n F t + \varphi_n) = \frac{1}{2} V_n e^{i\varphi_n} e^{i2\pi n F t} + \frac{1}{2} V_n e^{-i\varphi_n} e^{-i2\pi n F t}.$$

2.5.2 Properties of the Fourier Series

Fourier series has several properties (or rules) which represent so many theorems and will be considered systematically in Chap. 5 with the unified Fourier transform (which gives the Fourier series as a particularization). Here, we consider only a few of them.

- Let $s(t)$ be a periodic signal and $x(t) = s(t - t_0)$ a shifted version. Then, the relationship between the Fourier coefficients is

$$X_n = S_n e^{-i2\pi n F t_0}. \tag{2.50}$$

As a check, when t_0 is a multiple of the period $T_p = 1/F$, we find $x(t) = s(t)$, and indeed (2.50) yields $X_n = S_n$.

- The mean value in a period is the zeroth coefficient

$$m_s(T_p) = \frac{1}{T_p} \int_{t_0}^{t_0+T_p} s(t) dt = S_0.$$

- The power given by (2.12) can be obtained from the Fourier coefficients as follows (Parseval's theorem)

$$P_s = \frac{1}{T_p} \int_{t_0}^{t_0+T_p} |s(t)|^2 dt = \sum_{n=-\infty}^{+\infty} |S_n|^2. \quad (2.51)$$

In particular, for a real signal, considering the Hermitian symmetry (2.48), Parseval's theorem becomes

$$P_s = S_0^2 + 2 \sum_{n=1}^{\infty} |S_n|^2. \quad (2.51a)$$

2.5.3 Examples of Fourier Series Expansion

We consider a few examples. The related problems are:

1. Given a periodic signal $s(t)$, evaluate its Fourier coefficients S_n , i.e., evaluate the integral (2.46b) for any n ;
2. Given the Fourier coefficients S_n , evaluate the sum of series (2.46a), to find $s(t)$.

Problem 1 is often trivial, whereas the inverse problem 2 may be difficult.

Example 2.4 Let

$$s(t) = A_0 \cos(2\pi f_0 t + \varphi_0)$$

with A_0 and f_0 positive. Letting $F = f_0$ and using Euler's formulas, we get

$$s(t) = \frac{1}{2} A_0 e^{i\varphi_0} e^{i2\pi Ft} + \frac{1}{2} A_0 e^{-i\varphi_0} e^{-i2\pi Ft}.$$

Then, comparison with (2.46a) (by the uniqueness of Fourier coefficients) yields:

$$S_1 = \frac{1}{2} A_0 e^{i\varphi_0}, \quad S_{-1} = \frac{1}{2} A_0 e^{-i\varphi_0}, \quad S_n = 0 \quad \text{for } |n| \neq 1.$$

Example 2.5 A periodic signal consisting of equally-spaced rectangular pulses can be written in the form

$$s(t) = \sum_{n=-\infty}^{+\infty} A_0 \operatorname{rect}\left(\frac{t - nT_p}{dT_p}\right) = A_0 \operatorname{rep}_{T_p} \operatorname{rect}\left(\frac{t}{dT_p}\right), \quad 0 < d \leq 1$$

where d is the pulse duration normalized to the period (d is called the *duty cycle*). Considering that in the interval $(-\frac{1}{2}T_p, \frac{1}{2}T_p)$ the signal $s(t)$ is given by the zeroth term of the periodic repetition,

$$s(t) = A_0 \operatorname{rect}\left(\frac{t}{dT_p}\right), \quad -\frac{1}{2}T_p < t < \frac{1}{2}T_p,$$

we get

$$S_n = \frac{1}{T_p} \int_{-\frac{1}{2}dT_p}^{\frac{1}{2}dT_p} A_0 e^{-i2\pi n F t} dt.$$

This integral can be expressed by the sinc function (2.36), namely

$$S_n = S_0 \operatorname{sinc}(nd), \quad S_0 = A_0 d. \quad (2.52)$$

As a check, for $d = 1$ all the Fourier coefficients are zero for $n \neq 0$, and indeed $s(t)$ becomes a constant signal.

As an opposite limit case, suppose that the duty cycle d tends to zero, but holding the mean value at the fixed value $S_0 = A_0 d$. Then, at the limit each rectangular pulse becomes a delta function of area $S_0 T_p$, that is,

$$s(t) = \sum_{n=-\infty}^{+\infty} T_p S_0 \delta(t - nT_p) = T_p S_0 \operatorname{rep}_{T_p} \delta(t).$$

Then, all the Fourier coefficients S_n are equal to S_0 . The interpretation is that a “train” of delta functions has all the “harmonics” with the same amplitude S_0 . From this result, follows the remarkable identity

$$\sum_{n=-\infty}^{+\infty} e^{i2\pi n F t} = T_p \sum_{n=-\infty}^{+\infty} \delta(t - nT_p), \quad F = \frac{1}{T_p}. \quad (2.53)$$

Example 2.6 We want to find the signal $s(t)$ whose Fourier coefficients are given by

$$S_n = \begin{cases} A_0 & \text{for } |n| \leq n_0; \\ 0 & \text{for } |n| > n_0, \end{cases}$$

i.e., the signal that has only the first n_0 harmonics with the same amplitude.

From (2.46a) we get

$$s(t) = A_0 + A_0 \sum_{n=1}^{n_0} (e^{i2\pi n F t} + e^{-i2\pi n F t}) = A_0 + 2A_0 \sum_{n=1}^{n_0} \cos 2\pi n F t.$$

An alternative expression is obtained by letting $z = e^{i2\pi Ft}$ and noticing that

$$\sum_{n=1}^{n_0} e^{i2\pi n Ft} = \sum_{n=1}^{n_0} z^n = \frac{z(1 - z^{n_0})}{1 - z}.$$

Hence

$$\begin{aligned} s(t) &= A_0 \left[1 + \frac{z(1 - z^{n_0})}{1 - z} + \frac{z^{-1}(1 - z^{-n_0})}{1 - z^{-1}} \right] \\ &= A_0 \frac{z^{n_0 + \frac{1}{2}} - z^{-(n_0 + \frac{1}{2})}}{z^{\frac{1}{2}} - z^{-\frac{1}{2}}} = A_0 \frac{\sin 2\pi(n_0 + \frac{1}{2}) Ft}{\sin 2\pi \frac{1}{2} Ft}. \end{aligned}$$

The last term compared with definition (2.37) of the periodic sinc can be written in the form:

$$s(t) = A_0 N \operatorname{sinc}_N(N Ft), \quad N = 2n_0 + 1.$$

Thus, we have stated the following identity

$$1 + 2 \sum_{n=1}^{n_0} \cos 2\pi n Ft = N \operatorname{sinc}_N(N Ft), \quad N = 2n_0 + 1. \quad (2.54)$$

2.6 The Fourier Transform

An aperiodic signal $s(t)$, $t \in \mathbb{R}$, can be represented by the *Fourier integral*

$$s(t) = \int_{-\infty}^{+\infty} S(f) e^{i2\pi f t} df, \quad t \in \mathbb{R}, \quad (2.55a)$$

where the function $S(f)$ is evaluated from the signal as

$$S(f) = \int_{-\infty}^{+\infty} s(t) e^{-i2\pi f t} dt, \quad f \in \mathbb{R}. \quad (2.55b)$$

These relationships allow the passage from the time domain to the frequency domain, and vice versa. The function $S(f)$ is the *Fourier transform* (FT) of the signal $s(t)$, and the signal $s(t)$, when written in the form (2.55a), is the *inverse Fourier transform* of $S(f)$. Concisely, we write $S(f) = \mathcal{F}[s | f]$ and $s(t) = \mathcal{F}^{-1}[S | t]$ where \mathcal{F} and \mathcal{F}^{-1} are the operators defined by (2.55a, 2.55b). We also use the notation

$$s(t) \xrightarrow{\mathcal{F}} S(f), \quad S(f) \xrightarrow{\mathcal{F}^{-1}} s(t).$$

The above relationships can be established heuristically with a limit consideration from the Fourier series. With reference to (2.46a), (2.46b), we limit the given

aperiodic signal to the interval $(-\frac{1}{2}T_p, \frac{1}{2}T_p)$ and we repeat it periodically outside, then we take the limit with $T_p \rightarrow \infty$. From a mathematical viewpoint, the conditions on the existence of the Fourier transform and its inverse are formulated in several ways, often having no easy interpretation [2, 6]. A sufficient condition is that the signal be absolutely integrable, i.e.,

$$\int_{-\infty}^{+\infty} |s(t)| dt < \infty,$$

but this condition is too much stringent for Signal Theory where a very broad class of signals is involved, including “singular” signals as impulses, constant signals and periodic signals.

2.6.1 Interpretation

In the Fourier series, a *continuous-time* periodic signal is represented by a *discrete-frequency* function $S_n = S(nF)$. In the FT, this is no more true and we find a symmetry between the time domain and the frequency domain, which are both continuous. In (2.55a), a signal is represented as the sum of infinitely many exponential functions of the form

$$[S(f) df] e^{i2\pi ft}, \quad f \in \mathbb{R} \quad (2.56)$$

with frequency f and infinitesimal amplitude $S(f) df$.

In general, for a complex signal $s(t)$ the FT $S(f)$ has no peculiar symmetries. For a *real* signal, similarly to (2.48), we find that the Fourier transform has the *Hermitian symmetry*

$$S(-f) = S^*(f), \quad (2.57)$$

so that the portion of $S(f)$ for $f \geq 0$ completely specifies the signal. Letting

$$S(f) = R(f) + iX(f) = A_S(f)e^{i\beta_S(f)},$$

from (2.57) we find

$$R(f) = R(-f), \quad X(f) = -X(-f), \quad (2.57a)$$

which states that the real part of the FT is *even* and the imaginary part is *odd*. Analogously, we find for the modulus and the argument

$$A_S(f) = A_S(-f), \quad \beta_S(f) = -\beta_S(-f). \quad (2.57b)$$

These symmetries are illustrated in Fig. 2.16.

Continuing with the assumption of a *real signal*, the decomposition (2.55a) with both positive and negative frequencies can be set into a form with cosinusoidal terms

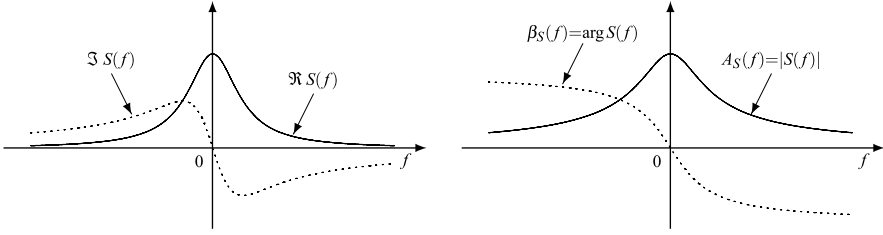


Fig. 2.16 Representation of the Fourier transform of a *real* signal $s(t)$, $t \in \mathbb{R}$, by real and imaginary parts, and by modulus and argument

with positive frequencies. In fact, by pairing the exponential terms (2.56) at frequency f with the terms at frequency $-f$, we get

$$\begin{aligned} & [S(f) df] e^{i2\pi ft} + [S(-f) df] e^{-i2\pi ft} \\ &= [S(f) df] e^{i2\pi ft} + [S^*(f) df] e^{-i2\pi ft} = 2\Re\{[S(f) df] e^{i2\pi ft}\} \\ &= 2[A_S(f) df] \cos(2\pi ft + \beta_S(f)), \quad f > 0. \end{aligned}$$

Hence, (2.55a) becomes

$$s(t) = \int_0^\infty 2A_S(f) \cos(2\pi ft + \beta_S(f)) df. \quad (2.58)$$

2.6.2 Properties of the Fourier Transform

The properties (or rules) of the FT will be seen in a unified form in Chap. 5 and in a specific form for continuous-time signals in Chap. 9. Here, we see the main rules. The formulation is simpler than with the Fourier series for the perfect symmetry between time and frequency domains.

- The *time-shifted* version $s(t - t_0)$ of a signal $s(t)$ gives the following FT pair

$$s(t - t_0) \xrightarrow{\mathcal{F}} S(f) e^{-i2\pi ft_0}. \quad (2.59a)$$

Symmetrically, the inverse FT of the *frequency-shifted* version $S(f - f_0)$ of $S(f)$ gives

$$S(f - f_0) \xrightarrow{\mathcal{F}^{-1}} s(t) e^{i2\pi f_0 t}. \quad (2.59b)$$

- The *convolution* $x * y(t)$ becomes the *product* for the FTs

$$x * y(t) \xrightarrow{\mathcal{F}} X(f)Y(f). \quad (2.60a)$$

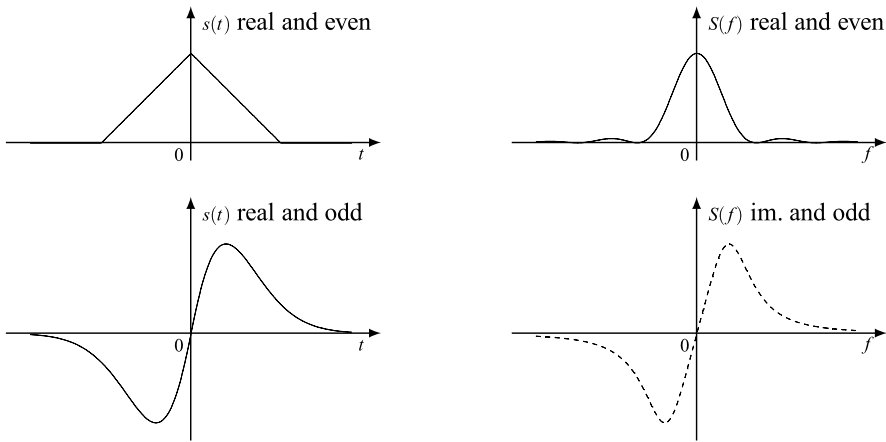


Fig. 2.17 Symmetric signals and the corresponding Fourier transforms

Symmetrically, the *products* $s(t) = x(t)y(t)$ becomes the *convolution*

$$S(f) = X * Y(f) = \int_{-\infty}^{+\infty} X(\lambda)Y(f - \lambda) d\lambda, \tag{2.60b}$$

where the operation is interpreted according to definition (2.38) for aperiodic continuous-argument functions, since $X(f)$ and $Y(f)$ belong to this class.

- Letting $t = 0$ and $f = 0$ in definitions (2.55a) and (2.55b), respectively, we get

$$s(0) = \int_{-\infty}^{+\infty} S(f) df = \text{area}(S), \quad S(0) = \int_{-\infty}^{+\infty} s(t) dt = \text{area}(s). \tag{2.61}$$

Hence, the signal area equals the FT evaluated at $f = 0$.

- The energy E_s of a signal $s(t)$, defined by (2.11), can be evaluated from the FT $S(f)$ as follows (Parseval Theorem):

$$E_s = \int_{-\infty}^{+\infty} |s(t)|^2 dt = \int_{-\infty}^{+\infty} |S(f)|^2 df. \tag{2.62}$$

For a real signal, $|S(f)|$ is an even function of f , and the energy evaluation can be limited to positive frequencies, namely

$$E_s = \int_{-\infty}^{+\infty} s(t)^2 dt = 2 \int_0^{\infty} |S(f)|^2 df.$$

However, we note the perfect symmetry of (2.62), which emphasizes the opportunity to deal with complex signals.

- As seen above, the symmetry $s(t) = s^*(t)$ (real signal) yields the Hermitian symmetry, $S(f) = S^*(-f)$. Moreover, see Fig. 2.17,

1. If the signal is *real and even*, the FT is *real and even*;
2. If the signal is *real and odd*, the FT is *imaginary and odd*.

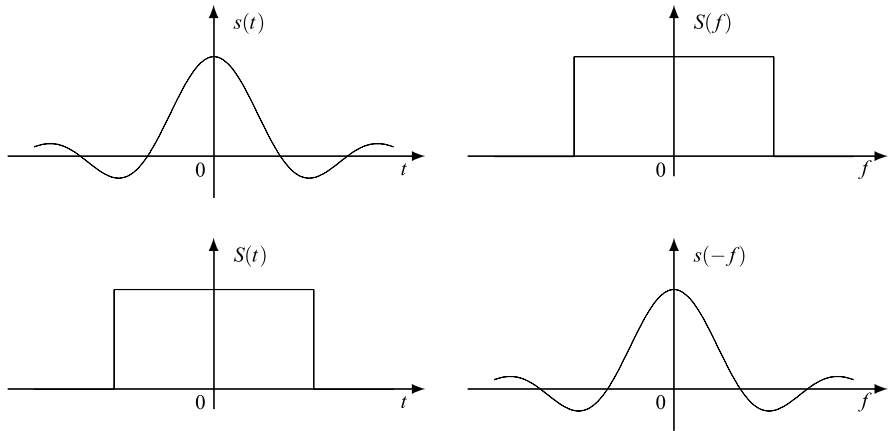


Fig. 2.18 Symmetry rule. If signal $s(t)$ has Fourier transform $S(f)$, then the signal $S(t)$ has transform $s(-f)$. In this specific case, $s(t)$ and $S(f)$ are even and $s(f) = s(-f)$

2.6.3 Symmetry Rule

Formulas (2.55a) and (2.55b), which express the signal and the FT, have a symmetrical structure, apart from a sign change in the exponential. This leads to the *symmetry rule*: If the FT of a signal $s(t)$ is $S(f)$, then, interpreting the FT as a signal $S(t)$, one obtains that the FT is $s(-f)$ (Fig. 2.18).

The symmetry rule is very useful in the evaluation, since, starting from the Fourier pair $(s(t), S(f))$, we get that also $(S(t), s(-f))$ is a consistent Fourier pair. The symmetry rule explains also the *symmetries* between the rules of the FT.

2.6.4 Band and Bandwidth of a Signal

In the time-domain, we have introduced the *extension* $e(s)$ and the *duration* $D(s) = \text{meas } e(s)$ of a signal. Symmetrically, in the frequency domain, we introduce the *spectral extension* $\mathcal{E}(s) = e(S)$, defined as the extension of the FT, and the *bandwidth*, defined as the measure of $\mathcal{E}(s)$:

$$B(s) = \text{meas } \mathcal{E}(s) = \text{meas } e(S). \quad (2.63)$$

Then, the property of the spectral extension is

$$\boxed{S(f) = 0, \quad f \notin \mathcal{E}(s).} \quad (2.63a)$$

For *real* signals, the Hermitian symmetry, $S(f) = S^*(-f)$, implies that the minimal extension \mathcal{E}_0 is symmetric with respect to the frequency origin and it will be

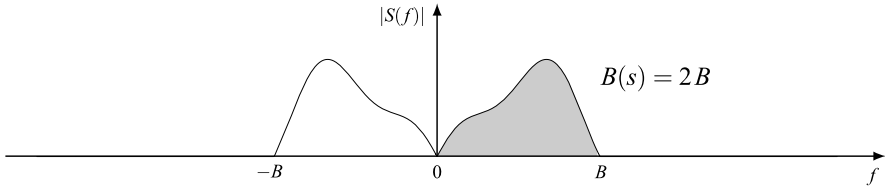


Fig. 2.19 Examples of limited spectral extension of a real signal; B represents the *band*

convenient to make such a choice also for an arbitrary extension $\mathcal{E}(s)$. Then, for a real *band-limited* signal we indicate the spectral extension in the form (Fig. 2.19):

$$e(S) = [-B, B]$$

for a finite frequency B , which is called the *band*³ of $s(t)$.

The first consequence of band limitation relies on the decomposition of a real signal into *sinusoidal* components (see (2.58)), i.e., $|S(f) df| \cos(2\pi ft + \arg S(f))$, $f > 0$, where $S(f) = 0$ for $f > B$, that is, the signal does not contain components with frequencies f greater than B . The second consequence will be seen with the *Sampling Theorem* at the end of the chapter.

2.7 Examples of Fourier Transforms

We develop a few examples of FTs. Note that the FT of some “singular” signals, as step signals and sinusoidal signals, can be written using the delta function, and should be interpreted in the framework of *distribution theory*.

2.7.1 Rectangular and Sinc Pulses

The FT of the rectangular pulse can be calculated directly from definition (2.55b), which yields

$$S(f) = A_0 \int_{-\frac{1}{2}D}^{\frac{1}{2}D} e^{-i2\pi ft} dt = \frac{A_0}{-i2\pi f} (e^{-i\pi f D} - e^{i\pi f D}) = A_0 \frac{\sin \pi f D}{\pi f}.$$

Then, using the sinc function,

$$A_0 \text{rect}(t/D) \xrightarrow{\mathcal{F}} A_0 D \text{sinc}(f D). \tag{2.64a}$$

³For real signals, it is customary to call as the *band* the half of the spectral extension measure.

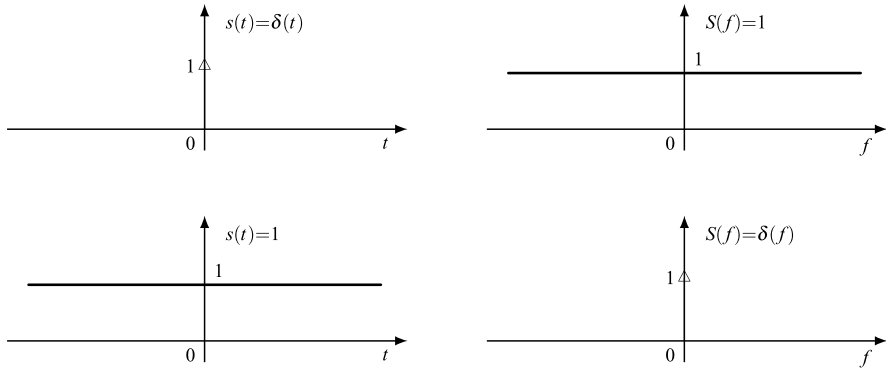


Fig. 2.20 Fourier transforms of the impulse and of the unit signal

In the direct evaluation of the FT of the sinc pulse, we encounter a difficult integral, instead we can apply the symmetry rule to the pair $(s(t), S(f))$ just evaluated. We get

$$S(t) = A_0 D \operatorname{sinc}(t D) \xrightarrow{\mathcal{F}} s(-f) = A_0 \operatorname{rect}(-f/D),$$

which is more conveniently written using the evenness of the rect function and making the substitutions $D \rightarrow 1/T$ and $A_0 D \rightarrow A_0$. Hence

$$A_0 \operatorname{sinc}(t/T) \xrightarrow{\mathcal{F}} A_0 T \operatorname{rect}(fT). \quad (2.64b)$$

This FT pair has been illustrated in Fig. 2.18 in connection with the symmetry rule.

2.7.2 Impulses and Constant Signals

The technique for the FT evaluation of the impulse $s(t) = \delta(t - t_0)$ is the usage of the sifting property (2.32) in definition (2.55b), namely

$$S(f) = \int_{-\infty}^{+\infty} \delta(t - t_0) e^{-i2\pi f t} dt = e^{-i2\pi f t_0}.$$

Hence

$$\delta(t - t_0) \xrightarrow{\mathcal{F}} e^{-i2\pi f t_0} \quad (2.65)$$

and particularly for $t_0 = 0$

$$\delta(t) \xrightarrow{\mathcal{F}} 1, \quad (2.65a)$$

that is, the FT of the impulse centered at the origin is unitary (Fig. 2.20).

Note that the sifting property (2.32) holds also in the frequency domain, namely

$$\int_{-\infty}^{+\infty} X(f)\delta(f - f_0) \, df = X(f_0),$$

where $X(f)$ is an arbitrary frequency function. Then, with $X(f) = \exp(i2\pi ft)$ we find

$$\int_{-\infty}^{+\infty} \delta(f - f_0)e^{i2\pi ft} \, df = e^{i2\pi f_0 t}.$$

Hence, considering the uniqueness of the Fourier transform,

$$e^{i2\pi f_0 t} \xrightarrow{\mathcal{F}} \delta(f - f_0). \quad (2.66)$$

In particular, for $f_0 = 0$

$$1 \xrightarrow{\mathcal{F}} \delta(f) \quad (2.66a)$$

which states that the FT of the unit signal is an impulse centered at the frequency origin (Fig. 2.20). Note that (2.66) could be obtained from (2.65) by the symmetry rule.

2.7.3 Periodic Signals

The natural tool for periodic signals is the Fourier series which represents the signal by a discrete-frequency function $S_n = S(nF)$. We can also consider the Fourier transform, but we obtain a “singular” result, however, expressed in terms of delta functions.

A first example of FT of a periodic signal is given by (2.66), which states that the FT of an exponential with frequency f_0 is the impulse applied at the frequency f_0 . A second example is given by sinusoidal signals, which can be decomposed into exponentials (see (2.21)). We find

$$\cos 2\pi Ft = \frac{1}{2}(e^{i2\pi Ft} + e^{-i2\pi Ft}) \xrightarrow{\mathcal{F}} \frac{1}{2}[\delta(f - F) + \delta(f + F)],$$

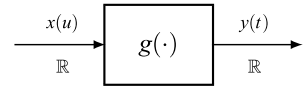
$$\sin 2\pi Ft = \frac{1}{2i}(e^{i2\pi Ft} - e^{-i2\pi Ft}) \xrightarrow{\mathcal{F}} \frac{1}{2i}[\delta(f - F) - \delta(f + F)].$$

More generally, for a periodic signal $s(t)$ that admits the Fourier series expansion, we find

$$s(t) = \sum_{n=-\infty}^{+\infty} S_n e^{i2\pi nFt} \xrightarrow{\mathcal{F}} \sum_{n=-\infty}^{+\infty} S_n \delta(f - nF). \quad (2.67)$$

Hence, the FT of a periodic signal consists of a train of delta functions at the frequencies $f = nF$ and with area given by the corresponding Fourier coefficients.

Fig. 2.21 Graphical representation of a continuous-time filter



2.7.4 Step Signals

First, it is convenient to consider the signum signal $\text{sgn}(t)$. In the appendix, we find that its FT is given by

$$\text{sgn}(t) \xrightarrow{\mathcal{F}} \frac{1}{i\pi f}.$$

This transform does not contain a delta function; anyway, it should be interpreted as a *distribution* [2].

For the FT of the unit step function, we use decomposition (2.22), which gives

$$1(t) = \frac{1}{2} + \frac{1}{2} \text{sgn}(t) \xrightarrow{\mathcal{F}} \frac{1}{2} \delta(f) + \frac{1}{i2\pi f}.$$

Then, in the passage from the “signum” signal to the step signal, in the FT we have to add a delta function of area equal to half the step amplitude, that is, equal to the *continuous component* of the step signal.

2.8 Signal Filtering

Filtering is the most important operation used to modify some characteristics of signals. Historically, its original target was the “filtering” of sinusoidal components in the sense of passing some of them and eliminating the others. With the technology evolution, filtering has a broader and more articulated purpose.

2.8.1 Time-Domain Analysis

A filter (linear, invariant and continuous-time) may be introduced as the system characterized by the input–output relationship (Fig. 2.21)

$$y(t) = \int_{-\infty}^{+\infty} g(t-u)x(u) du = x * g(t), \quad (2.68)$$

where

- $x(t)$, $t \in \mathbb{R}$, is the *input signal*,
- $y(t)$, $t \in \mathbb{R}$, is the *output signal* or the *filter response*,
- $g(t)$, $t \in \mathbb{R}$, is the *impulse response*, which characterizes the filter.

The interpretation of the impulse response is obtained by applying an impulse to the input. Indeed, letting $x(t) = \delta(t)$ in (2.68) and considering property (2.41a, 2.41b), we get

$$y(t) = \delta * g(t) = g(t).$$

Then, the impulse response is the *filter response to the impulse applied at the origin*.

The filter model stated by (2.68) does not entail considerations of physical constraints. A constraint is the *causality condition* which states that the filter cannot “respond” before the application of the input signal (otherwise the filter would predict the future!). This condition implies that the impulse response must be a *causal* signal, i.e.,

$$g(t) = 0, \quad t < 0,$$

since it is the response to the impulse applied at $t = 0$ and cannot start at negative times. A filter with this property will be called *causal*, otherwise *anticipatory* (or *non-causal*). Physically implemented filters are surely causal, as correct models of “real” filters, but in Signal Theory we often encounter anticipatory filters, used in a simplified analysis (see below).

For causal filters the input–output relationship can be written in the more specific forms

$$y(t) = \int_{-\infty}^t x(u)g(t-u) du = \int_0^{+\infty} g(u)x(t-u) du,$$

whereas for anticipatory filters the general form (2.68) must be used.

2.8.2 Frequency-Domain Analysis

In the frequency-domain, input–output relationship (2.68) becomes

$$Y(f) = G(f)X(f) \tag{2.69}$$

where

- $X(f)$ is the FT of the input signal, $Y(f)$ is the FT of the output signal,
- $G(f)$ is the FT of the impulse response, which is called the *frequency response*.⁴

The frequency response $G(f)$ completely specifies a filter as well as the impulse response $g(x)$. When $g(t)$ is real, the frequency response has the *Hermitian symmetry* $G(f) = G^*(-f)$. Relationship (2.69) clearly states the advantage of dealing with the frequency-domain analysis, where the convolution becomes a *product*. This relationship, written as an inverse FT,

$$y(t) = \int_{-\infty}^{+\infty} Y(f)e^{i2\pi ft} df = \int_{-\infty}^{+\infty} G(f)X(f)e^{i2\pi ft} df,$$

⁴We prefer to reserve the term *transfer function* to the Laplace transform of the impulse response.

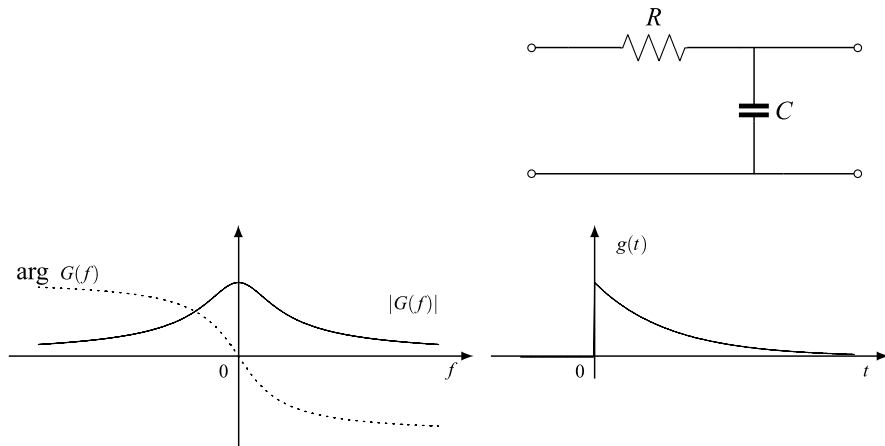


Fig. 2.22 The RC filter and the corresponding frequency and impulse responses

shows that each exponential component of the output signal is obtained from the corresponding component of the input signal as

$$[Y(f) df] e^{i2\pi ft} = G(f) [X(f) df] e^{i2\pi ft}, \quad f \in \mathbb{R}. \quad (2.70)$$

Hence, a filter modifies the complex amplitudes of the input signal components.

When both the input signal $x(t)$ and the impulse response $g(t)$ are real, the output signal $y(t)$ turns out to be real. If this is the case, considering the decomposition into sinusoidal components, we find

$$\begin{aligned} & 2|Y(f)| df \cos[2\pi ft + \varphi_Y(f)] \\ &= |G(f)| 2|X(f)| df \cos[2\pi ft + \varphi_X(f) + \varphi_G(f)], \quad f > 0. \end{aligned}$$

Hence, the filter modifies both the amplitude and the phase of the components.

Examples As a first example, we consider the RC filter of Fig. 2.22. To identify the frequency response from its definition (we recall that $G(f)$ is the Fourier transform of the impulse response), the following two steps are needed:

1. Applying a voltage impulse at the input, $e(t) = \delta(t)$, and evaluating the corresponding output voltage $v(t)$ (we need to solve the circuit in a transient regime). Then, the output voltage $v(t)$ gives the impulse response $g(t)$.
2. Evaluating the Fourier transform $G(f)$ of $g(t)$.

As known and as we shall see better in Chap. 9, it is more convenient to carry out the evaluation in a *symbolic form* which yields directly

$$G(f) = 1/(1 + i2\pi f RC).$$

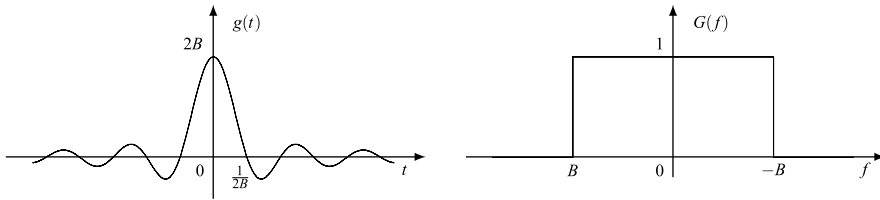


Fig. 2.23 Impulse response and frequency response of an *ideal low-pass* filter

Then, the inverse FT provides the impulse response which is given by

$$g(t) = \alpha 1(t)e^{-\alpha t}, \quad \alpha = 1/(RC).$$

This filter is causal, as expected, since it can be physically implemented.

As a second example, we consider the *ideal low-pass filter* which has the following frequency and impulse responses (Fig. 2.23):

$$G(f) = \text{rect}\left(\frac{f}{2B}\right) \xrightarrow{\mathcal{F}^{-1}} g(t) = 2B \text{sinc}(2Bt).$$

This filter is *anticipatory* and cannot be physically implemented. Nevertheless, it is a fundamental tool in Signal Theory (see Sampling Theorem).

2.9 Discrete Time Signals

In this second part of the chapter, we develop the topic of discrete signals.

Definition 2.3 A discrete-time signal is a complex function of a discrete variable

$$s : \mathbb{Z}(T) \rightarrow \mathbb{C}, \tag{2.71}$$

where the domain $\mathbb{Z}(T)$ is the set of the multiples of T

$$\mathbb{Z}(T) = \{\dots, -T, 0, T, 2T, \dots\}, \quad T > 0.$$

The signal (2.71) will usually be denoted in the forms

$$s(nT), \quad nT \in \mathbb{Z}(T) \quad \text{or} \quad s(t), \quad t \in \mathbb{Z}(T). \tag{2.72}$$

For *discrete-time* signals (more briefly, *discrete* signals), we will apply the same development seen for continuous signals. Most of the definitions are substantially the same; the main difference lies on the definitions expressed by integrals for continuous signals, which become sums for discrete signals.

In the final part of the chapter, discrete signals will be related to continuous signals by the Sampling Theorem. Discrete signals will be reconsidered in great detail, after the development of the Unified Theory in Chaps. 11, 12 and 13.

Notations In notations (2.72), the first one has the advantage of evidencing the discrete nature of the signal, whereas the second requires the specification of the domain $\mathbb{Z}(T)$, but is more in agreement with the notation for continuous signals, $s(t)$, $t \in \mathbb{R}$. The quantity $T > 0$ is the *spacing* (or *time-spacing*) between the instants where the signal is defined, and the reciprocal

$$F_p = 1/T \quad (2.73)$$

gives the signal *rate*, that is, the number of signal values per unitary time (values per second or v/s).

In textbooks and in other literature, it is customary to assume a unit spacing ($T = 1$) to simplify the notation in the form $s(n)$ or s_n with $n \in \mathbb{Z}$. We will not follow this consolidate convention for several reasons. First of all, by setting $T = 1$ we loose the application contest and the physical dimensions. Another motivation is that in the applications we often need to compare signals with different time-spacings (see multirate systems of Chap. 7), which is no more possible after the normalization $T = 1$. Finally, normalization represents a serious obstacle to a unified development.

2.9.1 Definitions

Most of the definitions introduced for continuous signals can directly be transferred to discrete signals, but sometimes with unexpected novelties.

Symmetries A discrete signal $s(nT)$ is *even*, if for any n , $s(nT) = s(-nT)$, $n \in \mathbb{Z}$ and it is *odd* if $s(nT) = -s(-nT)$, $n \in \mathbb{Z}$. An arbitrary discrete signal can always be decomposed into an even and an odd component

$$s(nT) = s_p(nT) + s_d(nT) \quad (2.73c)$$

exactly as for continuous signals.

A discrete signal $s(nT)$ is causal (Fig. 2.24) if it is zero for negative n ,

$$s(nT) = 0, \quad n < 0. \quad (2.74)$$

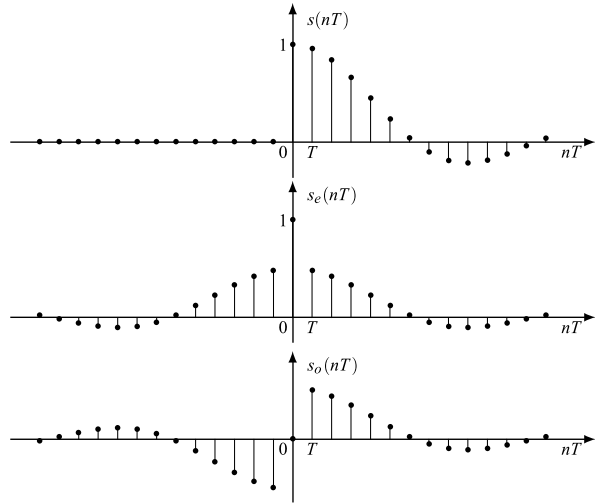
Relationships (2.6) between the even and odd components of a causal signal must be adjusted for discrete signal since $\text{sgn}(0) = 0$. The correct relationships are

$$\begin{aligned} s_d(nT) &= \text{sgn}(nT)s_p(nT), \\ s_p(nT) &= \text{sgn}(nT)s_d(nT) + s(0)\delta_{n0} \end{aligned} \quad (2.74a)$$

whereas in the continuous domain \mathbb{R} a single point has zero measure, and therefore the term related to $s(0)$ is irrelevant.

This is a general difference between the two classes, in so far two continuous signals, which coincide *almost everywhere*, must be considered as the same signal, whereas two discrete signals that differ even in a single point are really different.

Fig. 2.24 Decomposition of a causal discrete signal $s(nT)$ into even and odd parts



Time Shift Given a discrete signal $s(nT)$ and an integer n_0 , the signal $s(nT - n_0T)$ represents a shifted version of $s(nT)$ by the amount n_0T . The difference with respect to the continuous case, where the shift t_0 may be an arbitrary real number, is that now the shift $t_0 = n_0T$ must be a multiple of the spacing T .

Area and Mean Value The application of definition (2.9) would give zero for every discrete signal. To get a useful parameter, the right definition is

$$\text{area}(s) \triangleq \sum_{n=-\infty}^{+\infty} Ts(nT). \tag{2.75}$$

In this way, each value $s(nT)$ gives a contribution, $Ts(nT)$, to the area.

In the interpretation of this definition (and similar others), it is convenient to refer to a continuous signal $\tilde{s}(t)$, $t \in \mathbb{R}$, which is obtained from the given discrete signal $s(nT)$ by a *hold* operation, namely (Fig. 2.25)

$$\tilde{s}(t) = s(nT), \quad nT \leq t < (n+1)T. \tag{2.76}$$

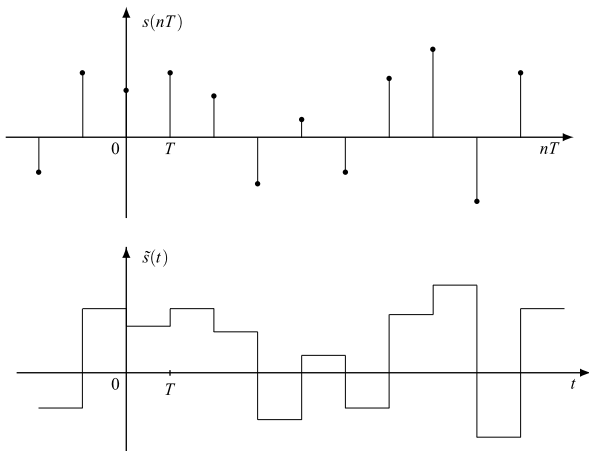
This continuous signal has the same area as $s(nT)$, but the area of $\tilde{s}(t)$ is evaluated according to (2.9) and the area of $s(nT)$ according to (2.75).

The *mean value* of a discrete signal $s(nT)$ is defined by the limit

$$m_s = \lim_{N \rightarrow +\infty} \frac{1}{(2N+1)T} \sum_{n=-N}^{+N} Ts(nT). \tag{2.77}$$

Remark The *hold signal* $\tilde{s}(t)$ is not completely useful to study discrete signals using continuous signal definitions. For instance, the FT applied to $\tilde{s}(t)$, $t \in \mathbb{R}$ does not give the FT of $s(t)$, $t \in \mathbb{Z}(T)$.

Fig. 2.25 Discrete signal and correspondent continuous signal obtained by a hold interpolation



Energy and Power A discrete signal has zero energy and zero power, if these parameters are interpreted in the sense of continuous signals. The appropriate definitions for discrete signals are

$$E_s = \lim_{N \rightarrow \infty} \sum_{n=-N}^N T |s(nT)|^2 = \sum_{n=-\infty}^{+\infty} T |s(nT)|^2, \tag{2.78a}$$

$$P_s = \lim_{N \rightarrow \infty} \frac{1}{(2N + 1)T} \sum_{n=-N}^N T |s(nT)|^2 \tag{2.78b}$$

which are in agreement with definitions (2.75) and (2.77). Moreover, E_s and P_s defined by (2.78a, 2.78b) equal respectively the energy and the power of the *hold signal* of Fig. 2.25.

Extension and Duration The *extension* $e(s)$ of a discrete signal may be defined as a set of consecutive points nT such that (Fig. 2.26)

$$s(nT) = 0, \quad nT \notin e(s).$$

The difference with respect to the extension of a continuous signal is that $e(s)$ is a subset of the domains $\mathbb{Z}(T)$ and therefore consists of *isolated* points.

The *duration* of a discrete signal is defined by

$$D(s) = \text{meas } e(s) = T \times \text{number of points of } e(s).$$

Here the *measure* is not the Lebesgue measure, which assigns zero to every set of isolated points, but the *Haar measure*, which assigns the finite value T to each point of the extension. Figure 2.26 shows an example of discrete signal with extension, $e(s) = \{-5T, \dots, 11T\}$, whose duration is $D(s) = 17T$.

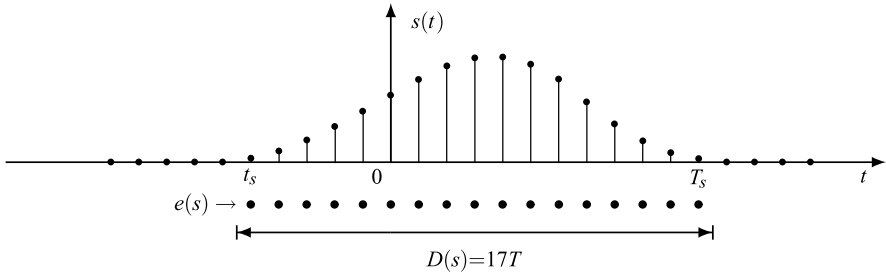


Fig. 2.26 Discrete signal with a limited extension: $e(s) = \{t_s, \dots, T_s\}$ with $t_s = -5T$ and $T_s = 11T$. The duration is $D(s) = 17T$

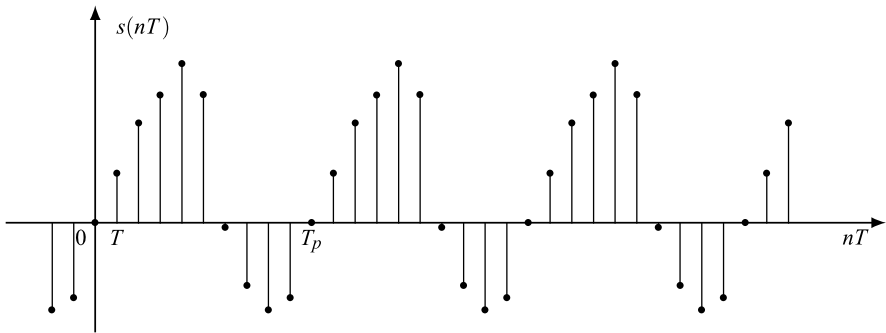


Fig. 2.27 Periodic discrete signal with period $T_p = 10T$

2.9.2 Periodic Discrete Signals

A discrete signal $s(nT)$ is *periodic* if

$$s(nT + NT) = s(nT), \quad \forall n \in \mathbb{Z}$$

where N is a natural number. Clearly, the period $T_p = NT$ must be a multiple of the spacing T . Figure 2.27 shows an example of a periodic discrete signal with period $T_p = 10T$.

As seen for continuous signals, some definitions must be modified for periodic signals. The rule is that the summations extended to the whole domain $\mathbb{Z}(T)$ *must be limited to a period*. For instance, the definition of energy given by (2.78a) for a periodic discrete signal is modified as *energy in a period*, namely

$$E_s = \sum_{n=n_0}^{n_0+N-1} T |s(nT)|^2,$$

where n_0 is an arbitrary integer (usually set to $n_0 = 0$).

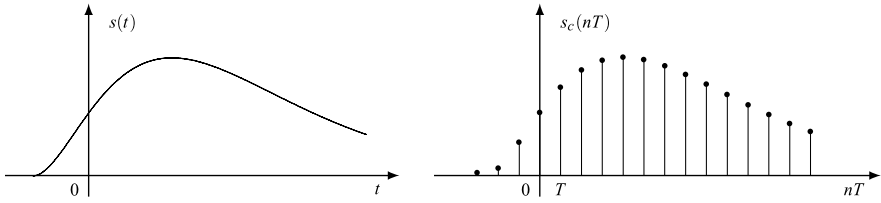


Fig. 2.28 Example of *sampling* of a continuous signal

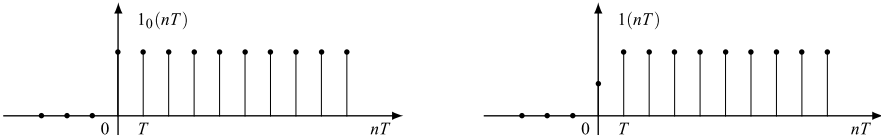


Fig. 2.29 Discrete step signal compared with sampled continuous step signal

As noted in the introduction (see Sect. 1.3), the class of periodic discrete signals is very important in applications, since they are the only signals that can be handled directly on a digital computer. The reason is that a periodic discrete signal $s(nT)$ with the period $T_p = NT$ is *completely specified by its finitely many values in a period*, say $s(0), s(T), \dots, s((N-1)T)$. For all the other classes, the signal specification involves infinitely many values.

2.10 Examples of Discrete Signals

Examples of discrete signals can autonomously be introduced, but frequently they are obtained from continuous signals with a domain *restriction* from \mathbb{R} into $\mathbb{Z}(T)$. This operation, called *sampling*, is stated by the simple relationship (Fig. 2.28)

$$s_c(nT) = s(nT), \quad nT \in \mathbb{Z}(T) \quad (2.79)$$

where $s(t), t \in \mathbb{R}$, is the reference continuous signal and $s_c(nT), nT \in \mathbb{Z}(T)$, is the discrete signal obtained by the sampling operation.

2.10.1 Discrete Step Signal

The *discrete unit step signal* (Fig. 2.29) is defined by

$$1_0(nT) = \begin{cases} 0 & \text{for } n < 0; \\ 1 & \text{for } n \geq 0. \end{cases} \quad (2.80)$$

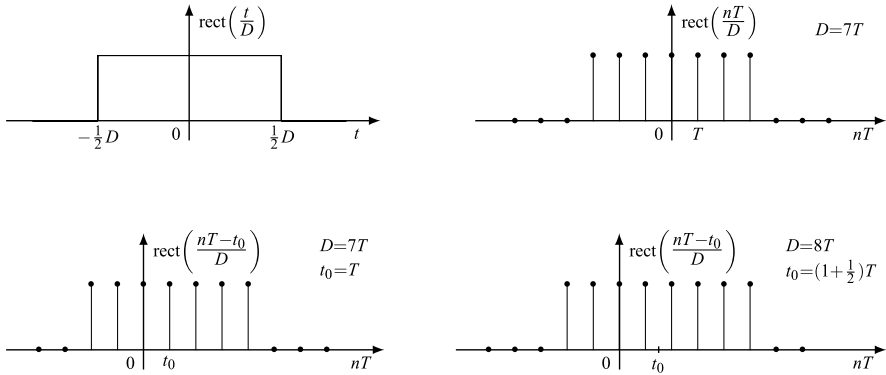


Fig. 2.30 Example of discrete rectangular pulses, compared with its continuous-time version. Above centered at the origin and below centered out of the origin

Note in particular that at the time origin $1_0(nT)$ takes a unit value. Instead, the signal obtained by sampling a unit step continuous signal is given by

$$1(nT) = \begin{cases} 0 & \text{for } n < 0; \\ \frac{1}{2} & \text{for } n = 0; \\ 1 & \text{for } n > 0, \end{cases}$$

as follows from the convention on discontinuities of continuous signals (see Sect. 2.1).

2.10.2 Discrete Rectangular Pulses

The *discrete rectangular pulse* with extension

$$e(r) = \{n_1 T, (n_1 + 1)T, \dots, n_2 T\}, \quad n_1 \leq n_2,$$

can be written in the form

$$r(nT) = \text{rect}\left(\frac{nT - t_0}{D}\right) \tag{2.81}$$

where

$$t_0 = \frac{n_1 + n_2}{2} T, \quad D = (n_2 - n_1 + 1)T \tag{2.81a}$$

are respectively the central instant and the duration. Note that expression (2.81) is not ambiguous since discontinuities of the function $\text{rect}(x)$ are not involved therein. Figure 2.30 shows a few examples of discrete rectangular pulses.

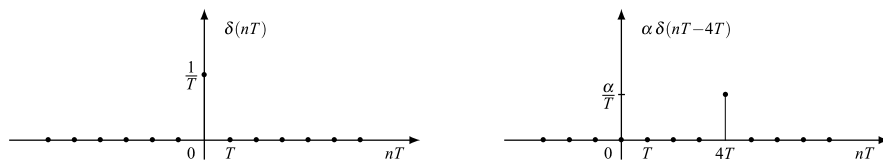


Fig. 2.31 The discrete impulse with unit area at the origin and with area α applied at $n_0T = 4T$

2.10.3 Discrete Impulses

We want a discrete signal with the same properties of the *impulse*, introduced for continuous signal by means of the delta function. However, in the discrete case the formalism of delta function (which is a distribution) is not necessary. In fact, the discrete signal defined by (Fig. 2.31)

$$\delta(nT) = \begin{cases} \frac{1}{T} & \text{for } n = 0; \\ 0 & \text{for } n \neq 0 \end{cases} \quad (2.82)$$

has exactly the same properties as the continuous impulse $\delta(t)$, namely the extension of $\delta(nT)$ is limited to the origin, i.e., $e(\delta) = \{0\}$, $\delta(nT)$ has unit area, $\delta(nT)$ has the *sifting property*

$$\sum_{n=-\infty}^{+\infty} Ts(nT)\delta(nT - n_0T) = s(n_0T), \quad (2.83a)$$

the *convolution* (see the next section) of an arbitrary signal $s(nT)$ with the impulse $\delta(nT)$ yields the signal itself

$$s(nT) = \sum_{k=-\infty}^{+\infty} Ts(kT)\delta(nT - kT). \quad (2.83b)$$

In general, the impulse with area α and applied at n_0T must be written in the form $\alpha\delta(nT - n_0T)$. Note that a discrete impulse is strictly related to the Kronecker delta, namely

$$T\delta(nT - n_0T) = \delta_{nn_0} = \begin{cases} 1 & \text{for } n = n_0; \\ 0 & \text{for } n \neq n_0. \end{cases} \quad (2.84)$$

2.10.4 Discrete Exponentials and Discrete Sinusoidal Signals

A discrete *exponential* signal has the general form

$$s(nT) = Ka^n \quad (2.85a)$$

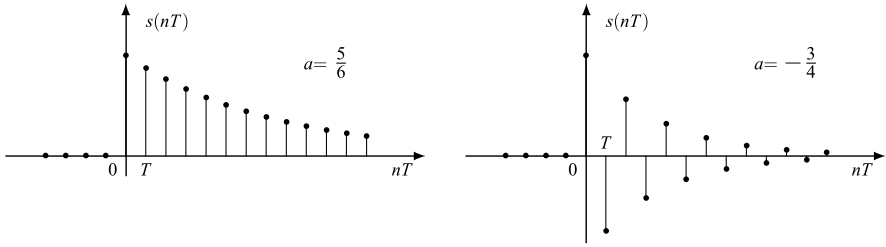


Fig. 2.32 Examples of discrete causal exponential

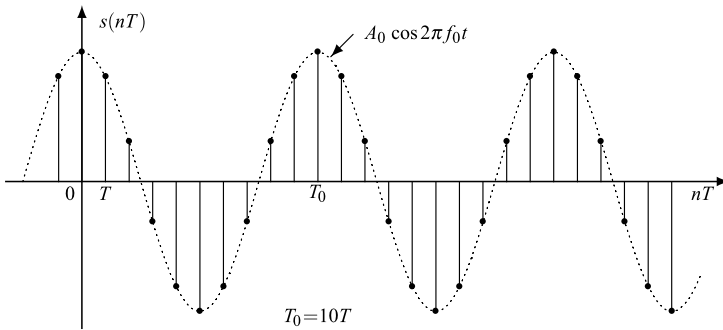


Fig. 2.33 Discrete sinusoidal signal with $f_0 T = 1/10$

where K and a are complex constants. In particular, when $|a| = 1$, it can be written as

$$Ae^{i2\pi f_0 nT} \tag{2.85b}$$

where A is a complex amplitude and f_0 is a real frequency (positive or negative).

A discrete *causal exponential* signal has the general form

$$K1_0(nT)a^n, \tag{2.86}$$

where K and a are complex constants. Figure 2.32 illustrates this signal for $K = 1$ and two values of a .

A discrete *sinusoidal* signal has the form (Fig. 2.33)

$$A_0 \cos(2\pi f_0 nT + \varphi_0) \tag{2.87}$$

where both A_0 and f_0 are real and positive, and can be expressed as the sum of two exponentials of the form (2.85b) (see (2.21)).

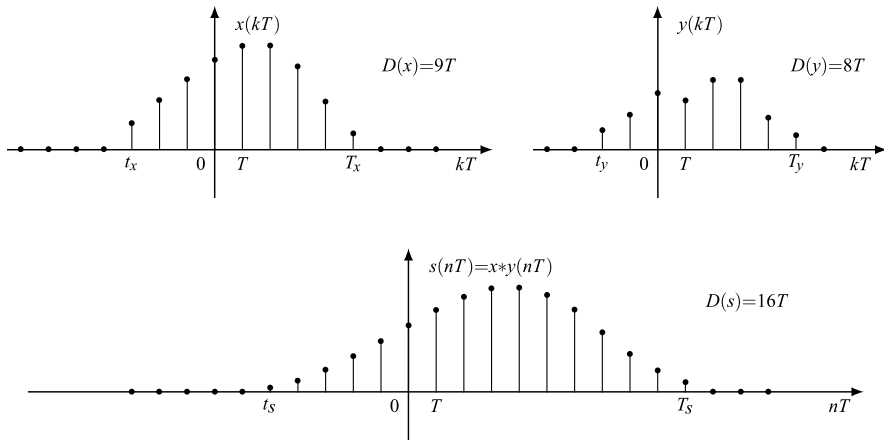


Fig. 2.34 Convolution of two time-limited discrete signals. Note that the convolution duration is $D(s) = D(x) + D(y) - T$

2.11 Convolution of Discrete Signals

As seen for continuous signals, we have different definitions for discrete aperiodic signals and for discrete periodic signals.

2.11.1 Aperiodic Discrete Signals

Given two discrete aperiodic signals $x(nT)$ and $y(nT)$, the convolution defines a new discrete signal $s(nT)$ according to

$$s(nT) = \sum_{k=-\infty}^{+\infty} T x(kT) y(nT - kT). \quad (2.88)$$

This is concisely denoted by $s = x * y$ or, more explicitly, by $s(nT) = x * y(nT)$.

Discrete convolution has the same properties as continuous convolution seen in Sect. 2.4 (rules on commutativity, area, etc.). Here, we outline only the extension rule. If $x(nT)$ and $y(nT)$ have the limited extensions

$$e(x) = \{n_x T, \dots, N_x T\}, \quad e(y) = \{n_y T, \dots, N_y T\}$$

then also their convolution $s(nT) = x * y(nT)$ has a limited extension given by

$$e(s) = \{n_s T, \dots, N_s T\} \quad \text{with } n_s = n_x + n_y, N_s = N_x + N_y. \quad (2.89)$$

Figure 2.34 shows an example, where $e(x) = \{-3T, \dots, 5T\}$ and $e(y) = \{-2T, \dots, 5T\}$. Then $e(s) = \{-5T, \dots, 10T\}$.

2.11.2 Periodic Discrete Signals

At this point, the right definition of the convolution for this class of signals should be evident. Given two periodic discrete signals $x(nT)$ and $y(nT)$ with the same period $T_p = NT$, their convolution is

$$s(nT) = \sum_{k=k_0}^{k_0+N-1} T x(kT)y(nT - kT), \quad (2.90)$$

where the summation is limited to a period. The result is a signal $s(nT)$ with the same period $T_p = NT$.

The “periodic discrete” convolution, often called the *cyclic convolution*, has the same properties as the other kind of convolutions.

2.12 The Fourier Transform of Discrete Signals

Discrete signals can be represented in the frequency domain by means of the FT, as seen for continuous signals. In the discrete case, the physical interpretation of the FT may be less evident, but nevertheless it is a very useful tool.

2.12.1 Definition

A discrete signal $s(nT)$, $nT \in \mathbb{Z}(T)$ can be represented in the form

$$s(nT) = \int_{f_0}^{f_0+F_p} S(f)e^{i2\pi fnT} df, \quad (2.91a)$$

where $S(f)$ is the FT of $s(nT)$, which is given by

$$S(f) = \sum_{n=-\infty}^{+\infty} T s(nT)e^{-i2\pi fnT}. \quad (2.91b)$$

In (2.91a), the integral is extended over an arbitrary period $(f_0, f_0 + F_p)$ of the FT. The FT $S(f)$ is a periodic function of the real variable f (Fig. 2.35) with period

$$F_p = 1/T.$$

This is a consequence of the periodicity of the exponential function $e^{-i2\pi fnT}$ with respect to f . Remarkable is the fact that the *period* of $S(f)$, expressed in cycles per second (or hertz), equals the *signal rate*, expressed in values per second.

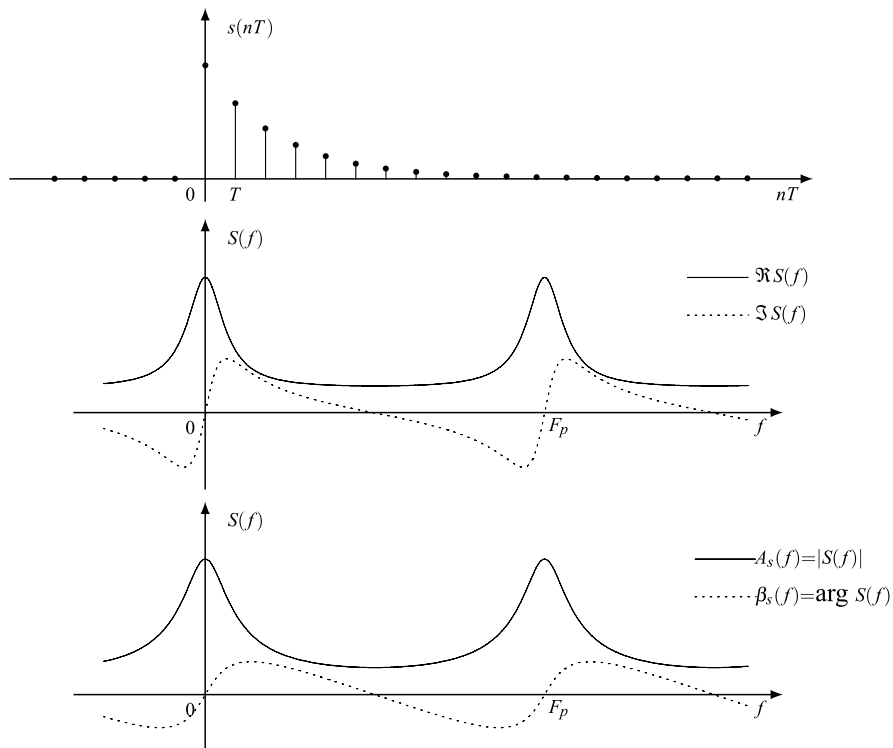


Fig. 2.35 Fourier transform of a real discrete time signal represented by real and imaginary parts, and by modulus and argument

As for continuous signals, we use the notations $S(f) = \mathcal{F}[s | f]$ and $s(nT) = \mathcal{F}^{-1}[S | nT]$ and also

$$s(nT) \xrightarrow{\mathcal{F}} S(f), \quad S(f) \xrightarrow{\mathcal{F}^{-1}} s(nT).$$

The operator $\xrightarrow{\mathcal{F}}$ represents a complex function of a discrete variable, $s(nT)$, by a periodic function of continuous variable, $S(f)$.

2.12.2 Interpretation

According to (2.91a), a discrete signal $s(nT)$ is represented as the sum of infinitely many exponentials of the form

$$[S(f) df] e^{i2\pi f nT}, \quad f \in [f_0, f_0 + F_p),$$

with infinitesimal amplitude $S(f) df$ and frequency f belonging to a period of the FT. The reason of this frequency limitation is due to the periodicity of discrete

exponentials. In fact, the components with frequency f and $f + kF_p$ are equal

$$[S(f) df] e^{i2\pi f n T} = [S(f + kF_p) df] e^{i2\pi(f + kF_p)nT}, \quad \forall k \in \mathbb{Z}.$$

We can therefore restrict the frequency range to a period, which may be $[0, F_p)$, that is,

$$s(nT) = \int_0^{F_p} S(f) e^{i2\pi f n T} df, \quad F_p = \frac{1}{T}. \quad (2.92)$$

The conclusion is that *the maximum frequency contained in a discrete signal $s(nT)$ cannot exceed the signal rate $F_p = 1/T$.*

For a *real* signal, $s^*(nT) = s(nT)$, the FT $S(f)$ has the *Hermitian symmetry*

$$S(f) = S^*(-f).$$

This symmetry, combined with the periodicity $S(f + F_p) = S(f)$, allows restricting the range from $[0, F_p)$ into $[0, \frac{1}{2}F_p)$. Moreover, from (2.92) we can obtain the form

$$s(nT) = \int_0^{\frac{1}{2}F_p} 2A_S(f) \cos(2\pi f n T + \beta_S(f)) df \quad (2.93)$$

where

$$A_S(f) = |S(f)| \quad \beta_S(f) = \arg S(f).$$

In the sinusoidal form (2.93), the maximum frequency is $\frac{1}{2}F_p$, which is called the *Nyquist frequency*.

2.12.3 Properties of the Fourier Transform

Here we consider only a few of the several properties (or *rules*).

- The shifted version of a discrete signal, $y(nT) = s((n - n_0)T)$, has FT

$$Y(f) = S(f) e^{-i2\pi f n_0 T}. \quad (2.94)$$

- The FT of *convolution*, $s(nT) = x * y(nT)$, is given by the product of the FTs

$$S(f) = X(f)Y(f). \quad (2.95)$$

Note the consistency of this rule: since $X(f)$ and $Y(f)$ are both periodic of period F_p , also their product is periodic with the same period, F_p .

- The FT of the *product* of two signals, $s(nT) = x(nT)y(nT)$, is given by the (cyclic) *convolution* of their FT (see (2.44))

$$S(f) = X * Y(f) = \int_{f_0}^{f_0 + F_p} X(\lambda)Y(f - \lambda) d\lambda. \quad (2.96)$$

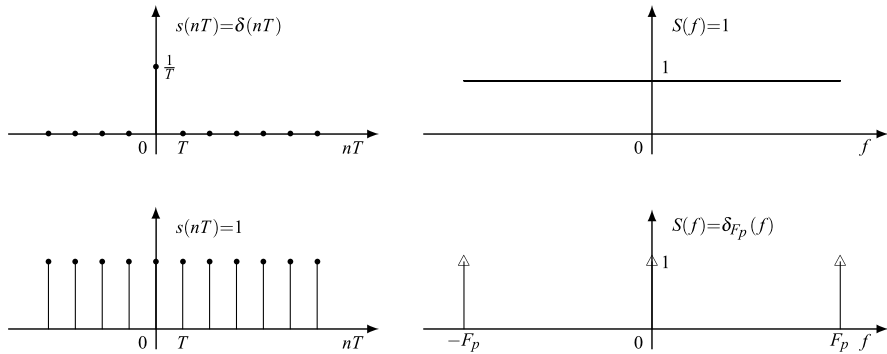


Fig. 2.36 Fourier transforms of the discrete impulse and of the discrete unit signal

- Parseval theorem allows evaluating the signal energy from the Fourier transform according to

$$E_s = \sum_{n=-\infty}^{+\infty} T |s(nT)|^2 = \int_{f_0}^{f_0+F_p} |S(f)|^2 df \quad (2.97)$$

where the integral is over an arbitrary period of $S(f)$.

2.12.4 Examples of Fourier Transforms

The explicit evaluation of the Fourier transform, according to (2.91b), requires the summation of a bilateral series; in the general case, this is not easy. The explicit evaluation of the inverse Fourier transform, according to (2.91a), requires the integration over a period.

Impulses and Constant Signals The FT evaluation of the impulse applied at n_0T is immediate

$$\delta(nT - n_0T) \xrightarrow{\mathcal{F}} e^{-i2\pi f n_0T}.$$

Note that with the notation $\delta(t - t_0)$ instead of $\delta(nT - n_0T)$ the above expression takes the same form as seen for the continuous case (see (2.65))

$$\delta(t - t_0) \xrightarrow{\mathcal{F}} e^{-i2\pi f t_0},$$

where now $t, t_0 \in \mathbb{Z}(T)$. In particular, for $t_0 = n_0T = 0$ we find (Fig. 2.36)

$$\delta(nT) \xrightarrow{\mathcal{F}} 1.$$

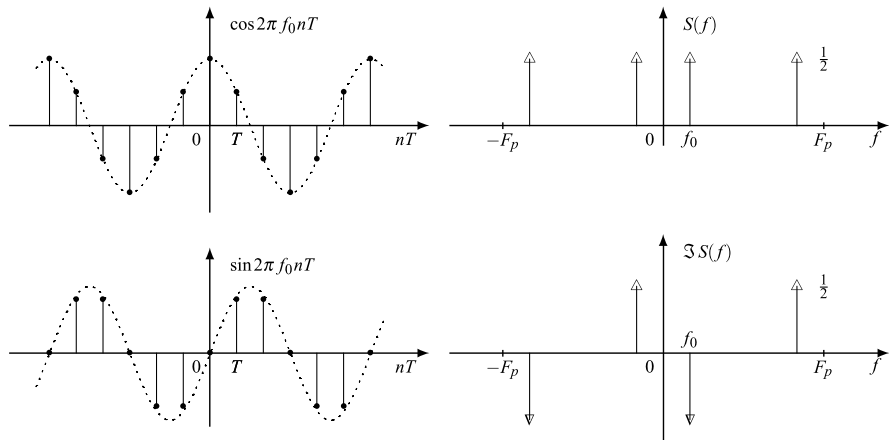


Fig. 2.37 Fourier transform of a cosinusoidal and of sinusoidal discrete signal

Less trivial is the FT evaluation of the unit signal, $s(nT) = 1$, since the definition (2.91b) gives

$$S(f) = T \sum_{n=-\infty}^{+\infty} e^{-i2\pi f nT},$$

where the series is not summable. To overcome the difficulty, we can use the identity (2.53) established in the contest of Fourier series and now rewritten in the form

$$\sum_{n=-\infty}^{+\infty} e^{-i2\pi f nT} = F_p \operatorname{rep}_{F_p} \delta(f), \quad F_p = 1/T. \tag{2.98}$$

Then, we find (Fig. 2.36)

$$1 \xrightarrow{\mathcal{F}} \operatorname{rep}_{F_p} \delta(f) \triangleq \delta_{F_p}(f). \tag{2.99}$$

Hence, the FT of the unit discrete signal, $s(nT) = 1$, consists of the periodic repetition of the frequency impulse $\delta(f)$. Remarkable is the fact that the delta function formalism allows the evaluation of the sum of a divergent series!

Exponential and Sinusoidal Signals If we replace f with $f - f_0$ in identity (2.98), we find the Fourier pair

$$e^{i2\pi f_0 nT} \xrightarrow{\mathcal{F}} \operatorname{rep}_{F_p} \delta(f - f_0) = \delta_{F_p}(f - f_0),$$

which gives the FT of the discrete exponential. Next, using Euler’s formulas, we obtain the FT of sinusoidal discrete signals (Fig. 2.37), namely

$$\cos 2\pi f_0 nT \xrightarrow{\mathcal{F}} \frac{1}{2} [\delta_{F_p}(f - f_0) + \delta_{F_p}(f + f_0)],$$

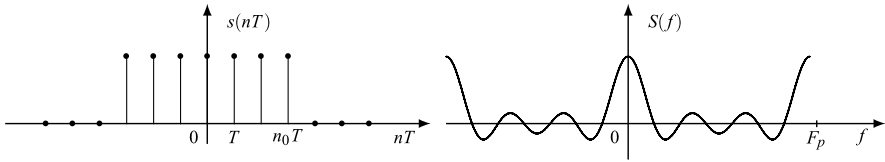


Fig. 2.38 Fourier transform of a discrete rectangular pulse

$$\sin 2\pi f_0 nT \xrightarrow{\mathcal{F}} \frac{1}{2i} [\delta_{F_p}(f - f_0) - \delta_{F_p}(f + f_0)].$$

Rectangular Pulses The discrete rectangular pulse of duration $(2n_0 + 1)T$

$$s(nT) = \begin{cases} A_0 & \text{for } |n| \leq n_0; \\ 0 & \text{for } |n| > n_0 \end{cases}$$

has as FT

$$S(f) = A_0 T \sum_{n=-n_0}^{n_0} e^{-i2\pi f nT}.$$

This finite sum can be expressed by means of the *periodic sinc* function, as seen in Example 2.6 of Sect. 2.5. The result is

$$S(f) = A_0 N T \operatorname{sinc}_N(f N T), \quad N = 2n_0 + 1.$$

Figure 2.38 illustrates $S(f)$ for $n_0 = 3$ ($N = 7$).

Causal Exponentials The FT of the signal $s(nT) = 1_0(n)a^n$ is

$$S(f) = T \sum_{n=0}^{+\infty} a^n e^{-i2\pi f nT} = T \sum_{n=0}^{+\infty} (a e^{-i2\pi f T})^n. \quad (2.100)$$

If $|a| < 1$ the geometrical series is convergent, since

$$|a e^{-i2\pi f T}| = |a| < 1$$

and the FT is given by

$$S(f) = \frac{T}{1 - a \exp(-i2\pi f T)}.$$

If $|a| > 1$ the geometrical series is divergent and the FT does not exist.

2.13 The Discrete Fourier Transform (DFT)

The DFT is commonly introduced to represent a finite sequence of values

$$s_0, s_1, \dots, s_{N-1} \quad (2.101a)$$

by another finite sequence of values

$$S_0, S_1, \dots, S_{N-1}. \quad (2.101b)$$

The two sequences are related by the relationships

$$s_n = \frac{1}{N} \sum_{k=0}^{N-1} S_k W_N^{nk}, \quad S_k = \sum_{n=0}^{N-1} s_n W_N^{-nk}, \quad (2.102)$$

where W_N is the N th root of the unity

$$W_N = \exp(i2\pi/N). \quad (2.103)$$

The first of (2.102) represents the inverse DFT (IDFT) and the second represents the DFT. They are a consequence of the orthogonality condition

$$\frac{1}{N} \sum_{m=0}^{N-1} W_N^{mk} W_N^{-nm} = \delta_{nk}.$$

Comments The DFT works with a finite number of values, and therefore it can be implemented on a digital computer. Its implementation is usually done by a very efficient algorithm, called the FFT (fast Fourier transform) (see Chap. 13).

In Signal Theory, the DFT represents the FT for periodic discrete signals and the finite sequence (2.101a) gives the *signal values in a period* and, analogously, the finite sequence (2.101b) gives the *Fourier transform values in a period*. However, the classical form (2.102) does not show clearly this assertion and the connection (or similarity) with the other FTs.

This will be seen after the development of the Unified Theory, in Chap. 11 and Chap. 13, where the DFT will be obtained as a special case of the unified Fourier transform.

2.14 Filtering of Discrete Signals

A discrete filter (linear, invariant) can be formulated as a system with the following input–output relationship (Fig. 2.39):

$$y(nT) = \sum_{k=-\infty}^{+\infty} T g(nT - kT)x(kT), \quad nT \in \mathbb{Z}(T) \quad (2.104)$$

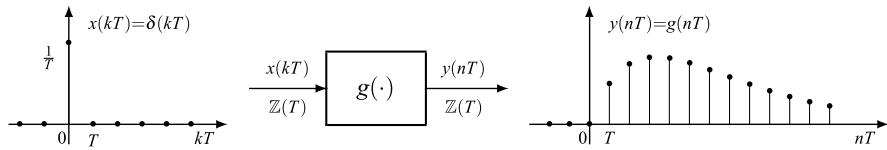


Fig. 2.39 Interpretation of impulse response of a discrete-time filter

where $x(kT)$ is the input signal, $y(nT)$ is the output signal and $g(nT)$ is the *impulse response* which specifies the filter.

We may recognize that (2.104) is a convolution, namely $y(nT) = g * x(nT)$, according to the definition given for (aperiodic) discrete signals in Sect. 2.11. As seen for continuous filters, the meaning of $g(nT)$ is the response of the filter to the discrete impulse $\delta(nT)$ defined by (2.82).

The input–output relationship (2.104) in the frequency domain becomes

$$Y(f) = G(f)X(f) \quad (2.105)$$

where $G(f)$ is the Fourier transform of the impulse response $g(nT)$, called the *frequency response* of the filter.

Thus, we recognize that the frequency-domain analysis of a discrete filter is exactly the same seen for a continuous filter in Sect. 2.8.

2.15 Sampling Theorem

The Sampling Theorem provides a connection between the classes of continuous and discrete signals.

2.15.1 The Operation of Sampling

In Sect. 2.3, we have seen that *sampling* gives a discrete signal $s_c(nT)$ starting from a continuous signal $s(t)$, $t \in \mathbb{R}$ according to the relationship

$$s_c(nT) = s(nT), \quad nT \in \mathbb{Z}(T).$$

The values $s(nT)$ are called the *samples* of $s(t)$, the spacing T is called the *sampling period* and $F_c = 1/T$ is the *sampling frequency* (it gives the number of samples per second).

Since sampling drops a portion of the original signal $s(t)$, it is evident that the recovery of $s(t)$ from its samples $s(nT)$ is not possible, in general. However, for a *band-limited* signal a perfect recovery becomes possible. This is stated by the *Sampling Theorem* which will now be formulated in the classical form. A very different formulation will be seen with the Unified Theory, in Chap. 8.

2.15.2 Formulation and Proof of Sampling Theorem

Theorem 2.1 Let $s(t)$, $t \in \mathbb{R}$ be a band-limited signal according to

$$S(f) = 0 \quad \text{for } |f| > B. \quad (2.106)$$

If the sampling frequency F_c is at least twice the band, $F_c \geq 2B$, then $s(t)$ can be recovered by its samples $s(nT)$, $n \in \mathbb{Z}$ according to the reconstruction formula

$$s(t) = \sum_{n=-\infty}^{+\infty} s(nT) \operatorname{sinc}[F_c(t - nT)]. \quad (2.107)$$

Proof Band-limitation stated by (2.106) allows writing the inverse FT in the form

$$s(t) = \int_{-\frac{1}{2}F_c}^{\frac{1}{2}F_c} S(f) e^{i2\pi f t} df. \quad (2.108a)$$

This, evaluated at $t = nT$, gives

$$s(nT) = \int_{-\frac{1}{2}F_c}^{\frac{1}{2}F_c} S(f) e^{i2\pi f nT} df. \quad (2.108b)$$

Next, consider the periodic repetition of the FT $S(f)$, with period F_c ,

$$S_p(f) = \sum_{k=-\infty}^{+\infty} S(f - kF_c). \quad (2.109)$$

Since $S_p(f)$ is periodic, it can be expanded into a Fourier series (this expansion has been considered for time functions, but it also holds for frequency functions). Considering that the period of $S_p(f)$ is F_c , we have

$$S_p(f) = \sum_{n=-\infty}^{+\infty} S_n e^{i2\pi f nT}, \quad T = 1/F_c, \quad (2.110a)$$

where

$$S_n = \frac{1}{F_c} \int_{-\frac{1}{2}F_c}^{\frac{1}{2}F_c} S_p(f) e^{-i2\pi f nT} df. \quad (2.110b)$$

Now, by the band-limitation, we find that the terms of the periodic repetition do not overlap (Fig. 2.40) and $S_p(f)$ equals $S(f)$ in the interval $(-\frac{1}{2}F_c, \frac{1}{2}F_c)$, that is, $S_p(f) = S(f)$, $-\frac{1}{2}F_c < f < \frac{1}{2}F_c$.

Then, replacing $S_p(f)$ with $S(f)$ in (2.110b) and comparing with (2.108b), we obtain

$$F_c S_n = s(-nT). \quad (2.110c)$$

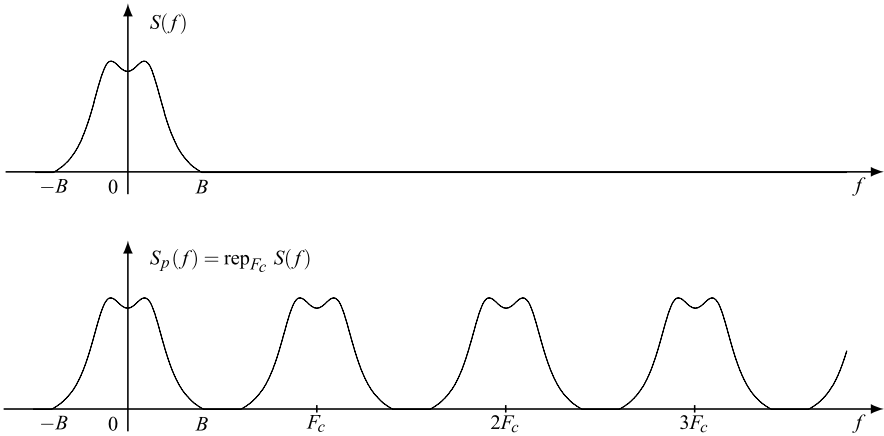


Fig. 2.40 Example of band-limited Fourier transform $S(f)$ and its periodic repetition with $F_c > 2B$

Finally, using series expansion (2.110a) in (2.108a), we find

$$s(t) = \sum_{n=-\infty}^{+\infty} \int_{-\frac{1}{2}F_c}^{\frac{1}{2}F_c} S_n e^{j2\pi f(t+nT)} df = \sum_{n=-\infty}^{+\infty} S_n F_c \operatorname{sinc}[F_c(t+nT)].$$

To complete the proof, it is sufficient to take into account (2.110c). □

2.16 Final Comments on Classical Theory

In this chapter, we have introduced and developed the two signal classes:

1. Continuous-time signals with domain \mathbb{R} , and
2. Discrete-time signals with domain $\mathbb{Z}(T)$.

A systematic comparison of definitions introduced in the time domain for the two classes brings to evidence the strong similarity, with the main difference that in the passage from class 1 to class 2 *integrals are replaced by summations*, specifically

$$\int_{-\infty}^{+\infty} s(t) dt \longrightarrow \sum_{n=-\infty}^{+\infty} Ts(nT).$$

In the frequency domain, the two classes give respectively: class 1 of continuous-frequency Fourier transforms, with domain \mathbb{R} , and class 2 of continuous-frequency Fourier transforms with domain \mathbb{R} and period $F_p = 1/T$. In this comparison, the rule of passing from time to frequency domain is not clear. To get this rule, we have to consider not only the domain, but also the periodicity.

On the other hand, we have realized that periodicity plays a fundamental role in definitions. In fact, from class 1 we have extracted the subclass 1(a) of periodic signals and used for them the integral limited to a period instead of the integral over the whole real axis, that is,

$$\int_{-\infty}^{+\infty} s(t) dt \longrightarrow \int_{t_0}^{t_0+T_p} s(t) dt.$$

Analogously, from class 2 we have extracted the subclass 2(a) of periodic signals with the substitution

$$\sum_{n=-\infty}^{+\infty} Ts(nT) \longrightarrow \sum_{n=n_0}^{n_0+N-1} Ts(nT).$$

In the frequency domain, the two subclasses of periodic signals give respectively: class 1(a) of discrete-frequency Fourier transforms, with domain $\mathbb{Z}(F)$, $F = 1/T_p$, and class 2(a) of discrete-frequency Fourier transforms, with domain $\mathbb{Z}(F)$ and period $F_p = 1/T$.

In conclusion, in order to find a link between time and frequency domains it is necessary to consider periodicity or aperiodicity. Only in this way, we find that the global class of signals, consisting of subclasses 1, 2, 1(a) and 2(a), has a full counterpart in the frequency domain consisting of subclasses of exactly the same type. This link will automatically be provided by the Unified Theory.

2.17 Problems

2.1 ★ [Sect. 2.1] Assuming that a continuous-time signal $s(t)$ is the mathematical model of an electrical voltage, find the physical dimensions of the following quantities: area, mean value, (specific) energy, and (specific) power.

2.2 ★ [Sect. 2.2] Show that the *area over a period* of a periodic signal defined by (2.17a) is independent of t_0 .

2.3 ★★ [Sect. 2.2] Show that the *mean value over a period* for a periodic signal, defined by (2.17b), is equal to the *mean value* defined in general by (2.10).

2.4 ★ [Sect. 2.3] Using the functions $1(x)$ and $\text{rect}(x)$ write a concise expression for the signal

$$s(t) = 3 \quad \text{for } t \in (-5, 1), \quad s(t) = t \quad \text{for } t \in (2, 4), \quad s(t) = 0 \quad \text{otherwise.}$$

2.5 ★ [Sect. 2.3] Find the extension, duration, area and energy of the signal of Problem 2.4.

2.6 ★ [Sect. 2.3] Find the energy of the causal exponential with $p_0 = 2 + i2\pi 5$.

2.7 ★ [Sect. 2.3] Write a mathematical expression of a triangular pulse $u(t)$ determined by the following conditions: $u(t)$ is even, has duration 2 and energy 10.

2.8 ★ [Sect. 2.3] An even-symmetric triangular pulse $u(t)$ of duration 4 and amplitude 2 is periodically repeated according to (2.16). Draw the periodic repetition in the following cases: $T_p = 8$, $T_p = 4$ and $T_p = 2$.

2.9 ★★ [Sect. 2.3] Write the derivative $r'(t)$ of the rectangular pulse $r(t)$ defined by (2.26). Verify that the integral of $r'(t)$ from $-\infty$ to t recovers $r(t)$.

2.10 ★★ [Sect. 2.3] Write the first and second derivatives of the rectified sinusoidal signal

$$s(t) = A_0 |\cos \omega_0 t|.$$

2.11 ★★ [Sect. 2.3] Find the (minimum) period of the signal

$$s(t) = 2 \cos \frac{2}{3} \omega_0 t + 3 \sin \frac{4}{5} \omega_0 t.$$

2.12 ★★ [Sect. 2.4] Show that the (acyclic) convolution of an arbitrary signal $x(t)$ with a sinusoidal signal $y(t) = A_0 \cos(\omega_0 t + \phi_0)$ is a sinusoidal signal with the same period as $y(t)$.

2.13 ★ [Sect. 2.4] Show that the derivative of the convolution $s(t)$ of two derivable signals $x(t)$ and $y(t)$ is given by $s' = x' * y = x * y'$.

2.14 ★★★ [Sect. 2.4] Evaluate the convolution of the following pulses:

$$x(t) = A_1 \text{rect}(t/2D), \quad y(t) = A_2 \exp(-t^2/D^2).$$

Hint. Express the result in terms of the normalized Gaussian distribution

$$\Phi(x) = \int_{-\infty}^x \frac{1}{\sqrt{2\pi}} e^{-\frac{1}{2}y^2} dy.$$

2.15 ★ [Sect. 2.4] Evaluate the convolution of the signals

$$x(t) = A_1 \text{sinc}(t/D), \quad y(t) = A_2 \delta(t) + A_3 \delta(t - 2D).$$

2.16 ★★★ [Sect. 2.4] Evaluate the (cyclic) convolution of the signal

$$x(t) = \text{rep}_{T_p} \text{rect}(t/T),$$

with $x(t)$ itself (auto-convolution). Assume $T_p = 4T$.

2.17 ★ [Sect. 2.5] Show that the Fourier coefficients have the same physical *dimensions* as the signal. In particular, if $s(t)$ is a voltage in volts, also S_n must be expressed in volts.

2.18 ★ [Sect. 2.5] Starting from the exponential form of the Fourier series and assuming a *real* signal, prove (2.49a) and (2.49b). Note that in this case S_0 is real.

2.19 ★ [Sect. 2.5] Show that if $s(t)$ is real and even, then its sine–cosine expansion (2.49a) becomes an *only cosine expansion*.

2.20 ★★★ [Sect. 2.5] Assume that a periodic signal has the following symmetry:

$$s(t) = -s(t - T_p/2).$$

Then, show that the Fourier coefficients S_n are zero for n even, i.e., the *even harmonics* disappear. *Hint*: use (2.50).

2.21 ★★ [Sect. 2.5] Evaluate the mean value, the root mean square value and the Fourier coefficients of the periodic signal

$$s(t) = \text{rep}_{T_p} \left[\text{rect} \left(\frac{t}{T_0} \right) A_0 \left(1 - \frac{|t|}{T_0} \right) \right]$$

in the cases $T_p = 2T_0$ and $T_p = T_0$.

2.22 ★ [Sect. 2.5] Check Parseval's Theorem (2.51a) for a sinusoidal signal (see Example 2.4).

2.23 ★ [Sect. 2.5] Evaluate the Fourier coefficients of the signal

$$s(t) = \text{rep}_{T_p} \left[\delta \left(t - \frac{1}{4} T_p \right) - \delta \left(t - \frac{3}{4} T_p \right) \right]$$

and find symmetries (if any).

2.24 ★ [Sect. 2.6] Find the physical dimension of the Fourier transform $S(f)$ when the signal is an electric voltage.

2.25 ★★ [Sect. 2.6] Show that if $s(t)$ is real, $S(f)$ has the Hermitian symmetry. *Hint*: use (2.55a, 2.55b).

2.26 ★★ [Sect. 2.6] Prove rule (2.60b) on the product of two signals.

2.27 ★★ [Sect. 2.6] Prove that the product $s(t) = x(t)y(t)$ of two strictly band-limited signal is strictly band-limited with

$$B(s) = B(x) + B(y).$$

Hence, in particular, the band of $x^2(t)$ is $2B(x)$.

2.28 ★ [Sect. 2.7] Evaluate the Fourier transform of the causal signal

$$s(t) = 1(t)e^{-t/T}, \quad T > 0$$

and then check that it verifies the Hermitian symmetry.

2.29 ★ [Sect. 2.7] Prove the relationship

$$s(t) \cos 2\pi f_0 t \xrightarrow{\mathcal{F}} \frac{1}{2}S(f - f_0) + \frac{1}{2}S(f + f_0) \quad (2.111)$$

called *modulation rule*.

2.30 ★ [Sect. 2.7] Using (2.111) evaluate the Fourier transform of the signal

$$s(t) = \text{rect}(t/T) \cos 2\pi f_0 t.$$

Then, draw graphically $S(f)$ for $f_0 T = 4$, checking that it is an even real function.

2.31 ★★ [Sect. 2.7] Using the rule on the product, prove the relationship

$$1(t) \cos 2\pi f_0 t \xrightarrow{\mathcal{F}} \frac{1}{4} \left[\delta(f - f_0) + \delta(f + f_0) + \frac{1}{i\pi(f - f_0)} + \frac{1}{i\pi(f + f_0)} \right].$$

2.32 ★★∇ [Sect. 2.7] The *scale change* (see Sect. 6.5) has the following rule

$$s(at) \xrightarrow{\mathcal{F}} (1/|a|)S(f/a) \quad a \neq 0. \quad (2.112)$$

Then, giving as known the pair $e^{-\pi t^2} \xrightarrow{\mathcal{F}} e^{-\pi f^2}$, evaluate the Fourier transform of the *Gaussian pulse*

$$u(t) = \frac{A_0}{\sqrt{2\pi}\sigma} \exp\left[-\frac{1}{2}\left(\frac{t}{\sigma}\right)^2\right].$$

2.33 ★★ [Sect. 2.7] Evaluate the Fourier transform of the periodic signal

$$s(t) = \text{rep}_{T_p} \text{rect}\left(\frac{t}{D}\right).$$

2.34 ★★ [Sect. 2.7] Prove the relationship

$$\text{triang}\left(\frac{t}{D}\right) = \text{rect}\left(\frac{t}{2D}\right) \left(1 - \frac{|t|}{D}\right) \xrightarrow{\mathcal{F}} D \text{sinc}^2(fD)$$

where the signal is the 2D-duration *triangular pulse*.

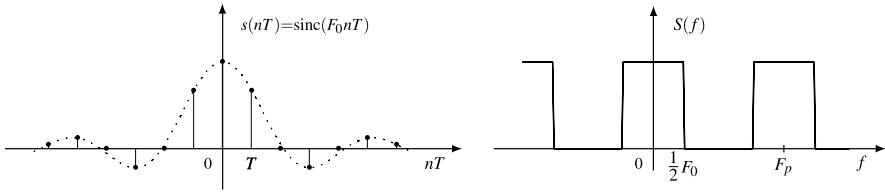


Fig. 2.41 Fourier transform of discrete sinc pulse

2.35 *** [Sect. 2.7] Consider the decomposition of a *real* signal in an even and an odd components

$$s(t) = s_e(t) + s_o(t).$$

Then, prove the relationship

$$s_e(t) \xrightarrow{\mathcal{F}} \Re S(f), \quad s_o(t) \xrightarrow{\mathcal{F}} j\Im S(f).$$

2.36 * [Sect. 2.12] Evaluate the Fourier transforms of the signals

$$s_1(nT) = \begin{cases} A_0, & \text{for } n = \pm 1; \\ 0, & \text{otherwise,} \end{cases} \quad s_2(nT) = \begin{cases} A_0, & \text{for } n = -1, 0, 1; \\ 0, & \text{otherwise,} \end{cases}$$

and check that $S_1(f)$ and $S_2(f)$ are (a) periodic with period $F_p = 1/T$, (b) real and (c) even.

2.37 * [Sect. 2.12] With the signals of the previous problem check the Parseval theorem (2.97).

2.38 * [Sect. 2.12] Show the relationship

$$\text{sinc}(nF_0T) \xrightarrow{\mathcal{F}} (1/F_0) \text{rep}_{F_p} \text{rect}(f/F_0),$$

illustrated in Fig. 2.41 for $F_0T = \frac{1}{2}$. *Hint: show that the inverse Fourier transform of $S(f)$ is $s(nT)$.*

2.39 ** [Sect. 2.15] Apply the Sampling Theorem to the signal

$$s(t) = \text{sinc}^3(Ft), \quad t \in \mathbb{R}$$

with $F = 4$ kHz.

Appendix: Fourier Transform of the Signum Signal $\text{sgn}(t)$

The Fourier transform definition (2.55b) yields

$$\int_{-\infty}^{+\infty} \text{sgn}(t)e^{-i2\pi ft} dt = \frac{2}{i} \int_0^{\infty} \sin 2\pi ft dt.$$

These integrals do not exist. However, $\text{sgn}(t)$ can be expressed as the inverse Fourier transform of the function $1/(i\pi f)$, namely

$$\text{sgn}(t) = \int_{-\infty}^{+\infty} \frac{1}{i\pi f} e^{i2\pi ft} df \triangleq x(t) \quad (2.113a)$$

provided that the integral is interpreted as a *Cauchy principal value*, i.e.,

$$x(t) = \int_{-\infty}^{+\infty} \frac{1}{i\pi f} e^{i2\pi ft} df = \lim_{F \rightarrow \infty} \int_{-F}^F \frac{1}{i\pi f} e^{i2\pi ft} df. \quad (2.113b)$$

Using Euler's formula, we get

$$x(t) = \int_{-\infty}^{+\infty} \frac{1}{i\pi f} \cos(2\pi ft) df + \int_{-\infty}^{+\infty} \frac{1}{\pi f} \sin(2\pi ft) df$$

where the integrand $(1/i2\pi f) \cos(2\pi f)$ is an odd function of f , and therefore the integral is zero. Then

$$x(t) = \int_{-\infty}^{+\infty} \frac{\sin(2\pi ft)}{\pi f} df.$$

Now, for $t = 0$ we find $x(0) = 0$. For $t \neq 0$, letting

$$2ft \rightarrow u, \quad df \rightarrow \frac{du}{2t},$$

we obtain

$$x(t) = \begin{cases} \int_{-\infty}^{+\infty} \frac{\sin(\pi u)}{\pi u} du & \text{for } t > 0; \\ \int_{+\infty}^{-\infty} \frac{\sin(\pi u)}{\pi u} du = -\int_{-\infty}^{+\infty} \frac{\sin(\pi u)}{\pi u} du & \text{for } t < 0. \end{cases}$$

It remains to evaluate the integral

$$I = \int_{-\infty}^{+\infty} \frac{\sin(\pi u)}{\pi u} du = \int_{-\infty}^{+\infty} \text{sinc}(u) du.$$

To this end, we use the rule (2.61) giving for a Fourier pair $s(t), S(f)$

$$\text{area}(S) = \int_{-\infty}^{+\infty} S(f) df = s(0)$$

with $s(t) = \text{rect}(t)$, $S(f) = \text{sinc}(f)$ (see (2.64a, 2.64b)). Hence, we obtain

$$\int_{-\infty}^{+\infty} \text{sinc}(f) \, df = s(0) = \text{rect}(0) = 1.$$

Combination of the above results gives $x(t) = \text{sgn}(t)$.

References

1. R.N. Bracewell, *The Fourier Transform and Its Applications*, 2nd edn. (McGraw–Hill, New York, 1986)
2. A. Papoulis, *The Fourier Integral and Its Applications* (McGraw–Hill, New York, 1962)
3. W. Rudin, *Functional Analysis* (McGraw–Hill, New York, 1991)
4. L. Schwartz, *Théorie des Distributions* (Hermann, Parigi, 1966)
5. G. Sansone, *Orthogonal Functions* (Interscience, New York, 1959)
6. E.C. Titchmarsh, *Introduction to the Theory of Fourier Integrals* (Oxford University Press, New York, 1937)
7. P.M. Woodward, *Probability and Information Theory, with Applications to Radar* (Pergamon/Macmillan & Co., New York, 1953)

Books on Classical Signal Theory

8. G. Cariolaro, *Teoria dei Segnali Determinati* (Patron, Bologna, 1977)
9. H.S. Carslaw, *Introduction to the Theory of Fourier's Series and Integrals*, 3rd edn. (Dover, New York, 1952)
10. G.R. Cooper, C.D. McGillem, *Methods of Signal and System Analysis* (Holt, Rinehart and Winston, New York, 1967)
11. G.R. Cooper, C.D. McGillem, *Continuous and Discrete Signal and System Analysis* (Holt, Rinehart and Winston, New York, 1974)
12. J.B. Cruz, M.E. Van Valkenburg, *Signals in Linear Circuits* (Houghton Mifflin, Boston, 1974)
13. H. Dym, H.P. McKean, *Fourier Series and Integrals* (Academic Press, New York, 1972)
14. L.E. Franks, *Signal Theory* (Prentice Hall, Englewood Cliffs, 1969)
15. R.A. Gabel, R.A. Roberts, *Signals and Linear Systems* (Wiley, New York, 1973)
16. D. Lindner, *Introduction to Signals and Systems* (McGraw–Hill, New York, 1999)
17. A.V. Oppenheim, A.S. Willsky, I.T. Young, *Signals and Systems* (Prentice Hall, Englewood Cliffs, 1983)
18. A. Papoulis, *Signal Analysis* (McGraw–Hill, New York, 1977)
19. A. Papoulis, *Circuits and Systems* (Holt, Rinehart and Winston, New York, 1980)
20. L.R. Rabiner, C.M. Rader (eds.), *Digital Signal Processing* (IEEE Press, New York, 1972)
21. M.J. Roberts, *Signals and Systems* (McGraw–Hill, New York, 2003)
22. L. Schwartz, *Information Transmission, Modulation and Noise: A Unified Approach to Communications Systems*, 3rd edn. (McGraw–Hill, New York, 1980)
23. J. Sherrick, *Concepts in Signals and Systems* (Prentice Hall, Englewood Cliffs, 2001)
24. W.M. Siebert, *Circuits, Signals and Systems* (McGraw–Hill, New York, 1986)
25. S. Soliman, M. Srinath, *Continuous and Discrete Signals and Systems* (Prentice Hall, Englewood Cliffs, 1990)

Part I
Classic Theory

Chapter 3

Unified Theory: Fundamentals

Guide to Reading This Chapter Notions concerning one-dimensional (1D) groups and related quantities may be regarded as elementary, but also multidimensional groups that are *separable* (in the Cartesian product of 1D groups) are elementary and require a slightly deeper effort than 1D groups. The difficulty is concentrated on *nonseparable* groups, which must be formulated in a special form, called *basis signature representation*. This consideration holds also for other topics, as cells and sum and intersection of groups.

The reader should be advised to tackle the chapter gradually, skimming over the more intricate topics by following the “jump” \Downarrow symbol, and considering only separable groups.

Alternatively, the reader willing to fully master the subject in all its details should study the whole chapter thoroughly, along Chap. 16, where groups and operations are further developed.¹

UT 3.1 The Philosophy of Unified Signal Theory

The Unified Signal Theory (UST) is an abstract formulation of signals and systems. Its few basic concepts allow for a completely general development, applicable to any kind of signal and system classes.

The key of the unification is based on the following definition.

Definition 3.1 A signal is a function

$$s : I \rightarrow \mathbb{C}, \tag{3.1}$$

¹The author suggests the reader to apply patience and perseverance in approaching the various foundational issues in this chapter (and in the next one, too), some of which are not exactly entertaining. However, we believe that effort and patience will be eventually rewarded when the reader will come to grips with the body of the UST. Once done with the (boring) fundamentals, the reader will hopefully realize that they allow for a very general and simple formulation of the various topics, and the whole theory will unfold in a smooth and straightforward way.

where I is a pair of Abelian groups, denoted in the form $I = I_0/P$, with I_0 the domain and P , a subgroup of I_0 , the periodicity. The codomain is always the set \mathbb{C} of complex numbers.

Signals (3.1) will be denoted in one of the forms

$$s(t), \quad t \in I \quad \text{or} \quad s(t), \quad t \in I_0/P,$$

where the codomain is not explicitly indicated since it is always \mathbb{C} . As we shall see, Definition 3.1 includes *aperiodic* signals, by letting the periodicity P degenerate to aperiodicity. The relevance of periodicity is already clear from the Classical Theory, where aperiodic and periodic signals required distinct definitions and developments. The possibility of unifying these different definitions lies just in treating aperiodicity as a degenerate form of periodicity.

The development of the UST, starting from the universal signal definition (3.1), needs a *linear functional* for the introduction of the fundamental operations of signal theory, like convolution and Fourier transform. Such a functional is the Haar integral, denoted as

$$\int_I dt s(t),$$

which is equipped with the proper topological requirements. Then, the *convolution* of two signals, $x(t)$ and $y(t)$, $t \in I$ can be defined as

$$x * y(t) = \int_I du x(t-u)y(u), \quad t \in I. \quad (3.2)$$

The Haar integral, moreover, can handle linear systems, here called *linear transformations*, according to the input–output relationship

$$y(t) = \int_I du h(t,u)x(u), \quad t \in U, \quad (3.3)$$

where $x(u)$, $u \in I$, is the input signal, $y(t)$, $t \in U$, is the output signal and $h(t,u)$ is the kernel which characterizes the linear transformation. Note that in general the output domain/periodicity U may be different from the input domain/periodicity I and this represents a relevant and not trivial generalization.

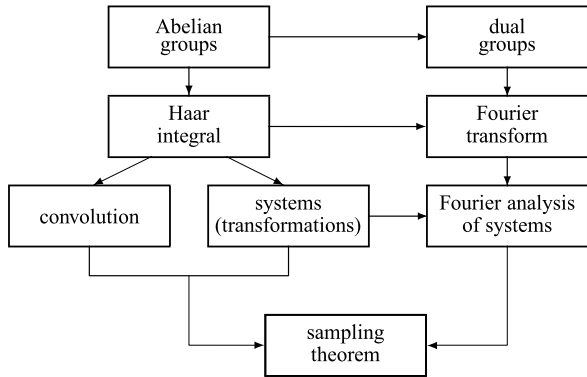
Finally, the Haar integral permits the introduction of the Fourier transform (FT), according to the general form

$$S(f) = \int_I dt \psi(f,t)s(t), \quad f \in \widehat{I} \quad (3.4)$$

and of the inverse FT, according to the symmetric form

$$s(t) = \int_{\widehat{I}} df \psi^*(f,t)S(f), \quad t \in I. \quad (3.5)$$

Fig. 3.1 Logical interconnections of topics in the Unified Theory



The kernel $\psi(f, t)$, which in (3.5) appears in the conjugate form, assumes a specific expression in dependence of the domain/periodicity I . In all the cases of interest, it has the familiar form

$$\psi(f, t) = e^{i2\pi ft}. \tag{3.6}$$

It is worth pointing out that the FT domain is defined as $\hat{I} = I_{0f}/P_f$, where both I_{0f} and P_f are Abelian groups. Therefore, FTs are not structurally different from signals: both are complex functions with domains and periodicities specified by Abelian groups.

The above are the very few basic notions upon which the UST is developed. The logical interconnection of the topics is illustrated in Fig. 3.1. For each topic, we can establish several results for signals and systems, with complete generality. For instance, in dealing with convolution, we shall formulate a dozen general rules, which in the Classical Theory are separately formulated for each signal class.

A unified approach will also be possible for the operations of sampling and interpolation, where two different signal classes are involved (continuous-time and discrete-time signals in the one-dimensional case). We shall establish a unified Sampling Theorem which gives the familiar theorem on the reconstruction of a one-dimensional continuous-time signal from its sample values as a special case, but it also includes the other cases of interest, e.g., the sampling and reconstruction of images.

A final comment is needed for a theory which is formulated in a very abstract form, but ultimately devoted to applications. Basic notions and related results are mathematically consistent since they are anchored on Topology. However, knowledge of Topology, which is a very difficult discipline, is not required for the comprehension of the UST. Topology is rather a reference guide and a precious source of useful results. In the author’s opinion, a Signal Theory developed with a full mathematical framework would risk to appear a bad duplicate of Topology, losing, perhaps, the essence of signals and systems. This “trade off” between mathematics and engineering is not unusual, e.g., topics such as probability, random variables and stochastic processes, in engineering books are typically developed without explicit reference to Measure Theory.

3.1.1 UST Implementation on a Specific Signal Class

Once the UST has been developed, to get explicit results for a specific signal class identified by a domain/periodicity $I = I_0/P$, a set of “implementation rules” is required. Specifically, we have to find the explicit form of:

1. The Haar integral on $I = I_0/P$,
2. The frequency domain/periodicity $\widehat{I} = I_{0f}/P_f$,
3. The Fourier transform kernel $\psi(f, t)$.

In practice, it will be convenient to fix a reference group G_0 and to form all the possible pairs I_0/P with the subgroups of G_0 . Then, we can carry out a systematic acquisition of the previous points and, in such a way, we implement the *Signal Theory on the groups of G_0* . The most important reference is the additive group \mathbb{R} of real numbers and its m -dimensional extension \mathbb{R}^m . However, we shall also see the UST implementation on *multiplicative* groups, which is quite unusual, but useful to remark the generality of the theory.

UT 3.2 Abelian Groups

3.2.1 Definition and Properties

An *Abelian group* is a nonempty set G in which a binary operation $+$ is defined, with the following properties:

- $u + v = v + u$, for all $u, v \in G$,
- $u + (v + z) = (u + v) + z$, for all $u, v, z \in G$,
- G contains an *identity* element, denoted by 0 , such that $u + 0 = u, u \in G$,
- To each $u \in G$ there corresponds an element $-u \in G$, such that $u - u = 0$, where $u - u$ stands for $u + (-u)$.

If a subset P of G is itself a group with respect to the same group operation, it is called a *subgroup* of G and G is a *supergroup* of P . The subset $\{0\}$, consisting of the identity element of G , is the *trivial* subgroup of G .

Examples of Abelian groups are:

- The additive group \mathbb{R} of the real numbers, where $+$ is the ordinary addition;
- The additive group \mathbb{Z} of the integers, and, more generally, the group of the multiples of T : $\mathbb{Z}(T) = \{nT \mid n \in \mathbb{Z}\}$ for all $T \in (0, \infty)$;
- The additive group \mathbb{Q} of rational numbers;
- The multiplicative group \mathbb{R}_p of positive real numbers, in which the group operation $+$ becomes the multiplication and the identity element is the unit;
- The multiplicative group \mathbb{C}^* of nonzero complex numbers, in which $+$ is the multiplication and the identity element is the complex number $1 + i0$;
- The q -adic group $\mathbb{Z}_q = \{0, 1, \dots, q - 1\}$, in which $+$ is the addition modulo q , and in particular the *dyadic* group $\mathbb{Z}_2 = \{0, 1\}$, where $+$ is the binary addition.

It is evident that $\mathbb{Z}(T)$ and \mathbb{Q} are subgroups of \mathbb{R} , but \mathbb{R}_p and \mathbb{Z}_q are not, since their group operation is different from the ordinary addition on \mathbb{R} .

A group whose set is discrete is called a *lattice*, and a group whose set is finite is called a *finite* group. Thus, \mathbb{Z} and $\mathbb{Z}(T)$ are lattices, and \mathbb{Z}_q is a finite group.

3.2.2 Multidimensional Groups

Given two Abelian groups G_1 and G_2 their *Cartesian product* $G_1 \times G_2$ is an Abelian group, whose set is the Cartesian product of the two sets and the group operation $+$ is defined by

$$(u_1, u_2) + (v_1, v_2) = (u_1 + v_1, u_2 + v_2), \quad u_1, v_1 \in G_1, \quad u_2, v_2 \in G_2,$$

where on the right hand side the first $+$ is the operation on G_1 and the second $+$ is the operation on G_2 . The identity element is $(0,0)$, with the first 0 the identity element of G_1 , etc. The above definition is easily generalized to the Cartesian product of an arbitrary number of factors.

For instance, from the additive group \mathbb{R} and its subgroups, we can obtain multidimensional groups of the form $\mathbb{R}^2 = \mathbb{R} \times \mathbb{R}$, $\mathbb{R}^3 = \mathbb{R} \times \mathbb{R} \times \mathbb{R}$, $\mathbb{R} \times \mathbb{Z}(T)$, etc. However, not all multidimensional groups are obtained as the Cartesian product of one-dimensional groups. An example of such a group is the so called *quincunx lattice* $\mathbb{Z}_2^1(d_1, d_2)$, which will be defined later on. Figure 3.2 shows three subgroups of \mathbb{R}^2 , a subgroup of \mathbb{R}^3 and a subgroup of \mathbb{C}^* .

3.2.3 Operations on the Subsets of a Group

Given two nonempty subsets, A and B , of a group G , the group operation $+$ allows the introduction of the following operations:

- *sum*: $A + B = \{a + b \mid a \in A, b \in B\}$,
- *reverse* of A : $-A = \{-a \mid a \in A\}$,
- *shift* of A : $A + p \stackrel{\Delta}{=} A + \{p\} = \{a + p \mid a \in A\}$, where $p \in G$ is the shift amount.

For instance, if $G = \mathbb{R}$, and $A = (a_1, a_2)$ and $B = (b_1, b_2)$ are intervals, we have

$$\begin{aligned} A + B &= (a_1 + b_1, a_2 + b_2), \\ -A &= (-a_2, -a_1), \\ A + p &= (a_1 + p, a_2 + p). \end{aligned}$$

We see that in general the sets $-A$ and $A + p$ are different from A . However, if A is the group G we find

$$-G = G, \quad G + p = G, \quad \text{for all } p \in G. \quad (3.7)$$

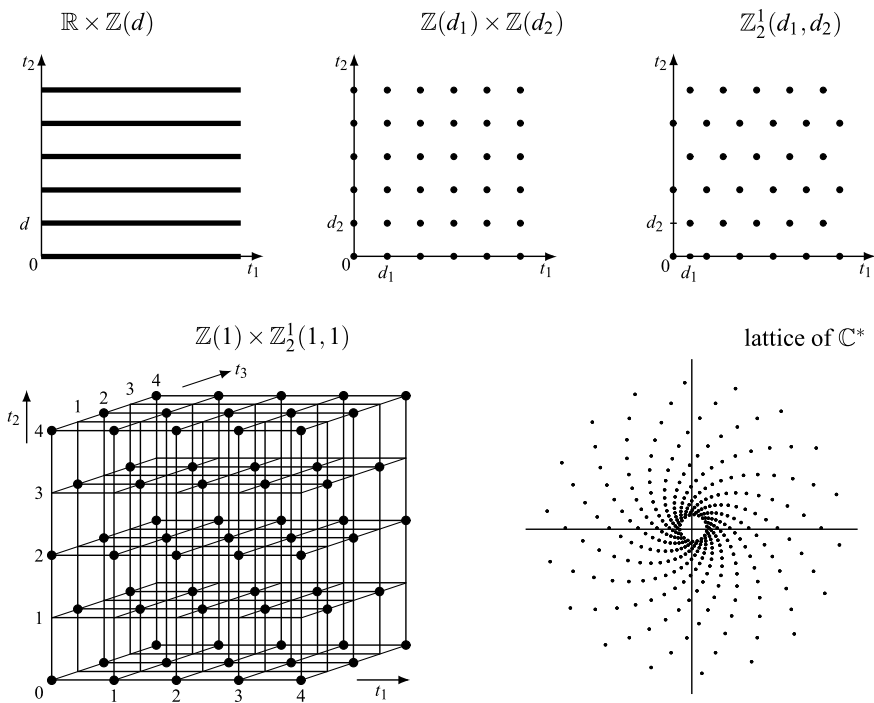


Fig. 3.2 Example of multidimensional groups: at the *top*, three subgroups of \mathbb{R}^2 ; and at the *bottom*, a subgroup of \mathbb{R}^3 and one of \mathbb{C}^*

Hence, the fundamental properties:

1. Every group is invariant with respect to the reverse operation,
2. Every group is shift-invariant with respect to the shift amounts belonging to the group.

For instance, if $G = \mathbb{Z}(T)$, we find $\mathbb{Z}(T) + 2T = \mathbb{Z}(T)$, $\mathbb{Z}(T) + (-5T) = \mathbb{Z}(T)$, but $\mathbb{Z}(T) + \frac{1}{2}T \neq \mathbb{Z}(T)$ since $\frac{1}{2}T \notin \mathbb{Z}(T)$.

3.2.4 Properties of Signals Defined on a Group

Group properties (3.7) have a direct consequence on the class $\mathcal{S}(G)$ of signals defined on a group G . In fact, if $s \in \mathcal{S}(G)$, the *reversed* signal (Fig. 3.3)

$$s_-(t) \triangleq s(-t), \quad t \in G \tag{3.8a}$$

is defined on $-G$, which coincides with G . Moreover, the *shifted* signal

$$s_p(t) \triangleq s(t - p), \quad t \in G \tag{3.8b}$$

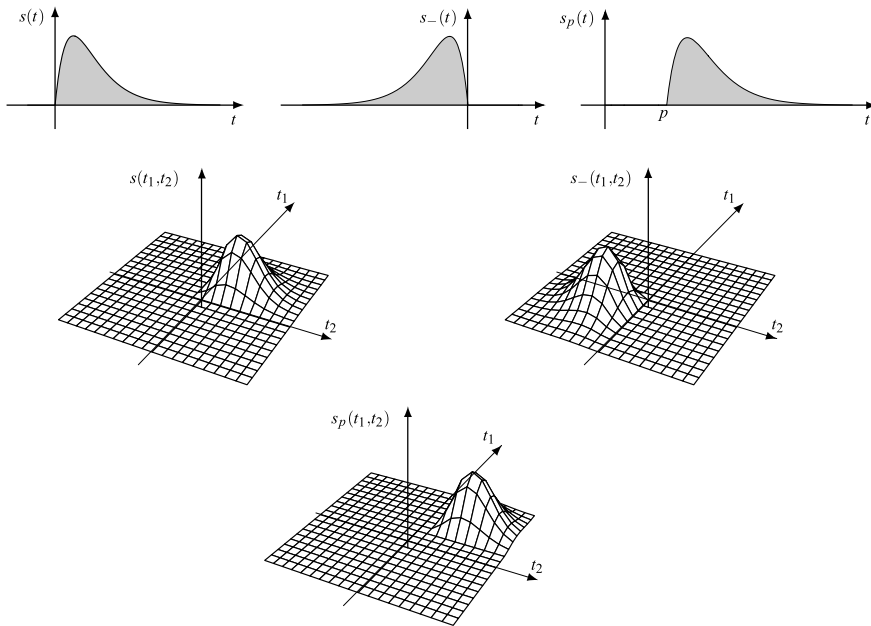


Fig. 3.3 Reversed signal and shifted signal illustrated on \mathbb{R} and \mathbb{R}^2

is defined on $G + p$, which coincides with G whenever $p \in G$.

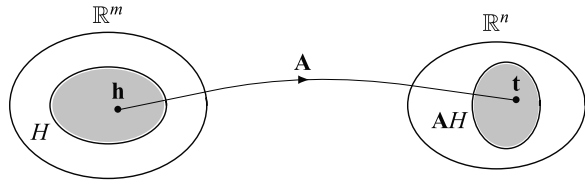
The conclusion is that the class $\mathcal{S}(G)$ is closed with respect to both the reverse and shifts of $p \in G$. Since these operations are fundamental for signals (both appear in a convolution), the above properties explain the reason for the choice of a group as signal domain. Note that the same properties are not verified when the domain is not a group. For example, if G is the 1D interval (t_1, t_2) , the domain becomes $(-t_2, -t_1)$ for s_- and $(t_1 + p, t_2 + p)$ for s_p and in both cases the signal domain changes, and, in fact, an interval is not a group.

UT 3.3 Overview of LCA Groups

Not all Abelian groups are useful for signals, the interest being confined to those groups where the Haar integral can be introduced. Topology gives a precise indication on these groups: they represent the class of *locally compact Abelian* (LCA) groups. The definition of LCA goes beyond the scope of this book and can be found in textbooks of Topology (see the bibliography [10–19] at the end of this chapter). In this context, we find, e.g., that the class of the subgroups of \mathbb{R} , as \mathbb{R} and \mathbb{Z} , are LCA, but others, as the group \mathbb{Q} of rational numbers, are not LCA, and for them the introduction of the Haar integral is not possible.

Since we intend to avoid the introduction of very abstract concepts (topological groups, compact groups, locally compact groups, etc.), we just identify the class

Fig. 3.4 Illustration of a linear mapping between \mathbb{R}^m and \mathbb{R}^n



of LCA groups and of the corresponding Haar integrals. In this regard, Topology gives a very simple and exhaustive guide for their identification (see in particular Theorem 3.3).

Given a reference LCA group G_0 , we denote by $\mathcal{G}(G_0)$ the class of all LCA subgroups of G_0 . The group G_0 will be called the *generator* of the class $\mathcal{G}(G_0)$. Note that $\mathcal{G}(G_0)$ is not empty since it contains at least G_0 and the trivial group $\{0\}$, which we know from Topology to be LCA. For brevity, we call a group $G \in \mathcal{G}(G_0)$ a “group of G_0 ”, although the correct term would be a “subgroup of G_0 ”.

In this section, most of the definitions on LCA groups are concentrated and, as a recommendation to the reader, the concepts herein may be acquired gradually.

3.3.1 Identification of LCA Groups

In the identification procedure, we can use the concept of *isomorphism* between groups which will be defined in the next section. Roughly speaking, isomorphism means a one-to-one correspondence. Now, if the groups H and G are isomorphic, symbolized $H \sim G$, Topology assures that if H is LCA, so is G (see Proposition 3.3). In this way, we can start from some *primitive* groups and generate the other LCA groups by isomorphism.

Now, to proceed we need to define linear transformations, which, in the context of sets, are set mappings.

Definition 3.2 Let \mathbf{A} be an $n \times m$ real matrix, then the relation $\mathbf{t} = \mathbf{A}\mathbf{h}$ maps a point \mathbf{h} of \mathbb{R}^m into a point \mathbf{t} of \mathbb{R}^n . If H is a nonempty subset of \mathbb{R}^m , then

$$\mathbf{A}H \triangleq \{\mathbf{A}\mathbf{h} \mid \mathbf{h} \in H\} \tag{3.9}$$

is a subset of \mathbb{R}^n obtained by mapping all the points of H . The set $\mathbf{A}H$ is called a *linear transformation* of the set H obtained with the matrix \mathbf{A} (Fig. 3.4).

Note that \mathbf{h} is an m -tuple $\mathbf{h} = (h_1, \dots, h_m)$, which in the matrix multiplication $\mathbf{t} = \mathbf{A}\mathbf{h}$ must be interpreted as a column vector. The result \mathbf{t} is a column vector of size n .

Another result of Topology is that in the identification of LCA groups, *without any restriction*, we can refer to the group \mathbb{R} and its subgroups and in general to \mathbb{R}^m and its subgroups (see Theorem 3.3). Then, groups are obtained by *linear transformation* of the form $G = \mathbf{A}H$, where H is a primitive group of \mathbb{R}^m and \mathbf{A} is an $m \times m$

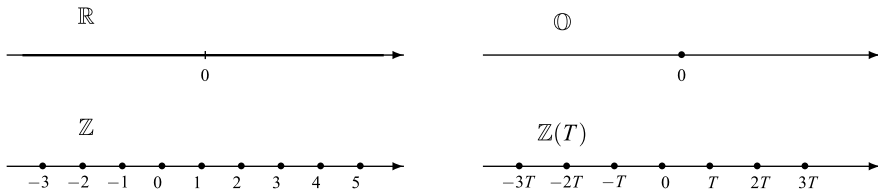


Fig. 3.5 The 1D primitive groups and the non-primitive group $\mathbb{Z}(T)$

real matrix. The linear transformation modifies the geometry of the groups but not the topology. So, if H is a continuum, so is G ; and if H is discrete, so is G .

In conclusion, the steps to find the LCA groups are:

1. Identification of the primitive groups,
2. Generation of the other LCA groups by linear transformations.

The generation is based on the following result, which will be proved in the next section:

Theorem 3.1 *All the LCA groups of \mathbb{R}^m can be generated from the primitive groups H , as follows*

$$G = \mathbf{G}H \iff G = \{\mathbf{G}\mathbf{h} \mid \mathbf{h} \in H\}, \tag{3.10}$$

where \mathbf{G} is a nonsingular real matrix of dimension $m \times m$.

The matrix \mathbf{G} is called the *basis* of the group, the primitive group H is the *signature* and the pair (\mathbf{G}, H) is a *representation* of the group G , symbolized

$$(\mathbf{G}, H) \mapsto G.$$

We now examine the 1D LCA groups of the class $\mathcal{G}(\mathbb{R})$ and then we will introduce the main definitions.

3.3.2 One-Dimensional LCA Groups: The Class $\mathcal{G}(\mathbb{R})$

The generator of 1D LCA groups is \mathbb{R} , the additive group of real numbers, and the primitive groups are

$$\mathbb{R}, \quad \mathbb{Z}, \quad \mathbb{O} \tag{3.11}$$

where \mathbb{Z} is the subgroup of integers and $\mathbb{O} = \{0\}$ is the *degenerate* subgroup (Fig. 3.5).

In the 1D case, the linear mapping $\mathbf{G}\mathbf{h}$ has the simple scalar form Th , where without restriction $T > 0$. This mapping, when applied to \mathbb{R} and \mathbb{O} , again gives

\mathbb{R} and \mathbb{O} . On the other hand, the application to the primitive group \mathbb{Z} gives $G = \{Th \mid h \in \mathbb{Z}\}$, that is, the set of the multiples of T , which we denote by $\mathbb{Z}(T)$, i.e.,

$$\mathbb{Z}(T) = \{hT \mid h \in \mathbb{Z}\}. \quad (3.12)$$

Hence, the only non-primitive groups of $\mathcal{G}(\mathbb{R})$ are $\mathbb{Z}(T)$ for every $T \in (0, \infty)$. This result is in agreement with a celebrated Bourbaki's theorem [1]:

Theorem 3.2 *The only LCA subgroups of \mathbb{R} are \mathbb{R} , $\mathbb{Z}(T)$ with $T \in (0, \infty)$, and the degenerate subgroup $\mathbb{O} = \{0\}$.*

Note that the class $\mathcal{G}(\mathbb{R})$ does not contain some subgroups of \mathbb{R} , as the group \mathbb{Q} of rationals.

3.3.3 Definitions and Classifications

The primitive groups of $\mathcal{G}(\mathbb{R}^m)$ have the form

$$H = \mathbb{R}^p \times \mathbb{Z}^q \times \mathbb{O}^r \quad \text{with } p + q + r = m, \quad p, q, r \in \mathbb{N}_0 \quad (3.13)$$

or a permutation of the m factors contained in H . These groups represent the *signature* in the generation of the other LCA groups of \mathbb{R}^m (\mathbb{N}_0 is the set of natural numbers, including 0).

Continuums, Lattices and Gratings. Dimensionality

In general, the signature determines the nature of the group:

- If $H = \mathbb{R}^m$, the group G is \mathbb{R}^m itself (the *continuous mD* group);
- If $H = \mathbb{Z}^m$, the group G is a *lattice* (a discrete *mD* group);
- If $H = \mathbb{R}^p \times \mathbb{Z}^{m-p}$ with $1 \leq p < m$ or a permutation of such factors, the group is a *grating* (a mixed *mD* group).

The signature also states the dimensionality² of the group, namely

$$\dim G = \dim H. \quad (3.14a)$$

Considering that $\dim \mathbb{R} = \dim \mathbb{Z} = 1$ and $\dim \mathbb{O} = 0$, we have more specifically if $H = \mathbb{R}^p \times \mathbb{Z}^q \times \mathbb{O}^r$

$$\dim G = \dim(\mathbb{R}^p \times \mathbb{Z}^q \times \mathbb{O}^r) = p + q. \quad (3.14b)$$

²We use “dimensionality” in place of “dimension”, reserving the latter for physical dimensions.

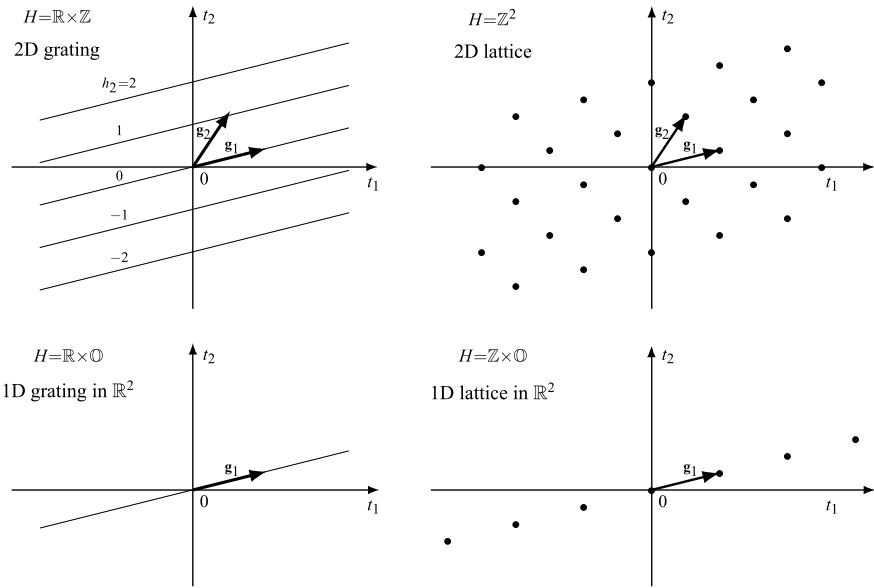


Fig. 3.6 Groups of \mathbb{R}^2 generated with the same basis and different signatures

Then, if H does not contain \mathbb{O} , the group is *full-dimensional*, otherwise *reduced-dimensional*,³ and more specifically, if H contains \mathbb{O} $m - n$ times, the group is said to be an *n-dimensional group in \mathbb{R}^m* .

Examples of 2D groups are illustrated in Fig. 3.6 which shows two full-dimensional groups: a 2D grating⁴ and a 2D lattice, and two reduced-dimensional groups: a 1D grating and a 1D lattice in \mathbb{R}^2 . Examples of 3D groups are illustrated in Fig. 3.7 which shows four 3D full-dimensional groups used in television scanning.

Full dimensional groups will be used as domains and periodicity of signals (normally periodicity will be expressed by lattices). Reduced-dimensional groups will not be used to define signals, but rather to express *partial periodicity*; for instance, signals of the form $s(t_1, t_2)$ which are periodic with respect to t_1 and aperiodic with respect to t_2 have a periodicity of the form $\mathbb{Z}(T_p) \times \mathbb{O}$. Zero-dimensional groups are used to express aperiodicity.

³Reduced-dimensional groups could be introduced by letting the basis matrix be singular, but we find it more convenient to work on the signature.

⁴The term “grating”, not used elsewhere, was suggested to the author by Peter Kraniuskas during a seminar in 1998 at Durford Mill, Petersfield, UK.

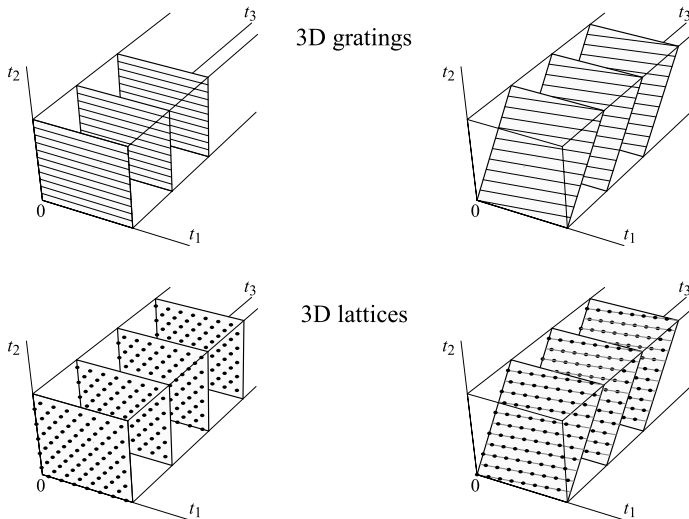


Fig. 3.7 Examples of 3D gratings (with signature $H = \mathbb{R} \times \mathbb{Z}^2$) and 3D lattices

Separable and Nonseparable Groups

A *separable* group is given by the Cartesian product of 1D groups, namely

$$G = G_1 \times G_2 \times \dots \times G_m \quad \text{with } G_i \in \mathcal{G}(\mathbb{R}). \tag{3.15}$$

For separable groups, the basis signature would not be necessary. However, they can be obtained from the general representation with a *diagonal* basis matrix. *Non-separable* groups cannot be expressed in the form (3.15) and the basis signature representation becomes necessary. The basis, in this case, is not diagonal.

Non-Uniqueness of Bases

It is important to remark that the basis of a group is not unique, and, for this reason, we use the symbol $(\mathbf{G}, H) \mapsto G$ to emphasize that representation (\mathbf{G}, H) identifies the group G . For instance, the basis of \mathbb{R}^m is any nonsingular matrix \mathbf{G} , and in particular the identity matrix. The problem of basis multiplicity will be considered in detail in Chap. 16. Here, we anticipate two important results for lattices [3]:

Proposition 3.1 *If G is a lattice with basis \mathbf{G} , all the other bases have the form $\mathbf{G}\mathbf{E}$, where \mathbf{E} is any matrix of integers \mathbf{E} such that $\det \mathbf{E} = \pm 1$.*

Proposition 3.2 *The bases of the sublattices G of a given lattice G_0 can be generated in the form*

$$\mathbf{G} = \mathbf{G}_0 \mathbf{A}, \tag{3.16}$$

where \mathbf{G}_0 is a basis of G_0 , and \mathbf{A} is a nonsingular matrix of integers. If $|\det \mathbf{A}| = 1$, then $G = G_0$, if $|\det \mathbf{A}| > 1$, G is a proper sublattice of G_0 (note that $\det \mathbf{A}$ is an integer).

It is often convenient to refer to “canonical” representations to economize on specifications and to simplify comparisons (see the examples below and Chap. 16).

Determinant and Density of a Group. Signal Rate

Given a representation (\mathbf{G}, H) of a group G , the absolute value of the basis determinant

$$d(\mathbf{G}) \triangleq |\det \mathbf{G}| \quad (3.17)$$

is called the *determinant* and its reciprocal $\mu(\mathbf{G}) \triangleq 1/|\det \mathbf{G}|$ the *density* of the group G . In general, $d(\mathbf{G})$ and $\mu(\mathbf{G})$ depend on the specific basis of the group, but, from Proposition 3.1, for a lattice G the determinant is independent of the basis \mathbf{G} , but becomes a quantity characteristic of the lattice, and consequently denoted by

$$d(G) = |\det \mathbf{G}|. \quad (3.18a)$$

The corresponding density $\mu(G)$ actually represents the lattice *density*, measured in number of points per unit volume of \mathbb{R}^m . For a signal defined on a lattice G the density

$$\mu(G) = \frac{1}{d(G)} \quad (3.18b)$$

is called the *signal rate*, measured in number of signal values per unit volume of \mathbb{R}^m . In particular, in the 1D case, the lattice $\mathbb{Z}(T)$ has determinant T and the signal rate $\mu(\mathbb{Z}(T)) = 1/T$ gives the number of signal values per second.

Now, a sublattice J of G has a smaller density than G . In fact, from Proposition 3.2 we have that the bases are related by $\mathbf{J} = \mathbf{G}\mathbf{A}$, where \mathbf{A} is an integer matrix. Then, we have

$$d(J) = d(G) d(\mathbf{A}), \quad (3.19)$$

where $d(\mathbf{A})$ is a positive integer N with $N \geq 2$ if J is a proper subgroup of G . The integer N is called the *index of J in G* , symbolized $(G : J)$ and given by

$$(G : J) = d(J)/d(G). \quad (3.19a)$$

3.3.4 Two-Dimensional LCA Groups: The Class $\mathcal{G}(\mathbb{R}^2)$

The multidimensional primitive groups are obtained as the Cartesian product of 1D primitive groups. Then, the primitive groups of $\mathcal{G}(\mathbb{R}^2)$ are (up to a permutation)

$$\mathbb{R}^2, \quad \mathbb{Z}^2, \quad \mathbb{R} \times \mathbb{Z}, \quad \mathbb{R} \times \mathbb{O}, \quad \mathbb{Z} \times \mathbb{O}, \quad \mathbb{O}^2, \quad (3.20)$$

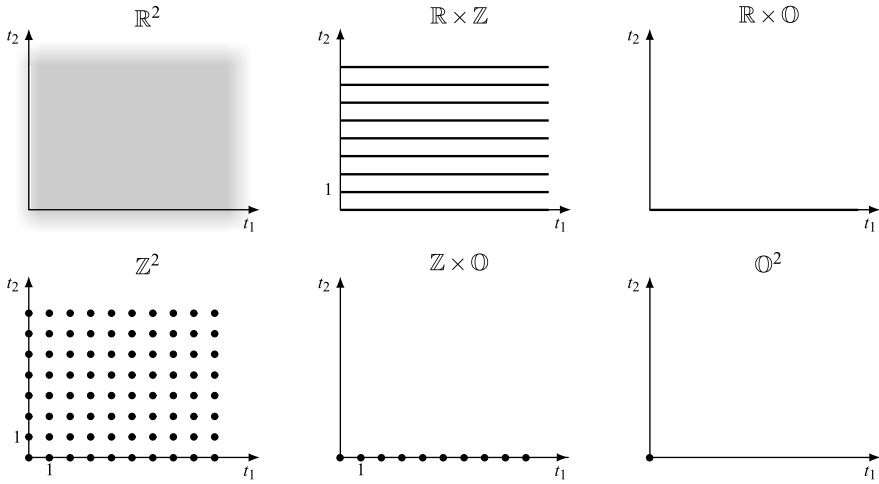


Fig. 3.8 The 2D primitive groups

which are illustrated in Fig. 3.8.

From the primitive groups (3.20), we can easily obtain 2D *separable* LCA groups by replacing \mathbb{Z} with its isomorphic version $\mathbb{Z}(d) \triangleq \{nd \mid n \in \mathbb{Z}\}$. Thus, we have the group

$$\mathbb{Z}(d_1, d_2) \triangleq \mathbb{Z}(d_1) \times \mathbb{Z}(d_2), \tag{3.21}$$

where in general d_1 and d_2 may be different. Other 2D separable LCA groups are $\mathbb{R} \times \mathbb{Z}(d)$ and $\mathbb{Z}(d) \times \mathbb{O}$.

⇓ Nonseparable Groups

To get 2D *nonseparable* groups we have to use the basis signature representation, according to Theorem 3.1, where the basis matrix has the general form

$$\mathbf{G} = \begin{bmatrix} g_{11} & g_{21} \\ g_{12} & g_{22} \end{bmatrix} = [\mathbf{g}_1 \quad \mathbf{g}_2]$$

with $\det \mathbf{G} = g_{11}g_{22} - g_{12}g_{21} \neq 0$. Considering that the primitive groups are separable, $H = H_1 \times H_2$, the linear transformation $G = \mathbf{G}H$ can be expressed in the form

$$G = \{h_1 \mathbf{g}_1 + h_2 \mathbf{g}_2 \mid h_1 \in H_1, h_2 \in H_2\},$$

where the columns \mathbf{g}_1 and \mathbf{g}_2 represent two vectors of \mathbb{R}^2 . The generic point $\mathbf{t} = (t_1, t_2)$ of G is given by $\mathbf{t} = h_1 \mathbf{g}_1 + h_2 \mathbf{g}_2$, and more explicitly

$$\mathbf{t} = \begin{bmatrix} t_1 \\ t_2 \end{bmatrix} = h_1 \begin{bmatrix} g_{11} \\ g_{12} \end{bmatrix} + h_2 \begin{bmatrix} g_{21} \\ g_{22} \end{bmatrix}, \quad h_1 \in H_1, h_2 \in H_2. \tag{3.22}$$

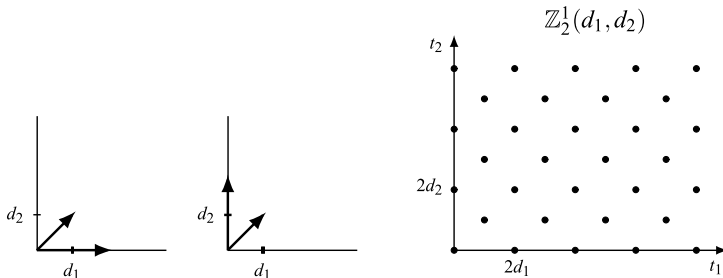


Fig. 3.9 The quincunx lattice with two of its possible bases

For concreteness, we now examine the nature of this linear transformation with all the 2D primitive groups. If $H = \mathbb{R}^2$, \mathbf{t} is given by all the combinations of the vectors \mathbf{g}_1 and \mathbf{g}_2 with real coefficients, and therefore spans \mathbb{R}^2 , that is $G = \mathbb{R}^2$. If $H = \mathbb{R} \times \mathbb{Z}$, the second coefficient h_2 is an integer, and, for each $h_2 \in \mathbb{Z}$, $\mathbf{t} = h_1\mathbf{g}_1 + h_2\mathbf{g}_2$ represents the equation of a line whose slope is given by the vector \mathbf{g}_1 , as shown in Fig. 3.6. Globally, the group G consists of a discrete set of equally-spaced parallel lines. This group is a *grating* which is a mixture between continuous and discrete. If $H = \mathbb{Z}^2$, both coefficients are integers, and G becomes a *lattice*. If $H = \mathbb{R} \times \mathbb{O}$, the second coefficient is zero and then $\mathbf{t} = h_1\mathbf{g}_1$, $h_1 \in \mathbb{R}$, which represents the zeroth line of the previous grating; thus G is a 1D *grating* in \mathbb{R}^2 . If $H = \mathbb{Z} \times \mathbb{O}$, the points $\mathbf{t} = h_1\mathbf{g}_1$ are restricted to $h_1 \in \mathbb{Z}$, and we have a 1D *lattice* in \mathbb{R}^2 . Finally, if $H = \mathbb{O}^2$, G is \mathbb{O}^2 itself. Of course, when $H = \mathbb{R} \times \mathbb{O}$ the vector \mathbf{g}_2 has no role in the generation since $h_2 = 0$.

Figure 3.6 illustrates four groups obtained with the same basis \mathbf{G} but with different signatures: a 2D grating, a 2D lattice, a 1D grating in \mathbb{R}^2 , and a 1D lattice in \mathbb{R}^2 .

A Fundamental Example: The Quincunx Lattice

The quincunx lattice, shown in Fig. 3.9, is perhaps the most important example of a nonseparable 2D lattice. It is a subgroup of $\mathbb{Z}(d_1, d_2)$, defined by the following basis signature representation

$$\mathbf{G} = \begin{bmatrix} 2d_1 & d_2 \\ 0 & d_2 \end{bmatrix}, \quad H = \mathbb{Z}^2 \tag{3.23}$$

and will be denoted by the symbol $\mathbb{Z}_2^1(d_1, d_2)$. The basis vectors are

$$\mathbf{g}_1 = \begin{bmatrix} 2d_1 \\ 0 \end{bmatrix}, \quad \mathbf{g}_2 = \begin{bmatrix} d_1 \\ d_2 \end{bmatrix}$$

and its generic point is (t_1, t_2) with $t_1 = 2d_1h_1 + d_2h_2$ and $t_2 = d_2h_2$. In particular, for $d_1 = d_2 = 1$, $\mathbb{Z}_2^1(1, 1)$ is a sublattice of \mathbb{Z}^2 and is given by the points of \mathbb{R}^2 whose coordinates (t_1, t_2) are *both even* or *both odd*.

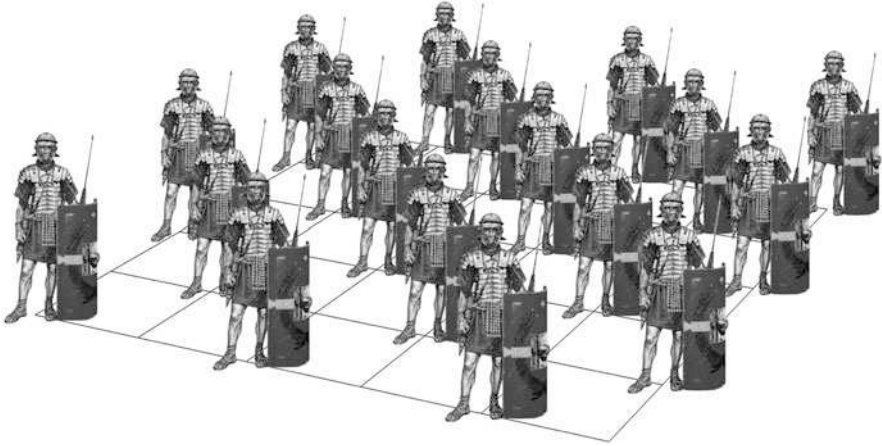


Fig. 3.10 “Obliquis ordinibus ad quincuncem dispositis”, Caius Julius Caesar, *De Bello Gallico*, VII, 73

Note the alternative bases for $\mathbb{Z}_2^1(d_1, d_2)$

$$\mathbf{G}_2 = \begin{bmatrix} d_1 & 0 \\ d_2 & 2d_2 \end{bmatrix}, \quad \mathbf{G}_3 = \begin{bmatrix} d_1 & d_1 \\ d_2 & 3d_2 \end{bmatrix}, \quad (3.24)$$

which show that the basis of a group is not unique (see Problem 3.8).

The quincunx⁵ lattice is pictorially illustrated in Fig. 3.10.

3.3.5 Gallery of 2D LCA Groups

We conclude this overview with a gallery of 2D LCA groups, which will be useful for illustration throughout the book. The gallery is collected in Fig. 3.11.

First, we have the separable groups

$$\begin{aligned} \mathbb{R}^2, \quad \mathbb{R} \times \mathbb{Z}(d), \quad \mathbb{Z}(d) \times \mathbb{R}, \quad \mathbb{Z}(d_1, d_2), \quad \mathbb{Z}(d) \times \mathbb{O}, \\ \mathbb{O} \times \mathbb{Z}(d), \quad \mathbb{O}^2. \end{aligned} \quad (3.25)$$

The bases of these groups are diagonal. For nonseparable groups, the basis can be chosen with the lower triangular form (see Chap. 16)

$$\mathbf{G} = \begin{bmatrix} a & 0 \\ b & c \end{bmatrix}.$$

⁵From Latin *quincunx*, denoting the disposition of number five on a die. The term was used to denote troop disposition, and nowadays is used in horticulture to indicate a vegetable arrangement.

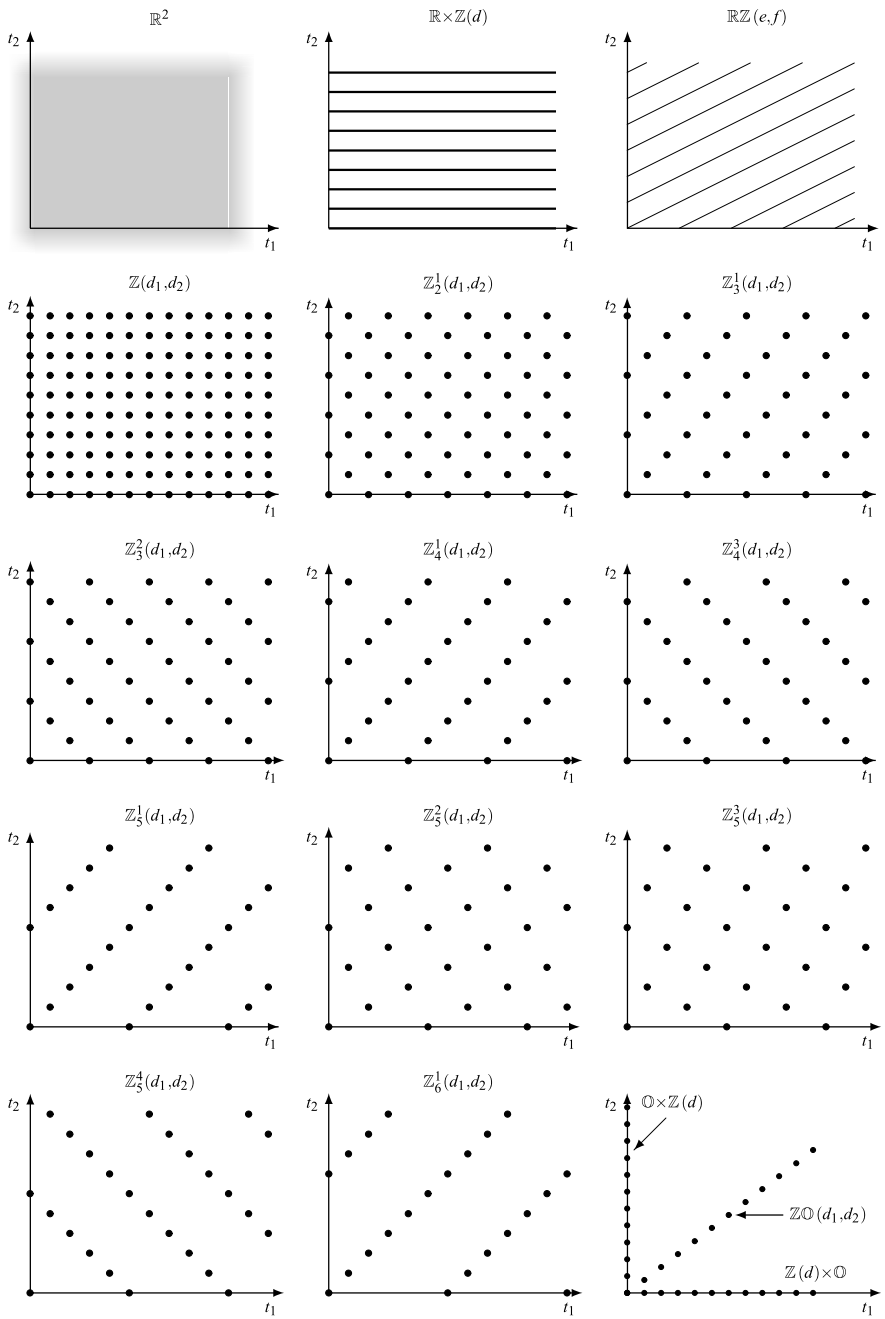


Fig. 3.11 Gallery of 2D groups considered for illustrations

The first example of nonseparable group of the gallery is the 2D grating, with representation

$$\mathbf{G} = \begin{bmatrix} 1 & 0 \\ e & f \end{bmatrix}, \quad H = \mathbb{R} \times \mathbb{Z} \quad (3.26a)$$

denoted by $\mathbb{R}\mathbb{Z}(e, f)$. Note that the point (t_1, t_2) in this grating is given by

$$(t_1, t_2) = (r, er + fn), \quad r \in \mathbb{R}, n \in \mathbb{Z}. \quad (3.26b)$$

Next, we consider the nonseparable sublattices of $\mathbb{Z}(d_1) \times \mathbb{Z}(d_2) \triangleq \mathbb{Z}(d_1, d_2)$. A general sublattice of this class will be denoted by $\mathbb{Z}_i^b(d_1, d_2)$, where i and b are integers, with $0 < b < i$. The corresponding bases are

$$\mathbf{G} = \begin{bmatrix} id_1 & 0 \\ bd_1 & d_2 \end{bmatrix} = \begin{bmatrix} d_1 & 0 \\ 0 & d_2 \end{bmatrix} \begin{bmatrix} i & 0 \\ b & 1 \end{bmatrix}. \quad (3.27)$$

These lattices are illustrated for some values of i and b . In particular, for $i = 1$ and $b = 0$, we have the *separable* lattice $\mathbb{Z}(d_1, d_2)$, and for $i = 2$ and $b = 1$ the *quincunx* lattice $\mathbb{Z}_2^1(d_1, d_2)$.

Finally, the figure shows the 1D lattices in \mathbb{R}^2 defined by

$$\mathbb{Z}\mathbb{O}(d_1, d_2) = \{(md_1, md_2) \mid m \in \mathbb{Z}\}. \quad (3.28)$$

UT↓ 3.4 The LCA Groups According to Topology

In the previous section, we have identified the class of LCA groups, and in this section we collect the result of Topology that justified our identification. First, we give the formal definition of an isomorphism.

Definition 3.3 Let $(H, +_H)$ and $(G, +_G)$ be two groups with their operations. An isomorphism of an H onto G is an *invertible* map $\alpha : H \rightarrow G$ such that

$$\alpha(t_1 +_H t_2) = \alpha(t_1) +_G \alpha(t_2), \quad t_1, t_2 \in H. \quad (3.29)$$

For instance, the isomorphism $\mathbb{Z} \sim \mathbb{Z}(T)$ is the map is $\alpha(h) = hT$. A less trivial example is the isomorphism between the additive group $(\mathbb{R}, +)$ of real numbers and the multiplicative group (\mathbb{R}_p, \cdot) of positive real numbers, where the map is $\alpha = \exp : \mathbb{R} \sim \mathbb{R}_p$ (see Sect. 3.8). For Topology, two isomorphic groups are essentially the same objects. This is not the case for Signal Theory where, e.g., the isomorphic groups $\mathbb{Z}(T_1)$ and $\mathbb{Z}(T_2)$ define different signal classes (with different spacings, different rates, etc.).

The importance of an isomorphism for the identification of LCA groups stems from the following statement [8].

Proposition 3.3 *If a group H is LCA and $G \sim H$, then also G is LCA.*

Finally, we note the fundamental role that groups we call *primitive* play in Topology. In fact, a theorem of Weil [9] states:

Theorem 3.3 *Every LCA group G is isomorphic to a group of \mathbb{R}^m of the form*

$$\boxed{G \sim \mathbb{R}^p \times \mathbb{Z}^q \times \mathbb{O}^r} \quad (p + q + r = m). \quad (3.30)$$

According to this theorem, all the LCA groups, *up to an isomorphism*, are given by the primitive groups of \mathbb{R}^m , and for Topology the search for LCA groups could stop here. But, in Signal Theory we want to have the explicit form of these groups. In Appendix A, we prove that the isomorphism map giving all the LCA groups of \mathbb{R}^m from the primitive groups of \mathbb{R}^m is *linear*, that is, of the form

$$\mathbf{t} = \alpha(\mathbf{h}) = \mathbf{G} \mathbf{h}, \quad \mathbf{h} \in H,$$

as anticipated in Theorem 3.1.

UT 3.5 Cells and Group Partitions

Cells play a fundamental role in an advanced signal theory. Broadly speaking, a cell is a subset of a group such that its shifted replicas cover the whole group without superposition. For instance, the interval $[0, 1)$ is a cell of the group \mathbb{R} since its shifted replicas $[0, 1) + k = [k, k + 1)$, with $k \in \mathbb{Z}$, cover \mathbb{R} without superposition.

In the literature, cells (usually called *unit cells*) are introduced in the context of lattices [3, 4]. Here we formulate a very general (and original) definition.

3.5.1 General Definition and Properties

Definition 3.4 Let G be an Abelian group and let C and P be nonempty subsets of G . The set C is a *cell* of G modulo P , denoted by⁶ $[G/P)$, if the shifted replicas of C , the sets

$$C + p \stackrel{\Delta}{=} \{c + p \mid c \in C\}, \quad p \in P, \quad (3.31)$$

represent a *partition* of G , that is,

$$\begin{aligned} (C + p) \cap (C + q) &= \emptyset, \quad p \neq q, \quad p, q \in P, \\ \bigcup_{p \in P} (C + p) &= G. \end{aligned} \quad (3.32)$$

⁶This symbol, proposed by the author, recalls that a cell of \mathbb{R} modulus $\mathbb{Z}(T)$ is given by the half-open interval $[0, T)$.

The partition of group G can be written synthetically in the form

$$\boxed{[G/P] + P = G.} \quad (3.33)$$

The modulus P is called the *set of repetition centers* (thinking that P is a lattice). A cell can be interpreted as follows: by shifting C over all the repetition centers, the group G is covered without superposition.

We note that:

1. If C is a cell, so is every shifted-replica $C + p_0$ with $p_0 \in G$, in particular with $p_0 \in P \subset G$. For this reason, the class (3.31) represents a *partition of the group G* into cells.
2. For a given pair G, P the cell partition is not unique.
3. If $P = \{0\}$, the unique cell is $C = G$.

The second equation of (3.32) can be rewritten in the alternative forms

$$G = \bigcup_{p \in P} (C + p) = \bigcup_{c \in C} \bigcup_{c \in P} (c + p) = C + P, \quad (3.34)$$

which clearly shows the symmetry between the cell C and the modulus P . Then

Proposition 3.4 *If C is a cell of G modulo P , then also P is a cell of G modulo C .*

The cells $[G/P]$ of main interest for signals are of two kinds:

- *Aperiodic* cells where P is a subgroup of G ,
- *Periodic* cells where P is itself an aperiodic cell (typically with a finite cardinality).

Remark Given G and P , the symbol $[G/P]$ does not identify a specific cell, rather, a class of cells. For instance $[\mathbb{R}/\mathbb{Z}(T_p)]$ may be the cell $[0, T_p)$ or $[-\frac{1}{2}T_p, \frac{1}{2}T_p)$, or any other interval of length T_p .

3.5.2 Aperiodic Cells

These cells have the form $[G/P]$, where G is an LCA group and P is an LCA subgroup of G .

A first example of an aperiodic cell has been seen at the beginning: the interval $[0, 1)$ is a cell of \mathbb{R} modulo \mathbb{Z} , that is, $[\mathbb{R}/\mathbb{Z}] = [0, 1)$. More generally, any interval $[t_0, t_0 + T_p)$ is a cell of \mathbb{R} modulo $\mathbb{Z}(T_p)$. As a second example, consider $G = \mathbb{Z}(T)$ and $P = \mathbb{Z}(4T)$; we find that $C = \{0, T, 2T, 3T\}$ is a cell $[\mathbb{Z}(T)/\mathbb{Z}(4T)]$ and, in fact, by repeating C over the centers $4kT$, with $k \in \mathbb{Z}$, we cover $\mathbb{Z}(T)$.

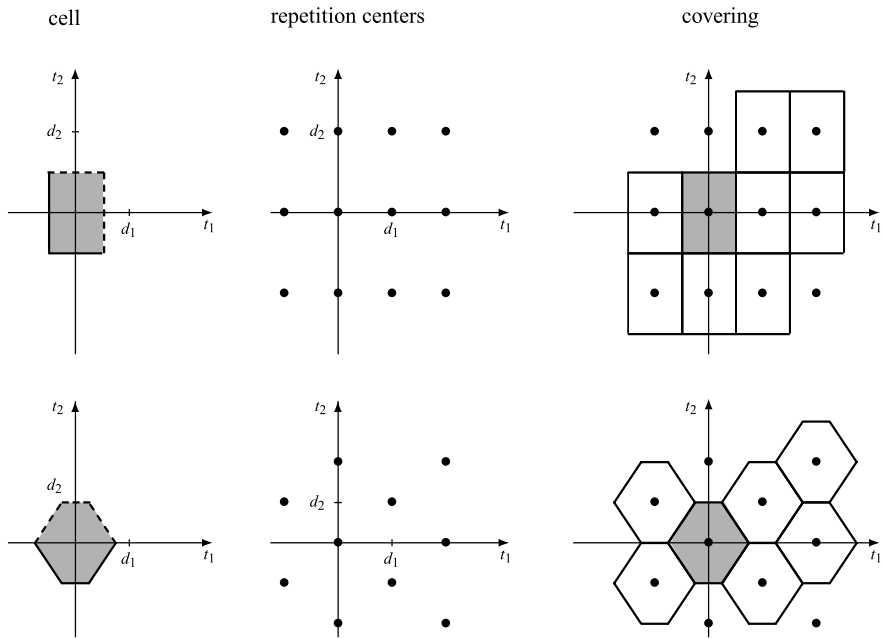


Fig. 3.12 Examples of 2D cells: cell of \mathbb{R}^2 modulo $\mathbb{Z}(d_1, d_2)$ and cell of \mathbb{R}^2 modulo $\mathbb{Z}_2^1(d_1, d_2)$

2D cells offer more expressive examples. For instance, if $G = \mathbb{R}^2$ and $P = \mathbb{Z}(d_1, d_2)$, a cell is given by the rectangle

$$[G/P] = \left[-\frac{1}{2}d_1, \frac{1}{2}d_1 \right) \times \left[-\frac{1}{2}d_2, \frac{1}{2}d_2 \right).$$

In fact, shifting this rectangle over the repetition centers (md_1, nd_2) gives the covering of \mathbb{R}^2 , as shown in Fig. 3.12. The figure also shows a cell $[\mathbb{R}^2/P]$, where P is the quincunx lattice $\mathbb{Z}_2^1(d_1, d_2)$; in this case the cell is hexagonal (Voronoi cell).

Terminology In the theory of lattices, the sets of the partition

$$P + c, \quad c \in [G/P] = C$$

are called the *cosets* of P in G , and C is called a *set of representatives*. For instance, with $G = \mathbb{Z}$ and $P = \mathbb{Z}(3)$, the sets $\mathbb{Z}(3) + 0, \mathbb{Z}(3) + 1, \mathbb{Z}(3) + 2$ are the cosets of $\mathbb{Z}(3)$ in \mathbb{Z} and the cell $\{0, 1, 2\}$ is the set of representatives. The cardinality of the set of representatives, that is, the size of the cell, is given by the index of P in G , that is, $(G : P) = d(P)/d(G)$ (see (3.19a)).

3.5.3 Periodic Cells

We begin with the following:

Definition 3.5 A subset A of a group G is *periodic* with periodicity P , if A is invariant with respect to the shifts of P , that is, if $A + p = A, \forall p \in P$.

The periodicity condition can also be written in the form

$$A + P = A.$$

It can be shown that P is always a subgroup of G . For instance, the union of the intervals $[4k, 4k + 1]$ with $k \in \mathbb{Z}$, which can be written in the form $A = [0, 1) + \mathbb{Z}(4)$, is a periodic subset of \mathbb{R} with periodicity $P = \mathbb{Z}(4)$.

Periodic cells can be conveniently introduced starting from three groups

$$P \subset P_0 \subset G, \tag{3.35}$$

which give the three partitions into aperiodic cells

$$G = [G/P_0) + P_0, \quad G = [G/P) + P, \quad P_0 = [P_0/P) + P.$$

Combination of the first and the third gives

$$G = [G/P_0) + [P_0/P) + P.$$

Hence, the set

$$\boxed{C = [G/P_0) + P} \tag{3.36}$$

has, by construction, periodicity P and moreover verifies the condition $G = C + R$ with $R = [P_0/P)$. Therefore, C is a periodic cell with *repetition centers* $R = [P_0/P)$.

Example 3.1 Assuming $G = \mathbb{R}$, $P_0 = \mathbb{Z}(1)$, $P = \mathbb{Z}(4)$, the periodic cell (3.36) is

$$C = [\mathbb{R}/\mathbb{Z}(1)) + \mathbb{Z}(4) = [0, 1) + \mathbb{Z}(4)$$

with repetition centers

$$R = [\mathbb{Z}(1)/\mathbb{Z}(4)) = \{0, 1, 2, 3\}.$$

In fact, the sets $C, C + 1, C + 2, C + 3$ form a partition of \mathbb{R} , as shown in Fig. 3.13.

Example 3.2 Figure 3.14 shows a 2D periodic cell identified by the groups

$$G = \mathbb{R}^2, \quad P_0 = \mathbb{Z}(1) \times \mathbb{Z}(1), \quad P = \mathbb{Z}(3) \times \mathbb{Z}(2).$$

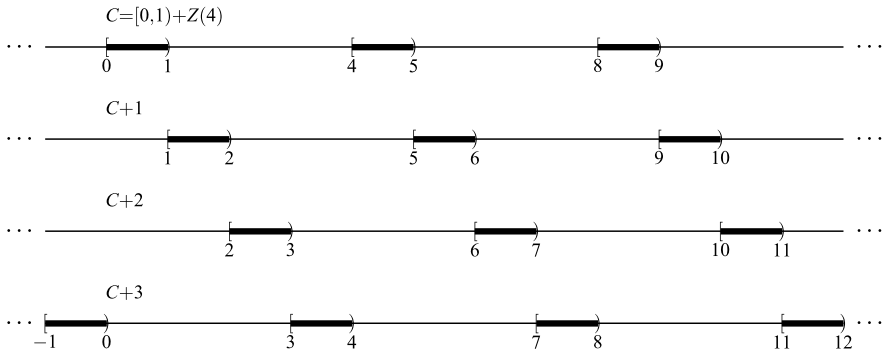


Fig. 3.13 Example of partition of \mathbb{R} with periodic cells

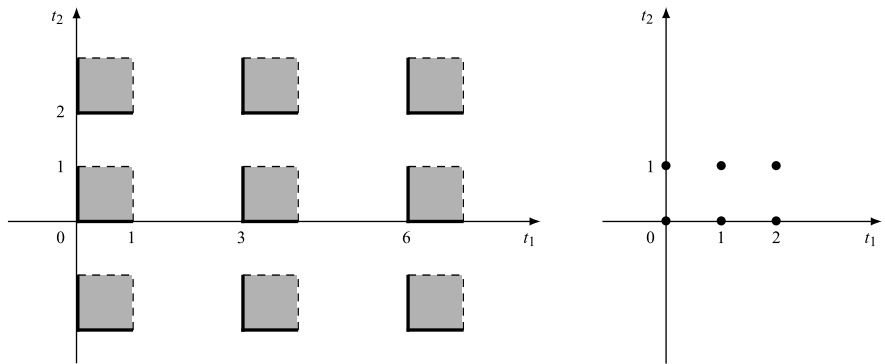


Fig. 3.14 Example of periodic cell and corresponding repetition centers

In this case, the periodic cell is given by the repetition of the square

$$C = [G/P_0] + P = [0, 1) \times [0, 1) + \mathbb{Z}(3) \times \mathbb{Z}(2), \tag{3.37}$$

with repetition centers

$$R = [P_0/P] = \{(0, 0), (1, 0), (2, 0), (0, 1), (1, 1), (2, 1)\}.$$

In fact, we can easily check that, shifting the set (3.37) around the six repetition centers, we obtain a covering of \mathbb{R}^2 .

⇓ 3.5.4 Cell Identification

We showed a few examples of cells, aperiodic and periodic, but not a general procedure to find them. Since periodic cells can be obtained using aperiodic ones

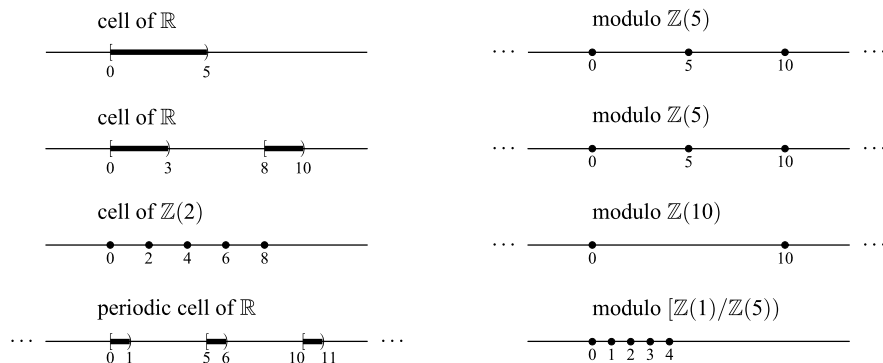


Fig. 3.15 Examples of cells on the groups of \mathbb{R}

(see (3.36)), the identification problem is confined to aperiodic cells. A general identification procedure will be seen in Chap. 16, where the idea is to start from some *primitive cells* and generate general cells by linear transformations. Here, we anticipate two rules which allow finding new cells from known ones.

Proposition 3.5 (Cartesian product) *If $C_1 = [G_1/P_1]$ and $C_2 = [G_2/P_2]$ are two cells of the groups G_1 and G_2 , then the Cartesian product $C_1 \times C_2$ is a cell of $G_1 \times G_2$ modulo $P_1 \times P_2$*

$$[G_1/P_1] \times [G_2/P_2] = [G_1 \times G_2/P_1 \times P_2].$$

Proposition 3.6 (Intersection) *Let G be a subgroup of G_0 , and let $C_0 = [G_0/P]$, where P is a subset of G . Then, the intersection*

$$C = G \cap C_0 = [G/P]$$

is a cell of G modulo P .

3.5.5 Cells on the Groups of \mathbb{R}

The cells of \mathbb{R} modulo $\mathbb{Z}(T_p)$ are in general the intervals (Fig. 3.15)

$$[t_0, t_0 + T_p) \quad \text{or} \quad (t_0, t_0 + T_p],$$

where t_0 is an arbitrary instant, and in particular the intervals

$$[0, T_p) \quad \text{and} \quad \left[-\frac{1}{2}T_p, \frac{1}{2}T_p\right).$$

These sets are *connected*, but we may find cells of the type $[\mathbb{R}/\mathbb{Z}(T_p))$, which are not connected. For instance, the set $[0, \frac{1}{2}T_p) \cup [\frac{3}{2}T_p, 2T_p)$, consisting of the union of two disjoint intervals, is a correct cell $[\mathbb{R}/\mathbb{Z}(T_p))$.

The cells of $\mathbb{Z}(T)$ modulo $\mathbb{Z}(T_p)$, with $T_p = NT$, consist typically of N consecutive points of $\mathbb{Z}(T)$, namely $\{n_0T, (n_0 + 1)T, \dots, (n_0 + N - 1)T\}$, where n_0 is an arbitrary integer. In particular, we have the cell

$$\mathbb{Z}_N(T) \triangleq \{0, T, \dots, (N - 1)T\}, \tag{3.38}$$

which is often a reference cell. But we may have cells not formed by consecutive points of $\mathbb{Z}(T)$. For instance, the set $\{2T, 4T, 5T, 6T, 8T\}$ is a cell $[\mathbb{Z}(T)/\mathbb{Z}(5T))$, as well as the set $\{0, T, 2T, 3T, 4T\}$. Figure 3.15 shows also a periodic cell of \mathbb{R} .

⇓ 3.5.6 Cells on the Groups of \mathbb{R}^m

First, we consider *primitive* cells of the forms $[\mathbb{R}^m/\mathbb{Z}^m)$ and $[\mathbb{R}^m/\mathbb{Z}^p \times \mathbb{O}^q)$ and then we obtain cells of the form $[\mathbb{R}^m/P)$, being P a sublattice of \mathbb{R}^m and other different types of cells.

Primitive Cells

We have seen that the interval $[0, 1)$ is a cell $[\mathbb{R}/\mathbb{Z})$, as any other interval of measure 1, e.g., $[-\frac{1}{2}, \frac{1}{2})$. Then, from Proposition 3.5 we have

$$[\mathbb{R}^m/\mathbb{Z}^m) = [\mathbb{R}/\mathbb{Z})^m = [0, 1)^m, \tag{3.39}$$

that is, a cell $[\mathbb{R}^m/\mathbb{Z}^m)$ is given by the m -dimensional cube $[0, 1)^m$.

To get primitive cells of the more general form $[\mathbb{R}^m/\mathbb{Z}^p \times \mathbb{O}^q)$ with $p + q = m$, it is sufficient to note that $[\mathbb{R}/\mathbb{O}) = \mathbb{R}$. Then

$$[\mathbb{R}^m/(\mathbb{Z}^p \times \mathbb{O}^q)) = [\mathbb{R}^p/\mathbb{Z}^p) \times [\mathbb{R}^q/\mathbb{O}^q) = [0, 1)^p \times \mathbb{R}^q, \tag{3.40}$$

which may be interpreted as a *multidimensional strip*. For instance,

$$[\mathbb{R}^2/(\mathbb{Z} \times \mathbb{O})) = [0, 1) \times \mathbb{R}, \quad [\mathbb{R}^2/\mathbb{O} \times \mathbb{Z}) = \mathbb{R} \times [0, 1)$$

are strips of the \mathbb{R}^2 plane, as shown in Fig. 3.16.

Cells $[\mathbb{R}^m/L)$ with L a Lattice. Fundamental Parallelepiped

A full-dimensional lattice L of \mathbb{R}^m is isomorphic to \mathbb{Z}^m , according to the isomorphism

$$\mathbf{t} = \mathbf{L}\mathbf{k}, \quad \mathbf{k} \in \mathbb{Z}^m,$$

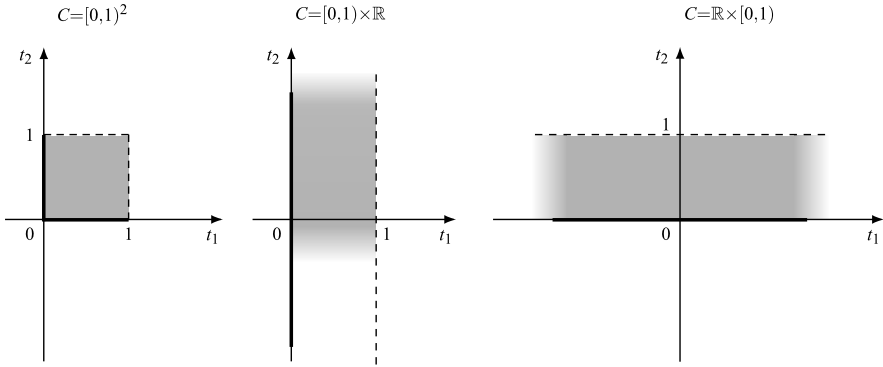


Fig. 3.16 Primitive cells of \mathbb{R}^2

where \mathbf{L} is a basis matrix for L . This map transforms the lattice \mathbb{Z}^m into the lattice L , but it can also be used to transform a primitive cell $[\mathbb{R}^m/\mathbb{Z}^m]$ into a cell $[\mathbb{R}^m/L]$, according to

$$[\mathbb{R}^m/L] = \{\mathbf{L}\mathbf{h} \mid \mathbf{h} \in [0, 1)^m\}. \quad (3.41)$$

With the partition of \mathbf{L} into its column vectors, $\mathbf{L} = [\mathbf{s}_1, \mathbf{s}_2, \dots, \mathbf{s}_m]$, we find more explicitly

$$[\mathbb{R}^m/L] = \{h_1\mathbf{s}_1 + \dots + h_m\mathbf{s}_m \mid 0 \leq h_1 < 1, \dots, 0 \leq h_m < 1\}. \quad (3.41a)$$

This cell is called the *fundamental parallelepiped* of the lattice L . Clearly, it depends on the basis \mathbf{L} of L and a different basis would give a different fundamental parallelepiped.

Figure 3.17 shows a 2D example of cell generation according to (3.41): the map

$$\mathbf{t} = \mathbf{L}\mathbf{h} \quad \text{with } \mathbf{L} = \begin{bmatrix} d_1 & 0 \\ 0 & d_2 \end{bmatrix} \begin{bmatrix} 3 & 1 \\ 0 & 1 \end{bmatrix}$$

transforms the signature $H = \mathbb{Z}^2$ into the lattice $L = \mathbb{Z}_3^1(d_1, d_2)$ and the square $[0, 1)^2$ into parallelepiped (a parallelogram in 2D). Thus, we obtain a cell of \mathbb{R}^2 modulo $\mathbb{Z}_3^1(d_1, d_2)$.

To get cells $[\mathbb{R}^m/L]$, with L a reduced-dimensional lattice with signature $\mathbb{Z}^p \times \mathbb{O}^q$, it is sufficient to replace the constraint $h_i \in [0, 1)$ with $h_i \in \mathbb{R}$ in the last q coordinates h_i , that is,

$$[\mathbb{R}^m/L] = \{\mathbf{L}\mathbf{h} \mid \mathbf{h} \in [0, 1)^p \times \mathbb{R}^q\}. \quad (3.42)$$

Note that the measure of cells (3.41) is given by the determinant of the lattice L , that is,

$$\text{meas}[\mathbb{R}^m/L] = |\det \mathbf{L}| = d(L), \quad (3.43)$$

whereas cells (3.42) have an infinite measure.

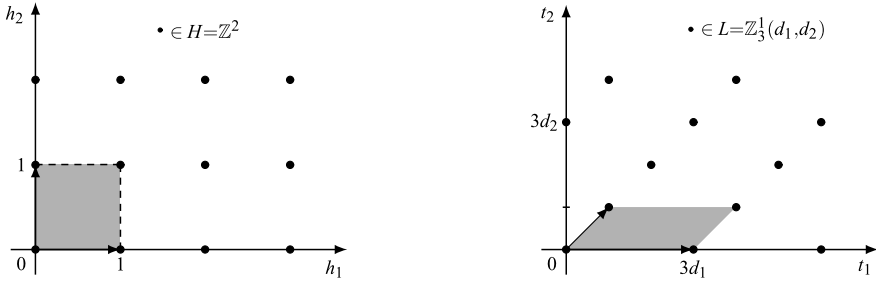


Fig. 3.17 Fundamental parallelepiped of $\mathbb{Z}_3^1(d_1, d_2)$ from primitive cell $[0, 1]^2$

Cells of the General Form $[G/L]$

From the cells $[\mathbb{R}^m/L]$, we can obtain the cells of the general form $[G/L]$, where G is an arbitrary supergroup of L , that is, $L \subset G \subset \mathbb{R}^m$. In fact, from Proposition 3.6 we have

$$C_0 = [\mathbb{R}^m/L] \Rightarrow C = G \cap C_0 = [G/L], \tag{3.44}$$

that is, from a cell of \mathbb{R}^m we find a cell of G by intersection.

The main case of interest is when both G and L are lattices. In this case, we first obtain a fundamental parallelepiped $[\mathbb{R}^m/L]$ and then the cell $[G/L]$. Note that $[G/L]$ has a finite cardinality given by

$$N = \text{meas}[G/L] = \frac{|\det(\mathbf{L})|}{|\det(\mathbf{G})|} = \frac{d(L)}{d(G)} = (G : L), \tag{3.45}$$

where $(G : L)$ is the index of L in G (see (3.19a)). Figure 3.18 shows two 2D examples of cells obtained with the above procedure. In the first example, a cell of $G = \mathbb{Z}(d_1, d_2)$ modulo $P = \mathbb{Z}(D_1, D_2)$, with $D_1 = 7d_1$ and $D_2 = 7d_2$, is generated. First, we find a cell C_0 of \mathbb{R}^2 modulo $\mathbb{Z}(D_1, D_2)$, which is given by the rectangle $[0, D_1] \times [0, D_2]$. Then, the intersection of C_0 with G gives the desired cell C . Note that the cardinality of C is $7 \times 7 = 49$, in agreement with (3.45).

In the second example, $L = \mathbb{Z}_2^1(D_1, D_2)$ and C_0 is a parallelogram with basis $2D_1$ and height D_2 . The intersection of C_0 with $G = \mathbb{Z}(d_1, d_2)$ gives the discrete cell C_0 . Note that in the figure $D_1 = 5d_1$ and $D_2 = 5d_2$, so $P = \mathbb{Z}_2^1(5d_1, 5d_2)$ is a sublattice of G . Since $d(L) = 2(5d_1)(5d_2)$ and $d(G) = d_1d_2$, the cardinality of C is $N = 50$.

Cell Applications

A first application of cells will be seen in connection with periodicity and then with the Haar integral. Other applications will be seen in the context of multirate systems

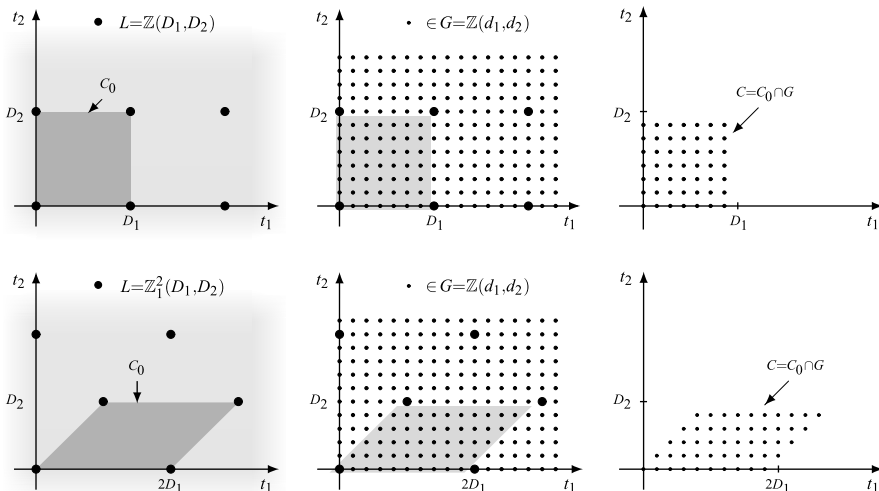


Fig. 3.18 Generation of discrete cells by intersection

(Chap. 7), where cells allow a very general definition of the so-called *polyphase decomposition*. Perhaps, the most relevant application of cells will be seen in the context of the Sampling Theorem (Chap. 8), where cells are used to formulate the band-limitation. Also, in subband decomposition (Chap. 14) and in wavelets (Chap. 15) cells are extensively used.

UT 3.6 Signal Periodicity and Quotient Groups

In the definition of signal given at the beginning (Definition 3.1), both the domain I_0 and the periodicity P are specified. We have already seen that the domain I_0 must be an LCA group and now we show that also the periodicity P must be an LCA subgroup of I_0 . We introduce the periodicity in a generalized sense to include the aperiodicity as a degenerate case, allowing to handle simultaneously periodic as well as aperiodic signals.

3.6.1 Periodicity as Shift Invariance

Let $s(t)$ be a signal defined on the domain I_0 , an LCA group. Then, $s(t)$, $t \in I_0$, is *shift invariant* with respect to the shift $p \in I_0$, if

$$s_p(t) = s(t), \quad t \in I_0, \tag{3.46}$$

where $s_p(t) \triangleq s(t - p)$ is the shifted version of s (see (3.8b) and Fig. 3.3). We have:

Theorem 3.4 Let P_0 be the shift-invariance set for a signal $s(t)$, $t \in I_0$, that is,

$$P_0 = \{p \in I_0 \mid s_p = s\}. \quad (3.46a)$$

Then P_0 is always a subgroup of the domain I_0 .

Proof A shift amount p in (3.46) must belong to the signal domain I_0 and therefore P_0 is a subset of I_0 . We have to prove that P_0 is an Abelian group. In fact, the condition $s_p(t) = s(t)$ is always verified with $p = 0$; hence $0 \in P_0$. If $p \in P_0$, then $s(t - p) = s(t)$, $\forall t \in I_0$, and setting $t' = t - p$, we find $s(t' + p) = s(t')$, $\forall t' \in I_0$; hence also $-p \in P_0$. Similarly, if $p, q \in P_0$, then $q - p \in P_0$, and, from the previous statement, also $q + p \in P_0$. \square

The shift-invariance group P_0 satisfies the condition $\{0\} \subseteq P_0 \subseteq I_0$, the limit cases being not excluded. Then, we have the following classification of signals into:

- *Constant* signals if $P_0 = I_0$;
- *Periodic* signals if $\{0\} \subset P_0 \subset I_0$;
- *Aperiodic* signals if $P_0 = \{0\}$.

To unify the terminology, we call P_0 the *maximal periodicity* of the signal. The term *periodicity* will refer to every subgroup P of P_0 . The reason is that, if the signal $s(t)$, $t \in I_0$, is shift-invariant on P_0 , it is also shift-invariant on $P \subseteq P_0$, that is,

$$s(t - p) = s(t), \quad p \in P.$$

Example 3.3 Consider the 1D discrete-time sinusoidal signal

$$s(t) = A_0 \cos 2\pi f_0 t, \quad t \in \mathbb{Z}(3)$$

with frequency $f_0 = \frac{1}{12}$. This signal is periodic with period $T_{p_0} = 12$ and, in fact, $\forall k \in \mathbb{Z}$

$$s(t - 12k) = A_0 \cos(2\pi(f_0 t - k)) = A_0 \cos 2\pi f_0 t = s(t).$$

The shift-invariance set is therefore $P_0 = \{12k \mid k \in \mathbb{Z}\} = \mathbb{Z}(12) \subset \mathbb{Z}(3)$, which represents the *maximal periodicity*. However, $s(t)$ has also period $T_p = 24$, since

$$s(t - 24k) = A_0 \cos(2\pi(f_0 t - 2k)) = s(t)$$

and also periods $T_p = 36, 48$, etc. Hence, the signal periodicities P are all the subgroups of $\mathbb{Z}(12)$, that is, $\mathbb{Z}(24)$, $\mathbb{Z}(36)$, $\mathbb{Z}(48)$, etc. The limit case $P = \{0\}$ is also a correct signal periodicity, since every signal is invariant with respect to the shift 0.

Note that the *maximal* periodicity, $\mathbb{Z}(12)$, which is a supergroup of the other admitted periodicities, corresponds to the *minimal* period $T_{p_0} = 12$.

3.6.2 Specification of a Signal by a Quotient Group

After the acquisition of group notions, the abstract signal definition finds now a full motivation: a signal $s(t)$ is a complex function with *domain* an LCA group I_0 and with periodicity S , a subgroup of I_0 . This ensures that $s(t)$ verifies the shift-invariance condition on P

$$\boxed{s(t - p) = s(t), \quad p \in P, \quad \forall t \in I_0.} \quad (3.47)$$

For a signal with domain I_0 and periodicity P we say, for brevity, that the signal is “defined” on the *quotient group* I_0/P and use the notations

$$s(t), t \in I_0/P \quad \text{or} \quad s \in \mathcal{S}(I_0/P). \quad (3.48)$$

Thus, we introduce the quotient group simply as a pair group/subgroup,⁷ where the group represents the domain and the subgroup the periodicity.

In a quotient group I_0/P , the group I_0 is called the *basis group* and the subgroup P the *modulus* of the quotient group. The condition

$$\boxed{\{0\} \subset P \subset I_0} \quad (3.49)$$

states that the periodicity P must be a subgroup of the domain I_0 , and it is called the *compatibility condition* of the quotient group I_0/P .

When $P = \{0\}$, I_0/P is a *degenerate* quotient group (isomorphic to I_0 itself), otherwise I_0/P is a *proper* quotient group. For instance, $\mathbb{R}/\mathbb{Z}(10)$ is a proper quotient group, $\mathbb{R}/\{0\}$ is a degenerate quotient group, while $\mathbb{Z}(2)/\mathbb{Z}(9)$ is not a quotient group since it violates the compatibility condition. Hereafter, a group will be called an *ordinary* group to distinguish it from a *quotient group*; the term *group* is used for both and the distinction will come from the context.

3.6.3 Choice of the Periodicity

We have seen that a signal has a *maximal periodicity* P_0 and several possible *periodicities* P , which are given by the class $\mathcal{G}(P_0)$ of the LCA subgroups of P_0 . Correspondingly, we may have several choices for the quotient groups I_0/P to represent the same signal, even if the natural choice is the maximal periodicity P_0 , which gives the full information on the signal shift-invariance. But if the signal is

⁷This is not the standard definition appearing in the mathematical literature, where a quotient group is defined as $I_0/P = \{P + p | p \in I_0\}$, which is not a pair of groups, but a single group. In Appendix B, we explain why it is not convenient to use the standard mathematical definition in Signal Theory.

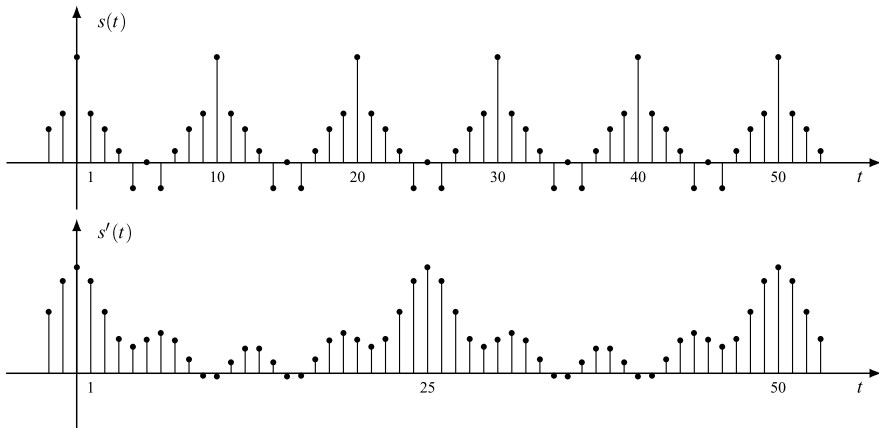


Fig. 3.19 Signal $s(t), t \in \mathbb{Z}$, has period equal to $T_p = 10$, while signal $s'(t), t \in \mathbb{Z}$, has period equal to $T'_p = 25$; the common period is 50

considered in the context of other signals, the common periodicity becomes the convenient choice. Thus, if $s_1(t)$ and $s_2(t)$ have respectively maximal periodicities P_1 and P_2 , the choice becomes

$$P = P_1 \cap P_2,$$

which is a subgroup of both P_1 and P_2 (see Sect. 3.9) and therefore is admitted as a correct periodicity for both signals.

For instance, if the two signals have minimum periods 10 and 25, we let $P = \mathbb{Z}(10) \cap \mathbb{Z}(25) = \mathbb{Z}(50)$, since a signal with period 10 is *also* periodic with period 50 and a signal with period 25 is *also* periodic with period 50 (Fig. 3.19).

In the limit case, when one of the two signals is aperiodic, say $P_2 = \{0\}$, then $P = P_1 \cap \{0\} = \{0\}$, and the joint analysis must be carried out considering both signals as aperiodic.

Role of Cells in Periodicity

There exists a connection between a signal representation by a quotient group I_0/P and the corresponding aperiodic cell $[I_0/P]$.

A signal $s(t), t \in I_0/P$, as a complex function defined on I_0 must be specified on the whole domain I_0 , but using its periodicity we can limit its specification (or knowledge) on a cell $C = [I_0/P]$. In fact, the knowledge of $s(t)$ on C allows obtaining $s(t)$ on every cell $C + p$ by the relation

$$s(t + p) = s(t), \quad t \in C, p \in P. \tag{3.50}$$

But, since the cells $C + p$ cover I_0 , the signal $s(t)$ becomes specified on the whole domain I_0 .

In conclusion, *the specification of a signal represented on the quotient group I_0/P can be limited to a cell $[I_0/P]$* . For instance, the specification of a signal $s(t)$, $t \in \mathbb{R}/\mathbb{Z}(10)$ can be limited to the interval $[0, 10)$ or $[-5, 5)$, which are both cells $[\mathbb{R}/\mathbb{Z}(10)]$. Similarly, the specification of $s(t)$, $t \in \mathbb{Z}(2)/\mathbb{Z}(10)$ can be limited to the set $\{0, 2, 4, 6, 8\}$ or to any other cell of $\mathbb{Z}(2)$ modulo $\mathbb{Z}(10)$. In the limit case of aperiodicity, $P = \{0\}$, the cell becomes

$$C = [I_0/\{0\}] = I_0, \quad (3.51)$$

and therefore the signal specification must be given on the whole domain I_0 .

According to identity (3.51), a degenerate quotient group can be identified with the domain, that is,

$$I_0/\{0\} = I_0. \quad (3.52)$$

UT 3.7 LCA Quotient Groups and Signal Classes

The LCA property must be considered also for quotient groups to make the theory development consistent (existence of the Haar integral, of the Fourier transform, etc.). In this section, with the help of Topology, we will search for LCA quotient groups and illustrate the corresponding signal classes.

From the class $\mathcal{G}(G_0)$ of the LCA subgroups of G_0 , a class of LCA quotient groups can be generated according to [8]:

Theorem 3.5 *Let G be an LCA group and P be an LCA subgroup of G . Then, the quotient group G/P is LCA.*

Thus, from $\mathcal{G}(G_0)$ we obtain the class of LCA quotient groups as

$$\mathcal{Q}(G_0) = \{G/P \mid P \subset G; P, G \in \mathcal{G}(G_0)\}. \quad (3.53)$$

Considering that an improper quotient group $G/\{0\}$ can be identified with G , the class $\mathcal{Q}(G_0)$ contains $\mathcal{G}(G_0)$.

3.7.1 Quotient Groups of \mathbb{R} and Related Signal Classes

Theorem 3.2 states that the class $\mathcal{G}(\mathbb{R})$ consists of \mathbb{R} , $\mathbb{Z}(T)$, with $T \in (0, \infty)$, and \mathbb{O} . Then, from Theorem 3.5 we obtain the class $\mathcal{Q}(\mathbb{R})$.

Corollary 3.1 *The LCA quotient groups on \mathbb{R} are*

$$\mathbb{R} = \mathbb{R}/\mathbb{O}, \quad \mathbb{R}/\mathbb{Z}(T), \quad \mathbb{Z}(T) = \mathbb{Z}(T)/\mathbb{O}, \quad \mathbb{Z}(T)/\mathbb{Z}(NT), \quad (3.54)$$

where $T > 0$.

Note that also the quotient groups \mathbb{R}/\mathbb{R} and $\mathbb{O}/\mathbb{O} = \mathbb{O}$ are LCA, but they are not useful for signals.

The previous corollary gives a clear and ultimate explanation on the existence of only four possible classes of 1D signals. In fact, excluding the trivial group \mathbb{O} as a signal domain, the corollary states that the definition of convolution and Fourier transform is possible only on these groups. Consequently, signals on the groups of \mathbb{R} are confined to the classes seen in the Classical Theory of Chap. 2:

1. *Aperiodic continuous-time signals* represented on $\mathbb{R} = \mathbb{R}/\mathbb{O}$,
2. *Aperiodic discrete-time signals* represented on $\mathbb{Z}(T) = \mathbb{Z}(T)/\mathbb{O}$,
3. *Periodic continuous-time signals* represented on $\mathbb{R}/\mathbb{Z}(T_p)$,
4. *Periodic discrete-time signals* represented on $\mathbb{Z}(T)/\mathbb{Z}(T_p)$.

In classes 2 and 4, the parameter T gives the signal *spacing* and in classes 3 and 4 the parameter T_p gives the signal *period*. Note that the compatibility condition (3.49) is always verified on $\mathbb{R}/\mathbb{Z}(T_p)$, that is, every period $T_p > 0$ is permitted for continuous-time signals, whereas on $\mathbb{Z}(T)/\mathbb{Z}(T_p)$ it requires that T_p to be a multiple of T . As a matter of fact, a periodic discrete-time signal must have an integer number of spacings in each period.

3.7.2 LCA Quotient Groups on \mathbb{R}^m

In Sect. 3.3, Theorem 3.1 identifies the class $\mathcal{G}(\mathbb{R}^m)$ of the LCA groups of \mathbb{R}^m . Then, by Theorem 3.5 we easily identify the class of the LCA quotient groups, explicitly

$$\mathcal{Q}(\mathbb{R}^m) = \{G/P \mid P \subset G, P, G \subset \mathcal{G}(\mathbb{R}^m)\}, \quad (3.55)$$

where both the basis G and the modulus P may be generated by a representation, say $(\mathbf{G}, H) \mapsto G$ and $(\mathbf{P}, K) \mapsto P$, according to

$$G = \{\mathbf{G} \mathbf{h} \mid \mathbf{h} \in H\}, \quad P = \{\mathbf{P} \mathbf{k} \mid \mathbf{k} \in K\}. \quad (3.56)$$

We shall always assume that: (i) *the domain G is a full-dimensional group*, whereas the periodicity P may have reduced dimensionality; (ii) *the periodicity P is a discrete group*. Then, in particular, when $K = \mathbb{O}$ the periodicity degenerates to aperiodicity. When P is a full-dimensional lattice, we have a *full periodicity* (periodicity with respect to all coordinates). In the intermediate cases, we have a *partial periodicity*. These ideas are better seen in the specific 2D cases.

3.7.3 Variety of Two-Dimensional Signals

Above we have seen that only four classes of 1D signals are possible. In the multidimensional case the signal variety becomes much richer and, to see this, it is sufficient to consider the simplest case of multidimensionality: $m = 2$.

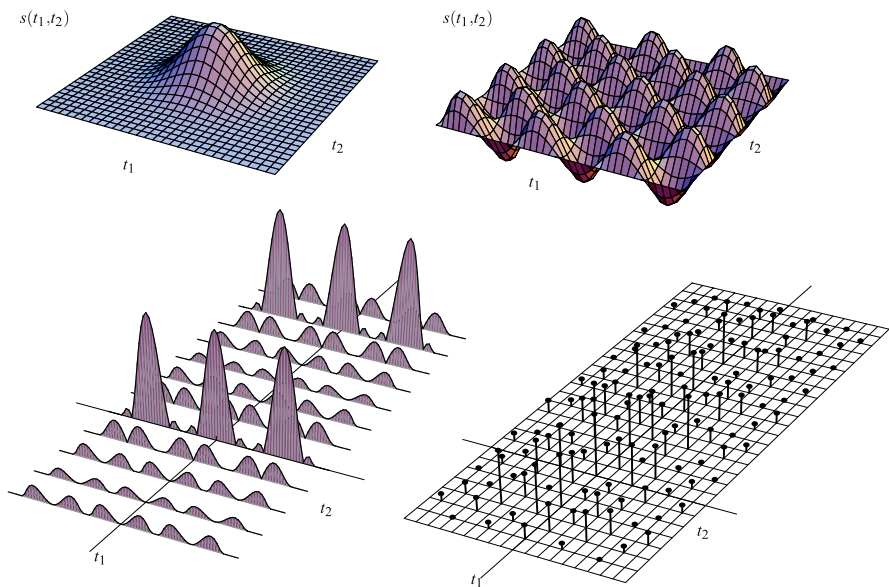


Fig. 3.20 Examples of 2D signals: above on \mathbb{R}^2 and on \mathbb{R}^2 with periodicity; below on the grating $\mathbb{R} \times \mathbb{Z}(d)$ and on the lattice $\mathbb{Z}_3^1(d_1, d_2)$

For the domain, we have three possible signatures

1. $H = \mathbb{R}^2$;
2. $H = \mathbb{Z}^2$;
3. $H = \mathbb{R} \times \mathbb{Z}$.

1. The domain is a 2D continuum, \mathbb{R}^2 itself, and correspondingly we have the class of *continuous* signals.
2. The domain is a 2D lattice L , and correspondingly we have the class of *discrete* signals. In the simplest case, L is a separable lattice such as $L = \mathbb{Z}(d_1, d_2)$, but in general L may be not separable, as shown in Fig. 3.11 with $L = \mathbb{Z}_3^2(d_1, d_2)$.
3. The domain is a 2D grating G , and correspondingly we have the class of *mixed-argument signals* with a mixture of continuous and discrete arguments. In the simplest case, the grating is separable, that is, $G = \mathbb{R} \times \mathbb{Z}(d_2)$, but in general G may be not separable, as shown in Fig. 3.11 with $G = \mathbb{R}\mathbb{Z}(e, f)$ (see (3.26a), (3.26b)).

The signal classes resulting from the three different types of domain are illustrated in Fig. 3.20.

For the *periodicity*, we have three possible signatures

- (a) \mathbb{O}^2 ;
- (b) \mathbb{Z}^2 ;
- (c) $\mathbb{O} \times \mathbb{Z}$.

- (a) The periodicity is the degenerate group \mathbb{O}^2 , and the 2D signal is *aperiodic*.

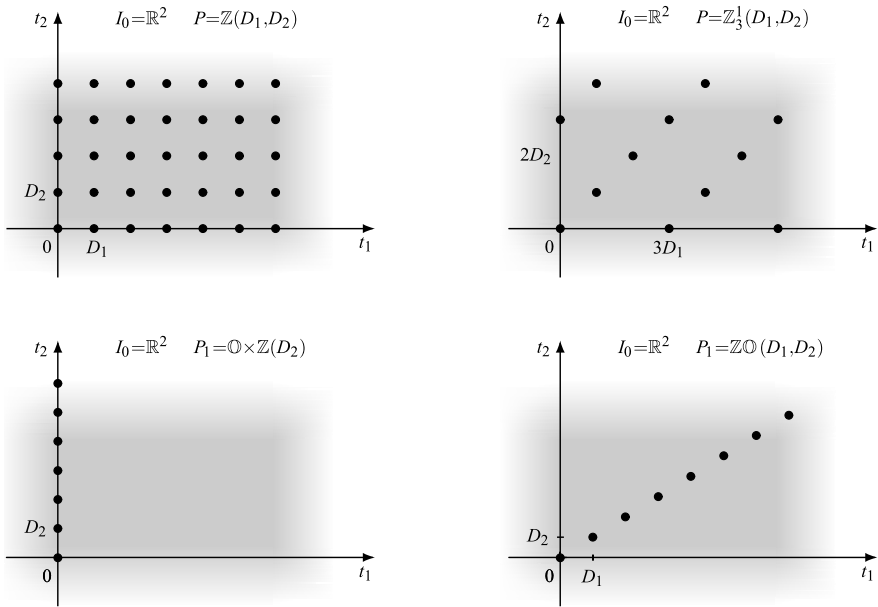


Fig. 3.21 Examples of full and partial periodicities for continuous 2D signals

(b) The periodicity is a 2D lattice P , and the signal is *fully periodic*. In the simplest case, P is separable, say $P = \mathbb{Z}(D_1, D_2)$, as shown in Fig. 3.21 in connection with the continuous domain $G = \mathbb{R}^2$ and in Fig. 3.22 in connection with the discrete domain $G = \mathbb{Z}(d_1, d_2)$. The corresponding signals $s(t_1, t_2)$ have period D_1 in t_1 and period D_2 in t_2 . In general, P is not separable, as shown in Figs. 3.21 and 3.22 with $P = \mathbb{Z}_3^1(D_1, D_2)$ and the interpretation of periodicity cannot be separated for each coordinate t_1, t_2 , but it holds globally in the form

$$s(t_1 - t_{10}, t_2 - t_{20}) = s(t_1, t_2), \quad (t_{10}, t_{20}) \in P. \tag{3.57}$$

(c) The periodicity is a 1D lattice P_1 , and the 2D signal is *partially periodic*. In the simplest case, P_1 is separable of the form (Fig. 3.21) $P_1 = \mathbb{O} \times \mathbb{Z}(D_2)$, which states that $s(t_1, t_2)$ is aperiodic in t_1 and periodic in t_2 with period D_2 . In the general case, P_1 is not separable, with points on a tilted line of the (t_1, t_2) -plane, and the periodicity must be interpreted in the global sense of (3.57).

As a final comment, we note that on \mathbb{R}^2 every lattice P is a candidate for periodicity (since $P \subset \mathbb{R}^2$), but on a discrete domain we have to pay attention to the compatibility condition $P \subset G$. For instance, with $G = \mathbb{Z}_2^1(d_1, d_2)$ and $P = \mathbb{Z}_3^1(D_1, D_2)$, the compatibility condition is $D_1 = 6N_1d_1$ and $D_2 = 6N_2d_2$ (in Fig. 3.22 $N_1 = 1, N_2 = 1$).

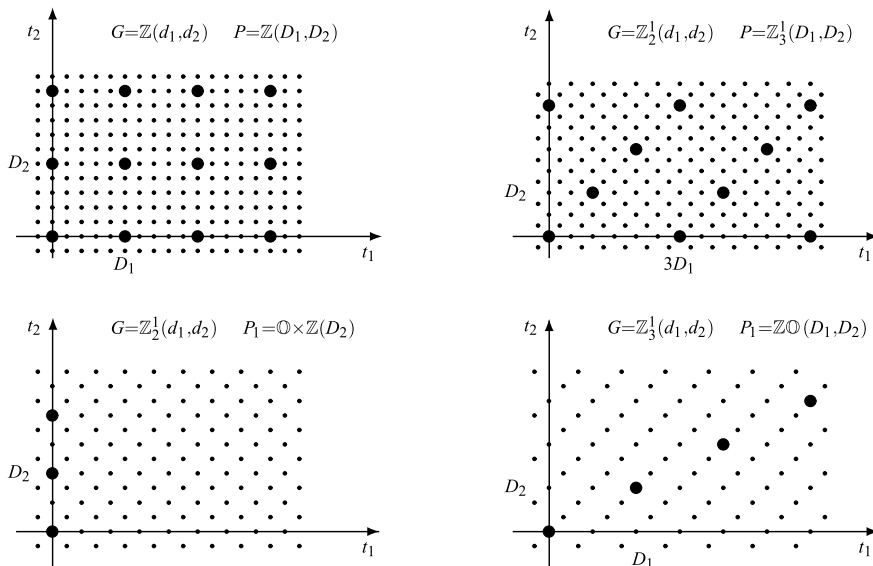


Fig. 3.22 Examples of full and partial periodicities for discrete 2D signals

Number of Signal Classes Versus Dimensionality

In the case of two-dimensional signals ($m = 2$), we have 3 types of domains and 3 forms of periodicities. The number of different signal classes is $3 \times 3 = 9$. The complete list is collected in Table 3.1. Not all these signal classes have the same practical relevance, but all of them find at least some applications.

In general, in \mathbb{R}^m we find $m + 1$ types of domains and $m + 1$ forms of periodicities, and the number of different signal classes is $\mathcal{N}_m = (m + 1)^2$. If in the counting we consider all the permutations, e.g., $\mathbb{R} \times \mathbb{Z}$ and $\mathbb{Z} \times \mathbb{R}$, the number of signal classes in \mathbb{R}^m becomes $\mathcal{N}'_m = (2^m)(2^m) = 4^m$.

	$m = 1$	$m = 2$	$m = 3$	$m = 4$	$m = 5$
\mathcal{N}_m	4	9	16	25	36
\mathcal{N}'_m	4	16	64	256	1024

3.7.4 Concluding Remarks on LCA Quotient Groups

We have identified the LCA quotient groups of \mathbb{R} and of \mathbb{R}^m having an arbitrary dimensionality m . The final question is: Do other LCA quotient groups exist? The full answer is given by the following theorem of Weil [9]:

Table 3.1 Regular groups on \mathbb{R}^2 and the corresponding signal classes

Signature	Separable group	General group	Signal class
1(a). $\mathbb{R}^2/\mathbb{O}^2$	\mathbb{R}^2	\mathbb{R}^2	Continuous-argument aperiodic
1(b). $\mathbb{R}^2/\mathbb{Z}^2$	$\mathbb{R}^2/\mathbb{Z}(D_1, D_2)$	\mathbb{R}^2/P	Continuous-argument periodic
1(c). $\mathbb{R}^2/\mathbb{O} \times \mathbb{Z}$	$\mathbb{R} \times [\mathbb{R}/\mathbb{Z}(D_2)]$	\mathbb{R}^2/P_1	Continuous-argument partially periodic
2(a). $\mathbb{Z}^2/\mathbb{O}^2$	$\mathbb{Z}(d_1) \times \mathbb{Z}(d_2)$	L	Discrete-argument aperiodic
2(b). $\mathbb{Z}^2/\mathbb{Z}^2$	$\mathbb{Z}(d_1, d_2)/\mathbb{Z}(D_1, D_2)$	L/P	Discrete-argument periodic
2(c). $\mathbb{Z}^2/\mathbb{O} \times \mathbb{Z}$	$\mathbb{Z}(d_1) \times [\mathbb{Z}(d_2)/\mathbb{Z}(D_2)]$	L/P_1	Discrete-argument partially periodic
3(a). $\mathbb{R} \times \mathbb{Z}/\mathbb{O}^2$	$\mathbb{R} \times \mathbb{Z}(d_2)$	G	Mixed-argument aperiodic
3(b). $\mathbb{R} \times \mathbb{Z}/\mathbb{Z}^2$	$\mathbb{R} \times \mathbb{Z}/\mathbb{Z}(D_1, D_2)$	G/P	Mixed-argument periodic
3(c). $\mathbb{R} \times \mathbb{Z}/\mathbb{O} \times \mathbb{Z}$	$\mathbb{R} \times [\mathbb{Z}(d_1)/\mathbb{Z}(D_2)]$	G/P_1	Mixed-argument partially periodic

Note: L : 2D lattice; P : 2D lattice; G : 2D grating; P_1 : 1D lattice (in \mathbb{R}^2)

Theorem 3.6 Every LCA group G is isomorphic to a group of \mathbb{R}^m of the form

$$G \sim \mathbb{R}^p \times \mathbb{Z}^q \times (\mathbb{R}/\mathbb{Z})^r \times \mathbb{F}_{N_1} \times \dots \times \mathbb{F}_{N_s} \tag{3.58}$$

for convenient p, q, r, s and N_1, \dots, N_s .

This fundamental result states substantially that every LCA group is related to the primitive groups of \mathbb{R} , that is, $\mathbb{R}, \mathbb{Z}, \mathbb{R}/\mathbb{Z}$, and $\mathbb{F}_N = \mathbb{Z}/\mathbb{Z}(N)$. It also states that every LCA group (not necessarily built from \mathbb{R}) is isomorphic to a group of the classes $\mathcal{Q}(\mathbb{R}^m)$ for a convenient m .

The conclusion is that the development of a signal theory can be confined to the classes $\mathcal{Q}(\mathbb{R}), \mathcal{Q}(\mathbb{R}^2), \dots$. In the other possible classes, signals may change their format, but not their topological nature. This will be seen in the next section for multiplicative groups.

⇓ 3.8 Multiplicative Groups

The purpose of this section is to show that the UST can be also developed on multiplicative groups, which sometimes have been considered in the field of images [5]. The reference multiplicative groups are \mathbb{R}_p , the group of positive real numbers (see Sect. 3.3), and \mathbb{C}^* , the group of nonzero complex numbers.

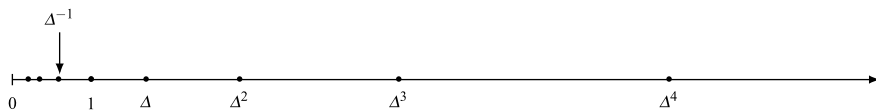


Fig. 3.23 The multiplicative group $\mathbb{Z}_p(\Delta)$

3.8.1 The Multiplicative Group \mathbb{R}_p and Its Subgroups

We begin by showing that (\mathbb{R}_p, \cdot) is really an Abelian group with respect to the multiplication “ \cdot ”. If a and b are positive real numbers, also $a \cdot b$ is a positive real number. The identity element of \mathbb{R}_p is 1, since $a \cdot 1 = a$. Finally, for every $a \in \mathbb{R}_p$ we can always find an element in \mathbb{R}_p , usually denoted by $1/a$, such that $a \cdot (1/a) = 1$.

Considering that the identity element is 1, the degenerate group in \mathbb{R}_p is $\mathbb{O}_p = \{1\}$. The discrete multiplicative groups have the form

$$\mathbb{Z}_p(\Delta) = \{\Delta^n | n \in \mathbb{Z}\}, \quad (3.59)$$

where $\Delta > 1$, and therefore their points are not equally spaced, but are in a geometric progression, as shown in Fig. 3.23.

The ordinary LCA groups of \mathbb{R}_p are

$$\mathbb{R}_p, \quad \mathbb{Z}_p(\Delta) \quad \text{with } \Delta \in (1, \infty), \quad \mathbb{O}_p, \quad (3.60)$$

which form the class $\mathcal{G}(\mathbb{R}_p)$. This statement is a consequence of the isomorphism linking \mathbb{R}_p to \mathbb{R} (see Sect. 3.3), that is,

$$\exp: \mathbb{R} \rightarrow \mathbb{R}_p, \quad (3.61)$$

which maps the elements of \mathbb{R} into the elements of \mathbb{R}_p and converts the addition “+” on \mathbb{R} into the multiplication “ \cdot ” on \mathbb{R}_p according to $\exp(a + b) = \exp(a) \cdot \exp(b)$, where a and b are elements of \mathbb{R} and $\exp(a)$ and $\exp(b)$ are elements of \mathbb{R}_p . The same isomorphism links $\mathbb{Z}(d)$ to $\mathbb{Z}_p(\Delta)$, with $\Delta = \exp(d)$, and \mathbb{O} to \mathbb{O}_p . On the other hand, from Theorem 3.2 we know that the only LCA groups on \mathbb{R} are \mathbb{R} , $\mathbb{Z}(d)$ and \mathbb{O} . Hence the conclusion that the only LCA groups in \mathbb{R}_p are given by (3.60).

Analogously, we can proceed to the identification of the LCA quotient groups $\mathcal{Q}(\mathbb{R}_p)$, generated by \mathbb{R}_p .

Note that $\mathbb{Z}_p(\Delta^N)$ with $N \geq 1$ is really a subgroup $\mathbb{Z}_p(\Delta)$, as requested by the compatibility of the quotient group $\mathbb{Z}_p(\Delta)/\mathbb{Z}_p(\Delta^N)$. In fact, (Fig. 3.24)

$$\mathbb{Z}_p(\Delta) = \{\dots, \Delta^{-3}, \Delta^{-2}, \Delta^{-1}, 1, \Delta, \Delta^2, \Delta^3, \dots\},$$

and, for instance,

$$\mathbb{Z}_p(\Delta^3) = \{\dots, \Delta^{-6}, \Delta^{-3}, 1, \Delta^3, \Delta^6, \Delta^9, \dots\}.$$

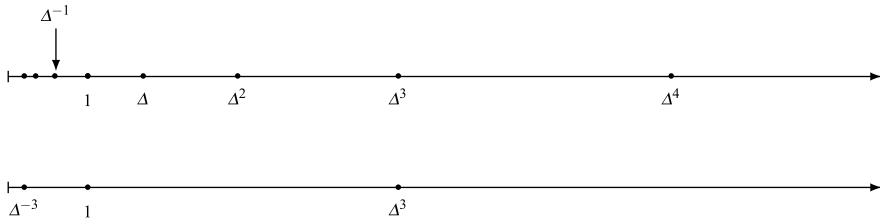


Fig. 3.24 The multiplicative group $\mathbb{Z}_p(\Delta)$ compared with its subgroup $\mathbb{Z}_p(\Delta^3)$

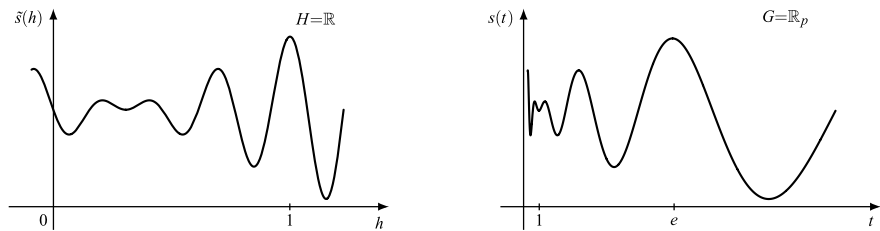


Fig. 3.25 Signal $s(h)$, $h \in \mathbb{R}$, and corresponding “isomorphic” signal $s(t)$, $t \in \mathbb{R}_p$

3.8.2 Signals on \mathbb{R}_p

From the list of the quotient groups of $\mathbb{Q}(\mathbb{R})$, we find that on \mathbb{R}_p we may have only four signal classes, namely

1. Aperiodic continuous signals with domain $I = \mathbb{R}_p$;
2. Periodic continuous signals with domain $I = \mathbb{R}_p/\mathbb{Z}_p(\Delta_p)$;
3. Aperiodic discrete signals with domain $I = \mathbb{Z}_p(\Delta)$;
4. Periodic discrete signals with domain $I = \mathbb{Z}_p(\Delta)/\mathbb{Z}_p(\Delta_p)$ with $\Delta_p = \Delta^N$.

Thus, we find exactly the same classes seen with the groups of \mathbb{R} .

In fact, the isomorphism (3.61), that is, $\alpha(h) = \exp(h)$ links signals defined on $H \in \mathbb{Q}(\mathbb{R})$ to signals defined on $G \in \mathbb{Q}(\mathbb{R}_p)$. Then, starting from a signal $\tilde{s}(h)$, $h \in H$, we find a corresponding signal $s(t)$, $t \in G$, and vice versa, by the relations

$$s(t) = \tilde{s}(\log t), \quad \tilde{s}(h) = s(\exp h). \tag{3.62}$$

Figure 3.25 shows an example of a pair related in this way.

The novelty lies in the signal behavior, as a consequence of multiplication “ \cdot ” acting on the domain. In particular, the periodicity condition, $s(t - p) = s(t)$, in \mathbb{R}_p assumes the form

$$s(t/p) = s(t), \quad p \in P,$$

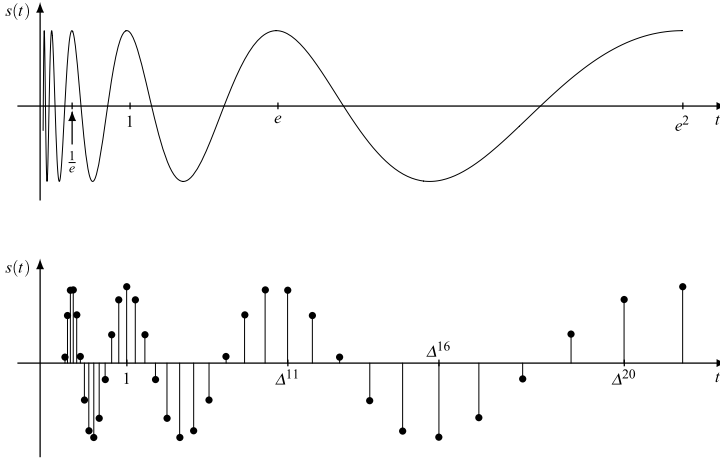


Fig. 3.26 Periodic signal on \mathbb{R}_p and its sampled version on $\mathbb{Z}_p(\Delta)$

where $t - p$ is replaced by t/p . Hence, with $P = \mathbb{Z}_p(\Delta_p)$ the explicit periodicity condition is

$$s(t/\Delta_p^k) = s(t), \quad \forall k \in \mathbb{Z}. \tag{3.63}$$

For instance, the signal on \mathbb{R}_p given by (Fig. 3.26)

$$s(t) = A_0 \cos(2\pi \log t), \quad t \in \mathbb{R}_p$$

verifies condition (3.63) with $\Delta_p = e$ and therefore can be formulated as a signal on the quotient group $\mathbb{R}_p/\mathbb{Z}_p(e)$.

Note that this signal has a compressed form for $0 < t < 1$ and an expanded form for $t > 1$ with zeros displayed in a geometric progression and is quite different with respect to a periodic signal on \mathbb{R} . Similar considerations hold for the discrete signals in $\mathbb{Z}_p(\Delta)$, whose behavior is compressed for $t < \Delta$ and expanded for $t > \Delta$.

3.8.3 The Multiplicative Group \mathbb{C}^* and Its Subgroups

We now consider the multiplicative group \mathbb{C}^* of nonzero complex numbers and the multiplicative group \mathbb{U} of complex numbers with unit modulus. The operation in these groups is the multiplication by complex numbers and the identity element is the complex unit $1 + i0$. Of course, \mathbb{U} is a subgroup of \mathbb{C}^* , as is \mathbb{R}_p .

Considering the Euler decomposition of a complex number

$$z = \rho e^{i\theta} \quad \text{with } \rho = |z|, \theta = \arg z, \tag{3.64}$$

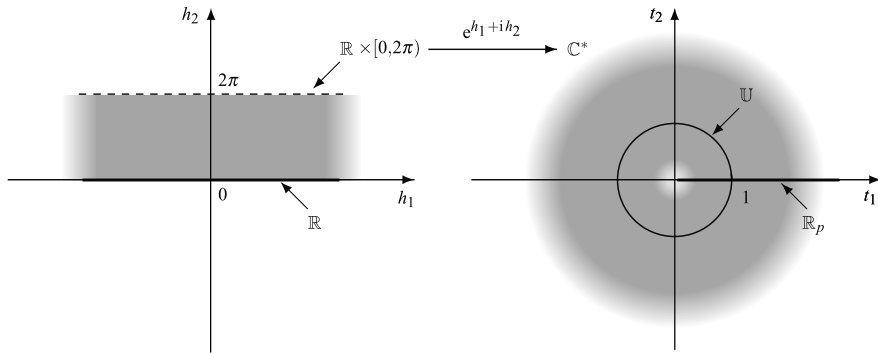


Fig. 3.27 Mapping of the \mathbb{R}^2 cell $\mathbb{R} \times [0, 2\pi)$ into \mathbb{C}^*

we find that if $z \in \mathbb{C}^*$, then $\rho \in \mathbb{R}_p$ and $e^{i\theta} \in \mathbb{U}$. Therefore, \mathbb{C}^* can be seen as the Cartesian product⁸

$$\boxed{\mathbb{C}^* = \mathbb{R}_p \times \mathbb{U}.} \tag{3.65}$$

We have seen that $\mathbb{R}_p \sim \mathbb{R}$ with the isomorphism map $\alpha = \exp(\cdot)$. On the other hand, we have

$$\mathbb{U} = \{e^{i\theta} \mid \theta \in [0, 2\pi)\}, \tag{3.66}$$

so that \mathbb{U} is isomorphic to the quotient group $\mathbb{R}/\mathbb{Z}(2\pi)$ with the isomorphism map $\exp(i\cdot)$. By composition, we have

$$\mathbb{C}^* = \mathbb{R}_p \times \mathbb{U} \sim \mathbb{R} \times \mathbb{R}/\mathbb{Z}(2\pi), \tag{3.67a}$$

where the isomorphism map is given by (3.64) that we rewrite using the standard notations as

$$(t_1, t_2) = \alpha(h_1, h_2) = e^{h_1+ih_2} \tag{3.67b}$$

with $(h_1, h_2) \in \mathbb{R} \times \mathbb{R}/\mathbb{Z}(2\pi)$ and $(t_1, t_2) \in \mathbb{C}^*$.

This isomorphism links a cell of \mathbb{R}^2 modulo $\mathbb{O} \times \mathbb{Z}(2\pi)$ with \mathbb{C}^* , as shown in Fig. 3.27 where the cell is the strip $\mathbb{R} \times [0, 2\pi)$ of \mathbb{R}^2 . Note that \mathbb{R} is mapped into \mathbb{R}_p , the vertical segment $[0, 2\pi)$ is mapped into the unit circle \mathbb{U} and $(0, 0)$ into $1 + i0$.

The isomorphism (3.67a), (3.67b) maps subgroups of $\mathbb{R} \times \mathbb{R}/\mathbb{Z}(2\pi)$ into subgroups of \mathbb{C}^* , as shown in Fig. 3.28. Specifically:

- (a) The separable grating $\mathbb{R} \times \mathbb{Z}(2\pi/N)/\mathbb{Z}(2\pi)$, given by N horizontal equally-spaced lines, is mapped onto N angularly equally-spaced half-lines leaving from the origin;

⁸When \mathbb{R}_p is regarded as a subgroup of \mathbb{C}^* it must be intended as $\mathbb{R}_p \times \mathbb{O}_p$, that is, as a 1D group in \mathbb{C}^* , which is a 2D group; similarly for \mathbb{U} .

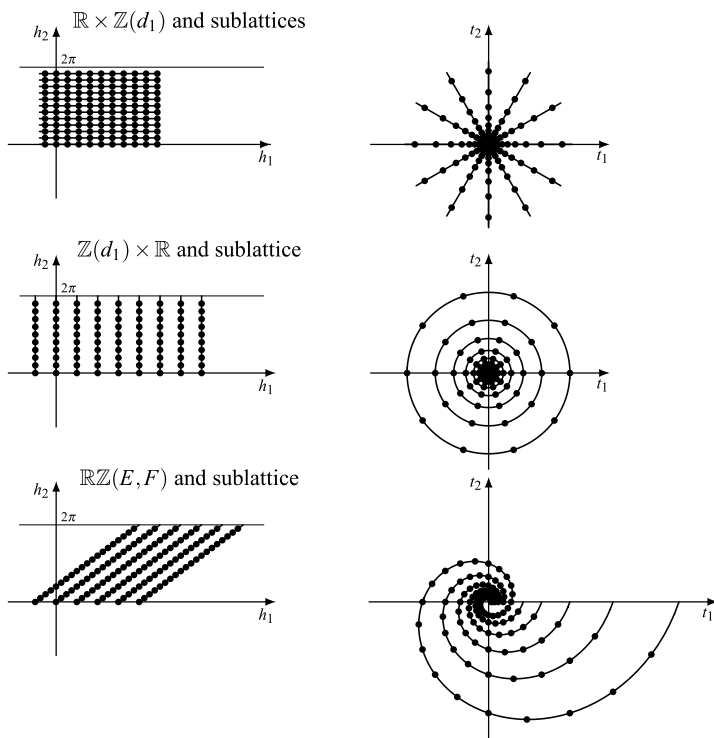


Fig. 3.28 Grating and lattice correspondence between $\mathbb{R}/\mathbb{Z}(2\pi)$ and \mathbb{C}^*

- (b) The separable grating $\mathbb{Z}(d_1) \times \mathbb{R}/\mathbb{Z}(2\pi)$, given by a vertical equally-spaced segments, is mapped onto infinitely many concentric circles, with radii in geometrical progression.
- (c) The tilted grating $\mathbb{R}\mathbb{Z}(\mu)/\mathbb{Z}(2\pi)$ (see Fig. 3.11) is mapped onto a sequence of spirals.

The figure also shows sublattices of the gratings and the corresponding sublattices in \mathbb{C}^* .

UT 3.9 Sum and Intersection of Groups

This topic will be fundamental for the theory of transformations (Chap. 6), particularly for multirate transformations (Chap. 7). The problem is that the sum $J + K$ of two LCA groups may not be an LCA group. For instance, $\mathbb{Z}(3) + \mathbb{Z}(\sqrt{2})$ is an Abelian group of \mathbb{R} , but it is not LCA. In general, the condition that assures that $J + K$ is LCA states that J and K are related in a *rational* way (in terms of their bases). The other problem is the evaluation of the sum and intersection when J and K are multidimensional lattices (which is the case of interest). This is an advanced

topic in the theory of integer matrices, which will be developed in Chap. 16. In this section, we develop the 1D case and give a guide for the general m D case.

3.9.1 Comparable and Rationally Comparable Groups

Given a reference LCA group G_0 , the groups of $\mathcal{G}(G_0)$ will be called *comparable* since they have the same group operation in common, and for every pair J, K of $\mathcal{G}(G_0)$ one can consider the expressions

$$J + K, \quad J \cap K, \quad J \subset K \quad \text{and} \quad J \supset K.$$

For instance, the sum $\mathbb{R} + \mathbb{Z}(T)$ makes sense, but not the sums $\mathbb{R}_p + \mathbb{Z}(T)$ and $\mathbb{R}^2 + \mathbb{Z}(T)$ because the groups do not have the same operation in common.

We recall the definition of the sum of two (comparable) groups

$$J + K = \{j + k \mid j \in J, k \in K\}, \quad (3.68)$$

whereas $J \cap K$ is defined as the usual set operation.

We are looking for conditions on *two comparable LCA groups* J and K which guarantee that their sum and intersection are LCA groups; in symbols,

$$J, K \in \mathcal{G}(G_0) \implies J + K, \quad J \cap K \in \mathcal{G}(G_0). \quad (3.69)$$

We note that if J is a subgroup of K , we have

$$J \subset K \implies J + K = K, \quad J \cap K = J. \quad (3.70)$$

This remark allows finding a general solution for an *ordered* pair (J, K) , which is defined as a pair such that $J \subset K$ or $J \supset K$.

Proposition 3.7 *The sum and intersection of two ordered groups J, K of $\mathcal{G}(G_0)$ are LCA groups, given by*

$$J + K = \max(J, K)_m, \quad J \cap K = \min(J, K). \quad (3.71)$$

For instance, in $\mathcal{G}(\mathbb{R})$, we find that

$$\begin{aligned} \mathbb{R} + \mathbb{Z}(3) &= \mathbb{R}, & \mathbb{R} \cap \mathbb{Z}(3) &= \mathbb{Z}(3), \\ \mathbb{Z}(2) + \mathbb{Z}(6) &= \mathbb{Z}(2), & \mathbb{Z}(2) \cap \mathbb{Z}(6) &= \mathbb{Z}(6). \end{aligned}$$

A crucial point happens when the pair (J, K) is not ordered, that is, when $J \not\subset K$ and $J \not\supset K$. Examples of non-ordered 1D pairs are $\mathbb{Z}(6), \mathbb{Z}(10)$ and $\mathbb{Z}(3), \mathbb{Z}(\sqrt{2})$.

At this point, we find it convenient to introduce the following definition:

Definition 3.6 Two comparable groups, J and $K \in \mathcal{G}(G_0)$, will be called *rationally comparable* if their sum $J + K$ is an LCA group.

The definition has interest mainly for lattices. The term “rationally comparable” will be immediately clear in the 1D case and later in the m D case.⁹

⇓ 3.9.2 Sum and Intersection on \mathbb{R}

We now evaluate the sum and the intersection of two groups of $\mathcal{G}(\mathbb{R})$. Considering that $\mathbb{R} + \mathbb{Z}(T) = \mathbb{R}$ and $\mathbb{R} \cap \mathbb{Z}(T) = \mathbb{Z}(T)$, the problem can be confined to lattices, and the solution is (see Appendix C):

Theorem 3.7 *If T_1/T_2 is rational, say $T_1/T_2 = N_1/N_2$ with N_1 and N_2 coprime, then*

$$\mathbb{Z}(T_1) \cap \mathbb{Z}(T_2) = \mathbb{Z}(N_2 T_1) = \mathbb{Z}(N_1 T_2), \quad (3.72a)$$

$$\mathbb{Z}(T_1) + \mathbb{Z}(T_2) = \mathbb{Z}(T_1/N_1) = \mathbb{Z}(T_2/N_2). \quad (3.72b)$$

If T_1/T_2 is irrational, $\mathbb{Z}(T_1) + \mathbb{Z}(T_2)$ cannot be written in the form $\mathbb{Z}(T)$ and therefore is not an LCA group, whereas the intersection is given by

$$\mathbb{Z}(T_1) \cap \mathbb{Z}(T_2) = \{0\} = \mathbb{O}.$$

The conclusion is that the sum of $\mathbb{Z}(T_1)$ and $\mathbb{Z}(T_2)$ is an LCA group if and only if the spacing ratio T_1/T_2 is rational. In this case, we can find an alternative formulation. Let

$$T = T_1/N_1 = T_2/N_2, \quad (3.73)$$

with N_1 and N_2 coprime, then

$$\mathbb{Z}(N_1 T) \cap \mathbb{Z}(N_2 T) = \mathbb{Z}(N_1 N_2 T), \quad \mathbb{Z}(N_1 T) + \mathbb{Z}(N_2 T) = \mathbb{Z}(T). \quad (3.74)$$

For instance, if $T_1 = 0.08$ and $T_2 = 0.3$, we have $T_1/T_2 = 0.08/0.3 = 4/15$. Then, with $T = 0.02$ we find $\mathbb{Z}(4T) \cap \mathbb{Z}(15T) = \mathbb{Z}(60T)$ and $\mathbb{Z}(4T) + \mathbb{Z}(15T) = \mathbb{Z}(T)$.

The intersection and sum are related to the *least common multiple* (lcm) and *greatest common divisor* (GCD). In fact, when the two lattices are written in the form $\mathbb{Z}(M_1 T)$ and $\mathbb{Z}(M_2 T)$, where in general M_1 and M_2 are not coprime, but have a common factor h , that is, $M_1 = hN_1$ and $M_2 = hN_2$ with N_1 and N_2 coprime, we have

$$\mathbb{Z}(M_1 T) \cap \mathbb{Z}(M_2 T) = \mathbb{Z}(MT) \quad \text{with } M = \text{lcm}(M_1, M_2),$$

$$\mathbb{Z}(M_1 T) + \mathbb{Z}(M_2 T) = \mathbb{Z}(hT) \quad \text{with } h = \text{GCD}(M_1, M_2).$$

⁹We shall see in Chap. 16 that if the bases \mathbf{J} and \mathbf{K} of the lattice J and K are such that \mathbf{JK}^{-1} is a rational matrix, then $J + K$ is LCA.

⇓ 3.9.3 Sum and Intersection on \mathbb{R}^m

To establish that the sum and intersection is LCA is not trivial already in the 1D case and becomes more complicated in the m D case, since in $\mathcal{G}(\mathbb{R}^m)$ we have three kinds of groups, instead of two, due to the presence of gratings. Also, the groups may have different dimensionalities. For the dimensionality, we have a very simple statement [6]

$$\boxed{\dim(J + K) + \dim(J \cap K) = \dim(J) + \dim(K)}. \quad (3.75)$$

Then, in particular, if J and K are full-dimensional, also $J + K$ and $J \cap K$ are full-dimensional.

For separable groups, the sum and intersection are easily found, considering that $J_1 \times J_2 + K_1 \times K_2 = (J_1 + K_1) \times (J_2 + K_2)$, etc. But for nonseparable groups, the problem becomes in general cumbersome. In the class of lattices (which is the case of main interest), we have a simple statement [7].

Theorem 3.8 *Let J and K be lattices of \mathbb{R}^m . Then the sum $J + K$ and the intersection $J \cap K$ are lattices of \mathbb{R}^m , if and only if there exists a lattice L_0 of \mathbb{R}^m that contains both J and K . Moreover, $J + K \in \mathcal{G}(L_0)$ and $J \cap K \in \mathcal{G}(L_0)$.*

The proof will be seen in Chap. 16, in the context of the theory of integer matrices. Also the technique for evaluating the sum and the intersection will be seen in that chapter. For the time being, we anticipate two other statements:

Proposition 3.8 *$J + K$ is the smallest lattice containing both J and K and $J \cap K$ is the largest lattice contained in both J and K .*

Proposition 3.9 *In the class $\mathcal{G}_m(L_0)$ of full-dimensional sublattices ($\mathcal{G}_m(L_0)$ is a subclass of $\mathcal{G}(\mathbb{R}^m)$), we have*

$$J, K \in \mathcal{G}_m(L_0) \implies J + K, \quad J \cap K \in \mathcal{G}_m(L_0) \quad (3.76)$$

and the following identity holds for the determinants

$$\boxed{d(J + K) d(J \cap K) = d(J) d(K)}. \quad (3.77)$$

Example 3.4 In the class $\mathcal{G}_2(\mathbb{Z}(d_1, d_2))$ where lattices have the form $\mathbb{Z}_a^i(d_1, d_2)$ (see the end of Sect. 3.3), both the sum and the intersection belong to this class. For instance, if $J = \mathbb{Z}_2^1(d_1, d_2)$ and $K = \mathbb{Z}_3^2(d_1, d_2)$, we find¹⁰

$$J + K = \mathbb{Z}_{10}^3(d_1, d_2), \quad J \cap K = \mathbb{Z}_1^0(d_1, d_2) = \mathbb{Z}(d_1, d_2),$$

¹⁰The evaluation technique of lattice sums and intersections will be seen in Chap. 16. The author has written a `Mathematica` program to compute them (see the introductory note of Chap. 16).

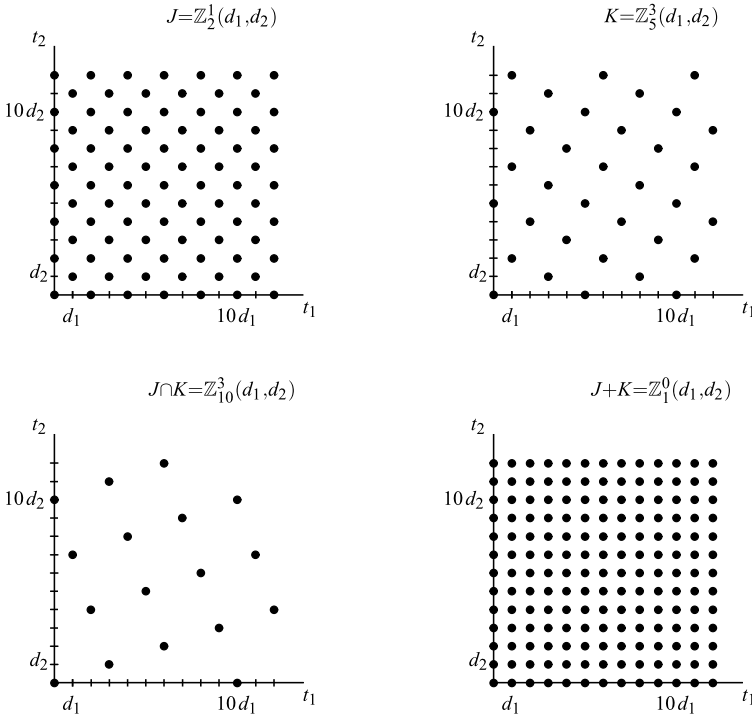


Fig. 3.29 Examples of sum and intersection of 2D full-dimensional lattices

as shown in Fig. 3.29.

Note that the above lattices verify the determinant identity (3.77). In fact,

$$\begin{aligned}
 d(J) &= 2d_1 d_2, & d(K) &= 5d_1 d_2, \\
 d(J + K) &= 10d_1 d_2, & d(J \cap K) &= d_1 d_2.
 \end{aligned}$$

Example 3.5 We now consider two lattices of the class $\mathcal{G}(\mathbb{Z}(d_1, d_2))$, but we suppose that one of them has a reduced dimensionality, specifically $J = \mathbb{Z}(2, 2)$ and $K = \mathbb{Z}\mathbb{O}(1, 1)$. Then, we easily find that

$$J \cap K = \mathbb{Z}\mathbb{O}(2, 2), \quad J + K = \mathbb{Z}_2^1(1, 1),$$

as shown in Fig. 3.30. Again, we can check the rule (3.75) on dimensionality; in fact,

$$\dim J = 2, \quad \dim K = 1, \quad \dim(J \cap K) = 1, \quad \dim(J + K) = 2.$$

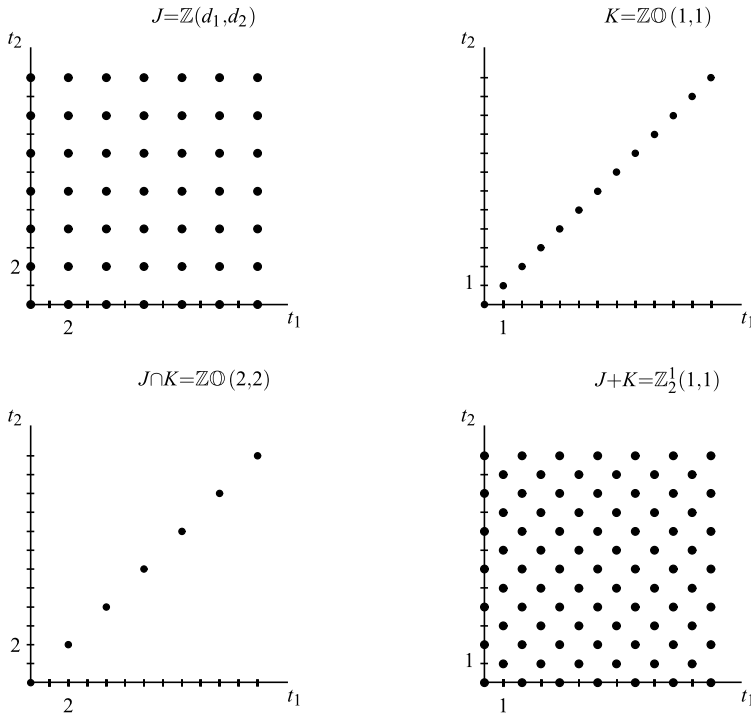


Fig. 3.30 Sum and intersection when one of the lattices is reduced-dimensional

3.9.4 Sum and Intersection of Quotient Groups

It is convenient to extend ordering and operations to quotient groups. Let $I = I_0/P_1$ and $U = U_0/P_2$ be quotient groups, where I_0, U_0, P_1 and P_2 are comparable ($\in \mathcal{G}(G_0)$). Then, we introduce the ordering for quotient groups in the following (conventional) way

$$\begin{aligned}
 I \subset U &\iff I_0 \subset U_0 \quad \text{and} \quad P_1 \subset P_2, \\
 I \supset U &\iff I_0 \supset U_0 \quad \text{and} \quad P_1 \supset P_2.
 \end{aligned}
 \tag{3.78}$$

For the sum and intersection, we let

$$\begin{aligned}
 I + U &\triangleq (I_0 + U_0)/(P_1 + P_2), \\
 I \cap U &\triangleq (I_0 \cap U_0)/(P_1 \cap P_2).
 \end{aligned}
 \tag{3.79}$$

Finally, a pair of LCA quotient groups I and U is rationally comparable, when both the pairs I_0, U_0 and the pairs P_1, P_2 are rationally comparable. Note that, from the standard relationships (3.70) we find

$$I \subset U \implies I + U = U, \quad I \cap U = I.$$

These generalizations to quotient groups will be useful for linear transformations in Chap. 6.

3.10 Problems

3.1 ★ [Sect. 3.2] Check that the additive set of complex numbers, \mathbb{C} , is an Abelian group.

3.2 ★ [Sect. 3.2] Prove the relations

$$\mathbb{Z}(2) + \mathbb{Z}(4) = \mathbb{Z}(2), \quad \mathbb{Z}(3) + \mathbb{R} = \mathbb{R}.$$

3.3 ★★★ [Sect. 3.2] Prove the relations

$$\mathbb{Z}(3) + \mathbb{Z}(5) = \mathbb{Z}(1), \quad \mathbb{Z}(6) + \mathbb{Z}(9) = \mathbb{Z}(3).$$

3.4 ★ [Sect. 3.2] Prove the relations

$$[0, 2) + \mathbb{Z}(2) = \mathbb{R}, \quad [0, 3) + \mathbb{Z}(2) = \mathbb{R}.$$

3.5 ★ [Sect. 3.2] Verify that \mathbb{C}^* is an Abelian group, where the group operation is the ordinary multiplication between complex numbers.

3.6 ★★ [Sect. 3.2] Verify that the 2D set \mathbb{Z}_2^1 consisting of the integer pairs (m, n) , with m, n both even or both odd, is a subgroup of \mathbb{R}^2 .

3.7 ★★★ [Sect. 3.3] With reference to representation (3.27), find the corresponding upper-triangular representation. *Hint: Use Proposition 3.1.*

3.8 ★ [Sect. 3.5] Check that the set $A = [0, 1) \cup [6, 7) \cup [12, 15)$ is a cell of \mathbb{R} modulo $\mathbb{Z}(5)$.

3.9 ★★ [Sect. 3.5] Verify the relationship $[I_0/P_0] + [P_0/P] + P = I_0$ for $I_0 = \mathbb{R}$, $P_0 = \mathbb{Z}(2)$ and $P = \mathbb{Z}(10)$.

3.10 ★ [Sect. 3.6] Find the periodicity of the continuous signal

$$s(t) = A_0 \cos 2\pi f_1 t + B_0 \sin 2\pi f_2 t, \quad t \in \mathbb{R}$$

for $f_1/f_2 = 3/5$ and $f_1/f_2 = \sqrt{2}/5$.

3.11 ★★★ [Sect. 3.6] Find the periodicity of the discrete signal

$$s(t) = A_0 \cos 2\pi f_1 t + B_0 \sin 2\pi f_2 t, \quad t \in \mathbb{Z}(2)$$

for $f_1 = 1/7$ and $f_2 = 1/4$.

3.12 *** [Sect. 3.6] Find the minimum period of the discrete signal

$$s(t) = s_1(t)s_2^3(t), \quad t \in \mathbb{Z}(3)$$

where $s_1(t)$ has period $T_{p1} = 9$ and $s_2(t)$ has period $T_{p2} = 12$.

3.13 ** [Sect. 3.8] Verify that any logarithmic function, \log_b , is an isomorphism from (\mathbb{R}_p, \cdot) onto $(\mathbb{R}, +)$.

3.14 *** [Sect. 3.9] Prove that if G_1 and G_2 are both subgroups of a group G , the sum $G_1 + G_2$ and the intersection $G_1 \cap G_2$ are subgroups of G .

The union $G_1 \cup G_2$ is not a group, in general, as we can check for the pair $G_1 = \mathbb{Z}(5)$ and $G_2 = \mathbb{Z}(3)$.

3.15 ** [Sect. 3.9] Evaluate

$$\mathbb{Z}(T_1) \cap \mathbb{Z}(T_2) \cap \mathbb{Z}(T_3) \quad \text{and} \quad \mathbb{Z}(T_1) + \mathbb{Z}(T_2) + \mathbb{Z}(T_3)$$

for $T_1 = 0.018$, $T_2 = 0.039$, $T_3 = 0.045$.

3.16 ** [Sect. 3.9] Reconsider Problems 3.10 and 3.11 using Theorem 3.7.

3.17 *** [Sect. 3.9] Find the periodicity of the discrete sinusoid

$$s(t) = A_0 \cos(2\pi f_0 t + \varphi_0), \quad t \in \mathbb{Z}(T)$$

considering f_0 as a parameter.

Appendix A: Proof of Theorem 3.1

Since the matrix \mathbf{G} in (3.10) is nonsingular, it defines a linear map $\mathbf{t} = \mathbf{G}\mathbf{h}$ with the inverse map $\mathbf{h} = \mathbf{G}^{-1}\mathbf{t}$ which represents an isomorphism. Hence, the group G defined by (3.10) is isomorphic to H , and therefore it is LCA.

We have to prove that all isomorphisms $\beta : H \rightarrow G$ have this linear form. For brevity, let us consider the specific case $L = 2$ and $H = \mathbb{R} \times \mathbb{Z}$. Then, from the isomorphism property (3.29), we have

$$\beta(\mathbf{h}_1 + \mathbf{h}_2) = \beta(\mathbf{h}_1) + \beta(\mathbf{h}_2) \in H \tag{3.80}$$

where on both sides $+$ is the group operation in \mathbb{R}^2 (the standard operation between vectors). Then, (3.80) states the *additivity* of β . Now, let

$$\mathbf{g}_1 = \beta(1, 0), \quad \mathbf{g}_2 = \beta(0, 1), \quad \mathbf{G} = [\mathbf{g}_1, \mathbf{g}_2].$$

We claim that

$$\beta(\mathbf{h}) = \mathbf{g}_1 r + \mathbf{g}_2 n = \mathbf{G} \begin{bmatrix} r \\ n \end{bmatrix}, \quad r \in \mathbb{R}, n \in \mathbb{Z}.$$

In fact, for $n = 0$ if $h = (1, 0) \in H$ and $r \in \mathbb{R}$, also $h = (r, 0) \in H$ and $\beta(r, 0) = r\beta(1, 0) = rg_1$.

Appendix B: The “True” Quotient Group

We have introduced the quotient group simply as a pair group/subgroup to represent simultaneously domain/periodicity of a signal. But the standard definition of quotient group is

$$I_0/P \triangleq \{P + p \mid p \in I_0\}. \quad (3.81)$$

So it is not a pair of groups, but a single group, whose elements are the subsets of I_0 of the form (3.81), called the *cosets* of P . The group operation \oplus between two elements of I_0/P , $P_p = P + p$ and $P_q = P + q$, is defined by $P_p \oplus P_q = P_{p+q}$ and the identity element of I_0/P is given by the subgroup P .

We now show that there is an equivalence between the class of signals defined on the “true” quotient group I_0/P and our class of signals with domain I_0 and periodicity P . Let \tilde{s} be a complex function on the “true” quotient group

$$\tilde{s} : I_0/P \rightarrow \mathbb{C}. \quad (3.82)$$

Then the domain of \tilde{s} is the class of the cosets of P . Now, letting

$$s(t) = \tilde{s}(P_t), \quad t \in I_0 \quad (3.83)$$

we obtain a function with domain I_0 and periodicity P . In fact, if $t_0 \in P$, we have $P_{t+t_0} = P + t + t_0 = P + t = P_t$. Conversely, if $s : I_0 \rightarrow \mathbb{C}$ is a complex function with periodicity P , the relation

$$\tilde{s}(P_t) = s(t), \quad P_t \in I_0/P \quad (3.84)$$

defines a function of the form (3.82).

In conclusion, (3.83) and (3.84) link with a one-to-one correspondence the class of signals defined on the “true” quotient group I_0/P and the class of signals with domain I_0 and periodicity P . Signal Theory could be completely developed on the basis of “true” quotient groups [2], but there is one catch. The management of functions having *as domain a class of subsets* turns out to be cumbersome. On the other hand, the one-to-one correspondence established above allows us to proceed, rigorously, with our nonstandard interpretation of quotient groups.

Appendix C: On the Sum $\mathbb{Z}(T_1) + \mathbb{Z}(T_2)$

This topic is related to the Bezout equation on polynomials. Here, we give a proof of (3.72b) by Alberto Vigato.

We claim that, if T_1/T_2 is rational, say $T_1/T_2 = M/N$ with M and N coprime, then $\mathbb{Z}(T_1) + \mathbb{Z}(T_2) = \mathbb{Z}(T_1/M)$. Dividing both sides of the equality by T_1/M we reduce the statement to proving that

$$\mathbb{Z}(M) + \mathbb{Z}(N) = \mathbb{Z}(1) \quad (3.85)$$

if and only if M and N are coprime.

We first assume that (3.85) holds. Then there exists a pair $a, b \in \mathbb{Z}$ such that $aM + bN = 1$. By taking $k = \text{GCD}(M, N)$ we can write $M = kM'$ and $N = kN'$ for convenient integers M' and N' . Rewriting the Bézout equation $k(aM' + bN') = 1$, we note that k divides 1; thus $k = 1$.

Vice versa, we have $\text{GCD}(M, N) = 1$. Let $\mathcal{P} = \{x, y \in \mathbb{Z} | xM + yN > 0\}$, we take $k = \min_{\mathcal{P}}(xM + yN)$ and $(a, b) \in \mathcal{P} : aM + bN = k$. From Euclidean division, $\exists q, r \in \mathbb{Z}$ with $0 \leq r < k$ such that $M = qk + r$. By rearranging $r = M - qk = M - q(aM + bN) = (1 - qa)M + (-qb)N$, we observe that r is a non-negative combination of M and N . Since k is the minimum positive combination, r must be 0; thus k divides M . Similarly, we also see that k divides N ; thus k divides $\text{GCD}(M, N) = 1$, so k must be 1.

References

1. N. Bourbaki, *General Topology, Parts 1 and 2* (Hermann, Paris, 1966)
2. G. Cariolaro, A unified signal theory (topological approach), in *Proc. of Italy–USA Seminar on Digital Signal Processing*, Portovenere, August 1981
3. J.W.S. Cassels, *An Introduction to the Geometry of Numbers* (Springer, Berlin, 1997)
4. E. Dubois, The sampling and reconstruction of time-varying imagery with application in video systems. *Proc. IEEE* **73**, 502–523 (1985)
5. E.P. Hansen, Theory of circular harmonic image reconstruction. *J. Opt. Soc. Am.* **71**, 304–308 (1981)
6. P. Halmos, *Measure Theory* (Van Nostrand, Princeton, 1950)
7. R. Manducchi, G.M. Cortellazzo, G.A. Mian, Multistage sampling structure conversion of video signals. *IEEE Trans. Signal Process.* **41**, 325–340 (1993)
8. W. Rudin, *Fourier Analysis on Groups* (Interscience, New York, 1962)
9. A. Weil, *L'Integration dans les Groupes Topologiques* (Hermann, Paris, 1940)

Additional Bibliography on Topological Groups

10. N. Bourbaki, *Integration* (Hermann, Paris, 1959)
11. N. Bourbaki, *Theory of Sets* (Addison–Wesley/Hermann, Reading, 1968)
12. A. Haar, Der Massbegriff in der Theorie der kontinuierlichen Gruppen. *Ann. Math.* **34**, 147–169 (1933)

13. E. Hewitt, K.A. Ross, *Abstract Harmonic Analysis*, vols. 1, 2 (Springer, Berlin, 1963)
14. P.J. Higgins, *Introduction to Topological Groups* (Cambridge University Press, London, 1974)
15. L.H. Loomis, *An Introduction to Abstract Harmonic Analysis* (Van Nostrand, New York, 1953)
16. L. Nachbin, *The Haar Integral* (Van Nostrand, Princeton, 1965)
17. A. Orsatti, *Introduzione ai Gruppi Abeliani Astratti e Topologici* (Pitagora Ed., Bologna, 1979)
18. L.S. Pontryagin, *Topological Groups* (Princeton University Press, Princeton, 1946)
19. M. Stroppel, *Locally Compact Groups* (European Mathematical Society, Zurich, 2006)

Chapter 4

Unified Theory: Signal Domain Analysis

Signal Definition Revisited The definition of a signal, introduced at the beginning of the previous chapter, can now be refined in terms of LCA property and dimensionality.

Definition 4.1 A signal $s(t)$ on an LCA quotient group $I = I_0/P$, symbolized $s(t)$, $t \in I$, is a complex function with domain I_0 , having the periodicity property

$$s(t + p) = s(t), \quad \forall p \in P.$$

UT 4.1 The Haar Integral

In Topology, the *Haar measure* is defined on the subsets of LCA groups, and from the measure, the *Haar integral* of complex functions over the group is introduced. This integral is then used to define convolution, Fourier transformation, etc. in a unified form.

In this section, we introduce the Haar integral of a signal $s(t)$, $t \in I$, and symbolize it in the form

$$\int_I dt s(t). \tag{4.1}$$

We follow the line of avoiding abstract notions of Topology, so we do not define the Haar measure and integral, but we give the expressions and the fundamental properties.¹

¹For a simple definition of the Haar integral, which avoids measure theory, we suggest the book by Higgins [9]. At the end of the previous chapter, you may find a bibliography on Topological Groups and the Haar integral.

4.1.1 Fundamental Properties. Existence and Uniqueness

The integral (4.1) has exactly the same properties as the ordinary (Lebesgue) integral on the real line. Specifically:

1. The Haar integral is a *linear functional*;
2. The Haar integral is not identically zero;
3. The Haar integral of a real nonnegative signal is real and nonnegative;
4. The Haar integral is *invariant with respect to the reflection operation*, that is, $s(t)$ and $s_{-}(t) = s(-t)$ have the same integral

$$\int_I dt s(-t) = \int_I dt s(t); \quad (4.2a)$$

5. The Haar integral is *shift-invariant*, that is, $s(t)$ and $s_p(t) = s(t - p)$ have the same integral

$$\int_I dt s(t - p) = \int_I dt s(t), \quad p \in I. \quad (4.2b)$$

The fundamental result is concerned with the existence and uniqueness of the Haar integral (see [13]).

Theorem 4.1 *On every LCA group it is possible to define an integral with properties 1–5. This integral is unique, up to a multiplicative positive constant.*

This theorem allows identifying the Haar integral (without constructing it from the Haar measure) in the specific cases, as soon as we find a functional with properties 1–5. For instance, the Lebesgue integral over \mathbb{R} verifies these properties and therefore it is the Haar integral on \mathbb{R} . On the other hand, the Lebesgue integral over $\mathbb{Z}(T)$ verifies 1, 3, 4, and 5, but not 2 because it is extended to a set of null (Lebesgue) measure and it is identically zero; therefore, it cannot represent the Haar integral on $\mathbb{Z}(T)$. The summation of the signal values over $\mathbb{Z}(T)$ verifies properties 1–5, and therefore it is the Haar integral over $\mathbb{Z}(T)$. In general, to introduce the Haar integral in a given signal class $\mathcal{S}(I)$, we use the following procedure:

- Formulate an expression of the integral for the class $\mathcal{S}(I)$.
- Check that it verifies properties 1–5 of Theorem 4.1.

Then, the expression is the Haar integral. As regards the multiplicative constant, we shall make a precise choice to remove ambiguities and to simplify formulas.

Sometimes the Haar integral is interpreted as the signal *area*. Then (4.2a, 4.2b) becomes

$$\text{area}(s) = \text{area}(s_{-}) = \text{area}(s_p). \quad (4.3)$$

As evident from the symbolism adopted in (4.1), the integral is *extended over the whole group I*. The *integral over a subset A* is obtained using the *indicator function*

$$\eta_A(t) = \begin{cases} 1, & \text{for } t \in A; \\ 0, & \text{for } t \notin A, \end{cases}$$

and it is given by

$$\int_A dt s(t) \triangleq \int_I dt s(t) \eta_A(t). \tag{4.4}$$

4.1.2 Further Properties

The following properties have a general validity.

Integral Over a Quotient Group If we know the Haar integral over an ordinary group I_0 , the Haar integral over the quotient group I_0/P is obtained by limiting the integration over a cell $[I_0/P)$, that is,

$$\int_{I_0/P} dt s(t) = \int_{[I_0/P)} dt s(t) = \int_{I_0} dt s(t) \eta_{[I_0/P)}(t), \tag{4.5}$$

where $\eta_{[I_0/P)}(t)$ is the indicator function of the cell.

Integral Over a Cartesian Product If $I = I_1 \times I_2$ is the Cartesian product of two LCA groups, it is an LCA group and the corresponding Haar integral is given by

$$\int_{I_1 \times I_2} dt s(t) = \int_{I_1} dt_1 \int_{I_2} dt_2 s(t_1, t_2), \tag{4.6}$$

which requires to evaluate first the integral with respect to t_2 and then with respect to t_1 . In particular, when the signal is the *tensor product* of two signals (*separable signal*), $s(t_1, t_2) = s_1(t_1)s_2(t_2)$, the integral is given by the product of two integrals, specifically

$$\int_{I_1 \times I_2} dt_1 dt_2 s_1(t_1)s_2(t_2) = \int_{I_1} dt_1 s_1(t_1) \int_{I_2} dt_2 s_2(t_2). \tag{4.7}$$

This rule is easily generalized to several factors.

Integral Over a Lattice If I is a lattice, the Haar integral is simply given as the summation of the signal values over the lattice, namely

$$\boxed{\int_I dt s(t) = d(I) \sum_{t \in I} s(t)}, \tag{4.8}$$

where $d(I)$ is an arbitrary positive constant. It is customary to set $d(I) = 1$, but we prefer the choice

$$d(I) = \text{determinant of } I. \tag{4.8a}$$

(see Sect. 3.3 for the definition of $d(I)$). For instance, in the 1D lattice $\mathbb{Z}(T)$ the determinant is given by the spacing T , then

$$\int_{\mathbb{Z}(T)} dt s(t) = T \sum_{t \in \mathbb{Z}(T)} s(t). \quad (4.9)$$

Integral Over a Finite Group If $I = I_0/P$ with I_0 a lattice and P a sublattice of I_0 , the combination of rules (4.5) and (4.8) gives

$$\boxed{\int_{I_0/P} dt s(t) = d(I_0) \sum_{t \in [I_0/P]} s(t)}, \quad (4.10)$$

meaning that the Haar integral is the summation of the signal values over a cell $[I_0/P]$ multiplied by the constant $d(I_0)$. Sometimes we simplify the notation $t \in [I_0/P]$ as $t \in I_0/P$ and then

$$\sum_{t \in I_0/P} s(t) \triangleq \sum_{t \in [I_0/P]} s(t). \quad (4.11)$$

Integral from Isomorphism If the integral over a group H is known, we can obtain the integral over an isomorphic group G . This is stated in Appendix A.

4.1.3 Integration Rules

Properties (4.2a, 4.2b) may be viewed as integration rules, which ensure that every variable change of the form $-t \rightarrow t$ and $t - p \rightarrow t$, and hence any combination $\pm t \pm p \rightarrow t$ is permitted.

If I_0 is an ordinary group and P is a sublattice of I_0 , the integral over I_0 can be evaluated in two steps according to the following rule [13, 15] (see Problem 4.1)

$$\int_{I_0} dt s(t) = \int_{I_0/P} du \sum_{p \in P} s(u - p). \quad (4.12a)$$

More generally, if $P \subset P_0 \subset I_0$ we have

$$\int_{I_0/P} dt s(t) = \int_{I_0/P_0} du \sum_{p \in P_0/P} s(u - p), \quad (4.12b)$$

where $s(t)$ has periodicity P .

Multirate Identity If I_0 and P are lattices, with P a sublattice of I_0 , it is possible to express the integral over I_0 in terms of the integral over P , namely

$$\boxed{\int_{I_0} dt s(t) = \frac{1}{N} \sum_{p \in [I_0/P]} \int_P du s(u + p)}, \quad (4.13)$$

where $N = (I_0 : P) = d(P)/d(I_0)$ is the cardinality of the cell $[I_0/P]$ given by the index of P in I_0 (see (3.45)). This identity plays a fundamental role in multirate systems, as we shall see in Chap. 7. It can be proved starting from (4.12a), (4.12b) and using (4.8) and (4.10) (see Problem 4.2).

4.1.4 Haar Measure

The Haar measure is preliminary to the construction of the Haar integral; however, if we know the expression of the Haar integral over a group I , we can obtain the measure of a subset A using the indicator function of A , namely

$$\text{meas}(A) = \int_A dt = \int_I dt \eta_A(t). \quad (4.14)$$

The integral properties (4.2a, 4.2b) ensure that the Haar measure is *reverse* and *shift* invariant, namely

$$\text{meas}(-A) = \text{meas}(A + p) = \text{meas} A. \quad (4.14a)$$

We also find that the measure of an ordinary group is infinity and the measure of a proper quotient group I_0/P is finite, since it is given by the measure of the cell $[I_0/P]$.

Concluding Remarks on Haar Integral

The rules introduced in this section allow the identification of the Haar integral in several cases. For instance, rule (4.8) allows the evaluation of the Haar integral on every kind of lattice and rule (4.10) on every kind of finite group. Also, in the illustration of the integration rules, we have seen the expressions of the Haar integral

on the groups of \mathbb{R} . In particular, for the primitive groups they are given by²

$$\begin{aligned} G = \mathbb{R}, \quad \int_{\mathbb{R}} dt s(t) &= \int_{-\infty}^{+\infty} s(t) dt \quad (\text{Lebesgue integral}), \\ G = \mathbb{Z}, \quad \int_{\mathbb{Z}} dt s(t) &= \sum_{t \in \mathbb{Z}} s(t) \quad (\text{series summation}). \end{aligned} \tag{4.15}$$

From these “primitive” integrals, using the rule (4.6) on the Cartesian product, we can build the Haar integral on primitive multidimensional groups, as \mathbb{R}^2 , $\mathbb{R} \times \mathbb{Z}$, etc. Conceptually, from the integral over the primitive groups, we can obtain the Haar integral on every other LCA groups by isomorphism. The explicit forms will be seen in the next sections for the groups of $\mathcal{Q}(\mathbb{R})$ and $\mathcal{Q}(\mathbb{R}^m)$, and also for multiplicative groups.

A final comment. For the reader that has no knowledge of the Lebesgue integral, we recall that this integral is introduced in a different way than the Riemann integral, but for the purpose of the present book they may be regarded as the same objects, specifically as *linear* functionals mapping a complex function to a complex number.

UT 4.2 Haar Integral on the Groups of \mathbb{R}

In the previous chapter (Sect. 3.3), we have identified the four types of LCA groups on \mathbb{R} that make up the class of LCA quotient groups $\mathcal{Q}(\mathbb{R})$, namely

$$\mathbb{R}, \quad \mathbb{Z}(T), \quad \mathbb{R}/\mathbb{Z}(T_p), \quad \mathbb{Z}(T)/\mathbb{Z}(T_p), \tag{4.16}$$

and the corresponding signal classes:

1. *Aperiodic continuous-time signals* represented on \mathbb{R} ,
2. *Aperiodic discrete-time signals* represented on $\mathbb{Z}(T)$,
- 1(a). *Periodic continuous-time signals* represented on $\mathbb{R}/\mathbb{Z}(T_p)$,
- 2(a). *Periodic discrete-time signal* represented on $\mathbb{Z}(T)/\mathbb{Z}(T_p)$.

Now, we give the Haar integral for each of these classes. The four expressions are collected in Table 4.1, and here we add a few comments.

- $I = \mathbb{R}$

We have the ordinary (Lebesgue) integral extended over \mathbb{R} . This statement has been obtained by the theorem on existence and uniqueness (Theorem 4.1).

- $I = \mathbb{R}/\mathbb{Z}(T_p)$

²The Haar integral on the trivial group $G = \mathbb{O}$ may be defined as $\int_{\mathbb{O}} dt s(t) = s(0)$. However, it will not be used, since \mathbb{O} is the domain of *constant signals*, which have no interest as a class (they find room in any other signal class).

Table 4.1 Expressions of Haar integral on \mathbb{R}

Group	Haar integral	Condition
$I = \mathbb{R}$	$\int_{\mathbb{R}} dt s(t) = \int_{-\infty}^{+\infty} s(t) dt$	
$I = \mathbb{R}/\mathbb{Z}(T_p)$	$\int_{\mathbb{R}/\mathbb{Z}(T_p)} dt s(t) = \int_{t_0}^{t_0+T_p} s(t) dt$	$t_0 \in \mathbb{R}$
$I = \mathbb{Z}(T)$	$\int_{\mathbb{Z}(T)} dt s(t) = \sum_{n=-\infty}^{+\infty} T s(nT)$	
$I = \mathbb{Z}(T)/\mathbb{Z}(T_p)$	$\int_{\mathbb{Z}(T)/\mathbb{Z}(T_p)} dt s(t) = \sum_{n=n_0}^{n_0+N-1} T s(nT)$	$T_p = NT, n_0 \in \mathbb{Z}$

We have again the ordinary integral, but limited to a cell $[\mathbb{R}/\mathbb{Z}(T_p)] = [t_0, t_0 + T_p)$; the instant t_0 is arbitrary since the result is independent of t_0 , due to the periodicity of the signal. This expression is obtained by the general rule (4.5), which gives the integral on a quotient group I_0/P from the integral on I_0 .

- $I = \mathbb{Z}(T)$

We have the sum of the signal values multiplied by the spacing T . This is a consequence of the rule (4.8) of the integral over a lattice (see (4.9)).

- $I = \mathbb{Z}(T)/\mathbb{Z}(T_p)$

The sum of the signal values is limited to a period, that is, to a cell (see rule (4.10))

$$[\mathbb{Z}(T)/\mathbb{Z}(NT)] = \{n_0, n_0 + 1, \dots, n_0 + N - 1\}$$

where $N = T_p/T$ and n_0 is an arbitrary integer.

We suggest the reader to check that all the above expressions are in agreement with the general properties of the Haar integral (and therefore they are actually Haar integrals).

UT 4.3 Haar Integral on the Groups of \mathbb{R}^m

In Sects. 3.3 and 3.7, we have identified the LCA groups of \mathbb{R}^m and, in particular, the class $\mathcal{Q}(\mathbb{R}^m)$ of quotient groups. Correspondingly, we have seen that the number of signal classes increases exponentially with the dimensionality m . In this section, we give an explicit formula of the Haar integral that is valid for all these classes.

4.3.1 General Expression

From the “primitive” integrals (4.15), we construct the Haar integral over a general m D quotient group in three steps:

1. Over the primitive m D group of \mathbb{R}^m ;

2. Over the *ordinary* groups G of $\mathcal{G}_m(\mathbb{R}^m)$;
 3. Over the quotient groups G/P of $\mathcal{Q}(\mathbb{R})$.
1. A primitive group of \mathbb{R}^m has the general form $H = H_1 \times H_2 \times \cdots \times H_m$, where each H_i may be \mathbb{R} or \mathbb{Z} . Hence, considering that H is a Cartesian product, from the composition rule (4.6), the integral over H is explicitly given by

$$\int_H d\mathbf{h} s(\mathbf{h}) = \int_{H_1} dh_1 \cdots \int_{H_m} dh_m s(h_1, \dots, h_m) \quad (4.17)$$

where the i th integral is

$$\int_{H_i} dh_i(\cdot) = \begin{cases} \int_{-\infty}^{+\infty} (\cdot) dh_i, & \text{if } H_i = \mathbb{R}, \\ \sum_{h_i=-\infty}^{+\infty} (\cdot), & \text{if } H_i = \mathbb{Z}. \end{cases} \quad (4.17a)$$

For instance, with $H = \mathbb{R}^2 \times \mathbb{Z}$ we have

$$\int_{\mathbb{R}^2 \times \mathbb{Z}} d\mathbf{h} s(\mathbf{h}) = \int_{-\infty}^{+\infty} \int_{-\infty}^{+\infty} \sum_{h_3=-\infty}^{+\infty} s(h_1, h_2, h_3) dh_1 dh_2.$$

2. An ordinary group G of \mathbb{R}^m specified by the basis–signature representation (\mathbf{G}, H) is generated according to (3.10), that is,

$$G = \{\mathbf{G}\mathbf{h} \mid \mathbf{h} \in H\}$$

where the basis \mathbf{G} is a nonsingular $m \times m$ matrix and the signature H is an m -dimensional primitive group. Then, the group G is isomorphic to its signature H , and we obtain the integral on G from the integral over H , as

$$\boxed{\int_G dt s(t) = d(\mathbf{G}) \int_H d\mathbf{h} s(\mathbf{G}\mathbf{h})} \quad (4.18)$$

where the multiplicative constant is $d(\mathbf{G}) = |\det(\mathbf{G})|$.

3. Having obtained the integral over an ordinary group G , we apply rule (4.5) to get the integral over a quotient group G/P , that is,

$$\boxed{\int_{G/P} dt s(t) = \int_{[G/P]} dt s(\mathbf{t}) = \int_G dt s(\mathbf{t}) \eta_{[G/P]}(\mathbf{t})} \quad (4.19)$$

where the integral is limited to a cell $[G/P]$.

This completes the evaluation of the Haar integral over a general group of $\mathcal{Q}(\mathbb{R}^m)$, where the final result is given by a mixture of ordinary integrals over \mathbb{R} and series summations. Moreover, for the consistency of the result some conceptual refinements are needed. In (4.18), the integral over an ordinary group appears to be dependent on the group basis \mathbf{G} , which is not unique. But in Appendix B we prove

that *the integral over G is independent of the basis \mathbf{G}* . In (4.19), the integral over a quotient group G/P is obtained by limiting the integral over a cell $C = [G/P]$, which is not unique. But again, in Appendix B we prove that *the integral over G/P is independent of the particular cell used in its evaluation*.

The choice of $d(\mathbf{G})$ as the positive constant in (4.18) finds the following motivations:

- To make sure that the Haar integral is independent of the group representation (see Appendix B);
- To simplify and harmonize formulas, particularly in connection with the frequency domain (see Chap. 5);
- To give the same physical dimensions to all signals of a given dimensionality m , when signals are interpreted in a physical context, as we can check in Table 4.1 for a 1D signal and in Table 4.2 for 2D signals.

4.3.2 Expressions Over Ordinary Groups

The general formula (4.18) of the integral over an ordinary group G gives the following expressions.

- Integral over \mathbb{R}^m .

It is the ordinary Lebesgue integral on \mathbb{R}^m

$$\int_{\mathbb{R}^m} d\mathbf{t} s(\mathbf{t}) = \int_{-\infty}^{+\infty} \cdots \int_{-\infty}^{+\infty} s(t_1, \dots, t_m) dt_1 \cdots dt_m. \quad (4.20)$$

This follows from (4.17), or from rules (4.6) on the Cartesian product.

- Integral over a lattice L (see rule (4.8)).

It is given by an m -dimensional summation

$$\int_L d\mathbf{t} s(\mathbf{t}) = d(L) \sum_{t_1=-\infty}^{+\infty} \cdots \sum_{t_m=-\infty}^{+\infty} s(t_1, \dots, t_m) \quad (4.21)$$

where $d(L)$ is the lattice determinant.

- Integral over a grating G .

⇓ This topic will be considered in detail in Chap. 16. Here, for completeness, we outline the result. Considering a grating G with signature $\mathbb{R}^p \times \mathbb{Z}^q$ and using the *canonical* basis

$$\mathbf{G}_0 = \begin{bmatrix} \mathbf{I} & \mathbf{0} \\ \mathbf{E} & \mathbf{F} \end{bmatrix}, \quad (4.22)$$

Table 4.2 Haar integrals for 2D signals

Signal class	Signatures	Group	Haar integral
1(a). continuous-argument aperiodic	$\mathbb{R}^2/\mathbb{O}^2$	\mathbb{R}^2	$\int_{-\infty}^{+\infty} \int_{-\infty}^{+\infty} s(t_1, t_2) dt_1 dt_2$
1(b). continuous-argument periodic	$\mathbb{R}^2/\mathbb{Z}^2$	\mathbb{R}^2/P	$\iint_P s(t_1, t_2) dt_1 dt_2$
1(c). continuous-argument partially periodic	$\mathbb{R}^2/\mathbb{O} \times \mathbb{Z}$	\mathbb{R}^2/P_1	$\iint_{P_1} s(t_1, t_2) dt_1 dt_2$
2(a). discrete-argument aperiodic	$\mathbb{Z}^2/\mathbb{O}^2$	L	$\sum_{(t_1, t_2) \in L} d(L) s(t_1, t_2)$
2(b). discrete-argument periodic	$\mathbb{Z}^2/\mathbb{Z}^2$	L/P	$\sum_{(t_1, t_2) \in [L/P]} d(L) s(t_1, t_2)$
2(c). discrete-argument partially periodic	$\mathbb{Z}^2/\mathbb{O} \times \mathbb{Z}$	L/P_1	$\sum_{(t_1, t_2) \in [L/P_1]} d(L) s(t_1, t_2)$
3(a). mixed-argument aperiodic	$\mathbb{R} \times \mathbb{Z}/\mathbb{O}^2$	G	$\int_{-\infty}^{+\infty} \sum_{n=-\infty}^{+\infty} E s(r, Fr + nE) dr$
3(b). mixed-argument periodic	$\mathbb{R} \times \mathbb{Z}/\mathbb{Z}^2$	G/P	$\int_0^{D_1} \sum_{n=0}^{N-1} E s(r, Fr + nE) dr$
3(c). mixed-argument partially periodic	$\mathbb{R} \times \mathbb{Z}/\mathbb{Z} \times \mathbb{O}$	G/P_1	$\int_0^{D_1} \sum_{n=-\infty}^{+\infty} E s(r, Fr + nE) dr$
3(d). mixed-argument partially periodic	$\mathbb{R} \times \mathbb{Z}/\mathbb{O} \times \mathbb{Z}$	G/P_1	$\int_{-\infty}^{+\infty} \sum_{n=0}^{N-1} E s(r, Fr + nE) dr$

Note: L : 2D lattice; P : 2D lattice; G : 2D grating; P_1 : 1D lattice (in \mathbb{R}^2)

the Haar integral is given by

$$\int_G dt s(\mathbf{t}) = d(\mathbf{F}) \int_{\mathbb{R}^p} d\mathbf{r} \sum_{\mathbf{n} \in \mathbb{Z}^q} s(\mathbf{r}, \mathbf{E}\mathbf{r} + \mathbf{F}\mathbf{n}). \tag{4.23}$$

This represents the general formula over an ordinary group and gives (4.20) and (4.21) as particularization.

4.3.3 Expressions for 2D Signals

In Sect. 3.7 (Table 3.1), we have seen explicitly the $\mathcal{N}_2 = (2 + 1)^2 = 9$ classes of 2D signals, and now, from the general formulas, we can write their Haar integrals. The complete results are collected in Table 4.2 and comments follow.

Integral of a Continuous 2D Signal

For aperiodic 2D signals, the integral is over \mathbb{R}^2 and it is given by the 2D ordinary (Lebesgue) integral. In the presence of a full periodicity P , the ordinary integral

is limited to a cell $[\mathbb{R}^2/P]$, which may be the fundamental parallelepiped of the lattice P (see Sect. 3.5). In the case of a partial periodicity, P_1 is a 1D lattice in \mathbb{R}^2 , and the cell $[\mathbb{R}^2/P_1]$ becomes a strip of the \mathbb{R}^2 plane (see Sect. 3.5).

Integral of a Discrete 2D Signal

For aperiodic 2D signals, the integral over a lattice L is simply given by the summation of the signal values multiplied by the lattice determinant $d(L)$. In general, a double series is involved in the summation. For instance, if $L = \mathbb{Z}_3^1(d_1, d_2)$, the generic point is $(t_1, t_2) = (m3d_1, (m+n)d_2)$, with $m, n \in \mathbb{Z}$, and then

$$\sum_{(t_1, t_2) \in L} d(L) s(t_1, t_2) = \sum_{m=-\infty}^{+\infty} \sum_{n=-\infty}^{+\infty} 3d_1 d_2 s(m3d_1, (m+n)d_2).$$

In the presence of a full periodicity P , the summation is limited to a cell $C = [L/P]$, which has a finite cardinality $d(P)/d(L)$ (see Sect. 3.5 for examples of such cells). When the periodicity is partial, the cell $[L/P_1]$ is given by the points of L belonging to a strip and has infinitely many points. For instance, with $L = \mathbb{Z}_3^1(d_1, d_2)$ and $P_1 = \mathbb{Z}(9d_1) \times \mathbb{O}$, we have explicitly

$$\sum_{(t_1, t_2) \in [L/P_1]} d(L) s(t_1, t_2) = 3d_1 d_2 \sum_{m=-\infty}^{+\infty} \sum_{n=0}^2 s(3md_1, (m+n)d_2).$$

Integral of a Mixed-Argument 2D Signal

The canonical representation of the grating given by (4.22) becomes

$$\mathbf{G}_0 = \begin{bmatrix} 1 & 0 \\ E & F \end{bmatrix}, \quad (t_1, t_2) = (r, Er + nF), \quad r \in \mathbb{R}, n \in \mathbb{Z} \quad (4.24)$$

where E and F are scalars. Then, the integral is given by

$$\int_G dt s(t) = F \int_{-\infty}^{+\infty} \sum_{n=-\infty}^{+\infty} s(r, Er + nF) dr. \quad (4.25)$$

In the presence of a full periodicity P , both the integral and the summation in (4.25) must be limited, whereas with a partial periodicity P_1 the limitation is confined to only one of the two coordinates.

4.3.4 Haar Integral with a Coordinate Change

In \mathbb{R}^m and its subgroups, it is possible to perform a coordinate change of the signal argument of the form

$$y(\mathbf{t}) = s(\mathbf{a}\mathbf{t}) \quad (4.26)$$

where $\mathbf{a} = [a_{rs}]$ is an $m \times m$ nonsingular real matrix and \mathbf{t} must be interpreted as a column vector. This coordinate change has the form

$$\mathbf{u} = \mathbf{a}\mathbf{t} \quad (\mathbf{t} = \mathbf{a}^{-1}\mathbf{u}) \quad (4.27)$$

where \mathbf{u} is the argument of the original signal $s(\mathbf{u})$ and \mathbf{t} is the argument after the coordinate change. In general, this operation changes the signal domain. If G is the domain of $s(\mathbf{u})$, the domain $G_{\mathbf{a}}$ of $y(\mathbf{t})$ is given by

$$G_{\mathbf{a}} = \{\mathbf{t} \mid \mathbf{a}\mathbf{t} \in G\} = \{\mathbf{a}^{-1}\mathbf{u} \mid \mathbf{u} \in G\} \quad (4.28)$$

and briefly $G_{\mathbf{a}} = \mathbf{a}G$. For the Haar integral we have:

Theorem 4.2 *The Haar integral after the coordinate change $\mathbf{u} = \mathbf{a}\mathbf{t}$ is given by*

$$\boxed{\int_{G_{\mathbf{a}}} d\mathbf{t} y(\mathbf{t}) = \int_{G_{\mathbf{a}}} d\mathbf{t} s(\mathbf{a}\mathbf{t}) = \frac{1}{d(\mathbf{a})} \int_G d\mathbf{u} s(\mathbf{u})}, \quad (4.29)$$

where $d(\mathbf{a}) = |\det \mathbf{a}|$.

The proof is given in Appendix C. Here, we simply note that when $G = \mathbb{R}^m$ the coordinate change transforms \mathbb{R}^m into \mathbb{R}^m itself, so that the domain does not change. Moreover, from (4.27) we have the relation for the differentials $d\mathbf{u} = d(\mathbf{a}) d\mathbf{t}$, where $d(\mathbf{a})$ is the Jacobian of the coordinate change.

When $I = G/P$ is a quotient group, the coordinate change modifies both the basis group and the modulus according to $G_{\mathbf{a}} = \mathbf{a}G$ and $P_{\mathbf{a}} = \mathbf{a}P$ and (4.29) still holds with G and $G_{\mathbf{a}}$ replaced respectively by G/P and $G_{\mathbf{a}}/P_{\mathbf{a}}$.

The coordinate change will be revisited on Chap. 6 in terms of transformations.

⇓ 4.4 Haar Integral Over Multiplicative Groups

In Sect. 3.8, we have introduced three multiplicative groups:

- The multiplicative group \mathbb{R}_p of positive real numbers, which is isomorphic to the additive group \mathbb{R} , according to

$$\exp : \mathbb{R} \rightarrow \mathbb{R}_p; \quad (4.30)$$

- The multiplicative group Γ of the complex numbers z with $|z| = 1$, which is isomorphic to $\mathbb{R}/\mathbb{Z}(2\pi)$, according to

$$\exp(i\cdot) : \mathbb{R}/\mathbb{Z}(2\pi) \rightarrow \Gamma;$$

- The multiplicative group \mathbb{C}^* of nonzero complex numbers, which is the Cartesian product of the two groups above

$$\mathbb{C}^* = \mathbb{R}_p \times \Gamma. \quad (4.31)$$

4.4.1 Haar Integral Over \mathbb{R}_p

The Haar integral over \mathbb{R}_p can be obtained by means of the isomorphism (4.30). The application of Theorem 4.10 of Appendix A, with $G = \mathbb{R}_p$, $H = \mathbb{R}$, $t = \alpha(h) = \exp(h)$, and $\mu_G = 1$, gives

$$\int_{\mathbb{R}_p} dt s(t) = \int_{\mathbb{R}} dh s(e^h) = \int_{-\infty}^{+\infty} s(e^h) dh.$$

Then, letting $t = e^h$ we obtain

$$\boxed{\int_{\mathbb{R}_p} dt s(t) = \int_0^{\infty} s(t) \frac{dt}{t}}, \quad (4.32)$$

where on the right the Lebesgue integral is over $(0, +\infty)$ and the signal is divided by the argument t .

The Haar integral over $\mathbb{R}_p/\mathbb{Z}_p(\Delta)$ is obtained by limiting the previous integral to a cell $[\mathbb{R}_p/\mathbb{Z}_p(\Delta)]$ (see (4.5)). Note that such a cell may be the interval $[1, \Delta)$ and, more generally, the interval $[h, h\Delta)$ with $h > 0$ arbitrary. In fact, recalling that the group operation is the multiplication, we find that the interval sequence $[ph, ph\Delta)$, with $p \in \mathbb{Z}_p(\Delta)$, is a partition of \mathbb{R}_p .

In conclusion, the Haar integral over $\mathbb{R}_p/\mathbb{Z}_p(\Delta)$ is given by

$$\int_{\mathbb{R}_p/\mathbb{Z}_p(\Delta)} dt s(t) = \int_h^{h\Delta} s(t) \frac{dt}{t}. \quad (4.33)$$

The evaluation of the integral over discrete groups is immediately found from (4.8). For convenience, we choose $d(I) = \log \Delta$, so that, Theorem 4.10 holds with $\mu_G = 1$, then

$$\int_{\mathbb{Z}_p(\Delta)} dt s(t) = \log \Delta \sum_{t \in \mathbb{Z}_p(\Delta)} s(t) = \log \Delta \sum_{n=-\infty}^{+\infty} s(\Delta^n). \quad (4.34)$$

Finally, the integral over $\mathbb{Z}_p(\Delta)/\mathbb{Z}_p(\Delta^N)$ is obtained from (4.34) by limiting the summation to a period.

4.4.2 Haar Integral Over Γ and \mathbb{C}^*

Considering the isomorphism $\alpha(h) = \exp(ih) : H = \mathbb{R}/\mathbb{Z}(2\pi) \rightarrow G = \Gamma$, from Theorem 4.10 we have that the Haar integral over Γ is given by (setting $\mu_G = 1$)

$$\int_{\Gamma} dt s(t) = \int_{\mathbb{R}/\mathbb{Z}(2\pi)} dh s(\alpha(h)) = \int_0^{2\pi} s(e^{ih}) dh. \quad (4.35)$$

Finally, we have the Haar integral on \mathbb{C}^* as a composition of the previous integrals (see the composition rule (4.6) and (4.31))

$$\int_{\mathbb{C}^*} dt s(t) = \int_{\mathbb{R}_p} dt_1 \int_{\Gamma} dt_2 s(t_1, t_2) = \int_0^{\infty} \int_0^{2\pi} s(t_1, e^{ih}) \frac{dt_1}{t_1} dh. \quad (4.36)$$

UT 4.5 Class of Signals and Vector Spaces

For any domain/periodicity $I = I_0/P$, we introduced the class $\mathcal{S}(I)$ of “all the signals defined on the group I_0 that have periodicity P ”. According to our convention, “signal” is synonymous with “complex function”. Hence, $\mathcal{S}(I)$ is a class of complex functions (including also generalized functions).

This class has an *algebraic structure*, since it is closed with respect to operations such as the sum and, more generally, a linear combination of signals with complex coefficients belongs to this class. We formalize this stating that $\mathcal{S}(I)$ is a *vector space* (or *linear space*) over the field of complex numbers \mathbb{C} .

An additional requirement may be a geometrical structure where signals can be compared and this is provided by the *inner product*. To this end, we have to restrict the class $\mathcal{S}(I)$ to the subclass $L_2(I)$ of square integrable signals, where the inner product can be defined by the Haar integral. Thus, the subclass $L_2(I)$ will be formalized as an *inner product vector space*. A final requirement is related to convergence and completeness, leading to the concept of a *Hilbert space*.

A preliminary remark on notation. In our convention, a signal is denoted either in the form $s(t)$, $t \in I$, or with the equivalent notation $s \in \mathcal{S}(I)$, but the latter is more convenient in approaching vector spaces, where s becomes a *vector* in the space.

Proposition 4.1 *For every quotient group I , the class $\mathcal{S}(I)$ is a vector space over the complex field \mathbb{C} .*

The above assertion can be easily proved by verifying that the following axioms of a vector space over \mathbb{C} hold for $\mathcal{S}(I)$:

1. *Commutativity*: $x + y = y + x$, for all $x, y \in \mathcal{S}(I)$.
2. *Associativity*: $(x + y) + z = x + (y + z)$ and $(ab)x = a(bx)$, for all $x, y, z \in \mathcal{S}(I)$ and $a, b \in \mathbb{C}$.
3. *Distributivity*: $a(x + y) = ax + ay$ and $(a + b)x = ax + bx$.

4. *Additive identity*: there exists 0 in $\mathcal{S}(I)$, such that $x + 0 = x$, for all x in $\mathcal{S}(I)$.
5. *Additive inverses*: for all x in $\mathcal{S}(I)$, there exists a $(-x)$ in $\mathcal{S}(I)$, such that $x + (-x) = 0$.
6. *Multiplicative identity*: $1 \cdot x = x$ for all x in $\mathcal{S}(I)$.

Note that in $\mathcal{S}(I)$ the element 0 is the signal which is identically zero. Conditions 1, 2, 4, and 5 assure that a vector space is an Abelian group.

We now introduce a few specific definitions related to the properties of vector spaces.

Subspaces A nonempty subset A of $\mathcal{S}(I)$ is a *subspace* of $\mathcal{S}(I)$ if A itself is a vector space with the same operations of addition and scalar multiplication. Note that the subset $\{0\}$ consisting of only the zero signal is a subspace.

Example 4.1 The class $E(I)$ of signals on I with even symmetry is a subspace. In fact, it is closed with respect to the sum and multiplication by a scalar. The same holds for the class $O(I)$ of the odd signals on I .

Span Given a nonempty subset $A \subset \mathcal{S}(I)$, the *span* of A is the subspace of $\mathcal{S}(I)$ consisting of all linear combinations of vectors in A . If A is countable, that is, $A = \{x_n \mid n \in \mathcal{N}\}$, where \mathcal{N} is an index set, the span is explicitly given by

$$\text{span}(A) = \left\{ \sum_{n \in \mathcal{N}} a_n x_n \mid a_n \in \mathbb{C} \right\}.$$

The index set \mathcal{N} may be finite or countably infinite, for example,

$$\mathcal{N} = \{0, 1, \dots, N-1\}, \quad \mathcal{N} = \mathbb{N}_0 \triangleq \{0, 1, 2, \dots\},$$

$$\mathcal{N} = \mathbb{Z} = \{\dots, -1, 0, 1, \dots\},$$

or a multidimensional extension of these forms.

Linear Independence The signals x_1, \dots, x_k are *linearly independent*, if

$$\sum_{n=1}^k a_n x_n = 0, \quad a_n \in \mathbb{C},$$

holds only if $a_n = 0$ for all n . Otherwise, these signals are *linearly dependent*. If there are infinitely many signals x_1, x_2, \dots , they are linearly independent if x_1, x_2, \dots, x_k are linearly independent, for each k .

Bases and Dimensionality A collection of signals in the vector space V , $\Phi = \{\varphi_n \mid n \in \mathcal{N}\}$ is a basis for V if

1. Φ consists of linear independent signals, and
2. $\text{span}(\Phi) = V$.

It can be shown [12] that every vector space V has a basis (with the exception of the trivial space $\{0\}$) and all the bases have the same cardinality. The common cardinality of the bases of V defines the dimension of the vector space V . Hence, V is *finite-dimensional* if $|\Phi|$ is finite, otherwise V is *infinite-dimensional*.

The Class of Real Signals $\mathcal{S}_{\mathbb{R}}(I)$ This is not a subspace of $\mathcal{S}(I)$ because the linear combination of real signals with complex coefficients is not a real signal, in general. The class $\mathcal{S}_{\mathbb{R}}(I)$ can be formalized as a vector space *over the real field* \mathbb{R} .

4.5.1 The Class of Integrable Signals

In the context of UST “integral” means “Haar integral”. As regards the existence of the Haar integral of a specific signal, we recall that a signal may be integrable or not. This is also the case of a signal defined on a lattice, where the Haar integral is given by the sum of a series, which may converge or not. The only case in which the integrability is assured is on finite groups, where the Haar integral is the sum of finitely many terms.

The Haar integral allows the introduction of the following subclasses of $\mathcal{S}(I)$. For every positive real number p , $L_p(I)$ is the subclass of signals for which the integral $\int_I dt |s(t)|^p$ exists and is finite. Within $L_p(I)$ the p -norm can be naturally defined as

$$\|s\|_p \triangleq \left\{ \int_I dt |s(t)|^p \right\}^{1/p}. \quad (4.37)$$

Analogously, we can define the classes $L_p(A)$, where A is a measurable subset of I (see (4.4)), and any statement on $L_p(I)$ can be equally stated for $L_p(A)$, unless otherwise noted. In particular, $L_1(I)$ is the subclass of *absolutely integrable signals* and $L_2(I)$ that of *square integrable signals*.

Proposition 4.2 *The class $L_p(I)$ with the ordinary operations of signal sum and multiplication by a complex scalar is a vector space on \mathbb{C} . Hence $L_p(I)$ is a subspace of the vector space $\mathcal{S}(I)$.*

The proof is given in Appendix D.

4.5.2 The Class $L_2(I)$ as an Inner Product Vector Space

Particularly important in Signal Theory is the $L_2(I)$ class, where the norm³ $\|s\| \triangleq \|s\|_2$ is given by

$$\|s\| = \sqrt{\int_I dt |s(t)|^2}. \quad (4.38)$$

In $L_2(I)$, it is possible to introduce the *inner product* of two signals in the form

$$\langle x, y \rangle \triangleq \int_I dt x(t)y^*(t). \quad (4.39)$$

The inner product $\langle x, y \rangle$ is also called the *cross-energy* E_{xy} between the signals x and y . For $x(t) = y(t)$, that is,

$$E_x \triangleq \langle x, x \rangle = \|x\|^2 = \int_I dt |x(t)|^2, \quad (4.40)$$

it becomes the *energy* (or self-energy) of $x(t)$, $t \in I$.

The reader can check that the inner product (4.39) verifies the axioms of inner product, that is, for x, y, z signals of $L_2(I)$ and $a \in \mathbb{C}$ the following properties hold:

1. $\langle x + y, z \rangle = \langle x, z \rangle + \langle y, z \rangle$;
2. $\langle ax, y \rangle = a \langle x, y \rangle$, $a \in \mathbb{C}$;
3. $\langle x, y \rangle^* = \langle y, x \rangle$;
4. $\langle x, x \rangle \geq 0$, and $\langle x, x \rangle = 0$ if and only if $x \equiv 0$.

It is clear that the inner product $\langle x, y \rangle$ is *linear* with respect to the first signal, while $\langle x, ay \rangle = a^* \langle x, y \rangle$. Then

Proposition 4.3 *The class $L_2(I)$ of square integrable functions is an inner product vector space over \mathbb{C} , with the inner product defined by (4.39).*

The inner product and the norm allow the introduction of orthogonality and orthonormality, and also of important inequalities. The following properties of inner product spaces can therefore be introduced for the class $L_2(I)$.

Inequalities on $L_2(I)$

A first inequality is the *Cauchy–Schwartz inequality* (briefly *Schwartz inequality*)

$$|\langle x, y \rangle| \leq \|x\| \|y\|, \quad (4.41a)$$

³From now on, we will mainly deal with the 2-norm and simply call it the norm for convenience.

where equality holds if and only if the two signals are proportional to each other, that is, $y(t) = \alpha x(t)$ with $\alpha \in \mathbb{C}$. Explicitly, by using (4.39), we have

$$\left| \int_I dt x(t)y^*(t) \right|^2 \leq \int_I dt |x(t)|^2 \int_I dt |y(t)|^2. \quad (4.41b)$$

An alternative form of (4.41a), (4.41b) is the *Schwartz–Gabor inequality* [7]

$$\left| \int_I dt [x(t)y^*(t) + x^*(t)y(t)] \right|^2 \leq 4 \int_I dt |x(t)|^2 \int_I dt |y(t)|^2, \quad (4.42)$$

where the equality holds if, and only if $y(t) = \beta x(t)$, with β real valued (see Problem 4.14), whereas in the Schwartz inequality the proportionality constant α may be complex.

Orthogonality

Two signals $x, y \in L_2(I)$ are said to be *orthogonal* (in symbols $x \perp y$) if

$$\langle x, y \rangle = 0.$$

Two subspaces A and B of $L_2(I)$ are called orthogonal, and symbolized $A \perp B$, if all the signals in A are orthogonal to all the signals in B . A countable set of signals $B = \{\beta_n \mid n \in \mathcal{N}\}$, such as a basis of $L_2(I)$, is called *orthogonal* if $\beta_i \perp \beta_j$ when $i \neq j$. If all the signals β_i have unit norm, the set $B = \{\beta_n \mid n \in \mathcal{N}\}$ is called *orthonormal*. Given a subspace A , the *orthogonal complement* of A in $L_2(I)$, denoted A^\perp , is the subset of signals that are orthogonal to all signals in A . Then, given a signal s in $L_2(I)$, there exist a unique signal $s_A \in A$ and a unique signal $s_A^\perp \in A^\perp$ such that $s = s_A + s_A^\perp$; s_A is called the *orthogonal projection of s onto A* . Thus, we can write $L_2(I)$ as the *direct sum* of the subspace and its orthogonal complement, symbolized

$$L_2(I) = A \oplus A^\perp.$$

The above concepts are illustrated in Fig. 4.1.

Theorem 4.3 (Projection Theorem) *Given a signal $s \in L_2(I)$ and a subspace $A \subset L_2(I)$, the closest signal to s in A is the orthogonal projection s_A of s onto A . In symbols,*

$$\arg \min_{y \in A} \|s - y\| = s_A \quad (4.43)$$

where

$$s = s_A + s_A^\perp$$

with $s_A \in A$, $s_A^\perp \in A^\perp$.

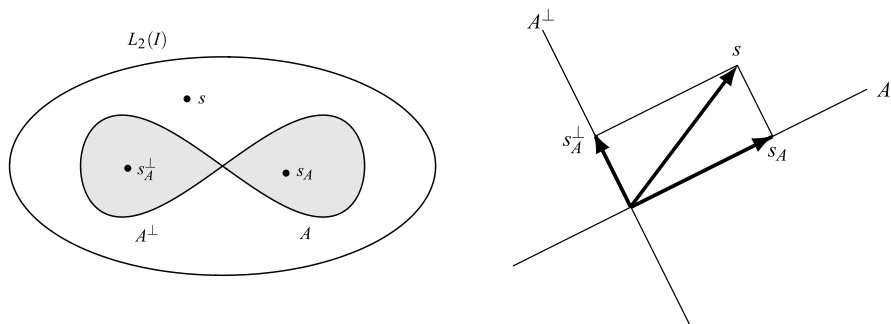


Fig. 4.1 In the space $L_2(I)$, the subspaces A and A^\perp are orthogonal to each other. A signal s in $L_2(I)$ is uniquely decomposed as $s = s_A + s_A^\perp$, where s_A is the *orthogonal projection* of s onto A and s_A^\perp is orthogonal to s_A

The proof is straightforward by considering the squared norm of $s - y$ and writing s as in (4.43) obtaining

$$\|s - y\|^2 = \|s_A - y + s_A^\perp\|^2 = \|s_A - y\|^2 + \|s_A^\perp\|^2$$

where the last equality is due to s_A^\perp being orthogonal to $s_A - y \in A$. Then the right hand side is minimized by taking $y = s_A$.

Example 4.2 We illustrate the above definitions and statements considering the classes of even and odd signals defined on an LCA quotient group I . Then, the environment is the class $L_2(I)$. The classes of even and odd signals are respectively

$$E(I) = \{s \mid s(-t) = s(t)\} \quad \text{and} \quad O(I) = \{s \mid s(-t) = -s(t)\}.$$

It is easy to see that $E' = E(I) \cap L_2(I)$ and $O' = O(I) \cap L_2(I)$ are subspaces of $L_2(I)$ and E' is orthogonal to O' . It is perhaps a little subtler to show that O' is the *orthogonal complement* to E' , that is, any signal orthogonal to all even signals must have odd symmetry. In fact, let s be such a signal. Then it can be decomposed (see Chap. 2) as

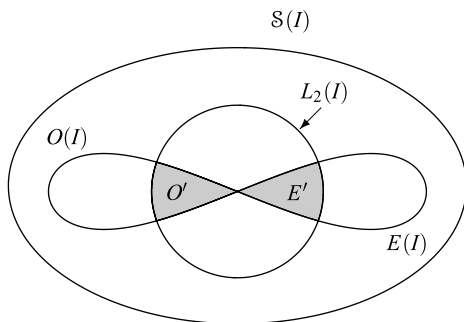
$$s(t) = s_E(t) + s_O(t)$$

with $s_E(t)$ even and $s_O(t)$ odd. By the inner product additivity, we have $\langle s, s_E \rangle = \langle s_E, s_E \rangle + \langle s_E, s_O \rangle$. Since it must be $\langle s, s_E \rangle = 0$ and $\langle s_E, s_O \rangle = 0$, we must also have $\langle s_E, s_E \rangle = 0$, which only holds if $s_E(t) = 0$, for all $t \in I$. Thus, $s = s_O$ is odd. Also $E' \cap O' = \{0\}$, which states that the class E' and O' have only the zero signal in common. These interrelations are illustrated in Fig. 4.2.

As a consequence of orthogonality, we have that every signal in $L_2(I)$ can be uniquely decomposed in an even component and an odd component, as summarized by

$$E \oplus O = L_2(I).$$

Fig. 4.2 The classes E' and O' of even and odd square integrable signals are orthogonal complements in $L_2(I)$



This was seen in the Classic Theory (Sects. 2.1 and 2.9), and will be reconsidered in Sect. 4.13 in the context of symmetries.

4.5.3 The Class $L_2(I)$ as a Hilbert Space

We have seen that the classes $L_2(I)$, where I is an arbitrary LCA quotient group, are inner product vector spaces. One more notion is needed in order to obtain a Hilbert space, that is, *completeness*. To this end, we consider sequences of signals $\{x_n\}$ in $L_2(I)$, which are said to *converge* to a signal x in $L_2(I)$ if $\|x_n - x\| \rightarrow 0$ as $n \rightarrow \infty$. A sequence of signals $\{x_n\}$ is called a *Cauchy sequence*, if $\|x_n - x_m\| \rightarrow 0$, when $n, m \rightarrow \infty$. If every Cauchy sequence in $L_2(I)$ converges to a signal in $L_2(I)$, then $L_2(I)$ is said to be *complete*, and, by definition, it is called a *Hilbert space*. The fundamental statement is

Proposition 4.4 *For every LCA quotient group I , the class of square summable signals $L_2(I)$ is a Hilbert space.*

For a general proof, see [13]. Here we show that the statement holds for two cases of particular interest.

The Class $L_2(I)$ on a Finite Group $I = I_0/P$ This class contains all the signals defined on I , that is, $L_2(I) = \mathcal{S}(I)$. In fact, signals of $\mathcal{S}(I)$ are specified by their values in a cell $[I_0/P]$ of finite cardinality N , that is, by N -tuples of complex numbers. For instance, a signal $s(t)$ of the class $L_2(\mathbb{Z}(T)/\mathbb{Z}(NT))$ is specified by the values in $\mathbb{Z}_N(T) = \{0, T, \dots, N-1\}$, that is, by the N -tuple of complex numbers $\mathbf{s} = (s_0, s_1, \dots, s_{N-1})$ with $s_i = s(iT)$. According to (4.39), the inner product in $L_2(\mathbb{Z}(T)/\mathbb{Z}(N))$ is

$$\langle x, y \rangle = \sum_{n=0}^{N-1} T x(nT) y^*(nT) = \langle \mathbf{x}, \mathbf{y} \rangle .$$

Then $L_2(I)$ is isomorphic to \mathbb{C}^N , which is known to be complete.

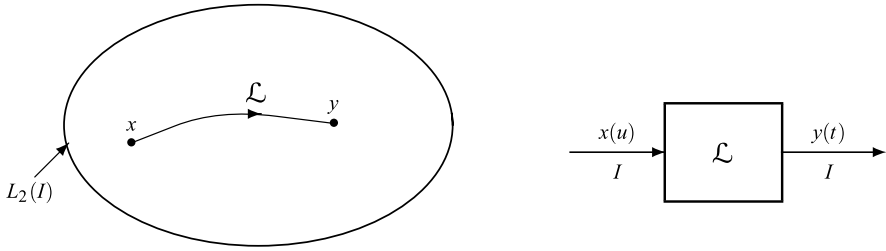


Fig. 4.3 Interpretation of a linear operator \mathcal{L} as a mapping (left) and graphical symbol (right)

The Class $L_2(\mathbb{Z}(T))$ This is a proper subclass of $\mathcal{S}(\mathbb{Z}(T))$, the class of discrete time signals, and in the literature it is usually called the *space of square summable sequences* and denoted by ℓ_2 . Also, it represents the classical example of an infinite dimensional Hilbert space introduced by Hilbert himself. The class $L_2(\mathbb{Z}(T))$ consists of the signals s such that $\|s\|^2 = \sum_{n=-\infty}^{+\infty} T|s(nT)|^2 < \infty$, which means that the series involved must converge to a finite limit. But, to form a Hilbert space a further condition is required, that is, for any sequence of signals $s_i = s_i(nT)$ of $L_2(\mathbb{Z}(T))$, such that $\|s_i - s_j\| \rightarrow 0$, there should exist a limit s in $L_2(\mathbb{Z}(T))$ such that $\|s_i - s\| \rightarrow 0$. This is proved in several textbooks, see, e.g., [8].

4.5.4 Linear Operators in Hilbert Spaces

This topic will be seen in great detail in Chap. 6 in the framework of linear transformations, and here we anticipate a few concepts on linear operators which form an important class of linear transformations.

A linear operator is a mapping $\mathcal{L} : H \rightarrow H$ in a Hilbert space H , in the present context $L_2(I)$, that verifies the linearity condition $\mathcal{L}[ax + by] = a\mathcal{L}[x] + b\mathcal{L}[y]$, where $x, y \in L_2(I)$ and $a, b \in \mathbb{C}$. In the mapping $y = \mathcal{L}[x]$, it is convenient to think of x and y as the *input signal* and the *output signal*, respectively, as sketched in Fig. 4.3.

A linear operator is governed by the following relationship

$$\mathcal{L} \quad y(t) = \int_I du h(t, u)x(u), \quad t \in I, \tag{4.44}$$

which gives the output signal $y(t)$, $t \in I$, starting from the input signal $x(u)$, $u \in I$; $h(t, u)$ is called the *kernel* of the linear operator \mathcal{L} . Note that in this relation we must keep the distinction between the input time $u \in I$ and the output time $t \in I$. The *cascade* of two operators \mathcal{L}_1 and \mathcal{L}_2 is defined as the operator $\mathcal{L} = \mathcal{L}_2\mathcal{L}_1$, which, starting from x , gives $y = \mathcal{L}_1[x]$ and $z = \mathcal{L}_2[y]$, so globally, $z = \mathcal{L}_2[\mathcal{L}_1[x]]$. It will be shown in Sect. 6.3 that the kernel of \mathcal{L} can be calculated from the component kernels $h_i(t, u)$ as

$$h(t, u) = \int_I dv h_2(t, v)h_1(v, u). \tag{4.45}$$

A trivial linear operator is the *identity* on I , symbolized \mathcal{J} , which maps every signal $x \in L_2(I)$ into itself, that is, $\mathcal{J}[x] = x$. Its kernel is given by

$$h_{\mathcal{J}}(t, u) = \delta_I(t - u)$$

where $\delta_I(t)$ is the *impulse* on I (see Sect. 4.9). Another simple operator is the reflector \mathcal{J}_- , which provides the axis inversion of a signal. Its kernel is $\delta_I(t + u)$.

The class of signals mapped by an operator \mathcal{L} is called the *image* of \mathcal{L} , symbolized

$$\text{im}(\mathcal{L}) = \{\mathcal{L}[s] \mid s \in L_2(I)\}. \quad (4.46)$$

Given an operator \mathcal{L} with a kernel $h(t, u)$, the *adjoint operator* (or Hermitian adjoint) \mathcal{L}^* is defined by the kernel (see Problem 4.8)

$$h_*(t, u) = h^*(u, t), \quad (4.47)$$

that is, the kernel of \mathcal{L}^* is obtained by swapping the variables t, u in the kernel of \mathcal{L} and taking the conjugate. This operator is used in the following classification:

1. An operator \mathcal{L} is *unitary* if $\mathcal{L}\mathcal{L}^* = \mathcal{J}$,
2. An operator \mathcal{L} is *Hermitian* if $\mathcal{L}^* = \mathcal{L}$.

Hence, the kernel of a Hermitian operator verifies the condition $h(u, t) = h^*(t, u)$. Two operators \mathcal{L}_1 and \mathcal{L}_2 are *orthogonal* if $\mathcal{L}_1\mathcal{L}_2 = 0$, where 0 is the zero operator.

An important class of linear operators is given by projectors [11, 12].

Definition 4.2 A *projector* is an *idempotent* operator, that is, with the property

$$\mathcal{P}^2 = \mathcal{P} \quad (4.48)$$

where \mathcal{P}^2 means $\mathcal{P}\mathcal{P}$.

Examples of projectors are $\mathcal{P}_E = \frac{1}{2}(\mathcal{J} + \mathcal{J}_-)$ and $\mathcal{P}_O = \frac{1}{2}(\mathcal{J} - \mathcal{J}_-)$ which extract from a signal the even and the odd components (see Problem 4.9), respectively. The meaning of a projector will be seen in the applications of the next sections and especially at the end of the chapter.⁴

⁴In the literature, the usual term is *projection* instead of *projector*, but we prefer to reserve “projection” to the application of a projector. A Hermitian projector is often called an *orthogonal* projector, for its specific properties. But we prefer to reserve “orthogonal” referring to a pair of projectors with the property $\mathcal{P}_1\mathcal{P}_2 = 0$.

Comments on the Topics Developed in This Section

Starting from the class $\mathcal{S}(I)$ of all signals defined on a quotient group I , we have introduced the class $L_p(I)$ and in particular $L_2(I)$, the class of square integrable signals. We have seen that $\mathcal{S}(I)$ is a *vector space* over \mathbb{C} and that $L_2(I)$ is a *subspace* of $\mathcal{S}(I)$. Moreover, $L_2(I)$ is an *inner product vector space* and also a *Hilbert space*. Using the inner product, in $L_2(I)$ we have introduced the concept of *orthogonal signals*.

In the Hilbert space $L_2(I)$, we have introduced the concept of a *linear operator*. We suggest the reader to revisit this concept and related definitions after the study of linear transformations, developed in Chap. 6.

UT 4.6 Signal Expansions into Orthogonal Functions

As an important application of the concepts related to Hilbert spaces, in this section we consider the expansion of a signal $s(t) \in L_2(I)$ in the form

$$\boxed{s(t) = \sum_{n \in \mathcal{N}} S_n \varphi_n(t)}, \quad (4.49)$$

where \mathcal{N} is an appropriate countable index set, $\Phi = \{\varphi_n(t), n \in \mathcal{N}\}$ is a basis of $L_2(I)$ and S_n are the expansion coefficients (or Fourier coefficients). The problem is the evaluation of S_n starting from the signal. The solution is particularly simple when the basis is orthonormal, but other forms of expansion are possible.⁵

Let I be an LCA group and \mathcal{N} a countable index set. For an orthogonal signal set $\Phi = \{\varphi_n(t) \mid t, n \in \mathcal{N}\}$, we can write

$$\int_I dt \varphi_m(t) \varphi_n^*(t) = \delta_{mn} K_n = \begin{cases} K_n, & \text{if } n = m; \\ 0, & \text{if } n \neq m, \end{cases} \quad (4.50)$$

where $K_n = \|\varphi_n\|^2$ and $0 < K_n < \infty$.

When $K_n = 1$ for all n , the set is said to be *orthonormal*. The class of orthogonal function is *complete* if all $L_2(I)$ signals are expandable according to (4.49). In this case, Φ is an *orthogonal basis* of $L_2(I)$.

A signal of $L_2(I)$ can be expanded into orthogonal functions in the form (4.49), where the coefficients S_n can be calculated from the signal $s(t)$ according to

$$S_n = (1/K_n) \int_I dt s(t) \varphi_n^*(t) = (1/K_n) \langle s, \varphi_n \rangle. \quad (4.51)$$

⁵Signal expansions will be further developed in Chap. 14 as a preliminary to filter banks and wavelets.

In fact, by multiplication of both sides of (4.49) by $\varphi_n^*(t)$ and using orthogonality conditions, (4.50) follows at once.

The orthogonality conditions allow obtaining the signal energy from the coefficients S_n , according to *Parseval's theorem*

$$E_s = \int_I dt |s(t)|^2 = \sum_{n \in \mathcal{N}} |S_n|^2 K_n. \quad (4.52)$$

4.6.1 Overview of Orthogonal Functions

As for any vector space, an orthogonal basis for $L_2(I)$ can always be found starting from a *basis*, that is, a family $\Phi = \{\varphi_n(t) \mid b \in \mathcal{N}\}$ of linear independent signals, such that $\text{span}(\Phi) = L_2(I)$, though the standard *Gram–Schmidt orthogonalization procedure* [10]. The so-obtained orthogonal basis $\Phi' = \{\varphi'_n(t) \mid n \in \mathcal{N}\}$ has necessarily the same cardinality as Φ (recall that the common cardinality of the bases defines the dimensionality of a vector space). From the orthogonal basis, it is easy to get an *orthonormal* basis by normalization, as $\varphi'_n(t)/\sqrt{K_n}$, where $K_n = \|\varphi'_n\|^2$.

We now see specific examples of orthogonal functions (in specific 1D domain/periodicities), and then we add some general ideas to construct orthogonal functions in the general multidimensional case.

Examples of Orthogonal Functions

The classical examples are sinusoidal and exponential functions on $I = \mathbb{R}/\mathbb{Z}(T_p)$ (Fig. 4.4), namely

$$\begin{aligned} \varphi_n(t) &= \cos 2\pi n Ft, & K_n &= 1/(2F), & \mathcal{N} &= \mathbb{N}_0 & \text{not complete;} \\ \varphi_n(t) &= \sin 2\pi n Ft, & K_n &= 1/(2F), & \mathcal{N} &= \mathbb{N} & \text{not complete;} \\ \varphi_n(t) &= e^{i2\pi n Ft}, & K_n &= 1/F, & \mathcal{N} &= \mathbb{Z} & \text{complete,} \end{aligned}$$

which are orthogonal on $I = \mathbb{R}/\mathbb{Z}(T_p)$ with $F = 1/T_p$. These classes provide the *Fourier series expansion*, seen in Sect. 2.5.

A class of orthogonal functions on $I = \mathbb{R}$ consists of the *cardinal* functions

$$\varphi_n(t) = \text{sinc}(Ft - n), \quad K_n = 1/F, \quad \mathcal{N} = \mathbb{Z}. \quad (4.53)$$

As seen in Chap. 2, the cardinal functions are related to the Sampling Theorem, where the signal recovery from sample values has the form

$$s(t) = \sum_{n=-\infty}^{+\infty} s(nT) \text{sinc}(Ft - n), \quad FT = 1, \quad (4.54)$$

and the coefficients are directly given by the sample values, $S_n = s(nT)$. Of course, the class of cardinal functions is not complete since expansion (4.54) holds only for

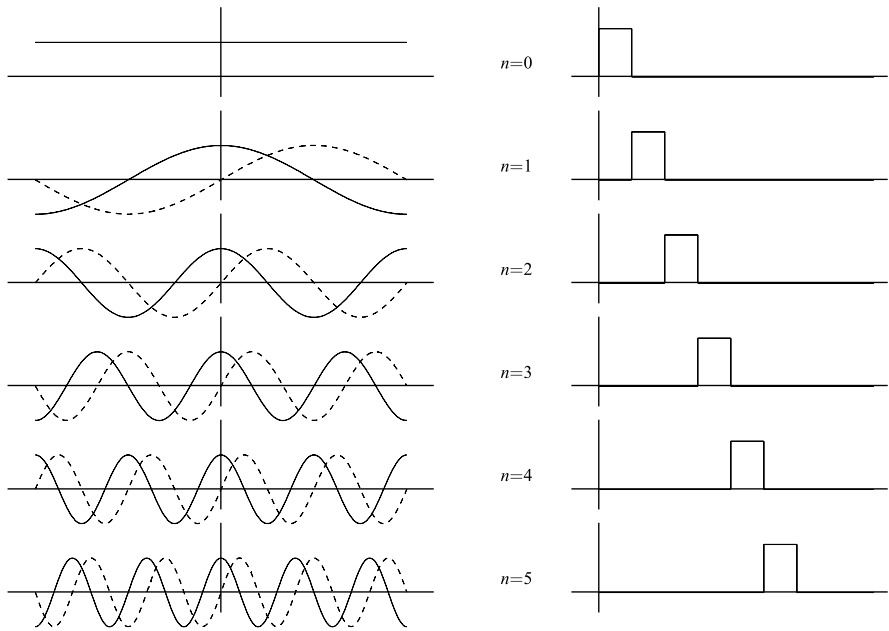


Fig. 4.4 Examples of orthogonal functions: sinusoidal functions and Block functions

band-limited signals and therefore not all signals of $L_2(\mathbb{R})$ admit such a representation. Another simple class of orthogonal functions on $I = \mathbb{R}$ is given by the *Block functions* (Fig. 4.4), which are nonoverlapping rectangular pulses. This class is not complete, either.

A more articulated class of rectangular orthogonal functions is given by *Walsh functions*. The definition of the Walsh function of order $n \in \mathcal{N}_0$, $wal(n, t)$, requires to express n in the binary form $n_0 n_1 \cdots n_{m-1}$, where

$$n = \sum_{r=0}^{m-1} 2^r n_r \quad (2^m \geq n),$$

then [2]

$$wal(n, t) = \prod_{r=0}^{m-1} \text{sgn}[\sin^{n_r} 2^{r+1} \pi t], \quad t \in \mathbb{R}/\mathbb{Z}(1)$$

where $\text{sgn}(x)$ is the signum function. These functions, which are periodic with period 1, are square-wave like for the presence of the signum function, as shown in Fig. 4.5. In the form $wal(n, Ft)$ they become orthogonal on $I = \mathbb{R}/\mathbb{Z}(T_p)$ with $F = 1/T_p$ and $K_n = 1/F$.

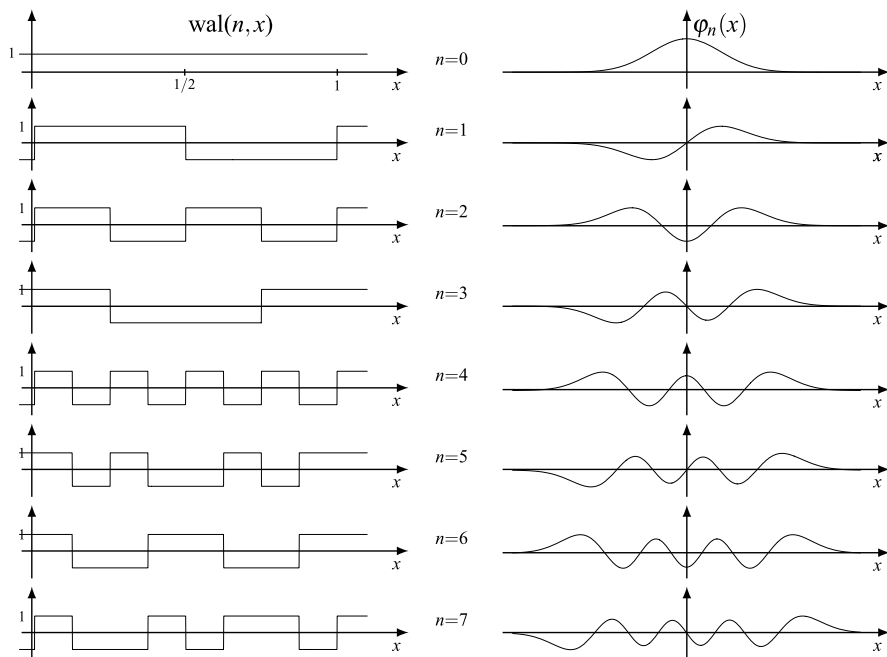


Fig. 4.5 The Walsh functions and Hermite–Gauss functions of the first orders

A complete class of orthonormal functions on \mathbb{R} are the *Hermite–Gauss* functions (Fig. 4.5)

$$\varphi_n(t) = \frac{\sqrt[4]{2}}{\sqrt{2^n n!}} H_n(\sqrt{2\pi}t) e^{-\pi t^2}, \quad n \in \mathbb{N}_0$$

where $H_n(t) = (-1)^n t^2 d^n e^{-t^2} / dt^n$ are the Hermite polynomials [1]. These functions form a complete orthonormal class with $K_n = 1$ and will be used in the context of the fractional Fourier transform at the end of Chap. 5.

Finally, an example of orthogonal functions on the finite group $\mathbb{Z}(1)/\mathbb{Z}(N)$ is given by the class

$$\varphi_n(t) = W_N^{nt}, \quad K_n = N, \quad \mathcal{N} = \{0, 1, \dots, N-1\} \quad (4.55)$$

where W_N is an N th root of unity

$$W_N = \exp(i2\pi/N). \quad (4.55a)$$

These functions are the discrete version of the exponential functions and appear in the DFT, that is, the Fourier transform on $\mathbb{Z}(T)/\mathbb{Z}(T_p)$.

Several other examples can be found in [14], where most classes are orthogonal on a finite interval of \mathbb{R} and only a few are orthogonal on the whole \mathbb{R} .

▽ Ideas How to Find Orthogonal Functions

In many cases, orthogonal functions, structured as bases, are used in signal expansions, but sometimes they are intentionally built for particular purposes. We now see a few cases of the latter type, where also multidimensional bases are derived.

Bases from Impulses The impulse $\delta_I(t)$, which will be introduced in Sect. 4.9, allows identifying an orthonormal basis when I is a lattice K or a finite group K/P (in the other cases, $\delta_I(t)$ is a generalized function not belonging to $L_2(I)$). In particular, if K is a lattice, the impulse is given by

$$\delta_K(t) = \begin{cases} 1/d(K), & \text{if } t = 0; \\ 0, & \text{if } t \neq 0, \end{cases} \quad t \in K.$$

Then, the functions

$$\delta_K(t - u), \quad u \in K, \quad (4.56)$$

form an orthogonal basis for $L_2(K)$. For the case $I = K/P$, see Problem 4.15.

Bases from the Fourier Kernel The Fourier kernel $\psi(f, t)$, which will be introduced in Chap. 5, allows the construction of orthonormal bases when I is a proper quotient group \mathbb{R}^m/P or a finite group L/P . In the first case, the orthogonal basis is given by

$$\psi(f, t) = e^{i2\pi ft}, \quad f \in P^*$$

where P^* is the *reciprocal* of the periodicity P . When $I = L/P$ the basis is given by

$$\psi(f, t) = e^{i2\pi ft}, \quad f \in [P^*/L^*].$$

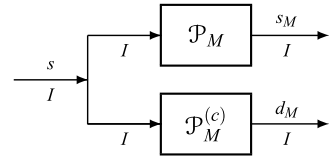
Bases from Sampling Theorem In the Sampling Theorem, which will be seen in Chap. 5, the interpolating function $q_0(t)$ allows defining an orthonormal basis (see Proposition 8.2).

Bases from Filter Banks and Wavelets In Chaps. 14 and 15, we shall see that filter banks and wavelets provide a large variety of orthonormal bases.

4.6.2 Orthogonal Projection and Least-Squares Approximation

Often, a signal s from the Hilbert space $L_2(I)$ has to be approximated by a vector lying in a finite dimensional subspace V_M . Given an *orthonormal* basis $\Phi = \{\varphi_n(t) \mid n \in \mathcal{N}\}$ of $L_2(I)$ we suppose that V_M is the subspace spanned by M functions of Φ .

Fig. 4.6 Approximation s_M and error d_M in an orthogonal expansion obtained from the signal s with projectors



To be more specific suppose that⁶ $\mathcal{N} = \mathbb{N}_0 = \{0, 1, 2, \dots\}$ and take the subfamily of the first M functions, $\Phi_M = \{\varphi_0, \varphi_1, \dots, \varphi_{M-1}\}$. Then, Φ_M is a basis of V_M and we compare the two expansions

$$s_M = \sum_{n=0}^{M-1} S_n \varphi_n, \quad s = \sum_{n=0}^{\infty} S_n \varphi_n \quad (4.57)$$

where $S_n = \langle s, \varphi_n \rangle$. Since the difference $d_M = s - s_M$ is easily seen to be orthogonal to Φ , s_M represents the orthogonal projection of s onto V_M . As we saw in the Projection Theorem (Theorem 4.3), s_M is the optimal solution, in the least-square sense. Observe that

$$\|s\|^2 = \|s_M\|^2 + \|d_M\|^2.$$

4.6.3 Projections by Projectors

We will now see that the orthogonal projections can be obtained by appropriate operators, the *orthogonal projectors*. Specifically, we show that (Fig. 4.6)

$$s_M = \mathcal{P}_M s, \quad d_M = \mathcal{P}_M^{(c)} s \quad (4.58)$$

where \mathcal{P}_M and $\mathcal{P}_M^{(c)}$ are *Hermitian projectors*, that is, Hermitian operators having the idempotency property.

Proposition 4.5 *Given the reduced orthonormal basis Φ_M , the Hermitian projector \mathcal{P}_M in (4.58) is defined by the kernel*

$$\mathcal{P}_M : \quad h_M(t, u) = \sum_{n=0}^{M-1} \varphi_n(t) \varphi_n^*(u), \quad t, u \in I, \quad (4.59)$$

and $\mathcal{P}_M^{(c)} = \mathcal{J} - \mathcal{P}_M$ is the complementary projector.

⁶This can be done without restriction since we suppose that the index set \mathcal{N} is countable. When \mathcal{N} is finite with cardinality N , we let $\mathcal{N} = \{0, 1, \dots, N-1\}$ and in the present context we suppose $M \leq N$.

Proof From the expression of s_M given by (4.57), we get

$$\begin{aligned} s_M(t) &= \sum_{n=0}^{M-1} \varphi_n(t) \int_I du s(u) \varphi_n^*(u) = \int_I du \sum_{n=0}^{M-1} \varphi_n(t) s(u) \varphi_n^*(u) \\ &= \int_I du h_M(t, u) s(u) \end{aligned} \quad (4.60)$$

where $h_M(t, u)$ is given by (4.59). \square

It is easy to check that \mathcal{P}_M is Hermitian and idempotent (using (4.45)) and the orthonormality of the $\varphi_n(t)$. As an example, with $\varphi_n(t) = (1/T_p)e^{i2\pi nt/T_p}$ (Fourier series) we have

$$h(t, u) = F \sum_{n=0}^{M-1} e^{i2\pi nF(t-u)}, \quad F = 1/T_p,$$

and the orthogonal projector \mathcal{P}_M is a filter on $\mathbb{R}/\mathbb{Z}(T_p)$ with impulse response given by $g(v) = F \sum_{n=0}^{M-1} e^{i2\pi nFv}$, $v \in \mathbb{R}/\mathbb{Z}(T_p)$. The corresponding frequency response is

$$G(kF) = F \sum_{n=0}^{M-1} \delta_{\mathbb{Z}(F)}(kF - nF) = \begin{cases} 1, & \text{if } 0 \leq k \leq M-1; \\ 0, & \text{otherwise,} \end{cases}$$

which means that the filter takes the first M harmonics and drops completely the other ones.

Concluding Remark on Orthogonal Expansion

We have seen the orthogonal expansion of a signal in a standard and preliminary form. The topic will be reconsidered and further developed in Chap. 14, where orthogonal expansions will be formulated in the framework of *generalized transforms*. In that context, also the generalization to *biorthogonal expansions* and to *frames* will be developed.

UT 4.7 Fundamental Symmetries

We consider the fundamental examples of symmetries, already seen in the Classic Theory for both continuous and discrete time signals.

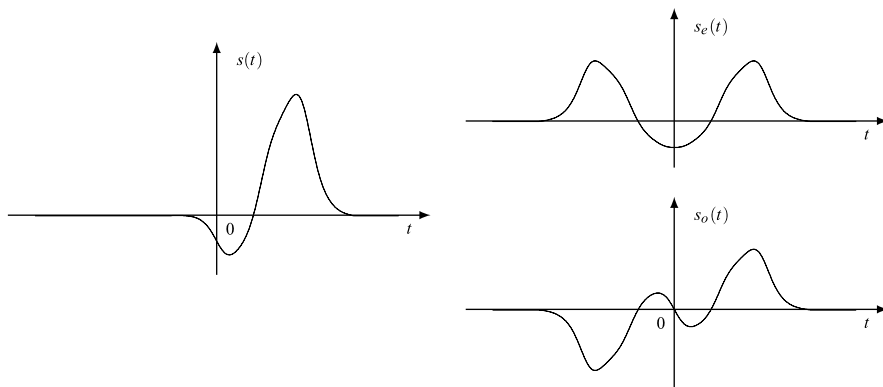


Fig. 4.7 Decomposition of a signal into even and odd components, illustrated on the domain $I = \mathbb{R}$

For signals defined on a generic group I , we can introduce the following symmetry pairs:

- 1(a) $s(t) = s(-t)$ (even symmetry)
- 1(b) $s(t) = -s(-t)$ (odd symmetry)
- 2(a) $s(t) = s^*(t)$ (real signal)
- 2(b) $s(t) = -s^*(t)$ (imaginary signal)
- 3(a) $s(t) = s^*(-t)$ (Hermitian symmetry)
- 3(b) $s(t) = -s^*(-t)$ (anti-Hermitian symmetry)

In general, a signal does not possess any of the previous symmetries, but it can always be decomposed into symmetric components.

Theorem 4.4 Every signal $s(t)$, $t \in I$, can be decomposed into two components, one with Symmetry (a) and one with Symmetry (b).

In fact, for Symmetries 1, it is well known that every signal can be decomposed into an even and an odd component (see Fig. 4.7), namely

$$s(t) = s_E(t) + s_O(t), \quad (4.61a)$$

where

$$s_E(t) = \frac{1}{2}[s(t) + s(-t)], \quad s_O(t) = \frac{1}{2}[s(t) - s(-t)]. \quad (4.61b)$$

A similar decomposition applies to Symmetries 3. Symmetries 2 give the familiar decomposition into real and imaginary part, namely

$$s(t) = \Re s(t) + i\Im s(t), \quad (4.62a)$$

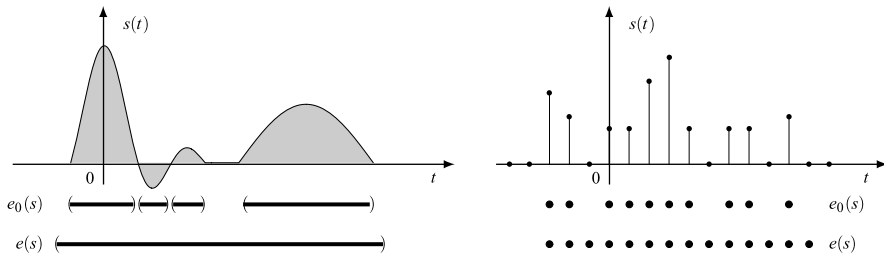


Fig. 4.8 Illustration of the *minimum extension* $e_0(s)$ and of the *extension* $e(s)$ of a signal on the continuous domain \mathbb{R} and on the discrete domain $\mathbb{Z}(T)$

where

$$\Re s(t) = \frac{1}{2}[s(t) + s^*(t)], \quad \Im s(t) = \frac{1}{2}[s(t) - s^*(t)]. \quad (4.62b)$$

Each of these symmetries can be viewed as an *invariance* of the signal with respect to a specific operation. As an example, the even symmetry states the signal invariance with respect to the reflection operation. The null element of this symmetry is the zero signal, which is both even and odd. These considerations will be formalized in the Symmetry Theory at the end of the chapter.

UT 4.8 Signal Extension and Duration

A signal is formally defined over a group but sometimes its information is confined to a subset of the group. We call this subset the signal *extension* and its Haar measure the signal *duration*.

We now give a precise definition of these concepts, whose importance is not limited to the signal domain analysis, but includes their role in the frequency domain, where they become the *band* and the *bandwidth*, respectively.

4.8.1 General Definitions

Definition 4.3 The *support* of a signal $s(t)$, $t \in I = I_0/P$, that is, the subset of I_0 where $s(t)$ is nonzero (Fig. 4.8),

$$e_0(s) = \{t \mid s(t) \neq 0\}, \quad (4.63)$$

will be called the *minimal extension* of the signal. The Haar measure of $e_0(s)$, $D_0(s) = \text{meas } e_0(s)$, is the *minimal duration* of $s(t)$.

Definition 4.4 Every subset of the domain I_0 containing the minimal extension (Fig. 4.8)

$$e(s) \supset e_0(s) \quad (4.64)$$

is an *extension* of $s(t)$ and $D(s) = \text{meas } e(s)$ is a *duration* of $s(t)$.

The convenience in considering an extension $e(s)$ instead of the minimal extension $e_0(s)$ is due to several reasons, which will be clear in the following. The main reason is that for $e(s)$ we can choose “simple” and structured subsets, as an interval on \mathbb{R} , a sequence of consecutive points on $\mathbb{Z}(T)$, and, in general, a cell.

The propriety of an extension $e(s)$ is that it ensures that the signal is identically zero outside $e(s)$

$$s(t) = 0, \quad t \notin e(s), \quad (4.65)$$

but within $e(s)$ the signal is not necessarily nonzero. Thus, knowing $e(s)$ we can limit the specification of a signal within $e(s)$.

Why Extension and Not Support? In the literature, it is customary to speak of the signal support, as defined by (4.63) or as the *closure* of $e_0(s)$. However, we prefer the more relaxed requirement (4.65), since it is more convenient to deal with. For clarity, we have introduced the specific term “extension”.

4.8.2 Extension and Duration of 1D Signals

We apply the general definitions to the four classes of 1D signals.

- $I = \mathbb{R}$

Commonly, the extension $e(s)$ is assumed as the *smallest interval* containing the minimal extension $e_0(s)$, say

$$e(s) = [t_s, T_s], \quad D(s) = T_s - t_s,$$

where t_s and T_s are the infimum and supremum of $e_0(s)$, respectively. Of course, we may have $t_s = -\infty$ and/or $T_s = +\infty$. For instance, $\text{rect}(t/T)$ has extension $[-\frac{1}{2}T, \frac{1}{2}T]$, while the step function $1(t)$ has extension $[0, +\infty)$.

- $I = \mathbb{Z}(T)$

In this case, $e(s)$ is a subset of $\mathbb{Z}(T)$, and the typical extension becomes a “discrete interval” (Fig. 4.8)

$$e(s) = [t_s, T_s] \cap \mathbb{Z}(T) = \{t_s, t_s + T, \dots, T_s - T, T_s\},$$

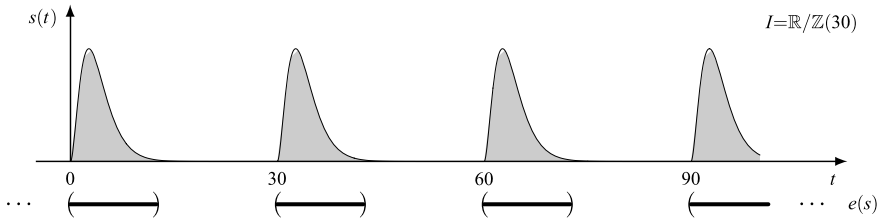


Fig. 4.9 Example of a signal that is duration-limited in a period

where the inclusion of t_s and T_s , becomes essential on $\mathbb{Z}(T)$, while it is irrelevant on \mathbb{R} . The duration is given by the number of points in $e(s)$ multiplied by the spacing T , that is,

$$D(s) = T_s - t_s + T.$$

This is more evident if we denote the extrema in the form $t_s = n_s T$, $T_s = N_s T$, so we have

$$D(s) = (N_s - n_s + 1)T.$$

In particular, if the signal consists of a single nonzero value, the duration becomes $D(s) = T$, with two nonzero values $e(s) = 2T$, etc. For instance, in the signal of Fig. 4.8(b), $n_s = -3$ and $N_s = 10$, then $D(s) = 14T$.

- $I = \mathbb{R}/\mathbb{Z}(T_p)$ and $I = \mathbb{Z}(T)/\mathbb{Z}(T_p)$

The extensions are always periodic sets and the maximum duration is given by the period, that is,

$$0 \leq D(s) \leq T_p.$$

In such a way, every periodic signal has a finite duration, provided that the signal is specified in a proper quotient group, otherwise its duration becomes infinite. When $D(s) < T_p$ (see Fig. 4.9), we say that the signal has a *limited duration in a period*.

4.8.3 Further Considerations on Signal Domain/Periodicity

The idea of an extension allows improving the choice of a signal domain and periodicity. We remark that in practice a signal may have a *natural* domain, intended as the set over which we know the signal values. For instance, the signal of a telephone call has a finite interval as its natural domain. Another example is the signal (luminance and chrominance) of a still image, where the natural domain is a 2D rectangle. In both cases, the natural domain is not a group.

On the other hand, in Signal Theory it is mandatory to choose a group as a signal domain. Hence, we have the problem of “completing” the signal definition outside

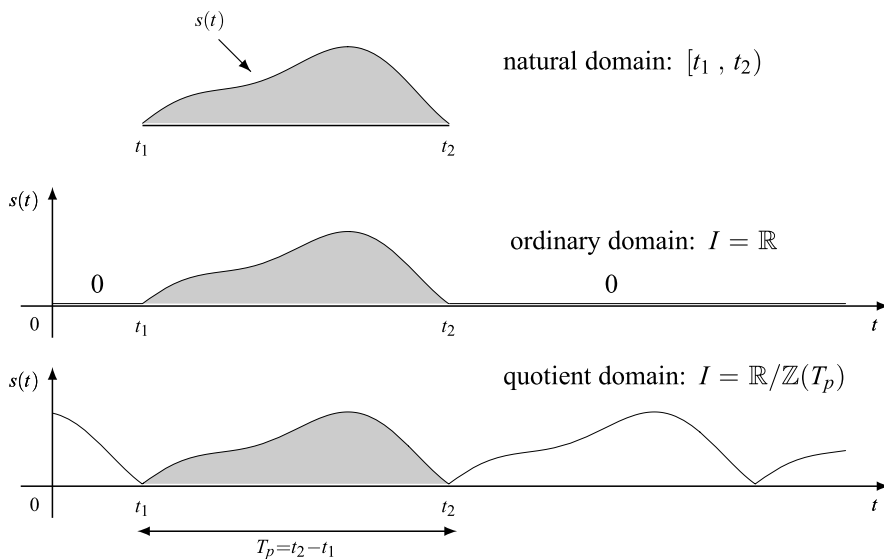


Fig. 4.10 Signal defined on an interval with its *aperiodic* and *periodic* versions

its natural domain. An obvious way is to extend the signal definition with *zero values* (Fig. 4.10), that is,

$$s(t) = 0, \quad t \in I_0, t \notin C, \tag{4.66}$$

where C is the natural domain and I_0 is an LCA group, such that $C \subset I_0$. In such a way, we obtain by construction a signal with a finite extension $e(s) = C$.

An alternative form, less usual but with some advantages, is extending the signal definition *by periodicity*. In this case, C must be a cell of I_0 of the form $C = [I_0/P)$ for a suitable modulus P . Then, we define the signal outside its natural domain C by

$$s(t + p) = s(t), \quad t \in I_0, p \in P. \tag{4.67}$$

Thus, we get a signal defined on a quotient group I_0/P .

Finally, we note:

Proposition 4.6 *The class of signals on an ordinary domain I_0 with a finite extension C can be linked by a one-to-one correspondence with the class of signals specified on I_0/P , provided that C is also a cell of I_0 modulo P .*

In fact, if $s_0(t)$ is defined on I_0 and has extension C , the periodic repetition

$$s(t) = \sum_{p \in P} s_0(t - p)$$

provides a signal with periodicity P . But, from $s(t)$ we can obtain $s_0(t)$ according to $s_0(t) = s(t)\eta_C(t)$, where $\eta_C(t)$ is the indicator function of the cell C .

UT 4.9 Convolution

We have recalled several times that convolution is one of the fundamental operations in Signal Theory. The Haar integral allows defining this operation in a unified way, that is, by giving a single definition, valid for all signal classes.

4.9.1 Definition and Interpretation

Definition 4.5 Given two signals x and y on the same group I , their convolution $x * y$ is a signal on I defined by

$$x * y(t) = \int_I du x(t - u)y(u), \quad t \in I. \quad (4.68)$$

The interpretation of convolution on an arbitrary group I is exactly the same as on the real line (see Sect. 2.4), but is revisited here for its importance. In (4.68), for a fixed $t \in I$, the integrand is the signal, written as function of the argument u ,

$$z_t(u) = x(t - u)y(u) = x_-(u - t)y(u), \quad u \in I \quad (4.69)$$

where $x_-(u) = x(-u)$ is the reverse of $x(u)$. Hence, we have a twofold operation: a signal reverse to get $x_-(u)$ and a shift of t , to get $x_-(u - t)$. By the reflection and shift properties (see Sect. 3.2), both $x_-(u)$ and $x_-(u - t)$, for every $t \in I$, are themselves defined on I and so is the product in (4.69). Once the product is obtained, its integral with respect to u gives the convolution evaluated at $t \in I$, that is,

$$x * y(t) = \int_I du z_t(u), \quad t \in I.$$

This integral can be put into a more specific form introducing the extensions. The extension of $x_-(u - t)$ is $e_0(x_-) + t = -e_0(x) + t$ and the extension of $z_t(u)$ is given by $e_0(z_t) = [-e_0(x) + t] \cap e_0(y)$, so that the integration can be limited to $e_0(z_t)$, that is,

$$x * y(t) = \int_{[-e_0(x) + t] \cap e_0(y)} du x(t - u)y(u). \quad (4.70)$$

In particular, we have $x * y(t) = 0$ whenever $e_0(z_t)$ is empty.

The above interpretation gives a guideline for the convolution evaluation. To this regard, it may be convenient to use several properties that are considered below.

Filter Interpretation The most important application of convolution is in filters. A *filter on the group I* is a system governed by the input–output relationship

$$y(t) = g * x(t) = \int_I du g(t - u)x(u), \quad t \in I \quad (4.71)$$

Fig. 4.11 Graphical representation of a filter on I

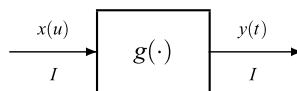


Table 4.3 Convolution Properties

Property	Relationship
1. commutativity	$x * y = y * x$
2. associativity	$(x * y) * z = x * (y * z)$
3. distributivity	$x * (y + z) = x * y + x * z$
4. area	$\text{area}(x * y) = \text{area}(x) \cdot \text{area}(y)$
5. 1 norm	$\ x * y\ _1 \leq \ x\ _1 \cdot \ y\ _1$
6. shift	$x_p * y_q = (x * y)_{p+q}$
7. minimal extension	$e_0(x * y) \subset e_0(x) + e_0(y)$
8. unit element	$\delta_I * x = x$

where $x(u), u \in I$, is the input, $y(t), t \in I$, is the output (or response) and $g(t), t \in I$, is the *impulse response* of the filter (Fig. 4.11).

Hence, a filter is a system governed by a convolution. More specifically, the filter processes every input signal x on I by performing the convolution of x with the signal g , specific of the filter, giving the output $y = g * x$.

4.9.2 Properties

Convolution properties are collected in Table 4.3 and are now commented. Strictly speaking, all the properties hold in the class $L_1(I)$ of absolutely integrable signals, but some of them have a more general validity.

Property 1 states that $*$ is a *commutative* operation, and it can be proved with the change of variable $v = t - u$ in the definition (4.68) and invoking properties (4.2a, 4.2b) of the Haar integral rules. Property 2 is the *associative* property, and it allows writing a repeated convolution in the form $x * y * z$ without ambiguity. Property 3 states the *distributive* property of convolution with respect to addition. Property 4 is obtained by integrating with respect to t and considering that $x(-(u - t))$ and $x(u)$ have the same area (see (4.3)). Property 5 states that the class $L_1(I)$ is closed under convolution; it can be proved using Hölder inequality [13]. Property 6 states that the convolution of the shifted versions, $x_p(t) = x(t - p)$ and $y_q(t) = y(t - q)$, produces the signal

$$x_p * y_q(t) = x * y(t - (p + q)).$$

Properties 7 and 8 deserve further discussions and will be the subject of the rest of this section and the next.

4.9.3 Extension of the Convolution

The extension of a convolution $x * y(t)$ can be evaluated without evaluating the convolution itself.

Theorem 4.5 *The minimal extension of a convolution is a subset of the sum of the minimal extensions of the convolution factors:*

$$e_0(x * y) \subset e_0(x) + e_0(y). \quad (4.72)$$

Proof In (4.72), the integrand extension can be written in the form

$$e_0(v_t) = \{u \mid x(t - u) \neq 0, y(u) \neq 0\} = \{u \mid t - u \in e_0(x), u \in e_0(y)\}.$$

Now, we prove that, if $t \notin e_0(x) + e_0(y)$, the set $e_0(v_t)$ is empty and then the integral is zero and $t \notin e_0(x * y)$. In fact, if $t \notin e_0(x) + e_0(y)$, we cannot find pairs (t_1, t_2) such that $t_1 \in e_0(x)$, $t_2 \in e_0(y)$ with $t_1 + t_2 = t$, and therefore no u value such that $t - u \in e_0(x)$ and $u \in e_0(y)$. Consequently, $e_0(v_t)$ is the empty set.

The theorem is concerned with *minimal* extensions. For *generic* extensions, the result can be put into the form

$$\boxed{e(x * y) = e(x) + e(y)}, \quad (4.73)$$

which will usually be considered in the following. □

⇓ 4.9.4 A Rule on Periodic Convolution

Consider two periodic signals $x(t), y(t), t \in G/P$, that are obtained as *periodic repetitions* of two aperiodic signals $a(t), b(t), t \in G$, that is,

$$x(t) = \text{rep}_P a(t), \quad y(t) = \text{rep}_P b(t),$$

where

$$\text{rep}_P a(t) \triangleq \sum_{p \in P} a(t - p).$$

Then, their convolution $x * y(t)$ can be obtained from the convolution $a * b(t)$ of the two aperiodic signals.

Theorem 4.6 *The convolution of the periodic repetition of two aperiodic signals $a(t), b(t), t \in G$, is given by the periodic repetition of the convolution of $a(t)$ and $b(t)$. In symbols,*

$$(\text{rep}_P a) * (\text{rep}_P b) = \text{rep}_P (a * b). \quad (4.74)$$

The theorem is proved in Appendix E using the transformation theory of Chap. 6.

UT 4.10 Impulses

The well known and important properties of the *delta* function $\delta(t)$ (which is introduced on the domain \mathbb{R}) can be extended to every signal class $\mathcal{S}(I)$. The signal of $\mathcal{S}(I)$ having the same properties as the delta function will be called the *impulse on I* and denoted by $\delta_I(t)$.

4.10.1 Convolution Algebra

Commutative, associative and distributive properties 1, 2 and 3 of Table 4.3, together with inequality 5, state that the class $L_1(I)$ of absolutely integrable signals forms a *commutative Banach algebra*, if multiplication is defined by convolution. In this context, the following result holds [13]:

Theorem 4.7 *The algebra of convolution on I has a unit if and only if the group I is discrete.*

Hence, if I is discrete there exists a signal δ_I of $L_1(I)$ such that $s * \delta_I = s$ for all $s \in L_1(I)$. If I is not discrete, such a signal of $L_1(I)$ does not exist, but can be introduced as a distribution (or generalized function). Anyway, the unitary element of convolution (as ordinary or generalized function) will be called the *impulse on I*. In conclusion, the impulse on I is defined as the signal that verifies the integral equation

$$\boxed{s * \delta_I(t) = s(t)}. \quad (4.75)$$

This impulse is said to be *applied at the origin* and to have *unit area* (and the reason will immediately be clear). In general, an impulse with area α and applied at t_0 has the form $\alpha \delta_I(t - t_0)$.

4.10.2 Properties

The main properties of impulses are:

Sifting Property By explicitly writing (4.75) and considering the commutative property, we obtain

$$\int_I du s(t - u) \delta_I(u) = \int_I du \delta_I(t - u) s(u) = s(t).$$

Hence, with the variable changes $t \rightarrow t_0$ and $u \rightarrow t$ and using the fact that the impulse is even (see below), we obtain

$$\boxed{\int_I dt s(t) \delta_I(t - t_0) = s(t_0)}, \quad (4.76)$$

which represents the *sifting property*. This means that by multiplying a signal by the impulse applied at t_0 and integrating, we obtain the signal value at t_0 .

Unit Area Using the convolution rule on area, from (4.75) we get: $\text{area}(\delta_I) \cdot \text{area}(s) = \text{area}(s)$. Hence, the impulse has unit area

$$\text{area}(\delta_I) = \int_I dt \delta_I(t) = 1. \quad (4.77)$$

Extension and Value at $t = 0$ Using the rule on extension, we find that the extension of the impulse δ_I on an ordinary group is limited to the origin, $e(\delta_I) = \{0\}$. More generally, on a quotient group $I = I_0/P$, the extension is given by the modulus

$$e(\delta_I) = P. \quad (4.78)$$

Hence

$$\delta_I(t) \neq 0 \quad \text{for } t \in P, \quad \delta_I(t) = 0 \quad \text{for } t \notin P. \quad (4.79)$$

Consequently, we see that $\delta_I(t)$ is an *even signal*

$$\delta_I(-t) = \delta_I(t). \quad (4.80)$$

The impulse on a discrete group is an ordinary function (see Theorem 4.7). In particular on a lattice, from (4.79) we have

$$\delta_I(t) = \begin{cases} 1/d(I), & \text{if } t = 0; \\ 0, & \text{if } t \neq 0, \end{cases} \quad (4.81)$$

where $d(I)$ is the lattice determinant. On a finite group $I = I_0/P$, we find

$$\delta_{I_0/P}(t) = \begin{cases} 1/d(I_0), & \text{if } t \in P; \\ 0, & \text{if } t \notin P. \end{cases} \quad (4.82)$$

Multiplication by a Signal If we multiply a signal $s(t)$ by the impulse $\delta_I(t - t_0) = 0$, we obtain

$$\boxed{s(t)\delta_I(t - t_0) = s(t_0)\delta_I(t - t_0)}, \quad (4.83)$$

and the result is an impulse with area $s(t_0)$. This rule should not be confused with the sifting property (4.76). The proof of (4.83) follows from the fact the $\delta_I(t - t_0) = 0$ for $t \neq t_0$ if I is an ordinary group and $\delta_I(t - t_0) = 0$ for $t \notin t_0 + P$ (see (4.79)).

Impulse on a Quotient Group The impulse on I_0/P is the periodic repetition of the impulse on I_0 , specifically

$$\delta_{I_0/P}(t) = \sum_{p \in P} \delta_{I_0}(t - p). \quad (4.84)$$

More generally, the impulse on I_0/P is related to the impulse on I_0/P_0 , with $P \subset P_0$,

$$\delta_{I_0/P_0}(t) = \sum_{p \in [P_0/P]} \delta_{I_0/P}(t - p), \quad (4.85)$$

where $[P_0/P]$ is a cell of P_0 modulo P . These relationships follow from integration rule (4.12a, 4.12b).

Impulse on Separable Groups The impulse on $I = I_1 \times I_2$ is the tensor product of the impulses on I_1 and I_2

$$\delta_{I_1 \times I_2}(t_1, t_2) = \delta_{I_1}(t_1) \delta_{I_2}(t_2). \quad (4.86)$$

This rule is a consequence of the integration rule (4.6).

⇓ 4.10.3 A Noble Identity for Impulses

The following identity is fundamental for transformations, and particularly for *multirate* transformations (see Chap. 7). It relates the impulses on two groups I_1 and I_2 with the impulse on $I_1 + I_2$ [6].

Theorem 4.8 *If (I_1, I_2) is a rationally comparable pair of groups, then*

$$\int_{I_1 \cap I_2} ds \delta_{I_1}(t - s) \delta_{I_2}(s - u) = \delta_{I_1 + I_2}(t - u), \quad t \in I_1, u \in I_2. \quad (4.87)$$

We call this identity *noble*, as it is used in the context of the so-called noble identities of multirate transformations. The assumption of *rationally comparable pair* assures that both the sum $I_1 + I_2$ and intersection $I_1 \cap I_2$ are LCA groups (see Sect. 3.9). It also holds for quotient groups (class $\mathcal{Q}(G_0)$) provided that the sum (+) and the intersection (\cap) are interpreted according to the conventions of Sect. 3.9.

The noble identity (4.87) is proved in Appendix F. Here, we confine ourselves to some structural checks on ordinary groups. On the left-hand side, the integration variable s occurs both in the first impulse, defined on I_1 , and in the second, defined on I_2 ; then, it must belong to both groups, that is, $s \in I_1 \cap I_2$. On the right hand side, we find the difference $t - u$, where $t \in I_1$ and $u \in I_2$; then $t - u$ belongs to the set

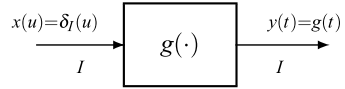
$$\{t - u \mid t \in I_1, u \in I_2\} = \{t + u \mid t \in I_1, u \in -I_2\} = I_1 + (-I_2) = I_1 + I_2,$$

where we have used the group property: $-I_2 = I_2$.

Finally, we note that if $I_1 \subset I_2$, we have (see (3.70)) $I_1 + I_2 = I_2$ and $I_1 \cap I_2 = I_1$. Then, (4.87) becomes

$$\int_{I_1} ds \delta_{I_1}(t - s) \delta_{I_2}(s - u) = \delta_{I_2}(t - u), \quad (4.88)$$

Fig. 4.12 Interpretation of the impulse response of a filter



which is a trivial consequence of the sifting property. A similar result holds if $I_1 \supset I_2$.

4.10.4 The Role of Impulses in Filters

We have introduced a filter on I as a system governed by input–output relation (4.71). Now, the impulse on I permits obtaining the interpretation of the impulse response $g(t)$, $t \in I$.

In general, $x(u)$, $u \in I$, is an arbitrary signal on I and $y(t)$, $t \in I$, is the corresponding response of the filter. When the input is given by the impulse, $x(u) = \delta_I(u)$, the corresponding output is given by

$$y(t) = g * \delta_I(t) = g(t), \quad t \in I.$$

Hence, the meaning of $g(t)$ as the *filter response to the impulse on I* (Fig. 4.12).

It is interesting to investigate what happens when the impulse response is itself an impulse, $g(t) = \delta(t)$. If this is the case, we find

$$y(t) = \delta_I * x(t) = x(t), \quad t \in I,$$

which states the coincidence $y(t) = x(t)$. Hence, a filter with impulse response $g(t) = \delta_I(t)$ does not modify the input signal, and therefore represents the *identity on I* (it is also called the *ideal all-pass filter*).

UT 4.11 One-Dimensional Convolution and Impulses

4.11.1 Convolution Expressions

The general expression of the convolution, given by (4.68), is now applied to the groups of \mathbb{R} , the class $\mathcal{Q}(\mathbb{R})$, to get as many explicit forms. To this end, we use the expressions of the Haar integral from Table 4.1. The four convolutions are collected in Table 4.4, where *continuous* times are denoted by t and u , as in the general definition, whereas *discrete* times are denoted by nT and kT to emphasize their discrete nature.

- $I = \mathbb{R}$

Table 4.4 Convolution on the groups of \mathbb{R}

Domain	Expression	Condition
$I = \mathbb{R}$	$x * y(t) = \int_{-\infty}^{+\infty} x(t-u)y(u) du$	
$I = \mathbb{R}/\mathbb{Z}(T_p)$	$x * y(t) = \int_{t_0}^{t_0+T_p} x(t-u)y(u) du$	$t_0 \in \mathbb{R}$
$I = \mathbb{Z}(T)$	$x * y(nT) = \sum_{k=-\infty}^{+\infty} Tx(nT - kT)y(kT)$	
$I = \mathbb{Z}(T)/\mathbb{Z}(T_p)$	$x * y(nT) = \sum_{k=k_0}^{k_0+N-1} Tx(nT - kT)y(kT)$	$T_p = NT, k_0 \in \mathbb{Z}$

We find the familiar expression of the convolution on the real line. We illustrate in particular the extension rule (Theorem 4.5), when the factor extensions are given by two intervals of \mathbb{R} , say

$$e(x) = [t_x, T_x], \quad e(y) = [t_y, T_y]. \quad (4.89)$$

The convolution extension is again an interval, namely

$$e(x * y) = [t_x + t_y, T_x + T_y]. \quad (4.89a)$$

Consequently, the duration is given by

$$D(x * y) = D(x) + D(y). \quad (4.89b)$$

Anyway, the rule of Theorem 4.5 is more general since it holds for every kind of extensions.

- $I = \mathbb{R}/\mathbb{Z}(T_p)$

We get the definition of Sect. 2.4.

- $I = \mathbb{Z}(T)$ and $I = \mathbb{Z}(T)/\mathbb{Z}(T_p)$

We get the definitions given for discrete signals in Chap. 2. In the literature, the convolution for periodic signals is usually called the *cyclic convolution*.

4.11.2 Impulses

In the groups of \mathbb{R} , the impulses are easily found and allow checking the general properties.

- $I = \mathbb{R}$

The impulse on \mathbb{R} is given by the *delta function*, also called the *Dirac delta* (Fig. 4.13)

$$\delta_{\mathbb{R}}(t) = \delta(t), \quad (4.90)$$

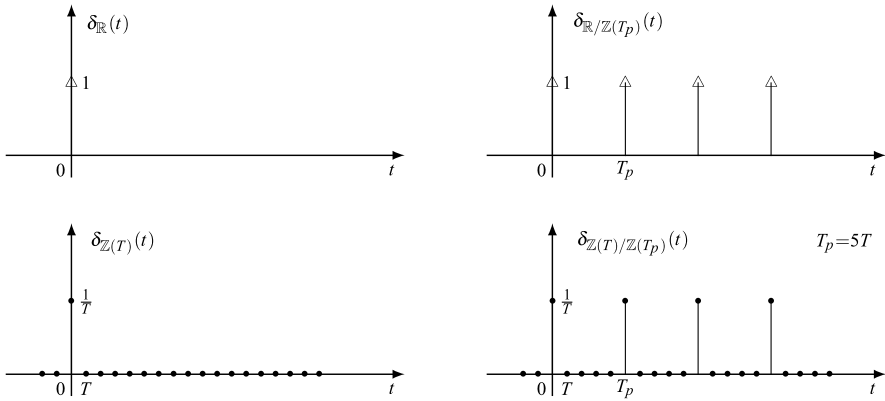


Fig. 4.13 Impulses on the groups of \mathbb{R} . In the representation of the delta function, the arrow length indicates the area (not the signal value!)

which verifies definition (4.75) and the other properties; in particular, it is zero outside the origin, so that $e(\delta_{\mathbb{R}}) = \{0\}$. As is well known, the delta function is a generalized function (or distribution), in agreement with Theorem 4.7.

- $I = \mathbb{R}/\mathbb{Z}(T_p)$

Using the rule (4.84) with $I_0 = \mathbb{R}$ and $P = \mathbb{Z}(T_p)$, we find

$$\delta_{\mathbb{R}/\mathbb{Z}(T_p)}(t) = \sum_{n=-\infty}^{+\infty} \delta(t - nT_p). \tag{4.91}$$

Then, the impulse on $\mathbb{R}/\mathbb{Z}(T_p)$ is a periodic repetition of delta functions, with repetition period T_p . Also in this case, the impulse is a generalized function.

- $I = \mathbb{Z}(T)$

In this case, the group is discrete, and therefore, from Theorem 4.7, the impulse is an ordinary function. Its expression is easily obtained by the properties of having extension $\{0\}$ and unit area. So, we find

$$\delta_{\mathbb{Z}(T)}(t) = \begin{cases} 1/T, & \text{if } t = 0; \\ 0, & \text{if } t \neq 0, \end{cases} \quad t \in \mathbb{Z}(T). \tag{4.92}$$

- $I = \mathbb{Z}(T)/\mathbb{Z}(T_p)$ with $T_p = MT$, $M \in \mathbb{N}$

The impulse is an ordinary function, which can be found by the rule (4.84) with $I_0 = \mathbb{Z}(T)$ and $P = \mathbb{Z}(T_p)$. We have

$$\delta_{\mathbb{Z}(T)/\mathbb{Z}(T_p)}(t) = \sum_{n=-\infty}^{+\infty} \delta_{\mathbb{Z}(T)}(t - nT) = \begin{cases} 1/T, & \text{if } t \in \mathbb{Z}(T_p); \\ 0, & \text{if } t \notin \mathbb{Z}(T_p). \end{cases} \tag{4.93}$$

UT 4.12 Multidimensional Convolution and Impulses

We shall give the expression of the convolution and of the impulses in the multidimensional case. We begin with the case where both the domains and the signals are separable; this gives very simple results, e.g., a 2D convolution is simply obtained by two 1D convolutions. But, in general, to get an explicit result is a difficult task. In fact, the evaluation of convolution may not be trivial, even in the 1D case, but in the multidimensional case it becomes a serious problem.

4.12.1 Convolution and Impulses with Separability

If the domain is separable, say $I = I_1 \times I_2$, and also the convolution factors are separable, $x(t_1, t_2) = x_1(t_1)x_2(t_2)$ and $y(t_1, t_2) = y_1(t_1)y_2(t_2)$, the result of convolution is a separable signal $s(t_1, t_2) = s_1(t_1)s_2(t_2)$, where

$$s_1(t_1) = x_1 * y_1(t_1), \quad s_2(t_2) = x_2 * y_2(t_2). \quad (4.94)$$

This result is a consequence of integration rule (4.7). In fact,

$$\begin{aligned} s(t_1, t_2) &= \int_{I_1 \times I_2} du_1 du_2 x(t_1 - u_1, t_2 - u_2)y(u_1, u_2) \\ &= \int_{I_1} du_1 x_1(t_1 - u_1, u_1)y_1(u_1) \int_{I_2} du_2 x_2(t_2 - u_2, u_2)y_2(u_2). \end{aligned}$$

For the impulse, using the rule (4.7) on separable signals, we have

$$\delta_{I_1 \times I_2}(t_1, t_2) = \delta_{I_1}(t_1)\delta_{I_2}(t_2). \quad (4.95)$$

These results can be easily extended to m factors.

Example 4.3 (Lazy pyramid) Consider the convolution of the 2D rectangular pulse

$$x(t_1, t_2) = \text{rect}(t_1)\text{rect}(t_2), \quad (t_1, t_2) \in \mathbb{R}^2$$

with itself, that is, the *self-convolution* $s(t_1, t_2) = x * x(t_1, t_2)$.

The signal is separable, $x(t_1, t_2) = x_0(t_1)x_0(t_2)$, with $x_0(t) = \text{rect}(t)$, $t \in \mathbb{R}$. Then, according to (4.94), it is sufficient to evaluate the self-convolution $s_0(t) = x_0 * x_0(t)$ of the 1D signal $x_0(t)$. Considering that $s_0(t)$ has a triangular form

$$s_0(t) \triangleq \text{triang}(t) = \begin{cases} 1 - |t|, & \text{if } |t| < 1; \\ 0, & \text{if } |t| > 1, \end{cases}$$

we find

$$s(t_1, t_2) = \text{triang}(t_1)\text{triang}(t_2). \quad (4.96)$$

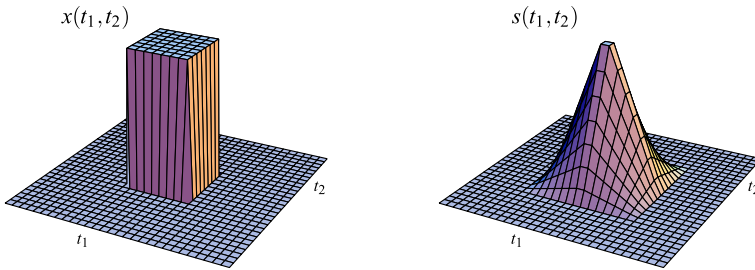
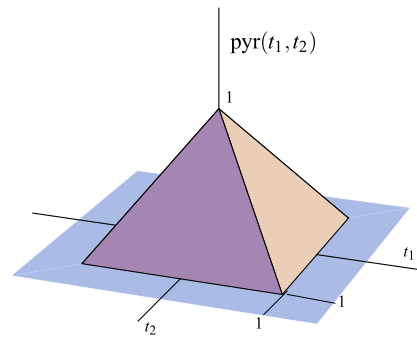


Fig. 4.14 2D rectangular pulse and its self-convolution

Fig. 4.15 The pyramidal signal



We realize that $s(t_1, t_2)$ has a quasi-pyramidal form (Fig. 4.14), called *lazy pyramid* by Bracewell [3]. In fact, it is like a pyramid, but one that has slumped along its four sloping edges.

We compare the lazy pyramid with the “true” pyramid, whose expression can be written in the form (Fig. 4.15)

$$\text{pyr}(t_1, t_2) = \begin{cases} 1 - |t_1|, & \text{if } |t_2| < |t_1| < 1; \\ 1 - |t_2|, & \text{if } |t_1| < |t_2| < 1; \\ 0, & \text{if } |t_1|, |t_2| > 1, \end{cases} \quad (4.97)$$

or in the compact form,

$$\text{pyr}(t_1, t_2) = \text{triang}(t_1) \text{rect}\left(\frac{t_2}{2t_1}\right) + \text{triang}(t_2) \text{rect}\left(\frac{t_1}{2t_2}\right). \quad (4.97a)$$

A cleared comparison is obtained by sectioning both signals along some vertical planes, as shown in Fig. 4.16, where we see that the lazy pyramid is close to the pyramid towards the basis (for both signals, the extension is the square $(-1, 1) \times (-1, 1)$) and the vertex, but it differs progressively towards the middle. Another difference is the area (volume): the lazy pyramid has $\text{area}(s) = \text{area}(s_0) \text{area}(s_0) = 1$, whereas the true pyramid has $\text{area}(\text{pyr}) = 4/3$. A final remarkable difference is that the pyramid signal is *not separable*!

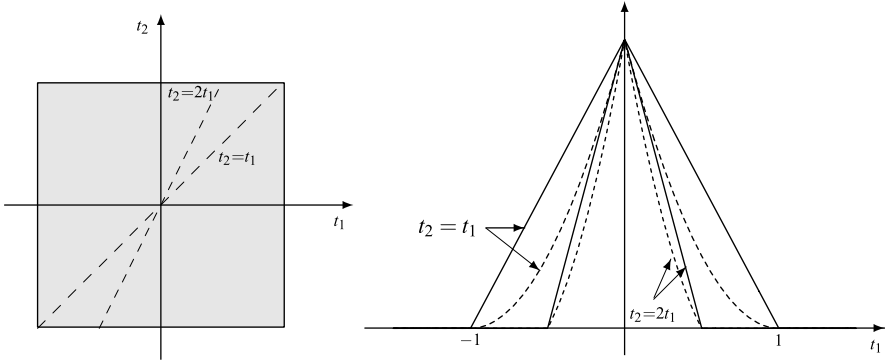


Fig. 4.16 Comparison of the true pyramid and lazy pyramid (*dashed lines*) along the planes $t_2 = t_1, t_2 = 2t_1$

4.12.2 Convolution Expressions

The expression of the Haar integral has been found on every group of \mathbb{R}^m , the class $\mathcal{Q}(\mathbb{R}^m)$, and therefore from the general definition (4.68) we can obtain the explicit forms of convolution. Here we give this form in a few cases.

$I = \mathbb{R}^m$ The Haar integral is the ordinary Lebesgue integral. Hence

$$x * y(t) = \int_{-\infty}^{+\infty} \cdots \int_{-\infty}^{+\infty} x(t_1 - u_1, \dots, t_m - u_m) y(u_1, \dots, u_m) du_1 \cdots du_m.$$

$I = mD$ lattice The Haar integral is the summation over the lattice points, multiplied by the lattice determinant. Hence

$$x * y(t_1, \dots, t_m) = d(I) \sum_{(t_1, \dots, t_m) \in I} x(t_1 - u_1, \dots, t_m - u_m) y(u_1, \dots, u_m). \quad (4.98)$$

Note that, in general, the mD summation cannot be split into m summations. Instead, when the lattice is separable, $I = \mathbb{Z}(d_1, \dots, d_m)$, the summation can be split into m summations; for instance, for $m = 2$ we have

$$\begin{aligned} &x * y(n_1 d_1, n_2 d_2) \\ &= d_1 d_2 \sum_{k_1=-\infty}^{+\infty} \sum_{k_2=-\infty}^{+\infty} x(n_1 d_1 - k_1 d_1, n_2 d_2 - k_2 d_2) y(k_1 d_1, k_2 d_2). \end{aligned}$$

$I = 2D$ grating Using the representation (4.24) in which the grating point is expressed in the form $(u_1, u_2) = (r, Er + Fn), r \in \mathbb{R}, n \in \mathbb{Z}$, we have

$$x * y(t_1, t_2) = F \int_{-\infty}^{+\infty} \sum_{n=-\infty}^{+\infty} x(t_1 - r, t_2 - Er - Fn) y(r, Er + Fn) dr.$$

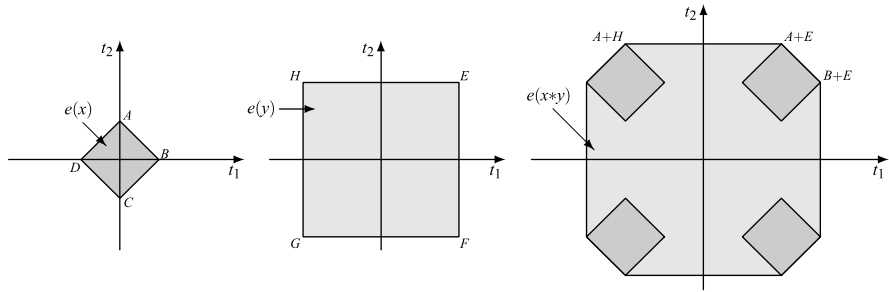


Fig. 4.17 Convolution extension of Example 4.4

Example 4.4 We want to find the extension of the convolution of the 2D rectangular pulses

$$x(t_1, t_2) = \text{rect}\left(\frac{t_1 + t_2}{2}\right) \text{rect}\left(\frac{t_1 - t_2}{2}\right),$$

$$y(t_1, t_2) = \text{rect}\left(\frac{t_1}{4}\right) \text{rect}\left(\frac{t_2}{4}\right), \quad (t_1, t_2) \in \mathbb{R}^2.$$

The extensions are (Fig. 4.17)

$$e(x) = \{(t_1, t_2) \mid -1 < t_1 + t_2 < 1, -1 < t_1 - t_2 < 1\},$$

$$e(y) = (-2, 2) \times (-2, 2),$$

that is, a tilted square and a square. The convolution extension is the set sum $e(x) + e(y)$ and can be found by evaluating the sum of all the four vertexes of $e(x)$ with all the four vertexes of $e(y)$; the resulting polygon is an octagon.

4.12.3 Impulses

We show that the impulses can be obtained from the general rules.

$I = \mathbb{R}^m$ The impulse is given by the m D delta function

$$\delta_{\mathbb{R}^m}(t_1, \dots, t_m) = \delta(t_1) \cdots \delta(t_m). \tag{4.99}$$

This expression is a consequence of rule (4.86) on separable groups.

$I = \mathbb{R}^m / P$ The impulse is the periodic repetition of m D delta functions (see (4.84))

$$\delta_{\mathbb{R}^m / P}(t) = \sum_{p \in P} \delta_{\mathbb{R}^m}(t - p). \tag{4.100}$$

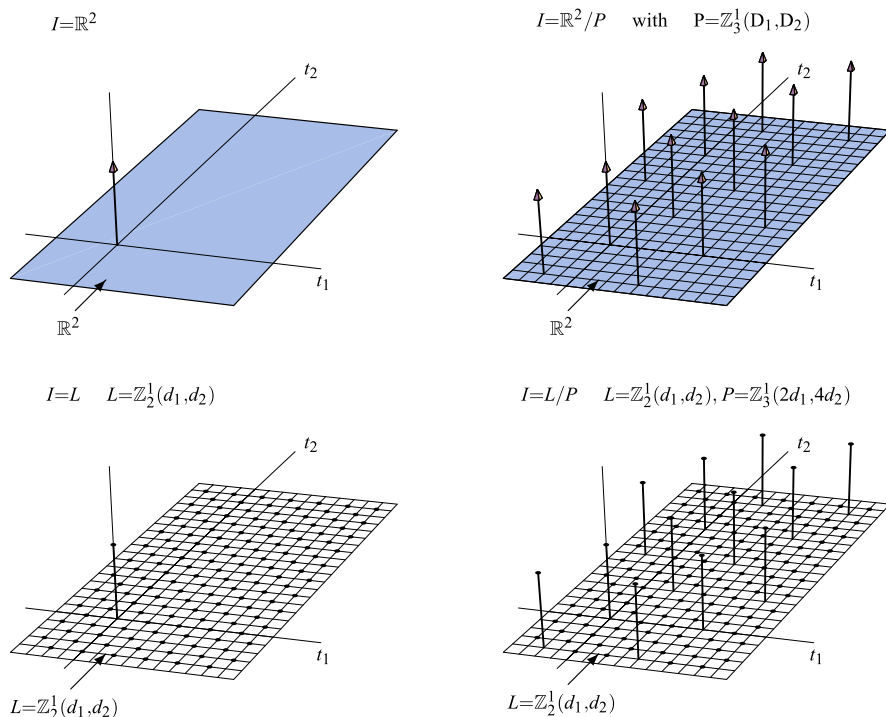


Fig. 4.18 Examples of 2D impulses $\delta_I(t_1, t_2)$

$I = L = mD$ lattice The impulse is the ordinary function

$$\delta_L(t) = \begin{cases} 1/d(L), & \text{if } t = 0; \\ 0, & \text{if } t \neq 0, \end{cases} \tag{4.101}$$

where $d(L)$ is the lattice determinant (see (4.81)).

$I = L/P = \text{finite group}$ The impulse is the periodic repetition of the impulse on L

$$\delta_{L/P}(t) = \sum_{s \in P} \delta_L(s - p). \tag{4.102}$$

Figure 4.18 shows four examples of 2D impulses. The impulse $\delta_{\mathbb{R}^2}(t_1, t_2)$ is indicated by a pyramidal arrow. The impulse $\delta_{\mathbb{R}^2/P}(t_1, t_2)$, with $P = \mathbb{Z}_3^1(D_1, D_2)$, is given by the periodic repetition of the impulse on \mathbb{R}^2 with repetition centers $\mathbb{Z}_3^1(D_1, D_2)$. The discrete impulse $\delta_L(t_1, t_2)$ and its periodic repetition $\delta_{L/P}(t_1, t_2)$, with $L = \mathbb{Z}_2^1(d_1, d_2)$ and $P = \mathbb{Z}_3^1(2d_1, 4d_2)$, are also shown.

UT↓ 4.13 Symmetry Theory

In Sect. 4.7, the standard symmetry pairs, namely even/odd, real/imaginary and Hermitian/anti-Hermitian, were introduced. In this section, we try to understand what these symmetries have in common with the target to get an answer to the question: *what is a symmetry?* We shall give a formal answer in the framework of linear spaces and operators. In this investigation, we are motivated by the famous sentence of the mathematician Emil Artin (1898–1962): “The investigation of symmetries of a given mathematical structure has always yielded the most powerful results”.⁷

4.13.1 Preliminary Considerations

Let H be the Hilbert space of square integrable signals $L_2(I)$ or a subspace of the same space. Then, a *symmetry* on H may be introduced as a *property* Π that some signals of H have and some others have not. Hence, the property Π identifies a subset of H

$$S = \{s \in H \mid s \text{ with property } \Pi\}.$$

For instance, the even symmetry is given by the property $s(-t) = s(t)$, which identifies the class of even signals

$$E = \{s \in H \mid s(-t) = s(t)\}.$$

Analogously, the odd symmetry $s(-t) = -s(t)$ identifies the class of odd signals

$$O = \{s \in H \mid s(-t) = -s(t)\}.$$

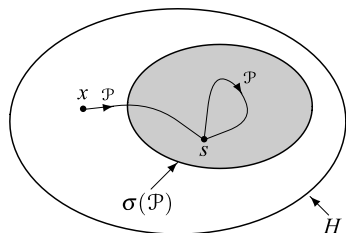
This viewpoint of thinking of a symmetry as a property is useful for the interpretation and, in fact, it corresponds to the common sense of what a symmetry means. However, it is difficult to proceed mathematically with properties, since at this level we do not have a consolidated algebra. The best solution we have found is to consider *a symmetry as a class of symmetric signals*. For instance, the class E of even signals will be considered as the even symmetry and so will be the class O .

Working with subclasses of the given class H , we can apply the algebra of sets, and the meaning, e.g., of the intersection of two symmetries becomes immediately clear. Furthermore, we can also make use of the algebra of linear spaces. In fact, we have seen in Sect. 4.5 that even and odd symmetries, intended as classes, have the structure of *subspaces* and this properties can be seen for other classes of “symmetric” signals.

Another advantage of this procedure is that symmetries can be generated by special linear operators, *projectors* and *reflectors*.

⁷The Symmetry Theory will not be used until Chap. 14. The main application will be seen in Chap. 15 with wavelets.

Fig. 4.19 H is the reference signal space and $\sigma(\mathcal{P})$ is the class of symmetric signals generated by the projector \mathcal{P} ; $s = \mathcal{P}[x]$ gives the projection of x onto $\sigma(\mathcal{P})$ and $s = \mathcal{P}[s]$ for any $s \in \sigma(\mathcal{P})$



4.13.2 General Definition of Symmetry

We recall from Definition 4.2 that a *projector* is an operator $\mathcal{P} : H \mapsto H$ with the idempotency property $\mathcal{P}^2 = \mathcal{P}$, where H is typically $L_2(I)$, but in general may be a subspace, $H \subset L_2(I)$.

Definition 4.6 Given a projector $\mathcal{P} : H \mapsto H$, the symmetry generated by \mathcal{P} is the subspace

$$\sigma(\mathcal{P}) = \{s \in H \mid \mathcal{P}[s] = s\}. \quad (4.103)$$

Hence, the subclass $\sigma(\mathcal{P})$ of symmetric signals in H is characterized by the property $\mathcal{P}[s] = s$, as shown in Fig. 4.19.

The interpretation of (4.103) is as follows: while in general the projector \mathcal{P} *changes* signals, that is, $\mathcal{P}[x] \neq x$, the application of \mathcal{P} leaves the signals having the symmetry $\sigma(\mathcal{P})$ unchanged. From the idempotency property, $\mathcal{P}^2 = \mathcal{P}$, it follows that, for every signal x , the output $y = \mathcal{P}[x]$ is a signal with the symmetry $\sigma(\mathcal{P})$ and indeed $\mathcal{P}[y] = \mathcal{P}^2[x] = \mathcal{P}[x] = y$. Hence, \mathcal{P} *extracts* the part of a signal with the symmetry $\sigma(\mathcal{P})$.

Note that, by definition (4.103), signals with the symmetry $\sigma(\mathcal{P})$ are eigenfunctions of the projector \mathcal{P} with eigenvalue $\lambda = 1$. Moreover, from the idempotency property, the projector \mathcal{P} generates its eigenfunctions starting from arbitrary signals.

Example 4.5 We illustrate the above definitions for the even (E) symmetry, which is generated by the projector

$$\mathcal{P}_E = \frac{1}{2}(\mathcal{J} + \mathcal{J}_-) \implies \mathcal{P}_E[x] = \frac{1}{2}x + \frac{1}{2}x_- \quad (4.104)$$

where \mathcal{J} is the identity operator, \mathcal{J}_- is the reflector operator (see Sect. 4.5) and $x_-(t) = x(-t)$ is the reflected version of $x(t)$. So, we see that \mathcal{P}_E “extracts the E part” of a signal as $s = \mathcal{P}_E(x)$ and, for an E signal, we find that $\mathcal{P}_E[s] = s$, that is, $\frac{1}{2}s + \frac{1}{2}s_- = s$, which is equivalent to $s(-t) = s(t)$, the standard definition of an even signal.

Analogous considerations hold for the odd (O) symmetry, where the projector

$$\mathcal{P}_O = \frac{1}{2}(\mathcal{J} - \mathcal{J}_-) \implies \mathcal{P}_O[x] = \frac{1}{2}x - \frac{1}{2}x_-, \quad (4.105)$$

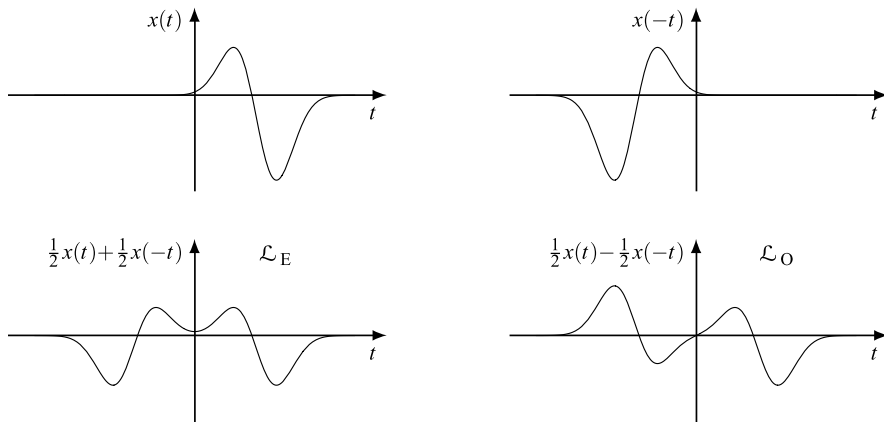


Fig. 4.20 Construction of E and O signals starting from an arbitrary signal $x(t)$

“extracts the O part” of a signal. So, from $\mathcal{P}_O[s] = s$ we obtain the standard definition of O symmetry $s(-t) = -s(t)$. Note also that $\mathcal{P}_E^2 = \mathcal{P}_E$ and $\mathcal{P}_O^2 = \mathcal{P}_O$, as required by the projector property.

Figure 4.20 illustrates the action of the projectors \mathcal{P}_E and \mathcal{P}_O . Starting from a general signal $x(t)$, the reflected version $x(-t)$ is first obtained, then \mathcal{P}_E gives the even part as $\frac{1}{2}x(t) + \frac{1}{2}x(-t)$ and \mathcal{P}_O the odd part as $\frac{1}{2}x(t) - \frac{1}{2}x(-t)$.

Example 4.6 The operator \mathcal{P}_c defined by the input–output relation

$$\mathcal{P}_c \quad y(t) = 1(t)x(t), \quad t \in \mathbb{R},$$

where $1(t)$ is the unitary step signal, provides the *causal* version of the signal $\mathcal{P}[x] = x_c$. Considering that $\mathcal{P}^2[x] = x_c$, the operator \mathcal{P}_c is a projector and generates the symmetry $\sigma(\mathcal{P}_c)$ of causal signals. The complementary symmetry is provided by the projector \mathcal{P}_a defined by $y(t) = 1(-t)x(t)$, which generates the symmetry of *anticausal* signals.

The purpose of this example is showing that symmetries must be intended in a generalized sense (usually causality is not called symmetry), but with the algebraic structure of classical symmetries.

Example 4.7 In the previous section, we have seen that an orthonormal basis allows defining an orthogonal projector \mathcal{P}_M (see Proposition 4.5). The symmetry generated by this projector is the subspace $\sigma(\mathcal{P}_M)$ spanned by the sub-basis Φ_M . The property of signals in $\sigma(\mathcal{P}_M)$ is that they have an M -term expansion provided by the basis Φ_M , while arbitrary signals have an infinite term expansion, in general.

4.13.3 Properties of a Symmetry

We complete the interpretation of a symmetry with some fundamental properties.

A first property is concerned with the *range space*, or *image*, of the projector generating the symmetry $\sigma(\mathcal{P})$. We recall that the *image* of a linear operator $\mathcal{L} : H \mapsto H$ is the subspace $\text{im}(\mathcal{L}) = \{\mathcal{L}[s] \mid s \in H\}$.

Proposition 4.7 *The image of a projector $\mathcal{P} : H \mapsto H$ is given by the symmetry it generates: $\text{im}(\mathcal{P}) = \sigma(\mathcal{P})$.*

This is a consequence of idempotency property. In fact, if $y = \mathcal{P}[s] \in \text{im}(\mathcal{P})$, then $\mathcal{P}[y] = \mathcal{P}^2[s] = \mathcal{P}[s] = y$. Next, the fundamental result:

Theorem 4.9 *Every subspace $S \subset H$ is a symmetry.*

Proof We have to find a projector \mathcal{P} such that $\sigma(\mathcal{P}) = S$. Now, every subspace S , as a vector space, has a basis $\mathbf{G}_S = \{\beta_n \mid n \in \mathcal{N}\}$ and, without restriction by Schmidt orthogonalization procedure, \mathbf{G}_S is assumed to be orthonormal, that is, $\langle \beta_m, \beta_n \rangle = \delta_{mn}$ [12]. Next, consider the kernel

$$h_B(t, u) = \sum_{n \in \mathcal{N}} \beta_n(t) \beta_n^*(u) \quad (4.106)$$

and the corresponding linear operator \mathcal{P} . The kernel of \mathcal{P}^2 can be evaluated by the composition law (4.45)

$$\begin{aligned} h_{12}(t_3, t_1) &= \int_I dt_2 h_B(t_3, t_2) h_B(t_2, t_1) \\ &= \sum_{m, n \in \mathcal{N}} \beta_m(t_3) \left\{ \int_I dt_2 \beta_m^*(t_2) \beta_n(t_2) \right\} \beta_n^*(t_1) = \sum_{m, n \in \mathcal{N}} \beta_m(t_3) \delta_{mn} \beta_n^*(t_1) \end{aligned}$$

where $\{\cdot\} = \delta_{mn}$ because of orthonormality. Hence $h_{12}(t_3, t_1) = \sum_{n \in \mathcal{N}} \beta_m(t_3) \times \beta_n^*(t_1) = h_B(t_3, t_1)$, which states that $\mathcal{P}^2 = \mathcal{P}$ and \mathcal{P} is a projector. The fact that $\sigma(\mathcal{P}) = S$ is evident by noting that

$$\mathcal{P}[s|t] = \int_I du h_B(t, u) s(u) = \sum_{n \in \mathcal{N}} \beta_n(t) \int_I du \beta_n^*(u) s(u) = s(t). \quad \square$$

A symmetry S defines a projector \mathcal{P} such that $S = \sigma(\mathcal{P})$, but \mathcal{P} is not unique. However, uniqueness is assured for Hermitian projectors [12].

Proposition 4.8 *Given a subspace S , there is a unique Hermitian projector that generates it.*

In the previous proof, the projector defined by (4.106) is Hermitian.

4.13.4 Complementary Projector and Binary Symmetries

A projector $\mathcal{P} : H \mapsto H$ identifies an operator $\mathcal{J}_H - \mathcal{P}$ that is itself a projector,

$$(\mathcal{J}_H - \mathcal{P})^2 = \mathcal{J}_H - \mathcal{P}, \quad (4.107)$$

which is called the *complementary projector* of \mathcal{P} (vice versa, \mathcal{P} is the complementary of $\mathcal{J}_H - \mathcal{P}$). Here, \mathcal{J}_H is the identity on H .

In this context, it is clear that two projectors \mathcal{P}_0 and \mathcal{P}_1 are complementary whenever

$$\mathcal{P}_0 + \mathcal{P}_1 = \mathcal{J}_H. \quad (4.108)$$

They also satisfy the orthogonality condition for operators

$$\mathcal{P}_0 \mathcal{P}_1 = \mathcal{P}_1 \mathcal{P}_0 = 0. \quad (4.109)$$

So, from (4.109), signals with the symmetry $\sigma(\mathcal{P}_0)$ have null components belonging to the complementary symmetry $\sigma(\mathcal{P}_1)$, and signals with the symmetry $\sigma(\mathcal{P}_1)$ have null components belonging to the symmetry $\sigma(\mathcal{P}_0)$. Note that $\sigma(\mathcal{P}_0)$ and $\sigma(\mathcal{P}_1)$ are disjoint, except for the zero signal $s(t) = 0$ which belongs to both. This allows the decomposition of an arbitrary signal x of H in the form

$$x = \mathcal{J}_H[x] = \mathcal{P}_0[x] + \mathcal{P}_1[x] = s_0 + s_1 \quad (4.110)$$

where s_0 belongs to the symmetry $\sigma(\mathcal{P}_0)$ and s_1 belongs to the complementary symmetry $\sigma(\mathcal{P}_1)$. Indeed, such a decomposition is unique, as immediately follows from (4.108) and from the property “ s_0/s_1 has the symmetry $\sigma(\mathcal{P}_0)/\sigma(\mathcal{P}_1)$ ”. This is illustrated in Fig. 4.21. Using the terminology of vector spaces we can write that H is the *direct sum* of the symmetries $\sigma(\mathcal{P}_0)$ and $\sigma(\mathcal{P}_1)$, symbolized

$$\sigma(\mathcal{P}_0) \oplus \sigma(\mathcal{P}_1) = H. \quad (4.111)$$

In the previous examples, we have seen projectors and the corresponding complementary projectors. The pairs of standard symmetries seen at the beginning of the section may be handled by each other complementary projectors.

A very relevant case is when the projectors \mathcal{P} and $\mathcal{J}_H - \mathcal{P}$ are *Hermitian*. Then, the symmetric components s_0 and s_1 become *orthogonal* (see Proposition 4.9).

About the Identity Operator

Usually the identity operator \mathcal{J} refers to the class of signals $\mathcal{S}(I)$, as the operator that is “transparent”, giving $\mathcal{J}[x] = x$ for every $x \in \mathcal{S}(I)$. In this case, its kernel is $h(t, u) = \delta_I(t - u)$, where δ_I is the impulse on I . In the present context, the identity is confined to a given subclass of $\mathcal{S}(I)$, specifically to a subspace H of $L_2(I)$. Then, considering a symmetry $S = \sigma(\mathcal{P})$, where by definition the signals

$$\sigma(\mathcal{P}_0) \oplus \sigma(\mathcal{P}_1) = H$$

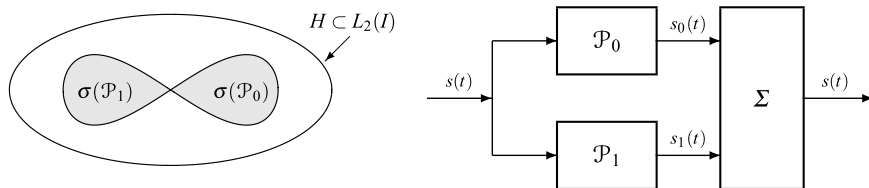


Fig. 4.21 Binary symmetry generated by a projector $\mathcal{P}_0 : H \mapsto H$ and by its complement $\mathcal{P}_1 = \mathcal{J}_H - \mathcal{P}_0$. A signal $s(t)$ is uniquely decomposed into the symmetric components $s_0(t)$ and $s_1(t)$

have the “transparency” property $\mathcal{P}[s] = s$, we realized that \mathcal{P} is the identity operator on S .

Having assumed that H is a subspace, the identity \mathcal{J}_H in (4.107) represents itself a projector and could be denoted by \mathcal{P}_H as well. Note that in Fig. 4.21, where the signal s is decomposed into the symmetric components $s_0 = \mathcal{P}_0[s]$ and $s_1 = \mathcal{P}_1[s]$, the reconstruction $s = s_0 + s_1$ holds if $s \in H$, otherwise the reconstruction gives $\mathcal{P}_H[s] = \mathcal{J}_H[s]$, that is, the projection of s onto H .

Note also that when H is a proper subspace of $L_2(I)$, the kernel of $\mathcal{P}_H = \mathcal{J}_H$ is no longer given by the impulse on I .

4.13.5 Symmetries in Terms of Reflectors

We now introduce another useful way to generate symmetries. A binary symmetry, interpreted as the pair $\sigma(\mathcal{P}_0), \sigma(\mathcal{P}_1)$, can be generated starting from a single operator $\mathcal{B} : H \mapsto H$ with the property

$$\boxed{\mathcal{B}^2 = \mathcal{J}_H}, \quad (4.112)$$

which will be called a *binary reflector* [11].

A binary reflector \mathcal{B} allows defining a pair of projectors as

$$\mathcal{P}_0 = \frac{1}{2}(\mathcal{J}_H + \mathcal{B}), \quad \mathcal{P}_1 = \frac{1}{2}(\mathcal{J}_H - \mathcal{B}). \quad (4.113)$$

In fact, from (4.112) we have that both \mathcal{P}_0 and \mathcal{P}_1 are projectors. Moreover, \mathcal{P}_0 and \mathcal{P}_1 are complementary and orthogonal, that is,

$$\mathcal{P}_0 + \mathcal{P}_1 = \mathcal{J}_H, \quad \mathcal{P}_0\mathcal{P}_1 = 0. \quad (4.114)$$

Given two complementary projectors \mathcal{P}_0 and \mathcal{P}_1 , the corresponding reflector \mathcal{B} can be obtained by solving (4.113),

$$\mathcal{B} = \mathcal{P}_0 - \mathcal{P}_1. \quad (4.115)$$

Note that to get the property $\mathcal{B}^2 = \mathcal{J}_H$, the projectors must be orthogonal. In fact, from (4.115) $\mathcal{B}^2 = \mathcal{P}_0^2 + \mathcal{P}_1^2 - \mathcal{P}_1\mathcal{P}_0 - \mathcal{P}_0\mathcal{P}_1 = \mathcal{P}_0 + \mathcal{P}_1 = \mathcal{J}$ if $\mathcal{P}_0\mathcal{P}_1 = \mathcal{P}_1\mathcal{P}_0 = 0$.

A binary reflector \mathcal{B} generates a *binary symmetry*,⁸ namely

$$\begin{aligned}\sigma(\mathcal{P}_0) &= \{s \mid \mathcal{P}_0[s] = s\} = \{s \mid \mathcal{B}[s] = s\}, \\ \sigma(\mathcal{P}_1) &= \{s \mid \mathcal{P}_1[s] = s\} = \{s \mid \mathcal{B}[s] = -s\}.\end{aligned}\tag{4.116}$$

Thus, the symmetry $\sigma(\mathcal{P}_0)$ consists of the eigenfunctions of \mathcal{P}_0 with eigenvalue $\lambda = 1$, or equivalently, of the eigenfunctions of \mathcal{B} with eigenvalue $\lambda = 1$. Similarly, the symmetry $\sigma(\mathcal{P}_1)$ consists of the eigenfunctions of \mathcal{P}_1 with eigenvalue $\lambda = 1$, or of the eigenfunctions of \mathcal{B} with eigenvalue $\lambda = -1$.

Finally, we note that, from (4.112), it follows that $\mathcal{B}^{-1} = \mathcal{B}$ and we can recover a signal after applying a reflector, whereas the application of a projector is not reversible.

As an example, the symmetry pair E/O is generated by the reflector

$$\mathcal{B}[x] = x_{-}\tag{4.117}$$

which represents the “time reflection” operation. Note that the “time reflection” operator is reversible. In fact, applying (4.117) twice, we recover the original signal, and therefore $\mathcal{B}^2 = \mathcal{J}_H$.

4.13.6 *M*-Ary Symmetries

We have seen that a pair of complementary and orthogonal projectors \mathcal{P}_0 and \mathcal{P}_1 generates a *binary symmetry* and that same symmetries can be generated by a single binary reflector with the property $\mathcal{B}^2 = \mathcal{J}$. This can be generalized to *M*-ary symmetries.

Definition 4.7 A set of *M* projectors $\mathcal{P}_i : H \mapsto H$, $i = 0, 1, \dots, M - 1$, form a *system of M-ary projectors* if

$$\mathcal{P}_i\mathcal{P}_j = 0 \quad \text{for } i \neq j, \quad \sum_{i=0}^{M-1} \mathcal{P}_i = \mathcal{J}_H,\tag{4.118}$$

that is, the \mathcal{P}_i are pairwise orthogonal and provide a *resolution of the identity* on *H* (see [12]).

A system of *M*-ary projectors defines an *M*-ary symmetry $\sigma(\mathcal{P}_i, i = 0, 1, \dots, M - 1)$, which allows the decomposition of a signal $s \in H$ into *M* symmetric components $s_i = \mathcal{P}_i[s]$. The decomposition is unique and thus the subspace *H* is given

⁸The term “binary symmetry” refers both to the individual symmetries, e.g., $\sigma(\mathcal{P}_0)$ is a binary symmetry, and to the pair $\sigma(\mathcal{P}_0), \sigma(\mathcal{P}_1)$.

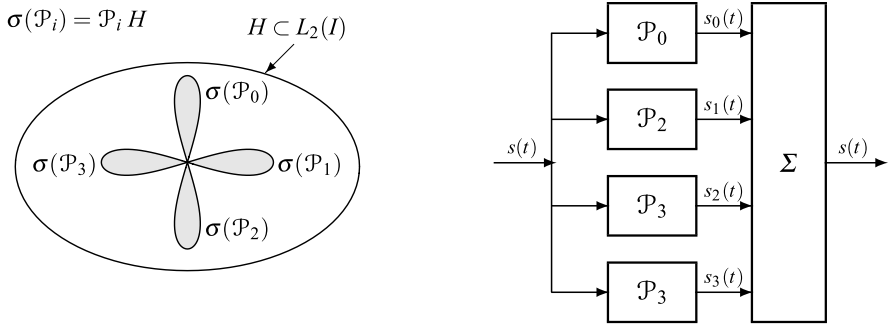


Fig. 4.22 Illustration of a *quaternary symmetry* generated by a system of quaternary projectors and corresponding decomposition of a signal $s(t)$ of a subspace $H \subset L_2(I)$ into four symmetric components $s_i(t)$

as the direct sum

$$\sigma(\mathcal{P}_0) \oplus \dots \oplus \sigma(\mathcal{P}_{M-1}) = H$$

as shown in Fig. 4.22 for $M = 4$.

Proposition 4.9 *If in the system of Definition 4.7 the M -ary projectors are Hermitian, the symmetric components $s_i = \mathcal{P}_i[s]$ are pairwise orthogonal, $s_i \perp s_j, i \neq j$.*

The proof is based on the identity of the inner product (see Problem 4.20)

$$\langle \mathcal{P}_i[x], \mathcal{P}_j[x] \rangle = \langle x, \mathcal{P}_i^* \mathcal{P}_j[x] \rangle, \tag{4.119}$$

where $\mathcal{P}_i \mathcal{P}_j^* = 0$ for $i \neq j$ by condition (4.118).

Also in the M -ary case, the symmetry can be obtained by a single reflector. An M -ary reflector \mathcal{B} is an operator with the property

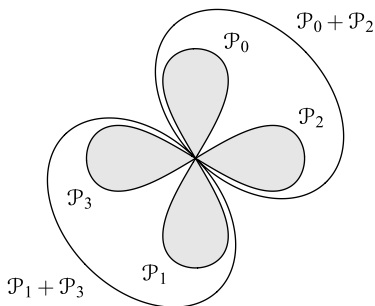
$$\boxed{\mathcal{B}^M = \mathcal{J}_H.} \tag{4.120}$$

Now, an M -ary reflector provides a system of M -ary projectors \mathcal{P}_i according to the relation

$$\mathcal{P}_i = \frac{1}{M} \sum_{s=0}^{M-1} \mathcal{B}^s W_M^s, \quad i = 0, 1, \dots, M - 1, \tag{4.121}$$

where $W_M = e^{i2\pi/M}$ and \mathcal{B}^s is \mathcal{B} applied s times (\mathcal{B}^0 must be intended as the identity operator \mathcal{J}_H). We can prove that the operators \mathcal{P}_i defined by (4.121) are projectors that verify conditions (4.118). For the proof, we use the orthogonality of the exponentials $W_M^k, k = 0, 1, \dots, M$ (the details are left to the reader).

Fig. 4.23 Quaternary symmetries $\sigma(\mathcal{P}_m)$ with marginal symmetries $\sigma(\mathcal{P}_0 + \mathcal{P}_2)$ and $\sigma(\mathcal{P}_1 + \mathcal{P}_3)$ (for brevity, a symmetry $\sigma(\mathcal{P})$ is indicated by the corresponding projector \mathcal{P})



Given a system of M -ary projectors \mathcal{P}_i , the M -ary reflector is obtained as (see Problem 4.20)

$$\mathcal{B} = \sum_{i=0}^{M-1} \mathcal{P}_i W_M^{-i}. \tag{4.122}$$

In conclusion, as seen for binary symmetries, M -ary symmetries can be generated by M projectors as well as by a single M -ary reflector.

It is remarkable that if M is not prime, the M -ary symmetries $\sigma(\mathcal{P}_i)$ can be grouped into *super-symmetries*. For instance, if $M = 4$ we find that

$$\mathcal{P}_0^{(2)} = \mathcal{P}_0 + \mathcal{P}_2 = \frac{1}{2}(\mathcal{J}_H + \mathcal{B}^2), \quad \mathcal{P}_1^{(2)} = \mathcal{P}_1 + \mathcal{P}_3 = \frac{1}{2}(\mathcal{J}_H - \mathcal{B}^2)$$

are projectors that generate two binary symmetries $\sigma(\mathcal{P}_0^{(2)})$ and $\sigma(\mathcal{P}_1^{(2)})$. We can check that $\sigma(\mathcal{P}_0), \sigma(\mathcal{P}_2) \subset \sigma(\mathcal{P}_0^{(2)})$ and $\sigma(\mathcal{P}_1), \sigma(\mathcal{P}_3) \subset \sigma(\mathcal{P}_1^{(2)})$, as illustrated in Fig. 4.23. In this sense, e.g., $\sigma(\mathcal{P}_0^{(2)})$ is a super-symmetry of $\sigma(\mathcal{P}_1)$ and $\sigma(\mathcal{P}_1)$ is a sub-symmetry of $\sigma(\mathcal{P}_0^{(2)})$.

M -ary symmetries can be obtained in several ways, autonomously or by combination of symmetries of smaller order, as we see in the following examples.

▽ *Example 4.8* The Fourier operator \mathcal{F} , which will be introduced in Chap. 5, verifies the condition $\mathcal{F}^4 = \mathcal{J}$. Hence, it is a quaternary reflector, and from (4.122) we obtain the corresponding projectors

$$\mathcal{P}_m = \sum_{s=0}^3 \mathcal{F}^s i^{ms}, \quad m = 0, 1, 2, 3.$$

Example 4.9 In Example 4.7, we have considered the projector \mathcal{P}_M obtained from an orthonormal basis $\Phi = \{\varphi_n \mid n \in \mathbb{N}_0\}$. The kernel of \mathcal{P}_M is obtained by summing the product $\varphi_n(t)\varphi_n^*(u)$ over the natural $0, 1, \dots, M-1$. By summing these products from M to $+\infty$ we obtain the kernel of the complementary projector $\mathcal{J} - \mathcal{P}_M$. In such a way, we have obtained a binary symmetry.

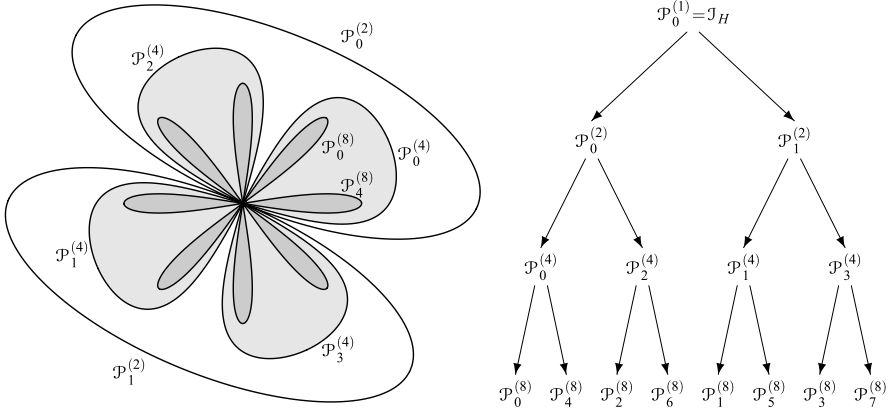


Fig. 4.24 Octal symmetries and corresponding quaternary and binary super-symmetries

To get an M -ary symmetry from the basis Φ it is sufficient to partition the index set \mathbb{N}_0 into M parts: $\mathcal{N}_0, \mathcal{N}_1, \dots, \mathcal{N}_{M-1}$. Then, the i th projector \mathcal{P}_i is defined by the kernel

$$\mathcal{P}_i : h_i(t, u) = \sum_{n \in \mathcal{N}_i} \varphi_n(t) \varphi_n^*(u), \quad i = 0, 1, \dots, M - 1.$$

Using orthonormality, we can check that the \mathcal{P}_i form a system of M -ary projectors and thus define an M -ary symmetry.

4.13.7 Hierarchies of Symmetries

A *hierarchy of symmetries* consists of several classes of symmetries displayed in a pyramidal order, where the symmetries of the first class contain those of the second, the symmetries of the second contain those of the third, and so on. Hierarchies can be expressed starting from the powers of an M -ary reflector \mathcal{B} , as we now show for the cases of an *octal* class.

Octal Symmetries

An octal symmetry (Fig. 4.24) is generated by a reflector \mathcal{B} of order 8, that is,

$$\mathcal{B}^8 = \mathcal{J}_H.$$

This reflector generates the 8 projectors

$$\mathcal{P}_m^{(8)} = \frac{1}{8} \sum_{r=0}^7 W_8^{mr} \mathcal{B}^r, \quad m = 0, 1, \dots, 7.$$

First, note that also \mathcal{B}^2 and \mathcal{B}^4 are reflectors, of order 4 and of order 2, respectively. Then we can relate the *octal* symmetry to two *quaternary* symmetries (generated by \mathcal{B}^2) and to the *binary* symmetries (generated by \mathcal{B}^4).

In order to establish the relation of the 8 octal symmetries with their quaternary super-symmetries, we note that

$$\mathcal{L}_m^{(8)} + \mathcal{L}_{m+4}^{(8)} = \frac{1}{8} \sum_{r=0}^7 (W_8^{mr} + W_8^{(m+4)r}) \mathcal{B}^r = \frac{1}{8} \sum_{r=0}^7 (W_8^{mr} + W_8^{mr} (-1)^r) \mathcal{B}^r$$

where the sum in brackets is zero for odd r and is $2W_8^{mr}$ for even r . So, we have

$$\mathcal{L}_m^{(4)} = \frac{1}{4} \sum_{s=0}^3 W_4^{ms} \mathcal{B}^{2s} = \mathcal{L}_m^{(8)} + \mathcal{L}_{m+4}^{(8)}, \tag{4.123}$$

which states that octal symmetry can be suitably grouped to obtain the quaternary symmetry generated by \mathcal{B}^2 .

Analogously, we can combine the four $\mathcal{L}_m^{(4)}$ as $\mathcal{L}_0^{(2)} = \mathcal{L}_0^{(4)} + \mathcal{L}_2^{(4)}$ and $\mathcal{L}_1^{(2)} = \mathcal{L}_1^{(4)} + \mathcal{L}_3^{(4)}$ to obtain the two binary super-symmetries. Hence, we have the overall relation between symmetries shown in Fig. 4.24.

Comments on Symmetry Theory

The Symmetry Theory developed in this section is completely original and not considered in other textbooks and perhaps it deserves a further development. It is “transversal” with respect to Signal Theory in the sense that it can be used for the reformulation of several results. The question is: Is it really useful? In the author’s opinion, the main interest lies in an elegant and compact *interpretation* of results obtained with other techniques, as we shall see in Chap. 14 with filter banks and in Chap. 15 with wavelets, and in general in the decomposition of signals.

But in some cases, Symmetry Theory can also be used as a *tool* to discover new results. As an example, it was used to find the exact (non-numerical) eigenvectors of the discrete Fourier transform (DFT) [5], a problem that was long recognized to be very challenging.

4.14 Problems

4.1 ★ [Sect. 4.1] Explicitly write (4.12a) with $I_0 = \mathbb{R}$ and $P = \mathbb{Z}(T_p)$ and (4.12b) with $I_0 = \mathbb{R}$, $P = \mathbb{Z}(T_p)$ and $P_0 = \mathbb{Z}(\frac{1}{3}T_p)$. Then, combine these formulas.

4.2 ★★ [Sect. 4.1] Explicitly write the multirate identity (4.13) with $I_0 = \mathbb{Z}$ and $P = \mathbb{Z}(5)$. Then, prove the identity in the general case, starting from (4.12a), (4.12b).

4.3 ★ [Sect. 4.2] Show that the ordinary integral over \mathbb{R} verifies the general properties of the Haar integral.

4.4 ★ [Sect. 4.2] Show that the Haar integral over $\mathbb{Z}(T)$ verifies the general properties of the Haar integral.

4.5 ★★★ [Sect. 4.3] Prove the identity

$$\int_{-\infty}^{+\infty} s(t) dt = \int_0^{T_p} \sum_{n=-\infty}^{+\infty} s(t - nT_p) dt,$$

which is a particular case of (4.12a) for $I_0 = \mathbb{R}$ and $P = \mathbb{Z}(T_p)$.

4.6 ★★ [Sect. 4.3] Using (4.6), explicitly write the integral of a signal (t_1, t_2) , $\in \mathbb{R} \times \mathbb{Z}(d)$. Then, evaluate the integral of the signal $s(t_1, t_2) = e^{-(t_1+t_2)}$ for $t_1, t_2 \geq 0$ and $s(t_1, t_2) = 0$ elsewhere.

4.7 ★★★ [Sect. 4.5] Prove that the inner product of an even real signal and an odd real signal on $\mathbb{Z}(T)/\mathbb{Z}(NT)$ is zero. *Hint*: consider the cases: N even and N odd separately.

4.8 ★★ [Sect. 4.5] The abstract definition of the *adjoint* of an operator \mathcal{L} is formulated through the inner product as an operator \mathcal{L}^* such that

$$\langle \mathcal{L}[x], y \rangle = \langle x, \mathcal{L}^*[y] \rangle, \quad \forall x, y \in L_2(I). \quad (4.124)$$

It can be shown that this condition uniquely define \mathcal{L}^* from \mathcal{L} [12].

Prove condition (4.124) through the kernels, where the kernel of \mathcal{L}^* is given by (4.47).

4.9 ★★★ [Sect. 4.5] Prove that the operators $\mathcal{L}_E = \frac{1}{2}(\mathcal{J} + \mathcal{J}_-)$ and $\mathcal{L}_O = \frac{1}{2}(\mathcal{J} - \mathcal{J}_-)$ are idempotent and orthogonal to each other.

4.10 ★★ [Sect. 4.5] Prove that the identity of the inner product in $L_2(I)$

$$\langle \mathcal{L}[x], \mathcal{K}[x] \rangle = \langle x, \mathcal{L}^*\mathcal{K}[x] \rangle$$

where \mathcal{L} and \mathcal{K} are arbitrary operators on $L_2(I)$ and \mathcal{L}^* is the adjoint of \mathcal{L} . *Hint*: use the abstract definition of the adjoint reported in Problem 4.8.

4.11 ★ [Sect. 4.6] Show that class (4.55) consists of orthogonal functions.

4.12 ★★∇ [Sect. 4.6] Show the orthogonality of the *cardinal functions* (4.53).

4.13 ★★ [Sect. 4.6] Show that cross-energies verify the inequality

$$0 \leq E_{xy}E_{yx} \leq E_xE_y.$$

4.14 *** [Sect. 4.6] Using the inequality for complex numbers

$$|z + z^*| \leq 2|z|, \quad (4.125)$$

prove Schwartz–Gabor inequality (4.42). Note that in (4.125) the equality holds if z is real.

4.15 * [Sect. 4.6] Formulate a basis on a finite group K/P starting from the impulse $\delta_{K/P}$.

4.16 ** [Sect. 4.8] Find the extension and duration of the signal

$$x(t) = \sum_{n=-\infty}^{+\infty} \text{rect}\left(\frac{t - nT_p}{dT_p}\right), \quad t \in \mathbb{R}/\mathbb{Z}(T_p)$$

where d is a positive real number. Discuss the result as a function of d .

4.17 * [Sect. 4.9] Prove the following relations for the minimal extension of the product and the sum of two signals

$$\begin{aligned} e_0(xy) &= e_0(x) \cap e_0(y), \\ e_0(x + y) &\subset e_0(x) \cup e_0(y). \end{aligned}$$

4.18 ** [Sect. 4.9] The signals $x(t)$ and $y(t)$, defined on $\mathbb{R}/\mathbb{Z}(10)$, have the following extensions

$$e(x) = [0, 1) + \mathbb{Z}(10), \quad e(y) = [0, 2) + \mathbb{Z}(10).$$

Find the extension of their convolution.

4.19 ** [Sect. 4.9] Consider the *self-convolution* $s(t) = x * x(t)$, $t \in \mathbb{R}/\mathbb{Z}(T_p)$, of the signal

$$x(t) = \sum_{n=-\infty}^{+\infty} \text{rect}\left(\frac{t - nT_p}{dT_p}\right), \quad t \in \mathbb{R}/\mathbb{Z}(T_p).$$

Find the extension as a function of the parameter d .

4.20 ** [Sect. 4.13] Prove that (4.122), where \mathcal{P}_i form a system of M -ary *orthogonal* projectors, defines an M -ary reflector, that is, an operator with the property $\mathcal{B}^M = \mathcal{J}_H$. *Hint*: first evaluate \mathcal{B}^2 using the orthogonality of the \mathcal{P}_i , then evaluate $\mathcal{B}^3 = \mathcal{B}^2\mathcal{B}$, etc.

Appendix A: Haar Integral Induced by an Isomorphism

If we know the Haar integral over an LCA group H , then we can derive the Haar integral over every $G \sim H$, by using the isomorphism.

Let $\alpha : H \rightarrow G$ be the isomorphism map. Let $s(t)$, $t \in G$, and let $\tilde{s}(h)$, $h \in H$, be the corresponding signal defined on H , which is given by (see (3.62))

$$\tilde{s}(h) = \tilde{s}(h), \quad h \in H.$$

Theorem 4.10 *The integral defined by*

$$\boxed{\int_G dt s(t) = \mu_G \int_H dh \tilde{s}(h)}, \quad (4.126)$$

where μ_G is an arbitrary positive constant, is a correct Haar integral over G .

Proof We have to show that the integral over G defined by (4.126) has the five identification properties listed as Properties 1–5 in Sect. 4.1. We now see that those properties follow from the Haar integral properties on H and isomorphism rules. Properties 1, 2 and 3 are evident. To prove Property 4, that is, that $s_-(t) = s(-t)$ and $s(t)$ have the same integral, it is sufficient to note that $\alpha(-h) = -\alpha(h)$. To prove Property 5, that is, that $s_{t_0}(t) = s(t - t_0)$ and $s(t)$ have the same integral, let $u = \beta(t)$ the inverse mapping and $u_0 = \beta(t_0)$ and note that $s(t - t_0) = s(\alpha(u) - t_0) = s(\alpha(u) - \alpha(u_0)) = \tilde{s}(u - u_0)$, where the last equality is obtained from the separability of the isomorphism map. But, from the shift-invariance of the Haar integral on H , we know that $\tilde{s}(u - u_0)$ and $\tilde{s}(u)$ have the same integral. \square

Appendix B: Integral Independence of a Group Representation

1. We want to prove that the integral defined by (4.18) is independent of the group representation $(\mathbf{G}, H) \mapsto G$, and this should be done for the three kinds of ordinary groups of $\mathcal{G}(\mathbb{R}^m)$, that is, $G = \mathbb{R}^m$, $G = \text{lattice}$ and $G = \text{grating}$.

When $G = \mathbb{R}^m$, (4.18) gives

$$\int_{\mathbb{R}^m} dt s(\mathbf{t}) = d(\mathbf{G}) \int_{\mathbb{R}^m} d\mathbf{h} s(\mathbf{G}\mathbf{h}), \quad (4.127)$$

where \mathbf{G} is an arbitrary regular matrix. The first is the ordinary integral of $s(\mathbf{t})$, evaluated with respect to an orthogonal coordinate system (with basis given by the identity matrix). In the second integral, we have the coordinate change $\mathbf{t} = \mathbf{G}\mathbf{h}$, which can be done without changing the result, provided that a multiplication by the *absolute value of the Jacobian determinant* is introduced. But, this factor is just $d(\mathbf{G})$.

When G is a lattice, we have the sum of all signal values on the lattice, which are independent of the lattice representation. On the other hand, also the lattice determinant $d(G)$ is independent of the basis \mathbf{G} .

The proof of independence when G is a grating is less trivial [4] and is omitted. It is based on the idea that, starting from an arbitrary representation $(\mathbf{G}, \mathbb{R}^p \times \mathbb{Z}^q)$, we finally obtain (working with a matrix partitioning) that the result is the same as with a *canonical representation* (see (16.14)).

2. The integral on a quotient group G/P is obtained by restricting the integration over a cell $[G/P]$. Now, suppose that we have evaluated the integral over a particular cell C , namely

$$\int_{G/P} dt s(\mathbf{t}) = \int_C dt s(\mathbf{t}),$$

and we compare the result obtained with another cell \tilde{C} . As we shall see in Chap. 16, \tilde{C} is related to C by the partition

$$\tilde{C} = \bigcup_{\mathbf{p} \in P_0} [C(\mathbf{p}) + \mathbf{p}]$$

where $\{C(\mathbf{p}), \mathbf{p} \in P_0\}$ is a suitable partition of C and $P_0 \subset P$. So, we have

$$\int_{\tilde{C}} dt s(\mathbf{t}) = \sum_{\mathbf{p} \in P_0} \int_{C(\mathbf{p}) + \mathbf{p}} dt s(\mathbf{t}) = \sum_{\mathbf{p} \in P_0} \int_{C(\mathbf{p})} dt s(\mathbf{t} - \mathbf{p}),$$

where $s(\mathbf{t} - \mathbf{p}) = s(\mathbf{t})$ for the periodicity of $s(t)$. Hence

$$\int_{\tilde{C}} dt s(\mathbf{t}) = \sum_{\mathbf{p} \in P_0} \int_{C(\mathbf{p})} dt s(\mathbf{t}) = \int_C dt s(\mathbf{t}),$$

where we have considered that $C(\mathbf{p})$ is a partition of C .

Appendix C: Proof of Theorem 4.2 on Coordinate Change in \mathbb{R}^m

Suppose that G is an ordinary group of \mathbb{R}^m with representation (\mathbf{G}, H) . After the coordinate change, the group becomes

$$G_{\mathbf{a}} = \{\mathbf{a}^{-1} \mathbf{u} \mid \mathbf{u} \in G\} = \{\mathbf{a}^{-1} \mathbf{G} \mathbf{h} \mid \mathbf{h} \in H\},$$

which states that a representation of $G_{\mathbf{a}}$ is $(\mathbf{G}_{\mathbf{a}}, H)$ with $\mathbf{G}_{\mathbf{a}} = \mathbf{a}^{-1} \mathbf{G}$.

Now, we can apply the general formula (4.18) to derive the Haar integral on $G_{\mathbf{a}}$, namely

$$\int_{G_{\mathbf{a}}} dt s_{\mathbf{a}}(\mathbf{t}) = d(\mathbf{G}_{\mathbf{a}}) \int_H d\mathbf{h} s_{\mathbf{a}}(\mathbf{G}_{\mathbf{a}} \mathbf{h}) \tag{4.128}$$

where

$$s_{\mathbf{a}}(\mathbf{G}\mathbf{a}\mathbf{h}) = s(\mathbf{a}\mathbf{G}\mathbf{a}\mathbf{h}) = s(\mathbf{G}\mathbf{h}).$$

On the other hand, the integral on G is

$$\int_G d\mathbf{u} s(\mathbf{u}) = d(\mathbf{G}) \int_H d\mathbf{h} s(\mathbf{G}\mathbf{h}). \quad (4.129)$$

Then, comparing (4.128) with (4.129) and considering that $d(\mathbf{G}\mathbf{a}) = d(\mathbf{a}^{-1})d(\mathbf{G})$, the conclusion follows.

Appendix D: Proof that $L_p(I)$ Is a Vector Space

It is sufficient to show that

1. $L_p(I)$ is closed with respect to the sum;
2. $L_p(I)$ is closed with respect to the multiplication by a scalar.

We begin by showing property 2, so let $x \in L_p(I)$, $\alpha \in C$ and $y = \alpha x$. Then

$$\int_I dt |y(t)|^p = \int_I dt |\alpha|^p |x(t)|^p = |\alpha|^p \int_I dt |x(t)|^p,$$

which exists and is finite. Hence property 2 is proved. To show property 1, let $x, y \in L_p(I)$, $z = x + y$. Then, by defining $A = \{t \in I : |x(t)| \geq |y(t)|\}$, we can write

$$|z(t)|^p = |x(t) + y(t)|^p \leq (|x(t)| + |y(t)|)^p$$

and

$$|x(t)| + |y(t)| \leq \begin{cases} 2|x(t)|, & \text{if } t \in A; \\ 2|y(t)|, & \text{if } t \notin A. \end{cases}$$

Therefore, we get

$$\int_I dt |z(t)|^p \leq \int_I dt (|x(t)| + |y(t)|)^p \leq \int_A dt 2^p |x(t)|^p + \int_{A^c} dt 2^p |y(t)|^p,$$

which exist and are finite by property 2, and hence property 1 is proved.

Appendix E: Proof of Theorem 4.6 on Periodic Convolution

With the language of transformations, the theorem claims that (i) the periodic repetitions (or up-periodization) $x(t)$, $y(t)$ of $a(t)$, $b(t)$, $t \in G$, followed by (ii) the convolution $c(t) = x * y(t)$ is equivalent to (iii) the convolution $s(t) = a * b(t)$ followed by (iv) the periodic repetition of $c(t)$, as shown in the top part of Fig 4.25.

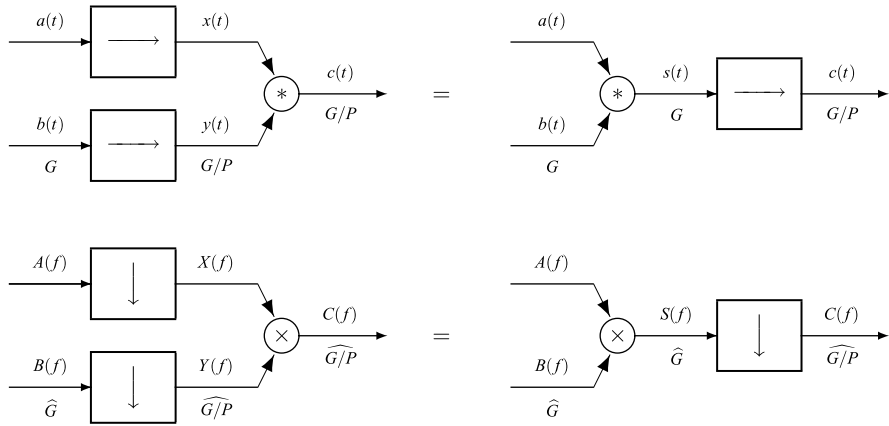


Fig. 4.25 Diagrams for the proof of Theorem 4.6

The proof is carried out in the frequency domain, where the up-periodization $G \rightarrow U = G/P$ becomes the $\widehat{G} \rightarrow \widehat{U}$ down-sampling and the convolution becomes a product, as shown in bottom part of Fig 4.13. Then we have to prove that (i') the down-sampling $\widehat{G} \rightarrow \widehat{U}$ of $A(f)$, $B(f)$, with equations

$$X(f) = A(f), \quad Y(f) = B(f), \quad f \in \widehat{U}$$

followed by (ii') the product $S(f) = X(f)Y(f)$, is equivalent to (iii') the product $C(f) = A(f)B(f)$, followed by (iv') the $\widehat{G} \rightarrow \widehat{U}$ down-sampling, with equation $S(f) = C(f)$, $f \in \widehat{U}$.

Now, the global relation of (i') and (ii') is

$$S(f) = A(f)B(f), \quad f \in \widehat{U},$$

and the global relation of (iii') and (iv') is just the same. This states the equivalence.

Appendix F: Proof of the Noble Identity on Impulse (Theorem 4.8)

We have already observed that if the pair (I_1, I_2) is ordered, that is, $I_1 \subset I_2$ or $I_1 \supset I_2$, the identity is trivial (see (4.88)). If one of the group is a *continuum*, then the pair is always ordered. Therefore, it remains to prove the identity in the case of *nonordered lattices* and *nonordered finite groups*. The proof is not easy and will be articulated in several steps with the main points illustrated by examples.

The main preliminaries are the determinant identity (3.77), that is,

$$d(J \cap K) d(J + K) = d(J) d(K), \tag{4.130}$$

and the following:

Lemma 4.1 *Let (J, K) be a pair of rationally comparable lattices, then for the sum $J + K$ the following partition holds*

$$J + p, \quad p \in [K/(J \cap K)] \stackrel{\Delta}{=} P. \quad (4.131)$$

Proof We start from the partitions of K modulo $J \cap K$, that is,

$$K = J \cap K + [K/(J \cap K)] = J \cap K + P,$$

which allows writing the sum in the form

$$J + K = J + J \cap K + P = J + P. \quad (4.132)$$

□

Here, we have considered that $J \cap K$ is a sublattice of J and then $J + J \cap K = J$. Now, (4.132) assures that partition (4.131) gives the covering of $J + K$, but not that the cosets $J + p$ are pairwise disjoint. To prove that this property holds, we evaluate the cardinality of P . In the partition of $J + K$ modulo J , given by

$$J + q, \quad q \in [(J + K)/J] \stackrel{\Delta}{=} Q, \quad (4.133)$$

the cardinality of Q is $d(J)/d(J + K)$, whereas the cardinality of P is $d(J \cap K)/d(K)$. But, by identity (4.130), these cardinalities coincide. This proves that (4.131) is itself a partition of $J + K$.

Example 4.10 Let

$$J = \mathbb{Z}(25), \quad K = \mathbb{Z}(40), \quad J + K = \mathbb{Z}(5), \quad J \cap K = \mathbb{Z}(200). \quad (4.134)$$

The determinant identity gives $200 \cdot 5 = 25 \cdot 40$. By Lemma 4.1 for the sum $J + K = \mathbb{Z}(5)$, we find the partition

$$\mathbb{Z}(25) + p, \quad p \in [\mathbb{Z}(40)/\mathbb{Z}(200)] = \{0, 40, 80, 120, 160\}$$

which is equivalent to (4.133)

$$\mathbb{Z}(25) + q, \quad q \in [\mathbb{Z}(5)/\mathbb{Z}(25)] = \{0, 5, 10, 15, 20\}.$$

Now, we realize that the two partitions coincide. In fact,

$$\mathbb{Z}(25) + 40 = \mathbb{Z}(25) + 15, \quad \mathbb{Z}(25) + 80 = \mathbb{Z}(25) + 5, \quad \text{etc.}$$

Identity Lemma 4.1 provides the following identity for every function $f(\cdot)$ defined on $J + K$

$$\sum_{v \in J + K} f(v) = \sum_{j \in J} \sum_{p \in [K/(J \cap K)]} f(j + p). \quad (4.135)$$

Proof of the Noble Identity for Lattices If we let $I_1 = A_1$ and $I_2 = A_2$, we have to prove that

$$\begin{aligned} h_a(t, u) &\stackrel{\Delta}{=} \int_{A_1 \cap A_2} ds \delta_{A_1}(t-s) \delta_{A_2}(s-u) \\ &= \delta_{A_1+A_2}(t-u) \stackrel{\Delta}{=} h_b(t, u), \quad t \in A_1, u \in A_2 \end{aligned} \quad (4.136)$$

where, considering that A_1 and A_2 are lattices, the Haar integral is explicitly given by (see (4.8))

$$h_a(t, u) = \sum_{s \in A_1 \cap A_2} d(A_1 \cap A_2) \delta_{A_1}(t-s) \delta_{A_2}(s-u) \quad (4.137)$$

with $t \in A_1$ and $u \in A_2$ being fixed arguments. We note that (see (4.79))

$$\delta_{A_1}(t-s) = 0, \quad t \neq s \quad \text{and} \quad \delta_{A_2}(s-u) = 0, \quad s \neq u,$$

and therefore $\delta_{A_1}(t-s) \delta_{A_2}(s-u) = 0$ for every s and $t \neq u$. Hence, also the sum is zero for $t \neq u$. On the other hand, $\delta_{A_1+A_2}(t-u) = 0$ for $t \neq u$. So, we have proved (4.136) for $t \neq u$.

Next, consider the case $t = u$ noting that this coincidence can be considered only for $t = u \in A_1 \cap A_2$. Since for $s \neq t = u$ the two impulses give a zero contribution, the summation can be limited to the single value $s = t = u$. Hence, we have to find

$$d(A_1 \cap A_2) \delta_{A_1}(0) \delta_{A_2}(0) = \delta_{A_1+A_2}(0)$$

which, considering that $\delta_I(0) = 1/d(I)$ (see (4.79)), is equivalent to

$$d(A_1 \cap A_2) d(A_1 + A_2) = d(A_1) d(A_2). \quad (4.138)$$

But, this is just the determinant identity.

Example 4.11 Consider the case in which

$$\begin{aligned} h_a(t, u) &= \sum_{s \in \mathbb{Z}(30)} 30 \delta_{\mathbb{Z}(6)}(t-s) \delta_{\mathbb{Z}(10)}(s-u), \\ h_b(t, u) &= \delta_{\mathbb{Z}(2)}(t-u). \end{aligned}$$

Now, we suggest the reader to check the different steps of the above proof by writing the arguments in the form $t = 6m, u = 10n, s = 30k$.

Proof of Noble Identity for Finite Groups Now, we let

$$I_1 = A_1/P_1, \quad I_2 = A_2/P_2, \quad (4.139)$$

and we first deal with the case $P_1 = P_2 = P$. Considering that (4.136) has been proved, we perform the summation

$$\sum_{r \in P} h_a(t - r, u) = \sum_{r \in P} h_b(t - r, u), \quad (4.140)$$

which is permitted since $t \in A_1$ and P is a sublattice of A_1 , and therefore $t - r \in A_1$. On the right-hand side, we obtain

$$\sum_{r \in P} h_b(t - r, u) \sum_{r \in P} \delta_{A_1+A_2}(t - r - u) = \delta_{(A_1+A_2)/P}(t - u),$$

where we have used (4.84). On the left-hand side, we find

$$\sum_{r \in P} \int_{A_1 \cap A_2} ds \delta_{A_1}(t - r - s) \delta_{A_2}(s - u) = \int_{A_1 \cap A_2} ds \delta_{A_1/P}(t - s) \delta_{A_2}(s - u).$$

Next, using integration rule (4.12a, 4.12b), we obtain

$$\begin{aligned} & \int_{A_1 \cap A_2} ds \delta_{A_1/P}(t - s) \delta_{A_2}(s - u) \\ &= \int_{(A_1 \cap A_2)/P} ds \sum_{p \in P} \delta_{A_1/P}(t - s - p) \delta_{A_2}(s - u + p) \\ &= \int_{(A_1 \cap A_2)/P} ds \delta_{A_1/P}(t - s) \sum_{p \in P} \delta_{A_2}(s - u + p) \\ &= \int_{(A_1 \cap A_2)/P} ds \delta_{A_1/P}(t - s) \delta_{A_2/P}(s - u), \end{aligned}$$

where we have considered that $\delta_{A_1/P}(t - s - p) = \delta_{A_1/P}(t - s)$, and we have used identity (4.84) again. At this point we have obtained the identity

$$\int_{(A_1 \cap A_2)/P} ds \delta_{A_1/P}(t - s) \delta_{A_2}(s - u) = \delta_{(A_1+A_2)/P}(t - u), \quad (4.141)$$

which proves (4.87) in the case $I_1 = A_1/P$, $I_2 = A_2/P$.

Finally, we develop the general case (4.139). Considering that (4.141) has been proved, we assume $P = P_1 \cap P_2$ and on the left-hand side we perform the summation

$$\sum_{p \in [P_1/P]} \sum_{q \in [P_2/P]} \int_{(A_1 \cap A_2)/P} ds \delta_{A_1/P}(t - p - s) \delta_{A_2}(s - u + q).$$

Next, using identity (4.85) for the first impulse, we obtain

$$\sum_{p \in [P_1/P]} \delta_{A_1/P}(t - p - s) = \delta_{A_1/P_1}(t - s).$$

Analogously, we deal with the second impulse. Therefore, once the summation has been carried out, the left-hand side gives

$$\int_{(A_1 \cap A_2)/P} ds \delta_{A_1/P_1}(t-s) \delta_{A_2/P_2}(s-u), \quad P = P_1 + P_2. \quad (4.142)$$

Next, the same summation is carried out on the right-hand side. Thus, we get

$$\begin{aligned} & \sum_{p \in [P_1/P]} \sum_{q \in [P_2/P]} \delta_{(A_1+A_2)/P}(t-p-u+q) \\ &= \sum_{q \in [P_2/P]} \delta_{(A_1+A_2)/P_1}(t-u+q) \\ &= \sum_{q \in [P_2/P]} \sum_{p \in P_1} \delta_{A_1+A_2}(t-u+q+r), \end{aligned}$$

where we have used identities (4.85) and (4.84). Finally, we recall that $P = P_1 \cap P_2$ and then identity (4.135) allows writing

$$\sum_{v \in P_1+P_2} \delta_{A_1+A_2}(t-u+v) = \delta_{(A_1+A_2)/(P_1+P_2)}(t-u). \quad (4.143)$$

In conclusion, starting from (4.141), we have carried out the same summation on both sides. So, we have obtained (4.142) for the left-hand side and (4.143) for the right-hand side. The equality of these two expressions proves identity (4.87) over finite groups.

Example 4.12 We suggest that the reader checks the steps leading to (4.142) and (4.143) with the basis groups given by (4.134) and with the moduli $P_1 = \mathbb{Z}(18)$ and $P_2 = \mathbb{Z}(60)$.

References

1. M. Abramowitz, I.A. Stegun, *Handbook of Mathematical Functions* (Dover, New York, 1970)
2. N.M. Blachman, Sinusoids versus Walsh functions. *Proc. IEEE* **62**(3), 346–354 (1974)
3. R.N. Bracewell, *Two-dimensional Imaging* (Prentice Hall, Englewood Cliffs, 1995)
4. G. Cariolaro, *Teoria dei Segnali Multidimensionali e Applicazioni alla HDTV* (Edizioni Scientifiche Telettra, Milan, 1991)
5. G. Cariolaro, T. Erseghe, P. Kraniuskas, N. Laurenti, Multiplicity of fractional Fourier transforms and their relationships. *IEEE Trans. Signal Process.* **48**, 227–241 (2000)
6. G. Cariolaro, P. Kraniuskas, L. Vangelista, A novel general formulation of up/downsampling commutativity. *IEEE Trans. Signal Process.* **53**, 2124–2134 (2005)
7. D. Gabor, Theory of communications. *J. Inst. Electr. Eng.* **93**, 429–457 (1946)
8. I. Gohberd, S. Gohbery, *Basic Operator Theory* (Birkhauser, Boston, 1981)
9. P.J. Higgins, *Introduction to Topological Groups* (Cambridge University Press, London, 1974)

10. R.A. Horn, C.R. Johnson, *Matrix Analysis* (Cambridge University Press, London, 1985)
11. G. Sartori, *Lezioni di Meccanica Quantistica*, 2nd edn. (Ed. Cortina, Padova, 1997)
12. S. Roman, *Advance Linear Algebra* (Springer, New York, 1992)
13. W. Rudin, *Fourier Analysis on Groups* (Interscience, New York, 1962)
14. G. Sansone, *Orthogonal Functions* (Interscience, New York, 1959)
15. A. Weil, *L'Integration dans les Groupes Topologiques* (Hermann, Paris, 1940)

Chapter 5

Unified Theory: Frequency Domain Analysis

UT 5.1 Introduction

In this chapter, the signal analysis moves from the signal domain to the frequency domain by means of the *Fourier transform* (FT), which is introduced in unified form using the Haar integral as

$$S(f) = \int_I dt s(t) \psi^*(f, t), \quad f \in \widehat{I}, \tag{5.1}$$

where I is the signal domain, \widehat{I} is the frequency domain and $\psi(f, t)$ is the *kernel*. From the FT $S(f)$, $f \in \widehat{I}$, the signal $s(t)$, $t \in I$, is recovered through the inverse FT, as

$$s(t) = \int_{\widehat{I}} df S(f) \psi(f, t), \quad t \in I. \tag{5.2}$$

Thus, the two expressions have the same structure, with the kernels conjugate to each other. Denoting with \mathcal{F} the operator defined by (5.1) and with \mathcal{F}^{-1} the operator defined by (5.2), we respectively symbolize the evaluation of the FT from the signal and the recovery of the signal from its FT as

$$s(t) \xrightarrow{\mathcal{F}} S(f), \quad S(f) \xrightarrow{\mathcal{F}^{-1}} s(t). \tag{5.3}$$

A preliminary problem is the evaluation of the frequency domain \widehat{I} and of the *kernel* $\psi(f, t)$. In the field of Topology, called Abstract Harmonic Analysis [10, 23], the kernel is obtained axiomatically by imposing the *separability* condition

$$\psi(f, t_1 + t_2) = \psi(f, t_1) \psi(f, t_2), \quad t_1, t_2 \in I \tag{5.4}$$

and the condition of unitary amplitude

$$|\psi(f, t)| = 1. \tag{5.5}$$

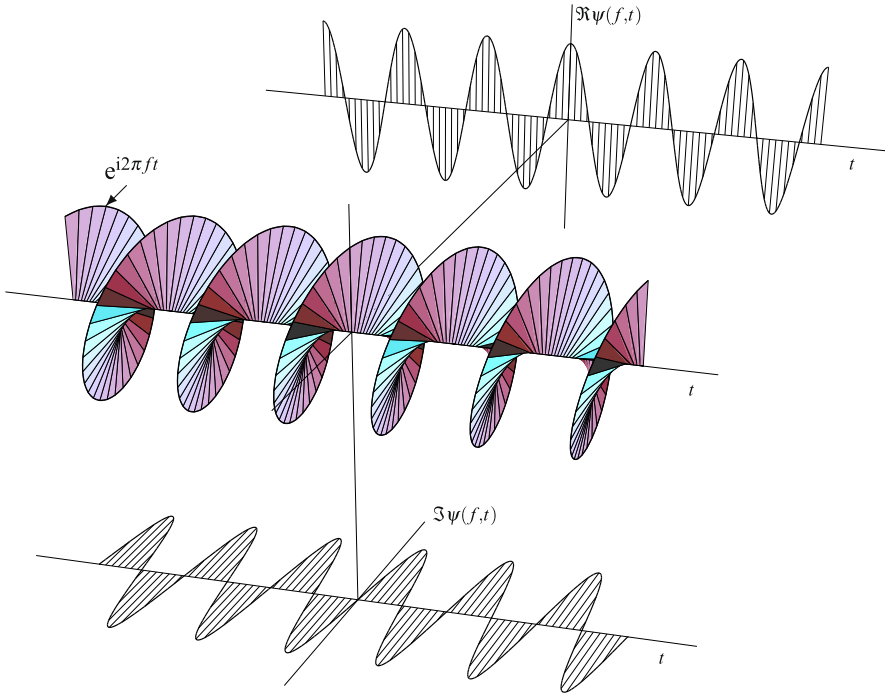


Fig. 5.1 Fourier transform kernel $\psi(f, t) = e^{i2\pi ft}$ on the groups of \mathbb{R} , shown as a function of t for a fixed frequency f

For a fixed f , each function $\psi_f(t) = \psi(f, t)$ that verifies the above conditions is called a *character* of the group I and the set of all characters identifies the kernel of the FT on the group I . Moreover, the range of the frequency f identifies the frequency domain \widehat{I} , which is called the *dual group*.

This identification procedure is carried out in Appendix A considering both the general case and the specific cases of interest. In particular, for the groups of \mathbb{R} , we find that the kernel has the familiar exponential form (Fig. 5.1)

$$\psi(f, t) = e^{i2\pi ft}. \tag{5.6}$$

Then, the FT and the inverse FT assume respectively the form

$$S(f) = \int_I dt s(t) e^{-i2\pi ft}, \quad f \in \widehat{I}, \tag{5.7a}$$

$$s(t) = \int_{\widehat{I}} df S(f) e^{i2\pi ft}, \quad t \in I. \tag{5.7b}$$

In the multidimensional case, that is, in the class $\mathcal{Q}(\mathbb{R}^m)$, the kernel is simply given by the product of m one-dimensional kernels

$$\psi(f_1, \dots, f_m; t_1, \dots, t_m) = \psi(f_1, t_1) \cdots \psi(f_m, t_m) = e^{i2\pi(f_1 t_1 + \dots + f_m t_m)}, \tag{5.8}$$

where (t_1, \dots, t_m) is the signal argument and (f_1, \dots, f_m) is the FT argument. Using (5.8), we can explicitly write the FT and its inverse in the mD case. But, to save space and formula proliferation, we can refer to (5.6) and (5.7a), (5.7b) *also for the mD case*, provided that t and f are interpreted as m -tuples and the product ft that appears in the exponential as¹

$$ft = f_1t_1 + \dots + f_mt_m. \quad (5.9)$$

The kernel depends on the group I , and so far we provided the expression for the groups of $\mathcal{Q}(\mathbb{R})$ and $\mathcal{Q}(\mathbb{R}^m)$. For other LCA groups the expression changes, as we shall see in Sect. 5.11 for multiplicative groups. For concreteness, in the following we will mainly refer to the groups of $\mathcal{Q}(\mathbb{R})$, where the FT is given by (5.7a), (5.7b), and to the groups of $\mathcal{Q}(\mathbb{R}^m)$, where, with the conventions made above, the FT is still given by (5.7a), (5.7b).

In the following sections, we will make explicit the frequency domains (dual groups) and realize that they have the same structure as the signal domain, specifically $\widehat{I} = I_{0_f}/S_f$, where I_{0_f} is the “true” FT domain and S_f is the periodicity. Then, all definitions and operations introduced in the signal domain are transferred to the frequency domain. In particular, the Haar integral used for the FT can be also used for the inverse FT.

Having established the frequency domain, we will carry out several rules, in unified way, that allow the full understanding and easy calculation of this powerful operation of Signal Theory.

UT 5.2 First Considerations on the Unified Fourier Transform

5.2.1 Invertibility of the FT and Orthogonality Conditions

The proof that the inverse transform allows effectively the signal recovery is not a simple problem and requires appropriate condition on the signal class (see [9, 24] [14, 23]). In a heuristic way, the correct recovery can be established starting from the following relations. For each pair (I, \widehat{I}) the Fourier kernel $\psi(f, t)$ is related to the impulses by the following relations

$$\int_I dt \psi(f, t) = \delta_{\widehat{I}}(f), \quad f \in \widehat{I}, \quad (5.10a)$$

$$\int_{\widehat{I}} df \psi(f, t) = \delta_I(t), \quad t \in I, \quad (5.10b)$$

¹This can be done without ambiguity in most of the cases. However, in some algebraic steps involving matrices, the m -tuples $\mathbf{t} = (t_1, \dots, t_m)$ and $\mathbf{f} = (f_1, \dots, f_m)$ must be interpreted as column vectors, and ft must be replaced by $\mathbf{f}^t \mathbf{t} = f_1t_1 + \dots + f_mt_m$, where \mathbf{f}^t is the transpose of \mathbf{f} .

that is, by integrating the kernel $\psi(f, t)$ with respect to time, we get the impulse in frequency, whereas integrating $\psi(f, t)$ with respect to frequency, we get the impulse in time. In Appendix B, we prove that, if conditions (5.10a), (5.10b) hold for the pair (I, \widehat{I}) , then (5.2) follows from (5.1).

Relations (5.10a), (5.10b) can be interpreted as orthogonality conditions in a generalized sense, as will be clear from the study of the specific cases. Together with impulse properties, the orthogonality conditions represent a fundamental tool for signal theory and, in fact, they will be exploited quite often.

Note that in the groups of \mathbb{R} the orthogonality conditions become

$$\int_I dt e^{i2\pi ft} = \delta_{\widehat{I}}(f), \quad f \in \widehat{I}, \quad (5.11a)$$

$$\int_{\widehat{I}} df e^{i2\pi ft} = \delta_I(t), \quad t \in I. \quad (5.11b)$$

As an example, when $I = \mathbb{R}/\mathbb{Z}(T_p)$, $\widehat{I} = \mathbb{Z}(F)$, we find

$$\int_0^{T_p} e^{i2\pi kFt} dt = \delta_{\mathbb{Z}(F)}(kF) = \begin{cases} 1/F, & \text{if } k = 0; \\ 0, & \text{if } k \neq 0, \end{cases}$$

which represents the orthogonality condition of exponential functions seen in Sect. 4.5. When $I = \mathbb{R}$, $\widehat{I} = \mathbb{R}$, we get

$$\int_{-\infty}^{+\infty} e^{i2\pi ft} dt = \delta_{\mathbb{R}}(f) = \delta(f),$$

which represents a fundamental identity in distribution theory [3, 11].

Fourier Transform of Some Singular Signals

To stress the importance of the orthogonality conditions, we now evaluate the FT of some signals, which we call “singular signals” since they are related to impulses or characters.

Letting $s(t) = \delta_I(t - t_0)$ in (5.11a) and using the sifting property (4.76), we find

$$\delta_I(t - t_0) \xrightarrow{\mathcal{F}} e^{-i2\pi ft_0}. \quad (5.12)$$

In particular, when $t_0 = 0$, we get $\psi(f, 0) = 1$. Then

$$\delta_I(t) \xrightarrow{\mathcal{F}} 1, \quad (5.12a)$$

that is, the FT of the impulse at the origin has unit value for all frequencies.

Analogously, letting $S(f) = \delta_{\widehat{I}}(f - f_0)$ in (5.11b), by the uniqueness of the inverse FT, we find

$$e^{i2\pi f_0 t} \xrightarrow{\mathcal{F}} \delta_{\widehat{I}}(f - f_0). \quad (5.13)$$

In particular, when $f_0 = 0$,

$$1 \xrightarrow{\mathcal{F}} \delta_{\widehat{I}}(f), \quad (5.13b)$$

that is, the unit signal has FT given by an impulse in the frequency origin.

The above Fourier pairs will be illustrated later by considering some specific cases.

5.2.2 Interpretation of the Fourier Transform

Now, we give an answer to a few fundamental questions. Why is the Fourier transform so important? Why is the Fourier kernel based on characters (which, in the case of main interest, are exponential functions)? These questions are strongly related to each other and both find an adequate answer in the context of the most important operation in signal processing, that is, *filtering*. In fact, in a filter a signal identified by a character exhibits a special kind of “transparency”, which is mathematically stated by the concept of eigenfunction.

Universal Signal Decomposition by Fourier Transform

The FT allows writing every signal $s(t)$, $t \in I$, as an inverse FT, that is, in the form

$$s(t) = \int_{\widehat{I}} df S(f) e^{i2\pi ft}, \quad t \in I, \quad (5.14)$$

where $\psi_f(t) = e^{i2\pi ft}$ are the characters of the signal domain I . In this expression, the signal is decomposed into terms of the form

$$s_f(t) = [df S(f)] e^{i2\pi ft}, \quad f \in \widehat{I}, \quad (5.14b)$$

that is, characters multiplied by the complex amplitude $[df S(f)]$. The “differential” df is infinitesimal if \widehat{I} is a continuum and is finite if \widehat{I} is discrete or finite.

Signal decomposition (5.14) is “universal” in the sense that *all signals defined on I have the same decomposition* in terms of characters. Indeed, this basic decomposition, has a paramount importance for signal processing, although recently more sophisticated decompositions were introduced (see wavelets in Chap. 15).

Characters as Filter Eigenfunctions

We recall from Sect. 4.9 that a filter on the domain I is a system governed by a convolution, $y(t) = g * x(t)$, and explicitly

$$y(t) = \int_I du g(t-u)x(u) = \int_I du g(u)x(t-u), \quad t \in I, \quad (5.15a)$$



Fig. 5.2 Interpretation of an *eigenfunction* $s_0(t)$ of a filter: the output signal is proportional to the input signal

where $x(t)$ is the input, $y(t)$ is the output and $g(t)$ is the filter *impulse response*. In the frequency domain, by the rule of convolution, which will be proved later on, (5.15a) becomes

$$Y(f) = G(f)X(f), \quad f \in \widehat{I}, \quad (5.15b)$$

where $G = \mathcal{F}[g]$ is called the filter *frequency response*.

A comparison of the relations (5.15a), (5.15b) suggests the convenience of working in the frequency domain. This is strictly related to the fact that characters (which form the Fourier kernel) are the filter eigenfunctions, that is, signals *having the property of passing unchanged through the filter*. More precisely, an eigenfunction is every (nonzero) signal $s_0(t)$, $t \in I$, that verifies the condition (Fig. 5.2)

$$\int_I du g(u)s_0(t-u) = \lambda s_0(t), \quad t \in I, \quad (5.16)$$

where the constant λ is called the *eigenvalue* corresponding to $s_0(t)$. Now, for a fixed frequency f , the signal $s_0(t) = e^{i2\pi ft} = \psi_f(t)$ verifies condition (5.16). In fact, using the character separability (5.4) in the form $\psi_f(u-t) = \psi_f(u)\psi_f(-t)$, we find that (5.16) holds with

$$\lambda = \int_I du g(u)e^{-i2\pi ft} = G(f). \quad (5.16a)$$

Therefore, the character $e^{i2\pi ft}$ with frequency f is a filter eigenfunction with eigenvalue given by the *frequency response evaluated at the same frequency* f , that is,

$$e^{i2\pi ft} \xrightarrow{\text{filter}} G(f)e^{i2\pi ft}. \quad (5.17)$$

This property represents the “transparency” claimed above: in the passage through the filter, the signal $e^{i2\pi ft}$ does not change, but only modifies its amplitude.

We may see that the above properties, upon which the success of Fourier transform is based, are ultimately due to the Fourier kernel *separability*. Note that for characters a second condition not exploited above is imposed, $|\psi_f(t)| = 1$. This means that we may find other separable functions, that are not constrained to take values on the unit circle of the complex plane and, nevertheless, they turn out to be filter eigenfunctions. Hence it is possible to introduce other *transforms*, having the same signal processing ability as the Fourier transform (see the Laplace transform and the z transform).

UT 5.3 The Frequency Domain

In general, a signal domain I is intended as a quotient group, $I = I_0/P$, with I_0 the true domain and P the periodicity. The dual group has the same structure, $\widehat{I} = I_{0f}/P_f$, with I_{0f} the true frequency domain and P_f the frequency periodicity.

The explicit relation between $I = I_0/P$ and its dual $\widehat{I} = I_{0f}/P_f$ is established by means of the reciprocal group.

5.3.1 The Reciprocal Group

Definition 5.1 The *reciprocal* J^* of an ordinary group J is the ordinary group defined from the kernel $\psi_f(t) = \psi(f, t)$ as

$$J^* \triangleq \{f \mid \psi_f(t) = 1, t \in J\}. \quad (5.18)$$

This is the abstract definition. For the groups of \mathbb{R} where the kernel is given by (5.6), considering that $e^{i2\pi ft} = 1$ if and only if ft is an integer, the reciprocal group is given by

$$J^* = \{f \mid ft \in \mathbb{Z}, t \in J\}, \quad (5.19)$$

where ft in the 1D case is the ordinary product and in the m D case it has to be interpreted as in (5.9).

We now list several properties of the reciprocal group that can be established by the definition (5.18) or more directly by (5.19). Then we will find explicitly the reciprocals of the groups of $\mathcal{G}(\mathbb{R})$ and of $\mathcal{G}(\mathbb{R}^m)$.

It can be shown that J^* is an LCA group. Moreover:

1. *The reciprocal of the reciprocal is the original group*

$$(J^*)^* = J. \quad (5.20)$$

2. *If K is a subgroup of J , then J^* is a subgroup of K^**

$$K \subset J \xrightarrow{*} K^* \supset J^*. \quad (5.21)$$

3. *If J and K are rationally comparable (see Sect. 3.9), then*

$$(J + K)^* = J^* \cap K^*, \quad (J \cap K)^* = J^* + K^*. \quad (5.22)$$

4. *If J is a lattice, so is J^* .*
5. *The reciprocal of the Cartesian product is the Cartesian product of the reciprocals*

$$J = J_1 \times J_2 \xrightarrow{*} J^* = J_1^* \times J_2^*. \quad (5.23)$$

5.3.2 The Dual Group

From the reciprocal group, the dual group can be easily obtained by using the following rule:

Theorem 5.1 *The dual \widehat{I} of a quotient group $I = I_0/P$ has the domain given by the reciprocal of the periodicity and the periodicity given by the reciprocal of the domain*

$$I = I_0/P \xrightarrow{\text{dual}} \widehat{I} = P^*/I_0^*. \quad (5.24)$$

Hence, in the passage to the dual, the role of the domain and of the periodicity is interchanged. The proof of the theorem, based on kernel properties, is given in Appendix C.

From Property 1 on reciprocals, we find that *the dual of the dual is the original group*

$$\widehat{\widehat{I}} \xrightarrow{\text{dual}} I. \quad (5.25)$$

This rule is a celebrated result of Topology, known as Duality Theorem of Pontryagin [21]. Considering (5.25) and the conventions on the sum and intersection reported in Sect. 3.9, the rules for reciprocals provide rules for duals:

1. The *dual of the dual is the original group*

$$\widehat{\widehat{I}} = I. \quad (5.26)$$

2. If I is a quotient group and U is a subgroup of I , then

$$U \subset I \xrightarrow{\text{dual}} \widehat{U} \supset \widehat{I}. \quad (5.27)$$

3. If I and U are rationally comparable (see Sect. 3.9), then \widehat{I} and \widehat{U} are rationally comparable and

$$\widehat{I+U} = \widehat{I} \cap \widehat{U}, \quad \widehat{I \cap U} = \widehat{I} + \widehat{U}. \quad (5.28)$$

4. If I is a finite group then so is \widehat{I} .

5. The dual of a Cartesian product is the Cartesian product of the duals

$$I = I_1 \times I_2 \xrightarrow{\text{dual}} \widehat{I} = \widehat{I}_1 \times \widehat{I}_2. \quad (5.29)$$

The latter property is a consequence of the separability of the kernel on $I_1 \times I_2$, given by $\psi_I(f_1, f_2; t_1, t_2) = \psi_{I_1}(f_1, t_1)\psi_{I_2}(f_2, t_2)$.

5.3.3 One-Dimensional Reciprocals and Duals

Now, we evaluate the reciprocals of the ordinary LCA groups of the class $\mathcal{G}(\mathbb{R})$, which are \mathbb{R} , $\mathbb{Z}(T)$ with $T \in (0, \infty)$ and \mathbb{O} . Letting $J = \mathbb{R}$ in (5.19), we find that

Table 5.1 Ordinary groups of \mathbb{R} and their duals

Group	Dual group
$\mathbb{R} = \mathbb{Z}(0)/\mathbb{Z}(\infty)$	$\mathbb{R} = \mathbb{Z}(0)/\mathbb{Z}(\infty)$
$\mathbb{Z}(T) = \mathbb{Z}(T)/\mathbb{Z}(\infty)$	$\mathbb{R}/\mathbb{Z}(F_p) = \mathbb{Z}(0)/\mathbb{Z}(F_p), F_p = 1/T$
$\mathbb{R}/\mathbb{Z}(T_p) = \mathbb{Z}(0)/\mathbb{Z}(T_p)$	$\mathbb{Z}(F) = \mathbb{Z}(F)/\mathbb{Z}(\infty), F = 1/T_p$
$\mathbb{Z}(T)/\mathbb{Z}(T_p), T_p = NT, N \in \mathbb{N}$	$\mathbb{Z}(F)/\mathbb{Z}(F_p), F_p = 1/T, F = 1/T_p$

the product ft must be an integer for any $t \in \mathbb{R}$. Then, the unique solution is $f = 0$. This states that the reciprocal of \mathbb{R} is \mathbb{O} . Next, from the rule $(J^*)^* = J$ we obtain that the reciprocal of \mathbb{O} is \mathbb{R} . When $J = \mathbb{Z}(T)$, the reciprocal is given by the solutions of the equation $fnT = \text{integer}$ for all n , which are given by $f = k/T$ with k an arbitrary integer. Therefore, the reciprocal of $\mathbb{Z}(T)$ is $\mathbb{Z}(1/T)$. To summarize, we have

$$\boxed{\mathbb{R}^* = \mathbb{O}, \quad \mathbb{Z}(T)^* = \mathbb{Z}(1/T), \quad \mathbb{O}^* = \mathbb{R}.} \tag{5.30}$$

To express this reciprocal in a unified form, we introduce the notation $\mathbb{R} \triangleq \mathbb{Z}(0)$ and $\mathbb{O} \triangleq \mathbb{Z}(\infty)$. Then, all the groups of \mathbb{R} and their reciprocal (5.30) can be written as

$$\mathbb{Z}(T), \quad \mathbb{Z}(T)^* = \mathbb{Z}(1/T), \quad T \in [0, \infty].$$

From reciprocals we obtain duals by rule (5.24). In compact notations, we have

$$\mathbb{Z}(T)/\mathbb{Z}(T_p) \xrightarrow{\text{dual}} \mathbb{Z}(F)/\mathbb{Z}(F_p) \quad \text{with } F = 1/T_p, F_p = 1/T.$$

As an example, to obtain the dual of \mathbb{R} we write $\mathbb{R} = \mathbb{Z}(0)/\mathbb{Z}(\infty)$ and we get $\widehat{\mathbb{R}} = \mathbb{Z}(1/\infty)/\mathbb{Z}(1/0) = \mathbb{Z}(0)/\mathbb{Z}(\infty) = \mathbb{R}$. Analogously, we proceed for the other cases. The results are reported in Table 5.1.

In conclusion, we have seen that on the groups of \mathbb{R} time and frequency domains have the same structure, namely $I = \mathbb{Z}(T)/\mathbb{Z}(T_p)$ and $\widehat{I} = \mathbb{Z}(F)/\mathbb{Z}(F_p)$, where the frequency spacing is given by the reciprocal of the time period and the frequency period is given by the reciprocal of the time spacing.

⇓ 5.3.4 Multidimensional Reciprocals and Duals

In the mD case, the arguments t and f become m -tuples and the reciprocal (5.19) is explicitly given by

$$J^* = \{(f_1, \dots, f_m) \mid f_1t_1 + \dots + f_mt_m \in \mathbb{Z}, (t_1, \dots, t_m) \in J\}. \tag{5.31}$$

For a separable group, we use (5.23) (extended to m factors), and, considering the 1D reciprocals given by (5.30), we find the reciprocal of any separable mD group.

For instance,

$$\begin{aligned} \mathbb{R}^2 &\xrightarrow{\star} \mathbb{O}^2, & \mathbb{R} \times \mathbb{Z}(2) &\xrightarrow{\star} \mathbb{O} \times \mathbb{Z}(1/2), \\ \mathbb{Z}(d_1, d_2) &= \mathbb{Z}(d_1) \times \mathbb{Z}(d_2) &\xrightarrow{\star} &\mathbb{Z}(1/d_1) \times \mathbb{Z}(1/d_2) = \mathbb{Z}(1/d_1, 1/d_2). \end{aligned}$$

In particular, for the primitive m D groups (see Sect. 3.3), we find

$$H = \mathbb{R}^p \times \mathbb{Z}^q \times \mathbb{O}^r \xrightarrow{\star} H^\star = \mathbb{O}^p \times \mathbb{Z}^q \times \mathbb{R}^r. \quad (5.32)$$

To get a general result we use the base–signature representation, which holds for both the original group J and its reciprocal J^\star , since both are groups of $\mathcal{G}(\mathbb{R}^m)$. Then, given a representation (\mathbf{J}, H) of J we have to find a representation of J^\star . Starting from (5.31) in Appendix D, we prove:

Theorem 5.2 *If J is a group of $\mathcal{G}(\mathbb{R}^m)$ with representation (\mathbf{J}, H) , the reciprocal group J^\star is a group of $\mathcal{G}(\mathbb{R}^m)$ identified by the representation*

$$(\mathbf{J}^\star, H^\star), \quad \mathbf{J}^\star \triangleq (\mathbf{J}')^{-1} \quad (5.33)$$

where \mathbf{J}^\star denotes the inverse of the transpose of \mathbf{J} and H^\star is the reciprocal of the signature H .

Note that, in general, the signature H has the primitive form (5.32) and, therefore, the evaluation of H^\star is straightforward. Note also, as a corollary, the relation between the determinants

$$\boxed{d(\mathbf{J}^\star) d(\mathbf{J}) = 1.} \quad (5.34)$$

Example 5.1 Consider the quincunx lattice $J = \mathbb{Z}_2^1(d_1, d_2)$, which is not separable and therefore its reciprocal J^\star must be evaluated using Theorem 5.2. The representation of J is given by (see Sect. 3.3)

$$\mathbf{J} = \begin{bmatrix} 2d_1 & d_1 \\ 0 & d_2 \end{bmatrix}, \quad H = \mathbb{Z}^2.$$

Then, we find

$$\mathbf{J}^\star = \begin{bmatrix} F_1 & 0 \\ -F_2 & 2F_2 \end{bmatrix}, \quad H^\star = \mathbb{Z}^2, \quad F_1 = 1/(2d_1), \quad F_2 = 1/(2d_2).$$

The reciprocal J^\star is drawn in Fig. 5.3 starting from the basis \mathbf{J}^\star , that is, from the vectors $(F_1, -F_2)$ and $(0, 2F_2)$. From the drawing we realize that also J^\star is a quincunx lattice, although the basis \mathbf{J}^\star has a form different from \mathbf{J} . However, we recall that the basis of a lattice is not unique (see Sect. 3.3).

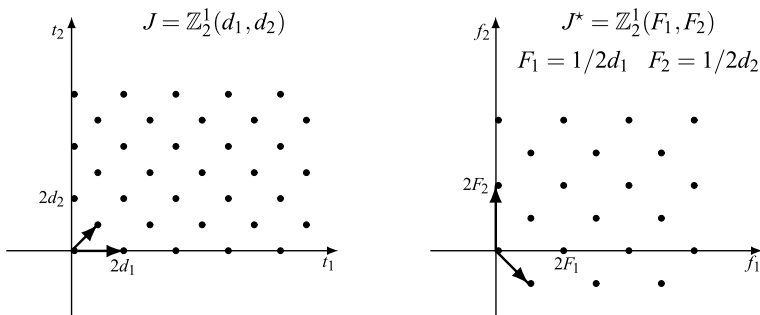


Fig. 5.3 The quincunx lattice and its reciprocal, itself a quincunx lattice

Other specific evaluations of reciprocals will be seen in Sect. 5.9 and in Chap. 16.

Having evaluated the reciprocals, the duals are obtained by Theorem 5.1. If both the domain and the periodicity are separable, then the evaluation is simple, being

$$I_1 \times I_2 = I_{01}/P_1 \times I_{02}/P_2 \xrightarrow{\text{dual}} \widehat{I}_1 \times \widehat{I}_2 = P_1^*/I_{01}^* \times P_2^*/I_{02}^*.$$

For instance, the dual of $I = \mathbb{R}^2 = \mathbb{R}/\mathbb{O} \times \mathbb{R}/\mathbb{O}$ is $\widehat{I} = \mathbb{R}/\mathbb{O} \times \mathbb{R}/\mathbb{O} = \mathbb{R}^2$ and the dual of $I = \mathbb{R}/\mathbb{Z}(D_1) \times \mathbb{R}/\mathbb{O}$ is $\widehat{I} = \mathbb{Z}(F_1)/\mathbb{O} \times \mathbb{R}/\mathbb{O}$. But, in general we have to use a base–signature representation for both the domain and the periodicity, say

$$(\mathbf{I}_0, H) \mapsto I_0, \quad (\mathbf{P}, K) \mapsto P. \tag{5.35}$$

Then, we find the reciprocal according to Theorem 5.2, that is,

$$(\mathbf{I}_0^*, H^*) \mapsto I_0^*, \quad (\mathbf{P}^*, K^*) \mapsto P^*. \tag{5.35a}$$

UT 5.4 Symmetry Between Signals and Fourier Transforms

Each LCA group I can be considered as a possible *signal domain*, but the rule (5.25) states that the dual of the dual is the original group. Therefore, the same group I can also be considered as a *frequency domain*, namely that of signals defined on \widehat{I} . As an example, the group $\mathbb{R}/\mathbb{Z}(5)$ is a signal domain (for periodic continuous-time signals with period 5) as well as a frequency domain (for signals defined on $\mathbb{Z}(1/5)$).

Therefore, for a given group I , the class $\mathcal{S}(I)$ of the complex functions defined on I and interpreted as *class of signals* defined on I , can also be interpreted as *class of Fourier transforms* of the signals defined on \widehat{I} . Broadly speaking, we can say that the “Fourier transform world” does not introduce any novelty with respect to the “signal world”. This symmetry is now presented in a more precise way.

The graph (5.3) states that: (i) starting from the signal $s(t)$ defined on I , the FT $S(f)$ defined on \widehat{I} is obtained by means of the operator \mathcal{F} (with kernel $e^{-i2\pi ft}$), and (ii) from the FT $S(f)$ we can recover $s(t)$ by means of the inverse operator \mathcal{F}^{-1}

(with kernel $e^{i2\pi ft}$). If in the second step we apply the direct operator \mathcal{F} , instead of the inverse operator \mathcal{F}^{-1} , we obtain $s(-t)$ instead of $s(t)$. Therefore, the FT of the FT of $s(t)$ gives the reversed signal $s(-t)$, that is, $\mathcal{F}^2[s|t] = s(-t)$. By further applications of the direct operator \mathcal{F} , we obtain $\mathcal{F}^3[s|f] = S(-f)$ and $\mathcal{F}^4[s|t] = s(t)$, as illustrated by the following graph

$$s(t) \xrightarrow{I} \xrightarrow{\mathcal{F}} S(f) \xrightarrow{\widehat{I}} \xrightarrow{\mathcal{F}} s(-t) \xrightarrow{I} \xrightarrow{\mathcal{F}} S(-f) \xrightarrow{\widehat{I}} \xrightarrow{\mathcal{F}} s(t). \quad (5.36)$$

Therefore, the operator \mathcal{F}^4 gives the original signal and represents the identity operator on I .

Symmetry Rule Let (s, S) be a Fourier pair on (I, \widehat{I}) , then, by considering S as a signal on \widehat{I} , also (S, s_-) is a valid Fourier pair on (\widehat{I}, I) , as summarized by the graph

$$\begin{array}{ccc} s(t) & \xrightarrow{\mathcal{F}} & S(f) \\ & & \widehat{I} \\ & & S(t) \xrightarrow{\mathcal{F}} s(-f) \\ & & I \end{array} \quad (5.37)$$

Examples of the application of this rule will be seen in Sect. 5.8 with 1D signals and in Sect. 5.10 with 2D signals.

5.4.1 Consequences of the Symmetry

The perfect symmetry between the “signal world” and the “Fourier transform world” allows transferring all basic concepts from the first to the second. In particular, the definitions of (a) cell, (b) Haar integral and measure, and (c) impulse need not be reformulated in the frequency domain. But, some terms are modified for convenience.

Spectral Extension and Bandwidth The *extension* and *duration* become *spectral extension* and *bandwidth*, respectively. Then, the *spectral extension* of a signal $s(t)$, $t \in I$, symbolized $\mathcal{E}(s)$, is defined as the extension of its FT $S(f)$, $f \in \widehat{I}$, namely

$$\mathcal{E}(s) \triangleq e(S). \quad (5.38)$$

The (Haar) measure of $\mathcal{E}(s)$ defines the *bandwidth* of $s(t)$ by

$$B(s) = \text{meas } \mathcal{E}(s).$$

We will distinguish between the *minimal* spectral extension, given

$$\mathcal{E}_0(s) = \{f \mid S(f) \neq 0\} \quad (5.39a)$$

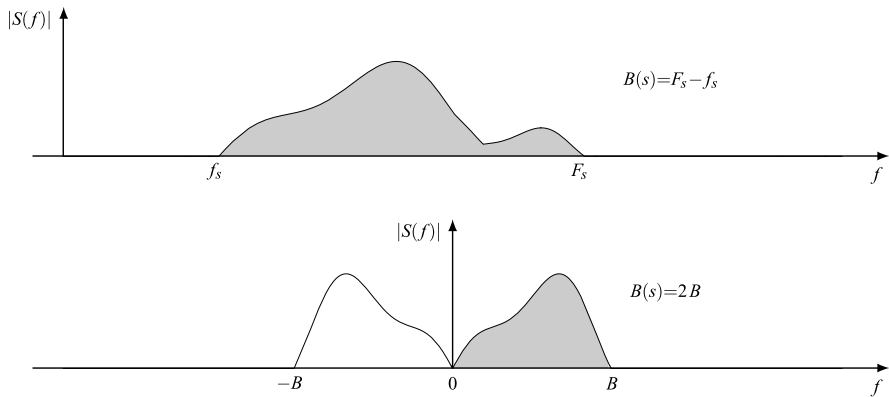


Fig. 5.4 Examples of limited spectral extension: for a complex signal (*above*) and for a real signal (*below*). For a real signal $B(s)$ is the *bandwidth*, while B is the *band*

and a *generic* spectral extension $\mathcal{E}(s)$, as any subset of \widehat{T} containing $\mathcal{E}_0(s)$. Clearly, $\mathcal{E}(s)$ is characterized by the property

$$\boxed{S(f) = 0, \quad f \notin \mathcal{E}(s).} \tag{5.39b}$$

As we shall see, the FT of a *real* signal has always the Hermitian symmetry $S^*(f) = S(-f)$, thus, if at a certain frequency f we have $S(f) = 0$, also $S(-f) = 0$ and, therefore, the minimal spectral support is always symmetric with respect to the frequency origin: $\mathcal{E}_0(s) = -\mathcal{E}_0(s)$. Then, we will pay attention of preserving this symmetry when choosing a generic spectral extension. For *real* signals it is customary to consider the *band* B , defined as half of the bandwidth $B(s)$ (Fig. 5.4)

$$B \triangleq \frac{1}{2} B(s) = \frac{1}{2} \text{meas } \mathcal{E}(s). \tag{5.40}$$

UT 5.5 Rules of the Fourier Transform

In this section, we establish several properties, or *rules*, for the FT. These rules correspond to so many theorems, and can be proved by using the FT definition, the kernel properties and the orthogonality conditions. We distinguish between *primitive* rules and *non-primitive* rules, which are obtained as combinations of the former. The collection of rules is summarized in Table 5.2.

5.5.1 Primitive Rules

There are six primitive rules.

Table 5.2 General rules of the Fourier transform

Rule	Signal	Transform
1. Linearity	$a_1 s_1(t) + a_2 s_2(t)$	$a_1 S_1(f) + a_2 S_2(f)$
2. Symmetry	$S(t)$	$s(-f)$
3. Reverse	$s(-t)$	$S(-f)$
4(a). Conjugate in time	$s^*(t)$	$S^*(-f)$
4(b). Conjugate in frequency	$s^*(-t)$	$S^*(f)$
5(a). Time shift	$s(t - t_0)$	$S(f)e^{-i2\pi f t_0}$
5(b). Frequency shift	$s(t)e^{i2\pi f_0 t}$	$S(f - f_0)$
6(a). Convolution in time	$x * y(t)$	$X(f)Y(f)$
6(b). Convolution in frequency	$x(t)y(t)$	$X * Y(f)$
7(a). Real part in time	$\Re s(t) = \frac{1}{2}[s(t) + s^*(t)]$	$\frac{1}{2}[S(f) + S^*(-f)]$
7(b). Real part in frequency	$\frac{1}{2}[s(t) + s^*(-t)]$	$\Re S(f)$
8(a). Imaginary part in time	$i \Im s(t) = \frac{1}{2}[s(t) - s^*(t)]$	$\frac{1}{2}[S(f) - S^*(-f)]$
8(b). Imaginary part in frequency	$\frac{1}{2}[s(t) - s^*(-t)]$	$i \Im S(f)$
9. Even part	$\frac{1}{2}[s(t) + s(-t)]$	$\frac{1}{2}[S(f) + S(-f)]$
10. Odd part	$\frac{1}{2}[s(t) - s(-t)]$	$\frac{1}{2}[S(f) - S(-f)]$
11(a). Correlation in time	$x * y^*(t)$	$X(f)Y^*(f)$
11(b). Correlation in frequency	$x(t)y^*(t)$	$X * Y^*(f)$

Note: \Re represents “real part”; \Im represents “imaginary part”

1. Linearity The operators \mathcal{F} and \mathcal{F}^{-1} are linear, as a consequence of the linearity of the Haar integral (see Sect. 4.1).

2. Symmetry This rule was already seen in Sect. 5.4.

3. Reverse Time reverse implies frequency reverse. This is a consequence of the kernel property $e^{i2\pi f(-t)} = e^{i2\pi(-f)t}$.

4. Conjugate Conjugate in one domain implies conjugate and reverse in the other domain. This is a consequence of the kernel property

$$e^{-i2\pi f t} = (e^{i2\pi f t})^*.$$

5. Shift A shift of a signal by t_0 implies a multiplication by the character on the FT

$$s(t - t_0) \xrightarrow{\mathcal{F}} S(f)e^{-i2\pi f t_0}.$$

This rule is proved using a variable substitution in the FT definition and recalling that Haar integral has the same properties as ordinary integral (see Sect. 4.1).

6. Convolution The convolution on the time domain gives the product in the frequency domain and vice-versa. This rule is a consequence of the kernel *separability* as seen in the introduction of this chapter. In fact, if we apply the Fourier transform to the convolution $s(t) = x * y(t)$, we obtain

$$S(f) = \int_I dt e^{-i2\pi ft} \int_I du x(t-u)y(u)$$

where $ft = f(t-u) + fu$, so that introducing the new integration variable $v = t-u$ gives

$$\begin{aligned} S(f) &= \int_I dt e^{-i2\pi f(t-u)} \int_I du x(t-u)e^{-i2\pi fu}y(u), \\ &= \int_I dv x(v)e^{-i2\pi fv} \int_I du e^{-i2\pi fu}y(u) = X(f)Y(f). \end{aligned}$$

5.5.2 Non-Primitive Rules

We now briefly discuss the other rules of Table 5.2, which are obtained from the primitive rules.

Rules 7 and 8. Real and Imaginary Parts For the proof, we recall that the real and imaginary parts are given by

$$\Re s(t) = \frac{1}{2}[s(t) + s^*(t)], \quad i\Im s(t) = \frac{1}{2}[s(t) - s^*(t)], \quad (5.41)$$

and then we apply the conjugation rule.

Rules 9 and 10. Even and odd parts Recall that the even and odd parts of a signal $s(t)$, $t \in I$, are given by

$$s_e(t) = \frac{1}{2}[s(t) + s(-t)], \quad s_o(t) = \frac{1}{2}[s(t) - s(-t)]$$

and then we apply the reverse rule.

Rule 11. Correlation This rule is a consequence of primitive Rules 4 and 10, as we shall see in Sect. 5.7, where the correlation is defined and developed.

5.5.3 Further Rules of the Fourier Transform

We outline other general rules of the Fourier transform.

Area and Value on the Origin

The signal area equals the value of the FT at the origin and, conversely, the FT area equals the value of the signal at the origin

$$\text{area}(s) = S(0), \quad \text{area}(S) = s(0). \quad (5.42)$$

The first is obtained by setting $f = 0$ in (5.7a) and the second by setting $t = 0$ in (5.7b). The usefulness of this rules should not be underestimated.

Parseval's Theorem

This theorem states that the energy of the signal equals the energy of its Fourier transform

$$E_s = \int_I dt |s(t)|^2 = \int_{\hat{I}} df |S(f)|^2 = E_S. \quad (5.43)$$

The theorem will be proved and discussed in Sect. 5.7 in the context of correlation.

▽ Poisson's Summation Formula

This rule relates the “samples” of a signal with the “samples” of the FT. Let I_0 , U_0 and P be ordinary groups with the ordering

$$P \subset U_0 \subset I_0 \quad (5.44a)$$

where U_0 is a lattice. Then, for reciprocals the ordering is reversed (see Sect. 5.3)

$$P^* \supset U_0^* \supset I_0^*, \quad (5.44b)$$

where U_0^* is a lattice.

Now, consider a signal $s(t)$, $t \in I_0/P$, and its FT $S(f)$, $f \in P^*/I_0^*$. Then, the signal $s(u)$, $u \in U_0/P$, gives the “samples” of $s(t)$ since the domain is restricted from I_0 to U_0 . Analogously, $S(\lambda)$, $\lambda \in U_0^*/I_0^*$, gives the “samples” of $S(f)$, since $U_0^* \subset P^*$.

Poisson's summation formula states that

$$\boxed{d(U_0) \sum_{u \in U_0/P} s(u) = \sum_{\lambda \in U_0^*/I_0^*} S(\lambda)} \quad (5.45)$$

where $d(U_0)$ is the determinant of the lattice U_0 . This rule is proved in Appendix E using the theory of linear transformations.

As an example, the samples $s(nT)$ of a continuous time signal $s(t)$, $t \in \mathbb{R}$, are related to the samples $S(kF_p)$ of the transform $S(f)$, $f \in \mathbb{R}$, by

$$\sum_{n=-\infty}^{+\infty} T s(nT) = \sum_{k=-\infty}^{+\infty} S(kF_p), \quad F_p = 1/T. \quad (5.46)$$

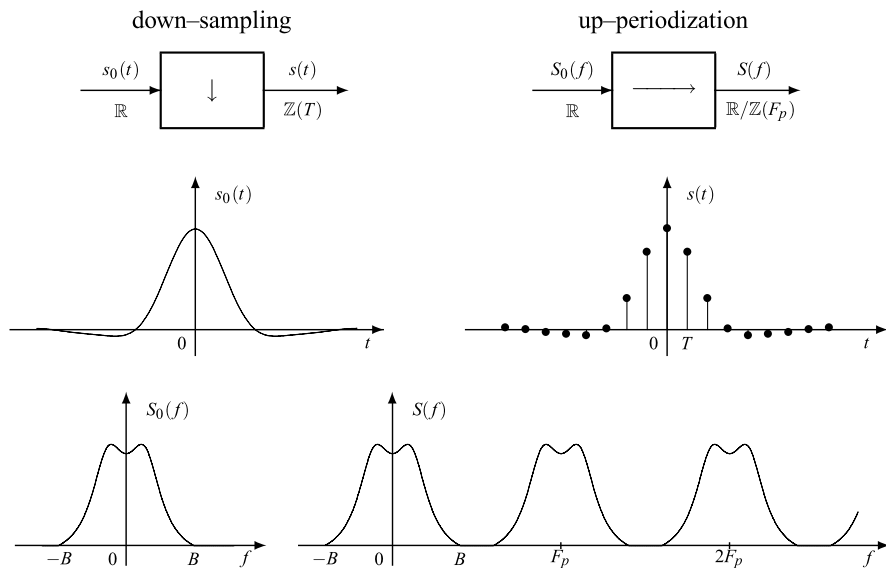


Fig. 5.5 Relation between the FT of a signal $s_0(t)$, $t \in I$, and of its down-sampled version $s(t)$, $t \in U$, illustrated for $I = \mathbb{R}$, $U = \mathbb{Z}(T)$

▽ **Fourier Transform After a Down-Sampling**

This and the next rule require the knowledge of elementary transformations, which will be developed in the following chapter.

Suppose that we know the FT $S_0(f)$, $f \in \widehat{I}$, of a signal $s_0(t)$, $t \in I$, and that we want to calculate the FT after a *restriction* of $s_0(t)$ from the group I into a subgroup U . In the theory of transformations, such a restriction is called a *down-sampling* and, more precisely, an $I \rightarrow U$ down-sampling, where $I = I_0/P$, $U = U_0/P$ and $U_0 \subset I_0$, with relationship $s(t) = s_0(t)$, $t \in U$. The Duality Theorem (Sect. 6.13) states that the corresponding operation in the frequency domain is a $\widehat{I} \rightarrow \widehat{U}$ up-periodization with relation

$$S(f) = \sum_{p \in [U_0^*/I_0^*]} S_0(f - p) \tag{5.47}$$

where the summation is extended over a cell of U_0^* modulo I_0^* (see the illustration of Fig. 5.5). In conclusion, from (5.47) we can calculate the FT after a down-sampling.

We now consider a 1D example of application. A 2D example will be seen in Sect. 5.10.

▽ *Example 5.2* We apply the rule to the case $I = \mathbb{R}$, $U = \mathbb{Z}(T)$, where $s_0(t)$, $t \in \mathbb{R}$, is a continuous-time signal and the result of the $\mathbb{R} \rightarrow \mathbb{Z}(T)$ down-sampling is a discrete-time signal $s(t)$, $t \in \mathbb{Z}(T)$. Since $U_0^* = \mathbb{Z}(T)^* = \mathbb{Z}(F_p)$ with $F_p = 1/T$

and $I_0^* = \mathbb{R}^* = \mathbb{O}$, we have $[U_0^*/I_0^*] = [\mathbb{Z}(F_p)/\mathbb{O}] = \mathbb{Z}(F_p)$. Then, (5.47) becomes

$$S(f) = \sum_{k=-\infty}^{+\infty} S_0(f - kF_p), \quad F_p = \frac{1}{T}. \quad (5.48)$$

For instance, from the Fourier pair

$$A_0 \operatorname{sinc}(F_0 t), \quad t \in \mathbb{R} \xrightarrow{\mathcal{F}} (A_0/F_0) \operatorname{rect}(f/F_0), \quad f \in \mathbb{R},$$

we obtain the Fourier pair

$$A_0 \operatorname{sinc}(F_0 t), \quad t \in \mathbb{Z}(T) \xrightarrow{\mathcal{F}} (A_0/F_0) \operatorname{rep}_{F_p} \operatorname{rect}(f/F_0), \quad f \in \mathbb{R}/\mathbb{Z}(F_p).$$

▽ Fourier Transform After a Periodic Repetition

Similarly to the previous case, we can find the FT after a periodic repetition (up-periodization) $I = I_0/P_1 \rightarrow U = I_0/P_2$ with $S_2 \supset P_1$, namely

$$s(t) = \sum_{p \in [P_2/P_1]} s_0(t - p), \quad (5.49)$$

starting from the FT of $s_0(t)$, $t \in I$. In fact, from the Duality Theorem, in the frequency domain we obtain the $\widehat{I} \rightarrow \widehat{U}$ down-sampling, with the relation

$$S(f) = S_0(f), \quad f \in \widehat{U}. \quad (5.50)$$

Example 5.3 If $I = \mathbb{R}$ and $U = \mathbb{R}/\mathbb{Z}(T_p)$, relation (5.49) becomes

$$s(t) = \sum_{k=-\infty}^{+\infty} s_0(f - kF_p).$$

Then, from (5.50)

$$S(kF) = S_0(kF), \quad kF \in \mathbb{Z}(F), \quad F = 1/T.$$

These relations are illustrated in Fig. 5.6.

UT 5.6 Symmetries in the Frequency Domain

We first consider the fundamental symmetries introduced in Sect. 4.13 in the signal domain and then we develop the *Symmetry Theory* in the frequency domain.

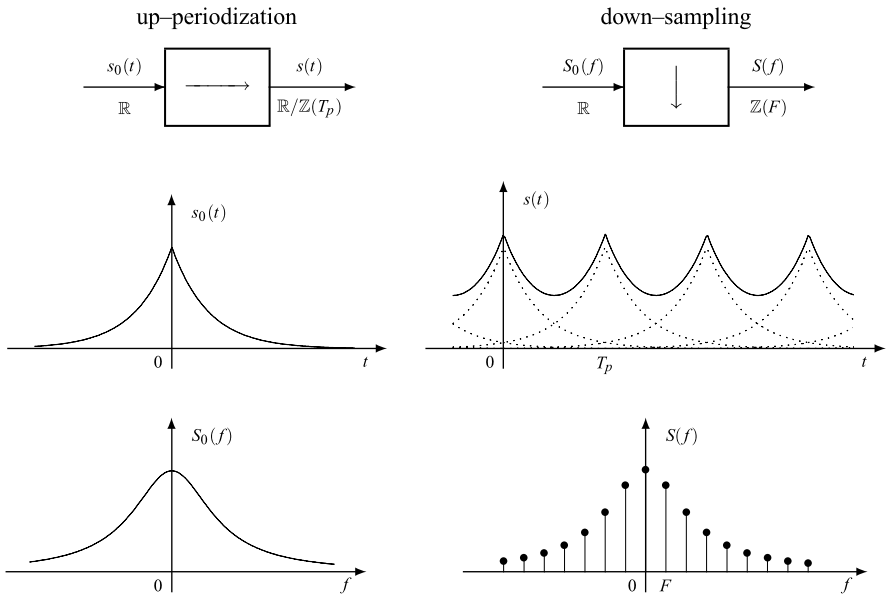


Fig. 5.6 Relation between the Fourier transform of a signal $s_0(t)$, $t \in I$, and the Fourier transform of its periodic version $s(t)$, $t \in U$, illustrated for $I = \mathbb{R}$, $U = \mathbb{R}/\mathbb{Z}(T_p)$

Table 5.3 Correspondence in the symmetries of signals and Fourier transforms

Signal		Fourier transform	
1(a). $s(t) = s(-t)$	Even	1(a). $S(f) = S(-f)$	Even
1(b). $s(t) = -s(-t)$	Odd	1(b). $S(f) = -S(-f)$	Odd
2(a). $s(t) = s^*(t)$	Real	3(a). $S(f) = S^*(-f)$	Hermitian
2(b). $s(t) = -s^*(t)$	Imaginary	3(b). $S(f) = -S^*(-f)$	Anti-Hermitian
3(a). $s(t) = s^*(-t)$	Hermitian	2(a). $S(f) = S^*(f)$	Real
3(b). $s(t) = -s^*(-t)$	Anti-Hermitian	2(b). $S(f) = -S^*(f)$	Imaginary

5.6.1 Symmetries of Fourier Transforms

The fundamental symmetries introduced in the signal domain generate as many symmetries in the frequency domain, as summarized in Table 5.3. Symmetries 1 (even and odd symmetries) are preserved in the frequency domain, as a consequence of Rule 3 of Table 5.2. Analogously, from Rule 4, Symmetries 2 in the signal domain become Symmetries 3 in the frequency domain and vice versa.

Figure 5.7 illustrates all the symmetries for continuous signals and the corresponding symmetries for the FT.

signal

transform

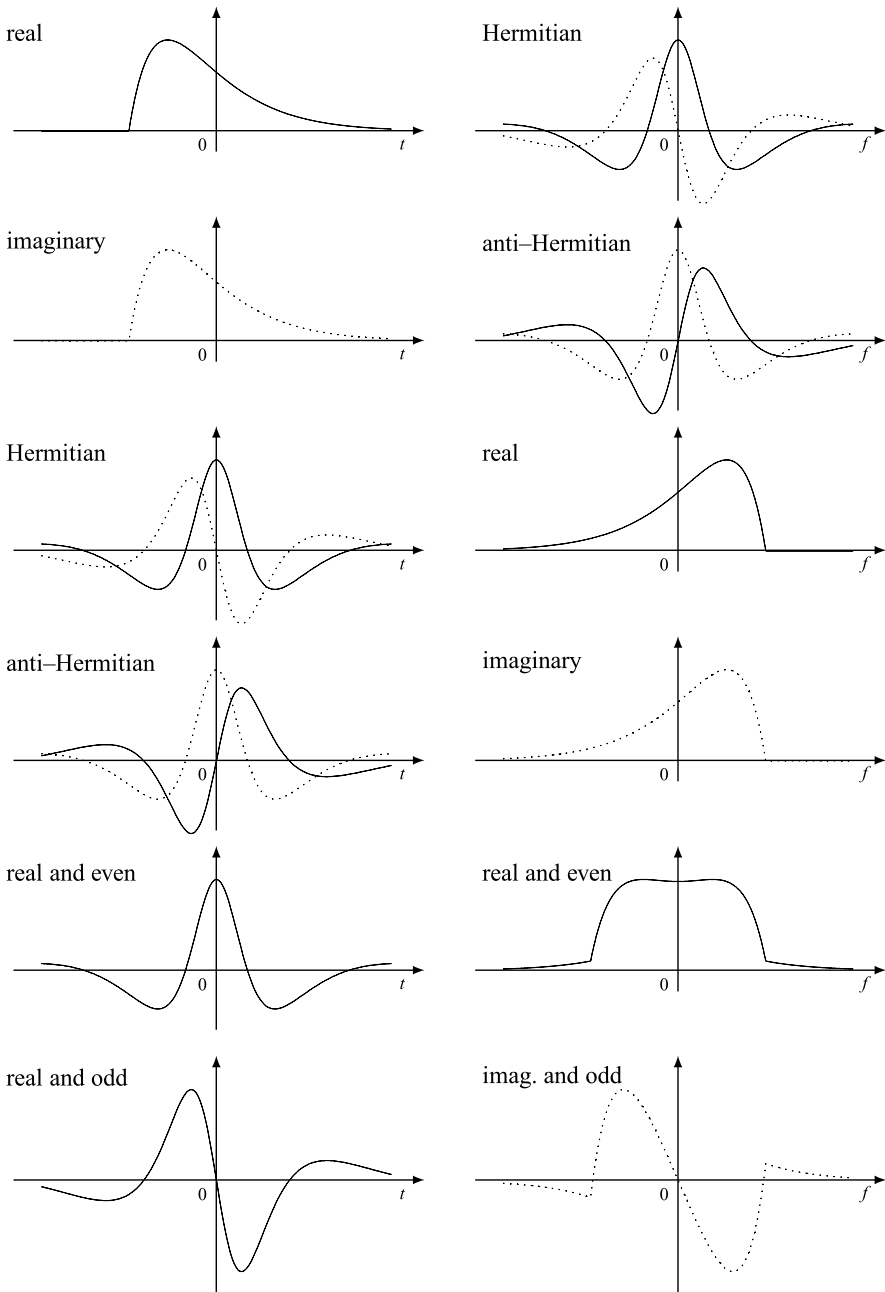


Fig. 5.7 Symmetries for signals and corresponding Fourier transforms for $I = \hat{T} = \mathbb{R}$

Particularly interesting is the symmetry “real signal”, which becomes “Hermitian symmetry” in the frequency domain

$$s(t) = s^*(t) \xrightarrow{\mathcal{F}} S(f) = S^*(-f).$$

Hence, in general, *the FT of a real signal is not real, but a function with the Hermitian symmetry*. By writing

$$S(f) = S_R(f) + iS_I(f) = A_S(f)e^{i\beta_S(f)},$$

the Hermitian symmetry basis becomes

$$S_R(f) = S_R(-f), \quad S_I(f) = -S_I(-f), \tag{5.51a}$$

$$A_S(f) = A_S(-f), \quad \beta_S(f) = -\beta_S(-f). \tag{5.51b}$$

Therefore, the Fourier transform of a real signal has even real part and even magnitude, odd imaginary part and odd argument.

The above statements can be summarized as follows:

<i>signal</i>	<i>Fourier transform</i>
complex	complex with no symmetry (in general)
real	complex with Hermitian symmetry
real and even	real and even
real and odd	imaginary and odd.

Decompositions into symmetric components are transferred into the frequency domain with the exchange of Symmetries 2 and 3. As an example, signal decomposition into real and imaginary parts gives

$$s = \Re s + i\Im s \xrightarrow{\mathcal{F}} \frac{1}{2}(S + S_-^*) + \frac{1}{2}(S - S_-^*), \tag{5.52}$$

that is, the FT decomposition into Hermitian and anti-Hermitian parts.

Real Signals We have seen that the FT of real signals has the Hermitian symmetry. Therefore, the *even part* and the *odd part* of a *real signal* respectively become

$$\begin{aligned} s_e(t) &= \frac{1}{2}[s(t) + s(-t)] \xrightarrow{\mathcal{F}} S_e(f) = \Re S(f), \\ s_o(t) &= \frac{1}{2}[s(t) - s(-t)] \xrightarrow{\mathcal{F}} S_o(f) = i\Im S(f). \end{aligned} \tag{5.53}$$

Thus, the decomposition of a real signal into even and odd parts implies the FT decomposition into real and imaginary parts.

This rule is useful when calculating new Fourier pairs (see Problem 5.24).

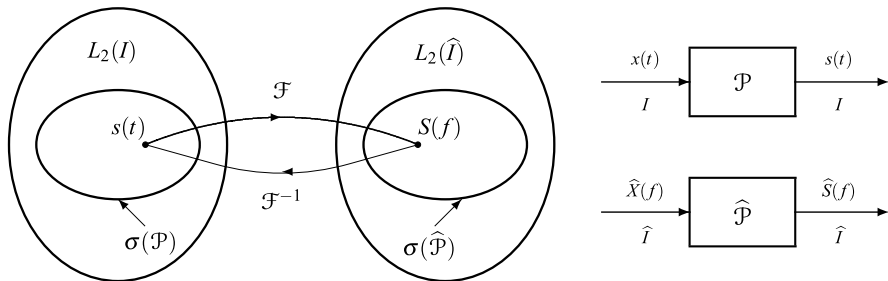


Fig. 5.8 $\hat{\mathcal{P}}$ is the projector dual of \mathcal{P} and $\sigma(\hat{\mathcal{P}})$ is the symmetry dual of $\sigma(\mathcal{P})$

5.6.2 Symmetry Theory in the Frequency Domain

In the previous chapter, we have introduced a general theory of symmetries in the time domain using the projector and reflector operators. This theory can be transferred to the frequency domain to establish and handle the symmetries of the Fourier transforms.

We recall that a projector \mathcal{P} applied to a signal $x \in L_2(I)$ extracts the symmetric component $s = \mathcal{P}[x]$. In the frequency domain, the *dual* projector $\hat{\mathcal{P}}$ extracts the symmetric component $S = \hat{\mathcal{P}}[X]$ of the FT $X \in L_2(\hat{I})$ of x , with S being the FT of s (Fig. 5.8).

To find the dual projector, we start from the original relation $s = \mathcal{P}[x]$ and express x as the inverse FT of X , that is, $x = \mathcal{F}^{-1}[X]$ and $S = \mathcal{F}[s]$. Thus, we get the graph

$$X \xrightarrow{\mathcal{F}^{-1}} x \xrightarrow{\mathcal{P}} s \xrightarrow{\mathcal{F}} S = X \xrightarrow{\hat{\mathcal{P}}} S$$

which globally gives S starting from X . The corresponding operator relation is

$$\hat{\mathcal{P}} = \mathcal{F}\mathcal{P}\mathcal{F}^{-1}. \tag{5.54}$$

We can check that $\hat{\mathcal{P}}$ is idempotent. In fact, $\hat{\mathcal{P}}^2 = \mathcal{F}\mathcal{P}\mathcal{F}^{-1}\mathcal{F}\mathcal{P}\mathcal{F}^{-1}$, where $\mathcal{F}^{-1}\mathcal{F} = \mathcal{J}$ and then $\mathcal{P}\mathcal{F}^{-1}\mathcal{F}\mathcal{P} = \mathcal{P}^2 = \mathcal{P}$.

In a similar way, we prove that the dual reflector operator is given by

$$\hat{\mathcal{B}} = \mathcal{F}\mathcal{B}\mathcal{F}^{-1}$$

and, if \mathcal{B} is M -ary, that is, $\mathcal{B}^M = \mathcal{J}$, also $\hat{\mathcal{B}}$ is an M -ary reflector. Thus, we can establish an M -ary symmetry for FTs on the frequency domain \hat{I} , starting from an M -ary symmetry for signals defined on I .

In general, the dual symmetry is different from the original symmetry, as we have seen with the fundamental symmetries, e.g., the *real symmetry* becomes the *Hermitian symmetry*. But, in some cases the dual symmetry coincides with the original one, as is for the even and odd symmetries. In that case, the corresponding symmetry is called *self-dual*.

We can check the self-duality for even/odd symmetries by evaluating the dual reflector $\widehat{\mathcal{B}}$. In this case, $\mathcal{B} = \mathcal{J}_-$ is the operator that gives the reflected signal $s_-(t) = s(-t)$ starting from $s(t)$. From (5.54) we have $\widehat{\mathcal{B}} = \mathcal{F}\mathcal{J}_-\mathcal{F}^{-1}$ and we have to find $\widehat{\mathcal{B}} = \mathcal{J}_-$. In fact, with the usual notations, if X is an FT, $\mathcal{F}^{-1}[X]$ gives the signal x , and $\mathcal{J}_-\mathcal{F}^{-1}[X]$ gives x_- . But, for the axis inversion rule, $\mathcal{F}[x_-]$ gives X_- and, globally, starting from X we obtain X_- , and then $\widehat{\mathcal{B}} = \mathcal{J}_-$.

UT 5.7 Energy and Correlation

5.7.1 Energy and Cross-Energy. Parseval's Theorem

The *energy* of a signal $x(t)$, $t \in I$, which is given by

$$E_x = \int_I dt |x(t)|^2 = \|x\|^2,$$

is generalized as the *cross-energy*

$$E_{xy} = \int_I dt x(t)y^*(t) = \langle x, y \rangle$$

for two signals $x(t)$ and $y(t)$ on the same domain I . Both of these quantities can be directly evaluated from the FTs.

Theorem 5.3 (Parseval's theorem) *The cross-energy of two signals equals the cross-energy of the corresponding Fourier transforms, $E_{xy} = E_{XY}$, namely*

$$\int_I dt x(t)y^*(t) = \int_{\widehat{I}} df X(f)Y^*(f). \quad (5.55)$$

In particular, for the energy $E_x = E_X$ and

$$\int_I dt |x(t)|^2 = \int_{\widehat{I}} df |X(f)|^2. \quad (5.55a)$$

This theorem, which will be proved below, states that the energy can be evaluated in the signal domain and in the frequency domain by the same formula. Using the notations introduced for the norm and inner product (see Sect. 4.5), the previous results can be expressed as

$$\langle x, y \rangle = \langle X, Y \rangle, \quad \|x\|^2 = \|X\|^2. \quad (5.55b)$$

These relations state that, in the passage from the class $L_2(I)$ of square-integrable signals to the class $L_2(\widehat{I})$ of square-integrable FTs, the inner product and the norm are preserved (*isometry*).

5.7.2 Correlation and Energy Spectral Density

For each pair of signals $x(t)$ and $y(t)$ on the same domain I , the *correlation* is defined as

$$c_{xy}(\tau) \triangleq \int_I dt x(t + \tau)y^*(t), \quad \tau \in I. \quad (5.56)$$

The corresponding FT

$$C_{xy}(f) \triangleq \int_I d\tau c_{xy}(\tau)e^{-i2\pi f\tau}, \quad f \in \widehat{I} \quad (5.57)$$

is called the *energy spectral density*. These two functions give a detailed description of the energy content of signals, the former in the signal domain and the latter in the frequency domain.

By applying a change of variable in (5.56), it is easily seen that the correlation can be expressed as the *convolution of the signal x with the signal y_-^** , the conjugate and reversed version of y , namely

$$\boxed{c_{xy}(\tau) = x * y_-^*(\tau)}. \quad (5.58)$$

Then, the computation of a correlation is substantially the same as that of a convolution. From the FT rules in the frequency domain, (5.58) becomes

$$\boxed{C_{xy}(f) = X(f)Y^*(f)}. \quad (5.59)$$

Now, the proof of Parseval's theorem is straightforward. If we set $\tau = 0$ in (5.56), we obtain the energy by evaluating the correlation at the origin

$$c_{xy}(0) = E_{xy}.$$

Moreover, the signal value at the origin equals the area of its FT and then

$$E_{xy} = \int_{\widehat{I}} df C_{xy}(f) = \int_{\widehat{I}} df X(f)Y^*(f). \quad (5.60)$$

This result justifies the term “energy spectral density” for the function $C_{xy}(f)$, since its integral gives the energy.

Finally, note that the correlation between signals x and y is not commutative, i.e., $c_{yx} \neq c_{xy}$ in general. The same holds for the spectral densities, $C_{yx}(f) \neq C_{xy}(f)$. Nevertheless, we have the following relations

$$c_{yx}(\tau) = c_{xy}^*(-\tau), \quad C_{yx}(f) = C_{xy}^*(f). \quad (5.61)$$

The previous results are now applied with $y = x$, so that the correlation becomes the self-correlation, $c_{xx}(\tau) = c_x(\tau)$, and the spectral density becomes the self-spectral density, $C_{xx}(f) = C_x(f)$. From (5.59) and (5.61), we find

$$C_x(f) = |X(f)|^2, \quad (5.62a)$$

$$c_x(\tau) = c_x^*(-\tau), \quad C_x(f) = C_x^*(f). \quad (5.62b)$$

Hence, the self-correlation has the Hermitian symmetry, while the self-spectral density is always a real function.

In the case of a *real* signal, the correlation is a real function and then the Hermitian symmetry becomes the even symmetry

$$x \text{ real} \implies c_x \text{ real and even} \implies C_x \text{ real and even.} \quad (5.63)$$

Interpretation of Energy and Correlation The “energy” between signals may or may not have a physical interpretation, and often this terminology is not appropriate, although its use is consolidated in Signal Theory. If a signal $v(t)$, $t \in \mathbb{R}$, represents a voltage applied to a resistor R , the energy dissipated therein is E_v/R and, in this case, E_v is proportional to the physical energy. If $v(t)$ and $i(t)$ represent the voltage and the current in a two-port device, then E_{vi} gives the physical energy entering the two-port device.

Similarly, the term “correlation” may be misleading, since it has not a statistical interpretation, rather from (5.56) it results that the correlation evaluated at τ equals the cross-energy of the signals $x(t)$ and $y_\tau(t) = y(t - \tau)$.

5.8 Explicit Forms of One-Dimensional Fourier Transforms

In this section, the FT, introduced and discussed in the previous sections in a unified form, is explicitly developed for the classes of 1D signals. To this end, we start from the expressions

$$\boxed{\begin{aligned} S(f) &= \int_I dt s(t) e^{-i2\pi ft}, & f \in \widehat{I}, \\ s(t) &= \int_{\widehat{I}} df S(f) e^{i2\pi ft}, & t \in I, \end{aligned}} \quad (5.64)$$

and we choose the groups I and \widehat{I} in the class $\mathcal{Q}(\mathbb{R})$. As shown explicitly in Table 5.1, these groups have substantially four different formats and, correspondingly, we find as many formats of signals and FTs.

5.8.1 The Four One-Dimensional Cases

In the explicit formulas, the following notation for time and frequency will be used

- t and f in the continuous case,
- nT and kF in the discrete case.

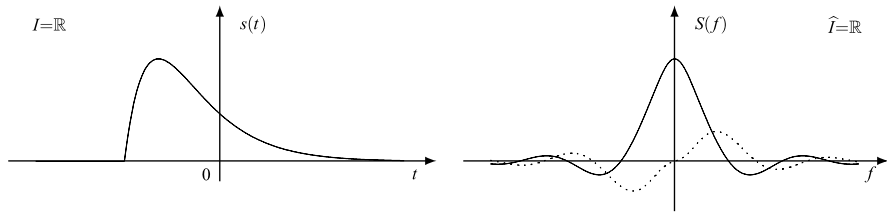


Fig. 5.9 Example of Fourier pair on \mathbb{R} with real $s(t)$

Of course, when we make these substitutions, the FT and its inverse lose the “beauty” of the symmetric form (5.64), sometimes even in a nontrivial way (see DFT).

Continuous Time Signals (Fig. 5.9)

$I = \mathbb{R}$ continuous time signal

$\hat{I} = \mathbb{R}$ continuous frequency FT

$$S(f) = \int_{-\infty}^{+\infty} s(t)e^{-i2\pi ft} dt, \quad s(t) = \int_{-\infty}^{+\infty} S(f)e^{i2\pi ft} df. \quad (5.65)$$

These are the classical expressions we have seen in Chap. 2. In both expressions, an ordinary integral is involved. This form of FT will be studied in detail in Chap. 9, where a rich gallery of Fourier pairs is also collected (see Table 9.2).

Periodic Continuous Time Signals (Fig. 5.10)

$I = \mathbb{R}/\mathbb{Z}(T_p)$ periodic continuous time signal

$\hat{I} = \mathbb{Z}(F)$, $F = 1/T_p$ discrete frequency FT

$$S(kF) = \int_0^{T_p} s(t)e^{-i2\pi kFt} dt, \quad s(t) = \sum_{k=-\infty}^{+\infty} FS(kF)e^{i2\pi kFt} \quad (5.66)$$

where the cell $[0, T_p)$ has been chosen (but the integral can be extended to any other cell of \mathbb{R} modulo $\mathbb{Z}(T_p)$). Expression (5.66b) is a form of the *Fourier series expansion* seen in the Classic Theory of Chap. 2. In fact, if we let

$$S_k = FS(kF), \quad (5.66a)$$

we get

$$S_k = \frac{1}{T_p} \int_0^{T_p} s(t)e^{-i2\pi kFt} dt, \quad s(t) = \sum_{k=-\infty}^{+\infty} S_k e^{i2\pi kFt}, \quad (5.66b)$$

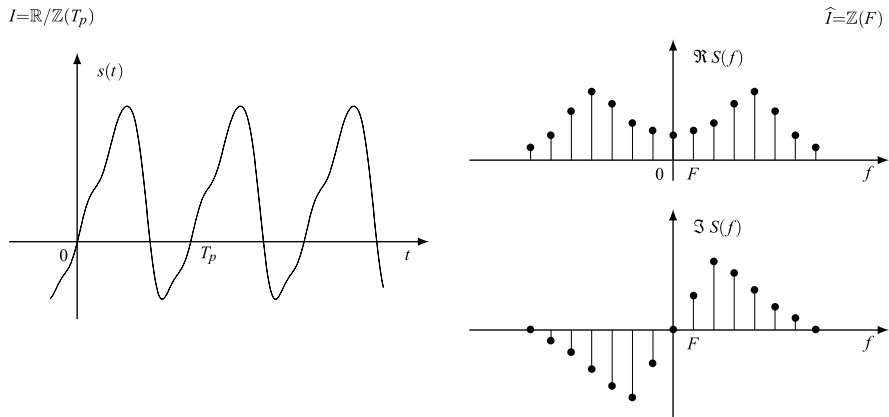


Fig. 5.10 Example of Fourier pair on $\mathbb{R}/\mathbb{Z}(T_p)$ with real $s(t)$. The FT values are proportional to the Fourier coefficients

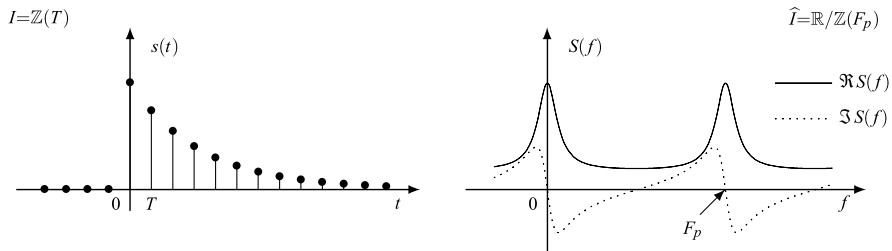


Fig. 5.11 Example of Fourier pair on $\mathbb{Z}(T)$ with real $s(t)$

which is exactly the exponential form of the Fourier series (see (2.46a), (2.46b)). This FT will be revisited in Chap. 10, where a gallery of Fourier pairs is collected (see Table 10.1).

Discrete Time Signals (Fig. 5.11)

$I = \mathbb{Z}(T)$ discrete time signal
 $\hat{I} = \mathbb{R}/\mathbb{Z}(F_p)$ periodic continuous frequency FT

$$S(f) = \sum_{n=-\infty}^{+\infty} T s(nT) e^{-i2\pi f n T}, \quad s(nT) = \int_0^{F_p} S(f) e^{i2\pi f n T} df, \quad (5.67)$$

where the cell $[0, F_p)$ with $F_p = 1/T$ has been chosen (but it can be replaced by any other cell of \mathbb{R} modulo $\mathbb{Z}(F_p)$). Expressions (5.67) are the same seen in Chap. 2 for discrete-time signals (see (2.91a), (2.91b)). This form of FT will be revisited in Chap. 11 together with the zeta transform (see the gallery of Fourier pairs of Table 11.1).

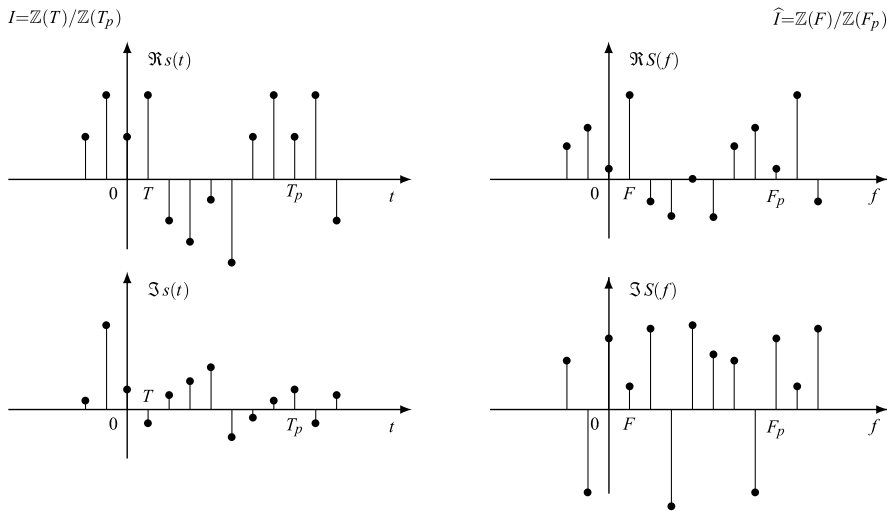


Fig. 5.12 Example of Fourier pair on $\mathbb{Z}(T)/\mathbb{Z}(T_p)$ with a complex signal $s(t)$ for $N = 8$ points per period

Periodic Discrete Time Signals (Fig. 5.12)

$I = \mathbb{Z}(T)/\mathbb{Z}(T_p)$ periodic discrete time signal

$\hat{I} = \mathbb{Z}(F)/\mathbb{Z}(F_p)$ periodic discrete frequency FT

$$S(kF) = \sum_{n=0}^{N-1} T s(nT) e^{-i2\pi kFnT}, \quad s(nT) = \sum_{k=0}^{N-1} F S(kF) e^{i2\pi kFnT}, \quad (5.68)$$

where

$$T_p = NT, \quad F_p = 1/T = NF, \quad N \in \mathbb{N}. \quad (5.68a)$$

The cells used in (5.68) are

$$\mathbb{Z}_N(T) \triangleq \{0, T, \dots, (N-1)T\}, \quad \mathbb{Z}_N(F) \triangleq \{0, F, \dots, (N-1)F\}.$$

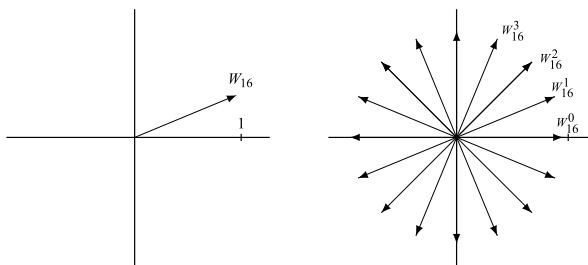
It is not trivial to recognize that these relations are equivalent to the expressions seen in Sect. 2.13 for the Discrete Fourier Transform (DFT). To show the equivalence, we express the exponential in terms of the N th root of unity (Fig. 5.13)

$$W_N = \exp(i2\pi/N).$$

Then, considering that $FT = 1/N$, (5.68) becomes

$$S(kF) = \sum_{n=0}^{N-1} T s(nT) W_N^{-kn}, \quad s(nT) = \sum_{k=0}^{N-1} F S(kF) W_N^{kn}. \quad (5.69)$$

Fig. 5.13 The principal N th root of unity and the whole root constellation, shown for $N = 16$



Finally, if we set as usual

$$T = 1, \quad s_n = s(nT), \quad S_k = S(kF),$$

we obtain the DFT form (2.102), i.e.,

$$S_k = \sum_{n=0}^{N-1} s_n W_N^{-kn}, \quad s_n = \frac{1}{N} \sum_{k=0}^{N-1} S_k W_N^{kn}. \quad (5.70)$$

We recall that these expressions play a fundamental role in computer processing, as we will see in more detail in Chaps. 12 and 13. A gallery of Fourier pairs is collected in Table 12.1.

5.8.2 Fourier Transform of Singular Signals

In Sect. 5.2, we obtained the general expression for the FT of some signals related to impulses and characters (singular signals), in particular we found that

$$\delta_I(t - t_0) \xrightarrow{\mathcal{F}} e^{-i2\pi f t_0}, \quad e^{i2\pi f_0 t} \xrightarrow{\mathcal{F}} \delta_{\hat{T}}(f - f_0). \quad (5.71)$$

Now, using Euler formulas (2.20) in (5.71), we obtain the FTs of sinusoidal signals, namely

$$\begin{aligned} \cos 2\pi f_0 t &\xrightarrow{\mathcal{F}} \frac{1}{2} [\delta_{\hat{T}}(f - f_0) + \delta_{\hat{T}}(f + f_0)], \\ \sin 2\pi f_0 t &\xrightarrow{\mathcal{F}} \frac{1}{2i} [\delta_{\hat{T}}(f - f_0) - \delta_{\hat{T}}(f + f_0)], \end{aligned}$$

and more generally,

$$A_0 \cos(2\pi f_0 t + \varphi_0) \xrightarrow{\mathcal{F}} \frac{1}{2} A_0 e^{j\varphi_0} \delta_{\hat{T}}(f - f_0) + \frac{1}{2} A_0 e^{-j\varphi_0} \delta_{\hat{T}}(f + f_0). \quad (5.72)$$

These results have a general validity on the groups of \mathbb{R} . By specifying the pair (I, \hat{T}) , we obtain more explicit formulas, as shown in Table 5.4.

Table 5.4 Singular 1D Fourier pairs

①	$s(t) = \delta_T(t), t \in I$	$S(f) = 1, f \in \hat{I}$
$I = \mathbb{R}$		$\hat{I} = \mathbb{R}$
$I = \mathbb{R}/\mathbb{Z}(T_p)$		$\hat{I} = \mathbb{Z}(F)$
$I = \mathbb{Z}(T)$		$\hat{I} = \mathbb{R}/\mathbb{Z}(F_p)$
$I = \mathbb{Z}(T)/\mathbb{Z}(T_p)$		$\hat{I} = \mathbb{Z}(F)/\mathbb{Z}(F_p)$
②	$s(t) = 1, t \in I$	$S(f) = \delta_{\hat{I}}(f), f \in \hat{I}$
$I = \mathbb{R}$		$\hat{I} = \mathbb{R}$
$I = \mathbb{R}/\mathbb{Z}(T_p)$		$\hat{I} = \mathbb{Z}(F)$
$I = \mathbb{Z}(T)$		$\hat{I} = \mathbb{R}/\mathbb{Z}(F_p)$
$I = \mathbb{Z}(T)/\mathbb{Z}(T_p)$		$\hat{I} = \mathbb{Z}(F)/\mathbb{Z}(F_p)$

Table 5.4 (Continued)

<p>③</p>	$\cos(2\pi f_0 t), t \in I$	$\frac{1}{2}[\delta_f(f-f_0) + \delta_f(f+f_0)], f \in \hat{I}$
$I = \mathbb{R}$ 	$\hat{I} = \mathbb{R}$ 	
$I = \mathbb{R}/\mathbb{Z}(T_p)$ 	$\hat{I} = \mathbb{Z}(F)$ 	
$I = \mathbb{Z}(T)$ 	$\hat{I} = \mathbb{R}/\mathbb{Z}(F_p)$ 	
$I = \mathbb{Z}(T)/\mathbb{Z}(T_p)$ 	$\hat{I} = \mathbb{Z}(F)/\mathbb{Z}(F_p)$ 	
<p>④</p>	$\sin(2\pi f_0 t), t \in I$	$\frac{1}{2j}[\delta_f(f-f_0) - \delta_f(f+f_0)], f \in \hat{I}$
$I = \mathbb{R}$ 	$\hat{I} = \mathbb{R}$ 	
$I = \mathbb{R}/\mathbb{Z}(T_p)$ 	$\hat{I} = \mathbb{Z}(F)$ 	
$I = \mathbb{Z}(T)$ 	$\hat{I} = \mathbb{R}/\mathbb{Z}(F_p)$ 	
$I = \mathbb{Z}(T)/\mathbb{Z}(T_p)$ 	$\hat{I} = \mathbb{Z}(F)/\mathbb{Z}(F_p)$ 	

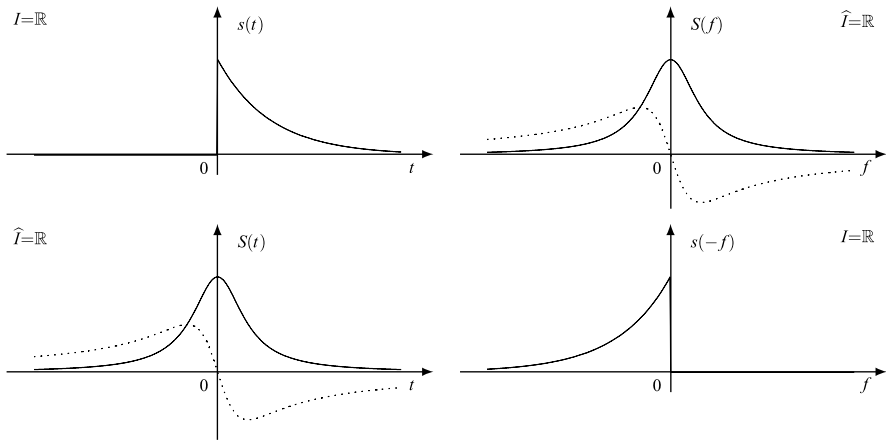


Fig. 5.14 Illustration of the Symmetry Rule for a continuous-time signal

Note that the above Fourier pairs are valid provided that t_0 and f_0 are compatible with the corresponding domains. For instance, the shift t_0 on $I = \mathbb{Z}(T)$ must be an integer multiple of T .

5.8.3 Application of the Symmetry Rule

The Symmetry Rule established in general form in Sect. 5.4 is now illustrated by two 1D examples.

Example 5.4 We consider a continuous-time signal, for which the graph (5.37) becomes

$$\begin{array}{ccc}
 s(t) & \xrightarrow{\mathcal{F}} & S(f) \\
 \mathbb{R} & & \mathbb{R} \\
 S(t) & \xrightarrow{\mathcal{F}} & s(-f) \\
 \mathbb{R} & & \mathbb{R}
 \end{array}$$

We apply this graph to the Fourier pair (Fig. 5.14)

$$1(t)e^{-\alpha t}, \quad t \in \mathbb{R} \quad \xrightarrow{\mathcal{F}} \quad \frac{1}{\alpha + i2\pi f}, \quad f \in \mathbb{R}. \tag{5.73a}$$

Then, the Symmetry Rule gives the new pair

$$\frac{1}{\alpha + i2\pi t}, \quad t \in \mathbb{R} \quad \xrightarrow{\mathcal{F}} \quad 1(-f)e^{\alpha f}, \quad f \in \mathbb{R}. \tag{5.73b}$$

In this case, the application is particularly simple because \mathbb{R} is self-dual, $\widehat{\mathbb{R}} = \mathbb{R}$.

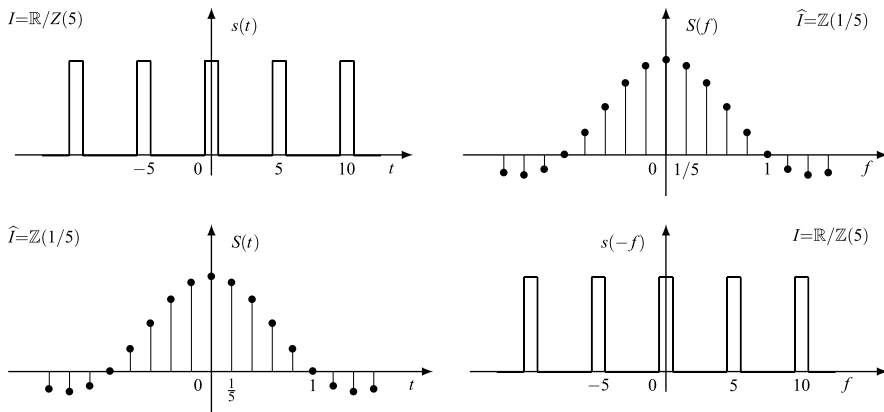


Fig. 5.15 Illustration of symmetry rule starting with a periodic continuous-time signal. Note that in this specific example it turns out that $s(-f) = s(f)$

Example 5.5 We now consider a periodic continuous-time signal with period $T_p = 5$. Since $I = \mathbb{R}/\mathbb{Z}(5)$ and $\hat{I} = \mathbb{Z}(1/5)$, the graph (5.37) becomes

$$\begin{array}{ccc} s(t) & \xrightarrow{\mathcal{F}} & S(f) \\ \mathbb{R}/\mathbb{Z}(5) & & \mathbb{Z}(1/5) \end{array} \quad \begin{array}{ccc} S(t) & \xrightarrow{\mathcal{F}} & s(-f) \\ \mathbb{Z}(1/5) & & \mathbb{R}/\mathbb{Z}(5) \end{array}$$

As a specific signal $s(t)$ we consider a “square wave” with duty cycle $d = 20\%$, which can be written in the form

$$s(t) = \text{rep}_5[\text{rect}(t)], \quad t \in \mathbb{R}/\mathbb{Z}(5)$$

where rep_5 is the periodic repetition with period 5. The FT results in

$$\begin{aligned} S(kF) &= \int_{\mathbb{R}/\mathbb{Z}(5)} dt s(t) e^{-i2\pi kFt} = \int_{-1/2}^{1/2} e^{-i2\pi kFt} dt \\ &= \frac{1}{-i2\pi kF} (e^{-i2\pi kF/2} - e^{i2\pi kF/2}) = \text{sinc}(k/5), \quad k \in \mathbb{Z}, \end{aligned}$$

which states the Fourier pair (Fig. 5.15)

$$\text{rep}_5[\text{rect}(t)], \quad t \in \mathbb{R}/\mathbb{Z}(5) \xrightarrow{\mathcal{F}} \text{sinc}(f), \quad f \in \mathbb{Z}(1/5).$$

Now, the application of a Symmetry Rule gives the new pair

$$\text{sinc}(t), \quad t \in \mathbb{Z}(1/5) \xrightarrow{\mathcal{F}} \text{rep}_5[\text{rect}(f)], \quad f \in \mathbb{R}/\mathbb{Z}(5),$$

where we have taken into account that $\text{rect}(f) = \text{rect}(-f)$.

This second example shows that when time and frequency domains are different ($I \neq \widehat{I}$), the application of the symmetry rule involves signals of two different classes, $\mathcal{S}(I)$ and $\mathcal{S}(\widehat{I})$. In fact, in the first pair the signal is periodic continuous, while in the second pair it is discrete aperiodic.

5.8.4 Decomposition of a Real Signal into Sinusoidal Components

For a *real* signal, the Hermitian symmetry of the FT allows obtaining a decomposition into sinusoids instead of exponentials. But, exponentials have both positive and negative frequencies, whereas sinusoids have only positive frequencies and in the manipulation we have to find a *pairing* between terms with frequencies $\pm f$.

The technique to obtain the sinusoidal representation from the exponential one is based on the Euler formula

$$e^{i2\pi ft} + e^{-i2\pi ft} = 2 \cos 2\pi ft.$$

Considering in general the presence of a component at zero frequency, we have to decompose the frequency domain into the form

$$\widehat{I} = \widehat{I}_z \cup \widehat{I}_+ \cup \widehat{I}_- \quad \text{with } \widehat{I}_- = -\widehat{I}_+, \quad (5.74)$$

where $\widehat{I}_z = \{0\}$, \widehat{I}_+ is the set of “positive” frequencies and \widehat{I}_- that of “negative” frequencies. We find in particular

$$\begin{aligned} I = \mathbb{R}, \quad \widehat{I} = \mathbb{R}, \quad \widehat{I}_+ = (0, +\infty), \quad \widehat{I}_- = (-\infty, 0), \\ I = \mathbb{Z}(T), \quad \widehat{I} = \mathbb{R}/\mathbb{Z}(F_p), \quad \widehat{I}_+ = \left(0, \frac{1}{2}F_p\right), \quad \widehat{I}_- = \left(-\frac{1}{2}F_p, 0\right). \end{aligned} \quad (5.75)$$

Now, from (5.14) we get

$$\begin{aligned} s(t) &= \int_{\widehat{I}_z} df S(f) e^{i2\pi ft} + \int_{\widehat{I}_+} df S(f) e^{i2\pi ft} + \int_{\widehat{I}_-} df S(f) e^{i2\pi ft} \\ &= S_0 + \int_{\widehat{I}_+} df [S(f) e^{i2\pi ft} + S(-f) e^{-i2\pi ft}] \end{aligned}$$

where the constant term is given by

$$S_0 = \int_{\widehat{I}_z} df S(f) e^{i2\pi ft} = \int_{\{0\}} df S(f).$$

Since the FT of a real signal has the Hermitian symmetry, we can write

$$S(f) = A_S(f) e^{i\beta_S(f)}, \quad (5.76)$$

where

$$A_S(f) = A_S(-f), \quad \beta_S(f) = -\beta_S(-f), \quad (5.76a)$$

and we obtain

$$s(t) = S_0 + \int_{\widehat{I}_+} df \, 2A_S(f) \cos[2\pi ft + \beta_S(f)], \quad t \in I. \quad (5.77)$$

In conclusion, a *real* signal can be decomposed into sinusoidal components of amplitude $[df \, 2A_S(f)]$, phase $\beta_S(f)$ and frequencies f limited to $f \in \widehat{I}_+$. Note that this decomposition holds also for discrete signals (see the problems at the end of this chapter).

5.8.5 Relation Between Duration and Bandwidth

We have previously defined the duration $D(s) = \text{meas } \mathcal{E}(s)$ and the bandwidth $B(s) = \text{meas } \mathcal{F}(s)$ of a signal. We can ask ourselves if there is a relation between these two measures (see Sect. 5.4). The qualitative answer is that *the smaller the duration of a signal, the larger its bandwidth, and vice versa*.

To get quantitative results, we need to refer to a specific signal class for which we can establish a relation of the form

$$D(s)B(s) = K \quad (5.78)$$

where K is a constant depending on the signal class and on the definitions of duration and bandwidth.² As an example, it is easy to show that relation (5.78) holds for the signal class generated in the form

$$s(t) = A s_0 \left(\frac{t - t_0}{a} \right), \quad t \in \mathbb{R},$$

where $s_0(t)$ is a reference signal and A , t_0 , a are parameters. In fact, we have $D(s) = aD(s_0)$, since the amplitude A and the translation t_0 do not affect the duration. Moreover, $S(f) = Aa S_0(af) \exp(-i2\pi f t_0)$ and then $B(s) = B(s_0)/a$, since the amplitude Aa and the rotation $\exp(-i2\pi f t_0)$, of unitary magnitude, do not affect the bandwidth. Therefore, the product $D(s)B(s) = D(s_0)B(s_0)$ depends only on the signal s_0 generating the class.

Other results will be given in Chap. 9.

²Simultaneous finite duration and finite bandwidth may be incompatible (see Sect. 9.5), so that one of the definitions must be relaxed using *conventional* duration and bandwidth (see Sect. 13.11).

5.8.6 Other Forms of 1D Fourier Transform

From Appendix A, it turns out that the Fourier kernel on \mathbb{R} is not unique, and its general form is given by

$$\psi(a, t) = e^{i\alpha at}, \quad a \in \mathbb{R}, t \in \mathbb{R}, \quad (5.79)$$

where $\alpha \neq 0$ is an arbitrary real constant. Considering that the Haar integral is unique, up to a multiplicative positive constant, expressions given by (5.64) should have the general form

$$\begin{aligned} S(a) &= H \int_I dt s(t) e^{i\alpha at}, \quad a \in \widehat{I}, \\ s(t) &= K \int_{\widehat{I}} da S(a) e^{-i\alpha at}, \quad t \in I, \end{aligned} \quad (5.80)$$

where H and K are positive constants related by [23]

$$2\pi KH = |\alpha|. \quad (5.80a)$$

Now, (5.64) represent the “form in f ” (frequency) and are obtained from (5.80) with $\alpha = -2\pi$ and $H = K = 1$. Another common choice is the “form in ω ” (angular frequency), which is obtained with $\alpha = -1$, $H = 1$ and $K = 1/(2\pi)$; it is not perfectly symmetric as (5.64) for the presence of the factor $1/(2\pi)$ in the inverse transform. A symmetric form in ω is possible with $H = K = 1/\sqrt{2\pi}$, which is frequently used in mathematics books (often with $\alpha = 1$ in place of $\alpha = -1$).

5.9 Explicit Forms of Multidimensional Fourier Transforms

As done for the 1D case, now from the “unified” FT we obtain the FT of multidimensional signals, defined on the groups of the class $\mathcal{Q}(\mathbb{R}^m)$. For the FT and inverse FT, we can refer to relations (5.7a), (5.7b) with the appropriate conventions on the m -tuples of arguments. Alternatively, we let

$$\mathbf{f} = (f_1, \dots, f_m) \in \widehat{I}, \quad \mathbf{t} = (t_1, \dots, t_m) \in I,$$

and we have more explicitly

$$\boxed{\begin{aligned} S(\mathbf{f}) &= \int_I d\mathbf{t} s(\mathbf{t}) e^{-i2\pi\mathbf{f}\mathbf{t}}, \quad \mathbf{f} \in \widehat{I}, \\ s(\mathbf{t}) &= \int_{\widehat{I}} d\mathbf{f} S(\mathbf{f}) e^{i2\pi\mathbf{f}\mathbf{t}}, \quad \mathbf{t} \in I. \end{aligned}} \quad (5.81)$$

In these relations, $\mathbf{f}'\mathbf{t}$ is a matrix product, where \mathbf{f} and \mathbf{t} are interpreted as column vectors and

$$\mathbf{f}'\mathbf{t} = [f_1 \dots f_m] \begin{bmatrix} t_1 \\ \vdots \\ t_m \end{bmatrix} = f_1 t_1 + \dots + f_m t_m.$$

To get specific results, the general procedure is the following. Given the signal domain/periodicity $I = I_0/S$, we have to find

1. The frequency domain/periodicity using the rule $I = I_0/P \xrightarrow{\text{dual}} \widehat{I} = P^*/I_0^*$;
2. The Haar integral on I and on \widehat{I} .

If both the domain and the periodicity of the signal are separable, so are the FT domain and periodicity, and the domain evaluation is straightforward according to the rule

$$I_1 \times I_2 = I_{01}/P_1 \times I_{02}/P_2 \xrightarrow{\text{dual}} \widehat{I}_1 \times \widehat{I}_2 = P_1^*/I_{01}^* \times P_2^*/I_{02}^*,$$

which is easily extended to the m D case. But, in general, we have to use a base-signature representation

$$(\mathbf{I}_0, H) \mapsto I_0, \quad (\mathbf{P}, K) \mapsto P, \quad (5.82)$$

and we find the reciprocal according to Theorem 5.2, that is,

$$(\mathbf{I}_0^*, H^*) \mapsto I_0^*, \quad (\mathbf{P}^*, K^*) \mapsto P^*. \quad (5.82b)$$

If I and \widehat{I} are separable, say $I = I_1 \times \dots \times I_m$ and $\widehat{I} = \widehat{I}_1 \times \dots \times \widehat{I}_m$, the Haar integrals can be expressed as combinations of 1D integrals, namely

$$S(f_1, \dots, f_m) = \int_{I_1} dt_1 \dots \int_{I_m} dt_m s(t_1, \dots, t_m) e^{-i2\pi(f_1 t_1 + \dots + f_m t_m)},$$

$$s(t_1, \dots, t_m) = \int_{\widehat{I}_1} df_1 \dots \int_{\widehat{I}_m} df_m S(f_1, \dots, f_m) e^{i2\pi(f_1 t_1 + \dots + f_m t_m)}$$

with $t_k \in I_k$ and $f_k \in \widehat{I}_k$. More specifically, if the signal itself is *separable*

$$s(t_1, \dots, t_m) = s_1(t_1) \dots s_m(t_m), \quad t_k \in I_k, \quad (5.83a)$$

then also the FT becomes *separable*, namely

$$S(f_1, \dots, f_m) = S_1(f_1) \dots S_m(f_m), \quad f_k \in \widehat{I}_k, \quad (5.83b)$$

where the k th factor $S_k(f_k)$ is the FT of $s_k(t_k)$. In the case of nonseparability, for the Haar integral we have to use the general expression given in Chap. 4.

We have seen in Sect. 3.7 that the variety of m D signals is very rich, with $(m+1)^2$ classes. We now give the explicit form of the FT and its inverse for the main classes. Other classes, in particular the FT on gratings, will be seen in Chap. 16.

Dimensionality In Chap. 4, we have assumed for signals that (i) the domain I_0 is a full-dimensional group, and (ii) the periodicity is a lattice (possibly with a reduced dimensionality). Now, we can check that (i) and (ii) hold also for the FT. To this end, it is sufficient to examine the signature. From (i), we have $H = \mathbb{R}^p \times \mathbb{Z}^q$ with $p + q = m$ and $K = \mathbb{O}^r \times \mathbb{Z}^s$ with $r + s = m$. Then, $K^* = \mathbb{R}^r \times \mathbb{Z}^s$, which states that the frequency domain S^* is a full-dimensional group. Analogously, $H^* = \mathbb{O}^p \times \mathbb{Z}^q$ and then the frequency periodicity is a lattice.

5.9.1 Fourier Transform on \mathbb{R}^m

The dual of \mathbb{R}^m is still \mathbb{R}^m , so (5.81) become

$$S(\mathbf{f}) = \int_{\mathbb{R}^m} d\mathbf{t} s(\mathbf{t}) e^{-i2\pi\mathbf{f}\mathbf{t}}, \quad \mathbf{f} \in \mathbb{R}^m, \quad (5.84a)$$

$$s(\mathbf{t}) = \int_{\mathbb{R}^m} d\mathbf{f} S(\mathbf{f}) e^{i2\pi\mathbf{f}\mathbf{t}}, \quad \mathbf{t} \in \mathbb{R}^m, \quad (5.84b)$$

where m -dimensional ordinary integrals appear. In these relations, the signal $s(\mathbf{t})$ is defined on a continuous domain, $\mathbf{t} \in \mathbb{R}^m$, and also the transform $S(\mathbf{f})$ is on a continuous domain, $\mathbf{f} \in \mathbb{R}^m$. The difficulty is in the evaluation of m D integrals, which sometimes is simplified by the structure of the function $s(\mathbf{t})$, as in the following case.

Signals on \mathbb{R}^2 with Circular Symmetry

A signal $s(t_1, t_2)$, $(t_1, t_2) \in \mathbb{R}^2$, has the *circular symmetry* (with respect to the origin) if it assumes the same values on the points of a circle centered at the origin, and therefore, it can be expressed in the form

$$s(t_1, t_2) = g(\sqrt{t_1^2 + t_2^2}) \quad (5.85)$$

for a suitable 1D function $g(a)$, $a \in [0, \infty)$. Just for reasons of symmetry, it can be guessed that circular symmetry is transferred to the FT, namely

$$S(f_1, f_2) = G(\sqrt{f_1^2 + f_2^2}) \quad (5.86)$$

for a suitable function $G(b)$, $b \in [0, \infty)$. The problem is to determine the function $G(b)$, which is not the FT of $g(b)$. The relation is [19]

$$G(b) = 2\pi \int_0^\infty da ag(a) J_0(2\pi ab) \quad (5.87a)$$

Table 5.5 Reciprocals L^* of 2D lattices $L = \mathbb{Z}_i^b(d_1, d_2)$ ($F_1 = 1/id_1, F_2 = 1/id_2$)

L	$\mathbb{Z}_2^1(d_1, d_2)$	$\mathbb{Z}_3^1(d_1, d_2)$	$\mathbb{Z}_3^2(d_1, d_2)$	$\mathbb{Z}_4^1(d_1, d_2)$	$\mathbb{Z}_4^3(d_1, d_2)$
L^*	$\mathbb{Z}_2^1(F_1, F_2)$	$\mathbb{Z}_3^1(F_1, F_2)$	$\mathbb{Z}_3^1(F_1, F_2)$	$\mathbb{Z}_4^1(F_1, F_2)$	$\mathbb{Z}_4^1(F_1, F_2)$
L	$\mathbb{Z}_5^1(d_1, d_2)$	$\mathbb{Z}_5^2(d_1, d_2)$	$\mathbb{Z}_5^3(d_1, d_2)$	$\mathbb{Z}_5^4(d_1, d_2)$	$\mathbb{Z}_6^1(d_1, d_2)$
L^*	$\mathbb{Z}_5^4(F_1, F_2)$	$\mathbb{Z}_5^2(F_1, F_2)$	$\mathbb{Z}_5^3(F_1, F_2)$	$\mathbb{Z}_5^1(F_1, F_2)$	$\mathbb{Z}_6^5(F_1, F_2)$

where $J_0(\cdot)$ is the Bessel function of the first kind and order zero. The relation giving $g(a)$ from $G(b)$ is perfectly symmetrical

$$g(a) = 2\pi \int_0^\infty db bG(b)J_0(2\pi ab). \tag{5.87b}$$

Expressions (5.87a), (5.87b) define the *Hankel transform* (see Chap. 17).

5.9.2 Fourier Transform on a Lattice

If I is a lattice L in \mathbb{R}^m its dual is $\hat{I} = \mathbb{R}^m/L^*$, where L^* is the reciprocal lattice. Then, (5.81) become

$$\begin{aligned} S(\mathbf{f}) &= \sum_{\mathbf{t} \in L} d(L)s(\mathbf{t})e^{-i2\pi\mathbf{f}\mathbf{t}}, \quad \mathbf{f} \in \mathbb{R}^m/L^*, \\ s(\mathbf{t}) &= \int_{\mathbb{R}^m/L^*} d\mathbf{f} S(\mathbf{f})e^{i2\pi\mathbf{f}\mathbf{t}}, \quad \mathbf{t} \in I. \end{aligned} \tag{5.88}$$

In these relations, the signal has a discrete domain, while the FT is a function with continuous frequency and periodicity given by the reciprocal lattice L^* . The evaluation of $S(\mathbf{f})$ is based on an m D series, while the evaluation of $s(\mathbf{t})$ on an m D integral extended to a cell $[\mathbb{R}^m/L^*]$.

If the lattice L is not separable, the reciprocal L^* is evaluated through the computation of the reciprocal basis L^* (see Theorem 5.2). An example of evaluation has been considered in Sect. 5.3 for the quincunx lattice, where also L^* is a quincunx lattice. That result can be generalized to the lattices $\mathbb{Z}_i^b(d_1, d_2)$ as follows

$$\mathbb{Z}_i^b(d_1, d_2) \xrightarrow{*} \mathbb{Z}_i^c(F_1, F_2), \quad F_1/id_1, F_2 = 1/id_2,$$

that is, the reciprocal belongs to the same class with the same index i . The integer c in the reciprocal is given as the solution to the integer equation $1 + cb = ki, k \in \mathbb{N}$ (see Chap. 16). The explicit evaluation is given in Table 5.5 for the first orders.

5.9.3 Fourier Transform on a Finite Group (DFT)

If $I = L/P$ is a finite group, where both L and P are full-dimensional lattices, the domains are

$$I = L/P \xrightarrow{\text{dual}} \widehat{I} = P^*/L^*$$

where also P^* and L^* are full-dimensional. Then, (5.81) become

$$\begin{aligned} S(\mathbf{f}) &= \sum_{\mathbf{t} \in [L/P]} d(L) s(\mathbf{t}) e^{-i2\pi \mathbf{f} \cdot \mathbf{t}}, \quad \mathbf{f} \in P^*/L^*, \\ s(\mathbf{f}) &= \sum_{\mathbf{f} \in [P^*/L^*]} d(P^*) S(\mathbf{f}) e^{i2\pi \mathbf{f} \cdot \mathbf{t}}, \quad \mathbf{t} \in L/P. \end{aligned} \quad (5.89)$$

The first summation is extended over a cell $C = [L/P]$ and the second over the reciprocal cell $C^* = [P^*/L^*]$. Both the signal and its FT are periodic and are fully specified in the cells C and C^* , respectively. We note that these cells are finite and have the same cardinality. In fact, (see Sect. 3.5)

$$|C| = d(S)/d(L), \quad |C^*| = d(L^*)/d(P^*) = d(P)/d(L). \quad (5.90)$$

The relations (5.89) represent the multidimensional DFT and IDFT and can be written in a more convenient form for an efficient numerical evaluation (see Chap. 13).

Proposition 5.1 *The Fourier kernel on a finite group L/P of \mathbb{R}^m assumes the form*

$$e^{i2\pi \mathbf{f} \cdot \mathbf{t}} = W_N^{\mathbf{f} \cdot \mathbf{t}}, \quad \mathbf{f} \cdot \mathbf{t} \in \mathbb{Z}(1/N)$$

where $N = (L : P)$ is the cardinality of $[L/P]$ and $W_N = \exp(i2\pi/N)$ is the N th root of 1.

Proof Let \mathbf{L} and \mathbf{P} be the bases of L and P , respectively, then the m D arguments \mathbf{t} and \mathbf{f} can be written as

$$\mathbf{t} = \mathbf{L}\mathbf{h}, \quad \mathbf{h} \in \mathbb{Z}^n, \quad \mathbf{f} = \mathbf{P}^*\mathbf{k}, \quad \mathbf{k} \in \mathbb{Z}^m$$

where $\mathbf{P}^* = (\mathbf{P}^{-1})'$. Since P is a sublattice of L , the basis \mathbf{P} can be written in the form

$$\mathbf{P} = \mathbf{L}\mathbf{A}$$

where \mathbf{A} is an integer matrix with $|\det \mathbf{A}| = (L : S) = N$ (see Chap. 16). Then, $\mathbf{A}^{-1} = (1/N)\mathbf{B}$ with \mathbf{B} an integer matrix. Thus,

$$\mathbf{f} \cdot \mathbf{t} = \mathbf{k}'(\mathbf{P}^*)'\mathbf{L}\mathbf{h} = \mathbf{k}'\mathbf{S}^{-1}\mathbf{L}\mathbf{h} = \mathbf{k}'\mathbf{A}^{-1}\mathbf{L}^{-1}\mathbf{L}\mathbf{h} = (1/N)\mathbf{k}'\mathbf{B}\mathbf{h}$$

where \mathbf{k} , \mathbf{B} and \mathbf{h} consist of integers, and therefore $\mathbf{k}'\mathbf{B}\mathbf{h} \in \mathbb{Z}$. □

Table 5.6 Basis signature representations with a coordinate change

Group	Base	Modulus
I	$(\mathbf{I}_0, H) \mapsto I_0$	$(\mathbf{P}, K) \mapsto P$
\widehat{I}	$(\mathbf{P}^*, K^*) \mapsto P^*$	$(\mathbf{I}_0^*, H^*) \mapsto I_0^*$
$I_{\mathbf{a}}$	$(\mathbf{a}^{-1}\mathbf{I}_0, H) \mapsto I_{0\mathbf{a}}$	$(\mathbf{a}^{-1}\mathbf{P}, K) \mapsto P_{\mathbf{a}}$
$\widehat{I}_{\mathbf{a}}$	$(\mathbf{a}'\mathbf{P}^*, K^*) \mapsto P_{\mathbf{a}}^*$	$(\mathbf{a}'\mathbf{I}_0^*, H^*) \mapsto I_{0\mathbf{a}}^*$

5.9.4 Fourier Transform After a Coordinate Change

In Sect. 4.3, we have considered the coordinate change on a signal $s(\mathbf{u})$, $\mathbf{u} \in I = I_0/P$, given by

$$s_{\mathbf{a}}(\mathbf{t}) = s(\mathbf{a}\mathbf{t}), \quad \mathbf{t} \in I_{\mathbf{a}} \tag{5.91}$$

where \mathbf{a} is a non-singular $m \times m$ real matrix. The coordinate change modifies the original domain/periodicity $I = I_0/P$ into $I_{\mathbf{a}} = I_{0\mathbf{a}}/P_{\mathbf{a}}$, where

$$I_{0\mathbf{a}} = \{\mathbf{t} \mid \mathbf{a}\mathbf{t} \in I_0\}, \quad P_{\mathbf{a}} = \{\mathbf{t} \mid \mathbf{a}\mathbf{t} \in P\}. \tag{5.92}$$

Correspondingly, $\widehat{I} = P^*/I_0^*$ is modified into $\widehat{I}_{\mathbf{a}} = P_{\mathbf{a}}^*/I_{0\mathbf{a}}^*$. Now, considering the rule for reciprocals, we can find the explicit representations for the groups $I_{0\mathbf{a}}^*$ and $P_{\mathbf{a}}^*$, as shown in Table 5.6.

For the FT, the coordinate change gives

$$\boxed{S_{\mathbf{a}}(\mathbf{f}) = \frac{1}{d(\mathbf{a})} S(\mathbf{a}^*\mathbf{f}), \quad \mathbf{f} \in \widehat{I}_{\mathbf{a}}.} \tag{5.93}$$

which states that a coordinate change on a signal with matrix \mathbf{a} becomes a coordinate change with matrix $\mathbf{a}^* = (\mathbf{a}^{-1})'$ on the FT.

To prove (5.93), we use the general formula (5.81) and we find

$$S_{\mathbf{a}}(\mathbf{f}) = \int_{I_{\mathbf{a}}} dt \psi(\mathbf{f}, \mathbf{t}) s_{\mathbf{a}}(t), \tag{5.94}$$

where $\psi(\mathbf{f}, \mathbf{t}) = \exp(-i2\pi\mathbf{f}'\mathbf{t})$. Then, we apply the integration rule of Theorem 4.2, which gives

$$S_{\mathbf{a}}(f) = \frac{1}{d(\mathbf{a})} \int_{I_{\mathbf{a}}} dt \psi(\mathbf{f}, \mathbf{t}) s(\mathbf{a}\mathbf{t}) = \frac{1}{d(\mathbf{a})} \int_I d\mathbf{u} \psi(\mathbf{f}, \mathbf{a}^{-1}\mathbf{u}) s(\mathbf{u}).$$

But, in the exponential $\mathbf{f}'[\mathbf{a}^{-1}\mathbf{u}] = [(\mathbf{a}^{-1})'\mathbf{f}]'\mathbf{u} = (\mathbf{a}^*\mathbf{f})'\mathbf{u}$. Hence, $\psi(\mathbf{f}, \mathbf{a}^{-1}\mathbf{u}) = \psi(\mathbf{a}^*\mathbf{f}, \mathbf{u})$, and (5.93) follows.

5.10 Examples of Multidimensional Fourier Transforms

In this section, the leading examples are on continuous-argument signals, that is with $I = \mathbb{R}^m$ and $\widehat{I} = \mathbb{R}^m$. Examples on other groups are obtained from the leading examples by application of the FT rules or carried out independently.

5.10.1 Fourier Transform of Multidimensional Singular Signals

In Sect. 5.2 we obtained the FT of some signals related to impulses and characters (singular signals). Here, we give their expressions in the m D case, as was done for the 1D case (see Table 5.1).

On the groups of \mathbb{R}^m (5.12) and (5.13) respectively become

$$\delta_I(\mathbf{t} - \mathbf{t}_0) \xrightarrow{\mathcal{F}} e^{-i2\pi\mathbf{f}'\mathbf{t}_0}, \quad e^{i2\pi\mathbf{f}'_0\mathbf{t}} \xrightarrow{\mathcal{F}} \delta_{\widehat{I}}(\mathbf{f} - \mathbf{f}_0). \quad (5.95)$$

Now, using the Euler formulas (2.20), in the second of (5.95) we obtain the FT of multidimensional sinusoidal signals, namely

$$\begin{aligned} \cos 2\pi\mathbf{f}'_0\mathbf{t} &\xrightarrow{\mathcal{F}} \frac{1}{2}[\delta_{\widehat{I}}(\mathbf{f} - \mathbf{f}_0) + \delta_{\widehat{I}}(\mathbf{f} + \mathbf{f}_0)], \\ \sin 2\pi\mathbf{f}'_0\mathbf{t} &\xrightarrow{\mathcal{F}} \frac{1}{2i}[\delta_{\widehat{I}}(\mathbf{f} - \mathbf{f}_0) - \delta_{\widehat{I}}(\mathbf{f} + \mathbf{f}_0)]. \end{aligned} \quad (5.96)$$

These results hold for all the groups of \mathbb{R}^m . By specification of the pair (I, \widehat{I}) , we obtain more explicit formulas, provided that the m D shifts \mathbf{t}_0 and \mathbf{f}_0 are compatible with the corresponding domains. For instance, for $I = \mathbb{R}^m/P$, considering that $\widehat{I} = P^*$, we see that \mathbf{f}_0 must belong to the reciprocal lattice P^* .

If I is a lattice L , that is, for an m D discrete sinusoid signal, the frequency domain is $\widehat{I} = \mathbb{R}^m/L^*$ and, therefore, each of the impulses in (5.96) becomes a periodic repetition of impulses on \mathbb{R}^m (see (4.84)), namely

$$\delta_{\mathbb{R}^m/L^*}(\mathbf{f} \pm \mathbf{f}_0) = \sum_{\mathbf{p} \in L^*} \delta_{\mathbb{R}^m}(\mathbf{f} \pm \mathbf{f}_0 - \mathbf{p}).$$

Note that the m D sinusoid in (5.96) is not separable. For instance, in the 2D case it is $\cos[2\pi(f_{01}t_1 + f_{02}t_2)]$. But, we can also consider the separable form $s(t_1, t_2) = \cos(2\pi f_{01}t_1) \cos(2\pi f_{02}t_2)$, $(t_1, t_2) \in I_1 \times I_2$, where I_1 and I_2 are 1D groups. In this case, the FT, obtained from rule (5.83a), (5.83b), is given by

$$S(f_1, f_2) = \frac{1}{4}[\delta_{\widehat{I}_1}(f_1 - f_{01}) + \delta_{\widehat{I}_1}(f_1 + f_{01})][\delta_{\widehat{I}_2}(f_2 - f_{02}) + \delta_{\widehat{I}_2}(f_2 + f_{02})],$$

and we find four “lines”, in place of two “lines”, as shown in Fig. 5.16 for $I = \mathbb{R}^2$ and $\widehat{I} = \mathbb{R}^2$.

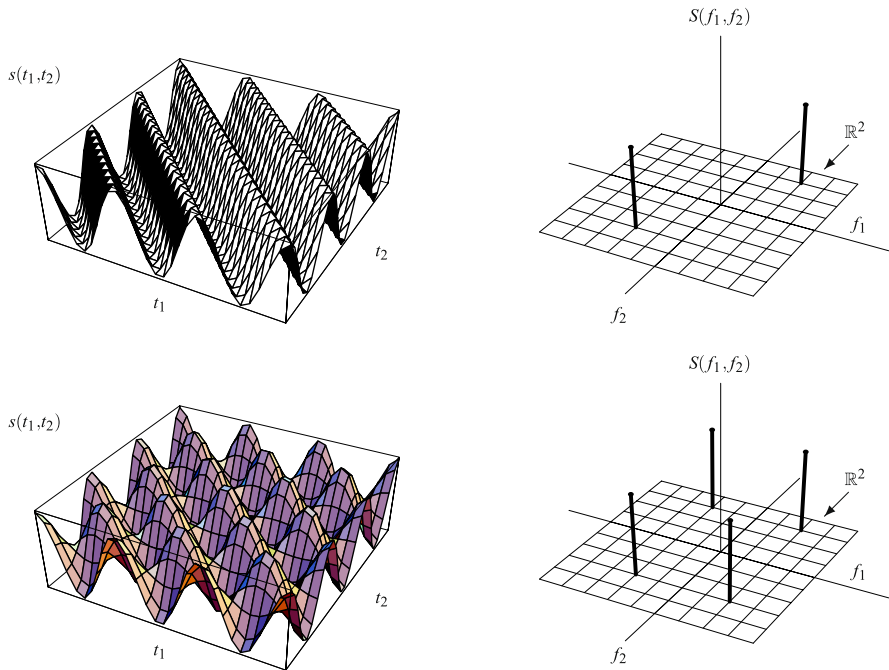


Fig. 5.16 Fourier transform of a 2D standard sinusoid and of a 2D “separable” sinusoid

5.10.2 Inverse Fourier Transform of Indicator Functions

We consider Fourier transforms of the kind

$$S(\mathbf{f}) = \eta_{\mathcal{B}}(\mathbf{f}) = \begin{cases} 1, & \text{if } \mathbf{f} \in \mathcal{B}; \\ 0, & \text{if } \mathbf{f} \notin \mathcal{B}, \end{cases}$$

which will be used in the definition of ideal filters (see Sect. 6.15), where \mathcal{B} is a subset of \mathbb{R}^m representing the filter *pass-band*. The inverse FT is simply given by

$$s(\mathbf{t}) = \int_{\mathcal{B}} e^{i2\pi\mathbf{f}\mathbf{t}} d\mathbf{f}, \quad \mathbf{t} \in \mathbb{R}^m, \tag{5.97}$$

and represents the *impulse response* of the filter.

We now develop some 2D cases. Suppose that \mathcal{B} is the rectangle $(-B_1, B_1) \times (-B_2, B_2)$, then

$$S_{\text{rect}}(f_1, f_2) = \text{rect}(f_1/2B_1)\text{rect}(f_2/2B_2),$$

which is separable. Then, we immediately find

$$s_{\text{rect}}(t_1, t_2) = 2B_1 \text{sinc}(2B_1t_1)2B_2 \text{sinc}(2B_2t_2). \tag{5.98a}$$

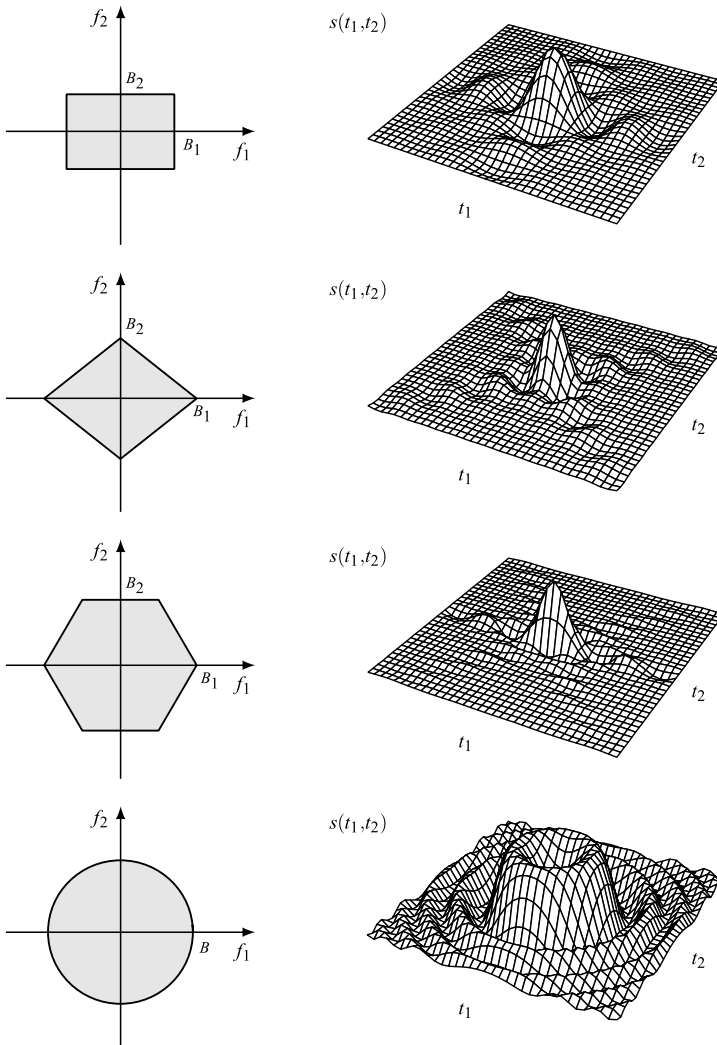


Fig. 5.17 Fourier transform given by the indicator function on a band \mathcal{B} (in gray) and corresponding inverse Fourier transform $s(t_1, t_2)$

As a second example, suppose that \mathcal{B} has a rhomboidal shape (Fig. 5.17) whose indicator function can be written in the form

$$S_{\text{rh}}(f_1, f_2) = \begin{cases} 1, & \text{if } 0 < |f_1|/B_1 + |f_2|/B_2 < 1; \\ 0, & \text{elsewhere.} \end{cases} \quad (5.98b)$$

The evaluation of the signal according to (5.97) can be done by partitioning the rhombus into four triangles and then combining the results. A more direct approach is based on a coordinate change, which maps a rectangle into a rhombus. The coor-

dinate change is

$$f_1 = \frac{1}{2} \left(u_1 - \frac{B_1}{B_2} u_2 \right), \quad f_2 = \frac{1}{2} \left(\frac{B_2}{B_1} u_1 - u_2 \right),$$

$$\mathbf{f} = \frac{1}{2} \begin{bmatrix} 1 & -B_1/B_2 \\ B_2/B_1 & 1 \end{bmatrix} \mathbf{u}$$

and, in fact, while (u_1, u_2) describes the rectangle $(-B_1, B_1) \times (-B_2, B_2)$, (f_1, f_2) describes the rhombus with vertexes $(B_1, 0)$, $(0, B_2)$, $(-B_1, 0)$, $(0, -B_2)$. Then, we have

$$S_{\text{rh}}(f_1, f_2) = S_{\text{rect}}(\mathbf{b}^{-1}(f_1, f_2)). \quad (5.99)$$

Note that in the argument of $S_{\text{rect}}(\cdot)$ we have to write the inverse coordinate change, since (f_1, f_2) describes the rhombus, and $\mathbf{b}^{-1}(f_1, f_2)$ describes the rectangle. Now, using rule (5.93) on a coordinate change with $\mathbf{a}^* = \mathbf{b}^{-1}$ in (5.99), we find

$$s_{\text{rh}}(t_1, t_2) = d(\mathbf{a}) s_{\text{rect}}(\mathbf{a}'(t_1, t_2)).$$

The explicit result is

$$s_{\text{rh}}(t_1, t_2) = 2B_1 B_2 \text{sinc}(B_1 t_1 - B_2 t_2) \text{sinc}(B_1 t_1 + B_2 t_2). \quad (5.100)$$

For a hexagonal form, a coordinate change is not useful, and we have to decompose \mathcal{B} into one rectangle and four triangles. The procedure is long and tedious and gives (see Problem 5.43)

$$s_{\text{hexagon}}(t_1, t_2) = 2B_3 \sin(2B_3 T_1) 2B_2 \text{sinc}(2B_2 t_2)$$

$$+ \frac{B}{2\pi t_2} \left\{ \text{sinc}(B_4 t_1 - B_2 t_2) \sin[\pi(B_4 t_1 + B_2 t_2)] \right.$$

$$\left. - \text{sinc}(B_4 t_1 + B_2 t_2) \sin[\pi(B_4 t_1 - B_2 t_2)] \right\}, \quad (5.101)$$

where B_1 and B_2 are defined in the figure, B_3 is half of the horizontal edges, $B = B_1 - B_3$ and $B_4 = B_1 + B_3$.

When \mathcal{B} is a circle of radius B , we have a circular symmetry and we can use (5.85) and (5.86). The result is (see Problem 5.44)

$$s_{\text{circle}}(t_1, t_2) = B(t_1^2 + t_2^2)^{-1/2} J_1(2\pi B \sqrt{t_1^2 + t_2^2}) \quad (5.102)$$

where $J_1(\cdot)$ is the Bessel function of the first kind of order 1.

The four impulse responses are shown in Fig. 5.17. Note that in the four cases we obtained *real* signals. The reason is that the sets \mathcal{B} considered above are *even*, that is, they have the property $-\mathcal{B} = \mathcal{B}$. Then, $S(\mathbf{f})$ is real and even, and so is the corresponding signal $s(\mathbf{t})$.

Fourier Transforms of a Pyramidal Signal

In Example 4.3, we have seen the *lazy* pyramid given by the separable signal $s_{\text{laz}}(t_1, t_2) = \text{triang}(t_1) \text{triang}(t_2)$. Recalling that $\text{triang}(t)$ has FT $\text{sinc}^2(f)$, we easily obtain the Fourier pair

$$s_{\text{laz}}(t_1, t_2) \xrightarrow{\mathcal{F}} \text{sinc}^2(f_1) \text{sinc}^2(f_2), \quad f_1, f_2 \in \mathbb{R}.$$

The true pyramid $\text{pyr}(t_1, t_2)$ defined by (4.97) is not separable, and therefore we have to calculate its FT by the general formula (5.84a), (5.84b). The signal is the sum of two symmetric terms. The first one is $\text{pyr}(t_1, t_2)_1 = \text{triang}(t_1) \text{rect}(t_2/2t_1)$ and has FT

$$\begin{aligned} \text{PYR}(f_1, f_2)_1 &= \int_{-\infty}^{+\infty} \int_{-\infty}^{+\infty} \text{pyr}(t_1, t_2)_1 e^{-i2\pi(f_1 t_1 + f_2 t_2)} dt_1 dt_2 \\ &= \int_{-\infty}^{+\infty} \text{triang}(t_1) \left[\int_{-\infty}^{+\infty} \text{rect}(t_2/2t_1) e^{-i2\pi f_2 t_2} dt_2 \right] e^{-i2\pi f_1 t_1} dt_1 \\ &= \int_{-1}^1 \underbrace{(1 - |t_1|) 2|t_1| \text{sinc}(2f_2 t_1)}_{\text{even in } t_1} e^{-i2\pi f_2 t_2} dt_1 \\ &= \frac{2}{\pi f_2} \int_0^1 (1 - t_1) \sin(2\pi f_2 t_1) \cos(2\pi f_1 t_1) dt_1, \end{aligned}$$

where we have used the well known rect – sinc pair and the definition of the sinc function. The evaluation of the integral gives

$$\text{PYR}(f_1, f_2)_1 = \frac{1}{4\pi^3 f_2} \left[\frac{\sin(2\pi(f_1 - f_2))}{(f_1 - f_2)^2} - \frac{\sin(2\pi(f_1 + f_2))}{(f_1 + f_2)^2} \right] - \frac{1}{\pi^2(f_1^2 - f_2^2)}.$$

Considering that the second term is symmetric, that is, $\text{PYR}(f_1, f_2)_2 = \text{PYR}(f_2, f_1)_1$, after a few simplifications we obtain

$$\text{PYR}(f_1, f_2) = \frac{\text{sinc}(2f_1 - 2f_2) - \text{sinc}(2f_1 + 2f_2)}{2\pi^2 f_1 f_2}. \quad (5.103)$$

The result is illustrated in Fig. 5.18. As a check, we can verify the rule $\text{area}(\text{pyr}) = \text{PYR}(0) = 4/3$, that is, the volume of a pyramid with unitary basis (see Problem 5.45).

5.10.3 Generation of Fourier Transforms on Several Domains

We now show that, starting from a Fourier pair on $(\mathbb{R}^2, \mathbb{R}^2)$, we can obtain several 2D Fourier pairs on different domains (I, \widehat{I}) , by application of Fourier transform rules.

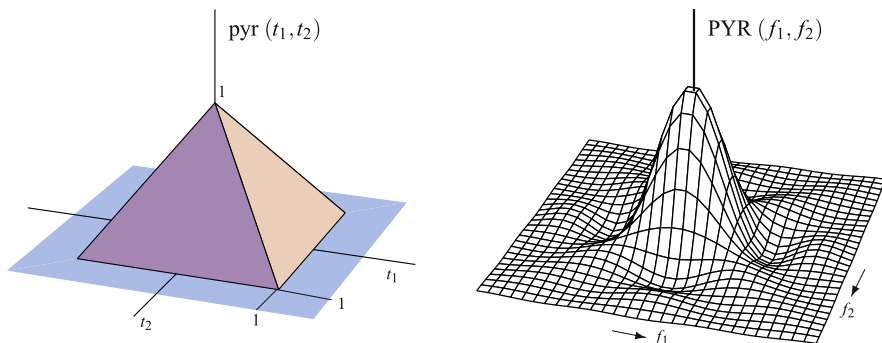


Fig. 5.18 The pyramidal signal and its Fourier transform

We consider the Fourier pair $s_0(t_1, t_2), S_0(f_1, f_2)$, where the FT is a “true” pyramid, that is, $S_0(f_1, f_2) = \text{pyr}(f_1, f_2)$, where the function pyr is defined by (4.97). The corresponding signal is given by $s_0(t_1, t_2) = \text{PYR}(t_1, t_2)$, where the function PYR is defined by (5.103). Then, we have the normalized Fourier pair

$$s_0(t_1, t_2) = \text{PYR}(t_1, t_2) \xrightarrow{\mathcal{F}} S_0(f_1, f_2) = \text{pyr}(f_1, f_2),$$

that is, the reverse of the pair shown in Fig. 5.18 (this choice is made to facilitate the drawing of the FTs) but, in this case, we introduce a scaling

$$s_0(t_1, t_2) \triangleq B_1 B_2 \text{PYR}(B_1 t_1, B_2 t_2) \xrightarrow{\mathcal{F}} S_0(f_1, f_2) \triangleq \text{pyr}(f_1/B_1, f_2/B_2), \tag{5.104}$$

where now $S_0(f_1, f_2)$ has a pyramidal shape with basis $(-B_1, B_1) \times (-B_2, B_2)$ and amplitude 1.

In the generation of new pairs, we first apply the rule on the FT *after a down-sampling* of Sect. 5.5, with the down-sampling $\mathbb{R}^2 \rightarrow L$, where L is a lattice. Then, we have the new Fourier pair (see (5.47))

$$s_1(t_1, t_2) = s_0(t_1, t_2), \quad (t_1, t_2) \in L, \\ S_1(f_1, f_2) = \sum_{(p_1, p_2) \in L^*} S_0(f_1 - p_1, f_2 - p_2), \quad (f_1, f_2) \in \mathbb{R}^2/L^*, \tag{5.105}$$

where the repetition centers are given by the reciprocal lattice L^* . In Fig. 5.19, $L = \mathbb{Z}_2^1(d_1, d_2)$ and $L^* = \mathbb{Z}_2^1(F_1, F_2)$ with $F_1 = 1/2d_1, F_2 = 1/2d_2$, and we have chosen $F_1 = 5B_1$ and $F_2 = 5B_2$, so that the terms of the repetition do not overlap.

As a second application of the same rule, we use the sampling $\mathbb{R}^2 \rightarrow \mathbb{R} \times \mathbb{Z}(d_2)$, that is, on a grating. Then, we have a 1D sampling along the second coordinate t_2 , and we find the new Fourier pair, shown in Fig. 5.19

$$s_2(t_1, t_2) = s_0(t_1, t_2), \quad (t_1, t_2) \in \mathbb{R} \times \mathbb{Z}(d_2), \\ S_2(f_1, f_2) = \sum_{p_2 \in \mathbb{Z}(F_2)} S_0(f_1, f_2 - p_2). \tag{5.106}$$

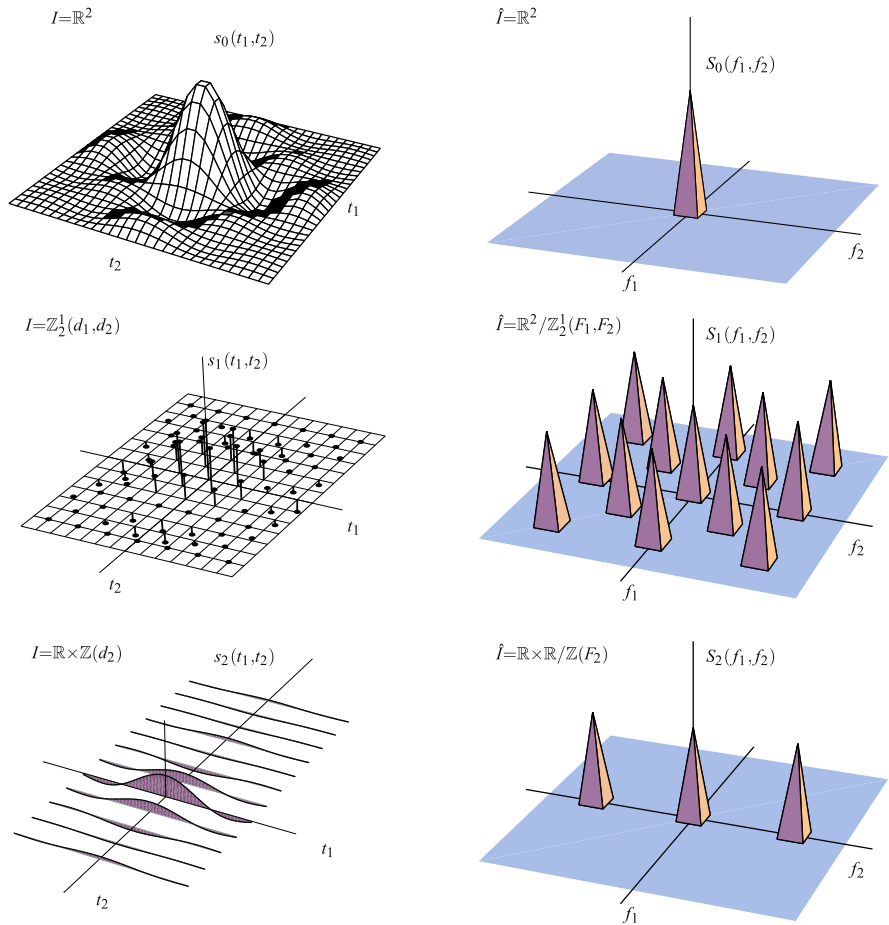


Fig. 5.19 Application of the rule of the Fourier transform after a down-sampling

In fact, the repetition centers of (5.47) are given by the cell $C^* = [U_0^*/I_0^*]$ with $I_0 = \mathbb{R}^2$, $U_0 = \mathbb{R} \times \mathbb{Z}(d_2)$. Hence $C^* = [\mathbb{O} \times \mathbb{Z}(F_2)/\mathbb{O} \times \mathbb{O}] = [\mathbb{O} \times \mathbb{Z}(F_2)]$, which states that the periodic repetition is limited to the second coordinate f_2 .

To obtain further Fourier pairs, we can apply the *Symmetry Rule*, stated by the graph (5.37), which can be used for each of the previous pairs. For instance, in (5.105) we have $I = L = \mathbb{Z}_2^1(d_1, d_2)$ and $\hat{I} = \mathbb{R}^2/\mathbb{Z}_3^2(F_1, F_2)$. So, if we interpret the FT $S_1(f_1, f_2)$ as a signal, say

$$s_4(t_1, t_2) = S_1(t_1, t_2) = \sum_{(p_1, p_2) \in \mathbb{Z}_2^1(F_1, F_2)} S_0(t_1 - p_1, t_2 - p_2),$$

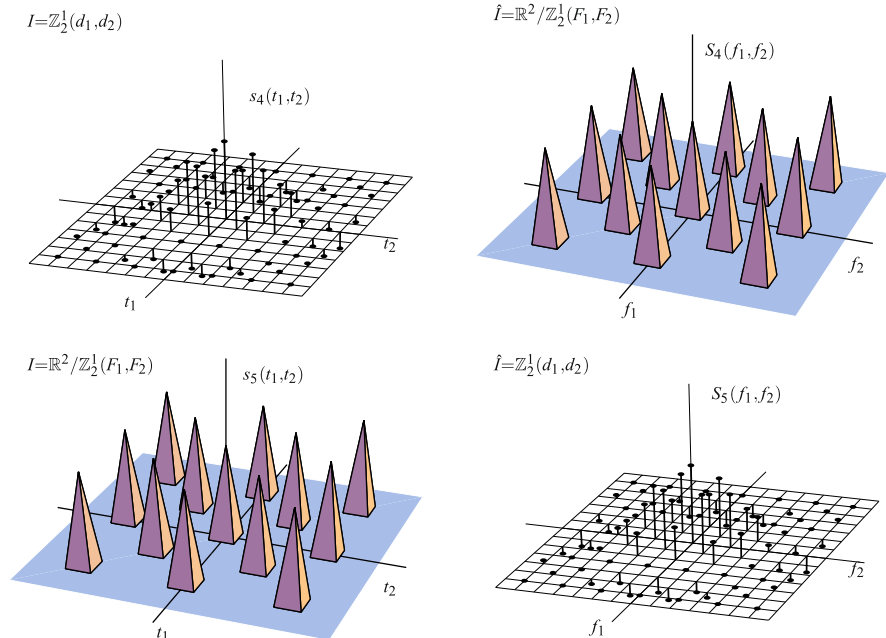


Fig. 5.20 Application of the Symmetry Rule

we obtain that the FT of $s_4(t_1, t_2)$ is given by

$$S_4(f_1, f_2) = s_1(-f_1, -f_2) = s_0(-f_1, -f_2), \quad (f_1, f_2) \in L,$$

as illustrated in Fig. 5.20.

Other pairs can be obtained by a *coordinate change* and using the rule given by (5.93). For instance, if we use the coordinate change

$$\mathbf{a} = \begin{bmatrix} 1 & -1 \\ 1 & 1 \end{bmatrix}, \quad \mathbf{a}^* = \frac{1}{2} \begin{bmatrix} 1 & 1 \\ -1 & 1 \end{bmatrix}$$

in (5.104), we obtain the Fourier pair

$$s_5(t_1, t_2) = s_0(t_1 - t_2, t_1 + t_2),$$

$$S_5(f_1, f_2) = \frac{1}{2} S_0\left(\frac{1}{2}(f_1 + f_2), \frac{1}{2}(-f_1 + f_2)\right), \quad (f_1, f_2) \in \mathbb{R}^2.$$

In this case, the application is particularly simple since a coordinate change transforms \mathbb{R}^2 into \mathbb{R}^2 , whereas in general it provides a modification of both signal and frequency domain according to the rules of Table 5.6.

↓ 5.11 Fourier Transform on Multiplicative Groups

Multiplicative groups were introduced in Sect. 3.8, and in Sect. 4.4 the corresponding Haar integrals were obtained. Now, we develop the FT on the group \mathbb{R}_p , i.e., the multiplicative group of positive real numbers. The FT on other multiplicative groups, as \mathbb{C}^* , can be obtained by composition.

5.11.1 Fourier Kernel and Dual Groups

As seen for the groups of \mathbb{R} in Sect. 5.8, the kernel of the FT is obtained from *characters*. Considering that the group operation is “ \cdot ”, the first of (5.4) becomes

$$\psi_f(t_1 \cdot t_2) = \psi_f(t_1)\psi_f(t_2), \quad t_1, t_2 \in \mathbb{R}_p, \quad (5.107)$$

and imposing that $|\psi_f(t)| = 1$, we find that the solutions can be written in the form

$$\psi_f(t) = e^{i2\pi f \log t}, \quad t \in \mathbb{R}_p, \quad (5.108)$$

where f is an arbitrary real number, $f \in \mathbb{R}$. This leads to the conclusion that the Fourier kernel on \mathbb{R}_p has the structure (5.108) and, moreover, that the dual of \mathbb{R}_p is \mathbb{R} . But, considering that \log is an isomorphism map, we can write $\log f$ instead of f , so that the kernel assumes the form

$$\boxed{\psi(f, t) = e^{i2\pi \log f \log t}}, \quad (5.109)$$

where now $f \in \mathbb{R}_p$. Hence, the dual of \mathbb{R}_p may be \mathbb{R} as well as \mathbb{R}_p . This is in agreement with the statement that *a dual group is determined up to an isomorphism* (see Appendix A).

For symmetry reasons, we choose (5.109) as the Fourier kernel and \mathbb{R}_p as the dual of \mathbb{R}_p .

To obtain the dual of the class quotient groups $\mathcal{Q}(\mathbb{R}_p)$, we first evaluate the reciprocals and then apply Theorem 5.1. On \mathbb{R}_p , the general definition (5.18) becomes

$$J^* = \{f \mid \log f \log t \in \mathbb{Z}, t \in J\}, \quad (5.110)$$

and we can write at once

$$\mathbb{R}_p^* = \mathbb{O}_p, \quad \mathbb{O}_p^* = \mathbb{R}_p, \quad \mathbb{Z}_p(\Delta)^* = \mathbb{Z}_p(\Phi), \quad (5.111)$$

where Δ and Φ are spacings with $\log \Delta \log \Phi = 1$. Then, by Theorem 5.1,

$$\widehat{\mathbb{R}_p} = \mathbb{R}_p, \quad \widehat{\mathbb{Z}_p(\Delta)} = \mathbb{R}_p/\mathbb{Z}_p(\Phi), \quad \text{etc.}$$

5.11.2 Fourier Transform on the Groups of $\mathbb{Q}(\mathbb{R}_p)$

Having obtained the expressions of the Haar integral, Fourier kernel and duals, we are ready to write the FT on the groups of \mathbb{R}_p . In particular, for $I = \mathbb{R}_p$ and $\widehat{I} = \mathbb{R}_p$ the general formula (5.1) reads

$$\begin{aligned} S(f) &= \int_{\mathbb{R}_p} dt e^{-i2\pi \log f \log t} s(t) \\ &= \int_0^\infty e^{-i2\pi \log f \log t} s(t) \frac{dt}{t}, \quad f \in \mathbb{R}_p. \end{aligned} \quad (5.112)$$

Analogously, the inverse FT is given by

$$s(t) = \int_0^\infty e^{i2\pi \log f \log t} S(f) \frac{df}{f}, \quad t \in \mathbb{R}_p. \quad (5.113)$$

With $I = \mathbb{Z}_p(\Delta)$ and $\widehat{I} = \mathbb{R}_p/\mathbb{Z}(\Phi_p)$, we obtain

$$\begin{aligned} S(f) &= \log \Delta \sum_{n=-\infty}^{+\infty} s(\Delta^n) e^{-i2\pi \log f \log \Delta^n}, \quad f \in \mathbb{R}/\mathbb{Z}(\Phi_p), \\ s(\Delta^n) &= \int_1^{\Phi_p} S(f) e^{i2\pi \log f \log \Delta^n} \frac{df}{f}, \quad \Delta^n \in \mathbb{Z}_p(\Delta), \end{aligned}$$

where Δ and Φ_p are related by $\log \Delta \log \Phi_p = 1$.

UT↓ 5.12 The Fractional Fourier Transform

The *fractional Fourier transform* is an emerging topic of Signal Theory and is herein introduced with a unified approach (of course!). Apart from possible applications, its development provides a further insight on the ordinary (non-fractional) FT.

In Sect. 5.4, we have seen that the repeated application of the Fourier operator \mathcal{F} gives

$$s(t) \underset{I}{\xrightarrow{\mathcal{F}}} S(f) \underset{\widehat{I}}{\xrightarrow{\mathcal{F}}} s(-t) \underset{I}{\xrightarrow{\mathcal{F}}} S(-f) \underset{\widehat{I}}{\xrightarrow{\mathcal{F}}} s(t), \quad (5.114)$$

which states in particular that \mathcal{F}^4 is the *identity* operator \mathcal{J} on I

$$\mathcal{F}^4 = \mathcal{J}.$$

Then, it is easy to understand the meaning of the integer powers \mathcal{F}^n of \mathcal{F} , including negative powers (recalling that \mathcal{F}^{-1} gives the inverse FT). For instance, we have $\mathcal{F}^{13} = \mathcal{F}^{12}\mathcal{F} = \mathcal{J}^3\mathcal{F} = \mathcal{F}$ and $\mathcal{F}^{-13} = \mathcal{F}^{-12}\mathcal{F}^{-1} = \mathcal{J}^{-3}\mathcal{F}^{-1} = \mathcal{F}^{-1}$.

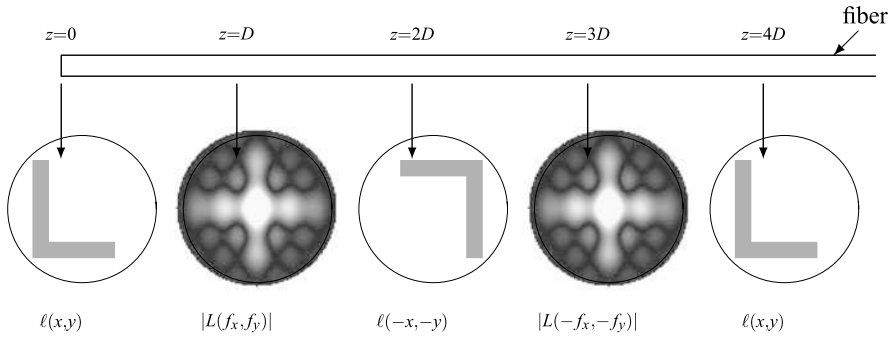


Fig. 5.21 Optical interpretation of 2D fractional Fourier transform. Specific example: fiber diameter 2 mm, distance $D = 50$ mm

The idea of the *fractional* Fourier transform lies in a generalization to an arbitrary *real power* a , \mathcal{F}^a , of the Fourier operator. Such a generalization has received considerable interest in the last decades for its promising applications in simultaneous time–frequency analysis [2, 13, 18] and in the field of Fourier optics [12, 15, 17].

Before developing the theory, we outline a nice physical interpretation of the fractional FT, based on the graph (5.114). In Fourier optics, it is well known that it is possible to implement an optical system, for instance, an optical fiber with a parabolic refraction index [15, 17], with the following behavior. By applying an image $\ell(x, y)$ at the reference coordinate $z = 0$, at an appropriate distance $z = 2D$ we observe the reversed image, that is, $\ell(-x, -y)$, and at $z = 4D$ the original image $\ell(x, y)$. Moreover, at the distance $z = D$ we observe the amplitude $|L(f_x, f_y)|$ of the FT, as shown in Fig. 5.21. Now, in such a system, at a distance $z = aD$ we get the amplitude of the fractional Fourier transform with the “fraction” a .

5.12.1 Technique for Defining a Fractional Operator

The technique³ to define a fractional operator \mathcal{F}^a relies on the eigenfunctions of the original operator \mathcal{F} . Specifically [5],

1. Finding a class of orthonormal eigenfunctions of the ordinary FT, say $\{\varphi_n(t), n \in \mathcal{N}\}$, and the corresponding eigenvalues $\{\mu_n, n \in \mathcal{N}\}$, where \mathcal{N} is an appropriated index set.
2. Writing the expansion of the kernel of \mathcal{F} by means of class 1, namely

$$\psi(f, t) = \sum_{n \in \mathcal{N}} \mu_n \varphi_n(f) \varphi_n^*(t). \quad (5.115)$$

³The technique can be used to define other fractional operators. In [7], it was used to define the fractional DCT.

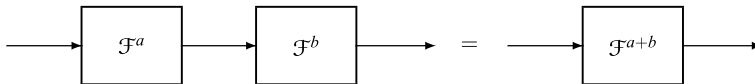


Fig. 5.22 Separability of fractional Fourier transform operator

3. The kernel of the fractional operator \mathcal{F}^a is obtained by replacing the eigenvalues μ_n with their a th power μ_n^a , that is,

$$\psi_a(f, t) = \sum_{n \in \mathbb{N}} \mu_n^a \varphi_n(f) \varphi_n^*(t), \quad f, t \in I, \quad f, t \in I. \tag{5.116}$$

Once the kernel is obtained, the *fractional Fourier transform with the fraction a* of a signal $s(t), t \in I$, is given by

$$S_a(f) = \int_I dt \psi_a(f, t) s(t), \quad f \in I. \tag{5.117}$$

Considering that $\mathcal{F}^{-a} \mathcal{F}^a = \mathcal{F}$, the *inverse* fractional FT with the fraction a is simply obtained by the fraction $-a$. Note that a is an arbitrary real number (notwithstanding the term “fractional”).

But, there are several remarks and conditions to outline. First, the existence of eigenfunctions requires that the dual group \hat{I} is the same as the original group I , that is, the group I must be *self-dual*: $\hat{I} = I$. An example of self-dual group is \mathbb{R} . Another self-dual group is $I = \mathbb{Z}(T)/\mathbb{Z}(T_p)$ with $T = 1/\sqrt{N}$ and $T_p = NT = \sqrt{N}$. Note that 1D lattices are never self-dual, since $\hat{\mathbb{Z}}(T) = \mathbb{R}/\mathbb{Z}(F_p)$, and the same also holds for m D lattices. Another reasonable condition is that the operator should have the separability property, illustrated in Fig. 5.22, namely

$$\mathcal{F}^{a+b} = \mathcal{F}^a \mathcal{F}^b, \quad a, b \in \mathbb{R}, \tag{5.118}$$

which means that the sequential application of $\mathcal{F}^{0.3}$ and $\mathcal{F}^{0.5}$ should be equivalent to the application of $\mathcal{F}^{0.8}$. Furthermore, \mathcal{F}^a must verify the *marginal conditions* $\mathcal{F}^0 = \mathcal{J}$, $\mathcal{F}^1 = \mathcal{F}$, $\mathcal{F}^2 = \mathcal{J}_-$, $\mathcal{F}^4 = \mathcal{J}$, and the *periodicity condition* $\mathcal{F}^{a+4} = \mathcal{F}^a$, which we have established for the integer powers (see (5.114)). These constraints for \mathcal{F}^a become constraints for its kernel $\psi_a(f, t)$, and we can see that, using the algebraic properties $\mu_n^{a+b} = \mu_n^a \mu_n^b$, all the above conditions are verified by the kernel $\psi_a(f, t)$ defined according to (5.116).

However, the above conditions do not allow the full identification of the kernel $\psi_a(f, t)$, and, in fact, we may find several kernels with these properties, and therefore several definitions of the fractional FT. The multiplicity, indeed, is a feature of all fractional operators (and also for scalars) and is twofold: first, the real power μ_n^a of a complex number μ_n is not unique and, second, the class of orthonormal eigenfunctions is not unique.

We now consider the class of eigenfunctions, which, surprisingly, exhibit a vast variety. Then, we classify the ambiguity of the real power μ_n^a .

5.12.2 Eigenfunctions of the Ordinary Fourier Transform

A (nonzero) signal $s_0(t)$, $t \in I$, is an *eigenfunction* of the Fourier operator \mathcal{F} if its FT $S_0 = \mathcal{F}[s_0]$ turns out to be proportional to $s_0(t)$, that is, $s_0(\lambda) = \mu s_0(\lambda)$, where μ is the *eigenvalue*. The explicit form is the integral equation

$$\int_I dt s_0(t) \psi^*(\lambda, t) = \mu s_0(\lambda), \quad \lambda \in I,$$

where $\psi(f, t)$ is the FT kernel on the group I .

Now, in self-dual groups it is easy to find a broad class of eigenfunctions. If $s(t)$, $t \in I$, is an arbitrary signal and $S(f)$, $f \in I$, is its FT, then

$$s_0(t) = s(t) + S(t) + s(-t) + S(-t), \quad t \in I, \quad (5.119)$$

is always an eigenfunction with unitary eigenvalue. In fact, from (5.114) we have that the FT of the FT is the reversed signal, and so on. Then, from (5.119) we have

$$S_0(f) = S(f) + s(-f) + S(-f) + s(f) = s_0(f).$$

For instance, starting from $s(t) = \text{rect}(t)$, $t \in \mathbb{R}$, and recalling that $S(f) = \text{sinc}(f)$, $f \in \mathbb{R}$, we find that $s_0(t) = 2\text{rect}(t) + 2\text{sinc}(t)$ is an eigenfunction of the FT on \mathbb{R} . It is easy to prove the following

Proposition 5.2 *The possible eigenvalues of the Fourier operator \mathcal{F} are the fourth roots of unity $\mu \in \{1, i, -1, -i\}$. The corresponding eigenfunctions are always even or odd functions.*

Proof If $s_0(t)$ is an eigenfunction with eigenvalue μ , from the graph (5.114) we find

$$s_0(t) \xrightarrow{\mathcal{F}} \mu s_0(t) \xrightarrow{\mathcal{F}} \mu^2 s_0(t) \xrightarrow{\mathcal{F}} \mu^3 s_0(t) \xrightarrow{\mathcal{F}} \mu^4 s_0(t).$$

On the other hand, \mathcal{F}^2 gives the reversed signal $s_0(-t)$ and \mathcal{F}^4 gives the original signal $s_0(t)$. Hence $\mu^2 s_0(t) = s_0(-t)$ and $\mu^4 s_0(t) = s_0(t)$. The latter gives $\mu^4 = 1$ and, considering that $\mu^2 = \pm 1$, from the first we find $\pm s_0(t) = s_0(-t)$. This completes the proof. \square

To define the functional \mathcal{F}^a we need a class of *orthonormal eigenfunctions* $\varphi_n(t)$, $n \in \mathcal{N}$, that is, functions with the property (see Sect. 4.5)

$$\int_I dt \varphi_m(t) \varphi_n^*(t) = \delta_{mn} \quad (5.120)$$

where \mathcal{N} may be \mathbb{N}_0 or a multidimensional extension of \mathbb{N}_0 , or a finite set (when I is finite). The existence of such a class on every self-dual group is ensured by theorems on linear vector spaces [22]. Moreover, the class is not unique, but there are infinitely many orthogonal classes of eigenfunctions (see [6] for an overview).

The best known orthonormal eigenfunction class on \mathbb{R} is given by the Hermite–Gauss functions (see Sect. 4.5)

$$\varphi_n(t) = \frac{\sqrt[4]{2}}{\sqrt{2^n n!}} H_n(\sqrt{2\pi}t) e^{-\pi t^2}, \quad n \in \mathbb{N}_0, \tag{5.121}$$

where $H_n(t)$ are the Hermite polynomials and the corresponding eigenvalues are $\mu_n = (-i)^n$. In particular, for $n = 0$ we have the important identity

$$e^{-\pi t^2} \xrightarrow{\mathcal{F}} e^{-\pi f^2}.$$

In the self-dual finite group $\mathbb{Z}(1/\sqrt{N})/\mathbb{Z}(\sqrt{N})$, several orthonormal classes have been proposed but all are based on a numerical evaluation (in this case, the number of eigenfunctions is finite and given by N) [4, 20]. Recently in [8], an orthonormal class of exact (not numerical) eigenfunctions was discovered.

5.12.3 Classification of Ambiguities

For a given set of orthonormal eigenfunctions, the kernel (5.116) is not unique. The reason is that μ_n^a is the real power of a complex number, which may assume infinitely many values. In fact, considering Proposition 5.2, we can write

$$\mu_n = e^{-i\frac{\pi}{2}h_n} \quad \text{with } h_n \in \{0, 1, 2, 3\} \tag{5.122}$$

where h_n is uniquely identified by μ_n . Then, the a th power has the general expression

$$\mu_n^a = e^{-i\frac{\pi}{2}(h_n+4k)a} \triangleq v_n(a, k), \quad k \in \mathbb{Z} \tag{5.123}$$

so that each μ_n^a assumes finitely many values if a is a rational number, and infinitely many if a is irrational. To remove this ambiguity in (5.123), we have to make a precise choice of the integer k to ensure a unique value to μ_n^a . In other words, we have to choose a sequence $k_n, n \in \mathbb{N}$, which we call the *generating sequence* of the fractional FT [5]. In such a way $\mu_n^a = v_n(a, k_n) = e^{-i\frac{\pi}{2}(h_n+4k_n)a}$ assumes a unique value for each $n \in \mathbb{N}$ and for each $a \in \mathbb{R}$.

In the literature, the following generating sequences have been considered:

1. $k_n = \lfloor n/4 \rfloor$, where $\lfloor \cdot \rfloor$ denotes the integer part, and
2. $k_n = 0, \forall n \in \mathbb{N}$.

Figure 5.23 illustrates the four eigenvalues of the standard (non-fractional) FT and the powers μ_n^a obtained with generating sequences 1 and 2.

In conclusion, to define a fractional FT without ambiguity we have to choose: (a) a set of orthonormal eigenfunctions, $\varphi_n(t), n \in \mathbb{N}$, and (b) a generating sequence k_n . Both choices must be done according to the applications of interest. Below we report interesting examples.

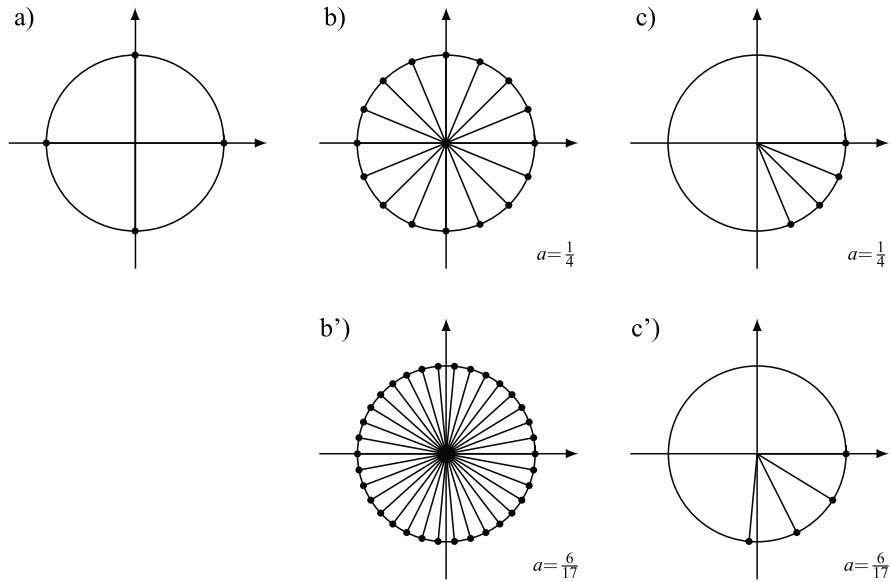


Fig. 5.23 (a) Eigenvalues of ordinary Fourier transform, (b) and (b') eigenvalue roots for chirp fractional Fourier transform, and (c) and (c') for weighted fractional Fourier transform

5.12.4 The chirp Fractional Fourier Transform

This fractional transform was obtained by Namias [16] by choosing the class of orthonormal eigenfunctions given by the Hermite–Gauss functions (5.121) with eigenvalues $\mu_n = (-i)^n$ and the zero generating sequence $k_n = 0$. Then, the a -powers of μ_n are given by

$$\mu_n^a = e^{-ia\frac{\pi}{2}n}. \tag{5.124}$$

Using (5.121) and (5.124) in (5.116), the series can be evaluated in closed form [16], and the result is

$$\psi_a(f, t) = K_a e^{i\pi(B_a(f^2+t^2)-2C_a ft)}, \tag{5.125}$$

where

$$K_a = \sqrt{1 - iB_a}, \quad B_a = \operatorname{ctg}\left(\frac{\pi}{2}a\right), \quad C_a = \operatorname{csc}\left(\frac{\pi}{2}a\right). \tag{5.125a}$$

Hence, the chirp fractional FT on \mathbb{R} has the expression

$$S_a(f) = K_a e^{i\pi B_a f^2} \int_{-\infty}^{+\infty} s(t) e^{i\pi(B_a t^2 - 2C_a ft)} dt. \tag{5.126}$$

Now, we may find that the evaluation of $S_a(f)$ can be carried out as follows (Fig. 5.24):

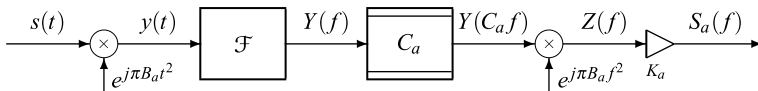


Fig. 5.24 Decomposition of the Fractional Fourier transform on \mathbb{R}

1. We let $y(t) = s(t)e^{i\pi B_a t^2}$.
2. We evaluate the ordinary Fourier transform $Y(f)$ of $y(t)$.
3. We get $S_a(f) = K_a e^{i\pi B_a f^2} Y(C_a f)$.

In step 1, we introduce a *chirp* modulation; in step 2, we evaluate an ordinary (non-fractional) Fourier transform; and in step 3, we complete the computation with another chirp modulation.

Following this procedure, we can evaluate, as an example, the chirp fractional FT of the rectangular signal $s(t) = \text{rect}(t)$, $t \in \mathbb{R}$. We find

$$S_a(f) = \frac{K_a}{\sqrt{2|B_a|}} e^{-i\pi f^2/B_a} \left\{ [A(f_+) - A(f_-)] + i \operatorname{sgn}(B_a) [B(f_+) - B(f_-)] \right\}, \tag{5.127}$$

where $A(x) + iB(x) \triangleq \int_0^x e^{i\frac{\pi}{2}y^2} dy$ is the Fresnel function [1] and $f_{\pm} = \pm\sqrt{|B_a|/2} - \operatorname{sgn}(B_a)\sqrt{2/|B_a|}C_a f$.

The result is illustrated in Fig. 5.25 for some values of the “fraction” a . We may see that, for small values of a , $S_a(f)$ resembles the original signal $\text{rect}(f)$. When a approaches 1, it resembles the ordinary transform $S(f) = \text{sinc}(f)$, but for intermediate value of a the shape is quite different from $s(t)$ and $S(f)$.

Optical Interpretation We reconsider the interpretation outlined at the beginning (see Fig. 5.21). It can be shown that, with appropriate conditions on the geometry and the refraction index profile [15, 17], the propagation *modes* are given by the 2D version $\varphi_n(x)\varphi_n(y)$ of (5.121) with eigenvalues $\mu_n^a = \exp(-i\frac{\pi}{2}a(z)n)$, where the “fraction” $a(z)$ is proportional to the distance z . The mode composition gives the image that one can observe along the fiber, which is given by the amplitude of the fractional FT $L_a(f_x, f_y)$ of the image $\ell(x, y)$ applied at $z = 0$.

5.12.5 The Weighted Fractional Fourier Transform

This fractional FT is obtained with the generating sequence $k_n = \lfloor n/4 \rfloor$, which gives for the a th eigenvalue power

$$\mu_n^a \in \left\{ 1, e^{ia\frac{\pi}{2}}, e^{ia\pi}, e^{ia\frac{3}{2}\pi} \right\}.$$

With this generating sequence, the specific choice of the eigenfunction class becomes irrelevant. In fact, the kernel (5.116) turns out to be given by four terms and

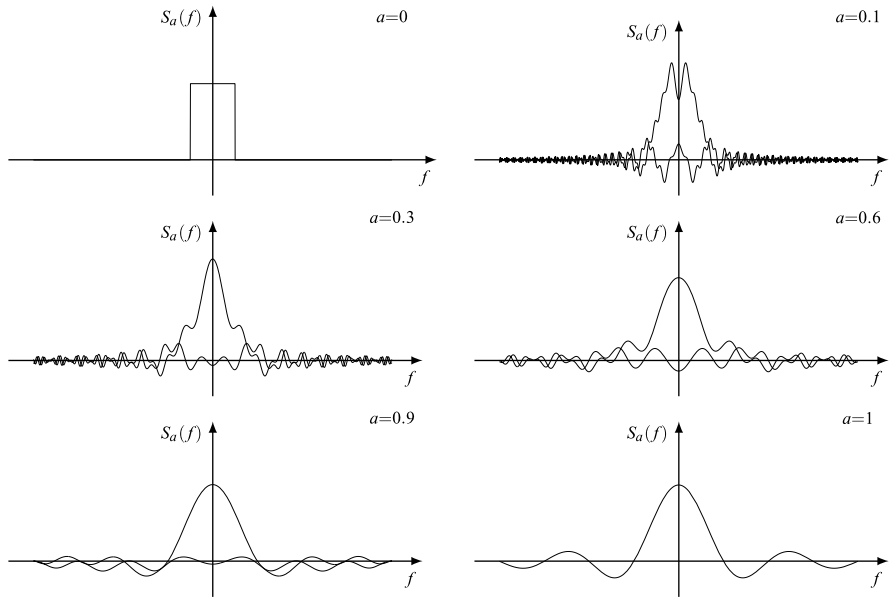


Fig. 5.25 Example of chirp fractional Fourier transform on \mathbb{R}

can be written in the form

$$\psi_a(f, t) = \beta_0(f, t) + e^{ia\frac{\pi}{2}} \beta_1(f, t) + e^{ia\pi} \beta_2(f, t) + e^{ia\frac{3}{2}\pi} \beta_3(f, t). \quad (5.128)$$

Since we know $\psi_a(f, t)$ explicitly for $a = 0, 1, 2, 3$ by the marginal conditions $\mathcal{F}^0 = \mathcal{J}$, $\mathcal{F}^1 = \mathcal{F}$, etc., from (5.128) we can form a systems of 4 equations whose solution ensures the identification of the functions $\beta_i(f, t)$. Then, we obtain the following expression for the weighted fractional FT [5]

$$S_a(f) = p_0(a)s(f) + p_1(a)S(f) + p_2(a)s(-t) + p_3(a)S(-f), \quad (5.129)$$

where $s(t)$ is the given signal, $S(f)$ is its ordinary FT and the weights are given by $p_m(a) = \frac{1}{4}[1 - e^{i2\pi a}]/[1 - e^{i(\pi/2)(a-m)}]$. The dependence on the “fraction” a appears only on the weights $p_m(a)$ of the linear combination.

Considering that (see (5.114)) $s = \mathcal{F}^0[s]$, $S = \mathcal{F}^1[s]$, etc., we can write (5.129) in the form

$$S_a(f) = \sum_{m=0}^3 p_m(a)\mathcal{F}^m[s|f],$$

and, in terms of operators $\mathcal{F}^a = \sum_{m=0}^3 p_m(a)\mathcal{F}^m$, as illustrated in Fig. 5.26.

Of course, the weighted fractional FT is very different from the chirp fractional FT; for example, for the rectangular signal compare Fig. 5.27 with Fig. 5.25.

Fig. 5.26 Interpretation of weighted fractional Fourier transform

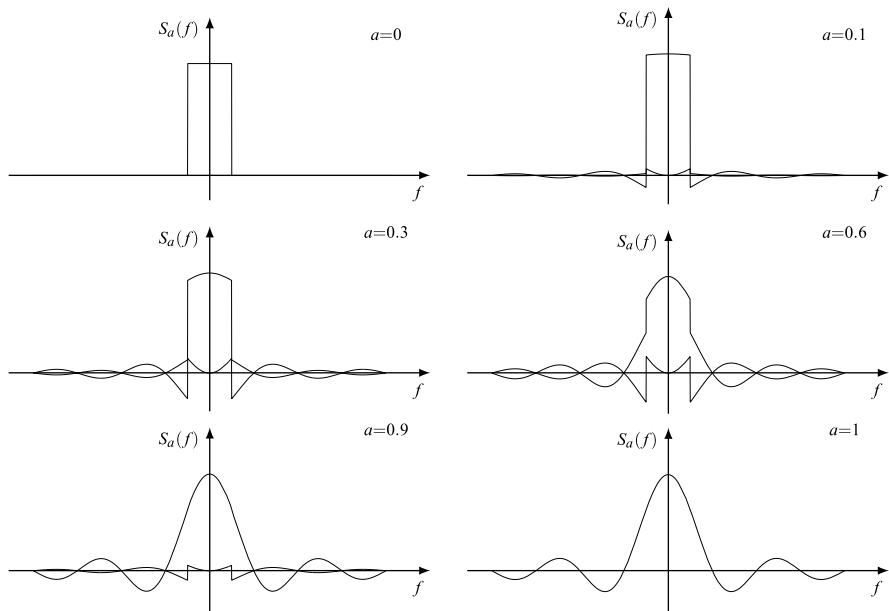
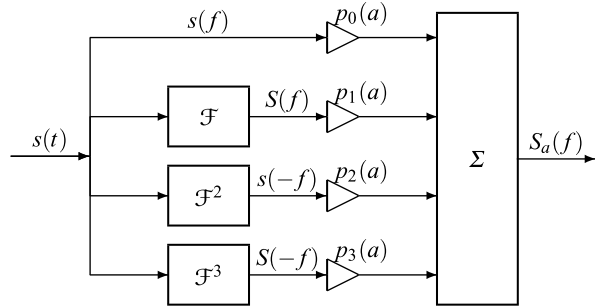


Fig. 5.27 Example of weighted fractional Fourier transform on \mathbb{R}

Finally, we note that the weighted fractional FT can be considered on any self-dual group. In the above example, we tacitly assumed $I = \mathbb{R}$. In the literature, it has also been considered on the finite group $\mathbb{Z}(1/\sqrt{N})/\mathbb{Z}(\sqrt{N})$ [4].

5.13 Problems

5.1 ★ [Sect. 5.2] Write and prove the orthogonality conditions (5.11a), (5.11b) for $I = \mathbb{Z}(T)/\mathbb{Z}(NT)$.

5.2 ★ [Sect. 5.3] Show that the 1D LCA groups, i.e., \mathbb{R} , $\mathbb{Z}(T)$ and \mathbb{O} , verify relation (5.21).

5.3 ★★ [Sect. 5.3] Starting from the general definition (5.18) of reciprocal, prove relation (5.21).

5.4 ★▽ [Sect. 5.3] Find the reciprocals of the following groups

$$\mathbb{R} + \mathbb{Z}(2), \quad \mathbb{Z}(6) + \mathbb{Z}(15), \quad \mathbb{Z}(12) \cap \mathbb{Z}(40), \quad \mathbb{O} \cap \mathbb{Z}(3).$$

5.5 ★★★ [Sect. 5.3] Prove that two *rationally comparable* groups J and K satisfy the relations

$$(J + K)^* = J^* \cap K^*, \quad (J \cap K)^* = J^* + K^*.$$

5.6 ★★ [Sect. 5.4] For any $n \in \mathbb{Z}$, find the result of the application of the operator \mathcal{F}^n on a signal $s(t)$, $t \in I$ (\mathcal{F}^n denotes a sequence of n applications of the operator \mathcal{F}).

5.7 ★ [Sect. 5.5] Prove Rule 11(a) of Table 5.2 using Rule 10(a).

5.8 ★ [Sect. 5.5] Write the Poisson summation formula with $I = \mathbb{Z}(T_0)$, $U = \mathbb{Z}(NT_0)$ and $P = \mathbb{O}$.

5.9 ★★ [Sect. 5.5] Evaluate the sum of the series

$$\sum_{n=0}^{\infty} \frac{1}{1 + an^2}$$

using Poisson's formula (5.46). *Hint:* consider $s(t) = \exp(-\alpha|t|)$, $t \in \mathbb{R}$ as the signal.

5.10 ★ [Sect. 5.5] Evaluate the Fourier transform of a periodic signal defined on \mathbb{R} , instead of $\mathbb{R}/\mathbb{Z}(T_p)$, starting from its Fourier series expansion.

5.11 ★ [Sect. 5.6] Find the symmetries of the signal

$$s(t) = i2\pi t 1(t)e^{-\alpha t}, \quad t \in \mathbb{R}.$$

5.12 ★★ [Sect. 5.6] Decompose the signal of the previous problem into symmetric components, according to Symmetries 1, 2 and 3.

5.13 ★★★ [Sect. 5.6] Decompose the signal

$$s(t) = \text{sinc}_N\left(\frac{t - t_0}{T_p}\right), \quad t \in \mathbb{R}/\mathbb{Z}(5T_p), \quad N = 5$$

into even and odd components, $s_e(t)$ and $s_o(t)$.

5.14 $\star\star\star\nabla$ [Sect. 5.6] Calculate the Fourier transforms of the signals $s(t)$, $s_e(t)$ and $s_o(t)$ of the previous problem. Then, check that they verify the corresponding symmetries, e.g., $S_e(f)$ must be real and even.

5.15 \star [Sect. 5.7] Prove the following rule on the extension of the correlation

$$e(c_{xy}) = e(x) + [-e(y)].$$

5.16 $\star\star$ [Sect. 5.7] Compute the correlation of the signals

$$x(t) = A_0 \operatorname{rect}(t/T), \quad y(t) = B_0 \exp(-|t|/T), \quad t \in \mathbb{R}.$$

5.17 $\star\star\star$ [Sect. 5.7] Calculate the energy spectral density of the two signals of the previous problem and verify their symmetries.

5.18 \star [Sect. 5.8] Show that, by substituting the expression of S_k given by the first of (5.70) in the second, we actually obtain s_n .

5.19 $\star\star$ [Sect. 5.8] Starting from (5.65), we can “prove” that *all continuous-time signals are constant valued*. Indeed

$$e^{i2\pi ft} = (e^{i2\pi})^{ft} = 1^{ft} = 1.$$

Therefore,

$$s(t) = \int_{-\infty}^{+\infty} S(f) \, df = \operatorname{area}(S) \quad !!!$$

Try to explain this paradox.

5.20 \star [Sect. 5.8] Calculate the Fourier transform of the signal

$$te^{-\alpha t} 1(t), \quad t \in \mathbb{R}, \quad \alpha > 0,$$

and then apply the Symmetry Rule.

5.21 $\star\star$ [Sect. 5.8] Calculate the Fourier transform of the discrete signal

$$e^{-\alpha|t|}, \quad t \in \mathbb{Z}(T), \quad \alpha > 0,$$

and then apply the Symmetry Rule.

5.22 $\star\star$ [Sect. 5.8] Referring to 3. of Table 5.4, define the *compatibility conditions* of a sinusoidal signal of the domains $\mathbb{Z}(T)$ and $\mathbb{Z}(T)/\mathbb{Z}(NT)$. In particular, determine in which domains the frequency $f_0 = \frac{7}{39} \frac{1}{T}$ is compatible.

5.23 [Sect. 5.8] Starting from the Fourier pair (5.73a), (5.73b) evaluate the Fourier transform of the even and odd part of $s(t)$. Note in particular that $s_e(t) = \frac{1}{2} \exp(-\alpha|t|)$.

5.24 ★ [Sect. 5.8] Evaluate the area of the signal

$$s(t) = A_0 \operatorname{sinc}(F_0 t), \quad t \in \mathbb{R}.$$

5.25 ★ [Sect. 5.8] Evaluate the Fourier transform of the *even part* and *odd part* of the signal

$$s(t) = 1(t)e^{-\alpha t}, \quad t \in \mathbb{R}, \quad \alpha > 0.$$

5.26 ★ [Sect. 5.8] Evaluate amplitude and phase of the Fourier transform of the signals

$$s_1(t) = A_0 \operatorname{rect}\left(\frac{t-t_0}{T}\right), \quad t \in \mathbb{R},$$

$$s_2(t) = A_0 \operatorname{rep}_{10}\left[\operatorname{rect}\left(\frac{t-2}{3}\right)\right], \quad t \in \mathbb{R}/\mathbb{Z}(10).$$

5.27 ★★ [Sect. 5.8] Evaluate the Fourier transform of the signal

$$s(t) = \operatorname{rect}(t/T) \sin 2\pi f_0 t, \quad t \in \mathbb{R}$$

in two different ways: (i) using Rule 6(b) and (ii) using the Euler formulas and then Rule 5(b).

5.28 ★ [Sect. 5.8] Write Parseval's theorem in the case $I = \mathbb{Z}(T)/\mathbb{Z}(10T)$.

5.29 ★ [Sect. 5.8] Write decomposition (5.77) for the causal exponential signal

$$s(t) = 1(t)e^{-3t}, \quad t \in \mathbb{R}.$$

5.30 ★★ [Sect. 5.8] Write decomposition (5.77) for the signal

$$s(t) = 5 + 1(t)e^{-3t}, \quad t \in \mathbb{R}.$$

5.31 ★★ [Sect. 5.8] Write decomposition (5.77) for the discrete signal

$$s(nT) = 2 + (1/3)^{|n|}, \quad nT \in \mathbb{Z}(T).$$

5.32 ★★ [Sect. 5.8] Show that on the discrete domain $\mathbb{Z}(T)$ the signals $x_0(nT) = z^n$, with z a complex constant, are filter eigenfunctions.

5.33 ★ [Sect. 5.8] Explain why sinusoids are not filter eigenfunctions, although the response to a sinusoid is still a sinusoid.

5.34 ★★★ [Sect. 5.8] Show that in the case of a continuous time signal $s(t)$, $t \in \mathbb{R}$, the constant term in the composition (5.77) is given by the so-called *continuous*

component (see Sect. 2.1)

$$S_0 = \lim_{T \rightarrow \infty} \frac{1}{2T} \int_{-T}^T s(t) dt,$$

provided that the limit exists and is finite.

5.35 ★ [Sect. 5.8] Write decomposition (5.74) in the case $I = \mathbb{R}/\mathbb{Z}(T_p)$ and then write the signal decomposition (5.77).

5.36 ★ [Sect. 5.8] Write decompositions (5.74) and (5.77) in the case $I = \mathbb{Z}(T)/\mathbb{Z}(T_p)$.

5.37 ★★★ [Sect. 5.8] The decomposition into “positive” and “negative” frequencies (5.74) is not unique. Prove that for $I = \mathbb{Z}(T)$, in place of decomposition indicated in (5.74), we can consider the alternative decomposition

$$\hat{I}_+ = \left(0, \frac{1}{2}F_p\right), \quad \hat{I}_- = \left(\frac{1}{2}F_p, F_p\right).$$

5.38 ★ [Sect. 5.8] Let $s(t)$, $t \in \mathbb{R}$, be a signal with the limited spectral extension $e(S) = (-B, B)$. Find the spectral extension of $s^2(t)$, $t \in \mathbb{R}$.

5.39 ★★ [Sect. 5.8] Find the spectral extension of the discrete signal

$$s(t) = A_0 \operatorname{sinc}(t/T_0), \quad t \in \mathbb{Z}(T), \quad T_0 = T/10.$$

5.40 ★ [Sect. 5.8] Find the spectral extension of the signal

$$s(t) = A_0 \sin^3(2\pi f_0 t) \cos(4\pi f_0 t), \quad t \in \mathbb{R}/\mathbb{Z}(T_0), \quad T_0 = 1/f_0.$$

5.41 ★★ [Sect. 5.8] Prove that the spectral extension of the previous signal does not change if the domain/periodicity $\mathbb{R}/\mathbb{Z}(T_0)$ is replaced by $\mathbb{R}/\mathbb{Z}(2T_0)$.

5.42 ★ [Sect. 5.9] Using (5.93), show that in 1D case the rule on the coordinate change becomes

$$s(at) \xrightarrow{\mathcal{F}} (1/|a|)S(f/a)$$

where a is an arbitrary nonzero real number.

5.43 ★★★ [Sect. 5.10] Prove that (5.97), when \mathcal{B} is hexagonal, yields (5.101).

5.44 ★★★ [Sect. 5.10] Prove that (5.97), when \mathcal{B} is circular, yields (5.102). *Hint:* use the Bessel function identity [1]: $d[x^{n+1}J_{n+1}(x)]/dx = x^{n+1}J_n(x)$.

5.45 ** [Sect. 5.10] Consider the Fourier transform of the pyramidal signal given by (5.103). Evaluate the value at the origin $\text{PYR}(0, 0)$. *Hint:* to evaluate the indeterminacy $0/0$, use the expansion $\sin(x) = x - x^3/6 + O(x^4)$.

Appendix A: Fourier Kernel from Characters

A *character* of an LCA group I is every continuous complex function on I , $\psi_f(t)$, $t \in I$, with the properties (see (5.4) and (5.5))

$$\psi_f(t_1 + t_2) = \psi_f(t_1)\psi_f(t_2), \quad t_1, t_2 \in I, \quad (5.130a)$$

$$|\psi_f(t)| = 1, \quad t \in I. \quad (5.130b)$$

The index f identifies a specific character ψ_f ; the collection of all the indexes f identifies a set, which represents the dual group \widehat{I} (the dual of I).⁴ In fact, it can be shown that the index set is always an LCA group [23]. Now, from the set of characters $\psi_f(t)$, with $t \in I$ and $f \in \widehat{I}$, we can define a function of two variables $\psi(f, t) = \psi_f(t)$, which represents the kernel of the FT on I .

From conditions (5.130a), (5.130b) the following important properties for the kernel $\psi(f, t)$, which generalize the properties of the exponential $e^{i2\pi ft}$, can be established

$$\psi(f, t_1 + t_2) = \psi(f, t_1)\psi(f, t_2), \quad (5.131a)$$

$$\psi(f, 0) = 1, \quad \psi(0, t) = 1, \quad (5.131b)$$

$$\psi(f, t) = \psi^*(f, -t) = 1/\psi(f, -t), \quad (5.131c)$$

$$\psi(f, -t) = \psi(-f, t), \quad (5.131d)$$

$$\psi(f_1 + f_2, t) = \psi(f_1, t)\psi(f_2, t). \quad (5.131e)$$

For instance, the first of (5.131b) is proved by fixing in (5.130a) $t_1 = t_2 = 0$; and (5.131c) is proved by letting $t_1 = -t_2 = t$. We see that the separability with respect to t leads to the separability with respect to f . Note that in (5.130a), (5.130b) and (5.131a), (5.131b), (5.131c), (5.131d), (5.131e) the group operation $+$ is not necessarily the same for I and \widehat{I} . In (5.131a), $+$ is the operation on I , whereas in (5.131e) $+$ is the operation on \widehat{I} . Finally, in (5.131b) the first 0 is the identity element of I and the second 0 is the identity element of \widehat{I} .

Fourier Kernel on \mathbb{R} When $I = \mathbb{R}$ in (5.130a), the group operation $+$ is the ordinary addition and the only continuous solution to the functional equation

⁴The dual group \widehat{I} is not unique, but two different dual groups are *isomorphic*.

$\psi(t_1 + t_2) = \psi(t_1)\psi(t_2)$ has the form $\psi(t) = e^{pt}$ with p an arbitrary complex number. But, constraint (5.130b) restricts p to be imaginary and this is sufficient to conclude that $\{e^{iat} \mid a \in \mathbb{R}\}$ is the character set and that \mathbb{R} is the dual of \mathbb{R} . On the other hand, we can denote the real number a in the form $a = 2\pi f$ with f still real, thus obtaining the form (5.6), that is, $\psi_{\mathbb{R}}(f, t) = e^{i2\pi ft}$.

Fourier Kernel on \mathbb{R}^m If a group is separable, $I = I_1 \times I_2$, the Fourier kernel on I is given by the product of the kernels on I_1 and I_2 (see [23]). Since \mathbb{R}^2 is separable, from this rule we find that the kernel on \mathbb{R}^2 is given by

$$\psi_{\mathbb{R}^2}(f_1, f_2; t_1, t_2) = \psi_{\mathbb{R}}(f_1, t_1)\psi_{\mathbb{R}}(f_2, t_2) = e^{i2\pi(f_1 t_1 + f_2 t_2)}.$$

The same form holds for all the subgroups of \mathbb{R}^2 , also not separable, since they have the group operation in common with \mathbb{R}^2 . The generalization to \mathbb{R}^m is immediate and gives (5.4).

Appendix B: Invertibility of the Fourier Transform

We prove that, from the FT calculated using (5.1), we can recover the signal using (5.2). Denoting the inverse transform by

$$\tilde{s}(t) = \int_{\hat{I}} df S(f)\psi^*(f, t),$$

and substituting the expression of $S(f)$ given by (5.1), we get

$$\tilde{s}(t) = \int_{\hat{I}} df \int_I du s(u)\psi^*(f, u)\psi(f, t),$$

where, from properties (5.131a), (5.131b), (5.131c), (5.131d), (5.131e) $\psi^*(f, u)\psi(f, t) = \psi(f, -u)\psi(f, t) = \psi(f, t - u)$. Hence

$$\tilde{s}(t) = \int_I du s(u) \int_{\hat{I}} df \psi(f, t - u) = \int_I du s(u)\delta_I(t - u) = s(t),$$

where we used the orthogonality condition (5.10a), (5.10b) and the sifting property of the impulse (4.76).

Appendix C: Proof of Theorem 5.1 on the Dual Group

We prove that if the function $\psi_f(t) = \psi(f, t)$ (with fixed f) is defined on I_0 and has periodicity P , then the function $\psi_t(f) = \psi(f, t)$ (with fixed t) is defined on P^* and has periodicity I_0^* . The periodicity of $\psi_f(t)$ yields $\psi_f(t + u) = \psi_f(t)$, $u \in P$, and, recalling that $\psi_f(t + u) = \psi_f(t)\psi_f(u)$, it follows that

$$\psi_f(u) = 1, \quad u \in P. \tag{5.132}$$

Thus, any frequency f satisfying (5.132) ensures the periodicity P with respect to the time domain u . The set of such frequencies is $P^* = \{f \mid \psi_f(u) = 1, u \in P\}$, which defines the domain of the kernel with respect to the frequency f .

Analogously, the possible periodicity of the function $\psi_t(f)$ with respect to f is expressed by the condition $\psi_t(f+v) = \psi_t(f)$, $t \in I_0$, which is equivalent to $\psi_t(v) = 1$, $t \in I_0$. The frequencies v that verify this condition form the reciprocal of I_0 . Therefore, the periodicity of the dual group is given by I_0^* .

Appendix D: Proof of Theorem 5.2 on the Representation of the Dual Group

To find the representation of the reciprocal J^* of an m D group J , we note that the condition $\mathbf{t} \in J$ in (5.31) can be expressed in the form $\mathbf{t} = \mathbf{J}\mathbf{h}$, $\mathbf{h} \in H$. Hence, we have

$$J^* = \{\mathbf{f} \mid \mathbf{f}'\mathbf{J}\mathbf{h} \in \mathbb{Z}, \mathbf{h} \in H\}.$$

Now, if we compare the expression of J^* with the expression of H^* , given by

$$H^* = \{\mathbf{v} \mid \mathbf{v}\mathbf{h} \in \mathbb{Z}, \mathbf{h} \in H\},$$

we find the relation between the frequencies \mathbf{v} of H^* and the frequencies \mathbf{f} of J^* , namely

$$\mathbf{v}' = \mathbf{f}'\mathbf{J} \rightarrow \mathbf{f} = (\mathbf{J}')^{-1}\mathbf{v}, \quad \mathbf{v} \in H^*.$$

This completes the proof.

Appendix E: Proof of Poisson's Summation Formula

For the proof we use the theory of elementary transformations and particularly the Duality Theorem of Sect. 6.13. Let us consider a signal $s(t)$, $t \in I$, that is, $I \rightarrow U$ down-sampled, where $I = I_0/P \rightarrow U = U_0/P$ and U_0 is a lattice. The relation is

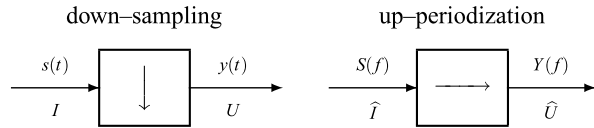
$$y(t) = s(t), \quad t \in U \tag{5.133a}$$

where $y(t)$ is the down-sampled signal (Fig. 5.28).

In the frequency domain, we have an $\hat{I} \rightarrow \hat{U}$ up-periodization, where $\hat{I} = P^*/I_0^*$, $\hat{U} = P^*/U_0^*$. The relation is (see (6.80))

$$Y(f) = \sum_{\lambda \in U_0^*/I_0^*} S(f - \lambda) = \sum_{\lambda \in U_0^*/I_0^*} S(f + \lambda), \quad f \in \hat{I}. \tag{5.133b}$$

Fig. 5.28 Diagram for the proof of Poisson's summation formula



Finally, the application of the rule $\text{area}(y) = Y(0)$ gives

$$\sum_{u \in U_0/P} d(U_0)s(u) = \sum_{\lambda \in U_0^*/I_0^*} S(\lambda). \quad (5.134)$$

This complete the proof.

References

1. M. Abramowitz, I.A. Stegun, *Handbook of Mathematical Functions* (Dover, New York, 1970)
2. L.B. Almeida, The fractional Fourier transform and time-frequency representations. *IEEE Trans. Signal Process.* **42**, 3084–3091 (1994)
3. H. Bremermann, *Distribution, Complex Variables, and Fourier Transforms* (Addison-Wesley, Reading, 1965)
4. C. Candan, M.A. Kutay, H.M. Ozaktas, The discrete fractional Fourier transform. *IEEE Trans. Signal Process.* **48**, 1329–1337 (2000)
5. G. Cariolaro, T. Erseghe, P. Kraniuskas, N. Laurenti, A unified framework for the fractional Fourier transform. *IEEE Trans. Signal Process.* **46**, 3206–3219 (1998)
6. G. Cariolaro, T. Erseghe, P. Kraniuskas, N. Laurenti, Multiplicity of fractional Fourier transforms and their relationships. *IEEE Trans. Signal Process.* **48**, 227–241 (2000)
7. G. Cariolaro, T. Erseghe, The fractional discrete cosine transform. *IEEE Trans. Signal Process.* **50**, 902–911 (2002)
8. T. Erseghe, G. Cariolaro, An orthonormal class of exact and simple DFT eigenfunctions with a high degree of symmetry. *IEEE Trans. Signal Process.* **51**, 2527–2539 (2003)
9. I.B. Gel'fand, G.E. Shilov, *Generalized Functions. Applications of Harmonic Analysis*, vol. 4 (Academic Press, Dordrecht, 1964)
10. E. Hewitt, K.A. Ross, *Abstract Harmonic Analysis, vols. 1, 2* (Springer, Berlin, 1963)
11. M.J. Lighthill, *Introduction to Fourier Analysis and Generalized Functions* (Cambridge University Press, Cambridge, 1958)
12. A.W. Lohmann, Image rotation, Wigner rotation, and the fractional Fourier transform. *J. Opt. Soc. Am. A* **10**(10), 2181–2186 (1993)
13. A.W. Lohmann, B.H. Soffer, Relationship between the Radon-Wigner and fractional Fourier transforms. *J. Opt. Soc. Am. A* **11**(6), 1798–1801 (1994)
14. L.H. Loomis, *An Introduction to Abstract Harmonic Analysis* (Van Nostrand, New York, 1953)
15. D. Mendlovic, H.M. Ozaktas, Fractional Fourier transforms and their optical implementation: I. *J. Opt. Soc. Am. A* **10**(9), 1875–1881 (1993)
16. V. Namias, The fractional order Fourier transform and its applications to quantum mechanics. *Inst. Math. Appl.* **25**, 241–265 (1980)
17. H.M. Ozaktas, D. Mendlovic, Fractional Fourier transforms and their optical implementation: II. *J. Opt. Soc. Am. A* **10**(12), 2522–2531 (1993)
18. H.M. Ozaktas, B. Barshan, D. Mendlovic, L. Onural, Convolution, filtering and multiplexing in fractional Fourier domains and their relation to chirp and wavelet transforms. *J. Opt. Soc. Am. A* **11**(2), 547–559 (1994)

19. A. Papoulis, *Systems and Transforms with Applications in Optics* (McGraw–Hill, New York, 1968)
20. S.C. Pei, M.H. Yeh, C.C. Tseng, Discrete fractional Fourier transform based on orthogonal projections. *IEEE Trans. Signal Process.* **47**, 1335–1348 (1999)
21. L. Pontryagin, *Topological Groups* (Princeton University Press, Princeton, 1946)
22. S. Roman, *Advance Linear Algebra* (Springer, New York, 1992)
23. W. Rudin, *Fourier Analysis on Groups* (Interscience, New York, 1962)
24. E.C. Titchmars, *Introduction to the Theory of Fourier Integrals* (Oxford University Press, New York, 1937)

Chapter 6

Unified Theory: Signal Transformations

UT 6.1 Definition of Signal Transformation

Here and elsewhere we consider complex signals defined on a “domain”, which should be intended as a domain/periodicity pair, that is, a quotient group.

Definition 6.1 A *signal transformation (tf)* is a quintuple (Fig. 6.1)

$$(I, U, C_I, C_U, \mathcal{T}), \tag{6.1}$$

where

- I is the input signal domain,
- U is the output signal domain,
- C_I is the class of input signals, $C_I \subset \mathcal{S}(I)$,
- C_U is the class of output signals, $C_U \subset \mathcal{S}(U)$,
- $\mathcal{T}: C_I \rightarrow C_U$ is an operator.¹

The operator \mathcal{T} , starting from the input signal $x \in C_I$, gives the output signal $y = \mathcal{T}[x] \in C_U$. With

$$y = \mathcal{T}[x], \tag{6.2a}$$

we denote the *input–output relationship* of the tf. It will also be written in the form²

$$y(t) = \mathcal{T}[x | t], \quad t \in U \tag{6.2b}$$

to indicate the output *response* value at the time³ t .

¹Several authors restrict the use of *operator* to mappings of the form $\mathcal{T}: C_I \rightarrow C_I$, which implies $U = I$ (see [6]).

²The input signal is denoted with x , instead of $x(u)$, to point out that the response value at any time t depends on the *whole behavior* of the input signal, and not only on its value at time u .

³It is customary to refer to “time”, but the correct terminology should be “signal argument”, since in general t may be multidimensional with a physical interpretation given by the context.

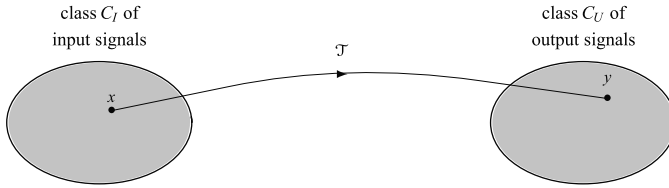
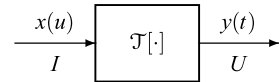


Fig. 6.1 The operator \mathcal{T} maps every input signal $x \in C_I$ into an output signal $y = \mathcal{T}[x] \in C_U$

Fig. 6.2 Representation of an $I \rightarrow U$ transformation with operator \mathcal{T}



To indicate explicitly the input and output domains of the tf, we will write “ $I \rightarrow U$ tf with operator \mathcal{T} ” or “ $I \rightarrow U$ tf with input–output relation $y = \mathcal{T}[x]$ ”. Note that in graphical representation the domains will be explicitly indicated (Fig. 6.2).

The quintuple (6.1) is usually simplified into the triplet

$$(I, U, \mathcal{T}) \tag{6.3}$$

since the input and output classes, C_I and C_U , are the classes of all signals defined on I and U , that is, $\mathcal{S}(I)$ and $\mathcal{S}(U)$, or they are deduced from the context.

6.1.1 Generality of the Definition

Note the great generality of the definition where no structural constraints are imposed on the elements of the triplet. The domains I and U may be equal (*equal-domain* tfs), as well as different (*different-domain* tfs). In the general case, they are quotient groups, namely

$$I = I_0/P_1, \quad U = U_0/P_2, \tag{6.4}$$

where I_0 and U_0 are domains and P_1 and P_2 periodicities; then, signal tfs may be periodic, but also aperiodic as soon as the periodicities become irrelevant. I and U may be one-dimensional as well as multidimensional, in general m -dimensional at the input and n -dimensional at the output.

Usually we will refer to one-input one-output transformations (*scalar* transformations), but multi-input multi-output transformations (*vector* transformations) are also included in the definition. So, in general, the input signal may have M components and the output signal N components, namely

$$x(u) = \begin{bmatrix} x_1(u) \\ \vdots \\ x_M(u) \end{bmatrix}, \quad y(t) = \begin{bmatrix} y_1(t) \\ \vdots \\ y_N(t) \end{bmatrix}, \tag{6.5}$$

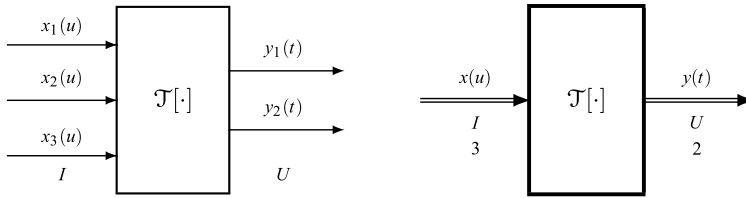


Fig. 6.3 Alternative representations of an $I \rightarrow U$ tf with 3 inputs and 2 outputs

where each $x_i(u)$ is defined on the input domain I , and each $y_j(t)$ on the output domain U . Figure 6.3 shows the graphical representations of an $I \rightarrow U$ tf with three inputs and two outputs.

6.1.2 Systems and Transformations

Transformations are linked to *systems*, the objects of System Theory based on state variables, and, in fact, they are both mathematical models of “physical” systems.

A *system* is a more structured model in so far as it describes not only the input–output relationship, but also the internal evolution of the system. This permits the formulation of concepts, like observability, stability, etc., which are not considered in transformations. Furthermore, a system by definition complies with the causality condition and is usually introduced with equal domains.

On the other hand, a *transformation* does not have structural constraints and, for this reason, it models more general signal operations, and it is preferred in Signal Theory. For instance, ideal filters cannot be modeled as systems, but only as transformations, and their usefulness is indeed basic to Signal Theory.

As said above, the quintuple (6.1) is usually simplified into the triplet (6.3), since the signal classes can be deduced from the context. The class specification is very important for linear tfs, where C_I and C_U become linear vector spaces equipped with inner-product (Banach and Hilbert spaces) [3]. Such a formulation would be straightforward in our context, since the concept of distance and inner-product can be introduced in a unified form by the Haar integral (see Sect. 4.5). However, this possibility will not be developed as a precise choice, to avoid a further mathematical heaviness.

6.1.3 Rate Diagram

For a signal $s(t)$, $t \in I$, defined on a lattice I , we have introduced the *rate* as

$$F = \mu(I) = 1/d(I), \tag{6.6}$$

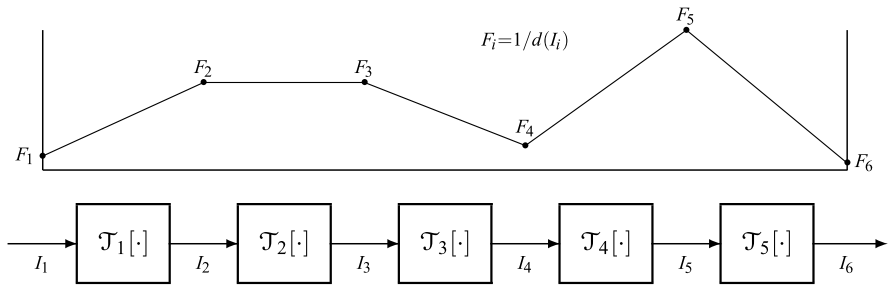


Fig. 6.4 A cascade of transformations on lattices with the rate diagram

where $d(I)$ is the lattice determinant. In particular, in the 1D case where $I = \mathbb{Z}(T)$, the rate is $F = 1/T$ and gives the number of signal values per second. In the general case, the meaning of F will depend on the context.

For an $I \rightarrow U$ tf, when both I and U are lattices, we find two rates: the input rate $F_1 = 1/d(I)$ and the output rate $F_2 = 1/d(U)$. So in general, a tf operates with two rates and, in particular, when $U = I$, we have a single rate. To emphasize the rate in the graphical representation, we introduce the *rate diagram* which simply connects the input rate to the output rate in the graphical representation.

The rate diagram is particularly useful in a cascade of tfs, where we may find several different rates, as shown in Fig. 6.4.

UT 6.2 Fundamental Definitions

6.2.1 Real and Complex Transformations

In general, the input and the output signals of a transformation are complex, so we normally consider *complex* tfs.

Definition 6.2 An $I \rightarrow U$ transformation is *real* if the response $y(t)$, $t \in U$, to any *real* input signal $x(u)$, $u \in I$, is a *real* signal.

Note that if the input signal of a real tf is a complex signal, the output is in general a complex signal. Note also that the word “real” is used here in the mathematical sense and does not refer to the physical realizability of the tf.

6.2.2 Invertible and Conditionally Invertible Transformations

An $I \rightarrow U$ tf with input–output relation $y = \mathcal{T}[x]$ is *invertible* if a $U \rightarrow I$ tf exists, that permits the recovery of the original signal x from y . Hence, if \mathcal{T}^{-1} denotes the

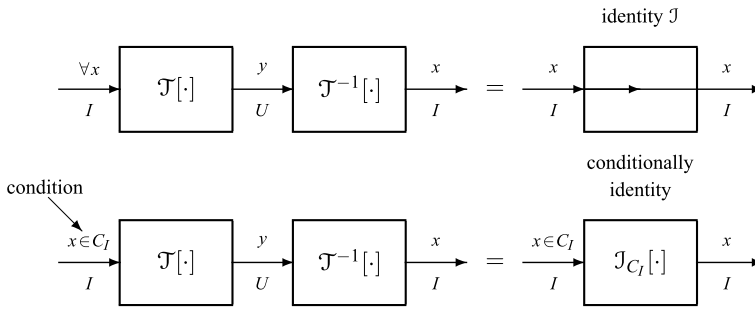


Fig. 6.5 Invertible transformation and conditionally invertible transformation

operator of the *inverse* tf, we must have

$$y = \mathcal{T}[x], \quad x = \mathcal{T}^{-1}[y] \tag{6.7}$$

and, by combination, $x = \mathcal{T}^{-1}\mathcal{T}[x]$. In other words, the cascade of the $I \rightarrow U$ tf followed by the inverse $U \rightarrow I$ tf must be equivalent to the $I \rightarrow I$ identity tf (Fig. 6.5). The invertibility condition can be written as

$$\mathcal{T}^{-1}\mathcal{T} = \mathcal{J}$$

where \mathcal{J} is the identity operator on I . Observe that the concept of invertibility *does not require* the equality of the domains ($I = U$), but it can also be considered for different-domain tfs ($I \neq U$).

The above definition tacitly refers to *unconditional invertibility*, in the sense that relationships (6.7) hold *for every input signal* x , without constraints on the class of the input signals. But sometimes it is convenient to relax the concept by introducing the *conditional invertibility*, where the signal recovery is limited to a given class C_I of input signals. Then, if $x \in C_I$, we find again $\mathcal{T}^{-1}\mathcal{T}[x] = x$, but if $x \notin C_I$, in general $\mathcal{T}^{-1}\mathcal{T}[x] \neq x$. Therefore, the cascade of the conditionally invertible tf followed by its inverse is no more equivalent to the identity on I , but to a *conditional identity* tf. The latter has an operator \mathcal{J}_{C_I} such that the perfect recovery $\mathcal{J}_{C_I}[x] = x$ is ensured only within the class C_I .

A relevant example of a conditionally invertible tf is the down-sampling. In fact, it is not possible to recover a signal from its sampled values unless the signal is band-limited. Therefore, the down-sampling is a conditionally invertible tf, where the condition is the band-limitation. The topic of invertibility will be revisited in Chap. 14 in the context of *generalized transforms*, where the conditional invertibility is formulated with specific statements (see Sect. 14.1).

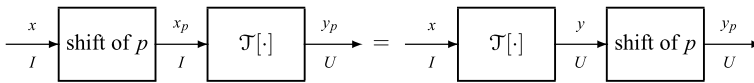


Fig. 6.6 Interpretation of the *shift-invariance* of an $I \rightarrow U$ transformation

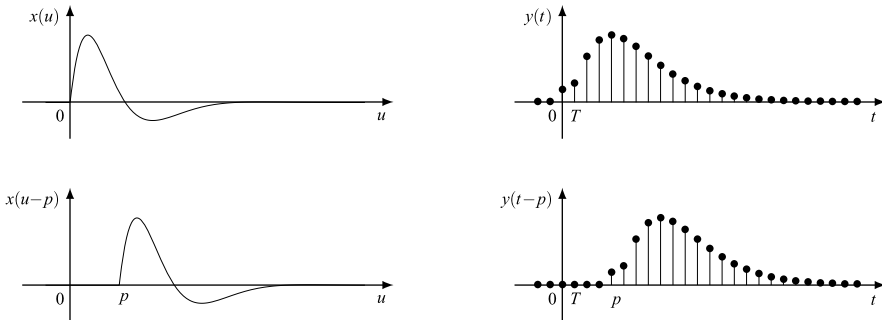


Fig. 6.7 Strict shift-invariance shown for an $\mathbb{R} \rightarrow \mathbb{Z}(T)$ tf. The input signal is shifted by $p = 4T$ and so is the response

6.2.3 Shift-Invariant Transformations

An $I \rightarrow U$ tf is shift-invariant if a shift applied to the input signal yields a shift of the same amount for the output signal, that is,

$$y = \mathcal{T}[x] \Rightarrow y_p = \mathcal{T}[x_p],$$

where $x_p = x(t - p)$ and $y_p = y(t - p)$, with p the shift amount (Fig. 6.6).

This property is illustrated in Fig. 6.7 for an $\mathbb{R} \rightarrow \mathbb{Z}(T)$ tf.

Definition 6.3 Let (I, U, \mathcal{T}) with $I = I_0/P_1$ and $U = U_0/P_2$ and let Π be the set of the shift amounts p such that

$$y = \mathcal{T}[x] \Rightarrow y_p = \mathcal{T}[x_p], \quad p \in \Pi. \tag{6.8}$$

Then, the tf is *shift-invariant on Π* . More specifically, with

$$\begin{aligned} \Pi = I_0 &: \text{strictly shift-invariant (SI);} \\ \Pi \subset I_0 &: \text{periodically shift-invariant (PI);} \\ \Pi = \{0\} &: \text{shift-variant.} \end{aligned} \tag{6.9}$$

Hence, in an SI tf, (6.8) holds for every shift p belonging to the input domain I_0 . In a PI tf, the shift-invariance is limited to a subgroup⁴ Π of I_0 . Finally, when (6.8) holds only for $p = 0$, the tf is shift-variant.

⁴It can be shown that Π is always a group (see Problem 6.3).

There is nothing else to add for equal-domain tfs ($I = U$), but in the general case, some consistency conditions must be added for the formulation of the shift-invariance to be completed. The reason is that a shift amount must belong to both signal domains and we can write $x_p(t) = x(t - p)$ only if $p \in I_0$, and $y_p(t) = y(t - p)$ only if $p \in U_0$. Therefore, Π must be a subgroup of both I_0 and U_0 , that is,

$$\boxed{\Pi \subset I_0 \cap U_0}, \quad (6.10)$$

which assures that, for $p \in \Pi$, both $x_p(t)$ and $y_p(t)$ have meaning. For instance, in an $\mathbb{R} \rightarrow \mathbb{Z}(T)$ tf (see Fig. 6.7), all shifts $p \in \mathbb{R}$ are permitted at the input, whereas at the output p must be a multiple of T , that is, $p \in \mathbb{Z}(T)$, and the shifts permitted at both input and output must belong to the intersection $\mathbb{R} \cap \mathbb{Z}(T) = \mathbb{Z}(T)$. Incidentally, note that this kind of tf cannot be SI since Π may be $\mathbb{Z}(T)$, at most, whereas the SI would require $\Pi = \mathbb{R}$.

When nontrivial periodicities are involved (see (6.4)), (6.10) must be completed by

$$P_1 \cap P_2 \subset \Pi \subset I_0 \cap U_0, \quad (6.11)$$

where P_1 and P_2 are respectively the input and output periodicities. In fact, the input and the output signals have the periodicity $P_1 \cap P_2$ in common, and therefore the shift-invariance is automatically ensured on $P_1 \cap P_2$ by the structure of the pairs I and U .

Finally, we note that conditions (6.10) and (6.11) require that the groups involved are *comparable* to assure that the intersection makes sense (see Sect. 3.9).

6.2.4 Linear Transformations

Definition 6.4 An $I \rightarrow U$ tf is *linear* if its operator \mathcal{L} verifies the two conditions

1. *Homogeneity* stated by

$$\mathcal{L}[cx] = c\mathcal{L}[x], \quad \forall c \in \mathbb{C}; \quad (6.12a)$$

2. *Additivity* stated by

$$\mathcal{L}[x_1 + x_2] = \mathcal{L}[x_1] + \mathcal{L}[x_2]. \quad (6.12b)$$

These two conditions are globally equivalent to the so-called *Superposition Principle* which can be stated as follows

$$\mathcal{L}[c_1x_1 + \cdots + c_nx_n] = c_1\mathcal{L}[x_1] + \cdots + c_n\mathcal{L}[x_n], \quad (6.12c)$$

where c_i are arbitrary complex constants. The superposition principle can be interpreted as follows: if $y_i = \mathcal{L}[x_i]$ denotes the output corresponding to the input

signal x_i , than the linear combination $x = c_1x_1 + \cdots + c_nx_n$ of signals x_i originates an output that is a linear combination of the responses: $y = c_1y_1 + \cdots + c_ny_n$.

Note that linearity does not put constraints on the $I \rightarrow U$ pair and can also be considered for different-domain tfs. The constraint is on the input and output signal classes C_I and C_U that must be *linear spaces* on the field of complex number \mathbb{C} . In fact, the Superposition Principle requires that all linear combinations of signals with complex coefficients be in the signal class both at the input and at the output; this is ensured by the properties of a linear space (see Sect. 4.5).

Linear tfs will be the main topic of the chapter.

UT 6.3 Linear Transformations

Linear tfs are by far the most important class of tfs, and they are used to model physical systems that obey the principle of superposition in the input/output mapping. Also, most of “mathematical” tfs (Fourier tf, Laplace tf, etc.) obey this principle.

6.3.1 Representation of the Operator

Under very general conditions, the operator of an $I \rightarrow U$ linear tf has the following integral representation

$$\mathcal{L} : \quad y(t) = \int_I du h(t, u)x(u), \quad t \in U, \quad (6.13)$$

where the *kernel*⁵ $h(t, u)$ is a complex function, $h : U \times I \rightarrow \mathbb{C}$, which characterizes the tf.

It is easy to check, using the linearity of the Haar integral, that the operator $\mathcal{L}[\cdot]$ represented by (6.13) satisfies the *homogeneity* condition: $\mathcal{L}[cx] = c\mathcal{L}[x]$ and the *additivity* condition $\mathcal{L}[x_1 + x_2] = \mathcal{L}[x_1] + \mathcal{L}[x_2]$. Therefore, a tf with the input–output relationship given by (6.13) verifies the Superposition Principle.

The kernel $h(t, u_0)$ has the following interpretation: By applying at the input the impulse $x(u) = \delta_I(u - u_0)$ and using the sifting property, (6.13) gives

$$\mathcal{L}[\delta_I(\cdot - u_0)|t] = h(t, u_0), \quad (6.14)$$

that is, $h(t, u_0)$ represents the output at time t when the input is given by the impulse centered at time u_0 (Fig. 6.8).

Note that $h(t, u)$, $(t, u) \in U \times I$, is a 2D signal if I and U are 1D, and it is in general an $(m + n)$ D if U is n D and I is m D.

⁵The term “kernel” is used in linear vector spaces with a different meaning.

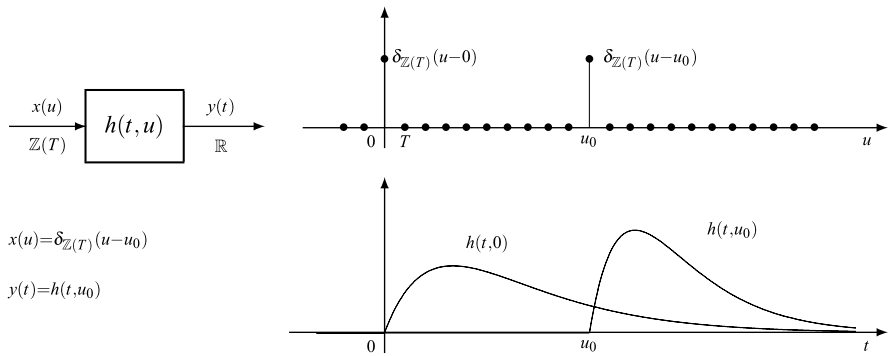


Fig. 6.8 Interpretation of the *impulse response* in a $\mathbb{Z}(T) \rightarrow \mathbb{R}$ linear tf: the application of the impulse $\delta_{\mathbb{Z}(T)}(u - u_0)$ gives as response $h(t, u_0)$

Terminology The function $h(t, u)$ will be called the *kernel* of the linear tf. When the kernel can be expressed in the form $h(t, u) = g(t - u)$, the function $g(t)$ will be called the *impulse response* and its Fourier transform $G(f)$ the *frequency response*. Several authors use impulse response for $h(t, u)$, but we prefer to reserve this term to the function $g(t)$.

Real Linear Transformations In general, $h(t, u)$ is a complex function and we have a complex linear tf. By applying Definition 6.2, it is easy to show that a linear tf is *real* if and only if its kernel $h(t, u)$ is a real function.

6.3.2 Examples of Input–Output Relationships

Linearity does not require that the input and output domains be equal. Each domain may be an ordinary or a quotient group, one-dimensional or multi-dimensional. To clarify the structure of relation (6.13), we develop a few remarkable cases.

For a linear $\mathbb{R} \rightarrow \mathbb{R}$ tf, the integral in (6.13) is an ordinary integral and the kernel h is a function of the continuous times, $t, u \in \mathbb{R}$. For a linear $\mathbb{Z}(T_1) \rightarrow \mathbb{Z}(T_2)$ tf, the integral becomes a summation and the kernel h is a function of the discrete times $t = nT_2, u = mT_1$, namely

$$y(nT_2) = \sum_{m=-\infty}^{+\infty} T_1 h(nT_2, mT_1)x(mT_1), \quad nT_2 \in \mathbb{Z}(T_2). \tag{6.15a}$$

For a linear $\mathbb{R} \rightarrow \mathbb{Z}(T)$ tf, we have

$$y(nT) = \int_{-\infty}^{+\infty} h(nT, u)x(u) du, \quad nT \in \mathbb{Z}(T), \tag{6.15b}$$

where $h(t, u)$ is discrete in t and continuous in u . For a linear $\mathbb{Z}(T) \rightarrow \mathbb{R}$ tf, the relation is

$$y(t) = \sum_{n=-\infty}^{+\infty} T_1 h(t, nT) x(nT), \quad t \in \mathbb{R}. \quad (6.15c)$$

Another example is a linear $\mathbb{R}/\mathbb{Z}(T_p) \rightarrow \mathbb{R}$ tf whose relation is

$$y(t) = \int_{t_0}^{t_0+T_p} h(t, u) x(u) du, \quad t \in \mathbb{R}, \quad (6.15d)$$

where $h(t, u)$ is continuous in both the arguments and periodic of period T_p with respect to u .

Next, consider the 2D $\mathbb{R}^2 \rightarrow \mathbb{Z}(T) \times \mathbb{Z}(T)$ tf, where the relation is

$$y(mT, nT) = \int_{-\infty}^{+\infty} \int_{-\infty}^{+\infty} h(mT, nT; u_1, u_2) x(u_1, u_2) du_1 du_2. \quad (6.15e)$$

In a multidimensional context, a change of signal dimensionality is possible. For instance, for a 1D \rightarrow 3D linear tf on $\mathbb{Z}(T) \rightarrow \mathbb{R}^3$ the relationship is

$$y(t_1, t_2, t_3) = \sum_{n=-\infty}^{+\infty} T h(t_1, t_2, t_3; nT) x(nT), \quad (t_1, t_2, t_3) \in \mathbb{R}^3. \quad (6.15f)$$

This kind of linear tf is encountered in the television reproduction and will be considered in Chap. 17.

6.3.3 Multi-Input Multi-Output (Vector) Linear Transformations

Representation (6.13) holds also for linear tfs with M inputs and N outputs (Fig. 6.9). In this case, the signals and the kernel become matrices, namely

$$y(t) = \int_I du \begin{matrix} N \times 1 \\ h(t, u) \\ N \times M \end{matrix} \begin{matrix} M \times 1 \\ x(u) \\ M \times 1 \end{matrix}, \quad t \in U, \quad (6.16)$$

where

$$\begin{aligned} x(u) &= \begin{bmatrix} x_1(u) \\ \vdots \\ x_M(u) \end{bmatrix}, & y(t) &= \begin{bmatrix} y_1(t) \\ \vdots \\ y_N(t) \end{bmatrix}, \\ h(t, u) &= \begin{bmatrix} h_{11}(t, u) & \cdots & h_{1M}(t, u) \\ \vdots & \ddots & \vdots \\ h_{N1}(t, u) & \cdots & h_{NM}(t, u) \end{bmatrix}, & u \in I, t \in U. \end{aligned} \quad (6.17)$$

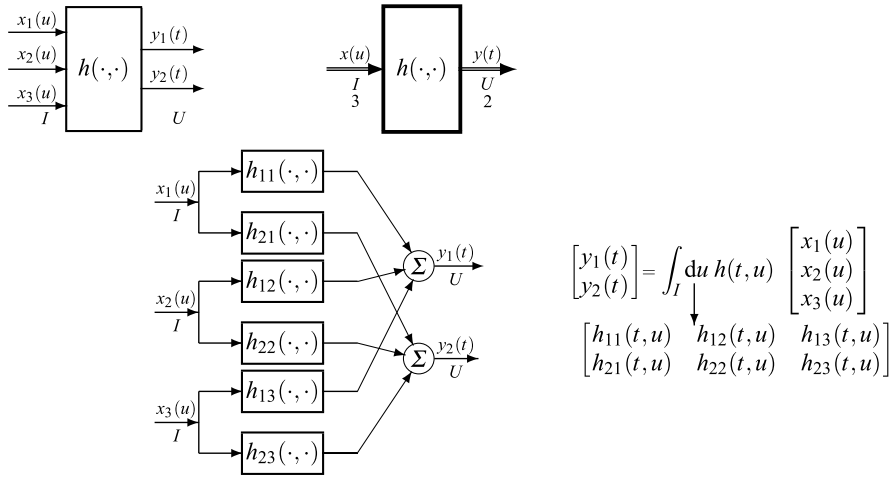


Fig. 6.9 Representation of an $I \rightarrow U$ linear tf with 3 inputs and 2 outputs; synthesis by scalar tfs

Using (6.17) in (6.16), we find the N scalar relationships

$$y_n(t) = \sum_{m=1}^M \int_I du h_{nm}(t, u)x_m(u), \quad n = 1, \dots, N.$$

These relationships permit a *synthesis* of the vector tf as a combination of scalar elementary tfs and interconnections. For instance, with $M = 3$ and $N = 2$ we obtain the synthesis of Fig. 6.9, which consists of $3 \times 2 = 6$ scalar linear tfs connected by $N = 3$ nodes and $M = 2$ adders.

The kernel $h(t, u)$ is an $N \times M$ matrix and cannot be interpreted as impulse response, but works as follows: the r th column ($r = 1, \dots, M$) of $h(t, u_0)$ is the response of the linear tf when the r th input is the impulse $\delta_I(u - u_0)$, and all the other inputs are zero.

6.3.4 Cascade of Linear Transformations: Kernel Composition

The cascade of two or more linear tfs is still a linear tf whose kernel can be calculated from the kernels of the component tfs. To organize the computation in a clear way, it is convenient to indicate the domains of the cascade by $I_1 \rightarrow I_2 \rightarrow I_3$, etc., and the corresponding signal arguments by t_1, t_2, t_3 , etc.

Consider then the cascade of two linear tfs on $I_1 \rightarrow I_2 \rightarrow I_3$ with kernels $h_1(t_2, t_1)$ and $h_2(t_3, t_2)$ (Fig. 6.10). To evaluate the kernel $h(t_3, t_1)$ of the resulting $I_1 \rightarrow I_3$ linear tf, we apply the impulse $x(\cdot) = \delta_{I_1}(\cdot - t_1)$ at the input of the first

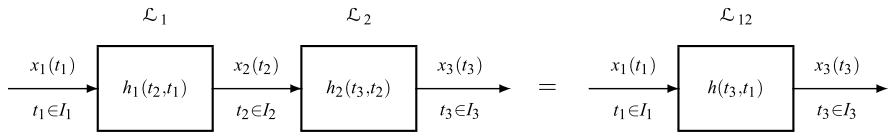


Fig. 6.10 Cascade of two linear tfs and equivalent linear tf

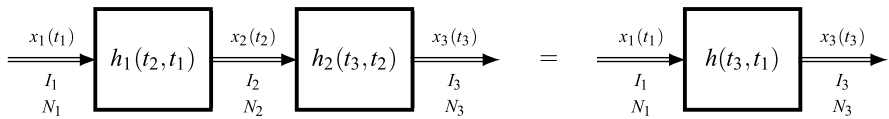


Fig. 6.11 Cascade of two multi-input multi-output linear transformations

linear tf. Then, we obtain $x_2(t_2) = h_1(t_2, t_1)$ in the middle, and the output becomes

$$\begin{aligned}
 x_3(t_3) &= \int_{I_2} dt_2 h_2(t_3, t_2)x_2(t_2) \\
 &= \int_{I_2} dt_2 h_2(t_3, t_2)h_1(t_2, t_1) = h(t_3, t_1), \quad t_3 \in I_3. \quad (6.18a)
 \end{aligned}$$

In fact, recalling the kernel interpretation, $x_3(t_3)$ gives the kernel of the cascade.

Similarly, for the cascade of three linear tfs on $I_1 \rightarrow I_2 \rightarrow I_3 \rightarrow I_4$, we obtain

$$h(t_4, t_1) = \int_{I_3} dt_3 \int_{I_2} dt_2 h_3(t_4, t_3)h_2(t_3, t_2)h_1(t_2, t_1), \quad t_4 \in I_4, t_1 \in I_1. \quad (6.18b)$$

As a mnemonic rule for the cascade of N linear tfs, one has to write the product of all the kernels, where $N + 1$ arguments t_i are involved; then, the kernel is obtained by integrating with respect to the $N - 1$ intermediate arguments.

The above rule holds also for vector tfs, as soon as the kernel composition rule is interpreted in the matrix sense. Figure 6.11 shows the cascade of two vector tfs on $I_1 \rightarrow I_2 \rightarrow I_3$ and vector signals with sizes N_1, N_2 and N_3 , respectively. The resulting $I_1 \rightarrow I_3$ tf has N_1 inputs, N_3 outputs and kernel given by

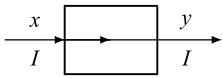
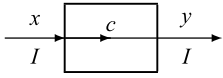
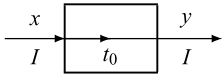
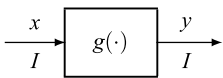
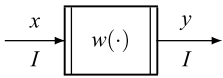
$$\boxed{h(t_3, t_1) = \int_{I_2} dt_2 \begin{matrix} h_2(t_3, t_2) \\ N_3 \times N_2 \end{matrix} \begin{matrix} h_1(t_2, t_1) \\ N_2 \times N_1 \end{matrix}} \quad (6.19)$$

where the integrand is the product of two matrices.

UT 6.4 Variety of Linear Transformations

In this section, we see a few examples of linear tfs, some simple but other less simple, with the purpose of showing the large and articulated variety of this class. Moreover, we will clarify a few misunderstandings that may occur in the interpretation of linearity.

Table 6.1 First examples of linear transformations

Transformation	Symbol	Kernel	Input–output relation
Identity		$\delta_I(t - u)$	$y(t) = x(t), t \in I$
Multiplication by a constant		$c\delta_I(t - u)$	$y(t) = cx(t), t \in I$
Shift		$\delta_I(t - t_0 - u)$	$y(t) = x(t - t_0), t \in I$
Filter		$g(t - u)$	$y(t) = g * x(t), t \in I$
Window		$w(t)\delta_I(t - u)$	$y(t) = w(t)x(t), t \in I$

6.4.1 Examples of Equal-Domain Linear Transformations

In Table 6.1, a few examples of very simple $I \rightarrow I$ tfs are collected. For each tf, we indicate the kernel, the input–output relation and the graphical representation which will be used in the following.

Identity on I It is the most simple tf, which maps any signal on I into itself.

Multiplication by a Constant c This is a linear tf with kernel $c\delta_I(t - u)$, where c is in general a complex constant.

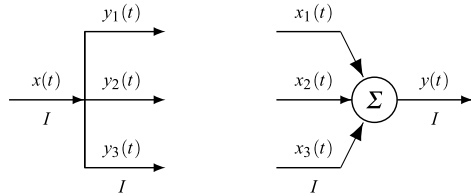
Shift (or Translation of $t_0 \in I$) This tf provides the shifted version of a signal.

Filter The kernel has the form $h(t, u) = g(t - u)$, where $g(t), t \in I$, is the filter *impulse response*. The input–output relation becomes a convolution between the input signal and the impulse response

$$y(t) = \int_I du g(t - u)x(u) = \int_I du g(u)x(t - u), \quad t \in I. \quad (6.20)$$

Note that the three previous tfs are special cases of filters.

Fig. 6.12 Elementary examples of vector linear transformations: *node* and *adder*



Window The input–output relation is $y(t) = x(t) w(t)$, $t \in I$, where $w(t)$ is a given signal defined on I , which gives the window *shape*. This tf generalizes the multiplication by a constant, which becomes a function of time. The kernel has the two alternative forms

$$h(t, u) = \delta_I(t - u) w(u) = \delta_I(t - u) w(t).$$

6.4.2 Examples of Linear Vector Transformations

Usually we refer to scalar tfs, but the generalization to vector tfs requires some effort.

The identity tf requires that the number of outputs equals the number of inputs (M -input M -output identity). Its kernel can be written as

$$h(t, u) = D\delta_I(t - u) \quad (6.21)$$

where $D = [\delta_{mn}]$ is the $M \times M$ identity matrix. Analogously, the M -input M -output shift of t_0 has a kernel given by $h(t, u) = D\delta_I(t - u - t_0)$. A generalization is the tf with different shifts t_m in the M branches, where the kernel has the form

$$h(t, u) = \text{diag}[\delta_I(t - u - t_1), \dots, \delta_I(t - u - t_M)].$$

The multiplication by a constant may have M inputs and N outputs and the “constant” becomes an $N \times M$ matrix of constants $c = \|c_{mn}\|$. In the M -input N -output filters and windows, $g(t)$ and $w(t)$ become $N \times M$ matrices.

Very basic examples of vector tfs are *nodes* and *adders* (Fig. 6.12). A node is a 1-input N -output tf that distributes the input signal to the N outputs. For instance, with $N = 3$ we have

$$y_1(t) = x(t), \quad y_2(t) = x(t), \quad y_3(t) = x(t),$$

which can be written in the standard form (6.17) with

$$x(t) = [x(t)], \quad y(t) = \begin{bmatrix} y_1(t) \\ y_2(t) \\ y_3(t) \end{bmatrix}, \quad h(t, u) = \begin{bmatrix} \delta_I(t - u) \\ \delta_I(t - u) \\ \delta_I(t - u) \end{bmatrix}.$$

An adder is an M -input 1-output tf with relationship (for $M = 3$)

$$y(t) = \sum_{m=1}^3 x_m(t) = \int_I du [\delta_I(t-u), \delta_I(t-u), \delta_I(t-u)] \begin{bmatrix} x_1(u) \\ x_2(u) \\ x_3(u) \end{bmatrix},$$

and therefore the kernel is $h(t, u) = [\delta_I(t-u), \delta_I(t-u), \delta_I(t-u)]$.

6.4.3 Is the Product of Signals a Linear tf?

In a window, the input–output relationship is given by the product

$$y(t) = w(t)x(t);$$

nevertheless, it has been formulated as a linear tf, although we are induced to think that a product implies nonlinearity. As a matter of fact, the *product of two signals* $x_1(t)$ and $x_2(t)$ with relationship

$$y(t) = x_1(t)x_2(t)$$

is a nonlinear tf. In fact, the additivity does not hold since the product of a sum does not equal the sum of the product. But also the homogeneity fails: if we multiply the input signal $\begin{bmatrix} x_1(t) \\ x_2(t) \end{bmatrix}$ by 3, that is, if we apply the signal $3\begin{bmatrix} x_1(t) \\ x_2(t) \end{bmatrix} = \begin{bmatrix} 3x_1(t) \\ 3x_2(t) \end{bmatrix}$, at the output we obtain $9y(t)$, instead of $3y(t)$.

Why is the window linear and the product nonlinear? The mismatch is due to the fact that the window must be regarded as a 1-input 1-output tf, where the shape $w(t)$ is a fixed signal, which is *inaccessible* from the input (it cannot be modified). Therefore, “a multiplication of the input signal by 3” means a multiplication limited to $x(t)$, which becomes $3x(t)$, leaving $w(t)$ unchanged; the final result is therefore $3y(t)$. Instead, a *product* must be intended as a 2-input 1-output tf, and therefore in the additivity check “a multiplication of the input signal by 3” means a multiplication by 3 of both the input components $x_1(t)$ and $x_2(t)$, and the additivity fails.

Another tf is the *tensor product* of signals defined by the relationship

$$y(t_1, t_2) = x_1(t_1)x_2(t_2), \quad t_1 \in I_1, t_2 \in I_2,$$

where $x_1(t_1)$, $t_1 \in I_1$ and $x_2(t_2)$, $t_2 \in I_2$ are 1D signals. The resulting signal $y(t_1, t_2)$ is 2D, with domain $I_1 \times I_2$, and therefore the tf provides a 1D \rightarrow 2D dimensionality conversion (see Chap. 16).

6.4.4 Transformations of the Signal Argument

The relation

$$y(t) = x(\beta t) \quad (a \neq 0)$$

represents a *scale change* of the signal argument, which will be studied in the next section. It formulates a first example of tf in which the output signal is obtained by *modifying the argument of the input signal*. Other relations in which the signal argument is modified may be $y(t) = x(t^2)$, or $y(t) = x(\sin \omega_0 t)$ and, more generally

$$y(t) = x(\beta(t)), \quad (6.22)$$

where $\beta(t)$ is a given real function.

At first glance, when the argument function $\beta(t)$ is nonlinear, such transformations may seem to be nonlinear, but this is a wrong impression: they are linear! In fact, if we multiply the input signal $x(t)$ by a constant c , at the output we obtain the signal $cx(\beta(t)) = cy(t)$ and the homogeneity condition holds. If $x(u)$ is decomposed as $x_1(u) + x_2(u)$, at the output we obtain $x_1(\beta(t)) + x_2(\beta(t)) = x(\beta(t))$ and also the additivity holds.

In conclusion, the tf is linear, and we can write its kernel explicitly. In fact, the kernel $h(t, u_0)$ can be identified as the response to the impulse $\delta_I(u - u_0)$, and, with $x(u) = \delta_I(u - u_0)$ from (6.22) we obtain $y(t) = \delta_I(\beta(t) - u_0)$. Hence

$$h(t, u_0) = \delta_I(\beta(t) - u_0). \quad (6.23)$$

For such tfs, it remains to investigate the domains and the nature of the function $\beta(t)$, which must be compatible with the input domain I to assure that the expression $x(\beta(t))$, $t \in I$, makes sense. A special case is when the argument function defines a group isomorphism (see Sect. 3.3), $\beta : I \sim U$, which states that the output domain is the isomorphic group $U = \beta(I)$.

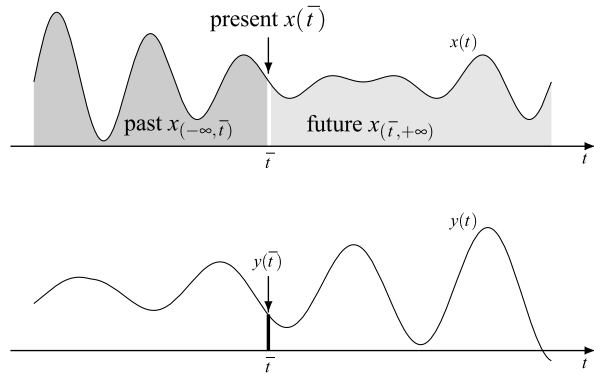
A Further Example of Linear Transformation In the overview of linear tfs, we have seen “simple” and also “very simple” tfs. To remove the impression that all linear tfs are of this kind, we now formulate a very articulate example, where input and output signals have a very different nature. Consider the model of a video camera, whose purpose is transforming a time-varying image into an electrical voltage, called the *video* signal. The input is a 3D signal, $\ell(x, y, t)$, with x, y the spatial coordinates and t the time, representing the time-varying image, and the output is the 1D video signal $u(t)$. Then, the tf has the format $\mathbb{R}^3 \rightarrow \mathbb{R}$ with a 3D \rightarrow 1D dimensionality change. We claim that this is a linear tf with the following input–output relationship

$$u(t) = \sum_{n=0}^{N-1} \sum_{k=-\infty}^{+\infty} \int_0^{D_x} \int_0^{D_y} \ell(v_x(t - nT_r - kT_q) - x, v_y(t - nT_r - kT_q) - y, t) dx dy$$

where $N, D_x, D_y, v_x, v_y, T_r, T_q$ are specific parameters of television scanning and, in particular, N is the number of lines per picture (see Chap. 17).

Here, we do not enter into the details of television scanning, but our purpose is to give the reader the impression that even a very complicated operation can be formulated with the theory of linear tfs.

Fig. 6.13 Partitioning of the input signal into “past”, “present” and “future”, with respect to time \bar{t} , for the output signal evaluation at the same time \bar{t}



6.4.5 Generalized Transforms

Transformations are introduced as mathematical models to represent systems of the real world. However, they can also be used to formulate “mathematical” transformations to obtain alternative signal representations. Such transformations are always linear and also invertible (to preserve signal information). We call them *generalized transforms*.

A first example is the Fourier transform, which, formulated as a transformation, has the form $(I, \hat{I}, \mathcal{F})$, where the output domain is the dual group \hat{I} and \mathcal{F} is the operator defined by the Fourier kernel $\psi^*(f, t)$. The inverse transformation is $(\hat{I}, I, \mathcal{F}^{-1})$, where \mathcal{F}^{-1} has kernel $\psi(f, t)$.

Other examples are the Laplace transform (see Chap. 9), the z transform (see Chap. 11) and the Hilbert transform (see Chap. 9 and Chap. 11). Further examples are the Radon transform, used for tomography [5] (see Chap. 17), the Hankel transform [4], the Mellin transform [1] (see Chap. 16), and the wavelet transform (see [2, 7] and Chap. 15).

The theory of generalized transforms will be developed in Chap. 14 in the context of wavelets and multiresolution analysis.

6.5 Other General Topics on Transformations

The groups of \mathbb{R} and \mathbb{R}^m , based on the ordinary addition, are also equipped with multiplication, which permits the introduction of the *scale change* on \mathbb{R} , which becomes a *coordinate change* in \mathbb{R}^m . Moreover, when the domain \mathbb{R} is interpreted as *time* domain, we can introduce the concept of *past* and *future*.

6.5.1 Causal and Anticipatory Transformations on \mathbb{R}

For systems operating on the “real” time, where “real” is in opposition to “virtual”, the constraint of *causality* holds. Broadly speaking, causality means that the effect

must follow the cause and, in the context of signals, that the output signal (effect) *cannot begin before the application* of the input signal (cause). In a transformation, this constraint must be explicitly introduced. As discussed in Sect. 6.1, this is one of the main differences with respect to a *system*, a model where causality is inside the definition.

The definition of causality requires that, given two points t_1 and t_2 of the signal domain, we can state that t_1 is “before” t_2 or “after” t_2 , that is, $t_1 < t_2$ or $t_1 > t_2$. Of course, this ordering is possible on \mathbb{R} , and also on $\mathbb{Z}(T)$, but not on \mathbb{R}^m for $m \geq 2$.

With reference to the time axis $\mathbb{R} = (-\infty, +\infty)$ and for a fixed time \bar{t} , we introduce the partition

$$\text{past} = (-\infty, \bar{t}), \quad \text{present} = \bar{t}, \quad \text{future} = (\bar{t}, +\infty).$$

Correspondingly, for a signal $x(t)$, $t \in \mathbb{R}$, we subdivide its evolution into (Fig. 6.13)

$$\text{past} = x_{(-\infty, \bar{t})}, \quad \text{present} = x(\bar{t}), \quad \text{future} = x_{(\bar{t}, +\infty)},$$

and denote the whole signal evolution by $x_{(-\infty, +\infty)}$. The same subdivision can be done on the discrete domain $\mathbb{Z}(T)$ for every $\bar{t} \in \mathbb{Z}(T)$.

Now, consider a general $I \rightarrow U$ tf, with $I, U \in \mathcal{G}(\mathbb{R})$, and write the input–output relations in the form

$$y(\bar{t}) = \mathcal{T}[x_{(-\infty, +\infty)} | \bar{t}], \quad \bar{t} \in U \quad (6.24)$$

to remark that the output value $y(\bar{t})$ at time \bar{t} depends on the whole input evolution $x_{(-\infty, +\infty)}$, comprising the past $x_{(-\infty, \bar{t})}$, the present $x(\bar{t})$, and the future $x_{(\bar{t}, +\infty)}$. Then, the tf is *causal* if the dependence of $y(\bar{t})$ is limited to the past and to the present, that is,

$$\boxed{y(\bar{t}) = \mathcal{T}[x_{(-\infty, \bar{t}]} | \bar{t}], \quad \forall \bar{t} \in U.} \quad (6.25)$$

If $y(\bar{t})$ also depends on the future, the tf is said *anticipatory*.

A refinement on the classification is the following. If the dependence of $y(\bar{t})$ is only limited to the present $x(\bar{t})$, the tf is *instantaneous* or *memoryless* (see Sect. 6.6). If the dependence is limited to a finite portion $x_{[t_0, \bar{t}]}$, the tf has a *finite memory* expressed by $\text{meas}[t_0, \bar{t}]$.

In conclusion, for a correct modeling of tfs working in the real time, we have to introduce the causality condition (6.25). However, in theoretical considerations, we often encounter important examples of anticipatory tfs as (see Sect. 6.15).

Causality for Linear Transformations

For a $I \rightarrow U$ linear tf on the groups of \mathbb{R} , the causality condition can be stated for the kernel $h(t, u)$ and takes the form

$$\boxed{h(t, u) = 0, \quad t < u.} \quad (6.26)$$

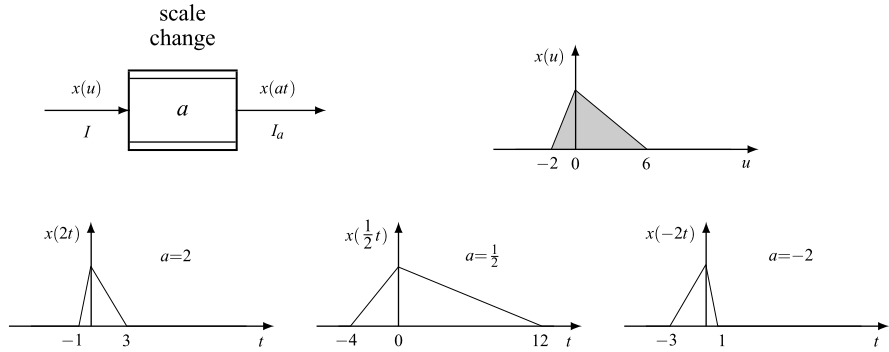


Fig. 6.14 Graphical symbol for scale change and elementary examples on \mathbb{R}

This is a necessary and sufficient condition for causality, as turns out from the interpretation of $h(t, u_0)$, that is, the response to the impulse $\delta_I(u - u_0)$. In fact, by contradiction, if $h(t, u_0) \neq 0$ for some $t < u_0$, the tf response would be different from zero before the impulse application at $u = u_0$, and therefore would be anticipatory. In Fig. 6.8, which refers to a $\mathbb{Z}(T) \rightarrow \mathbb{R}$ linear tf, the causality condition is verified.

For linear tfs whose kernel has the form $h(t, u) = g(t - u)$, where $g(t)$ is the impulse response, the causality condition (6.26) becomes

$$\boxed{g(t) = 0, \quad t < 0,} \tag{6.27}$$

that is, $g(t)$ must be a *causal signal*.

6.5.2 Scale Change on the 1D Groups

Let $x(t), t \in I$, be a signal with $I \in \mathcal{G}(\mathbb{R})$. Then, the relation

$$y(t) = x(at), \quad t \in I_a, \quad a > 0 \tag{6.28}$$

defines a time-scale change, more precisely:

- For $a > 1$ a *time-compression*,
- For $a < 1$ a *time-expansion*.

For $a < 0$, the scale change is combined with a time reverse, as shown in Fig. 6.14 for a triangular signal.

A scale change may be formulated as an $I \rightarrow I_a$ linear tf, with the kernel given by (see (6.23))

$$h(t, u) = \delta_I(at - u), \tag{6.29}$$

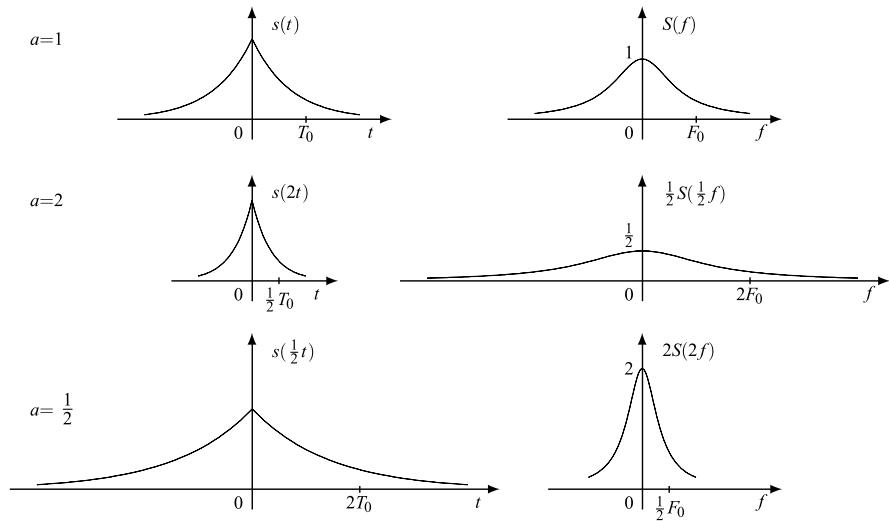


Fig. 6.15 Time compression (expansion) and consequent frequency expansion (compression) for $I = \mathbb{R}$

and the output domain given by

$$I_a = \{t|at \in I\}. \tag{6.30}$$

Hence, if $I = \mathbb{R}$, so is $I_a = \mathbb{R}$. For a discrete-time signal $x(v)$, $v \in \mathbb{Z}(T)$, the scale change $v = at \in \mathbb{Z}(T)$ implies a spacing change. In fact, letting $v = nT$, we obtain $t = v/a = nT/a \in \mathbb{Z}(T/a)$, so the original spacing T becomes T/a . A scale change modifies periodicity, and, using the unified notation, we see that $I = \mathbb{Z}(T)/\mathbb{Z}(T_p)$ is modified into $I_a = \mathbb{Z}(\frac{1}{a}T)/\mathbb{Z}(\frac{1}{a}T_p)$.

As seen in Sect. 5.9, a scale change in the time domain gives a scale change in the frequency domain, but with a reciprocal factor, specifically

$$Y(f) = (1/a)X(f/a), \quad f \in \widehat{I}_a. \tag{6.31}$$

Thus, a time expansion becomes a frequency compression, and vice versa, as shown in Fig. 6.15 for $I = \mathbb{R}$ and in Fig. 6.16 for $I = \mathbb{Z}(T)$.

6.5.3 Coordinate Change in \mathbb{R}^m

The scale change in \mathbb{R}^m becomes a *coordinate* change with relation

$$y(\mathbf{t}) = x(\mathbf{a}\mathbf{t}), \quad \mathbf{t} \in I_{\mathbf{a}}, \tag{6.32}$$

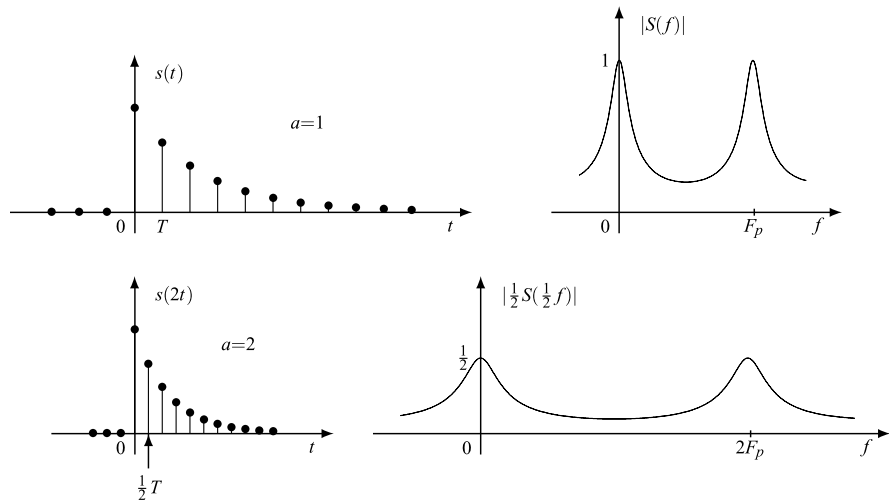


Fig. 6.16 Time compression and consequent frequency expansion for $I = \mathbb{Z}(T)$

where $\mathbf{a} = [a_{r,s}]$ is a non-singular $m \times m$ real matrix, and the signal arguments are related by

$$\mathbf{u} = \mathbf{a}\mathbf{t}, \quad \mathbf{t} = \mathbf{a}^{-1}\mathbf{u} \tag{6.33}$$

with \mathbf{u} the input argument and \mathbf{t} the output argument.

We have seen in Sect. 4.3 that a coordinate change modifies the domain/periodicity pair $I = I_0/P$ into $I_{0\mathbf{a}}/P_{\mathbf{a}}$, where

$$I_{0\mathbf{a}} = \{\mathbf{t} \mid \mathbf{a}\mathbf{t} \in I_0\} = \mathbf{a}I_0, \quad P_{\mathbf{a}} = \{\mathbf{t} \mid \mathbf{a}\mathbf{t} \in P\} = \mathbf{a}P.$$

A coordinate change can be modeled as an $I \rightarrow I_{\mathbf{a}}$ linear tf with the kernel (see Sect. 6.4)

$$h(\mathbf{t}, \mathbf{u}) = \delta_I(\mathbf{a}\mathbf{t} - \mathbf{u}).$$

In the frequency domain, relationship (6.32) becomes (see Sect. 5.9)

$$Y(\mathbf{f}) = \frac{1}{d(\mathbf{a})} X(\mathbf{a}^*\mathbf{f}), \quad \mathbf{f} \in I_{\mathbf{a}},$$

where \mathbf{a}^* is the inverse transpose of \mathbf{a} and $d(\mathbf{A}) = |\det(\mathbf{A})|$. Then, apart from the scale factor, we find that in the frequency domain we have a coordinate change with matrix \mathbf{a}^* instead of \mathbf{a} , as illustrated in Fig. 6.17.

UT 6.6 Nonlinear Transformations

It is very difficult to offer a systematic and complete framework for nonlinear tfs. We consider here only two classes of nonlinear transformations.

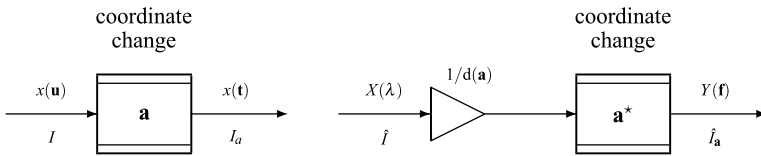


Fig. 6.17 Coordinate change on a signal and corresponding coordinate change on the Fourier transform

6.6.1 Nonlinear Transformations Without Memory

This is the simplest class of nonlinear tfs with equal domains ($I \rightarrow I$). The input-output relation has the form

$$y(t) = \mu[x(t)], \quad t \in I. \tag{6.34}$$

where $\mu[\cdot]$ is a function, called the *characteristic*, which specifies the tf. According to (6.34), the output signal value at time t depends only on the input signal value at the same time t . For this reason, the tf is said to be *without memory* or *instantaneous*. In several applications, $\mu(\cdot)$ is a polynomial, in others it is a piecewise function, as in the case of quantizers.

Figure 6.18 shows a few examples of nonlinear characteristics, which are commonly used to “rectify” a signal on $I = \mathbb{R}$. The figure also shows how a sinusoidal signal is modified by such rectifiers.

In the general case, the characteristic may be time-dependent, and the input-output relation becomes

$$y(t) = \mu[x(t), t], \quad t \in I. \tag{6.35}$$

An example of form (6.34) is $y(t) = x^2(t)$ or $y(t) = \text{sgn}[x(t)]$, while an example of (6.35) is $y(t) = [x(t) \cos \omega_0 t]^3$.

⇓ 6.6.2 Volterra Transformations

A more articulated class of nonlinear tfs of the general form $I \rightarrow U$ is given by *Volterra tfs*, where the output signal is the sum of a (Volterra) series

$$y(t) = y_1(t) + y_2(t) + y_3(t) + \dots \tag{6.36}$$

where (Fig. 6.19)

$$y_1(t) = \int_I du h_1(t, u)x(u), \quad t \in U,$$

$$y_2(t) = \int_I du_1 \int_I du_2 h_2(t, u_1, u_2)x(u_1)x(u_2),$$

Fig. 6.18 Nonlinear characteristics of “rectifier” type and corresponding responses to a sinusoidal input

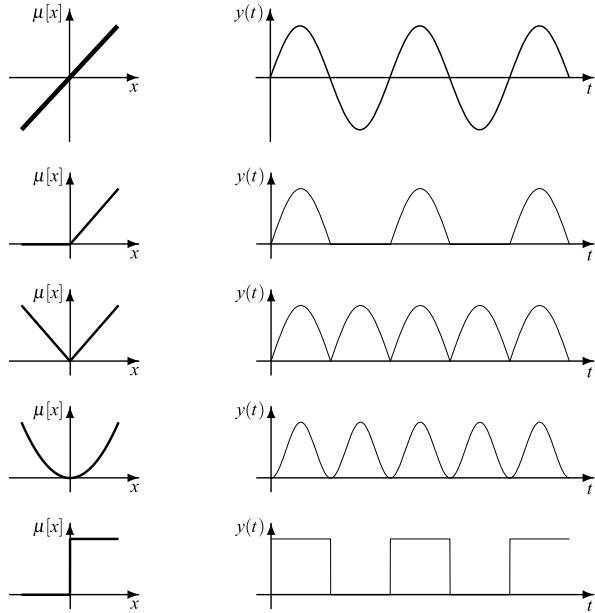
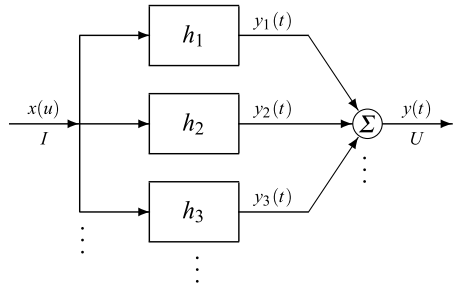


Fig. 6.19 $I \rightarrow U$ Volterra transformation



$$y_3(t) = \int_I du_1 \int_I du_2 \int_I du_3 h_3(t, u_1, u_2, u_3)x(u_1)x(u_2)x(u_3),$$

and h_1, h_2, h_3, \dots are the kernels that characterize the tf. The first output term y_1 is obtained from the input signal by a linear tf, while from the second on, the relation is not linear and the global relation is nonlinear.

In some cases, the sum has a finite number of terms (finite-order Volterra tfs). For instance, a filter with impulse response $g(t)$ followed by an instantaneous nonlinear tf with characteristic $\mu(x) = x^2$ can be represented as a Volterra tf of order two with the kernel

$$h_2(t, u_1, u_2) = g(t - u_1)g(t - u_2).$$

More generally, when μ is a polynomial with degree N , the Volterra tf becomes of order N .

Similarly to linear tfs, Volterra tfs can be defined on an arbitrary domain pair $I \rightarrow U$.

UT 6.7 Shift-Invariance in Linear Transformations

We apply the general definition of shift-invariance to linear tfs, where the degree of invariance will depend on the three objects, I , U and h , which specify a linear tf.

6.7.1 Periodical Shift-Invariance (PI)

We begin with this kind of shift-invariance because it represents the general case, including the SI with $\Pi = I_0$ and the shift-variance with $\Pi = \{0\}$.

Let $I = I_0/P_1$ and $U = U_0/P_2$ be *comparable* domains (see Sect. 3.9) and let Π be a subgroup of $I_0 \cap U_0$. Then, the PI on Π implies that

$$y = \mathcal{L}[x] \implies y_p = \mathcal{L}[x_p], \quad p \in \Pi. \quad (6.37)$$

For linear tfs in Appendix A, we prove

Theorem 6.1 *An $I \rightarrow U$ tf with kernel $h(t, u)$ is periodic shift-invariant (PI) on $\Pi \subset I_0 \cap U_0$ if and only if*

$$h(t + p, u + p) = h(t, u), \quad \forall p \in \Pi. \quad (6.38)$$

Condition (6.37) represents a *diagonal* form of periodicity for the kernel. If we regard $h(t, u)$ as a $2m$ D signal defined on the Cartesian product $U \times I$, we find that the periodicity stated by (6.38) is given by the $2m$ D subset of $U \times I$

$$\Pi_2 = \{(p, p) | p \in \Pi\}.$$

This set is not separable, but of *diagonal* type, and was classified in Sect. 3.7 as a lattice with a *reduced dimensionality*; in particular, if I and U are 1D, Π_2 is a 1D lattice in \mathbb{R}^2 . This lattice is illustrated in Fig. 6.20 in two 1D cases: on the left, with $I = \mathbb{Z}(3)$, $U = \mathbb{Z}(3)$ and $\Pi = \mathbb{Z}(12)$, the diagonal periodicity is $\Pi_2 = \mathbb{Z}\mathbb{O}(12, 12)$; on the right, with $I = \mathbb{Z}(3)$, $U = \mathbb{Z}(5)$ and $\Pi = \mathbb{Z}(15)$, the periodicity is $\Pi_2 = \mathbb{Z}\mathbb{O}(15, 15)$.

The diagonal form of periodicity is one of the main difficulties in the study of PIL tfs, particularly in the multirate case ($I \neq U$).

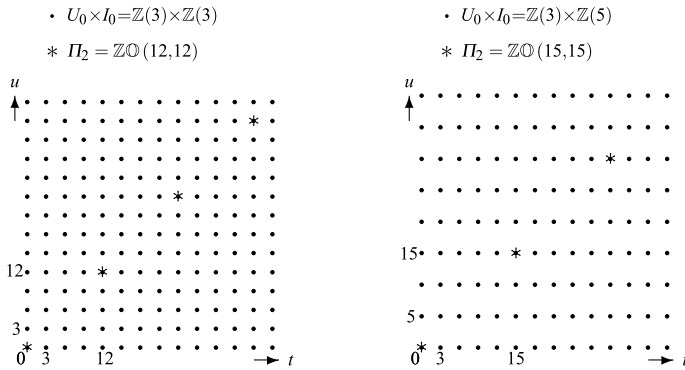


Fig. 6.20 Diagonal periodicity of the kernel $h(t, u)$ of a PIL transformation

6.7.2 Strict Shift-Invariance (SI)

The SI forces the condition (6.37) to hold for every shift p permitted at the input, $p \in I_0$, and the condition (6.38) to hold with $\Pi = I_0$, that is,

$$h(t + p, u + p) = h(t, u), \quad \forall p \in I_0.$$

A detailed analysis of this condition carried out in Appendix B leads to the conclusion that the kernel $h(t, u)$ must depend only on the difference $t - u$ of the arguments, and therefore it can be written as

$$h(t, u) = g(t - u) \tag{6.39}$$

for a convenient function $g(\cdot)$. Now, recalling the consistency condition (6.10), we have:

Theorem 6.2 *An $I \rightarrow U$ linear tf, with $I = I_0/P$ and $U = U_0/P$, is strictly shift-invariant (SI) if*

1. $I_0 \subset I_0 \cap U_0$, that is, $I_0 \subset U_0$.
2. The kernel has the form $h(t, u) = g(t - u)$.

For a SI linear tf, the input–output relationship becomes

$$y(t) = \int_I du g(t - u)x(u), \quad t \in U. \tag{6.40}$$

As we shall see in the following, the domain D of the function $g(v)$ may be different from both I and U , and therefore (6.40) does not represent a convolution. When $I = U$, it becomes a convolution, $y(t) = g * x(t)$, and the linear tf turns out to be a filter on I .

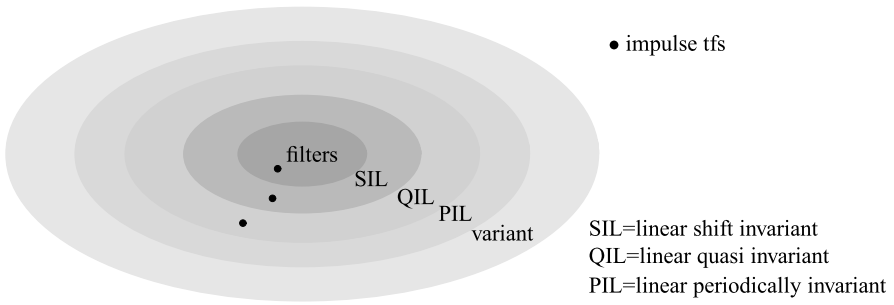


Fig. 6.21 Classification of linear transformations based on shift-invariance

6.7.3 Quasi Shift-Invariance (QI)

In Theorem 6.2, the SI requires two conditions: the compatibility condition $I_0 \subset U_0$ and the condition on the kernel

$$h(t, u) = g(t - u), \quad t \in U, u \in I. \tag{6.41}$$

It may happen (and *really* happens in several important cases) that the kernel verifies condition (6.41), but the domains fail the compatibility condition.

Condition (6.41), with or without compatibility, allows the introduction of a very broad and important class of linear tfs, which we call *quasi-invariant linear (QIL) tfs*. Here, “quasi” remarks the fact that the kernel exhibits the form adequate for SI, but the tf may be not SI (when $I_0 \not\subset I_0 \cap U_0$). A QIL tf may be regarded as a PI with a periodicity given by $\Pi_0 = I_0 \cap U_0$. In fact (see Appendix B for the proof),

Theorem 6.3 *An $I \rightarrow U$ linear tf is QI if it is PI with periodicity given by*

$$\Pi_0 = I_0 \cap U_0. \tag{6.42}$$

Note that (6.42) is the maximal periodicity permitted on the given domains. QIL tfs represent the main category of linear tfs and most of the chapter will be devoted to them.

Summary of Shift-Invariance and Classification

To summarize the previous definitions, it is convenient to classify linear tfs on the basis of shift-invariance, as shown in Fig. 6.21.

In the general case, the kernel $h(t, u)$ is an arbitrary complex function defined on $U \times I$ with no specific properties; also the domains I and U are arbitrary with no mutual constraints. When I and U become *rationally comparable*, the periodic invariance (PI) can be considered. Specifically, a linear tf is PI with periodicity Π

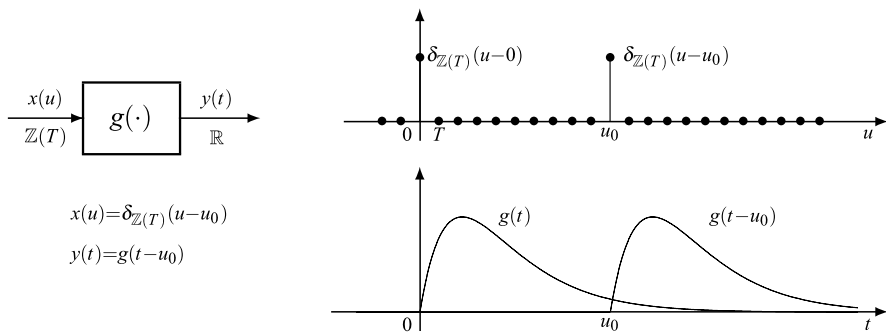


Fig. 6.22 Interpretation of the impulse response of a $\mathbb{Z}(T) \rightarrow \mathbb{R}$ transformation

if Π is a subgroup of $I_0 \cap U_0$, and the kernel verifies the condition (6.38). When the periodicity Π reaches the maximum admissible size $\Pi_0 = I_0 \cap U_0$, the linear tf becomes quasi-invariant (QI) and the kernel assumes the form $h(t, u) = g(t - u)$ (see Theorem 6.3). Finally, when $h(t, u) = g(t - u)$ and $\Pi_0 = I_0 \cap U_0 = I_0$, we have the strict invariance (SI).

In conclusion, QI tfs are a subclass of PI tfs, and SI tfs are a subclass of QI tfs. Finally, filters are a subclass of SI tfs. Impulse tfs indicated in Fig. 6.21 will be introduced later in Sect. 6.9.

UT 6.8 Quasi-Invariant Linear Transformations

6.8.1 Definition

The definition of QIL tfs has been motivated in Sect. 6.7 and is now formalized.

Definition 6.5 An $I \rightarrow U$ linear tf, where I and U are rationally comparable domains, is said to be *quasi-invariant linear* (QIL) if its kernel can be written in the form

$$h(t, u) = g(t - u), \quad t \in U, u \in I, \tag{6.43}$$

that is, if it depends only on the difference of the arguments.

The input–output relation of a QIL tf is therefore

$$\boxed{y(t) = \int_I du g(t - u)x(u), \quad t \in U.} \tag{6.44}$$

The function $g(t)$, $t \in D$, whose domain is given by the sum $I + U$ as stated below will be called *impulse response*. A QIL tf will be represented with the graphical symbol of Fig. 6.22.

Note that the input–output relation (6.44) resembles a convolution, but it is really a convolution only when the domains are equal. The interpretation of this relation is very articulated and will become clear only after the Decomposition Theorem of Sect. 6.11.

6.8.2 Domain of the Impulse Response and Periodicity

The impulse response $g(v)$ has been introduced in the form $g(t - u)$, $t \in U$, $u \in I$ (see (6.43)), and we now establish its domain D_0 and its periodicity P .

In general, I and U are quotient groups

$$I = I_0/P_1, \quad U = U_0/P_2. \quad (6.45)$$

Note that the difference $t - u = t + (-u)$ with $u \in I$ and $t \in U$ implies that the two groups have the same operation in common, and this is ensured if I and U are subgroups of a same group, that is, if I_0 and U_0 are *comparable* (see Sect. 3.9). The domain of the function $g(t - u)$ is the set

$$\begin{aligned} \{t - u \mid t \in U_0, u \in I_0\} &= \{t + u \mid t \in U_0, u \in -I_0\} \\ &= U_0 + (-I_0) = U_0 + I_0, \end{aligned}$$

that is, the *sum*

$$D_0 = I_0 + U_0. \quad (6.46a)$$

Furthermore, we want that the sum $D_0 = I_0 + U_0$ be an LCA group, and this requires that I_0 and U_0 be rationally comparable (see again Sect. 3.9).

As regards the periodicity of $g(t - u)$, we note that in the input–output relation (6.44), $x(u)$ has periodicity P_1 and $y(t)$ has periodicity P_2 . Hence, $x(u - p_1) = x(u)$ for $p_1 \in P_1$ and $y(t - p_2) = y(t)$ for $p_2 \in P_2$, and from (6.44) we find

$$y(t) = \int_I du g(t - p_2 - u + p_1)x(u) = \int_I du g(t - u)x(u),$$

for every $p_1 \in P_1$, $p_2 \in P_2$ and for every input signal. Therefore, the condition becomes

$$g(t - p_2 - u + p_1) = g(t - u), \quad p_1 \in P_1, p_2 \in P_2,$$

which states that periodicity of the impulse response is given by

$$P = P_1 + P_2. \quad (6.46b)$$

In conclusion, in a QIL tf with domain/periodicities given by (6.46a), (6.46b), (6.46c), the impulse response has the domain given by the sum of the domains and

periodicity given by the sum of the periodicities. If we define the sum of two quotient groups as done in Sect. 3.9, that is,

$$D = I + U \triangleq (I_0 + U_0)/(P_1 + P_2), \tag{6.46c}$$

we conclude that the impulse response $g(v)$ of $I \rightarrow U$ QIL tf is “defined” on the sum $I + U$ of the input and output “domains”.

Note that in general D may be different from both I and U .

6.8.3 Ordering and Classification of QIL tfs

In the theory of QIL tfs, a fundamental role is played by the *ordering* of the input domain I with respect to the output domain U . We first consider the case of *ordinary* domains, neglecting the periodicity. Then, the ordering may be

- $I = U$: equal domain
- $I \subset U$: upward
- $I \supset U$: downward
- $I \not\subset U, I \not\supset U$: unordered.

In the first three cases, the tfs are *ordered*, and in the latter case the tfs are *unordered*. For instance, $\mathbb{Z}(6) \rightarrow \mathbb{Z}(2)$ and $\mathbb{Z}(10) \rightarrow \mathbb{R}$ are upward, whereas $\mathbb{R} \rightarrow \mathbb{Z}(10)$ and $\mathbb{Z}(3) \rightarrow \mathbb{Z}(15)$ are downward, but the pair $\mathbb{Z}(5) \rightarrow \mathbb{Z}(12)$ is unordered, because $\mathbb{Z}(5)$ is not a subgroup of $\mathbb{Z}(12)$ and $\mathbb{Z}(12)$ is not a subgroup of $\mathbb{Z}(5)$.

The four cases listed above permit the introduction of as many classes of QIL tfs, namely *filters*, *interpolators*, *decimators* and *fractional interpolators*, as shown in Table 6.2 where for each class we use a specific graphical representation. The ordering determines the domain D of the impulse response $g(v)$: in *upward* tfs ($I \subset U$), we have $D = U$, in *downward* tfs ($I \supset U$), $D = I$. In any case, in *ordered* tfs, the domain D is the largest of the two groups, that is,

$$D = \max(I, U) \quad (I, U \text{ ordered}), \tag{6.47}$$

whereas in *unordered* tf D , it is different from both I and U .

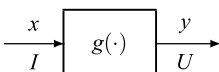
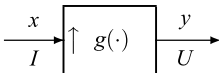
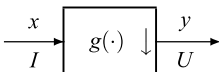
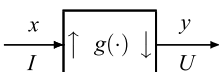
The ordering determines also the shift-invariance. If $I \subseteq U$, the SI condition $I \cap U = I$ holds, while in the other cases it does not hold and the tf is PI with periodicity $P_0 = I \cap U$, as shown in Table 6.2.

The classification of QIL tfs according to quotient groups is more articulated, but less interesting; the ordering $I \subset U$ has to be interpreted in the sense $I_0/P_1 \subset U_0/P_2 \iff I_0 \subset U_0, P_1 \subset P_2$, and similarly for the ordering $I \supset U$.

Domain Complexity of a QIL tf QIL tf involves three domains (interpreted as the domain/periodicity pairs): the *outer* domains I and U , and the *inner* domain $D = I + U$, which is the largest one. In fact,

$$D \supset I \quad \text{and} \quad D \supset U.$$

Table 6.2 Types of quasi-invariant linear (QIL) transformations

Transformation	Symbol	Ordering	$D = I + U$	$P = I \cap U$	Invariance
Filter		$I = U$	I	I	SI
Interpolator		$I \subset U$	U	I	SI
Decimator		$I \supset U$	I	U	PI
Fractional interpolator		$I \not\subset U$ $I \not\supset U$	$I + U$	$I \cap U$	PI

The tf starts on I and arrives at U , passing through the inner domain D , and in each passage the domain/periodicity may change. Considering in general quotient groups, $I = I_0/P_1$, $D = D_0/P$ and $U = U_0/P_2$, the simplest case is $I = D = U$, that is,

$$I_0 = D_0 = U_0, \quad P_1 = P = P_2, \tag{6.48a}$$

and the most articulated case is

$$I_0 \neq D_0 \neq U_0, \quad P_1 \neq P \neq P_2, \tag{6.48b}$$

where both the domains and the periodicities change.

Then, we define the *domain complexity* c of a QIL tf as the *number of diversities* \neq encountered in the above sequences, with the limit cases of (6.48a), where the complexity is $c = 0$, and of (6.48b), where the complexity is $c = 4$. As an example, in a $\mathbb{Z}(2)/\mathbb{Z}(20) \rightarrow \mathbb{R}/\mathbb{Z}(15)$ tf, the inner domain is $D = \mathbb{R}/\mathbb{Z}(5)$, and the sequence is $\mathbb{Z}(2) \neq \mathbb{R} = \mathbb{R}$, $\mathbb{Z}(20) \neq \mathbb{Z}(5) \neq \mathbb{Z}(15)$, and therefore the complexity is $c = 3$. The true meaning of the complexity c will be clear in Decomposition Theorem (see Sect. 6.11).

6.8.4 Identification of QIL Transformations

We have already remarked that QIL tfs are very articulated objects, as now confirmed in their identification.

In a QIL tf with equal domains (filter), the input–output relationship is a convolution $y(t) = g * x(t)$, $t \in I$. Then, if we let $x(u) = \delta_I(u)$, we find that the output is $y(t) = g(t)$. Therefore, $g(v)$ is really the *impulse response*, interpreted as the response of the filter to the impulse applied at the origin.

In general, the interpretation is not so simple, and the impulse response must be viewed as a *collection* of responses. For instance, in an $\mathbb{R} \rightarrow \mathbb{Z}(T)$ QIL tf (a decimator) the impulse response $g(t)$ is defined on \mathbb{R} and cannot be obtained as a single “output”, because the output signal is discrete. In this case, the identification of $g(v)$, $v \in \mathbb{R}$ requires the application of the collection of impulses $\{\delta_{\mathbb{R}}(u - u_0) | u_0 \in [0, T)\}$, which gives the outputs $\{g(t - u_0) | u_0 \in [0, T)\}$. In fact, from the latter where $t \in \mathbb{Z}(T)$ and $u_0 \in [0, T)$, we can obtain the whole $g(t)$, $t \in \mathbb{R}$, by composition.

The general case is carried out in Appendix C where we show that the identification requires the application of the impulse collection

$$\{\delta_I(u - u_0) | u_0 \in C\}, \quad C = [I_0/I_0 \cap U_0)$$

to obtain the output collection

$$\{g(t - u_0) | u_0 \in C\}, \quad (6.49)$$

which permits the whole identification of $g(v)$, $v \in D$. In Chap. 7, we shall see that (6.49) represents the *polyphase decomposition* of $g(v)$, $v \in D$.

Example 6.1 Consider the identification of a $\mathbb{Z}(2) \rightarrow \mathbb{Z}(3)$ QIL tf. Since $\mathbb{Z}(2) \cap \mathbb{Z}(3) = \mathbb{Z}(6)$ and $\mathbb{Z}(3) + \mathbb{Z}(2) = \mathbb{Z}(1)$, we have $C = [\mathbb{Z}(2)/\mathbb{Z}(6)] = \{0, 2, 4\}$. Then, to identify the impulse response $g(v)$, $v \in \mathbb{Z}(1)$, we have to apply the impulses (Fig. 6.23)

$$\delta_{\mathbb{Z}(2)}(u), \quad \delta_{\mathbb{Z}(2)}(u - 2), \quad \delta_{\mathbb{Z}(2)}(u - 4), \quad u \in \mathbb{Z}(2),$$

which give the outputs

$$g(t), \quad g(t - 2), \quad g(t - 4), \quad t \in \mathbb{Z}(3), \quad (6.49a)$$

which represents the *polyphase decomposition* of $g(v)$, $v \in \mathbb{Z}(1)$.

UT 6.9 Impulse and Elementary Transformations

In this section, we consider QIL tfs that modify a signal by simply reformatting its domains, without processing the signal itself. The most typical example of such tfs is the *down-sampling* which simply restricts the input domain I to a subgroup $U \subset I$.

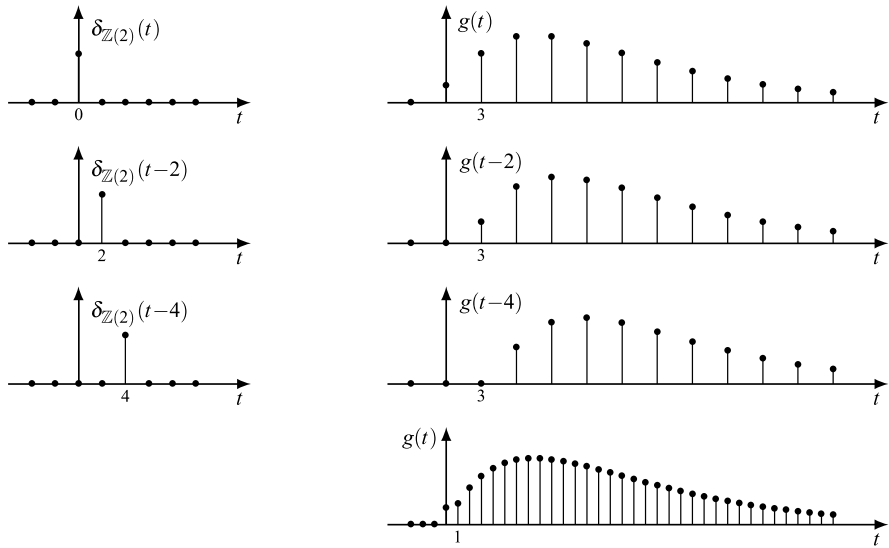
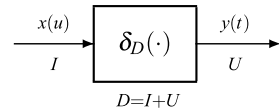


Fig. 6.23 Identification of the impulse response of a $\mathbb{Z}(2) \rightarrow \mathbb{Z}(3)$ QIL tf by application of three impulses

Fig. 6.24 Ideal transformation $I \rightarrow U$



6.9.1 Impulse Transformations

Definition 6.6 An *impulse* transformation is an $I \rightarrow U$ QIL tf, whose impulse response is the impulse on $D = I + U$ (Fig. 6.24)

$$g(t) = \delta_D(t), \quad t \in D. \tag{6.50}$$

The input–output relation of an impulse tf is obtained as a particular case of (6.44), namely

$$y(t) = \int_I du \delta_D(t - u) x(u), \quad t \in U, \tag{6.51}$$

where, in general, it is not possible to make simplifications using the sifting property since the impulse domain D is, in general, different from the integration domain I . Only if $I \supset U$, so that $D = I$, we obtain the relationship

$$y(t) = x(t), \quad t \in U,$$

Table 6.3 The four elementary transformations

Name	Symbol	Condition
Down-sampling		$I_0 \supset U_0$
Up-sampling		$I_0 \subset U_0$
Up-periodization		$P_1 \subset P_2$
Down-periodization		$P_1 \supset P_2$

which does not imply that the output equals the input since they are defined on different domains. The equality holds only when $I = U$, and in this case the impulse tf degenerates to the identity on I .

Since an impulse tf operates a simple domain reformatting, its behavior is strongly related to the *domain complexity* introduced in the previous section. In fact, we shall see that an impulse tf with complexity c can be decomposed into a cascade of c impulse tfs of complexity one, in which only one reformatting is performed.

6.9.2 Elementary Transformations

Definition 6.7 An *elementary* transformation is an impulse transformation with a unitary domain complexity.

The unitary complexity constraint leads on the domain/periodicities $I = I_0/P_1 \rightarrow U = U_0/P_2$ to only four possible elementary tfs, namely

- (a) down-sampling $I_0 \supset U_0, P_1 = P_2$;
- (b) up-sampling $I_0 \subset U_0, P_1 = P_2$;
- (c) up-periodization $I_0 = U_0, P_1 \subset P_2$;
- (d) down-periodization $I_0 = U_0, P_1 \supset P_2$.

We use the graphical symbols of Table 6.3 for the four elementary tfs.

Note that all elementary tfs are ordered, and specifically, (a) and (d) are downward, while (b) and (c) are upward. In (a), the domain is reduced and in (b) is enlarged, while the periodicity remains the same. On the other hand, in (c) and (d), the domains are the same, while periodicity is changed, reduced in (d) and enlarged

in (c). Note that, in the four elementary tfs, if the relations \subset and \supset degenerate to $=$, the corresponding tf becomes the identity.

In cases (a) and (d), where $D = I$, we can apply the sifting property in (6.51) to obtain

$$y(t) = x(t), \quad t \in U. \quad (6.52)$$

In cases (b) and (c), we have $D = U$, and (6.51) remains in the integral form

$$y(t) = \int_I du \delta_U(t - u)x(u), \quad t \in U, \quad (6.53)$$

and the possibility of simplifications depends on the specific case.

UT 6.10 Analysis of Elementary Transformations

We now examine in details the four elementary tfs and point out their effects on the input signals with illustration of 1D and 2D cases. The analysis will be done in great detail because it has an important role also in the frequency domain.

6.10.1 Down-Sampling

Down-sampling is a downward tf, so that $D = I$, and (6.51) gives

$$y(t) = x(t), \quad t \in U. \quad (6.54)$$

This simply implies that the output signal y is equal to the input signal x , but the equality is only confined to the *output domain* (the two signals are not equal, as already noted).

1D Down-Samplings We have two fundamental cases (Fig. 6.25):

- (a) $I_0 = \mathbb{R}$, $U_0 = \mathbb{Z}(T)$ which gives the sampling of a continuous-time signal into a discrete-time signal.
- (b) $I_0 = \mathbb{Z}(T_0)$, $U_0 = \mathbb{Z}(T)$ with $T = NT_0$ which gives the sampling of a discrete-time signal into a new discrete-time signal whose spacing is N times larger, preserving at the output one value for every N input values, with a rate reduction of N times. This form of down-sampling is often called *decimation*.

In both (a) and (b), the output spacing T is called the *sampling period* and its reciprocal the *sampling frequency*. The latter represents the number of samples per second that are picked up from the original signal to form the output signal.

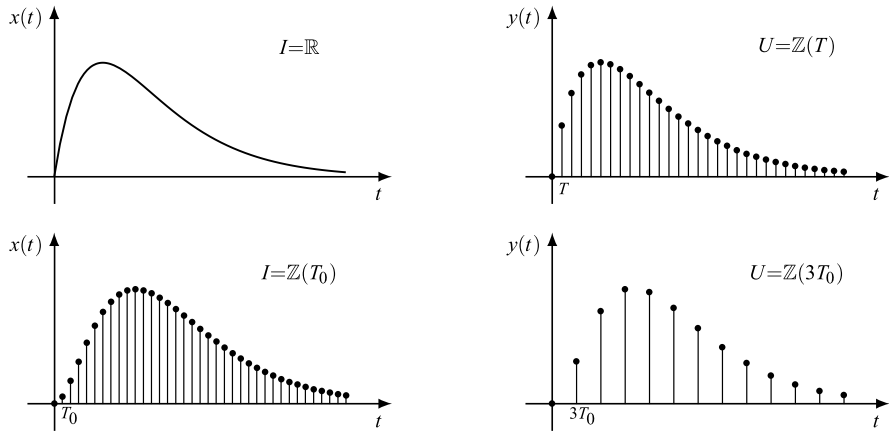


Fig. 6.25 Examples of 1D down-samplings: $\mathbb{R} \rightarrow \mathbb{Z}(T)$ and $\mathbb{Z}(T_0) \rightarrow \mathbb{Z}(3T_0)$

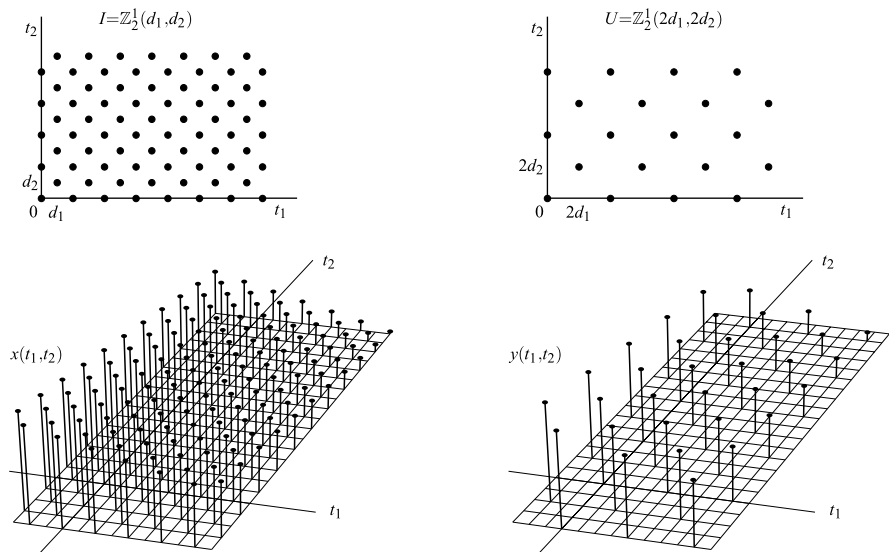


Fig. 6.26 Example of 2D down-sampling: above the domains and below the signals

2D Down-Samplings We have two fundamental cases:

- (a) $I_0 = \mathbb{R}^2 \rightarrow U_0$ with U_0 a 2D lattice which gives the sampling of a continuous-argument signal into a discrete-argument signal.
- (b) $I_0 \rightarrow U_0$ with I_0 a lattice and U_0 a sublattice of I_0 which gives the sampling of a discrete-argument signal into a new discrete-argument signal with a rate reduction from $F_1 = 1/d(I_0)$ to $F_2 = 1/d(U_0)$. Figure 6.26 illustrates this kind of down-sampling with $I_0 = \mathbb{Z}_2^1(d_1, d_2)$ and $U_0 = \mathbb{Z}_2^1(2d_1, 2d_2)$, where $d(I_0) = 2d_1d_2$ and $d(U_0) = 8d_1d_2$, and therefore the rate is reduced four times.

Another form of 2D down-sampling may be $\mathbb{R}^2 \rightarrow G$, with G a grating, which gives a mixed-argument signal starting from a continuous-argument signal $x(t_1, t_2)$.

When I and U are lattices, the rate reduction in the down-sampling is given by $d(U)/d(I) = (I : U)$ and will be called the *down-sampling ratio*.

6.10.2 Up-Sampling

This then determines an increase of the domain, from I_0 to U_0 with $U_0 \supset I_0$. Relation (6.51) remains in the integral form with $D = U$, namely

$$y(t) = \int_I du \delta_U(t - u)x(u) \quad t \in U. \quad (6.55)$$

For the interpretation of (6.55), let us consider the most interesting case when I and U are ordinary domains, $I = I_0$, $U = U_0$, and I_0 is a lattice. Then, we obtain (see (4.8))

$$y(t) = d(I) \sum_{u \in I} \delta_U(t - u)x(u), \quad t \in U, \quad (6.56)$$

where the impulse is zero for $t \neq u$, and we have

$$y(t) = \begin{cases} A_0 x(t), & \text{if } t \in I; \\ 0, & \text{otherwise,} \end{cases} \quad A_0 = d(I)\delta_U(0). \quad (6.57)$$

Thus the output signal is proportional to the input signal at the points of the *input domain* I , while it is zero at the other points of U . The constant $A_0 > 1$ represents an *amplification*.⁶

1D Up-Samplings We have two cases (Fig. 6.27):

- (a) $\mathbb{Z}(T) \rightarrow \mathbb{R}$ *up-sampling* where an input discrete-time signal is redefined as a continuous-time signal according to (6.56), namely

$$y(t) = T \sum_{n=-\infty}^{+\infty} \delta_{\mathbb{R}}(t - nT)x(nT)$$

as illustrated in Fig. 6.27; the amplification is infinite ($A_0 = \infty$). This up-sampling is sometimes called the *comb* [8].

⁶One could define the up-sampling without the “amplification”, as

$$y_0(t) = \begin{cases} x(t), & \text{if } t \in I; \\ 0, & \text{otherwise,} \end{cases} \quad (6.58)$$

but this is not a convenient choice because it leads to a lack of symmetry in the frequency domain. Moreover, this definition would not be consistent in the up-sampling from a discrete group into a continuous group, as in $\mathbb{Z}(T) \rightarrow \mathbb{R}$ up-sampling (see below).

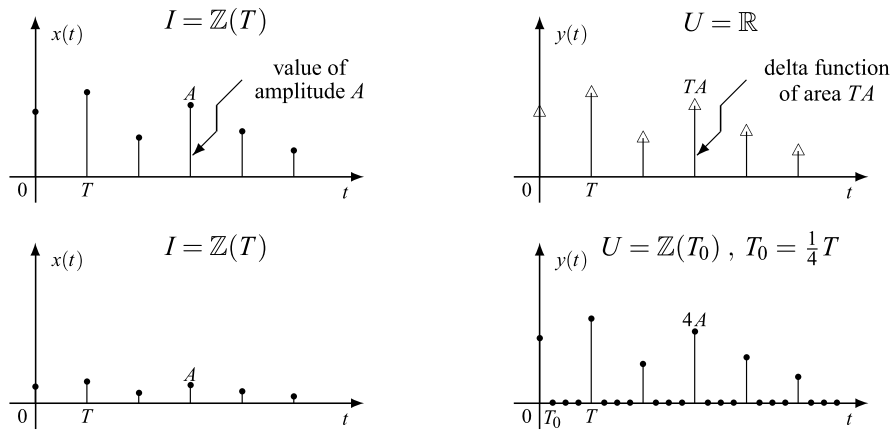


Fig. 6.27 1D examples of up-sampling: $\mathbb{Z}(T) \rightarrow \mathbb{R}$ and $\mathbb{Z}(T) \rightarrow \mathbb{Z}(T_0)$

(b) $\mathbb{Z}(T) \rightarrow \mathbb{Z}(T_0)$ up-sampling with $T_0 = T/N$ where the input–output relation is

$$y(nT_0) = \begin{cases} Nx(nT_0), & \text{if } nT_0 \in \mathbb{Z}(T); \\ 0, & \text{otherwise,} \end{cases} \quad A_0 = N,$$

and which is shown in Fig. 6.27 for $N = 4$.

2D Up-Samplings We have two fundamental cases:

(a) $I \rightarrow \mathbb{R}^2$ up-sampling where an input discrete-argument signal defined on a lattice I is redefined as a continuous-time signal, according to (6.56), namely

$$y(t) = d(I) \sum_{u \in I} \delta_{\mathbb{R}^2}(t - u)x(u);$$

the amplification is infinite ($A_0 = \infty$).

(b) $I \rightarrow U$ up-sampling with I and U lattices ($I \subset U$) where the input–output relation is

$$y(t) = \begin{cases} Nx(t), & \text{if } t \in I; \\ 0, & \text{otherwise,} \end{cases}$$

and the amplification is given by the index of U in I (see Sect. 3.3). In fact,

$$N = d(I)\delta_U(0) = \frac{d(I)}{d(U)} = \frac{\mu(U)}{\mu(I)} = (U : I).$$

This up-sampling is illustrated in Fig. 6.28 with $I = \mathbb{Z}_2^1(2d_1, 2d_2)$ and $U = \mathbb{Z}_2^1(d_1, d_2)$, where $N = 4$.

Other forms of 2D up-sampling are $L \rightarrow G$ with L a lattice and G a grating, in particular $\mathbb{Z}(d_1) \times \mathbb{Z}(d_2) \rightarrow \mathbb{R} \times \mathbb{Z}(d_2)$, in which the up-sampling is limited to the

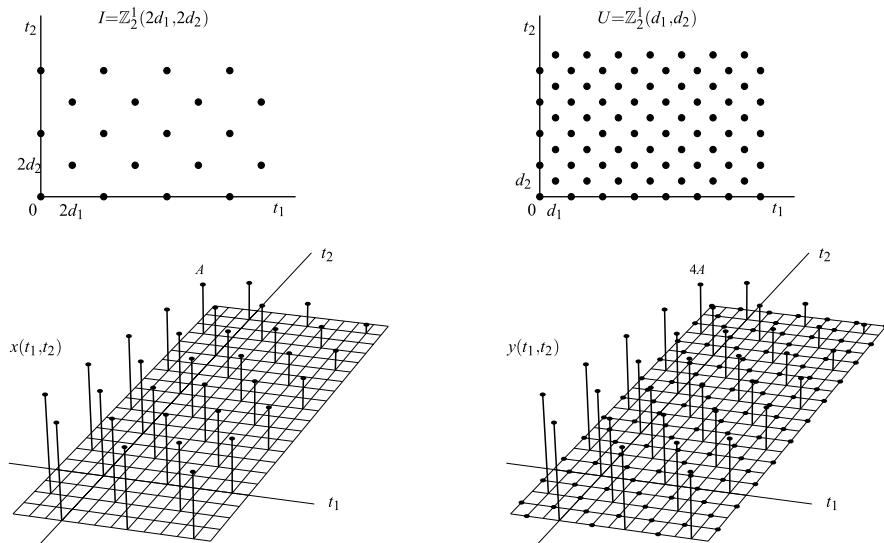


Fig. 6.28 Example of 2D up-sampling: above the domain and below the signals

first coordinate with relationship

$$y(t_1, t_2) = d_1 \sum_{n=-\infty}^{+\infty} \delta_{\mathbb{R}}(t_1 - nd_1)x(nd_1, t_2), \quad t_1 \in \mathbb{R}, t_2 \in \mathbb{Z}(d_2),$$

and the amplification is infinite.

When I and U are lattices, the rate increase in the up-sampling is given by the amplification $A_0 = d(U)/d(I) = (I : U)$ and will be called the *up-sampling ratio*.

6.10.3 Up-Periodization (or Periodic Repetition)

This tf produces a periodic signal from an aperiodic one and, more generally, a periodic signal with a larger periodicity, starting from a periodic signal. In general, with $I = I_0/P_1$, $U = I_0/P_2$, $P_1 \subset P_2$, the $I \rightarrow U$ up-periodization has the input–output relation

$$y(t) = \int_{I_0/P_1} du \delta_{I_0/P_2}(t - u)x(u), \quad t \in I_0/P_2. \tag{6.59}$$

To get a more specific result, we use identity (4.85), which gives the impulse on I_0/P_2 as a sum of impulses on I_0/P_1 , and then we can apply the sifting property. The result is

$$y(t) = \sum_{p \in [P_2/P_1]} x(t - p), \tag{6.60}$$

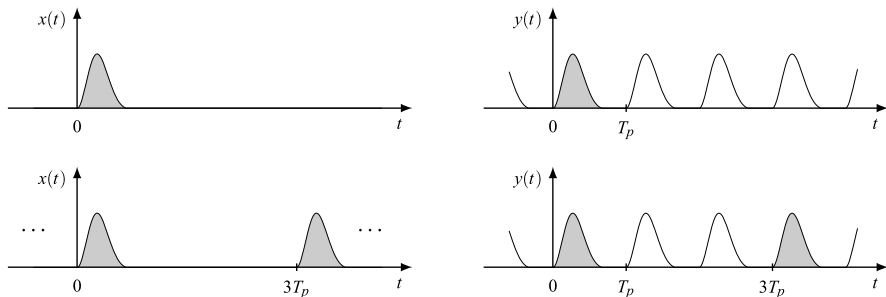


Fig. 6.29 Examples of 1D up-periodizations: $\mathbb{R} \rightarrow \mathbb{R}/\mathbb{Z}(T_p)$ and $\mathbb{R}/\mathbb{Z}(3T_p) \rightarrow \mathbb{R}/\mathbb{Z}(T_p)$

where the cell $[P_2/P_1)$ gives the *repetition centers*. According to (6.60), the output signal is obtained as a sum of the replicas of the input signal, shifted around the repetition centers.

1D Up-Periodization We have two cases (Fig. 6.29):

- (a) $P_1 = \mathbb{Z}(\infty)$, $P_2 = \mathbb{Z}(T_p)$ where the cell is $[P_2/P_1) = \mathbb{Z}(T_p)$, and (6.60) becomes

$$y(t) = \sum_{p \in \mathbb{Z}(T_p)} x(t - p) = \sum_{k=-\infty}^{+\infty} x(t - kT_p), \tag{6.61a}$$

which creates a periodic signal with period T_p starting from an aperiodic signal.

- (b) $P_1 = \mathbb{Z}(NT_p)$, $P_2 = \mathbb{Z}(T_p)$ where the cell is $[P_2/P_1) = \{0, T_p, \dots, (N - 1)T_p\}$, and (6.60) gives

$$y(t) = \sum_{p \in [\mathbb{Z}(T_p)/\mathbb{Z}(NT_p)]} x(t - p) = \sum_{k=0}^{N-1} x(t - kT_p), \tag{6.61b}$$

where the input has period NT_p and the output has a period T_p .

In Fig. 6.29, the terms $x(t - p)$ of the periodic repetition do not overlap, and therefore in each period we find a single term; then, the resulting signal is given by

$$y(t) = x(t), \quad 0 \leq t < T_p,$$

which completely defines $y(t)$ since $[0, T_p)$ is a cell of \mathbb{R} modulo $\mathbb{Z}(T_p)$. The non-overlapping is due to the limited extension of the signal $x(t)$. But in the general case, we may have overlapping, and the periodic repetition $y(t)$ for each t *must be computed as the sum of a series*, as stated by (6.61a). It is important to note that such a computation can be limited to a cell. For instance, if the input signal is (Fig. 6.30)

$$x(t) = A_0 e^{-t/D} 1(t), \quad t \in \mathbb{R},$$

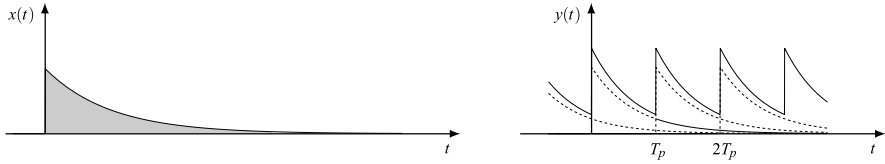


Fig. 6.30 A periodic repetition with overlapping terms: at each time t the output is the sum of a series

it is sufficient the evaluation in the interval $[0, T_p)$, namely

$$\begin{aligned} y(t) &= \sum_{k=-\infty}^{+\infty} A_0 e^{-(t-kT_p)/D} 1(t-kT_p) = \sum_{k=-\infty}^0 A_0 e^{-(t-kT_p)/D} \\ &= A_0 e^{-t/D} \sum_{k=0}^{\infty} (e^{-T_p/D})^k = \frac{A_0}{1 - e^{-T_p/D}} e^{-t/D}, \quad 0 \leq t < T_p, \end{aligned}$$

where we have considered that, for $0 \leq t < T_p$, the step signal $1(t - kT_p) = 0$ for $k > 0$.

2D Up-Periodization The standard case has the form $I_0 \rightarrow I_0/P$, where P is a 2D lattice and the relation is

$$y(t_1, t_2) = \sum_{(p_1, p_2) \in P} x(t_1 - p_1, t_2 - p_2), \quad (6.62)$$

where $x(t_1, t_2)$ is aperiodic and $y(t_1, t_2)$ has periodicity P . Figure 6.31 illustrates the $\mathbb{R}^2 \rightarrow \mathbb{R}^2/\mathbb{Z}_2^1(D_1, D_2)$ up-periodization, where the repetition centers lie on a quincunx lattice. When $P = \mathbb{Z}(D_1, D_2)$ is separable, (6.62) can be written in the “separable” form

$$y(t_1, t_2) = \sum_{m=-\infty}^{+\infty} \sum_{n=-\infty}^{+\infty} x(t_1 - mD_1, t_2 - nD_2). \quad (6.62a)$$

Another form is a *partial* periodic repetition in which the repetition centers are given by a 1D lattice P_1 . For instance, with $P_1 = \mathbb{Z}(D_1) \times \mathbb{O}$, the repetition acts only on the first coordinate t_1 , that is,

$$y(t_1, t_2) = \sum_{m=-\infty}^{+\infty} x(t_1 - mD_1, t_2).$$

If P_1 is “tilted” with the form $P_1 = \mathbb{Z}\mathbb{O}(D_1, D_2) = \{(mD_1, mD_2) | m \in \mathbb{Z}\}$, the periodic repetition becomes

$$y(t_1, t_2) = \sum_{m=-\infty}^{+\infty} x(t_1 - mD_1, t_2 - mD_2),$$

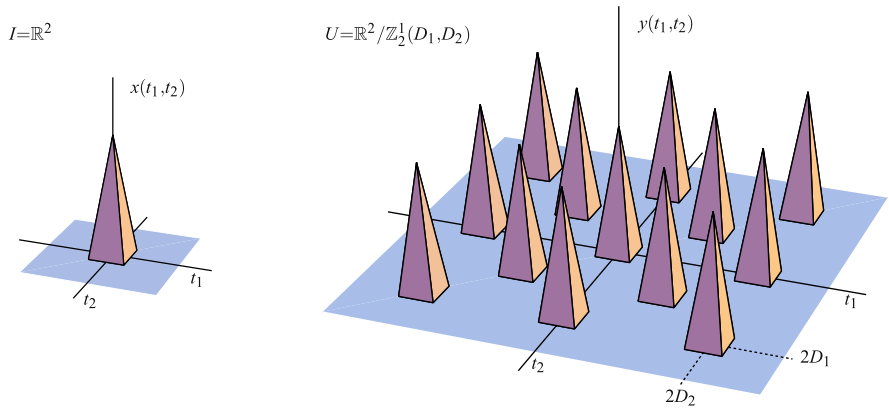


Fig. 6.31 2D periodic repetition with repetition centers given by a quincunx lattice

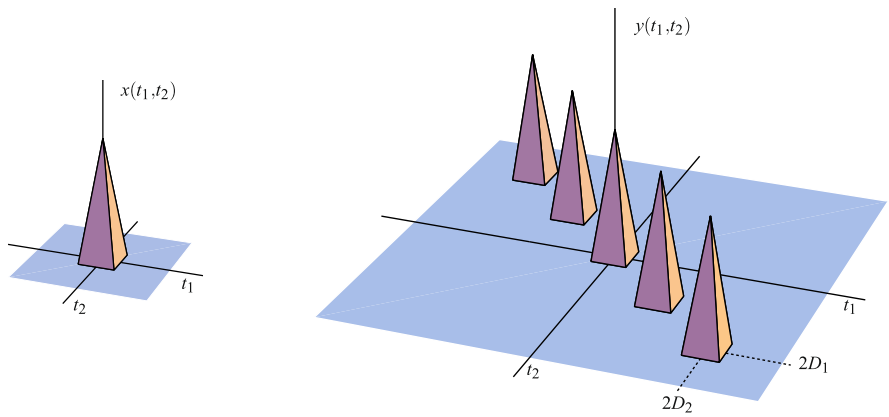


Fig. 6.32 2D periodic repetition with repetition centers given by a 1D lattice

as shown in Fig. 6.32 the case $\mathbb{R}^2 \rightarrow \mathbb{R}^2/\mathbb{Z}\mathcal{O}(D_1, D_2)$.

In the above examples, the original 2D signal is aperiodic, but in the general case of (6.60), it may be periodic and is transformed into a 2D signal with a greater periodicity ($P_2 \supset P_1$).

6.10.4 Down-Periodization

Since $I = I_0/P_1$ and $U = I_0/P_2$ with $P_1 \supset P_2$, we have $D = I$, and therefore the $I \rightarrow U$ down-periodization has the following relation

$$y(t) = \int_I du \delta_I(t - u)x(u) = x(t), \quad t \in I_0/P_2 = U. \quad (6.63)$$

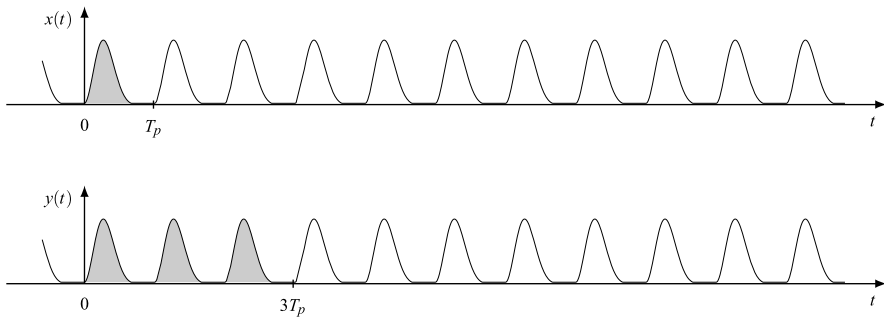


Fig. 6.33 Example of $\mathbb{R}/\mathbb{Z}(T_p) \rightarrow \mathbb{R}/\mathbb{Z}(3T_p)$ down-periodization

Then, a down-periodization does not modify the signal, and, in fact, $x(t)$ and $y(t)$ coincide on the common domain I_0 , but it changes the representation of the signal, which has periodicity P_1 at the input, but at the output it is regarded as having periodicity $P_2 \subset P_1$. This possibility is due to our definition of periodicity as the property of shift-invariance: a signal that is shift-invariant in P_0 is also shift-invariant in every $P \subset P_0$.

Since the signal is not modified, the down-periodization could appear to be a useless operation, but it has consequences on signal analysis. For instance, the Fourier transform of the original signal $x(t)$ and of the signal $y(t)$ after the down-periodization are different, as we shall see in Sect. 6.13.

1D Down-Periodizations

- (a) $P_1 = \mathbb{Z}(T_p)$, $P_2 = \mathbb{Z}(\infty)$. The input signal is periodic with period T_p , while at the output its periodicity is ignored.
- (b) $P_1 = \mathbb{Z}(T_p)$, $P_2 = \mathbb{Z}(NT_p)$. The signal, periodic at the input with period T_p , is considered to have a period N times larger at the output. Figure 6.33 illustrates the $\mathbb{R}/\mathbb{Z}(T_p) \rightarrow \mathbb{R}/\mathbb{Z}(3T_p)$ down-periodization: at the input the signal has period T_p , and at the output it is regarded as a signal with period $3T_p$.

6.10.5 Invertibility of Elementary Transformations

We investigate the problem of the recovery of the input signal after an elementary tf, that is, the *invertibility*. For down-periodization where the output signal equals the input signal, the conclusion is straightforward. But, the same conclusion holds for an up-sampling where the input signal values are preserved at the output (they are simply amplified). Therefore, both down-periodization and up-sampling are *unconditionally invertible* tfs (see Sect. 6.2).

Instead, down-sampling and up-periodization are not invertible. In the former, some values of the input signal are lost at the output, and in the latter the superposition of repetition terms does not permit the input signal recovery. However, we

can investigate the recovery under appropriate conditions, that is, the *conditional invertibility* (see Sect. 6.2).

For the up-periodization, a condition is easily formulated, that is, the “non-overlapping” of repetition terms is required. From (6.60), we find that such a condition is that the input signal extension $e(x)$ is contained in a cell C of I_0 modulo $[P_2/P_1]$, namely

$$e(x) \subset C = [P_2/P_1]. \quad (6.64)$$

This assures that, for each $t \in C$, the output signal $y(t)$ is given by a single term of the repetition, that is, $y(t) = x(t)$, $t \in C$, and this is sufficient for the whole signal recovery. For instance, in the $\mathbb{R} \rightarrow \mathbb{R}/\mathbb{Z}(T_p)$ up-periodization, the cell is $C = [\mathbb{R}/\mathbb{Z}(T_p)]$ (see Fig. 6.29), and in the $\mathbb{R}/\mathbb{Z}(3T_p) \rightarrow \mathbb{R}/\mathbb{Z}(T_p)$ up-periodization the cell is \mathbb{R} modulo $[\mathbb{Z}(T_p)/\mathbb{Z}(3T_p)] = \{0, T_p, 2T_p\}$, that is, the sequence of intervals $[0, T_p) + \mathbb{Z}(3T_p)$ (see Fig. 6.29). In conclusion, up-periodization is a conditionally invertible tf with the condition given by extension limitation (6.64).

For down-sampling, the formulation of conditional invertibility is less trivial and must be done in the frequency domain where it becomes an up-periodization. This will be seen in great detail in the context of the Sampling Theorem (Chap. 8), and we shall find that down-sampling is a conditionally invertible tf with the condition given by band-limitation.

UT 6.11 Decomposition of QIL Transformations

We have seen that in a QIL tf three domains are involved: the input domain I , the output domain U , and their sum $D = I + U$ where the impulse response is defined. Now we show that a QIL tf performs, in general, three distinct operations: a domain reformatting from I to D , a signal processing on the domain D , and a final domain reformatting from D to U .

6.11.1 Decomposition Theorem

The sum $D = I + U$ contains both I and U , by construction, so we have the ordering

$$I \subset D, \quad D \supset U. \quad (6.65)$$

Theorem 6.4 *An $I \rightarrow U$ QIL transformation with impulse response $g(v)$, $v \in D$, can be uniquely decomposed into the cascade of (Fig. 6.34):*

1. An $I \rightarrow D$ upward impulse tf;
2. A filter on D with impulse response $g(v)$, $v \in D$;
3. A $D \rightarrow U$ downward impulse tf.

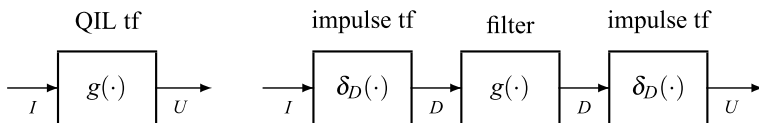


Fig. 6.34 Decomposition of an $I \rightarrow U$ QIL tf with impulse response $g(v)$, $v \in D = I + U$

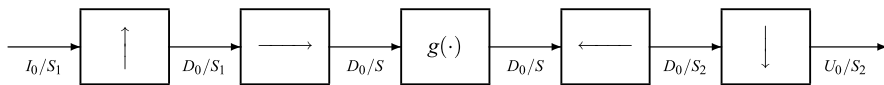


Fig. 6.35 Decomposition of a QIL tf into elementary tfs and a filter in the general case ($c = 4$)

Proof The cascade of Fig. 6.34 is equivalent to a linear tf whose kernel can be calculated using the composition rule (6.18b). The kernel of the first impulse tf is the impulse on $I + D = D$, that is, $h_1(t_2, t_1) = \delta_D(t_2 - t_1)$, and the filter has kernel $h_2(t_3, t_2) = g(t_3 - t_2)$. The kernel of the final impulse tf is the impulse on $D + U = D$, that is, $h_3(t_4, t_3) = \delta_D(t_4 - t_3)$. Then, the cascade kernel is given by

$$\int_D dt_3 \delta_D(t_4 - t_3) \int_D dt_2 g(t_3 - t_2) \delta_D(t_2 - t_1) = \int_D dt_3 \delta_D(t_4 - t_3) g(t_3 - t_1) = g(t_4 - t_1), \quad t_4 \in U, t_1 \in I, \quad (6.66)$$

where we have used the sifting property twice. Since (6.66) is equal to the kernel of the given tf, the theorem is proved. \square

The theorem permits confining the study of QIL tfs to that of very simple tfs, that is, filter and impulse tfs. The two impulse tfs, in turn, can be decomposed into elementary tfs. The $I \rightarrow D$ impulse tf, where $I = I_0/P_1$ and $D = D_0/P$ with $I_0 \subset D_0$ and $P_1 \subset P$, can be decomposed into

- 1(a) an $I_0/P_1 \rightarrow D_0/P_1$ up-sampling, and
- 1(b) a $D_0/P_1 \rightarrow D_0/P$ up-periodization.

Analogously, the $D \rightarrow U$ impulse tf, where $D = D_0/P$ and $U = U_0/P_2$ with $D_0 \supset U_0$ and $P \supset P_2$, can be decomposed as

- 2(a) a $D_0/P \rightarrow D_0/P_2$ down-periodization, and
- 2(b) a $D_0/P_2 \rightarrow U_0/P_2$ down-sampling.

The proof of these assertions can be made with the technique used in the proof of the Decomposition Theorem.

In conclusion, we obtain the decomposition of Fig. 6.35 into four elementary tfs and a filter. Some of the elementary tfs may degenerate to the identity and therefore can be dropped, and we can easily see that the number of relevant elementary tfs is just given by the *domain complexity* c , that is, the number of diversities encountered in the sequence (6.60).

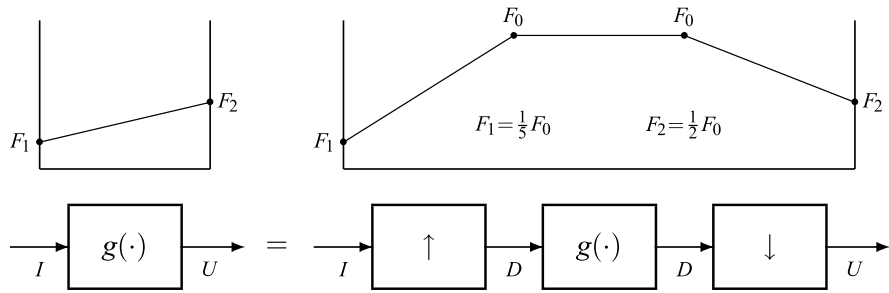


Fig. 6.36 Decomposition of a QIL tf on ordinary domains

Note that the order of the first two elementary tfs (and so is for the last two) in Fig. 6.35 cannot be changed since we have to assure the compatibility of quotient groups. In fact, in the inner group D_0/P_1 we have $P_1 \supset D_0$, whereas the order change would lead to I_0/P as the inner group for which the compatibility $P \subset I_0$ is not ensured.

It is worth noting that the decomposition shown in Fig. 6.35, having the full complexity $c = 4$, may have a scarce practical relevance, and the most interesting applications of Decomposition Theorem are concerned with ordinary domains where $c \leq 2$.

6.11.2 Decomposition of QIL tfs with Ordinary Domains

In this case, the domain complexity $c = c(I, U)$ is halved with respect to the general case ($c \leq 2$) since the periodicities are irrelevant ($P_1 = P_2 = P = \{0\}$). We have:

Corollary 6.1 A QIL tf on ordinary domains $I \rightarrow U$ with impulse response $g(v)$, $v \in D = I + U$, can be decomposed into the cascade of:

1. An $I \rightarrow D$ up-sampling,
2. A filter on D with impulse response $g(v)$, and
3. A $D \rightarrow U$ down-sampling, as shown in Fig. 6.36.

We actually have two elementary tfs when $I \rightarrow U$ is unordered ($c = 2$), while in ordered tfs ($c = 1$) we have only one elementary tf.

Figure 6.36 shows the decomposition of an unordered QIL tf. The rate diagram (see Sect. 6.1) refers to the discrete domains $\mathbb{Z}(5T_0) \rightarrow \mathbb{Z}(2T_0)$ where $D = \mathbb{Z}(T_0)$. The frequency $F_0 = 1/T_0$ represents the working rate of the filter, whereas the input and the output rates are $F_1 = F_0/5$ and $F_2 = F_0/2$, respectively. We remark that the decomposition and the corresponding rate diagram hold also in the multidimensional cases.

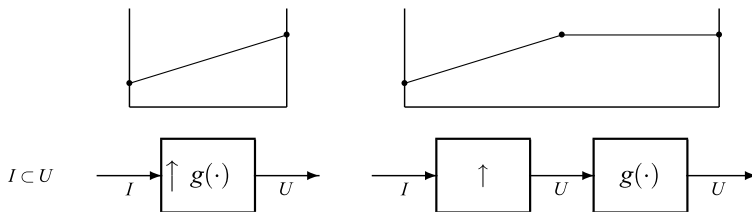


Fig. 6.37 Decomposition of an interpolator

6.11.3 Decomposition of Interpolators

Interpolators are upward QIL tfs, where $I \subset U$, $D = U$, that perform two distinct operations:

1. An $I \rightarrow U$ up-sampling, and
2. A filtering on the output domain U (Fig. 6.37).

In particular, when I is a lattice, we have the following input–output relation

$$y(t) = \sum_{u \in I} d(I) g(t - u)x(u) = \sum_{u \in I} x(u)g_0(t - u), \tag{6.67}$$

where

$$g_0(t) \triangleq d(I) g(t), \quad t \in U, \tag{6.67a}$$

has the role of the *interpolating function*. Relation (6.67) is interpreted as follows: to each input value $x(u)$ we associate the pulse $x(u)g_0(t - u)$ which is obtained by shifting by u the interpolating function and scaling its amplitude by $x(u)$, and the sum of all these contributions forms the output signal.

Note that there is no unique way to interpolate the input values since the form of interpolator depends on the choice of the interpolating function $g_0(t)$. This topic will be developed in detail in Chap. 8.

In the 1D case, we have two kinds of interpolators: (a) $\mathbb{Z}(T) \rightarrow \mathbb{R}$ which transforms a discrete signal into a continuous signal, and (b) $\mathbb{Z}(NT_0) \rightarrow \mathbb{Z}(T_0)$ which transforms a discrete-time signal into a new discrete signal with a rate N times greater.

6.11.4 Decomposition of Decimators

Decimators are downwards QIL tfs, where $I \supset U$, $D = I$, which perform a filtering on the input domain, followed by down-sampling (Fig. 6.38).

In the one-dimensional case, we have again two kinds of decimators: (a) $\mathbb{R} \rightarrow \mathbb{Z}(T)$ and (b) $\mathbb{Z}(T_0) \rightarrow \mathbb{Z}(NT_0)$.

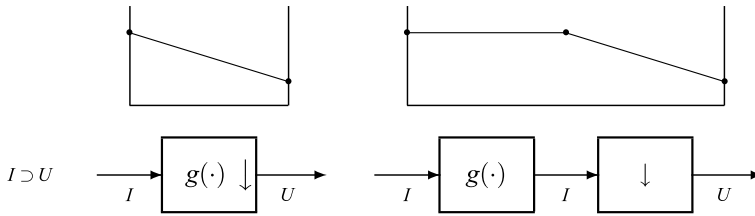


Fig. 6.38 Decomposition of a decimator

6.11.5 Decomposition of Fractional Interpolators

Fractional interpolators (or fractional decimators) are unordered QIL tfs, which represent the general case formulated in Corollary 6.1, where the domain D is different from both I and U . So, they perform an up-sampling followed by a filtering with a final down-sampling.

The 1D case has the form $I = \mathbb{Z}(N_1T_0) \rightarrow U = \mathbb{Z}(N_2T_0)$ with N_1 and N_2 coprimes. Then (see Sect. 3.9) the domain of the impulse response is $D = \mathbb{Z}(T_0)$. This case has been illustrated in Fig. 6.36 with $I = \mathbb{Z}(5T_0) \rightarrow U = \mathbb{Z}(2T_0)$.

In the 2D case with separable lattices $I = \mathbb{Z}(M_1d_1, M_2d_2) \rightarrow U = \mathbb{Z}(N_1d_1, N_2d_2)$, if both M_1, M_2 and N_1, N_2 are coprime, we have $D = \mathbb{Z}(d_1, d_2)$, and the rates are $F_0 = 1/(d_1d_2)$, $F_1 = F_0/M_1M_2$ and $F_2 = F_0/(N_1N_2)$.

In the general 2D case, the lattices have the form $I = \mathbb{Z}_i^b(M_1d_1, M_2d_2)$ and $\mathbb{Z}_j^c(N_1d_1, N_2d_2)$; also D has the same form, say $\mathbb{Z}_k^l(L_1d_1, L_2d_2)$, but the evaluation of the integers k, j, L_1, L_2 is not easy (it requires a matrix manipulation, see Chap. 16). For instance, with $I = \mathbb{Z}_2^1(d_1, d_2)$ and $I = \mathbb{Z}_3^3(d_1, d_2)$ we find $D = \mathbb{Z}(d_1, d_2)$. These lattices have been illustrated in Fig. 3.29.

⇓ 6.11.6 Generalization of Decomposition: Recomposition

We reconsider the decomposition of a QIL tf on ordinary domains, seen in Corollary 6.1, and introduce a greater inner domain

$$D_0 \supset D = I + U. \tag{6.68}$$

Theorem 6.5 *An $I \rightarrow U$ QIL tf on ordinary domains with impulse response $g(u)$, $u \in D$, can be decomposed into the cascade of:*

1. An $I \rightarrow D_0$ up-sampling,
2. A filter on D_0 with impulse response $g_0(t)$ satisfying the $D_0 \rightarrow D$ down-sampling condition

$$g_0(t) = g(t), \quad t \in D, \tag{6.69}$$

3. A $D_0 \rightarrow U$ down-sampling.

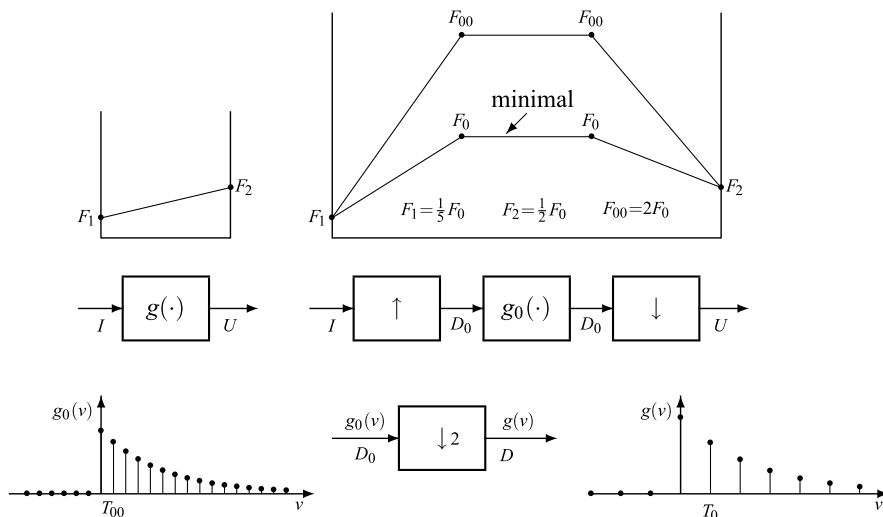


Fig. 6.39 Generalized decomposition on ordinary domains with interpretation of the impulse response

The proof is identical to the proof of Theorem 6.4. The decomposition of Corollary 6.1 is unique; in fact, the inner domain $D = I + U$ is uniquely determined by the outer domains I and U and also the filter is uniquely determined by the impulse response $g(v)$, $v \in D$, which is the same as in the original QIL tf. But, with the choice of an arbitrarily larger domain, $D_0 \supset D$, the decomposition is no more unique and the filter impulse response $g_0(t)$ has the down-sampling constraint (6.69) which requires that $g_0(t) = g(t)$ for $t \in D$ and $g_0(t)$ may be arbitrary elsewhere.

Figure 6.39 illustrates this generalized decomposition in the case where $I = \mathbb{Z}(5T_0) \rightarrow U = \mathbb{Z}(2T_0)$, $D = \mathbb{Z}(T_0)$, and we have chosen $D_0 = \mathbb{Z}(\frac{1}{2}T_0)$ as a bigger domain. The figure also shows the rate diagram, compared with the one of the standard decomposition.

Note that in the context of generalized decomposition, the standard one may be regarded as the *minimal* decomposition, that is, characterized by the minimal inner rate.

The generalized decomposition, interpreted in the reverse order, becomes useful for a cascade *recomposition*.

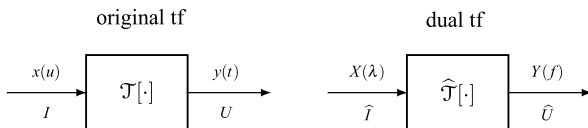
Theorem 6.6 *The cascade of QIL tfs on the ordinary domains*

$$I \rightarrow D_0 \rightarrow U \quad \text{with } D_0 \supset I + U = D \tag{6.70}$$

composed of

1. An $I \rightarrow D_0$ up-sampling,
2. A filter on D_0 with impulse response $g_0(v)$, $v \in D_0$, and
3. A $D_0 \rightarrow U$ down-sampling

Fig. 6.40 Dual of an $I \rightarrow U$ transformation with functional \mathcal{T} ; $\hat{\mathcal{T}}$ is the dual functional



is equivalent to an $I \rightarrow U$ QIL tf whose impulse response $g(v)$ is given by the $D_0 \rightarrow D$ down-sampled version of $g_0(v)$.

Note that the ordering specified by (6.70) is essential for the theorem validity; otherwise, the cascade is still a linear tf, but not necessarily QI (in general, it is PI, see Sect. 7.2).

UT 6.12 Transformations in the Frequency Domain (Dual tfs)

The analysis of tfs can be carried out in the frequency domain by considering, instead of the relations between signals, the relations between the corresponding Fourier transforms. As is well known, this analysis provides a powerful tool for the study of tfs, and particularly of linear tfs.

The link between the input and output FTs is explicitly given by a new tf, called the *dual transformation* (Fig. 6.40). Hereafter, we will consider only linear tfs.

6.12.1 The Dual of a Linear Transformation

The dual tf of an $I \rightarrow U$ linear tf with kernel h is obtained by the graph

$$\begin{matrix} X(\lambda) & \xrightarrow{\mathcal{F}^{-1}} & x(u) & \xrightarrow{h(t,u)} & y(t) & \xrightarrow{\mathcal{F}} & Y(f) \\ \hat{I} & & I & & U & & \hat{U} \end{matrix}, \quad (6.71)$$

and therefore it is given by the cascade of the three linear tfs. The first is the inverse FT, the second is the tf under consideration, and the third one gives the FT. Indeed, both the inverse Fourier transform and the Fourier transform can be formulated as linear tfs, respectively with kernels (see Sect. 6.4)

$$h_1(f, t) = e^{i2\pi ft}, \quad h_2(t, f) = e^{-i2\pi ft}. \quad (6.72)$$

Hence, recalling the composition rule of Sect. 6.3 for the kernel of a cascade of linear tfs, we have:

Theorem 6.7 *The dual of an $I \rightarrow U$ linear tf with the kernel $h(t, u)$ is an $\hat{I} \rightarrow \hat{U}$ linear tf with the kernel*

$$\hat{h}(f, \lambda) = \int_U dt \int_I du e^{-i2\pi ft} h(t, u) e^{i2\pi \lambda u}, \quad f \in \hat{U}, \lambda \in \hat{I}. \quad (6.73)$$

Therefore, the input-output relation of the dual tf is

$$Y(f) = \int_{\widehat{I}} d\lambda \widehat{h}(f, \lambda) X(\lambda), \quad f \in \widehat{U}, \lambda \in \widehat{I}. \quad (6.74)$$

On the other hand, the Fourier transform of the kernel $h(t, u)$, $(t, u) \in U \times I$, is

$$H(f, \lambda) = \int_U dt \int_I du e^{-i2\pi(f t + \lambda u)} h(t, u). \quad (6.75)$$

Then, comparing (6.73) with (6.75), we find

$$\boxed{\widehat{h}(f, \lambda) = H(f, -\lambda), \quad (f, \lambda) \in \widehat{U} \times \widehat{I}.} \quad (6.75a)$$

Thus, the dual kernel can be computed as a FT.

The symmetry between the original linear tf and the dual linear tf (compare (6.74) with (6.13)) allows transferring all the results obtained in the signal domain to the frequency domain. We point out, however, that the symmetry holds only at the general level of linear tfs, but when the form of the input–output relation is modified in specific cases, the symmetry may be lost. For instance, in a filter the input–output relation is given by a convolution, which becomes a product in the frequency domain; then the dual of an $I \rightarrow I$ filter is an $\widehat{I} \rightarrow \widehat{I}$ linear tf, but it is not a filter, as we will see immediately.

6.12.2 Dual of Filters and Windows

To find the dual of a filter on I , we can use Theorem 6.7 with $U = I$ and $h(t, u) = g(t - u)$. However, it is more straightforward recalling that the input–output filter relation is a convolution

$$y(t) = g * x(t), \quad t \in I, \quad (6.76a)$$

which in the frequency domain becomes

$$Y(f) = G(f)X(f), \quad f \in \widehat{I}. \quad (6.76b)$$

The conclusion is (Fig. 6.41) that the dual of a filter on I is a window on \widehat{I} with shape $G(f)$ given by the FT of the filter impulse response which, by definition, is called the *frequency response*.

Similarly, for a window on I , starting from the input–output relationship

$$y(t) = w(t)x(t), \quad t \in I, \quad (6.77a)$$

we find

$$Y(f) = W * X(f), \quad W(f) = \mathcal{F}[w | f], \quad f \in \widehat{I}. \quad (6.77b)$$

Thus (Fig. 6.41) the dual of a window on I with shape $w(t)$ is a filter on \widehat{I} with impulse response $W(f)$, the FT of $w(t)$.

Fig. 6.41 Dual of a filter and dual of a window

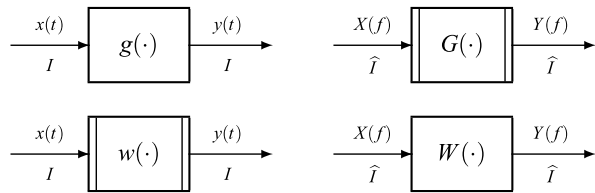
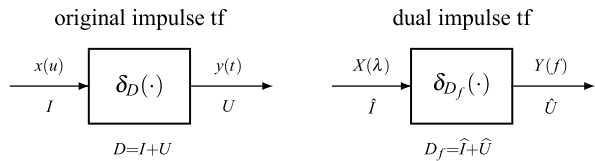


Fig. 6.42 Duality Theorem for impulse transformations



UT 6.13 Duality Theorem

This fundamental theorem states that *the dual of an impulse tf is still an impulse tf*. For its formulation, it is convenient to recall some facts about the three domains involved, I , U and $D = I + U$, and their duals.

The first fact is concerned with the *ordering*, namely (see (5.27))

$$I \supset U \xrightarrow{\text{dual}} \hat{I} \subset \hat{U}, \quad I \subset U \xrightarrow{\text{dual}} \hat{I} \supset \hat{U} \quad (6.78)$$

that is, the ordering is reversed when we pass to the frequency domain: “upward” becomes “downward”, and vice versa. The second fact is concerned with the operations of the *sum* and *intersection* which change their role in the passage to the frequency domain (see (5.28)), namely

$$D = I + U \xrightarrow{\text{dual}} \hat{I} \cap \hat{U}, \quad I \cap U \xrightarrow{\text{dual}} \hat{I} + \hat{U} = D_f. \quad (6.79)$$

6.13.1 Duals of Impulse Transformations

Owing to its importance we give the specific name of Duality Theorem to the following statement:

Theorem 6.8 *The dual of the $I \rightarrow U$ impulse transformation is the $\hat{I} \rightarrow \hat{U}$ impulse transformation (Fig. 6.42).*

In both tfs, the impulse response is defined on the sum of the domains, that is,

$$D = I + U, \quad D_f = \hat{I} + \hat{U}.$$

We also note that D_f is not the dual of $D = I + U$, but the dual of $I \cap U$ (see (6.79)).

Proof We use the Noble Identity established by (4.87), which permits writing the kernel of the original tf in an alternative form

$$h(t, u) = \delta_D(t - u) = \int_{I \cap U} ds \delta_U(t - s) \delta_I(s - u).$$

Using the latter form in the general expression (6.73), we obtain that the dual kernel is given by

$$\widehat{h}(f, \lambda) = \int_U dt \int_I du \int_{I \cap U} ds e^{i2\pi ft} \delta_U(t - s) \delta_I(s - u) e^{-i2\pi \lambda u}.$$

Here, we have used the sifting property twice. This permits dropping the first two integrals by setting $t = s$ and $s = u$, that is,

$$\widehat{h}(f, \lambda) = \int_{I \cap U} ds e^{-i2\pi(f-\lambda)s}.$$

Finally, we use the orthogonality condition (5.10a), (5.10b) to get

$$\widehat{h}(f, \lambda) = \delta_{\widehat{I \cap U}}(f - \lambda) = \delta_{\widehat{I} + \widehat{U}}(f - \lambda),$$

where the dual of intersection is given by the sum of the duals, $D_f = \widehat{I} + \widehat{U}$. This leads to the appropriate kernel for the $\widehat{I} \rightarrow \widehat{U}$ impulse tf. \square

6.13.2 Duals of Elementary Transformations

We can apply the Duality Theorem to the elementary tfs, which are a subclass of impulse tfs.

Corollary 6.2 *The dual of the $I \rightarrow U$ elementary transformation is the $\widehat{I} \rightarrow \widehat{U}$ elementary transformation.*

Thus, for the four elementary tfs we obtain the correspondences of Table 6.4.


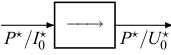

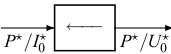

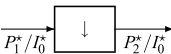


Down-Sampling Since $I = I_0/P$, $U = U_0/P$ with $I_0 \supset U_0$, the dual domains are

$$\widehat{I} = P^*/I_0^*, \quad \widehat{U} = P^*/U_0^* \quad \text{with } I_0^* \subset U_0^*.$$

Thus, the dual of the $I \rightarrow U$ down-sampling is the $\widehat{I} \rightarrow \widehat{U}$ up-periodization (periodic repetition) with the relationship

$$\boxed{Y(f) = \sum_{p \in \{U_0^*/I_0^*\}} X(f - p).} \quad (6.80)$$

Table 6.4 Duals of elementary transformations

Elementary transformation	Dual transformation
Down-sampling ($I_0 \supset U_0$) 	Up-periodization ($I_0^* \subset U_0^*$) 
Up-sampling ($I_0 \subset U_0$) 	Down-periodization ($I_0^* \supset U_0^*$) 
Up-periodization ($P_1 \subset P_2$) 	Down-sampling ($P_1^* \supset P_2^*$) 
Down-periodization ($P_1 \supset P_2$) 	Up-sampling ($P_1^* \subset P_2^*$) 

For instance, the dual of the $\mathbb{R} \rightarrow \mathbb{Z}(T)$ down-sampling is the $\mathbb{R} \rightarrow \mathbb{R}/\mathbb{Z}(F_p)$ up-periodization, and the input-output relation $y(t) = x(t)$, $t \in \mathbb{Z}(T)$, in the frequency domain becomes

$$Y(f) = \sum_{k=-\infty}^{+\infty} X(f - kF_p), \quad F_p = 1/T. \tag{6.80a}$$

In Chap. 8, we shall realize the importance of these fundamental relationships.

Up-Sampling Since $I = I_0/P$, $U = U_0/P$, with $U_0 \supset I_0$, we have

$$\widehat{I} = P^*/I_0^* \quad \text{and} \quad \widehat{U} = P^*/U_0^* \quad \text{with} \quad U_0^* \subset I_0^*,$$

which corresponds to a *down-periodization* with the relationship⁷

$$\boxed{Y(f) = X(f), \quad f \in \widehat{U}.} \tag{6.81}$$

Up-Periodization Since $I = I_0/P_1$, $U = I_0/P_2$ with $P_2 \supset P_1$, the dual domains are

$$\widehat{I} = P_1^*/I_0^*, \quad \widehat{U} = P_2^*/I_0^* \quad \text{with} \quad P_2^* \subset P_1^*.$$

⁷Notice that with the alternative definition of up-sampling (6.58), without amplification, the frequency-domain relationship would be $Y_0(f) = [d(U)/d(I)]X(f)$.

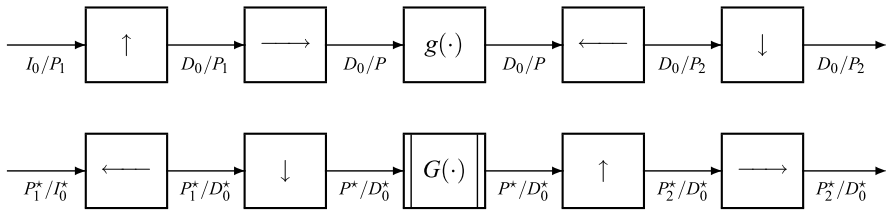


Fig. 6.43 Dual of a QLI transformation based on decomposition

Then, the dual of the $I \rightarrow U$ up-periodization is the $\widehat{T} \rightarrow \widehat{U}$ down-sampling with the relationship

$$\boxed{Y(f) = X(f), \quad f \in \widehat{U}.} \tag{6.82}$$

For instance, the dual of the $\mathbb{R} \rightarrow \mathbb{R}/\mathbb{Z}(T_p)$ up-periodization is the $\mathbb{R} \rightarrow \mathbb{Z}(F)$ down-sampling with $F = 1/T_p$.

Down-Periodization Since $I = I_0/P_1$, $U = I_0/P_2$, with $P_2 \subset P_1$, the dual domains are

$$\widehat{T} = P_1^*/I_0^*, \quad \widehat{U} = P_2^*/I_0^* \quad \text{with } P_2^* \supset P_1^*.$$

Then, the dual of the $I \rightarrow U$ down-periodization is the $\widehat{T} \rightarrow \widehat{U}$ up-sampling with the relationship

$$\boxed{Y(f) = \int_{\widehat{T}} du X(u) \delta_{\widehat{U}}(f - u), \quad f \in \widehat{U}.} \tag{6.83}$$

For instance, the dual of the $\mathbb{R}/\mathbb{Z}(T_p) \rightarrow \mathbb{R}$ down-periodization is the $\mathbb{Z}(F) \rightarrow \mathbb{R}$ up-sampling with $F = 1/T_p$.

UT 6.14 Duals of QIL Transformations

To find the dual of a QIL tf, we can apply the general procedure of Sect. 6.12. However, it is more convenient to use the Decomposition Theorem where duality can be applied to each component (elementary tfs and filter).

In the general case, the dual tf consists of the cascade shown in Fig. 6.43, and we realize that it is not a QIL tf because the dual of a filter is not a filter. This general case, when the domain complexity is $c = 4$, has a scarce relevance since in practice we have ordinary domains and the complexity is reduced to $c = 2$ or less. We now develop the three cases of interest.

6.14.1 Dual of an Interpolator

We saw that an $I \rightarrow U$ interpolator can be decomposed into an $I \rightarrow U$ up-sampling and a filter on U . Thus, the dual tf is the cascade of an $\widehat{I} \rightarrow \widehat{U}$ down-periodization and of a window on \widehat{U} . Therefore, the Fourier transforms are related as follows

$$X_1(f) = X(f), \quad Y(f) = G(f)X_1(f), \quad f \in \widehat{U},$$

and the global relation is

$$Y(f) = G(f)X(f). \quad (6.84)$$

This result is the same as in filters, but with the difference that (6.84) implies domain reformatting. For instance, for a $\mathbb{Z}(T) \rightarrow \mathbb{R}$ interpolator, $X(f)$ is periodic, while $G(f)$ and $Y(f)$ are aperiodic.

6.14.2 Dual of a Decimator

An $I \rightarrow U$ decimator can be decomposed into a filter on I and an $I \rightarrow U$ down-sampling. The dual tf is the cascade of a window on \widehat{I} and a $\widehat{I} \rightarrow \widehat{U}$ up-periodization. Then, the FT relation is

$$Y(f) = \sum_{\lambda \in A^*} G(f - \lambda)X(f - \lambda) \quad (6.85)$$

where $A^* = [U_0^*/I_0^*]$ is the reciprocal cell (see (6.80)).

For instance, the FT relation in an $\mathbb{R} \rightarrow \mathbb{Z}(T)$ decimator is

$$Y(f) = \sum_{k=-\infty}^{+\infty} G(f - kF_p)X(f - kF_p), \quad F_p = 1/T, \quad (6.86)$$

and in a $\mathbb{Z}(T_0) \rightarrow \mathbb{Z}(T)$ decimator

$$Y(f) = \sum_{k=0}^{N-1} G(f - kF_p)X(f - kF_p), \quad N = T/T_0, \quad F_p = 1/T. \quad (6.87)$$

6.14.3 Dual of a Rational Interpolator

This represents the most general case on ordinary domains, which are lattices. The decomposition gives the cascade of

1. An $I \rightarrow D$ up-sampler with $D = I + U$,
2. A filter on D , and

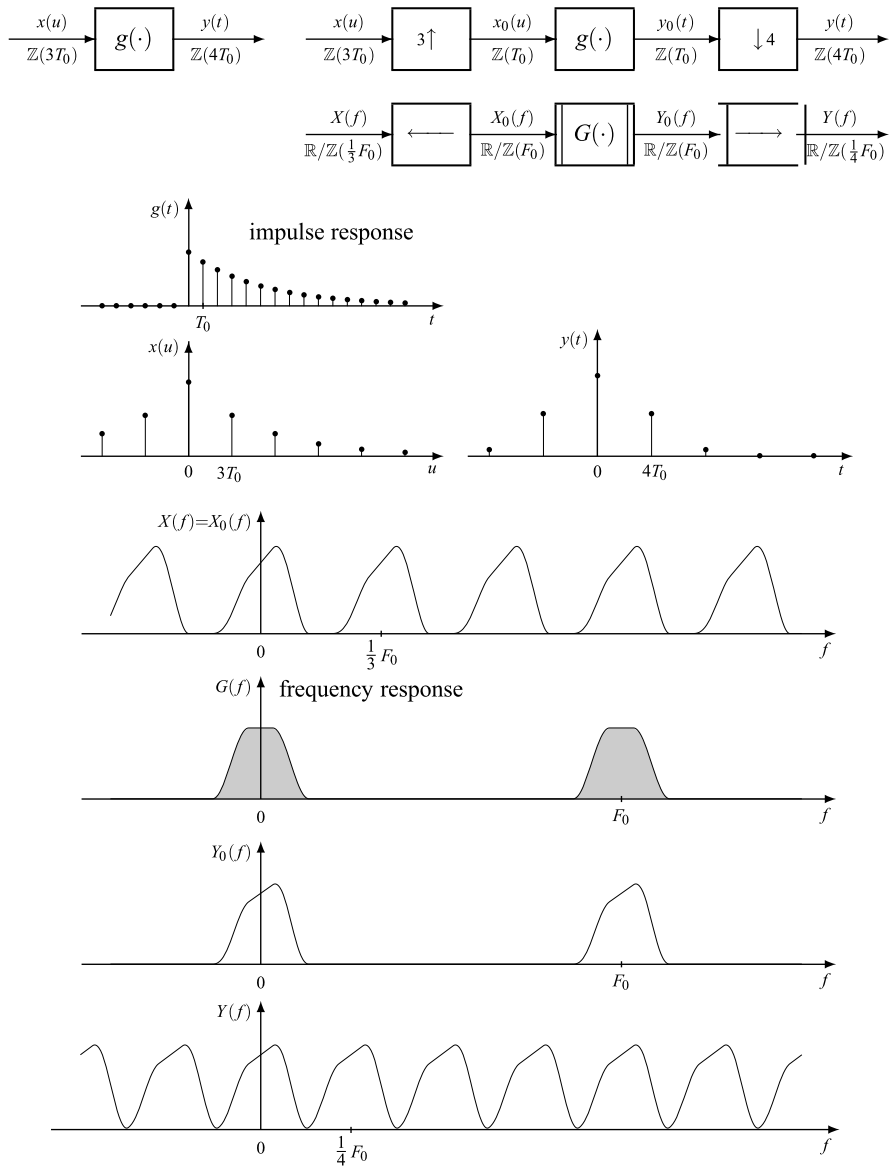


Fig. 6.44 Time and frequency analysis of a $\mathbb{Z}(3T_0) \rightarrow \mathbb{Z}(4T_0)$ rational interpolator

3. A $D \rightarrow U$ down-sampler.

Hence, in the frequency domain we find (Fig. 6.44):

- An $\widehat{T} \rightarrow \widehat{D}$ down-periodization with the relation $X_0(f) = X(f)$, $f \in \widehat{D}$,
- A window on D with the relation $Y_0(f) = G(f)X_0(f)$, $f \in \widehat{D}$, and

- An up-periodization with the relation

$$Y(f) = \sum_{p \in [U^*/D^*]} G(f - p)X(f - p), \quad f \in \widehat{U}.$$

Figure 6.44 illustrates the $\mathbb{Z}(3T_0) \rightarrow \mathbb{Z}(4T_0)$ fractional interpolator, where the dual domains are $\widehat{T} = \mathbb{R}/\mathbb{Z}(\frac{1}{3}F_0) \rightarrow \widehat{D} = \mathbb{R}/\mathbb{Z}(F_0) \rightarrow \widehat{U} = \mathbb{R}/\mathbb{Z}(\frac{1}{4}F_0)$ with $(F_0 = 1/T_0)$. All the FTs are defined on \mathbb{R} , but with different periods: $\frac{1}{3}F_0$ at the input, F_0 in the filter and $\frac{1}{4}F_0$ at the output. The global frequency relation is

$$Y(f) = \sum_{k=0}^3 G\left(f - k\frac{1}{4}F_0\right)X\left(f - k\frac{1}{4}F_0\right), \quad f \in \mathbb{R}/\mathbb{Z}\left(\frac{1}{4}F_0\right).$$

UT 6.15 Filters

Filters have been considered in several places (see, e.g., Sects. 4.9 and 5.2), but merit further investigations for their importance.

6.15.1 Signal-Domain Analysis

A filter on I is an $I \rightarrow I$ linear tf with the input–output relation

$$y(t) = \int_I du g(t - u)x(u) = x * g(t), \quad t \in I, \tag{6.88}$$

where $g(t)$, $t \in I$, is the *impulse response* with the meaning of *the filter response to the impulse centered at the origin*. This input–output relationship is used to define a filter, but it can be proved using the assumptions of linearity and shift-invariance. To this end, we write the input signal in the form (see Sect. 4.10)

$$x(t) = \int_I du x(u)\delta_I(t - u) \tag{6.88a}$$

where $x(t)$ is decomposed into the *impulse components* $[x(u) du]\delta_I(t - u)$. Because of the *shift-invariance*, the response to an impulse component is given by

$$[x(u) du]\delta_I(t - u) \xrightarrow{\text{filter}} [x(u) du]g(t - u). \tag{6.88b}$$

Finally, using the *linearity*, the global response is the superposition of the responses to impulse components, and we arrive at (6.88).

The above procedure is illustrated in Fig. 6.45 for a continuous-time filter.

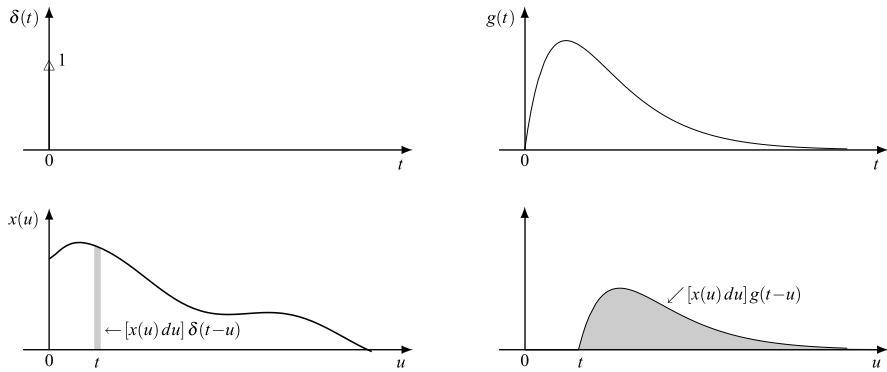


Fig. 6.45 Deduction of the input–output relationship of a filter on \mathbb{R}

6.15.2 Frequency Domain Analysis

The input–output relation (6.88) becomes

$$Y(f) = G(f)X(f) \quad (6.89)$$

where $G(f)$ is the *frequency response* defined as the FT of the impulse response. The frequency response $G(f)$ completely characterizes the filters, as well as the impulse response $g(t)$.

Relationship (6.89) clearly shows the convenience of the analysis in the frequency domain where the convolution is replaced by a product. We recall that this result does not come as a lucky coincidence, but was designed by the choice of the Fourier kernel, as discussed in Sect. 5.2. By rewriting that relation as an inverse FT, we obtain

$$y(t) = \int_{\hat{I}} df Y(f) e^{i2\pi ft} = \int_{\hat{I}} df G(f) X(f) e^{i2\pi ft}. \quad (6.90)$$

Thus, decomposing the integral we obtain for the elementary components

$$[Y(f) df] e^{i2\pi ft} = G(f) [X(f) df] e^{i2\pi ft}, \quad f \in \hat{I}. \quad (6.90a)$$

Therefore, a filter modifies the complex amplitude of each input component. This is in accordance with the fact that the exponentials are *eigenfunctions* of filters (see Sect. 5.2).

If the signal $x(t)$ and the impulse response are real, so is the output $y(t)$. In this case, we can decompose the signal into sinusoidal components. To this end, we write the FT in the form $X(f) = A_X(f) \exp[i\varphi_X(f)]$ and use the Hermitian symmetry $G^*(f) = G(-f)$. Then, from (6.90a) we find

$$\begin{aligned} & 2A_Y(f) df \cos[2\pi ft + \varphi_Y(f)] \\ &= A_G(f) 2A_X(f) df \cos[2\pi ft + \varphi_X(f) + \varphi_G(f)], \quad f \in \hat{I}_+, \quad (6.91) \end{aligned}$$

where \widehat{T}_+ is the set of “positive” frequencies introduced in Sect. 5.8 in the 1D case. Then, we have the relationships for the amplitudes and phases

$$A_Y(f) = A_G(f)A_X(f), \quad \varphi_Y(f) = \varphi_X(f) + \varphi_G(f). \quad (6.91a)$$

Therefore, both the phase and amplitude are modified by a filter. The possible constant term that may be present in the sinusoidal decomposition must be treated separately and is given by $Y_0 = A_G(0)X_0$. Note that in the sinusoidal decomposition we have a less simple behavior, compared to the exponential decomposition, ultimately this is due to the fact that sinusoids *are not filter eigenfunctions* (see Problem 5.33).

A similar decomposition can be obtained in the multidimensional case, but the specification of the “positive” frequencies becomes cumbersome.

6.15.3 Ideal Filters

Ideal filters do not alter the frequency components belonging to a given spectral extension \mathcal{B} , but completely suppress all the other components. The extension \mathcal{B} is called the *pass-band*, or simply the *band*, and its complement is the *stop-band*. Based on (6.89), the *unitary* ideal filters with band \mathcal{B} can be defined as

$$G(f) = \eta_{\mathcal{B}}(f) = \begin{cases} 1, & \text{if } f \in \mathcal{B}; \\ 0, & \text{if } f \notin \mathcal{B}, \end{cases} \quad (6.92)$$

that is, $G(f)$ is the *indicator function* of the set \mathcal{B} . The impulse response, obtained as the inverse Fourier transform of $G(f)$, is simply given by

$$g(t) = \int_{\mathcal{B}} df e^{i2\pi ft}. \quad (6.92a)$$

For a *real* filter, the band \mathcal{B} is always symmetric with respect to the frequency origin

$$-\mathcal{B} = \mathcal{B}. \quad (6.93)$$

If the frequency domain $\widehat{T} = I_{0f}/P_f$ has a relevant (non-degenerate) periodicity P_f , the band specification can be limited to a cell $C = [I_{0f}/P_f)$ and can be written in the form

$$\mathcal{B} = \mathcal{B}_0 + P_f \quad \text{with } \mathcal{B}_0 \subset C. \quad (6.94)$$

In this context, the cell C represents the *fundamental band*, where the specification of the ideal filter can be limited.

1D Ideal Filters

If $I = \mathbb{R}$, we have $\widehat{T} = \mathbb{R}$ and then the fundamental band is the whole real line: $C = \mathbb{R} = (-\infty, +\infty)$. Figure 6.46 shows the reference ideal filters on \mathbb{R} with the usual terminology.

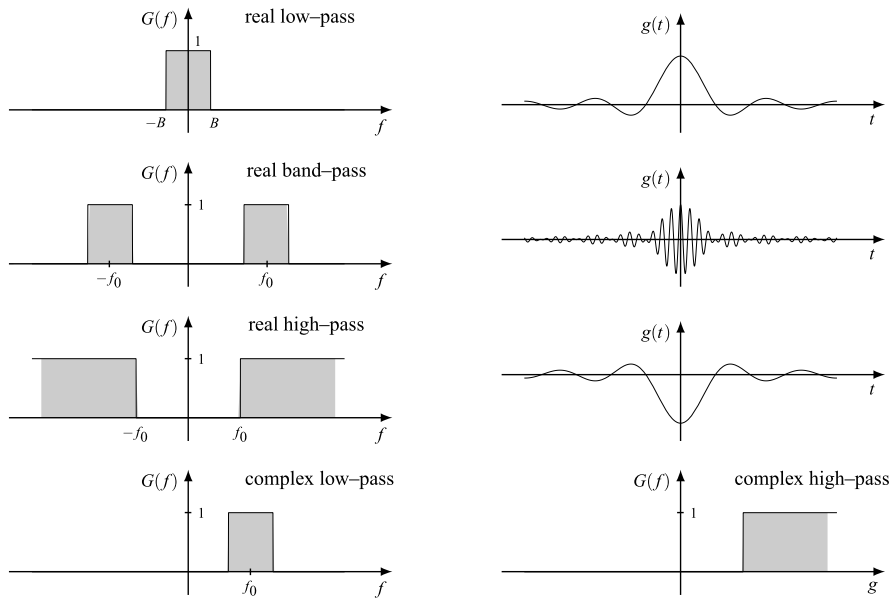


Fig. 6.46 Main examples of ideal filters on \mathbb{R}

With $\mathcal{B} = (-B, B)$ we have a *real low-pass filter*. The frequency and impulse responses are respectively

$$G(f) = \text{rect}(f/2B) \xrightarrow{\mathcal{F}^{-1}} g(t) = 2B \text{sinc}(2Bt).$$

The shifted version of the real low-pass filter, with band $\mathcal{B} = (f_0 - B, f_0 + B)$ and responses

$$G(f) = \text{rect}((f - f_0)/2B) \xrightarrow{\mathcal{F}^{-1}} g(t) = 2B \text{sinc}(2Bt) e^{-i2\pi f_0 t},$$

becomes a *complex band-pass filter*. To have a *real band-pass filter*, the band must have the negative frequency counterpart, that is,

$$\mathcal{B} = (-f_0 - B, -f_0 + B) \cup (f_0 - B, f_0 + B), \quad f_0 > B,$$

to ensure that the impulse response is real. In fact, we have

$$g(t) = 4B \text{sinc}(2Bt) \cos 2\pi f_0 t, \quad t \in \mathbb{R}.$$

The *complex high-pass filter* has band $\mathcal{B} = (f_0, +\infty)$ and the *real high-pass filter* has band $\mathcal{B} = (-\infty, -f_0) \cup (f_0, +\infty)$, $f_0 > 0$. Note that all the above ideal filters (real and complex) drop all the *exponential* components with frequency $f \notin \mathcal{B}$. The real ideal filters drop all sinusoidal components with frequencies $f \notin \mathcal{B}_+$, where \mathcal{B}_+ consists of the positive frequencies of \mathcal{B} .

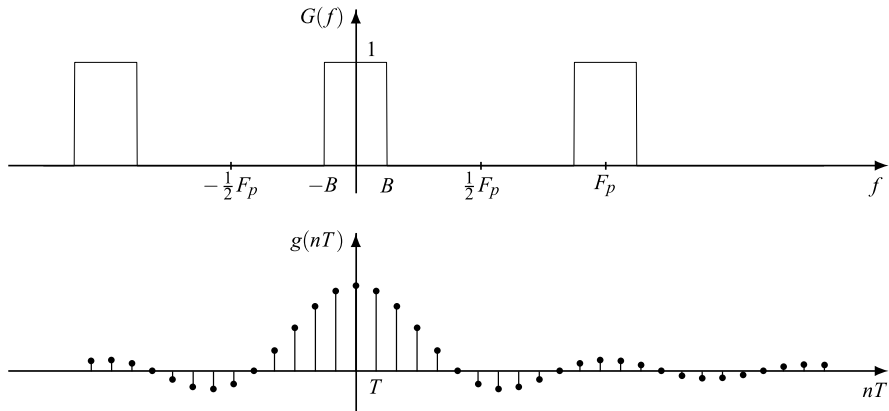


Fig. 6.47 Frequency and impulse responses of an ideal low-pass filter on $\mathbb{Z}(T)$

In the discrete case $I = \mathbb{Z}(T)$, we have $\widehat{I} = \mathbb{R}/\mathbb{Z}(F_p)$, with $F_p = 1/T$, and the frequency periodicity $P_f = \mathbb{Z}(F_p)$ is relevant. We may choose as the fundamental band $C = [\mathbb{R}/\mathbb{Z}(F_p))$ one of the cells $C = [-\frac{1}{2}F_p, \frac{1}{2}F_p)$ or $C = [0, F_p)$. Figure 6.47 illustrates the real low-pass filter on $\mathbb{Z}(T)$, where

$$\mathcal{B} = \mathcal{B}_0 + \mathbb{Z}(F_p) = (-B, B) + \mathbb{Z}(F_p)$$

and the responses are

$$G(f) = \text{rep}_{F_p} \text{rect}(f/2B) \xrightarrow{\mathcal{F}^{-1}} g(t) = 2B \text{sinc}(2Bt), \quad t \in \mathbb{Z}(T).$$

This filter drops all (discrete-time) exponential components with frequencies $f \notin (-B, B)$ and all (discrete-time) sinusoidal components with frequencies $f \notin (0, B)$.

Non-Causality of Ideal Filters We recall (Sect. 6.5) that the causality condition for filters is expressed by the causality condition of their impulse response, that is,

$$g(t) = 0, \quad t < 0. \tag{6.95}$$

Now, we realize that in all the examples seen above the impulse response is not causal, and therefore the ideal filters are anticipatory. This is a general statement for the ideal filters, and it can be proved by a theorem of Chap. 9 which states that if the stop-band has a positive measure, then the corresponding impulse response $g(t)$ may be zero only on a set of measure zero, i.e., $g(t) \neq 0$ almost everywhere, which is incompatible with causality (6.95).

2D Ideal Filters

In the continuous case $I = \mathbb{R}^2$, the frequency periodicity is irrelevant, and the fundamental band is the whole real plane $(f_1, f_2) \in \mathbb{R}^2$. The reference low-pass filter

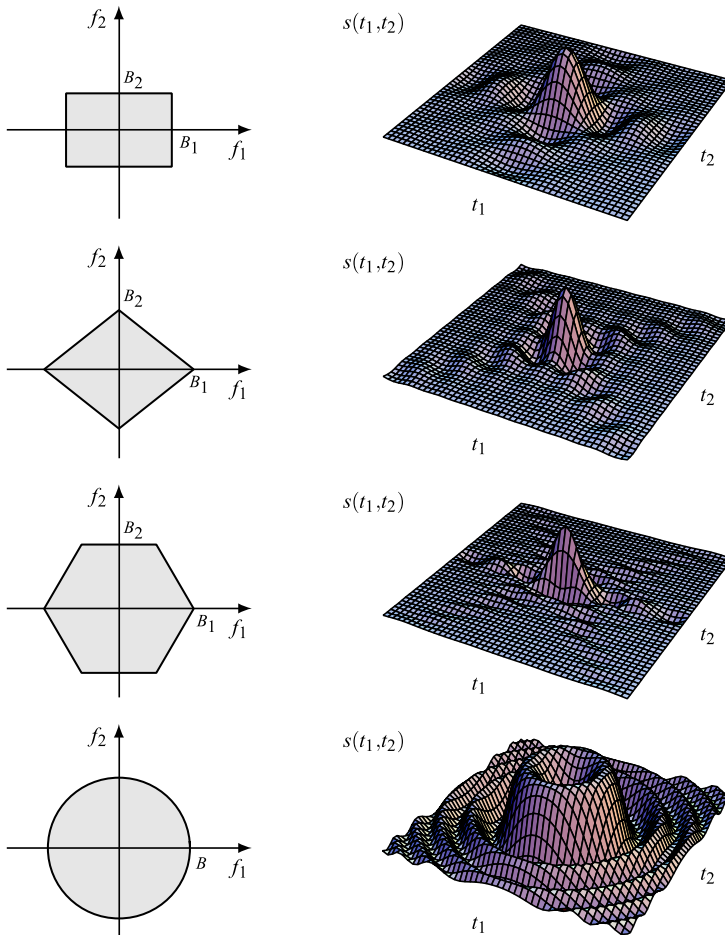


Fig. 6.48 Band \mathcal{B} and impulse response $g(t_1, t_2)$ of 2D ideal filters on \mathbb{R}^2

has a rectangular band

$$\mathcal{B} = (-B_1, B_1) \times (-B_2, B_2),$$

but we may also consider “nonseparable” ideal low-pass filters, as shown in Fig. 6.48. The condition of a *real* filter is that \mathcal{B} is an even subset of \mathbb{R}^2 , as stated by (6.93), that is, $(f_1, f_2) \in \mathcal{B} \Rightarrow (-f_1, -f_2) \in \mathcal{B}$. In the examples of Fig. 6.48, all filters verify this condition and therefore are real, and, in fact, the impulse responses $g(t_1, t_2)$ are real (the latter were calculated in Sect. 5.10).

The shifted version of a low-pass band \mathcal{B}_L , say $\mathcal{B}_P = \mathcal{B}_L + f_0$, gives a complex *band-pass* filter. A *real band-pass* filter has band

$$\mathcal{B} = -\mathcal{B}_P \cup \mathcal{B}_P = -(f_0 + \mathcal{B}_L) \cup (f_0 + \mathcal{B}_L),$$

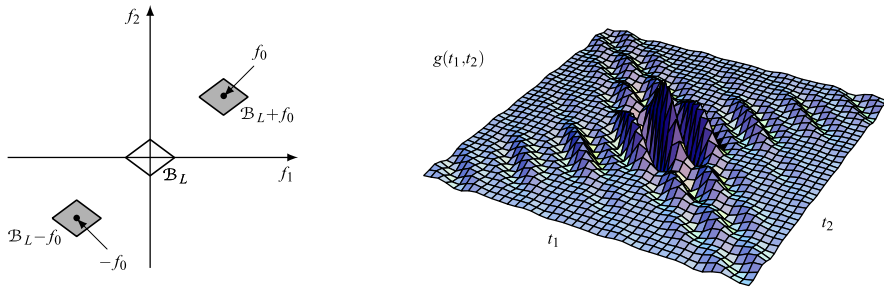


Fig. 6.49 Example of 2D discrete ideal filter illustrated by the band and the impulse response

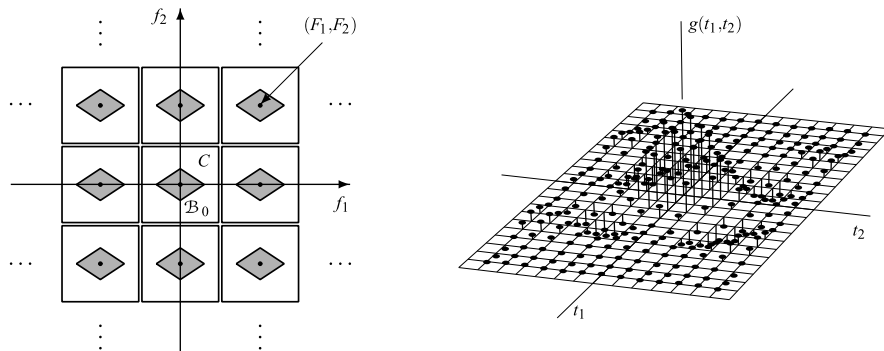


Fig. 6.50 Example of 2D band-pass ideal filter illustrated by the band and the impulse response

as shown in Fig. 6.49, where \mathcal{B}_L has a rhomboidal shape.

In the discrete case $I = L$ is a 2D lattice and $\widehat{T} = \mathbb{R}^2/L^*$, the fundamental band is $C = [\mathbb{R}^2/L^*]$. We can choose C as the fundamental parallelepiped (see Chap. 16) or its centered version. For instance, with $L = \mathbb{Z}(d_1, d_2)$ we find

$$L^* = \mathbb{Z}(F_1, F_2) \quad \text{with } F_1 = 1/d_1, F_2 = 1/d_2,$$

and the corresponding centered parallelepiped is the rectangle $(-\frac{1}{2}F_1, -\frac{1}{2}F_2) \times (\frac{1}{2}F_1, \frac{1}{2}F_2)$ (Fig. 6.50). In this case, to define an ideal filter, we choose a subset \mathcal{B}_0 of C and then we have the pass-band as

$$\mathcal{B} = \mathcal{B}_0 + L^* = \mathcal{B}_0 + \mathbb{Z}(F_1, F_2),$$

as shown in Fig. 6.50 where \mathcal{B}_0 is rhomboidal.

UT 6.16 Multi-Input Multi-Output QIL Transformations

The theory developed for QIL tfs holds also for multi-input multi-output tfs (or vector tfs), as well as for multidimensional tfs, but for vector tfs some concepts,

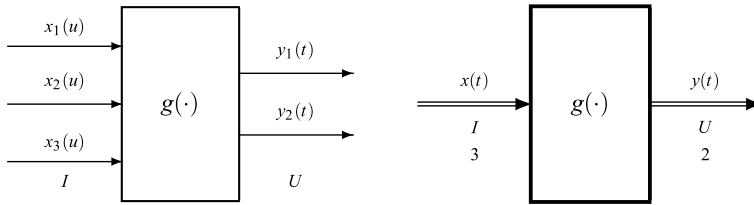


Fig. 6.51 3-input 2-output $I \rightarrow U$ QIL tf

very few indeed, must be revisited. A main constraint is on the impulse tfs, which must have *the same number of inputs and outputs*. For all the other tfs, this constraint is not required.

We concentrate our attention on QIL tfs which include impulse tfs. An M -input N -output QIL tf has the input–output relation (Fig. 6.51)

$$y(t) = \int_I du \underset{N \times M}{g(t-u)} \underset{M \times 1}{x(u)}, \quad t \in U, \tag{6.96}$$

where the impulse response is an $N \times M$ matrix. This matrix equation is equivalent to N scalar relations, namely

$$y_n(t) = \sum_{m=1}^M \int_I du g_{nm}(t-u)x_m(u), \quad t \in U, \quad n = 1, 2, \dots, N. \tag{6.96a}$$

6.16.1 Vector Impulse Transformations

The M -input M -output $I \rightarrow U$ impulse tf has the following impulse response

$$\mathbf{I}_M \delta_D(v), \quad v \in D = I + U,$$

where \mathbf{I}_M is the $M \times M$ identity matrix. Clearly, it is given by the *parallel* of M scalar $I \rightarrow U$ impulse tfs having the common impulse response $\delta_D(v)$. For instance, a 3-input 3-output down-sampler is given by the parallel of 3 scalar $I \rightarrow U$ down-samplers, as shown in Fig. 6.52.

With the above remark, all the results established for scalar impulse tfs are extended to vector impulse tfs, in particular the Duality Theorem.

Fig. 6.52 3-input 3-output $I \rightarrow U$ down-sampler

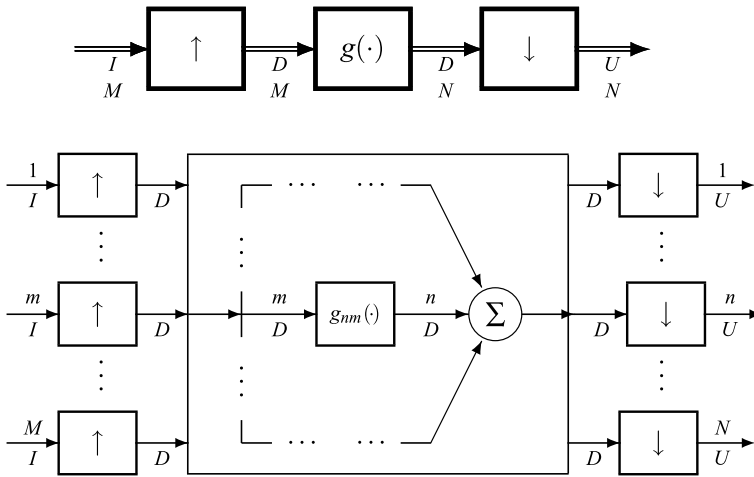
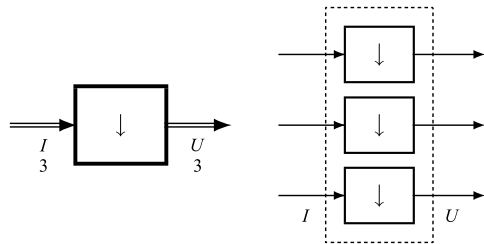


Fig. 6.53 Decomposition of an M -input N -output QIL tf on ordinary domains

6.16.2 Decomposition Theorem for Vector QIL tfs

For an M -input N -output QIL tf, the impulse response $g(v)$ is an $N \times M$ matrix $g(v)$. Then, using the identity

$$g(v) = \mathbf{I}_N g(v) \mathbf{I}_M$$

$N \times M$ $N \times M$

and reconsidering the proof of Theorem 6.4, we arrive at the following result:

Theorem 6.9 *An M -input N -output $I \rightarrow U$ QIL tf can be uniquely decomposed into the cascade of*

1. *An M -input M -output $I \rightarrow D$ impulse tf,*
2. *An M -input N -output filter on D with impulse response $g(v)$, $v \in D$, and*
3. *An N -input N -output $D \rightarrow U$ impulse tf.*

The theorem is illustrated in Fig. 6.53 for vector tfs on ordinary domains, where part 1 of the cascade becomes an $I \rightarrow D$ up-sampling and part 3 becomes a $D \rightarrow U$

down-sampling. A similar result holds also for the generalized decomposition and recomposition.

6.17 Problems

6.1 ★★ [Sect. 6.2] Consider the $\mathbb{R} \rightarrow \mathbb{R}$ tf with the following input–output relation

$$y(t) = e^{i2\pi f_0 t} x^2(t), \quad t \in \mathbb{R},$$

where $f_0 > 0$ is a constant frequency.

Check if the tf (i) is *real*, (ii) is *shift-invariant*, (iii) is *invertible*.

6.2 ★★ [Sect. 6.2] Consider the $\mathbb{R} \rightarrow \mathbb{R}$ tf with the input–output relationship

$$y(t) = e^{-\alpha|t|} x^2(t), \quad t \in \mathbb{R},$$

where $\alpha > 0$. Determine when the tf is *conditionally invertible* and express the inverse tf.

6.3 ★★ [Sect. 6.2] Prove that the set of shift-invariance Π defined by (6.8) of Definition 6.3 is always an Abelian group.

6.4 ★ [Sect. 6.4] Find the kernel of the $\mathbb{R} \rightarrow \mathbb{R}$ linear tf with the input–output relation

$$y(t) = \int_{-\infty}^t x(u) \, du, \quad t \in \mathbb{R}.$$

6.5 ★★ [Sect. 6.4] Find the kernel of the $\mathbb{R} \rightarrow \mathbb{Z}(T)$ linear tf with the input–output relation

$$y(t) = \int_{-\infty}^t x(u) \, du, \quad t \in \mathbb{Z}(T).$$

6.6 ★ [Sect. 6.4] Explain why a transformation with the input–output relation

$$y(t) = Ax(t) + B,$$

where A and B are constants and $B \neq 0$, is not linear.

6.7 ★★ [Sect. 6.4] Explain why the transformation that gives the conjugate of a signal is not linear, although it satisfies the additivity condition: $(x_1 + x_2)^* = x_1^* + x_2^*$.

6.8 ★★ [Sect. 6.4] Find the impulse response of the $I \rightarrow I$ linear tf with the input–output relation

$$y(t) = x(t) \cos \omega_0 t + x(t - t_0) \sin \omega_0 t.$$

6.9 **★★** [Sect. 6.4] Find the model of the operation that, starting from a signal $x(t)$, $t \in I$, gives its even and odd parts.

6.10 **★★★** [Sect. 6.4] Show that the necessary and sufficient condition for a linear tf to be real is that its kernel be real.

6.11 **★** [Sect. 6.4] Find the kernel of the cascade of a filter on $\mathbb{Z}(T)$ followed by a delay of $t_0 = 5T$.

6.12 **★** [Sect. 6.5] Prove the rule for the scale change in the frequency domain, given by relation (6.31), in the case $I = \mathbb{Z}(T)$.

6.13 **★** [Sect. 6.5] Find the time domain I_a and the frequency domain \widehat{I}_a after a scale change with $a = \frac{2}{5}$ in the cases $I = \mathbb{R}/\mathbb{Z}(10)$ and $I = \mathbb{Z}(3)/\mathbb{Z}(12)$.

6.14 **★** [Sect. 6.6] Classify the $\mathbb{R} \rightarrow \mathbb{R}$ tfs with the following input–output relations

$$y_1(t) = 1(x(t)), \quad y_2(t) = x(t)1(x(t) - A_0) \quad \text{with } A_0 > 0.$$

6.15 **★★** [Sect. 6.6] Show that the dual of a Volterra tf is still a Volterra tf.

6.16 **★** [Sect. 6.8] Calculate the response of the $\mathbb{Z}(T) \rightarrow \mathbb{R}$ QIL linear tf with the following impulse response

$$g(t) = \text{rect}(t/T - 1)$$

to the signal $x(t) = \exp(-2|t|/T)$.

6.17 **★** [Sect. 6.8] Find the domain of the impulse response of an $I \rightarrow U$ QIL linear tf with $I = \mathbb{Z}(6)/\mathbb{Z}(30)$ and $U = \mathbb{Z}(9)/\mathbb{Z}(90)$.

6.18 **★★** [Sect. 6.8] Find the kernel of the linear tfs given by the cascade of two QIL linear tf: $\mathbb{Z}(T) \rightarrow \mathbb{Z}(3T)$ and $\mathbb{Z}(3T) \rightarrow \mathbb{Z}(6T)$. Is the result a QIL linear tf?

6.19 **★★★** [Sect. 6.8] Repeat the previous problem with $\mathbb{R} \rightarrow \mathbb{Z}(T)$ and $\mathbb{Z}(T) \rightarrow \mathbb{R}$.

6.20 **★** [Sect. 6.8] Find the *domain complexity* of a $\mathbb{Z}(10)/\mathbb{Z}(30) \rightarrow \mathbb{R}/\mathbb{Z}(45)$ QIL tf.

6.21 **★★★** ∇ [Sect. 6.8] Find the *domain complexity* of a $\mathbb{Z}_2^1(d_1, d_2) \rightarrow \mathbb{Z}_3^2(2d_1, d_2)$ QIL tf. (for the evaluation of the sum of two lattices, see Chap. 16).

6.22 **★** [Sect. 6.9] Show that the cascade of two down-samplers is a down-sampler. Consider the case $\mathbb{R} \rightarrow \mathbb{Z}(T) \rightarrow \mathbb{Z}(5T)$ as an example.

6.23 **★★** [Sect. 6.9] The cascade of two impulse tfs with domains $I_1 \rightarrow I_2 \rightarrow I_3$ is not, in general, an impulse tf; for instance, the domains $\mathbb{R} \rightarrow \mathbb{Z}(T) \rightarrow \mathbb{R}$ do not lead to an impulse tf. Explain why.

6.24 ★★★ [Sect. 6.10] Prove that the inverse of an $\mathbb{R}/\mathbb{Z}(T_p) \rightarrow \mathbb{R}$ down-periodization is given by the cascade of a window on \mathbb{R} whose shape is the indicator function of the cell $[0, T_p)$, followed by an $\mathbb{R} \rightarrow \mathbb{R}/\mathbb{Z}(T_p)$ up-periodization.

6.25 ★★▽ [Sect. 6.10] Prove that the inverse of a $\mathbb{Z}(T) \rightarrow \mathbb{R}$ up-sampling is given by the cascade of a filter on \mathbb{R} with frequency response $G(f) - \text{rect}(fT)$, followed by an $\mathbb{R} \rightarrow \mathbb{Z}(T)$ down-sampling.

6.26 ★★▽ [Sect. 6.10] The down-sampling of a periodic signal $s(t)$, $t \in \mathbb{R}/\mathbb{Z}(10)$ with sampling period $T_0 = 3$ cannot be formulated as an $\mathbb{R}/\mathbb{Z}(10) \rightarrow \mathbb{Z}(3)/\mathbb{Z}(10)$ down-sampling because $\mathbb{Z}(3) \not\subset \mathbb{Z}(10)$. Nevertheless, a sampling with sampling period $T_0 = 3$ is possible. Formulate this operation.

6.27 ★ [Sect. 6.13] Find the dual of a $\mathbb{Z}(T) \rightarrow \mathbb{Z}(NT)$ down-sampling and write the corresponding input–output relation.

6.28 ★★ [Sect. 6.13] Consider the $\mathbb{R}/\mathbb{Z}(20) \rightarrow \mathbb{R}/\mathbb{Z}(60)$ down-periodization. Find (a) the impulse response, (b) the impulse response of the dual tf, and (c) the input–output relation of the dual tf.

6.29 ★ [Sect. 6.14] Find the dual tf of a $\mathbb{Z}(3T) \rightarrow \mathbb{Z}(5T)$ interpolator/decimator.

6.30 ★ [Sect. 6.14] Find the Fourier transform of the output of a window on \mathbb{R} with shape and input signal respectively given by

$$w(t) = \text{rect}(t/T), \quad x(t) = 1(t)e^{-\alpha t} \quad \text{with } \alpha = 1/T.$$

6.31 ★ [Sect. 6.15] Restate the axiomatic derivation of (6.88) for a discrete filter on $\mathbb{Z}(T)$.

6.32 ★ [Sect. 6.15] Prove the decomposition into sinusoidal components (6.90a) for a *real* filter with a *real* input.

6.33 ★ [Sect. 6.15] Find the impulse response of a discrete ideal filter with pass-band

$$e(G) = (-B, B) + \mathbb{Z}(F_p), \quad F_p = \frac{1}{T}, \quad B < \frac{1}{2}F_p.$$

6.34 [Sect. 6.15] Calculate the output of a discrete filter with impulse response

$$g(nT) = 1_0(n)a^n, \quad a \text{ real}$$

when the input is the discrete sinusoid $A_0 \cos(2\pi f_0 t + \varphi_0)$, $t \in \mathbb{Z}(T)$.

6.35 ★★ [Sect. 6.15] Prove that the impulse response of the ideal band-pass filter with the rhomboidal frequency response of Fig. 6.49 is given by (see (5.100))

$$g(t_1, t_2) = B_1 B_2 \operatorname{sinc}(B_1 t_1 - B_2 t_2) \operatorname{sinc}(B_1 t_1 + B_2 t_2) \cos(2\pi(f_{01} t_1 + f_{02} t_2)),$$

where $f_0 = (f_{01}, f_{02}) = (3B_1, 3B_2)$.

Appendix A: Proof of Theorem 6.1 on PIL tfs

Consider the input–output relation of an $I \rightarrow U$ linear tf given by

$$y(t) = \int_I du h(t, u)x(u), \quad t \in U. \quad (6.97)$$

If the input signal $x(u)$ is replaced by its shifted version $x_p(u) = x(u - p)$, we obtain

$$y'(t) = \int_I du h(t, u)x(u - p) = \int_I du h(t, u + p)x(u).$$

On the other hand, for the PI we must obtain $y'(t) = y(t - p)$. Hence

$$y(t - p) = \int_I du h(t, u + p)x(u),$$

which is equivalent to

$$y(t) = \int_I du h(t + p, u + p)x(u). \quad (6.98)$$

Since (6.97) and (6.98) must hold simultaneously *for every input signal*, we obtain that (6.38) is not only a sufficient, but also a necessary condition.

Appendix B: Proof of Theorem 6.2 on SI and of Theorem 6.3 on QI

Theorem 6.2 is a special case of Theorem 6.3 for $I_0 \subset U_0$. So, we carry out the proof of the second.

Assume that (6.39) holds. Then

$$h(t + p, u + p) = g(t + p - u - p) = g(t - u) = h(t, u) \quad (6.99)$$

for every $p \in I_0 \cap U_0 = \Pi_0$. The system is therefore PI on Π_0 . Conversely, if (6.99) holds for $\Pi = \Pi_0$, that is,

$$h(t + p, u + p) = h(t, u), \quad p \in I_0 \cap U_0, \quad (6.100)$$

then we can prove that the kernel can be written as

$$h(t, u) = g(t - u).$$

To this end define $g(v)$, $v \in I_0 + U_0$, in the following way: for any $v_0 \in I_0 + U_0$ there exist pairs (t_0, u_0) , $t_0 \in I_0$, $u_0 \in U_0$, such that $v_0 = t_0 + u_0$ and we pick one such pair (t_0, u_0) and let $g(v_0) = h(t_0, -u_0)$, so that $g(t_0 - u_0) = h(t_0, u_0)$. The definition is well-posed only if other choices of the pair (t_0, u_0) yield the same value of $g(v_0)$. To prove this, let (t_1, u_1) be a different pair such that $t_1 \in I_0$, $u_1 \in U_0$, $v_0 = t_1 + u_1$. Then, since $t_1 + u_1 = t_0 + u_0$, we have $t_1 - t_0 = u_0 - u_1$ and this quantity is in $I_0 \cap U_0$. Since (6.99) holds for any $p \in I_0 \cap U_0$, it also holds for $p = t_1 - t_0 = u_0 - u_1$ and yields

$$h(t_1, -u_1) = h(t_0 + p, -u_0 + p) = h(t_0, -u_0),$$

thus proving our statement.

Appendix C: On the Identification of PIL and QIL tfs

We recall the kernel interpretation of a general $I \rightarrow U$ linear tf: $h(t, u_0)$ is the tf response to the impulse applied at u_0 . Hence, for the identification it is required that we apply the input collection $\{x(u) = \delta_I(u - u_0) | u_0 \in I_0\}$ giving the output collection $\{y(t) = h(t, u_0) | u_0 \in I_0\}$. For a PIL tf, these collections are reduced by the PI condition. For instance, in a generic linear tf with input domain $I = \mathbb{R}$, we need the collection for every $u_0 \in \mathbb{R}$, but in the presence of a periodicity $P = \mathbb{Z}(T_s)$ the collection can be limited to $u_0 \in [0, T_s)$ since the other shifts provide replicas of $h(t, u_0)$.

Thus, we see that the identification of a PIL tf with a general input domain I_0 and periodicity P can be limited to a cell of I_0 modulo P . In the subclass of the QIL tfs whose periodicity is $P = I_0 \cap U_0$, the identification can be limited to the cell $C = [I_0 / (I_0 \cap U_0)]$. More specifically, we apply the input collection $\{\delta_I(u - u_0) | u_0 \in C\}$ to get the output collection $\{h(t, u_0) = g(t - u_0) | u_0 \in C\}$.

If the tf is upward ($I_0 \subset U_0$), we have $C = [I_0 / I_0] = \{0\}$ and a single application of $\delta_I(u)$ is sufficient to obtain $g(t)$, $t \in U$. Only in this case $g(t)$ has the meaning of the *response to the impulse applied at the origin*. In all the other cases, the term “impulse response” must be interpreted in a generalized sense.

References

1. R.N. Bracewell, *The Fourier Transform and Its Applications*, 2nd edn. (McGraw-Hill, New York, 1986)
2. I. Daubecheies, *Ten Lectures on Wavelets* (SIAM, Philadelphia, 1992)
3. L.E. Franks, *Signal Theory* (Prentice Hall, Englewood Cliffs, 1969)
4. A. Papoulis, *Systems and Transforms with Applications in Optics* (McGraw-Hill, New York, 1968)

5. J. Radon, Über die Bestimmung von Funktionen durch ihre Integralwerte längs gewisser Mannigfaltigkeiten, in *Berichte über die Verhandlungen der Königlichen Sächsischen Gesellschaft der Wissenschaften zu Leipzig (Reports on the proceedings of the Saxony Academy of Science)*, vol. 69 (Mathematisch-Physikalische Klasse, 1917), pp. 262–277
6. S. Roman, *Advance Linear Algebra* (Springer, New York, 1992)
7. M. Vetterli, J. Kovačević, *Wavelets and Subband Coding* (Prentice Hall, Englewood Cliffs, 1995)
8. P.M. Woodward, *Probability and Information Theory, with Applications to Radar* (Pergamon/Macmillan & Co., New York, 1953)

Chapter 7

Unified Theory: Multirate Transformations

UT 7.1 The Class of Multirate Transformations

Multirate tfs operate on discrete-argument signals defined over a lattice, and sometimes over a finite group. We recall from Sect. 6.1 that the rate of a discrete-argument signal $s(t)$, $t \in L$, is defined as the density of the lattice L

$$\mu(L) = 1/d(L) = 1/|\det L|.$$

In particular, for a 1D signal defined on $\mathbb{Z}(T)$ the rate is $\mu(L) = 1/T$ and represents the number of signal values per second. In multidimensional tfs, the interpretation of the rate depends on the context.

A multirate system is a $J \rightarrow K$ linear transformation, where the input and output domains are lattices with the same dimensionality, that is, lattices of \mathbb{R} in the 1D case and lattices of \mathbb{R}^m in the general m D case. Hence, the input–output relation has the form

$$y(t) = \int_J du h(t, u)x(u) = \sum_{u \in J} d(J) h(t, u)x(u), \quad t \in K, \quad (7.1)$$

where $x(u)$, $u \in J$, is the input signal, $y(t)$, $t \in K$, is the output signal and $h(t, u)$ is the *kernel* characterizing the system. Since in general the input domain J may be different from the output domain K , a $J \rightarrow K$ tf is a two-rate system.

A multirate tf may be not shift-invariant, but in general we assume at least the *periodical shift-invariance* (PI) and, more frequently, the *quasi shift-invariance*. We recall that for a linear tf the PI is stated by the kernel property¹

$$\boxed{h(t + p, u + p) = h(t, u), \quad p \in P,} \quad (7.2)$$

¹The periodicity of a transformation was denoted by Π in the previous chapter, but hereafter we use the symbol P .

where P is a lattice giving the *periodicity* of the tf. The compatibility condition requires that P be a sublattice of both the input and the output domain: $P \subset J \cap K$. The QI is a special case of PI, in which the kernel has the form

$$\boxed{h(t, u) = g(t - u)}, \quad (7.3)$$

where $g(\cdot)$ is defined on the sum $E = J + K$. The periodicity of a QIL tf is given by $P = J \cap K$. The input–output relation of a discrete $J \rightarrow K$ QIL tf is

$$y(t) = \int_J du g(t - u)x(u) = \sum_{u \in J} d(J) g(t - u)x(u), \quad t \in K.$$

7.1.1 The Basic Multirate Components

The building blocks of multirate tfs are very few. Most belong to the class of QIL tfs and a couple to the wider class of PIL tfs. The complete list is shown in Fig. 7.1 with the graphical representation. The QI building blocks are:

1. Filters, in which $J = K = E$ (single-rate tfs),
2. Interpolators, in which $J \subset K$ and $E = K$ (two-rate tfs),
3. Decimators, in which $J \supset K$ and $E = J$ (two-rate tfs),
4. Fractional interpolators, in which $J \not\supset K$ and $K \not\supset J$ and $E \neq J, K$ (three-rate tfs),
5. Samplers, whose impulse response is given by the impulse $\delta_{J+K}(v)$,
 - 5(a) Up-samplers, samplers in which $J \subset K$ and the impulse becomes $\delta_K(v)$,
 - 5(b) Down-samplers, samplers in which $J \supset K$ and the impulse becomes $\delta_J(v)$,
6. Serial-to-parallel (S/P) converters and parallel-to-serial (P/S) converters, which provide the *polyphase decomposition* and recomposition (these components will be introduced in Sect. 7.5).

The PI building blocks are:

7. Modulators, which multiply the input signal by a periodic carrier $\gamma(t)$,
 - 7(a) Exponential modulators (EMs), in which $\gamma(t)$ has the exponential form.

7.1.2 The Four Primitive Components of Multirate tfs

We recall explicitly the Decomposition Theorem for QIL tfs on ordinary domains, in particular on lattices (see Corollary 6.1 for scalar QIL tfs and Theorem 6.9 for vector QIL tfs).

Theorem 7.1 *A $J \rightarrow K$ QIL tf with impulse response $g(v)$, $v \in J + K = E$, can be uniquely decomposed as the cascade of (Fig. 7.2):*

1. A $J \rightarrow E$ up-sampler,

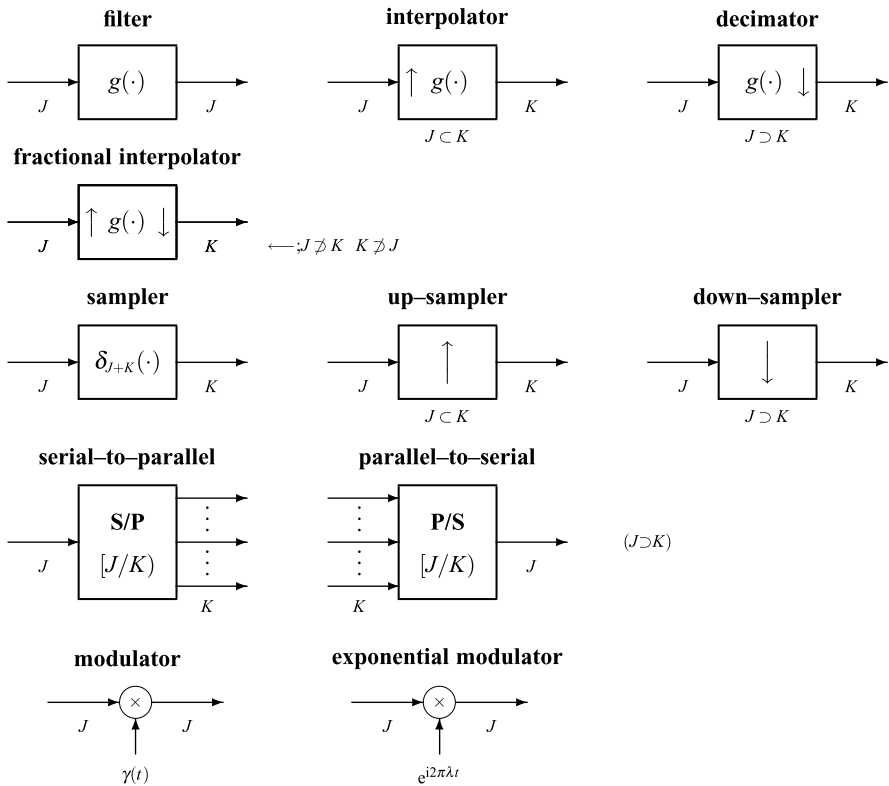


Fig. 7.1 Building blocks of multirate systems

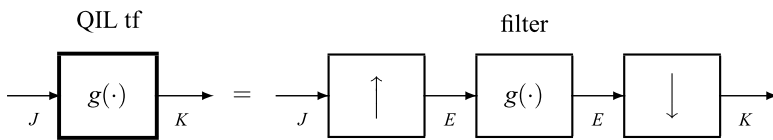


Fig. 7.2 Decomposition of a $J \rightarrow K$ QIL tf on lattices

2. A filter on E with impulse response $g(v)$, $v \in E$, and
3. An $E \rightarrow K$ down-sampler.

Then, all QIL tfs can be synthesized by only three basic QIL tfs: filters, up-samplers and down-samplers. On the other hand, the synthesis of PIL tfs can be done by adding the exponential modulators to the previous components [4, 6].

In conclusion, multirate systems can be built from the four *primitive* components:

- filters,
- up-samplers,
- down-samplers,
- exponential modulators.

This is very remarkable since the analysis of multirate systems can be limited to

these primitive components, and the analysis of non-primitive components is obtained by composition.

We now outline the analysis of the four primitive components, developed in the previous chapter.

Filters A filter on J is a single-rate system governed by the relations

$$y(t) = g * x(t), \quad t \in J, \quad Y(f) = G(f)X(f), \quad f \in \widehat{J}, \quad (7.4)$$

where the impulse response $g(t)$ is defined on J and the frequency response $G(f)$ on \widehat{J} . In the general mD case, $\widehat{J} = \mathbb{R}^m / J^*$ with J^* the reciprocal lattice.

Down-Samplers In the $J \rightarrow K$ down-sampler, the input–output relation is simply

$$y(t) = x(t), \quad t \in K, \quad (7.5)$$

where the equality is confined to the output domain $K \subset J$ (see Sect. 6.10). In the frequency domain, the relationship is (see Sect. 6.13)

$$Y(f) = \sum_{\lambda \in [K^*/J^*]} X(f - \lambda), \quad (7.6)$$

where the summation is over the reciprocal cell $[K^*/J^*]$.

Up-Samplers In the $J \rightarrow K$ up-sampler, where $J \subset K$, the relation is (see Sect. 6.10)

$$y(t) = \begin{cases} A_0 x(t), & \text{if } t \in J; \\ 0, & \text{if } t \notin J, \end{cases} \quad t \in K. \quad (7.7)$$

Thus, an up-sampler multiplies by A_0 the input signal values at the points t that J and K have in common, and inserts zeros in the rest of the output domain K . The constant A_0 in (7.7) is an amplification, given by the rate ratio

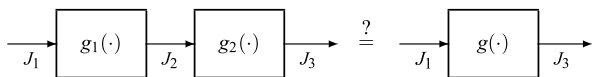
$$A_0 = (K : J) = \frac{d(J)}{d(K)} = \frac{\mu(K)}{\mu(J)} = \frac{\text{output rate}}{\text{input rate}}. \quad (7.7a)$$

The relationship in the frequency domain is simply (see Sect. 6.13)

$$Y(f) = X(f), \quad (7.8)$$

which has the subtle interpretation of *down-periodization*: the input FT $X(f)$ has periodicity J^* , whereas $Y(f)$ has periodicity $K^* \subset J^*$.

Fig. 7.3 Cascade of two QIL tfs and possible equivalent QIL tf



Exponential Modulators An exponential modulator (EM) on a lattice J has the following input–output relation²

$$y(t) = e^{i2\pi\lambda t} x(t), \quad t \in J, \quad (7.9)$$

where λ is a fixed frequency. The periodicity P of the carrier is determined by the frequency λ and, more specifically, if λ belongs to a reciprocal lattice, $\lambda \in P^*$, then P is the periodicity.

In the frequency domain, (7.9) provides a frequency shift of λ , namely

$$Y(f) = X(f - \lambda). \quad (7.10)$$

UT 7.2 Cascade of QIL Transformations

In multirate architectures, we often encounter the *cascade* connection of QIL tfs and we are interested in finding the equivalence of such a cascade. The cascade is equivalent to a linear tf, but the global QI is not assured.

We begin with the cascade of two arbitrary QIL tfs on the domains³ $J_1 \rightarrow J_2 \rightarrow J_3$. The problem is to establish when the cascade is equivalent to a $J_1 \rightarrow J_3$ QIL tf (Fig. 7.3). Note that in general to find the global $J_1 \rightarrow J_3$ linear tf we have to evaluate the global kernel $h_{13}(t_3, t_1)$ considering that the component kernels are $h_1(t_2, t_1) = g_1(t_2 - t_1)$ and $h_2(t_3, t_2) = g_2(t_3 - t_2)$. Then, using (6.19), we find

$$h_{13}(t_3, t_1) = \int_{J_2} dt \, g_2(t_3 - t_2) g_1(t_2 - t_1). \quad (7.11)$$

When we know that the cascade is globally QI, we can calculate its impulse response from the kernel as $g_{13}(t_3 - t_1) = h_{13}(t_3, t_1)$.

7.2.1 Composition Principle for QIL tfs

We recall that a $J \rightarrow K$ QIL tf is a specific case of $J \rightarrow K$ PIL tf, with the periodicity given by $P = J \cap K$. Now, in the cascade of Fig. 7.3, the first stage has

²In the mD case, λ and t are m -tuples, $(\lambda_1, \dots, \lambda_m)$, (t_1, \dots, t_m) , and the product λt must be interpreted as $\lambda_1 t_1 + \dots + \lambda_m t_m$, according to the conversion made in Chap. 5.

³We assume that the domains are lattices, but the statements of this section have a general validity, that is, for a cascade of QIL tfs on arbitrary domains (including quotient domains).

periodicity $P_{12} = J_1 \cap J_2$ and the second stage $P_{23} = J_2 \cap J_3$, and the periodicity of a cascade is given by the intersection of the periodicities

$$P_{123} = P_{12} \cap P_{23} = J_1 \cap J_2 \cap J_3$$

which represents the common periodicity of the two tfs. This is a first general result which states that the cascade of two QIL tfs on $J_1 \rightarrow J_2 \rightarrow J_3$ is equivalent to a PIL tf with periodicity given by the *intersection of the domains*. We call P_{123} the *global periodicity* of the cascade.

On the other hand, the equivalent tf is $J_1 \rightarrow J_3$ and for the QI it must have periodicity given by $P_{13} = J_1 \cap J_3$. We call P_{12} the *outer periodicity*, since it is determined by the *outer domains* of the cascade. The conclusion is that the cascade is QI as soon as the global periodicity P_{123} equals the outer periodicity P_{13} .

The generalization of this result is straightforward.

Theorem 7.2 *The cascade of K QIL tfs on the domains*

$$J_1 \rightarrow J_2 \rightarrow \cdots \rightarrow J_K \rightarrow J_{K+1}$$

is equivalent to a PIL tf with periodicity given by the intersection of the domains (global periodicity)

$$P_{12\dots K+1} = J_1 \cap J_2 \cap \cdots \cap J_K \cap J_{K+1}.$$

If the global periodicity equals the outer periodicity, that is, if

$$J_1 \cap J_2 \cap \cdots \cap J_K \cap J_{K+1} = J_1 \cap J_{K+1}, \quad (7.12)$$

the cascade is equivalent to a QIL tf.

In particular, for a cascade of two stages the condition of QI is

$$J_1 \cap J_2 \cap J_3 = J_1 \cap J_3, \quad (7.13a)$$

which is equivalent to

$$J_2 \supset J_1 \cap J_3. \quad (7.13b)$$

Alternatively, the conditions can be expressed in terms of the reciprocals lattices whose determinants give the signal rate along the cascade. Recalling that with reciprocals an intersection becomes a sum and the ordering is inverted (see Sect. 5.3), the above condition becomes

$$J_1^* + J_2^* + J_3^* = J_1^* + J_3^* \quad \Rightarrow \quad J_2^* \subset J_1^* + J_3^*. \quad (7.13c)$$

7.2.2 Examples

We consider a few examples where the domains are 1D lattices.

Example 7.1 Cascade of QIL tfs on $\mathbb{Z}(2) \rightarrow \mathbb{Z}(4) \rightarrow \mathbb{Z}(8)$. We find

$$P_{123} = \mathbb{Z}(2) \cap \mathbb{Z}(4) \cap \mathbb{Z}(8) = \mathbb{Z}(8), \quad P_{13} = \mathbb{Z}(2) \cap \mathbb{Z}(8) = \mathbb{Z}(8),$$

so that the equivalence to a QIL is verified.

The interpretation of this result is the following. The domain triplet is downward and both tfs are decimators. Also the resulting tf is downward and represents therefore a decimator. In conclusion, the cascade of two decimators on $\mathbb{Z}(2) \rightarrow \mathbb{Z}(4) \rightarrow \mathbb{Z}(8)$ is equivalent to a $\mathbb{Z}(2) \rightarrow \mathbb{Z}(8)$ decimator.

A similar conclusion holds when the domains are inverted: a cascade of two interpolators on $\mathbb{Z}(8) \rightarrow \mathbb{Z}(4) \rightarrow \mathbb{Z}(2)$ is equivalent to a $\mathbb{Z}(8) \rightarrow \mathbb{Z}(2)$ interpolator.

Example 7.2 Cascade of QIL tfs on $\mathbb{Z}(10) \rightarrow \mathbb{Z}(3) \rightarrow \mathbb{Z}(8)$. The global and the outer periodicities are respectively

$$P_{123} = \mathbb{Z}(10) \cap \mathbb{Z}(3) \cap \mathbb{Z}(8) = \mathbb{Z}(120), \quad P_{13} = \mathbb{Z}(10) \cap \mathbb{Z}(8) = \mathbb{Z}(40).$$

Hence, the cascade is not QI, but PI with periodicity $\mathbb{Z}(120)$.

Example 7.3 Cascade of QIL tfs on $\mathbb{Z}(7) \rightarrow \mathbb{Z}(T_2) \rightarrow \mathbb{Z}(15)$. This example is less trivial since we wish to study what happens when the inner domain $\mathbb{Z}(T_2)$ varies as a parameter. The condition for the equivalence to a QIL tf is

$$\mathbb{Z}(T_2) \supset \mathbb{Z}(7) \cap \mathbb{Z}(15) = \mathbb{Z}(105).$$

Hence, every inner domain $\mathbb{Z}(T_2)$ that is a superlattice of $\mathbb{Z}(105)$ leads to a QIL tf. The solutions in terms of T_2 are

$$T_2 = 105/h, \quad h = 1, 2, \dots$$

We arrive at the same conclusion if we work with reciprocals, but the procedure is more suitable for a discussion on the rate diagram. Using (7.13c) we find the condition

$$\mathbb{Z}(F_2) \subset \mathbb{Z}(F_1) + \mathbb{Z}(F_3) = \mathbb{Z}(F_0),$$

where $F_1 = 1/7 = 15F_0$, $F_3 = 1/15 = 7F_0$, $F_0 = 1/105$. For the QI, the inner rate $F_2 = 1/T_2$ must be a multiple of the rate $F_0 = 1/105$, that is,

$$F_2 = hF_0, \quad h = 1, 2, \dots \quad (7.14)$$

We examine this condition on the rate diagram (Fig. 7.4), where the outer rates are $F_1 = 15F_0$ and $F_3 = 7F_0$ and the QI inner rates F_2 , given by (7.14), are represented by the dots \bullet in the middle. Hence, for the QI a rate diagram must pass through one of these dots (otherwise the tf is PI).

Fig. 7.4 Permitted inner rates (•) for the cascade of two QIL tfs with outer domains $J_1 = \mathbb{Z}(7)$ and $J_3 = \mathbb{Z}(15)$. The minimal rate is $F_0 = 1/105$ and the outer rates are $F_1 = 15F_0$, $F_3 = 7F_0$

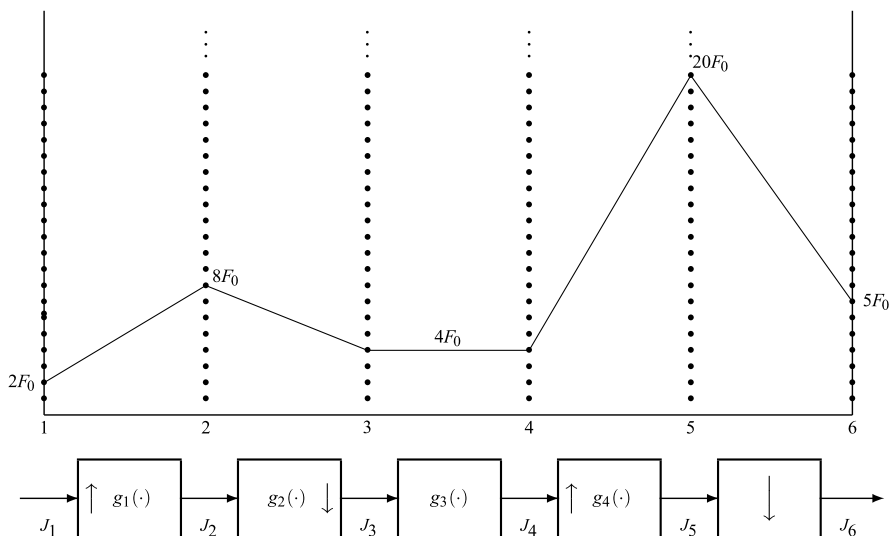
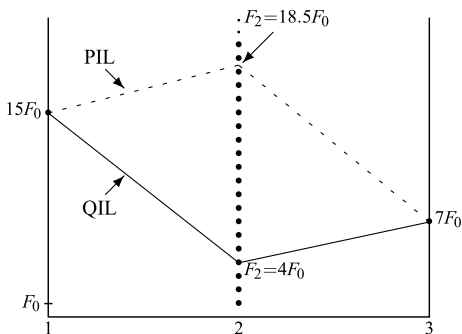


Fig. 7.5 Permitted inner rates (•) for the cascade of 5 QLI tfs with outer domains $J_1 = \mathbb{Z}(5)$, $J_5 = \mathbb{Z}(2)$. The minimal rate is $F_0 = 1/10$

The QI is assured only with this kind of paths. The figure shows a path of QI ($15F_0 \rightarrow 4F_0 \rightarrow 7F_0$) and a path ($15F_0 \rightarrow 18.5F_0 \rightarrow 7F_0$), where the QI is not assured.

Example 7.4 Figure 7.5 shows the rate diagram of the cascade of five QIL tfs with outer domains $J_1 = \mathbb{Z}(5)$ and $J_6 = \mathbb{Z}(2)$. By reasoning as in the previous example, we find that the QI condition for the cascade is that all the inner rates must be multiples of the rate F_0 determined by the outer domains, according to the relation

$$\mathbb{Z}(F_1) + \mathbb{Z}(F_6) = \mathbb{Z}(F_0), \quad F_1 = \frac{1}{2}, \quad F_6 = \frac{1}{5},$$

that is, $F_0 = 1/10$. The figure shows these QI rates (\bullet) and a path of QI given by

$$\begin{aligned} F_1 &= 2F_0, & F_2 &= 8F_0, & F_3 &= 4F_0, \\ F_4 &= 4F_0, & F_5 &= 20F_0, & F_6 &= 5F_0. \end{aligned}$$

General Consequences of Composition Principle

In the previous examples and particularly in the last, we have seen that the domain ordering for the overall QI may be quite articulated with an upward path followed by downward path, followed by an upward path, etc. However, QI must be checked in each specific case according to the rule stated above.

Nevertheless, there are some “sure” orderings that ensure the overall QI, namely

1. A sequence of upward domains (interpolators),
2. A sequence of downward domains (decimators),
3. A sequence of upward domains followed by a sequence of downward domains,
4. A sequence of downward domains followed by a sequence of upward domains, provided that the *separation domain is given by the intersection of the outer domains*.

Note that only in case 4 we find a condition for QI, whereas in the other cases the QI is always assured. Note also that “upward” ($J_n \subset J_{n+1}$) and “downward” ($J_n \supset J_{n+1}$) do not exclude “equal” ($J_n = J_{n+1}$), and therefore some parts of the paths may be “flat”.

UT 7.3 Standard Noble Identities

In the previous decompositions and recompositions of QIL tfs, we have seen that the domain ordering represents a strong constraint so that, in general, it is not allowed to reverse the order of the component tfs. From decomposition theorems one gets the impression that the natural paradigm should be: first “go upwards”, then “stay flat” (filtering), and finally “go downwards” (see Fig. 6.37 and also Fig. 6.39). Thus, in interpolators, we first have the up-sampling and then filtering; in decimators, first is the filtering and then down-sampling (see Fig. 6.38). Nevertheless, it is possible to change the above paradigm, but only in a few very precise cases. This possibility leads to the so-called *noble identities* which play a central role in multirate systems.

The standard *noble identities* are collected in Fig. 7.6. Notice that we follow a “signal-domain” approach, unusual in the literature, where the “z-domain” approach is commonly applied [9, 11].

For the up/down-sampling commutativity (NI1), our statement is the following: the cascade of a $J \rightarrow J + K$ up-sampler followed by a $J + K \rightarrow K$ down-sampler is equivalent to the cascade of a $J \rightarrow J \cap K$ down-sampler followed by a $J \cap K \rightarrow K$

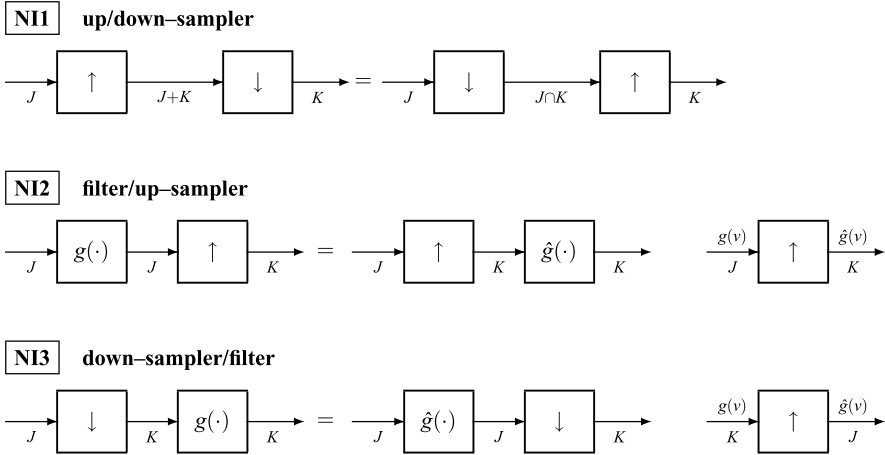


Fig. 7.6 The standard Noble Identities

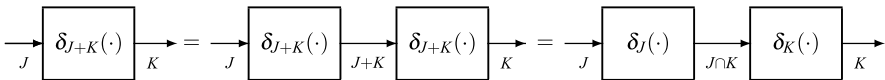


Fig. 7.7 Decompositions of an impulse transformation in the general case ($c = 4$)

up-sampler. This commutativity is well known in the theory of multirate systems, but in the multidimensional case it is usually presented through a heavy use of matrix theory [13, 15], while here it is presented in terms of sum and intersection of lattices, without considering their matrix representation [8].

The other two identities, also well known, allow the interchange of filters with up-samplers (down-samplers) provided that the impulse response of the filter is appropriately up-sampled.

7.3.1 Up/Down-Sampling Commutativity (N11)

Consider a general $J \rightarrow K$ impulse tf where J and K are not necessarily lattices. Then the impulse response of this tf is given by $\delta_{J+K}(v)$ and the application of the Decomposition Theorem (Theorem 6.4) assures that the tf can be decomposed as a $J \rightarrow J + K$ upward impulse tf followed by a $J + K \rightarrow K$ downward impulse tf. In fact, the inner filter has impulse response $\delta_{J+K}(v)$ and therefore represents an identity tf, which is irrelevant.

Theorem 7.3 A $J \rightarrow K$ impulse tf can be decomposed into the following equivalent cascades (Fig. 7.7):

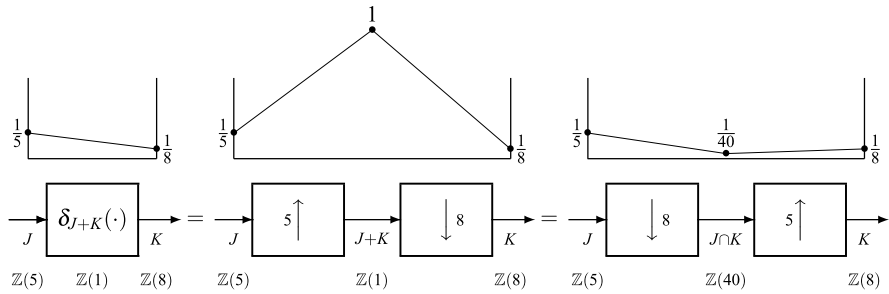


Fig. 7.8 Up/down-sampling commutativity

- (a) $A \rightarrow J + K$ upward impulse tf, followed by a $J + K \rightarrow K$ downward impulse tf,
- (b) $A \rightarrow J \cap K$ downward impulse tf, followed by a $J \cap K \rightarrow K$ upward impulse tf.

Proof As seen before, (a) is a direct consequence of the Decomposition Theorem. The kernel of (a) is

$$h_a(t, u) = \delta_{J+K}(t - u).$$

We now evaluate the kernel of decomposition (b) where the $J \rightarrow J \cap K$ tf has impulse response $\delta_J(v)$ since $J \cap K \subset J$, and the $J \cap K \rightarrow K$ tf has the impulse response $\delta_K(v)$ since $J \cap K \subset K$. Therefore, the overall kernel is

$$h_b(t, u) = \int_{J \cap K} ds \delta_K(t - s) \delta_J(s - u), \tag{7.15}$$

where we can use the Noble Identity for impulses of Sect. 4.10 to establish that $h_b(t, u) = h_a(t, u)$. Hence, both cascades are equivalent to the given impulse tf. \square

We recall that the operation of the sum (+) and intersection (\cap) have been extended to quotient groups (see Sect. 3.9), so that the theorem formulation is general, although the most interesting application is on lattices.

Corollary 7.1 *A $J \rightarrow K$ impulse tf on lattices can be decomposed into the following equivalent cascades:*

- (a) $A \rightarrow J + K$ up-sampling, followed by a $J + K \rightarrow K$ down-sampling,
- (b) $A \rightarrow J \cap K$ down-sampling, followed by a $J \cap K \rightarrow K$ up-sampling.

These decompositions are illustrated in Fig. 7.8 for the $\mathbb{Z}(5) \rightarrow \mathbb{Z}(8)$ impulse tf where the sum is $\mathbb{Z}(1)$ and the intersection is $\mathbb{Z}(40)$.

Attention must be paid to the fact that the corollary does not state that an up/down-sampling can always be commuted into a down/up-sampling. For instance,

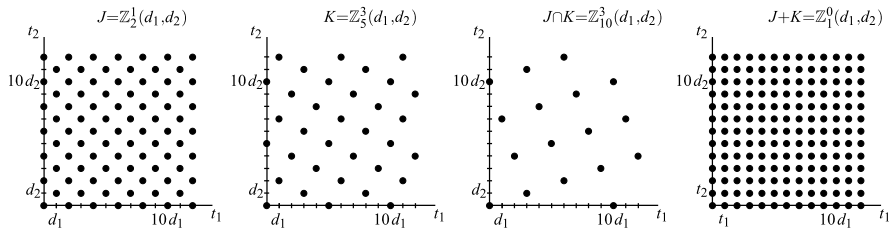


Fig. 7.9 Examples of 2D lattices of \mathbb{R}^2 for the commutativity of up/down-sampling

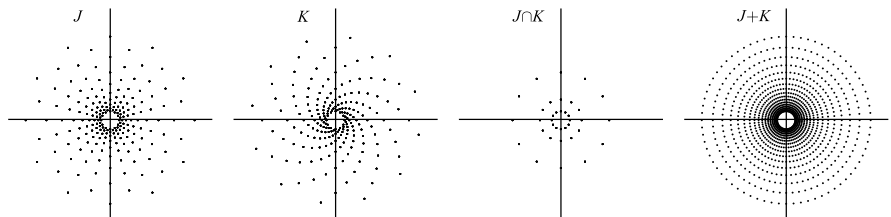


Fig. 7.10 Examples of lattices of \mathbb{C}^* for commutativity of up/down-sampling

the cascade of a $\mathbb{Z}(8) \rightarrow \mathbb{Z}(1)$ up-sampling and a $\mathbb{Z}(1) \rightarrow \mathbb{Z}(6)$ down-sampling cannot be commuted, since the cascade is equivalent to the $\mathbb{Z}(8) \rightarrow \mathbb{Z}(6)$ impulse tf and the sum $\mathbb{Z}(8) + \mathbb{Z}(6) = \mathbb{Z}(2)$ is different from $\mathbb{Z}(1)$.

For a correct application, we start from the *outer* domains J and K and evaluate the sum $J + K$ and the intersection $J \cap K$: the commutativity is possible only if the inner domain is given by the sum $J + K$. If this is the case, we can commute the up/down-sampling into a down/up-sampling with the inner domain given by the intersection $J \cap K$. In particular, in the 1D case we have that the up/down-sampling on $\mathbb{Z}(N_1 T_0) \rightarrow \mathbb{Z}(T_0) \rightarrow \mathbb{Z}(N_2 T_0)$ can be commuted with the down/up-sampling on $\mathbb{Z}(N_1 T_0) \rightarrow \mathbb{Z}(N_1 N_2 T_0) \rightarrow \mathbb{Z}(N_2 T_0)$ if and only if N_1 and N_2 are coprime.

Example 7.5 We apply Corollary 7.1 with $J = \mathbb{Z}_2^1(d_1, d_2)$ and $K = \mathbb{Z}_5^3(d_1, d_2)$. Then, we find that $J \cap K = \mathbb{Z}_{10}^3(d_1, d_2)$ and $J + K = \mathbb{Z}_1^0(d_1, d_2)$. These lattices are illustrated in Fig. 7.9.

Example 7.6 To stress the generality of up/down-sampling commutativity we consider sublattices of the multiplicative group \mathbb{C}^* (see Sect. 3.8), specifically we consider the lattices J and K determined by the matrices (Fig. 7.10)

$$\mathbf{G}_J = \begin{bmatrix} d & 0 \\ 0 & \frac{2\pi}{36} \end{bmatrix} \begin{bmatrix} 1 & 0 \\ 3 & 6 \end{bmatrix}, \quad \mathbf{G}_K = \begin{bmatrix} d & 0 \\ 0 & \frac{2\pi}{36} \end{bmatrix} \begin{bmatrix} 1 & 0 \\ 4 & 6 \end{bmatrix}$$

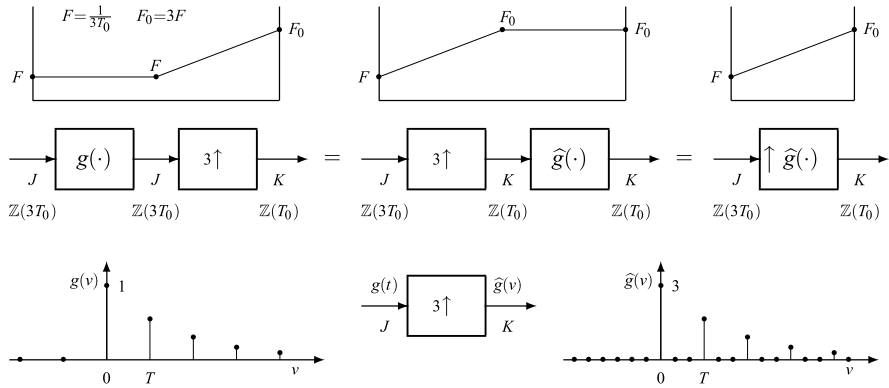


Fig. 7.11 Noble identity NI2 of a filter and an up-sampler, with interpretation of the impulse response $\widehat{g}(v)$

as the outer domains. Then, we find that the intersection $J \cap K$ and the sum $J + K$ have the basis matrices

$$\mathbf{G}_\cap = \begin{bmatrix} d & 0 \\ 0 & \frac{2\pi}{36} \end{bmatrix} \begin{bmatrix} 6 & 0 \\ 0 & 6 \end{bmatrix}, \quad \mathbf{G}_+ = \begin{bmatrix} d & 0 \\ 0 & \frac{2\pi}{36} \end{bmatrix} \begin{bmatrix} 1 & 0 \\ 0 & 1 \end{bmatrix}.$$

Another particular case of Theorem 7.3 is obtained when in the impulse tf only periodicities change, as outlined in Problem 7.2.

7.3.2 Filter/Up-Sampler Commutativity (NI2)

In this noble identity, the cascade filter/up-sampler can be inverted provided that the filter impulse response is appropriately changed.

Theorem 7.4 *The cascade of a filter on J with the impulse response $g(t)$, $t \in J$, followed by a $J \rightarrow K$ up-sampler is equivalent to the cascade of $J \rightarrow K$ up-sampler followed by a filter on K with impulse response*

$$\widehat{g}(v) = \int_J da \delta_K(v - a)g(a), \quad v \in K. \tag{7.16}$$

This noble identity is illustrated in Fig. 7.11 with $J = \mathbb{Z}(3T_0)$ and $K = \mathbb{Z}(T_0)$. Note that (7.16) gives the impulse response $\widehat{g}(v)$ as the *up-sampled version* of the original response $g(v)$.

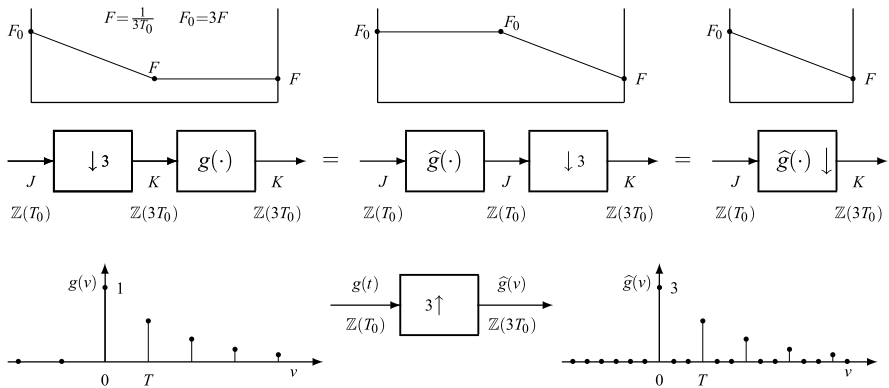


Fig. 7.12 Noble identity NI3 of a filter and a down-sampler, with interpretation of the impulse response $\hat{g}(v)$

Proof We evaluate the kernel $h(t, u)$ of the first cascade in which the component kernels are $g(s - u)$ and $\delta_K(t - s)$, respectively. Hence

$$h(t, u) = \int_J ds \delta_K(t - s)g(s - u).$$

Now, it is possible to introduce a variable change since $g(v)$ is defined on J and $\delta_K(v)$ on a larger domain. We get

$$h(t, u) = \int_J da \delta_K(t - u - a)g(a).$$

This proves that the cascade is equivalent to a QIL tf with the kernel given by (7.16). Since this $J \rightarrow K$ tf is upward ($J \subset K$), it can be decomposed as claimed in the second part of the theorem. \square

7.3.3 Down-Sampler/Filter Commutativity (NI3)

A third noble identity is concerned with a cascade down-sampler/filter.

Theorem 7.5 *The cascade of a $J \rightarrow K$ down-sampler followed by a filter on K with the impulse response $g(v)$, $v \in K$, is equivalent to a filter on J with the impulse response*

$$\hat{g}(v) = \int_K da \delta_J(v - a)g(a), \quad v \in J, \tag{7.17}$$

followed by a $J \rightarrow K$ down-sampler.

The result is illustrated in Fig. 7.12 with $J = \mathbb{Z}(T_0)$ and $K = \mathbb{Z}(3T_0)$. The proof is similar to the previous one.

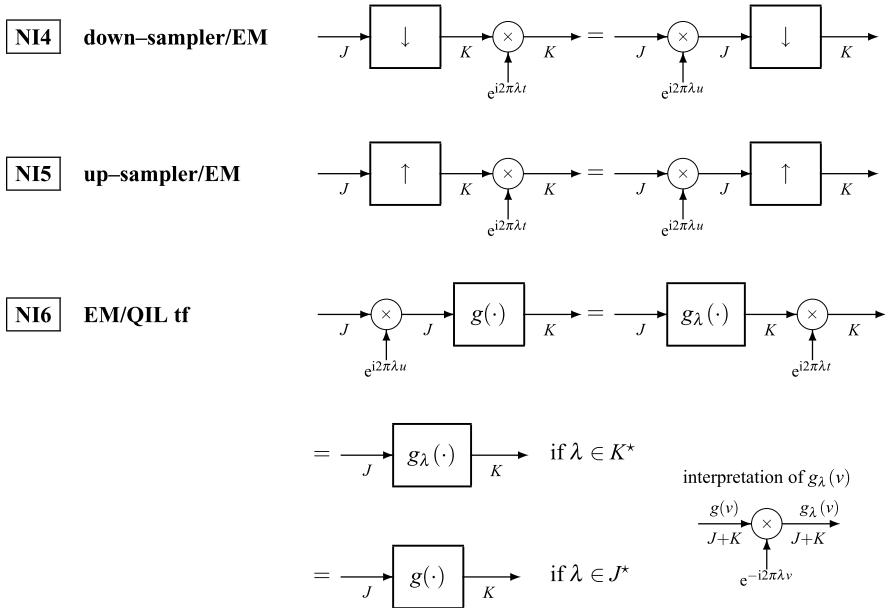


Fig. 7.13 Noble Identities with exponential modulators (EMs)

UT 7.4 Noble Identities with Modulators

The Noble Identities of the previous section are confined to the class of QIL tfs. In the more general class of PIL tfs, the exponential modulator (EM) provides other interesting Noble Identities which are illustrated in Fig. 7.13.

In spite of the fact that these Noble Identities are not considered in the literature, they find very interesting (and surprising) applications, as a carrierless modulation.

7.4.1 Set of Frequencies of an Exponential Modulator

We rewrite the relationship for an EM on a lattice J

$$y(t) = e^{i2\pi\lambda t} x(t), \quad t \in J,$$

where we assume that a periodicity P is assigned, and we want to find the *set of all possible frequencies* λ . For the compatibility condition, P must be a sublattice of the domain J , that is, $P \subset J$. We have:

Proposition 7.1 *The set of all possible frequencies for an exponential modulator (EM) on the lattice J with periodicity $P \subset J$ is given by the reciprocal lattice P^* ,*

but the specification can be limited to a reciprocal cell

$$\lambda \in C^* = [P^*/J^*]. \tag{7.18}$$

The number of frequencies in the reciprocal cell is finite and given by

$$N_{C^*} = (P^* : J^*) = (J : P). \tag{7.19}$$

In fact, the condition of periodicity P for the exponential carrier is

$$e^{i2\pi(t+p)\lambda} = e^{i2\pi t\lambda}, \quad t \in J, \tag{7.20}$$

which requires that $e^{i2\pi p\lambda} = 1$, that is, $p\lambda \in \mathbb{Z}$, which must be satisfied for every $p \in P$. Now, going back to the definition of the reciprocal (see Sect. 5.3 and (5.19)), we find that the set of the compatible frequencies λ is given by the reciprocal P^* . For instance, in the domain $J = \mathbb{Z}(T)$, the frequencies that assure the periodicity $P = \mathbb{Z}(5T)$ are given by the set $P^* = \mathbb{Z}(F)$ with $F = 1/(5T)$, that is, $\lambda = 0, \pm F, \pm 2F, \dots$. But, the frequency domain is $\hat{J} = \mathbb{R}/\mathbb{Z}(F_0)$ with $F_0 = 1/T = 5F$, and we can see that, e.g., the frequency $\lambda = 6F$ determines the same carrier as the frequency $\lambda = F$, namely $e^{i2\pi 6Ft} = e^{i2\pi Ft} e^{i2\pi 5Ft} = e^{i2\pi Ft}$ because $5Ft \in \mathbb{Z}$ for every $t \in \mathbb{Z}(T)$. Then, the frequencies can be limited to $\lambda \in \{0, F, 2F, 3F, 4F\}$ which represents a cell $[\mathbb{Z}(F)/\mathbb{Z}(5F)]$. To prove the general statement, we consider the partition $P^* = J^* + [P^*/J^*]$; then every frequency of P^* can be decomposed in the form $\lambda = \lambda_{J^*} + \lambda_{C^*}$ with $\lambda_{J^*} \in J^*$ and $\lambda_{C^*} \in [P^*/J^*]$, but $e^{i2\pi\lambda t} = e^{i2\pi\lambda_{J^*}t} e^{i2\pi\lambda_{C^*}t} = e^{i2\pi\lambda_{C^*}t}$, $t \in J$, where we have used the fact that $\lambda_{J^*}t \in \mathbb{Z}$.

Example 7.7 Consider an EM on $J = \mathbb{Z}_2^1(d_1, d_2)$ with periodicity $P = \mathbb{Z}_2^1(4d_1, 4d_2)$. The reciprocal lattices are (see Table 5.5)

$$J^* = \mathbb{Z}_2^1(4F_1, 4F_2), \quad P^* = \mathbb{Z}_2^1(F_1, F_2), \quad F_1 = 1/8d_1, \quad F_2 = 1/8d_2.$$

Then, all the frequencies $\lambda = (\lambda_1, \lambda_2) \in P^*$ are compatible with the periodicity P , but they can be limited to a cell $C^* = [P^*/J^*]$ which is illustrated in Fig. 7.14. This cell contains $N_{C^*} = 16$ points of the lattice P^* and, in fact, $d(J^*) = 32F_1F_2$ and $d(P^*) = 2F_1F_2$, so that $(P^* : J^*) = 16$.

To conclude the consideration on the possible frequencies we note:

Proposition 7.2 *An EM on a lattice J with frequency $\lambda \in J^*$ is irrelevant, that is, it degenerates into the identity.*

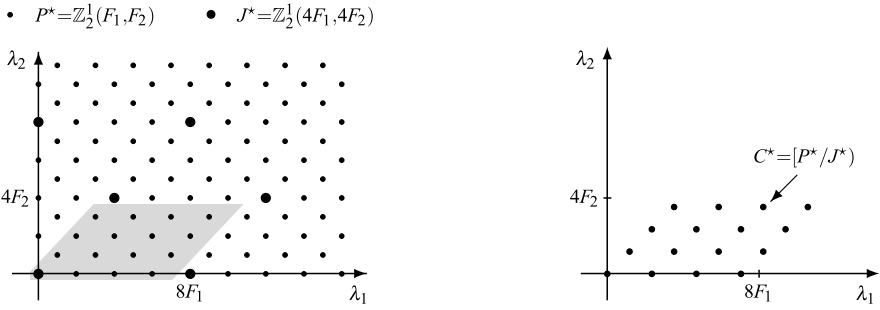


Fig. 7.14 Possible frequencies $(\lambda_1, \lambda_2) \in C^*$ of a 2D EM modulator on the lattice $J = \mathbb{Z}_2^1(d_1, d_2)$ with periodicity $P = \mathbb{Z}_2^1(4d_1, 4d_2)$ (the cell is evaluated through the fundamental parallelepiped)

7.4.2 Down-Sampler/EM Commutativity (NI4)

A $J \rightarrow K$ down-sampler followed by a modulator with an arbitrary carrier $\gamma(t)$, $t \in K$, has the global relationship

$$y(t) = \gamma(t)x(t), \quad t \in K.$$

A modulator on J with carrier $\tilde{\gamma}(t) \in J$ followed by a $J \rightarrow K$ down-sampler has the global relationship

$$\tilde{y}(t) = \tilde{\gamma}(t)x(t), \quad t \in K,$$

where only the values $\tilde{\gamma}(t)$, $t \in K$, give a contribution to the output, and therefore, if $\tilde{\gamma}(t) = \gamma(t)$ on K , the two relationships coincide. Note that the latter is a $J \rightarrow K$ down-sampling relationship. The conclusion holds in particular when $\tilde{\gamma}(t) = \gamma(t)$ is exponential. This proves NI4 of Fig. 7.13.

7.4.3 Up-Sampler/EM Commutativity (NI5)

A $J \rightarrow K$ up-sampler followed by a modulator with an arbitrary carrier $\gamma(t)$, $t \in K$, has the global relationship

$$y(t) = \begin{cases} A_0 \gamma(t)x(t), & \text{if } t \in J; \\ 0, & \text{if } t \in K \setminus J, \end{cases} \quad A_0 = (K : J).$$

A modulator with an arbitrary carrier $\tilde{\gamma}(t)$, $t \in K$, followed by a $J \rightarrow K$ up-sampler has the global relationship

$$\tilde{y}(t) = \begin{cases} A_0 \tilde{\gamma}(t)x(t) & \text{if } t \in J; \\ 0, & \text{if } t \in K \setminus J. \end{cases}$$

In both relationships, only the carrier values on J give a contribution to the output; hence, if $\tilde{\gamma}(t) = \gamma(t)$, $t \in J$, the two relationships coincide. This proves NI5 of Fig. 7.13.

7.4.4 EM/QIL tf Commutativity (NI6). Carrierless Modulation

An EM on J with frequency λ followed by an arbitrary $J \rightarrow K$ QIL tf with impulse response $g(v)$, $v \in J + K$, has the following input–output relation

$$y(t) = \int_J du g(t-u)x(u)e^{i2\pi\lambda u}, \quad t \in K.$$

Considering that $e^{i2\pi\lambda u} = e^{i2\pi\lambda t} e^{-i2\pi\lambda(t-u)}$, we can write

$$y(t) = e^{i2\pi\lambda t} \int_J du g_\lambda(t-u)x(u), \quad t \in K, \quad (7.21)$$

where

$$g_\lambda(v) = g(v)e^{-i2\pi\lambda v} \xrightarrow{\mathcal{F}} G_\lambda(f) = G(f + \lambda). \quad (7.21a)$$

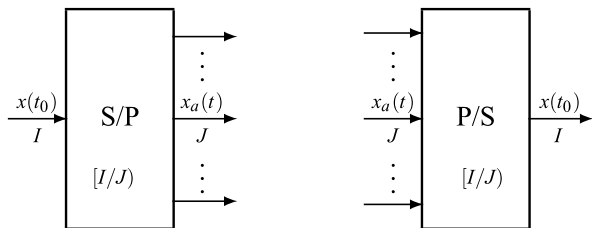
Hence, from (7.21), the original cascade is equivalent to a $J \rightarrow K$ QIL tf with impulse response $g_\lambda(v)$ followed by an EM on K with frequency λ , as shown in Fig. 7.13.

Noble Identity NI6 has several interesting particularizations. If $\lambda \in K^*$, with K^* the reciprocal of K , the EM at the output becomes irrelevant (see Proposition 7.2). This property is sometimes called *carrierless modulation* because it performs a modulation, but without a modulator! The same conclusion holds in a cascade of a $J \rightarrow K$ QIL tf followed by an EM. By NI6, we can transfer the EM at the input; if $\lambda \in J^*$, the EM becomes irrelevant and can be dropped, as shown in Fig. 7.13. An application of carrierless modulation will be seen in OFDM systems at the end of this chapter.

UT 7.5 The Polyphase Decomposition

The previous decompositions of multirate tf's were made in terms of cascade connections, that is, according to a *serial* architecture, but decompositions into a *parallel* architecture are by no means less interesting. The fundamental blocks for these new decompositions are the serial-to-parallel (S/P) and parallel-to-serial (P/S) conversions which are now introduced in a very general (and therefore abstract) form. In the field of multirate systems, an S/P conversion is usually called the *polyphase decomposition*, and in the field of telecommunications a P/S conversion is known as *multiplexing* (time-division multiplexing or TDM).

Fig. 7.15 Serial-to-parallel (S/P) and parallel-to-serial (P/S) conversions



7.5.1 S/P and P/S Conversions

Let I be a lattice and J a sublattice of I . The partition

$$I = J + [I/J] \quad (7.22)$$

permits the decomposition of every point t_0 of I in the form

$$t_0 = t + a \quad \text{with } t \in J \text{ and } a \in [I/J] \triangleq A. \quad (7.23)$$

Here, by definition of a cell, the sum $t + a$, with $t \in J$ and $a \in A$, spans without superposition the whole lattice I . The points $t \in J$ are infinitely many, whereas the cardinality of the cell A is finite and given by the ratio (see Sect. 3.5)

$$N = (I : J) = d(J)/d(I) = \mu(I)/\mu(J). \quad (7.24)$$

For instance, with $I = \mathbb{Z}(T_0)$ and $J = \mathbb{Z}(NT_0)$, a cell A is $\{0, T_0, \dots, (N-1)T_0\}$, and the ratio N represents the ratio of the spacings NT_0 and T_0 .

Now, using (7.23), we can decompose an arbitrary signal $x(t_0)$ defined on the lattice I into N signals (Fig. 7.15)

$$x_a(t) = x(t + a), \quad t \in J, a \in A \quad (7.25)$$

defined on the sublattice J which is N times sparser than I . The a th signal $x_a(t)$ consists of the values of the original signal picked up on the coset $J + a$. Globally, the N signals $x_a(t)$, $a \in A$, pick up all the values of $x(t_0)$ and therefore no information is lost. In fact, the recovery of $x(t_0)$ from $x_a(t)$ is possible according to the relationship

$$x(t + a) = x_a(t), \quad t \in J, a \in A, \quad (7.26)$$

where, as said above, $t + a$ spans without ambiguity all the points $t_0 \in I$.

From (7.24) we have that the rate $\mu(J)$ is N times smaller than the rate $\mu(I)$. In this context, we find it convenient to call $\mu(J)$ a *low rate* and the $\mu(I)$ a *high rate*. With this terminology, we can say that relationship (7.25) establishes the S/P conversion of a high-rate signal $x(t_0)$, $t_0 \in I$, into N low-rate signals $x_a(t)$, $t \in J$, and, analogously, the relationship (7.26) defines the P/S conversion of N low-rate signals $x_a(t)$ into a high-rate signal $x(t_0)$, $t_0 \in I$. We illustrate the above ideas in two specific cases.

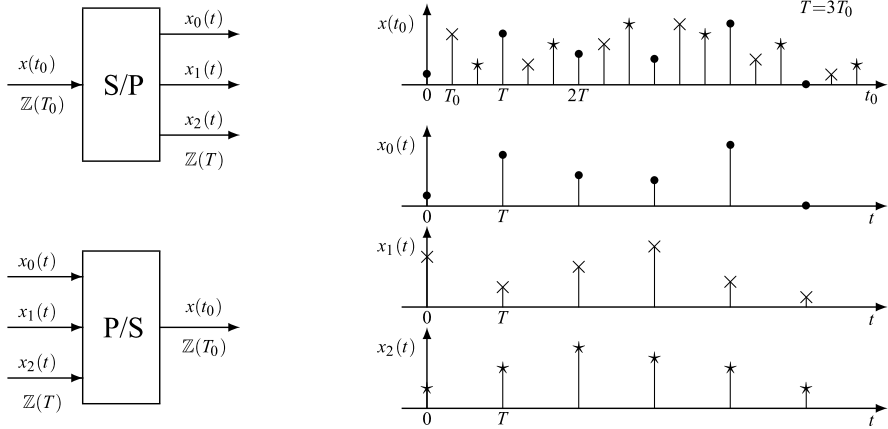


Fig. 7.16 S/P conversion of a signal $x(t_0)$ into three signals $x_0(t), x_1(t), x_2(t)$ and P/S conversion of $x_0(t), x_1(t), x_2(t)$ into $x(t_0)$

Example 7.8 Let $I = \mathbb{Z}(T_0)$ and $J = \mathbb{Z}(3T_0)$. Then the partition (7.22) becomes

$$\mathbb{Z}(T_0) = \mathbb{Z}(3T_0) + \{0, T_0, 2T_0\} \tag{7.27}$$

and allows the formulation of the S/P conversion of a signal $x(t_0), t_0 \in \mathbb{Z}(T_0)$, into three signals $x_a(t), t \in \mathbb{Z}(3T_0)$, as shown in Fig. 7.16. According to (7.27), the lattice $\mathbb{Z}(T_0)$ is partitioned into the sets (cosets)

$$\mathbb{Z}(3T_0), \quad \mathbb{Z}(3T_0) + T_0, \quad \mathbb{Z}(3T_0) + 2T_0, \tag{7.27a}$$

as shown in Fig. 7.17. Correspondingly $t_0 = nT_0 \in \mathbb{Z}(T_0)$ is decomposed as (see (7.25))

$$t_0 = t + a \quad \text{with } t \in \mathbb{Z}(3T_0) \text{ and } a \in \{0, T_0, 2T_0\}.$$

To emphasize this possibility, suppose that $T_0 = 1$, then we have the decomposition of an integer $n \in \mathbb{Z}$ into the form $n = 3k + a$, with $a = 0, 1, 2$. This decomposition is unique since k is the integer division $n/3$ and a the corresponding remainder.

Now, according to (7.25), starting from a signal $x(nT_0), n \in \mathbb{Z}$, we uniquely define 3 signals on $\mathbb{Z}(3T_0)$ by (Fig. 7.16)

$$\begin{aligned} x_0(3kT_0) &= x(3kT_0), & x_1(3kT_0) &= x(3kT_0 + T_0), \\ x_2(3kT_0) &= x(3kT_0 + 2T_0), \end{aligned}$$

which represent the polyphase decomposition of $x(nT_0)$. Note that the rate of $x(t_0)$ is $F_0 = 1/T_0$ and the rate of each $x_a(t)$ is $F = \frac{1}{3}F_0$.

Partition (7.27) allows also the formulation of the P/S conversion of three signals with rate F into a signal with rate $F_0 = 3F$.

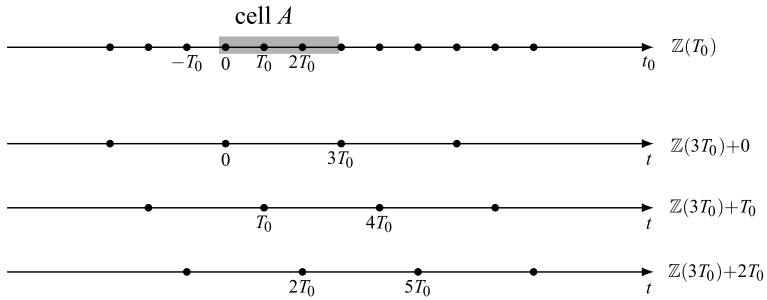


Fig. 7.17 Partition of $\mathbb{Z}(T_0)$ generated by the cell $A = [\mathbb{Z}(T_0)/\mathbb{Z}(3T_0)] = \{0, T_0, 2T_0\}$

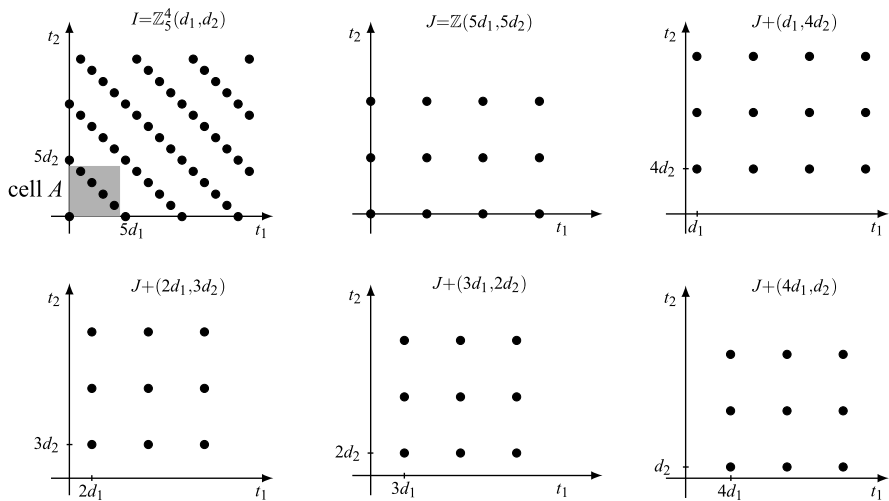


Fig. 7.18 Decomposition of the lattice $I = \mathbb{Z}_5^4(d_1, d_2)$ into the cosets of $J = \mathbb{Z}(5d_1, 5d_2)$

Example 7.9 Let $I = \mathbb{Z}_5^4(d_1, d_2)$ and $J = \mathbb{Z}(5d_1, 5d_2)$. Since $d(I) = 5d_1d_2$ and $d(J) = 25d_1d_2$, all the cells $A = [I/J]$ have size $d(J)/d(I) = 5$. An example of a cell $A = [I/J]$ is shown in Fig. 7.18. This cell generates the decomposition of the lattice $\mathbb{Z}_5^4(d_1, d_2)$ into the 5 cosets of $\mathbb{Z}(5d_1, 5d_2)$ shown in Fig. 7.18.

Correspondingly, we can decompose a signal on $\mathbb{Z}_5^4(d_1, d_2)$ into 5 signals on $\mathbb{Z}(5d_1, 5d_2)$, shown in Fig. 7.19.

Terminology and Remarks

1. We know that, given a lattice I and a sublattice J , the cell $[I/J]$ is not unique. Then we can choose different cells which define different S/P and P/S conversions. For instance, in Example 7.8, in place of $A = \{0, T_0, 2T_0\}$ we can choose $A = \{0, 4T_0, 2T_0\}$ as well. The specific cell A used will be called the *generating cell* (or simply, the *generator*) of S/P and P/S conversions.

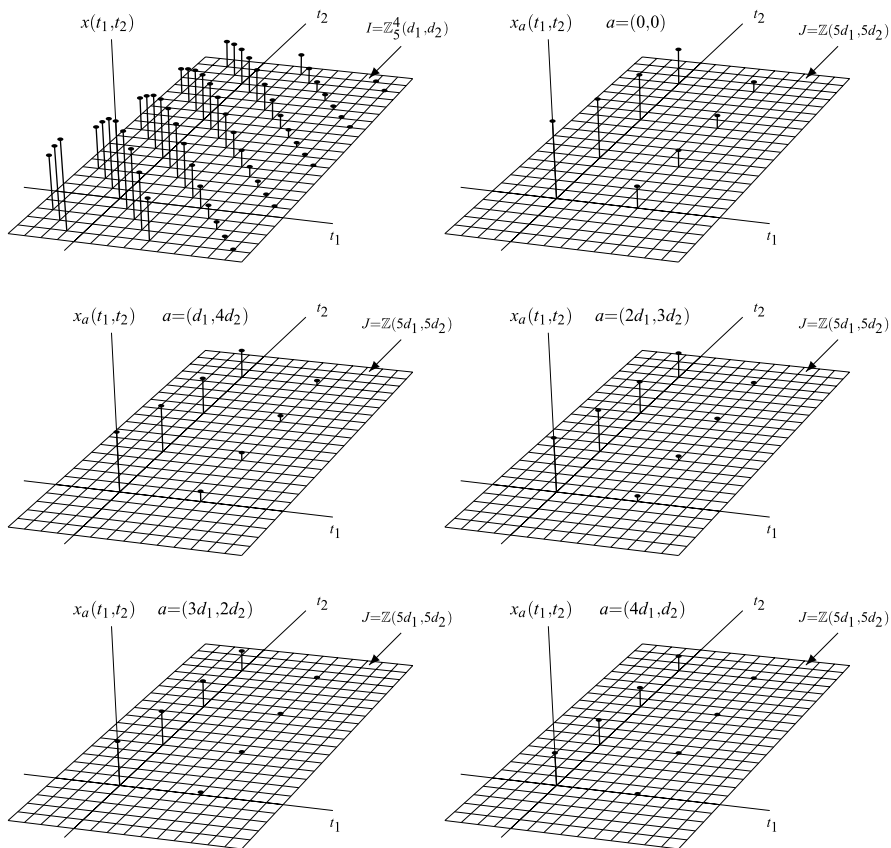


Fig. 7.19 Example of polyphase decomposition of a 2D signal

2. An S/P conversion can be iterated, in the sense that a new S/P conversion can be applied to each component $x_a(t)$. In this case, we work with three lattices I, J, K , with $K \subset J \subset I$, and the partition has the form

$$I = K + [J/K] + [I/J].$$

If $[I/J]$ has N points and $[J/K]$ has M points, we finally obtain the conversion of a signal on I into MN signals on K .

3. An S/P conversion can be applied to decompose a *vector* signal; in this case, each component of the decomposition becomes a vector signal with the same number of components as the original signal.
4. An S/P conversion can be applied to decompose a *multidimensional* signal; in this case, each component has the same dimensionality as the original signal.
5. S/P and P/S conversions can be formulated on *finite* groups where decompositions are done on the basis groups. Given three lattices I_0, J_0 and P with $P \subset J_0 \subset I_0$, the S/P conversion of $x(t_0), t_0 \in I_0/P$ into $x_a(t), t \in J_0/P$ is based

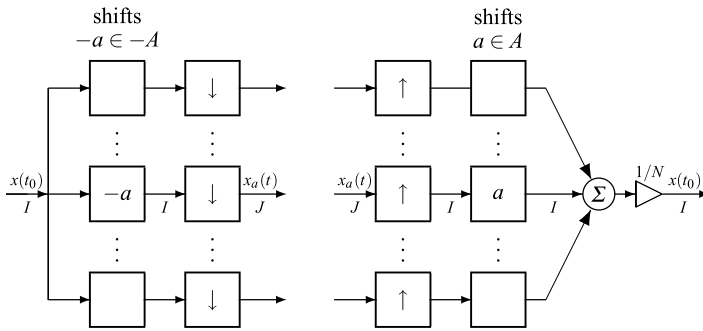


Fig. 7.20 System interpretation of S/P and P/S conversions. The size N of the cell $A = [I/J]$ gives the number of branches

on the partition $I_0 = J_0 + [I_0/J_0]$. Applications of S/P and P/S conversions on finite groups will be developed in Chaps. 12 and 13.

Historical Notes The polyphase decomposition was invented by Bellanger [2] and represents an important advancement in multirate signal processing. It allows great simplifications of theoretical results and also leads to computationally efficient implementation of digital components (both single and multirate). Nowadays, it is universally used; see the tutorial by Vaidyanathan [14].

7.5.2 S/P and P/S Conversions as QIL Transformations

We now show that S/P and P/S conversions can be classified as vector QIL tfs.

The S/P conversion is a 1-input N -output $I \rightarrow J$ tf with $J \subset I$ and then it is downward. The interpretation of the input–output relationship (7.25) is as follows:

1. In the a th branch, the signal $x(t_0)$, $t_0 \in I$, is shifted by $-a$ with $a \in A$; the result is $\tilde{x}_0(t_0) = x(t_0 + a)$, which is still defined on I ,
2. Each $\tilde{x}_a(t_0)$, $t_0 \in I$, is $I \rightarrow J$ down-sampled to get $x_a(t)$ defined on J .

This interpretation leads to the scheme of Fig. 7.20 and allows recognizing that the kernel of the a th branch is given by

$$h_a(t, u_0) = \delta_I(t - u_0 + a), \quad t \in J, \quad u_0 \in I,$$

which depends only on the difference $t - u_0$ and then has the QI property. The impulse response is $\delta_I(v_0 + a)$, $v_0 \in I$, and the global impulse response is the $N \times 1$ matrix (column vector)

$$g_{S/P}(v_0) = [\delta_I(v_0 + a_0), \delta_I(v_0 + a_1), \dots, \delta_I(v_0 + a_{N-1})]', \quad v_0 \in I, \quad (7.28)$$

where a_0, a_1, \dots, a_{N-1} are the points of the cell A .

In the above formulation, the order of operations 1 and 2 cannot be inverted, the reason being that a shift by $-a$ cannot be performed after the down-sampling since, in general, $-a \notin J$. For instance, with $I = \mathbb{Z}(T_0)$ and $J = \mathbb{Z}(3T_0)$ the shift of $-a = -2T_0$ cannot be done on the domain $\mathbb{Z}(3T_0)$, but only on the original domain $\mathbb{Z}(T_0)$.

We now consider the P/S conversion which is N -input 1-output $J \rightarrow I$ with $J \subset I$ and therefore upward. In the input–output relationship (7.26), we see the presence of a shift a in the a th branch, but, due to the above remark, this cannot be performed on the domain J . Therefore, a $J \rightarrow I$ up-sampling is needed before the shift operation. Finally, considering that the up-sampling introduces an amplification of $N = (I : J)$, a multiplication by $1/N$ is required to get exactly the original signal, as shown in Fig. 7.20. The kernel of the a th branch is $(1/N)\delta_I(t_0 - u - a)$, and the global impulse response is given by the $1 \times N$ matrix (row vector)

$$g_{P/S}(v_0) = \frac{1}{N} [\delta_I(v_0 - a_0), \delta_I(v_0 - a_1), \dots, \delta_I(v_0 - a_{N-1})], \quad v_0 \in I. \quad (7.29)$$

We can check that, starting from the general input–output relationship of a vector QIL tf given by (6.96) of Sect. 6.16 and inserting the corresponding impulse responses, namely (7.28) for S/P and (7.29) for P/S, the explicit forms (7.28) and (7.29) are finally obtained.

Since S/P and P/S conversions are QIL tfs, they can be classified on the basis of the domain ordering (see Sect. 6.8). The S/P conversion is *downward* and then it belongs to the class of vector interpolators. Analogously, the P/S conversion is *upward* and then it belongs to the class of vector decimators. Also, we can apply the decomposition theorem for vector QIL tfs (see Theorem 6.9) and so we may find just the decomposition anticipated in Fig. 7.20.

7.5.3 Frequency Domain Analysis

S/P and P/S conversions, as special QIL tfs, are characterized by their frequency responses, that is, the Fourier transform of the corresponding impulse response. Considering that

$$\delta_I(u_0 + a) \xrightarrow{\mathcal{F}} e^{i2\pi f a},$$

from (7.28) and (7.29), we find the frequency responses

$$\begin{aligned} \mathbf{G}_{S/P}(f) &= [e^{i2\pi f a_0}, \dots, e^{i2\pi f a_{N-1}}]', \\ \mathbf{G}_{P/S}(f) &= \frac{1}{N} [e^{-i2\pi f a_0}, \dots, e^{-i2\pi f a_{N-1}}]. \end{aligned} \quad (7.30)$$

Next, considering the frequency analysis of decimators of Sect. 6.14, for the S/P converter we find

$$\mathbf{X}(f) = \sum_{\lambda \in [J^*/I^*]} \mathbf{G}_{S/P}(f - \lambda) X(f - \lambda),$$

and in scalar form

$$X_a(f) = \sum_{\lambda \in [J^*/I^*]} e^{i2\pi(f-\lambda)a} X(f - \lambda), \quad a \in A, \quad (7.31)$$

where the reciprocal cell $A^* = [J^*/I^*]$ has the same cardinality N of the original cell $A = [I/J]$. Analogously, from the frequency analysis of interpolators (see Sect. 6.14), we obtain for the P/S converter

$$X(f) = \mathbf{G}_{P/S}(f) \mathbf{X}(f),$$

and in scalar form

$$X(f) = \frac{1}{N} \sum_{a \in [I/J]} e^{-i2\pi f a} X_a(f), \quad a \in A. \quad (7.32)$$

7.5.4 S/P and P/S Conversion on Finite Groups

Above we have supposed that the domains I and J are lattices, but the S/P and P/S conversion can be also considered on finite groups $I = I_0/P$ and $J = J_0/P$, where for compatibility

$$P \subset J_0 \subset I_0.$$

The theory on finite groups is substantially the same as on lattices, but it acquires special properties owing to the periodicity of signals.

The reference cell A is now given by $A = I_0/J_0$ (with cardinality N) and the basic S/P relation (7.25) is the same

$$x_a(t) = x(t + a), \quad t \in J_0/P, \quad a \in A, \quad (7.33)$$

where a periodic high rate signal $x(t_0)$, $t_0 \in I_0/P$, is converted to N periodic signals $x_a(t)$, $t_0 \in I_0/P$, with the same periodicity P . Considering the cell $[J_0/P]$ and denoting by L its cardinality, the cell $[I_0/P] = [I_0/J_0] + [J_0/P]$ has cardinality LM . Hence, recalling that a cell related to periodic signals gives the *number of signal values per period*, the basic relation (7.33) can be read as follows: the periodic signal $x(t_0)$, having NL values per period, is converted to N signals $x_a(t)$, each one having L values per period.

The rest of the theory on S/P and P/S works well also for signals on finite groups. In particular, the frequency domain relations (7.31) and (7.32) hold with the reciprocal cell given by $A^* = [J_0^*/I_0^*]$ (of cardinality N). Note that the frequencies f and λ become discrete, and in particular the signal $x(t_0)$, $t_0 \in I_0/P$, has Fourier transform $X(f)$, $f \in P^*/I_0^*$, so that $X(f)$ has ML frequencies per period.

A limit case is when the periodicity P coincides with the low rate domain J_0 . Then the low rate signals $x_a(t)$ become defined on J_0/I_0 , and therefore are constant signals, that is, the S/P conversion of a periodic signals $x(t_0)$, having N values per period, produces a vector of N constant signals.

An application of the S/P in the presence of periodicity will be seen in Chap. 13 in the parallel computation of the DFT, which is based on the Fast Fourier Transform (FFT). An application of the limit case $P = J_0$ will be considered at the end of Chap. 12 and also in Chap. 14.

UT 7.6 Parallel Architectures

The S/P and the P/S conversions (or polyphase decomposition and recomposition) are the fundamental tools for the construction of parallel architectures. In this section, we consider the parallel architecture of a general linear tf and, in the next sections, we develop the parallel architectures of QIL tfs and PIL tfs.

7.6.1 Parallel Architecture of a General Linear Transformation

The parallel decomposition of a general $I \rightarrow U$ linear tf, where I and U are lattices (or finite groups), is easily obtained by the application of an S/P conversion at the input and a P/S conversion at the output.

We start from the input–output relationship written in the form

$$y(t_0) = \int_I du_0 h(t_0, u_0)x(u_0), \quad t_0 \in U, \quad (7.34)$$

where the subscript 0 emphasizes that t_0 and u_0 will be regarded as “high-rate” arguments. Then, we choose a sublattice J of I and a sublattice K of U , and two cells to have the domain decompositions

$$I = J + [I/J], \quad U = K + [U/K]. \quad (7.35)$$

Correspondingly, we obtain the argument decompositions as

$$\begin{aligned} u_0 &= u + a, \quad u \in J, \quad a \in [I/J] \triangleq A, \\ t_0 &= t + b, \quad t \in K, \quad b \in [U/K] \triangleq B. \end{aligned} \quad (7.36)$$

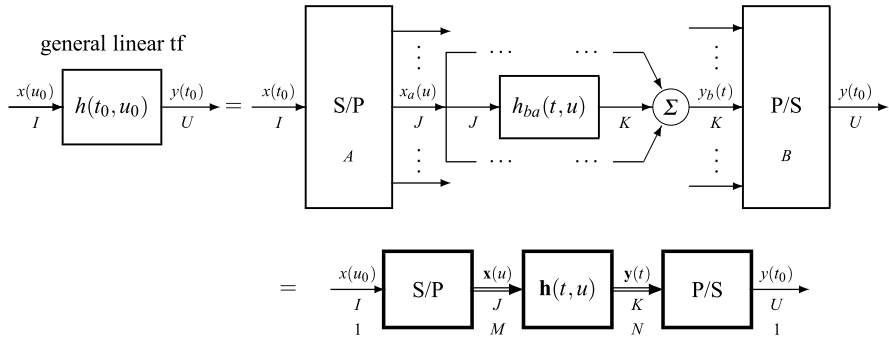


Fig. 7.21 Parallel architecture of an $I \rightarrow U$ linear tf with inner domains the sublattices J and K

At this point, we use the *multirate identity* of the Haar integral (see (4.13))

$$\int_I du_0 f(u_0) = \frac{1}{M} \sum_{a \in A} \int_J du f(u + a), \tag{7.37}$$

which express the integral over the lattice I in terms of an integral over the sublattice J (M is the cardinality of the cell $A = [I/J]$). Then, the application of (7.37) to (7.34) gives

$$y(t + b) = \frac{1}{M} \sum_{a \in A} \int_J du h(t + b, u + a)x(u + a), \quad t \in K, b \in B. \tag{7.38}$$

Next, we let

$$\begin{aligned} x_a(t) &= x(u + a), & y_b(t) &= y(t + b), \\ h_{ba}(t, u) &= (1/M)h(t + b, u + a), \end{aligned} \tag{7.39}$$

where the first line defines the S/P conversions of the input and output signals, respectively. Thus, (7.38) becomes

$$y_b(t) = \sum_{a \in A} \int_J du h_{ba}(t, u)x_a(u), \quad t \in K, b \in B. \tag{7.40}$$

If the cardinalities of the cells A and B are M and N , respectively, (7.40) represents the input–output relationship of an M -input N -output $J \rightarrow K$ linear tf which can be written in the compact form

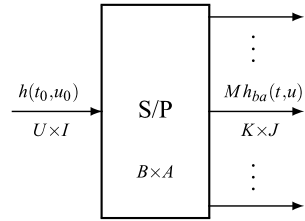
$$\mathbf{y}(t) = \int_J du \mathbf{h}(t, u) \mathbf{x}(u), \quad t \in K, \tag{7.40b}$$

$N \times 1 \quad N \times M \quad M \times 1$

where the $M \times 1$ column vector $\mathbf{x}(u)$ collects the input components $x_a(u)$ and the $N \times 1$ column vector $\mathbf{y}(t)$ collects the output components $y_b(t)$.

The above statements are illustrated in Fig. 7.21 and are summarized as:

Fig. 7.22 The kernel matrix $\mathbf{h}(t, u) = [h_{ba}(t, u)]$ as the S/P conversion of the kernel $h(t_0, u_0)$



Theorem 7.6 Given an $I \rightarrow U$ linear tf with the kernel $h(t_0, u_0)$, $(t_0, u_0) \in U \times I$, where I and U are lattices, choose a sublattice J of I and a sublattice K of U and two cells $A = [I/J]$ and $B = [U/K]$. Then, the tf can be decomposed into the cascade of:

1. An $I \rightarrow J$ S/P conversion generated by a cell $A = [I/J]$ with the relation $x_a(u) = x(u + a)$, $u \in J$, $a \in [I/J] \triangleq A$,
2. An M -input N -output $J \rightarrow K$ linear tf with the kernel

$$\mathbf{h}(t, u) = [h_{ba}(t, u)] = \frac{1}{M} [h(t + b, u + a)], \tag{7.41}$$

where M and N are the cardinalities of A and B , respectively, and

3. A $K \rightarrow U$ P/S conversion generated by a cell $B = [U/K]$ with relation $y(t + b) = y_b(t)$, $t \in K$, $b \in [U/K] \triangleq B$.

The elements $h_{ba}(t, u)$ of the $N \times M$ matrix $\mathbf{h}(t, u)$ are obtained as the S/P conversion of the original kernel $h(t_0, u_0)$. This conversion acts at multidimensional level as a $U \times I \rightarrow K \times J$ tf with generator given by the composite cell $B \times A$ (Fig. 7.22).

Note that the philosophy of a parallel architecture lies in the decomposition of a given tf into several branches, and the output signal is finally given by summing the contributions of each branch. In general, in Theorem 7.6 there is no constraint for the input and output lattices, $I \rightarrow U$, which may also have different dimensionality.

7.6.2 Examples

Example 7.10 With $I = \mathbb{Z}(2)$, $U = \mathbb{Z}(3)$, we can choose $J = \mathbb{Z}(4)$, $K = \mathbb{Z}(9)$ and $A = [I/J] = \{0, 2\}$, $B = [U/K] = \{0, 3, 6\}$. The polyphase vectors $\mathbf{x}(u)$, $\mathbf{y}(t)$ and the impulse response matrix $\mathbf{h}(u, t)$ are

$$\mathbf{x}(u) = \begin{bmatrix} x_0(t) \\ x_2(t) \end{bmatrix} = \begin{bmatrix} x(u) \\ x(u + 2) \end{bmatrix}, \quad \mathbf{y}(t) = \begin{bmatrix} y_0(t) \\ y_3(t) \\ y_6(t) \end{bmatrix} = \begin{bmatrix} y(t) \\ y(t + 3) \\ y(t + 6) \end{bmatrix},$$

$$\mathbf{h}(t, u) = \begin{bmatrix} h_{00}(t, u) & h_{02}(t, u) \\ h_{30}(t, u) & h_{32}(t, u) \\ h_{60}(t, u) & h_{62}(t, u) \end{bmatrix} = \frac{1}{3} \begin{bmatrix} h(t, u) & h(t, u + 2) \\ h(t + 3, u) & h(t + 3, u + 2) \\ h(t + 6, u) & h(t + 6, u + 2) \end{bmatrix}.$$

Example 7.11 Another example is with $I = \mathbb{Z}^2$, $U = \mathbb{Z}(2)$, $J = \mathbb{Z}(2, 2)$, $K = \mathbb{Z}(6)$, where the input signal is 1D and the output signal is 2D. Then $A = [I/J] = \{(0, 0)(0, 1)(1, 0)(1, 1)\}$, $B = [U/K] = \{0, 2, 4\}$ and

$$\mathbf{x}(u_1, u_2) = \begin{bmatrix} x(u_1, u_2) \\ x(u_1, u_2 + 1) \\ x(u_1 + 1, u_2) \\ x(u_1 + 1, u_2 + 2) \end{bmatrix}, \quad \mathbf{y}(t) = \begin{bmatrix} y(t) \\ y(t + 2) \\ y(t + 4) \end{bmatrix},$$

$\mathbf{h}(t; u_1, u_2)$

$$= \frac{1}{4} \begin{bmatrix} h(t; u_1, u_2) & h(t; u_1, u_2 + 1) & h(t; u_1 + 1, u_2) & h(t; u_1 + 1, u_2 + 1) \\ h(t + 2; u_1, u_2) & h(t + 2; u_1, u_2 + 1) & h(t + 2; u_1 + 1, u_2) & h(t + 2; u_1 + 1, u_2 + 1) \\ h(t + 4; u_1, u_2) & h(t + 4; u_1, u_2 + 1) & h(t + 4; u_1 + 1, u_2) & h(t + 4; u_1 + 1, u_2 + 1) \end{bmatrix}.$$

Note that the vectors and the matrix have been ordered following the lexicographical order.

Lexicographical Order In the 1D case, the discrete cells have a *natural* ordering, so that vectors and matrices that take the indices from a 1D cell are well defined. In the multidimensional case, we have no natural ordering, but we can use the *lexicographical order*. This name comes from the order given to words in a dictionary: a word of k letters, $\mathbf{a} = (a_1, \dots, a_k)$, appears in a dictionary before the word $\mathbf{b} = (b_1, \dots, b_k)$, symbolized $\mathbf{a} < \mathbf{b}$, if and only if the first a_i which is different from b_i comes before b_i in the alphabet. In our context, the alphabet is given by the set of integers. Then, we find, e.g., that $(1, 3) < (2, 1)$, $(0, 3, 2) < (1, 0, 1)$ and $(1, 1, 3) < (1, 2, 0)$.

7.6.3 Decompositions Limited to the Input or to the Output

In the parallel architecture of Fig. 7.21, J and K are arbitrary sublattices of I and U , respectively, but we have tacitly supposed that they are *proper* sublattices so that the cells $A = [I/J]$ and $B = [U/K]$ are not degenerate ($M, N \geq 2$). The corresponding configuration is referred to as the *input/output decomposition*. However, the theory holds also in the degenerate cases.

If we choose $K = U$ (and J a proper subset of I), the cell B becomes $[U/U] = \{0\}$, without the decomposition of the output signal, and we have the *input decomposition*, where the matrix (7.41) becomes

$$\mathbf{h}(t_0, u) = (1/M)[h_a(t_0, u)] = [h(t_0, u + a)], \quad a \in A,$$

with size $1 \times M$, that is, a row vector, as shown in Fig. 7.23.



Fig. 7.23 *Input decomposition and output decomposition of an $I \rightarrow U$ linear tf*

Analogously, if we choose $J = I$ (and K a proper subset of U), we find $A = [I/I] = \{0\}$ without the decomposition of the input signal, and we have the *output decomposition*, where the matrix (7.41) becomes

$$\mathbf{h}(t, u_0) = [h_b(t, u_0)] = [h(t + a, u_0)], \quad b \in B,$$

with size $N \times 1$, that is, a column vector.

UT 7.7 Parallel Architectures of QIL Transformations

We have seen that in the decomposition of a general $I \rightarrow U$ tf the domains may be arbitrary lattices. Here, in the decomposition of a QIL tf, the domains I and U must be *rationally comparable* to assure that the sum $I + U$ is LCA (see Sect. 3.9).

7.7.1 Parallel Architectures of a General QIL Transformation

The parallel architecture of a QIL tf, obtained with an input/output decomposition, can be implemented by QIL tfs. In fact, the original kernel has the form $h(t_0, u_0) = g(t_0 - u_0)$ and, with the argument decomposition (7.36), becomes

$$h_{ba}(t, u) = (1/M)g(t + b - u - a)$$

and can be reformulated in terms of impulse responses. Hence, given an $I \rightarrow U$ QIL tf with the impulse response $g(v_0)$, $v_0 \in I + U$, the corresponding parallel architecture has the impulse responses

$$g_{ba}(v) = (1/M)g(v + b - a), \quad v \in J + K, \quad a \in A, \quad b \in B, \quad (7.42)$$

which are obtained by an $I + U \rightarrow J + K$ S/P conversion of the original impulse response. This parallel decomposition is illustrated in Fig. 7.24. Note that the $N \times M$ matrix $\mathbf{g}(v)$, collecting the impulse responses (7.42) does not have NM distinct entries because $g_{ba}(v)$ depends only on the difference $b - a$. In the case $N = M$, the matrix $\mathbf{g}(v)$ is a *circulant* (see Problem 7.8).

Note that, given an $I \rightarrow U$ QIL tf, one may find infinitely many parallel architectures depending on the choice of the sublattices J, K and of the cells $A = [I/J]$, $B = [U/K]$, where the degenerate cases $J = I$ or $K = U$ are not excluded.

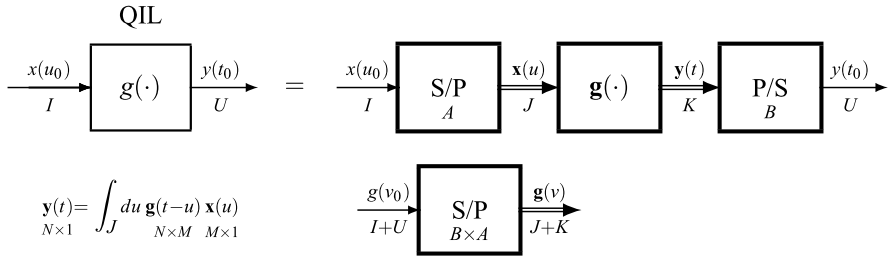


Fig. 7.24 Parallel architecture of an $I \rightarrow U$ QIL tf and interpretation of the impulse response matrix $\mathbf{g}(v)$, obtained as the S/P conversion of the original impulse response $g(v_0)$

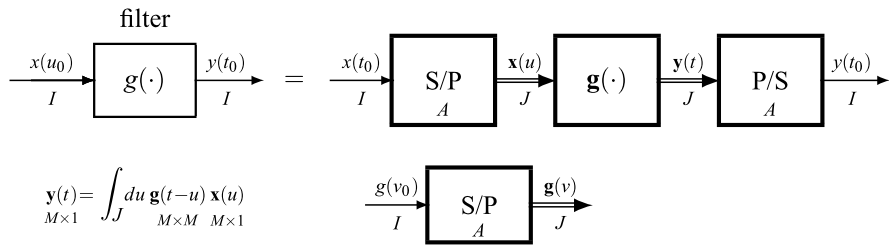


Fig. 7.25 Parallel architecture of a filter on I with inner domain J

7.7.2 Parallel Architecture of a Filter

For a filter on the lattice I , it is sufficient to choose a sublattice J of I , and correspondingly a cell $A = [I/J]$, which generates the S/P conversion at the input and the P/S conversion at the output. Hence, the filter is decomposed into the cascade of (Fig. 7.25):

1. An $I \rightarrow J$ S/P converter,
2. A M -input M -output filter on J with the impulse response

$$\mathbf{g}(v) = [g_{ba}(v)] = (1/M)[g(v + b - a)], \quad v \in J, \quad a, b \in A, \quad (7.43)$$

3. A $J \rightarrow I$ P/S converter.

The impulse responses $g_{ab}(v)$ are obtained by the S/P conversion of $g(v_0)$, $v_0 \in I$, namely

$$g_c(v) = (1/M)g(v + c), \quad v \in J, \quad c \in A.$$

Note that in (7.43) the matrix is $M \times M$, and then we have M^2 low-rate filters.

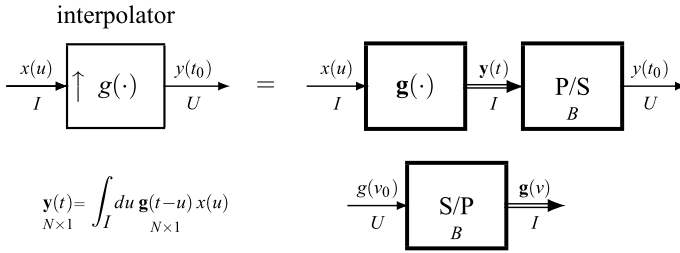


Fig. 7.26 Parallel architecture of an $I \rightarrow U$ interpolator with inner domain I

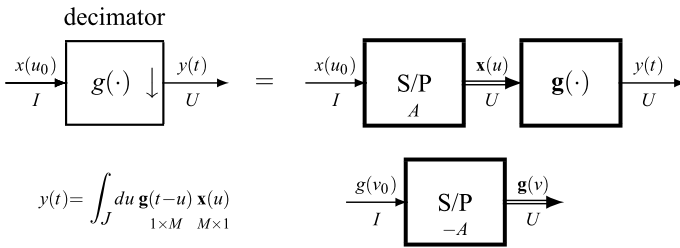


Fig. 7.27 Parallel architecture of an $I \rightarrow U$ decimator with inner domains U

7.7.3 Parallel Architecture of an Interpolator

One of the possible choices is to limit the decomposition to the output. Then, an $I \rightarrow U$ interpolator is decomposed as the cascade of (Fig. 7.26):

1. A 1-input N -output filter on I with the impulse response

$$\mathbf{g}(v) = [g_b(v)] = [g(v + b)], \quad v \in I, \quad b \in B = [U/I],$$

2. An $I \rightarrow U$ P/S converter,

where the N low-rate impulse responses $g_b(v)$ of the column vector $\mathbf{g}(v)$ are obtained as the $U \rightarrow I$ S/P conversion of $g(v_0)$, $v_0 \in U$ (N is the size of B).

7.7.4 Parallel Architecture of a Decimator

In this case, the conversion can be limited to the input. Then, the parallel architecture consists of (Fig. 7.27):

1. An $I \rightarrow U$ S/P converter,
2. An M -input 1-output filter with the impulse response given by the $1 \times M$ matrix:

$$\mathbf{g}(v) = [g_a(v)] = (1/M)[g(v - a)], \quad -a \in -A.$$

The M low-rate impulse responses $g_a(v)$ of the row vector $\mathbf{g}(v)$ are given by the $I \rightarrow U$ S/P conversion of the original impulse response $g(v_0)$, $v_0 \in I$, multiplied by $1/M$. Here, the generating cell is $-A$ instead of A (M is the size of the cell A).

About the Factor $1/M$ This factor, somewhat disturbing, is a consequence of the multirate identity (7.37) used for the input decomposition. Thus, it is present when the input decomposition is really applied, that is, in the decimator decomposition, but not in the interpolator decomposition.

UT 7.8 Parallel Architectures of PIL Transformations

We recall that an $I \rightarrow U$ linear tf is periodically invariant (PIL) if the kernel verifies the condition

$$h(t_0 + p, u_0 + p) = h(t_0, u_0), \quad p \in P, \quad (7.44)$$

where $P \subset I \cap U$ is the periodicity. It is assumed that I and U are rationally comparable.

We now show that a PIL tf can be decomposed into parallel architectures whose inner part is given by QIL tfs. In the decompositions, we choose as inner domain just the periodicity P .

7.8.1 Input Decomposition

To get the input decomposition, we apply Theorem 7.6 with $J = P$ and $K = U$. Then, the kernel components are given by

$$h_a(t_0, u) = (1/M)h(t_0, u + a), \quad a \in A = [I/P], \quad t_0 \in U, \quad u \in P,$$

where

$$a \in A = [I/P], \quad t_0 \in U, \quad u \in P,$$

and, using the periodicity condition (7.44) with $p = -u$, we find

$$h_a(t_0, u) = (1/M)h(t_0 - u, a) \stackrel{\Delta}{=} g_a(t_0 - u), \quad t_0 \in U, \quad u \in P.$$

Hence, the kernel components depend only on the difference $t_0 - u$, which assures the QI. Since $U \supset P$, such a parallel decomposition is upward and therefore involves interpolators.

Proposition 7.3 *An $I \rightarrow U$ PIL tf with the kernel $h(t_0, u_0)$ and periodicity P can be decomposed into the cascade of:*

1. An $I \rightarrow P$ S/P converter with the generator $A = [I/P]$ of cardinality M ,

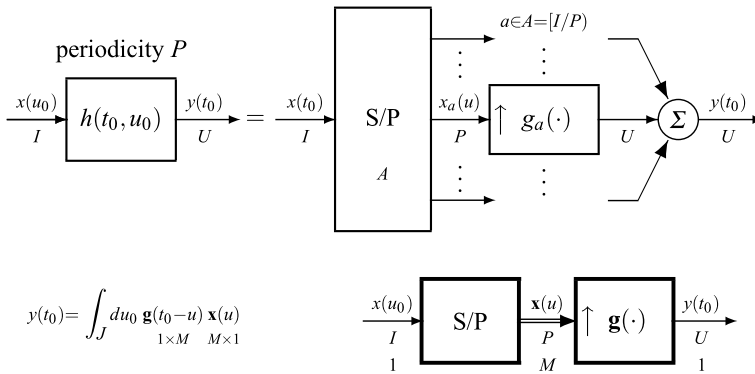


Fig. 7.28 Input decomposition of a PIL $I \rightarrow U$ tf with periodicity P with a bank of M interpolators, with M the cardinality of the cell $A = [I/P]$

2. An M -input 1-output $P \rightarrow U$ interpolator with the impulse response

$$\mathbf{g}(t_0) = [g_a(t_0)] \stackrel{\Delta}{=} (1/M)[h(t_0, a)], \quad t_0 \in U. \tag{7.45}$$

The decomposition is illustrated in Fig. 7.28.

7.8.2 Output Decomposition

We apply Theorem 7.6 with $J = I$ and $K = P$. Then:

Proposition 7.4 An $I \rightarrow U$ PIL tf with the kernel $h(t_0, u_0)$ and periodicity P can be decomposed into the cascade of:

1. A 1-input N -output $I \rightarrow P$ decimator with the impulse response

$$\mathbf{q}(u_0) = [q_b(u_0)] \stackrel{\Delta}{=} [h(b, -u_0)], \quad u_0 \in I, \quad b \in B,$$

2. A $P \rightarrow U$ P/S converter with the generator $B = [U/P]$ of cardinality N .

The decomposition is illustrated in Fig. 7.29.

Interpretation of the Impulse Responses The kernel $h(t_0, u_0)$ is defined on the lattice $U \times I$. The impulse response $g_a(t_0)$ of the interpolators (input decomposition) and the impulse response $q_b(u_0)$ of the decimators (output decomposition) are obtained by picking up values of $h(t_0, u_0)$.

To get insight, we investigate these impulse responses on the (t_0, u_0) -“plane”, where $h(t_0, u_0)$ is defined. We consider the 1D case $I = \mathbb{Z}(2)$, $U = \mathbb{Z}(3)$ and $P = \mathbb{Z}(12)$, where the “plane” is the lattice $\mathbb{Z}(3) \times \mathbb{Z}(2)$, shown in Fig. 7.30. In the input

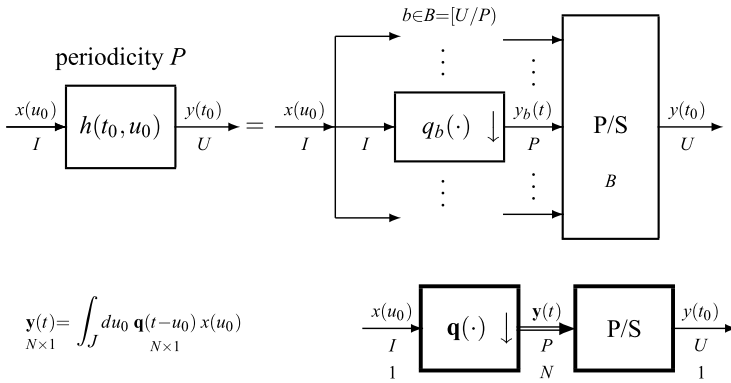


Fig. 7.29 Output decomposition of a PIL $I \rightarrow U$ tf with periodicity P with a bank of N decimators, with N the cardinality of the cell $B = [U/P]$

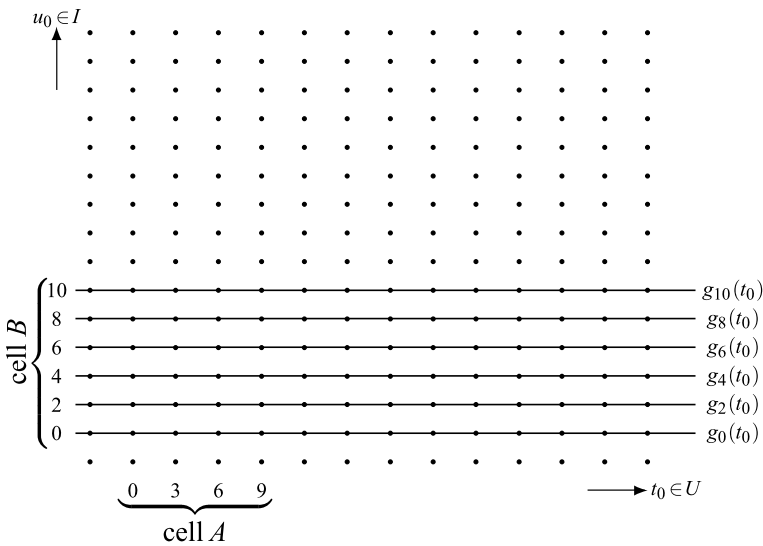


Fig. 7.30 Interpretation of the interpolators impulse responses in the input decomposition of a PIL tf on the “plane” $U \times I = \mathbb{Z}(3) \times \mathbb{Z}(2)$ with periodicity $P = \mathbb{Z}(12)$

decomposition, the cell is $A = [I/P] = [\mathbb{Z}(2)/\mathbb{Z}(12)] = \{0, 2, 4, 6, 8, 10\}$, and the impulse responses of the $M = 6$ interpolators are $g_a(t_0) = (1/6)h(t_0, a)$, $a \in A$, and can be read along the 6 horizontal “lines” $(t_0, 0)$, $(t_0, 2)$, \dots , $(t_0, 10)$ of the (t_0, u_0) -“plane”.

On the other hand, the 6 interpolators identify the original PIL tf. This means that the information on the kernel $h(t_0, u_0)$ is completely contained along these “lines” and, in fact, from these “lines” we can obtain all the other values of $h(t_0, u_0)$, using the periodicity. For instance, the value $h(27, 38)$ is obtained considering that $h(27 + 12n, 38 + 12n) = h(27, 38)$ with $n \in \mathbb{Z}$, and, choosing $n = -3$,

we have $h(27, 38) = h(9, 2)$, which corresponds to the impulse response $g_2(t_0) = (1/6)h(t_0, 2)$ with $t_0 = 9$. In the output decomposition, the cell is $B = [U/P] = [\mathbb{Z}(3)/\mathbb{Z}(12)] = \{0, 3, 6, 9\}$, and the impulse responses of the $N = 4$ decimators are $g_b(u_0) = h(b, -u_0)$, $b \in B$, and can be read along the vertical “lines” $(0, u_0)$, $(3, u_0)$, $(6, u_0)$, $(9, u_0)$.

Concluding Remarks

We have seen the parallel architecture of a general linear tf and several configurations for the subclasses of QIL tfs and PIL tfs. All these architectures play a fundamental role in the broad field of signal processing and in particular in sub-band coding, transmultiplexer and multiresolution analysis (see Chap. 14).

UT 7.9 Parallel Architectures with Modulators

In the previous section, PIL tfs have been decomposed into parallel architectures of QIL tfs where the periodic invariance was “distributed” between QIL tfs and the S/P and P/S conversions. In this section, we develop a parallel architecture of PIL tfs in terms of QIL tfs and exponential modulators (EMs) where the periodic invariance is essentially concentrated in the EMs.

The decomposition technique is based on the Fourier transform on finite groups (DFT) (see Sect. 5.9) where the finite groups are obtained in the form J/P and K/P with P being the periodicity of the given PIL tf. In the general case, the difficulty of the decomposition is due to the *diagonal form* of the kernel periodicity, that is, $h(t + p, u + p) = h(t, u)$. Here, we develop the ordered cases: $J \subset K$ and $K \supset J$ where the decomposition becomes simpler. The general case is developed in [5].

7.9.1 Parallel Architecture of a General Modulator

We begin with the decomposition of a general modulator with a periodic carrier $\gamma(t)$, $t \in J$, having the relation

$$y(t) = \gamma(t)x(t), \quad t \in J. \quad (7.46)$$

If $\gamma(t)$ has periodicity $P \subset J$, it can be represented on the finite group $I = J/P$ and expressed as the inverse Fourier transform (IDFT) in the form (see (5.89))

$$\gamma(t) = \sum_{\lambda \in \hat{I}} d(P^*) \Gamma(\lambda) e^{i2\pi\lambda t} \xrightarrow{\mathcal{F}} \Gamma(\lambda) = \sum_{t \in I} d(J) \gamma(t) e^{-i2\pi\lambda t},$$

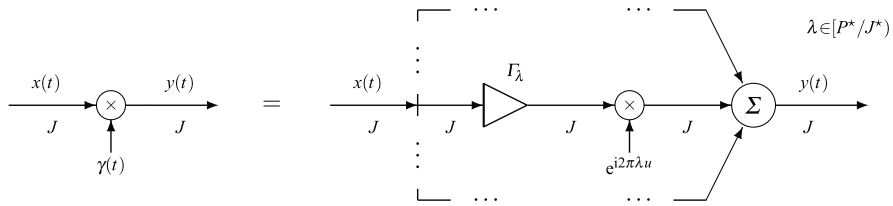


Fig. 7.31 Decomposition of a general modulator with periodicity P with exponential modulators

where $\hat{I} = P^*/J^*$ and the summations are extended over the cells $C^* = [P^*/J^*]$ and $C = [J/P]$, both having the finite cardinality $N = (P^* : J^*) = (J : P)$. Setting $\Gamma_\lambda = d(P^*) \Gamma(\lambda)$, we have

$$\gamma(t) = \sum_{\lambda \in [P^*/J^*]} \Gamma_\lambda e^{i2\pi\lambda t}, \tag{7.47}$$

and (7.46) becomes

$$y(t) = \sum_{\lambda \in [P^*/J^*]} \Gamma_\lambda e^{i2\pi\lambda t} x(t), \quad t \in J. \tag{7.48}$$

The interpretation of (7.48) shows that a general modulator can be synthesized by a finite number N of exponential modulators and multipliers, as shown in Fig. 7.31. In the frequency domain, (7.48) gives

$$Y(f) = \sum_{\lambda \in [P^*/J^*]} \Gamma_\lambda X(f - \lambda). \tag{7.49}$$

Now, we realize that a periodical carrier operating on a lattice provides a *multitone* modulation since it exhibits $N = (J : P)$ “tones”, whereas the exponential carrier $e^{i2\pi\lambda t}$ is *single-tone*, with the “tone” given by the frequency λ .

7.9.2 Parallel Architecture of a General PIL Transformation

In a $J \rightarrow K$ PIL tf with periodicity P , we have two cells which relate the input and output domains with the periodicity: the input cell $C_J = [J/P]$ with cardinality $N_J = (J : P)$ and the output cell $C_K = [K/P]$ with cardinality $N_K = (K : P)$. Correspondingly, we have the two parallel architectures shown in Fig. 7.32.

The *Input Decomposition* holds with $J \subset K$ and is based on the kernel decomposition

$$h(t, u) = \sum_{\lambda \in [P^*/J^*]} g_\lambda(t - u) e^{i2\pi\lambda u}, \tag{7.50}$$

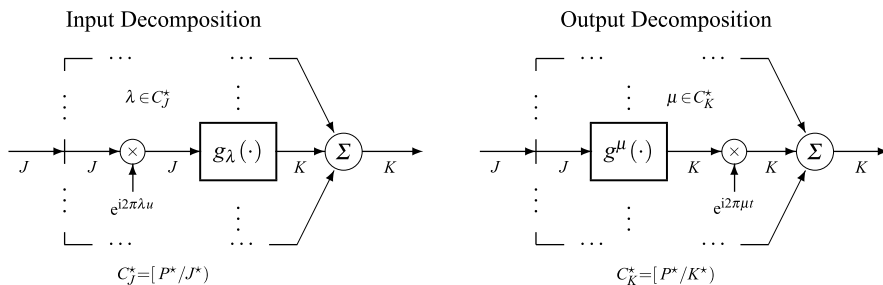


Fig. 7.32 Decompositions of a PIL tf into a bank of QIL tfs and exponential modulators

where

$$g_{\lambda}(v) = \frac{1}{N_J} \sum_{z \in [J/P]} h(v + z, z) e^{-i2\pi\lambda z}, \quad \lambda \in [P^*/J^*]. \tag{7.51}$$

In (7.50), the generic term has the form $h_{\lambda}(t, u) = g_{\lambda}(t - u) e^{i2\pi\lambda u}$, $t \in K$, $u \in J$, which represents a $J \rightarrow K$ QIL tf with impulse response $g_{\lambda}(v)$ preceded by an EM with frequency λ , as shown in Fig. 7.32. The proof of (7.50) is given in the Appendix.

The *Output Decomposition* holds with $J \supset K$ and is based on the kernel decomposition

$$h(t, u) = \sum_{\mu \in [P^*/K^*]} g^{\mu}(t - u) e^{i2\pi\mu t}, \tag{7.52}$$

where

$$g^{\mu}(v) = \frac{1}{N_K} \sum_{z \in [K/P]} h(z, v + z) e^{-i2\pi\mu z}. \tag{7.53}$$

Decompositions (7.50) and (7.52) are obtained by expressing the diagonal periodicity of the kernel via IDFT/DFT. The proof is given in the Appendix.

In Input Decomposition, the number N_J of branches is given by the cardinality of the cells $C_J = [J/P]$ and $C_J^* = [P^*/J^*]$, that is, by $N_J = (J : P)$. Similarly, the number of branches in Output Decomposition is given by $N_K = (K : P)$. However, both decompositions are redundant and not unique, in general. This can be seen by using Noble Identity NI6 on the EM/QIL tf commutativity, which allows transferring EMs from the input to the output, and vice versa. In these commutations, some EMs may become irrelevant with a consequent reduction of the branches.

Another remark is concerned with the limit case of periodicity $P = J \cap K \triangleq P_0$. In fact, we know that a $J \rightarrow K$ PIL tf with periodicity P_0 degenerates into a $J \rightarrow K$ QIL tf, and a decomposition with a single branch without EM is possible. But, if we apply the above decomposition to this limit case, we find several branches, in general.

Example 7.12 Consider a 1D PIL tf with $J = \mathbb{Z}(3)$, $K = \mathbb{Z}(5)$ and periodicity $P = \mathbb{Z}(45)$. Let $F = 1/45$, then the reciprocals are $J^* = \mathbb{Z}(15F)$, $K^* = \mathbb{Z}(9F)$ and $P^* = \mathbb{Z}(F)$. The Input Decomposition consists of $N_J = 15$ branches, where the EMs have frequencies

$$\lambda \in C_J^* = [P^*/J^*] = [\mathbb{Z}(F)/\mathbb{Z}(15F)] = \{0, F, 2F, \dots, 13F, 14F\}.$$

The Output Decomposition consists of $N_K = 9$ branches, where the EMs have frequencies

$$\mu \in C_K^* = [P^*/K^*] = [\mathbb{Z}(F)/\mathbb{Z}(9F)] = \{0, F, \dots, 8F\}.$$

If we consider the limit case of periodicity $P_0 = J \cap K = \mathbb{Z}(15)$, we find that Input Decomposition has $N_J = 5$ branches with frequencies $C_J^* = \{0, F, 2F, 3F, 4F\}$ with $F = 1/15$, and Output Decomposition has $N_K = 3$ branches with frequencies $C_K^* = \{0, F, 2F\}$. In both cases, we find the presence of EMs.

7.9.3 Minimal Decomposition

It is possible to formulate the *minimal* decomposition, that is, with the minimum number of branches [5]. To this end, the first step is the replacement of the kernel $h(t, u)$, which is defined on $K \times J$, with its $K \times J \rightarrow E \times J$ up-sampled version $\widehat{h}(t, u)$, where $E = K + J$. Then, the kernel can be decomposed in the form

$$h(t, u) = \sum_{\lambda \in [P^*/P_0^*]} p_\lambda(t - u) e^{i2\pi\lambda u}, \quad (7.54)$$

where $P_0 = J \cap K$ and

$$p_\lambda(v) = \frac{1}{N_J} \sum_{r \in C_J} \widehat{h}(v + r, r) e^{-i2\pi\lambda v}. \quad (7.54a)$$

Hence, we obtain the same scheme as in Input Decomposition, but with the number of branches given by $N_0 = (P_0 : P)$, where P is the periodicity of the given $J \rightarrow K$ PIL tf and $P_0 = J \cap K$ is the maximum periodicity compatible on the pair $J \rightarrow K$.

As a check of minimality, when $P = P_0$, the PI become the QI and, in fact, $N_0 = (P_0 : P_0) = 1$, and we have only one branch without the EM (since the EM has frequency $\lambda = 0$).

Example 7.13 With $J = \mathbb{Z}(3)$, $K = \mathbb{Z}(5)$ and $P = \mathbb{Z}(45)$, we have seen that the Input Decomposition has $N_J = 15$ branches and Output Decomposition has $N_K = 9$ branches. Now, the minimal decomposition has $N_0 = (P_0 : P) = (\mathbb{Z}(15) : \mathbb{Z}(45)) = 3$ branches with the frequency set $[P^*/P_0^*] = [\mathbb{Z}(F)/\mathbb{Z}(3F)] = \{0, F, 2F\}$ and $F = 1/45$.

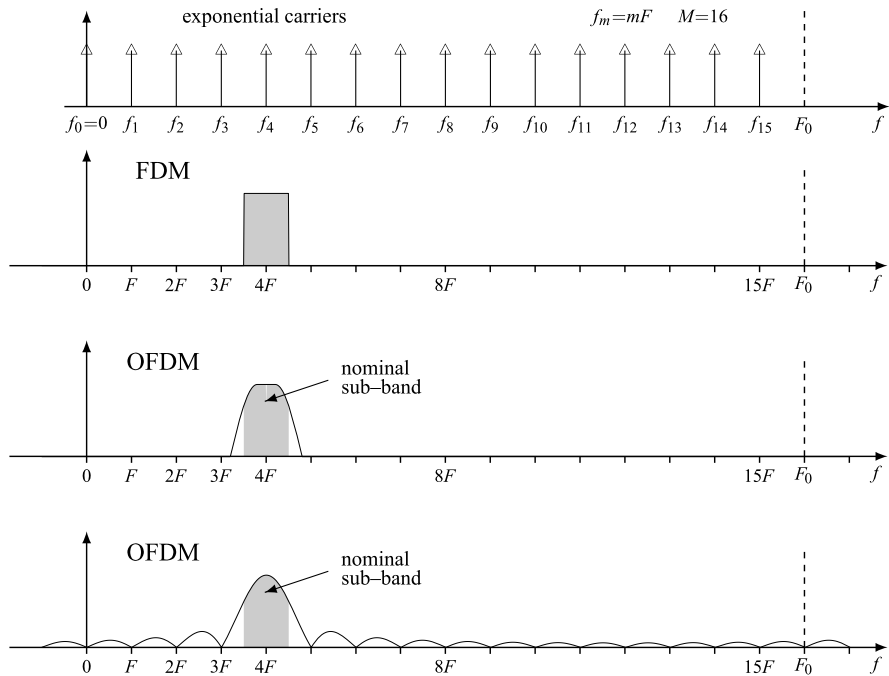


Fig. 7.33 Sub-channel allocation for the FDM and OFDM (in two versions)

7.10 Multirate Application to OFDM (Transmultiplexer)

The orthogonal frequency division multiplexing (OFDM) is one of the most interesting applications of multirate systems used for data transmission. It may be regarded as a generalization of the traditional frequency division multiplexing (FDM). Given a band $(f_0, f_0 + F_0)$, the data sequence to be transmitted is subdivided into M subsequences which are modulated by equally spaced carriers with frequencies (Fig. 7.33)

$$f_0, f_0 + F, \dots, f_0 + (M - 1)F, \tag{7.55}$$

where f_0 is a reference frequency and F is the frequency spacing ($F = F_0/M$). Finally, the modulated sequences are conveyed into a unique multiplexed signal. In the receiver, the M subsequences are recovered from the multiplexed signal.

In FDM, the subsequences are band-limited with a bandwidth F (see Fig. 7.33) and hence the recovery condition is clearly assured. However, the band limitation to the frequency spacing F is not required and, in general, the constraint for a correct recovery is provided by *orthogonality conditions* on the impulse responses of the sub-channels. In such a way, FDM becomes the OFDM.

In this section, we introduce the basic idea of OFDM and, using the previously described multirate theory, we develop efficient architectures. We recall that the OFDM has several other interesting properties, as the multi-path robustness ob-

tained by means of a cyclic prefix. This feature will be not developed here. The topic of the transmultiplexer will be reconsidered in Chap. 14, in the framework of sub-band decomposition.

The transmultiplexer finds its origin in an idea of Darlington [12], and was subsequently improved by Bellanger and Dauguet [1] and other authors [3, 10]. To emphasize the importance of this kind of modulation, it is sufficient to remark that the transmultiplexer format is used in radio and television broadcasting, in the transmission through old copper twisted pairs, under the acronym of ADSL (Asymmetrical Digital Subscriber Loop), and in the cellular telephone systems.

7.10.1 Basic OFDM Architectures

The OFDM system may be introduced in terms of a *basic* architecture which provides a direct insight of the frequency division multiplexing operation. Then, from the basic architecture, we will obtain *efficient* architectures.⁴

The Base-Band Architecture

Let $c_0(t), c_1(t), \dots, c_{M-1}(t)$ be M (complex) signals defined on the domain $\mathbb{Z}(T)$ with the rate $F = 1/T$ values per second. Then, an OFDM system provides the multiplexing of the M signals $c_m(t)$ into a single signal $v(t_0)$, $t_0 \in \mathbb{Z}(T_0)$, with the rate $F_0 = 1/T_0 = MF$. As was done in the polyphase decomposition, we call $F = 1/T$ the *low rate* and $F_0 = 1/T_0$ the *high rate*. The integer M is the *order* of the OFDM.

The sequence of operations required by the multiplexing is shown in Fig. 7.34.⁵ The first operation for each input signal $c_m(t)$ is an interpolation from the low rate domain $\mathbb{Z}(T)$ into the high rate domain $\mathbb{Z}(T_0)$ where all the M interpolators have the same impulse response $g(t_0)$, $t_0 \in \mathbb{Z}(T_0)$. Hence, the output of the m th interpolator is

$$x_m(t_0) = \int_{\mathbb{Z}(T)} du g(t_0 - u)c_m(u). \quad (7.56)$$

The second operation is a frequency shift of mF , obtained with an exponential modulation (EM) with carrier $e^{i2\pi mFt_0}$. The output of the m th modulator is given by

$$y_m(t_0) = e^{i2\pi mFt_0} x_m(t_0). \quad (7.57)$$

⁴In the formulation of the OFDM architecture, the reference frequency f_0 is always set to zero, so that the m th carrier frequency is given by $f_m = mF$, as in Fig. 7.33. The M -tuple of frequencies (7.55) is obtained with a final modulation not included in the architecture.

⁵In the illustrations, we use simplified notations: spacing T in place of domain $\mathbb{Z}(T)$, frequency f_m in place of the carrier $e^{i2\pi f_m t}$, etc.

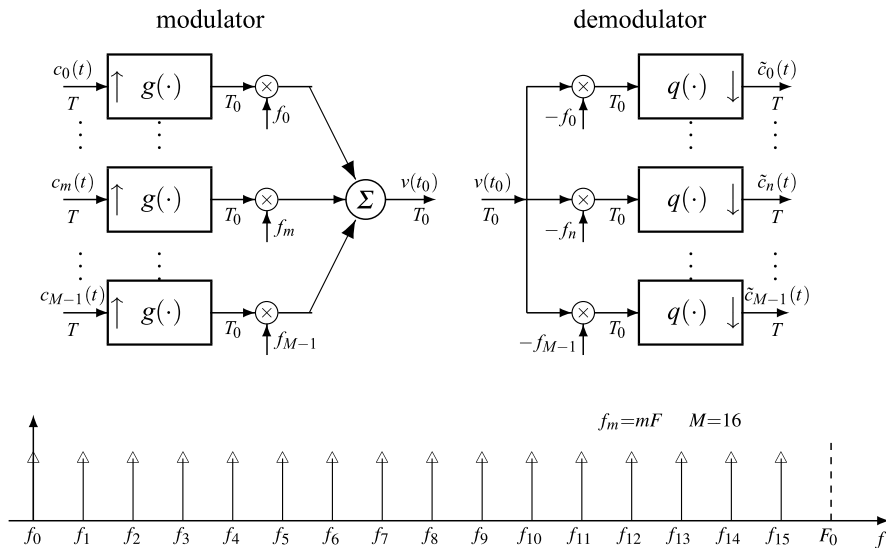


Fig. 7.34 The basic base-band architecture of an OFDM system

Finally, the sum

$$v(t_0) = \sum_{m=0}^{M-1} y_m(t_0) \tag{7.58}$$

gives the OFDM signal. The exponential carriers $e^{i2\pi mFt}$ have equally spaced frequencies mF , $m_0 = 0, 1, \dots, M - 1$, sharing the high-rate fundamental band $[0, MF)$ with $MF = F_0$.

The demultiplexing consists of the inverse operations, that is, frequency shifts by $-nF$ followed by decimators. The relations are

$$\begin{aligned} \tilde{y}_n(t_0) &= v(t_0)e^{-i2\pi nFt_0}, \\ \tilde{c}_n(t_0) &= \int_{\mathbb{Z}(T_0)} du_0 q(t_0 - u_0)\tilde{y}_n(u_0), \end{aligned} \tag{7.59}$$

where $q(t_0)$ is the impulse response of the decimators. Usually, a *correlation receiver* is considered, where

$$q(t_0) = g^*(-t_0). \tag{7.60}$$

The above operations are illustrated in Fig. 7.35 in the frequency domain for $M = 4$. Here, for simplicity, we consider an ideal interpolator with a rectangular frequency response on the low-rate fundamental band $[-\frac{1}{2}F, \frac{1}{2}F)$. In other words, the figure refers to a pure FDM. Note that, in general, all signals and components are complex.

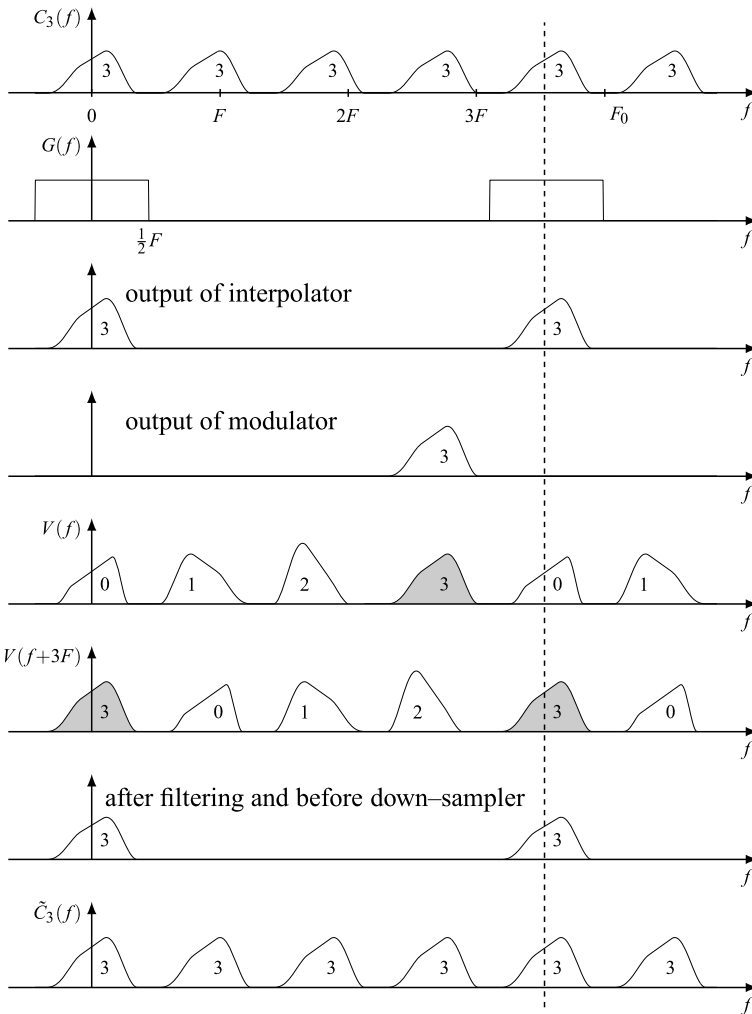


Fig. 7.35 Operations performed by the OFDM/FDM illustrated for $M = 4$ multiplexed signals

The Band-Pass Basic Architecture

In the previous scheme, both the transmitting and receiving filters have base-band characteristic with nominal band $[-\frac{1}{2}F, \frac{1}{2}F)$, or equivalently, $[0, F)$. Now according to Noble Identity NI6 of Sect. 7.4, each branch consisting of a base-band filter and an EM can be replaced by a *band-pass* filter without the modulator, specified by the relations

$$h_m(t_0) = g(t_0)e^{i2\pi mFt_0} \xrightarrow{\mathcal{F}} H_m(f) = G(f - mF). \quad (7.61)$$

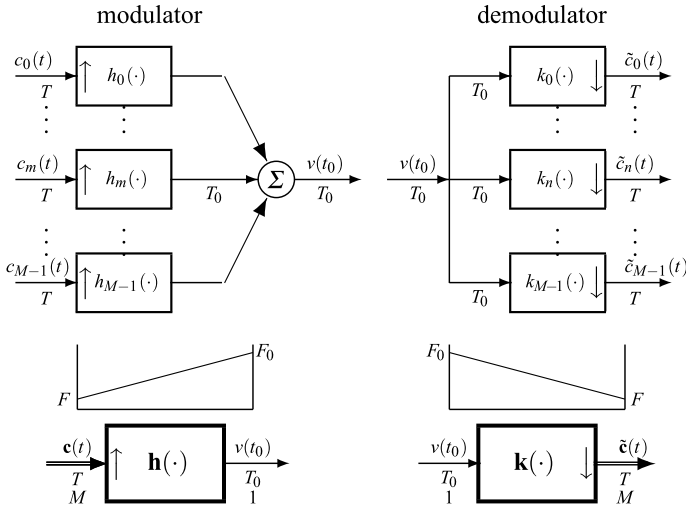


Fig. 7.36 The basic OFDM system architecture without modulators (carrierless); at the *top* the detailed scheme, at the *bottom* the compact scheme with the rate diagram

In this way, we obtain the *carrierless* architecture of Fig. 7.36, where the m th branch consists of a simple band-pass interpolator without a modulator (hence the term “carrierless”).

The global carrierless architecture consists of an M -input 1-output interpolator with the relation

$$v(t_0) = \int_{\mathbb{Z}(T)} du \mathbf{h}(t_0 - u) \mathbf{c}(u), \tag{7.62}$$

where $\mathbf{c}(u) = [c_0(u), \dots, c_{M-1}(u)]'$ is the column vector of the M inputs and $\mathbf{h}(t_0)$ is the row vector of the M impulse responses

$$\begin{aligned} \mathbf{h}(t_0) &= [h_0(t_0), h_1(t_0), \dots, h_{M-1}(t_0)] \\ &= g(t_0) [1, e^{i2\pi F t_0}, \dots, e^{i2\pi(M-1)F t_0}]. \end{aligned} \tag{7.63}$$

In a similar way, we obtain the carrierless architecture of the OFDM demodulator.

Orthogonality (or Perfect Reconstruction) Condition

The carrierless architecture is useful to establish the orthogonality conditions in a very simple way. In words, we impose that the direct connection of the modulator and the demodulator be equivalent to the M -input M -output identity filter on the domain $\mathbb{Z}(T)$. The corresponding impulse and frequency responses are respectively

$$\mathbf{b}(t) = \mathbf{I} \delta_{\mathbb{Z}(T)}(t) \xrightarrow{\mathcal{F}} \mathbf{B}(f) = \mathbf{I}, \tag{7.64}$$

where \mathbf{I} is the $M \times M$ identity matrix.

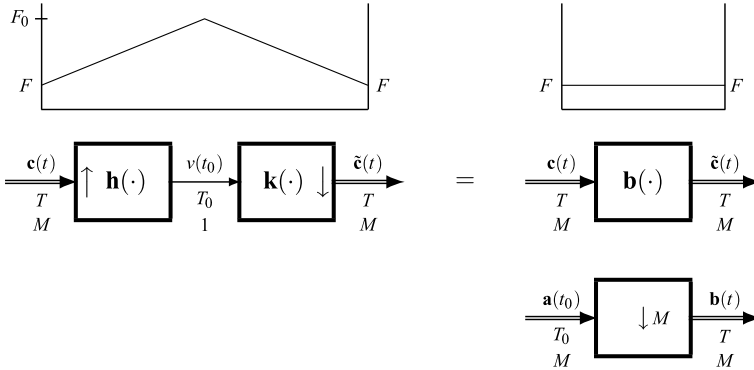


Fig. 7.37 Connection of modulator and demodulator to establish the orthogonality conditions

Now, we recall that the tandem of a $\mathbb{Z}(T) \rightarrow \mathbb{Z}(T_0)$ interpolator and a $\mathbb{Z}(T_0) \rightarrow \mathbb{Z}(T)$ decimator is equivalent to a filter on $\mathbb{Z}(T)$. The impulse response $\mathbf{b}(t)$, $t \in \mathbb{Z}(T)$, of the equivalent filter is the down-sampled version of the convolution $\mathbf{a}(t_0) = \mathbf{k} * \mathbf{h}(t_0)$, as illustrated in Fig. 7.37.

In the frequency domain, considering that the $\mathbb{Z}(T_0) \rightarrow \mathbb{Z}(T)$ down-sampling gives the $\mathbb{R}/\mathbb{Z}(F_0) \rightarrow \mathbb{R}/\mathbb{Z}(F)$ up-periodization, we find that the frequency response of the equivalent filter is given by $\mathbf{B}(f) = \text{rep}_F \mathbf{A}(f) = \text{rep}_F \mathbf{K}(f)\mathbf{H}(f)$, where $\text{rep}_F \mathbf{A}(f) = \sum_{k=0}^{M-1} \mathbf{A}(f - kF)$. Finally, imposing (7.64) we obtain the orthogonality conditions for the OFDM in terms of the band-pass filters

$$\mathbf{b}(t) = \mathbf{k} * \mathbf{h}(t) = \mathbf{I}\delta_{\mathbb{Z}(T)}(t), \quad \mathbf{B}(f) = \text{rep}_F \mathbf{K}(f)\mathbf{H}(f) = \mathbf{I}. \tag{7.65}$$

A more explicit form can be written in terms of the filters of the original base-band filter. Assuming a *correlation receiver*, defined by (7.60), we find

$$\int_{\mathbb{Z}(T_0)} du_0 g^*(u_0 - t)g(u_0)e^{i2\pi(m-n)Fu_0} = \delta_{nm}\delta_{\mathbb{Z}(T)}(t), \tag{7.66}$$

$$\text{rep}_F G^*(f)G(f - (m - n)F) = \delta_{nm}.$$

7.10.2 Fundamental Examples

We consider two examples of OFDM systems, both with a correlation receiver.

Perfectly Band-Limited OFDM This is the minimum bandwidth solution in which the *reference filter* is defined as

$$G(f) = \text{rep}_{F_0} \text{rect}(f/F), \quad g(t_0) = F \text{sinc}(Ft_0), \quad t \in \mathbb{Z}(T_0). \tag{7.67}$$

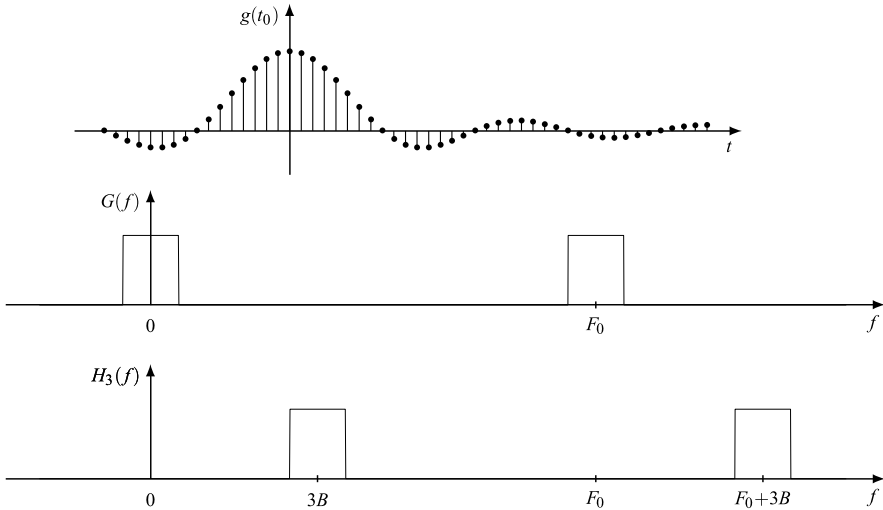


Fig. 7.38 Impulse and frequency responses of the interpolators in the OFDM/FDM system

The m th sub-channel has a bandwidth F centered at the frequency mF (Fig. 7.38). The check of the *orthogonality* is immediate in the frequency domain. In fact,

$$Q(f)G(f - (f_m - f_n)) = G^*(f)G(f - (m - n)F) = G(f)^2 \delta_{nm},$$

where $\text{rep}_F G(f)^2 = 1$.

Perfectly Time-Limited OFDM This is the dual example in which the reference filter has impulse response (Fig. 7.39)

$$g(nT_0) = \begin{cases} 1/T, & \text{if } 0 \leq n \leq M - 1; \\ 0, & \text{otherwise,} \end{cases} \quad (7.68)$$

and hence the frequency response can be expressed through the periodic sinc function (see (2.37))

$$G(f) = \text{sinc}_M(fT_0)e^{-i\pi(M-1)fT_0}. \quad (7.69)$$

The receiving filters are given by the anticausal version of $g(nT_0)$, i.e., $q(t_0) = g(-t_0)$. The sub-channels are not band-limited; however, their band-pass characteristics are concentrated around the carriers $f_n = nF$, as illustrated in Fig. 7.39.

The orthogonality condition can be easily stated in the time domain (see Problem 7.9).

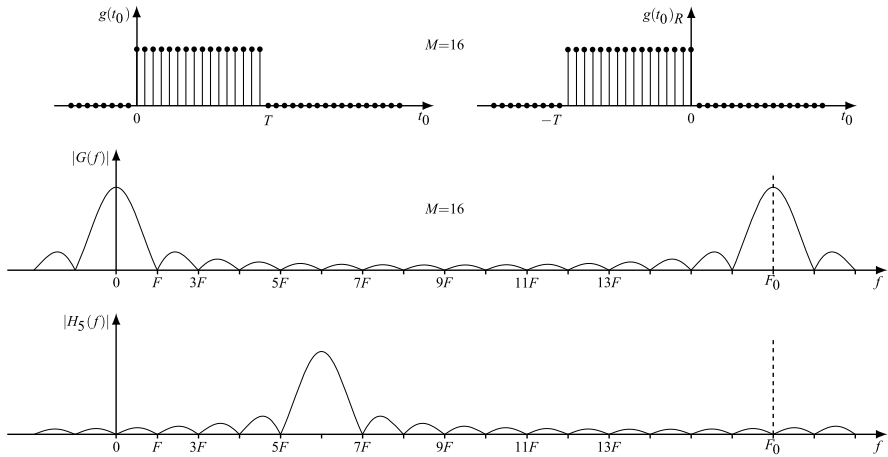


Fig. 7.39 Impulse and frequency responses of the filter in the perfectly time-limited OFDM

7.10.3 Efficient OFDM Architectures

In the basic OFDM architectures, all the components (filters and modulators) work at the high rate F_0 . Considering that $F_0 = MF$ and in practice M may be equal to 1024 or 2048 or even higher, the evaluation of the computational complexity of the *basic* scheme leads to the conclusion that their practical implementation is not feasible. Fortunately, easy to implement efficient architectures are available. In fact (Fig. 7.40):

Theorem 7.7 *An OFDM modulator of order M with input rate F and reference filter $g(t_0)$ is equivalent to the connection of*

1. *An M -point IDFT which processes the input vector $[S_0(t), \dots, S_{M-1}(t)]$ into the vector $[s_0(t), \dots, s_{M-1}(t)]$ for each low-rate time $t \in \mathbb{Z}(T)$ according to*

$$s_n(t) = \sum_{m=0}^{M-1} S_m(t) W_M^{mn}, \quad n = 0, \dots, M - 1, \quad (7.70)$$

2. *A low-rate filtering of $[s_0(t), \dots, s_{M-1}(t)]$ by an M -branch polyphase network (PPN), and*
3. *A P/S conversion of the M signals $v_n(t)$ into a high-rate signal $v(t_0)$.*

The impulse responses $g_n(t)$ of the PPN filters are the S/P conversion of the impulse response $g(t_0)$ of the reference filter.

We remark that, while in the basic architecture all the filters and modulators work on the high rate F_0 , in the new architecture both the IDFT (or DFT) and the PPN work at the low rate F . The consequent complexity reduction can be of several

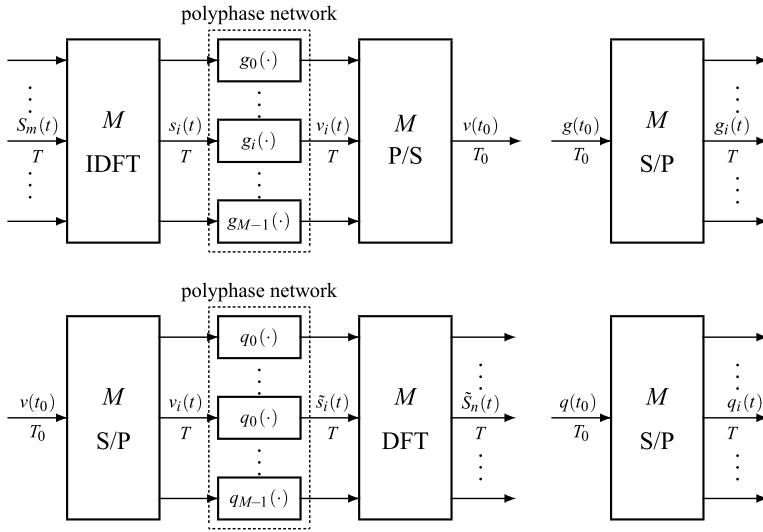


Fig. 7.40 Efficient architecture of the OFDM modulator and demodulator with interpretation of the low-rate impulse responses $g_i(t)$ and $q_i(t)$

orders of magnitude when N is large (as is in practice). A similar result holds for the demodulator.

Proof The theorem can be proved by comparing (in time or in frequency) the input–output relationship of the basic architecture with the input–output relationship of the cascade of 1, 2, and 3. Here, the proof is given in the time domain.

We start from the input–output relationship of the base-band architecture (see (7.56), (7.57) and (7.58)) after letting $c_m(u) = S_m(u)$

$$v(t_0) = \sum_{m=0}^{M-1} e^{i2\pi m F t_0} \int_{\mathbb{Z}(T)} du g(t_0 - u) S_m(u).$$

Then, we let $t_0 = t + iT_0$, $t \in \mathbb{Z}(T)$, $0 \leq i \leq M - 1$, to get

$$v(t + iT_0) = \sum_{m=0}^{M-1} e^{i2\pi m F t} e^{i2\pi m i F T_0} \int_{\mathbb{Z}(T)} du g(t + iT_0 - u) S_m(u),$$

where $e^{i2\pi m F t} = 1$ and $e^{i2\pi m i F T_0} = W_M^{mi}$. Finally, we let

$$v^{(i)}(t) \triangleq v(t + iT_0), \quad g^{(i)}(t) \triangleq g(t + iT_0), \quad t \in \mathbb{Z}(T).$$

Then

$$v^{(i)}(t) = \int_{\mathbb{Z}(T)} du g^{(i)}(t - u) s_i(u),$$

where

$$s_i(u) = \sum_{m=0}^{M-1} S_m(u) W_M^{mi}.$$

The interpretation of the last three relationships, read in the reverse order, proves Theorem 7.7. \square

Lattices and Cells in OFDM The essential parameters of an OFDM system are specified by two lattices, J and K with $J \subset K$, that is, the domains of the input signals $c_n(t)$ and of the multiplexed signal $v(t_0)$. The other parameters are obtained from J and K . The ratio

$$M = (K : J) = d(J)/d(K)$$

represents the order of the OFDM system, that is, the number of the input signals. The cell $A = [K/J)$ defines the P/S and S/P, that is, the *polyphase decomposition* of high-rate signals and the corresponding recomposition.

The reciprocal lattices J^* and K^* act on the frequency domain and determine other cells and partitions. The reciprocal cell $C^* = [J^*/K^*)$ contains the M frequencies of the exponential carriers.

Having this in mind, it is possible to introduce the multidimensional OFDM in which the generating lattices J and K become multidimensional [6, 7].

The Polyphase Network (PPN) In the efficient architecture, the PPN is uniquely determined by the impulse response $g(t_0)$ of the reference high-rate filter and by the rate ratio $M = F_0/F = T/T_0$. It consists of the parallel of M low-rate filters whose impulse responses $g_n(t)$ are obtained as the S/P conversion of $g(t_0)$, i.e.,

$$g_n(t) = g(t + nT_0), \quad n = 0, 1, \dots, M - 1. \quad (7.71)$$

The corresponding frequency responses are obtained from the theory of the S/P conversion developed in Sect. 7.5, and are given by

$$G_n(f) = \sum_{k=0}^{M-1} e^{i2\pi(f-kF)nT_0} G(f - kF). \quad (7.72)$$

7.10.4 Examples of Efficient Architectures

As illustration of the efficient implementation theorems, we now consider two fundamental examples. In particular, the first example will justify the term “polyphase”.

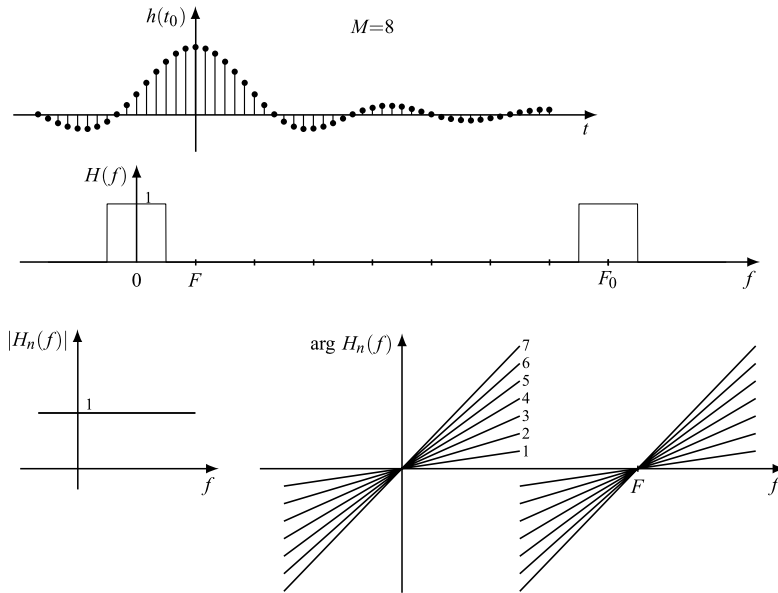


Fig. 7.41 Generating filter and amplitude and phase characteristics of the PPN filters in a perfectly band-limited OFDM (= FDM)

Perfectly Band-Limited OFDM (= FDM) The perfectly band-limited OFDM introduced in the previous section can be implemented according to Theorem 7.7. The reference filter is defined by

$$g(t_0) = F \operatorname{sinc}(Ft_0), \quad G(f) = \operatorname{rep}_{F_0} \operatorname{rect}(f/F), \quad (7.73)$$

and consequently, the impulse responses of the PPN filters are

$$g_n(t) = g(t + nT_0) = F \operatorname{sinc}(t/T + n/M), \quad (7.74)$$

as illustrated in Fig. 7.41 for $M = 8$. The frequency responses can be calculated from (7.72), and the result is an all-pass characteristic with a linear phase proportional to the order n , specifically

$$|G_n(f)| = 1, \quad \arg G_n(f) = 2\pi f n T_0 = 2\pi \frac{n}{M} \frac{f}{F}. \quad (7.75)$$

The PPN at the receiver has the complementary characteristic.

Perfectly Time-Limited OFDM Since the impulse response $g(t_0)$ of the reference filter has a rectangular mask (see (7.68)), the PPN filters are given by

$$g_n(t) = \begin{cases} 1/T, & \text{if } t = 0; \\ 0, & \text{if } t \neq 0, \end{cases} = \delta_{\mathbb{Z}(T)}(t), \quad G_n(f) = 1.$$

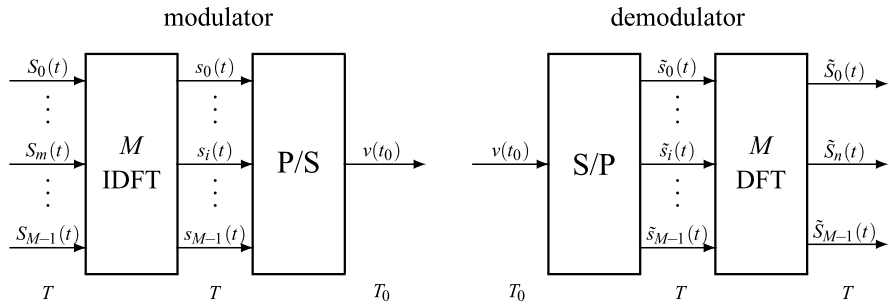


Fig. 7.42 Efficient implementation of a perfectly time-limited modulator and demodulator

Therefore, they are equivalent to the identity and are completely irrelevant. Hence, in the efficient implementation the PPN can be omitted! The same conclusions hold for the demodulator where the reference filter is the *anticausal* version $g(-t_0)$ and the generation of the PPN is obtained by a *causal* S/P converter.

Hence a perfectly time-limited OFDM can be simply implemented by an M -point IDFT followed by a P/S converter (Fig. 7.42).

7.11 Problems

7.1 **★** [Sect. 7.1] Show that an exponential modulator on a lattice J with a frequency $\lambda \in P^*$ is a PIL tf with periodicity P (P is a sublattice of J and P^* is the reciprocal lattice).

7.2 **★** [Sect. 7.3] Apply Theorem 7.3 to the case $\mathbb{R}/\mathbb{Z}(3) \rightarrow \mathbb{R}/\mathbb{Z}(5)$ and discuss the result by considering the signals in the cascades.

7.3 **★** [Sect. 7.4] Consider a $\mathbb{Z} \rightarrow \mathbb{Z}(T_0)$ interpolator with impulse response given by $g(t) = (1/10T_0) \text{sinc}(t/10T_0)$, $t \in \mathbb{Z}(T_0)$, followed by an EM with frequency $\lambda = 1/(5T_0)$. Apply Noble Identity NI6.

7.4 **★★** [Sect. 7.4] Consider a $J \rightarrow K$ down-sampler followed by a $K \rightarrow J$ up-sampler. Prove that the cascade is equivalent to a modulator on J with the carrier $\gamma(t)$, $t \in J$, given by the indicator function of K , multiplied by the amplification $A_0 = d(K)/d(J)$ of the up-sampler.

7.5 [Sect. 7.5] Study the S/P and P/S conversions on $\mathbb{Z}(T_0)/P \rightarrow \mathbb{Z}(T)/P$ with $T = 5T_0$ and $P = \mathbb{Z}(15T_0)$. Write all the cells involved and the frequency domain relationships.

7.6 **★** [Sect. 7.7] Explicitly write the parallel decomposition of an $I = \mathbb{Z}(2) \rightarrow U = \mathbb{Z}(5)$ QIL tf, choosing as inner domains $J = \mathbb{Z}(6)$ and $K = \mathbb{Z}(10)$.

7.7 ★★ [Sect. 7.7] In the previous problem, suppose that the impulse response of the $\mathbb{Z}(2) \rightarrow \mathbb{Z}(5)$ QIL tf is given by

$$g(n) = A_0 \operatorname{sinc}(n/10), \quad n \in \mathbb{Z}.$$

Find the frequency response of the corresponding 5-input 2-output $\mathbb{Z}(10) \rightarrow \mathbb{Z}(5)$ QIL parallel architecture.

7.8 ★★ [Sect. 7.7] Consider a $\mathbb{Z}(3) \rightarrow \mathbb{Z}(5)$ QIL tf and its parallel decomposition obtained with $J = \mathbb{Z}(15)$, $K = \mathbb{Z}(25)$. Write explicitly the matrix $\mathbf{g}(v)$ of decomposition (7.42) and show that its elements are a “circulant” replica of the elements of the first row.

7.9 ★★★ [Sect. 7.10] Prove the orthogonality condition of the perfect time-limited OFDM.

Appendix: Deduction of Parallel Architecture with EMs

To overcome the diagonal form of the PI, we introduce the auxiliary kernel

$$q(t - u, u) = h(t, u), \quad (t, u) \in K \times J. \quad (7.76)$$

Hence, the PI condition (7.44) becomes

$$q(t - u, u + p) = q(t - u, u), \quad p \in P, \quad (7.77)$$

which states that $q(v, u)$ has periodicity P with respect to its second argument. Now the domain of $q(v, z)$ is given by $D = \{(t - u, u) \mid t \in K, u \in J\}$, which defines a nonseparable lattice, in general. But, if $K \supset J$, the difference $t - u$ belongs to K and D becomes separable as $K \times J$. Then the function $q(v, z)$, $v \in K$, $z \in J$ has periodicity P in z and, for a fixed v , can be formulated as a signal on $I = J/P$. The DFT/IDFT of this signal are

$$Q(v, \lambda) = \sum_{z \in J/P} d(J) q(v, z) e^{-i2\pi\lambda z}, \quad q(v, z) = \sum_{\lambda \in P^*/J^*} d(P^*) Q(v, \lambda) e^{i2\pi\lambda z}.$$

Letting $g_\lambda(v) = [1/d(J)]Q(v, \lambda)$, the IDFT becomes

$$q(v, z) = \frac{1}{N_J} \sum_{\lambda \in P^*/J^*} g_\lambda(v) e^{i2\pi\lambda z}.$$

Finally, considering (7.76) we get (7.50) and (7.51). The proof of (7.52) is analogous.

References

1. M.G. Bellanger, J.L. Daguét, TDM–FDM transmultiplexer: digital polyphase and FFT. *IEEE Trans. Commun.* **COM-22**, 1199–1205 (1974)
2. M.G. Bellanger, G. Bonnerot, M. Coudress, Digital filtering by polyphase network: application to sample rate alteration and filter banks. *IEEE Trans. Acoust. Speech Signal Process.* **ASSP-24**, 109–114 (1976)
3. J.A.C. Bingham, Multicarrier modulator for data transmission: an idea whose time has come. *IEEE Commun. Mag.* 5–14 (1990)
4. C.S. Burrus, T.W. Parks, *DFT/FFT and Convolution Algorithms Theory and Implementation* (Wiley, New York, 1985)
5. G. Cariolaro, Theory of multidimensional periodically invariant linear system. CESP Report, Dept. Information Engineering, University of Padova, December 2003
6. G. Cariolaro, A.M. Cipriano, F. De Pellegrini, New Noble Identities for multidimensional multirate linear systems based on exponential modulators, in *Proceedings of SPACS 2003*, Osaka JP, December 2003
7. G. Cariolaro, V. Cellini, G. Donà, Theoretic group approach to multidimensional orthogonal frequency division multiplexing, in *ISPACS 2003*, Awaji Island, Japan, December 2003
8. G. Cariolaro, P. Kraniuskas, L. Vangelista, A novel general formulation of up/downsampling commutativity. *IEEE Trans. Signal Process.* **53**, 2124–2134 (2005)
9. T. Chen, P. P. Vaidyanathan, The role of integer matrices in multidimensional multirate systems. *IEEE Trans. Signal Process.* **SP-41**, 1035–1047 (1993)
10. J. Chow, J. Tu, J. Cioffi, A discrete multitone transceiver system for HDSL applications. *IEEE J. Sel. Areas Commun.* **9**, 895–908 (1991)
11. S. Coulombe, E. Dubois, Non-uniform perfect reconstruction filter banks over lattices with applications to transmultiplexers. *IEEE Trans. Signal Process.* 47 (1999)
12. S. Darlington, On digital single-sideband modulators. *IEEE Trans. Circuit Theory* **CT-17**, 409–414 (1970)
13. J. Kovačević, M. Vetterli, The commutativity of up/downsampling in two dimensions. *IEEE Trans. Inf. Theory* **37**(3) (1991)
14. P.P. Vaidyanathan, Multirate digital filters, filter banks, polyphase networks, and applications: a tutorial. *Proc. IEEE* **78**, 56–93 (1990)
15. P.P. Vaidyanathan, *Multirate Systems and Filter Banks* (Prentice Hall, Englewood Cliffs, 1993)

Chapter 8

Unified Theory: Sampling and Interpolation

UT 8.1 Equalization Conditions

As a preliminary to the recovery of a signal after a down-sampling, it is convenient to deal with the problem of the signal recovery after a general transformation.

For concreteness we may refer to a telecommunication system (see Sect. 1.1), where the information signal is first processed by the transmitter, then it is conveyed over a transmitting channel, and finally, it is processed by the receiver. In the ideal case, the target should be the exact recovery of the original signal $s(t)$ at the destination, according to the condition

$$s_0(t) = s(t), \quad t \in I, \tag{8.1}$$

where $s_0(t)$ is the final signal. Hence, the ideal target for a telecommunication system is the implementation of the identity tf (and so is for several other practical systems). Put into another form, the problem is the following. Let $r = \mathcal{L}[s]$ be the global relationship, where r is the received signal. Then, the ideal target of the receiver is to recover $s(t)$ from $r(t)$, performing in such a way the inverse tf with the operator \mathcal{L}^{-1} (see Sect. 6.1).

Condition (8.1), although a useful reference, is much too stringent because it imposes the *equalization condition* for all possible signals defined on the domain I (class $\mathcal{S}(I)$). The condition is relaxed to the form

$$s_0(t) = s(t), \quad t \in I, s \in \mathcal{S}_c(I), \tag{8.2}$$

which restricts the equalization to a subclass $\mathcal{S}_c(I)$ of the class $\mathcal{S}(I)$ and the target becomes the *conditional* identity (see again Sect. 6.1). Typically, $\mathcal{S}_c(I)$ is a subclass of band-limited signals.

In several cases, the condition is further relaxed into the form

$$s_0(t) = A_0 s(t - t_0), \quad t \in I, s \in \mathcal{S}_c(I), \tag{8.3}$$

where a scale factor and a delay in the recovered signal are accepted. In the latter form, the equalization is known as *Heaviside's condition*. In any case, the above

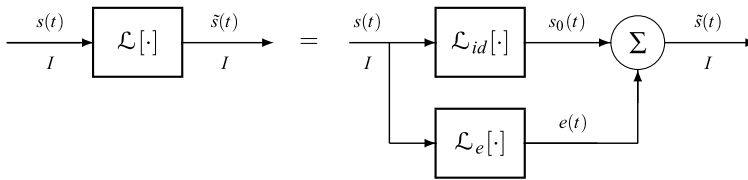


Fig. 8.1 Decomposition of a transformation into the “ideal” tf and the “error” tf

conditions (and similar others) are ideal, in the sense that they cannot be exactly implemented in practice, but only with some degree of approximation. Therefore, it becomes important to compare the true result, say $\tilde{s}_0 = \mathcal{L}[s]$, with the ideal one, $s_0 = \mathcal{L}_{id}[s]$. The difference

$$e = \tilde{s} - s_0 = \mathcal{L}[s] - \mathcal{L}_{id}[s] \quad (8.4)$$

gives the error (or distortion)¹ between the true recovered signal \tilde{s} and the *useful signal* s_0 . This error e may be put in direct relationship with the original signal s , as shown in Fig. 8.1, and we can write

$$e = \tilde{s} - s_0 = \mathcal{L}[s] - \mathcal{L}_{id}[s] \triangleq \mathcal{L}_e[s], \quad (8.4a)$$

where $\mathcal{L}_e[\cdot]$ relates the error to the signal.

In practice, the complete error behavior $e(t)$, $t \in I$, may have no interest and a global parameter, as the signal/error ratio (SER)

$$\Lambda = \frac{E_{s_0}}{E_e} = \frac{\text{useful signal energy}}{\text{error energy}} \quad (8.5)$$

is considered. This parameter must be large enough, say $\Lambda \geq 10^5$ (50 dB), in order that the recovery accuracy be accepted in practical applications.

In sampling and related topics, our approach will first deal with an ideal target and then possible errors are investigated. Now, we develop some usual reference conditions.

8.1.1 Perfect Equalization Condition

The condition $s_0(t) = s(t)$, $t \in I$, implies the identity tf on I , which is given as a *unitary all-pass* filter with impulse and frequency responses

$$g(v) = \delta_I(v), \quad G(f) = 1, \quad (8.6)$$

as shown in Fig. 8.2 for $I = \mathbb{R}$.

¹We are neglecting the *noise* which is always present in “real” systems.

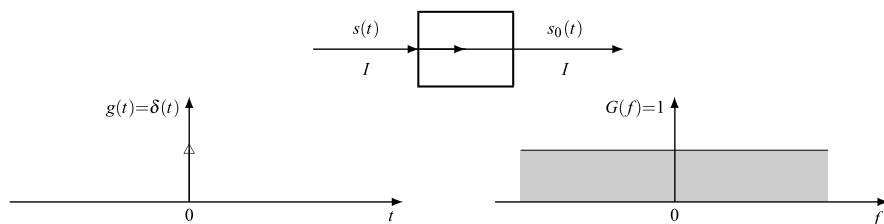


Fig. 8.2 The all-pass filter which performs the perfect equalization

If the condition is relaxed into the form

$$\boxed{s_0(t) = s(t), \quad t \in I, \quad s \in S_c(I),} \quad (8.7)$$

the identity becomes *conditioned* within the signal class \mathcal{J} , and it is interesting to investigate the different forms of tfs in dependence on the condition $s \in S_c(I)$.

Suppose that \mathcal{J} is the class of *band-limited* signals according to

$$S(f) = 0, \quad f \notin \mathcal{E}_0,$$

where \mathcal{E}_0 is a fixed spectral extension (a subset of the frequency domain). Then, the conditioned identity becomes a filter with the frequency response given by the indicator function of \mathcal{E}_0 , that is,

$$G(f) = \eta_{\mathcal{E}_0}(f) = \begin{cases} 1, & \text{if } f \in \mathcal{E}_0; \\ 0, & \text{if } f \notin \mathcal{E}_0. \end{cases} \quad (8.8)$$

In fact, if s is a signal of this class, we find $S_0(f) = G(f)S(f) = S(f)$, and, considering the uniqueness of the inverse FT, we get the perfect recovery: $s_0(t) = s(t)$, $t \in I$. Note that condition (8.8) may be relaxed into the form

$$G(f) = \begin{cases} 1, & \text{if } f \in \mathcal{E}_0; \\ \text{arbitrary,} & \text{if } f \notin \mathcal{E}_0, \end{cases} \quad (8.9)$$

so that (8.8) may be viewed as a minimal solution. Thus, we find that a conditioned identity is not unique. The filters that formalize these conditioned identities are illustrated in Fig. 8.3 for $I = \mathbb{R}$ and $\mathcal{E}_0 = (-B, B)$.

An alternative condition is that \mathcal{J} is the class of *time-limited* signals, according to $s(t) = 0$, $t \notin e_0$, where e_0 is a subset of the signal domain. In this case, the conditioned identity becomes a window whose shape $w(t)$ is given by (in the minimal case) $w(t) = \eta_{e_0}(t)$.

Heaviside's Condition

When the perfect recovery is relaxed into the form (8.3), that is (Fig. 8.4),

$$s_0(t) = A_0 s(t - t_0), \quad t \in I, \quad s \in S_c(I), \quad (8.10)$$

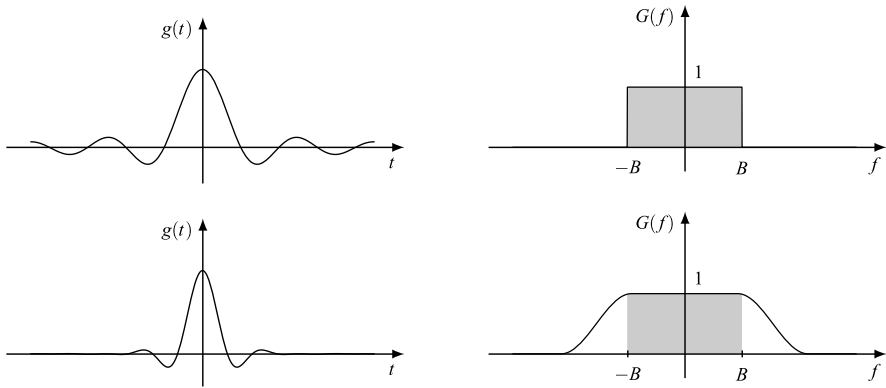


Fig. 8.3 Perfect equalizers for band-limited signals with band $(-B, B)$

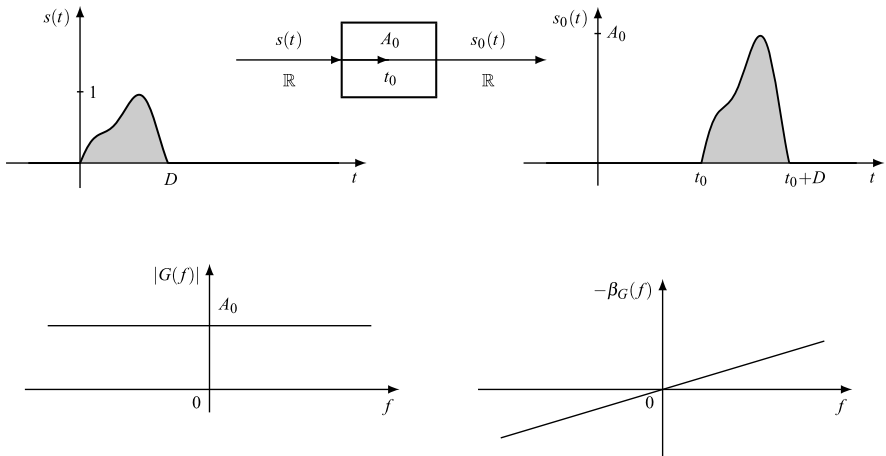


Fig. 8.4 Heaviside condition shown for $I = \mathbb{R}$

we have the *Heaviside condition*. If $S_c(I)$ is the class of all signals on I , that is, $S_c(I) = \mathcal{S}(I)$, it is easy to find that the condition is verified by a filter with responses

$$g(t) = A_0 \delta_I(t - t_0), \quad t \in I, \quad \boxed{G(f) = A_0 e^{-i2\pi f t_0}, \quad f \in \widehat{I}.} \quad (8.11)$$

Therefore, the Heaviside condition in the frequency domain requires that the amplitude response $A_G(f) = |G(f)|$ be constant and the phase response be proportional to the frequency at every frequency $f \in \widehat{I}$, namely²

$$A_G(f) = A_0, \quad \beta_G(f) = -2\pi f t_0. \quad (8.11c)$$

²We tacitly assume that A_0 is real and positive.

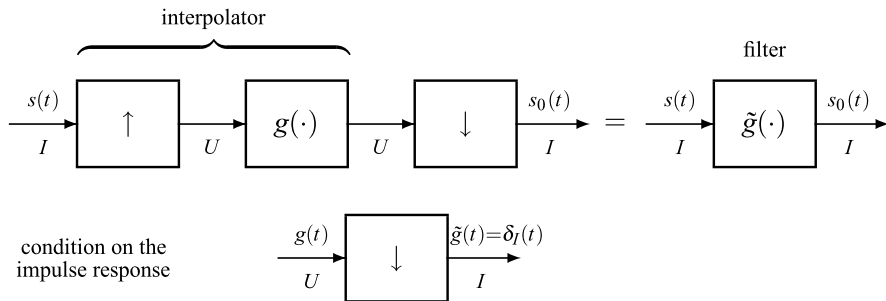


Fig. 8.5 Equalization after an upward transformation

8.1.2 Equalization After an Upward Transformation: Nyquist Criterion

We consider the signal recovery after an upward $I \rightarrow U$ tf ($U \supset I$), where the recovery is performed by a downward $U \rightarrow I$ tf. This problem is encountered in digital transmission and in multirate systems.

Specifically, we examine the scheme of Fig. 8.5 where an $I \rightarrow U$ interpolator with impulse response $g(t)$, $t \in U$, is followed by an $U \rightarrow I$ down-sampler (in the figure, the interpolator is decomposed into an $I \rightarrow U$ up-sampler followed by a filter on U). We want to establish the condition for a perfect recovery, that is,

$$s_0(t) = s(t), \quad t \in I. \tag{8.12}$$

We prove

Proposition 8.1 *When an $I \rightarrow U$ interpolator is followed by a $U \rightarrow I$ down-sampler, the perfect recovery condition holds if and only if the impulse response $g(t)$, $t \in U$, of the interpolator verifies the down-sampling condition*

$$g(t) = \delta_I(t) = \begin{cases} 1/d(I), & \text{if } t = 0; \\ 0, & \text{if } t \neq 0, \end{cases} \quad t \in I, \tag{8.13}$$

and the frequency response $G(f)$ verifies the periodic repetition condition

$$\boxed{\sum_{p \in I^*/U^*} G(f - p) = 1, \quad f \in \hat{I},} \tag{8.14}$$

which represents the Nyquist criterion.

Proof We have seen that the overall tf must be the ideal all-pass filter with responses $\tilde{g}(v) = \delta_I(v)$, $v \in I$, and $\tilde{G}(f) = 1$, $f \in \hat{I}$. On the other hand, the overall tf can be identified by the Recomposition Theorem seen in Sect. 6.11, which states that

the overall tf is equivalent to a filter on I , whose impulse response $\tilde{g}(v)$, $v \in I$, is given by the down-sampled version of the interpolator impulse response $g(v)$, $v \in I$. Hence, (8.13) follows. In the frequency domain, the $U \rightarrow J$ down-sampling becomes the $\widehat{U} \rightarrow \widehat{J}$ up-periodization, and (8.13) gives (8.14). \square

In conclusion, we have found two forms of equalization condition for the scheme of Fig. 8.5: in the signal domain the condition is given by (8.13), and in the frequency domain it is given by the Nyquist criterion. If the strict equalization condition is replaced by the Heaviside condition, the Nyquist criterion becomes (see (8.11))

$$\sum_{p \in I^*/U^*} G(f - p) = A_0 e^{-i2\pi f t_0}, \quad f \in \widehat{I}. \quad (8.15)$$

Above we have tacitly assumed ordinary domains. In the general case of quotient groups $I = I_0/P$, $U = U_0/P$, (8.13) becomes

$$g(t) = \delta_{I_0/P}(t) = \sum_{s \in P} \delta_{I_0}(t - s),$$

and in (8.14) $p \in I^*/U^*$ must be replaced by $p \in I_0^*/U_0^*$.

Reference Case $I = \mathbb{Z}(T)$ and $U = \mathbb{R}$. The interpolator impulse response $g(v)$, $v \in \mathbb{R}$, must verify the condition

$$g(nT) = \begin{cases} 1/T, & \text{if } n = 0; \\ 0, & \text{if } n \neq 0, \end{cases} \quad n \in \mathbb{Z}, \quad (8.16)$$

and the interpolator frequency response $G(f)$, $f \in \mathbb{R}$, the condition

$$\sum_{k=-\infty}^{+\infty} G(f - kF_c) = 1, \quad f \in \mathbb{R}/\mathbb{Z}(F_c), \quad F_c = 1/T. \quad (8.17)$$

In particular, if the interpolator is duration-limited, from (8.16) we find that every impulse response with

$$e(g) \subset (-T, T) \quad \text{and} \quad g(0) = 1/T$$

verifies the equalization condition. On the other hand, if the interpolator is band-limited, that is, if $G(f)$ has a limited extension, the Nyquist criterion (8.17) leads to interesting solutions. The first one is given by the *ideal low-pass* interpolator (Fig. 8.6), specified by the responses

$$g(t) = T \operatorname{sinc}(t/T), \quad G(f) = \operatorname{rect}(fT), \quad (8.18)$$

which represents the minimal band solution of the Nyquist criterion with band $B = F_c/2 = 1/(2T)$. For this reason, $F_c/2$ (half the sampling frequency) is called

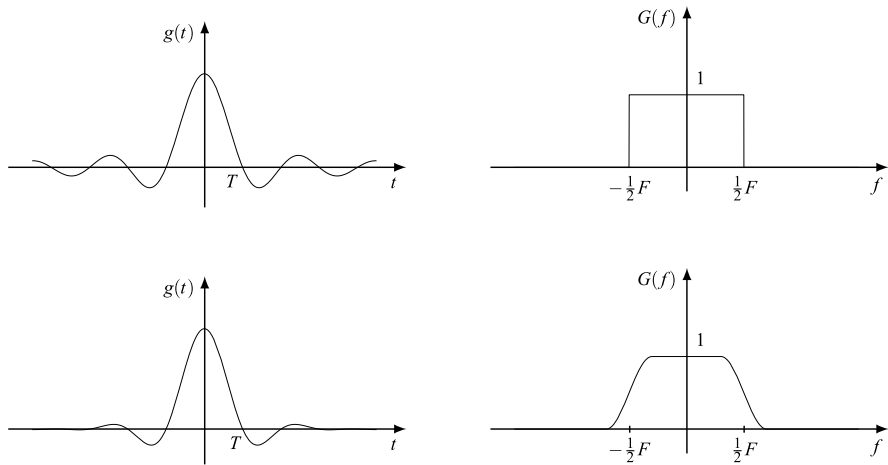


Fig. 8.6 Band-limited solutions of the Nyquist criterion; above with an ideal low-pass (minimal bandwidth solution) and below with a raised cosine

the *Nyquist frequency*. But in the band-limited class, we may find other interesting and articulated solutions. The most referenced is the *raised cosine* characteristic (Fig. 8.6) where the vertical lines of the rectangular shape are replaced by a cosine roll-off, as we shall see in detail in Sect. 9.6. To check the Nyquist criterion on this characteristic, it is sufficient to note that in the periodic repetition (8.17) in a period, say $(-\frac{1}{2}F_c, \frac{1}{2}F_c)$, we find (for band-limitation) only the terms with $k = -1$, $k = 0$ and $k = 1$. Then, using the roll-off symmetry (see Fig. 9.7), we find that the sum gives 1 over all the period. But due to the periodicity, it is identically equal to 1 on all \mathbb{R} .

UT 8.2 Interpolation Theory

The interpolation is an operation in which a discrete signal is processed to produce a continuous signal and, in general, a signal on a denser domain. This operation is performed by a $J \rightarrow I$ interpolator, where J is a discrete domain (lattice or finite group) and I is typically (but not necessarily) a continuous domain. The input-output relation is (see Sect. 6.11)

$$\tilde{s}(t) = \sum_{u \in J} s(u)g_0(t - u), \quad t \in I, \tag{8.19}$$

where $g_0(t) = d(J)g(t)$, $t \in I$, is the *interpolating function* and $g(t)$ is the impulse response. In (8.19), the interpolated signal $\tilde{s}(t)$, $t \in I$ is constructed starting from the values $s(u)$, $u \in J$.

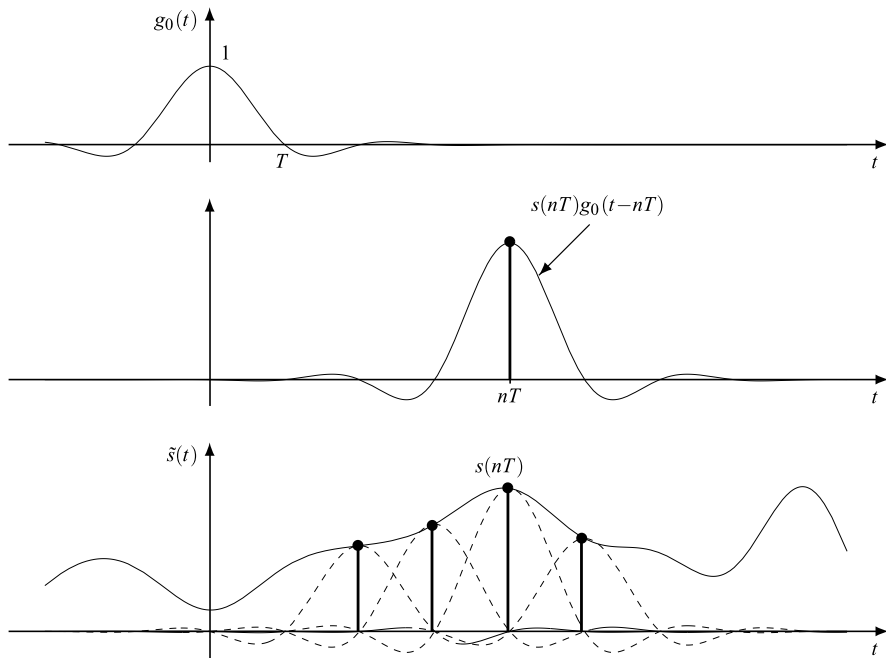


Fig. 8.7 Mechanism of interpolation provided by a $\mathbb{Z}(T) \rightarrow \mathbb{R}$ interpolator

In the reference case $\mathbb{Z}(T) \rightarrow \mathbb{R}$, the interpolated signal is given

$$\tilde{s}(t) = \sum_{n=-\infty}^{+\infty} s(nT)g_0(t-nT), \quad t \in \mathbb{R}, \quad (8.20)$$

where the interpolating function $g_0(t)$ is defined on \mathbb{R} . Figure 8.7 illustrates how the interpolation works according to (8.20): the interpolating function $g_0(t)$ is shifted at the instant nT and weighted by the discrete value $s(nT)$ to get the n th contribution $s(nT)g_0(t-nT)$; the interpolated signal is finally obtained by summing all contributions.

8.2.1 Correct Interpolation Condition

The interpolation of a signal is not unique and depends on the choice of the interpolating function. Among the possible choices, it will be convenient to *preserve the integrity of the original values* in the final interpolated signal. This condition, illustrated in Fig. 8.8 in the case $\mathbb{Z} \rightarrow \mathbb{R}$, will be called the *correct interpolation condition*.

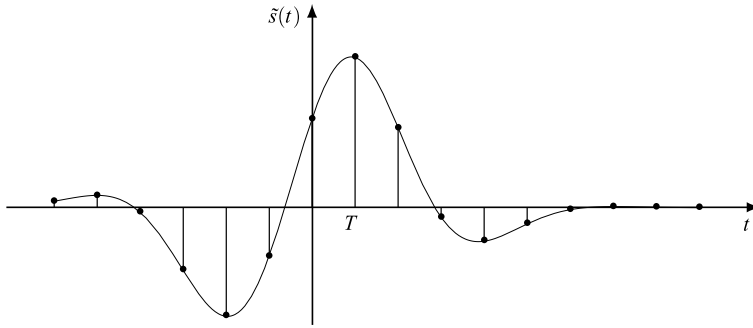
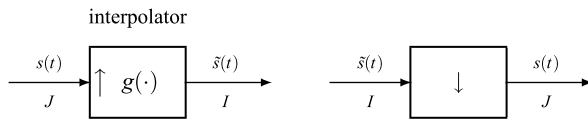


Fig. 8.8 Example of interpolation that verifies the *correct interpolation* condition

Fig. 8.9 Correct interpolation condition: the down-sampling of the interpolated signal must give the original signal values



In the general case of a $J \rightarrow I$ interpolation, the *correct interpolation condition* is given by

$$\tilde{s}(t) = s(t), \quad t \in J, \tag{8.21}$$

which requires that *the $I \rightarrow J$ sampled version of the interpolating signal be equal to the original signal*. This condition is formalized with the appropriate tfs in Fig. 8.9, which leads immediately to the conclusion that the cascade of the $J \rightarrow I$ interpolator followed by the $I \rightarrow J$ down-sampler must be equivalent to the identity tf on J . Thus, we arrive at the conclusion of the previous section concerning the signal recovery after an upward tf (compare Fig. 8.9 with Fig. 8.5).

The correct interpolation condition can be established in terms of the impulse response or of the frequency response of interpolator:

1. *Signal-domain condition*: the sampled version of the impulse response $g(t)$, $t \in I$, must be the impulse on J

$$g(t) = \delta_J(t), \quad t \in J. \tag{8.22}$$

In particular, when I and J are ordinary groups, the more explicit form is

$$g(t) = \delta_J(t) = \begin{cases} 1/d(J), & \text{if } t = 0; \\ 0, & \text{if } t \neq 0, \end{cases} \quad t \in J. \tag{8.22a}$$

2. *Frequency-domain condition*: the periodic repetition of the frequency response $G(f)$, $f \in \hat{I}$, must be unitary

$$\sum_{p \in J_0^*/I_0^*} G(f - p) = 1. \tag{8.23}$$

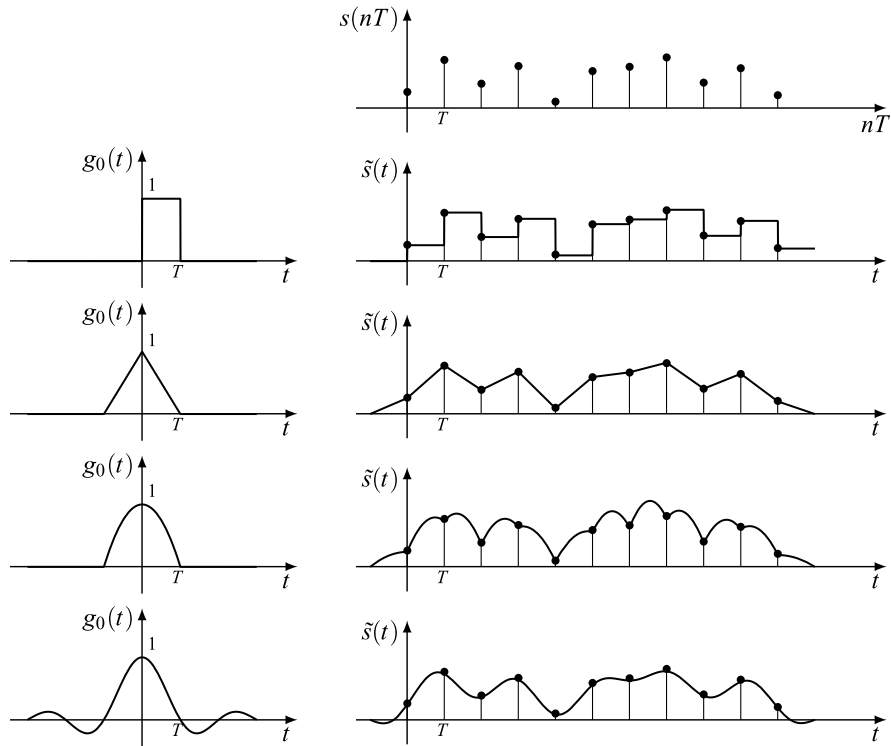


Fig. 8.10 Examples of $\mathbb{Z}(T) \rightarrow \mathbb{R}$ interpolations

Then, we find again the Nyquist criterion.

8.2.2 Reference Case and Examples

With $J = \mathbb{Z}(T)$ and $I = \mathbb{R}$, the correct interpolating condition on the interpolation function $g_0(t) = Tg(t)$, $t \in \mathbb{R}$, and on the frequency response are respectively

$$g_0(nT) = \begin{cases} 1, & \text{if } n = 0; \\ 0, & \text{if } n \neq 0, \end{cases} \quad \sum_{k=-\infty}^{+\infty} G(f - kF_c) = 1. \quad (8.24)$$

We now illustrate a few examples of interpolations (Fig. 8.10). The first example is the *hold interpolation* where the interpolating function $g_0(t)$ is a unitary rectangle from 0 and T and the interpolated signal is given by $\tilde{s}(t) = s(nT)$, $nT < t < nT + T$. This is a very simple form in which the continuous-time signal is obtained by “holding” the discrete values $s(nT)$ for a time T .

A second form is the *linear interpolation* in which the interpolated signal is obtained by a linear connection of the discrete values $s(nT)$; this requires a triangular

interpolating function. In the third example, the interpolating function is parabolic: $g_0(t) = [1 - (t/T)^2]$ for $-T < t < T$. The final example is obtained with the sinc function, namely $g_0(t) = \text{sinc}(t/T)$, which is related to the Fundamental Sampling Theorem (see below).

In all the above examples, the interpolating function verifies the correct interpolation condition.

UT 8.3 Signal Recovery After a Down-Sampling

From now on, we develop the main problem of the signal recovery after a down-sampling. Then, we consider an $I \rightarrow J$ sampler followed by $J \rightarrow I$ interpolator, where typically (but not necessarily) I is a continuum and J is a lattice. The sampling relationship is

$$s_c(t) = s(t), \quad t \in J, \quad (8.25)$$

where $s(t)$, $t \in I$, is the original signal and $s_c(t)$, $t \in J$, is the sampled signal which consists of the sample values of $s(t)$. The interpolator produces the *interpolated* signal as

$$\tilde{s}(t) = \sum_{u \in J} g_0(t - u)s(u), \quad t \in I, \quad (8.26)$$

where $g_0(t)$, $t \in I$, is the interpolating function. The target is the *correct reconstruction*

$$\tilde{s}(t) = s(t), \quad t \in I, \quad (8.27)$$

from the samples. Note that (8.27) must hold for every $t \in I$, and particularly for $t \in J$. Hence, the correct reconstruction *implies the correct interpolation condition*.

In a more general sampling/interpolation scheme, a *pre-filter* is present at the beginning. This scheme will be examined in the second part of the chapter.

First, as a preparation, we deal with the reference case, $\mathbb{R} \rightarrow \mathbb{Z}(T)$, arriving at the *Fundamental Sampling Theorem*. Then, we will examine the general case, arriving at the *Unified Sampling Theorem*. Next, we will apply the Unified Sampling Theorem to several cases, one-dimensional and multidimensional. In the final part of the chapter, we shall consider the (unavoidable) errors that we find in practice in the non-ideal reconstruction.

8.4 The Fundamental Sampling Theorem

We develop the case $I = \mathbb{R}$ and $J = \mathbb{Z}(T)$. First, we examine the sampling/interpolation scheme (Fig. 8.11), both in the time and in the frequency domain, then we introduce appropriate conditions for the exact recovery of the signal.

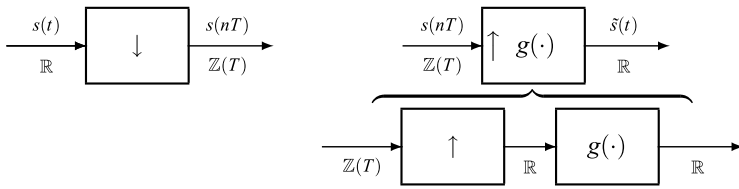


Fig. 8.11 $\mathbb{R} \rightarrow \mathbb{Z}(T)$ sampling followed by a $\mathbb{Z}(T) \rightarrow \mathbb{R}$ interpolator (the interpolator is decomposed in the standard form)

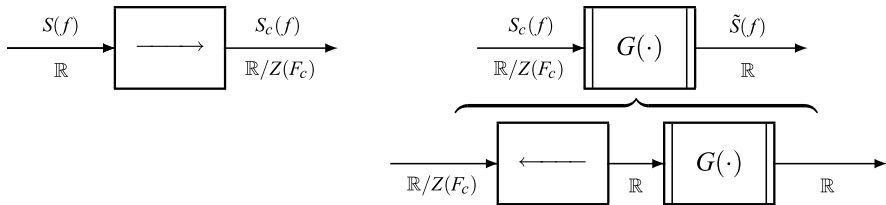


Fig. 8.12 Dual scheme of the sampling/interpolation of the previous figure

8.4.1 Sampling/Interpolation Analysis

The sampling relationship is

$$s_c(nT) = s(nT), \tag{8.28}$$

where T has the meaning of *sampling period*. The interpolator, for the moment with an arbitrary impulse response $g(t)$, $t \in \mathbb{R}$, is governed by (see Sect. 6.11)

$$\tilde{s}(t) = \int_{\mathbb{Z}(T)} du g(t-u)s_c(u) = \sum_{n=-\infty}^{+\infty} s_c(nT)g_0(t-nT), \tag{8.29}$$

where $g_0(t) \triangleq Tg(t)$, $t \in \mathbb{R}$, is the *interpolating function*. Considering (8.28), from (8.29) we obtain

$$\tilde{s}(t) = \sum_{n=-\infty}^{+\infty} s(nT)g_0(t-nT), \quad t \in \mathbb{R}, \tag{8.30}$$

which gives the interpolated signal in terms of the sample values of the original signal. This is the overall relation of the sampling/interpolation scheme and is a special case of (8.26).

In the frequency domain (Fig. 8.12), the $\mathbb{R} \rightarrow \mathbb{Z}(T)$ down-sampling becomes the $\mathbb{R} \rightarrow \mathbb{R}/\mathbb{Z}(F_c)$ up-periodization with the relation

$$S_c(f) = \sum_{k=-\infty}^{+\infty} S(f-kF_c), \quad f \in \mathbb{R}/\mathbb{Z}(F_c), \tag{8.31}$$

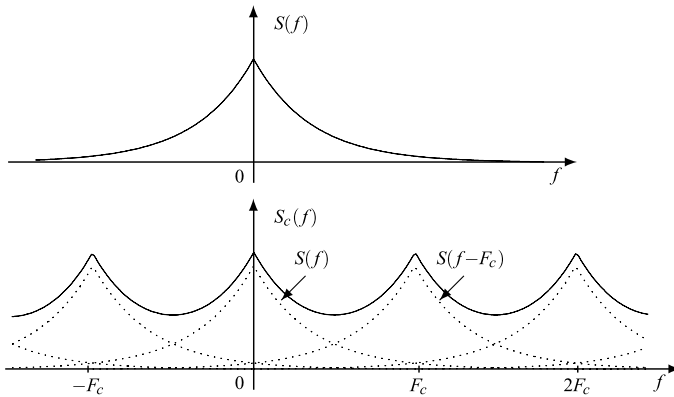


Fig. 8.13 Collision (*aliasing*) of the periodic repetition terms when $S(f)$ is not band-limited

where the period $F_c = 1/T$ of the FT has the meaning of the *sampling frequency* and is expressed in samples per second (sps). The interpolator has the same relation as a filter, that is,

$$\tilde{S}(f) = G(f)S_c(f), \quad f \in \mathbb{R}. \tag{8.32}$$

In fact, we can decompose the $\mathbb{Z}(T) \rightarrow \mathbb{R}$ interpolator into a $\mathbb{Z}(T) \rightarrow \mathbb{R}$ up-sampling and a filter on \mathbb{R} , but in the frequency domain the up-sampling becomes a down-periodization, which is irrelevant for the FT (see Sect. 6.9). For this reason, here and in the following, the irrelevant down-periodization will be included in the window, as shown in Fig. 8.12. The combination of the previous relationships gives

$$\tilde{S}(f) = \sum_{k=-\infty}^{+\infty} S(f - kF_c)G(f), \quad f \in \mathbb{R}. \tag{8.33}$$

In the above analysis, no assumption has been made on the signal and on the parameters (sampling period T , sampling frequency F_c and interpolator impulse response $g(t)$). Now, we introduce the fundamental assumption—the band-limitation.

8.4.2 Band-Limitation and Alias-Free Condition

The periodic repetition (8.31) consists of the terms $S(f - kF_c)$, $kF_c \in \mathbb{Z}(F_c)$, where $S(f)$ is the *useful* term and $S(f - kF_c)$ with $k \neq 0$ are the *lateral* terms. The extension of $S(f - kF_c)$ is

$$e(S) + kF_c, \quad kF_c \in \mathbb{Z}(F_c).$$

Thus in general, we find a superposition with a collision of the useful term with the lateral terms, as shown in Fig. 8.13. This collision is called *aliasing*.

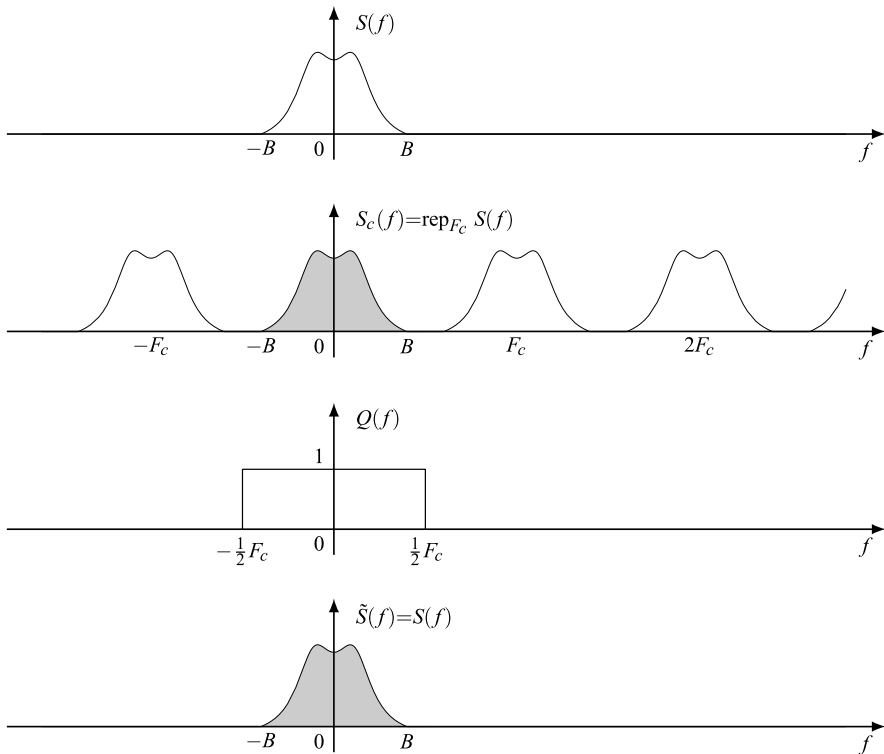


Fig. 8.14 Possibility of the exact recovery of the Fourier transform $S(f)$ from its periodic repetition $S_c(f)$ (with band limitation, $B < \infty$, and $F_c \geq 2B$)

The non-collision condition, which guarantees the integrity of the useful term, requires the *band-limitation*, according to

$$e(S) = (-B, B), \quad B < \infty, \quad (8.34a)$$

where B is the band.³ Then, *if the sampling frequency is at least twice the band*,

$$F_c \geq 2B, \quad (8.34b)$$

the lateral terms do not collide with the useful term (alias-free condition), and it will be possible to recover the FT $S(f)$ from the periodic repetition $S_c(f)$. This statement is illustrated in Fig. 8.14.

Note that band-limitation (8.34a) is necessary, but not sufficient. In fact, if $F_c < 2B$, notwithstanding the band-limitation, the aliasing is present and the exact FT recovery fails.

³We recall the convention made in Sect. 5.4 for *real* signals: the *band* B is half the *bandwidth* $B(s) = \text{meas } e(S)$. Note that the symmetric extension (8.34a), (8.34b) holds for a real signal, but does not imply a real signal.



Fig. 8.15 Exact signal recovery from its samples by an interpolator filter under the hypothesis of band limitation and $F_c \geq 2B$

8.4.3 Fourier Transform Recovery and Signal Recovery

Now, we assume that conditions (8.34a), (8.34b) hold. Then, the multiplication of $S_c(f)$ by the unitary window $Q(f) = \text{rect}(f/F_c)$ yields

$$S_c(f)Q(f) = \sum_{k=-\infty}^{+\infty} S(f - kF_c)Q(f) = S(f).$$

In fact,

$$S(f - kF_c)Q(f) = \begin{cases} S(f)Q(f) = S(f), & \text{if } k = 0; \\ 0, & \text{if } k \neq 0. \end{cases} \quad (8.35)$$

Hence, reconsidering the scheme of Fig. 8.12 with⁴ $G(f) = Q(f)$, we obtain

$$\tilde{S}(f) = S(f), \quad (8.36)$$

that is, the perfect recovery in the frequency domain. But, considering the uniqueness of the inverse FT, we have also the signal recovery $\tilde{s}(t) = s(t)$ (Fig. 8.15). In conclusion, the signal recovery from its samples is possible by an interpolator with the frequency response $Q(f)$ and interpolating function given by $q_0(t) = \text{sinc}(F_c t)$, $t \in \mathbb{R}$. Finally, using the above results, we find

$$s(t) = \sum_{n=-\infty}^{+\infty} s(nT) \text{sinc}[F_c(t - nT)], \quad t \in \mathbb{R}. \quad (8.37)$$

Thus, we have proved:

Theorem 8.1 (Fundamental Sampling Theorem) *Let $s(t)$, $t \in \mathbb{R}$, be a band-limited signal with spectral extension $e(S) = (-B, B)$. If the sampling frequency $F_c = 1/T$ verifies the condition $F_c \geq 2B$, the signal $s(t)$ can be exactly recovered from its samples $s(nT)$ by an interpolator with the frequency response*

$$Q(f) = \text{rect}(f/F_c). \quad (8.38)$$

⁴We denote by $G(f)$ a generic frequency response and by $Q(f)$ the ideal frequency response that allows the exact recovery.

8.4.4 Comments

The proof of the theorem is constructive in the sense that it states not only that *it is possible*, but also *how* the recovery can be implemented.

We may state two distinct, but equivalent interpretations of the Fundamental Sampling Theorem. According to the *reconstruction formula* (8.37), the n th sample $s(nT)$ is multiplied by the interpolating function centered at nT , thus obtaining the term $s_n(t) = s(nT)g_0(t - nT)$; then the reconstruction is given by the sum of all terms, as already illustrated in Fig. 8.7. The interpolating function verifies the correct interpolation condition

$$q_0(nT) = \begin{cases} 1, & \text{if } n = 0; \\ 0, & \text{if } n \neq 0, \end{cases} \quad (8.39)$$

which assures that the n th term $s_n(t)$ does not interfere with the other terms at the sampling instant nT .

Note that the reconstruction according to (8.37) at any time t requires the knowledge of the samples for $nT < t$ (past), but also for $nT \geq t$ (present and future). The consequence is that a *real time* perfect reconstruction is not possible in practice.

This conclusion may seem in contradiction with the reconstruction provided by the interpolator which receives the samples at the input and produces the correct output at any time t . But, there is no contradiction because (8.38) defines an *anticipatory* filter (see Sect. 6.15) so that also the interpolator cannot be implemented in real time. This discussion will be completed later on.

Remark The proof of the Fundamental Sampling Theorem is articulated in two steps: the recovery of the FT and consequent recovery of the signal. It is very different from the classical approach seen in Chap. 2 which is based on mathematical manipulations. Our approach does not require such manipulations since it is based on the theory of tfs, mainly on the Duality Theorem. Moreover, it is not linked to the special case $\mathbb{Z}(T) \rightarrow \mathbb{R}$ and, in fact, the same formulation will also be used for the Unified Sampling Theorem.

8.4.5 Other Choices of the Interpolator

The interpolator of the Fundamental Sampling Theorem is defined by (Fig. 8.16), that is,

$$q(t) = F_c \operatorname{sinc}(F_c t), \quad Q(f) = \operatorname{rect}(f/F_c) \quad (8.40)$$

with pass-band $(-F_N, F_N)$, where $F_N = \frac{1}{2}F_c$ is the *Nyquist frequency*.

If the sampling frequency is not the minimal $F_c = 2B$, but $F_c > 2B$, the spectral separation in the periodic repetition has a margin, and the rectangular frequency

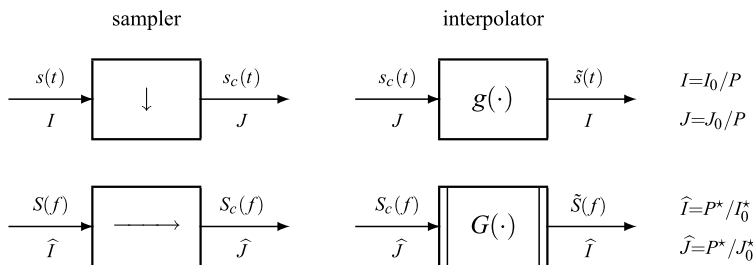


Fig. 8.16 Sampling–interpolation general scheme and dual scheme

response $Q(f)$ can be replaced by

$$Q_\alpha(f) = \begin{cases} 1, & \text{if } |f| < B; \\ \alpha(f), & \text{if } B < |f| < F_c - B; \\ 0, & \text{if } |f| > F_c - B, \end{cases} \quad (8.41)$$

where $\alpha(f)$ is an arbitrary function. In fact, the FT recovery, stated by (8.35), still holds with $Q(f)$ replaced by $Q_\alpha(f)$.

In theoretical considerations, it is customary to refer to the minimal solution $Q(f)$, but in practice, it is convenient to assure a margin and refer to $Q_\alpha(f)$, where $\alpha(f)$ is chosen with a graceful roll-off between the pass-band and the stop-band with a benefit in filter implementation. In any case, the roll-off must guarantee the correct interpolation condition (see (8.23)) and the usual reference is the raised-cosine shape (see Chap. 9).

UT 8.5 The Unified Sampling Theorem

In this section, we develop the analysis of the $I \rightarrow J$ down-sampler followed by an $J \rightarrow I$ interpolator, where I, J is an arbitrary quotient group pair (rationally comparable) with (Fig. 8.16)

$$I = I_0/P \rightarrow J = J_0/P \quad (I_0 \supset J_0), \quad (8.42)$$

arriving at the Unified Sampling Theorem. This will be an obvious generalization of the $I = \mathbb{R} \rightarrow J = \mathbb{Z}(T)$ case with the addition of some *compatibility conditions* which do not explicitly appear in the Fundamental Sampling Theorem.

8.5.1 Signal Domain Analysis

The sampling relationship is

$$s_c(t) = s(t), \quad t \in J = J_0/P, \quad (8.43)$$

which provides a restriction from the input domain I_0 into the output domain J_0 , with J_0 a subgroup of I_0 . In this context, the input signal is typically aperiodic ($P = \{0\}$), but we may have also a relevant periodicity P which is preserved after the down-sampling. It is remarkable that the three groups in (8.42) must verify the compatibility condition

$$P \subset J_0 \subset I_0. \quad (8.44)$$

The $J \rightarrow I$ interpolator, as a special QIL tf, has the input–output relationship

$$\tilde{s}(t) = \int_J du g(t-u)s_c(u), \quad t \in I, \quad (8.45)$$

where the impulse response is defined on the output domain I , that is, $g(t)t \in I$. In particular, if J is discrete (a lattice or a finite group), the relationship can be written in the form

$$\tilde{s}(t) = \sum_{u \in J} s_c(u)g_0(t-u), \quad (8.46)$$

where

$$g_0(t) \triangleq d(J_0)g(t), \quad t \in I, \quad (8.46a)$$

is the *interpolating function*.

Considering (8.43), in (8.46), $s_c(u)$ can be replaced by the samples $s(u)$ of the input signal. Hence

$$\boxed{\tilde{s}(t) = \sum_{u \in J} s(u)g_0(t-u), \quad t \in I,} \quad (8.47)$$

which represents the global relationship of the sampling/interpolation scheme.

8.5.2 Frequency Domain Analysis

The Duality Theorem states that the down-sampling $I \rightarrow J$ becomes the $\hat{I} \rightarrow \hat{J}$ up-periodization with

$$\hat{I} = P^*/I_0^* \rightarrow \hat{J} = P^*/J_0^* \quad (I_0^* \subset J_0^*) \quad (8.48)$$

and the relationship (see Sect. 6.13)

$$S_c(f) = \sum_{p \in R} S(f-p), \quad (8.49)$$

where the set of *repetition centers* R is given by a cell of J_0^* modulo I_0^* , namely

$$R = [J_0^*/I_0^*]. \quad (8.49a)$$

Hence, the frequency domain is the reciprocal P^* of the signal periodicity, and the frequency periodicity increases from I_0^* into J_0^* according to the up-periodization (8.49). In the frequency domain, the compatibility condition (8.44) becomes

$$P^* \supset J_0^* \supset I_0^*. \quad (8.50)$$

The interpolator has the same relation as a filter, that is,

$$\tilde{S}(f) = G(f)S_c(f), \quad f \in \widehat{I}, \quad (8.51)$$

where $G(f)$, $f \in \widehat{I}$, is the frequency response. Finally, by combination we have

$$\boxed{\tilde{S}(f) = \sum_{p \in R} S(f-p)G(f), \quad f \in \widehat{I}.} \quad (8.52)$$

In this analysis, no assumptions have been made, and in general, the correct recovery $\tilde{s}(t) = s(t)$ is not verified. To realize this condition, we have to make appropriate assumptions on the input signal and on the interpolator. Both will be introduced using the concept of a *cell*.

8.5.3 Alias-Free Condition

The generic term $S(f-p)$ of the periodic repetition (8.52) has extension

$$e(S) + p, \quad p \in R = [J_0^*/I_0^*], \quad (8.53a)$$

and the condition of no collision of the *lateral* terms $S(f-p)$, $p \neq 0$, with the useful term $S(f)$ is given by

$$e(S) \cap [e(S) + p] = \emptyset, \quad p \neq 0, p \in R. \quad (8.54)$$

On the other hand, we note that the $P^*/I_0^* \rightarrow P^*/J_0^*$ up-periodization identifies a cell partition of P^* modulo $R = [J_0^*/I_0^*]$ (see (8.49)). By calling C_0 a reference cell of this partition, by the definition of a cell we find that the cells $C_0 + p$, $p \in R$, do not overlap, that is,

$$C_0 \cap (C_0 + p) = \emptyset, \quad p \neq 0, p \in R.$$

Hence, if the spectral extension $e(S)$ is contained in the reference cell (Fig. 8.17), that is,

$$\boxed{e(S) \subset C_0,} \quad (8.55)$$

then $e(S) + p \subset C_0 + p$, and the non-collision (8.54) condition is verified.

In conclusion, the alias-free condition requires the existence of a cell C_0 containing the spectral extension $e(S)$. Thus, (8.55) states the general form of the *band-limitation*.

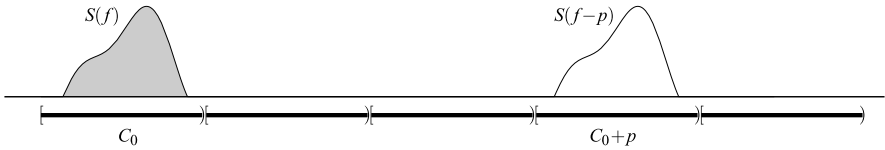
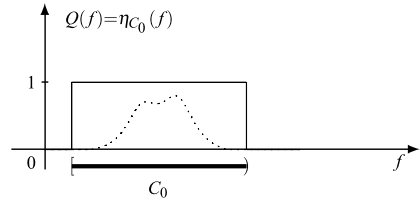


Fig. 8.17 Alias-free condition expressed by means of a cell partition of the frequency domain

Fig. 8.18 The frequency response of the interpolator of the Unified Sampling Theorem is given by the indicator function of the reference cell C_0



Partition of the Frequency Domain The alias-free conditions are based on the partition of the frequency domain P^* into cells of the form

$$P^* = C_0 + R, \quad R = [J_0^*/I_0^*], \tag{8.56}$$

where C_0 is a reference cell and R is the set of repetition centers. To write the explicit form of the cell C_0 , we start from the ordering (8.50) which allows the following decomposition of P^* (see Sect. 3.5)

$$P^* = [P^*/J_0^*] + [J_0^*/I_0^*] + I_0^*,$$

and by comparison with (8.56), we get that the cell C_0 is given by

$$C_0 = [P^*/J_0^*] + I_0^*. \tag{8.57}$$

Now, C_0 is aperiodic if $I_0^* = \mathbb{O}$; otherwise it is a periodic cell.

For instance, in the $\mathbb{R} \rightarrow \mathbb{Z}(T)$ sampling $P^* = \mathbb{O}^* = \mathbb{R}$, $I_0^* = \mathbb{R}^* = \mathbb{O}$ and $J^* = \mathbb{Z}(F_c)$, the reference cell is the aperiodic cell $C_0 = [\mathbb{R}/\mathbb{Z}(F_c)]$; in the $\mathbb{Z}(T_0) \rightarrow \mathbb{Z}(T)$ sampling $P^* = \mathbb{O}^* = \mathbb{R}$, $I_0^* = \mathbb{Z}(F_0)$ and $J^* = \mathbb{Z}(F_c)$ with $F_0 = 1/T_0$, $F_c = 1/T$, the reference cell is the periodic cell $C_0 = [\mathbb{R}/\mathbb{Z}(F_c)] + \mathbb{Z}(F_0)$.

8.5.4 Fourier Transform and Signal Recovery

For the FT recovery, the interpolator must be chosen with the frequency response given by the indicator function of the reference cell C_0 (Fig. 8.18)

$$Q(f) \triangleq \eta_{C_0}(f) = \begin{cases} 1, & \text{if } f \in C_0; \\ 0, & \text{if } f \notin C_0. \end{cases} \tag{8.58}$$

In fact, $\tilde{S}(f)$ is given by

$$\tilde{S}(f) = \sum_{p \in \mathbb{R}} Q(f)S(f - p), \tag{8.59}$$

where, by the alias-free condition, we have

$$Q(f)S(f - p) = \begin{cases} S(f), & \text{if } p = 0; \\ 0, & \text{if } p \neq 0. \end{cases}$$

Hence, the exact recovery of the FT, $\tilde{S}(f) = S(f)$, follows. Finally, using the inverse FT uniqueness, we find the exact recovery of the signal

$$\tilde{s}(t) = s(t), \quad t \in I. \tag{8.60}$$

At this point we have proved:

Theorem 8.2 (Unified Sampling Theorem) *Let $s(t)$, $t \in I$, be a signal which is down-sampled in the form $I = I_0/P \rightarrow J = J_0/P$.*

If the signal is band-limited according to

$$e(S) \subset C_0, \tag{8.61}$$

where C_0 is a convenient cell of the frequency domain P^ of the form (8.57), then the signal can be exactly recovered by a $J \rightarrow I$ interpolator with the frequency response $Q(f) = \eta_{C_0}(f)$.*

This theorem is comprehensive of a sequence of theorems we encounter in the literature, where the reference case $I = \mathbb{R}$, $J = \mathbb{Z}(T)$ is the best known. In the next sections, the theorem will be applied to several cases (1D and mD).

UT 8.6 Further Considerations on the Unified Sampling Theorem

8.6.1 Reconstruction Formula

The input–output relationship of sampling/interpolation after the signal recovery, $\tilde{s}(t) = s(t)$, can be rewritten in the form

$$\boxed{s(t) = \sum_{u \in J} s(u)q_0(t - u), \quad t \in I,} \tag{8.62}$$

where the interpolating function is obtained as the inverse FT of (8.58), namely

$$q_0(t) = d(J_0) q(t) = d(J_0) \int_{\hat{I}} df \eta_{C_0}(f) e^{i2\pi ft}$$

$$= d(J_0) \int_{C_0} df e^{i2\pi ft}. \quad (8.63)$$

8.6.2 Orthogonal Basis from the Interpolating Function

The interpolating function $q_0(t)$, $t \in I$, provides an orthogonal basis for the signals on I , and the reconstruction formula (8.62) may be viewed as an orthogonal expansion of the signal $s(t)$, $t \in I$, where the Fourier coefficients are directly given by the sampled values $s(u)$, $u \in J$.

Proposition 8.2 *The family of functions $\{q_0(t - v) \mid v \in J\}$ forms an orthogonal basis for band-limited signals defined on I with*

$$\int_I dt q_0(t - v) q_0^*(t - u) = d(J_0)^2 \delta_J(u - v), \quad u, v \in J. \quad (8.64)$$

For instance, in the standard $\mathbb{R} \rightarrow \mathbb{Z}(T)$ sampling where $q_0(t) = \text{sinc}(t/T)$, we have

$$\int_{-\infty}^{+\infty} \text{sinc}\left(\frac{t-u}{T}\right) \text{sinc}\left(\frac{t-v}{T}\right) dt = T^2 \delta_{\mathbb{Z}(T)}(u - v) = T \delta_{uv}.$$

Proof We use the Parseval's theorem for the inner product in (8.64). Considering that $q_0(t - v) \xrightarrow{\mathcal{F}} d(J_0) Q(f) e^{-i2\pi f v}$, we get

$$\begin{aligned} \int_I q_0(t - v) q_0^*(t - u) &= d(J_0)^2 \int_I df |Q(f)|^2 e^{i2\pi f(u-v)} \\ &= d(J_0)^2 \int_I df |\eta_{C_0}(f)|^2 e^{i2\pi f(u-v)} \\ &= d(J_0)^2 \int_{C_0} df e^{i2\pi(u-v)} = d(J_0) q_0(u - v), \quad u, v \in J, \end{aligned}$$

where the last passage follows from (8.63). On the other hand, we have seen that the correct reconstruction implies that the interpolation function verifies the correct interpolation condition given by (8.22), that is, $q(t) = (1/d(J_0))q_0(t) = \delta_J(t)$. Hence, $q_0(u - v) = d(J_0)\delta_J(u - v)$. \square

8.6.3 Energy of Samples

When the assumptions of the Unified Sampling Theorem hold, the energy of the samples $s_c(t)$, $t \in J$, equals the energy of the original signal $s(t)$, $t \in I$, namely

$$\int_J dt |s_c(t)|^2 = \int_I dt |s(t)|^2. \quad (8.65)$$

For instance, for the $\mathbb{R} \rightarrow \mathbb{Z}(T)$ sampling, we have

$$\sum_{n=-\infty}^{+\infty} T |s(nT)|^2 = \int_{-\infty}^{+\infty} |s(t)|^2 dt. \tag{8.65a}$$

Relation (8.65) can be proved using the orthogonal condition (8.64).

8.6.4 Interpolator Design: Efficiency

The $J \rightarrow I$ interpolator of the Unified Sampling Theorem is defined by

$$q(t) = \int_{C_0} df e^{i2\pi ft}, \quad Q(f) = \eta_{C_0}(f), \tag{8.66}$$

and therefore it is uniquely determined by the reference cell C_0 . The interpolating function $q_0(t)$ is obtained as the impulse response $q(t)$ multiplied by the scale factor $d(J_0)$, that is,

$$q_0(t) = d(J_0) q(t), \quad t \in I.$$

If the signal $s(t)$ is *real*, its spectral extension is always symmetric with respect to the frequency origin, $e(S) = -e(S)$, and it will be convenient to impose such a condition on the reference cell,⁵ that is,

$$-C_0 = C_0. \tag{8.67}$$

This condition assures that the interpolator is a *real tf*, that is, with $q(t)$, $t \in I$, real and with $Q(f)$, $f \in \widehat{I}$, having the Hermitian symmetry $Q(f) = Q^*(-f)$.

When the cell C_0 properly contains (with a margin) the spectral extension $e(S)$, the frequency response $Q(f)$ is required to be zero only at the frequencies where the spectrum repetition appears, that is,

$$Q(f) = \begin{cases} 1, & \text{if } f \in e(S); \\ 0, & \text{if } f \in e(S) + q, q \in R \setminus I_0^*; \\ \text{arbitrary,} & \text{elsewhere.} \end{cases}$$

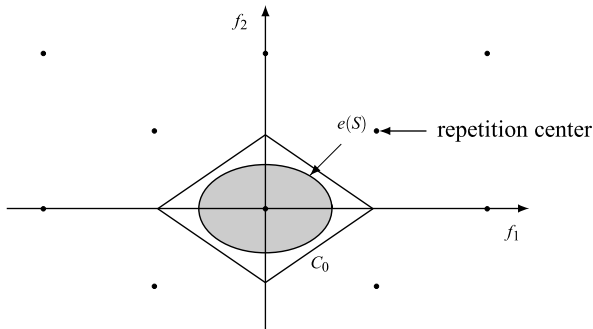
In practice, the arbitrary part will be chosen with a gradual roll-off between the pass-band $e(S)$ and the stop-band $e(S) + q$ (see considerations on the Fundamental Sampling Theorem).

The ratio

$$\eta_{si} \triangleq \frac{\text{meas } e(S)}{\text{meas } C_0} \tag{8.68}$$

⁵If the frequency domain \widehat{I} is a continuum, the symmetry $-C_0 = C_0$ may hold *almost everywhere*, that is, with the exception of some border points with measure zero.

Fig. 8.19 Illustration of the efficiency η_{si} in the $\mathbb{R}^2 \rightarrow \mathbb{Z}_2^1(d_1, d_2)$ sampling: η_{si} is given by the ratio between the area of the elliptical extension $e(S)$ and the area of the rhomboidal cell C_0



may be regarded as the *efficiency* of a given sampling/interpolation scheme. The meaning of efficiency is shown in Fig. 8.19 in the 2D case with $I = \mathbb{R}^2$, $J = \mathbb{Z}_2^1(d_1, d_2)$ where also the repetition centers are given by a quincunx lattice $\mathbb{Z}_2^1(F_1, F_2)$. In particular, in the 1D cases, it is given by

$$\eta_{si} = \frac{B(s)}{F_c} = \frac{\text{bandwidth}}{\text{sampling frequency}}. \tag{8.68a}$$

In practice, a high efficiency assures computational savings.

8.6.5 Historical Note

The first investigation on the Sampling Theorem is due to Cauchy in 1841 [1], who developed the following idea. For a (real) periodic signal containing only N harmonics, the Fourier series expansion is

$$s(t) = A_0 + \sum_{n=1}^N [A_n \cos 2\pi n Ft + B_n \sin 2\pi n Ft].$$

Then the signal knowledge at $2N + 1$ instants t_n , possibly not equally spaced, permits writing $2N + 1$ equations, where $s(t_n)$ are the known terms and the coefficients A_n and B_n are the $2N + 1$ unknowns. The solution of this system identifies the coefficients A_n and B_n , and we have the signal recovery from the sample values $s(t_n)$. The corresponding formulation is not simple and, perhaps, this explain why Cauchy’s result was not so successful.

The first one to formulate a modern version of the sampling theorem, essentially the fundamental one, was Nyquist in 1924 [4]. But the importance of Sampling Theorem was fully pointed out by Shannon in 1948 [5, 6]. The extension of the theorem to multidimensional signals was considered by Peterson and Middleton in 1962 [3]. For several years, the production of sampling theorems continued, all related to specific forms (most of them can be obtained as a corollary of Theorem 8.2). The unified formulation given by Theorem 8.2 was first presented by the author in 1974 [2].

Table 8.1 Parameters in $\mathbb{R} \rightarrow \mathbb{Z}(T)$ sampling

Term	Parameter
Original domains	$I = \mathbb{R}, \widehat{I} = \mathbb{R}$
Domains after sampling	$J = \mathbb{Z}(T), \widehat{J} = \mathbb{R}/\mathbb{Z}(F_c) \ (F_c = 1/T)$
Compatibility condition	None
Typical reference cell	$C_0 = [-\frac{1}{2}F_c, \frac{1}{2}F_c)$
Repetition centers	$R = \mathbb{Z}(F_c)$
Interpolating function	$q_0(t) = \text{sinc}(F_c t), t \in \mathbb{R}$

8.6.6 Handling of the Unified Sampling Theorem

Given a class of band-limited signals on $I = I_0/P$ with the common spectral extension $e(S)$, the application of the Unified Sampling Theorem requires choosing:

1. A subgroup J_0 of I_0 with the constraint $J_0 \supset P$ (quotient group compatibility).
2. A cell C_0 of the frequency domain P^* given by (8.57), containing the spectral extension $e(S)$.

These choices are not unique and are done with the target of maximizing the sampling/interpolation efficiency and having in mind that the ideal target is $C_0 = e(S)$, which provides a unitary efficiency. But, in practice a margin is introduced to optimize the interpolator implementation.

In the following sections, the above procedure will be illustrated in several application cases.

8.7 $\mathbb{R} \rightarrow \mathbb{Z}(T)$ Sampling

This case has been seen in Sect. 8.4 as the Fundamental Sampling Theorem, and can be obtained from the Unified Sampling Theorem as a particular case, as summarized in Table 8.1.

We remark in particular that the frequency domain is $\widehat{I} = \mathbb{R}$, and it must be partitioned into cells modulo $\mathbb{Z}(F_c)$, where typically the reference cell is the interval $C_0 = [-\frac{1}{2}F_c, \frac{1}{2}F_c)$. Thus, if the spectral extension is $e(S) = (-B, B)$, the alias-free condition is $F_c \geq 2B$. This is the standard case already seen with the Fundamental Sampling Theorem, but the variety of the cells of \mathbb{R} modulo $\mathbb{Z}(F_c)$ leads to several other interesting cases.

8.7.1 Sampling of Unimodal Signals

In the context of sampling and interpolation, a signal will be called *unimodal* (or with unimodal spectrum) when its spectral extension $e(S)$ is an interval and *multi-modal* when $e(S)$ consists of several intervals.

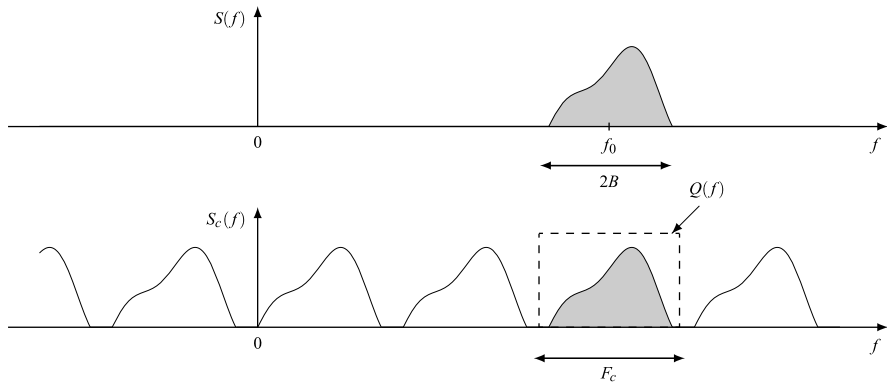


Fig. 8.20 Example of unimodal spectrum with indication of frequency response of the interpolator that recovers the original spectrum from the periodic repetition

The formulation with the symmetric extension $e(S) = (-B, B)$ tacitly refers to *real low-pass* signals, but more generally, a unimodal spectrum may be a non-centered interval (Fig. 8.20)

$$e(S) = (f_0 - B, f_0 + B). \quad (8.69a)$$

If $f_0 \neq 0$, the signal is surely a complex one. The reference cell for the extension (8.69a) is given by

$$C_0 = \left[f_0 - \frac{1}{2}F_c, f_0 + \frac{1}{2}F_c \right), \quad (8.69b)$$

and the alias-free condition is still given by $F_c > 2B$, but the interpolator frequency response and interpolating function become respectively

$$Q(f) = \text{rect}[(f - f_0)/F_c], \quad q_0(t) = \text{sinc}(F_c t) e^{i2\pi f_0 t}. \quad (8.69c)$$

The corresponding theorem may be regarded as the *Sampling Theorem for complex signals*, whereas the Fundamental Sampling Theorem refers to *real* signals. The minimum sampling frequency is obtained when we choose the cell $C_0 = e(S)$, and it is given by

$$F_{c \min} = 2B = \text{meas } e(S) = B(s), \quad (8.69e)$$

that is, the *bandwidth* (not the *half-band*) of the signal.

8.7.2 Sampling of Bimodal Signals

We recall (see Sect. 3.5) that a cell of \mathbb{R} modulo $\mathbb{Z}(F_c)$ is typically an interval, as in (8.69b), but it may also be the union of intervals with global measure F_c .

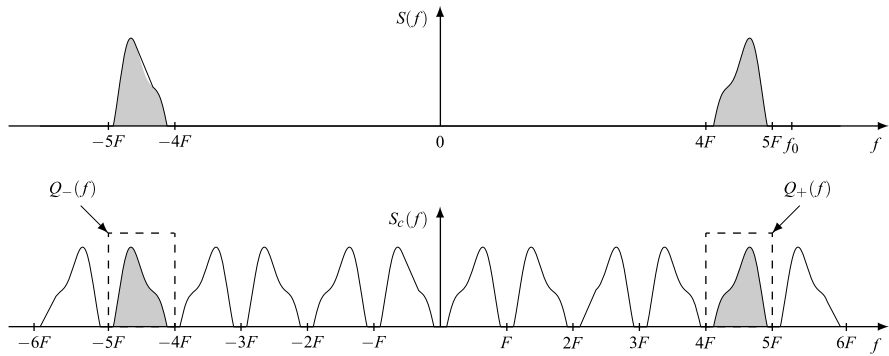


Fig. 8.21 Example of unimodal spectrum with indication of frequency response of the interpolator that recovers the original spectrum form the periodic repetition

This allows the formulation of an $\mathbb{R} \rightarrow \mathbb{Z}(T)$ sampling for multimodal signals. For instance, the set

$$C_0 = [-5F, -4F) \cup [4F, 5F), \quad F = \frac{1}{2} F_c,$$

is a cell of \mathbb{R} modulo $\mathbb{Z}(T_c)$. Now, if a signal has a bimodal spectrum contained in this cell, as shown in Fig. 8.21, it verifies the alias-free condition, and therefore it can be exactly recovered after an $\mathbb{R} \rightarrow \mathbb{Z}(T)$ sampling with $T = 1/F_c$. In this case, the interpolator frequency response is given by

$$Q(f) = \text{rect}\left(\frac{f + f_0}{F}\right) + \text{rect}\left(\frac{f - f_0}{F}\right), \quad f_0 = \frac{9}{4} F_c.$$

This situation holds for *real* band-pass signals, such as modulated signals, whose spectral extension consists of two intervals symmetrically displayed with respect to the frequency origin, say

$$e(S) = e_-(S) \cup e_+(S), \quad e_+(S) = (f_1, f_1 + B), \quad e_-(S) = -e_+(S). \quad (8.70)$$

Then, the reference cell is given by

$$C_0 = (-C_{0+}) \cup C_{0+} \quad \text{with } C_{0+} = (mF, (m + 1)F), \quad F = \frac{1}{2} F_c$$

with m an arbitrary natural. The alias-free condition becomes

$$mF \leq f_1 < f_1 + B \leq (m + 1)F. \quad (8.71)$$

In particular, if the spectral extension coincides with the cell, that is, if (8.71) holds with equality, the minimum sampling frequency is again

$$F_{c \min} = 2B = \text{meas } e(S) \stackrel{\Delta}{=} B(s).$$

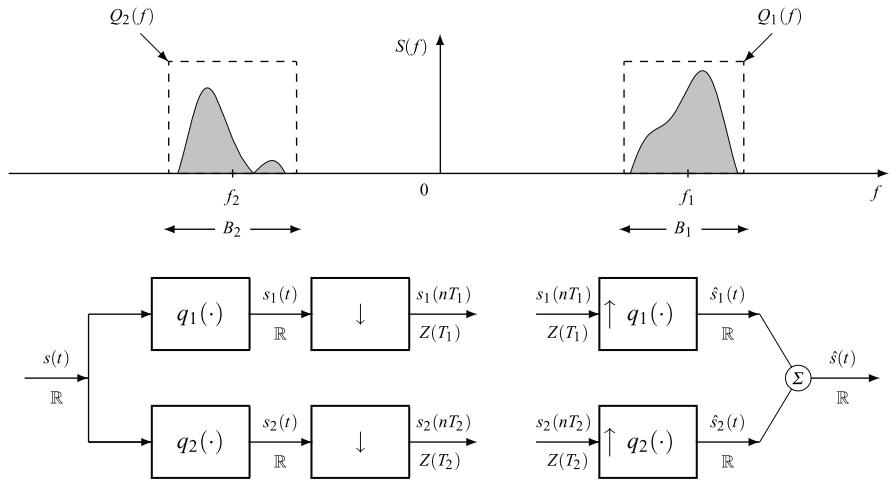


Fig. 8.22 Example of bimodal spectrum and corresponding sampling–interpolation scheme based on mode decomposition

As an example, if $e_+(S) = (20 \text{ kHz}, 24 \text{ kHz})$, equality (8.71) holds in the strict sense with $B = F = 4 \text{ kHz}$, $f_1 = 20 \text{ kHz}$, $m = 5$, and the minimum sampling frequency is $F_{c \min} = 2B = 8 \text{ ksps}$. Instead, if $e_+(S) = (19 \text{ kHz}, 23 \text{ kHz})$, equality (8.71) holds in the strict sense and $2B = 8 \text{ ksps}$ is no more sufficient for the exact signal recovery; the reason is that $[-23 \text{ kHz}, -19 \text{ kHz}] \cup [19 \text{ kHz}, 23 \text{ kHz}]$ is not a cell.

8.7.3 Separation of Spectral Modes

We have just seen that a multimodal extension is not a cell in general, and therefore it is not possible to use $F_c = \text{meas } e(S)$ as the sampling frequency. However, by changing the sampling/interpolation scheme, it is possible to use exactly

$$\boxed{F_{c \min} = \text{meas } e(S) \text{ sps.}} \tag{8.72}$$

In fact, suppose that the spectral extension consists of the N disjoint intervals

$$e_k(S) = (f_k - B_k, f_k + B_k), \quad k = 1, \dots, N \tag{8.73}$$

so that the bandwidth is given by

$$B(s) = \text{meas } e(S) = 2B_1 + \dots + 2B_N.$$

To achieve the minimal condition (8.72), and then a unitary efficiency, we have to use a composite scheme in which the signal is *not directly* sampled, but it is first

decomposed into N signals $s_k(t)$, $t \in \mathbb{R}$, by N pass-band filters having unitary frequency responses over the extensions $e_k(S)$. In such a way, we obtain N unimodal signals, and we can use separately, for each mode, the unimodal sampling theorem. Thus, the component $s_k(t)$ is $\mathbb{R} \rightarrow \mathbb{Z}(T_k)$ down-sampled with a sampling frequency $F_k = 1/T_k = B_k$, and subsequently it is recovered by an interpolator with a unitary frequency response over $e_k(S)$, as shown in Fig. 8.22 for $N = 2$. Note that the N down-samplers produce N sample sequences with a rate $2B_1 + \dots + 2B_N$ sps that is equal to the bandwidth $B(s)$, and we obtain a unitary sampling/interpolator efficiency. The penalty to pay for achieving a unitary efficiency frequency lies in the fact that the scheme requires a pre-filtering for the mode separation.

Multiplexing of Several Sample Sequences In practical applications, the sampling/interpolation schemes considered above are completed with other intermediate operations, such as the transmission over a channel (typically, the sampling is performed at the transmitter and the interpolation at the receiver). In this context, the spectral mode separation which provides several sample sequences requires a *multiplexing* into a unique sequence to permit the use of a common transmission channel.

The topic of multiplexing, and subsequent demultiplexing, of discrete-time signals will be seen in details in Chap. 11. For the moment, we put into evidence the conclusion that the velocity (in sps) of the multiplexed sequence is given by *the sum of the velocities of the individual sequences*.

8.8 $\mathbb{Z}(T_0) \rightarrow \mathbb{Z}(T)$ Sampling

The $\mathbb{Z}(T_0) \rightarrow \mathbb{Z}(T)$ down-sampling provides a rate reduction (in number of values per second). For instance, Fig. 8.23 shows the $\mathbb{Z}(T_0) \rightarrow \mathbb{Z}(3T_0)$ down sampling, where the rate is reduced from F_0 to $\frac{1}{3}F_0$, with $F_0 = 1/T_0$.

In this “discrete” sampling, the compatibility condition

$$\mathbb{Z}(T) \subset \mathbb{Z}(T_0)$$

is not irrelevant since it requires that the sampling period T be a multiple of the original time-spacing T_0 , say $T = NT_0$ with $N \in \mathbb{N}$. In the frequency domain, the compatibility condition becomes

$$\mathbb{Z}(F_c) \supset \mathbb{Z}(F_0), \quad F_0 = 1/T_0, \quad F_c = 1/T = F_0/N. \quad (8.74)$$

Table 8.2 gives the parameters of the $\mathbb{Z}(T_0) \rightarrow \mathbb{Z}(T)$ sampling which will be now discussed.

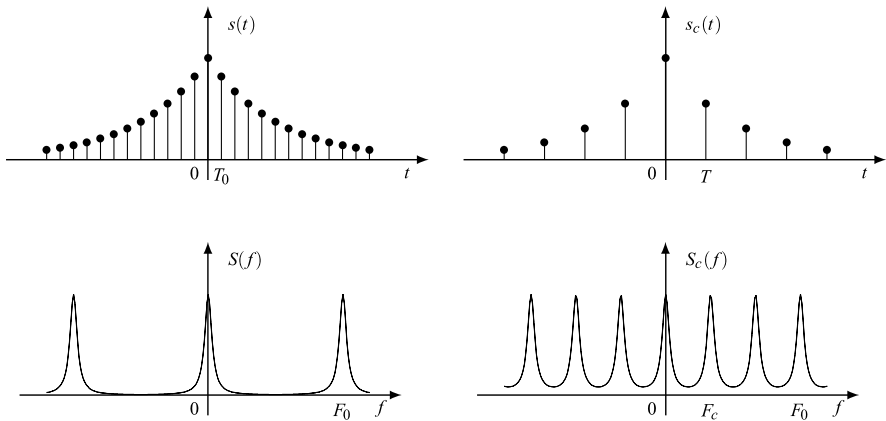


Fig. 8.23 $\mathbb{Z}(T_0) \rightarrow \mathbb{Z}(T)$ sampling and consequent $\mathbb{R}/\mathbb{Z}(F_0) \rightarrow \mathbb{R}/\mathbb{Z}(F_c)$ periodic repetition in frequency domain, shown for $T = 3T_0$

Table 8.2 Parameters in $\mathbb{Z}(T_0) \rightarrow \mathbb{Z}(T)$ sampling

Term	Parameter
Original domains	$I = \mathbb{Z}(T_0), \widehat{I} = \mathbb{R}/\mathbb{Z}(F_0), F_0 = 1/T_0$
Domains after sampling	$J = \mathbb{Z}(T), \widehat{J} = \mathbb{R}/\mathbb{Z}(F_c)$
Compatibility condition	$T = NT_0, F_c = F_0/N, N \in \mathbb{N}$
Typical reference cell	$C_0 = [-\frac{1}{2}F_c, \frac{1}{2}F_c) + \mathbb{Z}(F_0)$
Repetition centers	$R = \{0, F_c, \dots, (N - 1)F_c\}$
Interpolating function	$q_0(t) = \text{sinc}(F_c t), t \in \mathbb{Z}(T_0)$

8.8.1 Cells Partition of the Frequency Domain

The periodic repetition induced in the frequency domain by the $\mathbb{Z}(T_0) \rightarrow \mathbb{Z}(T)$ down-sampling is

$$S_c(f) = \sum_{k=0}^{N-1} S(f - kF_c) = \sum_{p \in P} S(f - p), \tag{8.75a}$$

where the set of repetition centers is finite

$$R = [\mathbb{Z}(F_c)/\mathbb{Z}(F_0)] = \{0, F_c, \dots, (N - 1)F_c\}. \tag{8.75b}$$

Here, the novelty is that the original transform $S(f)$ is already periodic, and therefore the cells of the frequency domain of $\widehat{I} = \mathbb{R}/\mathbb{Z}(F_c)$ must be periodic sets with periodicity $\mathbb{Z}(F_0)$. The reference cell may be

$$C_0 = \left[-\frac{1}{2}F_c, \frac{1}{2}F_c \right) + \mathbb{Z}(F_0), \tag{8.75c}$$

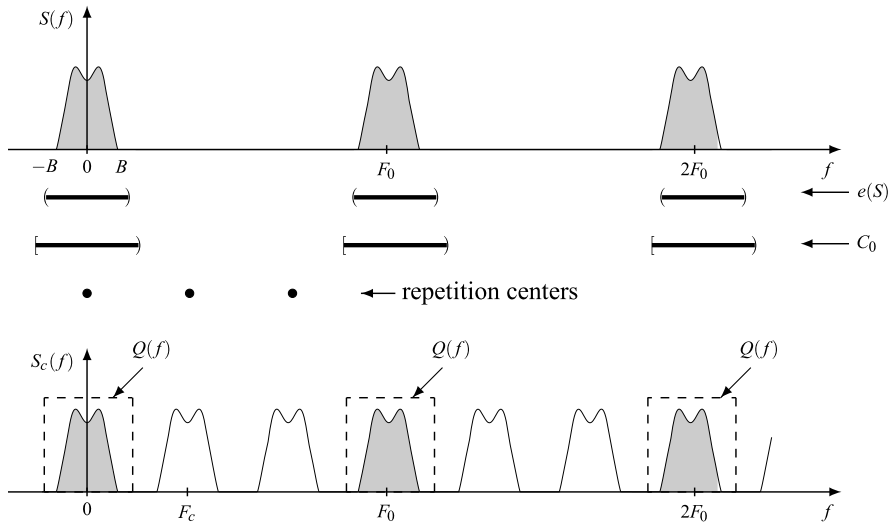


Fig. 8.24 Periodic repetition in frequency domain in the $\mathbb{Z}(T_0) \rightarrow \mathbb{Z}(T)$ down-sampling with $T = 3T_0$

and in fact, the sets $C_0 + p$, $p \in \mathbb{R}$, provide a partition of \mathbb{R} .

To be specific, let us consider the case $\mathbb{Z}(T_0) \rightarrow \mathbb{Z}(3T_0)$, where (Fig. 8.24)

$$C_0 = \left[-\frac{1}{2}F_c, \frac{1}{2}F_c \right) + \mathbb{Z}(F_0), \quad F_0 = 3F_c, \quad R = \{0, F_c, 2F_c\}. \quad (8.76)$$

The alias-free condition (8.55) requires that

$$e(S) \subset \left[-\frac{1}{2}F_c, \frac{1}{2}F_c \right) + \mathbb{Z}(F_0), \quad (8.77)$$

and it is verified as soon as

$$e(S) = (-B, B) + \mathbb{Z}(F_0) \quad \text{with } F_c \geq 2B.$$

The result is similar to the one of the $\mathbb{R} \rightarrow \mathbb{Z}(T)$ sampling, but with the difference that now $2B$ is the *bandwidth in a period*.

8.8.2 The Interpolator

The frequency response of the interpolator is given, according to the general rule, by the indicator function of the reference cell. Thus, from (8.76) we find (Fig. 8.25)

$$Q(f) = \text{rep}_{F_0} \text{rect}(f/F_c), \quad f \in \mathbb{R}/\mathbb{Z}(F_0). \quad (8.78)$$

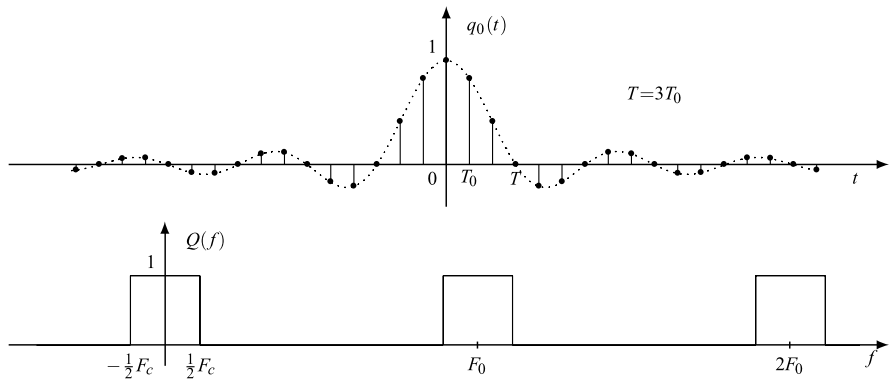


Fig. 8.25 Interpolating function and frequency response for the $\mathbb{Z}(T_0) \rightarrow \mathbb{Z}(T)$ sampling

The interpolation is provided according to

$$s(t) = \sum_{n=-\infty}^{+\infty} s(nT)q_0(t - nT), \quad t \in \mathbb{Z}(T_0), \tag{8.79}$$

where

$$q_0(t) = \text{sinc}(F_c t), \quad t \in \mathbb{Z}(T_0). \tag{8.78a}$$

Again, note the similarity with the Fundamental Sampling Theorem, but with the difference that now the interpolation provides a discrete signal (defined on $\mathbb{Z}(T_0)$), and therefore $q_0(t)$ is a discrete-time function.

8.8.3 Efficiency

The choice of the sampling frequency is constrained by the two conditions

$$F_c \geq 2B, \quad F_c = F_0/N, \quad N \in \mathbb{N}, \tag{8.79}$$

the first is alias-free and the second is the compatibility condition. Then, if and only if the bandwidth $2B$ is a divisor of F_0 (the period of $S(f)$), we can choose $F_c = 2B$, thus obtaining unitary efficiency. For instance, if $2B = \frac{1}{5}F_0$, we can choose $F_c = \frac{1}{5}F_0$, that is, we can apply the $\mathbb{Z}(T_0) \rightarrow \mathbb{Z}(5T_0)$ down-sampling to get $\eta_{si} = 100\%$. Instead, if $2B = \frac{3}{10}F_0$, we have to choose $F_c = \frac{1}{2}F_0$, and the sampling becomes $\mathbb{Z}(T_0) \rightarrow \mathbb{Z}(2T_0)$ with efficiency 60%.

This conclusion holds for the *direct sampling*, but with a composite scheme it is always possible to achieve unitary efficiency (see problems).

Table 8.3 Parameters in $\mathbb{R}/\mathbb{Z}(T_p) \rightarrow \mathbb{Z}(T)/\mathbb{Z}(T_p)$ sampling

Term	Parameter
Original domains	$I = \mathbb{R}/\mathbb{Z}(T_p), \hat{I} = \mathbb{Z}(F), F = 1/T_p$
Domains after sampling	$J = \mathbb{Z}(T)/\mathbb{Z}(T_p), \hat{J} = \mathbb{Z}(F_c)/\mathbb{Z}(F_c)$
Compatibility condition	$T_p = NT, F_c = NF, F_c = \frac{1}{T}$
Typical reference cell	$C_0 = \{-N_0F, \dots, 0, \dots, N_0F\}, N + 2N_0 + 1$
Repetition centers	$R = \mathbb{Z}(F)$
Interpolating functions	$q_0(t) = \text{sinc}_N(F_c t), t \in \mathbb{R}/\mathbb{Z}(T_p)$

8.9 $\mathbb{R}/\mathbb{Z}(T_p) \rightarrow \mathbb{Z}(T)/\mathbb{Z}(T_p)$ Sampling

Here the novelty is the presence of a periodicity in the original signal, which is preserved after the down-sampling. Then, the compatibility condition is that the sampling period T be a divisor of the period T_p , or equivalently, that the sampling frequency F_c be a multiple of the fundamental frequency F , that is,

$$T = T_p/N, \quad F_c = NF. \quad (8.80)$$

The frequency domain $\hat{I} = \mathbb{Z}(F)$ is discrete and the reference cell may be given by N consecutive frequencies of $\mathbb{Z}(F)$: $C_0 = \{n_0F, \dots, (n_0 + N - 1)F\}$, and the repetition centers are given by the lattice $R = \mathbb{Z}(F_c)$.

If the signal to be sampled is *real*, the cell C_0 is symmetric, as shown in Table 8.3; therefore, it always consists of an odd number of points, $N = 2N_0 + 1$. Then, the alias-free condition is that the real periodic signal contains *only the first N_0 harmonics* (see historical note).

The frequency response of the interpolator can be written in the usual form

$$Q(f) = \text{rect}(f/F), \quad f \in \mathbb{Z}(F), \quad (8.81)$$

but now the frequency is discrete. The interpolation formula is

$$s(t) = \sum_{n=0}^{N-1} s(nT)q_0(t - nT), \quad t \in \mathbb{R}/\mathbb{Z}(T_p), \quad (8.82)$$

where the interpolating function can be written in terms of the periodic sinc (see (2.37))

$$q_0(t) = \text{sinc}_N(F_c t), \quad t \in \mathbb{R}/\mathbb{Z}(T_p), \quad (8.82a)$$

where N is odd, which assures that $q_0(t)$ has period $T_p = NT$.

The sampling theorem for real periodic signals now outlined can be sketched as follows: a real periodic signal containing only the first N_0 harmonics can be recovered starting from $N = 2N_0 + 1$ *samples per period*.

We suggest the reader to formulate the $\mathbb{Z}(T_0)/\mathbb{Z}(T_p) \rightarrow \mathbb{Z}(T)/\mathbb{Z}(T_p)$ sampling theorem, which turns out to be clear from the previous 1D cases.

Table 8.4 Prototypes of multidimensional sampling

Signal domain	Frequency domain	Reference cell C_0	Repetition centers R
1. $\mathbb{R}^m \rightarrow L$	$\mathbb{R}^m \rightarrow \mathbb{R}^m/L^\star$	$[\mathbb{R}^m/L^\star)$	L^\star
2. $L_0 \rightarrow L$	$\mathbb{R}^m/L_0 \rightarrow \mathbb{R}^m/L^\star$	$[\mathbb{R}^m/L^\star) + L_0^\star$	$[L^\star/L_0^\star)$
3. $\mathbb{R}^m/P \rightarrow L/P$	$P^\star \rightarrow P^\star/L^\star$	$[P^\star/L^\star)$	L^\star
4. $L_0/P \rightarrow L/P$	$P^\star/L_0^\star \rightarrow P^\star/L^\star$	$[P^\star/L^\star) + L_0^\star$	$[L^\star/L_0^\star)$

8.10 Multidimensional Sampling

Multidimensional sampling can be handled on the basis of the Unified Sampling Theorem. Of course, the variety of the forms in the multidimensional case becomes very broad.

Excluding the presence of mixed groups (gratings) which will be briefly considered at the end of this section, we find four prototypes of sampling, which are collected in Table 8.4, where L and L_0 denote mD lattices and, as usual, P is the signal periodicity. For each prototype, the frequency domain, the reference cell C_0 and the repetition centers are indicated. The expression of C_0 is obtained from (8.57).

1. $\mathbb{R}^m \rightarrow L$ sampling. This is the most typical form, where a continuous aperiodic mD signal is converted into an aperiodic discrete mD signal. The reference cell $C_0 = [\mathbb{R}^m/L^\star)$ is aperiodic, and the repetition centers are given by the reciprocal lattice. The corresponding 1D sampling is $\mathbb{R} \rightarrow \mathbb{Z}(T)$, seen in Sect. 8.7.
2. $L_0 \rightarrow L$ sampling with $L_0 \supset L$, where an aperiodic discrete mD signal is sampled into an aperiodic discrete mD signal with a rate reduction from $d(L_0^\star)$ to $d(L^\star)$. The reference cell C_0 is periodic, $C_0 = [\mathbb{R}^m/L) + L_0^\star$, and the set of repetition centers is finite, $R = [L^\star/L_0)$ with cardinality $d(L_0^\star)/d(L_0)$. The corresponding 1D sampling is $\mathbb{Z}(T_0) \rightarrow \mathbb{Z}(T)$, seen in Sect. 8.8.
3. $\mathbb{R}^m/P \rightarrow L/P$ sampling, where a periodic continuous mD signal is converted to a periodic discrete mD signal. The frequency domain P^\star is discrete and the reference cell $C_0 = [P^\star/L^\star)$ is aperiodic. The corresponding 1D sampling is $\mathbb{R}/\mathbb{Z}(T_p) \rightarrow \mathbb{Z}(T)/\mathbb{Z}(T_p)$, developed in Sect. 8.9.
4. $L_0/P \rightarrow L/P$ sampling, where a periodic discrete mD signal is converted to a periodic discrete mD signal with a rate reduction. The reference cell $C_0 = [P^\star/L^\star) + L_0^\star$ is periodic and the set of repetition centers R is finite. The corresponding 1D sampling is $\mathbb{Z}(T_0)/\mathbb{Z}(T_p) \rightarrow \mathbb{Z}(T)/\mathbb{Z}(T_p)$.

The main application of multidimensional sampling is the conversion of images (possibly time-varying), as in television and cinema, as we shall see in Chap. 17.

In this section, we develop form 1, starting with the case in which L is separable and then considering the nonseparable case. Then, we briefly develop the sampling on a grating.

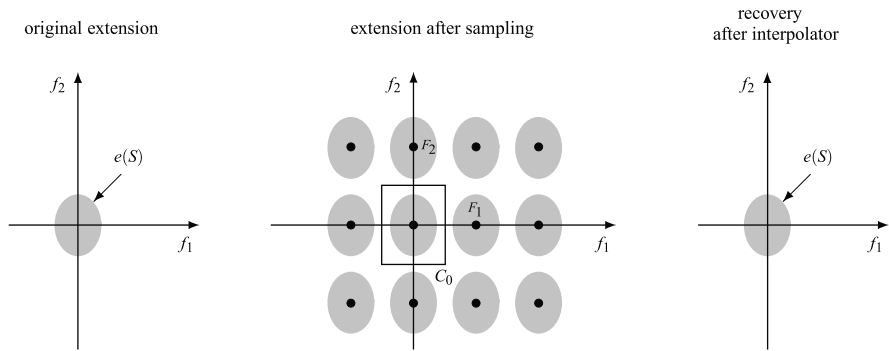


Fig. 8.26 Elliptical spectral extension $e(S)$ contained in a rectangular cell C_0 in the $\mathbb{R}^2 \rightarrow \mathbb{Z}(d_1, d_2)$ sampling

8.10.1 Sampling on a Separable Lattice

In the sampling

$$\mathbb{R}^m \rightarrow \mathbb{Z}(d_1, \dots, d_m) = \mathbb{Z}(d_1) \times \dots \times \mathbb{Z}(d_m), \tag{8.83}$$

we can use the explicit results obtained for the $\mathbb{R} \rightarrow \mathbb{Z}(T)$ sampling and proceed by composition. In the frequency domain, sampling (8.83) becomes the periodic repetition

$$\mathbb{R}^m \rightarrow \mathbb{R}^m / \mathbb{Z}(F_1, \dots, F_m) \quad \text{with } F_k = 1/d_k. \tag{8.84}$$

Thus, we may choose a separable reference cell

$$C_0 = C_{01} \times \dots \times C_{0m}, \tag{8.85}$$

where C_{0k} are cells of \mathbb{R} modulo $\mathbb{Z}(d_k)$, and in particular

$$C_{0k} = \left[-\frac{1}{2}F_k, \frac{1}{2}F_k \right) \quad \text{with } F_k = 1/d_k. \tag{8.85a}$$

The alias-free condition continues to have the standard form $e(S) \subset C_0$, where the signal spectral extension $e(S)$ is not necessarily separable. This is shown in Fig. 8.26 where $e(S)$ has an elliptical form and the cell has the rectangular form

$$C_0 = \left[-\frac{1}{2}F_1, \frac{1}{2}F_1 \right) \times \left[-\frac{1}{2}F_2, \frac{1}{2}F_2 \right). \tag{8.86}$$

The repetition centers are given by the lattice $\mathbb{Z}(F_1, F_2)$, so that the generic center is (rF_1, sF_2) with $r, s \in \mathbb{Z}$.

From (8.85), we have that the interpolator has a separable frequency response given by

$$Q(f_1, \dots, f_m) = \eta_{C_0}(f_1, \dots, f_m) = \eta_{C_{01}}(f_1) \cdots \eta_{C_{0m}}(f_m), \tag{8.87a}$$

and so is the impulse response $q(t_1, \dots, t_m) = q_1(t_1) \cdots q(t_m)$ where

$$q_k(t_k) = \int_{\eta_{C_{0k}}} df_k e^{i2\pi f_k t_k}, \quad t_k \in \mathbb{R}. \quad (8.87b)$$

Considering that the determinant of $L = \mathbb{Z}(d_1, \dots, d_m)$ is $d(L) = d_1 \cdots d_m$, the interpolating function is given by $q_0(t_1, \dots, t_m) = d_1 q_1(t_1) \cdots d_m q_m(t_m)$. In particular with the reference cell (8.85a), we find

$$q_0(t_1, \dots, t_m) = \text{sinc}(F_1 t_1) \cdots \text{sinc}(F_m t_m).$$

The interpolating formula becomes (written for brevity in the 2D case)

$$s(t_1, t_2) = \sum_{p=-\infty}^{+\infty} \sum_{r=-\infty}^{+\infty} s(pd_1, rd_2) \text{sinc}(F_1 t_1 - p) \text{sinc}(F_2 t_2 - r).$$

In conclusion, we have seen that the sampling from a continuous m D signal into a discrete m D signal defined on a separable lattice can be developed by an m -fold composition of the 1D sampling $\mathbb{R} \rightarrow \mathbb{Z}(T)$. Note that the above results do not require that the signal itself be separable, that is, of the form $s(t_1, \dots, t_m) = s_1(t_1) \cdots s_m(t_m)$, but they hold in general for nonseparable signals.

8.10.2 Sampling on a Nonseparable Lattice

The general $\mathbb{R}^m \rightarrow L$ sampling, with L an arbitrary m D lattices, in the frequency domain becomes the $\mathbb{R}^m \rightarrow \mathbb{R}^m/L^*$ up-periodization, L^* being the reciprocal lattice. If L is not separable, so is L^* , and the repetition centers do not form an orthogonal array.

The motivation of the sampling on nonseparable lattices lies mainly in the fact that cells of the form $[\mathbb{R}^m/L^*]$ provide a variety which permits better tailoring of the spectral extension with an improvement of the efficiency. Consider, e.g., the 2D example of Fig. 8.26 where the spectral extension $e(S)$ has an efficiency of at most $\pi/4$. On the other hand, with a sampling on a nonseparable lattice we may find a shape C_0 closer to the spectral extension $e(S)$ and improve the efficiency of a cell.

The general theory of this sampling/interpolation must be done on the basis of the Unified Sampling Theorem with the particularization of Table 8.5.

In general, the reference cell C_0 is not separable, and so is the frequency response of the interpolator. As said above, the main topic of this sampling is the simultaneous choice of an appropriate lattice L which, in general, is not separable, and of an appropriate cell of the class $[\mathbb{R}^m/L^*]$. This will be better seen in the sampling of images developed in Chap. 17.

Table 8.5 Parameters in $\mathbb{R}^m \rightarrow L$ sampling (L is an m D lattice)

Term	Parameter
Original domains	$I = \mathbb{R}^m, \widehat{I} = \mathbb{R}^m$
Domains after sampling	$J = L, \widehat{J} = \mathbb{R}^m/L^*$
Compatibility condition	None
Typical reference cell	$C_0 = [\mathbb{R}^m/L^*]$
Repetition centers	$R = L^*$
Interpolating function	$q_0(t) = d(L) \int_{[\mathbb{R}^m/L^*]} df e^{i2\pi ft}, t \in \mathbb{R}^m$

Table 8.6 Parameters in $\mathbb{R}^2 \rightarrow \mathbb{Z}(d) \times \mathbb{R}$ sampling

Term	Parameter
Original domains	$I = \mathbb{R}^2, \widehat{I} = \mathbb{R}^2$
Domains after sampling	$J = \mathbb{Z}(d) \times \mathbb{R}, \widehat{J} = \mathbb{R}/\mathbb{Z}(F_c) \times \mathbb{R}$
Compatibility condition	None
Typical reference cell	$C_0 = [-\frac{1}{2}F_c, \frac{1}{2}F_c] \times \mathbb{R}$
Repetition centers	$R = \mathbb{Z}(F_c) \times \mathbb{O}$
Interpolating function	$q_0(t_1, t_2) = \text{sinc}(F_c t_1) \delta(t_2), (t_1, t_2) \in \mathbb{R}^2$

8.10.3 Sampling on a Grating

The form

$$\mathbb{R}^m \rightarrow G$$

with G an m D grating with signature $\mathbb{Z}^q \times \mathbb{R}^p$ ($p + q = m$) may be regarded as a *partial* sampling since this operation is only confined to the first q of the m possible directions.

For simplicity, we limit the development to the 2D separable case $\mathbb{R}^2 \rightarrow \mathbb{Z}(d) \times \mathbb{R}$ where the sampling of a $s(t_1, t_2), (t_1, t_2) \in \mathbb{R}^2$ is confined to the first coordinate t_1 . The corresponding sampling/interpolation parameters are illustrated in Table 8.6.

For the $\mathbb{Z}(d) \times \mathbb{R} \rightarrow \mathbb{R}^2$ interpolator, the input–output relationship is given by

$$s(t_1, t_2) = \sum_{n=-\infty}^{+\infty} s(nd, t_2) q_0(t_1 - nd),$$

where the interpolating function is 1D and given by $g_0(t_1) = \text{sinc}(F t_1 - n)$. The general case will be developed in Chap. 16.

UT 8.11 Errors in Sampling/Interpolation

According to the Unified Sampling Theorem, the exact signal recovery requires:

1. Band-limitation,
2. Alias-free condition, and
3. An ideal interpolator.

If these conditions are not verified (and in practice they are never fully verified), the recovered signal has an error

$$e(t) \triangleq \tilde{s}(t) - s(t), \quad (8.88)$$

where $\tilde{s}(t)$ is the interpolated signal, given by (8.47), that is,

$$\tilde{s}(t) = \sum_{u \in J} s(u) g_0(t - u). \quad (8.89)$$

8.11.1 In-Band and Out-Band Errors

The lack of band-limitation creates aliasing in the periodic repetition, and consequently the *useful term* cannot be separated from the lateral terms. Although we suppose operating with an ideal interpolator having unitary shape over the reference cell C_0 , the aliasing causes a two-fold error. The first error (the *in-band error*) is the contributions of the lateral terms within the cell C_0 . And the second error (the *out-band error*) is due to the fact that the useful term $S(f)$ extends outside the cell, and then it is partially filtered (the interpolator operates within the cell). These two errors are shown in Fig. 8.27 for the $\mathbb{R} \rightarrow \mathbb{Z}(T)$ sampling with $C_0 = [-\frac{1}{2}F_c, \frac{1}{2}F_c]$ as a reference cell.

In the frequency domain, the error is given by (see (8.52))

$$E(f) = \tilde{S}(f) - S(f) = \sum_{p \in P} S(f - p) Q(f) - S(f) = E_{\text{out}}(f) + E_{\text{in}}(f),$$

where

$$E_{\text{out}}(f) = [Q(f) - 1]S(f) = \text{out-band error}, \quad (8.90a)$$

$$E_{\text{in}}(f) = \sum_{p \neq 0} S(f - p) Q(f) = \text{in-band error}. \quad (8.90b)$$

We see that $E_{\text{out}}(f)$ is extended outside C_0 , whereas $E_{\text{in}}(f)$ is extended over C_0 .

The practical evaluation of the error is made globally in terms of the signal-to-error ratio (SER)

$$\Lambda = \frac{\mathcal{E}_s}{\mathcal{E}_e} = \frac{\text{signal energy}}{\text{error energy}} \quad (8.91)$$

which must be sufficiently large, for instance, $\Lambda = 10^4 = 40$ dB, for the recovery accuracy to be accepted. The evaluation of the SER is easy in the frequency domain

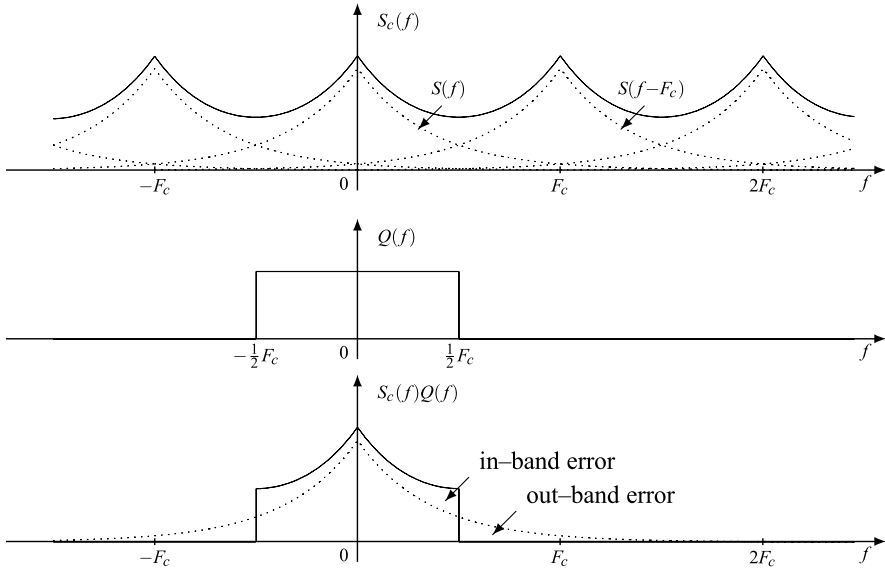


Fig. 8.27 *In-band and out-band errors illustrated for the $\mathbb{R} \rightarrow \mathbb{Z}(T)$ sampling and with an ideal interpolator*

where the energies are evaluated by Parseval’s theorem, that is,

$$\mathcal{E}_s = \int_{\hat{T}} df |S(f)|^2, \quad \mathcal{E}_e = \int_{\hat{T}} df |E(f)|^2. \tag{8.92}$$

The energies of out-band and in-band errors are respectively

$$\begin{aligned} \mathcal{E}_{\text{out}} &= \int_{\hat{T}} df |E_{\text{out}}(f)|^2 = \int_{f \notin C_0} df |S(f)|^2, \\ \mathcal{E}_{\text{in}} &= \int_{\hat{T}} df |E_{\text{in}}(f)|^2 = \int_{C_0} df |\tilde{S}(f) - S(f)|^2, \end{aligned} \tag{8.93}$$

and allow the calculation of the global error energy simply as

$$\mathcal{E}_e = \mathcal{E}_{\text{out}} + \mathcal{E}_{\text{in}}, \tag{8.94}$$

where the errors $e_{\text{out}}(t)$ and $e_{\text{in}}(t)$ are spectrally disjoint, and therefore their cross-energy is zero.

It is important to relate the two energies \mathcal{E}_{out} and \mathcal{E}_{in} and their role in the SER Λ . The out-band energy \mathcal{E}_{out} requires the evaluation of the integral outside the reference cell C_0 , whereas the in-band energy \mathcal{E}_{in} requires the preliminary evaluation of a series, which is a difficult task. We shall see that in practice $\mathcal{E}_{\text{out}} \approx \mathcal{E}_{\text{in}}$, but before we develop an example.

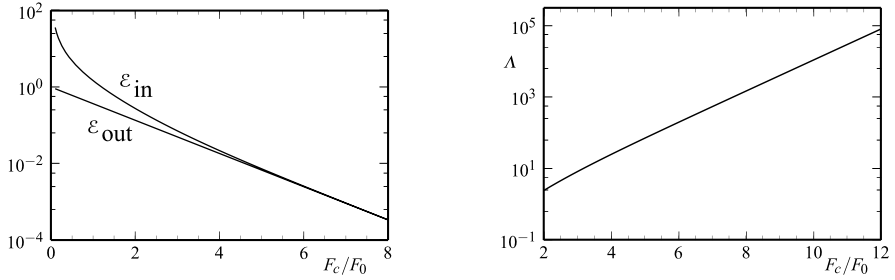


Fig. 8.28 In-band and out-band energies and SER on function of the normalized sampling frequency

Example 8.1 Consider the $\mathbb{R} \rightarrow \mathbb{Z}(T)$ sampling of the signal

$$s(t) = A_0 \frac{1}{1 + (F_0 t / 2\pi)} \xrightarrow{\mathcal{F}} S(f) = S_0 e^{-|f|/F_0}, \quad S_0 = \frac{A_0}{2F_0}.$$

This signal is not band-limited, so we want to study the in-band and out-band errors (see Fig. 8.27 for their illustration). The energy of the out-band error is

$$\mathcal{E}_{\text{out}} = \int_{|f| > \frac{1}{2}F_c} |S(f)|^2 df = 2S_0^2 \int_0^{F_c} e^{-2f/F_0} df = S_0^2 F_0 e^{-F_c/F_0} = \mathcal{E}_s e^{-F_c/F_0}.$$

The FT of the in-band error is

$$\begin{aligned} E_{\text{in}}(f) &= \sum_{n \neq 0} S(f - nT) Q(f) \\ &= S_0 \left[\sum_{n=1}^{\infty} e^{(f-nF_c)/F_0} + \sum_{n=0}^{\infty} e^{(f+nF_c)/F_0} - e^{f/F_0} \right] Q(f) \\ &= S_0 \frac{e^{-F_c/F_0}}{1 - e^{-F_c/F_0}} (e^{f/F_0} + e^{-f/F_0}) Q(f). \end{aligned}$$

Hence, we get the energy by the second equation of (8.93). After few passages we find

$$\mathcal{E}_{\text{in}} = \mathcal{E}_s 2 [\exp(F_c/F_0) - 1]^{-2} [\sinh(F_c/F_0) + F_c/F_0].$$

The plot of \mathcal{E}_{out} and \mathcal{E}_{in} as a function of F_c/F_0 is illustrated in Fig. 8.28 where also the SER Λ is represented. Note that the two energies become very close for moderately large F_c/F_0 .

This example shows that in practice, when the sampling frequency is large enough, the contribution of the in-band and out-band errors are very close, that is,

$$\mu = \mathcal{E}_{\text{in}}/\mathcal{E}_{\text{out}} \approx 1. \quad (8.95)$$

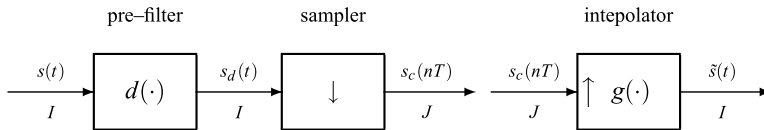


Fig. 8.29 Sampling–interpolation with a pre-filtering

This statement has a general “practical” validity and may be used as a guide for the sampling of non-band-limited signals.

8.11.2 Benefit of Pre-Filtering

The frequency analysis of the sampling error suggests that the in-band error can be reduced by the introduction of a filter that removes the frequency components outside the cell C_0 . Then in the sampling/interpolation scheme, we introduce a *pre-filter* before the down-sampling, as shown in Fig. 8.29.

To make a clear analysis of this scheme, we assume that both the pre-filter and the interpolator have an ideal frequency response over the cell C_0 , that is,

$$D(f) = G(f) = \eta_{C_0}(f).$$

Now, by construction, the output of the pre-filter $s_d(t)$ has spectral extension over C_0 . Hence, $s_d(t)$ verifies the Unified Sampling Theorem assumptions and can be exactly recovered at the end, that is,

$$\tilde{s}(t) = s_d(t). \tag{8.96}$$

Therefore, the in-band error disappears, although the original signal $s(t)$ is not band-limited, and we find

$$\mathcal{E}_e = \int_{f \notin C_0} df |S(f)|^2 = \mathcal{E}_{\text{out}}, \tag{8.97}$$

where \mathcal{E}_{out} is the out-band error energy. Taking the indication given by (8.95), we conclude that the pre-filter introduction halves the error energy, so the SER is improved by 3 dB.

8.11.3 Sampling of Non-Band-Limited Signals

To begin with, we consider the $\mathbb{R} \rightarrow \mathbb{Z}(T)$ sampling of a unimodal spectrum signal, where the choice is confined to the sampling frequency F_c . If the signal is strictly band-limited according to $e(S) = (-B, B)$, the *natural choice* is $F_c = 2B$, and we

know that in such a way we obtain a perfect recovery. But if the signal is not band-limited, we have no natural choice for the sampling frequency F_c , and a criterion will be based on assuring a reconstruction *with a sufficiently large SER*, say $\Lambda \geq \Lambda_{\min}$. To this end, we use the concept of a *conventional band* B_c which replaces the concept of a *strict band* B of band-limited signals. The conventional band B_c is defined by the condition that the energy outside the cell $(-B_c, B_c)$ is a fraction ε of the global signal energy, that is,

$$\mathcal{E}_{\text{out}} = \int_{f \notin (-B_c, B_c)} |S(f)|^2 df = \varepsilon \int_{-\infty}^{+\infty} |S(f)|^2 df. \quad (8.98)$$

Now, taking as reference a sampling scheme with a pre-filter and letting $F_c = 2B_c$, we find that the error energy is just given by (8.97). Hence

$$\Lambda = \mathcal{E}_s / \mathcal{E}_{\text{out}} = 1/\varepsilon.$$

For instance, if we want $\Lambda_{\min} = 40 \text{ dB} = 10^4$ we have to choose a conventional band B_c such that $\varepsilon = 10^{-4}$.

On the other hand, if we use a sampling scheme without a pre-filter, we have to recall that Λ is reduced by 3 dB; hence to guarantee $\Lambda = 40 \text{ dB}$ we have to reduce ε to 0.5×10^{-4} with a consequent increase of the conventional band B_c .

In conclusion, to handle the $\mathbb{R} \rightarrow \mathbb{Z}(T)$ sampling of a non-band-limited signal, we have to find the SER as a function of the sampling frequency, $\Lambda = \Lambda(F_c)$. Since $\Lambda(F_c)$ always increases with F_c , for every fixed Λ_{\min} , we can find the minimum sampling frequency $F_{c,\min}$ that assures this SER.

The above ideas can be extended to multidimensional sampling. For instance, if we consider the $\mathbb{R}^2 \rightarrow \mathbb{Z}_2^1(d_1, d_2)$ sampling, we fix a prototype reference cell C_0 which is convenient for the class of signals we are considering. The size of C_0 is determined by two sampling frequencies $F_{c1} = 1/d_1$ and $F_{c2} = 1/d_2$. Then, the SER

$$\Lambda = \mathcal{E}_s / \int_{(f_1, f_2) \notin C_0} |S(f_1, f_2)|^2 df_1 df_2$$

is an increasing function of both F_{c1} and F_{c2} and allows the evaluation of the frequencies that ensures a given SER Λ_{\min} .

8.12 The “Real” Sampling

The ideal tfs considered in the previous chapters, and particularly the *down-sampling*, are very abstract models which may not accurately describe the corresponding “real” operations. In particular, the “real” sampling of a continuous-domain signal is never confined to picking up isolated values, as happens in the “ideal” sampling, but finite portions of the signal. In this section, we deal with some realistic models of the “real” sampling, and we shall see that also in these models the “ideal” sampling will play a fundamental role and is a guide to choosing the parameters also in the “real sampling”.

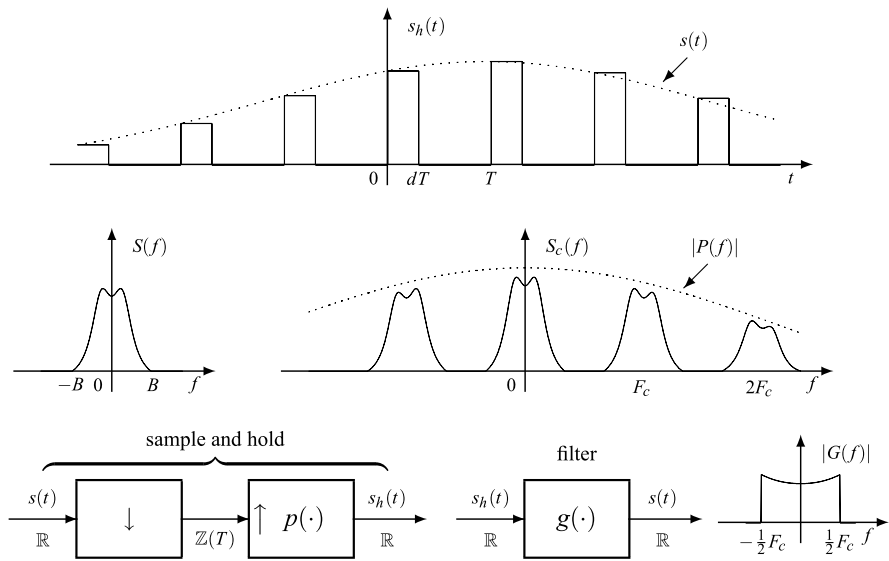


Fig. 8.30 Illustration of sample-and-hold and its equivalent scheme; the filter $g(\cdot)$ permits the recovery of the original signal

8.12.1 Sample-and-Hold

In this operation, a continuous-time signal $s(t)$, $t \in \mathbb{R}$, is sampled at the instants nT (sampling) and each value $s(nT)$ is held for a fraction d of the sampling period T . Hence, the resulting signal $s_h(t)$ consists of rectangular pulses of amplitude $s(nT)$ and extension $(nT, nT + dT)$, where d is called the *duty cycle* (Fig. 8.30). Therefore, the signal obtained with the sample-and-hold operation can be written in the form

$$s_h(t) = \sum_{n=-\infty}^{+\infty} s(nT) p_0(t - nT), \quad t \in \mathbb{R}, \tag{8.99}$$

where $p_0(t) = 1$ for $0 < t < dT$ and $p_0(t) = 0$ elsewhere. Note that the sampled-and-held signal $s_h(t)$ is still a continuous-time signal with domain \mathbb{R} .

An inspection of (8.99) shows that it corresponds to the input–output relationship of an $\mathbb{Z}(T) \rightarrow \mathbb{R}$ interpolator with impulse response

$$p(t) = (1/T) p_0(t). \tag{8.100}$$

Therefore, a sample-and-hold operation is equivalent to (Fig. 8.30): (i) an $\mathbb{R} \rightarrow \mathbb{Z}(T)$ “ideal” sampler followed by (ii) a $\mathbb{Z}(T) \rightarrow \mathbb{R}$ interpolator with the impulse response given by (8.100).

Now using this equivalent scheme, it is easy to establish when and how the original signal $s(t)$ can be recovered by the sampled-and-held signal $s_h(t)$. In fact, it is sufficient to recall that the Fundamental Sampling Theorem requires an interpolator

with frequency response $Q(f) = \text{rect}(f/F_c)$. Then, it will be sufficient to add to the sample-and-hold scheme a filter with the frequency response $G(f)$ such that

$$P(f)G(f) = (1/T)P_0(f)G(f) = Q(f). \quad (8.101)$$

In fact, the cascade is equivalent to the interpolator of the Fundamental Sampling Theorem, and therefore, if the original signal $s(t)$ is band-limited with band B and $F_c = 1/T \geq 2B$, the output of $G(f)$ gives the perfect recovery of $s(t)$.

In conclusion, if a band-limited signal is sampled-and-held, the resulting signal can be recovered with a filter having the frequency response

$$G(f) = Q(f)/P(f) = TQ(f)/P_0(f). \quad (8.102)$$

In particular, when $p(t)$ is a rectangular pulse, we have

$$G(f) = \frac{\text{rect}(f/F_c)}{d \text{sinc}(f dT)} e^{i\pi f dT}. \quad (8.102a)$$

In general, the fundamental pulse $p_0(t)$ may have an arbitrary shape. Then the recovery filter has a frequency response given by (8.102) with $P_0(f)$ given by the FT of $p_0(t)$. Note that the sample-and-hold operation may be viewed as a pulse amplitude modulator (PAM) which is frequently encountered in digital transmissions.

The above consideration can be easily extended to multidimensional samplings, say $\mathbb{R}^m \rightarrow L$, where the impulse $p_0(t)$ becomes a multidimensional pulse. The recovery is still performed by an m D filter designed according to

$$G(f) = d(L)Q(f)/P_0(f), \quad (8.102b)$$

where $Q(f)$ is the frequency response of the Unified Sampling Theorem interpolator and $d(L)$ is the lattice determinant.

8.12.2 Natural Sampling

In this form of “real sampling”, the signal $s(t)$, $t \in \mathbb{R}$, is preserved on the intervals $(nT, nT + dT)$ and dropped outside (Fig. 8.31). The operation can be modeled by a window with the periodic shape

$$v(t) = \text{rep}_T p_0(t) = \sum_{k=-\infty}^{+\infty} p_0(t - kT),$$

where $p_0(t)$ is a unitary rectangular pulse with extension $(0, dT)$. The resulting signal is

$$s_n(t) = s(t)v(t) = \begin{cases} s(t), & \text{if } kT < t < kT + dT; \\ 0, & \text{elsewhere.} \end{cases} \quad (8.103)$$

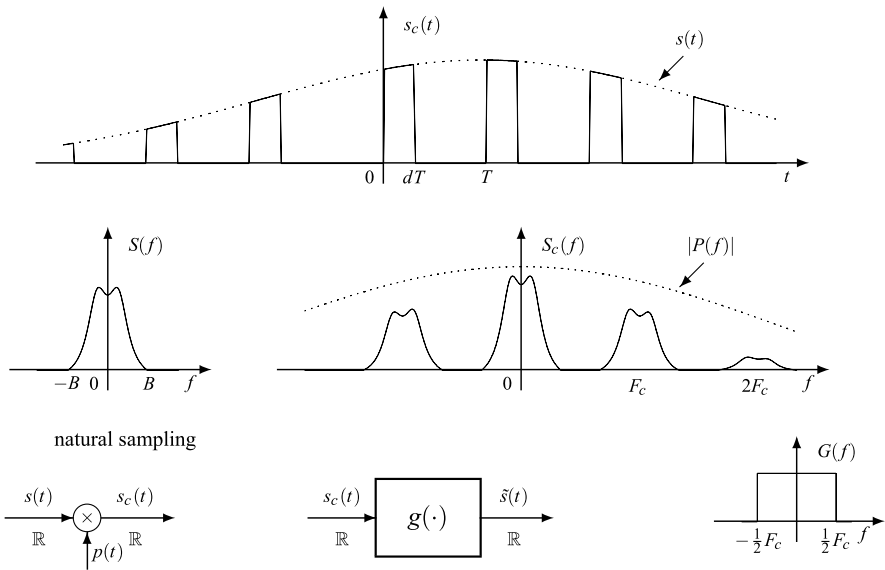


Fig. 8.31 Illustration of natural sampling and its equivalent scheme. On the *right*, the giving recovery signal filter

Again, the signal obtained by a natural sampling is continuous, that is, $s_n(t)$, $t \in \mathbb{R}$. To investigate the possibility of the recovery of the original signal $s(t)$ from the naturally sampled signal $s_n(t)$, we pass to the frequency domain. Then, the product $s_n(t) = s(t)v(t)$ becomes the convolution

$$S_n(f) = S * V(f) = \int_{\mathbb{R}} d\lambda S(f - \lambda)V(\lambda). \tag{8.104}$$

However, in this form we do not realize the nature of the operation since the periodicity $v(t)$ is not explicitly taken into account. Then, we reformulate $v(t)$, $t \in \mathbb{R}$, as a periodic signal $\tilde{v}(t)$, $t \in \mathbb{R}/\mathbb{Z}(T)$. This is irrelevant in the time domain, where $v(t)$ must be considered as the $\mathbb{R}/\mathbb{Z}(T) \rightarrow \mathbb{R}$ down-periodization of $\tilde{v}(t)$. But in the frequency domain, we find the $\mathbb{Z}(F_c) \rightarrow \mathbb{R}$ interpolation (see Sect. 6.13) with the relationship

$$V(f) = \sum_{k=-\infty}^{+\infty} F_c \tilde{V}(kF_c) \delta(f - kF_c) = \sum_{k=-\infty}^{+\infty} V_k \delta(f - kF_c), \tag{8.105}$$

where $V_k = F_c \tilde{V}(kF_c)$ are the Fourier coefficients of $\tilde{v}(t)$. Now, (8.105) shows the presence of “lines” of $V(f)$, which can be used to get a more explicit result from (8.104), namely

$$S_n(f) = \sum_{k=-\infty}^{+\infty} V_k S(f - kF_c). \tag{8.106}$$

Hence, the natural sampling gives a *weighted repetition* of the FT, which is very similar to the *periodic repetition* provided by the ideal sampling.

Now, it is easy to establish the perfect recovery of $s(t)$ from $s_n(t)$. If the sampling frequency verifies the alias-free condition, $F_c \geq 2B$, the terms of the weighted repetition (8.106) do not collide, and it is possible to recover the useful term $V_0 S(f)$ from $S_n(f)$. The recovery is obtained with a filter having the frequency response

$$G(f) = (1/V_0) \text{rect}(f/F_c) = (1/V_0) Q(f). \quad (8.107)$$

Also in this case, it is easy to extend the conclusions to the multidimensional sampling.

8.13 Problems

8.1 ★ [Sect. 8.1] Make explicit the Nyquist criterion for $I = \mathbb{Z}(T)$ and $U = \mathbb{Z}(T_0)$ with $T = NT_0$.

8.2 ★ [Sect. 8.1] Verify that an interpolator whose frequency response $G(f)$, $f \in \mathbb{R}$, has an *isosceles triangle shape* over $(-F_c, F_c)$, satisfies the correct interpolation condition.

8.3 ★★★ [Sect. 8.1] Consider the frequency response $G(f)$, $f \in \mathbb{R}$, defined for $f > 0$ as follows:

$$G(f) = \begin{cases} 1, & \text{if } 0 < f < \frac{1}{2}F_c(1-r); \\ \alpha(f), & \text{if } \frac{1}{2}F_c(1-r) < f < \frac{1}{2}F_c(1+r); \\ 0, & \text{if } f > \frac{1}{2}F_c(1+r), \end{cases} \quad 0 \leq r \leq 1,$$

and extended by the even symmetry for $f < 0$.

Find the conditions on the function $\alpha(f)$ such that $G(f)$ verifies the Nyquist criterion (8.17).

8.4 ★★ [Sect. 8.4] In Fig. 8.13, the Fourier transform

$$S(f) = A_0 \exp(-|f|T_0), \quad f \in \mathbb{R}.$$

is drawn. Calculate its periodic repetition $S_c(f)$, $f \in \mathbb{R}/\mathbb{Z}(F_c)$. Recall that it is sufficient to perform the evaluation over a period, such as $[0, F_c)$.

8.5 ★ [Sect. 8.4] Find the minimum sampling frequency (for a perfect reconstruction) of the signal:

$$s(t) = A_0 \text{sinc}^2(F_0 t), \quad t \in \mathbb{R},$$

with $F_0 = 2$ MHz.

8.6 ** [Sect. 8.4] Find the alias-free condition (8.34a, 8.34b) for the signal

$$s(t) = A_0 \operatorname{sinc}(F_0 t) \cos(2\pi f_0 t),$$

with $F_0 = 2$ kHz and $f_0 = 1$ MHz.

8.7 *** [Sect. 8.4] Show that, if the hypotheses of the Fundamental Sampling Theorem are verified, the energy of samples equals the energy of the signal:

$$\sum_{n=-\infty}^{+\infty} T |s(nT)|^2 = \int_{-\infty}^{+\infty} |s(t)|^2 dt.$$

8.8 * [Sect. 8.7] Find the spectral extension of the signal

$$s(t) = A_0 \operatorname{sinc}^2(F_0 t) \cos(2\pi f_0 t),$$

with $f_0 = 10 F_0$. Then express the efficiency η_{si} that can be achieved with a *direct* down-sampling.

8.9 * [Sect. 8.7] Referring to the sampling of Fig. 8.21, find the interpolating function.

8.10 ** [Sect. 8.7] Find the smallest cell of \mathbb{R} modulo $\mathbb{Z}(F_c)$ containing the extension

$$e(S) = (-23 \text{ kHz}, -19 \text{ kHz}) \cup (19 \text{ kHz}, 23 \text{ kHz})$$

and then calculate the efficiency η_{si} .

8.11 *** [Sect. 8.7] Consider a bimodal symmetric spectrum with the extension indicated in (8.70). Evaluate the smallest cell C_0 containing such an extension for any value of the ratio f_0/B .

8.12 *** [Sect. 8.7] Referring to Fig. 8.22 suppose that the signal $s(t)$, $t \in \mathbb{R}$, is real. Show that the signal $s_2(t)$ in the lower branch of the block diagram is the conjugate of the signal $s_1(t)$ in the upper branch, and in particular $\tilde{s}_2(t) = \tilde{s}_1^*(t)$.

8.13 ** [Sect. 8.8] Consider a discrete signal $s(t)$, $t \in \mathbb{Z}(T_0)$ with extension $e(S) = (-B, B) + \mathbb{Z}(F_0)$ and $B = \frac{1}{7}F_0$. Find the minimum sampling frequency.

8.14 *** [Sect. 8.8] Consider a discrete signal with extension

$$e(S) = (-B, B) + \mathbb{Z}(F_0). \quad (8.108)$$

Find the minimum sampling frequency with a *direct* down-sampling as a function of B/F_0 .

8.15 *** [Sect. 8.8] Consider the down-sampling of a discrete signal with extension (8.108) with $B = \frac{3}{11}F_0$. Find a scheme that, using a pre-filtering, allows a correct down-sampling with $2B$ samples/s.

8.16 * [Sect. 8.9] The signal

$$s(t) = \text{rep}_{F_p} \text{rect}(t/dT_p), \quad t \in \mathbb{R}/\mathbb{Z}(T_p),$$

with $T_p = 1$ ms and $d = 20\%$, is filtered by an ideal low-pass filter with band $B_0 = 3.5$ kHz and then down-sampled with an $\mathbb{R}/\mathbb{Z}(T_p) \rightarrow \mathbb{Z}(T)/\mathbb{Z}(T_p)$ sampling.

Find the minimum number of samples per period and write the expression of the recovered signal.

8.17 ** [Sect. 8.9] Make explicit the Unified Sampling Theorem for discrete periodic signals, that is, with $\mathbb{Z}(T_0)/\mathbb{Z}(T_p) \rightarrow \mathbb{Z}(T)/\mathbb{Z}(T_p)$.

8.18 ** [Sect. 8.10] Prove that, if the reference cell C_0 in the 2D sampling verifies the symmetry condition

$$-C_0 = C_0,$$

then the interpolator is *real*, i.e., with a real impulse response.

8.19 ** [Sect. 8.10] Consider an $\mathbb{R}^2 \rightarrow \mathbb{Z}(d_1, d_2)$ sampling and assume that the reference cell C_0 is a parallelogram, instead of a rectangle.

Write the frequency response of the interpolator specified by this cell.

8.20 *** [Sect. 8.10] Consider the sampling $\mathbb{R}^2 \rightarrow \mathbb{Z}_2^1(d_1, d_2)$ and assume the reference cell C_0 is a rhombus.

Determine the impulse response of the interpolator specified by this cell.

8.21 ** [Sect. 8.11] Consider the $\mathbb{R} \rightarrow \mathbb{Z}(T)$ sampling of the signal

$$s(t) = 1(t)e^{-\alpha t}, \quad t \in \mathbb{R}.$$

Find the sampling frequency F_c that ensures $\Lambda_{\min} = 48$ dB, using a pre-filter and assuming $F_0 = \alpha/2\pi = 1$ MHz.

8.22 ** [Sect. 8.11] As in the previous problem, but without the pre-filter (assume $\mu = 1$).

8.23 *** [Sect. 8.11] Evaluate the ratio μ defined in (8.95) for the signal:

$$s(t) = \frac{A_0}{1 + (F_0 t)^2}.$$

8.24 ** [Sect. 8.11] Consider the down-sampling $\mathbb{R} \rightarrow \mathbb{Z}(T)$ with a pre-filter (see Fig. 8.29), with

$$D(f) = e^{-|f|/F_0} \text{rect}(f/F_c), \quad G(f) = \text{rect}(f/F_c).$$

Show that this scheme is equivalent to a filter on \mathbb{R} and find the equivalent filter.

8.25 * [Sect. 8.11] In the $\mathbb{R} \rightarrow \mathbb{Z}(T)$ sampling, verify that, if $e(S) \subset (-F_c, F_c)$, the in-band energy \mathcal{E}_{in} equals the out-band energy \mathcal{E}_{out} .

8.26 * [Sect. 8.12] Consider the *sample-and-hold* with the fundamental pulse

$$p_0(t) = \cos 2\pi \frac{t}{T_0} \text{rect}\left(\frac{t}{dT}\right),$$

where $T_0 = 2dT$ and $d = 20\%$. Find the frequency response of the filter that allows the perfect reconstruction of the signal.

8.27 ** [Sect. 8.12] A real signal $s(t)$, $t \in \mathbb{R}$, with bandwidth $B = 4$ kHz is *sampled-and-held* with $F_c = 2B$ and then filtered with a real pass-band filter with band-pass $(3F_c - B, 3F_c + B)$ and unitary frequency response over the band.

Find the signal expression at the filter output.

References

1. A.L. Cauchy, Mémoire sur diverses formules de analyse. Comptes Rendus **12**, 283–298 (1841)
2. G. Cariolaro, A unified signal theory (topological approach), in *Proc. of Italy–USA Seminary on Digital Signal Processing*, Portovenere, Italy, August 1981
3. D.P. Petersen, D. Middleton, Sampling and reconstruction of wave-number-limited functions in N -dimensional Euclidean spaces. *Inf. Control* **5**, 279–323 (1962)
4. H. Nyquist, Certain factors affecting telegraph speed. *Bell Syst. Tech. J.* **3**, 324–346 (1924)
5. B.M. Oliver, J.R. Pierce, C.E. Shannon, The Philosophy of PCM. *Proc. IRE* **36**, 1324–1332 (1948)
6. C.E. Shannon, Communication in the presence of noise. *Proc. IRE* **37**, 10–21 (1949)

Part III
Specific Classes of Signals
and Applications

Chapter 9

Signals Defined on \mathbb{R}

UT 9.1 The Time Domain

9.1.1 The Additive Group \mathbb{R} of the Real Numbers

This LCA group exhibits some peculiarities that in general we do not find in other groups, such as

- shifts and periods have no structural constraints;
- a scale change maps \mathbb{R} into itself;
- the dual group of \mathbb{R} is still \mathbb{R} , that is, \mathbb{R} is self-dual.

The measure on \mathbb{R} is the ordinary Lebesgue measure. *Cells* of the form $[\mathbb{R}/\mathbb{Z}(T_p)]$ are typically intervals as $[t_0, t_0 + T_p)$ or $(t_0, t_0 + T_p]$, but sometimes the union of open intervals with total measure T_p .

9.1.2 Integral and Convolution

The Haar integral over \mathbb{R} (see Sect. 4.1) is the usual (Lebesgue) integral

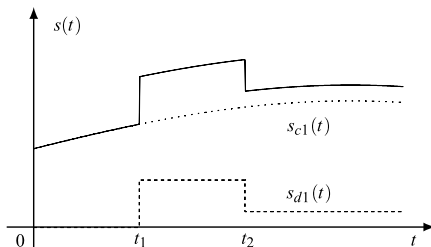
$$\int_{\mathbb{R}} dt s(t) = \int_{-\infty}^{+\infty} s(t) dt = \text{area}(s).$$

Consequently, the *convolution* is

$$x * y(t) = \int_{-\infty}^{+\infty} x(t-u)y(u) du = \int_{-\infty}^{+\infty} y(t-u)x(u) du \quad (9.1)$$

and has all the general properties established in Sect. 4.9. For the evaluation and the interpretation of this operation, the reader can refer to Sect. 2.4. The convolution

Fig. 9.1 Decompositions of a discontinuous signal into a continuous signal and piecewise constant signal by using the *step function*



evaluation can also be carried out via FT, following the graph

$$x * y(t) \xrightarrow{\mathcal{F}} X(f)Y(f) \xrightarrow{\mathcal{F}^{-1}} x * y(t).$$

The *impulse*, defined in general as the unitary element of the convolution algebra is given by the delta function, $\delta_{\mathbb{R}}(t) = \delta(t)$, and is a generalized function (see Sect. 2.3 and Theorem 4.7).

9.1.3 Discontinuous Signals

The class of signals defined on \mathbb{R} includes discontinuous signals, where at a discontinuity point t_i , it is convenient to define the signal by the *semi-value*

$$s(t_i) \triangleq \frac{1}{2}[s(t_i+) + s(t_i-)].$$

This convention is motivated by the fact that, at discontinuities, the inverse FT converges to the semi-value; in such a way we obtain $s(t) = \mathcal{F}^{-1}[S|t]$ for every $t \in \mathbb{R}$.

A discontinuous signal $s(t)$ having only type-2 discontinuities can be decomposed into a continuous signal $s_c(t)$ and a *piecewise constant* signal $s_d(t)$, collecting the discontinuities of $s(t)$, of the form

$$s_d(t) = \sum_i d_i 1(t - t_i), \quad d_i = s(t_i+) - s(t_i-), \tag{9.2}$$

where $1(t)$ is the step function, and d_i are the discontinuity sizes. The continuous part is given by $s_c(t) = s(t) - s_d(t)$, as shown in Fig. 9.1.

An alternative decomposition can be made in terms of the “*signum*” function $\text{sgn}(\cdot)$, where the discontinuous part becomes

$$\tilde{s}_d(t) = \sum_i \frac{1}{2} d_i \text{sgn}(t - t_i), \tag{9.3}$$

and, in fact, $\frac{1}{2}d_i \text{sgn}(t - t_i)$ has the same discontinuity size as $d_i 1(t - t_i)$. The two decompositions differ for the management of dc component: the discontinuous part (9.2) has in general a dc component given by $\sum_i d_i$, whereas (9.3) has no dc component (see Problem 9.1).

9.1.4 Time Differentiation and Integration

For signals defined on \mathbb{R} , it is possible to consider the differentiation and the integration, namely

$$s'(t) = \frac{ds(t)}{dt}, \quad y(t) = \int_{-\infty}^t s(u) du.$$

We recall that the delta function allows one to handle the differentiation of discontinuous functions. As an example, the differentiation of the discontinuous part of a signal (defined by (9.2) or (9.3)) is given by

$$s'_d(t) = \sum_i d_i \delta(t - t_i).$$

9.1.5 Scale Change

The scale change

$$y(t) = x(at), \quad a \neq 0, \tag{9.4}$$

has the peculiarity to transform a signal defined on \mathbb{R} into a signal still defined on \mathbb{R} . This relationship was illustrated in Sect. 6.5.

Note that a scale change modifies the area in the following way:

$$\text{area}(y) = (1/|a|) \text{area}(x).$$

In particular, the scale change applied to the impulse gives

$$\delta(at) = (1/|a|)\delta(t) \tag{9.4a}$$

with the consequence that the area of the impulse $\delta(at)$ is not 1, but rather $1/|a|$.

9.1.6 Zero Counting with Delta Function

The “function” $\delta(x)$ is identically zero for $x \neq 0$, where it has a concentrated area. Now, if the argument is a time function, $x = g(t)$, the resulting signal $\delta(g(t))$ is zero everywhere with the exception of the instants where $g(t) = 0$. The explicit result is

$$\delta(g(t)) = \sum_n \frac{1}{|g'(t_n)|} \delta(t - t_n), \tag{9.5}$$

where t_n are the zeros of $g(t)$, and we suppose that $g(t)$ has a nonzero derivative at the zero t_n . The presence of the factor $1/|g'(t_n)|$ can be explain as follows: in the

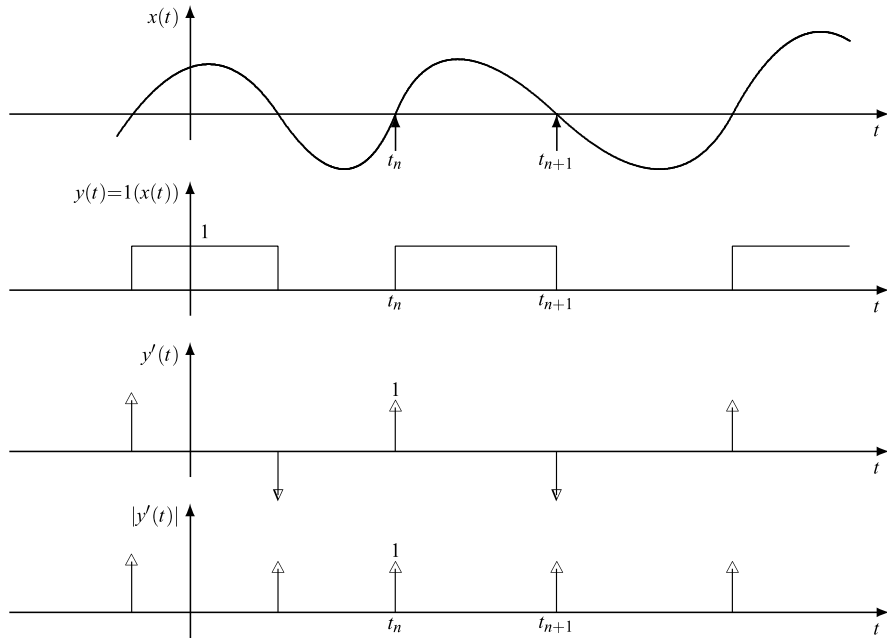


Fig. 9.2 Zero counting property of the delta function

neighborhood of each t_n , we can write

$$g(t) \simeq g(t_n) + g'(t_n)(t - t_n) = g'(t_n)(t - t_n), \quad |t - t_n| < \varepsilon,$$

and, using (9.4a), we find that the area is given by $1/|g'(t_n)|$.

Identity (9.5) has several applications related to the property of the delta function to sift the zeros of a function. For instance, consider the composite signal (Fig. 9.2)

$$y(t) = 1(x(t)), \quad t \in \mathbb{R}, \quad (9.6)$$

where $1(\cdot)$ is the step function. Clearly $y(t)$ consists of rectangular pulses that connect the “crossings” of $x(t)$ with the time axis. Each pulse starts at an up-crossing (crossing with a positive slope) and ends at a down-crossing. Then, by differentiating (9.6) we get (see (2.34))

$$y'(t) = \delta(x(t))x'(t) = \sum_n a_n \delta(t - t_n),$$

where $a_n = x'(t_n)/|x'(t_n)| = \text{sgn}[x'(t_n)]$. Therefore, we find a sequence of delta functions applied at the crossings of $x(t)$ with area 1 for the up-crossings (crossing with a positive slope) and -1 for the down-crossings. In conclusion, $y'(t)$ has the

counting property

$$\int_{T_1}^{T_2} |y'(t)| dt = \text{number of crossings of } x(t) \text{ in } [T_1, T_2]$$

as shown in Fig. 9.2.

UT 9.2 The Frequency Domain

The dual group of \mathbb{R} is \mathbb{R} itself, $\widehat{\mathbb{R}} = \mathbb{R}$, and we find a perfect symmetry between the time and the frequency domains. Consequently, we can transfer all the considerations made in the time domain (on discontinuities, derivatives, etc.) into the frequency domain.

9.2.1 The Fourier Transform

The FT and its inverse are given by

$$S(f) = \int_{-\infty}^{+\infty} s(t)e^{-i2\pi ft} dt, \quad f \in \mathbb{R}, \tag{9.7a}$$

$$s(t) = \int_{-\infty}^{+\infty} S(f)e^{i2\pi ft} df, \quad t \in \mathbb{R}. \tag{9.7b}$$

Then, starting from a continuous-time signal $s(t)$, $t \in \mathbb{R}$, we obtain a continuous-frequency transform $S(f)$, $f \in \mathbb{R}$.

The inverse FT (9.7b) represents the signal as a sum of *exponential* components $df S(f)e^{i2\pi ft}$ of infinitesimal amplitude and frequency $f \in \mathbb{R}$, with both negative and positive frequencies. For a *real* signal, using the consequent Hermitian symmetry of the FT, the representation can be done in terms of *sinusoidal* components, having only *positive frequencies*, namely (see Sect. 5.8)

$$s(t) = S_0 + 2 \int_0^{\infty} A_S(f) \cos[2\pi ft + \beta_S(f)] df, \tag{9.8}$$

where

$$S_0 = m_s = \lim_{T \rightarrow \infty} \frac{1}{2T} \int_{-T}^T s(t) dt \tag{9.8a}$$

is the signal mean value, and $A_S(f) = |S(f)|$, $\beta_S(f) = \arg S(f)$.

Table 9.1 Specific rules of Fourier transform on \mathbb{R}

Signal	Fourier transform	
Time differentiation	$\frac{ds(t)}{dt}$	$i2\pi f S(f)$
Frequency differentiation	$-i2\pi t s(t)$	$\frac{dS(f)}{df}$
Time integration	$\int_{-\infty}^t s(u) du$	$\frac{1}{i2\pi f} S(f) + \frac{1}{2} S(0)\delta(f)$
Frequency integration	$\frac{1}{-i2\pi t} s(t) + \frac{1}{2} s(0)\delta(t)$	$\int_{-\infty}^f S(\lambda) d\lambda$

9.2.2 Specific Rules of the Fourier Transform on \mathbb{R}

The continuous nature of time and frequency domains allows the formulation of a few specific rules on the Fourier transform, which are to be added to the general rules of Table 5.2. These additional rules are collected in Table 9.1.

Differentiation The FT of $y(t) = ds(t)/dt$ is given by the FT of $s(t)$ multiplied by $i2\pi f$

$$\frac{ds(t)}{dt} \xrightarrow{\mathcal{F}} (i2\pi f) S(f). \tag{9.9a}$$

This rule is obtained by differentiating both sides of (9.7b) and can be iterated, giving

$$\frac{d^n s(t)}{dt^n} \xrightarrow{\mathcal{F}} (i2\pi f)^n S(f). \tag{9.9b}$$

This property states the *operational* nature of the FT: it allows one to solve a differential equation in the time domain by solving an algebraic equation in the frequency domain. Identical considerations hold for the frequency differentiation. The validity of these rules requires that integration and differentiation can be interchanged.

Integration For the signal $y(t)$ obtained by integration

$$y(t) = \int_{-\infty}^t s(u) du, \tag{9.10}$$

we have obviously $s(t) = dy(t)/dt$ and then from the differentiation rule

$$S(f) = i2\pi f Y(f) \implies Y(f) = \frac{1}{i2\pi f} S(f).$$

However, this passage does not hold in general, since it requires that area (s) = $S(0) = 0$. To find the general rule, we observe that (9.10) can be written as a convolution of $s(t)$ and the unit step signal. Then

$$y(t) = 1(\cdot) * s(t) \xrightarrow{\mathcal{F}} Y(f) = \left[\frac{1}{i2\pi f} + \frac{1}{2} \delta(f) \right] S(f)$$

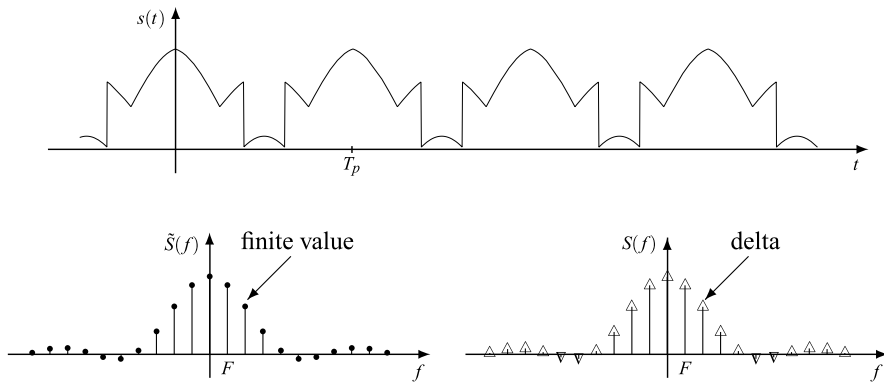


Fig. 9.3 Fourier transforms of a periodic signal: $\tilde{S}(f)$ refers to the signal represented on $\mathbb{R}/\mathbb{Z}(T_p)$, and $S(f)$ to the signal represented on \mathbb{R}

where we have used the expression of the FT of $1(t)$ established in Sect. 2.7. In conclusion, if $S(0) \neq 0$, the impulse $\frac{1}{2}S(f)\delta(f) = \frac{1}{2}S(0)\delta(f)$ must be added in the previous relation, as done in Table 9.1.

9.2.3 Periodic Signals. Spectral Lines

The natural representation of a periodic continuous signal is given by a quotient group $\mathbb{R}/\mathbb{Z}(T_p)$, but sometimes in connection with aperiodic signals we need a representation on \mathbb{R} . We now compare the two representations in the frequency domain.

To formalize the problem, we denote by $\tilde{s}(t)$ the periodic signal (of period T_p) represented on the quotient group $\mathbb{R}/\mathbb{Z}(T_p)$ and by $s(t)$, $t \in \mathbb{R}$, the same signal represented on \mathbb{R} . From the theory of elementary tfs (see Sect. 6.10) we know that $s(t)$ is obtained from $\tilde{s}(t)$ by an $\mathbb{R}/\mathbb{Z}(T_p) \rightarrow \mathbb{R}$ down-periodization (Fig. 9.3). Correspondingly, in the frequency domain we find a $\mathbb{Z}(F) \rightarrow \mathbb{R}$ up-sampling (with $F = 1/T_p$); the relation is (see Sect. 6.13)

$$S(f) = \sum_{k=-\infty}^{+\infty} F \tilde{S}(kF) \delta(f - kF), \quad f \in \mathbb{R}, \tag{9.11}$$

where $\tilde{S}(kF)$, $kF \in \mathbb{Z}(F)$, and $S(f)$, $f \in \mathbb{R}$, are respectively the FT of the signal, represented as periodic and as aperiodic. We recall that $F \tilde{S}(kF) = S_k$ give the *Fourier coefficients* of $\tilde{s}(t)$ (see Sect. 5.8).

In particular, if the periodic signal is given by a periodic repetition of a pulse $p(t)$, $t \in \mathbb{R}$, we find (see Sect. 5.5)

$$s(t) = \text{rep}_{T_p} p(t) \xrightarrow{\mathcal{F}} S(f) = \sum_{k=-\infty}^{+\infty} F P(kF) \delta(f - kF), \tag{9.12}$$

where $P(f)$, $f \in \mathbb{R}$, is the FT of $p(t)$. In conclusion, the FT on \mathbb{R} of a periodic signal consists of equally spaced impulses (*lines*), with spacing given by $F = 1/T_p$.

A periodic signal represents a limiting case in which the spectrum consists only of lines, but in general we may find lines mixed with a continuous spectrum. The presence of a line is due to an exponential component $A_i \exp(i2\pi f_i t)$; in particular a line at the origin, $A_0\delta(f)$, is due to a dc-component $A_0 = m_s$ (see (9.8a)). For real signals, the lines are always in pairs, $A_i\delta(f - f_i) + A_i^*\delta(f + f_i)$ with $f_i \neq 0$, and are due to the presence of a sinusoidal component $2|A_i|\cos(2\pi f_i t + \arg A_i)$.

9.2.4 Further Rules

Causal Version The FT of the causal version of a signal $s(t)$

$$s_c(t) = 1(t)s(t), \quad t \in \mathbb{R},$$

can be obtained by the product rule, which gives $S_c(f) = U * S(f)$, where $U(f) = (1/2)\delta(f) + 1/(i2\pi f)$ is the FT of the unit step signal (see Sect. 2.7). Hence,

$$S_c(f) = \frac{1}{2}S(f) + \frac{1}{2i}\widehat{S}(f), \quad (9.13)$$

where the integral

$$\widehat{S}(f) = \int_{-\infty}^{+\infty} \frac{S(\lambda)}{\pi(f - \lambda)} d\lambda \quad (9.13a)$$

represents the *Hilbert transform* of $S(f)$ (see Sect. 9.10).

Modulated Signals The signal

$$v(t) = s(t) \cos \omega_0 t, \quad \omega_0 = 2\pi f_0,$$

is a particular form of *amplitude modulation*. To obtain the FT of $v(t)$, we can use again the product rule, which implies the calculation of a convolution in the frequency domain. But it is more convenient to decompose the cosine by the Euler formulas, namely $v(t) = \frac{1}{2}s(t)e^{i2\pi f_0 t} + \frac{1}{2}s(t)e^{-i2\pi f_0 t}$, and use the frequency shifting rule. Thus,

$$s(t) \cos \omega_0 t \xrightarrow{\mathcal{F}} \frac{1}{2}S(f - f_0) + \frac{1}{2}S(f + f_0). \quad (9.14a)$$

Therefore, a cosine multiplication acts as a double frequency shifts of $\pm f_0$, as shown in Fig. 9.4. Analogously,

$$s(t) \sin \omega_0 t \xrightarrow{\mathcal{F}} \frac{1}{2i}S(f - f_0) - \frac{1}{2i}S(f + f_0). \quad (9.14b)$$

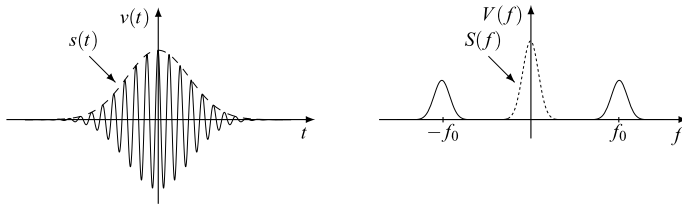


Fig. 9.4 *Modulation rule:* the signal multiplication by $\cos(2\pi f_0 t)$ provides a double frequency shift in the Fourier transform

9.3 Remarkable Examples

9.3.1 The Causal Exponential

The signal

$$1(t)e^{p_0 t}, \quad t \in \mathbb{R}, \tag{9.15}$$

where $p_0 = -\alpha + i\omega_0$ is in general a complex number, plays a fundamental role in filtering (see Sects. 9.8 and 9.9). Its FT exists if $\Re p_0 < 0$ and is given by

$$1(t)e^{p_0 t} \xrightarrow{\mathcal{F}} S(f) = \frac{1}{i\omega - p_0}, \quad \omega = 2\pi f. \tag{9.16}$$

Instead, if $\Re p_0 > 0$, the FT does not exist. If $\Re p_0 = 0$, we have a limit case that can be solved by means of the frequency-shift rule. Specifically, letting $p_0 = i\omega_0 = i2\pi f_0$, we obtain

$$1(t)e^{i2\pi f_0 t} \xrightarrow{\mathcal{F}} U(f - f_0) \quad \text{with } U(f) = \frac{1}{2}\delta(f) + \frac{1}{i2\pi f}, \tag{9.16a}$$

where $U(f)$ is the FT of $1(t)$.

From the Fourier pair (9.16) other interesting pairs can be derived. For instance, using the rule on “real part of the signal” (see Table 5.2), that is, $\Re s(t) \xrightarrow{\mathcal{F}} \frac{1}{2}[S(f) + S^*(-f)]$, we obtain

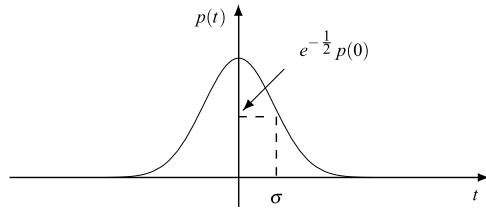
$$1(t)e^{-\alpha t} \cos \omega_0 t \xrightarrow{\mathcal{F}} \frac{\alpha + i\omega}{(\alpha + i\omega)^2 + \omega_0^2}, \quad \omega = 2\pi f. \tag{9.16b}$$

Analogously, using the rule $\Im s(t) \xrightarrow{\mathcal{F}} \frac{1}{2i}[S(f) - S^*(-f)]$, we obtain

$$1(t)e^{-\alpha t} \sin \omega_0 t \xrightarrow{\mathcal{F}} \frac{\omega_0}{(\alpha + i\omega)^2 + \omega_0^2}, \quad \omega = 2\pi f. \tag{9.16c}$$

Finally, applying the “frequency differentiation” rule n times, we obtain

$$1(t) \frac{t^n}{n!} e^{p_0 t} \xrightarrow{\mathcal{F}} \frac{1}{(i\omega - p_0)^{n+1}}. \tag{9.16d}$$

Fig. 9.5 The Gaussian pulse

9.3.2 The Gaussian Pulse and the Chirp Signal

The Gaussian function $\varphi(x) = (1/\sqrt{2\pi}) \exp(-x^2/2)$ plays a fundamental role in probability theory, but it also has a remarkable importance in Signal Theory.

The standard form of the Gaussian pulse (of unit area) is

$$p(t) = \frac{1}{\sigma} \varphi\left(\frac{t}{\sigma}\right) = \frac{1}{\sqrt{2\pi}\sigma} e^{-\frac{1}{2}(t/\sigma)^2}, \quad (9.17)$$

where σ^2 is the second *moment* given by $\sigma^2 = \int_{-\infty}^{+\infty} t^2 p(t) dt$, and σ , called root-mean square (rms) duration, gives the pulse “dispersion” about its central instant $t = 0$ (Fig. 9.5).

The derivatives of the Gaussian pulse can be expressed in the form

$$p^{(n)}(t) = (-1)^n \sigma^{-n} He_n(t/\sigma) \varphi(t/\sigma), \quad n = 0, 1, 2, \dots,$$

where $He_n(x) = 2^{-n/2} H_n(x/\sqrt{2})$ are modified versions of Hermite polynomials [1]; in particular, $He_1(x) = x$ and $He_2(x) = x^2 - 1$. The integral of a Gaussian pulse is expressed by the normalized Gaussian distribution function, $\Phi(x) = \int_{-\infty}^x \varphi(u) du$, namely

$$\int_{-\infty}^t p(u) du = \Phi\left(\frac{t}{\sigma}\right).$$

The FT of $p(t)$ can be evaluated using the moment theorem [7] and is given by

$$P(f) = e^{-2\pi^2\sigma^2 f^2}. \quad (9.18)$$

Thus, the FT also has a Gaussian shape. In particular, for $\sigma = 1/\sqrt{2\pi}$, we find

$$e^{-\pi t^2} \xrightarrow{\mathcal{F}} e^{-\pi f^2}, \quad (9.19)$$

which states that $e^{-\pi t^2}$ is an eigenfunction of the FT (see Sect. 5.12). A remarkable property of the Gaussian pulse is its minimality in duration-bandwidth product (see Sect. 9.5).

Till now we have tacitly assumed that σ and σ^2 are real and positive (and this is usually the case), but the Fourier pair given by (9.17) and (9.18) holds also when σ and σ^2 become complex (provided that $\Re\sigma^2 \geq 0$). Figure 9.6 shows an example

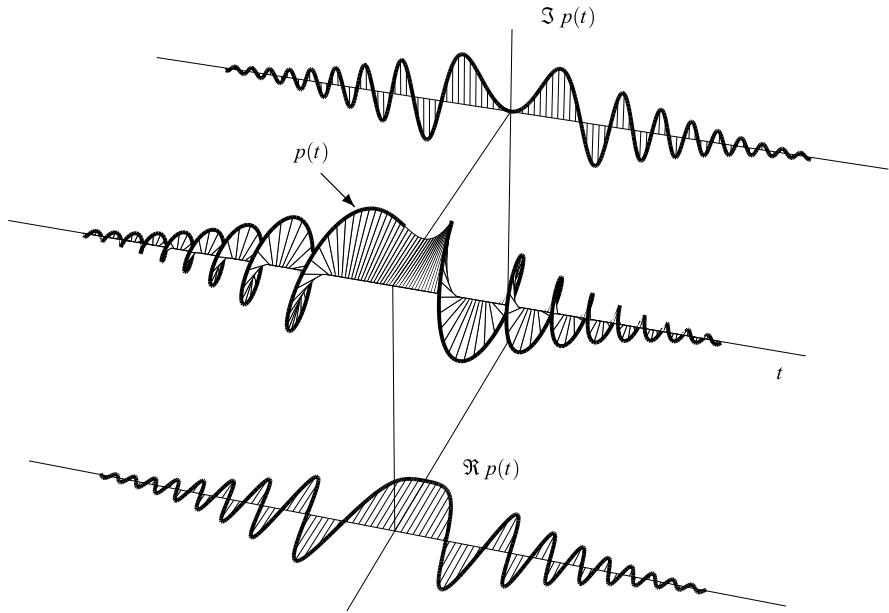


Fig. 9.6 Example of complex Gaussian pulse

with $\sigma^2 = 0.2 + i3.6$. In particular, when σ^2 is imaginary, say $\sigma^2 = i\beta/(2\pi)$, we have the *chirp* signal. The corresponding Fourier pair is

$$p_c(t) = e^{i\pi t^2/\beta} \xrightarrow{\mathcal{F}} P_c(f) = \sqrt{i\beta} e^{-i\pi f^2\beta}, \tag{9.20}$$

where $\sqrt{i\beta} = e^{i\text{sgn}\beta(\pi/4)}|\beta|$.

The chirp signal and, in general, the complex Gaussian pulse are encountered in optical propagation [6], particularly in fiber optics, and also in the *fractional* Fourier transform (see Sect. 5.12).

9.3.3 The Raised Cosine

The “raised cosine” function plays an important role in system design, and therefore it will be seen in detail. The *raised cosine* function is defined by (for $x > 0$)

$$\text{rcos}(x, \alpha) = \begin{cases} 1, & 0 < x < x_1, \\ \cos^2 \frac{\pi}{2} \left(\frac{x-x_1}{\alpha} \right), & x_1 < x < x_2, \\ 0, & x > x_2, \end{cases} \tag{9.21}$$

where

$$0 \leq \alpha \leq 1, \quad x_1 = \frac{1}{2}(1 - \alpha), \quad x_2 = \frac{1}{2}(1 + \alpha).$$

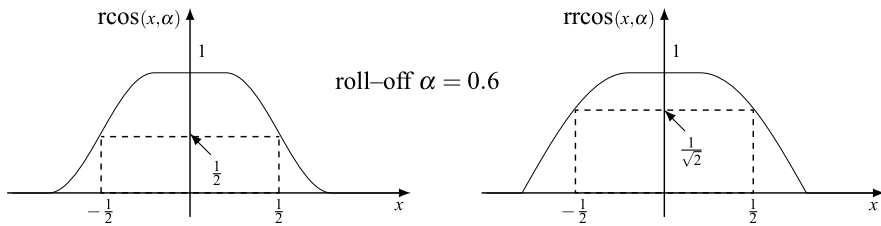


Fig. 9.7 The raised cosine and the square-root raised cosine functions

For negative values of x , the function is *extended by evenness* (Fig. 9.7), that is, $\text{rcos}(-x, \alpha) = \text{rcos}(x, \alpha)$. The parameter α is called the *roll-off*. The function is unitary in the central part for $|x| < x_1$ and zero for $|x| > x_2$. In the range $x_1 < x < x_2$ (and symmetrically in the range $-x_2 < x < -x_1$) it exhibits a roll-off connecting the unit to the zero value. The roll-off is centered at the point $(-\frac{1}{2}, \frac{1}{2})$ and can be written in the alternative forms

$$\cos^2 \frac{\pi}{2} \left(\frac{x - x_1}{\alpha} \right) = \frac{1}{2} + \frac{1}{2} \cos \pi \left(\frac{x - x_1}{\alpha} \right) = \frac{1}{2} - \frac{1}{2} \sin \frac{\pi}{\alpha} \left(x - \frac{1}{2} \right), \quad (9.22)$$

where the term $\frac{1}{2}$ explains the “raised.” For $\alpha = 0$, the roll-off disappears, and the raised cosine degenerates into a rectangle, $\text{rcos}(x, 0) = \text{rect}(x)$, whereas for $\alpha = 1$, the roll-off is displayed on the whole interval $(-1, 1)$ with a raised cosine shape.

A constructive definition of the raised cosine is determined by the conditions: (1) the roll-off connects the points $(x_1, 1)$ and $(x_2, 0)$ with a cosine function in a quarter of a period, (2) the function is continuous with its derivative, and (3) the derivative is zero at x_1 and at x_2 .

Related to the raised cosine function is its square root

$$\text{rrcos}(x, \alpha) = \sqrt{\text{rcos}(x, \alpha)}$$

which is explicitly given by (for $x > 0$)

$$\text{rrcos}(x, \alpha) = \begin{cases} 1, & 0 < x < x_1, \\ \cos \frac{\pi}{2} \left(\frac{x - x_1}{\alpha} \right), & x_1 < x < x_2, \\ 0 & x > x_2. \end{cases} \quad (9.23)$$

The two functions are used to express the frequency responses of filters, written in the form

$$R(f) = \text{rcos}(f/F, \alpha), \quad R_r(f) = \text{rrcos}(f/F, \alpha), \quad (9.24)$$

where $\frac{1}{2}F$ is the *Nyquist frequency*.¹ The reason is that the frequency response $R(f)$ verifies the Nyquist criterion (see Sect. 8.1), and, in fact, the periodic repetition with

¹In digital transmissions F represents the symbol rate and in sampling/interpolation F is the sampling frequency.

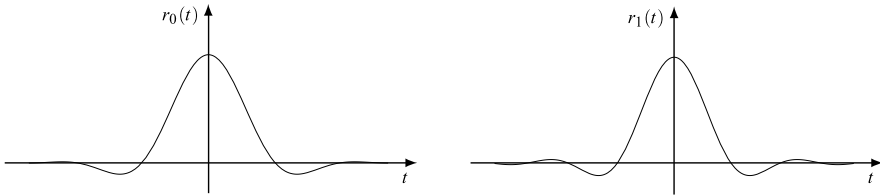


Fig. 9.8 Inverse Fourier transforms of raised cosine and square-root raised cosine for $\alpha = 0.6$

period F gives

$$\text{rep}_F R(f) = \sum_{k=-\infty}^{+\infty} R(f - kF) = 1.$$

The square-root raised cosine frequency response is used to equally subdivide a raised cosine response, that is, $R(f) = R_r(f)R_r(f)$. A typical application is in a telecommunication system, where the first $R_r(f)$ is at the transmitter, and the second $R_r(f)$ at the receiver [10].

To express the inverse FTs, we introduce the functions (Fig. 9.8)

$$\text{ircos}(t, \alpha) = \text{sinc}(t) \frac{\pi}{4} \left[\text{sinc}\left(\alpha t + \frac{1}{2}\right) + \text{sinc}\left(\alpha t - \frac{1}{2}\right) \right], \tag{9.25a}$$

$$\begin{aligned} \text{irrcos}(t, \alpha) &= \frac{\sin \pi(t - \frac{1}{4})}{4t} \text{sinc}\left(\alpha t + \frac{1}{4}\right) \\ &+ \frac{\sin \pi(t + \frac{1}{4})}{4t} \text{sinc}\left(\alpha t + \frac{1}{4}\right). \end{aligned} \tag{9.25b}$$

In Appendix D we prove the relationships

$$\text{rcos}(f, \alpha) \xrightarrow{\mathcal{F}^{-1}} \text{ircos}(t, \alpha), \tag{9.26a}$$

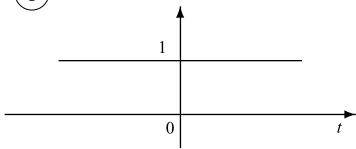
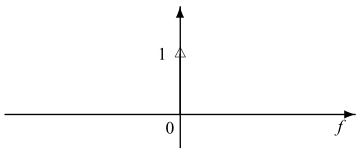
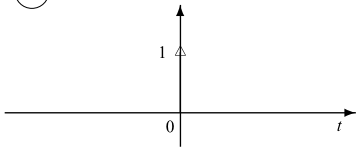
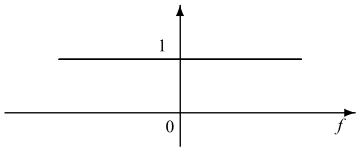
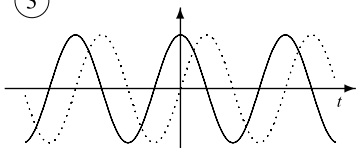
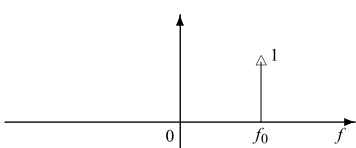
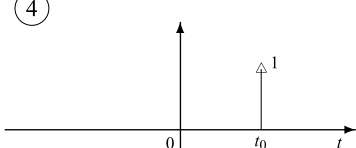
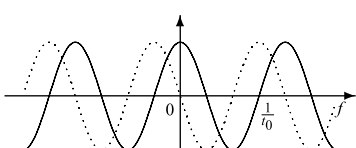
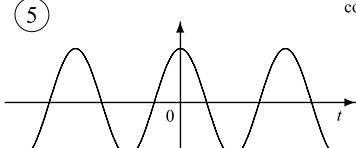
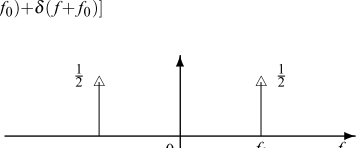
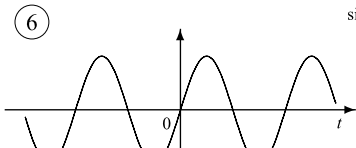
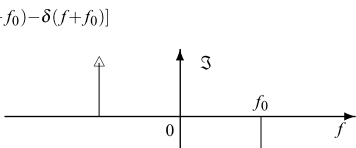
$$\text{rrcos}(f, \alpha) \xrightarrow{\mathcal{F}^{-1}} \text{irrcos}(t, \alpha). \tag{9.26b}$$

Then, in particular considering the nonnormalized frequency response $R(f)$ given by (9.24), we find that the corresponding impulse response is $r(t) = \mathcal{F}^{-1}[R|t] = F \text{ircos}(Ft, \alpha)$. We can check the $r(t)$ verifies the correct interpolation condition (see Sect. 8.2) and has a *fast damping* (see Sect. 9.6).

9.4 Gallery of Fourier Pairs

Table 9.2 collects several Fourier pairs, some already considered and some others now developed. In this collection it is convenient to have in mind the Symmetry

Table 9.2 Fourier pairs on \mathbb{R}

<i>Signal</i>	<i>Fourier transform</i>
① 	$1 \quad \delta(f)$ 
② 	$\delta(t) \quad 1$ 
③ 	$e^{i2\pi f_0 t} \quad \delta(f-f_0)$ 
④ 	$\delta(t-t_0) \quad e^{-i2\pi f_0 t}$ 
⑤ 	$\cos(2\pi f_0 t) \quad \frac{1}{2} [\delta(f-f_0) + \delta(f+f_0)]$ 
⑥ 	$\sin(2\pi f_0 t) \quad \frac{1}{2i} [\delta(f-f_0) - \delta(f+f_0)]$ 

real part
 imaginary part

Table 9.2 (Continued)

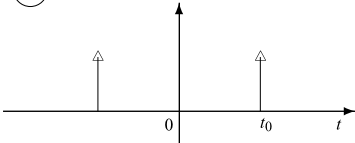
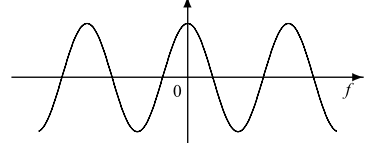
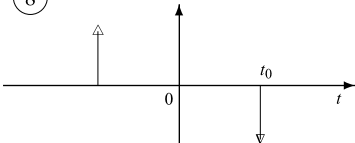
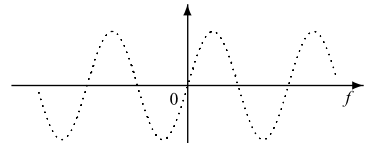
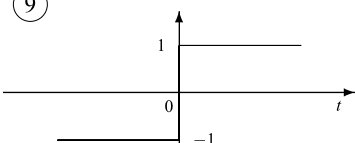
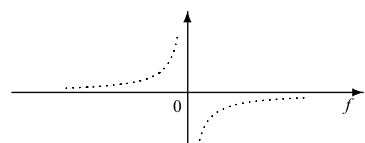
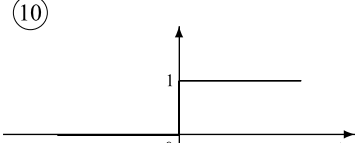
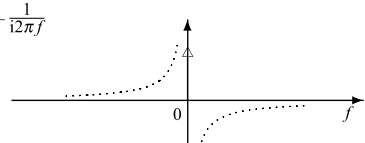
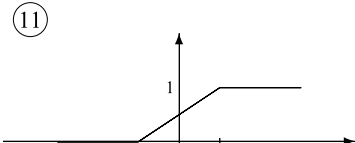
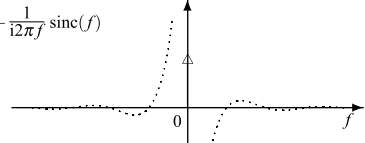
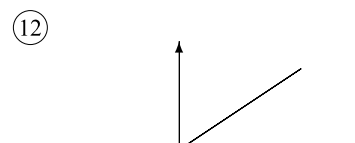
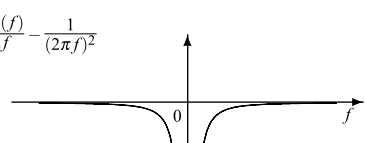
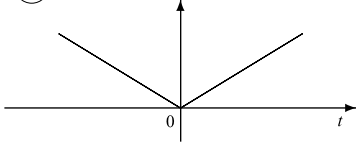
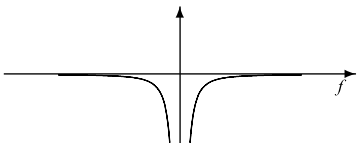
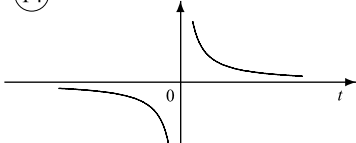
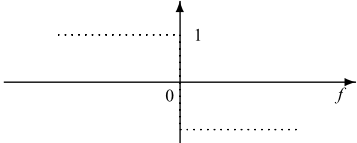
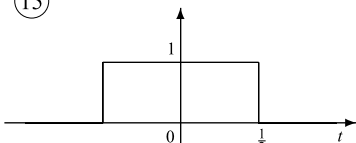
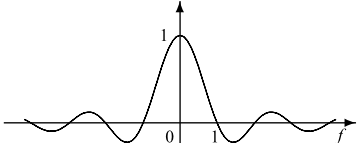
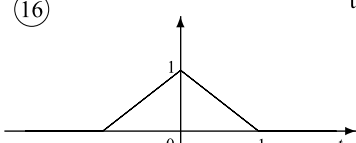
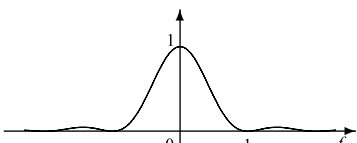
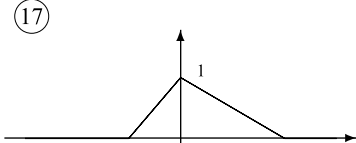
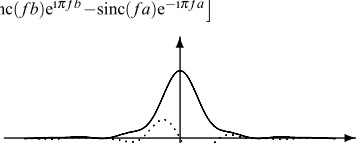
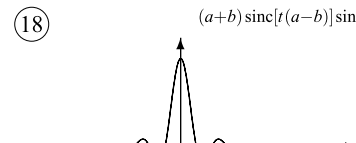
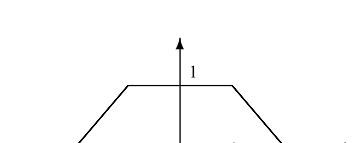
<i>Signal</i>	<i>Fourier transform</i>
(7) 	$\delta(t+t_0) + \delta(t-t_0) \quad 2 \cos(2\pi f t_0)$ 
(8) 	$\delta(t+t_0) - \delta(t-t_0) \quad 2i \sin(2\pi f t_0)$ 
(9) 	$\text{sgn}(t) \quad \frac{1}{i\pi f}$ 
(10) 	$1(t) \quad \frac{1}{2} \delta(f) + \frac{1}{i2\pi f}$ 
(11) 	$\frac{1}{2} \delta(f) + \frac{1}{i2\pi f} \text{sinc}(f)$ 
(12) 	$t1(t) \quad i \frac{1}{4\pi} \frac{d\delta(f)}{df} - \frac{1}{(2\pi f)^2}$ 
——— real part imaginary part

Table 9.2 (Continued)

Signal	Fourier transform
(13) 	$ t \quad -\frac{2}{(2\pi f)^2}$ 
(14) 	$\frac{1}{\pi i} \quad -i \operatorname{sgn}(f)$ 
(15) 	$\operatorname{rect}(t) \quad \operatorname{sinc}(f)$ 
(16) 	$\operatorname{triang}(t) \quad \operatorname{sinc}^2(f)$ 
(17) 	$\frac{1}{i2\pi f} [\operatorname{sinc}(fb)e^{i\pi fb} - \operatorname{sinc}(fa)e^{-i\pi fa}]$ 
(18) $(a+b) \operatorname{sinc}[t(a-b)] \operatorname{sinc}[t(a+b)]$ 	

— real part

..... imaginary part

Table 9.2 (Continued)

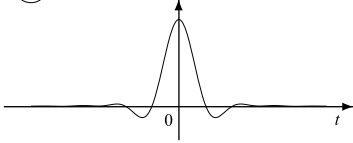
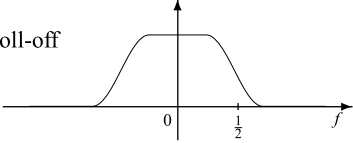
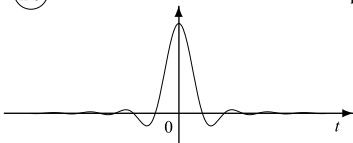
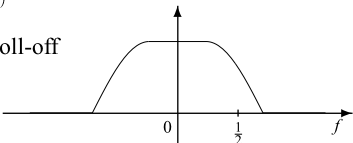
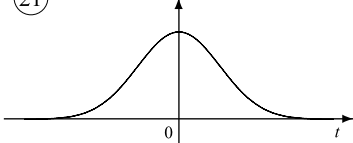
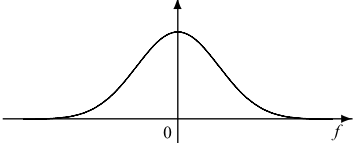
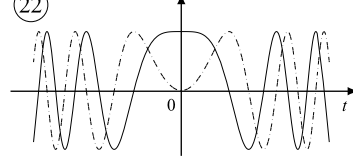
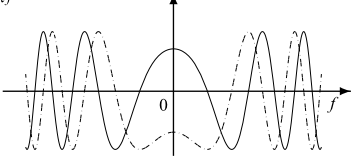
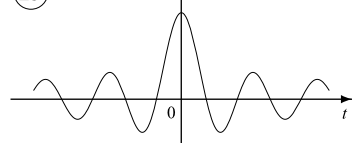
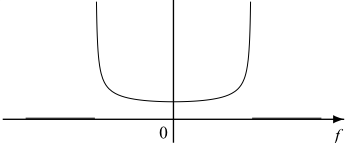
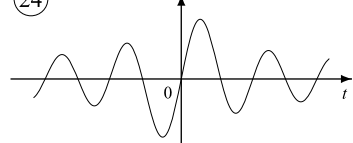
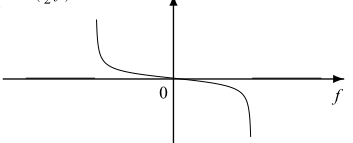
Signal	Fourier transform
<p>(19)</p> 	<p>$\text{ircos}(t,r)$ $\text{rcos}(f,r)$</p> <p>r: roll-off</p> 
<p>(20)</p> 	<p>$\text{irrcos}(t,r)$ $\text{rrcos}(f,r)$</p> <p>r: roll-off</p> 
<p>(21)</p> 	<p>$e^{-\pi t^2}$ $e^{-\pi f^2}$</p> 
<p>(22)</p> 	<p>$e^{i\pi t^2}$ $e^{i\pi/4} e^{-i\pi f^2}$</p> 
<p>(23)</p> 	<p>$J_0(2\pi t)$ $\frac{1}{\pi\sqrt{1-f^2}} \text{rect}(\frac{1}{2}f)$</p> 
<p>(24)</p> 	<p>$J_1(2\pi t)$ $\frac{-if}{\pi\sqrt{1-f^2}} \text{rect}(\frac{1}{2}f)$</p> 
<p>————— real part</p>	<p>..... imaginary part</p>

Table 9.2 (Continued)

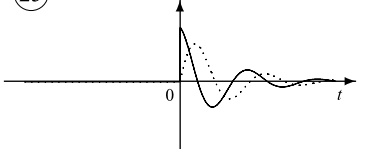
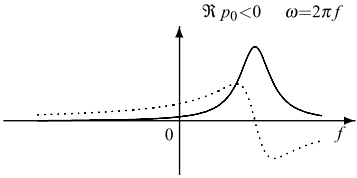
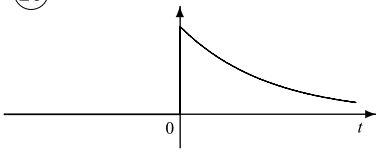
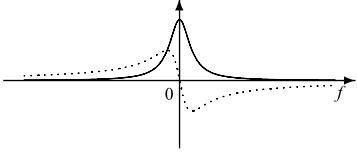
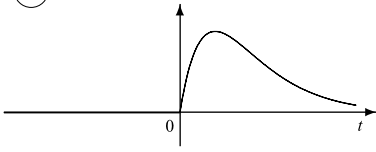
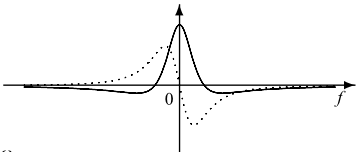
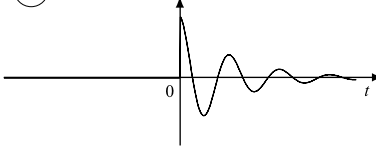
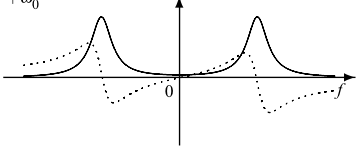
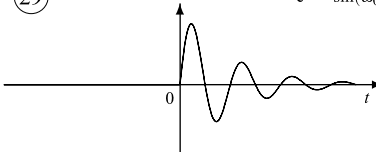
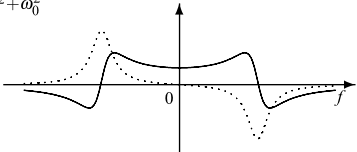
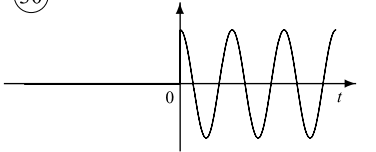
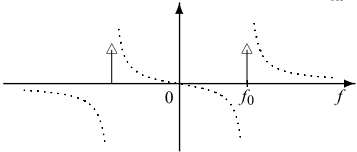


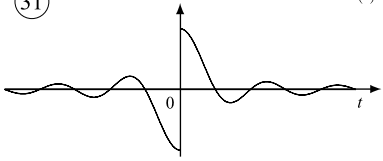
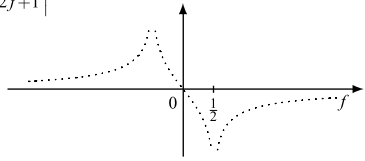
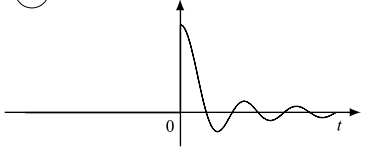
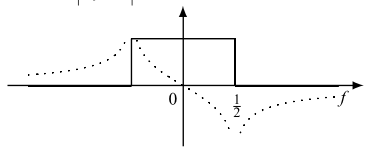
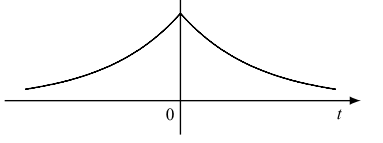
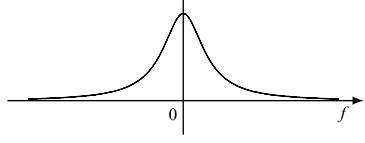
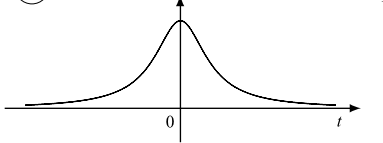
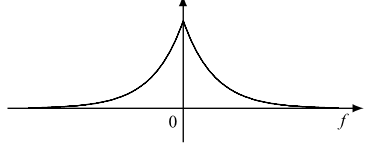
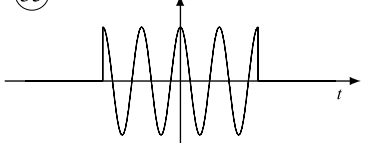
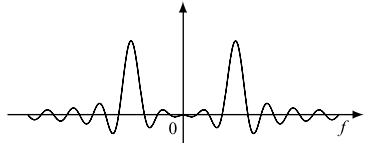
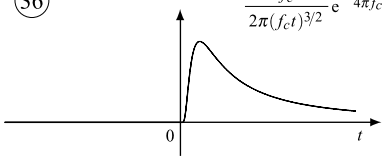
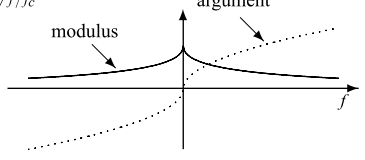
<i>Signal</i>		<i>Fourier transform</i>	
(25)	$e^{p_0 t} 1(t)$ 	$\frac{1}{i\omega - p_0}$	$\Re p_0 < 0 \quad \omega = 2\pi f$ 
(26)	$e^{-\alpha t} 1(t)$ 	$\frac{1}{\alpha + i2\pi f}$	$\alpha > 0$ 
(27)	$t e^{-\alpha t} 1(t)$ 	$\frac{1}{(\alpha + i2\pi f)^2}$	
(28)	$e^{-\alpha t} \cos(\omega_0 t) 1(t)$ 	$\frac{\alpha + i\omega}{(\alpha + i\omega)^2 + \omega_0^2}$	
(29)	$e^{-\alpha t} \sin(\omega_0 t) 1(t)$ 	$\frac{\omega_0}{(\alpha + i\omega)^2 + \omega_0^2}$	
(30)	$\cos(2\pi f_0 t) 1(t)$ 	$\frac{1}{2} [U(f - f_0) + U(f + f_0)]$	$U(f) = \frac{1}{2} \delta(f) + \frac{1}{i\omega}$ 
 real part		 imaginary part	

Table 9.2 (Continued)

<i>Signal</i>	<i>Fourier transform</i>
<p>(31) </p>	$i \frac{1}{\pi} \log \left \frac{2f-1}{2f+1} \right $ 
<p>(32) </p>	$\frac{1}{2} \text{rect}(f) + i \frac{1}{2\pi} \log \left \frac{2f-1}{2f+1} \right $ 
<p>(33) </p>	$\frac{2\alpha}{\alpha^2 + (2\pi f)^2}$ 
<p>(34) </p>	$\pi e^{-2\pi f }$ 
<p>(35) </p>	$\frac{1}{2} T \text{sinc}[T(f+f_0)] + \frac{1}{2} T \text{sinc}[T(f-f_0)]$ 
<p>(36) </p>	$e^{-(1+i)\sqrt{f/f_c}}$ 

— real part

..... imaginary part

Rule (Sect. 5.4), which in \mathbb{R} assumes the simple form

$$\begin{array}{ccc} s(t) & \xrightarrow{\mathcal{F}} & S(f) \\ & & S(t) \xrightarrow{\mathcal{F}} s(-f) \\ \mathbb{R} & & \mathbb{R} \end{array}$$

since $\widehat{\mathbb{R}} = \mathbb{R}$. Then, for each Fourier pair $(s(t), S(f))$ on \mathbb{R} , ones get a new pair $(S(t), s(-f))$ on \mathbb{R} .

We now briefly comment each Fourier pair.

(1)–(8) *singular signals*. These signals, already considered in Sect. 5.4, are now reconsidered for the sake of completeness. They are based on the primitive pairs

$$\delta(t - t_0) \xrightarrow{\mathcal{F}} e^{-i2\pi f t_0}, \quad e^{i2\pi f_0 t} \xrightarrow{\mathcal{F}} \delta(f - f_0), \quad (9.27)$$

which give, as particular cases, the FT of $\delta(t)$ (for $t_0 = 0$) and of the unit constant signal, for $f_0 = 0$.

(9), (10) *sign and unit step*. The deduction of these pairs was made in Sect. 2.7.

(11)–(13) *ramp signals*. (11) is a unit step signal, but with a linear roll-off in the range $-\frac{1}{2} e \frac{1}{2}$. It can be written in the integral form

$$\int_{-\infty}^t \text{rect}(u) du, \quad (9.28)$$

and therefore its FT can be obtained by the integration rule of Table 9.1. For the signal $t1(t)$, we can use the frequency differentiation rule. The signal $|t|$ may be regarded as the even part of the *real* signal $2t1(t)$; then recalling the decomposition rule for a real signal $s(t) = s_e(t) + s_o(t)$, we get (see Sect. 5.6)

$$s_e(t) \xrightarrow{\mathcal{F}} \Re S(f), \quad s_o(t) \xrightarrow{\mathcal{F}} \Im S(f). \quad (9.29)$$

(14) *Hilbert kernel*. This pair is obtained from (9) by the Symmetry Rule.

(15) *rect*. The derivation is straightforward (see Sect. 2.7).

(16), (17) *triangular pulses*. Fourier pair (16) can be obtained from the definition using integration by parts. In alternative, recall that an isosceles triangle over $(-1, 1)$ is the self-convolution of $\text{rect}(t)$, then apply $s * s(t) \xrightarrow{\mathcal{F}} S^2(f)$. For a general triangular pulse, see Problem 9.7.

(18) *frequency trapezoidal shape*. See Problem 9.7.

(19), (20) *raised cosine and square-root raised cosine*. See Sect. 9.3.

(21) *Gaussian pulse* and (22) *chirp signal*. See Sect. 9.3.

(23), (24) *Bessel functions* of the first kind. To get the FT of the signal $s(t) = J_n(2\pi t)$, we use the integral representation of the Bessel functions given by

$$J_n(z) = \frac{1}{2\pi} \int_0^{2\pi} e^{-in\theta + iz \sin\theta} d\theta.$$

The result is [8]

$$S(f) = (-i)^n \frac{T_n(f)}{\pi \sqrt{1-f^2}} \operatorname{rect}\left(\frac{1}{2}f\right),$$

where $T_n(x) = \cos(n \arccos x)$ are the Chebyshev polynomials of the first kind.

(25)–(30) *causal exponential*. See Sect. 9.3.

(31), (32) *causal and sign version of sinc*. For the causal version, the rule (9.13) can be used. For pair (32), note that the signal can be expressed as twice the *odd part* of the previous signal, so that the second of (9.29) can be applied.

(33), (34) *even versions*. (33) is obtained by application of the first of (9.29) to pair (26). For pair (34), apply Symmetry Rule to (33).

(35) *modulated pulse*: see (9.14a), (9.14b).

(36) *low loss cable response*: see Sect. 9.9.

9.4.1 On Fourier Transform Calculation

For the calculation of the FT and its inverse, two cases must be distinguished: (a) we know the mathematical expression of the signal, and (b) we have a registration of the signal. In the latter case, which is the most frequent in practice, the FT is computed *numerically* by means of the “Fast Fourier Transform” (see Chap. 13).

When the signal mathematical expression is known, the FT can be directly derived from definition (9.7a), but the calculation may be not straightforward for the presence of an integral within infinite limits. If necessary, one can resort to *tables* of transform pairs, such as Table 9.2. For a rich collection, see [1] and particularly [3]. When this search fails, the FT must be computed numerically with the methods of Chap. 13.

UT 9.5 Duration and Bandwidth

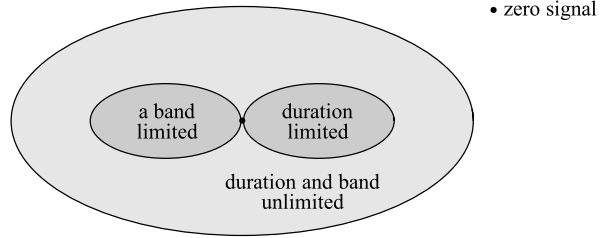
The *extension* $e(s)$ of a signal was introduced in Sect. 4.8, and the *spectral extension* $\mathcal{E}(s) = e(S)$ in Sect. 5.4. Their Haar measures give respectively the *duration* $D(s)$ and the *bandwidth* $B(s)$. These general definitions can be applied to the class of signals on \mathbb{R} , where the Haar measure becomes the ordinary Lebesgue measure, both in time and in frequency domain. The continuous nature of both domains allows one to obtain some interesting and deep results.

9.5.1 Incompatibility of Band and Duration-Limitation

We consider the *minimal* extensions (supports) $e_0(s)$ and $\mathcal{E}_0(s)$ and their complements

$$\bar{e}_0(s) = \{t | s(t) = 0\}, \quad \bar{\mathcal{E}}_0(s) = \{f | S(f) = 0\}. \tag{9.30}$$

Fig. 9.9 Duration and band classification for signals on \mathbb{R}



The incompatibility is based on the following result:

Theorem 9.1 *The set $\bar{e}_0(s)$ and $\bar{E}_0(s)$ cannot have both positive measure, unless $s(t)$ and, consequently, $S(f)$ are identically zero.*

This theorem is a reformulation, in the frame of Signal Theory, of results on analytical functions, which are summarized in Appendix A.

We begin by observing that, with the exclusion of pathological sets (such as the Cantor set), a subset of \mathbb{R} has measure zero when it is countable, and it has positive measure when it is a limited or unlimited interval or a combination of intervals. The fundamental consequence is the incompatibility between bandwidth and duration limitation. In fact, if a signal has a finite duration, the extension complement $\bar{e}_0(s)$ has a positive measure. If this is the case, the spectral extension complement $\bar{E}_0(s)$ has a zero measure, and therefore the FT $S(f)$ is zero at most in a countable set of frequencies; this excludes band limitation. Analogously, we can state that a band-limited signal cannot be duration-limited.

In this context, continuous-time signals can be classified as follows (Fig. 9.9):

- (1) strictly-time limited and consequently with infinite bandwidth;
- (2) strictly-band limited and consequently with infinite duration;
- (3) time unlimited and band unlimited.

A remarkable consequence of the incompatibility, already seen in Chap. 6, is that *an ideal filter is always anticipatory*.

9.5.2 Rms Duration and Bandwidth: Uncertainty Principle

We have remarked several times that narrow signals have a wide spectrum, and conversely. To get a quantitative measure of this fact, we introduce the root mean square (rms) duration D_q and bandwidth B_q that are defined by

$$\begin{aligned}
 D_q^2 &= \int_{-\infty}^{+\infty} t^2 |s(t)|^2 dt \Big/ \int_{-\infty}^{+\infty} |s(t)|^2 dt, \\
 B_q^2 &= \int_{-\infty}^{+\infty} f^2 |S(f)|^2 df \Big/ \int_{-\infty}^{+\infty} |S(f)|^2 df,
 \end{aligned}
 \tag{9.31}$$

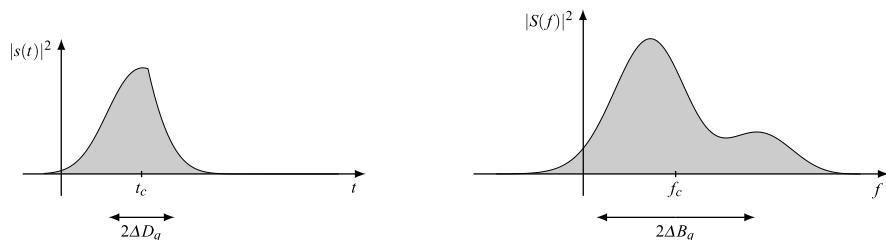


Fig. 9.10 Meaning of centroid abscissas t_c and f_c and “variances” ΔD_q^2 and ΔF_q^2

where the denominators give the energy E_S (Parseval’s theorem). Now, if the signal $s(t)$ vanishes at infinity faster than $1/\sqrt{t}$, that is, if

$$\lim_{t \rightarrow \pm\infty} t |s(t)|^2 = 0, \quad (9.32)$$

then the rms bandwidth and duration are constrained by

$$\boxed{B_q D_q \geq 1/(4\pi)}, \quad (9.33)$$

where the equality holds only for the real Gaussian shaped pulses

$$s_0(t) = A_0 e^{-\alpha t^2}, \quad \alpha > 0. \quad (9.34)$$

A more stringent form of bound (9.33) is obtained by measuring the dispersions of the functions $|s(t)|^2$ and $|S(f)|^2$ with respect to their *centroid abscissas*, which are defined by

$$t_c = \int_{-\infty}^{+\infty} t |s(t)|^2 dt / E_S, \quad f_c = \int_{-\infty}^{+\infty} f |S(f)|^2 df / E_S. \quad (9.35)$$

Then, D_q^2 and B_q^2 are replaced by the “variances”

$$\Delta D_q^2 = D_q^2 - t_c^2, \quad \Delta B_q^2 = B_q^2 - f_c^2, \quad (9.36a)$$

and it is easy to show that their direct expressions are

$$\Delta D_q^2 = \int_{-\infty}^{+\infty} (t - t_c)^2 |s(t)|^2 dt / E_S, \quad \Delta B_q^2 = \int_{-\infty}^{+\infty} (f - f_c)^2 |S(f)|^2 df / E_S.$$

The meaning of these parameters are sketched in Fig. 9.10. The improved bound is

$$\boxed{B_q D_q \geq \Delta B_q \Delta D_q \geq 1/(4\pi)}. \quad (9.37)$$

The proof of (9.33) and (9.37), based on the Schwartz–Gabor inequality, is given in Appendix C, where it is also shown that the product $B_q D_q$ can be calculated, in

alternative to (9.31), according to the relation

$$4\pi B_q D_q = \sqrt{E_{S'} E_{s'}} / E_s, \quad (9.38)$$

where $E_{S'}$ and $E_{s'}$ are the energies of $S' = dS(f)/df$ and $s' = ds(t)/dt$, respectively. Also, the centroid abscissas have the alternative expressions

$$t_c = \frac{i}{2\pi} \frac{E_{S'S}}{E_S}, \quad f_c = -\frac{i}{2\pi} \frac{E_{s's}}{E_s}, \quad (9.39)$$

where $E_{S'S}$ and $E_{s's}$ are the cross-energies.

In Quantum Mechanics inequalities (9.33) and (9.37) (read in a probabilistic context) states the Heisenberg uncertainty principle [4, 5]. In Signal Theory it explains the reciprocity between bandwidth and duration.

Velocity Variation of a Signal The derivative $s'(t)$ of signal $s(t)$, $t \in \mathbb{R}$, may be viewed as the velocity variation. If the signal is strictly band-limited over $(-B, B)$, it is easily seen that the velocity is bounded as follows:

$$\boxed{|s'(t)| \leq 2\pi B \int_{-B}^B |S(f)| df.} \quad (9.40)$$

To this end, we express the velocity $s'(t)$ as the inverse FT of $i2\pi f S(f)$ (see (9.9a), (9.9b)); then

$$|s'(t)| = \left| \int_{-B}^B i2\pi f S(f) e^{i2\pi f t} df \right| \leq 2\pi \int_{-B}^B |f S(f)| df,$$

and (9.40) follows from the observation that $|f| \leq B$ in $(-B, B)$.

UT 9.6 Asymptotic Behavior of Signals and Fourier Transforms

The reciprocity between band and duration is now investigated in term of “regularity,” and we find that the more regular is the FT, the more fast is the damping of the signal, and conversely. This topic is formulated with a slightly different approach in [9, 12] for the asymptotic behavior of the FT.

9.6.1 Formulation of Damping

To formulate the *damping*, we introduce appropriate notation and terminology. Let $a(t)$ be a function such that

$$\lim_{t \rightarrow \infty} a(t)t^\alpha = \lambda \neq 0, \quad (9.41)$$

that is, $a(t)$ is *infinitesimal of order α* with respect to $1/t$. Then, as customary with infinitesimals, we write $a(t) = O(t^{-\alpha})$. If $\lambda = 0$, $a(t)$ is infinitesimal *at least* of order α , and we write $a(t) \leq O(t^{-\alpha})$. The above condition requires that the limit (9.41) exists. We relax this condition by assuming that the function $t^\alpha a(t)$ is bounded, namely

$$t^\alpha |a(t)| < \lambda, \quad |t| > T_0, \quad T_0 \text{ large}, \quad (9.42)$$

and we use the above symbol also in this case. For instance, with $a(t) = K|t|^{-2}$ the limit (9.41) exists with $\alpha = 2$, while with $a(t) = \text{sinc}^2(t)$ the limit (9.41) does not exist, but $|\text{sinc}^2(t)|t^2 = [\sin(\pi t)/\pi]^2 \leq 1/\pi^2$, so (9.42) holds with $\alpha = 2$. In both cases we write $a(t) = O(t^{-2})$, and we say that $a(t)$ has a t^{-2} damping.

Now, we see that the damping of a signal essentially depends on the “regularity” of its FT, stated in terms of differentiability and absolute integrability. Specifically:

Lemma 9.1 *If the Fourier transform $S(f)$, $f \in \mathbb{R}$, of a signal $s(t)$, $t \in \mathbb{R}$, is absolutely integrable, i.e., $S \in L_1(\mathbb{R})$, then the signal is continuous and infinitesimal as $|t| \rightarrow \infty$:*

$$\lim_{|t| \rightarrow \infty} s(t) = 0.$$

Lemma 9.2 *If $S(f)$ is absolutely integrable and differentiable with an absolutely integrable derivative $S^{(1)}(f)$, then*

$$\lim_{|t| \rightarrow \infty} |t|s(t) = 0 \iff s(t) \leq O(t^{-1}).$$

Theorem 9.2 *If a Fourier transform $S(f)$ is absolutely integrable n times differentiable and $S^{(1)}(f), \dots, S^{(n)}(f)$ are absolutely integrable, then*

$$\lim_{|t| \rightarrow \infty} |t|^n s(t) = 0 \iff s(t) \leq O(t^{-n}).$$

These statements are proved in Appendix B. Note that Lemma 9.2 holds also when $S(f)$ has a finite number of discontinuities, and similarly Theorem 9.2 holds when $S^{(n)}(f)$ has a finite number of discontinuities.

9.6.2 Fourier Transform Regularity and Signal Damping

Now we establish the damping of a pulse from the number of times its FT is differentiable.

We begin with observing that, if the FT $S(f)$ exhibits *only one discontinuity* at the frequency f_1 , then it can be decomposed in the following way (Fig. 9.11):

$$S(f) = S_c(f) + S_d(f), \quad S_d(f) = \frac{1}{2}d_1 \text{sgn}(f - f_1), \quad (9.43)$$

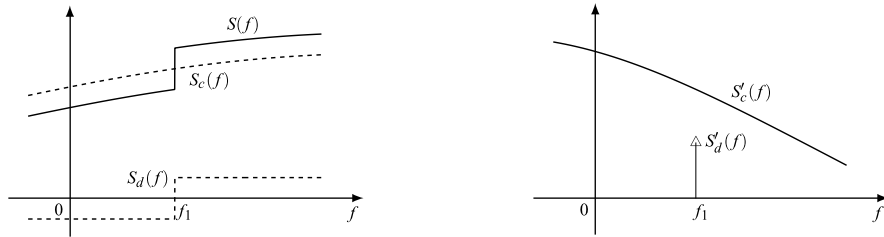


Fig. 9.11 Decomposition of a discontinuous Fourier transform $S(f)$ and of its derivative $S'(f)$

where $d_1 = S(f_1+) - S(f_1-)$ is the discontinuity size. This decomposition was seen in the time domain (see Sect. 9.1), but for symmetry, it also holds in the frequency domain.

In (9.43) suppose that the continuous part $S_c(f)$ has an absolute integrable derivative $S'_c(f)$. Then, its inverse FT, say $s_{c1}(t)$, is given by $s_{c1}(t) = (-i2\pi t)s_c(t)$, and, by Lemma 9.2, $s_{c1}(t) \leq O(t^{-1})$, so that $s_c(t) = s_{c1}(t)/(-i2\pi t) \leq O(t^{-2})$, while

$$s_d(t) = d_1 e^{i2\pi f_1 t} / (-i2\pi t) = O(t^{-1}).$$

Therefore the component $s_d(t)$ dominates, and

$$s(t) = s_c(t) + s_d(t) = O(t^{-1}). \tag{9.44}$$

The same conclusion holds if the FT has finitely many discontinuities.

The assumptions to arrive at (9.44) are:

- (1) the FT $S(f)$ has a finite number of discontinuities,
- (2) the continuous part $S_c(f)$ has an absolute integrable derivative $S'_c(f)$.

To summarize these assumptions, we say that $S(f)$ has *regularity degree 1*. Note that (1) implies that $S'(f)$ is *impulsive*, in the sense that it contains delta lines (see Fig. 9.11). The conclusion is that, if an FT has a regularity degree 1, the signal has a damping of the form $O(t^{-1})$.

The generalization is:

Definition 9.1 A function $S(f)$ has *regularity degree n* if

- (1) $S(f)$ possesses $n - 1$ absolutely integrable derivatives $S', S'', \dots, S^{(n-1)}$.
- (2) $S^{(n-1)}(f)$ has a finite number of discontinuities, and its continuous part $S_c^{(n-1)}(f)$ has an absolutely integrable derivative $S_c^{(n)}(f)$.

In practice, in the evaluation of the regularity degree n , one can refer to the following rule of thumb: evaluate the derivatives of $S(f)$ until you find discontinuities (step $n - 1$) and then the presence of impulses (step n).

Using Definition 9.1 in Appendix B, we prove the fundamental theorem, which generalizes what was seen above with $n = 1$.

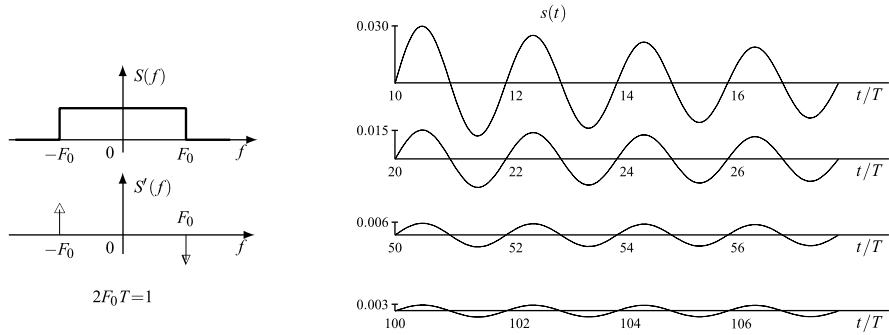


Fig. 9.12 $1/t$ damping for a pulse with a rectangular Fourier transform

Theorem 9.3 *If the Fourier transform $S(f)$, $f \in \mathbb{R}$, has regularity degree n , then the signal $s(t)$, $t \in \mathbb{R}$, is infinitesimal as $|t|^{-n}$ for $|t| \rightarrow \infty$, that is,*

$$s(t) = O(t^{-n}).$$

Note that Theorem 9.3 holds also in the limit, that is when $S(f)$ is infinitely differentiable (regularity degree $n = \infty$). In this case, $s(t) = O(t^{-n})$ with n arbitrarily large. For instance, the FT $P(f)$ of the Gaussian pulse $p(t)$ (see (9.18)) has regularity degree $n = \infty$, and, in fact, $p(t)$ decays as $|t| \rightarrow \infty$ faster than $O(t^{-n})$ with n arbitrarily large.

A noteworthy application of this theorem can be found in the digital transmission theory, where band limitation and fast damping pulses are required [10], and also in interpolation theory. Now, we consider some specific cases.

Regularity Degree 1: Pulse with $1/t$ Damping

The previous theorem, for $n = 1$, assures that, if the FT is discontinuous in a finite number of points (and therefore it is differentiable in a generalized sense), the damping has the form $s(t) = O(t^{-1})$. As an example, the FT $S(f) = \text{rect}(f/(2F_0))$ has two discontinuity points at $f = \pm F_0$ (Fig. 9.12), and decomposition (9.43) assumes the form

$$S_c(f) = 0, \quad S_d(f) = \frac{1}{2} \text{sgn}(f + F_0) - \frac{1}{2} \text{sgn}(f - F_0).$$

Then, the damping has the form $1/t$, and, in fact, the corresponding signal is

$$s(t) = 2F_0 \text{sinc}(2F_0t) = 2F_0 \frac{\sin 2\pi F_0t}{2\pi F_0t}.$$

Figure 9.12 illustrates the damping for high values of F_0t . Note that $1/t$ damping is very weak; as an example, doubling the time t , the amplitude reduces only to half, and to get a reduction to 1%, we must wait 100 reference times.

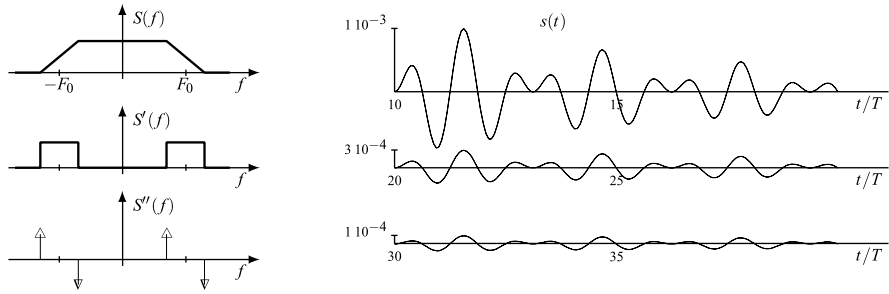


Fig. 9.13 $1/t^2$ damping for a pulse with a trapezoidal Fourier transform

Regularity Degree 2: Pulse with $1/t^2$ Damping

Theorem 9.3 with $n = 2$ assumes that if the FT $S(f)$ is differentiable and its derivative $S'(f)$ has a finite number of discontinuities (and $S''(f)$ is impulsive), the damping has the form $1/t^2$.

These assumption holds, e.g., for a triangular FT, and, in fact, the corresponding signal has a $\text{sinc}^2(Ft)$ -type behavior. The same happens for a trapezoidal FT, as in Fig. 9.13, which is obtained as the convolution between a $\text{rect}(f/2F_0)$ -type and a $\text{rect}(f/2F_1)$ -type, whose signal has the form (see Sect. 2.4)

$$A_0 \text{sinc}(2F_0t) \text{sinc}(2F_1t).$$

The $1/t^2$ damping is quite stronger than the $1/t$ damping, and to get a reduction to 1%, we must wait only 10 reference times.

Regularity Degree 3: Pulse with $1/t^3$ Damping

To have this kind of damping, the FT $S(f)$ must have the first and the second derivatives, with the second derivative having a finite number of discontinuities (and the third derivative exhibits impulses).

The reference function that meets these requirements is the “raised cosine”

$$S(f) = \text{rcos}(f/F, \alpha), \quad F = F_0/2, \tag{9.45}$$

defined by (9.21), where F_0 is the Nyquist frequency, and the cosine shape *roll-off* is extended between the frequencies $f_1 = F_0(1 - \alpha)$ and $f_2 = F_0(1 + \alpha)$.

Figure 9.14 shows the first three derivatives of $S(f)$. Note that $S''(f)$ is discontinuous and $S'''(f)$ exhibits impulses. The continuous part $S'''_c(f)$ of $S'''(f)$ is in $L_1(\mathbb{R})$, then $S(f)$ has regularity degree $n = 3$, and the pulse damping has the form $1/t^3$. In fact, the inverse FT of (9.45) gives the pulse (see (9.25a))

$$\begin{aligned} s(t) &= F \text{rcos}(Ft, \alpha) \\ &= (\pi/4)F \text{sinc}(Ft) \left[\text{sinc}\left(F\alpha t + \frac{1}{2}\right) + \text{sinc}\left(F\alpha t - \frac{1}{2}\right) \right]. \end{aligned} \tag{9.46}$$

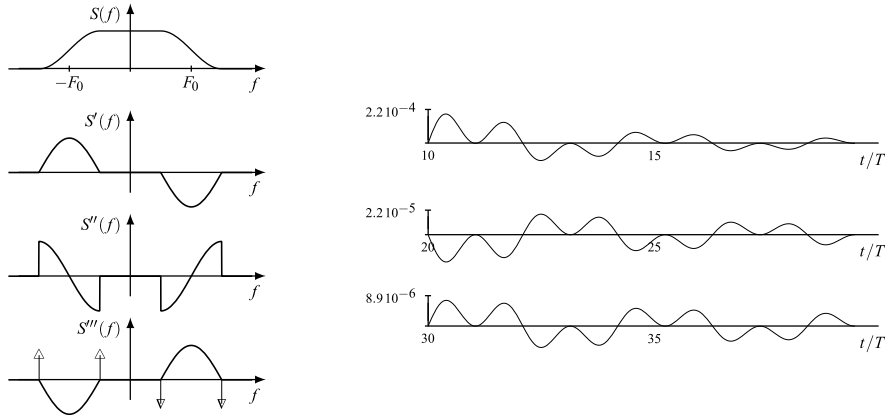


Fig. 9.14 $1/t^3$ damping for a pulse with a raised-cosine Fourier transform

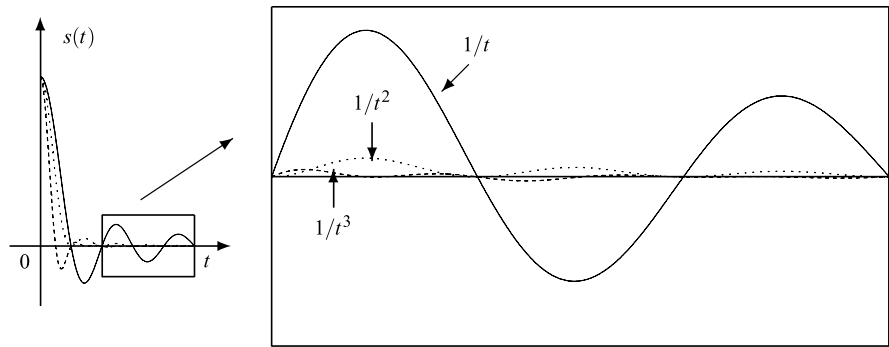


Fig. 9.15 Comparison of pulse dampings with $1/t$, $1/t^2$, and $1/t^3$ decays

For $0 < \alpha \leq 1$, the pulse has a $1/t^3$ damping, and to get a reduction to 1%, it is sufficient to wait only 5 reference times. A comparison between this damping and the previous ones is shown in Fig. 9.15. The strong damping explains why the raised cosine is a good reference in systems design.

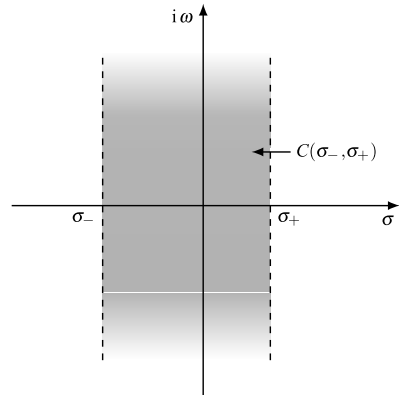
9.6.3 Asymptotic Behavior of Fourier Transforms

The Symmetry Rule allows one to transfer the previous results to FT damping.

Theorem 9.4 *If a signal $s(t)$, $t \in \mathbb{R}$, has regularity degree n , then its Fourier transform $S(f)$, $f \in \mathbb{R}$, is infinitesimal as $|f|^{-n}$ for $|f| \rightarrow \infty$.*

As an example, if a signal has regularity degree $n = 5$, the FT has a $1/f^5$ damping.

Fig. 9.16 General convergence region of a Laplace transform



UT 9.7 The Laplace Transform

For continuous signals, the Laplace transform (LT) is alternative and, in some respects, complementary to the Fourier transform (FT). It represents of a continuous signal by a *complex function of a complex variable*, $S_L(p)$, $p \in \mathbb{C}$, instead of a complex function of a real variable, $S(f)$, $f \in \mathbb{R}$.

9.7.1 Definition

A signal $s(t)$, $t \in \mathbb{R}$, can be represented by the function

$$S_L(p) = \int_{-\infty}^{+\infty} s(t)e^{-pt} dt, \quad p \in \Gamma, \tag{9.47}$$

where $p = \sigma + i\omega$ is a complex variable, and Γ is the region of the complex plane \mathbb{C} in which the integral converges (*convergence region*). The function $S_L(p)$ is called the *bilateral Laplace transform* of $s(t)$.

The following can be proved:

- (1) the convergence region Γ is always a vertical strip of the complex plane (Fig. 9.16)

$$\Gamma = \{\sigma_- < \Re p < \sigma_+\} \stackrel{\Delta}{=} \mathbb{C}(\sigma_-, \sigma_+),$$

possibly not limited on the left ($\sigma_- = -\infty$) and/or on right ($\sigma_+ = +\infty$);

- (2) inside the convergence region, the LT is an *analytic function*.

The inversion formula is

$$s(t) = \frac{1}{2\pi i} \int_{\sigma_- - i\infty}^{\sigma_+ + i\infty} S_L(p)e^{pt} dp, \quad t \in \mathbb{R}, \tag{9.48}$$

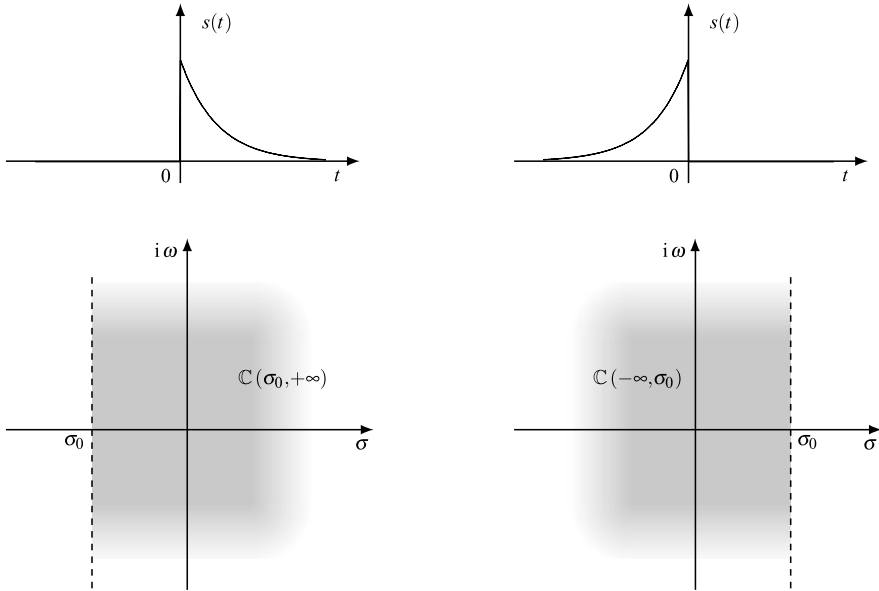


Fig. 9.17 Causal exponential and anticausal exponential with the convergence regions of the corresponding Laplace transforms

where the integration path is arbitrary inside the convergence region, that is, with $\sigma_- < \sigma < \sigma_+$. To prove (9.48), we let $p = \sigma + i2\pi f$, and we see from (9.47) that $\tilde{S}(f) = S_L(\sigma + i2\pi f)$ is the FT of the signal $\tilde{s}(t) = e^{-\sigma t}s(t)$. The inverse FT is

$$\tilde{s}(t) = \int_{-\infty}^{+\infty} S_L(\sigma + i2\pi f)e^{i2\pi f t} df, \tag{9.48b}$$

and then

$$s(t) = \int_{-\infty}^{+\infty} S_L(\sigma + i2\pi f)e^{\sigma t + i2\pi f t} df. \tag{9.48c}$$

This result can be written as a line integral with $p = \sigma + i2\pi f$ and $i2\pi df = dp$, so that when f varies from $-\infty$ to $+\infty$, p assumes values along the vertical line $\Re p = \sigma$, as indicated in (9.48).

9.7.2 A Few Examples

Example 9.1 The causal exponential (Fig. 9.17) $s(t) = 1(t)e^{p_0 t}$, where $p_0 = \sigma_0 + i\omega_0$ is an arbitrary complex number, gives

$$S_L(p) = \int_0^\infty e^{(p_0 - p)t} dt = \lim_{T \rightarrow \infty} \int_0^T e^{(p_0 - p)t} dt$$

$$= \lim_{T \rightarrow \infty} \frac{1}{p_0 - p} [e^{(p_0 - p)T} - 1], \quad p \neq p_0,$$

where $\lim_{T \rightarrow \infty} e^{(p_0 - p)T} = 0$ for $\Re(p_0 - p) < 0$, and the limit does not exist for $\Re(p_0 - p) > 0$. Consequently,

$$S_L(p) = \frac{1}{p - p_0}, \quad p \in \mathbb{C}(\sigma_0, \infty),$$

where the convergence region Γ is the right half-plane with abscissas greater than σ_0 .

Example 9.2 The *anticausal* exponential (Fig. 9.17) $s(t) = 1(-t)e^{p_0 t}$ gives analogously

$$S_L(p) = -\frac{1}{p - p_0}, \quad p \in \mathbb{C}(-\infty, \sigma_0),$$

and the convergence region is the left half-plane with abscissas smaller than σ_0 .

Example 9.3 The *bilateral* exponential $s(t) = s_1(t) + s_2(t) = 1(-t)e^{p_1 t} + 1(t)e^{p_2 t}$ consists of a causal part and of an anticausal part with LTs

$$S_{L1}(p) = -\frac{1}{p - p_1}, \quad p \in \Gamma_1 = \mathbb{C}(-\infty, \sigma_1),$$

$$S_{L2}(p) = \frac{1}{p - p_2}, \quad p \in \Gamma_2 = \mathbb{C}(\sigma_2, +\infty).$$

Therefore,

$$S_L(p) = -\frac{1}{p - p_1} + \frac{1}{p - p_2}, \quad p \in \Gamma = \Gamma_1 \cap \Gamma_2. \quad (9.49)$$

Then, for $\Re p_1 > \Re p_2$, the LT is given by (9.49) with convergence region $\Gamma = \{\Re p_2 < \Re p < \Re p_1\} = \mathbb{C}(\sigma_1, \sigma_2)$, while for $\Re p_1 \leq \Re p_2$, the convergence region is empty, and therefore the LT does not exist.

Example 9.4 The LT of the unit step signal is given by

$$1(t) \xrightarrow{\mathcal{L}} 1/p, \quad p \in \mathbb{C}(0, +\infty),$$

while the LT of the anticausal unit step signal is

$$1(-t) \xrightarrow{\mathcal{L}} -1/p, \quad p \in \mathbb{C}(-\infty, 0).$$

Note that $1(t)$ and $-1(-t)$ have the same LT, $1/p$, but different convergence regions.

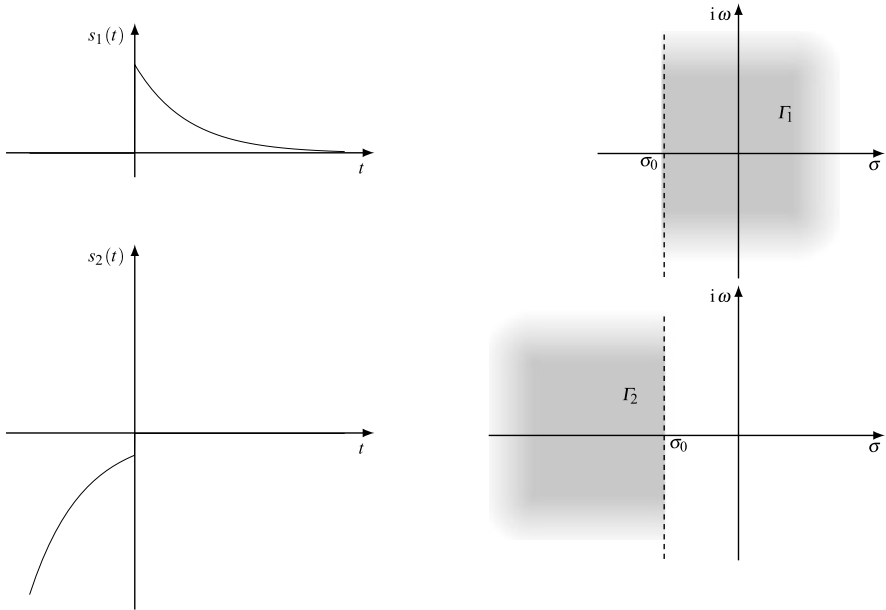


Fig. 9.18 Signals with the same Laplace transforms but with different convergence regions

9.7.3 On the Uniqueness of the Inverse Laplace Transform

The latter example shows that two different signals may have the same LT $S_L(p)$, and therefore the recovery of $s(t)$ from $S_L(p)$ is ambiguous. We give another example of ambiguity: the signals (Fig. 9.18)

$$s_1(t) = 1(t)e^{p_0t}, \quad s_2(t) = -1(-t)e^{p_0t}$$

have the same LT

$$S_{L1}(p) = S_{L2}(p) = 1/(p - p_0),$$

but they have distinct convergence regions, namely $\Gamma_1 = \mathbb{C}(\sigma_0, +\infty)$, $\Gamma_2 = \mathbb{C}(-\infty, \sigma_0)$, $\sigma_0 = \Re p_0$. Now, starting from the same function $S_{L1}(p) = S_{L2}(p)$ and applying inversion formula (9.48) with an integration path inside Γ_1 , we obtain the causal signal $s_1(t)$, whereas with an integration path inside Γ_2 we obtain the anticausal signal $s_2(t)$.

The general conclusion is that the specification of the convergence region removes the ambiguity, that is the pair $(S_L(p), \Gamma)$ allows the signal recovery, as summarized by

$$s(t) \xrightarrow{\mathcal{L}} S_L(p), \quad p \in \Gamma, \quad S_L(p), \quad p \in \Gamma \xrightarrow{\mathcal{L}^{-1}} s(t).$$

9.7.4 Relations with the Fourier Transform

By letting $p = i2\pi f$ in definition (9.47) we obtain

$$S_L(i2\pi f) = \int_{-\infty}^{+\infty} s(t)e^{-i2\pi ft} dt = S(f),$$

that is, the LT evaluated for $p = i2\pi f$ gives the FT evaluated at the frequency f . Analogously, by substituting in the definition of the FT $S(f)$ the real variable f with the complex variable $p/i2\pi$, we obtain

$$\boxed{S\left(\frac{p}{i2\pi}\right) = S_L(p)}. \quad (9.50)$$

However, these substitutions are not allowed in general, and we have to distinguish the following cases.

Case 1: $S_L(p)$ Exists, and $S(f)$ Exists

If the convergence region Γ contains the imaginary axis of the complex plane

$$\sigma_- < 0 < \sigma_+, \quad (9.51)$$

the substitution $p = i2\pi f$ allows us to obtain the FT from the LT by

$$\boxed{S(f) = S_L(i2\pi f)}$$

and the LT from the FT, according to (9.50).

As an example, for the causal exponential, we have found

$$S_L(p) = 1/(p - p_0), \quad p \in \mathbb{C}(\sigma_0, +\infty). \quad (9.52a)$$

Therefore, if $\Re p_0 = \sigma_0 < 0$, the FT also exists and is given by (see (9.16))

$$S(f) = 1/(i2\pi f - p_0). \quad (9.52b)$$

We note that the condition $\sigma_0 < 0$ guarantees that the exponential is “damping,” as is necessary for the existence of the FT.

Case 2: $S_L(p)$ Exists, $S(f)$ Does Not Exist

If the convergence region does not contain the imaginary axis, the LT exists, while the FT does not exist. The existence of the LT can be explained by the fact that the

complex variable $p = \sigma + i\omega$ allows the introduction of a damping function in the integrand

$$S_L(\sigma + i\omega) = \int_{-\infty}^{+\infty} s(t)e^{-\sigma t} e^{-i\omega t} dt,$$

which, for a suitable σ , guarantees the convergence, although the signal grows exponentially. For the FT, this opportunity is not possible.

Reconsidering the previous example, if $\sigma_0 > 0$, the LT is given by (9.52a), while the (9.52b) is no longer valid. In fact, the exponential signal diverges when t diverges, and the existence of the FT is excluded.

Case 3: $S_L(p)$ Exists, $S(f)$ Exists in a Generalized Sense

In some singular cases a signal admits FT (in the generalized sense), although the convergence region of the LT does not contain the imaginary axis; in such a case, however, $S(f)$ cannot be obtained from $S_L(p)$ with the simple substitution $p = i2\pi f$. As an example, for the unit step signal $1(t)$, we have

$$S_L(p) = \frac{1}{p}, \quad \Re p > 0, \quad S(f) = \frac{1}{i2\pi f} + \frac{1}{2}\delta(f),$$

where the condition $\Re p > 0$ excludes the imaginary axis from the convergence region. In fact, the integral giving the FT does not converge, but the formalism of the delta function allows us to write its expression.

Case 4: $S(f)$ Exists, $S_L(p)$ Does Not Exist

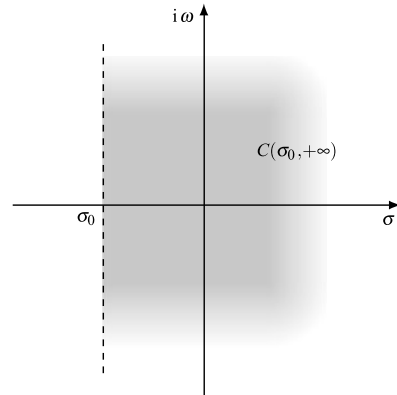
The previous cases induce to think that the existence conditions for the LT are less stringent than for the FT. However, we find remarkable examples in which the FT exists and the LT does not. Consider the Fourier pair

$$\text{sinc}(t) \xrightarrow{\mathcal{F}} \text{rect}(f),$$

and we prove, by contradiction, that $s(t) = \text{sinc}(t)$ does not admit Laplace transform. Let us suppose that the couple $S_L(p)$, $p \in \Gamma$, exists; then, considering the even symmetry of $\text{sinc}(t)$, the convergence region Γ should have the symmetric form $\Gamma = \{-\sigma_0 < \Re p < \sigma_0\}$ with $\sigma_0 > 0$. If this is the case, Γ contains the imaginary axis, and therefore $S_L(p)$ allows the evaluation of the FT as $S_L(i2\pi f) = \text{rect}(f)$. But this conclusion is absurd because $S_L(p)$ is an analytic function for every $p \in \Gamma$, and therefore it would be continuous together with all its derivatives, while for $p = i2\pi f$, we have found a discontinuous function.

The same proof excludes the existence of the LT for all signals having a discontinuous FT or with discontinuous derivatives. For instance, the ircos pulse given by (9.46) has a raised cosine FT, but its LT does not exist because, for $p = i2\pi f$, its second derivative is discontinuous.

Fig. 9.19 Convergency region of a *unilateral* Laplace transform



9.7.5 The Unilateral Laplace Transform

The traditional form of the Laplace transform is

$$S_L(p) = \int_0^{\infty} s(t)e^{-pt} dt, \quad p \in \Gamma. \quad (9.53)$$

This form is called the *unilateral* form because the integration is limited to nonnegative t , whereas in the *bilateral* form (9.47) the integration is over \mathbb{R} .

The *bilateral* form is more general since it can be considered for all continuous-time signals, casual and noncasual. When $s(t)$ is causal, (9.47) gives (9.53) as a particular case. The causality has a consequence on the convergence region, which becomes a left half-plane (Fig. 9.19)

$$\Gamma = \{\sigma_0 < \Re p < +\infty\} = \mathbb{C}(\sigma_0, +\infty)$$

in place of a vertical string. With this peculiarities the unilateral LT can be perfectly viewed in the frame of the more general bilateral LT, having care on the applicability of certain rules, in particular the time-shifting rule, where a negative shift applied to a causal signal gives a signal that is no more causal.

9.7.6 A Comparison Between Fourier and Laplace Transforms

Both the FT and the LT have a very large diffusion in the analysis of signals and systems, each of them offering advantages and some disadvantages. However, in most cases, the tradition plays a fundamental role in the choice.

In the field of telecommunications the FT is generally preferred because it allows one to represent the signals on the whole time axis in a simple way, whereas the LT is more suitable for representing causal signals, although the bilateral form is valid for all signals. The FT has also the advantage of working with functions of a real

variable instead of a complex one, where the real variable has the very relevant physical meaning of *frequency*.

In the study of systems, electrical circuits, and automatic controls, the LT is preferred because the need of representing the signals over the whole time axis is weaker, and, very often, the analysis is limited to causal signals. Furthermore one can take advantage of the remarkable properties of the Laplace transform (analyticity, residue theorem). In particular, in the synthesis of circuits and in the study of the stability the LT is not only a preference, but becomes an essential tool.

9.8 Properties of the Laplace Transform

9.8.1 General Rules

The properties of the LT are similar to the properties of the FT and are mainly based on the kernel separability

$$e^{p(t_1+t_2)} = e^{pt_1} e^{pt_2},$$

which converts a *convolution* operation in a domain into a product in the dual domain. The collection of the rules is given in Table 9.3.

A remarkable difference with respect to the FT lies on the fact that the LT domain is complex and loses the perfect symmetry of the FT. Another difference is the specification of the convergence region, not needed for the FT. A collection of Laplace transforms is given in Table 9.4.

For a more complete collection, we suggest the following references: Angot [2], Abramowitz and Stegun [1], and Erdelyi [3]. Note that all collections refer to the unilateral LT.

9.8.2 On the Inversion Formula

The calculation of the inverse LT by (9.48), involving an integration along a vertical line inside the convergence region, is in general very difficult. On the contrary, taking advantage of the Cauchy theorem on analytical functions, the calculation is often confined to the evaluation of the *residues*.

In particular, if the function $S_L(p)$ has a finite number of *poles* p_1, \dots, p_n , as happens for the important class of rational functions, the calculation can be made in the following way. Let us suppose that the convergence region is of the type $\mathbb{C}(\sigma_0, +\infty)$. Then, if a pole p_k is *simple*, the evaluation of the residue

$$R_k = S_L(p)(p - p_k)|_{p=p_k} = \left. \frac{dS_L(p)}{dp} \right|_{p=p_k}$$

Table 9.3 Rules on the Laplace transform

Rule	Signal	Laplace transform
1. linearity	$a_1 s_1(t) + a_2 s_2(t)$	$a_1 S_{1L}(p) + a_2 S_{2L}(p)$
2. coordinate reverse	$s(-t)$	$S_L(-p), p \in -\Gamma_s$
3. conjugation	$s^*(t)$	$S_L^*(p^*), p \in \Gamma_s$
4. real part	$\Re s(t) = \frac{1}{2}[s(t) + s^*(t)]$	$\frac{1}{2}[S_L(p) + S_L^*(p^*)]$
5. imaginary part	$\Im s(t) = \frac{1}{2}[s(t) - s^*(t)]$	$\frac{1}{2}[S_L(p) - S_L^*(p^*)]$
6. even part	$\frac{1}{2}[s(t) + s(-t)]$	$\frac{1}{2}[S_L(p) + S_L(-p)],$
7. odd part	$\frac{1}{2}[s(t) - s(-t)]$	$\frac{1}{2}[S_L(p) - S_L(-p)],$
8(a). time shift	$s(t - t_0)$	$S_L(p) \exp(-pt_0)$
8(b). p shift	$s(t) \exp(p_0 t)$	$S_L(p - p_0), p \in \Gamma_s + p_0$
9(a). time differentiation	$\frac{ds(t)}{dt}$	$p S_L(p), p \in \Gamma_s$
9(b). time integration	$\int_{-\infty}^t s(u) du$	$\frac{1}{p} S_L(p)$
10. p differentiation	$-ts(t)$	$\frac{dS_L(p)}{dp}, p \in \Gamma_s$
11(a). time convolution	$x * y(t)$	$X_L(p)Y_L(p), p \in \Gamma_x \cap \Gamma_y$
11(b). p convolution	$x(t)y(t)$	$X_L * Y_L(p), p \in \Gamma_x \cap \Gamma_y$
12. correlation	$x * y_-(t)$	$X_L(p)Y_L^*(p^*), p \in \Gamma_x \cap \Gamma_y$
13. scale change	$s(at)$	$\frac{1}{ a } S_L\left(\frac{p}{a}\right)$

Note: p convolution: $X_L * Y_L(p) = \frac{1}{i2\pi} \int_{\sigma-i\infty}^{\sigma+i\infty} X_L(q)Y_L(p-q) dq$

gives the following contribution to the inverse LT

$$s_k(t) = R_k e^{p_k t} 1(t).$$

More generally, if the pole p_k has multiplicity $m + 1$, we let

$$S_{Lk}(p) = S_L(p)(p - p_k)^{m+1},$$

and the contribution becomes

$$s_k(t) = \frac{1}{m!} \left. \frac{d^m [e^{pt} S_{Lk}(p)]}{dp^m} \right|_{p=p_k}.$$

As an example, if

$$S_L(p) = \frac{p + 1}{(p - 1)^3(p + 2)}, \quad p \in \mathbb{C}(1, +\infty),$$

it is found

$$s(t) = 1(t) \left\{ \left[-\frac{1}{27} + \frac{1}{9}t + \frac{1}{3}t^2 \right] e^t + \frac{1}{27} e^{-2t} \right\}.$$

Table 9.4 Laplace transforms of some causal signals

Signal	Transform	Convergence region
$\delta(t)$	1	$\mathbb{C}(0, +\infty)$
$1(t)$	$\frac{1}{p}$	$\mathbb{C}(0, +\infty)$
$t1(t)$	$\frac{1}{p^2}$	$\mathbb{C}(0, +\infty)$
$t^n 1(t)$	$\frac{n!}{p^{n+1}}$	$\mathbb{C}(0, +\infty), n \in \mathbb{N}_0$
$t^\alpha 1(t)$	$\frac{\Gamma(\alpha+1)}{p^{\alpha+1}}$	$\mathbb{C}(0, +\infty), \Re\alpha > -1$
$\frac{1}{\sqrt{t}} 1(t)$	$\sqrt{\frac{\pi}{p}}$	$\mathbb{C}(0, +\infty)$
$e^{p_0 t} 1(t)$	$\frac{1}{p-p_0}$	$\mathbb{C}(\sigma_0, +\infty), \sigma_0 = \Re p_0$
$t^n e^{p_0 t} 1(t)$	$\frac{n!}{(p-p_0)^{n+1}}$	$\mathbb{C}(\sigma_0, +\infty), \sigma_0 = \Re p_0$
$\cos \omega_0 t 1(t)$	$\frac{p}{p^2 + \omega_0^2}$	$\mathbb{C}(0, +\infty), \omega_0 \in \mathbb{R}$
$\sin \omega_0 t 1(t)$	$\frac{\omega_0}{p^2 + \omega_0^2}$	$\mathbb{C}(0, +\infty)$
$e^{\alpha t} \cos \beta t 1(t)$	$\frac{p-\alpha}{(p-\alpha)^2 + \beta^2}$	$\mathbb{C}(\sigma_0, +\infty), \sigma_0 = \Re\alpha + \Im\beta$
$e^{\alpha t} \sin \beta t 1(t)$	$\frac{\beta}{(p-\alpha)^2 + \beta^2}$	$\mathbb{C}(\sigma_0, +\infty), \sigma_0 = \Re\alpha + \Im\beta$
$\frac{e^{\alpha t} - e^{\beta t}}{t} 1(t)$	$\log \frac{p-\beta}{p-\alpha}$	$\mathbb{C}(\sigma_0, +\infty), \sigma_0 = \max\{\Re\alpha, \Re\beta\}$
$\frac{\sin \alpha t}{t} 1(t)$	$\arctan(\frac{\alpha}{p})$	$\mathbb{C}(\sigma_0, +\infty), \sigma_0 = \Im\alpha$
$\text{sinc}(\frac{t}{T}) 1(t)$	$\frac{T}{\pi} \arctan(\frac{\pi}{pT})$	$\mathbb{C}(\sigma_0, +\infty), T \in \mathbb{R}$
$\text{rect}(\frac{t-t_0}{T})$	$e^{-pt_0} \frac{\sinh(\frac{1}{2}pT)}{p}$	$\mathbb{C}(0, +\infty)$

The residues method can also be utilized with an infinite number of singularities and with convergence regions different from the ones considered above [2, 7].

UT 9.9 Continuous-Time Filters

The filters for continuous-time signals were introduced in Chap. 2 and developed in a general form at the end of Chap. 6. In this section we get deeper insight into this topic.

As for the general case, the specification of a filter on \mathbb{R} can be made in terms of the *impulse response* $g(t), t \in \mathbb{R}$, or *frequency response* $G(f), f \in \mathbb{R}$. The latter is usually decomposed in the form $A_G(f) = |G(f)|, \beta_G(f) = \arg G(f)$. But, an alternative specification is given by the *transfer function* $G_L(p), p \in \Gamma$, which is defined as the *Laplace transform of the impulse response*. The three forms of specification are equivalent.

We recall that the input–output relationship of a filter on \mathbb{R} is given by the convolution

$$y(t) = \int_{-\infty}^{+\infty} g(t-u)x(u) du, \quad t \in \mathbb{R},$$

which becomes, in the domains f and p ,

$$Y(f) = G(f)X(f), \quad Y_L(p) = G_L(p)X_L(p).$$

Related to the impulse response is the *unit step response*, which is simply given as the integral of the impulse response

$$u(t) = \int_{-\infty}^t g(a) da,$$

which gives

$$u(t) \xrightarrow{\mathcal{L}} \frac{1}{p}G_L(p).$$

9.9.1 The Exponential Mode

In Sect. 5.8 we have seen that exponentials are the *eigenfunctions* of the filters and that the correspondent eigenvalues are given by the frequency response. As a consequence, the response to the exponential

$$x(t) = X e^{i2\pi f t}, \quad t \in \mathbb{R}, \quad (9.54a)$$

is an exponential with the same frequency,

$$y(t) = Y e^{i2\pi f t} \quad \text{with } Y = G(f)X. \quad (9.54b)$$

This result plays a fundamental role in *symbolic calculus* of electrical circuits, where *sinusoids are replaced by exponentials*. In this way the identification of the frequency response $G(f)$ of the circuit becomes very simple, namely

$$G(f) = Y/X, \quad (9.54c)$$

where X is an (arbitrary) complex amplitude of the input exponential, and Y is the corresponding complex amplitude of the output.

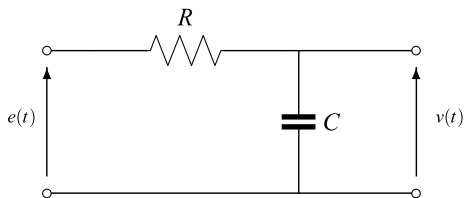
The input exponential can be considered in the more general form

$$x(t) = X e^{p t}, \quad p \in \Gamma, \quad (9.54d)$$

and again it turns out to be an eigenfunction

$$y(t) = Y e^{p t} \quad \text{with } Y = G_L(p)X. \quad (9.54e)$$

Then, the transfer function is identified as $G_L(p) = Y/X$, $p \in \Gamma$, where the convergence region Γ is given by the values of p that produce a finite amplitude response Y .

Fig. 9.20 The RC filter

To illustrate the previous considerations, we consider the RC filter of Fig. 9.20. If the input is an exponential voltage $e(t) = Ee^{i2\pi ft}$, the output voltage also is an exponential $v(t) = Ve^{i2\pi ft}$, where the amplitude is given by $V = E/(1 + i2\pi fRC)$. Hence, from (9.54c) we identify the frequency response

$$G(f) = V/E = 1/(1 + i2\pi fRC).$$

Next, by taking the inverse FT we find the impulse response, which is given by

$$g(t) = \alpha 1(t)e^{-\alpha t}, \quad \alpha = 1/RC.$$

Analogously, we can identify the transfer function by applying at the input an exponential voltage of the general form (9.54d).

9.9.2 Causality Conditions and Realizable Filters

We stated in Sect. 6.5 that a filter is *causal* if and only if its impulse response is a causal signal: $g(t) = 0, t < 0$. This simple time condition becomes somewhat complicated in the frequency domain. We recall that a causal signal, not containing a dc component, can be decomposed into an even part $g_e(t)$ and an odd part $g_o(t)$ that are related by (see (2.6))

$$g_o(t) = g_e(t) \operatorname{sgn}(t). \quad (9.55a)$$


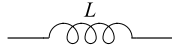

Then, keeping in mind that the FT of $\operatorname{sgn}(t)$ is $1/(i\pi f)$, in the frequency domain we obtain

$$iG_o(f) = \frac{1}{\pi} \int_{-\infty}^{+\infty} \frac{G_e(\lambda)}{f - \lambda} d\lambda = \widehat{G}_e(f), \quad (9.55b)$$

where $\widehat{G}_e(f)$ denotes the Hilbert transform of $G_e(f)$ (see Sect. 9.10). Now, if we suppose that $g(t)$ is *real*, from Rules (5) and (6) of Table 5.2 we find $G_e(f) = \Re G(f)$ and $G_o(f) = \Im G(f)$. The conclusion is that the real and the imaginary parts of a real causal filter are related by the Hilbert transform, which will be introduced in the next section. This conclusion does not hold in general, because it requires that the impulse response $g(t)$ has not a dc component.

The causality condition, which is obviously verified by all physically “realizable” filters, implies a constraint between the real and the imaginary parts of the

Table 9.5 Continuous-time filter components

Component	Graphical symbol	Relationship	Symbolic relationship
Resistance		$v(t) = Ri(t)$	$V(p) = RI(p)$
Inductance		$v(t) = L \frac{di(t)}{dt}$	$V(p) = pLI(p)$
Capacitance		$v(t) = \frac{1}{C} \int^t i(u) du$	$V(p) = \frac{1}{pC} I(p)$

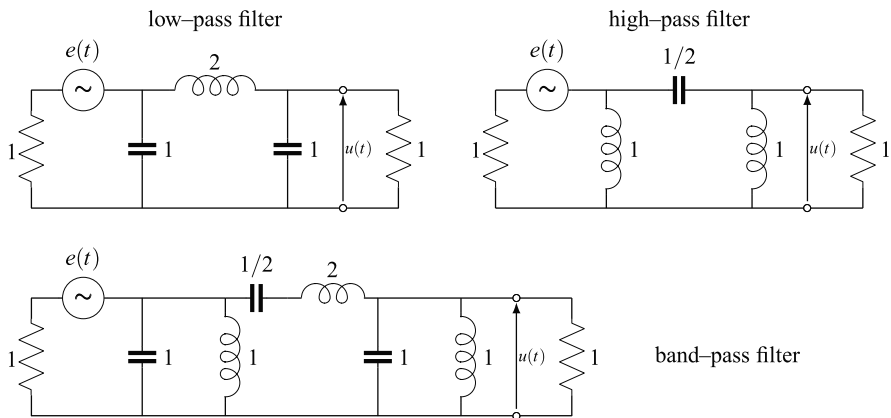


Fig. 9.21 Examples of RLC filters: Butterworth filters. $e(t)$ is the input, and $u(t)$ is the output

frequency response. The same conclusions hold for the amplitude and phase characteristics $A_G(f)$ and $\beta_G(f)$; so that it is not possible, for causal filters, to constrain amplitude and phase simultaneously. Under certain hypotheses (minimal phase filters), the amplitude characteristic $A_G(f)$ uniquely determines the phase characteristic $\beta_G(f)$ [7].

We now consider the standard components of electrical filters (and electrical networks), which are surely casual. The components of *lumped constant* filters are reported in Table 9.5. Conceptually, each component itself is a filter whose input is the applied voltage and output is the corresponding current. Combination of these components allows one to obtain *real* filters, whose transfer function $G_L(p)$ is always a rational function of the variable p . Figure 9.21 shows examples belonging to the class of Butterworth filters.

We can also consider *distributed constant* filters, which consist of antennas, transmission lines, or a coaxial cables. As an example, a coaxial cable with negligible losses has a transfer function given by

$$G_L(p) = \exp(-\sqrt{p/p_0} - pt_0), \quad p \in \mathbb{C}(0, +\infty), \quad (9.56)$$

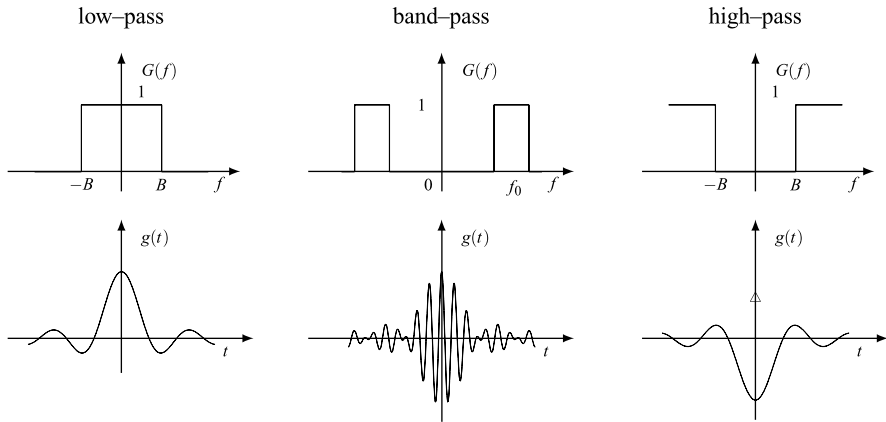


Fig. 9.22 Fundamental examples of ideal filters on \mathbb{R} with zero phase shift

where p_0 is a real constant, and t_0 is a delay. Note that in this case the transfer function is no more a rational function of p , rather a transcendental function.

9.9.3 Ideal Filters and Phase-Shifters

Ideal filters were introduced in Sect. 6.15. Figure 9.22 illustrated the three fundamental classes: (1) *low-pass* filter, (2) *pass-band* filter, and (3) *high-pass* filter. As established in the considerations of Sect. 9.7 on the existence of LT and FT, *ideal filters do not admit transfer function*.

Ideal phase-shifters are all-pass filters with unit amplitude characteristic and a constant phase characteristic $\beta_G(f) = \beta_0$. A phase shifter with such characteristic is in general *complex* since a constant phase violates the Hermitian symmetry. In fact, in a *real* phase shifter $\beta_0(f)$ must be an odd function of f , and then its phase characteristic must have the form

$$\beta_G(f) = \beta_0 \operatorname{sgn}(f), \tag{9.57a}$$

and consequently the frequency response becomes

$$G(f) = e^{i\beta_0 \operatorname{sgn}(f)} = \begin{cases} e^{i\beta_0}, & f > 0, \\ e^{-i\beta_0}, & f < 0. \end{cases} \tag{9.57b}$$

Figure 9.23 compares a complex phase shifter and a real phase shifter.

In particular, for a real phase-shifter with $\beta_0 = -\pi/2$, we find that the responses are given by

$$G(f) = -i \operatorname{sgn}(f), \quad g(t) = \frac{1}{\pi t}. \tag{9.57c}$$

This filter will be used in the next section to introduce the Hilbert transform.

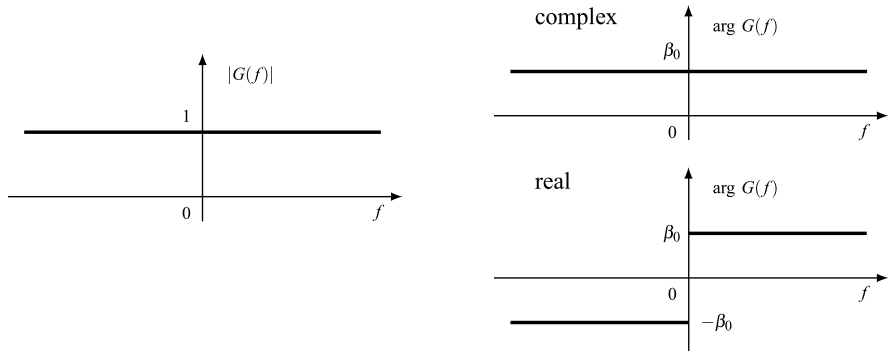


Fig. 9.23 Amplitude and phase characteristics of a *complex* and a *real* phase-shifter

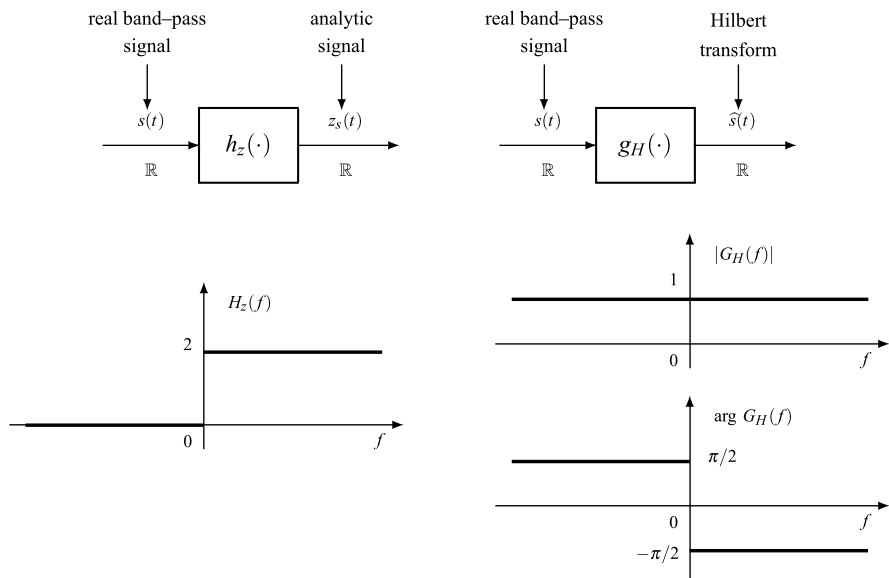


Fig. 9.24 Filters giving the *analytic signal* and the *Hilbert transform*

9.10 Analytic Signal and Hilbert Transform

In Modulation Theory the *analytic signal* and the *Hilbert transform* are introduced for an efficient analysis of *pass-band* signals and particularly of modulated signals. These auxiliary signals can be defined as the response of appropriate ideal filters, whose specifications are given in Fig. 9.24.

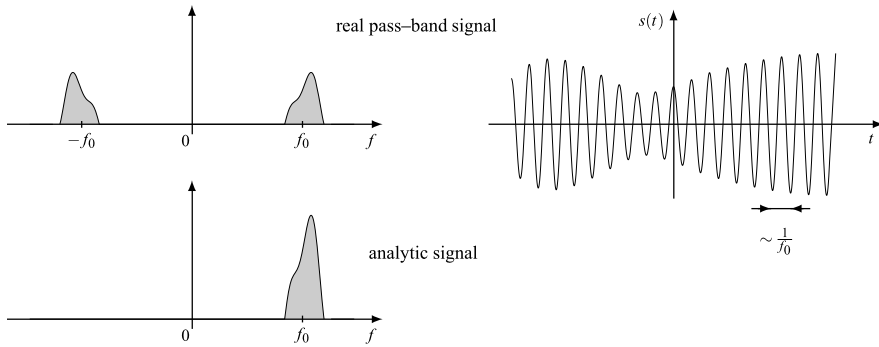


Fig. 9.25 Spectrum of a real pass-band signal $s(t)$ and of the corresponding analytic signal

9.10.1 Analytic Signal

The *analytic signal* $z_s(t)$, $t \in \mathbb{R}$, of a *real signal* $s(t)$, $t \in \mathbb{R}$, can be defined as the response of the complex filter with frequency response

$$H_z(f) = 2 \cdot 1(f), \quad f \in \mathbb{R}, \tag{9.58}$$

to the given signal $s(t)$. This filter eliminates all negative frequency components and double the positive frequency components. Therefore, by construction, the analytic signal has as spectral extension $e(Z_s) = [0, +\infty)$. As a consequence, if $s(t)$ is a real pass-band signal composed by two symmetrical spectral modes (see Sect. 8.7), the correspondent analytic signal is *unimodal*, that is, with only the positive frequency mode, as illustrated in Fig. 9.25.

Let us consider, as an example, a sinusoidal signal decomposed in the form

$$v(t) = A_0 \cos(2\pi f_0 t + \varphi_0) = \frac{1}{2} A_0 e^{i\varphi_0} e^{i2\pi f_0 t} + \frac{1}{2} A_0 e^{-i\varphi_0} e^{-i2\pi f_0 t}.$$

Now, filter (9.58) drops the component with the negative frequency $-f_0$ and doubles the component with positive frequency f_0 , and the output becomes the exponential

$$z_v(t) = A_0 e^{i(2\pi f_0 t + \varphi_0)}. \tag{9.59}$$

The real part of the analytic signal gives the original signal

$$\boxed{s(t) = \Re z_s(t)}, \tag{9.60}$$

so that, in spite of the elimination of the negative frequency mode, the analytic signal $z_s(t)$ contains the same information as the original signal $s(t)$. To prove (9.60), it is sufficient to note

$$\begin{aligned}\Re z_s(t) &\xrightarrow{\mathcal{F}} \frac{1}{2} [Z_s(f) + Z_s^*(-f)] = 1(f)S(f) + 1(-f)S^*(-f) \\ &= [1(f) + 1(-f)]S(f) = S(f),\end{aligned}$$

where $S^*(-f) = S(f)$ since $s(t)$ is assumed to be real.

The analytic signal can be viewed as a generalization of the symbolic calculus of electrical circuits, in which the sinusoidal regime is replaced by the exponential regime. In any case the advantage lies on the simplification of the spectral structure (a single mode in place of two modes).

9.10.2 The Hilbert Transform

The Hilbert transform $\widehat{s}(t)$ of a real signal $s(t)$ can be defined as the response to $s(t)$ of the *real* $-\pi/2$ phase-shifter (Hilbert filter). This filter has frequency response (see Fig. 9.24)

$$G_H(f) = -i \operatorname{sgn}(f) = e^{-i\frac{\pi}{2} \operatorname{sgn}(f)}. \quad (9.61)$$

Since the corresponding impulse response is $g_H(t) = 1/(\pi t)$, the Hilbert transform is explicitly given by

$$\widehat{s}(t) = \frac{1}{\pi} \int_{-\infty}^{+\infty} \frac{s(u)}{t-u} du. \quad (9.62)$$

In alternative, the Hilbert transform can be obtained from the analytic signal. In fact,

$$z_s(t) = s(t) + i\widehat{s}(t), \quad (9.63)$$

that is, $\widehat{s}(t)$ is the imaginary part of $z_s(t)$ (Fig. 9.26),

$$\boxed{\widehat{s}(t) = \Im z_s(t)}. \quad (9.64)$$

The proof of this assertion is similar to the proof of (9.60). We have

$$\begin{aligned}\Im z_v(t) &\xrightarrow{\mathcal{F}} \frac{1}{2i} [Z_v(f) - Z_v^*] = \frac{1}{2i} [1(f) - 1(-f)]S(f) \\ &= -i \operatorname{sgn}(f)S(f) = G_H(f)S(f).\end{aligned}$$

From the Hilbert transform $\widehat{s}(t)$ it is possible to recover the original signal $s(t)$. In fact, the *Hilbert filter* (9.61) is all-pass, and therefore it admits the *inverse* filter, which is given by

$$\frac{1}{G_H(f)} = i \operatorname{sgn}(f) \xrightarrow{\mathcal{F}^{-1}} -\frac{1}{\pi t}$$

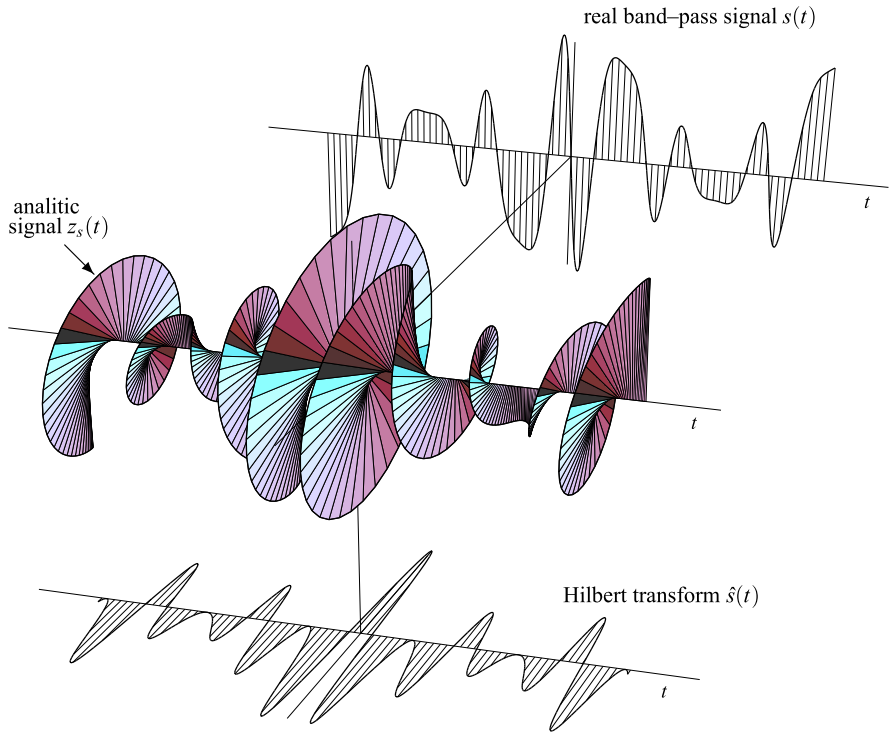


Fig. 9.26 Example of analytic signal and related Hilbert transform

and represents an ideal $\pi/2$ phase-shifter. Therefore, the Hilbert filter adds a $-\pi/2$ phase shift (to the components with positive frequencies), while the inverse filter adds a $\pi/2$ shift, thus restoring the original signal.

We remark that the recovery is possible only if the signal $s(t)$ does not contain a dc component. In fact, the sign function is zero at the origin, so that $G_H(0) = 0$ with the consequence that the Hilbert filter *drops out* the dc component, which therefore cannot be recovered.

9.10.3 Forward and Inverse Hilbert Transforms

As we have seen, a signal free of a dc component can be recovered from its Hilbert transform through a filter with impulsive response $-1/(\pi t)$. Therefore the following relationships hold:

$$\widehat{s}(t) = \frac{1}{\pi} \int_{-\infty}^{+\infty} \frac{s(u)}{t-u} du, \quad s(t) = -\frac{1}{\pi} \int_{-\infty}^{+\infty} \frac{\widehat{s}(u)}{t-u} du. \quad (9.65)$$

Table 9.6 Properties of the Hilbert transform

Property	Signal	Hilbert transform
1. antisymmetry	$\widehat{s}(t)$	$-s(t)$
2. reversal	$s(-t)$	$-\widehat{s}(t)$
3. scale change	$s(at), a \neq 0$	$\widehat{s}(at) \operatorname{sgn}(a)$
4. shift	$s(t - t_0)$	$\widehat{s}(t - t_0)$
5. convolution	$x * y(t)$	$\widehat{x} * y(t) = \widehat{y} * x(t)$
6. filtering	$y(t) = g * x(t)$	$\widehat{y}(t) = \widehat{g} * x(t) = g * \widehat{x}(t)$
7. time differentiation	$\frac{ds(t)}{dt}$	$\frac{d\widehat{s}(t)}{dt}$
8. product ^a	$a(t)p(t)$	$a(t)\widehat{p}(t)$

^aIn the hypothesis given below

To remove the divergence in these relationships for $t = u$, we must take the Cauchy principal value of the integral, that is,

$$\widehat{s}(t) = \lim_{\varepsilon \rightarrow 0} \frac{1}{\pi} \left\{ \int_{-\infty}^{t-\varepsilon} \frac{s(u)}{t-u} du + \int_{t+\varepsilon}^{+\infty} \frac{s(u)}{t-u} du \right\}.$$

As regards the computation of the Hilbert transform, we note that rarely it is possible to evaluate convolution in (9.65) and a convenient way is to pass to the frequency domain following the graph

$$s(t) \xrightarrow{\mathcal{F}} S(f) \xrightarrow{G_H(f)} -i \operatorname{sgn}(f) S(f) \xrightarrow{\mathcal{F}^{-1}} \widehat{s}(t). \tag{9.66}$$

Another way is to calculate the analytic signal, and then we obtain the Hilbert transform as $\widehat{s}(t) = \Im z_s(t)$, but also in this case we resort to the frequency domain.

9.10.4 Properties of the Hilbert Transform

Some properties of the Hilbert transform are collected in Table 9.6. Their deduction is quite immediate considering the definition based on the ideal phase-shifter.

Let us consider, as an example, a generic filter with relationship $y(t) = g * x(t)$. To calculate the Hilbert transform of the output, it is sufficient to note that

$$Y(f)G_H(f) = G(f)[G_H(f)X(f)] = X(f)[G_H(f)G(f)],$$

so that $\widehat{y}(t)$ can be obtained by applying $\widehat{x}(t)$ to the original filter or by applying $x(t)$ to a filter with impulse response $\widehat{g}(t)$. This proves Rule 5 of Table 9.6.

The product rule does not hold in general but requires that the spectral extensions of the signals verify the conditions

$$e(A) \subset (-f_0, f_0), \quad e(P) \subset (-\infty, -f_0) \cup (+f_0, +\infty)$$

for a suitable frequency $f_0 > 0$. In other words, the two real signals must have *separate bands*, with $a(t)$ pass-band and $p(t)$ pass-band or high-pass. For the proof of this result, see [11].

9.11 Problems

9.1 ** [Sect. 9.1] Consider the signal

$$s(t) = A_0 \text{rect}_+(t/D) \cos 2\pi t/T_0$$

and find the decompositions into continuous and discontinuous parts in the cases: (a) $D = 3T_0$ and (b) $D = 3.25T_0$.

9.2 * [Sect. 9.4] Starting from the pair (9.19), find the Fourier transform of the signal

$$s_1(t) = A_0 e^{-t^2/T^2}.$$

9.3 ** [Sect. 9.4] Find the Fourier transform of the signal

$$s_2(t) = A_0 \int_{-\infty}^t e^{-u^2/T^2} du.$$

9.4 ** [Sect. 9.4] Find the Fourier transform of the signal

$$s_3(t) = t e^{-t^2/T^2}.$$

9.5 * [Sect. 9.4] Find the Fourier transform of the signal

$$s_4(t) = 1(t)t^2 e^{-t/T} \sin \omega_0 t.$$

9.6 * [Sect. 9.4] Find the Fourier transform of the signal

$$s_5(t) = A_0 \text{sinc}(f_1 t) \cos 2\pi f_2 t.$$

9.7 ** [Sect. 9.4] The derivative of a triangular pulse is given by the sum of two rectangular pulses. Use this remark to find its Fourier transform from pairs (17) of Table 9.2.

9.8 ** [Sect. 9.4] Prove Fourier pair (18) using the technique suggested in the previous problem.

9.9 ** [Sect. 9.5] Check that for a Gaussian pulse, relation (9.37) holds with equality sign.

9.10 ** [Sect. 9.5] Evaluate the product $B_q D_q$ for the triangular pulse

$$p(t) = A_0 \text{triang}(t/D).$$

9.11 ** [Sect. 9.5] Check bounds (9.33) and (9.37) for the signal

$$s(t) = 1(t)t e^{-t/T}, \quad T > 0.$$

9.12 * [Sect. 9.6] Find the first three derivatives of the function (9.45) and then establish that the damping of the correspondent pulse is of type $1/t^3$.

9.13 ** [Sect. 9.6] Find the damping of a pulse whose FT is given by the convolution of the raised-cosine transform (9.45) with $\text{rect}(f/(2F_0))$.

9.14 * [Sect. 9.8] Find the Laplace transform of the signal

$$s_1(t) = 1(t)t^2 e^{-t/T_0}, \quad t \in \mathbb{R}.$$

9.15 ** [Sect. 9.8] Find the Laplace transform of the signal

$$s_2(t) = 1(t)A_0 \cos \omega_0 t, \quad t \in \mathbb{R}.$$

9.16 ** [Sect. 9.8] Find the inverse Laplace transform of the function

$$S_L(p) = \frac{(p+1)}{p^2+p+1}, \quad p \in \mathbb{C} \left(-\frac{1}{2}, +\infty \right).$$

9.17 *** [Sect. 9.8] As in the previous problem, but with convergence region given by $\mathbb{C}(-\infty, -\frac{1}{2})$.

9.18 *** [Sect. 9.9] Find the frequency response $G(f)$ of a *real causal filter* such that

$$\Re G(f) = \text{rect}(f/2B).$$

9.19 * [Sect. 9.9] Explicitly write the impulse responses of the ideal filters whose frequency responses are shown in Fig. 9.22.

9.20 [Sect. 9.9] Find the responses of an ideal low-pass filter when the input is: (1) a unit step and (2) a rectangular pulse. *Hint*: Use the *sine integral* function

$$\text{Si}(x) \triangleq \int_0^x \frac{\sin(y)}{y} dy.$$

9.21 *** [Sect. 9.9] Show that the impulse response of the ideal *real* phase-shifter of β_0 is

$$g(t) = \delta(t) \cos \beta_0 - \frac{1}{\pi t} \sin \beta_0.$$

9.22 ★★ [Sect. 9.9] Find the frequency response of a low-loss coaxial cable (see (9.56)).

9.23 ★ [Sect. 9.10] Show that the following is a Hilbert pair:

$$s(t) = \text{sinc}(Ft), \quad \widehat{s}(t) = \frac{1 - \cos 2\pi Ft}{\pi Ft}.$$

9.24 ★★ [Sect. 9.10] Show that the following is a Hilbert pair:

$$s(t) = \text{rect}\left(\frac{t}{T}\right), \quad \widehat{s}(t) = \frac{1}{\pi} \log \left| \frac{2t + T}{2t - T} \right|.$$

9.25 ★★ [Sect. 9.10] Find the analytic signal associated to the signal

$$s(t) = \text{sinc}^2\left(\frac{t}{T}\right) \cos 2\pi f_0 t \quad \text{with } f_0 T > 1.$$

Appendix A: Proof of the Theorem 9.1 on Band-Duration Incompatibility

We recall the following statements from the theory of analytic functions [2]:

(1) Let γ be a curve (open or closed) of finite length ℓ , and Ω a region of the complex plane \mathbb{C} . Let $f(t, z)$ be a function of two complex variables defined for $t \in \gamma$, $z \in \Omega$, continuous in $\gamma \times \Omega$, analytic with respect to z in the region Ω . Then, the integral

$$F(z) = \int_{\gamma} f(t, z) dt$$

represents an analytic function in Ω , and

$$F'(z) = \int_{\gamma} f'_z(t, z) dt.$$

(2) (*restricted identity principle*) If $f(z)$ is analytic in Ω and zero in a subset E and if an accumulation point of E belongs to Ω , then $f(z)$ is identically zero in Ω .

Applying (1) and (2), we sketch a proof of the Theorem 9.1. Specifically, we prove that if a signal $s(t)$ is absolutely integrable, $s \in L_1(\mathbb{R})$, and is strictly band-limited, and if the support complement $\bar{e}_0(s)$ contains an accumulation point of E , then $\bar{e}_0(s) = \mathbb{R}$, that is, the signal is identically zero. In fact, the absolute integrability assures the existence of the FT, so that we can write

$$s(t) = \int_{-B}^B S(f) e^{i2\pi ft} df \quad \xrightarrow{\mathcal{F}} \quad S(f) = \int_{-\infty}^{+\infty} s(t) e^{-i2\pi ft} dt. \quad (9.67)$$

Therefore, since $s \in L_1(\mathbb{R})$, from the second of (9.67) it follows that $S(f)$ is a continuous function. Then, application of statement (1) to the first of (9.67) yields that $s(t)$ is an analytic function for every $t \in \mathbb{R}$. Moreover, from statement (2) it follows that if $\bar{e}_0(s)$ contains an accumulation point of E , then $\bar{e}_0(s) = \mathbb{R}$.

Appendix B: Proof of Theorems on Asymptotic Behavior

Proof of Lemma 9.1 If $h \rightarrow 0$, we have

$$|s(t+h) - s(t)| \leq \int_{-\infty}^{+\infty} |S(f)| |e^{i2\pi f(t+h)} - e^{i2\pi ft}| df,$$

where the integrand converges to 0 as $h \rightarrow 0$. Moreover,

$$|S(f)| |e^{i2\pi f(t+h)} - e^{i2\pi ft}| \leq 2|S(f)| \in L_1(\mathbb{R}).$$

Now, the dominated convergence theorem assures that also the left-hand side $\rightarrow 0$ and $s(t)$ is a continuous function. Moreover,

$$\|s(t)\|_{\infty} = \max \|s(t)\| = \max \left| \int_{-\infty}^{+\infty} S(f) e^{i2\pi ft} dt \right| \leq \int_{-\infty}^{+\infty} |S(f)| df = \|S(f)\|_1.$$

Finally, from

$$\begin{aligned} -s(t) &= e^{-i\pi} \int_{-\infty}^{+\infty} S(f) e^{i2\pi ft} dt = \int_{-\infty}^{+\infty} S(f) e^{i2\pi(f-1/(2t))} df \\ &= \int_{-\infty}^{+\infty} S(f+1/(2t)) e^{i2\pi ft} df \end{aligned}$$

it follows that

$$\begin{aligned} 2|s(t)| &= \left| \int_{-\infty}^{+\infty} [S(f) - S(f+1/(2t))] e^{i2\pi ft} df \right| \\ &\leq \int_{-\infty}^{+\infty} |S(f) - S(f+1/(2t))| df = \|S - S_{1/(2t)}\|_1. \end{aligned}$$

As $t \rightarrow \pm\infty$, the right-hand side goes to 0 by the continuity of the shift operator, and hence the conclusion. \square

Proof of Lemma 9.2 and of Theorem 9.2 Since $S(f)$ and $S'(f)$ are absolutely integrable, their inverse FTs $s(t)$ and $s_1(t)$ exist. Next, we integrate by parts:

$$s(t) = \int_{-\infty}^{+\infty} S(f) e^{i2\pi ft} df = \frac{1}{i2\pi t} S(f) e^{i2\pi ft} \Big|_{-\infty}^{+\infty} - \frac{1}{i2\pi t} \int_{-\infty}^{+\infty} S'(f) e^{i2\pi ft} df$$

$$= -\frac{1}{i2\pi t} \int_{-\infty}^{+\infty} S'(f)e^{i2\pi ft} df = \frac{1}{i2\pi t} s_1(t),$$

where the first part of the integral vanishes because $S(f)$ is absolutely integrable. Then $\lim_{f \rightarrow \pm\infty} S(f) = 0$. Finally, from Lemma 9.1 we have $\lim_{t \rightarrow \pm\infty} ts(t) = \lim_{t \rightarrow \pm\infty} -\frac{1}{i2\pi} s_1(t) = 0$.

The proof of Theorem 9.2 is based on a recursive application of Lemma 9.2. \square

Proof of Theorem 9.3 The regularity degree of order n assures that the $(n - 1)$ th derivative has the following decomposition:

$$S^{(n-1)}(f) = S_c^{(n-1)}(f) + S_d^{(n-1)}(f),$$

where

$$S_d^{(n-1)}(f) = \sum_i \frac{1}{2} d_i \operatorname{sgn}(f - f_i).$$

Then, the inverse FT of $S_d^{(n-1)}(f)$ is

$$s_{d,n-1}(t) = \sum_i \frac{1}{2} d_i \frac{e^{i2\pi f_i t}}{-i2\pi t}.$$

From the frequency differentiation rule it follows that $s_{d,n-1}(t) = (-i2\pi t)^{n-1} s_d(t)$, and therefore $s_d(t) = O(t^{-n})$. On the other hand, for the continuous part $s_{c,n}(t)$, Theorem 9.2 assures that $s_c(t) \leq O(t^{-n})$. Then, by combination $s(t) = s_c(t) + s_d(t)$ is $O(t^{-n})$. \square

Appendix C: Proof of Uncertainty Principle Inequality

We recall the Schwartz–Gabor inequality (see Sect. 4.5)

$$\left| \int_{-\infty}^{+\infty} [x(t)y^*(t) + x^*(t)y(t)] dt \right|^2 \leq 4 \int_{-\infty}^{+\infty} |x(t)|^2 dt \int_{-\infty}^{+\infty} |y(t)|^2 dt, \quad (9.68)$$

where the equality holds if and only if $x(t)$ and $y(t)$ are proportional: $y(t) = Kx(t)$ with K real. We apply (9.68) to the signals $x(t) = s'(t)$, $y(t) = ts(t)$, namely

$$\begin{aligned} \left| \int_{-\infty}^{+\infty} [ts(t)s'(t)^* + ts'(t)s(t)^*] dt \right|^2 &\leq 4 \int_{-\infty}^{+\infty} |s'(t)|^2 dt \int_{-\infty}^{+\infty} t^2 |s(t)|^2 dt \\ &= 4 \int_{-\infty}^{+\infty} |s'(t)|^2 dt D_q^2 E_s, \end{aligned} \quad (9.69)$$

where $s'(t)$ has FT $i2\pi f S(f)$, and therefore,

$$\int_{-\infty}^{+\infty} |s'(t)|^2 dt = (2\pi)^2 \int_{-\infty}^{+\infty} f^2 |S(f)|^2 df = (2\pi)^2 B_q^2 E_s.$$

Considering that $s(t)s'(t)^* + s'(t)s(t)^* = d|s(t)|^2/dt$ and integrating by parts, the first term of (9.69) yields

$$\int_{-\infty}^{+\infty} t \frac{d|s(t)|^2}{dt} dt = t|s(t)|^2 \Big|_{-\infty}^{+\infty} - \int_{-\infty}^{+\infty} |s(t)|^2 dt = -E_s,$$

where we have used assumption (9.32). Combination of the results yields $E_s^2 \leq 4(2\pi)^2 D_q^2 B_q^2 E_s^2$, that is, (9.33). Considering (9.68), the equality holds when $s'(t) = Kts(t)$ with K real. The unique solution of this differential equation is $s(t) = C \exp(\frac{1}{2}Kt^2)$, but condition (9.32) implies that $K < 0$.

In (9.37) $\Delta D_q \leq D_q$ and $\Delta B_q \leq B_q$, and hence the first inequality. To prove the second, we apply (9.33) to the Fourier pair

$$s_0(t) = s(t + t_c)e^{-i2\pi f_c t} \xrightarrow{\mathcal{F}} S_0(f) = S(f + f_c)e^{i2\pi(f+f_c)t_c}.$$

So we get $B_q(S_0)D_q(s_0) \leq 1/(4\pi)$, where $B_q(S_0)$ and $D_q(s_0)$ refer to the signal $s_0(t)$. But $E_{s_0} = E_s$ and

$$\begin{aligned} E_{s_0} D_q^2(s_0) &= \int_{-\infty}^{+\infty} t^2 |s_0(t)|^2 dt = \int_{-\infty}^{+\infty} t^2 |s(t + t_c)|^2 dt \\ &= \int_{-\infty}^{+\infty} (t - t_c)^2 |s(t)|^2 dt = E_s \Delta D_q^2(s), \end{aligned}$$

and analogously we find $E_{s_0} B_q^2(S_0) = E_s \Delta B_q^2(S)$. Hence, $\Delta B_q(s)\Delta D_q(S) \leq 1/(4\pi)$.

Next, we prove (9.38), showing that

$$D_q^2 = \frac{E_{S'}}{(2\pi)^2 E_s}, \quad B_q^2 = \frac{E_{S'}}{(2\pi)^2 E_s}. \quad (9.70)$$

The energy of $S'(f) = \mathcal{F}[-i2\pi ts(t)|f]$ is

$$E_{S'} = \int_{-\infty}^{+\infty} |S'(f)|^2 df = \int_{-\infty}^{+\infty} |-i2\pi ts(t)|^2 dt = (2\pi)^2 D_q^2 E_s,$$

which proves the first (9.70). The proof of the second one is similar, considering the energy of $s'(t)$. For the proof of (9.39), consider the auxiliary signal $x(t) = |s(t)|^2$. Then, applying the FT rules, we have

$$E_s t_c = \int_{-\infty}^{+\infty} t x(t) dt = \frac{1}{-i2\pi} \frac{dX(f)}{df} \Big|_{f=0},$$



Fig. 9.27 Derivative $R'_0(f)$ of raised cosine for $\alpha = 0.6$

but $X(f)$ is given by the correlation $C_S(f)$ of $S(f)$, and its derivative at $f = 0$ is given by the cross-energy (see Sect. 5.7). The second of (9.37) follows by symmetry.

Appendix D: Inverse Fourier Transform of Raised Cosine

We prove the Fourier pairs (9.26a), (9.26b). The proof, based on FT definition (9.7b) is cumbersome. An easier proof is based on the frequency integration rule.

Letting $R_0(f) = r\cos(f, \alpha)$, we find that the derivative $X(f) = R'_0(f)$ is different from zero only on the two roll-off parts (Fig. 9.27) and can be written in the form

$$X(f) = R'_0(f) = P\left(f + \frac{1}{2}\right) - P\left(f - \frac{1}{2}\right), \tag{9.71}$$

where (see (9.22))

$$P(f) = \frac{\pi}{2\alpha} \cos\left(\frac{\pi}{\alpha} f\right) \text{rect}\left(\frac{f}{\alpha}\right). \tag{9.72}$$

Hence,

$$R_0(f) = \int_{-\infty}^f X(\lambda) d\lambda.$$

But from the frequency integration rule we obtain

$$r_0(t) = \frac{1}{-i2\pi t} x(t) + \frac{1}{2} x(0) \delta(t) = \frac{1}{-i2\pi t} x(t), \tag{9.73}$$

where $x(0) = \text{area}(X) = 0$. Then, from (9.71) we find

$$x(t) = p(t)e^{-i\pi t} - p(t)e^{i\pi t} = -2i \sin \pi t p(t)$$

and by combination $r_0(t) = p(t) \text{sinc}(t)$. Next, we evaluate the inverse FT $P(f)$ starting from (9.72). Considering that $\text{sinc}(\alpha t) \rightarrow (1/\alpha) \text{rect}(f/\alpha)$ and expressing the cosine by the Euler formula, one gets

$$p(t) = \frac{\pi}{2} \text{sinc}\left(\alpha t - \frac{1}{2}\right) + \frac{\pi}{2} \text{sinc}\left(\alpha t + \frac{1}{2}\right),$$

and (9.26a) follows.

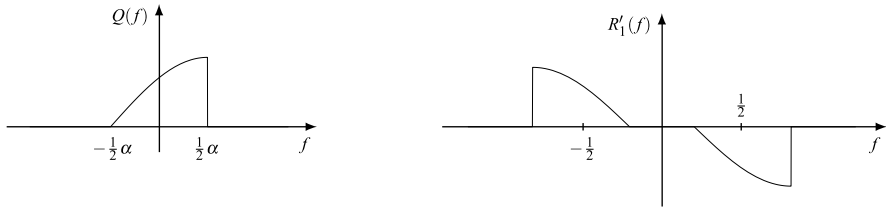


Fig. 9.28 Derivative $R'_1(f)$ of root-raised cosine, for $\alpha = 0.6$

For the second formula, we use the same technique. We let $R_1(f) \triangleq \text{rrcos}(f, \alpha)$ and write the derivative in the form (Fig. 9.28)

$$\begin{aligned} X_1(f) \triangleq R'_1(f) &= -Q\left(f - \frac{1}{2}\right) + Q\left(-f - \frac{1}{2}\right) \\ &= -Q\left(f - \frac{1}{2}\right) + Q^*\left(-f - \frac{1}{2}\right), \end{aligned} \tag{9.74}$$

where

$$Q(f) = \frac{\pi}{2\alpha} \sin\left(\frac{\pi}{2\alpha} f + \frac{\pi}{4}\right) \text{rect}(f/\alpha). \tag{9.75}$$

Next, the integration rule again yields (9.73), where now

$$x(t) = -q(t)e^{-i\pi t} + q^*(t)e^{-i\pi t} = -2i\Im[q(t)e^{i\pi t}].$$

Hence, $r_1(t) = \frac{1}{\pi t} \Im[q(t)e^{i\pi t}]$. The evaluation of $q(t)$, which is not immediate, finally gives (9.26b). Note that

$$\lim_{t \rightarrow 0} r_1(t) = 1 - \alpha \left(\frac{4}{\pi} - 1\right)$$

as we can check by calculating the area of $R_1(f)$.

References

1. M. Abramowitz, I.A. Stegun, *Handbook of Mathematical Functions* (Dover, New York, 1970)
2. A. Angot, *Compléments de Mathématiques* (Editions de la Revue d'Optiques, Paris, 1957)
3. A. Erdelyi, W. Magnus, F. Oberhettinger, F.G. Tricomi, *Tables of Integral Transforms* (McGraw-Hill, New York, 1954)
4. D. Gabor, Theory of communications. *J. Inst. Electr. Eng.* **93**, 429–457 (1946)
5. C.W. Helstrom, J.W.S. Lin, J.P. Gordon, Quantum-mechanical communication theory. *Proc. IEEE* **58**, 1578–1598 (1970)
6. H.M. Ozaktas, B. Barshan, D. Mendlovic, L. Onural, Convolution, filtering and multiplexing in fractional Fourier domains and their relation to chirp and wavelet transforms. *J. Opt. Soc. Am. A* **11**(2), 547–559 (1994)

7. A. Papoulis, *The Fourier Integral and Its Applications* (McGraw–Hill, New York, 1962)
8. A. Papoulis, *Systems and Transforms with Applications in Optics* (McGraw–Hill, New York, 1968)
9. A. Papoulis, *Signals Analysis* (McGraw–Hill, New York, 1984)
10. J.G. Proakis, *Digital Communications*, 3rd edn. (McGraw–Hill, New York, 1995)
11. H.E. Rowe, *Signals and Noise in Communications Systems* (Van Nostrand, Princeton, 1965)
12. M. Vetterli, J. Kovačević, *Wavelets and Subband Coding* (Prentice Hall, Englewood Cliffs, 1995)

Chapter 10

Signals on $\mathbb{R}/\mathbb{Z}(T_p)$

UT 10.1 The Time Domain

A continuous-time signal that verifies the periodicity condition

$$s(t - t_0) = s(t), \quad t \in \mathbb{R}, \quad t_0 \in \mathbb{Z}(T_p),$$

can be formulated both on \mathbb{R} and on the quotient group $\mathbb{R}/\mathbb{Z}(T_p)$. In the first case the signal appears to be a “singular” signal, namely with infinite energy, Fourier transform composed of delta functions, etc. In the second case the signal is treated more appropriately: the energy (given by the energy in one period) becomes finite, the Fourier transform becomes an ordinary (discrete) function, etc.

10.1.1 Integral and Convolution

The *Haar integral* on $\mathbb{R}/\mathbb{Z}(T_p)$ (see Sect. 4.2) is the ordinary integral extended over one period

$$\int_{\mathbb{R}/\mathbb{Z}(T_p)} dt s(t) = \int_{t_0}^{t_0+T_p} s(t) dt, \quad t_0 \in \mathbb{R}.$$

Therefore, the convolution becomes

$$x * y(t) = \int_{t_0}^{t_0+T_p} x(t - u)y(u) du = \int_{t_0}^{t_0+T_p} y(t - u)x(u) du. \quad (10.1)$$

The *impulse*, defined as the unit element of the convolution algebra (see Sect. 4.10), consists of a sequence of delta functions applied at the points of $\mathbb{Z}(T_p)$

$$\delta_{\mathbb{R}/\mathbb{Z}(T_p)}(t) = \sum_{n=-\infty}^{+\infty} \delta(t - nT_p).$$

10.1.2 Differentiation and Integration

Differentiating a signal defined on $\mathbb{R}/\mathbb{Z}(T_p)$,

$$s'(t) = \frac{ds(t)}{dt},$$

gives a signal on $\mathbb{R}/\mathbb{Z}(T_p)$. The integration

$$y(t) = \int_{t_0}^t s(u) du, \quad t_0 \in \mathbb{R}, \quad (10.2)$$

yields a periodic signal *only if* $s(t)$ *has a zero mean value in a period*; otherwise $y(t)$ becomes aperiodic.

10.1.3 Scale Change

The relation

$$y(t) = x(at), \quad a \neq 0, \quad (10.3)$$

converts a signal $x(t)$ defined on $\mathbb{R}/\mathbb{Z}(T_p)$ into a signal defined on the new quotient group $\mathbb{R}/\mathbb{Z}(T_p/|a|)$. For example, if $a = \frac{1}{3}$, we have a time *expansion*, and the period becomes $3T_p$.

UT 10.2 The Frequency Domain

The dual of $\mathbb{R}/\mathbb{Z}(T_p)$ is

$$\widehat{\mathbb{R}/\mathbb{Z}(T_p)} = \mathbb{Z}(F), \quad F = 1/T_p,$$

where F is called the *fundamental frequency*. The *fundamental band* \mathcal{B} is the whole discrete frequency domain $\mathbb{Z}(F)$, whereas the nonnegative band and the positive band are respectively (Fig. 10.1)

$$\mathcal{B}_0 = \{0, F, 2F, 3F, \dots\}, \quad \mathcal{B}_+ = \{F, 2F, 3F, \dots\}.$$

10.2.1 The Fourier Transform

The Fourier transform and its inverse are given by

$$S(kF) = \int_{t_0}^{t_0+T_p} s(t) e^{-i2\pi kFt} dt, \quad kF \in \mathbb{Z}(F), \quad (10.4a)$$

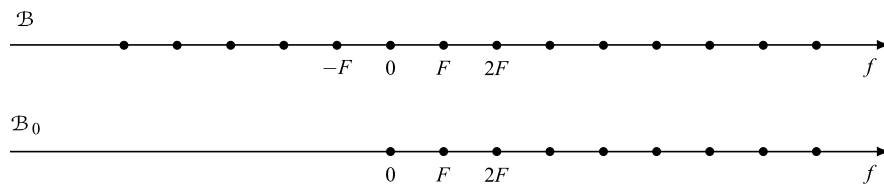


Fig. 10.1 Fundamental band \mathcal{B} and *nonnegative* band \mathcal{B}_0 for signals on $\mathbb{R}/\mathbb{Z}(T_p)$

$$s(t) = \sum_{k=-\infty}^{+\infty} FS(kF)e^{i2\pi kFt}, \quad t \in \mathbb{R}/\mathbb{Z}(T_p). \quad (10.4b)$$

Hence, starting from a continuous-time periodic signal $s(t)$, $t \in \mathbb{R}/\mathbb{Z}(T_p)$, the Fourier transform gives a discrete-frequency function $S(f)$, $f \in \mathbb{Z}(F)$. The inverse transform expresses the signal as a sum of *exponentials*

$$FS(kF)e^{i2\pi kFt}$$

with finite amplitude and frequency $kF \in \mathbb{Z}(F)$, that is, with both positive and negative frequencies.

For *real* signals, the Hermitian symmetry $S(-kF) = S^*(kF)$ allows a representation in terms of *positive frequency sinusoids*. In fact, letting

$$S(kF) = A_S(kF)e^{i\beta_S(kF)}, \quad (10.5)$$

the general relationship (5.77) with $\widehat{I}_z = \{0\}$ and $\widehat{I}_+ = \{F, 2F, \dots\}$ gives

$$s(t) = S_0 + 2 \sum_{k=1}^{\infty} FA_S(kF) \cos[2\pi kFt + \beta_S(kF)], \quad (10.6)$$

where $S_0 = FS(0)$ is the mean value in a period.

10.2.2 Relation with Fourier Series

Letting

$$S_k \triangleq FS(kF), \quad (10.7)$$

(10.4b) gives the usual *Fourier series expansion* of a periodic signal

$$s(t) = \sum_{k=-\infty}^{+\infty} S_k e^{i2\pi kFt}, \quad (10.8a)$$

and (10.4a) gives the *Fourier coefficients*

$$S_k = \frac{1}{T_p} S(kF) = \frac{1}{T_p} \int_{t_0}^{t_0+T_p} s(t) e^{-i2\pi k F t} dt \tag{10.8b}$$

from the signal. The pairs (10.4a), (10.4b) and (10.8a), (10.8b) are substantially equivalent, although the former allows the direct application of the general FT rules. For example, the Parseval theorem (see Sect. 5.7 gives

$$\int_{t_0}^{t_0+T_p} |s(t)|^2 dt = \sum_{k=-\infty}^{+\infty} F |S(kF)|^2, \tag{10.9a}$$

whereas, in terms of Fourier coefficients (10.8a), (10.8b) it becomes

$$\frac{1}{T_p} \int_{t_0}^{t_0+T_p} |s(t)|^2 dt = \sum_{k=-\infty}^{+\infty} |S_k|^2. \tag{10.9b}$$

10.2.3 Symmetries

Symmetry pairs (even and odd, real and imaginary signals, Hermitian and anti-Hermitian), seen in general in Sect. 5.6, hold for the Fourier transform on $\mathbb{R}/\mathbb{Z}(T_p)$ and therefore for the Fourier coefficients.

Figure 10.2 illustrates in particular the following symmetries:

real signal	Hermitian Fourier transform
even real signal	even real Fourier transform
odd real signal	odd imaginary Fourier transform

10.2.4 Specific Fourier Transform Rules on $\mathbb{R}/\mathbb{Z}(T_p)$

As seen in Sect. 9.1 for signals on \mathbb{R} , differentiation and integration can be considered also on $\mathbb{R}/\mathbb{Z}(T_p)$, but only in the time domain, since the frequency domain is discrete.

Time Differentiation and Integration The rules are substantially the same seen in Sect. 9.2, namely

$$\begin{aligned} \frac{ds(t)}{dt} &\xrightarrow{\mathcal{F}} i2\pi f S(f), \\ y(t) = \int_{t_0}^t s(u) du &\xrightarrow{\mathcal{F}} Y(f) = \frac{1}{i2\pi f} S(f), \quad f \neq 0. \end{aligned}$$

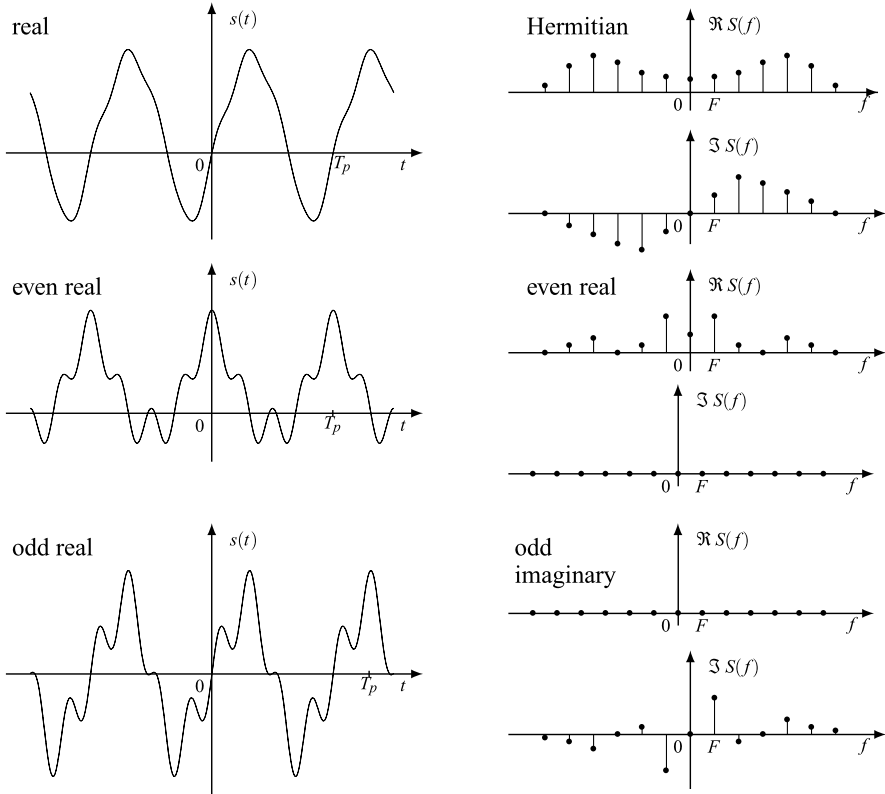


Fig. 10.2 Symmetries of periodic signals and of their Fourier transforms

The integration rule requires that the mean value of $s(t)$ is zero, that is, $S_0 = FS(0) = 0$; otherwise the integral $y(t)$ is not periodic. In the second rule, the indeterminacy in the origin is removed by calculating the mean value Y_0 , and then $Y(0) = FY_0$.

Relationship with the Fourier Transform on \mathbb{R} Applying the Duality Theorem (see Sect. 6.13) with $I = \mathbb{R}$ and $U = \mathbb{R}/\mathbb{Z}(T_p)$, we obtain:

Proposition 10.1 *If $s(t), t \in \mathbb{R}/\mathbb{Z}(T_p)$, is the $\mathbb{R} \rightarrow \mathbb{R}/\mathbb{Z}(T_p)$ periodic repetition of a pulse $p(t), t \in \mathbb{R}$, then the transform $S(f), f \in \mathbb{Z}(F)$, is the $\mathbb{R} \rightarrow \mathbb{Z}(F)$ down-sampling of $P(f), f \in \mathbb{R}$:*

$$s(t) = \text{rep}_{T_p} p(t) \xrightarrow{\mathcal{F}} S(kF) = P(kF).$$

Duration and Bandwidth

The extension $e(s)$ of a signal on $\mathbb{R}/\mathbb{Z}(T_p)$ is always a periodic set, which can be expressed in the form $e(s) = J + \mathbb{Z}(T_p)$, where J is a subset of $[0, T_p)$. The duration $D(s) = \text{meas } e(s)$ is evaluated *within a period* (see Sect. 4.2), and therefore $D(s) \leq T_p$. In particular, we have that a periodic signal is strictly *time-limited in a period* if $D(s) < T_p$.

The spectral extension $\mathcal{E}(s) = e(S)$ is a subset of $\mathbb{Z}(F)$. For a real low-pass signal, $e(S)$ has the symmetric form $e(S) = \{-N_0F, \dots, -F, 0, F, \dots, N_0F\}$, where N_0F is the greatest *harmonic frequency* of the signal.

As we have seen on \mathbb{R} , it is possible to prove the incompatibility between the strict duration and strict band limitation, that is, the incompatibility of having $D(s) < T_p$ and $B(s) < \infty$ at the same time.

Fourier Transform Damping

The considerations seen for continuous aperiodic signals about signal and FT damping (see Sect. 9.6) here are only valid for the FT. Omitting details, we find that, if the signal has *regularity degree* n , then the Fourier transform decays with the low $O(1/f^n)$ and then that the Fourier coefficients S_k with the low $O(1/k^n)$. We suggest the reader to check this statement in the following examples.

10.3 Gallery of Fourier Pairs

Table 10.1 collects examples of Fourier pairs on $\mathbb{R}/\mathbb{Z}(T_p)$. We note that the FT evaluation is based on an integral between finite limits, while the inverse transform is based on a summation of a series. A very useful rule for computation is given by Proposition 10.1.

The Symmetry Rule (see Sect. 5.4) takes the form

$$\begin{array}{ccc}
 s(t) & \xrightarrow{\mathcal{F}} & S(f) \\
 & & S(t) \xrightarrow{\mathcal{F}} s(-f) \\
 \\
 \mathbb{R}/\mathbb{Z}(T_p) & & \mathbb{Z}(F) \\
 & & \mathbb{Z}(T) \quad \mathbb{R}/\mathbb{Z}(F_p)
 \end{array}$$

Hence, from a Fourier pair on $\mathbb{R}/\mathbb{Z}(T_p)$ one obtains a pair on $\mathbb{Z}(T)$, and conversely (compare Table 10.1 and Table 11.1 of the next chapter).

(1)–(6) These pairs were considered in Sect. 5.4 (see also Table 5.2. We recall that the impulse on $\mathbb{R}/\mathbb{Z}(T_p)$ is given by a periodic repetition of delta functions, while the impulse on $\mathbb{Z}(F)$ is $1/F = T_p$ at the origin and zero otherwise.

(7)–(10) In these examples the signals are given by a periodic repetition, and therefore Proposition 10.1 can be applied. For example, the square wave is the

Table 10.1 Fourier pairs on $\mathbb{R}/\mathbb{Z}(T_p)$

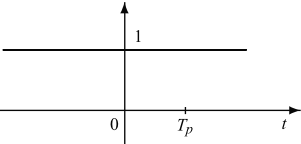
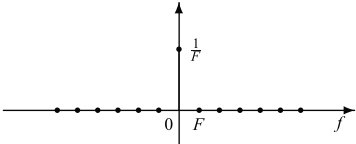
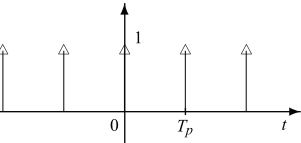
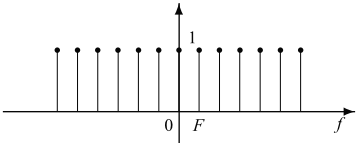
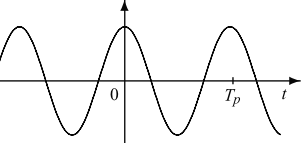
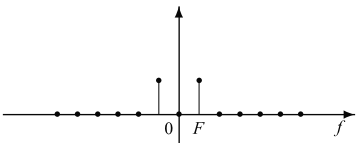
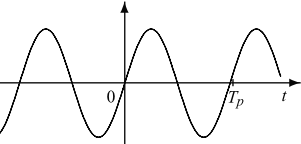
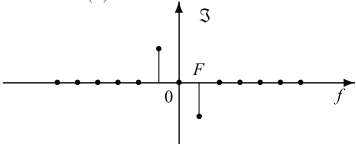
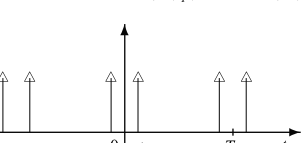
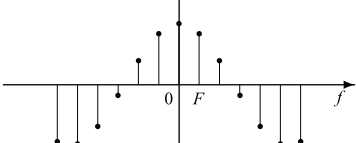
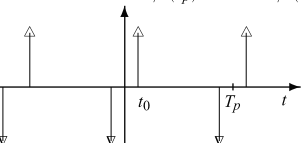
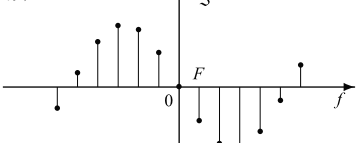
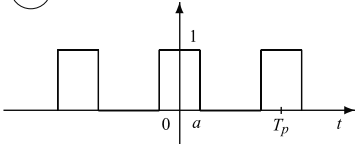
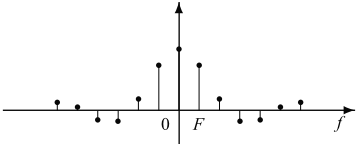
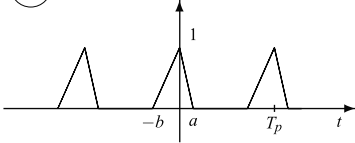
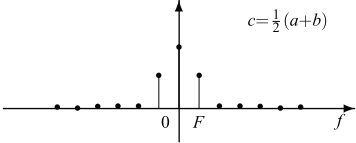
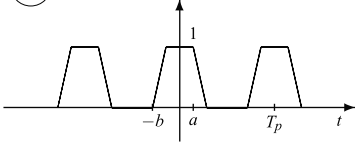
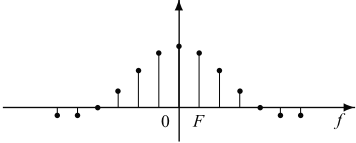
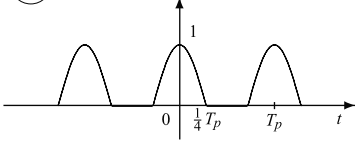
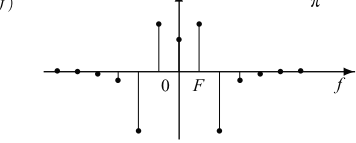
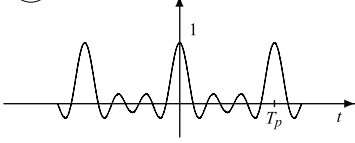
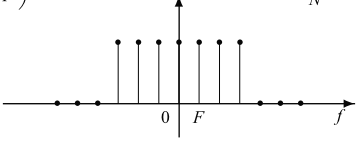
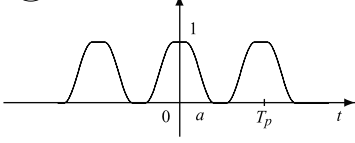
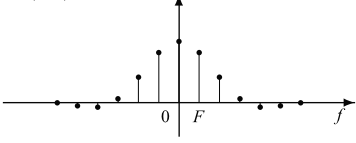
Signal	Fourier transform
① 	$1 \quad \delta_{\mathbb{Z}(F)}(f)$ 
② 	$\delta_{\mathbb{R}/\mathbb{Z}(T_p)}(t) \quad 1$ 
③ 	$\cos(2\pi f_0 t) \quad \frac{1}{2} [\delta_{\mathbb{Z}(F)}(f-f_0) + \delta_{\mathbb{Z}(F)}(f+f_0)]$ 
④ 	$\sin(2\pi f_0 t) \quad \frac{1}{2i} [\delta_{\mathbb{Z}(F)}(f-f_0) - \delta_{\mathbb{Z}(F)}(f+f_0)]$ 
⑤ 	$\delta_{\mathbb{R}/\mathbb{Z}(T_p)}(t-t_0) + \delta_{\mathbb{R}/\mathbb{Z}(T_p)}(t+t_0) \quad 2 \cos(2\pi t_0 f)$ 
⑥ 	$\delta_{\mathbb{R}/\mathbb{Z}(T_p)}(t-t_0) - \delta_{\mathbb{R}/\mathbb{Z}(T_p)}(t+t_0) \quad 2i \sin(2\pi t_0 f)$ 

Table 10.1 (Continued)

<i>Signal</i>	<i>Fourier transform</i>
<p>⑦</p> 	<p>$c \operatorname{sinc}(2af)$ $c=2a$</p> 
<p>⑧</p> 	<p>$c \operatorname{sinc}^2(bf) + \operatorname{sinc}^2(af) - i \operatorname{sinc}(2bf) + i \operatorname{sinc}(2af)$ $c = \frac{1}{2}(a+b)$</p> 
<p>⑨</p> 	<p>$c \operatorname{sinc}[f(b-a)] \operatorname{sinc}[f(b+a)]$ $c=(a+b)$</p> 
<p>⑩</p> <p style="text-align: center;">cosinusoidal pulses</p> 	<p>$c \frac{\cos(2\pi f)}{1-(4af)^2}$ $c = \frac{T_p}{\pi}$</p> 
<p>⑪</p> <p style="text-align: center;">$\operatorname{sinc}_N(NFt)(t)$</p> 	<p>$c \operatorname{rect}\left(\frac{f}{NF}\right)$ $c = \frac{T_p}{N}$</p> 
<p>⑫</p> <p style="text-align: center;">raised cosine pulses</p> 	<p>$c \operatorname{sinc}(\lambda) \frac{\cos(\pi r \lambda)}{1-(2r\lambda)^2}$ $\lambda=2af \quad c=2a$</p> 

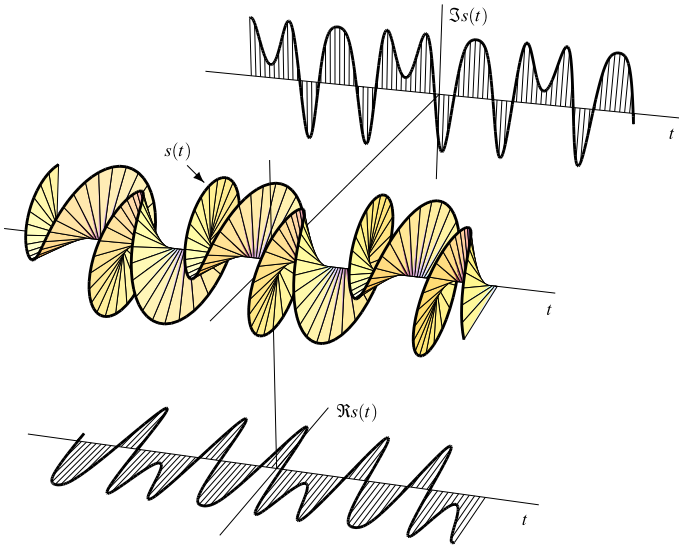


Fig. 10.3 The sinusoidal modulated exponential

repetition of the rectangular pulse $p(t) = \text{rect}(t/2a)$, whose transform is $P(f) = 2a \text{sinc}(f2a)$. Therefore, its Fourier transform is

$$S(kF) = 2a \text{sinc}(kF2a), \quad kF \in \mathbb{Z}(F).$$

(11) This pair was considered in Sect. 2.5.

(12) See pair (19) of Table 9.2.

10.3.1 Example: A Periodic Modulated Signal

Consider the exponential signal (Fig. 10.3)

$$s(t) = \exp(iA \sin 2\pi Ft), \quad t \in \mathbb{R}/\mathbb{Z}(T_p), \tag{10.10a}$$

in which the exponent is a sinusoid (A_0 is a real amplitude). Its Fourier coefficients are

$$\begin{aligned} S_k &= \frac{1}{T_p} \int_0^{T_p} e^{iA_0 \sin 2\pi Ft} e^{-i2\pi kFt} dt \\ &= \frac{1}{2\pi} \int_0^{2\pi} e^{i(A_0 \sin u - ku)} du = J_k(A_0), \end{aligned} \tag{10.10b}$$

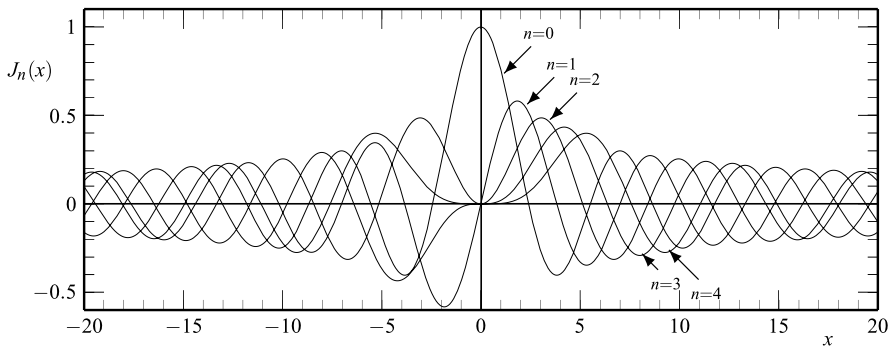


Fig. 10.4 The Bessel functions of the first kind

where $J_k(\cdot)$ are the *Bessel functions* of the first kind [1]. Therefore, the Fourier series expansion of signal (10.10a) is

$$e^{iA_0 \sin 2\pi Ft} = \sum_{n=-\infty}^{+\infty} J_n(A_0) e^{i2\pi n Ft}. \tag{10.10c}$$

The Bessel functions of the first kind (of integer index) may be defined by the integral

$$J_n(x) = \frac{1}{\pi} \int_0^\pi e^{i(nu - x \sin u)} du$$

and are shown in Fig. 10.4 for the first orders.

They have the following properties:

- (1) $J_k(A_0) = J_k^*(A_0)$,
- (2) $J_{-k}(A_0) = (-1)^k J_k(A_0)$,
- (3) $J_k(-A_0) = J_{-k}(A_0)$,
- (4) $\sum_{k=-\infty}^{+\infty} J_k^2(A_0) = 1$.

These properties are remarkable results of Bessel function theory but can be easily proved from Fourier transform rules. In fact, signal (10.10a), (10.10b), (10.10c) has the Hermitian symmetry, and therefore its Fourier coefficients $S_k = J_k(A_0)$ are real. Next, consider that a shift of $t_0 = \frac{1}{2}T_p$ on the signal gives the conjugate signal; then, for the time-shift rule,

$$s\left(t - \frac{1}{2}T_p\right) = s^*(t) \xrightarrow{\mathcal{F}} S(kF) e^{-i\pi k F T_p} = S^*(-kF),$$

which for the (real) Fourier coefficients gives $S_k(-1)^k = S_{-k}$, thus obtaining (2). Moreover, if we replace A_0 with $-A_0$, we obtain the conjugate signal, and so we prove (3). Finally, (4) can be deduced from Parseval’s theorem, written in the form (10.9b), as soon as we note that the signal energy in one period is T_p .

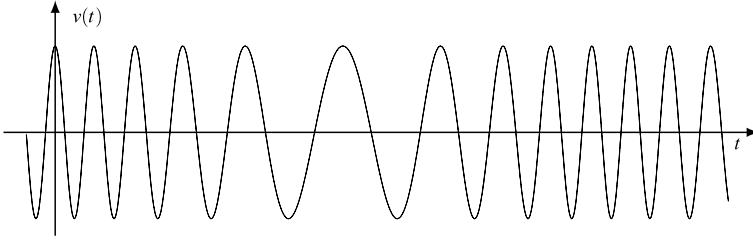


Fig. 10.5 Example of frequency-modulated signal

Exponential signal (10.10a), (10.10b), (10.10c) is encountered in Modulation Theory [2, 3], specifically in phase or frequency-modulated signals of the form (Fig. 10.5)

$$v(t) = V_0 \cos(2\pi f_0 t + A_0 \sin 2\pi F t). \quad (10.11)$$

UT 10.4 Filtering of Periodic Signals

Consider the input–output relationship of a filter on \mathbb{R}

$$y(t) = \int_{-\infty}^{+\infty} g(t-u)x(u) du, \quad t \in \mathbb{R}. \quad (10.12)$$

Then, it is easy to see that if the input is periodic with period T_p , the output is periodic with the same period, while the impulse response $g(t)$, $t \in \mathbb{R}$, is in general aperiodic. As regards the representation of the three signals, there are two possibilities.

The first is to represent the input and output on \mathbb{R} , even if they are both periodic, and (10.12) has to be seen in this sense. The second possibility is to represent the three signals (including the impulse response) on $\mathbb{R}/\mathbb{Z}(T_p)$. In fact, using the integration rule (see (4.12a), (4.12b))

$$\int_{-\infty}^{+\infty} f(u) du = \int_{t_0}^{t_0+T_p} \sum_{k=-\infty}^{+\infty} f(u - kT_p) du$$

in (10.12) and taking into account that $x(u)$ is periodic and then $x(u - kT_p) = x(u)$, we get

$$y(t) = \int_{t_0}^{t_0+T_p} g_p(t-u)x(u) du, \quad t \in \mathbb{R}/\mathbb{Z}(T_p), \quad (10.13)$$

where

$$g_p(t) = \sum_{k=-\infty}^{+\infty} g(t - kT_p), \quad t \in \mathbb{R}/\mathbb{Z}(T_p). \quad (10.13a)$$

Now, in (10.13) all the three signals are represented on $\mathbb{R}/\mathbb{Z}(T_p)$.

In the frequency domain, from (10.13) we obtain

$$Y(f) = G_p(f)X(f), \quad f \in \mathbb{Z}(F), \quad (10.14)$$

where $G_p(f) = G(f)$, $f \in \mathbb{Z}(F)$, is the $\mathbb{R} \rightarrow \mathbb{Z}(F)$ down-sampled version of the original frequency response. Therefore, in the frequency domain we can use the original frequency response $G(f)$, $f \in \mathbb{R}$, whose values are considered only for $f \in \mathbb{Z}(F)$.

10.5 Problems

10.1 **★★** [Sect. 10.1] In the previous chapter we have seen that a discontinuous signal on \mathbb{R} can be decomposed into a continuous signal and a piecewise constant signal. Find the decomposition for a signal defined on $\mathbb{R}/\mathbb{Z}(T_p)$.

10.2 **★** [Sect. 10.1] Find conditions on the signal

$$s(t) = A_1 \operatorname{rep}_{T_p} \operatorname{rect}\left(\frac{t}{dT_p}\right) + A_2 \operatorname{rep}_{T_p} \operatorname{rect}\left(\frac{t}{dT_p} - \frac{1}{2}\right), \quad d = 20\%,$$

which assure that its integral, defined by (10.2), is still periodic. Then, evaluate $y(t)$ and its Fourier transform.

10.3 **★** [Sect. 10.2] Compute the Fourier coefficients of the “two-wave” rectified sinusoid

$$s(t) = |\cos 2\pi F_0 t|, \quad t \in \mathbb{R}/\mathbb{Z}(T_p).$$

10.4 **★★** [Sect. 10.3] A signal with minimum period T_0 can be represented on $\mathbb{R}/\mathbb{Z}(T_0)$, but also on $\mathbb{R}/\mathbb{Z}(3T_0)$. Let $s_1(t)$ and $s_3(t)$ be the two representations. Find the relationship between $S_1(f)$ and $S_3(f)$.

10.5 **★★★** [Sect. 10.3] Using the Fourier series expansion of the signal (10.10a), prove that the modulated signal (10.11) can be written in the form

$$v(t) = \sum_{k=-\infty}^{+\infty} V_0 J_k(A_0) \cos[2\pi(f_0 + kF)t].$$

References

1. A. Angot, *Compléments de Mathématiques* (Editions de la Revue d'Optiques, Paris, 1957)
2. A. Papoulis, *The Fourier Integral and Its Applications* (McGraw-Hill, New York, 1962)
3. J.G. Proakis, *Digital Communications*, 3rd edn. (McGraw-Hill, New York, 1995)

Chapter 11

Signals on $\mathbb{Z}(T)$

UT 11.1 The Time Domain

The domain of discrete-time aperiodic signals is the additive group $\mathbb{Z}(T)$, where T is the signal *spacing*, and its reciprocal $F_p = 1/T$ is the signal *rate*. We recall that:

- time shifts and periods are constrained to belong to $\mathbb{Z}(T)$;
- the measure of a given subset of $\mathbb{Z}(T)$ is equal to the cardinality of the subset itself multiplied by T ;
- *cells* on $\mathbb{Z}(T)$ typically consist of N consecutive points (see Sect. 3.5).

11.1.1 Integral and Convolution

The *Haar integral* on $\mathbb{Z}(T)$ is the sum of the signal values multiplied by the spacing T (see Sect. 4.2)

$$\int_{\mathbb{Z}(T)} dt s(t) = \sum_{n=-\infty}^{+\infty} T s(nT).$$

As a consequence, the *convolution* is given by

$$x * y(nT) = \sum_{k=-\infty}^{+\infty} T x(nT - kT) y(kT). \tag{11.1}$$

The *impulse*, defined as the unit element of convolution algebra (see Sect. 4.10), is given by

$$\delta_{\mathbb{Z}(T)}(nT) = \frac{1}{T} \delta_{n0} = \begin{cases} \frac{1}{T}, & n = 0, \\ 0, & n \neq 0, \end{cases}$$

then, it is an ordinary function (see Theorem 4.7).

11.1.2 Increment and Running Sum

Differentiation and integration are not defined on $\mathbb{Z}(T)$, but are replaced respectively by the *increment*

$$\Delta s(nT) = s((n+1)T) - s(nT) \quad (11.2)$$

and the *running sum*

$$y(nT) = \sum_{k=-\infty}^n Ts(kT). \quad (11.3)$$

The increment normalized to the spacing T , $\Delta s(nT)/T$, has the meaning of *rate variation* of the signal. The running sum is given by the convolution of $s(nT)$ with the discrete step signal $1_0(nT)$ as

$$y(nT) = s * 1_0(nT). \quad (11.3a)$$

11.1.3 Scale Change

Given a discrete signal $x(t)$, $t \in \mathbb{Z}(T)$, the relation

$$y(u) = x(au), \quad a \neq 0, \quad u \in \mathbb{Z}(T/|a|), \quad (11.4)$$

defines a discrete signal on the domain $\mathbb{Z}(T/|a|)$. For instance, the signal $y(u) = x(3u)$ is defined on $\mathbb{Z}(T/3)$. Scale change (11.4) was discussed in Sect. 6.5.

UT 11.2 The Frequency Domain

The dual of $\mathbb{Z}(T)$ results in

$$\widehat{\mathbb{Z}(T)} = \mathbb{R}/\mathbb{Z}(F_p), \quad F_p = 1/T.$$

Because of the periodicity, the specification in the frequency domain can be limited to a cell $[\mathbb{R}/\mathbb{Z}(F_p)]$, typically chosen as (Fig. 11.1)

$$\mathcal{B} = [0, F_p) \quad \text{or} \quad \mathcal{B}_c = \left[-\frac{1}{2}F_p, \frac{1}{2}F_p\right), \quad (11.5a)$$

which we call *fundamental bands*. For *real signals* owing to the Hermitian symmetry of the FT, the specification can be confined to the nonnegative band

$$\mathcal{B}_0 = \{0\} \cup \mathcal{B}_+ \quad \text{with} \quad \mathcal{B}_+ = \left(0, \frac{1}{2}F_p\right), \quad (11.5b)$$

where \mathcal{B}_+ is the *positive half-band*.

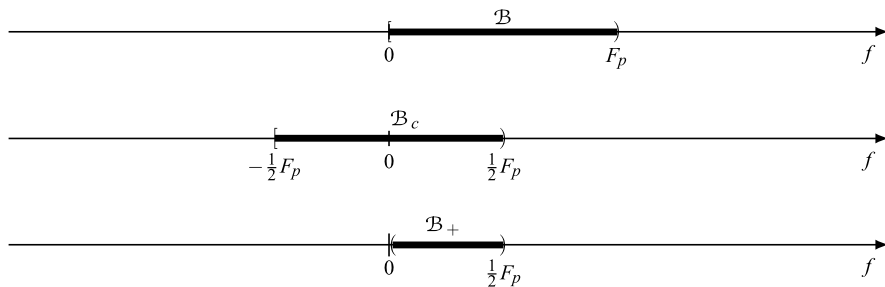


Fig. 11.1 Fundamental band \mathcal{B} , centered fundamental band \mathcal{B}_c , and positive half-band \mathcal{B}_+

11.2.1 Fourier Transform on $\mathbb{Z}(T)$

The FT and inverse FT are respectively given by

$$S(f) = \sum_{n=-\infty}^{+\infty} Ts(nT)e^{-i2\pi fnT}, \quad f \in \mathbb{R}/\mathbb{Z}(F_p), \quad (11.6a)$$

$$s(nT) = \int_{f_0}^{f_0+F_p} S(f)e^{i2\pi fnT} df, \quad nT \in \mathbb{Z}(T). \quad (11.6b)$$

According to (11.6a), from a discrete-time signal $s(nT)$, $nT \in \mathbb{Z}(T)$, one obtains a continuous-frequency function with period $F_p = 1/T$, $S(f)$, $f \in \mathbb{R}/\mathbb{Z}(F_p)$. According to (11.6b), the signal is represented as a sum of discrete *exponentials*

$$df S(f)e^{i2\pi fnT}, \quad f \in [f_0, f_0 + F_p),$$

with infinitesimal amplitudes and frequency range within the *cell* $[f_0, f_0 + F_p)$, which is usually chosen equal to one of the fundamental bands, \mathcal{B} or \mathcal{B}_c . The motivation of this choice is discussed in the next section.

For *real* signals, the Hermitian symmetry of the FT yields a signal representation in terms of *sinusoidal* components with frequencies limited to the positive half-band \mathcal{B}_+ . To this end, in (11.6b) we take the centered fundamental band $\mathcal{B}_c = [-\frac{1}{2}F_p, \frac{1}{2}F_p)$ as integration domain with the following partition:

$$\mathcal{B}_c = \{0\} \cup \mathcal{B}_+ \cup (-\mathcal{B}_+), \quad \text{where } \mathcal{B}_+ = \left(0, \frac{1}{2}F_p\right).$$

Then, the general result (5.77) found in Chap. 5 reads

$$s(t) = S_0 + 2 \int_0^{\frac{1}{2}F_p} A_S(f) \cos[2\pi fnT + \beta_S(f)] df, \quad (11.7)$$

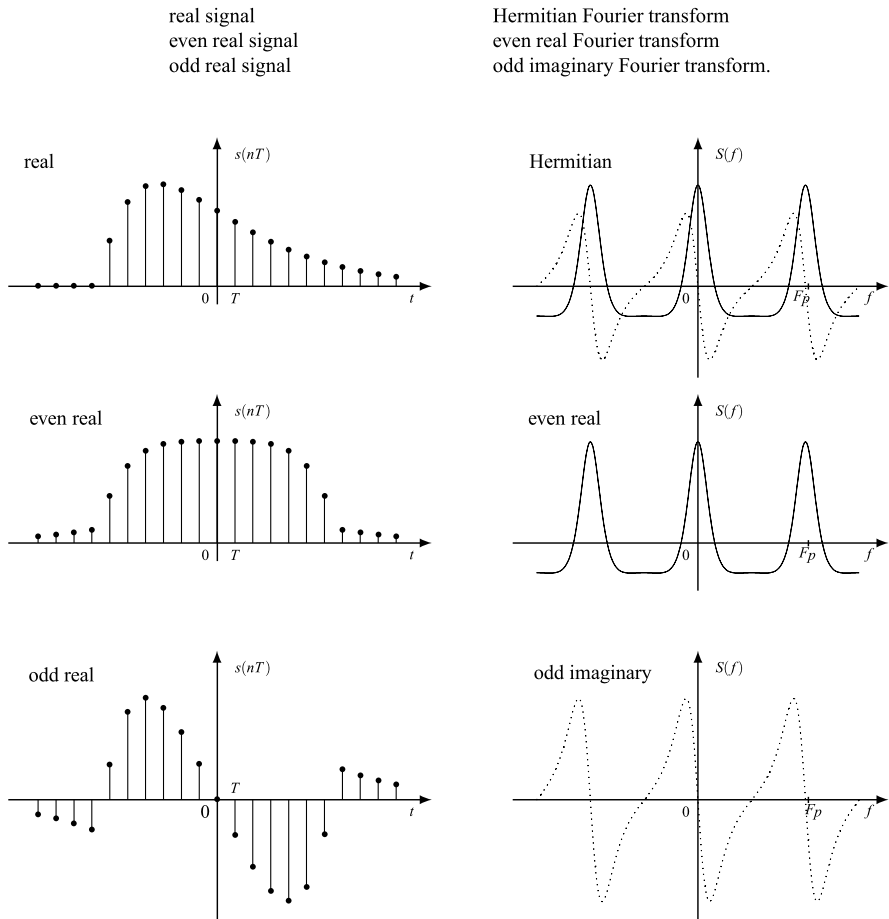


Fig. 11.2 Symmetries for discrete-time signals and their Fourier transforms

where S_0 is the *mean value* of $s(t)$,

$$S_0 = m_s = \lim_{N \rightarrow \infty} \frac{1}{(2N + 1)T} \sum_{n=-N}^N T s(nT). \tag{11.7a}$$

11.2.2 Symmetries

The standard symmetries considered in Sect. 5.6 are further emphasized for the presence of periodicity in the FT. In particular, in Fig. 11.2 the following symmetric

pairs are illustrated:

real signal	Hermitian Fourier transform
even real signal	even real Fourier transform
odd real signal	odd imaginary Fourier transform.

Note that with these symmetries the specification of the FT can be limited to the nonnegative half-band $\mathcal{B}_0 = [0, \frac{1}{2}F_p]$.

11.2.3 Specific Rules of the Fourier Transform on $\mathbb{Z}(T)$

To the general rules of Table 5.2 we can add the following specific rules.

Frequency Differentiation and Integration By differentiating both members of (11.6a) with respect to f we obtain the rule

$$-i2\pi nTs(nT) \xrightarrow{\mathcal{F}} \frac{dS(f)}{df}. \tag{11.8a}$$

The integration rule is

$$y(nT) = \frac{1}{-i2\pi nT} s(nT) \xrightarrow{\mathcal{F}} Y(f) = \int_{f_0}^f S(\lambda) d\lambda$$

and requires that $s(0) = 0$; otherwise the FT $Y(f)$ is not periodic. This is the symmetric rule of the one considered in Sect. 10.2 for signals on $\mathbb{R}/\mathbb{Z}(T_p)$.

Increment and Running Sum The FT of the *increment* signal is easily obtained using the time-shifting rule; in fact,

$$\Delta s(t) = s(t + T) - s(t) \xrightarrow{\mathcal{F}} \Delta S(f) = S(f)[e^{i2\pi fT} - 1]. \tag{11.9a}$$

Less simple is to find the rule to calculate the FT $Y(f)$ of the *running sum* $y(nT)$ defined in (11.3). The formulation is based on the FT $U_0(f)$ of the discrete step signal (see (11.3a)), which will be calculated in the next section. The result is

$$Y(f) = U_0 * S(f) = \frac{1}{2}S(f) + S_1(f) + \frac{1}{2}T \text{area}(S), \tag{11.10}$$

where

$$S_1(f) = T \frac{1}{2i} \int_{f_0}^{f_0+F_p} S(\lambda) \tan[\pi(f - \lambda)T] df. \tag{11.10a}$$

Relation with the Fourier Transform on \mathbb{R} By applying the Duality Theorem (see Sect. 6.13) with $I = \mathbb{R}$ and $U = \mathbb{Z}(T)$ one gets:

Proposition 11.1 *If a discrete signal $s(nT)$ is the $\mathbb{R} \rightarrow \mathbb{Z}(T)$ down-sampling of the continuous signal $s_0(t)$, $t \in \mathbb{R}$, the FT of $s(nT)$ is the $\mathbb{R} \rightarrow \mathbb{R}/\mathbb{Z}(F_p)$ up-periodization (periodic repetition) of the FT of $s_0(t)$, namely*

$$s(nT) = s_0(nT) \xrightarrow{\mathcal{F}} S(f) = \text{rep}_{F_p} S_0(f), \quad F_p = 1/T. \quad (11.11)$$

Up-Sampling of a Discrete-Time Signal This operation appears very often in the study of discrete-time signals and systems. From the Duality Theorem with $I = \mathbb{Z}(T)$ and $U = \mathbb{Z}(T_0)$ one obtains:

Proposition 11.2 *Let $T = NT_0$, and let $y(nT_0)$ be the $\mathbb{Z}(T) \rightarrow \mathbb{Z}(T_0)$ up-sampling of $s(nT)$, given by (see Sect. 6.10)*

$$y(nT_0) = \begin{cases} Ns(nT), & n \in \mathbb{Z}(N), \\ 0, & \text{elsewhere.} \end{cases}$$

Then, $Y(f)$ is the $\mathbb{R}/\mathbb{Z}(F_p) \rightarrow \mathbb{R}/\mathbb{Z}(NF_p)$ down-periodization of $S(f)$, given by

$$Y(f) = S(f), \quad f \in \mathbb{R}/\mathbb{Z}(NF_p), \quad F_p = 1/T.$$

It should be noted that the two FTs coincide, but while $S(f)$ is considered with period F_p , $Y(f)$ is considered with period NF_p , according to the idea of *down-periodization*.

11.2.4 Presence of Lines in the Fourier Transform

Considering that

$$Ae^{i2\pi f_0 nT} \xrightarrow{\mathcal{F}} A\delta_{\mathbb{R}/\mathbb{Z}(F_p)}(f - f_0) = \sum_{k=-\infty}^{+\infty} A\delta(f - kF_p - f_0),$$

we find that, if a line is present at the frequency f_0 , lines are also present at all the frequencies $f_0 + kF_p$ with the same amplitude, but only one of them falls into the fundamental band \mathcal{B} , as shown in Fig. 11.3.

In particular, the presence in the signal of a *constant component*, given by (11.7a), implies the presence of a line at the origin and consequently also at the frequencies multiple of F_p . In general, a periodic component with period $T_p = MT$ exhibits M lines in the fundamental band $\mathcal{B} = [0, F_p)$.

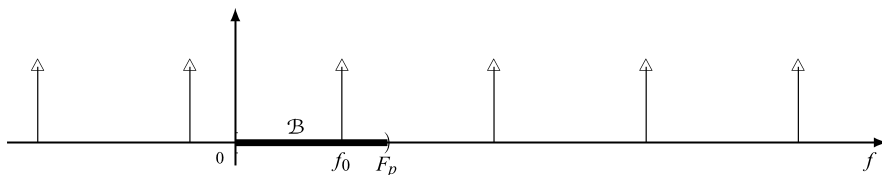


Fig. 11.3 Form of a line on $\mathbb{Z}(T)$. Only one “delta” falls into the fundamental band \mathcal{B}

11.2.5 Duration, Band, Dumping and Rate Variation

We recall that in the domain $\mathbb{Z}(T)$ the duration must be a multiple of T , while the bandwidth is constrained by the condition $0 \leq B(s) \leq F_p$. The incompatibility between the simultaneous strict limitation of duration and band implies that no signal can have simultaneously $D(s) < \infty$ and $B(s) < F_p$ (the zero signal excepted).

The asymptotic behavior of the signal is related to the differentiability of the FT: if $S(f)$ has $m - 1$ derivatives and, more precisely, has *regularity degree* m (see Sect. 9.6), the signal dumping has the “decay” rate $m O(1/t^m) = O(1/n^m)$ as $|t| = |n|T \rightarrow \infty$.

The *rate variation* is constrained by the bandwidth. Specifically, for a signal with spectral extension $(-B, B) + \mathbb{Z}(F_p)$, the constraint is

$$\left| \frac{\Delta s(nT)}{T} \right| \leq 2\pi B \int_{-B}^B |S(f)| df \tag{11.12}$$

that is perfectly similar to that of continuous signals (see (9.40)). For the proof, we express the increment as an inverse FT (see (11.9a))

$$\frac{\Delta s(nT)}{T} = \frac{1}{T} \int_{-B}^B S(f) (e^{i2\pi fT} - 1) e^{-i2\pi f nT} df.$$

Hence, considering that $e^{i2\pi fT} - 1 = e^{i\pi fT} \text{sinc}(fT) i2\pi fT$, we obtain

$$\left| \frac{\Delta s(nT)}{T} \right| \leq \int_{-B}^B |S(f)| |2\pi f| df \leq 2\pi B \int_{-B}^B |S(f)| df.$$

11.3 Remarkable Examples

Signals on $\mathbb{Z}(T)$ are usually obtained by down-sampling signals defined on \mathbb{R} . It is important to bear in mind that a periodicity $\mathbb{Z}(T_0)$ of a signal on \mathbb{R} , if present, is also preserved after an $\mathbb{R} \rightarrow \mathbb{Z}(T)$ down-sampling only if $\mathbb{Z}(T_0) \subset \mathbb{Z}(T)$, i.e., if the period T_0 is multiple of the spacing T . In general, the period T_p after a down-sampling is given by

$$\mathbb{Z}(T_p) = \mathbb{Z}(T_0) \cap \mathbb{Z}(T). \tag{11.13}$$

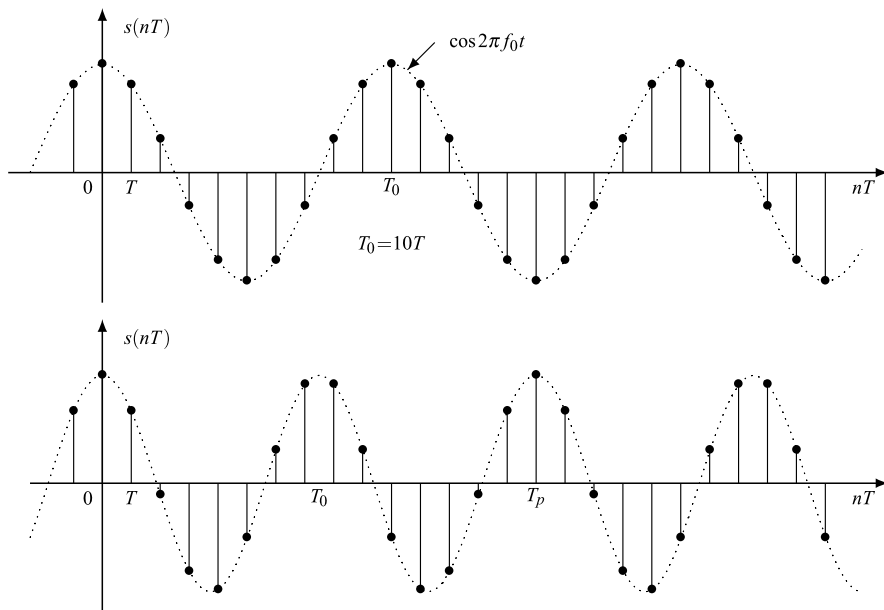


Fig. 11.4 Comparison of the period T_0 of a continuous sinusoid and the period T_p of its sampled version: above $T_p = T_0 = 10T$, below $T_0 = (7 + \frac{1}{2})T$ and $T_p = 2T_0 = 15T$

Then

- (1) if T_0 is multiple of T , $T_0 = KT$, then $T_p = T_0$;
- (2) if $T_0 = (K/N)T$ with K and N coprime, then $T_p = NT_0 = KT$;
- (3) if T_0/T is an irrational number, then the signal after the down-sampling becomes aperiodic.

11.3.1 Discrete Exponentials and Discrete Sinusoids

These signals have, respectively, the forms

$$Ae^{i2\pi f_0 nT}, \quad A_0 \cos(2\pi f_0 nT + \varphi_0). \quad (11.14)$$

In the exponential the amplitude A is in general a complex number, while the frequency f_0 is real (possibly negative). In the sinusoid (Fig. 11.4) both the amplitude A_0 and the frequency f_0 are real and positive. The quantity $T_0 = 1/|f_0|$ is the period of the corresponding continuous signals, but in general it is not the period of the discrete signals (11.14). The periodicity is in general given through (11.13). Hence, if $f_0 T = T/T_0 = K/N$ is a rational number, with K and N coprime, then the period turns out to be

$$T_p = NT_0 = KT.$$

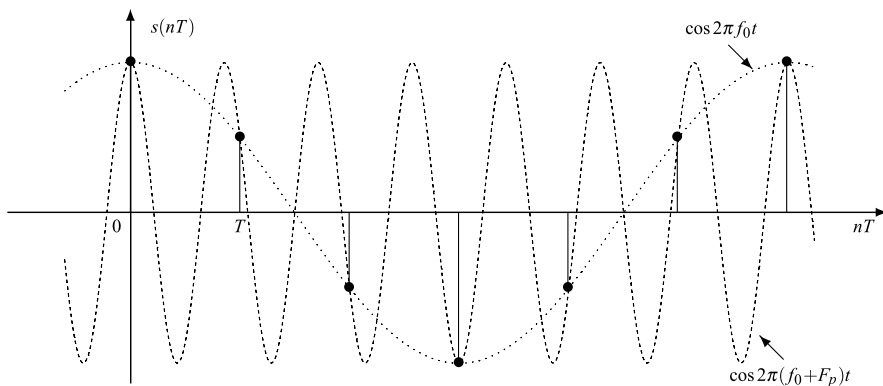


Fig. 11.5 Illustration of the frequency ambiguity of a discrete sinusoid

Therefore, the continuous signal and the corresponding discrete signal have the same period only if $N = 1$, as shown in Fig. 11.4, where $T_0/T = 10$. But, if $N > 1$, the discrete signal has a period N times greater than the period of the continuous signal. In Fig. 11.4 (below), $T_0/T = 15/2$, and then the discrete sinusoid has the period twice the one of the corresponding continuous sinusoid.

A remarkable feature of these signals is the *ambiguity* of a frequency f_0 with respect to the values spaced of multiples of F_p . In fact, considering that

$$e^{i2\pi(f_0+kF_p)nT} = e^{i2\pi f_0 nT}, \quad F_p = 1/T,$$

we find that two discrete exponentials with frequencies f_0 and $f_0 + kF_p$ represent the same discrete signal. As a consequence, without restriction, f_0 can be chosen in the fundamental band $\mathcal{B} = [0, F_p)$ or $\mathcal{B}_c = (-\frac{1}{2}F_p, \frac{1}{2}F_p)$. This explains why in the inverse transform (11.6b) the integral is limited to an interval of measure F_p .

A similar conclusion holds for the discrete sinusoid (11.14), as illustrated in Fig. 11.5, where two continuous sinusoids, $\cos 2\pi f_0 t$ and $\cos 2\pi(f_0 + F_p)t$, yield the same samples. Moreover, recalling that for a sinusoid the frequency f_0 is positive, it may be confined to the positive half-band $\mathcal{B}_+ = (0, \frac{1}{2}F_p)$, because

$$A_0 \cos(2\pi f_0 t + \varphi_0) \quad \text{and} \quad A_0 \cos[2\pi(F_p - f_0)t + \varphi_0], \quad t \in \mathbb{Z}(T),$$

represent the same discrete sinusoid. Again, this fact explains why in (11.6b) the integral is limited to the interval $(0, \frac{1}{2}F_p)$.

11.3.2 Discrete Step Signal

We observed in Sect. 2.10 that the discrete step signal (Fig. 11.6)

$$1_0(nT) = \begin{cases} 1, & n \geq 0, \\ 0, & n < 0, \end{cases} \quad (11.15)$$

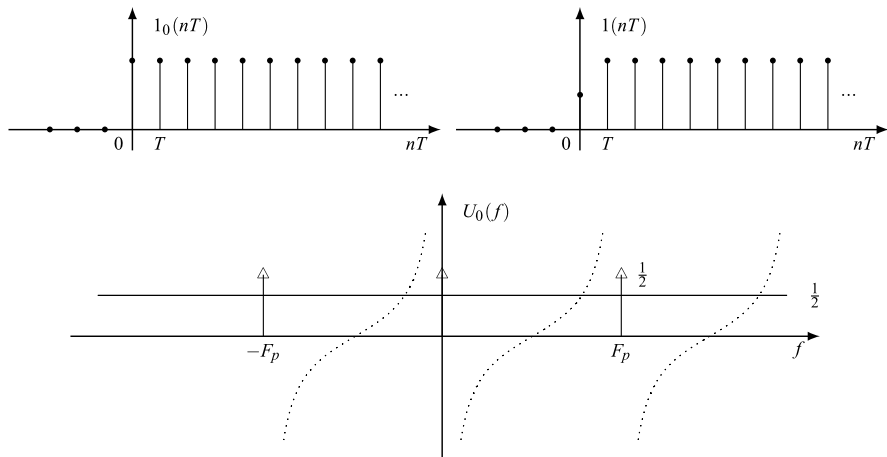


Fig. 11.6 Discrete step signal $1_0(nT)$ compared with the sampled version of continuous step signal $1(t)$. $U_0(f)$ is the Fourier transform of $1_0(nT)$

does not coincide exactly with the sampled version of the continuous step signal $1(t)$, $t \in \mathbb{R}$, because $1_0(0) = 1$, while $1(0) = \frac{1}{2}$. Consequently, the decomposition by means of the *sgnum* function is slightly different from the decomposition of $1(t)$ (see Sect. 2.3), giving

$$1_0(nT) = \frac{1}{2} + \frac{1}{2} \operatorname{sgn}(nT) + \frac{1}{2} T \delta_{\mathbb{Z}(T)}(nT), \quad (11.16)$$

where the impulse is introduced to ensure that $1_0(0) = 1$.

To evaluate the FT $U(f)$ of $1_0(nT)$, we first evaluate the FT of $\operatorname{sgn}(nT)$. Letting $z = \exp(i2\pi fT)$, we obtain

$$\begin{aligned} \sum_{n=-\infty}^{+\infty} T \operatorname{sgn}(nT) z^{-n} &= - \sum_{n=-\infty}^{-1} T z^{-n} + \sum_{n=1}^{\infty} T z^{-n} = T \left[-\frac{z}{1-z} + \frac{z^{-1}}{1-z^{-1}} \right] \\ &= T \frac{z^{-1} - z}{(1-z^{-1})(1-z)} = T \frac{z^{\frac{1}{2}} + z^{-\frac{1}{2}}}{z^{\frac{1}{2}} - z^{-\frac{1}{2}}}. \end{aligned}$$

Then, the Euler formulas gives

$$\operatorname{sgn}(nT) \xrightarrow{\mathcal{F}} -iT \cot(\pi fT). \quad (11.17)$$

Next, from decomposition (11.16) one gets

$$1_0(nT) \xrightarrow{\mathcal{F}} \frac{1}{2} \delta_{\mathbb{R}/\mathbb{Z}(F_p)}(f) + T \frac{1}{2i} \cot(\pi fT) + T \frac{1}{2}. \quad (11.18)$$

Finally, using this Fourier pair in (11.10), we can prove the rule on the running sum, given by (11.10).

11.3.3 Discrete Causal Exponential

The signal

$$s(nT) = 1_0(nT)p_0^n, \quad p_0 = \rho_0 e^{i\theta_0}, \tag{11.19}$$

has FT only if $|p_0| = \rho_0 < 1$. Indeed, this condition assures that the series giving the FT,

$$S(f) = \sum_{n=0}^{\infty} T(p_0 z^{-1})^n = T \frac{1}{1 - p_0 z^{-1}}, \quad z = e^{i2\pi fT}, \tag{11.20}$$

is convergent. If $|p_0| > 1$, the series is not convergent, and the FT does not exist. If $|p_0| = 1$, the FT exists in a generalized sense: for instance, for $p_0 = 1$, (11.19) becomes the step signal whose FT is given by (11.18).

A signal related to the causal exponential is $y(nT) = np_0^n 1_0(nT)$. Its FT is obtained by applying the rule on frequency differentiation to (11.20), namely

$$np_0^n 1_0(nT) \xrightarrow{\mathcal{F}} T p_0 \frac{z}{(z - p_0)^2}, \quad z = e^{i2\pi fT}, \tag{11.21}$$

which holds for $|p_0| < 1$.

11.4 Gallery of Fourier Pairs

Table 11.1 collects several examples of Fourier pairs, some have been already considered, while some others are now developed. The Symmetry Rule (Sect. 5.4) has the form

$$\begin{array}{ccc} s(t) & \xrightarrow{\mathcal{F}} & S(f) \\ & & S(t) \xrightarrow{\mathcal{F}} s(-f) \\ \mathbb{Z}(T) & \mathbb{R}/\mathbb{Z}(F_p) & \\ & \mathbb{R}/\mathbb{Z}(T_p) & \mathbb{Z}(F) \end{array}$$

Then, starting from a Fourier pair on $\mathbb{Z}(T)$, with the substitutions $F_p \rightarrow T_p, T \rightarrow F$, one obtains a Fourier pair on $\mathbb{R}/\mathbb{Z}(T_p)$. In this way we can use a pair of Table 11.1 to find a pair for Table 10.1 of the previous chapter. Alternatively, we can start from a pair on $\mathbb{R}/\mathbb{Z}(T_p)$ to find a pair on $\mathbb{Z}(T)$ (see Sect. 10.3).

(1)–(6) *singular signals*: these examples were discussed in a general form in Sect. 5.8.

(7) (8) *sign and step functions*: see above.

(9) *discrete Hilbert kernel*: see Sect. 11.7.

(10) *causal cosine*: see Problem 11.2.

(11), (12) *causal exponential*: see above.

Table 11.1 Fourier pairs on $\mathbb{Z}(T)$

<i>Signal</i>	<i>Fourier transform</i>
①	$1 \quad \delta_{\mathbb{R}/\mathbb{Z}(F_p)}(f)$
②	$\delta(t) \quad 1$
③	$\cos(2\pi f_0 t) \quad \frac{1}{2} [\delta_{\mathbb{R}/\mathbb{Z}(F_p)}(f-f_0) + \delta_{\mathbb{R}/\mathbb{Z}(F_p)}(f+f_0)]$
④	$\sin(2\pi f_0 t) \quad \frac{1}{2i} [\delta_{\mathbb{R}/\mathbb{Z}(F_p)}(f-f_0) - \delta_{\mathbb{R}/\mathbb{Z}(F_p)}(f+f_0)]$
⑤	$\delta(t-t_0) + \delta(t+t_0) \quad 2 \cos(2\pi t_0 f)$
⑥	$-\delta(t-t_0) + \delta(t+t_0) \quad 2i \sin(2\pi t_0 f)$
——— real part imaginary part

Table 11.1 (Continued)

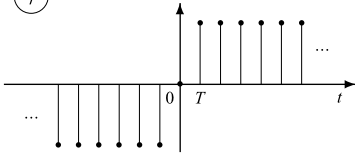
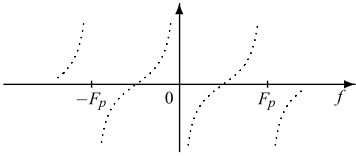
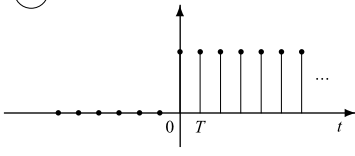
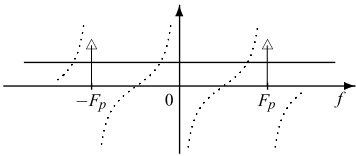
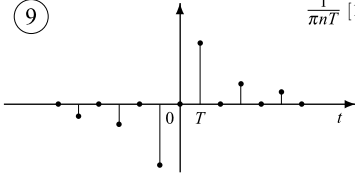
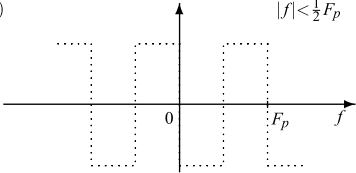
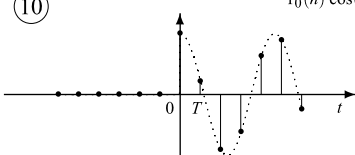
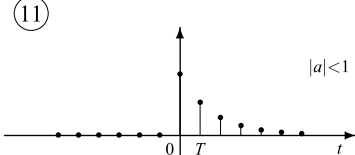
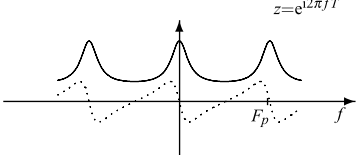
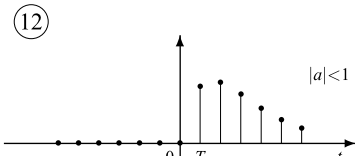
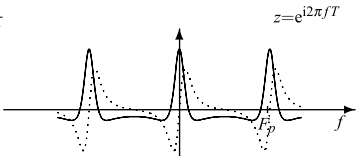
<i>Signal</i>	<i>Fourier transform</i>
<p>⑦</p> 	<p>$\text{sgn}(nT) \quad -iT \cotg(\pi fT)$</p> 
<p>⑧</p> 	<p>$1_0(nT) \quad U_0(f) = \frac{1}{2} \delta_{\mathbb{R}/Z(F_p)}(f) + T \frac{1}{2\pi} \cotg(\pi fT) + \frac{1}{2} T$</p> 
<p>⑨</p> 	<p>$\frac{1}{\pi nT} [1 - (-1)^n] \quad -i \text{sgn}(f)$</p> <p style="text-align: right;">$f < \frac{1}{2} F_p$</p> 
<p>⑩</p> 	<p>$1_0(n) \cos(2\pi f_0 nT) \quad \frac{1}{2} U_0(f-f_0) + \frac{1}{2} U_0(f+f_0)$</p> <p>$U_0(f)$: Fourier transform of $1_0(nT)$, see above</p>
<p>⑪</p>  <p style="text-align: right;">$a < 1$</p>	<p>$1_0(n) a^n \quad T \frac{z}{z-a}$</p> <p style="text-align: right;">$z = e^{i2\pi fT}$</p> 
<p>⑫</p>  <p style="text-align: right;">$a < 1$</p>	<p>$1_0(n) n a^n \quad T \frac{z}{(z-a)^2}$</p> <p style="text-align: right;">$z = e^{i2\pi fT}$</p> 
<p>— real part</p>	<p>..... imaginary part</p>

Table 11.1 (Continued)

<i>Signal</i>	<i>Fourier transform</i>
<p>(13)</p>	<p>$\text{rect}\left(\frac{nT}{2T_0}\right)$ $2T_0 \text{sinc}_N(f2T_0)$ $2T_0 = NT$</p>
<p>(14)</p>	<p>$2T \sum_{n=1}^{N_0} \left(1 - \frac{n}{N_0}\right) \cos(2\pi f n T) + T$</p>
<p>(15)</p>	<p>$\text{sinc}(2F_0 n T)$</p>
<p>(16)</p>	<p>$\text{sinc}^2(2F_0 n T)$</p>
<p>(17)</p>	<p>$\frac{1}{\pi} \frac{\cos(2a\pi t)}{1-(4at)^2}$ half sine wave $a = \frac{1}{4T}$</p>
<p>(18)</p>	<p>$J_n(A_0)$ $T e^{iA_0 \sin(2\pi f T)}$</p>

real part
 imaginary part

(13), (14) *rectangular and triangular pulses*. For the rectangular pulse, use the definition or apply the symmetry rule to the pair (11) of Table 10.1. For the triangular pulse, see Problem 11.3.

(15)–(17) apply the Symmetry Rule to the corresponding pairs of Table 10.1 or use Proposition 11.1.

(18) $J_n(A_0)$ *signal*: this is the symmetrical pair of (11.40) of the previous chapter.

11.4.1 On Fourier Transform Calculation

The evaluation of an FT on $\mathbb{Z}(T)$ requires the summation of a series, while the evaluation of the inverse requires a finite integration. Simplifications are often possible by using the general rules of Table 5.2 and also the specific rules of Sect. 11.2. When the discrete signal is obtained by a down-sampling of a continuous signal, we can use Proposition 11.1, but in this case the FT is obtained as a series (the periodic repetition), which must be summed up to get a closed-form result for $S(f)$.

In any case an efficient numerical evaluation, also valid for the inverse FT, is available by means of the FFT algorithm of Chap. 13.

UT 11.5 The z -Transform

The z -transform provides a representation of a discrete signal by a *complex function of a complex variable* $S_z(z)$, $z \in \mathbb{C}$, and it is alternative to the Fourier transform $S(f)$, $f \in \mathbb{R}/\mathbb{Z}(F_p)$. The aim of this section is to introduce the z -transform and to point out similarities and differences with respect to the FT. Although the subject is quite similar to the Laplace transform, here it will be developed autonomously.

11.5.1 Definition

A discrete-time signal $s(nT)$ can be represented by the function

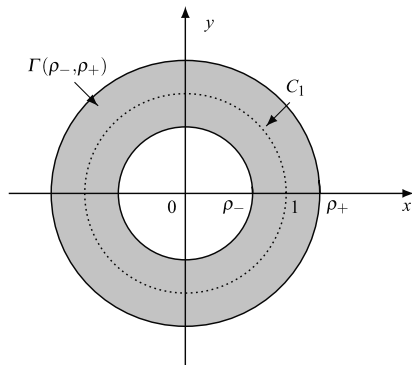
$$S_z(z) = \sum_{n=-\infty}^{+\infty} T s(nT) z^{-n}, \quad z \in \Gamma, \quad (11.22)$$

where

$$z = \rho \exp(i\theta)$$

is a complex variable, and Γ is the region of the complex plane \mathbb{C} in which the series converges (*convergence region*). The function $S_z(z)$ is called the *bilateral z -transform* of $s(nT)$. It can be proved that [2, 5]

Fig. 11.7 Generic region of convergence of z -transform



- (1) the convergence region Γ is always an *annular region* centered at the origin (Fig. 11.7)

$$\Gamma = \{\rho_- < |z| < \rho_+\} \triangleq \Gamma(\rho_-, \rho_+),$$

possibly degenerating to a disk (when $\rho_- = 0$, $0 < \rho_+ < \infty$), or to the complement of a disk (when $0 < \rho_- < \infty$, $\rho_+ = \infty$), or to the whole complex plane with the exception of the origin (when $\rho_- = 0$, $\rho_+ = \infty$).

- (2) inside the convergence region the z -transform is an *analytic function*.

The inversion formula is given by

$$s(nT) = \frac{1}{2\pi iT} \oint_{C_0} S_z(z) z^{n-1} dz, \quad nT \in \mathbb{Z}(T), \quad (11.23)$$

where C_0 is an arbitrary counterclockwise oriented closed path of the convergence region that includes the origin. Typically, C_0 is a circle of radius ρ centered at the origin with $\rho_- < \rho < \rho_+$.

To prove (11.23), we let $z = \rho e^{i2\pi fT}$ with $\rho_- < \rho < \rho_+$, and we see from (11.22) that $\tilde{S}(f) = S_z(\rho e^{i2\pi fT})$ is the FT of the discrete signal

$$\tilde{s}(nT) = \rho^{-n} s(nT). \quad (11.23a)$$

The inverse FT is (see (11.6b))

$$\tilde{s}(nT) = \int_0^{F_p} S_z(\rho e^{i2\pi fT}) e^{i2\pi f nT} df,$$

and then

$$s(nT) = \int_0^{F_p} S_z(\rho e^{i2\pi fT}) \rho^n e^{i2\pi f nT} df. \quad (11.23b)$$

This can be written as a contour integral with $z = \rho e^{i2\pi fT}$ and $dz = \rho e^{i2\pi fT} i2\pi T df = zi2\pi T df$, so that, as f varies in $[0, F_p)$, z assumes values along the circle $|z| = \rho$ counterclockwise (see Fig. 11.10), as indicated in (11.23).

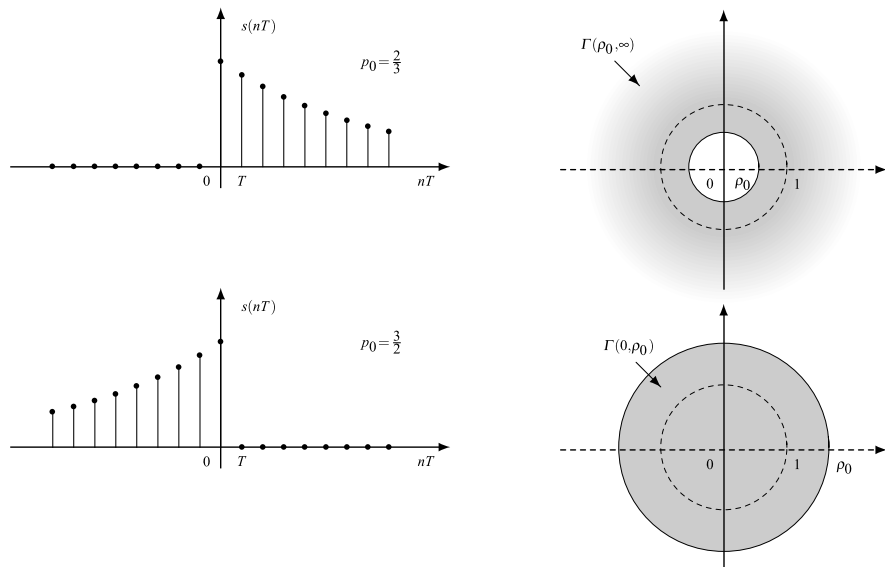


Fig. 11.8 The *causal* and *anticausal* discrete exponentials and the convergence regions of their z -transforms

11.5.2 Examples

Example 11.1 The *causal* discrete exponential (Fig. 11.8)

$$s(nT) = 1_0(nT)p_0^n,$$

where $p_0 = \rho_0 \exp(i\theta_0)$ is an arbitrary complex number, has z -transform

$$S_z(z) = T \sum_{n=0}^{\infty} (p_0 z^{-1})^n = T \frac{1}{1 - p_0 z^{-1}} \quad \text{for } |p_0 z^{-1}| < 1.$$

Then

$$1_0(nT)p_0^n \xrightarrow{z} T \frac{1}{1 - p_0 z^{-1}}, \quad z \in \Gamma(|p_0|, \infty),$$

where the convergence region Γ is the complement of a disk of a radius $\rho_0 = |p_0|$.

Example 11.2 The *anticausal* discrete exponential (Fig. 11.8) has the z -transform

$$1_0(-nT)p_0^n \xrightarrow{z} T \frac{1}{1 - p_0^{-1}z}, \quad z \in \Gamma(0, |p_0|),$$

where the convergence region is the disk with radius $\rho_0 = |p_0|$.

Example 11.3 The *bilateral* exponential

$$s(nT) = s_1(nT) + s_2(nT) = 1_0(-nT)p_1^n + 1_0(nT)p_2^n$$

has both causal and anticausal parts, having the z -transform

$$S_{z1}(z) = T \frac{1}{1 - p_1^{-1}z}, \quad z \in \Gamma(0, \rho_1), \quad \rho_1 = |p_1|,$$

$$S_{z2}(z) = T \frac{1}{1 - p_2z^{-1}}, \quad z \in \Gamma(\rho_2, \infty), \quad \rho_2 = |p_2|.$$

Then

$$S_z(z) = T \left[\frac{1}{1 - p_1^{-1}z} + \frac{1}{1 - p_2z^{-1}} \right], \quad z \in \Gamma(0, \rho_1) \cap \Gamma(\rho_2, \infty).$$

If $\rho_2 < \rho_1$, the convergence region is the annular region $\Gamma(\rho_2, \rho_1)$; if $\rho_2 \geq \rho_1$, the convergence region is empty, and the signal has no z -transform.

Example 11.4 La z -transform of the discrete step signal is

$$1_0(nT) \xrightarrow{z} T \frac{1}{1 - z^{-1}}, \quad z \in \Gamma(1, \infty),$$

while the z -transform of the *anticausal* step signal is

$$1_0(-nT) \xrightarrow{z} T \frac{1}{1 - z}, \quad z \in \Gamma(0, 1).$$

11.5.3 On the Uniqueness of the Inverse z -Transform

While the z -transform is uniquely determined by the signal, the z -transform $S_z(z)$ alone does not determine uniquely the signal. For instance, the signals (Fig. 11.9)

$$s_1(nT) = 1_0(nT)p_0^n, \quad s_2(nT) = -1_0(-nT - T)p_0^n$$

have the same z -transform $S_{z1}(z) = S_{z2}(z) = T/(1 - p_0z^{-1})$, so that the signal recovery is ambiguous. To remove the ambiguity, the function $S_z(z)$ must be considered *together with the convergence region*. In the above example the function $S_z(z)$ is the same, but the signals are distinguished by the different convergence regions, given respectively by $\Gamma_1 = \Gamma(\rho_0, \infty)$ and $\Gamma_2 = \Gamma(0, \rho_0)$ with $\rho_0 = |p_0|$.

In conclusion, a signal identifies a (z -transform, convergence region) pair, and this pair identifies a signal. In symbols,

$$s(nT) \xrightarrow{z} S_z(z), \quad z \in \Gamma, \quad S_z(z), \quad z \in \Gamma \xrightarrow{z^{-1}} s(nT).$$

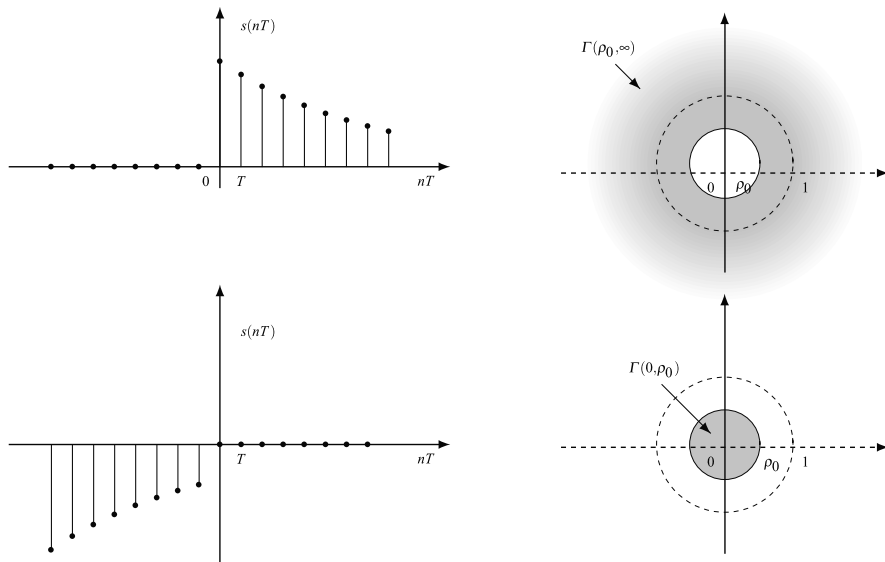


Fig. 11.9 Examples of signals with the same z-transform but different convergence regions

11.5.4 Relation with the Fourier Transform

By setting

$$z = e^{i2\pi fT} \tag{11.24}$$

in definition (11.22), one gets

$$S_z(e^{i2\pi fT}) = \sum_{n=-\infty}^{+\infty} T s(nT) e^{-i2\pi f nT} = S(f). \tag{11.25}$$

Then, the z-transform evaluated on the unit circle gives formally the FT. Analogously, if the FT is rewritten in the form

$$\tilde{S}(e^{i2\pi fT}) = \sum_{n=-\infty}^{+\infty} T s(nT) e^{-i2\pi f nT} = S(f), \tag{11.26}$$

substitution (11.24) yields $\tilde{S}(z) = S_z(z)$, and from the FT written in the form (11.26) one obtains the z-transform.

Map (11.24) relates a period of the frequency domain $\mathbb{R}/\mathbb{Z}(F_p)$ to the circle C_1 of the complex plane, as depicted in Fig. 11.10.

However, the above substitutions cannot be performed in general, and the following cases must be examined.

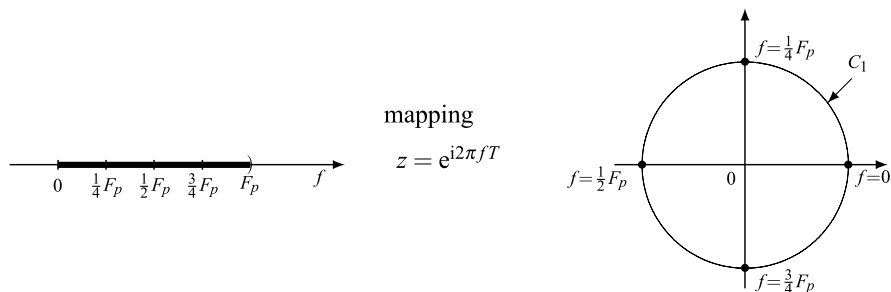


Fig. 11.10 Mapping of the frequency interval $[0, F_p]$ onto the unit circle C_1

Case 1: Both $S_z(z)$ and $S(f)$ Exist

If the convergence region Γ of the z -transform includes the circle C_1 , that is, $\rho_- < 1 < \rho_+$, then substitution (11.24) is allowed and gives the FT from the z -transform

$$\boxed{S(f) = S_z(e^{i2\pi fT})}. \tag{11.27}$$

For instance, for the discrete causal exponential, where

$$S_z(z) = T \frac{1}{1 - \rho_0 z^{-1}}, \quad z \in \Gamma(\rho_0, \infty), \tag{11.28a}$$

if $\rho_0 = |\rho_0| < 1$, the FT also exists and is obtained by using (11.27), namely

$$S(f) = \frac{1}{1 - \rho_0 \exp(-i2\pi fT)}. \tag{11.28b}$$

Condition $\rho_0 < 1$ guarantees that the exponential is sufficiently damped, as needed for the existence of the FT.

Case 2: $S_z(z)$ Exists, $S(f)$ Does Not Exist

If the convergence region does not include the circle C_1 , the z -transform exists, and the FT does not exist. In the previous example, if $\rho_0 > 1$, the z -transform exists and is given by (11.28a), whereas (11.28b) does not hold, because the exponential diverges as nT diverges. The existence of the z -transform is justified because the complex variable $z = \rho \exp(i2\pi fT)$ introduces an adequate damping

$$S_z(\rho e^{i2\pi fT}) = \sum_{n=-\infty}^{+\infty} Ts(nT)\rho^{-n}e^{-i2\pi fnT}.$$

In other words, the z -transform computes the FT of the signal $s(nT)\rho^{-n}$ instead of the signal $s(nT)$.

Case 3: $S_z(z)$ Exists, $S(f)$ Exists in a Generalized Sense

In some cases, the signal admits FT in a generalized sense, although the convergence region of the z -transform does not include the circle C_1 . In such cases, $S(f)$ cannot be obtained from $S_z(z)$ by the direct substitution (11.24). For instance, for the step signal $1_0(nT)$, we have found

$$S_z(z) = \frac{1}{1 - z^{-1}}, \quad |z| > 1,$$

$$S(f) = \frac{1}{2} \delta_{\mathbb{R}/\mathbb{Z}(F_p)}(f) + T \frac{1}{2i} \cot(\pi f T) + \frac{1}{2} T,$$

and clearly the second is not given by the mapping $z = \exp(i2\pi f T)$ of the first. The condition $|z| > 1$ excludes the circle C_1 from the convergence region. Indeed, the FT of the step signal does not exist as an ordinary function, but only as a distribution.

Case 4: $S(f)$ Exists, $S_z(z)$ Does Not Exist

On the basis of the previous cases one may think that the z -transform exists under broader conditions than the FT. However, we can give remarkable counterexamples. Let us consider the pair (15) in Table 11.1,

$$\text{sinc}(nF_0T) \xrightarrow{\mathcal{F}} (1/F_0) \text{rep}_{F_p} \text{rect}(f/F_0).$$

Now, this signal does not admit z -transform as can be proved, by contradiction, following the same argument used for the Laplace transform in Sect. 9.7: the region of convergence should include the circle C_1 , where $S_z(z) = S(e^{i2\pi f T})$, but $S(f)$ is discontinuous, while $S_z(z)$ is an analytic function, which gives the contradiction.

11.5.5 The Unilateral z -Transform

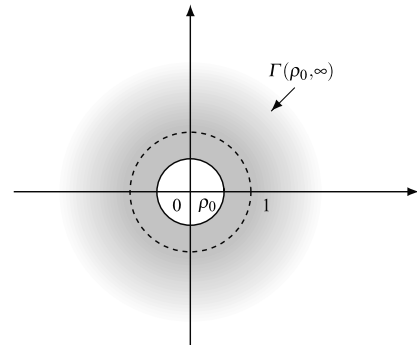
The z -transform is traditionally introduced in the *unilateral* form as

$$S_z(z) = \sum_{n=0}^{\infty} Ts(nT)z^{-n}, \quad z \in \Gamma. \quad (11.29)$$

Conceptually, the *bilateral* form (11.22) is preferable for its generality, because it can be considered for every discrete-time signal, whereas the unilateral form (11.29) can be applied only to *causal* signals. The causality of the signal has a consequence on the convergence region, which becomes the region outside a disk centered at the origin, $\Gamma = \Gamma(\rho_0, \infty)$, as shown in Fig. 11.11.

With these peculiarities, the unilateral z -transform can be perfectly framed into the more general bilateral z -transform, even though some attention must be paid in the application of some rules (as the time-shift rule).

Fig. 11.11 Typical convergence region of the unilateral z -transform



11.5.6 Comparison with the Fourier Transform

Substantially we can repeat what reported in the previous chapter on the comparison between Fourier and Laplace transforms. Both the Fourier and the z -transform are widely used in the study of discrete-time signals and systems, and they exhibit some advantages and some drawbacks.

In the analysis of signals not related to systems, the FT may be preferred for its capability of representing signals on the whole time axis, whereas the z -transform is more suitable to represent causal signals. Moreover, the FT has the important advantage of operating with functions of a real variable, with the precise physical meaning of *frequency*. Also, in the computer signal processing the FT is preferred, since operating with complex variables is more computationally expensive.

In the study of discrete-time systems, circuits and controls the z -transform is preferred for its remarkable properties (analyticity, residue theorem) and can be profitably used. In particular, in circuit synthesis and in stability analysis the use of the z -transform becomes mandatory.

UT 11.6 Properties of the z -Transform

11.6.1 General Properties

The properties of the z -transform are analogous to the properties of the Fourier transform and mostly of the Laplace transform. The main properties are due to the separability of the kernel

$$z^{(n_1+n_2)} = z^{n_1} z^{n_2},$$

which converts a *convolution* in one domain into a product in the dual domain. The main difference is that the z -transform operates with a complex variable, whereas the Fourier transform operates with a real variable. We have seen that, to remove the ambiguity of the signal recovery from the z -transform, the specification of the convergence region is required.

Table 11.2 General rules of z -transform

Rule	Signal	z transform
1. linearity	$a_1s_1(nT) + a_2s_2(nT)$	$a_1S_{1z}(z) + a_2S_{2z}(z)$
2(a). time reversal	$s(-nT)$	$S_z(z^{-1}), z \in \Gamma'_s \quad \Gamma'_s \triangleq \Gamma_s(1/\rho_+, 1/\rho_-)$
2(b). z reversal	$(-1)^n s(nT)$	$S_z(-z), z \in \Gamma_s$
3. conjugate	$s^*(nT)$	$S_z^*(z^*), z \in \Gamma_s$
4. real part	$\Re s(nT) = \frac{1}{2}[s(nT) + s^*(nT)]$	$\frac{1}{2}[S_z(z) + S_z^*(z^*)], z \in \Gamma_s$
5. imaginary part	$\Im s(nT) = \frac{1}{2}[s(nT) - s^*(nT)]$	$\frac{1}{2}[S_z(z) - S_z^*(z^*)], z \in \Gamma_s$
6. even part	$\frac{1}{2}[s(nT) + s(-nT)]$	$\frac{1}{2}[S_z(z) + S_z(z^{-1})], z \in \Gamma_s \cap \Gamma'_s$
7. odd part	$\frac{1}{2}[s(nT) - s(-nT)]$	$\frac{1}{2}[S_z(z) - S_z(z^{-1})], z \in \Gamma_s \cap \Gamma'_s$
8. shift	$s(nT - n_0T)$	$z^{-n_0} S_z(z)$
9. multiplic. by p_0^n	$p_0^n s(nT)$	$S_z(\frac{z}{p_0}), z \in \Gamma(p_0 \rho_-, p_0 \rho_+)$
10. running sum	$\sum_{k=-\infty}^n T s(kT)$	$T \frac{1}{1-z^{-1}} S_z(z)$
11. multiplic. by n	$ns(nT)$	$-z \frac{dS_z(z)}{dz}$
12(a). time convolution	$x * y(nT)$	$X_z(z)Y_z(z), z \in \Gamma_x \cap \Gamma_y$
12(b). z convolution	$x(nT)y(nT)$	$X_z * Y_z(z)$

Note: convolution in z : $X_z * Y_z(z) = \frac{1}{i2\pi T} \oint_{C_0} X_z(q)Y_z(\frac{z}{q}) \frac{dq}{q}, z \in \Gamma(\rho_x - \rho_y, \rho_x + \rho_y)$

The rules of the z -transform are collected in Table 11.2. We remark that most rules should require a specific examination, in particular with regards to the convergence region. There are *other rules*, similar to the ones seen for the Fourier transform. For instance, the rule giving the signal area in terms of the z transform is $\text{area}(s) = S_z(1)$, while the Parseval theorem is expressed in the form

$$E_{xy} = \sum_{n=-\infty}^{+\infty} T x(nT)y^*(nT) = \frac{1}{i2\pi T} \oint_{C_0} X(z)Y^*\left(\frac{1}{z^*}\right) \frac{dz}{z}. \tag{11.30}$$

Table 11.3 collects some remarkable examples of z -transforms.

11.6.2 On the Inversion Formula

The evaluation of the inverse z -transform according to (11.23) requires the computation of an integral along a closed path inside the convergence region. This may be very complicated, at least in general. A powerful tool is given by the Cauchy theorem on analytic functions, which allows the calculation through *residues*. In particular, from (11.23) one gets [5]

$$s(nT) = \frac{1}{i2\pi T} \Sigma \{ \text{residues di } S_z(z)z^{n-1} \text{ for poles inside } C_1 \}.$$

Table 11.3 Examples of z -transforms pairs

Signal	z transform	Convergence region
$\delta(nT)$	1	$\Gamma[0, \infty)$
$\delta(nT - n_0T)$	Tz^{-n_0}	$\Gamma(0, \infty), n_0 > 0$ $\Gamma[0, \infty), n_0 \leq 0$
$1_0(nT)$	$T \frac{1}{1-z^{-1}}$	$\Gamma(1, \infty)$
$1_0(-(n+1)T)$	$T \frac{1}{1-z^{-1}}$	$\Gamma(0, 1)$
$1_0(-nT)$	$T \frac{1}{1-z}$	$\Gamma(0, 1)$
$p_0^n 1_0(nT)$	$T \frac{1}{1-p_0z^{-1}}$	$\Gamma(p_0 , \infty)$
$p_0^n 1_0(-nT)$	$T \frac{1}{1-p_0z}$	$\Gamma(0, p_0 ^{-1})$
$np_0^n 1_0(nT)$	$T \frac{pz^{-1}}{(1-p_0z^{-1})^2}$	$\Gamma(p_0 , \infty)$
$n^2 p_0^n 1_0(nT)$	$T \frac{p_0z^{-1}(1+p_0z^{-1})}{(1-p_0z^{-1})^3}$	$\Gamma(p_0 , \infty)$
$\cos \omega_0 nT 1_0(nT)$	$T \frac{1 - (\cos \omega_0 T)z^{-1}}{1 - (2 \cos \omega_0 T)z^{-1} + z^{-2}}$	$\Gamma(1, \infty)$
$\sin \omega_0 nT 1_0(nT)$	$T \frac{\sin \omega_0 T z^{-1}}{1 - (2 \cos \omega_0 T)z^{-1} + z^{-2}}$	$\Gamma(1, \infty)$
$(-1)^{n+1} \frac{p_0^n}{n} 1_0(nT - T)$	$T \log(1 + p_0 z^{-1})$	$\Gamma(p_0 , \infty)$
$1_0(nT) - 1_0(nT - NT)$	$T \frac{1-z^{-N}}{1-z^{-1}}$	$\Gamma(0, \infty)$

This approach is quite easily practicable if $S_z(z)$ is a rational function, but can be used more generally.

For rational functions, we may apply other techniques, as the partial *fraction expansion*, which allows one to express the z -transform as the sum of simple terms, whose inverse transforms are causal exponential signals or, more generally, of the form [3]

$$s_k(nT) = 1_0(nT)n^m p_k^n \quad \text{with } m = 0, 1, 2, \dots$$

11.6.3 Relation with the Laplace Transform

When a discrete signal $y(t), t \in \mathbb{Z}(T)$, is obtained by down-sampling a continuous signal $x(t), t \in \mathbb{R}$, it is possible to relate the z -transform $Y_z(z)$ of $y(t)$ to the Laplace transform $X_L(p)$ of $x(t)$. In principle, the relations are given by the graph

$$\begin{aligned}
 X_L(p), \quad p \in \Gamma &\xrightarrow{\mathcal{L}^{-1}} x(t), \quad t \in \mathbb{R}, \\
 y(t) = x(t), \quad t \in \mathbb{Z}(T) &\xrightarrow{z} Y_z(z), \quad z \in \Gamma_z,
 \end{aligned}
 \tag{11.31}$$

where $X_L(p)$ is given, and the first step consists in the evaluation of $x(t)$ as the inverse Laplace transform of $X_L(p)$. Then, the down-sampling gives $y(t), t \in \mathbb{Z}(T)$,

and, finally, the z -transform $Y_z(z)$ is computed. Considering that the inverse Laplace transform is given by (9.48), we find

$$Y_z(z) = \sum_{n=-\infty}^{+\infty} \frac{T}{i2\pi} \int_{\Sigma-i\infty}^{\Sigma+i\infty} X_L(p) (e^{pT} z^{-1})^n dp, \quad (11.32)$$

where in general it is not possible to exchange the order of the summation and of the integral.

A more explicit result is obtained passing through the Fourier transform, where the time down-sampling becomes a periodic repetition, namely

$$Y(f) = \sum_{k=-\infty}^{+\infty} X(f - kF_p), \quad F_p = 1/T.$$

Hence, considering that $X_L(p) = X(p/i2\pi)$ and writing $Y(f)$ in the exponential form (11.26), we obtain

$$\tilde{Y}(e^{i2\pi fT}) = \sum_{k=-\infty}^{+\infty} X_L(i2\pi f - i2\pi kF_p).$$

Finally, the substitutions $i2\pi f = p$, $z = e^{i2\pi fT} = e^{pT}$ yield

$$Y_z(z) = \sum_{k=-\infty}^{+\infty} X_L(p - i2\pi kF_p), \quad z = e^{pT}. \quad (11.33)$$

Thus, given the Laplace transform $X_L(p)$, we evaluate the right-hand side in (11.33), and then, in the result, we set $e^{pT} = z$.

This method has the advantage of relating the complex planes p and z by $z = e^{pT}$, but its implementation is not straightforward, and (11.32) is often preferable.

Example 11.5 Consider the Laplace pair

$$x(t) = 1(t)t \xrightarrow{\mathcal{L}} X_L(p) = \frac{1}{p^2}, \quad p \in \mathbb{C}(0, +\infty).$$

Now, to get the z -transform of the down-sampled version $y(nT) = 1(nT)nT = 1_0(nT)nT$, according to (11.33), we have to evaluate

$$Y_z(z) = \sum_{k=-\infty}^{+\infty} \frac{1}{(p - i2\pi kF_p)^2} = \sum_{k=-\infty}^{+\infty} \frac{T^2}{(pT - i2\pi k)^2}.$$

The sum of this series can be found in specialized textbooks (see, e.g., [4]), but this seems to be a lucky case. Instead, using (11.31), we get directly

$$Y_z(z) = T^2 \frac{z^{-1}}{(1 - z^{-1})^2}, \quad |z| > 1.$$

UT 11.7 Filters on $\mathbb{Z}(T)$

Filters for discrete-time signals were introduced at the end of Chap. 2 and developed in a general way at the end of Chap. 6. In this section we give some further insight.

As in the general case, a filter on $\mathbb{Z}(T)$ can be specified by its *impulse response* $g(nT)$, $nT \in \mathbb{Z}(T)$, or by its *frequency response* $G(f)$, $f \in \mathbb{R}/\mathbb{Z}(F_p)$, usually expressed in terms of amplitude and phase: $A_G(f) = |G(f)|$ and $\beta_G(f) = \arg G(f)$. Because of the periodicity of $G(f)$, the specification can be confined to the fundamental band $\mathcal{B} = [0, F_p)$ and, if the filter is *real*, to the nonnegative half-band $\mathcal{B}_0 = [0, \frac{1}{2}F_p)$. An alternative specification is given by the *transfer function*, $G_z(z)$, $z \in \Gamma$, defined as the z -transform of the impulse response. Thus, we have three different ways of specification. In particular, if Γ includes the circle C_1 , from the transfer function one obtains the frequency response, according to (see (11.27))

$$G(f) = G_z(e^{i2\pi fT}). \quad (11.34)$$

We recall that the input–output relation is given by the convolution

$$y(nT) = \sum_{k=-\infty}^{+\infty} T g(nT - kT)x(kT),$$

which leads to the following expressions in the f and z domains

$$Y(f) = G(f)X(f), \quad Y_z(z) = G_z(z)X_z(z).$$

11.7.1 Discrete Exponential Regime

As in the continuous case, the exponentials are still filter *eigenfunctions* in the discrete case (see Sect. 5.2). Consequently, the application of the discrete exponential

$$x(nT) = X e^{i2\pi f nT} \quad (11.35a)$$

gives at the output an exponential with the same frequency and with corresponding eigenvalue given by the frequency response, namely

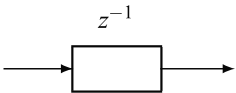
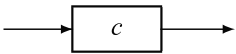
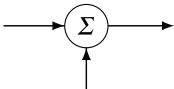
$$y(nT) = Y e^{i2\pi f nT} \quad \text{with } Y = G(f)X. \quad (11.35b)$$

Then, the exponential regime allows the identification of the frequency response in a very simple way, as the ratio

$$G(f) = Y/X, \quad (11.35c)$$

where X is the (arbitrary) complex amplitude of the input, and Y is the corresponding complex amplitude of the output. The ratio gives the frequency response evaluated at the same frequency of the exponential.

Table 11.4 Discrete filter components

Component	Graphic symbol	Relationship	Symbolic relationship
Elementary delay		$y_n = x_{n-1}$	$Y(z) = z^{-1} X(z)$
Multiplier by c		$y_n = cx_n$	$Y(z) = cX(z)$
Adder		$s_n = x_n + y_n$	$S(z) = X(z) + Y(z)$

More generally, the input exponential may have the form

$$x(nT) = Xz^n, \quad z \in \Gamma, \tag{11.35d}$$

which is again an eigenfunction, and, therefore, the output results in

$$y(nT) = Yz^n \quad \text{with } Y = G_z(z)X. \tag{11.35e}$$

In such a way we identify the transfer function $G_z(z)$, $z \in \Gamma$, where the convergence region Γ is given by all the values of z for which the response Yz^n has finite amplitude.

11.7.2 Causality Condition and Realizable Filters

In the time domain the causality condition is very simple: $g(nT) = 0, n < 0$. On the contrary, it becomes somewhat complicated in the frequency domain. For a thorough discussion of the topic, we refer the reader to [2]. Anyway, the causality condition leads to link the amplitude $A_G(f)$ to the phase $\beta_G(f)$, so that they cannot be chosen independently.

For discrete causal filters, we make a distinction between *finite* impulse response (FIR) and *infinite* impulse response (IIR).¹ FIR filters have impulse response with a limited extension, $e(g) = \{0, T, \dots, (N - 1)T\}$, whereas the extension of IIR filters is upper unbounded.

The discrete-time filters with constant parameters can be implemented by combining the components of Table 11.4, as we now illustrate with some simple examples.

¹This distinction could be made for continuous-time filters too, but only in the discrete case we can implement FIR filters, whereas they are not realizable in the continuous case with the standard components (R, L, C), but require “distributed” components, as lines, coaxial cables, etc.

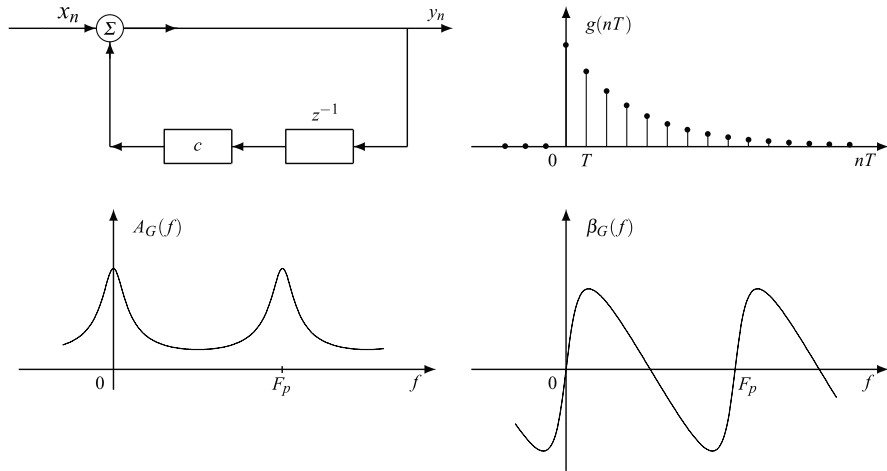


Fig. 11.12 First-order IIR filter and corresponding impulse and frequency responses

11.7.3 Example of IIR Filter

Figure 11.12 shows an example of a *first-order* IIR filter (the order is the number of elementary delays). Here, it is convenient to use the compact notation $s_n = s(nT)$. Then, for this filter, we find the relations

$$y_n = cs_n + x_n, \quad s_n = y_{n-1},$$

which give

$$y_n = cy_{n-1} + x_n, \tag{11.36}$$

where the output at time n depends on both the output at time $n - 1$ and the input at time n . This is a *finite difference* recursive equation, which can be solved analogously to a differential equation. The solution by means of the exponential regime is straightforward. Letting $x_n = Xz^n$ and $y_n = Yz^n$, from (11.36) we obtain

$$Yz^n = cYz^{n-1} + Xz^n,$$

that is, $Y = cYz^{-1} + X$. Hence, the transfer function is given by

$$G_z(z) = \frac{Y}{X} = \frac{1}{1 - cz^{-1}}, \quad z \in \Gamma(|c|, \infty).$$

If $|c| < 1$, the convergence region includes the circle C_1 , and the transfer function gives the frequency response with $z = \exp(i2\pi fT)$. The inverse transform gives the impulse response, specifically (see (11.28a))

$$g_n = g(nT) = (1/T)1_0(nT)c^{n/T}.$$

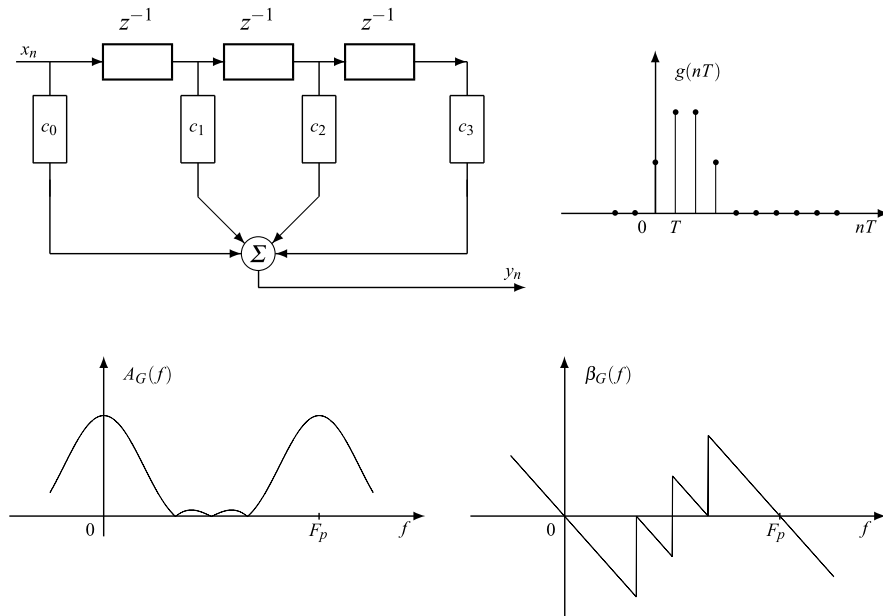


Fig. 11.13 Third-order FIR filter and its impulse and frequency responses

This signal has extension $e(g) = \{0, T, 2T, \dots\}$, and therefore the filter is IIR.

Figure 11.12 shows the impulse response and the frequency response, in terms of amplitude and phase, for $c = 1/2$.

11.7.4 Example of FIR Filters

Figure 11.13 shows an example of a *third-order* FIR filter. Proceeding as above, one gets the difference equation

$$y_n = c_0x_n + c_1x_{n-1} + c_2x_{n-2} + c_3x_{n-3},$$

which is nonrecursive, because the output y_n depends only on the input values $x_n, x_{n-1}, x_{n-2}, x_{n-3}$. In the exponential regime for the complex amplitude we obtain

$$Y = (c_0 + c_1z^{-1} + c_2z^{-2} + c_3z^{-3})X,$$

and therefore

$$G_z(z) = c_0 + c_1z^{-1} + c_2z^{-2} + c_3z^{-3}, \quad z \neq 0.$$

By inverse transforming one gets the impulse response

$$g_n = \begin{cases} c_n/T, & n = 0, 1, 2, 3, \\ 0 & \text{elsewhere,} \end{cases}$$

whose extension $e(g) = \{0, T, 2T, 3T\}$ confirms that the filter is FIR.

11.7.5 Ideal Filters

In the discrete case we find the same types of ideal filters as in the continuous case, i.e., (1) *low-pass* filter, (2) *band-pass* filter, and (3) *high-pass* filter. Their frequency responses are obtained as periodical repetitions of the frequency response of the corresponding continuous filters (see Sect. 6.15 for a general formulation of ideal filters). We recall that ideal filters *do not admit transfer function* (see Sect. 11.5).

The discrete low-pass filter has the frequency response

$$G(f) = \text{rep}_{F_p} \text{rect}(f/(2B)), \quad (11.37)$$

where the *band* B is constrained by $B < \frac{1}{2}F_p$.

As a limiting case, one obtains *all-pass filters*. In particular, the frequency response

$$G(f) = A_0 e^{-i2\pi f t_0}, \quad f \in \mathbb{R}/\mathbb{Z}(T_p), \quad t_0 \in \mathbb{Z}(T),$$

represents an all-pass filter satisfying, for any $A_0 \neq 0$ and $t_0 \in \mathbb{Z}(T)$, the Heaviside conditions (see Sect. 6.15). Another ideal filter is the *phase shifter*, which has unitary amplitude $A_G(f) = 1$ and a given phase characteristic $\beta_G(f) = \beta_0(f)$. For the sake of compatibility on $\mathbb{Z}(T)$, $\beta_0(f)$ must be periodic with period F_p . In particular, a *real* ideal shifter with a constant shift β_0 has phase characteristic that must be an odd function of f (for the Hermitian symmetry of $G(f)$) and can be written in the form

$$\beta_G(f) = \beta_0 \text{sgn}(f), \quad |f| < F_p/2. \quad (11.38)$$

11.7.6 The Discrete Hilbert Transform

The Hilbert transform $\widehat{s}(nT)$ of a discrete signal $s(nT)$ can be defined as *the response to $s(nT)$ of a real phase-shifter of $-\pi/2$* (discrete Hilbert filter). Hence, the definition is exactly the same as in the continuous case (see Sect. 9.10), but with the constraint imposed by the periodicity in the frequency domain. Then, the discrete Hilbert filter has frequency response (Fig. 11.14)

$$G_H(f) = -i \text{sgn}(f), \quad f \in \mathcal{B}_c = \left[-\frac{1}{2}F_p, \frac{1}{2}F_p \right) \quad (11.39a)$$

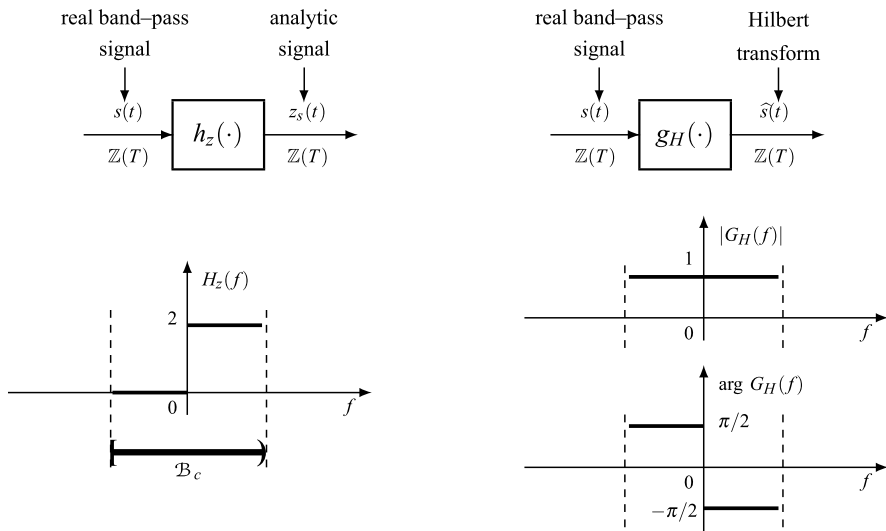


Fig. 11.14 Filters giving the discrete *analytic signal* and *Hilbert transform*. The specification coincides with the continuous case in the centered band \mathcal{B}_c (see Fig. 9.24) but is extended by periodicity outside

which is extended by periodicity outside \mathcal{B}_c . The corresponding impulse response results in

$$g_H(nT) = \begin{cases} 0, & n \text{ even,} \\ \frac{2}{\pi nT}, & n \text{ odd.} \end{cases} \tag{11.39b}$$

In conclusion, the discrete Hilbert transform is given by

$$\widehat{s}(nT) = \sum_{k=-\infty}^{+\infty} \frac{2}{\pi(2k+1)} s(nT - (2k+1)T). \tag{11.40}$$

From the Hilbert transform the signal recovery is obtained by a *real phase-shifter* of $\pi/2$, whose impulse response is $-g_H(nT)$. Then the inverse discrete Hilbert transform is

$$s(nT) = - \sum_{k=-\infty}^{+\infty} \frac{2}{\pi(2k+1)} \widehat{s}(nT - (2k+1)T). \tag{11.41}$$

The perfect analogy with the continuous case can be extended to the analytic signal (see Sect. 9.10). Then the analytic signal² of a discrete signal $s(nT)$ is the

²“Analytic” is only used for analogy with the continuous case, since analytic functions are not defined on a discrete domain.

response $z_s(nT)$ of the filter

$$H_z(f) = 21(f), \quad f \in \mathcal{B}_c = \left[-\frac{1}{2}F_p, \frac{1}{2}F_p \right), \quad (11.42)$$

that is, with the same frequency response as in the continuous case, but limited to the fundamental band \mathcal{B}_c . This filter cuts the negative frequency components and doubles the positive frequency components, where the frequencies are confined to \mathcal{B}_c , where $(-\frac{1}{2}F_p, 0)$ gives the negative frequencies and $(0, \frac{1}{2}F_p)$ the positive frequencies. Following this line, we can state the properties seen in the continuous case (see Table 9.6), in particular, the relation $z_v(t) = s(t) + \widehat{1s}(t)$.

UT 11.8 Interpolators and Decimators

The increasing importance of discrete-time signal processing motivates a deeper understanding on interpolators and decimators, introduced in Chap. 6 in a general form. In the 1D case, the analysis can be carried out in the time and frequency domains, but also in the z -domain. We shall use the notation

$$T = NT_0, \quad F = 1/T, \quad F_0 = 1/T_0 = NF,$$

and sometimes we call F the *low rate* and F_0 the *high rate* (in values per second). For the z -variable, we use the notation z for signals on $\mathbb{Z}(T)$ and z_0 for signals on $\mathbb{Z}(T_0)$; then in the unit circle

$$z_0 = e^{i2\pi fT_0} \quad \text{and} \quad z = e^{i2\pi fT} = z_0^N. \quad (11.43)$$

The main goal of this section is to establish the z -domain relations, whereas time and frequency domain analysis (already seen in the general case) will be given for completeness. Following the Decomposition Theorem, we begin with the analysis of filters, up-samplers and down-samplers, and then we obtain the analysis of interpolators and decimators by composition of the results.

11.8.1 Filters, Up-Samplers and Down-Samplers

For a filter on $\mathbb{Z}(T_0)$, the z -domain relation is given by

$$\boxed{Y_z(z_0) = G_z(z_0)X_z(z_0), \quad \Gamma_y = \Gamma_g \cap \Gamma_x,}$$

where $G_z(z_0)$ is the transfer function of the filter.

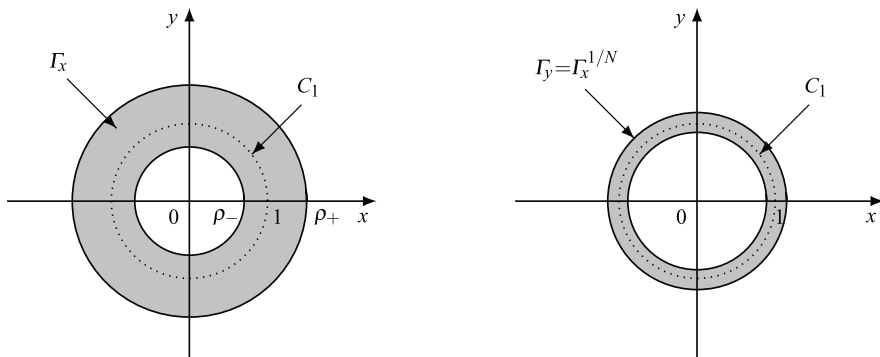


Fig. 11.15 Convergence regions in an down-sampler with rate ratio $N = 3$

Up-Samplers

For a $\mathbb{Z}(T) \rightarrow \mathbb{Z}(T_0)$ up-sampler, the input-output relation is given by

$$y(nT_0) = \begin{cases} Nx(nT_0), & n \in \mathbb{Z}(N), \\ 0 & \text{elsewhere,} \end{cases}$$

where $N = T/T_0 = F_0/F$ is the rate ratio. Then, applying the z -transform, we find

$$\begin{aligned} Y_z(z_0) &= \sum_{n=-\infty}^{+\infty} T_0 y(nT_0) z_0^n = \sum_{m=-\infty}^{+\infty} NT_0 x(mNT_0) z_0^{-mN} \\ &= \sum_{m=-\infty}^{+\infty} T x(mT) z_0^{-mN} = X_z(z_0^N). \end{aligned}$$

If the convergence region of the input is $\Gamma_x = \Gamma(\rho_-, \rho_+) = \{\rho_- < |z| < \rho_+\}$, then the convergence region of the output is

$$\Gamma_y = \{\rho_- < |z_0^N| < \rho_+\} = \{\rho_-^{1/N} < |z_0| < \rho_+^{1/N}\} \triangleq \Gamma_x^{1/N},$$

where the notation $\Gamma_x^{1/N}$ is not ambiguous since the N th root is applied to the radii ρ_- and ρ_+ . Figure 11.15 shows the effect of this operation for an annular region Γ_x containing the unit circle C_1 .

In conclusion, for an up-sampler, the complete relation is

$$\boxed{Y_z(z_0) = X_z(z_0^N), \quad \Gamma_y = \Gamma_x^{1/N}.} \tag{11.44}$$

In the frequency domain we found simply $Y(f) = X(f)$, which is less expressive than (11.44), where the rate change appears explicitly.

Down-Samplers

For a $\mathbb{Z}(T_0) \rightarrow \mathbb{Z}(T)$ down-sampler with $T = NT_0$, the input–output relation is simply $y(nT) = x(nT)$. The relation in the frequency domain is given by (6.80), namely

$$Y(f) = \sum_{k=0}^{N-1} X(f - kF), \quad f \in \mathbb{R}/\mathbb{Z}(F), \quad (11.45)$$

where $X(f)$, $f \in \mathbb{R}/\mathbb{Z}(NF)$, and $Y(f)$, $f \in \mathbb{R}/\mathbb{Z}(F)$. Now, we use this relation to pass to the z -domain by replacing the argument f of the FTs by appropriate exponentials (see (11.26)), that is, $e^{i2\pi fT}$ or $e^{i2\pi fT_0}$ in dependence of the rate. In (11.45), $Y(f)$ refers to a low rate, and $X(f)$ to a high rate. Thus, we obtain

$$\tilde{Y}(e^{i2\pi fT}) = \sum_{k=0}^{N-1} \tilde{X}(e^{i2\pi(f-kF)T_0}) = \sum_{k=0}^{N-1} \tilde{X}(e^{i2\pi fT_0} W_N^{-k}), \quad W_N = e^{i2\pi/N}.$$

Finally, we replace the exponentials with the variables z_0 and $z = z_0^N$ (see (11.43)), and we find

$$Y_z(z_0^N) = \sum_{k=0}^{N-1} X_z(z_0 W_N^{-k}). \quad (11.46)$$

It remains to relate the convergence regions. The input and output z -transforms are respectively

$$X(z_0) = \sum_{n=-\infty}^{+\infty} T_0 x(nT_0) z_0^{-n}, \quad Y(z) = \sum_{m=-\infty}^{+\infty} T y(mT) z^{-m},$$

with $mT = nNT_0$ and $z = z_0^N$. Clearly, the second series is obtained by dropping summation terms from the first (apart from a scale factor). Now, if the first series converges at the point z_0 , that is, $z_0 \in \Gamma_x = \{\rho_- < z_0 < \rho_+\}$, then also the second converges³ at $z = z_0^N$, but $Y(z)$ may also converge at other values of z not belonging to Γ_x . Then, $\Gamma_y \supseteq \{\rho_- < |z_0| < \rho_+\} = \{\rho_-^N < z_0^N < \rho_+^N\} \triangleq \Gamma_x^N$. In conclusion, after a down-sampling we find

$$\Gamma_y \supseteq \Gamma_x^N. \quad (11.47)$$

Figure 11.16 shows the region Γ_x^N when Γ_x contains the unit circle C_1 .

³We recall that in the z -transform the convergence region is determined by the *absolute convergence*. Otherwise, with ordinary convergence, dropping of series terms might have unpredictable effects on the series sum.

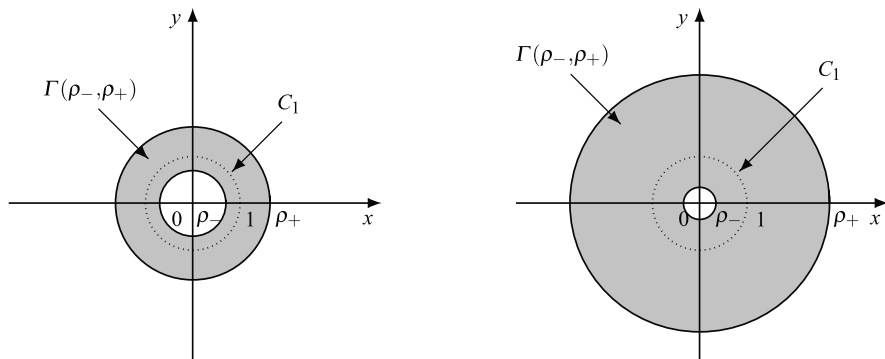


Fig. 11.16 Convergence regions in an down-sampler with rate ratio $N = 3$

Remark 11.1 It is easy to find examples in which $\Gamma_y \supset \Gamma_x^N$ (in the strict sense), but in the important case of rational functions the equality $\Gamma_y = \Gamma_x^N$ always holds (see Problem 11.12).

11.8.2 Interpolators

In a $\mathbb{Z}(T) \rightarrow \mathbb{Z}(T_0)$ interpolator the input is low-rate, $F = 1/T$, and the output is high-rate, $F_0 = NF$, according to the relation

$$y(nT_0) = \sum_{k=-\infty}^{+\infty} Tg(nT_0 - kT)x(kT), \tag{11.48}$$

where the impulse response $g(mT_0)$ is high-rate.

In the frequency domain we simply find

$$Y(f) = G(f)X(f), \quad f \in \mathbb{R}/\mathbb{Z}(F_0), \tag{11.49}$$

where $X(f)$ has period F , while $G(f)$ and $Y(f)$ have period $F_0 = NF$. The above relations are illustrated in Fig. 11.17 for $N = 3$.

To get the relation in the z -domain, we use the Decomposition Theorem, which states that a $\mathbb{Z}(T) \rightarrow \mathbb{Z}(T_0)$ interpolator can be decomposed into an up-sampler followed by a filter on $\mathbb{Z}(T_0)$ (Fig. 11.18). Then, denoting by $\bar{y}(nT_0)$ the intermediate signal and using the previous results, we find

$$\begin{aligned} \bar{Y}_z(z_0) &= X_z(z_0^N), & \Gamma_{\bar{y}} &= \Gamma_x^{1/N}, \\ Y_z(z_0) &= G_z(z_0)\bar{Y}_z(z_0), & \Gamma_y &= \Gamma_g \cap \Gamma_{\bar{y}}. \end{aligned}$$

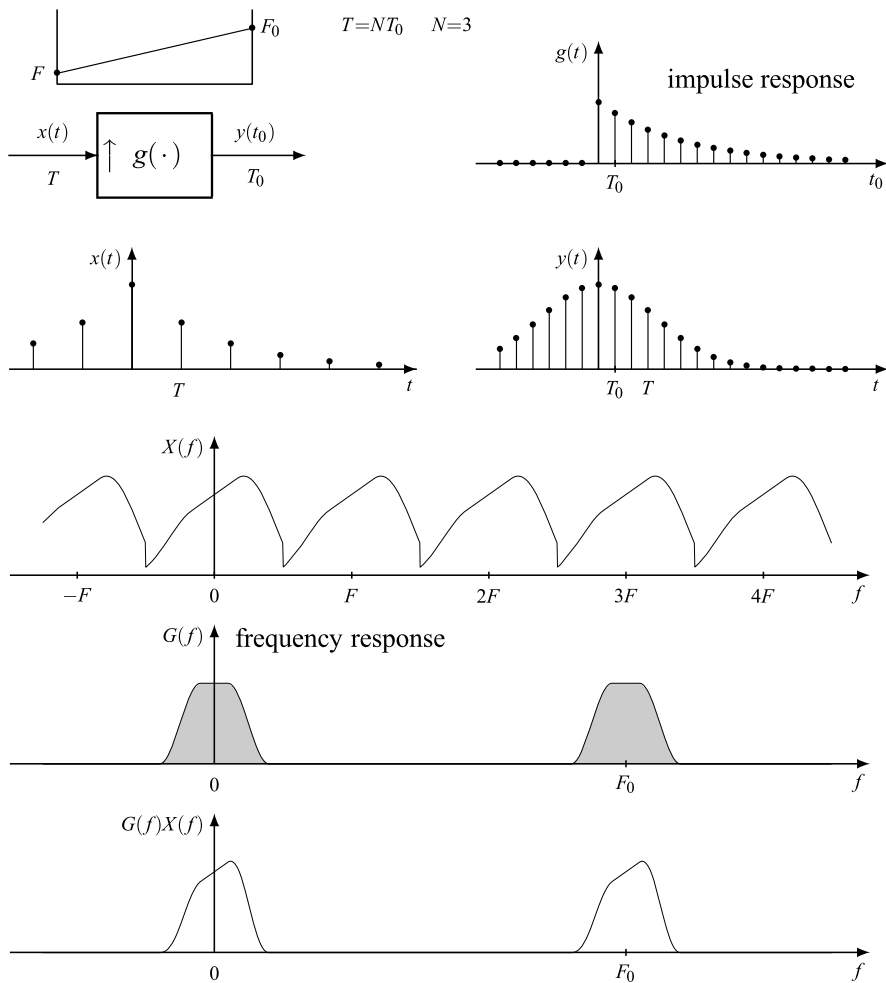


Fig. 11.17 Signals and Fourier transforms in a $\mathbb{Z}(T) \rightarrow \mathbb{Z}(T_0)$ interpolator

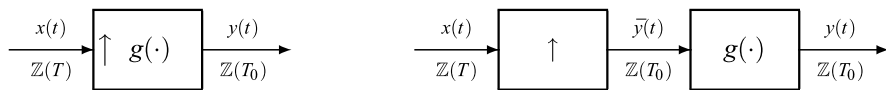


Fig. 11.18 Decomposition of a $\mathbb{Z}(T) \rightarrow \mathbb{Z}(T_0)$ interpolator

By combination, the following z -transform relation is obtained:

$$Y_z(z_0) = G_z(z_0)X(z_0^N), \quad \Gamma_y = \Gamma_g \cap \Gamma_x^{1/N}, \quad (11.50)$$

where $G_z(z_0)$ is the *transfer function* of the interpolator.

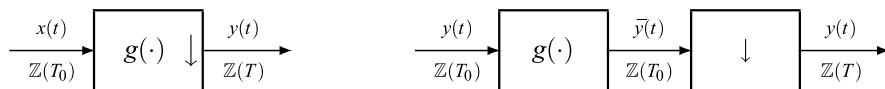


Fig. 11.19 Decomposition of a $\mathbb{Z}(T_0) \rightarrow \mathbb{Z}(T)$ decimator

11.8.3 Decimators

In a $\mathbb{Z}(T_0) \rightarrow \mathbb{Z}(T)$ decimator the input is high-rate and the output is low-rate according to the relation

$$y(nT) = \sum_{k=-\infty}^{+\infty} T_0 g(nT - kT_0)x(kT_0),$$

where the impulse response $g(mT_0)$ is high-rate. The corresponding relation in the frequency domain was established and discussed in Sect. 6.14.

To get the relation in the z -domain, we use the Decomposition Theorem, which states that a $\mathbb{Z}(T_0) \rightarrow \mathbb{Z}(T)$ decimator can be decomposed into a filter on $\mathbb{Z}(T_0)$, followed by a $\mathbb{Z}(T_0) \rightarrow \mathbb{Z}(T)$ down-sampler (Fig. 11.19). Thus, denoting the intermediate signal by $\bar{y}(t)$, one gets

$$\begin{aligned} \bar{Y}_z(z_0) &= G_z(z_0)Z_z(z_0), & \Gamma_{\bar{y}} &= \Gamma_g \cap \Gamma_x, \\ Y_z(z_0^N) &= \sum_{k=0}^{N-1} \bar{Y}_z(z_0 W_N^{-k}), & \Gamma_y &\supseteq \Gamma_{\bar{y}}^N, \end{aligned}$$

and by combination

$$\boxed{Y_z(z_0^N) = \sum_{k=0}^{N-1} G_z(z_0 W_N^{-k})X_z(z_0 W_N^{-k}), \quad \Gamma_y \supseteq (\Gamma_g \cap \Gamma_x)^N,} \tag{11.51}$$

where $G_z(z_0)$ is the *transfer function* of the decimator.

11.8.4 Fractional Interpolators

A $\mathbb{Z}(T_1) \rightarrow \mathbb{Z}(T_2)$ fractional interpolator, with $T_1 = N_1 T_0$, $T_2 = N_2 T_0$, and N_1, N_2 coprime, has the following input–output relation

$$y(nT_2) = \sum_{k=-\infty}^{+\infty} T_1 g(nT_1 - kT_2)x(kT_1),$$

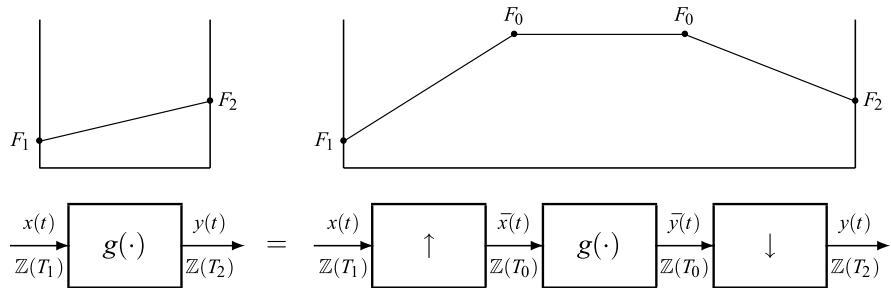


Fig. 11.20 Decomposition of a fractional interpolator

where the input has rate $F_1 = 1/T_1 = F_0/N_1$, the output has rate $F_2 = 1/T_2 = F_0/N_2$, and the impulse response $g(mT_0)$ has the high rate F_0 . The frequency-domain relation was discussed in Sect. 6.14.

To establish the z -relation, we apply the Decomposition Theorem, which states that a $\mathbb{Z}(T_1) \rightarrow \mathbb{Z}(T_2)$ interpolator can be decomposed into a $\mathbb{Z}(T_1) \rightarrow \mathbb{Z}(T_0)$ up-sampler, a filter on $\mathbb{Z}(T_0)$, and a final $\mathbb{Z}(T_0) \rightarrow \mathbb{Z}(T_2)$ down-sampler (Fig. 11.20). Denoting the intermediate signals by $\bar{x}(nT_0)$ and $\bar{y}(nT_0)$, we find the following relations for the three stages of the decomposition:

$$\begin{aligned} \bar{X}_z(z_0) &= X_z(z_0^{N_1}), & \Gamma_{\bar{x}} &= \Gamma_x^{1/N_1}, \\ \bar{Y}_z(z_0) &= G_z(z_0)\bar{X}(z_0), & \Gamma_{\bar{y}} &= \Gamma_g \cap \Gamma_{\bar{x}}, \\ Y_z(z_0) &= \sum_{k=0}^{N_2-1} \bar{Y}_z(z_0 W_{N_2}^{-k}), & \Gamma_y &\supseteq \Gamma_{\bar{y}}^{N_2}, \end{aligned}$$

and by combination

$$Y_z(z_0) = \sum_{k=0}^{N_2-1} G_z(z_0 W_{N_1}^{-k}) X_z(z_0^{N_1} W_{N_2}^{-kN_1}), \quad \Gamma_y \supseteq (\Gamma_g \cap \Gamma_x^{1/N_1})^{N_2},$$

where $G_z(z_0)$ is the *transfer function* of the fractional interpolator.

11.9 Signal Multiplexing

Given N discrete signals with the same rate F , we can construct a single discrete signal with rate $F_0 = NF$. This operation is called *time-division multiplexing* (TDM) and can be viewed as a parallel-to-serial conversion (P/S) and the inverse operation (demultiplexing) as a series-to-parallel conversion (S/P). These conversions were introduced in Chap. 7 (Sect. 7.5) in the general multidimensional case and are synonymous of *polyphase decomposition* and recomposition [1, 6]. In this section they are reviewed in the 1D case in the framework of multiplexing. We recall from

Sect. 7.5 that the P/S and S/P conversions are specified by two lattices I and J , with $J \subset I$, and a cell $C = [I/J]$. Then, the super-lattice I is partitioned into the form

$$I = J + [I/J]. \quad (11.52)$$

11.9.1 P/S and S/P Conversions

In the 1D case, $I = \mathbb{Z}(T_0)$ and $J = \mathbb{Z}(T)$. As in the previous section, we use the notation

$$T = NT_0, \quad F = 1/T, \quad F_0 = NF$$

with $T = NT_0$, and we call F the *low rate* and F_0 the *high rate*.

For the conversions, we choose the standard cell

$$C = [\mathbb{Z}(T_0)/\mathbb{Z}(T)] = \{0, T_0, \dots, (N-1)T_0\}.$$

Thus, (11.52) becomes $\mathbb{Z}(T_0) = \mathbb{Z}(T) + \{0, T_0, \dots, (N-1)T_0\}$, which states that $\mathbb{Z}(T_0)$ can be partitioned into its N distinct *cosets*

$$\mathbb{Z}(T), \mathbb{Z}(T) + T_0, \dots, \mathbb{Z}(T) + (N-1)T_0.$$

In the P/S conversion the N low-rate signals

$$x_0(t), x_1(t), \dots, x_{N-1}(t), \quad t \in \mathbb{Z}(T),$$

are converted (multiplexed) to the high-rate signal $x(t_0)$, $t_0 \in \mathbb{Z}(T_0)$, by displaying the values of $x_0(t)$ over $\mathbb{Z}(T)$, the values of $x_1(t)$ over $\mathbb{Z}(T) + T_0$, the values of $x_2(t)$ over $\mathbb{Z}(T) + 2T$, etc., as shown in Fig. 11.21. In the S/P conversion, starting from the high-rate signal $x(t_0)$, $t_0 \in \mathbb{Z}(T_0)$, the signal $x_0(t)$ is obtained by picking up the values of $x(t_0)$ at $t \in \mathbb{Z}(T)$, the signal $x_1(t)$ by picking up the values at $t \in \mathbb{Z}(T) + T_0$, and so on.

The corresponding relations are

$$\text{P/S conversion} \quad x(v + iT_0) = x_i(v), \quad (11.53)$$

$$\text{S/P conversion} \quad x_i(v) = x(v + iT_0), \quad (11.54)$$

where $i = 0, 1, \dots, N-1$, and $v \in \mathbb{Z}(NT_0)$.

We recall that the S/P and P/S are QIL tfs, the first is one-input N -output, and the second N -input one-output. The impulse responses are obtained as a particular case of (7.29) and (7.28) with

$$I = \mathbb{Z}(T_0) \quad \text{and} \quad [I/J] = \{0, T_0, \dots, (N-1)T_0\},$$

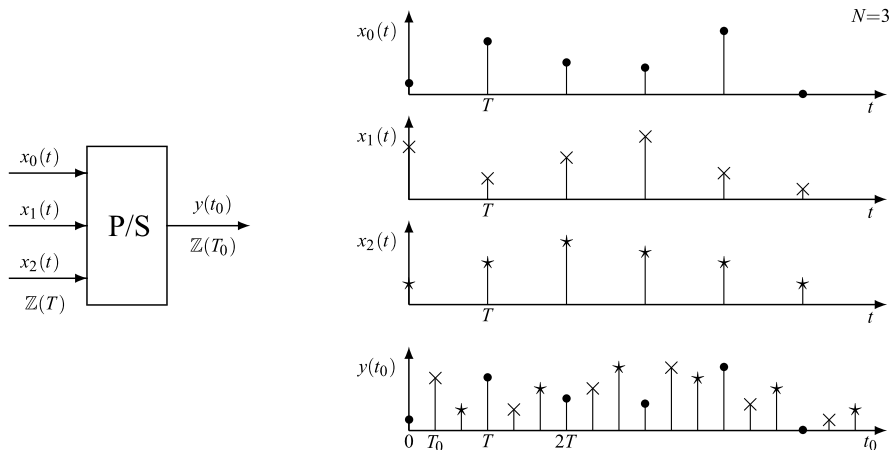


Fig. 11.21 Illustration of the P/S conversion of three signals $x_0(t)$, $x_1(t)$, $x_2(t)$, $t \in \mathbb{Z}(T)$, to a single signal $y(t_0)$, $t_0 \in \mathbb{Z}(T_0)$, with $T_0 = T/3$

namely

$$\mathbf{g}(v_0)_{P/S} = \frac{1}{N} [\delta_{\mathbb{Z}(T_0)}(v_0), \delta_{\mathbb{Z}(T_0)}(v_0 - T_0), \dots, \delta_{\mathbb{Z}(T_0)}(v_0 - (N - 1)T_0)], \quad (11.55a)$$

$$\mathbf{g}(v_0)_{S/P} = [\delta_{\mathbb{Z}(T_0)}(v_0), \delta_{\mathbb{Z}(T_0)}(v_0 + T_0), \dots, \delta_{\mathbb{Z}(T_0)}(v_0 + (N - 1)T_0)]', \quad (11.55b)$$

where $'$ denotes transposition.

In the unified formulation we showed that the two conversions can be decomposed into elementary tfs (up-samplers and down-samplers) and time shifters. In the present 1D case, the decomposition is shown in Fig. 11.22, where time shifters of $\pm iT_0$ are denoted by $z_0^{\mp i}$. In the P/S conversion (demultiplexing) the i th signal is delayed by iT_0 to be displayed on the times $\mathbb{Z}(T) + iT_0$, but this operation cannot be performed directly on the signal $x_i(t)$, $t \in \mathbb{Z}(T)$, because a delay of iT_0 is not permitted in the domain $\mathbb{Z}(T)$. This explains the presence of a $\mathbb{Z}(T) \rightarrow \mathbb{Z}(T_0)$ up-sampler, which creates the required framework. The up-sampler has an amplification of N , which is compensated by a multiplication by $1/N$.

Finally, we remark that the conversions are the inverse of each other, and therefore the cascade S/P and P/S gives the (scalar) identity, while the cascade P/S and S/P gives the N -input N -output identity. The P/S conversion contains *delays*, and the S/P *negative delays*. The S/P is not causal, but it can be easily transformed into a *causal* S/P by adding a delay of NT_0 at each branch, so that z_0^i becomes $z_0^i z_0^{-N} = z_0^{-(N-i)}$.

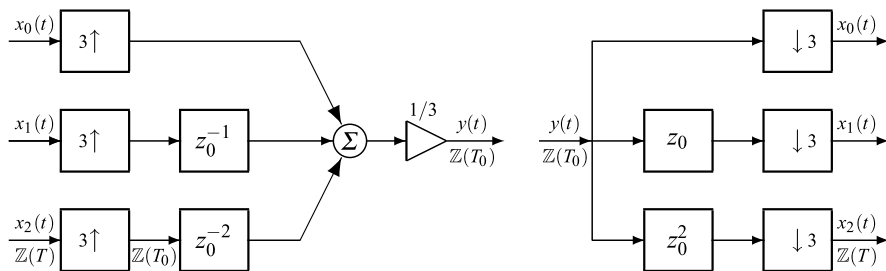


Fig. 11.22 Structure of P/S and S/P conversions for $N = 3$

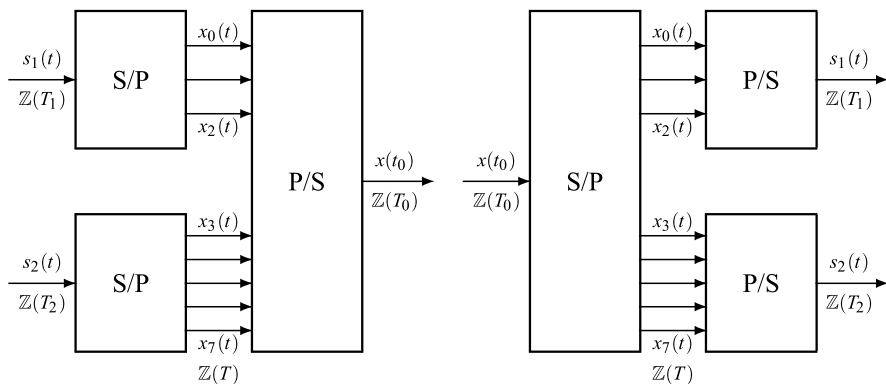


Fig. 11.23 Multiplexing of signals with different rates $F_1 = 3F, F_2 = 5F$

11.9.2 Multiplexing of Signals with Different Rates

The P/S conversion has the constraint that the signals to be multiplexed must have the *same rate* $F = 1/T$. But, with combination of P/S and S/P conversions, it is possible to obtain the multiplexing with different rates, provided that their rate ratios are *rational*.

To begin with, we consider the multiplexing of two signals $s_1(t), t \in \mathbb{Z}(T_1)$, and $s_2(t), t \in \mathbb{Z}(T_2)$, with the specific rate ratio $F_2/F_1 = T_1/T_2 = 5/3$. The multiplexing is provided by preliminary S/P conversions of the two signals to signals having the common rate $F = F_1/3 = F_2/5$. Specifically (Fig. 11.23), $s_1(t)$ is S/P converted to 3 signals $x_0(t), x_1(t), x_2(t)$ with rate $F = F_1/3$, and $s_2(t)$ is S/P converted to 5 signals $x_3(t), \dots, x_7(t)$, again with rate $F = F_2/5$. Then, all the 8 signals $x_i(t)$ have the same rate F , and they can be multiplexed to a signal $x(t_0), t_0 \in \mathbb{Z}(T_0)$, with rate $F_0 = 8F_1$. As expected, we have $F_0 = 8F = 3F + 5F = F_1 + F_2$. The demultiplexing procedure is trivial, as shown in Fig. 11.23.

In this preliminary example, the intermediate rate $F = 1/T$ is determined by $\mathbb{Z}(T) = \mathbb{Z}(T_1) \cap \mathbb{Z}(T_2)$ or equivalently by $\mathbb{Z}(F) = \mathbb{Z}(F_1) + \mathbb{Z}(F_2)$. This suggests the following general solution. Given M signals $s_m(t), t \in \mathbb{Z}(T_m)$, with rates $F_m =$

$1/T_m$, where the domains $\mathbb{Z}(T_m)$ are *rationally comparable* (see Sect. 3.9), evaluate the intermediate rate F through

$$\mathbb{Z}(F) = \mathbb{Z}(F_1) + \cdots + \mathbb{Z}(F_M).$$

Let $N_m = F_m/F$. Then the final rate is $F_0 = F_1 + \cdots + F_M$. The multiplexing scheme consists of M S/P converters, in which the m th converter decomposes $s_m(t)$ into N_m signals at the rate $F = F_m/N_m$, and a final P/S, which conveys the $N_1 + \cdots + N_m$ signals at the rate F into a single signal at the rate F_0 .

11.10 Polyphase Decomposition in z -Domain

The *polyphase decomposition* is usually introduced as an algebraic manipulation in the z domain. For a given a z -transform

$$X(z_0) = \sum_{m=-\infty}^{+\infty} T_0 x(mT_0) z_0^{-m},$$

we let $m = nN + i$, $i = 0, 1, \dots, N - 1$, $n \in \mathbb{Z}$. Then

$$X(z_0) = \frac{1}{N} [X_0(z_0^N) + X_1(z_0^N)z_0^{-1} + \cdots + X_{N-1}(z_0^N)z_0^{-(N-1)}], \quad (11.56a)$$

where the functions of z_0^N , given by

$$X_i(z_0^N) = \sum_{n=-\infty}^{+\infty} T x(nT + iT_0) z_0^{-mN}, \quad (11.56b)$$

are called the *polyphase components* of $X(z_0)$.

In this book we prefer a time-domain approach, where the polyphase decomposition is provided by the S/P conversion and the polyphase “recomposition” by the P/S conversion. The explicit relations are given by (11.53) and (11.54), which are now rewritten as

- *polyphase decomposition* of $x_0(t)$, $t_0 \in \mathbb{Z}(T_0)$:

$$x_i(v) = x(v + iT_0), \quad v \in \mathbb{Z}(T), \quad i = 0, 1, \dots, N - 1; \quad (11.57a)$$

- *polyphase recomposition* of $x_i(t)$, $t \in \mathbb{Z}(T)$:

$$x(v + iT_0) = x_i(v), \quad v \in \mathbb{Z}(T), \quad i = 0, 1, \dots, N - 1. \quad (11.57b)$$

In our terminology, the polyphase decomposition of a high-rate signal is given by N low-rate signals (polyphase components).

We now obtain the z -domain analysis from the time-domain analysis. From the impulse responses (11.55a), (11.55b) we easily obtain the *frequency responses*

$$\begin{aligned} G_{P/S}(f) &= \frac{1}{N} [1, z_0^{-1}, z_0^{-2}, \dots, z_0^{-(N-1)}] = \mathbf{G}_{P/S}(z_0), \\ G_{S/P}(f) &= [1, z_0^1, z_0^2, \dots, z_0^{(N-1)}]' = \mathbf{G}_{S/P}(z_0), \end{aligned} \tag{11.58}$$

where $z_0 = e^{i2\pi f T_0}$. The same expressions gives the *transfer functions*, provided that the variable z_0 is not confined to the unit circle C_1 .

To get the relation for the polyphase components, we recall that the S/P and P/S conversions belong to the class of vector decimators and vector interpolators, respectively (see Sect. 6.16). Then we can apply the results of the previous section (which hold in the vector case too).

To get the z -domain relation of the P/S conversion, we use (11.50), which gives (with simplified notation)

$$X(z_0) = \mathbf{G}_{P/S}(z_0)\mathbf{X}(z_0^N),$$

where $\mathbf{X}(z_0^N)$ is the vector of the $X_i(z_0^N)$. Hence, considering that $\mathbf{G}_{P/S}(\cdot)$ is $1 \times N$ and $\mathbf{X}(\cdot)$ is $N \times 1$, we get

$$X(z_0) = \frac{1}{N} \sum_{i=0}^{N-1} z_0^{-i} X_i(z_0^N). \tag{11.59}$$

Analogously for the S/P conversion, using (11.51), we obtain

$$\mathbf{X}(z_0^N) = \sum_{k=0}^{N-1} \mathbf{G}_{S/P}(z_0 W_N^{-k}) X(z_0 W_N^{-k}),$$

which explicitly is

$$X_i(z_0^N) = \sum_{k=0}^{N-1} z_0^i W_N^{-ki} X(z_0 W_N^{-k}). \tag{11.60}$$

This formulation not only allows us to obtain the traditional form of the polyphase decomposition, seen at the beginning as a simple algebraic manipulation, but also the explicit form of each polyphase component $X_i(z_0^N)$ in terms of $X(z_0)$, which cannot be obtained by a trivial algebraic manipulation.

Convergence Regions Inspection on the transfer functions (11.58) shows that their convergence region is the whole complex plane \mathbb{C} (with $z_0 \neq 0$ in (11.59) and (11.60) for the P/S). Then, considering (11.50) and (11.51), we find: in the S/P conversion: $\Gamma_{x_i} \supseteq \Gamma_x^N$ and in the P/S conversion, $\Gamma_x = \Gamma_{x_0}^{1/N} \cap \Gamma_{x_1}^{1/N} \cap \dots \cap \Gamma_{x_{N-1}}^{1/N}$.

11.10.1 Application: Parallel Architecture of an Interpolator

As seen in Chap. 7, the polyphase decomposition is widely used in multirate systems to find alternative architectures. Here, we consider the application to a $\mathbb{Z}(T) \rightarrow \mathbb{Z}(T_0)$ interpolator. In the serial decomposition (given by the Decomposition Theorem) we find a $\mathbb{Z}(T) \rightarrow \mathbb{Z}(T_0)$ up-sampler followed by a high-rate filter. The parallel decomposition is obtained by the polyphase decomposition and consists of (Fig. 11.24):

- (1) a bank of N low-rate filters,
- (2) a final P/S conversion. The impulse responses $g_i(t)$, $t \in \mathbb{Z}(T)$, of the N low-rate filter is obtained as the S/P conversion of the original impulse response $g(t_0)$, $t_0 \in \mathbb{Z}(T_0)$.

This parallel architecture was established in the general case in Sect. 7.5, and here, as an exercise, it is reconsidered in the specific $\mathbb{Z}(T) \rightarrow \mathbb{Z}(T_0)$ case. We begin with the input–output relation of the interpolator given by

$$y(t_0) = \int_{\mathbb{Z}(T)} du g(t_0 - u)x(u), \quad t_0 \in \mathbb{Z}(T_0),$$

and we decompose the output time t_0 in the form $t_0 = t + iT_0$, $t \in \mathbb{Z}(T)$, $i = 0, 1, \dots, N - 1$. Then, we obtain

$$y_i(t) = \int_{\mathbb{Z}(T)} du g_i(t - u)x(u), \quad t \in \mathbb{Z}(T), \quad (11.61)$$

where

$$y_i(t) = y(t + iT_0), \quad g_i(t) = g(t + iT_0), \quad t \in \mathbb{Z}(T). \quad (11.62)$$

The interpretation of these relations leads to the architecture of Fig. 11.24. In particular, the second of (11.62) states that the impulse responses $g_i(t)$ are the polyphase components of the original impulse response $g(t_0)$, $t_0 \in \mathbb{Z}(T_0)$. By this interpretation, using (11.60), we can obtain the transfer functions and the frequency responses of the “polyphase” filters, which are given by

$$G_i(z_0^N) = \frac{1}{N} \sum_{k=0}^{N-1} z_0^i W_N^{-ki} G(z_0 W_N^{-k}), \quad (11.63a)$$

$$G_i(f) = \frac{1}{N} \sum_{k=0}^{N-1} e^{i2\pi(f-kF)iT_0} G(f - kF). \quad (11.63b)$$

We complete the exercise by explicitly finding the parallel architecture of an *ideal low-pass* interpolator, with impulse and frequency responses (Fig. 11.25)

$$g(t_0) = F \operatorname{sinc}(Ft_0), \quad t \in \mathbb{Z}(T_0), \quad G(f) = \operatorname{rep}_{F_0} \operatorname{rect}(f/F), \quad f \in \mathbb{R}/\mathbb{Z}(F_0),$$

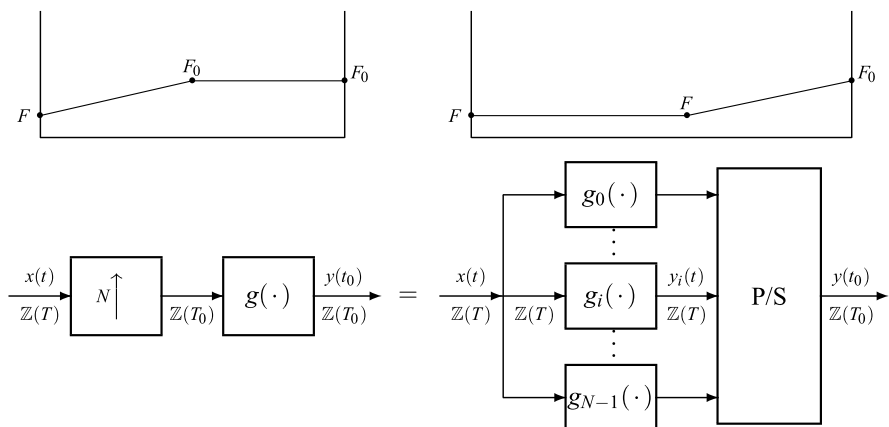


Fig. 11.24 Synthesis of an interpolator: by an up-sampler and a high-rate filter (serial architecture) and by a bank of low-rate filters (polyphase network), followed by a P/S conversion (parallel architecture)

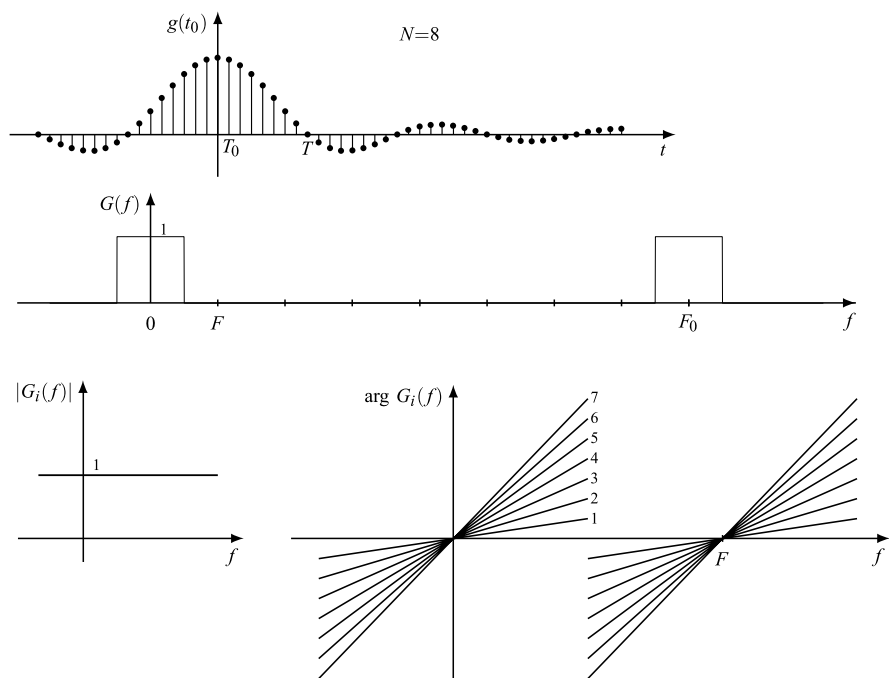


Fig. 11.25 Ideal band-limited interpolator and its polyphase decomposition

where $F = F_0/N$. As remarked in Sect. 11.7, a transfer function cannot be given for ideal filters, but the polyphase decomposition can be carried out both in the time and frequency domains. In particular, the impulse responses of the polyphase filters

are

$$g_i(t) = g(t + iT_0) = F \operatorname{sinc}(Ft + iFT_0), \quad FT_0 = 1/N.$$

We evaluate the frequency response $G_i(f)$ of the polyphase filters using (11.63b). Since $G_i(f)$ has period F , its evaluation can be limited to the centered band $(-\frac{1}{2}F, \frac{1}{2}F)$, and we find $G_i(f) = (1/N)e^{i2\pi f_i T_0}$, $f \in (-\frac{1}{2}F, \frac{1}{2}F)$. Hence,

$$|G_i(f)| = 1, \quad \arg G_i(f) = 2\pi f_i T_0 = 2\pi \frac{if}{NF}, \quad f \in \left(-\frac{1}{2}F, \frac{1}{2}F\right).$$

Then, the polyphase filters are unit all-pass, each one with a linear phase characteristic, as shown in Fig. 11.25 for $N = 8$. The N filters have N distinct phases, and this justifies the term “polyphase.” This decomposition was used in a synthesis of transmultiplexer at the end of Chap. 7.

11.11 Problems

11.1 **★★** [Sect. 11.4] Evaluate the *running sum* $y(nT)$ of the causal exponential $1_0(nT)a^n$ and its Fourier transform.

11.2 **★★** [Sect. 11.4] Prove the discrete modulation rule

$$s(nT) \cos(2\pi f_0 nT) \xrightarrow{\mathcal{F}} \frac{1}{2}S(f - f_0) + \frac{1}{2}S(f + f_0)$$

and apply it to the signal $s(nT) = 1_0(nT)$.

11.3 **★★** [Sect. 11.4] Evaluate the Fourier transform of a discrete triangular pulse (see pair 14 of Table 11.1).

11.4 **★★** [Sect. 11.4] Find the Fourier transform of the signal

$$s(nT) = \begin{cases} 1, & n = 0, 3, 6, \dots, \\ 0 & \text{elsewhere.} \end{cases}$$

Hint: use Proposition 11.2.

11.5 **★** [Sect. 11.6] Find the z -transform of the signal

$$s_1(nT) = 1_0(nT)n^2 a^n.$$

11.6 **★★** [Sect. 11.6] Find the z -transform of the signal

$$s_2(nT) = 1_0(nT)n \cos 2\pi f_0 nT.$$

11.7 ★ [Sect. 11.6] Find the z -transform of the signal

$$s_3(nT) = a^{|n|}.$$

11.8 ★ [Sect. 11.7] Find the impulse response of the discrete low-pass filter with frequency response (11.37).

11.9 ★★ [Sect. 11.7] Show that the impulse response of the discrete Hilbert filter is given by (11.39b).

11.10 ★ [Sect. 11.7] Show that the impulse response of the filter, whose frequency response is defined by (11.42), is given by

$$h_z(nT) = \frac{1}{T} \operatorname{sinc}\left(\frac{1}{2}n\right) i^n.$$

11.11 ★★ [Sect. 11.7] Prove that the impulse response of the *discrete real* phase shifter of β_0 is

$$g(nT) = -\frac{\sin \beta_0}{\pi nT} + \frac{2 \sin(\beta_0 + n\pi)}{\pi nT}, \quad n \neq 0,$$

while $g(0) = 0$.

11.12 [Sect. 11.8] Show that if the input to a $\mathbb{Z}(T_0) \rightarrow \mathbb{Z}(T)$ down-sampler is causal with the rational z -transform

$$X(z) = \frac{Tz^{-1}}{(1 - \frac{1}{3}z^{-1})(1 - \frac{1}{4}z^{-1})},$$

the equality $\Gamma_y = \Gamma_x^N$ holds for the convergence regions.

References

1. M.G. Bellanger, J.L. Daguet, TDM-FDM transmultiplexer: digital polyphase and FFT. IEEE Trans. Commun. **COM-22**, 1199–1205 (1974)
2. A.V. Oppenheim, R.W. Schaffer, *Digital Signal Processing* (Prentice Hall, Englewood Cliffs, 1975)
3. A. Papoulis, *Circuits and Systems* (Holt, Rinehart and Winston, New York, 1980)
4. A.P. Prudnikov, Yu.A. Brychkov, O.I. Marichev, *Integrals and Series*, vol. 5 (Gordon & Breach, New York, 1986)
5. L.R. Rabiner, B. Gold, *Theory and Application of Digital Signal Processing* (Prentice Hall, Englewood Cliffs, 1975)
6. P.P. Vaidyanathan, Multirate digital filters, filter banks, polyphase networks, and applications: a tutorial. Proc. IEEE **78**, 56–93 (1990)

Chapter 12

Signals on $\mathbb{Z}(T)/\mathbb{Z}(T_p)$

UT 12.1 The Time Domain

A periodic discrete-time signal

$$s(t - t_0) = s(t), \quad t \in \mathbb{Z}(T), \quad t_0 \in \mathbb{Z}(T_p), \quad (12.1)$$

with period $T_p = NT$, can be formulated on the domain $\mathbb{Z}(T)$ or on the quotient group $\mathbb{Z}(T)/\mathbb{Z}(T_p)$. In the first case the signal turns out to be “singular” because, for example, its energy is infinite and its FT is composed by a train of delta functions. In the second case the definitions give more appropriate quantities; in particular, the signal energy (the energy in a period) turns out to be finite, and the FT exhibits only finite values.

12.1.1 Integral and Convolution

The *Haar integral* on $\mathbb{Z}(T)/\mathbb{Z}(T_p)$ (Sect. 4.2) is given by the sum of the signal values in a period, multiplied by the spacing T ,

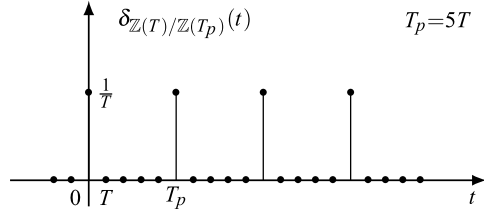
$$\int_{\mathbb{Z}(T)/\mathbb{Z}(T_p)} dt s(t) = \sum_{n=0}^{N-1} Ts(nT).$$

Consequently, the *convolution* (often called *cyclic convolution*) is given by

$$x * y(nT) = \sum_{k=0}^{N-1} Tx(nT - kT)y(kT). \quad (12.2)$$

The *impulse*, defined as the unit element of the convolution algebra (Sect. 4.10), has values equal to $1/T$ at the points $\mathbb{Z}(T_p) = \mathbb{Z}(NT)$ and zero elsewhere, as shown

Fig. 12.1 The impulse on $\mathbb{Z}(T)/\mathbb{Z}(T_p)$



in Fig. 12.1 for $T_p = 5T$. It can be written in terms of impulses on $\mathbb{Z}(T)$ as

$$\delta_{\mathbb{Z}(T)/\mathbb{Z}(T_p)}(nT) = \sum_{k=-\infty}^{+\infty} \delta_{\mathbb{Z}(T)}(nT - kT_p).$$

UT 12.2 The Frequency Domain

It is obtained by

$$I = \mathbb{Z}(T)/\mathbb{Z}(T_p) \xrightarrow{\text{dual}} \hat{I} = \mathbb{Z}(F)/\mathbb{Z}(F_p), \quad (12.3)$$

where spacings and periods are related by

$$T_p = NT, \quad F_p = NF, \quad F_p T_p = N, \quad \boxed{FT = 1/N}. \quad (12.4)$$

Here, we have remarked that the product of the time spacing T and the frequency spacing is not unitary. Considering the periodicity in both domains, the signal and the FT specification can be limited to the cells

$$\begin{aligned} C &= [\mathbb{Z}(T)/\mathbb{Z}(NT)] = \{0, T, \dots, (N-1)T \triangleq \mathbb{Z}_N(T)\}, \\ \hat{C} &= [\mathbb{Z}(F)/\mathbb{Z}(NF)] = \{0, F, \dots, (N-1)F \triangleq \mathbb{Z}_N(F)\}. \end{aligned} \quad (12.5)$$

Note that with the choice $T = 1/\sqrt{N}$, $T_p = \sqrt{N}$, the group $I = \mathbb{Z}(T)/\mathbb{Z}(T_p)$ becomes *self-dual* and we have $\hat{I} = I$.

12.2.1 The Fourier Transform (DFT)

The FT and the inverse FT are

$$S(kF) = \sum_{n=0}^{N-1} T s(nT) e^{-i2\pi kFnT}, \quad (12.6a)$$

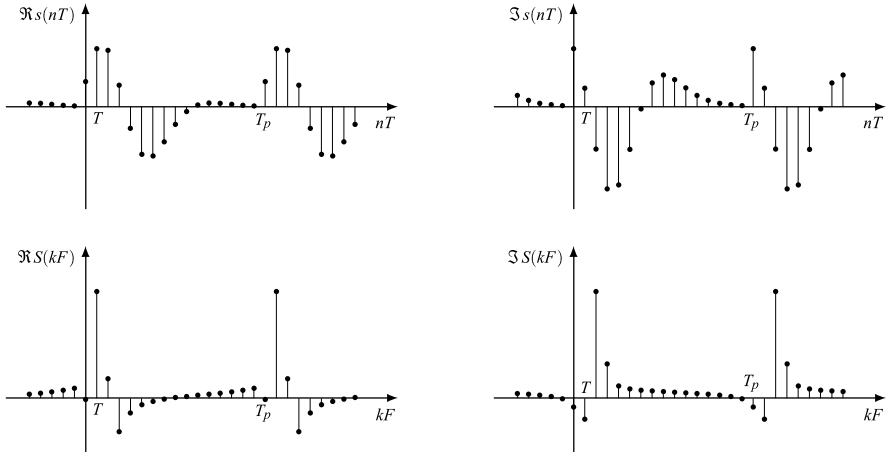


Fig. 12.2 The DFT of a discrete complex signal with period $T_p = 16T$

$$s(nT) = \sum_{k=0}^{N-1} FS(kF)e^{i2\pi kFnT}. \tag{12.6b}$$

Then, from a periodic discrete-time signal we obtain a periodic discrete-frequency FT. The number of points per period N is the same for both the signal and its FT, as stated by (12.4). Figure 12.2 shows an example of Fourier pair with $N = 16$ points per period, when both $s(nT)$ and $S(kF)$ are complex. The Fourier transform (12.6a) is usually called the *discrete Fourier transform* (DFT), and its inverse (12.6b) the *inverse discrete Fourier transform* (IDFT). In particular, the IDFT represents the signal as the sum of discrete *exponentials*

$$FS(kF)e^{i2\pi kFnT}$$

with finite amplitudes and frequencies kF belonging to the dual cell $\widehat{C} = \mathbb{Z}_N(F)$ (see (12.5)).

For *real* signals, it is possible to get a representation in terms of discrete *sinusoids* using the Hermitian symmetry of the DFT. Letting

$$S(kF) = A_S(kF)e^{i2\beta_S(kF)}, \tag{12.7}$$

from the general relationship (5.77), we find:

- for N odd ($N = 2M + 1$),

$$s(nT) = FS(0) + 2 \sum_{k=1}^M FA_S(kF) \cos[2\pi kFnT + \beta_S(kF)]; \tag{12.8a}$$

- for N even ($N = 2M$),

$$s(nT) = FS(0) + FS(MF)(-1)^n$$



Fig. 12.3 $\mathbb{R}/\mathbb{Z}(T_p) \rightarrow \mathbb{Z}(T)/\mathbb{Z}(T_p)$ down-sampling and its dual transformation

$$+ 2 \sum_{k=1}^{M-1} FA_S(kF) \cos[2\pi kFnT + \beta_S(kF)]. \quad (12.8b)$$

12.2.2 Computational Rules

The DFT and IDFT have no convergence problem, since they are given by a finite summation. However, the usual rules on the FT may be useful; note that these rules become particularly simple since both I and \hat{I} are finite groups with the same number of points per period.

Symmetry Rule From a Fourier pair $s(nT), S(kF)$ on $\mathbb{Z}(T)/\mathbb{Z}(T_p)$ we obtain the pair $S(kF), s(-nT)$ on $\mathbb{Z}(F)/\mathbb{Z}(F_p)$ according to the graph

$$\begin{array}{ccc} s(t) & \xrightarrow{\mathcal{F}} & S(f) \\ \mathbb{Z}(T)/\mathbb{Z}(T_p) & & \mathbb{Z}(F)/\mathbb{Z}(F_p) \\ & & S(t) \xrightarrow{\mathcal{F}} s(-f). \end{array}$$

Energy The Parseval theorem has the symmetric form

$$E_s = \sum_{n=0}^{N-1} T |s(nT)|^2 = \sum_{k=0}^{N-1} F |S(kF)|^2 = E_S. \quad (12.9)$$

Hence, the energy in the frequency domain has the same expression as in the time domain.

12.2.3 Relationship with the FT on $\mathbb{R}/\mathbb{Z}(T_p)$

The Duality Theorem with

$$I = \mathbb{R}/\mathbb{Z}(T_p), \quad U = \mathbb{Z}(T)/\mathbb{Z}(T_p)$$

yields (Fig. 12.3):



Fig. 12.4 $\mathbb{Z}(T) \rightarrow \mathbb{Z}(T)/\mathbb{Z}(T_p)$ up-periodization and its dual transformation

Proposition 12.1 *Let $s(nT)$ be the $\mathbb{R}/\mathbb{Z}(T_p) \rightarrow \mathbb{Z}(T)/\mathbb{Z}(T_p)$ down-sampled version of $\tilde{s}(t)$, $t \in \mathbb{R}/\mathbb{Z}(T_p)$. Then its FT $S(kF)$ is given by the $\mathbb{Z}(F) \rightarrow \mathbb{Z}(F)/\mathbb{Z}(F_p)$ up-periodization of $\tilde{S}(kF)$, namely*

$$s(nT) = \tilde{s}(nT) \xrightarrow{\mathcal{F}} S(kF) = \sum_{m=-\infty}^{+\infty} \tilde{S}(kF - mF_p) = \text{rep}_{F_p} \tilde{S}(kF).$$

12.2.4 Relationship with the FT on $\mathbb{Z}(T)$

Again, the Duality Theorem with

$$I = \mathbb{Z}(T), \quad U = \mathbb{Z}(T)/\mathbb{Z}(T_p)$$

yields (Fig. 12.4):

Proposition 12.2 *Let $s(nT)$, $nT \in \mathbb{Z}(T)/\mathbb{Z}(T_p)$, be the $\mathbb{Z}(T) \rightarrow \mathbb{Z}(T)/\mathbb{Z}(T_p)$ periodic repetition of $\tilde{s}(nT)$, $nT \in \mathbb{Z}(T)$. Then the FT of $s(nT)$ is the $\mathbb{R}/\mathbb{Z}(F_p) \rightarrow \mathbb{Z}(F)/\mathbb{Z}(F_p)$ down-sampling of the FT of $\tilde{s}(nT)$, namely*

$$S(kF) = \tilde{S}(kF), \quad kF \in \mathbb{Z}(F)/\mathbb{Z}(F_p).$$

12.2.5 Alternative Forms and Normalizations of DFT and IDFT

Letting

$$W_N = e^{i2\pi/N}$$

and considering that

$$e^{\pm i2\pi nTkF} = W_N^{\pm kn},$$

the DFT and the IDFT take the form

$$\boxed{S(kF) = \sum_{n=0}^{N-1} T s(nT) W_N^{-kn}, \quad s(nT) = \sum_{k=0}^{N-1} F S(kF) W_N^{kn},} \quad (12.10)$$

where spacings and periods are related by (12.4). Therefore, it is not possible to normalize simultaneously both time and frequency spacings ($T = F = 1$), but, for instance, we can make the choice

$$T = 1, \quad F = 1/N \quad (T_p = N, F_p = 1),$$

which gives the relationships

$$S_k = \sum_{n=0}^{N-1} s_n W_N^{-kn}, \quad s_n = \frac{1}{N} \sum_{k=0}^{N-1} S_k W_N^{kn}, \quad (12.11)$$

where $s_n = s(nT)$ and $S_k = S(kF)$. An alternative choice is

$$T = 1/N, \quad F = 1 \quad (T_p = 1, F_p = N),$$

which gives

$$S_k = \frac{1}{N} \sum_{n=0}^{N-1} s_n W_N^{-kn}, \quad s_n = \sum_{k=0}^{N-1} S_k W_N^{kn}. \quad (12.12)$$

Also, the ‘‘symmetric’’ choice is possible:

$$T = 1/\sqrt{N}, \quad F = 1/\sqrt{N} \quad (T_p = \sqrt{N}, F_p = \sqrt{N}), \quad (12.13a)$$

which gives

$$S_k = \frac{1}{\sqrt{N}} \sum_{n=0}^{N-1} s_n W_N^{-kn}, \quad s_n = \frac{1}{\sqrt{N}} \sum_{k=0}^{N-1} S_k W_N^{kn}. \quad (12.13b)$$

In the literature we find all the *normalized* forms written above (sometimes with sign + at the DFT exponential and – at the IDFT exponential). However, in this book we prefer the *nonnormalized* form (12.6a), (12.6b) or the equivalent (12.10), which is fully symmetric and gives easier relationships with the FT defined over other domains.

12.3 Gallery of Signals and Fourier Transforms on $\mathbb{Z}(T)/\mathbb{Z}(T_p)$

A signal $s(t)$ on $\mathbb{Z}(T)/\mathbb{Z}(T_p)$ is completely specified by its values in the *cell* $C = \mathbb{Z}_N(T)$, and the DFT $S(f)$ on $\mathbb{Z}(F)/\mathbb{Z}(F_p)$ by its values in the dual cell $\widehat{C} = \mathbb{Z}_N(F)$ (see (12.5)).

The signal $s(t)$ can be obtained in different ways starting from a signal $s_0(t)$ defined on another domain *by defining its values on a period* as

$$s(t) = s_0(t), \quad t \in C = \mathbb{Z}_N(T), \quad (12.14)$$

and then extending the definition to all $\mathbb{Z}(T)/\mathbb{Z}(T_p)$ by periodicity. This operation is straightforward. However, the symmetric relationship between the FTs

$$S(f) = S_0(f), \quad f \in \widehat{C} = \mathbb{Z}_N(F), \quad (12.15)$$

is *verified only in very particular cases*, because the down-sampling operation in time stated by (12.14) implies some conceptual operations which may appear irrelevant (at a point that one may not pay attention to them), but they have a relevant consequence in the frequency domain.

12.3.1 Sampling a Continuous-Time Periodic Signal

Starting from a continuous-time periodic signal $s_0(t)$, $t \in \mathbb{R}/\mathbb{Z}(T_0)$, we can obtain a signal $s(t)$, $t \in \mathbb{Z}(T)/\mathbb{Z}(T_p)$, where we recall that T must be a submultiple of T_p .

The simplest case is where the period T_0 of the continuous-time signal is equal to the desired final period, that is, $T_p = T_0$. Then, we get $s(t)$ by an $\mathbb{R}/\mathbb{Z}(T_p) \rightarrow \mathbb{Z}(T)/\mathbb{Z}(T_p)$ down-sampling. The corresponding relationship in the frequency domain is given by Proposition 12.1, namely

$$S(f) = \text{rep}_{F_p} S_0(f), \quad f \in \mathbb{Z}(F)/\mathbb{Z}(F_p). \quad (12.16)$$

If the spectral extension of $S_0(f)$ is contained in the cell \widehat{C} , then (12.15) holds because the terms of the periodic repetition do not overlap; otherwise *aliasing* occurs, and the two FTs are different even inside the cell \widehat{C} .

If the period T_0 is a submultiple of T_p , that is, $T_p = MT_0$, the signal $s(t)$ is still obtained by down-sampling $s_0(t)$, but the frequency domain relationship is somewhat different. In fact, the signal $s_0(t)$, $t \in \mathbb{R}/\mathbb{Z}(T_0)$, must be *down-periodized* with an $\mathbb{R}/\mathbb{Z}(T_0) \rightarrow \mathbb{R}/\mathbb{Z}(MT_0)$ tf, which is irrelevant in the time domain, but in the frequency domain it becomes a $\mathbb{Z}(F_0) \rightarrow \mathbb{Z}(F)$ up-sampling with $F_0 = MF$. This is the first example in which the tf is irrelevant in the time domain, but not in the frequency domain.

Finally, if the period T_0 is not a submultiple of T_p , from $s_0(t)$ it is possible to get a signal on $\mathbb{Z}(T)/\mathbb{Z}(T_p)$, but with a complicated procedure. Indeed, it is required to *down-periodize* the signal $s_0(t)$ by a unitary window $w(t)$ on $[0, T_p)$, namely

$$s_w(t) = s_0(t)w(t), \quad t \in \mathbb{R},$$

to limit the extension within the interval $[0, T_p)$. The signal obtained in such a way is periodically repeated as follows:

$$s_{wp}(t) = \sum_{n=-\infty}^{+\infty} s_w(t - nT_p),$$

and only at this point can we apply the $\mathbb{R}/\mathbb{Z}(T_p) \rightarrow \mathbb{Z}(T)/\mathbb{Z}(T_p)$ down-sampling.

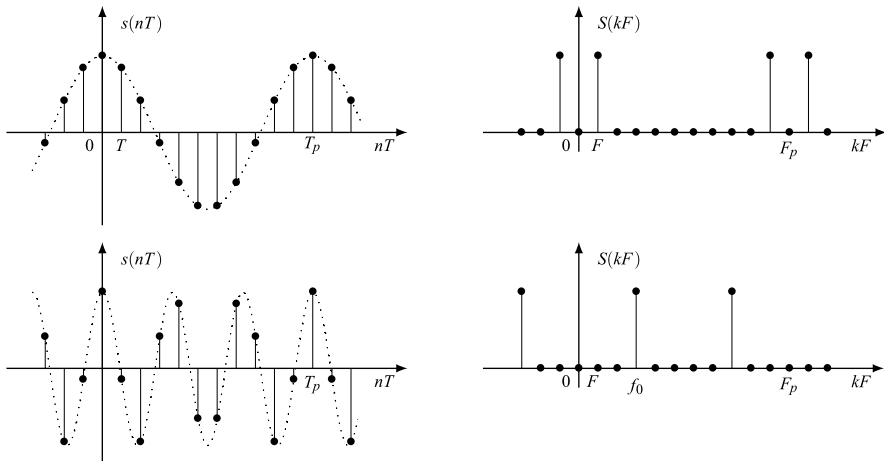


Fig. 12.5 DFT for a discrete sinusoid with period $T_p = 11T$ and with frequencies $f_0 = F$ and $f_0 = 3F$

As a consequence of this sequence of operations, the relationship between the original FT $S_0(f)$ and the final FT $S(f)$ turns out to be cumbersome.

Example 12.1 The continuous-time sinusoidal signal (Fig. 12.5)

$$s_0(t) = A_0 \cos 2\pi f_0 t = A_0 \cos 2\pi(t/T_0), \quad T_0 = (1/f_0), \quad (12.17)$$

has minimum period T_0 .

If $T_p = T_0$, the corresponding discrete-time signal, obtained by an $\mathbb{R}/\mathbb{Z}(T_0) \rightarrow \mathbb{Z}(T)/\mathbb{Z}(T_p)$ down-sampling, is

$$s(nT) = A_0 \cos 2\pi f_0 nT, \quad nT \in \mathbb{Z}(T)/\mathbb{Z}(T_p),$$

and its FT is

$$S(f) = \frac{1}{2} A_0 \delta_{\mathbb{Z}(F)/\mathbb{Z}(F_p)}(f - f_0) + \frac{1}{2} A_0 \delta_{\mathbb{Z}(F)/\mathbb{Z}(F_p)}(f + f_0). \quad (12.18)$$

In the cell \widehat{C} we find only two nonzero values at the frequencies (Fig. 12.5)

$$f_0 = F, \quad F_p - f_0 = (N - 1)F.$$

If T_p is a multiple of T_0 , e.g., $T_p = 3T_0$, (12.18) holds but with a different interpretation. In the fundamental band the frequencies become

$$f_0 = 3F, \quad F_p - f_0 = F_p - 3F,$$

and we note the up-sampling domain due to the down-periodization in the time domain. In particular it introduces two zeros between 0 and f_0 .

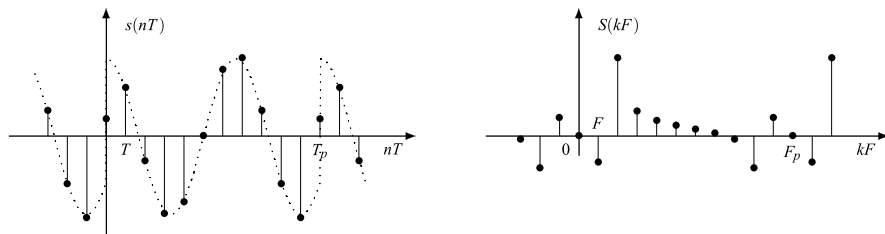


Fig. 12.6 DFT of a signal obtained by down-sampling a truncated sinusoid and extended elsewhere by periodicity. The sinusoid is not truncated to its natural period, and this causes some artefacts in the DFT

If T_p is not a multiple of T_0 , the values *in a period* can be obtained directly by down-sampling from $s_0(t)$, but *outside the period* those values must be repeated and cannot be obtained from the continuous-time sinusoid. By doing this we conceptually *truncate (with a window operation) and periodically repeat*. Then, in the frequency domain we obtain a result quite different than before, as shown in Fig. 12.6.

12.3.2 Periodic Repetition of a Discrete-Time Signal

To get a signal on $\mathbb{Z}(T)/\mathbb{Z}(T_p)$, we can also start from a signal $s_0(t)$, $t \in \mathbb{Z}(T)$, and apply a periodic repetition.

In the simplest case, the signal $s_0(t)$ is time limited to the basic cell C ; then the periodic repetition does not exhibit aliasing, and we obtain straightforwardly the desired signal as in (12.14). In the frequency domain, the $\mathbb{Z}(T) \rightarrow \mathbb{Z}(T)/\mathbb{Z}(T_p)$ periodic repetition becomes the $\mathbb{R}/\mathbb{Z}(F_p) \rightarrow \mathbb{Z}(F)/\mathbb{Z}(F_p)$ down-sampling (see Proposition 12.2), and, as a consequence, (12.15) holds true.

If the signal is not time limited to C , we can again take the values on C , but this conceptually implies the presence of a window, so that we work on the signal

$$s_w(t) = w(t)s_0(t), \quad t \in \mathbb{Z}(T),$$

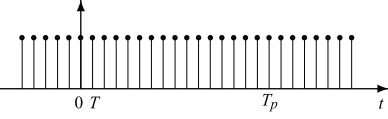


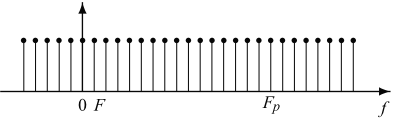
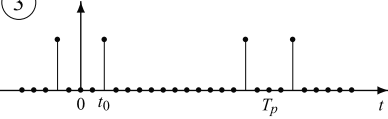
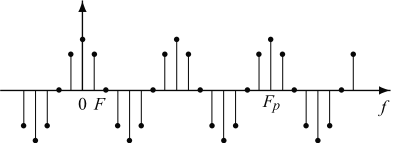
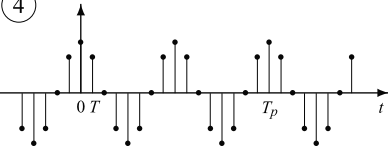
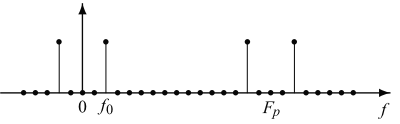
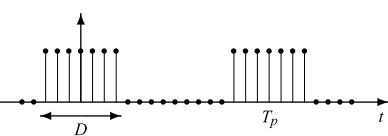
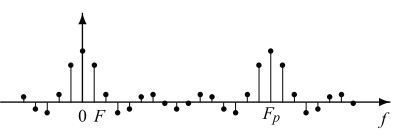
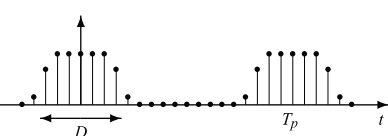
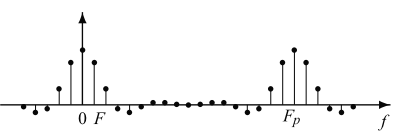
and correspondingly, in the frequency domain we get the convolution $S_w(f) = W * S_0(f)$, $f \in \mathbb{R}/\mathbb{Z}(F_p)$.

Finally, the FT of the desired signal is obtained from $S_w(f)$ by an $\mathbb{R}/\mathbb{Z}(F_p) \rightarrow \mathbb{Z}(F)/\mathbb{Z}(F_p)$ down-sampling, and the results may be quite different with respect to the one obtained by sampling directly $S_0(f)$, so that (12.15) does not hold anymore.

12.3.3 Examples of Fourier Pairs

Examples of Fourier pairs on $\mathbb{Z}(T)/\mathbb{Z}(T_p)$ have been presented in a unified view in Sect. 5.8 (see Table 5.4). Table 12.1 collects further examples.

Table 12.1 Fourier pairs on $\mathbb{Z}(T)/\mathbb{Z}(T_p)$

Signal		Fourier transform
<p>①</p> 	1	<p>$\delta_{\mathbb{Z}(F)/\mathbb{Z}(F_p)}(f)$</p> 
<p>②</p> 	$\delta_{\mathbb{Z}(T)/\mathbb{Z}(T_p)}(t)$	<p>1</p> 
<p>③</p> 	$\delta_{\mathbb{Z}(T)/\mathbb{Z}(T_p)}(t-t_0) + \delta_{\mathbb{Z}(T)/\mathbb{Z}(T_p)}(t+t_0)$	<p>$2 \cos 2\pi f t_0$</p> 
<p>④</p> 	$2 \cos 2\pi f_0 t$	<p>$\delta_{\mathbb{Z}(F)/\mathbb{Z}(F_p)}(f-f_0) + \delta_{\mathbb{Z}(F)/\mathbb{Z}(F_p)}(f+f_0)$</p> 
<p>⑤</p> 	$\text{rep}_{T_p} \text{rect}(\frac{t}{D})$	<p>$D \text{sinc}_M(fD)$ ($M = D/T$ odd)</p> 
<p>⑥</p> 	$\text{rep}_{T_p} \text{rcos}(\frac{t}{D}, r)$	

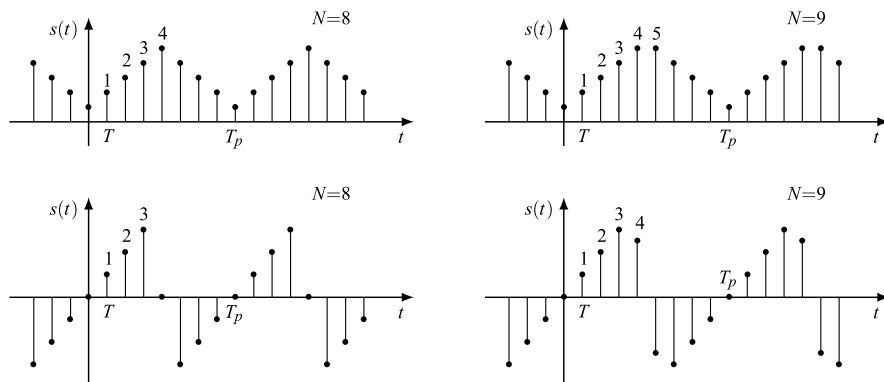


Fig. 12.7 Essential signal values in the presence of even (*above*) and odd (*below*) symmetry

UT 12.4 Symmetries

To the signals on $\mathbb{Z}(T)/\mathbb{Z}(T_p)$ and their FTs we can apply the fundamental symmetries of Sect. 5.6, but with relevant consequences due to the nature of the domain (discrete with periodicity).

12.4.1 Cardinality Reduction in the Presence of Symmetries

We introduce the *cardinality* of a signal as the *cardinality of the set of values required for its specification*. Then, the cardinality of a signal on $\mathbb{Z}(T)/\mathbb{Z}(T_p)$ is finite and given by the number of points in a period. We find that also the DFT has the same cardinality. In the presence of a symmetry, the cardinality is reduced since the signal specification is limited to some *essential* values, while the other nonessential (redundant) values can be obtained by the symmetry.

Even Symmetry For an *even* signal, considering the periodicity, we can write

$$s(t) = s(-t) \implies s(t) = s(T_p - t),$$

where the first states the evenness *with respect to the origin*, and the second *with respect to the half of the period* (Fig. 12.7). Hence, a signal on $\mathbb{Z}(T)/\mathbb{Z}(T_p)$ has always two symmetry centers per period. If $N = T_p/T$ is even, the center $\frac{1}{2}T_p = \frac{1}{2}NT$ belongs to the domain, whereas if N is odd, $\frac{1}{2}T_p$ does not (but the symmetry can be formulated also in this case, see below). The number of essential values (cardinality) is

$$\frac{1}{2}N + 1 \quad \text{for } N \text{ even,} \quad \frac{1}{2}(N + 1) \quad \text{for } N \text{ odd.}$$

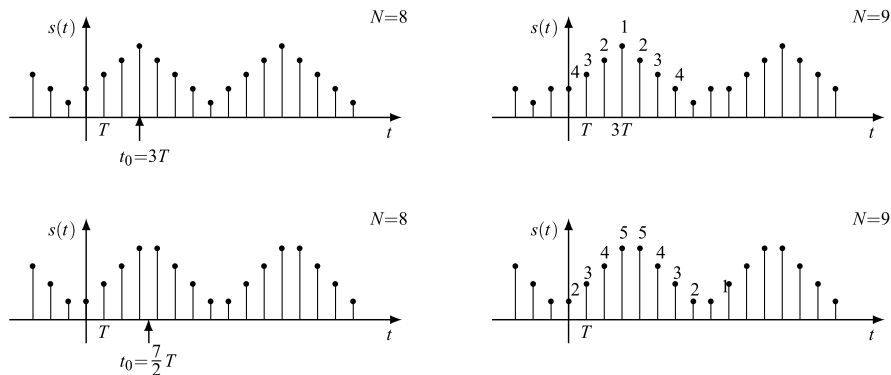


Fig. 12.8 Signals with the even symmetry *out of the origin*

Odd Symmetry For an *odd* signal, we have

$$s(t) = -s(-t) \implies s(t) = -s(T_p - t).$$

If N is even, $\frac{1}{2}T_p$ belongs to the domain, and we have the constraints (Fig. 12.7)

$$s(0) = 0, \quad s\left(\frac{1}{2}T_p\right) = 0, \tag{12.19}$$

while for N odd, only the first constraint holds. Then, the cardinality is

$$\frac{1}{2}N - 1 \quad \text{for } N \text{ even}, \quad \frac{1}{2}(N + 1) \quad \text{for } N \text{ odd}.$$

For the Hermitian and anti-Hermitian symmetries, the previous symmetries hold respectively for the real or imaginary part, so that we can use the previous results.

These considerations for a signal on $\mathbb{Z}(T)/\mathbb{Z}(T_p)$ can be applied to the DFT whose domain $\mathbb{Z}(F)/\mathbb{Z}(F_p)$ has the same structure (and cardinality). It can be shown that, if a signal with given symmetry Σ has cardinality N_0 , its DFT with the dual symmetry $\widehat{\Sigma}$ has the same cardinality N_0 .

12.4.2 Symmetries Out of the Origin

The even and odd symmetries till now considered are *about the origin*, but they can also be formulated about another time “out of the origin.” The *even symmetry about the time* t_0 is given by

$$s(-t + t_0) = s(t + t_0), \tag{12.20}$$

which implies that $t_0 \in \mathbb{Z}(T)$. Figure 12.8 (at the top) shows two examples of signals, which are even about $t_0 = 3T$. However, it is possible to state the evenness

about time t_0 that is an odd multiple of $\frac{1}{2}T$, as shown at the bottom of Fig. 12.8, where $t_0 = \frac{7}{2}T \notin \mathbb{Z}(T)$. To include this possibility, (12.20) must be rewritten in the form

$$\boxed{s(-t) = s(t + 2t_0)}, \quad (12.21)$$

which implies the less stringent condition $2t_0 \in \mathbb{Z}(T)$. Using the periodicity, (12.21) gives

$$s(-t) = s(t + T_p + 2t_0) = s(t + 2t'_0), \quad t'_0 = t_0 + \frac{1}{2}T_p = t_0 + \frac{1}{2}NT.$$

Hence, a signal that is even about t_0 is also even about $t_0 + \frac{1}{2}T_p$.

In the frequency domain the symmetry becomes

$$S(-f) = S(f)e^{i2\pi f 2t_0} \Rightarrow S(-f)e^{-i2\pi f t_0} = S(f)e^{i2\pi f t_0},$$

which states that the function $S(f)e^{i2\pi f t_0}$ is even (about the frequency origin).

Similar considerations hold for the odd symmetry about t_0 , which is stated by

$$s(-t) = -s(t + 2t_0). \quad (12.22)$$

12.4.3 The Cosine DFT

If a signal is *real and even*, also its FT is *real and even* (see Sect. 5.6). This statement holds in general, in particular on finite groups where the *periodicity* holds in both domains.

Now, we want to see the consequence of this symmetry (real + even) on the DFT. We suppose that the number of points per period is even, say $2N = T_p/T$, and we choose the cells (of cardinality $2N$)

$$K = \{-(N-1)T, \dots, 0, \dots, NT\}, \quad \widehat{K} = \{-(N-1)F, \dots, 0, \dots, NF\}.$$

Then

$$\begin{aligned} S(kF) &= \sum_{n=-(N-1)}^N T s(nT) e^{-i2\pi kn/2N} \\ &= Ts(0) + \sum_{n=1}^{N-1} Ts(nT) [e^{-i2\pi kn/2N} + e^{i2\pi kn/2N}] + Ts(NT) e^{-i\pi k}, \end{aligned}$$

which can be written in the compact form

$$\boxed{S(kF) = T \sum_{n=0}^N \mu_n s(nT) \cos 2\pi \frac{nk}{2N}}, \quad (12.23a)$$

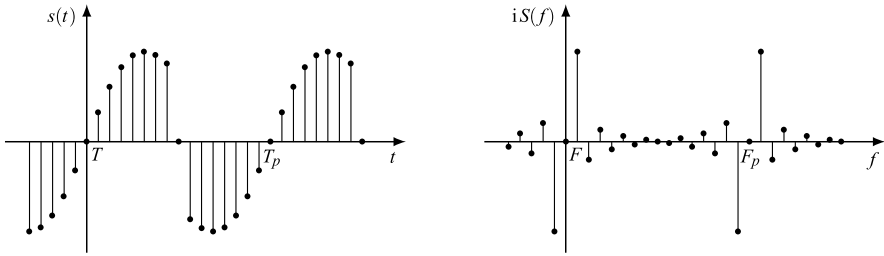


Fig. 12.9 DFT of an odd real signal with $2N = 16$ values per period

where

$$\mu_n = \begin{cases} 1, & n = 0, N, \\ 2, & n = 1, \dots, N - 1. \end{cases}$$

Analogously, for the IDFT, we obtain

$$s(nT) = F \sum_{k=0}^N \mu_k S(kF) \cos 2\pi \frac{nk}{2N}. \quad (12.23b)$$

We call (12.23a) the *cosine* DFT and (12.23b) the *cosine* IDFT. They work as follows: given a real sequence $s(0), s(T), \dots, s(NT)$ of length $N + 1$, the cosine DFT produces a real sequence $S(0), S(F), \dots, S(NF)$ of the same length $N + 1$ using only real operations.

12.4.4 The Sine DFT

For a real and odd signal, the FT is imaginary and odd. Then, considering, as above, $2N$ points per period and using the cells (12.5), we obtain

$$S(kF) = Ts(0) + \sum_{n=1}^{N-1} Ts(nT) [e^{-i2\pi kn/2N} - e^{i2\pi kn/2N}] + Ts(NT)e^{-i\pi k}. \quad (12.24)$$

However, for an odd signal with $2N$ points per period, we have the constraints (12.19), namely $s(0) = 0$ and $s(NT) = 0$ (Fig. 12.9). Hence, (12.24) becomes

$$iS(kF) = 2 \sum_{n=1}^{N-1} Ts(nT) \sin 2\pi \frac{kn}{2N}, \quad (12.25a)$$

where $iS(kF)$ is real since $S(kF)$ is imaginary. Analogously, considering that also in the frequency domain we have the constraints $S(0) = 0$ and $S(NF) = 0$, we find,

for the IDFT,

$$s(nT) = 2 \sum_{n=1}^{N-1} F iS(kF) \sin 2\pi \frac{kn}{2N}. \quad (12.25b)$$

Relations (12.25a), (12.25b) represent respectively the *sine* DFT and the *sine* IDFT. Starting for a real sequence $s(T), s(2T), \dots, s((N-1)T)$ of length $N-1$, the sine DFT produces an imaginary sequence $iS(F), iS(2F), \dots, iS((N-1)F)$ of length $N-1$, *working with only real operations*.

Remark We obtain the cosine and the sine DFT starting from the ordinary DFT, and in such a way we have established the inversion formulas, giving the cosine IDFT and the sine IDFT, respectively. An alternative approach would consist of giving directly (autonomously) their definitions and then obtaining the inversion formulas using the orthogonality of cosine and sine functions.

UT 12.5 The Discrete Cosine Transform (DCT)

The DCT is very similar to the “cosine” DFT. Starting from a real sequence s_n and using real operations, the DCT gives a real sequence S_k of the same length. The forward transform (DCT) and the inverse transform (IDCT) are respectively

$$S_k = \varepsilon_k \frac{1}{\sqrt{N}} \sum_{n=0}^{N-1} s_n \cos \frac{2\pi(2n+1)k}{4N}, \quad k = 0, \dots, N-1, \quad (12.26a)$$

$$s_n = \frac{1}{\sqrt{N}} \sum_{k=0}^{N-1} \varepsilon_k S_k \cos \frac{2\pi(2n+1)k}{4N}, \quad n = 0, \dots, N-1, \quad (12.26b)$$

where N is the sequence length, and

$$\varepsilon_k = \sqrt{\mu_k} = \begin{cases} 1, & k = 0, \\ \sqrt{2} & \text{elsewhere.} \end{cases} \quad (12.27)$$

An example of DCT pair is shown in Fig. 12.10 for $N = 16$.

The DCT is not used for a signal representation in the frequency domain, since to this end, the DFT, possibly in the cosine form, is more suitable. Its tremendous importance lies on the property of permitting a very efficient representation of images. In fact, the DCT is used in most international standards for image (video) compression/coding [6, 8–11].

The purpose of this section is the DCT settlement in the context of discrete periodic signals, showing that it is essentially a DFT with the constraint of some symmetries. The properties deriving from these symmetries will explain, at an intuitive level, the “compressing” capability of the DCT.

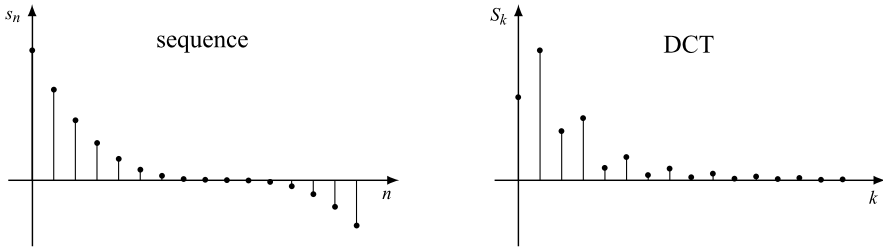


Fig. 12.10 Example of DCT for a sequence of length $N = 16$

12.5.1 Deduction of the DCT from the Cosine DFT

To design the DCT, one can start from a signal $s(t)$, $t \in \mathbb{Z}(T)/\mathbb{Z}(T_p)$, with $4N$ points per period, to which three simultaneous symmetries are imposed.

The first two symmetries are “even” and “real” that allow one to consider the “cosine” DFT and IDFT, namely

$$\begin{aligned} S(kT) &= T \sum_{n=0}^{2N} \mu_n s(nT) \cos 2\pi \frac{nk}{4N}, \\ s(nT) &= F \sum_{k=0}^{2N} \mu_k S(kF) \cos 2\pi \frac{nk}{4N}, \end{aligned} \quad (12.28)$$

where now

$$\mu_n = \begin{cases} 1, & n = 0, 2N, \\ 2 & \text{elsewhere.} \end{cases}$$

In this form, with $4N$ instead of $2N$, the sequences $s(nT)$ and $S(kF)$ have length $2N + 1$.

At this point the third symmetry¹ is introduced: *zero at the even instants* (Fig. 12.11)

$$s(2nT) = 0, \quad n \in \mathbb{Z}. \quad (12.29)$$

Hence, (12.28) become

$$\begin{aligned} S(kT) &= 2T \sum_{n=0}^{N-1} s((2n+1)T) \cos 2\pi \frac{(2n+1)k}{4N}, \\ s((2n+1)T) &= F \sum_{k=0}^{2N} \mu_k S(kF) \cos 2\pi \frac{(2n+1)k}{4N}, \end{aligned} \quad (12.30)$$

¹“Symmetry” is intended in the generalized sense introduced at the end of Chap. 4.

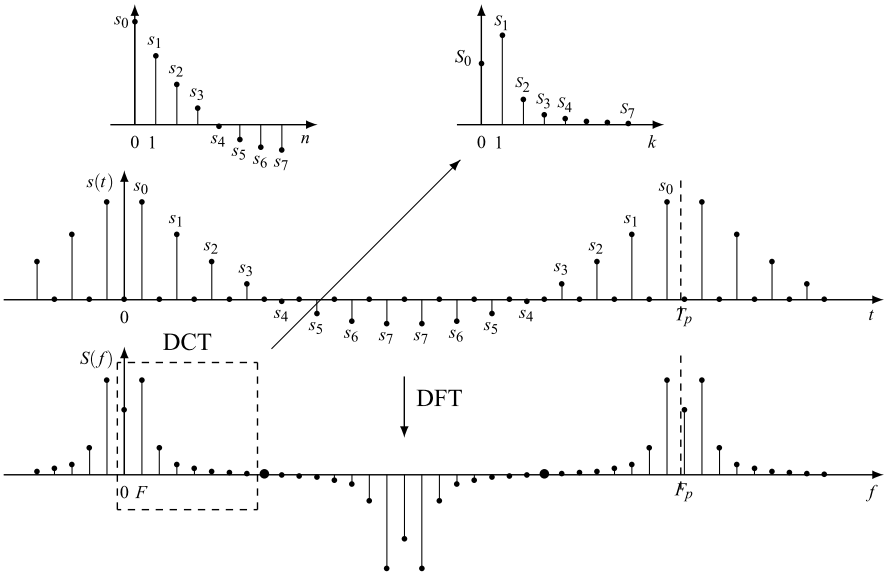


Fig. 12.11 Deduction of DCT as the “cosine” DFT with $4N$ points of a *real even signal with zeros at even points*

where we have considered that $\mu_n = 2$ for every n odd. Now, in (12.30) we find N values of the signal and $2N + 1$ values of the transform. For the reduction of the latter, we search for the consequence of (12.29) in the frequency domain. To this end, we note that the $\mathbb{Z}(T)/\mathbb{Z}(T_p) \rightarrow \mathbb{Z}(2T)/\mathbb{Z}(T_p)$ down-sampling of $s(nT)$ gives a zero signal and the dual $\mathbb{Z}(F)/\mathbb{Z}(F_p) \rightarrow \mathbb{Z}(F)/\mathbb{Z}(\frac{1}{2}F_p)$ up-periodization gives a zero FT. Hence, expressing the up-periodization, we find

$$S(f) + S\left(f - \frac{1}{2}F_p\right) = 0.$$

Since $S(f)$ is even with period F_p , we can write

$$S(-f) = -S\left(f - \frac{1}{2}F_p\right) = -S\left(f + \frac{1}{2}F_p\right), \tag{12.31}$$

which must be interpreted as odd symmetry with respect to $\frac{1}{4}F_p = NF$ (see (12.22)). Hence, the “third” symmetry for the FT becomes the *odd symmetry with respect to a quarter of a period*, which implies

$$S(NF) = 0; \quad S(2NF + kF) = -S(kF), \quad k = 1, 2, \dots, N - 1.$$

Using these relations and considering that the cosine terms have the same symmetry, from the second of (12.30) we obtain

$$s((2n+1)T) = F \sum_{k=0}^{N-1} (\mu_k + \mu_{2N-k}) S(kF) \cos 2\pi \frac{(2n+1)k}{4N}.$$

Finally, noting that $\mu_k + \mu_{2N-k} = 2\mu_k$ for every k , the relation pair is obtained:

$$\begin{aligned} S(kF) &= 2T \sum_{n=0}^{N-1} s((2n+1)T) \cos 2\pi \frac{(2n+1)k}{4N}, \\ s((2n+1)T) &= 2F \sum_{k=0}^{N-1} \mu_k S(kF) \cos 2\pi \frac{(2n+1)k}{4N}, \end{aligned} \quad (12.32)$$

which is substantially the pair (12.26a), (12.26b).

Letting

$$S_k = \alpha_k S(kF), \quad s_n = s((2n+1)T),$$

where α_k is arbitrary, and choosing *symmetrical spacings* defined by (12.13a) with $4N$ instead of N , that is, $T = F = 1/\sqrt{4N}$, one gets

$$\boxed{\begin{aligned} S_k &= \alpha_k \frac{1}{\sqrt{N}} \sum_{n=0}^{N-1} s_n \cos 2\pi \frac{(2n+1)k}{4N}, \\ s_n &= \frac{1}{\sqrt{N}} \sum_{k=0}^{N-1} \frac{\mu_k}{\alpha_k} S_k \cos 2\pi \frac{(2n+1)k}{4N}. \end{aligned}} \quad (12.33)$$

Considering that these relations are not symmetric, one could choose

$$\alpha_k = 1 \quad \forall k \quad (\text{uniform weights}), \quad (12.33a)$$

but to get (12.26a), (12.26b), the choice is $\alpha_k = \varepsilon_k = \sqrt{\mu_k}$.²

12.5.2 DCT Examples

For numerical computations, it is not convenient to use the DCT formula (12.26a), but rather the DFT with the constraint of the three symmetries. Hence, given a real sequence s_0, s_1, \dots, s_{N-1} :

²This choice yields the property that the DCT and IDCT matrices are each others transpose.

- (1) We compose the *associate* signal $s(nT)$, $nT \in \mathbb{Z}(T)/\mathbb{Z}(T_p)$, where the spacing T is arbitrary (but at the end we set $T = 1/\sqrt{4N}$), and $T_p = 4T$. The given sequence, together with the three symmetries, identifies the *associate* signal, as shown in Fig. 12.11.
- (2) We calculate the DFT of the associate signal, having $4N$ values per period; the resulting DFT is a function $S(kF)$, $kF \in \mathbb{Z}(F)/\mathbb{Z}(F_p)$, which still has $4N$ values per period.
- (3) The DCT sequence S_0, S_1, \dots, S_{N-1} is finally given by the first quarter of a period of $S(kF)$.

This procedure is illustrated in Table 12.2 in a few cases. Here we use the choice $\alpha_k = 1$, instead of the standard form (12.26a, 12.26b), which in this context appears to be artificial. In (1) the sequence s_n is constant, but the associated signal is not constant. However, the final DCT is an impulse at the origin. This example allows one to assert that a “quasi-constant” sequence will have a DCT with values “concentrated around the origin.” In (2) the sequence s_n is an impulse, but the DCT is not a constant, being given by a cosine in its first fourth of a period. Comparison of (1) and (2) shows that for the DCT a Symmetry Rule, as the rule seen for the FT, does not hold. In (3) the sequence s_n has only the nonzero value s_1 ; the corresponding DCT is given by a 3/4 of period of a cosine. In (4) a constant DCT S_k is assumed, but the IDCT is not given by an impulse.

12.5.3 Properties of the DCT

To obtain the DCT properties, it is convenient to make reference to the *associated* signal and the corresponding DFT. Below we denote by $S(kF)$ the DCT obtained from (12.33) with uniform weights ($\alpha_k = 1$) and by \tilde{S}_k the standard DCT given by (12.26a).

Energy Application of the Parseval theorem (12.9) to the associate signal yields

$$\sum_{n=0}^{N-1} s_n^2 = \sum_{k=0}^{N-1} \mu_k S_k^2 = \sum_{k=0}^{N-1} \varepsilon_k \tilde{S}_k^2. \quad (12.34)$$

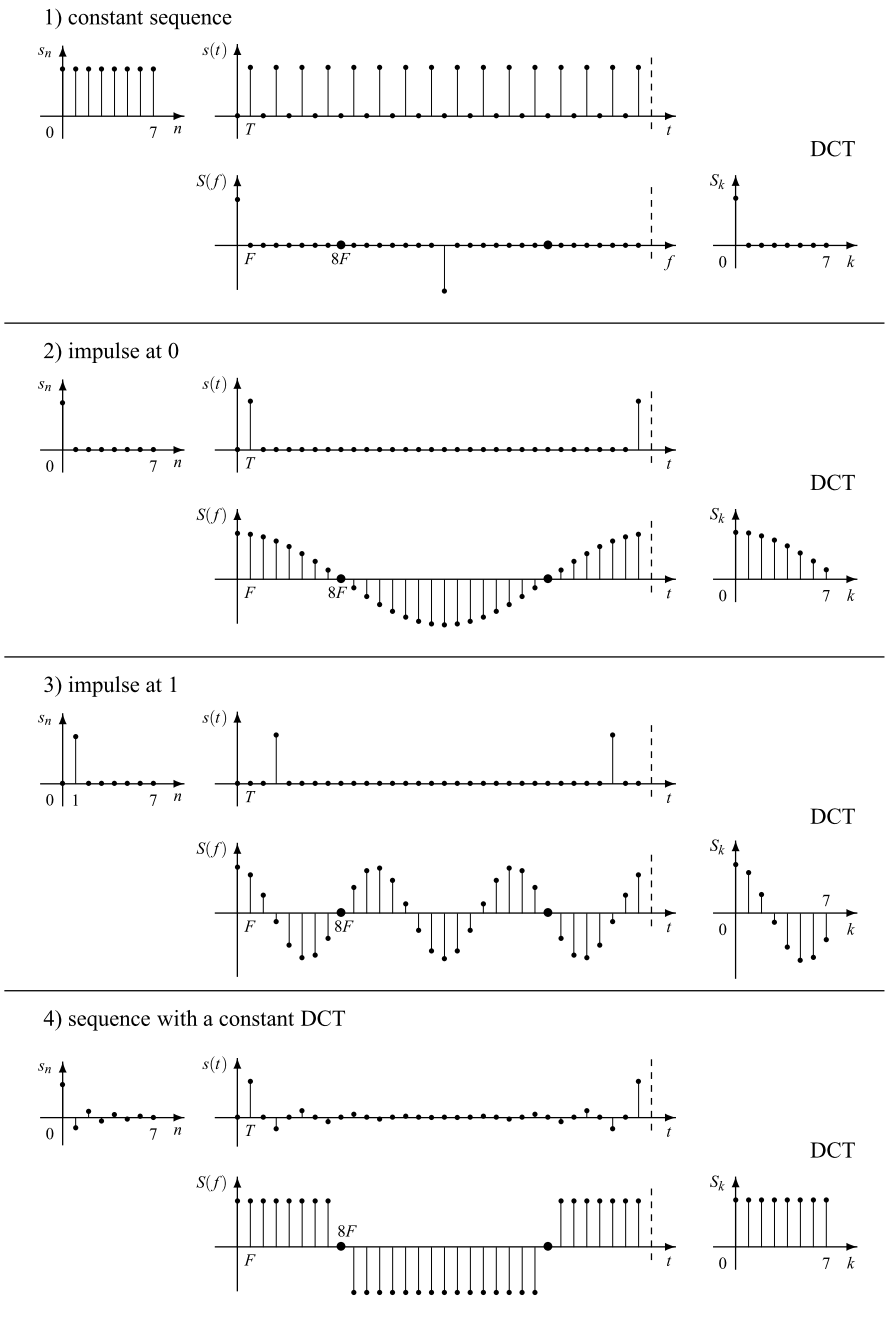
Area Application of area rule (for the Fourier transform) to the associate signal yields

$$\frac{1}{N} \sum_{n=0}^{N-1} s_n = S_0 = \tilde{S}_0,$$

whereas application to the DFT of the associate signal, and considering that $s(0) = 0$, gives

$$\sum_{k=0}^{N-1} \mu_k S_k = \sum_{k=0}^{N-1} \varepsilon_k \tilde{S}_k = 0.$$

Table 12.2 Example of DCT pairs



Orthogonality Conditions Considering that the DCT and IDCT are the inverse of each other, the following orthogonality conditions hold:

$$\begin{aligned} \frac{1}{N} \sum_{k=0}^{N-1} \mu_k \cos 2\pi \frac{(2m+1)k}{4N} \cos 2\pi \frac{(2n+1)k}{4N} &= \delta_{mn}, \\ \frac{1}{N} \sum_{n=0}^{N-1} \mu_k \cos 2\pi \frac{(2n+1)h}{4N} \cos 2\pi \frac{(2n+1)k}{4N} &= \delta_{hk}. \end{aligned} \quad (12.35)$$

A Fundamental Property The DFT associated to the DCT is an even function with respect to a quarter of a period. This implies the condition

$$\boxed{S(NF) = 0}. \quad (12.36)$$

Hence, for the symmetry conditions imposed to the associate signal, the associate DCT is forced to cross the zero level at a quarter of a period. This consideration (which cannot be rigorous since the domain is discrete) explains why the DCT, as a tendency, concentrates the energy about the origin. Example 2 of Table 12.2 is appropriate to this regard: for a sequence formed by an impulse at the origin, the DFT, which does not have the symmetry constraints of the DCT, gives a constant sequence and then with a uniform energy density. Instead, the DCT takes its values from a quarter of cosine with a final zero value.

A full characterization of the DCT properties should be done in a statistical framework. To this purpose, it is worth noting that the DCT (an input-independent orthogonal transform) is very close to the Karhunen–Loève transform (the input-dependent optimal orthogonal transform) for highly correlated sources, as the ones used to model real images. This property was first noticed by Ahmed et al. [1] for a first-order separable Markov image model with high values of the correlation between adjacent pixels. A formal proof can be found in Jain [7].

The DCT properties for the image coding are now illustrated.

12.5.4 Role of DCT in Image Compression

In coding systems, based on the DCT, an image is partitioned into small blocks of size 8×8 . The DCT is evaluated on the 8 lines of each block and then along the columns of the resulting block. In such a way a separable 2D DCT is performed, producing an 8×8 block S_{ij} , $i = 0, \dots, 7$, $j = 0, \dots, 7$.

Figure 12.12 shows the image of *Lenna*, a test image used in image processing (with a resolution of 512×512 pixels) and the representation of the DCT modulus. More specifically, the subimage at the top represents the terms S_{00} at the left, the terms S_{01} at the right, and so on, following the figure from top to bottom and from left to right. Note that the energy decreases going on from low frequencies (S_{00} and a neighborhood). Finally, note that the S_{00} part is a low-pass down-sampled version of the original image.



Fig. 12.12 Original image of *Lenna* and its bidimensional DCT. Below: an example of 8×8 block of *Lenna* and its DCT (courtesy of Roberto Rinaldo)

Figure 12.12 also shows an 8×8 block, taken starting from position (248, 248), and the corresponding DCT. It is evident how the image energy concentrates at the low frequencies.

Figure 12.13 compares the DCT with the DFT of *Lenna* and clear evidences the better capability of the DCT to concentrate the energy toward low frequencies. This property is used in coding schemes, where the low-frequency part is quantized with high accuracy, whereas the high-frequency content is only roughly coded.

12.5.5 The Discrete Sine Transform (DST)

The DST is obtained from the DFT by imposing suitable symmetries, in a similar way as seen from the DCT. The direct transform (DST) and the inverse transform (IDST) are given by

$$S_k = \sqrt{\frac{2}{N+1}} \sum_{n=0}^{N-1} s_n \sin 2\pi \frac{(n+1)(k+1)}{2(N+1)}, \quad (12.37a)$$

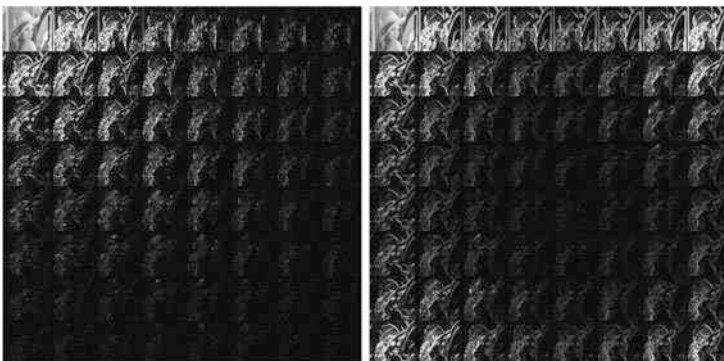


Fig. 12.13 Comparison of the DCT (left) and the DFT of *Lenna*

$$s_n = \sqrt{\frac{2}{N+1}} \sum_{k=0}^{N-1} S_k \sin 2\pi \frac{(n+1)(k+1)}{2(N+1)}, \tag{12.37b}$$

where s_n and S_k are real sequences.

To design (12.37a), (12.37b), we start from a DFT on $2(N+1)$ points and impose the “real” and “odd” symmetries. Then, we write the “sine” DFT and IDFT (see (12.25a), (12.25b)), namely

$$iS(kF) = 2 \sum_{n=0}^N T s(nT) \sin 2\pi \frac{nk}{2(N+1)},$$

$$s(nT) = 2 \sum_{k=0}^N FiS(kF) \sin 2\pi \frac{nk}{2(N+1)},$$

where both $s(nT)$ and $iS(kF)$ are real. The odd symmetry, which holds also for the DFT, imposes that $s(0) = 0$ and $S(0) = 0$, which become redundant, and, therefore, they are dropped by letting

$$s_n = s((n+1)T), \quad S_k = S((k+1)F), \quad n, k = 0, 1, \dots, N-1.$$

Finally, letting $T = F = 1/\sqrt{2(N+1)}$, we arrive at (12.37a), (12.37b). Hence, the deduction of the DST is more straightforward than the DCT.

The DST has no the same practical relevance as the DCT, and, in fact, *it has no capability of concentrating the energy toward the low frequencies*. On the contrary, the condition $S(0) = 0$ leads to think that it “removes” energy from the low frequencies. However, the DST would have the advantage to be perfectly symmetric with respect to the IDST.

12.6 Matrix Form of the DFT and of Other Transforms

The DFT and other transforms as the DCT are often presented as a matrix multiplication of the form

$$\mathbf{S} = \mathbf{W}\mathbf{s}, \quad (12.38)$$

where \mathbf{s} is a vector of size N , \mathbf{W} is an $N \times N$ matrix, called DFT matrix, and \mathbf{S} represents the DFT of the vector \mathbf{s} . Similarly, the IDFT is written in the form $\mathbf{s} = \mathbf{W}^{-1}\mathbf{S}$. We add that these are the common forms used in practical applications. Here we connect this formulation to the previous one, where the DFT was applied to a periodic discrete-time signal. To this end, we use the S/P and P/S conversions for periodic signals.

12.6.1 S/P and P/S conversions on $\mathbb{Z}(T)/\mathbb{Z}(T_p)$

In Sect. 7.5 we have seen that these conversions can be applied to periodic signals, that is, on finite groups. In the 1D case, the S/P conversion becomes a tf on $\mathbb{Z}(T)/\mathbb{Z}(T_p) \rightarrow \mathbb{Z}(MT)/\mathbb{Z}(T_p)$, where $T_p = NT$, and M must be a submultiple of N , that is, $N = LM$ with L a natural. This operation works as follows: a signal $s(t)$, $t \in \mathbb{Z}(T)/\mathbb{Z}(T_p)$, with $N = LM$ values per period, is subdivided into M signals $s_m(t)$, $t \in \mathbb{Z}(MT)/\mathbb{Z}(LMT)$, each with L values per period. The input–output relation has the usual form

$$s_m(t) = s(t + mT), \quad m = 0, 1, \dots, M - 1, t \in \mathbb{Z}(LT)/\mathbb{Z}(T_p). \quad (12.39)$$

Here, we consider the limit case, where $M = N$ and $L = 1$, and the S/P conversion produces a constant vector signal.

12.6.2 Matrix Form of the Transform of Periodic Signals

Consider the DFT of a signal $s(t)$, $t \in \mathbb{Z}(T)/\mathbb{Z}(T_p)$, written in the form

$$S(nF) = \sum_{n=0}^{N-1} T s(nT) W_N^{-kn}. \quad (12.40)$$

By applying a $\mathbb{Z}(T)/\mathbb{Z}(NT) \rightarrow \mathbb{Z}(NT)/\mathbb{Z}(NT)$ S/P conversion on the signal and a $\mathbb{Z}(F)/\mathbb{Z}(NF) \rightarrow \mathbb{Z}(NF)/\mathbb{Z}(NF)$ S/P conversion on the DFT, we find the constant vectors

$$\mathbf{s} = \begin{bmatrix} s_0 \\ \vdots \\ s_{N-1} \end{bmatrix}, \quad \mathbf{S} = \begin{bmatrix} S_0 \\ \vdots \\ S_{N-1} \end{bmatrix},$$

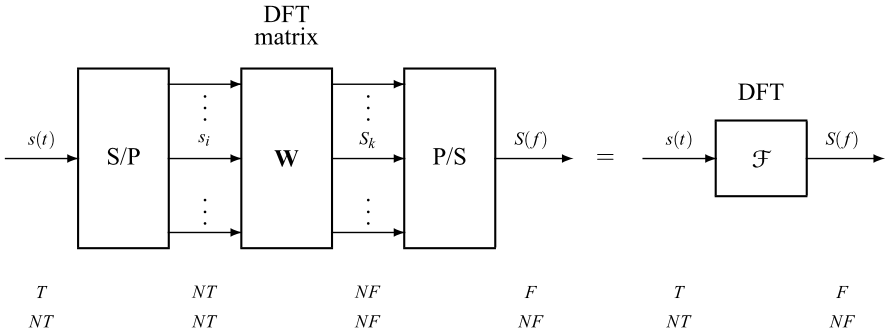


Fig. 12.14 Parallel architecture of the DFT, which becomes a multiplication by a constant matrix (the sequence of spacings and periods are indicated at the *bottom*)

where

$$s_n = s(t + nT), t \in \mathbb{Z}(NT)/\mathbb{Z}(NT), \quad S_k = S(f + kF), f \in \mathbb{Z}(NF)/\mathbb{Z}(NF),$$

are independent of t and f . Introducing the $N \times N$ matrix

$$\mathbf{W} = [W_{kn}] = [TW_N^{-kn}],$$

(12.40) can be written in the compact form $\mathbf{S} = \mathbf{W}\mathbf{s}$, anticipated in (12.38). The procedure to pass from periodic signals to constant vectors is illustrated in (Fig. 12.14).

The matrix formulation of the DFT can be also applied to aperiodic signals in a new context. A signal $s(t)$ on $\mathbb{Z}(T)$ is subdivided into blocks of N consecutive values obtaining a sequence of vectors \mathbf{s}_n . Then, for each n , the DFT matrix is applied and gives a sequence $\mathbf{S}_n = \mathbf{W}\mathbf{s}_n$ of DFT. This procedure is called *block transform* and will be seen in Chap. 14.

The consideration seen for the DFT can be applied as well to the DCT and similar transforms.

12.7 Fractional DFT and DCT

We have seen that the domains $I = \mathbb{Z}(T)/\mathbb{Z}(T_p)$ and $\hat{I} = \mathbb{Z}(F)/\mathbb{Z}(F_p)$, with the choice $T = 1/\sqrt{N}$, $T_p = \sqrt{N}$, become equal. Then, it is possible to consider the *fractional* DFT following the general ideas of the *fractional Fourier transform* developed in Sect. 5.12. Now we have a simplification because the fractional form can be established working with a square matrix instead of operators. The first step is the diagonalization of the DFT matrix \mathbf{W} , that is, $\mathbf{W} = \mathbf{U}\mathbf{\Lambda}\mathbf{U}^*$, where \mathbf{U} collects the orthonormal eigenvectors, and $\mathbf{\Lambda}$ is a diagonal matrix containing the eigenvalues λ_i as diagonal entries. Then, the matrix of the fractional DFT is obtained as

$$\mathbf{W}^\alpha = \mathbf{U}\mathbf{\Lambda}^\alpha\mathbf{U}^*,$$

where a is the “fraction” (a real number), and $\mathbf{\Lambda}^a$ contains the fractional eigenvalues given by λ_i^a . As seen in general in Sect. 5.12, there is the problem of *multiplicity* in the definition [3, 4]. Here, it is due to the multiplicity of the eigenvalues and to the ambiguity of the power to a real number λ_i^a . As regards the eigenvectors, an interesting choice is the *exact DFT eigenvectors* obtained in [5] using the Theory of Symmetries (see Sect. 4.13).

Similar considerations can be done for the fractional DCT starting from the $N \times N$ matrix defined by the first of (12.33), that is,

$$\mathbf{C} = [\alpha_k 1/\sqrt{N} \cos[2\pi(2n+1)k/4N]], \quad n, k = 0, 1, \dots, N-1.$$

The complete development of the fractional DCT has been carried out in [2].

12.8 Problems

12.1 ** [Sect. 12.3] Evaluate the DFT of the $\mathbb{Z}(T) \rightarrow \mathbb{Z}(T)/\mathbb{Z}(T_p)$ up-periodization of the unitary rectangular pulse on $[0, D) \cap \mathbb{Z}(T)$ with $D = MT \leq T_p$.

12.2 * [Sect. 12.3] The signal $s_0(t) = \cos 2\pi t/T_0$, $t \in \mathbb{Z}(T)/\mathbb{Z}(T_0)$, is truncated on the interval $[0, \alpha T_0)$ and repeated with period $T_p = \alpha T_0$, giving the signal $s(t)$, $t \in \mathbb{Z}/\mathbb{Z}(T_p)$. Find the DFT of $s(t)$.

12.3 ** [Sect. 12.3] In the previous problem suppose that α is a natural. Check that the DFT $S(f)$ consists of two impulses and explain why.

12.4 * [Sect. 12.3] Show that the discrete chirp signal $s(nT) = W_{2N}^{n^2}$ has period NT for N even and period $2NT$ for N odd.

12.5 ** [Sect. 12.5] Show that the sequence s_n that has a constant DCT (see Table 12.2) is given by

$$s_n = A_0 \frac{2N-1}{\sqrt{N}} \operatorname{sinc}_{(2N-1)} \left(\frac{(2N-1)(2n+1)}{2N} \right).$$

Take uniform weights and use identity (2.54).

12.6 ** [Sect. 12.5] Suppose that the DCT and IDCT, given by (12.33), hold. Then, prove orthogonality conditions (12.35).

References

1. N. Ahmed, T. Natarajan, K.R. Rao, Discrete cosine transform. IEEE Trans. Comput. C-23, 90–93 (1974)

2. G. Cariolaro, T. Erseghe, The fractional discrete cosine transform. *IEEE Trans. Signal Process.* **50**, 902–911 (2002)
3. G. Cariolaro, T. Erseghe, P. Kraniuskas, N. Laurenti, A unified framework for the fractional Fourier transform. *IEEE Trans. Signal Process.* **46**, 3206–3219 (1998)
4. G. Cariolaro, T. Erseghe, P. Kraniuskas, N. Laurenti, Multiplicity of fractional Fourier transforms and their relationships. *IEEE Trans. Signal Process.* **48**, 227–241 (2000)
5. T. Erseghe, G. Cariolaro, An orthonormal class of exact and simple DFT eigenfunctions with a high degree of symmetry. *IEEE Trans. Signal Process.* **51**(10), 2527–2539 (2003)
6. B. Haskell, A. Puri, A.N. Netravali, *Digital Video: An Introduction to MPEG-2* (Chapman & Hall, London, 1997)
7. A.K. Jain, *Fundamentals of Digital Image Processing* (Prentice Hall, Englewood Cliffs, 1999)
8. J.L. Mitchell, *MPEG Video Compression Standard* (Chapman & Hall, London, 1997)
9. W.B. Pennebaker, J.L. Mitchell, *JPEG Still Image Data Compression Standard* (Van Nostrand/Reinhold, London, 1993)
10. P.P. Vaidyanathan, *Multirate Systems and Filter Banks* (Prentice Hall, Englewood Cliffs, 1993)
11. M. Vetterli, J. Kovačević, *Wavelets and Subband Coding* (Prentice Hall, Englewood Cliffs, 1995)

Chapter 13

Signal Analysis via Digital Signal Processing

13.1 Introduction

In the middle of the last century the introduction of digital computers represented a tremendous opportunity in several fields, in particular in signal processing. However, the problem of *computational complexity* was soon clear in so far as elementary forms of processing required an unacceptable computational time. This was particularly true for the computation of the Fourier transform and, in fact, its evaluation, e.g., on a thousand points, required some hours of computer time. Therefore, scientists, such as Cooley and Tuckey in 1965 [1, 2], were strongly motivated in searching for fast algorithms able to reduce the computational complexity. In this context the Fast Fourier Transform (FFT) was formulated, and nowadays it is the most important tool in digital signal processing (and not only in this area).

As a historical note, Gauss was probably the first, at the beginning of the nineteenth century, to use an FFT-like algorithm in the evaluation of the orbit of the asteroid Ceres.

In this chapter we begin by showing that the direct evaluation of the DFT in N points requires about N^2 operations. Then, we present the FFT, which is an efficient algorithm of DFT computation, where the complexity is reduced to $N \log_2 N$ operations.

The algorithm of computational reduction will be based on the parallel architectures and, essentially *on the polyphase decomposition*, which will be applied iteratively to arrive at very simple building blocks. Also, the theory of *elementary transformations* and particularly the Duality Theorem play a fundamental role in the management of computational complexity reduction.

In the second part of the chapter, the usage of DFT/FFT is applied to evaluate FTs, convolutions, and other operations. This application is not trivial because it requires, as a preliminary, the passage from signals defined in a continuous or discrete domain to signals defined on finite groups and in particular on $\mathbb{Z}(T)/\mathbb{Z}(T_p)$.

UT 13.2 Computational Complexity of the DFT

Consider the N -point DFT written in the normalized form

$$S_k = \sum_{n=0}^{N-1} s_n W_N^{-kn}, \quad k = 0, 1, \dots, N-1, \quad (13.1)$$

and we want to evaluate its *computational complexity* in terms of number of operations. We suppose that the N roots of unit

$$W_N^0 = 1, W_N, W_N^2, \dots, W_N^{N-1} \quad (13.2)$$

have been saved in a memory; then the evaluation of W_N^{-kn} simply requires to identify the corresponding value in (13.2) and therefore does not require any computation. For instance, with $N = 8$, $k = 3$, and $n = 4$ it is sufficient to recognize that $W_8^{3 \cdot 4} = W_8^{12} = W_8^4$.

From (13.1), $N-1$ complex additions and N complex multiplications are needed to compute S_k for a given k . Since the computation must be carried out for the N values of k , the DFT computation requires $(N-1)N \simeq N^2$ complex additions and N^2 complex multiplications. We express the result by saying that the *computational complexity* $\mathcal{C}(N)$ of the DFT has the form N^2 :

$$\mathcal{C}(N) = N^2 \text{ operations.}$$

We can also note that the number of data accesses (read/write) increases with the same law N^2 .

The computation of the IDFT

$$s_n = \frac{1}{N} \sum_{k=0}^{N-1} S_k W_N^{kn} \quad (13.3)$$

has the same computational complexity of N^2 operations.

UT 13.3 Introduction to the FFT

The FFT is an algorithm for the fast computation of the DFT, which reduces the complexity from N^2 to $N \log_2 N$ when N is a power of 2.

In this section we show, in a preliminary form,¹ how the complexity can be reduced. In the next sections we consider a more general formulation, based on the *parallel* computation of the DFT.

¹For an alternative introduction, we suggest the tutorial paper [4].

The target is the numerical computation of the expression

$$s(n) = \sum_{k=0}^{N-1} S(k) W^{nk}, \quad n = 0, 1, \dots, N-1, \quad (13.4)$$

where $W \triangleq W_N = \exp(i2\pi/N)$. This expression allows us to handle both the DFT and the IDFT.

To show how the operation saving is achieved, we consider the case $N = 8$. Since $N = 2^3$, we can write the index n and k in the binary form

$$n = 4n_2 + 2n_1 + n_0 \rightarrow n_2n_1n_0, \quad k = 4k_2 + 2k_1 + k_0 \rightarrow k_2k_1k_0,$$

where the new indexes assume the values 0 and 1. In such a way, (13.4) becomes

$$s(n_2n_1n_0) = \sum_{k_0=0}^1 \sum_{k_1=0}^1 \sum_{k_2=0}^1 S(k_2k_1k_0) W^{n(4k_2+2k_1+k_0)}, \quad (13.5)$$

where $W^{n(4k_2+2k_1+k_0)} = W^{n4k_2} W^{n2k_1} W^{nk_0}$.

Substituting the binary representation of n in the three factors yields

$$\begin{aligned} W^{n4k_2} &= W^{(4n_2+2n_1+n_0)4k_2} = [W^{8(2n_2+n_1)k_2}] \cdot W^{4n_0k_2}, \\ W^{n2k_1} &= W^{(4n_2+2n_1+n_0)2k_1} = [W^{8n_2k_1}] \cdot W^{(2n_1+n_0)2k_1}, \\ W^{nk_0} &= W^{(4n_2+2n_1+n_0)k_0}, \end{aligned}$$

where we have used the identity $W^8 = \exp(i2\pi 8/8) = \exp(i2\pi) = 1$ and the fact that the factors in square brackets are unitary. Therefore, (13.5) becomes

$$s(n_2n_1n_0) = \underbrace{\sum_{k_0=0}^1 \sum_{k_1=0}^1 \sum_{k_2=0}^1 S(k_2k_1k_0) W^{4n_0k_2} W^{(2n_1+n_0)2k_1} W^{(4n_2+2n_1+n_0)k_0}}_{S_3(n_0n_1n_2)}. \quad (13.6)$$

In this expression it is convenient to carry out the summation in the order indicated in (13.6). Starting from the coefficients $S(k) = S(k_2k_1k_0)$ we recursively evaluate

$$S_1(n_0k_1k_0) = \sum_{k_2 \in \{0,1\}} S(k_2k_1k_0) W^{4n_0k_2}, \quad (13.7a)$$

$$S_2(n_0n_1k_0) = \sum_{k_1 \in \{0,1\}} S_1(n_0k_1k_0) W^{(2n_1+n_0)2k_1}, \quad (13.7b)$$

$$S_3(n_0 n_1 n_2) = \sum_{k_0 \in \{0,1\}} S_2(n_0 n_1 k_0) W^{(4n_2 + 2n_1 + n_0)k_0}. \quad (13.7c)$$

At the end, S_3 gives the desired result

$$s(n) = s(n_2 n_1 n_0) = S_3(n_0 n_1 n_2).$$

For $N = 8$, the direct computation of (13.5) requires $N^2 = 64$ multiplications and so many additions, whereas using (13.6), this number is reduced to 24. For instance, in (13.7a) for $n_0 k_1 k_0$ fixed, one addition and one multiplication are needed (for $k_2 = 0$, the multiplication is by 1, and therefore it is not counted). Since $n_0 k_1 k_0$ assumes 8 values, the computation of $S_1(n_0 k_1 k_0)$ requires 8 additions and 8 multiplications. The same computation must be repeated for each one of the expressions (13.7a), (13.7b), (13.7c) and therefore the balance is of $3 \cdot 8 = 24$ additions and $3 \cdot 8 = 24$ multiplications.

In general with $N = 2^m$, (13.6) consists of m recurrences of the form (13.7a), (13.7b), (13.7c), each one requiring N additions and N multiplications; for the multiplication, the actual number of recurrences is reduced to $m - 1$. Hence, we find

$$\begin{aligned} \sigma(N) &= Nm = N \log_2 N \quad \text{additions,} \\ \mu(N) &= N(m - 1) = N(\log_2 N - 1) \quad \text{multiplications.} \end{aligned} \quad (13.8)$$

13.3.1 FFT Computational Complexity

We have seen that for the FFT with $N = 2^m$ points, the computational complexity is

$$\boxed{\mathcal{C}(N) = N \log_2 N \text{ operations}}$$

in place of $\mathcal{C}(N) = N^2$ operations of the direct DFT computation.

It is interesting to explicitly visualize this complexity to have a concrete impression on the FFT fastness. In Table 13.1, $N \log_2 N$ is compared with N^2 , and also the corresponding computation time is compared, assuming $1 \mu\text{s}$ for a single operation. For instance, with $N = 2^{13} = 8192$ we find that the FFT requires only one tenth of a second, instead of more than one minute for the direct DFT evaluation.²

13.3.2 FFT Implementations

The Cooley and Takey algorithm was extended to an arbitrary natural N , although the maximum operation saving is achieved when N is a power of 2. For an N -point

²To the author's knowledge, the largest FFT implemented is found in the NASA SETI (Search for Extra-terrestrial intelligence) project with N equal to $2^{30} \simeq 10^9$.

Table 13.1 Computational complexity of DFT and FFT

	Size N	DFT		FFT	
		$\mathcal{C}(N) = N^2$	Time	$\mathcal{C}(N) = N \log_2 N$	Time
2^4	16	256	256 μ s	64	64 μ s
2^5	32	1 024	1 ms	160	160 μ s
2^6	64	4 096	4 ms	384	384 μ s
2^7	128	16 384	16.4 ms	896	896 μ s
2^8	256	65 536	65.5 ms	2 048	2 ms
2^9	512	262 144	0.26 s	4 608	4.6 ms
2^{10}	1 024	1 048 576	1 s	10 240	10 ms
2^{11}	2 048	4 194 304	4.2 s	22 528	22 ms
2^{12}	4 096	1.6×10^6	16.8 s	49 152	49 ms
2^{13}	8 192	6.7×10^7	1 min 7 s	106 496	0.1 s
2^{14}	16 384	2.6×10^8	4 min 28 s	229 376	0.2 s
2^{15}	32 768	1×10^9	17 min 54 s	491 520	0.5 s
2^{16}	65×10^3	4.2×10^9	1 h 11 min 35 s	1×10^6	1 s
2^{17}	131×10^3	1.7×10^{10}	4 h 44 min	2.2×10^6	2 s
2^{20}	1×10^6	1×10^{12}	12 days 18 hours	2×10^7	21 s
2^{24}	1.6×10^7	2.8×10^{14}	9 years	4×10^8	6 min 42 s
2^{27}	1.3×10^8	1.8×10^{16}	572 years	3.6×10^9	1 h 23 min
2^{30}	1.1×10^9	1.1×10^{18}	36 558 years	3.2×10^{10}	8 h 57 min

FFT, the usage format has the form

$$s = [s_0, s_1, \dots, s_{N-1}] \xrightarrow{\text{FFT}} S = [S_0, S_1, \dots, S_{N-1}], \tag{13.9a}$$

$$S = [S_0, S_1, \dots, S_{N-1}] \xrightarrow{\text{IFFT}} s = [s_0, s_1, \dots, s_{N-1}], \tag{13.9b}$$

where the vectors are related by

$$S_k = \alpha_N \sum_{n=0}^{N-1} s_n W_N^{-kn}, \quad 0 \leq k \leq N - 1, \tag{13.10a}$$

$$s_n = \beta_N \sum_{k=0}^{N-1} S_k W_N^{kn}, \quad 0 \leq n \leq N - 1. \tag{13.10b}$$

The coefficients α_N and β_N may be (see Sect. 11.2)

$$\begin{aligned} \alpha_N &= 1, & \beta_N &= 1/N, \\ \alpha_N &= 1/N, & \beta_N &= 1, \\ \alpha_N &= 1/\sqrt{N}, & \beta_N &= 1\sqrt{N}. \end{aligned} \tag{13.11}$$

A small, but intriguing, problem is that the index 0 is not accepted in most computer programs, so attention must be paid with vector management. We now give explicitly the FFT usage of most popular computer packages.

The FFT in FORTRAN The standard implementation is based on real arithmetic. The usage is

```
CALL FFT(C, D, N, Index)
```

where C is the vector of the real part, D is the vector of the imaginary part, N the number of points, $\text{Index} = -1$ for FFT computation, and $\text{Index} = 1$ for IFFT computation. The final result is stored in the same vectors C and D . Since the index 0 is not accepted, we have to set $C(n+1) = \Re s_n$, $D(n+1) = \Im s_n$, $0 \leq n \leq N-1$. Then, with $\text{Index} = -1$ expression (13.9b) is computed with $\Re S_k = C(k+1)$, $\Im S_k = D(k+1)$. Analogously, with $\text{Index} = 1$ expression (13.10b) is computed.

The FFT in MATLAB[®] Given a complex sequence s , the usage is

$$S = \text{fft}(s), \quad s = \text{ifft}(S).$$

MATLAB[®] introduces the normalization factor $1/N$ in the IDFT.

The FFT in Mathematica[®] The complex sequence s must be written in the `List` format. Then, the usage is

$$S = \text{FourierInverse}[s], \quad s = \text{Fourier}[S].$$

Mathematica[®] inverts the roles of DFT and IDFT and uses the symmetrical normalization factor $1/\sqrt{N}$.

UT 13.4 The FFT as a Parallel Computation

The computational complexity reduction performed by the FFT, seen in a preliminary form, is now framed in the *parallel computation* using the technique of multirate tfs. The leading idea is that the DFT computation can be subdivided into the computation of two DFTs on half points, with the final combination of the results. This idea is iterated until DFTs of size 2 are obtained. The N -point DFT could be subdivided into an arbitrary number of parts, but the subdivision into two parts (when possible) is the most efficient one. In any case we have a computational saving.

In this section we consider the one-dimensional case, whereas the multidimensional case will be developed in the next sections.

13.4.1 Time Decimation

We want to compute the DFT $S(f)$ of a signal $s(t)$, $t \in \mathbb{Z}(T)/\mathbb{Z}(T_p)$, with N points per period. Suppose that the number of point N is factorizable as

$$N = ML.$$

Then, $s(t)$, $t \in \mathbb{Z}(T)/\mathbb{Z}(T_p)$, can be S/P converted into M signals

$$s_0(t), s_1(t), \dots, s_{M-1}(t), \quad t \in \mathbb{Z}(MT)/\mathbb{Z}(T_p),$$

each one with $L = N/M$ points per period. Their Fourier transforms

$$S_0(f), S_1(f), \dots, S_{M-1}(f), \quad f \in \mathbb{Z}(F)/\mathbb{Z}\left(\frac{1}{M}F_p\right),$$

are M DFTs on L points. Now, the DFT $S(f)$ can be calculated from the M DFTs $S_m(f)$. Indeed, the frequency analysis of S/P conversion (see Sect. 12.6) gives

$$S(f) = \frac{1}{M} \sum_{m=0}^{M-1} S_m(f) e^{-i2\pi f m T}. \quad (13.12)$$

The procedure now outlined is shown in Fig. 13.1, and is based on the following steps:

- (1) an S/P conversion (or polyphase decomposition) of the given signal $s(t)$ into M signals,
- (2) the separate computation of the M DFTs $S_m(f)$, and
- (3) the combination, according to (13.12), of the $S_m(f)$ to get $S(f)$.

We recognize that the tf in step (3) is the dual of a P/S conversion, since it relates the FTs of the signals $s_m(t)$ and $s(t)$. This dual tf, denoted by $\widehat{\text{P/S}}$ in Fig. 13.1, is formed by M parallel branches, where the m -branch consists of a $\mathbb{Z}(F)/\mathbb{Z}(LF) \rightarrow \mathbb{Z}(F)/\mathbb{Z}(MLF)$ down-periodization followed by a multiplier by $e^{-i2\pi f m T}$; a final adder collects the contribution of the M branches.

The above procedure is called *time decimation* since the S/P conversion includes $\mathbb{Z}(T) \rightarrow \mathbb{Z}(MT)$ down-sampling, which is also called “time decimation.”

We now examine the operation balance, where $\sigma(N)$ and $\mu(N)$ denote respectively the numbers of additions and multiplications in an N -point DFT.

The S/P conversion of step (1) has no complexity. Step (2) requires M L -point DFT computations, with a complexity of $M\sigma(L)$ additions and $M\mu(L)$ multiplications. Finally, in step (3), for every frequency f , $M - 1$ additions and $M - 1$ multiplications are required (for $m = 0$, the multiplication by 1 is not counted). The frequencies f are N , since the global DFT is on N points. Therefore, the budget is

$$\boxed{\begin{aligned} \sigma(N) &= M\sigma(L) + (M - 1)N, \\ \mu(N) &= M\mu(L) + (M - 1)N. \end{aligned}} \quad (13.13)$$

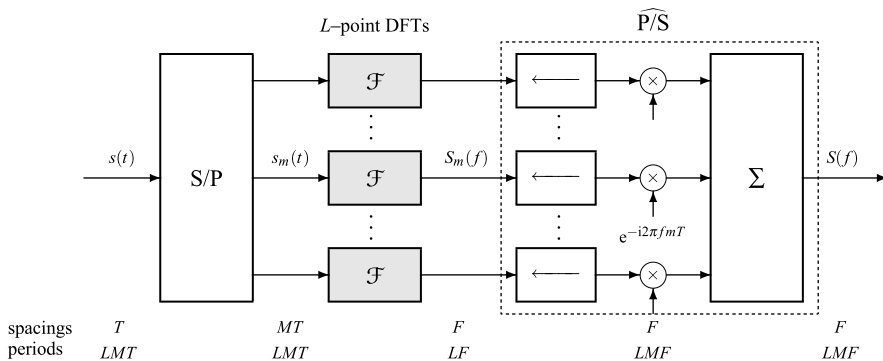


Fig. 13.1 Parallel DFT computation using *time decimation*

The parallel scheme, based on the time decimation, is shown in Fig. 13.2 for $N = 16$, $M = 2$, and $L = 8$. From the signal $s(t)$, $t \in \mathbb{Z}(T)/\mathbb{Z}(T_p)$, with $N = 16$ points per period, the signals $s_0(t)$ and $s_1(t)$, $t \in \mathbb{Z}(2T)/\mathbb{Z}(T_p)$, are obtained by taking the values at the even and odd instants, respectively. The DFTs $S_0(f)$ and $S_1(f)$, defined on $\mathbb{Z}(F)/\mathbb{Z}(\frac{1}{2}F_p) = \mathbb{Z}(F)/\mathbb{Z}(8F)$, have 8 values per period and are combined according to (13.12), which becomes

$$S(kF) = \frac{1}{2} [S_0(kF) + S_1(kF)W_N^{-k}]. \tag{13.14}$$

In this relation, the exponential has period $N = 16$, and the two DFTs are down-periodized to $N = 16$ values per period; therefore the 8 values of each DFT are used twice.

The computation of (13.14) requires $N = 16$ operations (additions + multiplications) to be added to the operations required for the two DFTs on $\frac{1}{2}N = 8$ points. The overall budget is

$$\sigma(16) = 2\sigma(8) + 16, \quad \mu(16) = 2\mu(8) + 16,$$

in agreement with (13.13).

Recombination via DFT By considering the general case, we note that the *recombination* of the DFT $S_m(f)$ stated by (13.12) resembles an M -point DFT. But, in general, it is not a DFT. However, rearranging (13.12) using an S/P conversion, the recombination by L M -point DFTs becomes possible.

13.4.2 Frequency Decimation

The S/P conversion can also be applied to the FT $S(f)$, $f \in \mathbb{Z}(F)/\mathbb{Z}(F_p)$, which is defined on a discrete domain like the signal. Assuming again that $N = ML$, the S/P

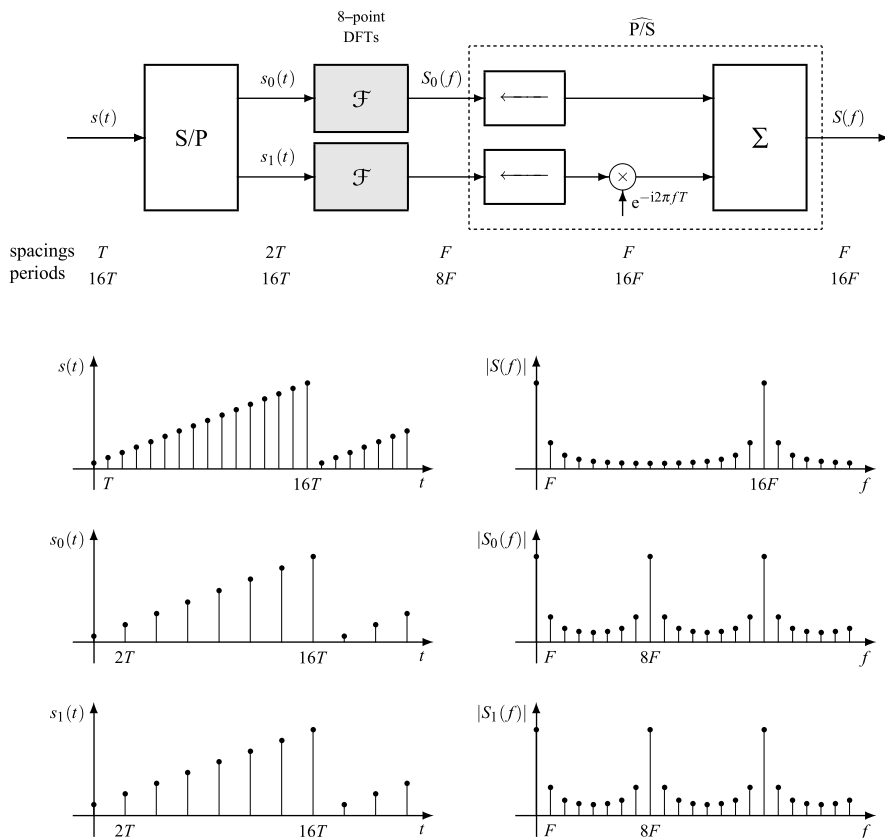


Fig. 13.2 Time decimation in the binary case for $N = 16$

conversion of $S(f)$ is given by

$$S'_m(f) = S(f + mF), \quad f \in \mathbb{Z}(LF)/\mathbb{Z}(F_p), \quad m = 0, 1, \dots, M - 1, \quad (13.15)$$

where each $S'_m(f)$ has M values per period. Since the target of the computation is $S(f)$, the previous conversion must be considered in the reverse sense, that is, the P/S conversion of the $S'_m(f)$ to obtain $S(f)$, as shown in Fig. 13.3.

Finally, we want to find how to get the signals $s'_m(t) = \mathcal{F}^{-1}[S'_m|t]$ from $s(t) = \mathcal{F}^{-1}[S|t]$. The required tf is the *antidual* of the S/P conversion, that is, the time tf whose dual is the S/P conversion governed by (13.15). We recall (see Sect. 7.5) that the m -branch of an S/P conversion consists of (with the present notation):

- (a) a shift of $-mF$

$$\tilde{S}_m(f) = S(f + mF), \quad f \in \mathbb{Z}(F)/\mathbb{Z}(F_p),$$

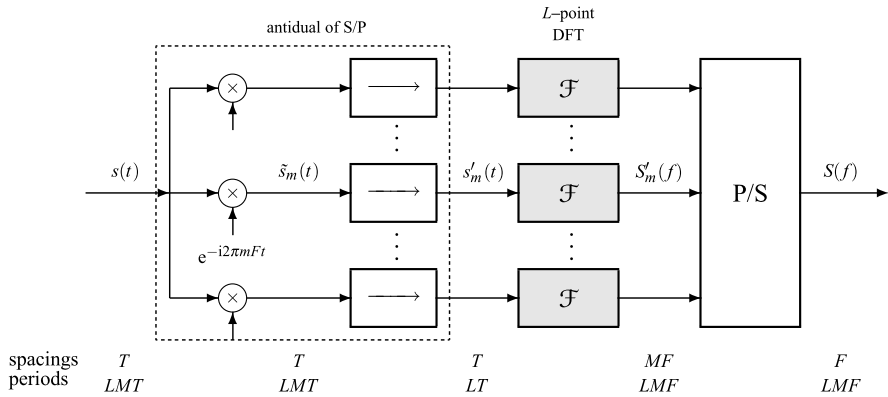


Fig. 13.3 Parallel DFT computation using the *frequency decimation*

(b) a $\mathbb{Z}(F)/\mathbb{Z}(F_p) \rightarrow \mathbb{Z}(LF)/\mathbb{Z}(F_p)$ down-sampling

$$S'_m(f) = \tilde{S}_m(f), \quad f \in \mathbb{Z}(LF)/\mathbb{Z}(F_p). \tag{13.16}$$

Taking the inverse FT in these relationships, we find

$$\begin{aligned} \tilde{s}_m(t) &= s(t)e^{-i2\pi m F t}, \quad t \in \mathbb{Z}(T)/\mathbb{Z}(T_p), \\ s'_m(t) &= \sum_{k=0}^{M-1} \tilde{s}_m\left(t - k \frac{1}{M} T_p\right), \quad t \in \mathbb{Z}(T)/\mathbb{Z}\left(\frac{1}{M} T_p\right) \end{aligned}$$

where we consider that a frequency down-sampling becomes a time up-periodization. Hence, the global relationship of the anti dual S/P converter is

$$s'_m(t) = \sum_{k=0}^{M-1} s\left(t - k \frac{1}{M} T_p\right) e^{-i2\pi m F (t - k \frac{1}{M} T_p)}, \quad t \in \mathbb{Z}(T)/\mathbb{Z}\left(\frac{1}{M} T_p\right). \tag{13.17}$$

From the above considerations we conclude that parallel DFT computation, based on the *frequency decimation*, can be performed as follows:

- (1) Apply to the signal $s(t)$, $t \in \mathbb{Z}(T)/\mathbb{Z}(T_p)$, the anti-dual S/P conversion to get the components $s'_m(t)$, $t \in \mathbb{Z}(T)/\mathbb{Z}(\frac{1}{M} T_p)$, according to (13.17);
- (2) Compute the FTs $S'_m(f)$ of the M components $s'_m(t)$, which are L -point DFTs;
- (3) Apply the P/S conversion of the $S'_m(f)$ to get $S(f)$.

In step (1) the construction of the $s'_m(t)$ requires $M - 1$ multiplications for each t , and, since t assumes N values, $(M - 1)N$ multiplications are required. The up-periodization requires $M - 1$ additions for every t and every m ; but t assumes L values, since the $s'_m(t)$ have L values per period, and m assumes M values. Hence, we find globally $(M - 1)LM = (M - 1)N$ additions. In conclusion, the budget is

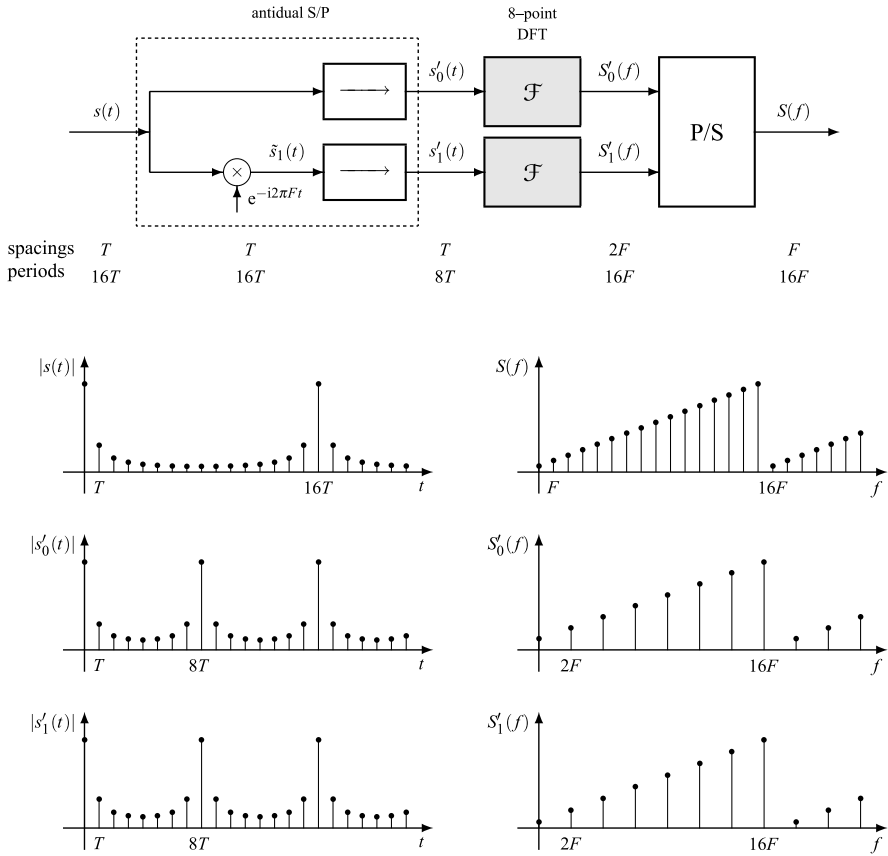


Fig. 13.4 Frequency decimation in the binary case for $N = 16$

still given by (13.13), that is, *the frequency decimation and the time decimation have the same computational complexity.*

The frequency decimation is illustrated in Fig. 13.4 for $N = 16$, $M = 2$, and $L = 2$. The components $s'_m(t)$ are computed according to (13.16), which gives

$$\begin{aligned} \tilde{s}_0(t) &= s(t), & \tilde{s}_1(t) &= s(t)e^{-i2\pi Ft}, \\ s'_0(t) &= \tilde{s}_0(t) + \tilde{s}_0\left(t - \frac{1}{2}T_p\right), & s'_1(t) &= \tilde{s}_1(t) + \tilde{s}_1\left(t - \frac{1}{2}T_p\right). \end{aligned} \tag{13.18}$$

These operations are those of antidual S/P conversion, which becomes the S/P conversion of the FT $S(f)$ in the frequency domain, according to

$$S(f + mF) = S'_m(f), \quad m = 0, 1.$$

The first line of (13.18) requires N multiplications to give the signal $\tilde{s}_1(t)$ in a period (which has N points), whereas the two up-periodizations require 8 additions

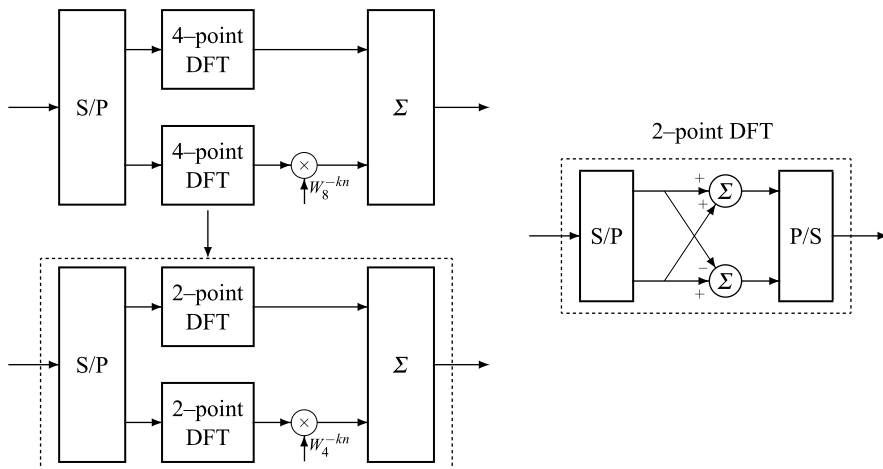


Fig. 13.5 Iterations with time decimations in the binary case with $N = 8$

each, since $s'_0(t)$ and $s'_1(t)$ have only $\frac{1}{2}N = 8$ per period. Globally we find $N = 16$ multiplications and $N = 16$ additions, in agreement with the general case.

13.4.3 Decimation Iterations

The parallel computation allows the computation of a DFT with $N = LM$ points by M L -point DFTs, with the additional computation to combine the results (in the time decimation) or to construct the components (in the frequency decimation). This procedure can be iterated several times, sequentially, to decompose the DFT computation into smaller and smaller DFTs.

The iteration is now explicitly shown for the case of the time decimation; for the frequency decimation case, the procedure is perfectly similar. Suppose that $N = 2^3 = 8$; then the 8-point DFT is subdivided into two branches, each having a 4-point DFT (Fig. 13.5). Then, each 4-point DFT is further subdivided into two branches, each containing a 2-point DFT, and the iteration is stopped. A 2-point DFT is explicitly given by

$$S(0) = T[s(0) + s(T)], \quad S(F) = F[s(0) - s(T)]$$

and requires only 2 additions and no multiplication:

$$\sigma(2) = 2, \quad \mu(2) = 0.$$

Hence, in the iterative procedure the computation complexity is *practically confined to the extra computation* to combine the results. For $M = 2$, the general equa-

tion is (13.13) and can be written as

$$\sigma(N) = 2\sigma\left(\frac{1}{2}N\right) + N, \quad \mu(N) = 2\mu\left(\frac{1}{2}N\right) + N. \quad (13.19)$$

In particular, starting from $N = 8$, the additions are

$$\sigma(8) = 2\sigma(4) + 8, \quad \sigma(4) = 2\sigma(2) + 4,$$

and, considering that $\sigma(2) = 2$, we have

$$\sigma(8) = 2[2\sigma(2) + 4] + 8 = 24 \quad \text{additions.}$$

Analogously, for the number of multiplications, we get

$$\mu(8) = 2[2\mu(2) + 4] + 8 = 16 \quad \text{multiplications.}$$

In the general binary case, with $N = 2^n$, letting $\sigma_m = \sigma(2^m)$, from the first of (13.19) we obtain the recurrence

$$\sigma_m = 2\sigma_{m-1} + 2^m, \quad m \geq 2, \quad (13.20)$$

where $\sigma_1 = \sigma(2) = 2$ is the initial condition. The recurrence solution is immediate and given by $\sigma_m = m2^m$, but considering that $m = \log_2 N$, we get

$$\sigma(N) = N \log_2 N. \quad (13.21a)$$

For multiplications, the recurrence is again (13.20), but the initial condition is $\mu(2) = 0$, and the explicit result is

$$\mu(N) = N(\log_2 N - 1). \quad (13.21b)$$

13.4.4 Iterations with $N = a^m$

If the number of points is a power of a , at the end of the iteration process we find a -point DFTs. The computational complexity is evaluated using (13.13) and gives for multiplications (see Problem 13.2),

$$\mu(N) = \frac{1}{a}N\mu(a) + (a-1)N(\log_a N - 1), \quad (13.22)$$

where $\mu(a)$ is the initial condition, that is, the number of multiplications for an a -point DFT. The same result holds for additions with $\sigma(a)$ different from $\mu(a)$.

Equation (13.22) gives, in particular,

$$\begin{aligned} a = 2 &\implies \mu(N) = \frac{1}{2}N\mu(2) + N(\log_2 N - 1), \\ a = 3 &\implies \mu(N) = \frac{1}{3}N\mu(3) + 2N(\log_3 N - 1), \\ a = 4 &\implies \mu(N) = \frac{1}{4}N\mu(4) + 3N(\log_4 N - 1). \end{aligned} \quad (13.23)$$

UT↓ 13.5 Computation of the Multidimensional DFT

In this section we extend the parallel computation of the DFT to the multidimensional case, thus arriving at the multidimensional FFT. As we will see, in this extension, a fundamental role is played by lattices and related finite groups and cells. This fact lies in the background in the one-dimensional case, but it must be explicitly emphasized in the multidimensional case.

We first recall the multidimensional DFT, that is, *the Fourier transform on finite groups*.

13.5.1 The Multidimensional DFT

Let $I = J/P$ be an arbitrary finite group. Then the DFT and IDFT on I have the form (see Sect. 5.9)

$$S(f) = \sum_{t \in J/P} d(J)s(t)\psi^*(f, t), \quad f \in P^*/J^*, \quad (13.24a)$$

$$s(t) = \sum_{f \in P^*/J^*} d(P^*)S(f)\psi(f, t), \quad t \in J/P, \quad (13.24b)$$

where P^*/J^* is the dual group, and $\psi(f, t)$ is the Fourier kernel given by

$$\psi(f, t) = e^{i2\pi ft} = e^{i2\pi(f_1t_1 + \dots + f_mt_m)}.$$

The specification of a signal on the finite group J/P can be limited to a cell $C = [J/P]$ whose cardinality is given by $N = (J : P) = d(P)/d(J)$. Then, the “period” of the 1D case becomes in general a cell. Since the frequency domain/periodicity P^*/J^* is still a finite group, also the specification of the DFT can be limited to a dual cell $\widehat{C} = [P^*/J^*]$, which has the same cardinality as C , namely

$$N = \frac{d(P)}{d(J)} = \frac{d(J^*)}{d(P^*)} = (J : P) = (P^* : J^*), \quad (13.25)$$

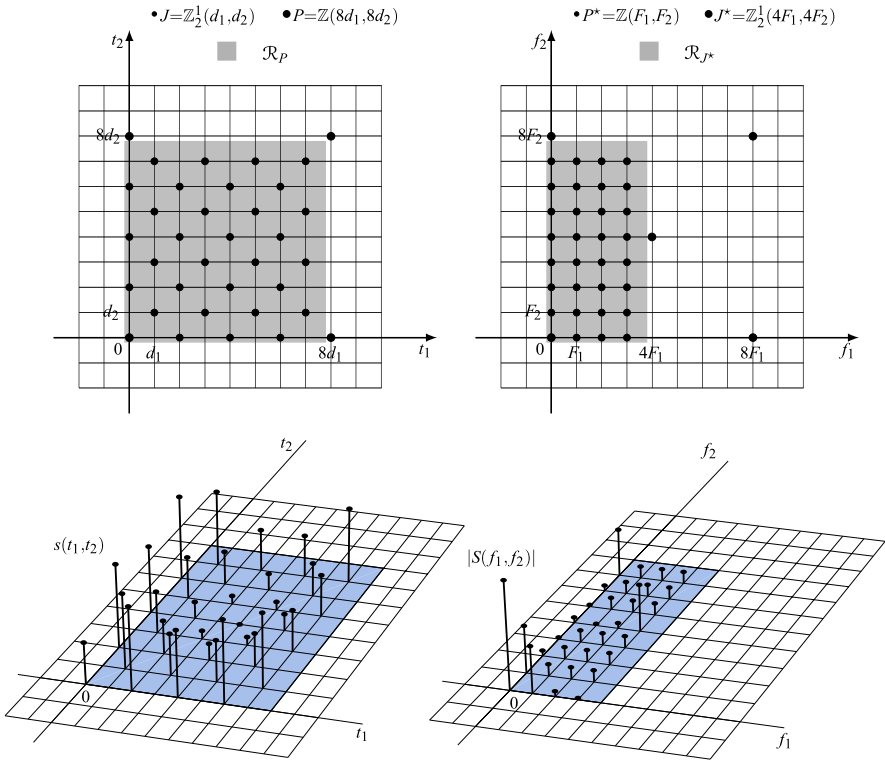


Fig. 13.6 Example of cells for signal and DFT specifications

which generalizes the 1D relation $N = T_p/T = F_p/F$. Figure 13.6 shows an example of signal and DFT specification on the corresponding cells in a 2D case (see Example 13.1). As shown in Proposition 5.1, the Fourier kernel can be expressed by the N th root $W_N = \exp(i2\pi/N)$ of unit in the form

$$\psi(f, t) = W_N^{ft}, \quad ft \in \mathbb{Z},$$

and then it assumes only the N values $W_N^0, W_N^1, \dots, W_N^{N-1}$, as in the 1D case. Hence, once stored these N values, we see that also in the general case the direct DFT and IDFT computation has a complexity of N^2 .

Cell Identification The signal and the DFT specifications require the identification of discrete cells of the form $C = [J/P]$, where J is a lattice, and P is a sublattice of J . We recall that, for a given pair J/P , we may find a large variety of cells. In the present context it is convenient to refer to “rectangular” cells, given as the intersection of J with a rectangle \mathcal{R}_P related to P (see Sect. 16.9),

$$C = J \cap \mathcal{R}_P. \tag{13.26a}$$

We illustrate this in the 2D case. If $P = \mathbb{Z}(N_1d_1, N_2d_2)$, the rectangle is given by $\mathcal{R}_P = [0, N_1d_1) \times [0, N_2d_2)$, and, in general, if $P = \mathbb{Z}_i^a(N_1d_1, N_2d_2)$, the rectangle is

$$\mathcal{R}_P = [0, iN_1d_1) \times [0, N_2d_2) \quad \text{or} \quad \mathcal{R}_P = [0, N_1d_1) \times [0, iN_2d_2). \quad (13.26b)$$

(For the definition of the lattice $\mathbb{Z}_i^a(\cdot, \cdot)$, see Sect. 3.3.) This procedure can also be applied to the dual cell \widehat{C} since it has the same structure as C .

Example 13.1 Figure 13.6 refers to the following 2D lattices and reciprocals:

$$\begin{aligned} J &= \mathbb{Z}_2^1(d_1, d_2), & P &= \mathbb{Z}(8d_1, 8d_2), \\ J^* &= \mathbb{Z}_2^1(4F_1, 4F_2), & P^* &= \mathbb{Z}(F_1, F_2), \quad F_1 = 1/(8d_1), \quad F_2 = 1/(8d_2). \end{aligned}$$

The cardinality N is

$$\begin{aligned} (J : P) &= d(P)/d(J) = 8d_1 8d_2 / (2d_1 d_2) = 32, \\ (P^* : J^*) &= d(J^*)/d(P^*) = 2(4F_1 4F_2) / (F_1 F_2) = 32. \end{aligned}$$

A cell $C = [J/P)$ is given by the intersection of J with the rectangle $\mathcal{R}_P = [0, 8d_1) \times [0, 8d_2)$. A dual cell \widehat{C} is given by the intersection of P^* with the rectangle $\mathcal{R}_{J^*} = [0, 4F_1) \times [0, 8F_2)$. In Fig. 13.6 the rectangles \mathcal{R}_P and \mathcal{R}_{J^*} are given by the gray areas.

13.5.2 Decimation Procedure

Given the finite group J/P , which defines the signal domain/periodicity, for the decimation procedure, we have to choose an “intermediate” lattice K that gives the domain of the “decimated” signals. Hence, three lattices J , K , and P are involved, such that

$$P \subset K \subset J. \quad (13.27)$$

All the other entities (finite groups, cells, and cardinality) are generated from these lattices. Specifically, we have:

before decimation

- $I = J/P$: domain/periodicity of the given signal $s(t)$,
- $\widehat{I} = P^*/J^*$: domain/periodicity of the DFT $S(f)$ to be computed,
- $C = [J/P)$: cell where $s(t)$ is specified,
- $\widehat{C} = [P^*/J^*)$: cell where $S(f)$ is specified,
- $N = |C| = |\widehat{C}|$: signal and DFT cardinality.

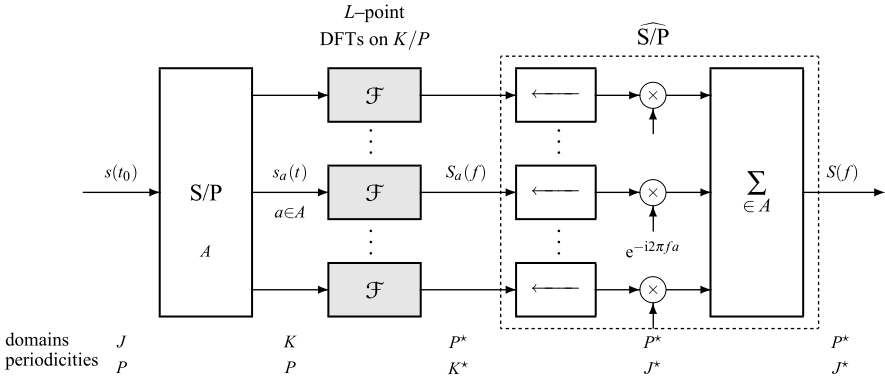


Fig. 13.7 Parallel DFT computation on an arbitrary finite group using *time decimation*

after decimation

- $U = K/P$: domain/periodicity of the components $s_m(t)$,
- $\widehat{U} = P^*/K^*$: domain/periodicity of the DFTs,
- $Q = [K/P]$: cell where the components are specified,
- $\widehat{Q} = [P^*/K^*]$: cell where the DFTs are specified,
- $L = |Q| = |\widehat{Q}|$: cardinality of components and of their DFTs.

to be used in the S/P conversion

- $A = [J/K]$: generating cell,
- $M = |A| = d(K)/d(J)$: number of subdivisions.

The reader can check that in the 1D case the three lattices and their reciprocals are

$$\begin{aligned}
 J &= \mathbb{Z}(T), & K &= \mathbb{Z}(MT), & P &= \mathbb{Z}(NT), \\
 P^* &= \mathbb{Z}(F), & K^* &= \mathbb{Z}(LF), & J^* &= \mathbb{Z}(NF), & F &= 1/(NT),
 \end{aligned}$$

and

$$\begin{aligned}
 I &= \mathbb{Z}(T)/\mathbb{Z}(NT), & \widehat{I} &= \mathbb{Z}(F)/\mathbb{Z}(NT), & F &= 1/(NT), \\
 C &= [J/P] = \{0, T, \dots, (N-1)T\} \stackrel{\Delta}{=} \mathbb{Z}_N(T), & \widehat{C} &= [P^*/J^*] = \mathbb{Z}_N(F), \\
 U &= \mathbb{Z}(MT)/\mathbb{Z}(NT), & \widehat{U} &= \mathbb{Z}(F)/\mathbb{Z}(MF), \\
 Q &= [K/P] = \mathbb{Z}_L(MT), & \widehat{Q} &= [P^*/K^*] = \mathbb{Z}_L(MF), \\
 A &= [J/K] = \mathbb{Z}_L(MT).
 \end{aligned}$$

The parallel computation is carried out according to the scheme of Fig. 13.7, which is essentially the same as in the 1D case. The S/P conversion, specified by the

cell $A = [J/K]$, gives the decimated components according to

$$s_a(t) = s(t + a), \quad a \in A, \quad t \in K/P, \quad (13.28)$$

whose number M is given by the size of the cell A , namely

$$\boxed{M = (J : K) = (J : P)/(K : P) = N/L.} \quad (13.29)$$

In the “time” decimation the DFTs $S_a(f)$, $f \in P^*/K^*$, of the components $s_a(t)$ are calculated according the general DFT formula (13.24a). Then the M DFTs are combined by the dual S/P conversion ($\widehat{S/P}$ conversion). Equation (13.12) of the $\widehat{S/P}$ conversion in the 1D case (see Sect. 7.5) in the general case becomes

$$S(f) = \frac{1}{M} \sum_{a \in A} S_a(f) e^{-i2\pi f a}, \quad (13.30)$$

where

$$e^{-i2\pi f a} \in \{W_N^0, W_N^1, \dots, W_N^{L-1}\}. \quad (13.30a)$$

The computational complexity is still given by (13.13), that is,

$$\mu(N) = M\mu(L) + (M - 1)L \quad \text{multiplications}, \quad (13.31)$$

and the same holds for additions. Analogously, the frequency decimation approach can be generalized.

The previous general procedure is now applied to 2D finite groups. We begin with *separable* lattices, and then we consider nonseparable lattices.

13.6 The FFT on Separable Lattices

The general form of 2D *separable* lattices, in agreement with ordering (13.27), is

$$J = \mathbb{Z}(d_1, d_2), \quad K = \mathbb{Z}(M_1 d_1, M_2 d_2), \quad P = \mathbb{Z}(N_1 d_1, N_2 d_2) \quad (13.32a)$$

with $N_1 = L_1 M_1$ and $N_2 = L_2 M_2$. The reciprocals are

$$P^* = \mathbb{Z}(F_1, F_2), \quad K^* = \mathbb{Z}(L_1 F_1, L_2 F_2), \quad J^* = \mathbb{Z}(N_1 F_1, N_2 F_2) \quad (13.32b)$$

with $F_1 = 1/(N_1 d_1)$ and $F_2 = 1/(N_2 d_2)$. With the notation $\mathbb{Z}_N(d) = \{0, d, \dots, (N - 1)d\}$ the specification of the cells for $s(t_1, t_2)$ and $S(f_1, f_2)$ is

$$C = [J/P] = \mathbb{Z}_{N_1}(d_1) \times \mathbb{Z}_{N_2}(d_2), \quad \widehat{C} = [P^*/J^*] = \mathbb{Z}_{N_1}(F_1) \times \mathbb{Z}_{N_2}(F_2),$$

both of size $N = N_1 N_2$.

The DFT to be computed is

$$S(f_1, f_2) = \sum_{(t_1, t_2) \in C} d(J) s(t_1, t_2) e^{-i2\pi(f_1 t_1 + f_2 t_2)}, \quad (f_1, f_2) \in \widehat{C},$$

and it is easy to show that the *direct* computation has the complexity of $N^2 = N_1^2 N_2^2$ operations.

Following the scheme of Fig. 13.7, the signal $s(t_0) = s(t_{10}, t_{20})$ is S/P converted to the signals

$$\begin{aligned} s_a(t) &= s(t + a), \quad t \in K/P = \mathbb{Z}(M_1 d_1, M_2 d_2) / \mathbb{Z}(N_1 d_1, N_2 d_2), \\ a \in A &= [J/K] = \mathbb{Z}_{M_1}(d_1) \times \mathbb{Z}_{M_2}(d_2), \end{aligned} \quad (13.33)$$

whose number is $M = M_1 M_2$. Then, the M DFTs have the form

$$S_a(f_1, f_2) = \sum_{(t_1, t_2) \in Q} d(K) s_a(t_1, t_2) e^{-i2\pi(f_1 t_1 + f_2 t_2)}, \quad (f_1, f_2) \in \widehat{Q}, \quad (13.34)$$

where the cells are

$$\begin{aligned} Q &= [K/P] = \mathbb{Z}_{L_1}(M_1 d_1) \times \mathbb{Z}_{L_2}(M_2 d_2), \\ \widehat{Q} &= [P^*/K^*] = \mathbb{Z}_{L_1}(F_1) \times \mathbb{Z}_{L_2}(F_2), \end{aligned}$$

both of size $L = L_1 L_2$. The M DFTs are finally combined according to (13.30), giving

$$S(f_1, f_2) = \frac{1}{M} \sum_{(a_1, a_2) \in A} S_a(f_1, f_2) e^{-i2\pi(f_1 a_1 + f_2 a_2)}, \quad (f_1, f_2) \in \widehat{C}. \quad (13.35)$$

Several strategies can be followed in the choice of decimation parameters. We will describe two examples of strategies.

13.6.1 Row Partition

In (13.32a), (13.32b) we choose

$$L_1 = N_1, \quad L_2 = 1, \quad M_1 = 1, \quad M_2 = N_2.$$

Then

$$\begin{aligned} J &= \mathbb{Z}(d_1, d_2), & K &= \mathbb{Z}(d_1, N_2 d_2), & P &= \mathbb{Z}(N_1 d_1, N_2 d_2), \\ P^* &= \mathbb{Z}(F_1, F_2), & K^* &= \mathbb{Z}(N_1 F_1, F_2), & J^* &= \mathbb{Z}(N_1 F_1, N_2 F_2). \end{aligned}$$

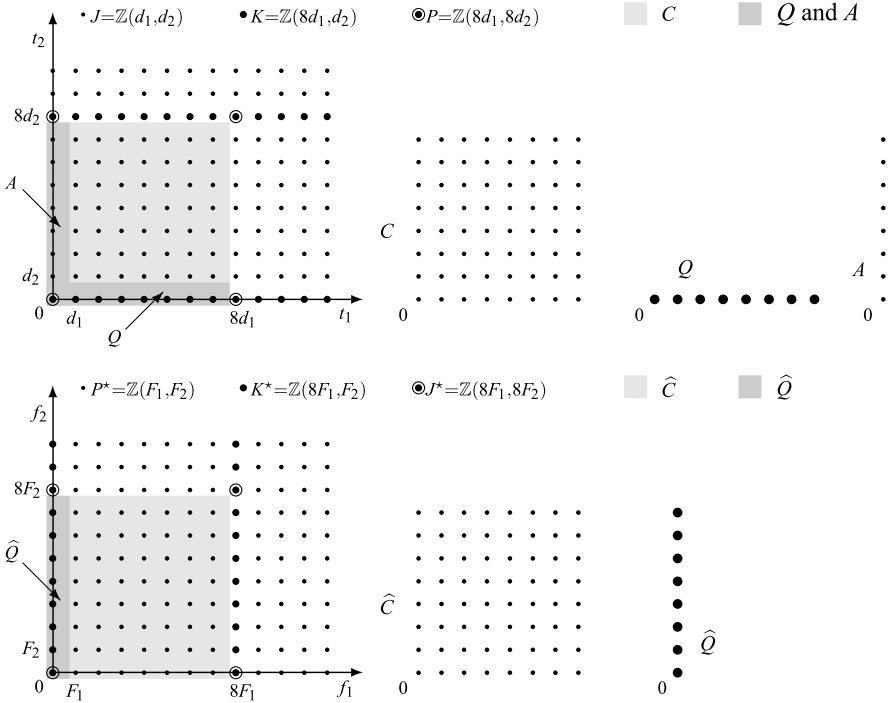


Fig. 13.8 Lattices and cells in the “row partition” for the bidimensional DFT

The cells are shown in Fig. 13.8 and can be written as

$$C = \mathbb{Z}_{N_1}(d_1) \times \mathbb{Z}_{N_2}(d_2), \quad \hat{C} = \mathbb{Z}_{N_1}(F_1) \times \mathbb{Z}_{N_2}(F_2),$$

$$A = \{0\} \times \mathbb{Z}_{N_2}(d_2), \quad Q = \mathbb{Z}_{N_1}(d_1) \times \{0\}, \quad \hat{Q} = \{0\} \times \mathbb{Z}_{N_2}(F_2).$$

Here A and Q consist respectively of column 0 and row 0 of the cell C . Equations (13.34) and (13.35) become

$$S_a(f_1, 0) = \sum_{t_1 \in \mathbb{Z}_{N_1}(d_1)} d(K) s_a(t_1, 0) e^{-i2\pi f_1 t_1}, \quad f_1 \in \mathbb{Z}_{N_1}(F_1), \quad (13.36a)$$

$$S_a(f_1, f_2) = \frac{1}{M} \sum_{a_2 \in \mathbb{Z}_{N_2}(d_2)} S_a(f_1, 0) e^{-i2\pi f_2 a_2}, \quad f_2 \in \mathbb{Z}_{N_2}(F_2), \quad (13.36b)$$

which are essentially 1D DFTs. The computational steps are:

- (1) for each $a \in A$, a 1D DFT on N_1 points is computed, picking up the signal values *along the rows* (see (13.36a)),
- (2) for each frequency $f_1 \in \mathbb{Z}_{N_1}(F_1)$, a 1D DFT on N_2 points is computed *along the columns* (see (13.36b)).

The computational complexity is evaluated as follows. Let $\mu(N)$ denote the complexity of a 1D FFT on N points. In step (1) the complexity is $N_2\mu(N_1)$, since $a \in A$ assumes N_2 values. In step (2) the complexity is $N_1\mu(N_2)$, since the frequencies f_1 are N_1 . Hence, the global complexity is

$$N_2\mu(N_1) + N_1\mu(N_2).$$

But, if $\mu(N) = N \log_2 N$, we find

$$N_2N_1 \log_2 N_1 + N_1N_2 \log_2 N_2 = N_1N_2 \log_2(N_1N_2),$$

where N_1N_2 is the cardinality of the 2D DFT we are computing.

The conclusions are:

- (1) a 2D DFT computation on separable lattices can be carried out using a 1D FFT algorithm,
- (2) in the binary case ($N_1 = 2^{m_1}$ and $N_2 = 2^{m_2}$) the global computation complexity has the standard law $N \log_2 N$ with $N = N_1N_2$.

13.6.2 Block Partition

If $N_1 = N_2 \stackrel{\Delta}{=} N_0$ is a power of 2, the cell C can be partitioned into 2×2 parts by choosing (Fig. 13.9)

$$K = \mathbb{Z}(2d_1, 2d_2), \quad M_1 = M_2 = 2, \quad L_1 = L_2 = \frac{1}{2}N.$$

The other cells become

$$A = \mathbb{Z}_2(d_1) \times \mathbb{Z}_2(d_2) = \{(0, 0), (0, d_2), (d_1, 0), (d_1, d_2)\},$$

$$Q = \mathbb{Z}_{N/2}(2d_1) \times \mathbb{Z}_{N/2}(2d_2), \quad \widehat{Q} = \mathbb{Z}_{N/2}(F_1) \times \mathbb{Z}_{N/2}(F_2),$$

as shown in Fig. 13.9 for $N_1 = N_2 = 8$.

The parallel computation starts with 4 DFTs on $\frac{1}{2}N_0 \times \frac{1}{2}N_0$ points. In the second iteration the DFTs are on $\frac{1}{4}N_0 \times \frac{1}{4}N_0$ points, in the third iteration on $\frac{1}{8}N_0 \times \frac{1}{8}N_0$ points, etc. until we arrive at 2×2 -point DFTs. For instance, with $N_0 \times N_0 = 16 \times 16$ we have: in the first iteration 8×8 points, in the second 4×4 points, and in the third 2×2 points.

This block partition has the advantage that the final 2×2 -point DFTs do not require multiplications.

13.7 The FFT on Nonseparable Lattices

The FFT can be implemented on nonseparable lattices with substantially the same computational complexity as on separable lattices and, ultimately, using one-dimensional FFTs.

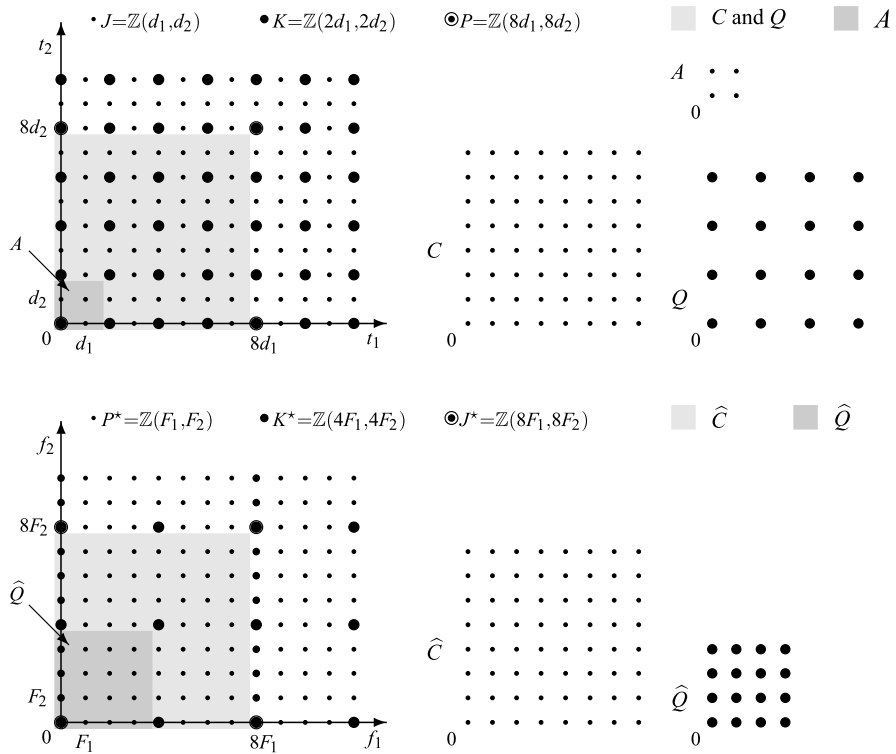


Fig. 13.9 Lattices and cells in the “block partition” for the bidimensional DFT

Consider a general 2D lattice (see Fig. 3.11)

$$J = \mathbb{Z}_i^b(d_1, d_2),$$

where i and b are coprime with $0 < b < i$, and a separable sublattice of the form

$$P = \mathbb{Z}(iN_1d_1, iN_2d_2).$$

Then, we consider a 2D signal $s(t_1, t_2)$ with domain J and periodicity P with the purpose of implementing the time decimation and its iterations to develop an FFT algorithm. To this end, it is fundamental to perform the decimation *from the non-separable lattice J into a separable lattice K* . In this way the iteration procedure, from the second step on, becomes the same as the one done on a separable lattice. The separable lattice K is easily found as

$$K = \mathbb{Z}(id_1, id_2),$$

which represents the *largest separable sublattice of J* (see Proposition 16.6).

Once the triplet of lattices J, K, P has been identified, for the decimation, it is sufficient to evaluate the parameters listed at the beginning. Without loss of gener-

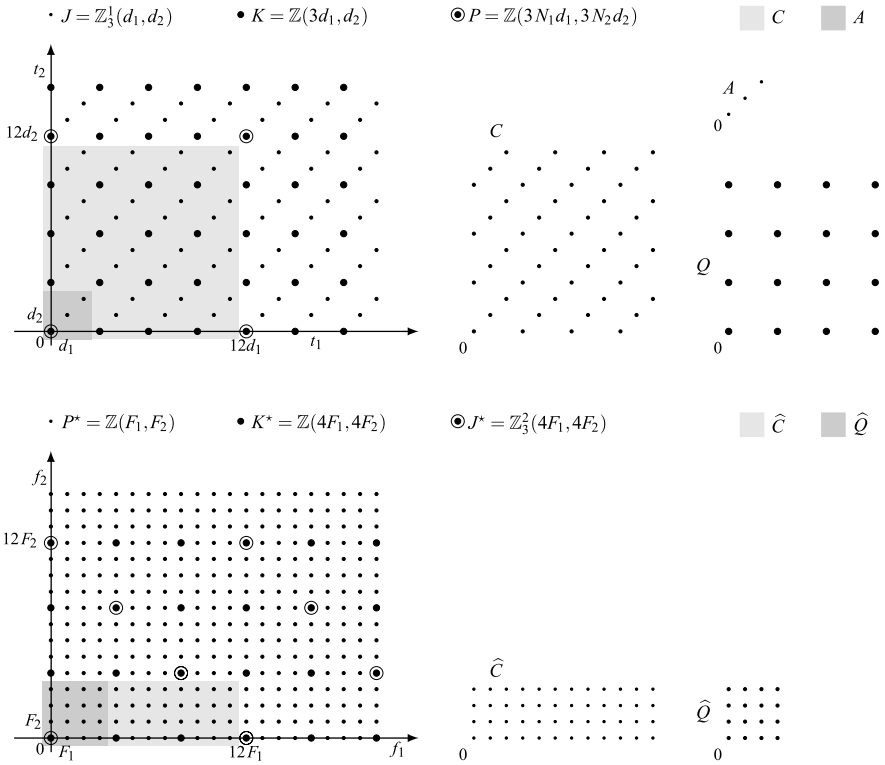


Fig. 13.10 Lattices and cells for the decimation on a nonseparable lattice

ality, for clarity, we develop the case $i = 3, b = 1$, that is, we start with the lattices

$$J = \mathbb{Z}_3^1(d_1, d_2), \quad K = \mathbb{Z}(3d_1, 3d_2), \quad P = \mathbb{Z}(3N_1d_1, 3N_2d_2), \quad (13.37)$$

which are illustrated in Fig. 13.10 for $N_1 = 4$ and $N_2 = 4$. The cardinality of the DFT is given by

$$N = (J : P) = \frac{d(P)}{d(J)} = \frac{3N_1d_1 3N_2d_2}{3d_1d_2} = 3N_1N_2 = 48.$$

To find the discrete cells involved in the parallel computation, we can use the “intersection” procedure outlined in Sect. 13.5. A discrete cell $C = [J/P]$ is given by the intersection of J with the rectangle $\mathcal{R}_P = [0, 3N_1d_1) \times [0, 3N_2d_2)$. In Fig. 13.10, where $N_1 = 4$ and $N_2 = 4$, C consists of $N = 3N_1N_2 = 48$ points of J . Analogously, we find that a cell $A = [J/K]$ for the S/P conversion is given by $J \cap \mathcal{R}_K$ with $\mathcal{R}_K = [0, 3d_1) \times [0, 3d_2)$; hence $A = \{(0, 0), (d_1, d_2), (2d_1, 2d_2)\}$. A cell $Q = [K/P] = K \cap \mathcal{R}_P$ is also given by the intersection $Q = C \cap J$ and consists of $|Q| = N_1N_2 = 16$ points.

The reciprocals of the lattices (13.37) are (see Table 5.5)

$$\begin{aligned} P^* &= \mathbb{Z}(F_1, F_2), \quad F_1 = 1/(3N_1d_1), \quad F_2 = 1/(3N_2d_2), \\ K^* &= \mathbb{Z}(F'_1, F'_2) = \mathbb{Z}(N_1F_1, N_2F_2), \quad F'_1 = 1/(3d_1), \quad F'_2 = 1/(3d_2), \\ J^* &= \mathbb{Z}_3^2(F'_1, F'_2) = \mathbb{Z}_3^2(N_1F_1, N_2F_2), \end{aligned}$$

which are shown in Fig. 13.10. A dual cell $\widehat{C} = [P^*/J^*]$ is obtained as the intersection of P^* with the rectangle $\mathcal{R}_{J^*} = [0, 3N_1F_1) \times [0, N_2F_2)$. As a check, note that $|\widehat{C}| = |C| = 3N_1N_2 = 48$. Finally, a cell $\widehat{Q} = [P^*/K^*]$ is given as the intersection of P^* with the rectangle $\mathcal{R}_{K^*} = [0, N_1F_1) \times [0, N_2F_2)$ and has $|\widehat{Q}| = N_1N_2 = 16$ points.

Now, we follow the general decimation scheme of Fig. 13.1 with the parameters of the specific case. The given signal $s(t)$, $t \in J/P$, is specified in the cell C of $3N_1N_2 = 48$ points. Then, by following the scheme, we have:

- (1) An S/P conversion generated by the cell A of cardinality $M = 3$, which produces three components $s_a(t)$, $a \in A$, defined on K/P . Each component is specified on the cell Q of $L = N_1N_2 = 16$ points.
- (2) Three 12-point DFTs, which give $S_a(f)$, $a \in A$, defined on P^*/K^* . Each $S_a(f)$ is specified on the cell \widehat{Q} of $L = N_1N_2 = 16$ points.
- (3) The \widehat{P}/\widehat{S} conversion of the three $S_a(f)$ into $S(f)$.

The computational complexity is confined to steps (2) and (3). The DFTs in the scheme are on separable groups, K/P at the input and P^*/K^* at the output. Denoting by $\mu(L)$ the computation complexity of an L -point DFT on separable groups, the complexity of step (2) is $3\mu(N_1N_2)$ operations. In the \widehat{P}/\widehat{S} conversion we find, for each frequency, $M - 1 = 2$ additions and $M - 1 = 2$ multiplication (by $e^{-i2\pi fa}$). Since the number of frequencies (given by the cell \widehat{C}) is $N = 3N_1N_2$, the complexity of step (2) is

$$2N = 2 \cdot 3N_1N_2 \quad \text{operations.}$$

Hence, the global complexity of the decimation procedure is

$$\mathcal{C} = 3\mu(N_1N_2) + 2 \cdot 3N_1N_2 \quad \text{operations.} \quad (13.38)$$

On the other hand, we have seen that the DFT on separable lattice (when N_1 and N_2 are powers of 2) the complexity for the FFT is

$$\mu(N_1N_2) = N_1N_2 \log_2 N_1N_2.$$

Then, the complexity (13.38) becomes

$$\begin{aligned} \mathcal{C} &= 3N_1N_2 \log_2 N_1N_2 + 2 \cdot 3N_1N_2 \\ &= N \log_2(N/3) + 2N = N \log_2(4N/3), \end{aligned}$$

which is not far from the standard law $N \log_2 N$.

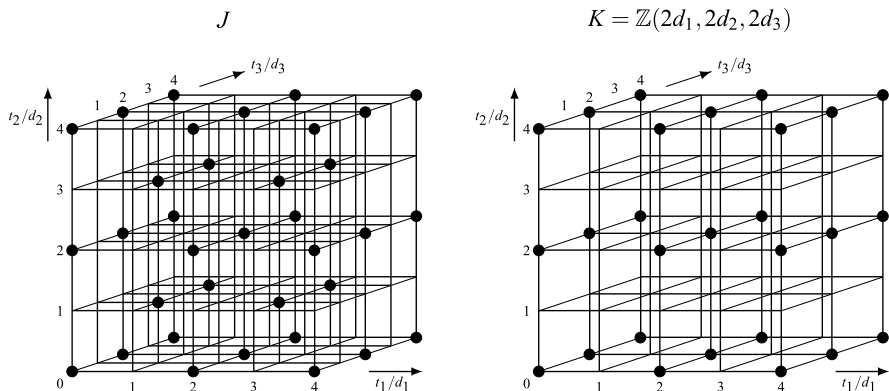


Fig. 13.11 3D nonseparable lattice J and largest separable sublattice K contained in J

13.7.1 Concluding Remark on Multidimensional FFT

The procedure seen for the 2D lattice $J = \mathbb{Z}_3^1(d_1, d_2)$ can be easily extended to an arbitrary 2D lattice of the form $J = \mathbb{Z}_i^b(d_1, d_2)$ by performing the decimation from J into the separable lattice $\mathbb{Z}(id_1, id_2)$ and then proceeding on separable lattices. It can be also extended to m D nonseparable lattices; the problem is to find the largest separable sublattice K of the given lattice J (see Proposition 16.6). For instance, with $m = 3$ an example of nonseparable lattice J is generated by the upper-triangular matrix (Fig. 13.11)

$$\mathbf{J} = \begin{bmatrix} d_1 & 0 & 0 \\ 0 & d_2 & 0 \\ 0 & 0 & d_3 \end{bmatrix} \begin{bmatrix} 2 & 0 & 1 \\ 0 & 2 & 1 \\ 0 & 0 & 2 \end{bmatrix},$$

and the largest separable sublattice of J is

$$K = \mathbb{Z}(2d_1, 2d_2, 2d_3).$$

Considering that $(J : K) = 2$, the cell $A = [J/K)$ consists of 2 points, namely $A = \{(0, 0, 0), (d_1, d_2, d_3)\}$.

UT 13.8 DFT Computation via FFT

From this section we begin with the applications of the FFT algorithm, starting with the computation of the DFT.

The FFT has been formulated as the fast computation of the DFT, although its use is typically for the computation of the FT of continuous-time signals. However, the *passage through the DFT is conceptually necessary*, so it will be useful to examine

in detail the DFT/FFT relationship. It is very important to remark that the DFT deals with a *periodic* signal $s(t)$ and produces a *periodic* function $S(f)$, namely

$$\boxed{s(t), \quad t \in \mathbb{Z}(T)/\mathbb{Z}(T_p) \xrightarrow{\text{DFT}} S(f), \quad f \in \mathbb{Z}(F)/\mathbb{Z}(F_p),}$$

where $N = T_p/T = F_p/F$, and

$$S(kF) = \sum_{n=0}^{N-1} Ts(nT)W_N^{-nk}, \quad kF \in \mathbb{Z}(F)/\mathbb{Z}(F_p), \quad (13.39a)$$

$$s(nT) = \sum_{k=0}^{N-1} FS(kF)W_N^{nk}, \quad nT \in \mathbb{Z}(T)/\mathbb{Z}(T_p). \quad (13.39b)$$

Instead, the FFT deals with *finite* sequences

$$\boxed{s = [s_0, s_1, \dots, s_{N-1}] \xrightarrow{\text{FFT}} S = [S_0, S_1, \dots, S_{N-1}].}$$

Then, in the DFT computation via FFT we have to consider the *values in a period*.

Comparison of (13.39a), (13.39b) with (13.10a), (13.10b) yields

$$\alpha_N s_n = Ts(nT), \quad \beta_N S_k = FS(kF), \quad 0 \leq n, k \leq N-1. \quad (13.40)$$

Then the input vector is loaded with the N signal values of the interval $[0, T_p)$, and the FFT produces the N DFT values of the interval $[0, F_p)$. This does not represent a limitation since the other values of the function $S(f)$, for every $f \in \mathbb{Z}(F)$, can be obtained by the periodicity. In other words, a “reduction” to the cells (“periods”) $\mathbb{Z}(T) = \{0, T, \dots, (N-1)T\}$ and $\mathbb{Z}(F) = \{0, F, \dots, (N-1)F\}$ is needed, as shown in Fig. 13.12.

Analogous considerations hold for the IDFT.

13.9 FFT Computation of a Fourier Transform on \mathbb{R}

We have seen that the DFT computation is quite trivial, since it is only based on the interpretation of the data loaded and produced by the FFT. In the other cases, in which the signal is not discrete and periodic, the FT computation must be carried out through a discrete and periodic version of the signal for the applicability of the DFT/FFT. This preliminary passage is the most critical and must be carried out with a lot of attention.

This is now developed in the case of the most common usage of the FFT, that is, the computation of the FT of a continuous-time signal

$$S(f) = \int_{-\infty}^{+\infty} s(t)e^{-i2\pi ft} dt, \quad f \in \mathbb{R}.$$

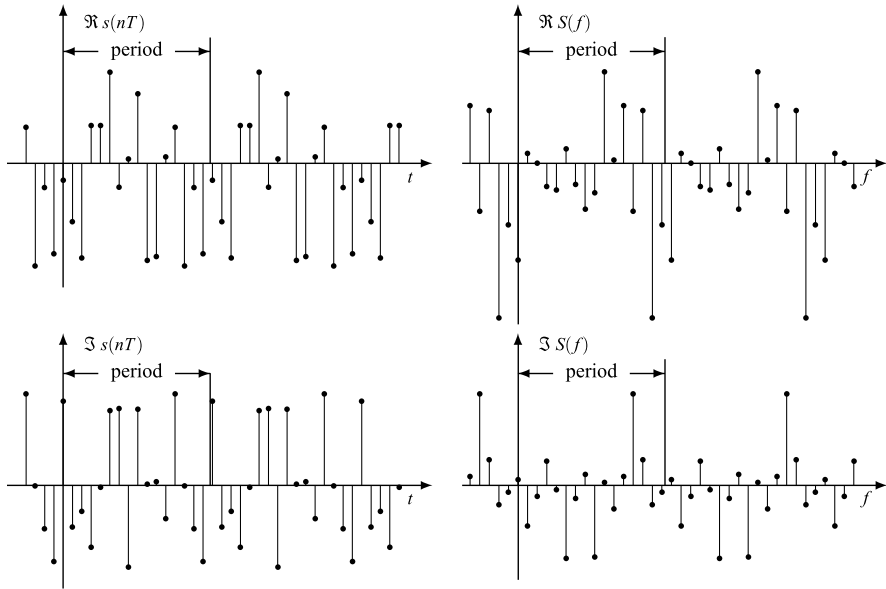


Fig. 13.12 Fourier transform (DFT) of a discrete-time periodic signal. The FFT takes the signal values in *one period*, and produces the DFT values in *one period*

13.9.1 Choice of Parameters

For the conversion of a continuous aperiodic signal to a discrete periodic signal, the following operations are needed (Fig. 13.13):

- (1) an $\mathbb{R} \rightarrow \mathbb{Z}(T)$ down-sampling,
- (2) a $\mathbb{Z}(T) \rightarrow \mathbb{Z}(T)/\mathbb{Z}(T_p)$ up-periodization,

which in the frequency domain become

- (1) an $\mathbb{R} \rightarrow \mathbb{R}/\mathbb{Z}(F_p)$ up-periodization with $F_p = 1/T$,
- (2) an $\mathbb{R}/\mathbb{Z}(F_p) \rightarrow \mathbb{Z}(F)/\mathbb{Z}(F_p)$ down-sampling with $F = 1/T_p$,

where

$$T_p = NT, \quad F_p = NF, \quad F_p T_p = N. \quad (13.41)$$

The order of (1) and (2) can be changed, but in any case we arrive at a discrete periodic signal

$$s_{cp}(t), \quad t \in \mathbb{Z}(T)/\mathbb{Z}(T_p) \xrightarrow{\mathcal{F}} S_{cp}(f), \quad f \in \mathbb{Z}(F)/\mathbb{Z}(F_p). \quad (13.42)$$

In this Fourier pair we need to choose the spacing T and the period $T_p = NT$. The choice of T is based on the *bandwidth*, and the choice of T_p is based on the *duration*.

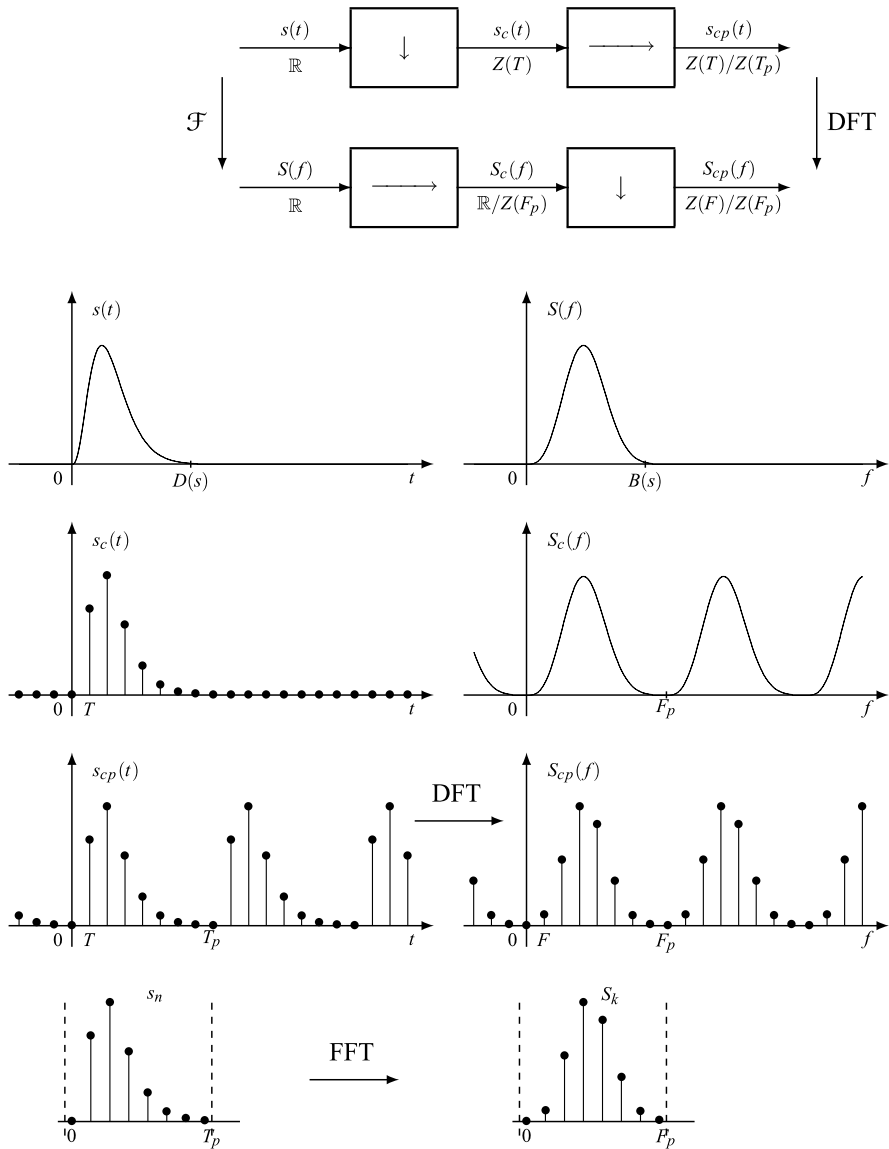


Fig. 13.13 Illustration of the computation of the Fourier transform of a continuous-time signal via FFT. This computation conceptually needs to obtain a discrete-time periodic signal, to which DFT can be applied to. In this figure, $S(f)$ is simplified (it does not correspond to the Fourier transform of $s(t)$) and has been chosen in order to show more clearly the procedure

Now, we assume that the signal is both duration-limited, $D(s) < \infty$, and is band-limited, $B(s) < \infty$. As is well known, these assumptions cannot hold simultaneously (see Sect. 9.5), with the consequence that $D(s)$ and/or $B(s)$ must be *con-*

ventionally defined. But, for the moment, we suppose that the consequence of the nonstrict limitation is negligible.

The choice of the sampling frequency $F_p = 1/T$ relies upon the bandwidth $B(s)$ according to

$$F_p = 1/T \geq B(s). \quad (13.43)$$

This guarantees that in the frequency $\mathbb{R} \rightarrow \mathbb{R}/\mathbb{Z}(F_p)$ up-periodization the repetition terms do not overlap (*alias-free* condition, see Sampling Theorem in Sect. 8.4). The choice of the period T_p relies upon the duration $D(s)$ according to

$$T_p \geq D(s). \quad (13.44)$$

In such a way, in the time $\mathbb{Z}(T) \rightarrow \mathbb{Z}(T)/\mathbb{Z}(T_p)$ up-periodization the terms do not overlap.

By combination of (13.43) and (13.44) we find the condition on the number of signal values per period

$$N = F_p T_p \geq B(s) D(s). \quad (13.45)$$

Moreover, it will be convenient that N be a power of 2, that is, $N = 2^m$.

Now, it is easy to check that with the above choice, the FT $S(f)$ is correctly computed at N frequencies. In fact, the alias-free condition ensures that $S(f) = S_c(f)$, $f \in \mathcal{E}(s)$, whereas, by definition, it turns out that $S(f) = 0$, $f \notin \mathcal{E}(s)$. Moreover, the frequency $\mathbb{R} \rightarrow \mathbb{Z}(F)$ down-sampling gives $S_{cp}(f) = S_c(f)$, $f \in \mathbb{Z}(F)$, and therefore

$$S(f) = S_{cp}(f), \quad f \in \mathcal{E}(s) \cap \mathbb{Z}(F). \quad (13.46)$$

In the time domain we find analogously

$$s(t) = s_{cp}(t), \quad t \in e(s) \cap \mathbb{Z}(T). \quad (13.47)$$

Hence, the Fourier pair $(s(t), S(f))$, when confined to the discrete domains and to the extensions, coincides with the DFT pair $(s_{cp}(nT), S_{cp}(kF))$, and the FFT can be applied.

This conclusion holds with band and duration limitation, but, as noted above, this assumption cannot hold in the strict sense, and consequently we shall find an approximate computation. This point will be investigated later on.

13.9.2 Extensions of the Forms $[0, D)$ and $[0, B)$

If the time extension of the signal $s(t)$ is in the interval $[0, T_p)$, as in Fig. 13.13, the FFT loading is immediate: the input vector consists of the first N points starting from the origin, according to (see (13.40))

$$\alpha_N s_n = T s(nT), \quad 0 \leq n \leq N - 1. \quad (13.48)$$

If the spectral extension is the interval $[0, F_p)$, the FFT gives directly the values of $S(f)$ as

$$FS(kF) = \beta_N S_k, \quad 0 \leq k \leq N - 1, \quad (13.49)$$

whereas $S(kF) = 0$ for the other k 's.

13.9.3 Generic Extensions: $[t_0, t_0 + D)$ and $[f_0, f_0 + B)$

In this general case the FFT loading must be modified, using the periodicity of the version $s_{cp}(nT)$ in (13.47), which allows one to transfer the values of s into the interval $[0, T_p)$. Letting $t_0 = n_0T$, then (13.47) can be written in the form

$$s(nT) = s_{cp}(nT), \quad n = n_0, n_0 + 1, \dots, n_0 + N - 1, \quad (13.50)$$

where the index n can be replaced by $n_N \triangleq n \bmod N$. Hence,

$$s(nT) = s_{cp}(n_N T),$$

and the loading becomes

$$\alpha_N s_{n_N} = Ts(nT), \quad n = n_0, n_0 + 1, \dots, n_0 + N - 1,$$

where the index n_N takes all the values from 0 to $N - 1$. For instance, for $n_0 = 21$ and $N = 8$, the expression $\alpha_8 s_{n_8} = Ts(nT)$, $n = 21, 22, \dots, 28$, generates the input vector

$$\begin{aligned} & \alpha_8 [s_0, s_1, s_2, s_3, s_4, s_5, s_6, s_7] \\ & = T[s(24T), s(25T), s(26T), s(27T), s(28T), s(21T), s(22T), s(23T)]. \end{aligned}$$

In fact, $n = 21$ gives $\alpha_8 s_{21_8} = \alpha_8 s_5 = Ts(21T)$, which must be stored in position 5, $n = 22$ gives $\alpha_8 s_{22_8} = \alpha_8 s_6 = Ts(22T)$, which must be stored in position 6, etc.

Analogously, in the frequency domain, we let $f_0 = k_0F$, and in place of (13.49) we set

$$\beta_N S(kF) = S_{k_N}, \quad k = k_0, k_0 + 1, \dots, k_0 + N - 1.$$

An alternative way of writing/reading with generic extension is based on the *shifting rules*, which allow one to transfer the extensions to $[0, D)$ and $[0, B)$. Then, in place of $s(t)$ with extension $[t_0, t_0 + D)$, we deal with the shifted signal

$$y(t) = s(t + t_0)$$

whose extension is $[0, D)$. But the time-shifted signal $y(t)$ has still $[f_0, f_0 + B)$ as the spectral extension. To move the spectral extension to $[0, B)$, we use the frequency shifting rule, introducing the signal

$$v(t) = y(t) \exp(-i2\pi f_0 t) = s(t + t_0) \exp(-i2\pi f_0 t), \quad (13.51)$$

and finally we have $e(v) = [0, D)$ and $\varepsilon(v) = [0, B)$. Then, we compute $V(f)$ via FFT, and we obtain $S(f)$ by

$$S(f) = V(f - f_0) \exp(-i2\pi f t_0). \quad (13.52)$$

13.9.4 Fourier Transform of a Real Signal

If the signal $s(t)$ is *real*, its FT has the Hermitian symmetry, $S(f) = S^*(-f)$, and its spectral extension is always symmetric, $\mathcal{E}(s) = (-B, B)$, where $B = \frac{1}{2}B(s)$ is the *band*, as illustrated in Fig. 13.14.

Given N (usually a power of 2), let $M = \frac{1}{2}N - 1$; then³

$$\begin{aligned} FS(kF) &= \beta_N S_k, & 0 \leq k \leq M, \\ FS(-kF) &= \beta_N S_{N-k}, & -M \leq -k \leq -1, \end{aligned} \quad (13.53)$$

while the value $S_{N/2}$ can be used considering that $S(kF)$ is zero outside its extension. The first $M + 1$ values of the output vector give the nonnegative frequency components, while reverse values give the negative frequency components. Note that the latter are redundant and can be used to check the Hermitian symmetry $S_k = S_{N-k}^*$.

In the context of real signals, to get a full efficiency, the FFT can be used for the *simultaneous computation of two real signals* $s_1(t)$ and $s_2(t)$. To this end, we introduce the complex signal $z(t) = s_1(t) + is_2(t)$, then we compute $Z(f)$, and, finally, we have (see Table 5.2, rules 7a and 8a)

$$S_1(f) = \frac{1}{2}[Z(f) + Z^*(-f)], \quad S_2(f) = \frac{1}{2i}[Z(f) - Z^*(-f)].$$

13.9.5 Computation of the Inverse Fourier Transform

If the signal is complex, the inverse FT computation is perfectly similar to that of the forward transform. Instead, if the signal is *real*, we have to load the input data with the Hermitian symmetry format (Fig. 13.14 refers to a real signal). The IDFT vector is given by the periodic function $S_{cp}(kF)$ in the period $[0, F_p)$, which is obtained from $S(f)$, only in the first half period, while in the second, it is obtained by the Hermitian symmetry. For instance, with $N = 8$ the FFT input vector is given by

$$S(0), S(F), S(2F), S(3F), S(4F), S^*(3F), S^*(2F), S^*(F).$$

From the output vector, which gives the $s(t)$ values, we have to check that the imaginary part is zero.

³In FFT packages where real and imaginary parts are introduced separately, it is important to fill the imaginary part with N zeros.

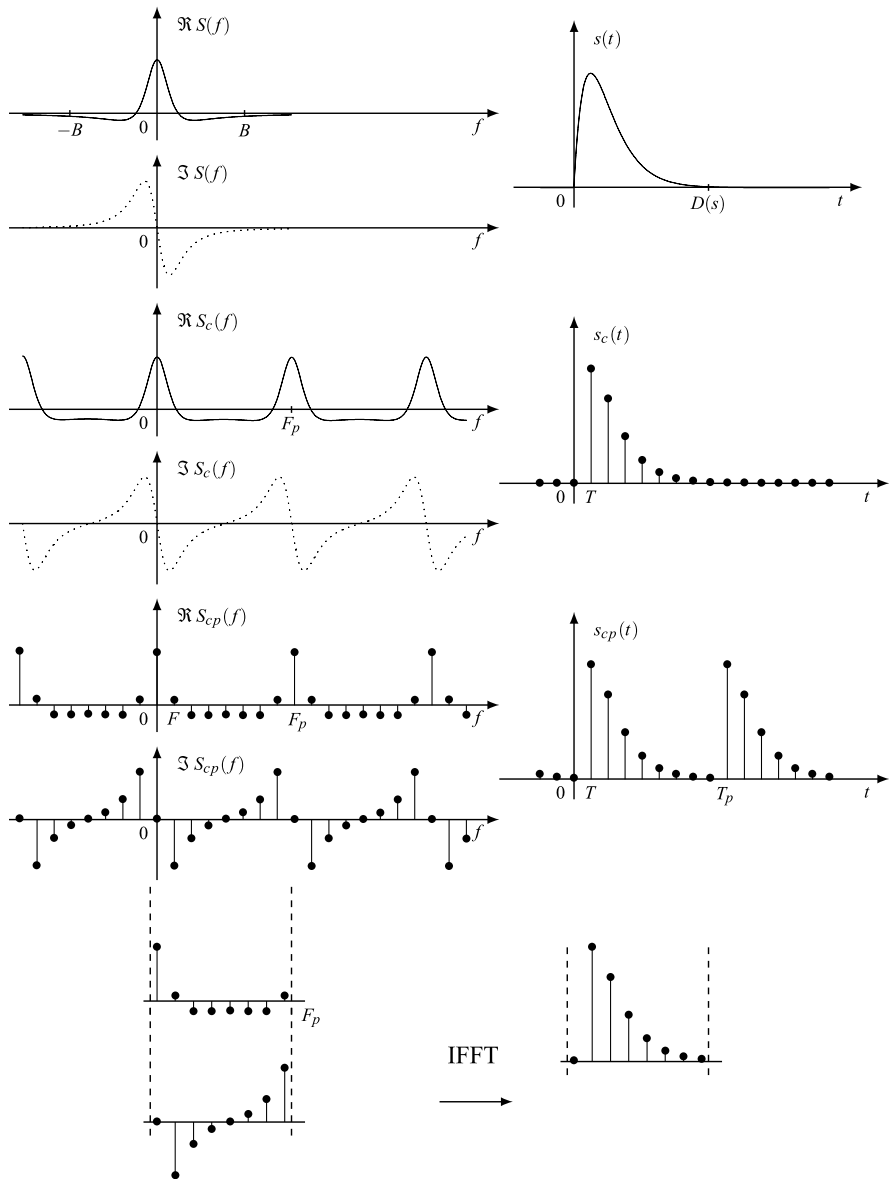
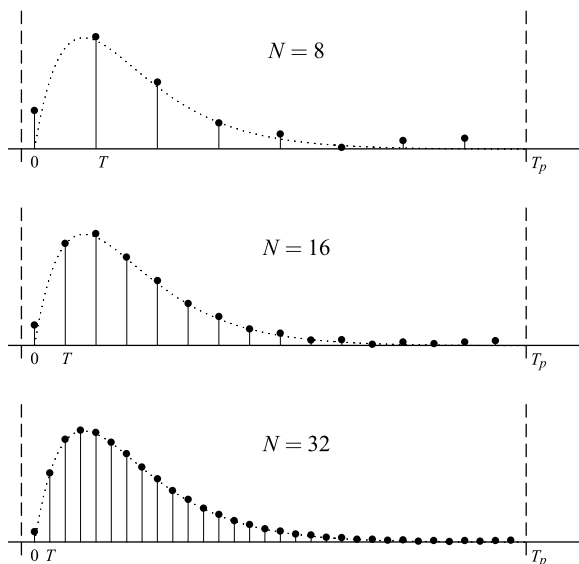


Fig. 13.14 Illustration of the FFT computation of the inverse Fourier transform of a continuous-time *real* signal. This computation conceptually needs to obtain a discrete-frequency periodic Fourier transform

Figure 13.15 shows an example of computation of the inverse FT of

$$S(f) = T_0 \frac{1}{(1 + i2\pi f T_0)^2}, \quad f \in \mathbb{R},$$

Fig. 13.15 Inverse Fourier transform computation via FFT for different numbers of points N (dashed curve shows the exact values)



and shows the result for a few values of N . This example serves only as a check, since we know that the inverse transform is given by $s(t) = 1(t)(t/T_0) \exp(-t/T_0)$, $t \in \mathbb{R}$, and so we can have an accuracy check with different N . In this case we see that with $N = 32$ we reach an acceptable result (but in general N should be much larger).

UT 13.10 Other FFT Utilizations

Other examples of application of the FFT are the computation of:

- the Fourier transform of a continuous periodic signal,
- the Fourier transform of a discrete-time signal and its inverse,
- the convolution and, particularly, the response of a filter,
- the Hilbert transform,
- the DCT.

In (a) we find a simplification with respect to the previous application, since the signal is already periodic and therefore the choice of the period T_p becomes natural. In (b) we find another simplification, since the signal is already discrete and the choice of the spacing T is implicit. The other applications are discussed below.

It is worth recalling that the FFT is also widely used for multidimensional signals.

13.10.1 Computation of Convolution

The computational complexity of a convolution is effectively reduced with the usage of the FFT. In fact, consider the (cyclic) convolution of two signals defined on $\mathbb{Z}(T)/\mathbb{Z}(T_p)$, given by (10.1) and, in normalized form, by

$$s_n = \sum_{k=0}^{N-1} x_{n-k} y_k. \quad (13.54)$$

Then, we see that the direct computation requires N^2 operations. Instead, if we pass to the frequency domain according to the graph

$$(x_n, y_n) \xrightarrow{\text{DFT}} (X_k, Y_k) \longrightarrow S_k = X_k Y_k \xrightarrow{\text{IDFT}} s_n$$

and use the FFT, the complexity is:

- $2N \log_2 N$ operations to compute X_k, Y_k ,
- N multiplications to compute $S_k = X_k Y_k$, and
- $N \log_2 N$ operations to compute the IDFT of S_k .

Then, the global complexity is

$$\mathcal{C}(N) = 3N \log_2 N + N,$$

which is less than N^2 for $N \geq 16$.

For the computation of a continuous-time convolution, a preliminary step is the choice of durations and bandwidths, which must be common to both signals and also to the final result, the convolution. To this end, the rule on the convolution extension (see Sect. 4.9) must be borne in mind. Specifically, if both the signals to be convolved have extension $[0, D)$, the convolution will have extension $[0, 2D)$. Then, the common extension is $[0, 2D)$. In practice, we have to load the input vectors with signal values for a half and to fill with zeros the second half.

13.10.2 Computation of Hilbert Transform

In Sect. 9.10 we have seen that the Hilbert transform $\hat{s}(t)$, $t \in \mathbb{R}$, can be obtained as the response of a real ideal-shifter of $-\pi/2$. So, it is given by a convolution, which can be computed via FFT as seen above. In alternative, $\hat{s}(t)$ is given as the imaginary part of the analytic signal

$$\hat{s}(t) = \Im z_s(t). \quad (13.55)$$

We develop this second possibility. Considering that $Z_s(f) = 21(f)S(f)$, the computation of $\hat{s}(t)$ can be articulated as follows:

- (1) compute $S(f)$ via FFT,
- (2) evaluate $Z_s(f) = 21(f)S(f)$,
- (3) compute the inverse transform $z_s(t)$ of $Z_s(f)$ via FFT, and
- (4) take the imaginary part of $z_s(t)$, which gives $\hat{s}(t)$.

The global computational complexity is $2C(N) = 2N \log_2 N$. This procedure can be applied as well to the computation of the discrete Hilbert transform (see Sect. 11.7).

13.10.3 Computation of DCT

In Sect. 12.5 we have seen that the DCT S_0, S_1, \dots, S_{N-1} of a real sequence s_0, s_1, \dots, s_{N-1} can be obtained from the DFT of an auxiliary signal $s(nT)$ defined on $\mathbb{Z}(T)/\mathbb{Z}(4NT)$, which is obtained as follows (see Fig. 12.11):

- (1) let $s(2nT) = 0$,
- (2) display the N values s_n on the instants $T, 3T, \dots, (2N+1)T$, and
- (3) complete the signal in a period using the even symmetry.

Then, the DCT sequence is obtained from the values of the DFT $S(kF)$, $kF \in \mathbb{Z}(F)/\mathbb{Z}(4NF)$, in the *first quarter* of a period. Of course, this DFT is evaluated by the FFT.

For instance, for $N = 8$, the FFT must be loaded with the vector

$$[0, s_0, 0, s_1, 0, \dots, s_6, 0, s_7, 0, s_7, 0, s_6, 0, \dots, s_1, 0, s_0]$$

of length $4N = 32$. The resulting 32-point DFT vector has the form

$$[S_0, S_1, S_2, S_3, S_4, S_5, S_6, S_7, S_7, S_6, \dots],$$

and the first 8 values give the DCT sequence. This procedure is clearly redundant, because it requires a $4N$ -point FFT to compute an N -point DCT.

A nonredundant procedure, using an N -point FFT, is based on the following considerations. Once composed the auxiliary signal $s(t)$, $t \in \mathbb{Z}(T)/\mathbb{Z}(4NT)$, consider the other auxiliary signals (Fig. 13.16):

- the signal $u(t) = s(t + T)$, which moves the zeros of $s(t)$ from the even instants to the odd instants.
- the signal $v(t)$ obtained by the $\mathbb{Z}(T)/\mathbb{Z}(4NT) \rightarrow \mathbb{Z}(4T)/\mathbb{Z}(4NT)$ down-sampling of $u(t)$. Note that $v(t)$ has N points per period.

Now, the DFT $V(f)$ of $v(t)$ is the $\mathbb{Z}(F)/\mathbb{Z}(4NF) \rightarrow \mathbb{Z}(F)/\mathbb{Z}(NF)$ up-periodization of $U(f)$. The relationships are

$$U(f) = S(f)e^{i2\pi fT},$$

$$V(f) = U(f) + U\left(f - \frac{1}{4}F_p\right) + U\left(f - \frac{1}{2}F_p\right) + U\left(f - \frac{3}{4}F_p\right),$$

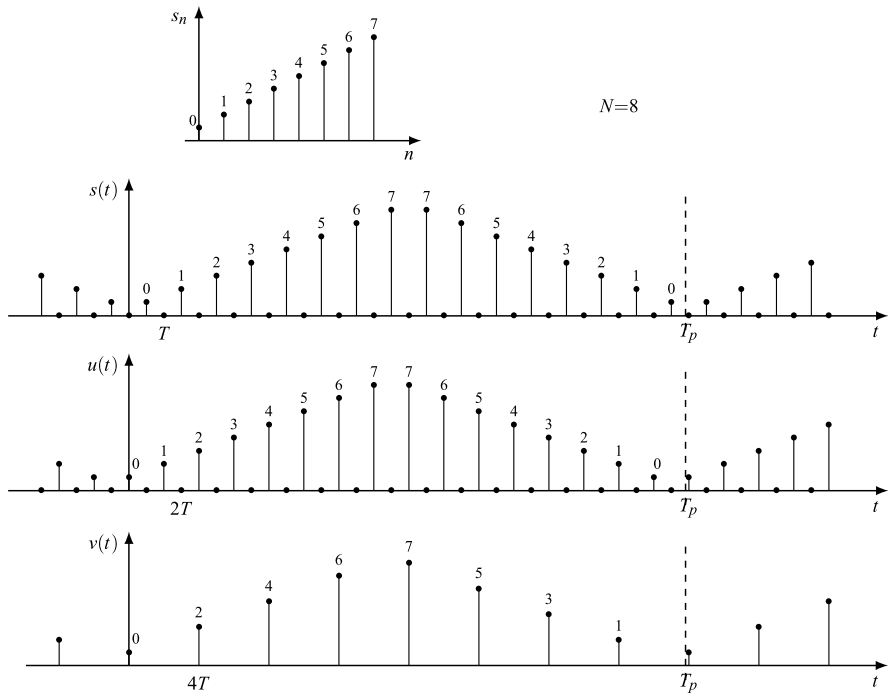


Fig. 13.16 Associated signal construction to compute an N -DCT by an N -DFT

and by combination

$$\begin{aligned}
 V(f) &= e^{i2\pi fT} \left[S(f) - iS\left(f - \frac{1}{4}F_p\right) - S\left(f - \frac{1}{2}F_p\right) + iS\left(f - \frac{3}{4}F_p\right) \right] \\
 &= e^{i2\pi fT} \left[2S(f) - 2iS\left(f - \frac{1}{4}F_p\right) \right], \tag{13.56}
 \end{aligned}$$

where $F_p = 1/T$, and we have used the symmetry (12.31) of $S(f)$.

We recall that $S(f)$ is a real function, and therefore it can be “extracted” from (13.56) as

$$S(f) = \frac{1}{2} \Re[V(f)e^{-i2\pi fT}]. \tag{13.57}$$

In this way, $S(f)$ and then the N -point DCT are obtained using an N -point DFT.

We organize the computation noting that the values of $v(t)$ in a period can be obtained by the given sequence s_n as (for N even, see Fig. 13.16)

$$v(4mT) = \begin{cases} s_{2m}, & 0 \leq m \leq \frac{1}{2}N - 1, \\ s_{N-2m-1}, & \frac{1}{2}N \leq m \leq N - 1. \end{cases} \tag{13.58}$$

In other words, the even values of s_n are displayed in the first half period and the odd values, in reverse sense, on the second half. Then, the procedure is:

- (1) construct $v(t)$ according to (13.58),
- (2) compute the DFT $v(t) \rightarrow V(f)$ via FFT, and
- (3) extract $S(f)$ from $V(f)$ according to (13.57).

Then, the DCT is given by $S_k = S(kF) = \frac{1}{2} \Re[V(kF)e^{-i2\pi kFT}]$, where $e^{-i2\pi kFT} = W_{4N}^{-k}$. For instance, for an 8-point DCT, the vector for the FFT is (see Fig. 13.16)

$$v = [s_0, s_2, s_4, s_6, s_7, s_5, s_3, s_1],$$

and, once obtained the FFT $V_k, k = 0, \dots, 7$, the DCT sequence is given by $S_k = \frac{1}{2} \Re[W_{32}^{-k} V_k]$. The procedure can be inverted for the IDCT computation, namely

- (1) using (13.56), evaluate $V(kF)$ from $S(kF) = S_k$,
- (2) compute the IDFT $V(f) \rightarrow v(t)$ via IFFT, and
- (3) obtain the sequence s_n from $v(t)$ by inverting (13.58).

UT 13.11 Conventional Durations and Bandwidths

For the computer processing of continuous-time signals, in particular for the FFT usage, both durations and bandwidths must be *finite*. However, that finiteness cannot hold simultaneously in both domains in the strict sense, and the introduction of “practically” finiteness is necessary.

For a non-time-limited signal $s(t), t \in \mathbb{R}$, infinitesimal as $|t| \rightarrow \infty$, we can introduce a *conventionally limited* extension $\tilde{e}(s)$ with the criterion that the signal is “negligible” outside $\tilde{e}(s)$. Then, from the conventional extension we obtain the conventional duration. Symmetric consideration can be done in the frequency domain.

Now, we introduce two criteria by which “negligible” is stated in a quantitative form. There are several other criteria that are dictated by the context of the specific applications. In any case, the target is an acceptable accuracy of the result with an acceptable computational complexity.

13.11.1 Criteria of “Negligible” Amplitudes

The assumption is that the signal is infinitesimal as $t \rightarrow \pm\infty$. Let s_M be the reference amplitude, which may be $s_M = \sup |s(t)| < \infty$ when the signal is amplitude limited, and let b a fixed number with $0 < b < 1$. Then, an *amplitude conventional (AC) extension* is a set $e_b(s)$ such that (Fig. 13.17)

$$|s(t)| \leq bs_M, \quad t \notin e_b(s). \quad (13.59)$$

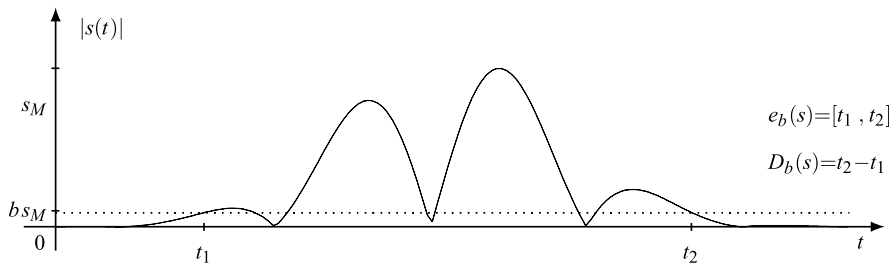


Fig. 13.17 Conventional extension $e_b(s)$ and duration $D_b(s)$ according to amplitudes

The measure $D_b(s) = \text{meas } e_b(s)$ will be called the *amplitude conventional (AC) duration*. In practice we choose $b \ll 1$, e.g., $b = 10^{-2}$ (40 dB), and as AC extension the smallest interval that verifies condition (13.59).

In the frequency domain we proceed analogously. We assume that $S(f)$ is infinitesimal as $f \rightarrow \pm\infty$ and a reference finite amplitude S_M may be $S_M = \sup |S(f)|$. Then, a set $\mathcal{E}_b(s)$ such that

$$|S(f)| < b S_M, \quad f \in \mathcal{E}_b(s),$$

is called the *AC spectral extension*, and its measure $B_b(s)$ the AC bandwidth. For a real signal, we choose a symmetric interval and consider the *AC band* $B_b = \frac{1}{2} B_b(s)$ in place of $B_b(s)$.

The above definition does not exclude strict-sense limitations. If the signal is strictly duration-limited, we set $e_b(s) = e(s)$, and if it is strictly band-limited, we set $\mathcal{E}_b(s) = \mathcal{E}(s)$. At least one of the extensions is conventional.

Example 13.2 We apply the above definitions to the causal exponential

$$s(t) = 1(t) A_0 \exp\left(-\frac{t}{T_0}\right) \xrightarrow{\mathcal{F}} S(f) = A_0 T_0 \frac{1}{1 + i2\pi f T_0},$$

which is neither duration-limited nor band-limited. For the AC extension, we choose $s_M = A_0$, and, considering the signal causality, we assume the form $(0, D_b)$ for $e_b(s)$. Since for $t > 0$, the signal is decreasing, D_b is given by the solution of $s(D_b) = b s_M$, that is,

$$A_0 \exp(-D_b/T_0) = b A_0 \implies D_b = T_0 \log(1/b).$$

For instance, for $b = 1\%$, we find $D_b = 4.6 T_0$.

Since the signal is real, we consider a symmetric AC spectral extension, that is, $(-B_b, B_b)$. Considering that

$$|S(f)| = A_0 T_0 / \sqrt{1 + (2\pi f T_0)^2}$$

is decreasing for $f > 0$, B_b is given by the solution of $S(B_b) = bS_M$, that is,

$$B_b = \frac{1}{2\pi T_0} \frac{\sqrt{1-b^2}}{b} \simeq \frac{1}{2\pi T_0 b}.$$

For instance, for $b = 1\%$, we find $B_b = 15.9/T_0$.

Example 13.3 The rectangular pulse $s(t) = A_0 \text{rect}(t/D) \xrightarrow{\mathcal{F}} A_0 D \text{sinc}(Df)$ has a finite ordinary extension, so we set $e_b(s) = e(s) = [-\frac{1}{2}D, \frac{1}{2}D]$ and $D_b = D$. The spectral extension is therefore conventional, and, considering the AC form, we set $e_b(s) = (-B_b, B_b)$, which is determined by the condition

$$S_M |\text{sinc}(Df)| \leq bS_M, \quad |f| > B_b. \quad (13.60)$$

Now, the evaluation of the smallest interval that verifies (13.60) is based on the solution of a transcendental equation (which can be solved numerically). However, this is not useful, and we can search for an approximate evaluation. Considering that $|\text{sinc}(x)| \leq 1/(\pi x)$, we evaluate B_b according to

$$S_M 1/|\pi Df| \leq bS_M, \quad |f| > B_b.$$

Thus, we find

$$B_b = 1/(\pi Db).$$

For instance, for $b = 1\%$, we obtain $B_b = 31.8/D$.

13.11.2 Criteria of “Negligible” Energy

The conventional bandwidth B^b determined by the criterion that the signal energy is negligible outside $(-B^b, B^b)$ was introduced and discussed in Sect. 8.11, in connection with error in sampling. The definition of *energy conventional* (EC) bandwidth is

$$\int_{f \notin (-B^b, B^b)} |S(f)|^2 df = b \int_{-\infty}^{+\infty} |S(f)|^2 df.$$

A similar definition may be used for the EC duration D^b ; specifically, we determine two instants t_1 and t_2 such that

$$\int_{t_1}^{t_2} |s(t)|^2 dt = b \int_{-\infty}^{+\infty} |s(t)|^2 dt.$$

Then, $D^b = t_2 - t_1$. Of course, for a given accuracy b , the EC duration D^b is not unique, and, in practice, symmetries and the context suggest a better choice.

13.11.3 Duration \times Bandwidth

The product $D(s)B(s)$ or $D(s)B$ for a real signal depends on the definitions of these parameters; one of them, at least, is conventional.

Once refined the definitions, the product turns out to be characteristic of the class of the signals

$$s(t) = A_0 s_0 \left(\frac{t - t_0}{a} \right), \quad a > 0,$$

which is generated by the parameters A_0 , t_0 , and a , starting from a reference signal $s_0(t)$, $t \in \mathbb{R}$. In fact, using the rules on scale change and on time shift (see Sect. 6.5), we find that $D(s) = aD(s_0)$ and $B(s) = (1/a)B(s_0)$. Hence,

$$D(s)B(s) = D(s_0)B(s_0) = K$$

depends only on the reference signal s_0 and on the definition adopted for $D(s)$ and $B(s)$.

Example 13.4 For the Fourier pair

$$A_0 1(t) e^{-t/T_0} \xrightarrow{\mathcal{F}} A_0 T_0 / (1 + i2\pi f T_0),$$

we have found that the AC duration D_b and the AC band B_b are given by

$$D_b = T_0 \log(1/b), \quad B_b = 1/(2\pi T_0 b),$$

whereas the EC duration D^b and the EC band B^b are given by

$$D^b = \frac{1}{2} T_0 \log \frac{1}{b}, \quad B^b = \frac{1}{2\pi T_0} \tan \frac{\pi}{2} (1 - b).$$

Then, the corresponding products are

$$D_b B_b = \frac{1}{2\pi b} \log \frac{1}{b}, \quad D^b B^b = \frac{1}{4\pi} \left(\log \frac{1}{b} \right) \tan \frac{\pi}{2} (1 - b).$$

Table 13.2 gives these products as functions of the accuracy b , expressed in decibels, that is, $-20 \log_{10} b$. Note that the same results hold for the symmetrical pair

$$\frac{A_0 F_0}{1 + i2\pi t F_0} \xrightarrow{\mathcal{F}} A_0 1(-f) e^{-f/F_0}.$$

Interpretation The Unified Sampling Theorem (see Sect. 8.4) states that the bandwidth $B(s)$ represents the minimal sampling frequency for the perfect reconstruction, and, to this end, the number of sample values $s(nT)$, with $T = 1/B(s)$,

Table 13.2 Conventional durations and bands of causal exponential

Precision <i>b</i> dB	Duration		Band		Product	
	D_b/T_0	D^b/T_0	B_bT_0	B^bT_0	D_bB_b	D^bB^b
30	3.45	1.73	5.0	3.2	17.4	5.5
40	4.61	2.30	15.9	10.1	73.3	23.3
50	5.76	2.88	50.3	32.0	289.7	92.2
60	6.91	3.45	159.2	101.3	1099	350.0
70	8.06	4.03	503.2	320.4	4056	1291

would be infinite. However, if we neglect the sample values outside the (conventional) duration, their number becomes finite and given by the product $K = D(s)B(s)$.

In conclusion, the product $K = D(s)B(s)$ represents the *number of sample values required for the reconstruction of the signals according to a specified accuracy*. For this reason, K is sometimes called the number of degrees of freedom of the signal.

13.11.4 Extension Estimation in Practical Cases

The FT computation via FFT requires the *preliminary* knowledge of the spectral extension, which is one of the targets of the computation itself. This difficulty is overcome mainly by experience and by the context. Let us consider a couple of contexts:

- (1) The signal has been saved by a tape recorder. In this case the bandwidth is determined by the tape recorder or by the instrumentation previously used. It is worth observing that the conventional 3-dB bandwidth used for amplifiers is not sufficient, but a larger bandwidth, may be a 40-dB bandwidth or more, is appropriate.
- (2) The signal is known by its time expression, and we want to evaluate numerically its FT that we are not able to calculate explicitly. In this case we search for an approximate Fourier pair which allows an evaluation of $D(s)$ and $B(s)$.

It is clear that the computation based on these suggestions requires a check after the computation, guided by the experience.

UT 13.12 Use of Windows

In a conventional extension the signal is “neglected” outside the extension, where the signal is set to zero, although it is not identically zero. This corresponds to a

truncation of the signal that is a multiplication by a *unitary rectangular window* spread over the extension. The problem becomes critical in some applications when a portion of a signal is analyzed, e.g., in speech recognition where the analysis is carried out sequentially on segments of words. It is intuitive that the rectangular window is not the best choice to obtain a finite-duration signal.

Given a sampled signal $s_c(t)$, $t \in \mathbb{Z}(T)$, we can take N consecutive samples in the form

$$s_w(t) = w(t)s_c(t), \quad t \in \mathbb{Z}(T), \quad (13.61)$$

where the window (shape) $w(nT)$ is zero outside $[0, (N - 1)T]$. In the frequency domain, (13.61) becomes

$$S_w(f) = W * S_c(f), \quad f \in \mathbb{R}/\mathbb{Z}(F_p), \quad F_p = 1/T. \quad (13.62)$$

Now it is clear that the closer is $W(f)$ to the impulse $\delta_{\mathbb{R}/\mathbb{Z}(F_p)}(f)$, the closer is $S_w(f)$ to $S(f)$.

The simplest is the *rectangular window*

$$w(t) = 1, \quad t = 0, T, \dots, (N - 1)T,$$

and $w(t) = 0$ elsewhere. Its FT is given by

$$W(f) = NT e^{-i\pi f(N-1)T} \text{sinc}_N(fNT), \quad f \in \mathbb{R}/\mathbb{Z}(F_p). \quad (13.63)$$

Figure 13.18 shows the amplitude $|W(f)|$, in dB, for $T = 1$ and $N = 21$. Note the presence of a *principal lobe* with width $2/(NT)$ and *secondary lobes*. The amplitude of the first secondary lobe is only 13 dB less than that of the principal lobe. The effect of a rectangular window is a “smoothing,” mainly due to the width of the principal lobe. The secondary lobes may have a shadow effect on frequency components having small amplitudes (*leakage* effect).

To avoid these effects, several nonrectangular windows have been proposed, the most popular of which are collected in Fig. 13.18. The main parameters of a window are:

- normalized duration N ,
- the ratio ΔF of the main lobe, which can be expressed in the form αF , where $F = F_p/N$ is frequency spacing, and
- the rate r_1/r_0 between the amplitude of the first secondary lobe and of the primary lobe (in dB).

We may see the importance of the lobe ratio r_1/r_0 at the cost of an increase of the main lobe width ΔF .

To show the windowing effect, we consider the computation of the Fourier transform of the signal

$$s(t) = \cos 2\pi f_0 t + 0.05 \cos 2\pi f_1 t, \quad t \in \mathbb{Z}(T), \quad f_0 T = 0.3, \quad f_1 T = 0.2.$$

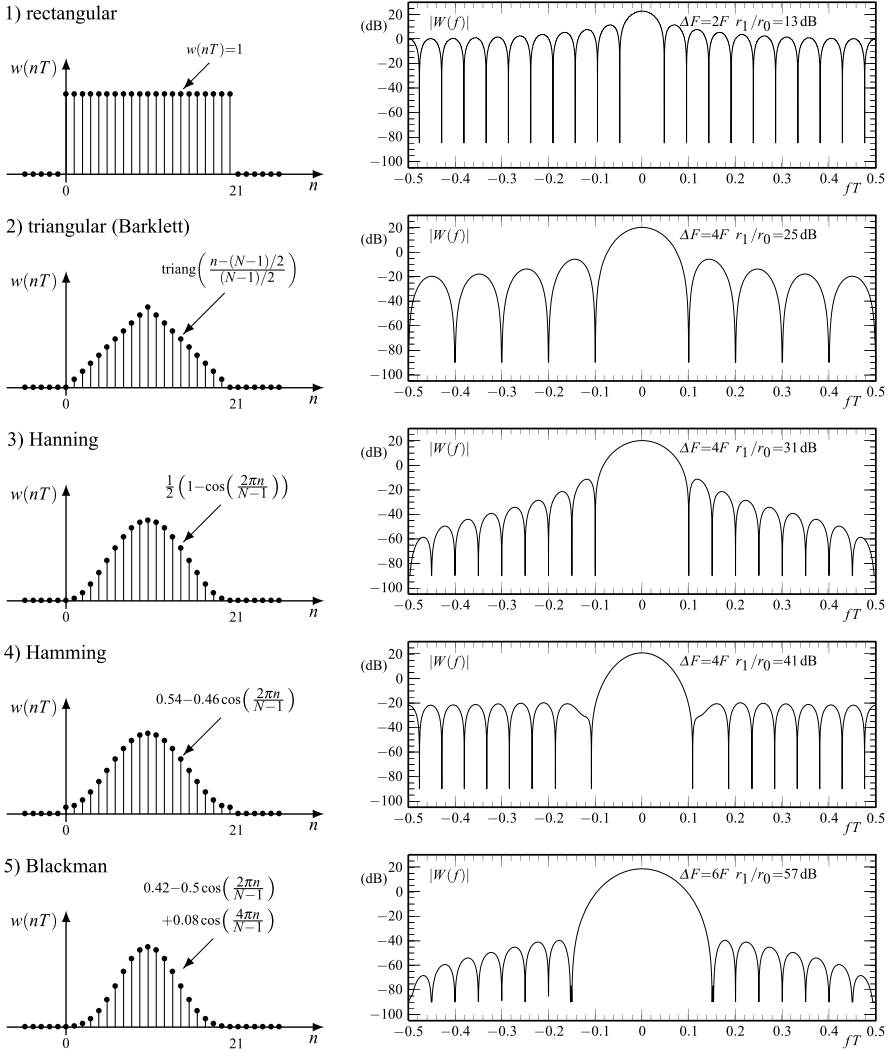


Fig. 13.18 Fundamental windows for $N = 21$. ΔF is the width of the main lobe ($F = F_p/N$), r_1 is the amplitude of the first secondary lobe

The spectrum of this signal, considered on $\mathbb{Z}(T)$, exhibits two impulses at the frequencies $f_0 = 0.3/T$ and $f_1 = 0.2/T$. Figure 13.19 shows the modulus (in dB) of the FT of the windowed version of $s(t)$, using the windows of Fig. 13.18. For the windows, we have chosen a normalized duration $N = 101$, and the FTs have been computed via FFT, after a windowing and a (conceptual) $\mathbb{Z}(T)/\mathbb{Z}(NT)$ up-periodization with $N = 512$. The figure shows the 512 FFT values (interpolated for clarity) of $S_w(f)$ in the fundamental band $(-\frac{1}{2}NF, \frac{1}{2}NF)$. Note how the use of an

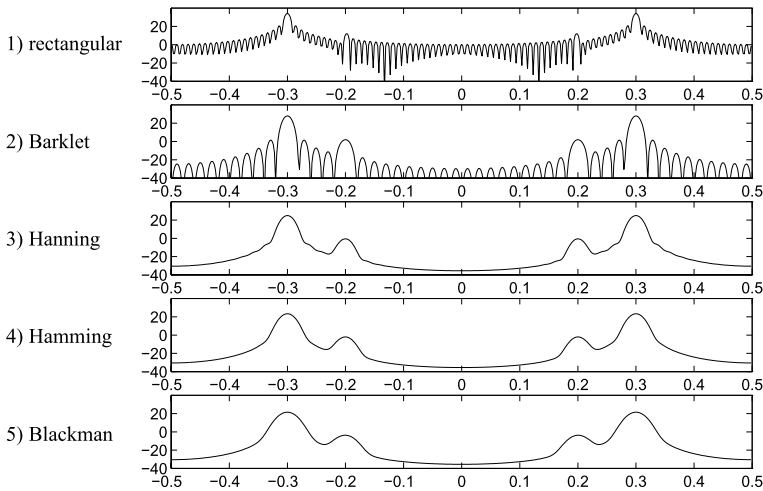


Fig. 13.19 Fourier transform after a window processing

appropriate window is essential to recognize the presence of a sinusoidal component with a small amplitude.

For more details on this topic, we suggest references [3, 5, 6].

13.13 Problems

13.1 ★ [Sect. 13.4] Show that with $N = 2^m$ the general solution of recurrence (13.19) is

$$\mu(N) = \frac{1}{2}N\mu(2) + N(\log_2 N - 1) \quad (13.64)$$

with $\mu(2)$ the initial condition.

13.2 ★★ [Sect. 13.4] Prove (13.22) concerning the parallel computation of an a -point DFT.

13.3 ★ [Sect. 13.4] Gauss dedicated several years to compute the orbit of the asteroid Ceres. In particular, he was engaged on a 12-point DFT and found it convenient to use the decompositions $12 = 3 \cdot 4$ and $12 = 3 \cdot 2 \cdot 2$ (Fig. 13.20).

Discuss the advantage of such decompositions with respect to the direct 12-point DFT computation.

13.4 ★★ [Sect. 13.8] In the previous chapter (Sect. 12.4) we have introduced the *cosine* DFT. Organize its numerical computation and evaluate the number of operations.

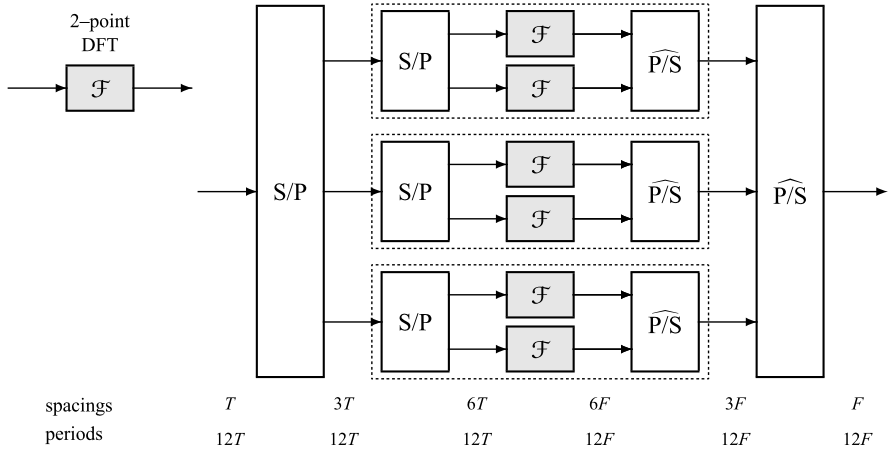


Fig. 13.20 The parallel computation used by Gauss for a 12-point DFT

13.5 ★★ [Sect. 13.8] In the previous chapter (Sect. 12.4) we have introduced the *sine* DFT. Organize its numerical computation and evaluate the number of operations.

References

1. J.W. Cooley, J.W. Tukey, An algorithm for the machine computation of complex Fourier series. *Math. Comput.* **19**, 297–301 (1965)
2. J.W. Cooley, P.A.W. Lewis, P.D. Welch, Historical notes on the fast Fourier transform. *IEEE Trans. Audio Electroacoust.* **15**, 76–79 (1967)
3. F. Harris, On the use of windows for harmonic analysis with the discrete Fourier transform. *Proc. IEEE* **66**, 51–83 (1978)
4. P. Kraniuskas, A plain man’s guide to the FFT. *IEEE Signal Process. Mag.* 22–35 (1994)
5. L.R. Rabiner, B. Gold, *Theory and Application of Digital Signal Processing* (Prentice Hall, Englewood Cliffs, 1975)
6. L.R. Rabiner, C.M. Rader (eds.), *Digital Signal Processing* (IEEE Press, New York, 1972)

Chapter 14

Signal Expansions, Filter Banks, and Subband Decomposition

UT 14.1 Generalized Transforms

A generalized transform performs a signal representation in a new environment as the frequency domain for the Fourier transform. The kernel of a generalized transform becomes an arbitrary function of two variables, instead of the familiar exponential of the Fourier transform, and is chosen in dependence of the specific application. The possibility of recovering the signal from the generalized transform (invertibility) must be assured. Another generalization regards the inverse transform, the kernel of which may be not trivially related to that of the forward transform, whereas in the case of the Fourier transform the kernels are simply the conjugate of each other.

14.1.1 Definition

Definition 14.1 Let I and U be LCA groups, possibly quotient groups. Then an $I \rightarrow U$ generalized transform is a double linear mapping

$$\Theta: L_2(I) \mapsto L_2(U), \quad \Phi: L_2(U) \mapsto L_2(I), \quad (14.1)$$

where $L_2(I)$ and $L_2(U)$ are the Hilbert spaces of square-integrable functions.

The group I is called the *signal domain*, and the group U the *transform domain*; Θ is called the *operator* of the *forward transform*, and Φ the *operator* of the *inverse transform*.¹

¹Most authors prefer to reserve the term “operator” to the case $L_2(I) \mapsto L_2(I)$, and in the general case they use the term “transformation” (see [9]).



Fig. 14.1 Domains and kernels in a general *transform* and in its *inverse transform*

Considering the linearity of the mappings, the evaluation of a generalized transform pair (s, S) has the form (Fig. 14.1)

$$\Theta \quad S(u) = \int_I dt s(t)\theta(u, t), \quad u \in U, \quad (14.2a)$$

$$\Phi \quad s(t) = \int_U du S(u)\varphi(t, u), \quad t \in I, \quad (14.2b)$$

where $\theta(u, t)$, $(u, t) \in U \times I$, is the kernel of the transform, and $\varphi(t, u)$, $(t, u) \in I \times U$, is the kernel of the inverse transform. The function $S(u)$, $u \in U$, gives the *transform* of the signal $s(t)$, $t \in I$, and, from the transform, the original signal can be recovered by the *inverse transform*. In symbols,

$$s(t) \xrightarrow{\Theta} S(u), \quad S(u) \xrightarrow{\Phi} s(t). \quad (14.3)$$

Kernels related in the forms

$$\theta(u, t) = \varphi^*(t, u) \quad (14.4)$$

are called *self-reciprocal* [4].

The possibility of the signal recovery from the transform requires stringent conditions, which in turn pose a serious constraint on the choice of the transform domain U for any given signal domain I (see the FT, where U must be chosen as the dual group). However, for the time being with, we do not make assumptions on the domains I and U .

We can easily see that the Fourier transform introduced in Chap. 5 is a special case of a generalized transform with transform domain given by the dual group $U = \widehat{I}$, forward kernel $\theta(f, t) = e^{-i2\pi ft}$, and inverse kernel $\varphi(t, f) = e^{i2\pi ft}$, which are self-reciprocal. Other examples have been listed in Chap. 6, Sect. 6.4. Further examples, as the *wavelet transform* and the *Radon transform*, will be seen in the next chapters.

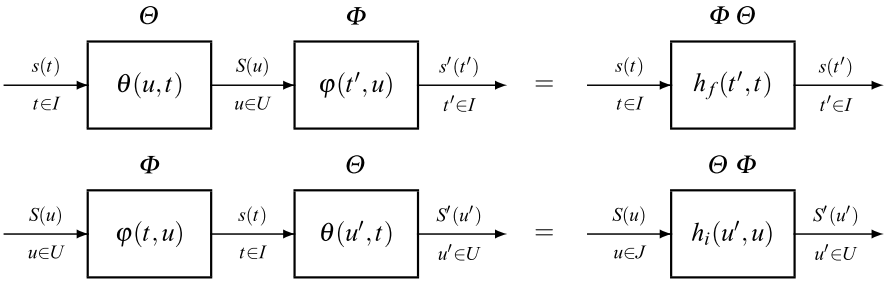


Fig. 14.2 Cascades to establish the reconstruction conditions of a general transform. *Above*, the forward reconstruction condition (FRC); *below*, the inverse reconstruction (IRC)

14.1.2 Invertibility Conditions

In Chap. 6 we have introduced the notion of an $I \rightarrow U$ linear transformation.² Now, the forward transform with relationship (14.2a) defines an $I \rightarrow U$ linear transformation with kernel $\theta(u, t)$, and the inverse transform with relationship (14.2b) defines a $U \rightarrow I$ linear transformation with kernel $\varphi(t, u)$. If we connect the two transformations in the indicated order (Fig. 14.2, we obtain an $I \rightarrow I$ linear transformation with kernel

$$\Phi \Theta \quad h_f(t', t) = \int_U du \varphi(t', u)\theta(u, t). \tag{14.5}$$

In general, the connection produces a signal $\tilde{s}(t)$ that is different from the original signal $s(t)$, but if the two kernels verify the condition

$$\boxed{\int_U du \varphi(t', u)\theta(u, t) = \delta_I(t' - t)}, \tag{14.6}$$

where $\delta_I(\cdot)$ is the impulse on I , the cascade becomes equivalent to the identity on I , symbolically $\Phi \Theta = \mathcal{J}_I$, and one obtains the exact reconstruction of $s(t)$ from its transform $S(u)$. Then (14.6) is called *perfect reconstruction condition*.

We can also consider the connection of the $U \rightarrow I$ linear transformation with kernel $\varphi(t, u)$ followed by the $I \rightarrow U$ linear transformation with kernel $\theta(u, t)$, that is, Φ followed by Θ . The cascade gives a $U \rightarrow U$ linear transformation with kernel

$$\Theta \Phi \quad h_i(u', u) = \int_I dt \theta(u', t)\varphi(t, u). \tag{14.7}$$

²The terms “transform” and “transformation” may be confused. We use “transformation” thinking of a model of a system, and “transform” as a mathematical operation, usually accomplished by the inverse operation (inverse transform). “Transform” is also used to denote the result of the application of a transform.

Here, we start with the transform $S(u)$ to get the signal $s(t)$, from which we get in general a new transform $S'(u)$. But, if the kernels verify the condition

$$\boxed{\int_I dt \theta(u', t) \varphi(t, u) = \delta_U(u' - u),} \quad (14.8)$$

the cascade becomes equivalent to the identity on U , that is, $\Theta\Phi = \mathcal{J}_U$, and we obtain the exact reconstruction of the transform, $S'(u) = S(u)$, from the signal $s(t)$.

Condition (14.8) is called *biorthogonality condition*, and when the kernels are self reciprocal, $\theta(u, t) = \varphi^*(t, u)$, it is called *orthogonality condition*. The terms biorthonormality and orthonormality are also used.

To unify the terminology, condition (14.6) will be called *forward reconstruction condition* (FRC), and condition (14.8) *inverse reconstruction condition* (IRC). In general, the two conditions are not equivalent, and appropriate assumptions should be made to ensure the equivalence. This will be seen gradually in the next sections.

14.1.3 Reconstruction Limited to a Subclass of Signals

In Chap. 6, Sect. 6.2, we have introduced the concept of *conditionally invertible* transformations, where the signal can be recovered under the condition that it belongs to a subclass of the possible input signals. For linear transformations, which we are considering in the present context of generalized transforms, we can formulate some specific statements in terms of images and projectors.

Consider the *images* of the inverse transform Φ and of the forward cascade $\Phi\Theta$, which are given respectively by

$$\text{im}(\Phi) = \{\Phi[S] \mid S \in L_2(U)\}, \quad \text{im}(\Phi\Theta) = \{\Phi\Theta[s] \mid s \in L_2(I)\},$$

and both are subspaces of $L_2(I)$. Now, if the IRC holds, that is, if $\Theta\Phi = \mathcal{J}_U$, any transform $S \in L_2(U)$ can be uniquely recovered as $S = \Theta[s]$ from $s = \Phi[S]$, and hence Θ is surjective. Then

$$\text{im}(\Phi) = \text{im}(\Phi\Theta) \stackrel{\Delta}{=} H.$$

If H is a proper subspace of $L_2(I)$, the FRC does not hold, and in general the inverse transform Φ gives the *projection of the signal onto the subspace H* , instead of the perfect reconstruction.

Proposition 14.1 *In a generalized transform Θ, Φ , where the IRC holds and $H = \text{im}(\Phi)$ is a proper subspace of $L_2(I)$, the forward cascade is equivalent to the projector*

$$\mathcal{P}_H = \Phi\Theta : L_2(I) \mapsto H. \quad (14.9)$$

The kernel of the projector is

$$\mathcal{P}_H \quad h_H(t', t) = \int_U du \varphi(t', u)\theta(u, t). \tag{14.10}$$

If $H = \text{im}(\Phi) = L_2(I)$, the projector \mathcal{P}_H becomes the identity on I , and also the FRC holds.

Proof We have to prove that \mathcal{P}_H is idempotent, that is, $\mathcal{P}_H^2 = \mathcal{P}_H$ (see Definition 4.2). The proof is very simple in terms of operator algebra. In fact,

$$\mathcal{P}_H^2 = (\Phi \Theta)(\Phi \Theta) = \Phi(\Theta \Phi)\Theta = \Phi \mathcal{J}_U \Theta = \Phi \Theta = \mathcal{P}_H. \quad \square$$

Example 14.1 Consider the generalized transform where $I = \mathbb{R}$, $U = \mathbb{Z}$, and

$$\begin{aligned} \Theta \quad S(n) &= \int_n^{n+1} s(t) dt, \quad n \in \mathbb{Z}, \\ \Phi \quad \tilde{s}(t) &= \sum_{n \in \mathbb{Z}} S(n) \text{rect}_+(t - n), \quad t \in \mathbb{R}. \end{aligned}$$

In words, $S(n)$ is given by the area of the signal in the interval $[n, n + 1)$, and $\tilde{s}(t)$ is obtained from the transform $S(n)$ with a “hold” operation with interpolating function $\varphi(t) = \text{rect}_+(t)$.

The IRC holds, and, in fact,

$$\int_{\mathbb{R}} \varphi(t - n')\varphi(t - n) dt = \delta_{n'n},$$

whereas the FRC does not hold as one can see from Fig. 14.3. The image of Φ is the subclass of $L_2(\mathbb{R})$

$$H = \text{im}(\Phi) = \left\{ \tilde{s}(t) = \sum_{n \in \mathbb{Z}} S(n) \text{rect}_+(t - n) \mid S(n) \in L_2(\mathbb{Z}) \right\}$$

given by the piecewise constant signals over the intervals $[n, n + 1)$, and therefore it is a proper subspace of $L_2(\mathbb{R})$.

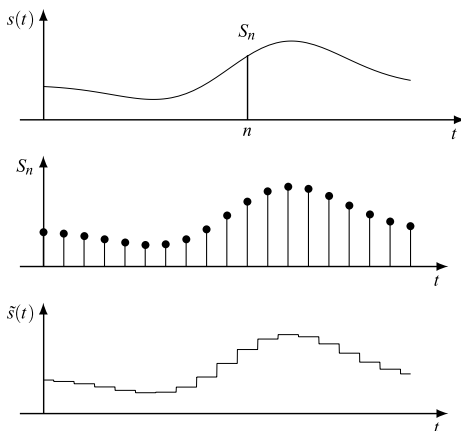
The forward cascade $\Phi \Theta$ gives the projector \mathcal{P}_H that approximates an arbitrary signal with a piecewise constant signal.

14.1.4 Inner Products and Parseval’s Relations

The transform $S(u)$ defined by (14.2a) can be expressed as an inner product in the space $L_2(I)$, where

$$\langle x, y \rangle = \int_I dt x(t)y^*(t). \tag{14.11}$$

Fig. 14.3 Generalized transform where the reconstruction is limited to the subclass H of piecewise constant signals. The reconstructed signal $\tilde{s}(t)$ is the projection of $s(t)$ onto H



In fact, $S(u) = \langle s, \theta^*(u, \cdot) \rangle$, $u \in U$, where the transform variable u is intended as a parameter, and the integration is performed with respect to $t \in I$. Analogously, the inverse transform $s(t)$ given by (14.2b) can be expressed as an inner product in the space $L_2(U)$, where

$$\langle X, Y \rangle = \int_U du X(u)Y^*(u), \tag{14.12}$$

and we have $s(t) = \langle S, \varphi^*(t, \cdot) \rangle$, $t \in I$.

To find a general Parseval’s relation, we introduce the *dual*³ transform $\tilde{S}(u)$, which is obtained by rearranging the reciprocal kernels, namely $\tilde{\theta}(u, t) = \varphi^*(t, u)$ and $\tilde{\varphi}(t, u) = \theta^*(u, t)$. Then, following (14.2a), (14.2b), we get the pair

$$\tilde{\Theta} = \Phi^* \quad \tilde{S}(u) = \int_I dt s(t)\varphi^*(t, u), \quad u \in U, \tag{14.13a}$$

$$\tilde{\Phi} = \Theta^* \quad s(t) = \int_U df \tilde{S}(u)\theta^*(u, t), \quad t \in I. \tag{14.13b}$$

In general, the dual transform $\tilde{S}(u)$ is different from the original transform $S(u)$, but the recovery condition of the signal $s(t)$ from $\tilde{S}(u)$ is ensured. In fact, the orthogonality condition for (14.13a), (14.13b) is still given by (14.6). When the kernels are self-reciprocal, (14.13a), (14.13b) become (14.2a), (14.2b), and the dual transform coincides with the original one.

Now, we prove that, if the FRC holds, the inner product of $S(u)$ and $\tilde{S}(u)$ gives

$$\boxed{\langle S, \tilde{S} \rangle = \langle s, s \rangle = \|s\|^2}, \tag{14.14a}$$

³Caution must be paid on this term, because in this book “dual” is used throughout for quantities related to the Fourier transform, while here it has a different meaning.



Fig. 14.4 Domains, functions, and kernels of the transform and its inverse

which represents a generalized Parseval’s relation. When the kernels are self-reciprocal, $\tilde{S} = S$, we find the standard Parseval’s relation

$$\langle S, S \rangle = \|S\|^2 = \langle s, s \rangle = \|s\|^2. \tag{14.14b}$$

To prove (14.14a), we use (14.2a) and (14.13a) to get

$$\begin{aligned} \langle S, \tilde{S} \rangle &= \int_U du S(u) \tilde{S}^*(u) \\ &= \int_U du \left\{ \int_I dt s(t) \theta(u, t) \right\} \left\{ \int_I dt' s(t') \varphi^*(t', u) \right\}^* \\ &= \int_I dt \int_I dt' \left\{ \int_U du \theta(u, t) \varphi(t', u) \right\} s(t) s^*(t') \\ &= \int_I dt \int_I dt' \delta_I(t - t') s(t) s^*(t') = \int_I dt |s(t)|^2, \end{aligned}$$

where we have changed the integration order and used the FRC (14.6).

UT 14.2 Signal Expansions as Generalized Transforms

For convenience, we reconsider the *forward transform* and the *inverse transform* introduced in Sect. 14.1, but with the arguments written in the form we use for the polyphase decomposition, namely (Fig. 14.4)

$$\Theta \quad S(u_0) = \int_I dt_0 s(t_0) \theta(u_0, t_0), \quad u_0 \in U, \tag{14.15a}$$

$$\Phi \quad s(t_0) = \int_U du_0 S(u_0) \varphi(t_0, u_0), \quad t_0 \in I. \tag{14.15b}$$

Now, a signal expansion may be viewed as an inverse transform, where the domain U is discrete (a lattice or a finite group). In fact, in this case (14.2b) can be written in the form

$$\boxed{ \Phi \quad s(t_0) = \sum_{u_0 \in U} S_{u_0} \varphi_{u_0}(t_0), \quad t_0 \in I, } \tag{14.16a}$$

where the *coefficients* S_{u_0} are obtained from the forward transform as

$$\Theta \quad S_{u_0} = d(U)S(u_0) = d(U) \int_I dt_0 \theta_{u_0}(t_0)s(t_0) \quad (14.16b)$$

with

$$\theta_{u_0}(t_0) = \theta(u_0, t_0), \quad \varphi_{u_0}(t_0) = \varphi(t_0, u_0). \quad (14.17)$$

With the new symbolism the FRC (14.6) and the IRC (14.8) become respectively

$$\begin{aligned} \text{(FRC)} \quad & \sum_{u_0 \in U} d(U) \varphi_{u_0}(t'_0) \theta_{u_0}(t_0) = \delta_I(t'_0 - t_0), \\ \text{(IRC)} \quad & \int_I dt_0 \theta_{u'_0}(t_0) \varphi_{u_0}(t_0) = \delta_U(u'_0 - u_0). \end{aligned} \quad (14.18)$$

If U is a lattice, the impulse is explicitly given by

$$\delta_U(u'_0 - u_0) = \delta_{u_0, u'_0} / d(U) = \begin{cases} 1/d(U), & u'_0 = u_0, \\ 0, & u'_0 \neq u_0, \end{cases}$$

and the IRC can be written in the form

$$\langle \theta_{u'_0}(\cdot), \varphi_{u_0}^*(\cdot) \rangle = \int_I dt_0 \theta_{u'_0}(t_0) \varphi_{u_0}(t_0) = \delta_U(u'_0 - u_0) = \delta_{u_0 u'_0} / d(U), \quad (14.19)$$

where $\delta_{u'u}$ is the Kronecker symbol.

Generalized Bases The forward transform Θ and the inverse transform Φ are expressed in terms of two families of functions from the classes $L_2(I)$ and $L_2(U)$, respectively

$$\Phi = \{\varphi_{u_0} | u_0 \in U\} \quad \text{and} \quad \Theta = \{\theta_{u_0} | u_0 \in U\} \quad (14.20)$$

that may be viewed as *generalized bases*. As seen in Chap. 4, a *basis* must consist of independent functions, but here this condition is not required, and the families may be redundant, and in general they may represent *frames*. When the kernels are reciprocal, that is, $\theta_{u_0}(t_0) = \varphi_{u_0}^*(t_0)$, the IRC becomes an *orthogonal condition*,⁴ and the family Φ becomes an *orthogonal basis*. But, in general, the families Φ and Θ form *biorthogonal bases*. In this classification we will be more precise in the following.

⁴The terms “orthogonal” and “orthonormal” will often used interchangeably, unless we want to stress the normalization and then we use “orthonormal.” The same applies to the terms “biorthogonal” and “biorthonormal.”

Limited Reconstruction If the correct reconstruction is limited to a proper subclass of signals, $H = \text{im}(\Phi) \subset L_2(I)$, the FRC given by (14.18) must be modified as

$$\sum_{u_0 \in U} d(U) \varphi_{u_0}(t'_0) \theta_{u_0}(t_0) = h_H(t'_0, t_0), \quad (14.21)$$

where $h_H(t'_0, t_0)$ is the kernel of the projector $\mathcal{P}_H : L_2(I) \mapsto H$.

This may be viewed as the general case, since it includes the case $H = L_2(I)$, where $h_H(t'_0, t_0) = \delta_I(t'_0 - t_0)$ as in (14.18).

Example 14.2 Consider the sampling and interpolation formulas of the *Fundamental Sampling Theorem*, written in the form

$$\begin{aligned} S(nT) &= \int_{\mathbb{R}} dt_0 s(t_0) \delta(t_0 - nT) = s(nT), \quad nT \in \mathbb{Z}(T), \\ s(t_0) &= \int_{\mathbb{Z}(T)} du_0 \frac{1}{T} \text{sinc}\left(\frac{t_0 - u_0}{T}\right) S(nT) \\ &= \sum_{nT \in \mathbb{Z}(T)} s(nT) \text{sinc}\left(\frac{t_0 - nT}{T}\right), \quad t_0 \in \mathbb{R}, \end{aligned} \quad (14.22)$$

which are a special case of (14.15a), (14.15b) with $I = \mathbb{R}$, $U = \mathbb{Z}(T)$, and

$$\theta(nT, t_0) = \theta_{nT}(t_0) = \delta(t_0 - nT), \quad \varphi(t_0, nT) = \varphi_{nT}(t_0) = \frac{1}{T} \text{sinc}\left(\frac{t_0 - nT}{T}\right).$$

This expansion has been considered in Sect. 4.6 and is based on the orthogonality of the *cardinal functions* $\varphi_{nT}(t_0) = \text{sinc}((t_0 - nT)/T)$.

In this case the IRC given by (14.18) holds. In fact,

$$\int_{\mathbb{R}} dt_0 \delta(t_0 - n'T) \frac{1}{T} \text{sinc}\left(\frac{t_0 - nT}{T}\right) = \frac{1}{T} \text{sinc}(n' - n) = \frac{1}{T} \delta_{n',n},$$

but the forward kernel (14.5) is given by

$$h_H(t'_0, t_0) = \sum_{nT \in \mathbb{Z}(T)} T \frac{1}{T} \text{sinc}\left(\frac{t'_0 - nT}{T}\right) \delta(t_0 - nT) \neq \delta(t'_0 - t_0). \quad (14.23)$$

The reason is that the cardinal functions do not form a *complete* basis, being the reconstruction limited to the class of band-limited signals

$$H(B) = \{s \mid \mathcal{E}(s) \subset (-B, B), 2B \leq 1/T\} \quad (14.24)$$

with band $B \leq 1/(2T)$ (note that $H(B)$ forms a *subspace* of $L_2(I)$). The kernel (14.23) defines a projector $\mathcal{P}_H : H(B) \mapsto L_2(I)$, which represents the identity operator for the class $H(B)$.

In conclusion: if the expansion is applied to a band-limited signal of the class H , the reconstruction is correct (according to the Sampling Theorem), otherwise the reconstruction gives a projection of the signal onto $H(B)$.

14.3 Interpretation of Expansions: The Matrix Viewpoint

The formulation of signal expansions in terms of generalized transforms is very general but somewhat abstract and needs a test on simple cases to get familiarity and to achieve more insight. The *matrix viewpoint*, when possible, is the adequate tool.

The matrix viewpoint is directly applicable on finite groups and, with some caution, on discrete groups, where the dimensionality becomes infinite. In the former case, transformation operators and bases are finite-dimensional and can be handled with ordinary matrices (of finite size), while in the latter case it is necessary to handle matrices with infinite dimensions. To facilitate the comprehension, we consider the simplest signals, which are defined on $\mathbb{Z}/\mathbb{Z}(N)$ and are isomorphic to the vectors of \mathbb{C}^N .

14.3.1 Finite-Dimensional Generalized Expansions

A signal $s(t)$, $t \in \mathbb{Z}/\mathbb{Z}(M)$, can be represented as a (column) vector $\mathbf{s} = [s_0, s_1, \dots, s_{M-1}]'$, which collects the values of $s_n = s(n)$ in a period. A generalized transform

$$\begin{aligned}\Theta: L_2(\mathbb{Z}/\mathbb{Z}(M)) &\mapsto L_2(\mathbb{Z}/\mathbb{Z}(N)), \\ \Phi: L_2(\mathbb{Z}/\mathbb{Z}(N)) &\mapsto L_2(\mathbb{Z}/\mathbb{Z}(M))\end{aligned}$$

is represented by two matrices Θ and Φ with entries respectively

$$\theta(u_0, t_0) = \theta_{u_0}(t_0), \quad \varphi(t_0, u_0) = \varphi_{u_0}(t_0),$$

where both u_0 and t_0 can be limited to a period, that is, with $u_0 = 0, 1, \dots, N-1$ and $t_0 = 0, 1, \dots, M-1$. Then Θ is $N \times M$, and Φ is $M \times N$. For instance, for $M = 2$ and $N = 3$, the matrices are

$$\Theta = \begin{bmatrix} \theta_0(0) & \theta_0(1) \\ \theta_1(0) & \theta_1(1) \\ \theta_2(0) & \theta_2(1) \end{bmatrix}, \quad \Phi = \begin{bmatrix} \varphi_0(0) & \varphi_1(0) & \varphi_2(0) \\ \varphi_0(1) & \varphi_1(1) & \varphi_2(1) \end{bmatrix},$$

and in $\theta_{u_0}(t_0)$ the subscript u_0 is the *row index*, whereas in $\varphi_{u_0}(t_0)$ it is the *column index*.

The input output relation (14.2a), (14.2b) can be written in the simple matrix form

$$\mathbf{S} = \Theta \mathbf{s}, \quad \mathbf{s} = \Phi \mathbf{S}, \quad (14.25)$$

where $\mathbf{s} = [s_0, \dots, s_{M-1}]'$ collects the signal values in a period, and $\mathbf{S} = [S_0, \dots, S_{N-1}]'$ collects the values of the transform in a period.

The orthogonality condition (14.18) becomes (where now $I = \mathbb{Z}/\mathbb{Z}(M)$ and $U = \mathbb{Z}/\mathbb{Z}(N)$)

$$\text{(FRC)} \quad \sum_{u_0=0}^{N-1} \varphi_{u_0}(t'_0) \theta_{u_0}(t_0) = \delta_{t'_0 t_0},$$

$$\text{(IRC)} \quad \sum_{t_0=0}^{M-1} \theta_{u'_0}(t_0) \varphi_{u_0}(t_0) = \delta_{u'_0 u_0}.$$

These relations can be written in matrix form as

$$\begin{array}{cc} \boldsymbol{\Phi} & \boldsymbol{\Theta} \\ M \times N & N \times M \end{array} = \mathbf{I}_M, \quad \begin{array}{cc} \boldsymbol{\Theta} & \boldsymbol{\Phi} \\ N \times M & M \times N \end{array} = \mathbf{I}_N, \quad (14.26)$$

where \mathbf{I}_M and \mathbf{I}_N are the identity matrices.

It is important to see how the inner products work with this symbolism. The FRC is expressed by the inner product

$$\langle \varphi_{(\cdot)}(t'_0), \theta_{(\cdot)}^*(t_0) \rangle = \sum_{u_0=0}^{N-1} \varphi_{u_0}(t'_0) \theta_{u_0}(t_0), \quad (14.27)$$

where the summation is made with respect to $u_0 = (\cdot)$. Then the rows of $\boldsymbol{\Phi}$ are multiplied by the columns of $\boldsymbol{\Theta}$. Analogously, in the IRC the inner product is

$$\langle \theta_{u'_0}(\cdot), \varphi_{u_0}^*(\cdot) \rangle = \sum_{t_0=0}^{M-1} \theta_{u'_0}(t_0) \varphi_{u_0}(t_0), \quad (14.28)$$

where the rows of $\boldsymbol{\Theta}$ are multiplied by the columns of $\boldsymbol{\Phi}$.

Now, consider the *generalized bases* introduced in (14.20) (which are denoted by the same symbol used for the correspondent matrix). The basis $\boldsymbol{\Phi}$ is formed by the *column vectors* of the matrix $\boldsymbol{\Phi}$, and the basis $\boldsymbol{\Theta}$ by the *row vectors* of the matrix $\boldsymbol{\Theta}$.

Self-Reciprocal Case The condition $\theta(u_0, t_0) = \varphi^*(t_0, u_0)$ implies that the matrix $\boldsymbol{\Theta}$ becomes the conjugate transpose of $\boldsymbol{\Phi}$, namely

$$\boldsymbol{\Theta} = \boldsymbol{\Phi}^*, \quad (14.29)$$

and all the operations can be written in terms of either matrix (we choose $\boldsymbol{\Phi}$). Then, (14.26) becomes

$$\boldsymbol{\Phi} \boldsymbol{\Phi}^* = \mathbf{I}_M, \quad \boldsymbol{\Phi}^* \boldsymbol{\Phi} = \mathbf{I}_N,$$

and the inner products (14.27) and (14.28) become respectively

$$\langle \varphi_{(\cdot)}(t'_0), \varphi_{(\cdot)}(t_0) \rangle, \quad \langle \varphi_{u'_0}^*(\cdot), \varphi_{u_0}^*(\cdot) \rangle.$$

14.3.2 The Case $M = N$: Biorthogonality and Orthogonality

We specialize the discussion to the case $M = N$, where Θ and Φ become square matrices, and the bases become ordinary (not generalized). Now, an ordinary basis in \mathbb{C}^M consists of M independent vectors, say $\{\varphi_0, \varphi_1, \dots, \varphi_{M-1}\}$, which implies that the correspondent matrix Φ is invertible. Then the FRC and IRC given by (14.26) become equivalent

$$\Phi\Theta = \mathbf{I}_M \quad \Leftrightarrow \quad \Theta\Phi = \mathbf{I}_M,$$

where $\Theta = \Phi^{-1}$. The condition can be written in the scalar form $\langle \theta_i, \varphi_j^* \rangle = \delta_{ij}$, where θ_i is the i th row of Θ , and φ_j is the j th column of Φ , both intended as vectors.

We are now ready to give the following definition:

Definition 14.2 Two sets of vectors $\{\varphi_0, \varphi_1, \dots, \varphi_{M-1}\}$ and $\{\theta_0, \theta_1, \dots, \theta_{M-1}\}$ form *biorthogonal bases* if they are independent and pairwise orthogonal, $\theta_i \perp \varphi_j$, $i \neq j$. Equivalently: the matrix Θ with rows θ_i and the matrix Φ with columns φ_j form biorthogonal bases if $\Theta\Phi = \Phi\Theta = \mathbf{I}_M$.

The self-reciprocity is stated by the condition $\theta_i = \varphi_i^*$, which reads that the i th row of Θ is given by the conjugate transpose of the i th column of Φ . This corresponds to the standard *orthogonality condition*

$$\Phi^*\Phi = \mathbf{I}_M,$$

where the columns of the same matrix are pairwise orthogonal: $\varphi_i \perp \varphi_j$, $i \neq j$.

We now illustrate the above definition in the case $M = 2$, and, for graphical reasons, we suppose that the space is \mathbb{R}^2 instead of \mathbb{C}^2 . We begin with orthonormality, where $\Phi = [\varphi_0, \varphi_1]$ with $\varphi_0 \perp \varphi_1$. Figure 14.5 shows the basis

$$\Phi = [\varphi_0, \varphi_1] = \frac{1}{\sqrt{2}} \begin{bmatrix} 1 & 1 \\ -1 & 1 \end{bmatrix}. \quad (14.30)$$

Note that in this case the transform is given by

$$S = \Phi^* s \quad \rightarrow \quad \begin{bmatrix} S_0 \\ S_1 \end{bmatrix} = \begin{bmatrix} \langle s, \varphi_0 \rangle \\ \langle s, \varphi_1 \rangle \end{bmatrix},$$

where $S_i = \langle s, \varphi_i \rangle$ is the orthogonal projection of s onto the vector φ_i .

Next, we consider the basis

$$\Theta = \begin{bmatrix} \theta_0 \\ \theta_1 \end{bmatrix} = \begin{bmatrix} 1 & -1 \\ 0 & \sqrt{2} \end{bmatrix}, \quad (14.31)$$

whose rows are not orthogonal, as shown in Fig. 14.6. The transform is now given by

$$S = \Theta s \quad \rightarrow \quad \begin{bmatrix} S_0 \\ S_1 \end{bmatrix} = \begin{bmatrix} \langle s, \theta_0 \rangle \\ \langle s, \theta_1 \rangle \end{bmatrix}.$$

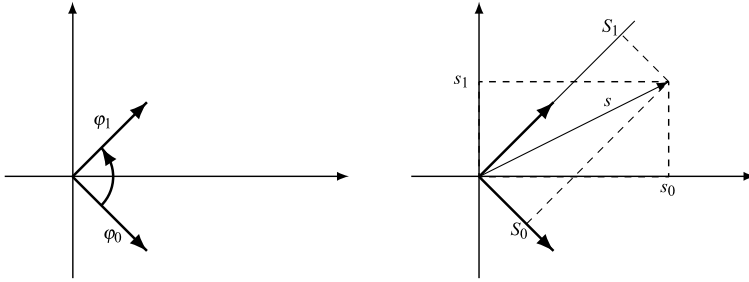
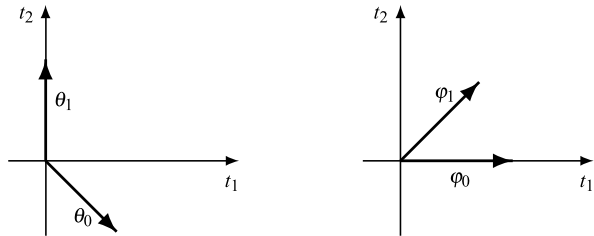


Fig. 14.5 Example of an *orthogonal basis* in \mathbb{R}^2 and of an *orthogonal expansion* of $s = \{s_0, s_1\}$ with transform $S = \{S_0, S_1\}$

Fig. 14.6 Example of *biorthogonal bases* in \mathbb{R}^2 : $\theta_1 \perp \varphi_0$ and $\theta_0 \perp \varphi_1$



Considering that Θ is regular, the information on s is preserved in S , but for the recovery of the signal from the transform, Φ^* is not the right matrix, and we need the matrix

$$\Phi = \Theta^{-1} = [\varphi_0, \varphi_1] = \begin{bmatrix} 1 & \sqrt{2}/2 \\ 0 & \sqrt{2}/2 \end{bmatrix}, \tag{14.32}$$

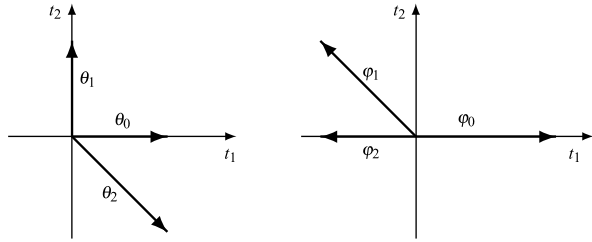
where $\varphi_0 \perp \theta_1$ and $\varphi_1 \perp \theta_0$, and we have the biorthogonality.

While with orthogonality the norm is preserved, $\|S\|^2 = \|s\|^2$, with biorthogonality the norm is not preserved. However, the biorthogonality has the advantage of a larger choice, since it is less constrained.

14.3.3 The Case $N > M$: Frames

In an M -dimensional space the ordinary bases must have the same dimensionality as the space. When this number is larger, we can still have a representative set, but the vectors are no longer linearly independent with the presence of redundancy. A representative set of vectors of size $N > M$ is called a *frame*. Since frames are less constrained than bases, their flexibility leads to very important applications, and nowadays they represent a consolidated tool in several fields [7].

Fig. 14.7 Example of *frames* and the corresponding *dual frames* in \mathbb{R}^2



A simple example of a frame and of the corresponding *dual frame* (see below) is given by

$$\Theta = \begin{bmatrix} \theta_0 \\ \theta_1 \\ \theta_2 \end{bmatrix} = \begin{bmatrix} 1 & 0 \\ 0 & 1 \\ 1 & -1 \end{bmatrix}, \quad \Phi = [\varphi_0, \varphi_1, \varphi_2] = \begin{bmatrix} 2 & -1 & -1 \\ 0 & 1 & 0 \end{bmatrix}, \quad (14.33)$$

as shown in Fig. 14.7.

Since the matrices are no longer square, the problem of inversion must be posed in terms of generalized inverse, so it will be convenient to recall the following general statement [5].

Lemma 14.1 *If a complex matrix \mathbf{A} is $m \times n$ and has rank n , then \mathbf{A} has a left inverse, an $n \times m$ matrix \mathbf{B}_L such that $\mathbf{B}_L \mathbf{A} = \mathbf{I}_n$. If \mathbf{A} has rank m , then it has a right inverse, an $m \times n$ matrix \mathbf{B}_R such that $\mathbf{A} \mathbf{B}_R = \mathbf{I}_m$. Left inverse and right inverse are not unique.*

Then, considering that in the relation $\Phi \Theta = \mathbf{I}_M$, both Θ and Φ must have the maximum rank M , in the present context, Θ is the right inverse of Φ (as can be checked in (14.33)). However, we have to bear in mind that a right inverse is not unique.

14.3.4 General Frames

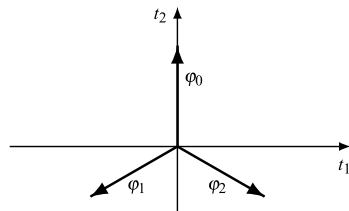
We have introduced frames in a finite-dimensional space, but they can be considered more generally in a Hilbert space [7].

Definition 14.3 A family of functions $\Phi = \{\varphi_n(t) \mid n \in \mathcal{N}\}$ is called a *frame* if there exist two constants $0 < A \leq B < \infty$ such that

$$A \|s\|^2 \leq \sum_{n \in \mathcal{N}} |\langle s, \varphi_n \rangle|^2 \leq B \|s\|^2 \quad \forall s, \quad (14.34)$$

where A and B are called *frame bounds*. The family Θ that allows the reconstruction is called the *dual frame*.

Fig. 14.8 The Mercedes Benz frame



The bounds, which are central for the issue of stable reconstruction, allow a detailed classification of frames [7]. In particular, *tight frames* have equal frame bounds, $A = B$, *unit-norm frames* have all vectors φ_n with unit norm, and so on. In particular, in a unit-norm tight frame, the bound represents the redundancy in the frame, as by picking $s = \varphi_m$ in (14.34) we have

$$A = 1 + \sum_{n \neq m} |\langle \varphi_m, \varphi_n \rangle|^2.$$

Example 14.3 (Mercedes Benz frame) This represents a celebrated example of frame given by (Fig. 14.8)

$$\Phi = [\varphi_0, \varphi_1, \varphi_2] = \begin{bmatrix} 0 & -\sqrt{3}/2 & \sqrt{3}/2 \\ 1 & -1/2 & -1/2 \end{bmatrix}.$$

This frame is representative of several important classes of frames and is also used in quantum information theory (with the name of Perez–Wooters frame).

UT 14.4 Expansions with Periodic Invariance (PI)

A very relevant case, for the implementation with filter banks, is represented by signal expansions when the periodic invariance holds. We recall from Chap. 6 that a linear transformation on rationally comparable domains $I \rightarrow U$ is PI if the kernel has the property

$$h(t_0 + p, u_0 + p) = h(t_0, u_0), \quad p \in P,$$

where P is the *periodicity*,⁵ which is always a subgroup of both I and U , that is, $P \subset I \cap U$. Here we suppose that both the forward and inverse transforms have a periodicity P , as stated by the conditions

$$\begin{aligned} \theta(u_0 + p, t_0 + p) &= \theta(u_0, t_0), \\ \varphi(t_0 + p, u_0 + p) &= \varphi(t_0, u_0), \end{aligned} \quad p \in P \subset I \cap U. \quad (14.35)$$

⁵The periodicity of a transformation was denoted by Π in Chap. 6, but in Chap. 7 and also in this chapter we use the symbol P .

With notation (14.17), the PI conditions become

$$\begin{aligned}\theta_{u_0+p}(t_0+p) &= \theta_{u_0}(t_0), \\ \varphi_{u_0+p}(t_0+p) &= \varphi_{u_0}(t_0),\end{aligned}\quad t_0 \in I, u_0 \in U, p \in P.$$

Alternatively, perfectly symmetrical relations can be obtained with the notation $\tilde{\theta}_{t_0}(u_0) = \theta(u_0, t_0)$ and $\tilde{\varphi}_{t_0}(u_0) = \varphi(u_0, t_0)$, where I is a lattice.

14.4.1 New Formulation of Expansions

In a PI transform a fundamental role is played by the cells

$$A = [I/P], \quad B = [U/P], \quad (14.36)$$

which allow the polyphase decomposition of the high-rate argument kernel in the form

$$t_0 = a + p, a \in A, p \in P, \quad u_0 = b + p, b \in B, p \in P. \quad (14.37)$$

Their cardinalities will be denoted by $M = |A|$ and $N = |B|$. With these decompositions, the kernels take the form

$$\theta_{u_0}(t_0) = \theta_{b+p}(t_0) = \theta_b(t_0 - p), \quad \varphi_{u_0}(t_0) = \varphi_{b+p}(t_0) = \varphi_b(t_0 - p), \quad (14.38)$$

and expansion (14.16a), (14.16b) becomes

$$s(t_0) = \sum_{b \in B} \sum_{p \in P} S_{b+p} \varphi_b(t_0 - p), \quad t_0 \in I, \quad (14.39)$$

where

$$S_{b+p} = d(U) \int_I dt_0 s(t_0) \theta_b(t_0 - p), \quad b \in B, p \in P. \quad (14.40)$$

As a consequence of the PI, the families $\Phi = \{\varphi_{u_0}(t_0) \mid u_0 \in U\}$ and $\Theta = \{\theta_{u_0}(t_0) \mid u_0 \in U\}$ can be expressed through the finite families

$$\Theta_B = \{\theta_b(t_0) \mid b \in B\}, \quad \Phi_B = \{\varphi_b(t_0) \mid b \in B\},$$

having the cardinality N of the cell B .

The reconstruction conditions can be expressed in terms of the functions of the subfamilies Θ_B and Φ_B . In fact, the FRC, given by the first of (14.18), becomes

$$d(U) \sum_{b \in B} \sum_{p \in P} \varphi_b(t'_0 - p) \theta_b(t_0 - p) = \delta_I(t'_0 - t_0). \quad (14.41)$$

Analogously, the IRC given by (14.19), becomes

$$\boxed{d(U) \int_I dt_0 \theta_{b'}(t_0 - p') \varphi_b(t_0 - p) = \delta_{bb'} \delta_{pp'},} \tag{14.42}$$

where we have used the fact that $u'_0 = b' + p' = u_0 = b + p$ if and only if $p' = p$ and $b' = b$.

When also I is a lattice, similar results can be obtained by decomposing the argument t_0 in the form $a + p$ with $a \in A$ and $p \in P$.

An important comment is concerned with biorthogonality condition (14.42): the p -translated versions (with $p \in P$) of the subfamilies Θ_B and Φ_B form biorthogonal bases and, more generally, frames. This will represent a key property in filter banks and wavelets.

14.4.2 Examples of Expansions with Periodic Invariance

In Chap. 4 we have seen several examples of orthonormal bases for the expansion of continuous- and discrete-time signals. Here, we see other examples, related to the topic of this chapter, with the purpose to check the new viewpoint (expansion as a generalized transform).

Examples from the Fourier Transform

We consider the four classes of 1D signals, where the FT $I \rightarrow \hat{I}$ has the following input and output domains:

$$\begin{aligned} \mathbb{R} &\rightarrow \mathbb{R}, & \mathbb{R}/\mathbb{Z}(T_p) &\rightarrow \mathbb{Z}(F), & \mathbb{Z}(T) &\rightarrow \mathbb{R}/\mathbb{Z}(F_p), \\ \mathbb{Z}(T)/\mathbb{Z}(T_p) &\rightarrow \mathbb{Z}(F)/\mathbb{Z}(F_p). \end{aligned}$$

Then we find that with the FT a discrete expansion is possible only for periodic signals.

With $I = \mathbb{R}/\mathbb{Z}(T_p) \rightarrow U = \mathbb{Z}(F)$, the inverse FT gives the well-known Fourier series expansion, seen in Chaps. 5 and 10. With $I = \mathbb{Z}(T)/\mathbb{Z}(T_p) \rightarrow U = \mathbb{Z}(F)/\mathbb{Z}(F_p)$, the inverse FT gives the IDFT (inverse discrete FT), seen in Chaps. 5 and 12.

Other Examples

Next, we consider two examples for the class $L_2(\mathbb{Z})$, usually denoted by ℓ_2 , which are special cases of the general formulation with $I = U = \mathbb{Z}$. Following the standard

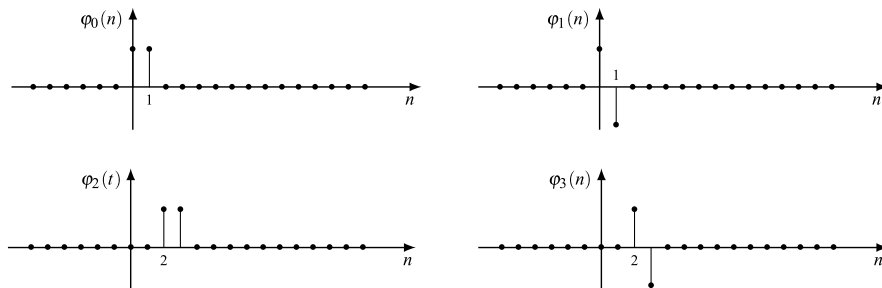


Fig. 14.9 The functions of the Haar basis of the first orders

notation, we let $t = n$ and $u = k$, so that the expansion has the form

$$s(n) = \sum_{k \in \mathbb{Z}} S_k \varphi_k(n) \quad \text{with} \quad S_k = \sum_{n \in \mathbb{Z}} \theta_k(n) s(n). \quad (14.43)$$

In both examples below the kernels are self-reciprocal, $\theta_k(n) = \varphi_k^*(-n)$, and the simple orthogonality holds, namely

$$\sum_{n \in \mathbb{Z}} \varphi_{k'}(n) \varphi_k^*(n) = \delta_{\mathbb{Z}}(k' - k) = \delta_{k'k}. \quad (14.44)$$

Example 14.4 (Haar basis) The discrete *Haar basis* is defined by

$$\varphi_{2k}(n) = \begin{cases} \frac{1}{\sqrt{2}}, & n = 2k, \\ \frac{1}{\sqrt{2}}, & n = 2k + 1, \\ 0 & \text{otherwise,} \end{cases} \quad \varphi_{2k+1}(n) = \begin{cases} \frac{1}{\sqrt{2}}, & n = 2k, \\ -\frac{1}{\sqrt{2}}, & n = 2k + 1, \\ 0 & \text{otherwise,} \end{cases} \quad (14.45)$$

and illustrated in Fig. 14.9.

We see that even-indexed functions are translated versions of each other and so are the odd-indexed functions, specifically

$$\varphi_{2k}(n) = \varphi_0(n - 2k), \quad \varphi_{2k+1}(n) = \varphi_1(n - 2k). \quad (14.45a)$$

It is easy to check that the Haar basis verifies the orthonormality condition (14.44) and also is complete [14]. The Haar basis verifies the PI condition with $P = \mathbb{Z}(2)$ and is completely specified by the subfamily $\Phi_B = \{\varphi_0, \varphi_1\}$.

Example 14.5 (Discrete sinc basis) The discrete *sinc basis* is related to the Sampling Theorem for discrete signals. It has a periodicity $\mathbb{Z}(N)$, where $N \geq 2$, and therefore is specified by N functions which are given by (Fig. 14.10)

$$\varphi_k(n) = \frac{1}{\sqrt{N}} \operatorname{sinc}\left(\frac{n}{2N}\right) \cos(2\pi f_k n), \quad k = 0, \dots, N - 1, \quad (14.46)$$

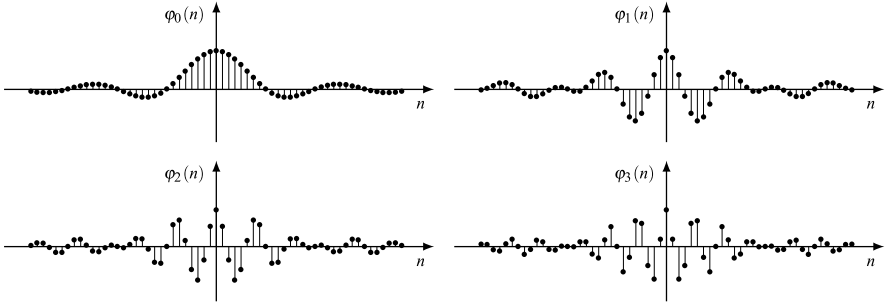


Fig. 14.10 The sinc basis functions for $M = 4$

where $f_k = k/(2N) + 1/(4N)$. Then, the functions are extended to any order as

$$\varphi_{\ell N+k}(n) = \varphi_k(n - \ell N), \quad k = 0, \dots, N - 1, \ell \in \mathbb{Z}. \tag{14.46a}$$

The sinc basis is orthogonal and complete [14], but the proof of these properties must be done in the frequency domain (see Problem 14.10).

14.4.3 Summary of Expansion with Periodic Invariance

It is convenient to summarize the steps made to arrive at the expansion in the presence of PI.

- (1) We started from a *generalized transform* Θ, Φ with arbitrary input and output domains $I \rightarrow U$ and with the operators Θ and Φ defined by relations (14.2a), (14.2b).
- (2) *Assumption that U is a lattice.* The kernels can be written in the form (14.17)

$$\theta_{u_0}(t_0) = \theta(u_0, t_0), \quad \varphi_{u_0}(t_0) = \varphi(t_0, u_0). \tag{14.47}$$

- (3) *Introduction of the PI condition.* With the polyphase decomposition

$$u_0 = b + p, \quad b \in B = [U/P], p \in P, \quad |B| = N,$$

the kernels can be written as

$$\theta_{u_0}(t_0) = \theta_{b+p}(t_0) = \theta_b(t_0 - p), \quad \varphi_{u_0}(t_0) = \varphi_{b+p}(t_0) = \varphi_b(t_0 - p),$$

and the expansion becomes (see (14.39) and (14.40))

$$s(t_0) = \sum_{b \in B} \sum_{p \in P} S_{b+p} \varphi_b(t_0 - p), \quad t_0 \in I, \tag{14.48}$$

with

$$S_{b+p} = d(U) \int_I dt_0 s(t_0) \theta_b(t_0 - p), \quad b \in B, p \in P. \quad (14.49)$$

The FRC and IRC take the form (see (14.41) and (14.42))

$$\sum_{b \in B} d(U) \sum_{p \in P} \varphi_b(t'_0 - p) \theta_b(t_0 - p) = \delta_I(t'_0 - t_0), \quad (14.50a)$$

$$d(U) \int_I dt_0 \theta_{b'}(t_0 - p') \varphi_b(t_0 - p) = \delta_{bb'} \delta_{pp'}. \quad (14.50b)$$

Two generalized bases are specified in the form (after the PI condition)

$$\Theta = \{\theta_b(t_0 - p) \mid b \in B, p \in P\}, \quad \Phi = \{\varphi_b(t_0 - p) \mid b \in B, p \in P\}. \quad (14.51)$$

Summary with Self-Reciprocal Kernels

- (1) *Generalized transform* $\Theta = \Phi^*$ with *self-reciprocal* kernels $\theta(u_0, t_0) = \varphi^*(t_0, u_0)$.
- (2) *Assumption that U is a lattice*, $\theta_{u_0}(t_0) = \varphi_{u_0}^*(t_0)$.
- (3) *Introduction of the PI condition*. The expansion becomes

$$s(t_0) = \sum_{b \in B} \sum_{p \in P} S_{b+p} \varphi_b(t_0 - p) \quad (14.52)$$

with

$$S_{b+p} = d(U) \int_I dt_0 s(t_0) \varphi_b^*(t_0 - p).$$

In particular, the IRC (biorthogonality) becomes the *orthogonality*

$$d(U) \int_I dt_0 \varphi_{b'}^*(t'_0 - p') \varphi_b(t_0 - p) = \delta_{b'b} \delta_{p'p} \quad (14.53)$$

and is expressed by the single orthogonal basis Φ .

UT↓ 14.5 Symmetry Theory Interpretation of Signal Expansions

Signal expansion can be conveniently interpreted with the Symmetry Theory formulated in Chap. 4, the interpretation being particularly useful when the PI holds. Now, we first show that, in the presence of PI, a signal expansion can be viewed as a decomposition into a finite number of components. Then we show that these components can be obtained by appropriated *projectors* and may be interpreted as *symmetric components*. Finally, we show that the projectors can be implemented by multirate components (decimators and interpolators).

These considerations anticipate basic concepts of subband decomposition, multiresolution analysis, and wavelets.

14.5.1 Expansions with PI Viewed as Decomposition

A PI expansion can be viewed as a decomposition of a signal in the form

$$s(t_0) = \sum_{b \in B} s_b(t_0), \quad (14.54)$$

where the *components* are given by

$$s_b(t_0) = \sum_{p \in P} S_{b+p} \varphi_b(t_0 - p), \quad b \in B, \quad (14.55)$$

with

$$S_{b+p} = d(U) \int_I dt_0 \theta_b(t_0 - p) s(t_0), \quad p \in P. \quad (14.56)$$

Relations (14.54) and (14.55) are obtained by splitting relation (14.48) giving the signal from its Fourier coefficients. This form of decomposition will be used in subband decomposition and in wavelets. We now show that the components $s_b(t_0)$ can be obtained by projectors.

14.5.2 Projectors and Symmetries with Periodic Invariance

We refer directly to a PI expansion in which the correct reconstruction is limited to a proper subclass $H = \text{im}(\Phi)$ of $L_2(I)$, and the bases verify the PI with the structure given by (14.51). Then, for the kernels of the projectors, the following statement holds:

Theorem 14.1 *If the bases Θ and Φ verify the IRC condition (14.50b), the kernels*

$$\mathcal{P}_b: h_b(t'_0, t_0) = d(U) \sum_{p \in P} \varphi_b(t'_0 - p) \theta_b(t_0 - p), \quad b \in B, \quad (14.57)$$

define a system of N projectors $\{\mathcal{P}_b, b \in B\}$, that is, operators with the properties

$$\mathcal{P}_b^2 = \mathcal{P}_b, \quad \sum_{b \in B} \mathcal{P}_b = \mathcal{P}_H, \quad (14.58)$$

where \mathcal{P}_H is the projector $L_2(I) \mapsto H$.

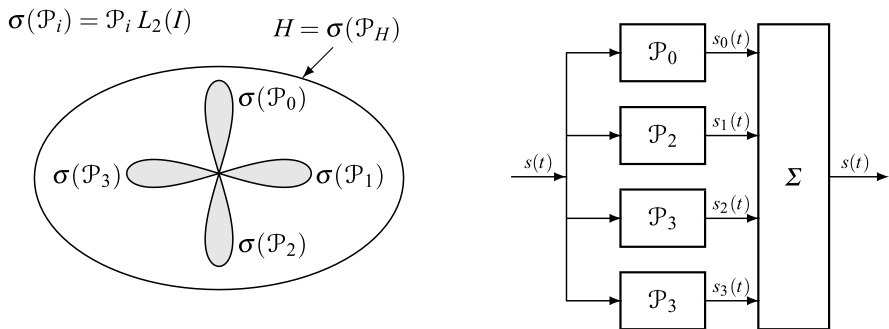


Fig. 14.11 Symmetry generated by the PI bases Θ and Φ with $N = 4$ (quaternary symmetry). The system of projectors \mathcal{P}_i decomposes a signal of a subclass $H \subset L_2(I)$ into four symmetric components $s_i(t)$ that belong to the subspaces $\sigma(\mathcal{P}_i)$ of H

Corollary 14.1 *If the bases are self-reciprocal, that is, $\theta_b(t_0 - p) = \varphi_b^*(t_0 - p)$, and the kernels verify the IRC, then the kernels*

$$\mathcal{P}_b: h_b(t'_0, t_0) = d(U) \sum_{p \in P} \varphi_b(t'_0 - p) \varphi_b^*(t_0 - p)$$

define a system of N Hermitian projectors $\{\mathcal{P}_b, b \in B\}$.

The proof is given in Appendix A.

Note that a basis Φ can be conveniently partitioned in the form

$$\Phi = \{\Phi_b \mid b \in B\} \quad \text{with } \Phi_b = \{\varphi_b(t_0 - p) \mid p \in P\}, \tag{14.59}$$

where Φ_b generates the projector \mathcal{P}_b , and $\text{span}(\Phi_b) = \text{im}(\mathcal{P}_b) = \sigma(\mathcal{P}_b)$.

The projectors \mathcal{P}_b decompose a signal $s(t)$, $t \in I$, of the class $H \subset L_2(I)$ into the N symmetric components given by

$$s_b(t'_0) = \mathcal{P}_b[s \mid t'_0] = \int_I dt_0 h_b(t'_0, t_0) s(t_0), \tag{14.60}$$

as illustrated in Fig. 14.11. The “symmetry” (intended in the sense of Chap. 4) is established by the projector property $\mathcal{P}_b^2 = \mathcal{P}_b$, which gives $\mathcal{P}_b[s_b] = s_b$. This property is specific and unique for the signals belonging to the subspace defined by

$$\sigma(\mathcal{P}_b) = \{s \in H \mid s = \mathcal{P}_b[s]\}. \tag{14.61}$$

It is important to remark that the information on the component $s_b(t_0)$ is confined to its Fourier coefficients given by (14.56), and, in fact, they allow the reconstruction of the symmetric components $s_b(t_0)$ according to (14.55). In general, and in particular in subband decomposition, the extraction of the symmetric components may have no interest, since elaboration and coding are rather applied to the coefficients. Nevertheless, it is important to have in mind, at each step, which part of the signal is being processed, and this is just given by the symmetric components $s_b(t_0)$.

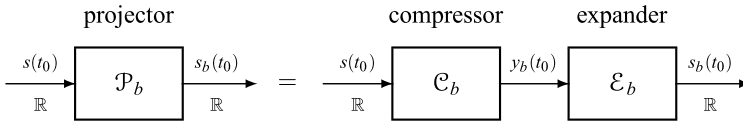


Fig. 14.12 General synthesis of a projector \mathcal{P}_b by a *compressor* \mathcal{C}_b and an *expander* \mathcal{E}_b

14.5.3 Synthesis of the Projectors \mathcal{P}_b

Projectors are redundant operators and can be decomposed in the form

$$\mathcal{P}_b = \mathcal{E}_b \mathcal{C}_b, \tag{14.62}$$

where \mathcal{E}_b and \mathcal{C}_b represent appropriate transformations, which we call *compressor* and *expander*,⁶ respectively. Then, a signal s is first “compressed” as $y_b = \mathcal{C}_b[s]$ and then “expanded” as $s_b = \mathcal{E}_b[y_b]$ to get the symmetric component s_b (Fig. 14.12). The decomposition is not unique, and hence we may find infinitely many compressors and expanders that achieve the synthesis (14.62). In the case of signal expansion, the compression gives the Fourier coefficients $S_b(u_0)$ of the symmetric component $s_b(t_0)$, and the expansion gives the reconstruction of $s_b(t_0)$ from the coefficients. In this case the *compression* consists of representing a signal, which is typically continuous, e.g., with $I = \mathbb{R}$, by a discrete signal given by the sequence of its Fourier coefficients. A very efficient compression is obtained when the PI condition holds. In fact, we now show that, under this condition, the compressor is a decimator and the expander is an interpolator.

We have seen that the projectors \mathcal{P}_b decompose a signal $s(t)$, $t \in I$, into the N symmetric components given by (14.60). Considering the definition (14.57) of $h_b(t_0, t'_0)$, relation (14.60) can be decomposed into the relations

$$S_{b+p} = d(U) \int_I dt_0 \theta_b(t_0 - p) s(t_0), \tag{14.63a}$$

$$X_{b+p}(t_0 - p) = S_{b+p} \varphi_b(t_0 - p), \tag{14.63b}$$

$$s_b(t_0) = \sum_{p \in P} X_{b+p}(t_0 - p), \tag{14.63c}$$

whose interpretation is shown in Fig. 14.13. In the first relation the Fourier coefficients S_{b+p} of the signal $s(t_0)$ are evaluated; then the coefficients X_{b+p} are obtained by the basis functions $\varphi_b(t_0 - p)$ and finally the symmetric components $s_b(t_0)$ are obtained by combining all contributions running over $p \in P$. We realize that the synthesis of the projector \mathcal{P}_b shown in Fig. 14.13 is somewhat complicated and that, furthermore, it contains infinitely many branches.

⁶Some authors, e.g., Vaidyanathan [12], use these terms to denote down-sampling and up-sampling, respectively.

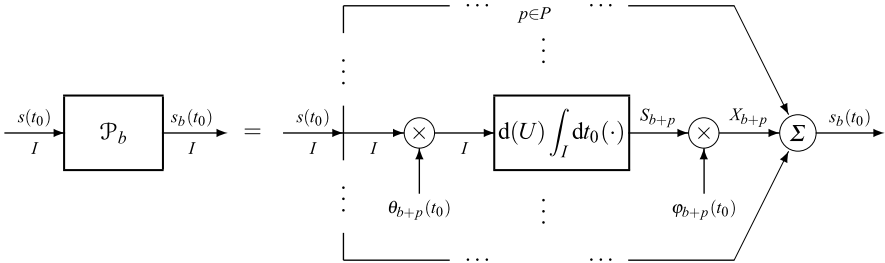


Fig. 14.13 A first synthesis of the projector \mathcal{P}_b with infinite branches (the cardinality of P is infinite)

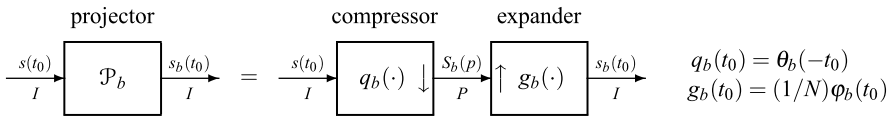


Fig. 14.14 Efficient synthesis of the projector \mathcal{P}_b given by a $I \rightarrow P$ decimator followed by a $P \rightarrow I$ interpolator. The impulse responses are obtained from the basis functions as indicated at the margin

However, a drastic simplification is obtained by a reinterpretation through the techniques (and the way of thinking) of multirate systems. To this end, we interpret the Fourier coefficients as a signal on P , which we call *coefficient signal*, given by

$$S_b(p) = (1/d(U))S_{b+p}, \quad p \in P. \tag{14.64}$$

Then (14.63a) becomes

$$S_b(p) = \int_I dt_0 \theta_b(t_0 - p)s(t_0), \quad p \in P. \tag{14.65}$$

Moreover, combination of relation (14.63a), (14.63b), (14.63c) gives

$$s_b(t_0) = \sum_{p \in P} d(U) \varphi_b(t_0 - p)S_b(p) = \frac{d(U)}{d(P)} \int_P dp \varphi_b(t_0 - p)S_b(p), \tag{14.66}$$

where $d(U)/d(P) = 1/N$. The interpretation of these formulas are: (14.65) is the relation of an $I \rightarrow P$ decimator with impulse response $q_b(t_0) = \theta_b(-t_0)$, and (14.66) is the relation of a $P \rightarrow I$ interpolator with impulse response $g_b(t_0) = (1/N)\varphi_b(t_0)$, $t_0 \in I$. Thus, we obtain the synthesis of \mathcal{P}_b consisting of simple multirate components, as shown in Fig. 14.14.

Note that the transition from the first to the second scheme conceptually consists in a *space to time conversion*: in the first scheme the coefficients are spatially displayed in the infinitely many branches, while in the second they are conveyed in a unique signal. The relation of the space to time conversion is given by (14.64).

We summarize the results.

Theorem 14.2 *If the bases Θ and Φ of the expansion verify the condition of PI, the synthesis of the projectors \mathcal{P}_b giving the symmetric components $s_b(t_0)$, $b \in B$, is obtained by an $I \rightarrow P$ decimator followed by a $P \rightarrow I$ interpolator. The corresponding impulse responses are given by*

$$q_b(t_0) = \theta_b(-t_0), \quad g_b(t_0) = (1/N)\varphi_b(t_0), \quad (14.67)$$

where N is the cardinality of the cell B .

Self-Reciprocal Case We have seen that when the bases verify the condition $\theta_b(t_0) = \varphi_b^*(t_0)$, the projectors \mathcal{P}_b become Hermitian, and hence the N symmetric components are *pairwise orthogonal*, that is, $s_{b'} \perp s_b$ with $b' \neq b$ (see Proposition 4.9).

Corollary 14.2 *If the basis Φ is orthogonal and verifies the PI condition, that is, it has the structure $\Phi = \{\varphi_b(t_0 - p) \mid b \in B, p \in P\}$, the synthesis of the Hermitian projectors \mathcal{P}_b , giving the symmetric components $s_b(t_0)$, is obtained by an $I \rightarrow P$ decimator followed by a $P \rightarrow I$ interpolator. The corresponding impulse responses are given by*

$$q_b(t_0) = \varphi_b^*(-t_0), \quad g_b(t_0) = (1/N)\varphi_b(t_0). \quad (14.68)$$

Moreover, the components $s_b(t_0)$ are pairwise orthogonal.

14.6 Subband Decomposition from Generalized Transforms

In this section we show that a PI generalized transform can be implemented via a filter bank with the goal of a reduced computational complexity. This conclusion is in agreement with the statements of Chap. 7 on parallel architectures, where we have seen that PI transformations can be implemented, in several ways, with filter banks.

It is also in agreement with the considerations of the previous section, where we have interpreted a signal expansion as a decomposition into symmetric components that can be obtained by multirate components.

In the previous section we have seen the decomposition of a signal $s(t_0)$, $t_0 \in I$, into a finite number of “symmetric” components starting from a signal expansion under the assumption that the PI condition holds. The components $s_b(t_0)$, $t_0 \in I$, are obtained as the projection of $s(t) \in L_2(I)$ onto distinct subspaces of $L_2(I)$. We have also seen that each projector can be implemented by a decimator followed by an interpolator. On the other hand, a signal expansion may be viewed as a generalized transform, and therefore we have found a method for implementing a PI generalized transform by multirate components. Collecting these ideas, we soon arrive at the implementation of a PI generalized transform using filter banks of decimators and interpolators, known as *subband decomposition* architecture. A related implementation is given by the *transmultiplexer* architecture, which will be seen in the next section.

14.6.1 Formulation of Subband Decomposition Architecture

We reconsider the steps in the decomposition from the previous section and the synthesis of the projectors. We have considered a forward transform $\Theta : L_2(I) \mapsto L_2(U)$, where U is a lattice and the transform is given by

$$\Theta \quad S(u_0) = \int_I dt_0 \theta_{u_0}(t_0) s(t_0). \quad (14.69)$$

Using the PI with periodicity $P \subset U$, we have decomposed the *transform argument* in the form

$$\boxed{u_0 = b + p, \quad b \in B = [U/P], \quad p \in P,} \quad (14.70)$$

which leads to a *polyphase decomposition*. Then the forward transform is written as

$$\Theta \quad S_b(p) = S(b + p) = \int_I dt_0 \theta_b(t_0 - p) s(t_0). \quad (14.71)$$

Now, the relation $S_b(p) = S(b + p)$ defines the P/S conversion (see Sect. 7.5) of the transform $S(u_0)$, $u_0 \in U$, into N components $S_b(p)$, $p \in P$, where N is the cardinality of the cell B . We have interpreted (14.71) as the relation of an $I \rightarrow P$ decimator with impulse response $q_b(t_0) = \theta_b(-t_0)$.

The inverse transform Φ has been written in the form

$$\Phi \quad s(t_0) = \int_I du_0 \varphi_{u_0}(t_0) S(u_0) = \sum_{b \in B} \int_P dp \frac{1}{N} \varphi_b(t_0 - p) S_b(p), \quad (14.72)$$

where the last integral defines a $P \rightarrow I$ interpolator with impulse response $g_b(t_0) = (1/N)\varphi_b(t_0)$.

Proposition 14.2 *A PI transform Θ with kernel $\theta(u_0, t_0)$, $t_0 \in I$, $u_0 \in U$, and periodicity P can be implemented by a bank of N $I \rightarrow P$ decimators with impulse responses given by*

$$q_b(t_0) = \theta(b, -t_0) = \theta_b(-t_0), \quad b \in B = [U/P], \quad t_0 \in I. \quad (14.73)$$

The N outputs $S_b(u)$, $u \in P$, conveyed by a P/S converter with generator $B = [U/P]$, produce the transform $S(u_0)$, $u_0 \in U$. The inverse transform $\Phi = \Theta^{-1}$ with a kernel $\varphi(t_0, u_0)$, $t_0 \in I$, $u_0 \in U$, and periodicity P can be implemented as follows. First, the transform $S(u_0)$ is S/P converted into its N polyphase components $S_b(u)$, $u \in P$. Then, the components are filtered by a bank of $NP \rightarrow I$ interpolators with impulse responses given by

$$g_b(t_0) = (1/N)\varphi(t_0, b) = (1/N)\varphi_b(t_0), \quad b \in B, \quad t_0 \in I. \quad (14.74)$$

The output of the bank produces the inverse transform $s(t_0)$, $t_0 \in I$. The down-sampling and the up-sampling ratios are given by $M = (I : P)$.

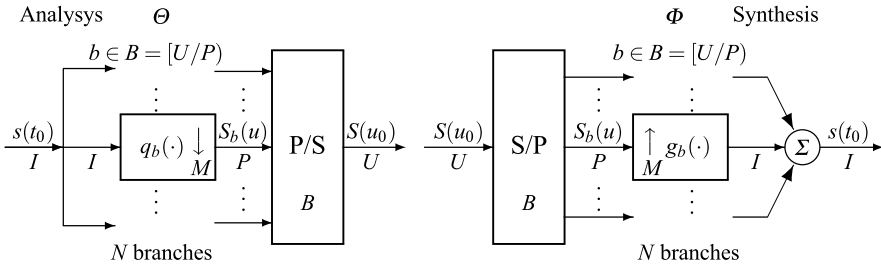


Fig. 14.15 PI transform implemented through a bank of decimators and inverse PI transform implemented through a bank of interpolators (subband architecture). The number of branches is given by the size N of the cell B , and the down-sampling and up-sampling ratios are given by the size M of the cell $A = [I/P]$

The implementation is illustrated in Fig. 14.15. The parts concerning the forward and the inverse transform are called *Analysis* and *Synthesis*, respectively.

A subband decomposition architecture is identified by two subfamilies of functions, which essentially contain the filters impulse responses, namely

$$\begin{aligned} \Theta_B &= \{\theta_b(t_0) \mid b \in B\} \quad \text{with } \theta_b(t_0) = q_b(-t_0), \\ \Phi_B &= \{\varphi_b(t_0) \mid b \in B\} \quad \text{with } \varphi_b(t_0) = Ng_b(t_0). \end{aligned} \tag{14.75}$$

The FRC (14.41) and the IRC (14.42) can be expressed in terms of the filters, namely

$$\begin{aligned} d(U) \sum_{b \in B} \sum_{p \in P} Ng_b(t'_0 - p)q_b(p - t_0) &= \delta_I(t'_0 - t_0), \\ d(U) \int_I dt_0 Nq_{b'}(p' - t_0)Ng_b(t_0 - p) &= \delta_{pp'}\delta_{bb'}. \end{aligned} \tag{14.76}$$

Finally, note that the *number of branches* $N = (U : P)$ may be different from the down-sampling and up-sampling ratios, both given by $M = (I : P)$. This peculiarity will be discussed in the next section.

Self-Reciprocal Case When the transform kernels are self-reciprocal, $\theta(u_0, t_0) = \varphi^*(t_0, u_0)$, in the subband architecture the impulse responses become related as

$$q_b(t_0) = Ng_b^*(-t_0), \quad t_0 \in I, b \in B. \tag{14.77}$$

Hence, the synthesis filters are uniquely determined by the analysis filters.

Remark In Chap. 7, Sect. 7.8, we have developed two architectures of PI transformations by applying the polyphase decomposition at the *input* or at the *output* of the transformation. The architecture of Fig. 14.15 can be obtained from those architectures by applying the *output decomposition* to the forward transform and the *input decomposition* to the inverse transform.

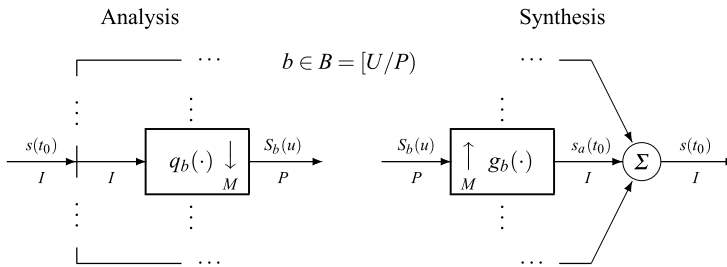


Fig. 14.16 Direct connection of the bank of decimators to the bank of interpolators. The decimators give the components $S_b(u)$ of the transform $S(u)$, and the interpolators recover the signal $s(t_0)$ directly from the transform components

14.6.2 Direct Connection of Filter Banks

The subband scheme of Fig. 14.15 gives the full implementation of a generalized transform $S(u_0)$ starting from the signal $s(t_0)$. The reconstruction side starts from the global transform $S(u_0)$ for the recovery of the signals $s(t_0)$. In subband decomposition, the global transform $S(u_0)$ may be of no interest, rather the attention is focused on its polyphase components $S_b(u)$, and the signal is directly recovered from these components. In other words, the P/S and the S/P conversions are dropped, and the scheme consists only of filter banks, as shown in Fig. 14.16.

Conceptually, the direct connection may be viewed as a one-input N -output $I \rightarrow P$ generalized transform, where the input $s(t)$ is scalar, and the output is a vector $\mathbf{S}(u)$ collecting the components $S(u)$. Analogously, the inverse transform becomes N -input one-output $P \rightarrow I$.

14.6.3 From Filter Banks to PI Transforms

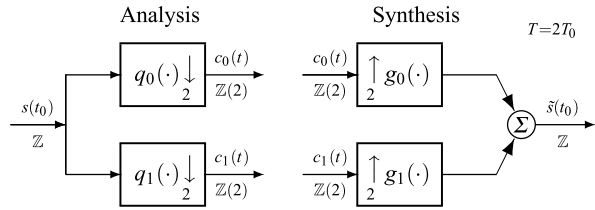
From the vast literature on subband decomposition we can obtain a variety of generalized transforms with the PI property.

Consider in general the filter banks of the Analysis and of the Synthesis, as depicted in Fig. 14.16, where we assume the perfect reconstruction. Then, from the Analysis scheme we can define a forward transform Θ and from the Synthesis scheme the corresponding inverse transform Φ . From the schemes we get: the signal domain I , the cell B and its cardinality N , and the periodicity P , and we have to find the transform domain U and the kernels $\theta(u_0, t_0)$ and $\varphi(t_0, u_0)$. The transform domain is generated in the form

$$U = B + P = [U/P] + P. \tag{14.78}$$

For the kernels, we consider (14.75), that is, $\theta(b, -t_0) = q_b(t_0)$ and $\varphi(t_0, b) = Ng_b(t_0)$, where $b \in B$, $t_0 \in I$, and the definition with respect to one of the arguments

Fig. 14.17 Subband architecture with two-channel filter banks, implementing the discrete Haar basis



is limited to the cell B . To complete the identification on U , we use the periodicity property

$$\theta(b + p, t_0) = q_b(-t_0 + p), \quad \varphi(t_0, b + p) = N g_b(t_0 + p), \quad (14.79)$$

where $b + p = u_0$ with $b \in B$ and $p \in P$ completes the definition on U .

14.6.4 Examples of Implementation of Generalized Transforms

We illustrate a few examples of filter bank implementation of PI transforms, according to the subband architecture.

Example 14.6 (Discrete Haar basis) Using the notation of (14.43), we see that the Haar basis given by (14.45) has periodicity $\mathbb{Z}(2)$. Hence, we have

$$I = \mathbb{Z}, \quad U = \mathbb{Z}, \quad P = \mathbb{Z}(2), \quad B = \{0, 1\}.$$

In the subband decomposition architecture the Analysis consists of a two-channel filter bank as shown in Fig. 14.17, where the impulse responses are given by $q_b(n) = \varphi_b(-n)$, $b = 0, 1$. In the Synthesis we have the impulse responses $g_b(n) = \frac{1}{2}\varphi_b(n)$, $b = 0, 1$.

Example 14.7 (Discrete sinc basis) This basis, defined by (14.46), verifies the periodicity condition with $P = \mathbb{Z}(N)$. In fact, with $p = Ni$ in (14.46a) we find

$$\varphi_{\ell N+k+iN}(n) = \varphi_k(n - k - i),$$

that is, $\varphi_{r+p}(n - p) = \varphi_r(n)$ for all $p \in \mathbb{Z}(N)$. Then

$$I = \mathbb{Z}, \quad U = \mathbb{Z}, \quad P = \mathbb{Z}(N), \quad B = \{0, 1, \dots, N - 1\}.$$

The subband implementation consists of $N\mathbb{Z} \rightarrow \mathbb{Z}(N)$ decimators with impulse responses $q_k(n) = \varphi_k(-n) = \varphi_k(n)$ at the Analysis side. In the Synthesis we have $N\mathbb{Z}(N) \rightarrow \mathbb{Z}$ interpolators with $g_k(n) = (1/N)\varphi_k(n)$, $k = 0, 1, \dots, N - 1$.

14.7 Transmultiplexer from Generalized Transforms

The subband architecture was obtained by the polyphase decomposition of the transform $S(u_0)$ working on the argument u_0 , as stated by (14.70). The transmultiplexer architecture is obtained by the *polyphase decomposition of the signal* $s(t_0)$, $t_0 \in I$, where the input domain I is assumed to be a lattice. Then, if the PI holds with a given periodicity $P \subset I$, the input argument is decomposed as

$$\boxed{t_0 = a + p, \quad a \in A = [I/P], \quad p \in P,} \quad (14.80)$$

and the kernels of the generalized transform Θ, Φ are written in the form

$$\tilde{\theta}_{t_0}(u_0) = \theta(u_0, t_0), \quad \tilde{\varphi}_{t_0}(u_0) = \varphi(t_0, u_0).$$

Hence, the forward transform becomes

$$\Theta \quad S(u_0) = \int_I dt_0 \tilde{\theta}_{t_0}(u_0) s(t_0), \quad u_0 \in U.$$

The polyphase decomposition is then obtained using the *multirate identity* of the Haar integral (see (4.13)), which gives

$$\begin{aligned} S(u_0) &= \frac{1}{M} \sum_{a \in A} \int_P dp \tilde{\theta}_{a+p}(u_0) s(a+p) \\ &= \frac{1}{M} \sum_{a \in A} \int_P dp \tilde{\theta}_a(u_0 - p) s_a(p), \end{aligned} \quad (14.81)$$

where M is the cardinality of the cell A , and

$$s_a(p) = s(a+p), \quad a \in A, \quad p \in P, \quad (14.82)$$

is the polyphase decomposition of the signal, and the substitution $\tilde{\theta}_a(u_0 - p) = \tilde{\theta}_{a+p}(u_0)$ is a consequence of the PI.

The inverse transform is now written as

$$\Phi \quad s_a(p) = \int_U du_0 \tilde{\varphi}_{a+p}(u_0) S(u_0) = \int_U du_0 \tilde{\varphi}_a(u_0 - p) S(u_0), \quad (14.83)$$

where again the PI is used. The transmultiplexer architecture is now obtained by interpretation of the above relations.

Proposition 14.3 *A PI transform Θ with kernel $\theta(u_0, t_0)$, $t_0 \in I$, $u_0 \in U$, and periodicity P can be implemented by an S/P converter with generator $A = [I/P]$, followed by a bank of M $P \rightarrow U$ interpolators with impulse responses given by*

$$\tilde{g}_a(u_0) = (1/M)\theta(u_0, a) = (1/M)\tilde{\theta}_a(u_0), \quad a \in A, \quad u_0 \in U. \quad (14.84)$$

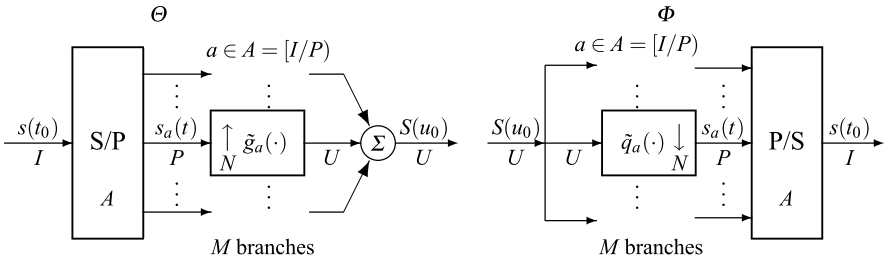


Fig. 14.18 PI transform implemented through a bank of interpolators and inverse PI transform implemented through a bank of decimators (transmultiplexer architecture). The number of branches is given by the size M of the cell A and the down-sampling and up-sampling ratios by the size N of the cell $B = [U/P]$

The inverse PI transform Φ with a kernel $\varphi(t_0, u_0)$, $t_0 \in I$, $u_0 \in U$, and periodicity P can be implemented by a bank of M $U \rightarrow P$ decimators with impulse responses given by

$$\tilde{q}_a(u_0) = \varphi(a, -u_0) = \tilde{\varphi}_a(-u_0), \quad a \in A, u_0 \in U. \quad (14.85)$$

The output of the bank, converted through a P/S, produces the inverse transform $s(t_0)$, $t_0 \in I$. The up-sampling and down-sampling ratios are given by $N = (U : P)$.

The implementation is illustrated in Fig. 14.18.

A transmultiplexer identifies two subfamilies of functions, specified by the filter impulse responses as

$$\begin{aligned} \Theta_A &= \{\tilde{\theta}_a(u_0) \mid a \in A\} && \text{with } \tilde{\theta}_a(u_0) = M\tilde{g}_a(u_0), \\ \Phi_A &= \{\tilde{\varphi}_a(u_0) \mid a \in A\} && \text{with } \tilde{\varphi}_a(u_0) = \tilde{q}_a(-u_0). \end{aligned} \quad (14.86)$$

The FRC condition can be expressed in terms of the filters

$$\int_U du_0 M\tilde{g}_a(u_0 - p')\tilde{q}_{a'}(p - u_0) = \delta_{aa'}\delta_{pp'}, \quad (14.87)$$

and the IRC as

$$d(I) \sum_{a \in A} \sum_{p \in P} M\tilde{g}_a(p - u'_0)\tilde{q}_a(p - u_0) = \delta_U(u'_0 - u_0). \quad (14.88)$$

It is evident that the structure of these relations shows an inversion of roles with respect to the subband decomposition architecture.

Remark In Chap. 7 (see Sect. 7.8) we have developed the parallel architecture of PI transformations, obtained by applying the polyphase decomposition at the *input* or at the *output*. The transmultiplexer architecture could be obtained by applying the *input* decomposition to the forward transform and the *output* decomposition to the inverse transform.

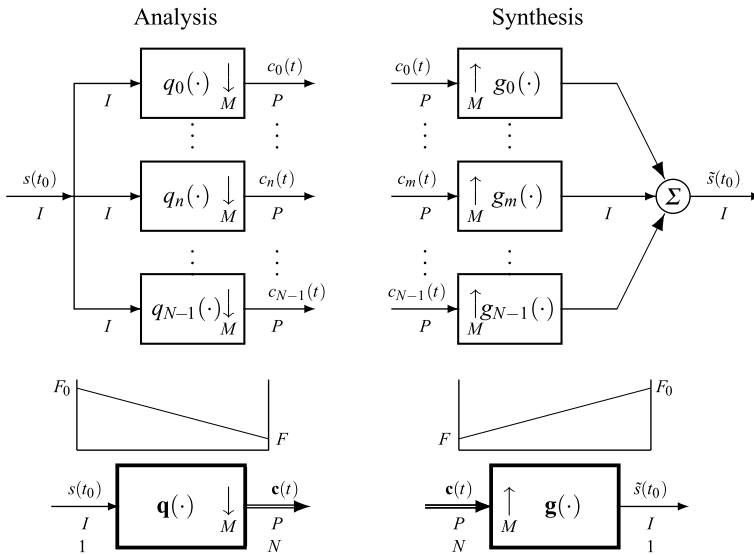


Fig. 14.19 Analysis and Synthesis in subband architecture: at the *top* the detailed scheme; at the *bottom* the compact scheme with the rate diagram

The transmultiplexer was considered in Sect. 7.10 of Chap. 7 as an efficient architecture of the orthogonal frequency division multiplexing (OFDM). That approach was developed in the context of telecommunications, while here the context is more related to DSP. Of course, the architectures are the same, as can be seen by comparing Fig. 14.18 with Fig. 7.36.

14.8 General Formulation of Subband Decomposition

In the previous sections we have obtained subband decomposition as an implementation architecture of PI transforms. Now, we develop the specific theory of subband decomposition in a general form, and, in the next sections, we will see applications to specific cases (1D and multidimensional). In this context the *partial* architecture is usually considered, so that the expansion side, called *Analysis*, simply consists of a decimator bank, and the reconstruction side, called *Synthesis*, consists of an interpolator bank, as shown in Fig. 14.19.⁷

Specification of the System A subband decomposition system is specified by:

⁷In the figure and in the forthcoming theory we slightly modify the symbolism. The indexes $b \in B$ are replaced by the natural $n \in \mathbb{Z}_N$ to facilitate the matrix notation. The subband components $S_b(u)$ are denoted by $c_n(t)$ leaving the uppercase to the FT.

- (1) two ordered lattices I and P of \mathbb{R}^m , with P a sublattice of I , that is, $P \subset I$,
- (2) the number of branches N ,
- (3) the impulse responses $q_n(t_0)$ and $g_m(t_0)$, $t_0 \in I$.

It will be convenient to collect the impulse responses in vectors (to get compact expressions), specifically

$$\mathbf{q}(t) = \underset{N \times 1}{[q_0(t), \dots, q_{N-1}(t)]'}, \quad \mathbf{g}(t) = \underset{1 \times N}{[g_0(t), \dots, g_{N-1}(t)]}. \quad (14.89)$$

Also the N subband components will be collected in a (column) vector $\mathbf{c}(t)$ (see Fig. 14.19). For convenience, we call I the *high-rate* domain and P the *low-rate* domain. The corresponding frequency domains have the structure

$$\widehat{I} = \mathbb{R}^m / I^*, \quad \widehat{P} = \mathbb{R}^m / P^*,$$

where I^* and P^* are the reciprocal lattices. The rates are

$$F_0 = \mu(I) = d(I^*) = \text{high rate}, \quad F = \mu(P) = d(P^*) = \text{low rate}. \quad (14.90)$$

(As usual, we use the subscript 0 to denote quantities related to the high rate and no subscript for the low rate.) A fundamental parameter is the *rate ratio* given by

$$M = F_0/F = d(P^*)/d(I^*) = (P^* : I^*) = (I : P), \quad (14.91)$$

which may differ from the number of branches, as discussed below.

14.8.1 The Idea of Subband Decomposition (in the Case $M = N$)

The original idea of subband decomposition is to subdivide a high-rate band \mathcal{B}_0 into N subbands $\mathcal{B} + \lambda_0, \mathcal{B} + \lambda_1, \dots, \mathcal{B} + \lambda_{N-1}$, where \mathcal{B} is a reference subband, N times smaller than \mathcal{B}_0 , and λ_i are regularly spaced frequencies (repetition centers). The bands and the repetition centers can be conveniently defined in terms of cells, namely

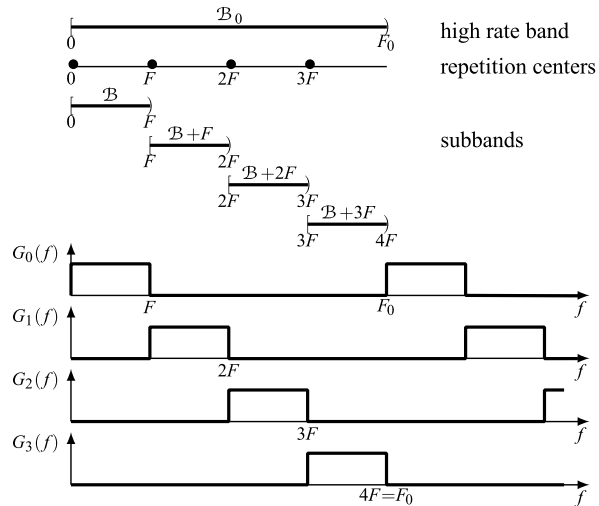
$$\begin{aligned} \mathcal{B}_0 &= [\mathbb{R}^m / I^*], & \mathcal{B} &= [\mathbb{R}^m / P^*], \\ A^* &= [P^* / I^*] = \{\lambda_0, \lambda_1, \dots, \lambda_{N-1}\}. \end{aligned} \quad (14.92)$$

We illustrate the idea of subband decomposition in the 1D case, where the lattices I and P and their reciprocals are

$$\begin{aligned} I &= \mathbb{Z}(T_0), & P &= \mathbb{Z}(T) \quad \text{with } T = NT_0, \\ I^* &= \mathbb{Z}(F_0), & P^* &= \mathbb{Z}(F) \quad \text{with } F_0 = 1/T_0, F = 1/T = F_0/N. \end{aligned} \quad (14.93)$$

The bands in (14.92) have some degrees of freedom (in agreement with the concept of cell). A choice may be the intervals, illustrated in Fig. 14.20 in the ideal case for

Fig. 14.20 Subband decomposition in the 1D case with $M = N = 4$ and ideal frequency responses



$N = 4$,

$$\mathcal{B}_0 = [\mathbb{R}/\mathbb{Z}(F_0)] = [0, F_0), \quad \mathcal{B} = [\mathbb{R}/\mathbb{Z}(F)] = [0, F), \quad (14.94a)$$

or the centered intervals

$$\mathcal{B}_0 = [\mathbb{R}/\mathbb{Z}(F_0)] = \left[-\frac{1}{2}F_0, \frac{1}{2}F_0\right), \quad \mathcal{B} = [\mathbb{R}/\mathbb{Z}(F)] = \left[-\frac{1}{2}F, \frac{1}{2}F\right), \quad (14.94b)$$

the second being more useful to deal with real signals. The set of repetition centers may be chosen as $A^* = \{0, F, \dots, (N - 1)F\}$, so that $\lambda_i = iF$. In the ideal case the frequency responses of the filters are unitary over each subband.

14.8.2 Number of Branches and Rate Ratio: Bases Versus Frames

In the scheme of Fig. 14.19, for generality, we let the rate ratio M be different from the number of branches N . Note that M is the down-sampling ratio of the decimators and the up-sampling ratio of the interpolators. To understand the role of these parameters, we compare the two 1D Analysis schemes of Fig. 14.21, where we suppose that the input signal on $\mathbb{Z}(T_0)$ has $F_0 = 1000$ values/s (v/s). In the first scheme, where $M = N = 2$, the input signal is decomposed into $N = 2$ low-rate signals of $F = 500$ v/s that can be recomposed into a 1000 v/s signal by a P/S conversion. In the second scheme, where $N = 3$ and $M = 2$, the input signal is decomposed into $N = 3$ signals with $F = 500$ v/s that can be recomposed into a 1500 v/s signal (note that the spacing at the output of the 3-input P/S becomes $\frac{2}{3}T_0$, instead of T_0).

In general, the comparison of N with M allows the following classification:

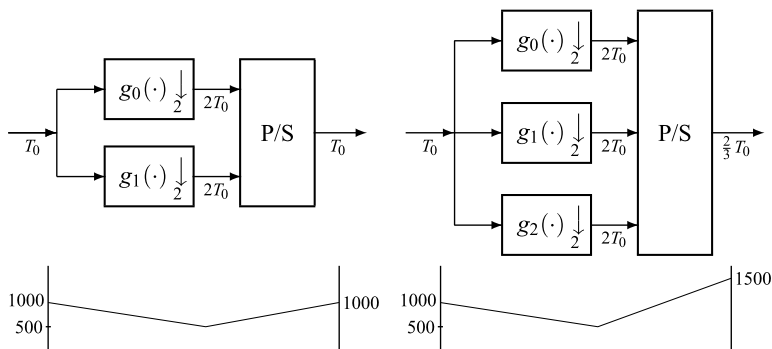


Fig. 14.21 Examples of subband decomposition with non-redundant branches ($M = N = 2$) and with redundant branches ($N = 3, M = 2$)

- (1) If $M = N$ (number of branches equal to the rate ratio), the subband decomposition system is said to be *nonredundant* or *critically sampled*.
- (2) If $N > M$ (number of branches greater than the rate ratio), the subband decomposition system is said to be *redundant* or *oversampled*.

There are differences: in (1) the recomposition by the S/P converter leads to the output domain $U = I$. In (2) the recomposition leads to a different domain $U \neq I$, denser than I , with redundant rate

$$\text{rate}(U) = \frac{N}{M} \text{rate}(I) > \text{rate}(I).$$

Since the inner domain P is a subgroup of I (for decimator condition) and also a subgroup of U (for interpolator condition), the periodicity of the Analysis is $P_{12} = I \cap P = P$, and the periodicity of the Synthesis is $P_{23} = P \cap U = P$. We also have that the global periodicity is $P_{123} = I \cap P \cap U = P$ (see Chap. 7). These conclusions hold both for redundant and nonredundant schemes.

As we shall see, a nonredundant scheme is a candidate for the realization of a *basis* (orthogonal or biorthogonal), whereas a redundant scheme leads to *frames*.

14.9 Fundamental Relations of Subband Decomposition

The task is the formulation of the input–output relationship of Analysis and Synthesis schemes, with the final goal of establishing perfect recovery conditions and, more generally, the recovery with an acceptable degree of accuracy. In the formulation, the complete specification of the system is assumed as given. A very different task is the *design*, where the specification must be discovered with the goal of brilliant performances. In any case a detailed and diversified analysis is preliminary to the design.

The study may be carried out in the time domain (or, better, in the signal domain, this being our preference) and in the frequency or z -domain, also called modulation domain [14]. Another possibility is the analysis in the polyphase domain.

In the literature, subband decomposition and, in general, multirate systems are developed in the z -domain with reference to the 1D case. In the author's opinion, the signal-domain analysis is more general and easier (when the unified approach is followed). So, we begin with the formulation in the signal domain, but the final interpretation (subdivision in subbands) and the specification will be necessarily established in the frequency domain.

In the analysis we follow the general scheme of Fig. 14.19 without simplification. In particular, we let the rate ratio M differ from the number of branches (the unique simplification with $M = N$ is that some matrices become square instead of rectangular).

14.9.1 Signal-Domain Analysis

The Analysis scheme consists of a one-input N -output decimator on $I \rightarrow P$ and the Synthesis of an N -input one-output interpolator on $P \rightarrow I$. Both these systems are QIL transformations and therefore can be handled according to the theory of QIL transformations developed in Chaps. 6 and 7, where we have used a standard form of input–output relation without subdivision of the operations of filtering and down-sampling or up-sampling.

In the Analysis, the input signal $s(t_0)$ is high-rate, and the output consists of N low-rate signals $c_n(t_0)$ (subband components) with relationship

$$c_n(t) = \int_I dt_0 q_n(t - t_0) s(t_0), \quad t \in P, \quad n = 0, 1, \dots, N - 1, \quad (14.95)$$

where $q_n(t_0)$, $t_0 \in I$, are the N impulse responses of the decimators.

In the Synthesis, the N inputs are the subband components, and the output is a replica $\tilde{s}(t_0)$ of the original high-rate signal $s(t_0)$ with relationship

$$\tilde{s}(t_0) = \sum_{m=0}^{N-1} \int_P du g_m(t_0 - u) c_m(u), \quad t_0 \in I, \quad (14.96)$$

where $g_m(t_0)$, $t_0 \in I$, are the impulse responses of the interpolators.

Relationships (14.95) and (14.96) can be written in the compact form

$$\mathbf{c}(t) = \int_I dt_0 \mathbf{q}(t - t_0) s(t_0), \quad t \in P, \quad (14.97a)$$

$N \times 1 \qquad \qquad \qquad N \times 1$

$$\tilde{s}(t_0) = \int_P du \mathbf{g}(t_0 - u) \mathbf{c}(u), \quad (14.97b)$$

$1 \times N \qquad \qquad \qquad N \times 1$

where $\mathbf{c}(t) = [c_0(u), \dots, c_{N-1}(u)]'$ is the vector of the N subband components, and $\mathbf{q}(t_0)$ and $\mathbf{g}(t_0)$ are the vectors collecting the high-rate impulse responses (see (14.89)).

In several applications, the impulse responses are related by the self-reciprocal condition

$$N\mathbf{g}(t_0) = \mathbf{q}^*(-t_0). \quad (14.98)$$

Perfect Reconstruction Condition The task of the Synthesis is to recover the high-rate signal from its subband components to get (in the ideal case)

$$\tilde{s}(t_0) = s(t_0), \quad t_0 \in I. \quad (14.99)$$

To establish the *perfect reconstruction condition* (FRC) (14.99), we have to impose that the Analysis/Synthesis cascade be equivalent to the identity on I . Now, using the kernel composition rule formulated in (6.19), we find that the global kernel is given by $\int_P dt \mathbf{g}(t'_0 - t)\mathbf{q}(t - t_0)$. Then, the FRC (14.99) becomes explicitly

$$\int_P dt \mathbf{g}(t'_0 - t)\mathbf{q}(t - t_0) = \delta_I(t'_0 - t_0), \quad t'_0, t_0 \in I. \quad (14.100)$$

It can be shown that this condition is perfectly equivalent to the FRC given by the second of (14.76) for the families of Θ and Φ (which was written in scalar form).

With a nonperfect reconstruction, the recovered signal has the form

$$\tilde{s}(t_0) = d * s(t_0) + a(t_0), \quad (14.101)$$

where $d * s(t_0)$ is a filtered version of $s(t_0)$, and $a(t_0)$ is the *aliasing*; the first component represents the SI part, and $a(t_0)$ is the PI part. Thus, the perfect recovery condition can be split into the *alias-free condition* $a(t_0) = 0$ and into the *distortion-free condition* $d(t_0) = \delta_I(t_0)$, but this separation will be clearer in the frequency domain.

A final comment: the condition (14.99) may be relaxed in the form $\tilde{s}(t_0) = A_0 s(t_0 - \tau_0)$, accepting a scale factor A_0 and a delay τ_0 (see Sect. 8.1, Heaviside condition), but in the following we will neglect this generalization.

14.9.2 Frequency Domain Analysis

For the Analysis, we recall that an $I \rightarrow P$ decimator with impulse response $\mathbf{q}(t_0)$ is decomposed into an $I \rightarrow I$ filter with impulse response $\mathbf{q}(t_0)$ and an $I \rightarrow P$ down-sampler. This decomposition is useful to find the frequency domain relationship (see Sect. 6.14), which is given by

$$\mathbf{C}(f) = \sum_{\lambda \in A^*} \mathbf{Q}(f - \lambda)S(f - \lambda), \quad f \in \widehat{P}, \quad (14.102)$$

where $\mathbf{Q}(f)$ is the frequency response of the filter, and the repetition centers are given by the reciprocal cell $A^* = [P^*/I^*]$. The cardinality of this cell is given by the rate ratio $M = (I : P) = (P^* : I^*)$, and therefore A^* consists of M distinct frequencies

$$A^* = \{\lambda_0, \lambda_1, \dots, \lambda_{M-1}\}.$$

At the Synthesis side, the $P \rightarrow I$ interpolator with impulse response $\mathbf{g}(t_0)$ is decomposed into a $P \rightarrow I$ up-sampler and an $I \rightarrow I$ filter with impulse response $\mathbf{g}(t_0)$, but the frequency domain relationship is exactly the same as in a filter, that is,

$$\tilde{S}(f) = \mathbf{G}(f)\mathbf{C}(f), \quad f \in \tilde{I}, \quad (14.103)$$

which corresponds to the signal domain relation (14.97b).

Example 14.8 Consider the two Analysis schemes of Fig. 14.21. The first is nonredundant with $M = N = 2$, $I = \mathbb{Z}(T_0)$, and $P = \mathbb{Z}(2T_0)$. Then, $A^* = \{0, F\}$ with $F = 1/(2T_0)$ and the frequency domain relation (14.102) gives

$$\mathbf{C}(f) = \mathbf{Q}(f)S(f) + \mathbf{Q}(f - F)S(f - F) \quad (14.104)$$

and in scalar form

$$\begin{aligned} C_0(f) &= Q_0(f)S(f) + Q_0(f - F)S(f - F), \\ C_1(f) &= Q_1(f)S(f) + Q_1(f - F)S(f - F). \end{aligned}$$

The second scheme is redundant with $N = 3$, $M = 2$, $I = \mathbb{Z}(T_0)$, and $P = \mathbb{Z}(2T_0)$. We have the same parameters $F_0 = 1/T_0$ and $F = 1/(2T_0)$ of the previous case and in particular the same cell $A^* = \{0, F\}$, and hence the same relation (14.104), but now $\mathbf{C}(f)$ and $\mathbf{Q}(f)$ are 3×1 , and therefore the number of scalar equations becomes $N = 3$.

Inspection on the Analysis relationship (14.102) shows that the subdivision into “subbands” is jointly operated by the decimators, whose down-sampling provides, in the frequency domain, the periodic repetition around the repetition centers λ of the reciprocal cell A^* . According to (14.102), the band \mathcal{B}_0 of the high-rate domain I (see (14.92)) is partitioned into the subband form $\mathcal{B} + \lambda$, $\lambda \in A^*$, where \mathcal{B} is the reference subband of the low-rate domain P . A clear interpretation of the subdivision in subbands is obtained with ideal filters for $M = N$ (see Fig. 14.20).

Self-Reciprocal Filters In the frequency domain, condition (14.98) becomes

$$N\mathbf{G}(f) = \mathbf{Q}^*(f), \quad (14.105)$$

where it may be useful to recall that $*$ stands for transpose conjugate.

Perfect Reconstruction Conditions Combination of (14.102) and (14.103) gives the global frequency relation of Analysis–Synthesis

$$\tilde{S}(f) = \mathbf{G}(f) \sum_{\lambda \in A^*} \mathbf{Q}(f - \lambda) S(f - \lambda). \quad (14.106)$$

Considering that in the reciprocal cell we can choose $\lambda_0 = 0$, we obtain

$$\begin{aligned} \tilde{S}(f) &= \mathbf{G}(f) \mathbf{Q}(f) S(f) + \sum_{\lambda \neq 0} \mathbf{G}(f) \mathbf{Q}(f - \lambda) S(f - \lambda) \\ &\triangleq D(f) S(f) + H(f). \end{aligned} \quad (14.107)$$

Now, with reference to decomposition (14.101), we have a clear meaning: $D(f)S(f)$ is the SI component, and $H(f)$ is the PI component. The perfect reconstruction condition is now split into the forms

$$\begin{aligned} \mathbf{G}(f) \mathbf{Q}(f - \lambda) &= 0 \quad \forall \lambda \neq 0 \quad \text{alias-free,} \\ D(f) = \mathbf{G}(f) \mathbf{Q}(f) &= 1 \quad \text{distortion-free,} \end{aligned} \quad (14.108)$$

and globally

$$\boxed{\begin{cases} \mathbf{G}(f) \mathbf{Q}(f) = 1 \\ \mathbf{G}(f) \mathbf{Q}(f - \lambda) = 0 \quad \forall \lambda \neq 0 \end{cases} \quad \text{perfect reconstruction.} \quad (14.109)$$

A trivial solution of (14.109), for $M = N$, is provided by ideal filters with frequency response (see Fig. 14.20)

$$Q_i(f) = G_i(f) = \eta_{\mathcal{B}}(f - \lambda_i), \quad \lambda_i \in A^*,$$

but interesting solutions can be found also with realizable filters, and in particular with FIR filters.

14.9.3 Comparison with the Literature

The application of the Unified Signal Theory leads to results that are often different, although equivalent, from the ones of the literature. The main difference is in the formulation of multirate systems, where we apply the Haar integral and avoid the normalization of the time and frequency domains.

Here, we emphasize the differences concerning decimators and interpolators, that is, the components of subband decomposition. To be specific, we consider the 1D case, where the domains involved are $I = \mathbb{Z}(T_0)$ and $P = \mathbb{Z}(T)$ with $T = NT_0$, and to simplify the discussion, we let $T_0 = 1$, so that $I = \mathbb{Z}$ and $P = \mathbb{Z}(N)$.

For a $\mathbb{Z} \rightarrow \mathbb{Z}(N)$ decimator, we write the input–output relation in the form

$$c(kN) = \int_{\mathbb{Z}} dt_0 g(kN - t_0)s(t_0) = \sum_{n \in \mathbb{Z}} g(kN - n)s(n), \quad kN \in \mathbb{Z}(N), \quad (14.110)$$

and for a $\mathbb{Z}(N) \rightarrow \mathbb{Z}$ interpolator,

$$\tilde{s}(n) = \int_{\mathbb{Z}(N)} dt g(n - t)c(t) = \sum_{k \in \mathbb{Z}} Ng(n - kN)c(k), \quad n \in \mathbb{Z}. \quad (14.111)$$

Here $s, \tilde{s}, q,$ and g have domain \mathbb{Z} , while c has domain $\mathbb{Z}(N)$. In the literature it is customary, and very consolidated, to define *all 1D discrete signals on the domain \mathbb{Z}* . Hence, in the present case, instead of $c(kN)$, we have to write $c[k]$ (the use of square brackets is also consolidated for denoting discrete signals). Moreover, a simple summation is written for an interpolator, without the weight N . Hence, the previous relations are written as

$$\begin{aligned} c[k] &= \sum_{n \in \mathbb{Z}} q[kN - n]s[n], \\ \tilde{s}[n] &= \sum_{k \in \mathbb{Z}} \tilde{g}[n - kN]c[k], \end{aligned} \quad (14.112)$$

where

$$\tilde{g}[n] = Ng(n). \quad (14.113)$$

Both formulations have advantages and drawbacks. A drawback is that writing $c[k]$ instead of $c(kN)$, the information on the signal rate is lost. On the other hand, (14.112) have the advantage of working directly with *filter coefficients*, whereas in (14.111) we have to introduce the factor N . Another advantage of (14.112) is simpler relations with basis functions, e.g.,

$$\varphi_i[n] = \tilde{g}_i[n] \quad \text{and} \quad \theta_i[n] = q_i[-n],$$

whereas we have to write $\varphi_i(n) = Ng(n)$ and $\theta_i(n) = q_i(-n)$, in agreement with (14.113). A remarkable advantage of the unified approach is the complete generality, with the same relations for one-dimensional and multidimensional cases.

In the frequency domain, relations (14.110) and (14.111) become

$$\begin{aligned} C(f) &= \sum_{k=0}^{N-1} Q(f - kF)S(f - kF), \quad F = 1/N, \\ \tilde{S}(f) &= G(f)C(f), \end{aligned} \quad (14.114)$$

and the corresponding relations in the literature are written as

$$\begin{aligned} \tilde{C}(e^{i\omega}) &= \frac{1}{N} \sum_{k=0}^{N-1} Q(e^{i(\omega-2\pi k)/N})S(e^{i(\omega-2\pi k)/N}), \\ \tilde{S}(e^{i\omega}) &= G(e^{iN\omega})C(e^{iN\omega}), \end{aligned} \quad (14.115)$$

with the presence of the factor $1/N$. This factor is not present in (14.114), because $C(f)$ is defined by

$$C(f) = \int_{\mathbb{Z}(N)} dt c(t) e^{-i2\pi ft} = \sum_{n \in \mathbb{Z}} N c(nN) e^{-i2\pi f n N}, \quad (14.116)$$

whereas

$$\tilde{C}(e^{i\omega}) = \sum_{n \in \mathbb{Z}} \tilde{c}[n] e^{-i\omega n}. \quad (14.117)$$

Consider in particular the perfect reconstruction condition in the frequency domain, given by (14.109): in the literature we find that 1 is replaced by N , and this is explained by comparing (14.116) with (14.117).

14.10 Polyphase Decomposition in Subband Decomposition

It is very useful to represent the Analysis and the Synthesis by the polyphase decomposition (PD). We recall from Chap. 7 that, in the time domain, the idea of the PD is to decompose a high-rate signal $s(t_0)$, $t_0 \in I$, into M low-rate components, given by the S/P conversion of $s(t_0)$, namely

$$s^{(i)}(t) = s(t + \tau_i), \quad i = 0, 1, \dots, M - 1, t \in P. \quad (14.118)$$

The shifts τ_i are the elements of a cell $A = [I/P]$ of cardinality given by the rate ratio M , namely

$$A = [I/P] = \{\tau_0, \tau_1, \dots, \tau_{M-1}\}. \quad (14.119)$$

In (14.118) the high-rate argument $t_0 \in I$ is decomposed in the form

$$t_0 = t + \tau_i, \quad i = 0, 1, \dots, M - 1, \quad (14.120)$$

where $t \in P$ is a low-rate argument. An alternative decomposition is

$$t_0 = t - \tau_j \quad j = 0, 1, \dots, M - 1, \quad (14.121)$$

which refers to the cell $-A = \{-\tau_0, -\tau_1, \dots, -\tau_{M-1}\}$ instead of A , leading to the polyphase components $s^{(i)}(t) = s(t - \tau_i)$.⁸

⁸In the 1D case, the decomposition (14.120) leads to an *anticipatory* S/P conversion, which is the standard one in the present theory, while decomposition (14.121) leads to a *causal* S/P conversion. This terminology refers to time arguments, that is, when causality makes sense.

14.10.1 Polyphase Decomposition of Analysis/Synthesis

The difficulty of the formulation is that in Analysis and Synthesis, the PD is applied to vectors and matrices instead of scalar signals. For clarity, we find it convenient to start from scalar relations, and *then* we write the matrix form.

The scalar relation of the Analysis is given by (14.95), where we apply the multirate identity (see (7.37))

$$\int_I dt_0 f(t_0) = \frac{1}{M} \sum_{j=0}^{M-1} \int_P du f(u + \tau_j). \tag{14.122}$$

Hence, we get

$$c_n(t) = \frac{1}{M} \sum_{j=0}^{M-1} \int_P du q_n^{(j)}(t - u) s^{(j)}(u), \tag{14.123}$$

where

$$q_n^{(j)}(t) = q_n(t - \tau_j), \quad s^{(j)} = s(t + \tau_j). \tag{14.123a}$$

Now, we introduce the vector $\mathbf{s}(u) = [s(u + \tau_0), \dots, s(u + \tau_{M-1})]'$ and the $N \times M$ matrix with entries $q_n^{(j)}(t)$, where n is the *row index*, and j is the *column index*, that is,

$$\begin{aligned} \mathbf{q}_\pi(t) &= \begin{bmatrix} q_0^{(0)}(t) & \cdots & q_0^{(M-1)}(t) \\ \vdots & \ddots & \vdots \\ q_{N-1}^{(0)}(t) & \cdots & q_{N-1}^{(M-1)}(t) \end{bmatrix} \\ &= \begin{bmatrix} q_0(t - \tau_0) & \cdots & q_0(t - \tau_{M-1}) \\ \vdots & \ddots & \vdots \\ q_{N-1}(t - \tau_0) & \cdots & q_{N-1}(t - \tau_{M-1}) \end{bmatrix} \end{aligned} \tag{14.124}$$

(the subscript π stands for “polyphase”). Hence, (14.123) becomes

$$\boxed{\mathbf{c}(t) = \frac{1}{M} \int_P du \mathbf{q}_\pi(t - u) \mathbf{s}(u) = \frac{1}{M} \mathbf{q}_\pi * \mathbf{s}(t),} \tag{14.125}$$

$\begin{matrix} N \times 1 & & N \times M & & M \times 1 \end{matrix}$

where we emphasize that the operation involved is an ordinary convolution.

The decomposition is illustrated in Fig. 14.22, where the input signal $s(t)$ is decomposed, with generator A , into its M polyphase components $s^{(i)}(t)$ that are low-rate filtered on P to produce the N subband components $c_n(t)$. Note that the polyphase matrix is obtained with generator $-A$.

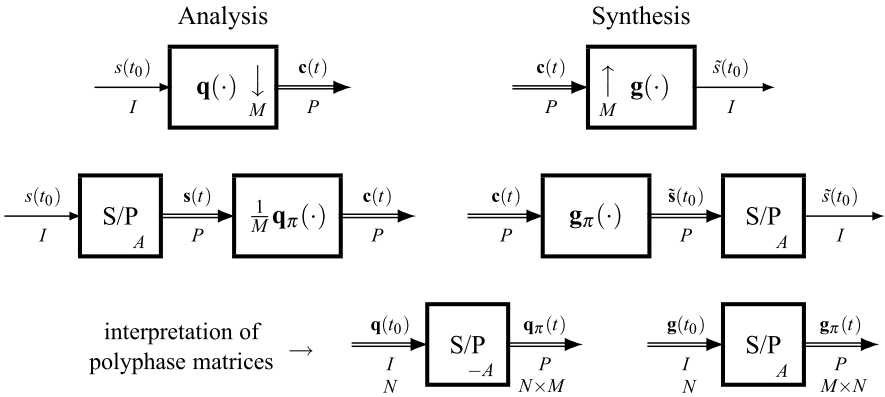


Fig. 14.22 Polyphase decomposition of Analysis and Synthesis in subband architecture. In the P/S and S/P blocks the cells A and $-A$ of the conversions are indicated

For the Synthesis, we use decomposition (14.120) in relationship (14.96) and find

$$\tilde{s}^{(j)}(t) = \sum_{m=0}^{M-1} \int_P du g_m^{(j)}(t-u)c_m(u), \quad (14.126)$$

where

$$\tilde{s}^{(j)}(t) = \tilde{s}(t + \tau_j), \quad g_m^{(j)}(t) = g_m(t + \tau_j). \quad (14.126a)$$

By introducing the (column) vector $\tilde{\mathbf{s}}(u)$ of the polyphase components of $\tilde{s}(t_0)$ and the $M \times N$ polyphase matrix $\mathbf{g}_\pi(t)$ with entries $g_m^{(j)}(t)$, where now j is the row index and m is the column index, that is,

$$\begin{aligned} \mathbf{g}_\pi(t) &= \begin{bmatrix} g_0^{(0)}(t) & \cdots & g_{N-1}^{(0)}(t) \\ \vdots & \ddots & \vdots \\ g_0^{(M-1)}(t) & \cdots & g_{N-1}^{(M-1)}(t) \end{bmatrix} \\ &= \begin{bmatrix} g_0(t + \tau_0) & \cdots & g_{N-1}(t + \tau_0) \\ \vdots & \ddots & \vdots \\ g_0(t + \tau_{M-1}) & \cdots & g_{N-1}(t + \tau_{M-1}) \end{bmatrix}, \end{aligned} \quad (14.127)$$

we obtain

$$\boxed{\tilde{\mathbf{s}}(t) = \int_P du \mathbf{g}_\pi(t-u) \mathbf{c}(u) = \mathbf{g}_\pi * \mathbf{c}(t).} \quad (14.128)$$

$M \times 1 \qquad \qquad M \times N \qquad N \times 1$

The synthesis PD is illustrated in Fig. 14.22, where the N components $c_n(t)$ are low-rate filtered on P , and the M outputs are P/S converted to form the high-rate

signal $\tilde{s}(t_0)$. Both the P/S conversion and the polyphase matrix $\mathbf{g}_\pi(t)$ are obtained with generator A .

14.10.2 Frequency Domain Analysis with Polyphase Decomposition

The polyphase networks are simply filters on the low-rate domain P , as stated by the convolutions in (14.125) and (14.128), and therefore the frequency domain relationships are immediate:

$$\mathbf{C}(f) = \frac{1}{M} \mathbf{Q}_\pi(f) \mathbf{S}(f), \quad \tilde{\mathbf{S}}(f) = \mathbf{G}_\pi(f) \mathbf{C}(f). \quad (14.129)$$

$N \times 1$ $N \times M$ $M \times 1$ $M \times 1$ $M \times N$ $N \times 1$

It remains to relate the polyphase vector $\mathbf{S}(f)$ to the original FT $S(f)$ and the frequency responses of the polyphase network to the ones of the original Synthesis/Analysis filters. To this end, we recall from Sect. 7.5 the frequency domain relations of an $I \rightarrow P$ S/P conversion operating with cell A and reciprocal cell A^* , given by

$$A = [I/P] = \{\tau_0, \tau_1, \dots, \tau_{M-1}\}, \quad A^* = [P^*/I^*] = \{\lambda_0, \lambda_1, \dots, \lambda_{M-1}\},$$

where we can choose $\tau_0 = 0$ and $\lambda_0 = 0$. The frequency response of the S/P is (see (7.30))

$$\mathbf{G}_{\text{S/P}}(f)_A = [e^{i2\pi f \tau_0}, \dots, e^{i2\pi f \tau_{M-1}}]', \quad (14.130)$$

where the subscript A remarks the generator cell of the S/P conversion.

Now, for the high-rate signal $s(t_0)$, $t_0 \in I$, with polyphase components $s^{(j)}(t) = s(t + \tau_j)$, $i = 0, 1, \dots, M - 1$, the Fourier relation is (see (7.31))

$$\boxed{S^{(j)}(f) = \sum_{\lambda \in A^*} e^{i2\pi(f-\lambda)\tau_j} S(f - \lambda), \quad \tau_j \in A,} \quad (14.131)$$

and in matrix form

$$\mathbf{S}(f) = \sum_{\lambda \in A^*} \mathbf{G}_{\text{S/P}}(f - \lambda)_A S(f - \lambda). \quad (14.131a)$$

This relates the polyphase vector $\mathbf{S}(f)$ to the FT $S(f)$ of $s(t_0)$.

Self-Reciprocal Filters Conditions (14.98) and (14.105) seen for the impulse and frequency responses, for the polyphase matrices, respectively, become

$$N \mathbf{g}_\pi(t) = \mathbf{q}_\pi^*(-t), \quad N \mathbf{G}_\pi(f) = \mathbf{Q}_\pi^*(f). \quad (14.132)$$

The proof of these very simple relations requires a lot of attention (recall that $*$ means conjugate transpose).

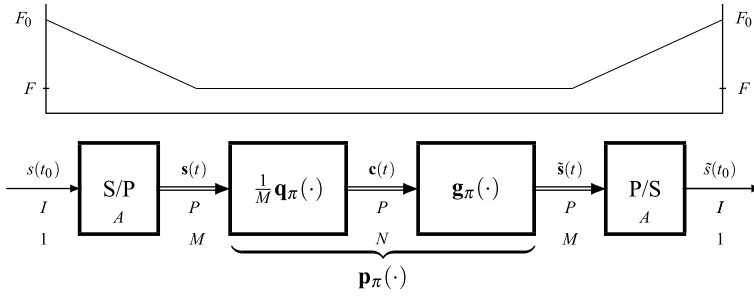


Fig. 14.23 Connection of the Analysis and Synthesis schemes after the polyphase decomposition

14.10.3 Perfect Reconstruction in Terms of Polyphase Decomposition

We now consider the direct connection of the subband architecture when the PD is used for the Analysis/Synthesis schemes (Fig. 14.23). Considering that S/P and P/S are invertible transformations, we realized that the perfect reconstruction condition $\tilde{s}(t_0) = s(t_0)$ is equivalent to the perfect reconstruction condition of the polyphase components, that is, $\tilde{s}(t) = s(t)$. Hence, the cascade of the two polyphase blocks must be equivalent to the $M \times M$ identity on P

$$\mathbf{p}_\pi(t) = \mathbf{g}_\pi * \frac{1}{M} \mathbf{q}_\pi(t) = \mathbf{I}_M \delta_P(t) \tag{14.133}$$

and in the frequency domain

$$\mathbf{P}_\pi(f) = \mathbf{G}_\pi(f) \frac{1}{M} \mathbf{Q}_\pi(f) = \mathbf{I}_M. \tag{14.133a}$$

While the formulation of perfect reconstruction is immediate, it is less trivial to impose the alias-free condition. The problem can be formulated as follows. Consider Fig. 14.23, where the inner part is an $M \times M$ filter $\mathbf{p}_\pi(t) = \mathbf{g}_\pi * \mathbf{q}_\pi / M$, and search for conditions on the matrix $\mathbf{p}_\pi(t)$ such that the global cascade (including S/P and P/S) is equivalent to a high-rate filter $d(t_0)$ on I . If this is the case, the cascade is SI, and the PI aliasing is not present. This approach is developed in Appendix B, where we arrive at precise conditions on the matrix $\mathbf{p}_\pi(t)$ (circulant or pseudo-circulant matrix).

14.11 Perfect Reconstruction Conditions and Biorthogonality

In the theory of generalized transforms we have considered the correct reconstruction of the signal from the transform and the correct reconstruction of the transform

Table 14.1 Perfect reconstruction condition (FRC) and biorthogonality condition (IRC) in subband coding expressed in terms of filter responses

Domain	Perfect reconstruction condition (FRC)	Self-reciprocity
Time domain	$\int_P dt \mathbf{g}(t'_0 - t) \mathbf{q}(t - t_0) = \delta_I(t'_0 - t_0)$	$N \mathbf{g}(t_0) = \mathbf{q}^*(-t_0)$
Frequency domain	$\mathbf{G}(f) \mathbf{Q}(f - \lambda) = \delta_{\lambda 0}$	$N \mathbf{G}(f) = \mathbf{Q}^*(f)$
Polyphase domain	$\mathbf{g}_\pi * \frac{1}{M} \mathbf{q}_\pi(t) = \mathbf{I}_M \delta_P(t)$	$N \mathbf{g}_\pi(t) = \mathbf{q}_\pi^*(-t)$
Polyphase freq. domain	$\mathbf{G}_\pi(f) \frac{1}{M} \mathbf{Q}_\pi(f) = \mathbf{I}_M$	$N \mathbf{G}_\pi(f) = \mathbf{Q}_\pi^*(f)$
Biorthogonality condition (IRC)		
Time domain	$\mathbf{q} * \mathbf{g}(t) = \mathbf{I}_N \delta_P(t)$	$N \mathbf{g}(t_0) = \mathbf{q}^*(-t_0)$
Frequency domain	$\sum_{\lambda \in A^*} \mathbf{Q}(f - \lambda) \mathbf{G}(f - \lambda) = \mathbf{I}_N$	$N \mathbf{G}(f) = \mathbf{Q}^*(f)$
Polyphase domain	$\frac{1}{M} \mathbf{q}_\pi * \mathbf{g}_\pi(t) = \mathbf{I}_N \delta_P(t)$	$N \mathbf{g}_\pi(t) = \mathbf{q}_\pi^*(-t)$
Polyphase freq. domain	$\frac{1}{M} \mathbf{Q}_\pi(f) \mathbf{G}_\pi(f) = \mathbf{I}_N$	$N \mathbf{G}_\pi(f) = \mathbf{Q}_\pi^*(f)$

from the signal. The corresponding conditions were called FRC and IRC, respectively. In the context of filter banks, FRC is called the *perfect reconstruction condition*, and in the context of signal expansions, IRC is called the *biorthogonality condition*.

In the theory of subband decomposition we have seen the perfect reconstruction conditions in several forms: (14.100) in the time domain, (14.109) in the frequency domain, and (14.133) and (14.133a) in the polyphase domain. The results are summarized in Table 14.1.

We now consider the inverse condition, that is, the IRC, with the final target to state the equivalence of the FRC and IRC.

14.11.1 Inverse Reconstruction Condition in Subband Decomposition

We consider the Synthesis followed by the Analysis, as shown in Fig. 14.24. The Synthesis is represented by an N -input one-output $P \rightarrow I$ interpolator with impulse response $\mathbf{g}(t_0)$ and the Analysis by a one-input N -output $I \rightarrow P$ with impulse response $\mathbf{q}(t_0)$. In order to realize the IRC, the cascade must be equivalent to the N -input N -output identity on P . Then, the condition is

$$\int_I dt_0 \mathbf{q}(t'_0 - t_0) \mathbf{g}(t_0 - t) = \mathbf{I}_N \delta_P(t'_0 - t). \quad (14.134)$$

Now, one can check that (14.134) is the matrix form of the IRC condition seen in (14.42) but written in terms of the basis functions instead of impulse responses.

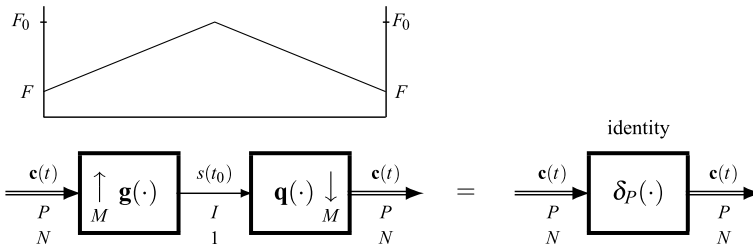


Fig. 14.24 Connection of the Synthesis and Analysis schemes to establish the inverse reconstruction condition (IRC) or biorthogonality

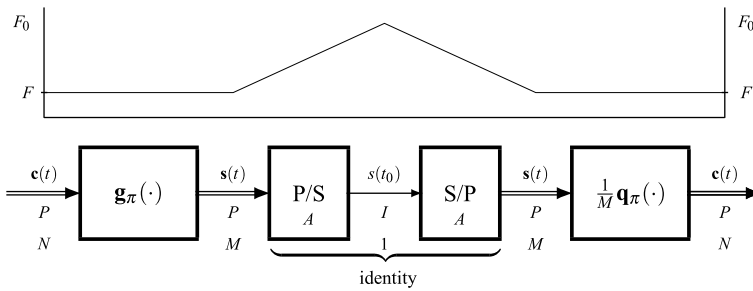


Fig. 14.25 Connection of the Synthesis and Analysis schemes after the polyphase decomposition

Considering that both $\mathbf{g}(t_0)$ and $\mathbf{q}(t_0)$ are defined on I , in (14.42) we can perform an appropriated variable change to obtain

$$\int_I dt_0 \mathbf{q}(t - t_0) \mathbf{g}(t_0) = \mathbf{I}_N \delta_P(t). \tag{14.135}$$

The interpretation is a convolution between $\mathbf{q}(t_0)$ and $\mathbf{g}(t_0)$, performed on the high-rate domain I , but with the final argument t evaluated at the low-rate domain P . This domain restriction corresponds to an $I \rightarrow P$ down-sampling.

In the frequency domain, the convolution gives $\mathbf{Q}(f)\mathbf{G}(f)$, and the down-sampling gives a periodic repetition. In conclusion the relation is

$$\sum_{\lambda \in [P^*/I^*]} \mathbf{Q}(f - \lambda) \mathbf{G}(f - \lambda) = \mathbf{I}_N,$$

where $A^* = [P^*/I^*]$ is the reciprocal cell.

In the polyphase domain we can use the representation of the forward polyphase analysis to get the scheme of Fig. 14.25, where the filter $\mathbf{g}_\pi(t)$ can be directly connected to the filter $\mathbf{q}_\pi(t)$. Hence, we get the condition $\frac{1}{M} \mathbf{q}_\pi * \mathbf{g}_\pi(t) = \mathbf{I}_N \delta_P(t)$ or, equivalently,

$$\frac{1}{M} \mathbf{Q}_\pi(f) \mathbf{G}_\pi(f) = \mathbf{I}_N. \tag{14.136}$$

In conclusion, we have established the IRC in subband decomposition in the different domains, as summarized in Table 14.1.

Note that, for the filters, the perfect reconstruction is determined up to a multiplicative constant. In fact, if $q_b(t_0)$ and $g_b(t_0)$ verify perfect reconstruction, also $q_b(t_0)K$ and $g_b(t_0)/K$ verify the same condition.

When subband decomposition is issued to perform signal expansions, the results and conditions obtained in terms of filters can be expressed in terms of basis functions. The relations linking the two viewpoints are given by Proposition 14.2, specifically

$$\theta_b(t_0) = q_b(-t_0), \quad \varphi_b(t_0) = Ng_b(t_0), \quad t_0 \in I, b \in B. \quad (14.137)$$

Usually $\theta_b(t_0)$ and $\varphi_b(t_0)$ are normalized as $[\theta_b] = 1$ and $[\varphi_b] = 1$, so we have *biorthonormality* and in particular *orthonormality*. Hence, also the corresponding filters become constrained by normalization.

14.11.2 Biorthogonality Versus Perfect Reconstruction

The promised equivalence of biorthogonality and perfect reconstruction is obtained from the polyphase analysis in the frequency domain, where we have found

$$\begin{aligned} \text{(FRC)} \quad \mathbf{G}_\pi(f) \frac{1}{M} \mathbf{Q}_\pi(f) &= \mathbf{I}_M, \\ \text{(IRC)} \quad \frac{1}{M} \mathbf{Q}_\pi(f) \mathbf{G}_\pi(f) &= \mathbf{I}_N. \end{aligned} \quad (14.138)$$

The problem of the equivalence can be posed in the following way. The design of the Analysis and Synthesis filters, specified by the polyphase matrices $\mathbf{Q}_\pi(f)$ and $\mathbf{G}_\pi(f)$, can be primarily done with the goal of achieving the FRC, that is, the perfect reconstruction condition. Since there is room for other constraints, we can impose that the solution achieves the further goal of the IRC.

In the case of *critically sampled* systems, where $M = N$, the polyphase matrices become square, and we have notable simplifications. In fact, the relations have the structures $\mathbf{A}\mathbf{B} = \mathbf{I}_N$ and $\mathbf{B}\mathbf{A} = \mathbf{I}_N$, which are both verified by $\mathbf{B} = \mathbf{A}^{-1}$. Hence:

Theorem 14.3 *In a critically sampled subband decomposition ($M = N$), the perfect reconstruction condition is achieved by choosing the polyphase analysis matrix $(1/M)\mathbf{Q}_\pi(f)$ as the inverse of the synthesis polyphase matrix, that is,*

$$\boxed{(1/M)\mathbf{Q}_\pi(f) = \mathbf{G}_\pi^{-1}(f) \quad \forall f.} \quad (14.139)$$

The perfect reconstruction is equivalent to the biorthogonality!

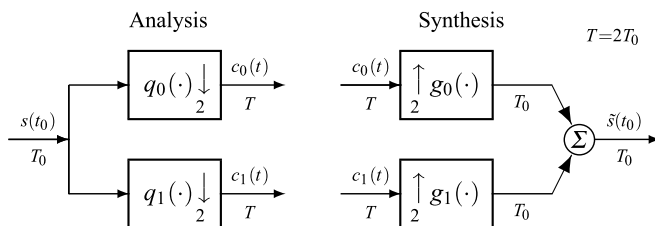


Fig. 14.26 Subband architecture with two-channel filter banks, implementing the discrete Haar basis

In the case of oversampled (or redundant) subband decomposition ($N > M$), the polyphase matrices are no more square, and the problem must be posed in terms of left inverse and right inverse. To this end, we refer to Lemma 14.1 introduced in Sect. 14.10. Now, it is reasonable to suppose that the $M \times N$ matrix $\mathbf{G}_\pi(f)$ and the $N \times M$ matrix $\mathbf{Q}_\pi(f)$ are maximum rank, given by M . Then, from the first of (14.138) we find that $(1/M)\mathbf{Q}_\pi(f)$ is a right inverse of $\mathbf{G}_\pi(f)$.

Theorem 14.4 *In an oversampled subband decomposition ($M < N$), given the synthesis polyphase matrix $\mathbf{G}_\pi(f)$, the perfect reconstruction condition (14.138) is achieved by choosing the analysis polyphase matrix $(1/M)\mathbf{Q}_\pi(f)$ as a right inverse of $\mathbf{G}_\pi(f)$. Equivalently, given the analysis polyphase matrix $(1/M)\mathbf{Q}_\pi(f)$, the perfect reconstruction condition (14.138) is achieved by choosing the synthesis polyphase matrix $\mathbf{G}_\pi(f)$ as a left inverse of $(1/M)\mathbf{Q}_\pi(f)$.*

Note that when $N = M$, the left inverse coincides with the right inverse.

For $N > M$, the application of Lemma 14.1 is no longer possible because it would require a rank N instead of M . We explain this considering the inverse scheme of Fig. 14.25, where we suppose that $M = 3$ and $N = 5$. In the synthesis polyphase network, the input $\mathbf{c}(t)$ has $N = 5$ components, and the output $\mathbf{s}(t)$ has $M = 3$ components, with a compression of information. Thus, the recovery of $\mathbf{c}(t)$ from $\mathbf{s}(t)$ is not possible. This is in general, but if $\mathbf{c}(t)$ is redundant, as happens in the direct connection where it is produced by the analysis polyphase network, a correct recovery is possible.

14.12 Two-Channel Filter Banks

We apply the previous general theory on subband decomposition to the simplest case, 1D subband decomposition with two-channel filter banks (Fig. 14.26), where the parameters are $M = N = 2$, and

$$I = \mathbb{Z}(T_0), \quad P = \mathbb{Z}(T), \quad q_0(t_0), q_1(t_0), g_0(t_0), g_1(t_0),$$

so that we have a *critically sampled* scheme. The study of this simple system is very important in itself but also for its relation with wavelets.

14.12.1 Frequency Domain Analysis

In the present case, the general input and output relations (14.102) and (14.103) become

$$\begin{aligned} \mathbf{C}(f) &= \mathbf{Q}(f)S(f) + \mathbf{Q}(f - F)S(f - F), \quad f \in \mathbb{R}/\mathbb{Z}(F), \\ \tilde{S}(f) &= \mathbf{G}(f)\mathbf{C}(f), \quad f \in \mathbb{R}/\mathbb{Z}(F_0), \end{aligned} \quad (14.140)$$

where $F_0 = 2F$, and

$$\mathbf{Q}(f) = \begin{bmatrix} Q_0(f) \\ Q_1(f) \end{bmatrix}, \quad \mathbf{G}(f) = [G_0(f)G_1(f)].$$

Then, in scalar form,

$$\begin{aligned} \begin{bmatrix} C_0(f) \\ C_1(f) \end{bmatrix} &= \begin{bmatrix} Q_0(f)S(f) + Q_0(f - F)S(f - F) \\ Q_1(f)S(f) + Q_1(f - F)S(f - F) \end{bmatrix}, \\ \tilde{S}(f) &= G_0(f)C_0(f) + G_1(f)C_1(f). \end{aligned}$$

By combination of (14.140),

$$\tilde{S}(f) = \mathbf{G}(f)\mathbf{Q}(f)S(f) + \mathbf{G}(f)\mathbf{Q}(f - F)S(f - F) \quad (14.141)$$

and, explicitly,

$$\tilde{S}(f) = D(f)S(f) + B(f)S(f - F), \quad (14.142)$$

where

$$\begin{aligned} D(f) &= G_0(f)Q_0(f) + G_1(f)Q_1(f), \\ B(f) &= G_0(f)Q_0(f - F) + G_1(f)Q_1(f - F). \end{aligned}$$

The first term $D(f)S(f)$ represents a filtering of the input signal, and the second one, due to the down-sampling of 2, gives the aliasing. The *alias-free condition* is

$$\boxed{B(f) = G_0(f)Q_0(f - F) + G_1(f)Q_1(f - F) = 0.} \quad (14.143)$$

With this condition the recovered signal is a filtered version of the input signal (it does not contain extra frequency components), but in general it causes a distortion. The *distortion-free condition* is

$$\boxed{D(f) = G_0(f)Q_0(f) + G_1(f)Q_1(f) = 1.} \quad (14.144)$$

The above two conditions ensure *perfect reconstruction*.

14.12.2 Alias-Free Conditions

The choice of the four filters forming a two-channel filter bank is based on several criteria and constraints, as distortion cancellation, perfect reconstruction, and the biorthogonality or orthogonality of the related subfamilies. An FIR choice is often imposed. The most usual constraint is alias cancellation.

QMF Choice I

A choice made at the beginning of the history of filter banks by Croiser et al. [2] is that the analysis filters are related as

$$Q_1(f) = Q_0(f - F), \quad (14.145)$$

which states that if $Q_0(f)$ is low-pass with nominal band $(-F/2, F/2)$, then $Q_1(f)$ is high-pass with nominal band $(F/2, 3F/2)$. Filters that verify this condition are called *quadrature mirror filters* (QMFs)⁹ for the reason that $|Q_1(f)|$ is the mirror image of $|Q_0(f)|$ with respect to the frequency $\frac{1}{2}F = \frac{1}{4}F_0$. For the synthesis, the choice is $G_1(f) = -G_0(f - F)$, which again states a QMF relation. Then, for the alias-free condition (14.143), the four filters become related as

$$2G_0(f) = Q_0(f), \quad 2G_1(f) = -Q_1(f) = -Q_0(f - F) \quad (14.146)$$

and are completely determined by the low-pass prototype filter $Q_0(f)$, with a remarkable advantage in the design. With alias cancellation, the global relation becomes $\tilde{S}(f) = D(f)S(f)$ with *distortion transfer function*

$$D(f) = Q_0^2(f) - Q_0^2(f - F). \quad (14.147)$$

Then, with choice (14.146), the global system becomes strict shift invariant, but in general it is affected by distortion. Note that in (14.147) $D(f)$ verifies the condition $D(f - F) = -D(f)$, which implies that the impulse response $d(nT_0)$ is zero for n even (see Problem 14.21).

Considering that the inverse FT of $Q_0(f - F)$ is given by $(-1)^n q_0(nT_0)$, the impulse responses of choice (14.146) are related as

$$2g_0(nT_0) = q_0(nT_0), \quad 2g_1(nT_0) = -q_1(nT_0) = (-1)^n q_0(nT_0).$$

Note that $q_i(nT_0)$ is not given by $2g_i^*(-nT_0)$, and therefore the filters are not self-reciprocal.

⁹This term was introduced by Croisier, Esteban, and Galand [2] in the context of speech analysis. Subsequently, QMF was used also for multichannel filter banks to indicate alias-free conditions. But some confusion exists in the literature concerning the use of this term [11].

QMF Choice II

The disadvantage of Choice I is that it is not compatible with the FIR condition, except for the trivial case of length 2 (see below Haar basis). We now see an alternative choice, where the filter are self-reciprocal,

$$q_i(nT_0) = 2g_i^*(-nT_0) \xrightarrow{\mathcal{F}} Q_i(f) = 2G_i^*(f), \quad (14.148)$$

and allow the FIR realization with perfect reconstruction. The choice relates the synthesis filters as

$$\boxed{g_1(nT_0) = (-1)^n g_0^*(-(n-1)T_0) \xrightarrow{\mathcal{F}} G_1(f) = -e^{-i2\pi f T_0} G_0^*(f-F)}. \quad (14.149)$$

Then, again, the four filters are determined by a unique prototype filter, given by the low-pass filter $g_0(nT)$ of the Synthesis.

We can check that (14.149) leads to an *alias-free two-channel filter bank*. In fact, considering that the frequency responses have period $2F = F_0 = 1/T_0$, we find

$$G_1(f-F) = -e^{i2\pi(f+F)T_0} G_0^*(f-2F) = e^{-i2\pi f T_0} G_0(f)$$

and

$$\begin{aligned} B(f) &= \frac{1}{2} [G_0(f)G_0^*(f-F) + G_1(f)G_1^*(f-F)] \\ &= \frac{1}{2} [G_0(f)G_0^*(f-F) - G_0^*(f)G_0(f) = 0], \\ D(f) &= \frac{1}{2} [|G_0(f)|^2 + |G_1(f)|^2] = \frac{1}{2} [|G_0(f)|^2 + |G_0(f-F)|^2]. \end{aligned}$$

Then, the perfect reconstruction condition, after Choice II, is

$$\boxed{D(f) = \frac{1}{2} [|G_0(f)|^2 + |G_0(f-F)|^2] = 1,} \quad (14.150)$$

which is called the *power complementary property*. This is the starting point of Smith and Barnwell procedure for the design of perfect reconstruction filter banks [10].

We have seen in Theorem 14.3 that the perfect reconstruction ensures the biorthogonality, which becomes the orthogonality with the self-reciprocal condition (14.148). Then:

Proposition 14.4 *In a two-channel filter bank on $\mathbb{Z}(T_0) \rightarrow \mathbb{Z}(2T_0)$, let the Analysis and Synthesis filter be chosen as (14.148) and (14.149) (Choice II), where the prototype filter is given by the Synthesis low-pass filter $g_0(nT_0)$. If this filter has the power complementary property*

$$|G_0(f)|^2 + |G_0(f-F)|^2 = 2, \quad (14.151)$$

then

- (1) *The two-channel filter bank is orthogonal and perfect reconstruction;*
- (2) *The family of functions obtained from the impulse responses and their $2T_0$ -translates $\{\varphi_i((n - 2k)T_0) = 2g_i((n - 2k)T_0) \mid i = 0, 2, k \in \mathbb{Z}\}$ forms an orthonormal basis of $L_2(\mathbb{Z}(T_0))$.*

14.12.3 Polyphase Domain Analysis

In this domain the Analysis and the Synthesis are represented by the polyphase matrices (see (14.124) and (14.127))

$$\mathbf{q}_\pi(t) = \begin{bmatrix} q_0^{(0)}(t) & q_0^{(1)}(t) \\ q_1^{(0)}(t) & q_1^{(1)}(t) \end{bmatrix} = \begin{bmatrix} q_0(t) & q_0(t - T_0) \\ q_1(t) & q_1(t - T_0) \end{bmatrix},$$

$$\mathbf{g}_\pi(t) = \begin{bmatrix} g_0^{(0)}(t) & g_0^{(1)}(t) \\ g_1^{(0)}(t) & g_1^{(1)}(t) \end{bmatrix} = \begin{bmatrix} g_0(t) & g_0(t + T_0) \\ g_1(t) & g_1(t + T_0) \end{bmatrix},$$

where $t \in \mathbb{Z}(2T_0)$. Note that $\mathbf{q}_\pi(t)$ is obtained with the cell $-A = \{0, -T_0\}$, while $\mathbf{g}_\pi(t)$ with the cell $A = \{0, T_0\}$.

In the frequency domain we obtain, with the abbreviated notation $G_i = G_i(f)$, $G_i^- = G_i(f - F)$, and $z_0 = e^{i2\pi f T_0}$,

$$\mathbf{Q}_\pi(f) = \begin{bmatrix} Q_0 + Q_0^- & z_0^{-1}(Q_0 - Q_0^-) \\ Q_1 + Q_1^- & z_0^{-1}(Q_1 - Q_1^-) \end{bmatrix},$$

$$\mathbf{G}_\pi(f) = \begin{bmatrix} G_0 + G_0^- & G_1 - G_1^- \\ z_0(G_0 + G_0^-) & z_0(G_1 - G_1^-) \end{bmatrix}.$$

These matrices can be factored in the forms

$$\mathbf{Q}_\pi(f) = \begin{bmatrix} Q_0 & Q_0^- \\ Q_1 & Q_1^- \end{bmatrix} \begin{bmatrix} 1 & 1 \\ 1 & -1 \end{bmatrix} \begin{bmatrix} 1 & 0 \\ 0 & z_0^{-1} \end{bmatrix},$$

$$\mathbf{G}_\pi(f) = \begin{bmatrix} 1 & 0 \\ 0 & z_0 \end{bmatrix} \begin{bmatrix} 1 & 1 \\ 1 & -1 \end{bmatrix} \begin{bmatrix} G_0 & G_1 \\ G_0^- & G_1^- \end{bmatrix}.$$

Now, we calculate the global polyphase matrix using the above identities. Preliminarily, considering the definition of $B(f)$, given by (14.143), and of $D(f)$, given by (14.144), we find

$$\begin{bmatrix} G_0 & G_1 \\ G_0^- & G_1^- \end{bmatrix} \begin{bmatrix} Q_0 & Q_0^- \\ Q_1 & Q_1^- \end{bmatrix} = \begin{bmatrix} D(f) & B(f) \\ B(f - F) & D(f - F) \end{bmatrix}.$$

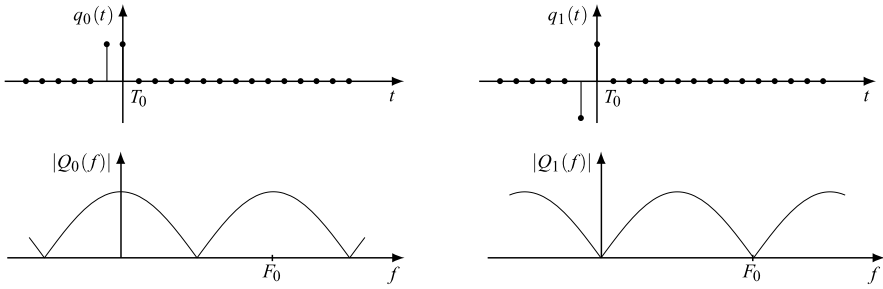


Fig. 14.27 The Haar FIR filters of a two-channel filter bank

Then, the polyphase matrix given by (14.133a) becomes

$$\mathbf{P}_\pi(f) = \frac{1}{2} \begin{bmatrix} 1 & 0 \\ 0 & z_0 \end{bmatrix} \begin{bmatrix} 1 & 1 \\ 1 & -1 \end{bmatrix} \begin{bmatrix} D(f) & B(f) \\ B(f-F) & D(f-F) \end{bmatrix} \begin{bmatrix} 1 & 1 \\ 1 & -1 \end{bmatrix} \begin{bmatrix} 1 & 0 \\ 0 & z_0^{-1} \end{bmatrix}.$$

In the condition of alias-free $B(f) = 0$ we obtain

$$\mathbf{P}_\pi(f) = \frac{1}{2} [D(f) + D(f-F)] \mathbf{I}_2,$$

and when also the distortion-free condition holds, $D(f) = 1$, we get

$$\mathbf{P}_\pi(f) = \mathbf{I}_2$$

in agreement with the general condition (14.133a).

14.12.4 Examples

Example 14.9 A remarkable example of Analysis FIR filters is obtained from the Haar basis. The impulse responses are (Fig. 14.27)

$$q_0(nT_0) = \frac{1}{T_0} \begin{cases} \frac{1}{\sqrt{2}}, & n = -1, 0, \\ 0 & \text{otherwise,} \end{cases} \quad q_1(nT_0) = \frac{1}{T_0} \begin{cases} -\frac{1}{\sqrt{2}}, & n = -1, \\ \frac{1}{\sqrt{2}}, & n = 0, \\ 0 & \text{otherwise,} \end{cases} \quad (14.152)$$

and the frequency responses are given by

$$Q_0(f) = \frac{1}{\sqrt{2}}(z_0 + 1), \quad Q_1(f) = \frac{1}{\sqrt{2}}(-z_0 + 1), \quad z_0 = e^{i2\pi f T_0}.$$

If we choose the Synthesis filters according to (14.146), that is, $2G_0(f) = Q_0(f)$ and $2G_1(f) = -Q_1(f)$, the alias-free conditions are verified for all the filters of

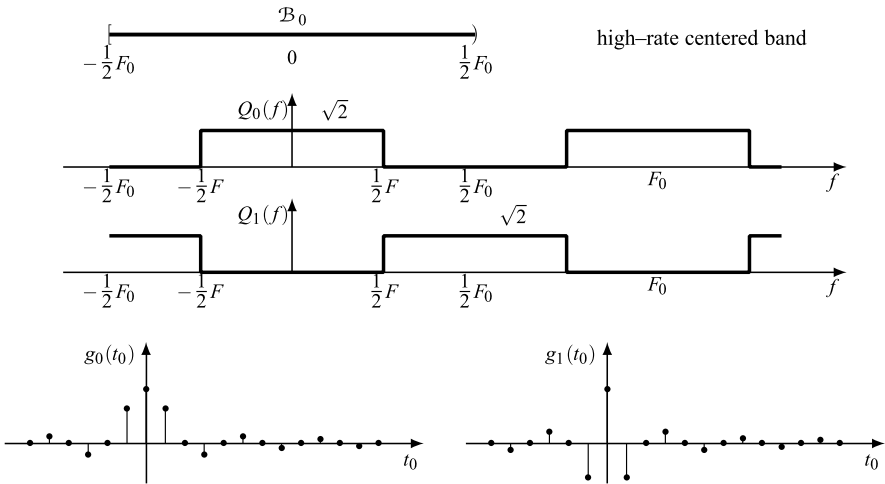


Fig. 14.28 Ideal filters of a two-channel filter bank subband decomposition in the 1D case

Choice I. The distortion transfer function is

$$D(f) = Q_0^2(f) - Q_0^2(f - F) = \frac{1}{2}(1 + z_0)^2 - \frac{1}{2}(1 - z_0)^2 = 1 .$$

Then, also the distortion-free condition and the power-complementary property hold.

Example 14.10 An example of Analysis IIR filters is given by the ideal filters (shown in Fig. 14.20 for $M = 4$ with a noncentered band) with symmetric (even) frequency responses on centered bands (Fig. 14.28)

$$Q_0(f) = \text{rep}_{F_0} A_0 \text{rect}(f/F), \quad Q_1(f) = \text{rep}_{F_0} A_0 \text{rect}((f - F)/F),$$

where $F = \frac{1}{2}F_0$. The inverse FT of these responses are easily found and given by

$$q_0(nT_0) = FA_0 \text{sinc}(n/2), \quad q_1(nT_0) = (-1)^n FA_0 \text{sinc}(n/2), \quad n \in \mathbb{Z}.$$

The constant A_0 is chosen to ensure normalization, that is, $[Q_0] = [Q_1] = 1$, which gives $A_0 = \sqrt{2}$. The filters are in agreement with Choice II and therefore are perfect reconstructions.

14.12.5 Results and Applications of Two-Channel Filter Banks

Two-channel filter banks are important for a variety of reasons. They play a fundamental role in the construction of *dyadic* multiresolution transforms, as will be seen

Table 14.2 Coefficients of the Daubechies length-4 orthogonal analysis and synthesis filters (values rounded up to 7-digit precision)

n	$q_0(n)$	$q_1(n)$	$2g_0(n)$	$2g_1(n)$
-2	0	0	-0.129410	-0.482963
-1	0.482963	-0.129410	0.2241439	0.836516
0	0.836516	-0.2241439	0.836516	-0.2241439
1	0.2241439	0.836516	0.482963	-0.129410
2	-0.129410	-0.482963	0	0

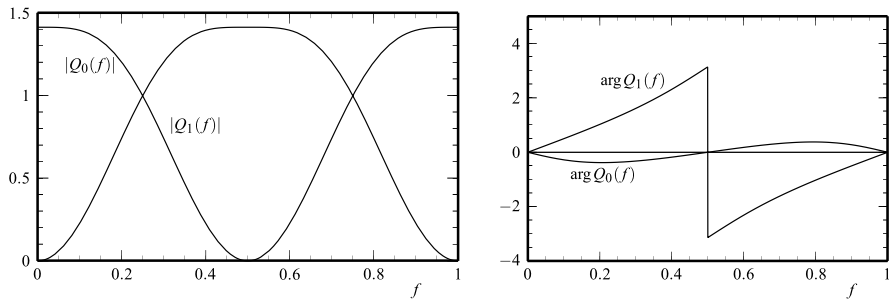


Fig. 14.29 Amplitude and phase responses of Daubechies length-4 filters

in Sect. 14.15. Moreover, iterative applications of two-channel filter banks represent a natural way to provide a variety of interesting subband structures [11]. Also, 1D filter banks are used to implement multidimensional separable filter banks (see Sect. 14.14).

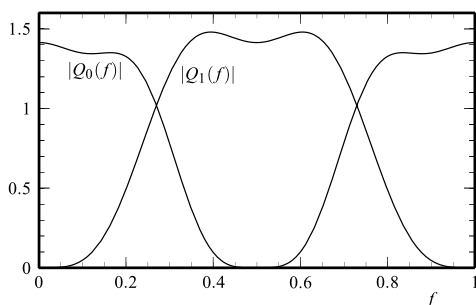
A remarkable importance has the fact that in applications the use of *finite-impulse response* (FIR) is particularly convenient because of the easier implementation compared to *infinite-impulse response* (IIR) filters. Then, the search for FIR *orthogonal* filter banks has played a central role in the digital signal processing community. An exhaustive report on this development can be found in specific textbooks as [12, 14]. An important contribution to the topics came from the discovery of the conceptual link between wavelets and filter banks by Daubechies [3] and Mallat [8].

Here, we give an example of FIR implementation of *orthogonal* filter banks due to Daubechies, where the FIR length is $L = 4$. The Analysis and Synthesis coefficients are listed in Table 14.2, while Fig. 14.29 shows the magnitude and the phase of the frequency responses. It is easy to verify that these filters satisfy the perfect reconstruction property and the orthogonal condition.

However, in digital processing, especially in image processing, FIR orthogonal filter banks have an important drawback, the *nonlinearity* of phase. In fact, with FIR orthogonal filter banks the linearity of phase is possible only with length $L = 2$, that is, with the Haar filters. To remove this drawback, the solution is the *biorthogonality*. As a matter of fact, it is possible to design FIR biorthogonal filter banks with linear

Table 14.3 Coefficients of the Cohen–Daubechies–Feauveau 9–7 symmetric biorthogonal analysis and synthesis filters (values rounded up to 7-digit precision)

n	$q_0(n)$	$q_1(n)$	$2g_0(n)$	$2g_1(n)$
–4	0.0378287	0	0	0.0378287
–3	–0.0238492	0.064539	–0.064539	0.0238492
–2	–0.110624	–0.0406897	–0.0406897	–0.110624
–1	0.3774026	–0.4180924	0.4180924	–0.3774026
0	0.8526986	0.7884848	0.7884848	0.8526986
1	0.3774026	–0.4180924	0.4180924	–0.3774026
2	–0.110624	–0.0406897	–0.0406897	–0.110624
3	–0.0238492	0.064539	–0.064539	0.0238492
4	0.0378287	0	0	0.0378287

Fig. 14.30 Amplitude response of Cohen—Daubechies—Feauveau 9–7 symmetric biorthogonal analysis filters $q_0(n)$, $q_1(n)$. The phase responses are zero and therefore linear

phase, which is obtained with real symmetric (even) or antisymmetric (odd) impulse responses [11].

Here we give an example of FIR biorthogonal filter banks. Table 14.3 lists the filter coefficients, where the length is $L = 9$. Figure 14.30 shows the impulse and the frequency responses. Note that all the four impulse responses are even and that phases are identically zero.

14.13 One-Dimensional Multichannel Subband Decomposition

In this section the previous theory of subband decomposition is applied to the 1D case, which is the most important for applications. The simplifications we obtain for 1D subband decomposition are not very *relevant* at the level of general analysis, but become *relevant* for final explicit results and for filter design. In the 1D case the z -domain analysis turns out to be very useful, especially for the filter specification.

Finally, in the 1D case the problem of the FRC (perfect reconstruction) and the IRC (orthogonality or biorthogonality) equivalence can be clearly stated in terms of the polyphase matrices, and several explicit solutions are available (see [12]).

In 1D subband decomposition with N branches and rate ratio M the signal domains are

$$I = \mathbb{Z}(T_0), \quad P = \mathbb{Z}(MT_0), \quad U = \mathbb{Z}(T'_0) = \mathbb{Z}(T_0M/N), \quad (14.153)$$

and the frequency domains are

$$\hat{I} = \mathbb{R}/\mathbb{Z}(F_0), \quad \hat{P} = \mathbb{R}/\mathbb{Z}(F), \quad \hat{U} = \mathbb{R}/\mathbb{Z}(F'_0)$$

with $F_0 = 1/T_0$, $F = F_0/M$, $F'_0 = (N/M)F_0$. The reference cells are

$$\begin{aligned} A &= [I/P] = \{0, T_0, \dots, (M-1)T_0\}, \\ A^* &= [P^*/I^*] = \{0, F, \dots, (M-1)F\}, \\ B &= [I/U] = \{0, T'_0, \dots, (N-1)T'_0\}, \\ B^* &= [P^*/U^*] = \{0, F', \dots, (N-1)F'\}. \end{aligned} \quad (14.154)$$

For $N = M$, the subband decomposition is *critically sampled*, and for $N > M$, it is *oversampled*. The bands $\mathcal{B}_0 = [0, F_0)$ and $\mathcal{B} = [0, F)$ have been illustrated in Fig. 14.20 with $M = L = 4$.

In the 1D case we have no particular simplification with respect to the general case seen in the previous sections. In particular, the relations of the Analysis and Synthesis given by (14.102) and (14.103) remain substantially the same, that is,

$$\begin{aligned} \mathbf{C}(f) &= \sum_{k=0}^{M-1} \mathbf{Q}(f - kF)S(f - kF), \quad f \in \mathbb{R}/\mathbb{Z}(F), \\ \tilde{\mathbf{S}}(f) &= \mathbf{G}(f)\mathbf{C}(f), \quad f \in \hat{I}. \end{aligned} \quad (14.155)$$

From (14.109) and (14.108) we obtain that the distortion-free condition and the alias-free condition become respectively

$$\begin{aligned} \mathbf{G}(f)\mathbf{Q}(f) &= 1, \\ \mathbf{G}(f)\mathbf{Q}(f - kF) &= 0, \quad k = 1, 2, \dots, M-1. \end{aligned} \quad (14.156)$$

In the PD the cells may be chosen as in (14.154). Then, the elements of the polyphase matrix $\mathbf{Q}_\pi(f)$ and $\mathbf{G}_\pi(f)$ are respectively

$$\begin{aligned} Q_n^{(j)}(f) &= \sum_{k=0}^{M-1} e^{-i2\pi(f-kF)jT_0} Q_n(f - kF), \\ G_n^{(j)}(f) &= \sum_{k=0}^{M-1} e^{-i2\pi(f-kF)jT_0} G_n(f - kF). \end{aligned} \quad (14.157)$$

The study of 1D subband decomposition is completed in Appendix B with the alias-free condition. In Appendix C the z -domain analysis is also developed, which may be useful to compare our results with the ones of the literature.

14.14 Multidimensional Filter Banks

The theory of this chapter is comprehensive of the multidimensional case. In fact, both the generalized transform and the signal expansion have been developed according to the Unified Signal Theory, and the results therein are completely general and can be particularized to 1D, 2D, and so on. The same considerations hold for filter banks, which were illustrated mainly in the 1D case, but the results have a general validity. Note that the capability to formulate unified results is essentially due to the use of the Haar integral, but also the role of cells must not be underestimated. In the multidimensional case the only attention to pay is to write vectors and matrices using the lexicographical order (see Sect. 7.6 and the problems at the end of this chapter).

To illustrate the problems in the study and design of multidimensional filter banks, we consider the subband decomposition architecture in the 2D case. From Fig. 14.15, or its simplified version of Fig. 14.16, we find that structural parameters are simply given by three domains

$$I, \quad U, \quad \text{and} \quad P, \quad P \subseteq I \cap U,$$

which can be chosen from the class of 2D lattices $\mathcal{L}_2(\mathbb{Z}^2)$ and, more generally, from the class $\mathcal{L}(\mathbb{Z}(d_1, d_2))$. From the domains we obtain the cells $A = [I/P]$ and $B = [U/P]$. The cardinality $M = |A| = (I : P)$ gives the down-sampling ratio of the Analysis decimators and the up-sampling ratio of the Synthesis interpolators. The cardinality $N = |B| = (U : P)$ gives the number of branches of the subband decomposition architecture. If $M = N$, the architecture is *critically sampled*; if $N > M$, it is *oversampled*.

For the frequency domain analysis, one has to evaluate the reciprocal lattices I^* , U^* , P^* , which give the *periodicities* of the Fourier transform, and the reciprocal cells $A^* = [P^*/I^*]$ and $B^* = [P^*/U^*]$, which give the *repetition centers* (see (14.102) and (14.106)) and the *polyphase decomposition* (see (14.131)). As regards the evaluation of the 2D cells and their reciprocal, we can use either Proposition 16.9 or the theory of Chap. 16, where the technique of finding *orthogonal* cells is developed (see Sect. 16.9).

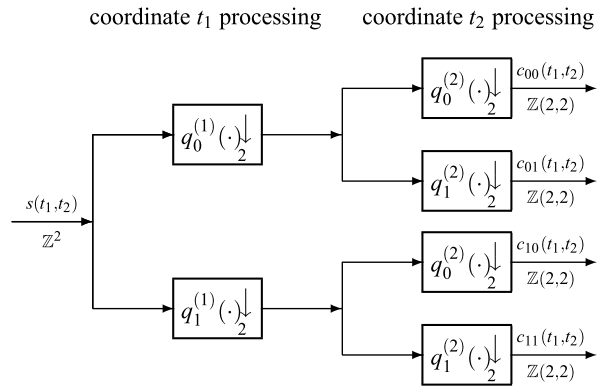
The above resume refers to the general 2D case, where the lattices and the cells may be not separable. A drastic simplification is obtained in the separable case, where the idea is to apply all known one-dimensional techniques separately along one dimension at a time.

14.14.1 Separable 2D Implementation

The domains become $I = I_1 \times I_2$, $U = U_1 \times U_2$, $P = P_1 \times P_2$, where the factors are 1D lattices of the class $\mathcal{L}_1(\mathbb{Z})$ and, more generally, of the class $\mathcal{L}_1(\mathbb{Z}(d))$. Without restriction we can assume that the domains have the form

$$I = \mathbb{Z} \times \mathbb{Z}, \quad U = \mathbb{Z}(M_1/N_1) \times \mathbb{Z}(M_2/N_2), \quad P = \mathbb{Z}(M_1) \times \mathbb{Z}(M_2),$$

Fig. 14.31 Separable 2D two-channel filter bank obtained with 1D two-channel filter banks



where M_1, N_1 and M_2, N_2 are coprime, and the case of critical sampling is obtained with $M_1 = N_1$ and $M_2 = N_2$. The cells become separable $A = A_1 \times A_2$ with $A_i = [\mathbb{Z}/\mathbb{Z}(M_i)] = \{0, 1, \dots, M_i - 1\}$ and $B = B_1 \times B_2$ with $B_i = [\mathbb{Z}(M_i/N_i)/\mathbb{Z}(M_i)] = \{0, M_i/N_i, 2M_i/N_i, \dots, (N_i - 1)/N_i\}$.

Also the filters are assumed separable, with impulse responses expressed by the form (called *tensor product*)

$$q_{b_1 b_2}(t_1, t_2) = q_{b_1}(t_1)q_{b_2}(t_2), \quad g_{b_1 b_2}(t_1, t_2) = g_{b_1}(t_1)g_{b_2}(t_2)$$

with $t_i \in I_i, b_i \in B_i, i = 1, 2$.

In conclusion, the 2D filter bank is determined by two 1D filter banks. It is easy to prove the following:

Proposition 14.5 *Given two arbitrary 1D filter banks that verify the perfect reconstruction condition, the 2D filter bank, with domains obtained by Cartesian product and filters obtained by tensor product, verifies the perfect reconstruction condition.*

An illustration of a 2D two-channel filter bank obtained in such a way is shown in Fig. 14.31. The signal $s(t_1, t_2)$ to be processed is in general nonseparable. The first filter bank, with filters $q_0^{(1)}(t_1)$ and $q_1^{(1)}(t_1)$, acts along the coordinate t_1 and the second filter bank pair, with filters $q_0^{(2)}(t_2)$ and $q_1^{(2)}(t_2)$, acts along the coordinate t_2 . Finally, the subband components $c_{ij}, i, j = 0, 1$, are obtained on the domain $\mathbb{Z}(2, 2)$.

14.14.2 Nonseparable 2D Implementation

The separable case is easy to implement by using the consolidated experience especially with FIR filters. However, it has the following drawback. To see this, we reconsider the implementation of Fig. 14.31, where in the first stage the filter may have length L_1 and in the second, length L_2 . Then, the number of free design variables is $L_1 + L_2$. On the other hand, the nonseparable solution has $L_1 L_2$ free design variables that are better suited for the tailoring of subband components.

But choosing a nonseparable solution, the advantages come at the price of a more difficult design and with a substantially higher complexity. The conclusion is that the problem is still open.

14.15 Tree-Structured Filter Banks

A simple way to construct filter banks is to cascade appropriately filter banks of smaller size according to a *tree architecture*. We outline this possibility considering as building blocks two-channel filter banks, which represent the more common construction, and thinking of band subdivision.

14.15.1 Full Tree Architecture

A first case is shown in Fig. 14.32, where cascading of two-channel filter banks is iterated $J = 2$ times giving a tree with $2^2 = 4$ leaves. In the first stage the fundamental band \mathcal{B}_0 of size F_0 is subdivided into two parts, with a down-sampling of 2, and in the second stage each half band is subdivided into two parts, again with down-sampling of 2. The band subdivision is illustrated in the figure in the ideal case. The $\mathbb{Z}(T_0) \rightarrow \mathbb{Z}(2T_0)$ decimator of the first stage provides the subdivision of the band $[0, F_0)$ into the half-bands $[0, \frac{1}{2}F_0)$ and $[\frac{1}{2}F_0, F_0)$ with their repetition (recall that the domain/periodicity of the frequency responses $Q_0^{(1)}(f)$ and $Q_1^{(1)}(f)$ is $\mathbb{R}/\mathbb{Z}(F_0)$). In the second stage, the $\mathbb{Z}(2T_0) \rightarrow \mathbb{Z}(4T_0)$ provides the subdivision into quarter bands, since the period of $Q_0^{(2)}(f)$ and $Q_1^{(2)}(f)$ is $\frac{1}{2}F_0$. To see the global effect, we can apply the rule that “the frequency response of a cascade of two decimators is simply given by the product of the two frequency responses of the stages” (see Sect. 7.2). Hence, following the four paths of the tree, we find the global frequency responses

$$Q_i^{(1)}(f)Q_j^{(2)}(f), \quad i, j = 0, 1,$$

which give the subdivision of the original reference band $[0, F_0)$ into the equal-size subbands $[i\frac{1}{4}F_0, (i+1)\frac{1}{4}F_0)$. In general, with J iterations, the tree has 2^J leaves with bandwidth $F_0/2^J$.

The obvious advantage of a tree filter bank is the easy implementation starting from a prototype two-channel filter bank.¹⁰

¹⁰In the formulation of tree filter bank we label differently the basic two-channel filter banks at the different stages, whereas other textbooks do not make any distinction, since a single prototype of basic filter bank, e.g., with the same FIR coefficients, is commonly used. We remark, however, that at different stages the filters act with different rates, and they must be regarded as different objects.

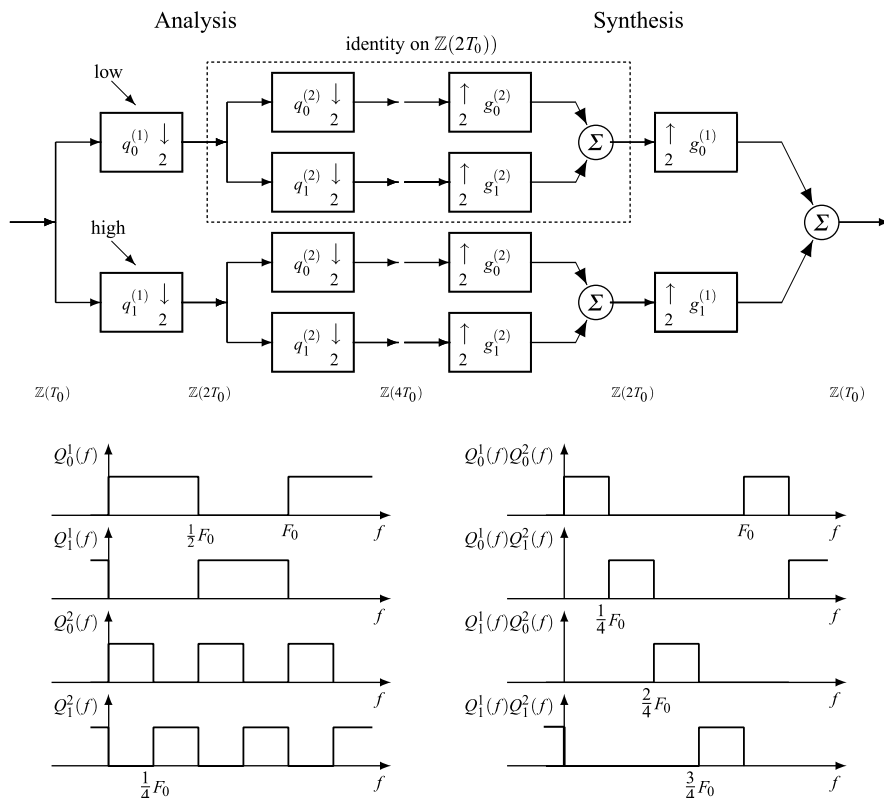


Fig. 14.32 Full tree filter bank of the second order

Perfect Reconstruction We assume that the building blocks (two-channel filter banks) verify the perfect reconstruction. Then, it is easy to see that the perfect reconstruction holds for the whole tree (the assumption of ideal filters, as in Fig. 14.32, is not needed and is made only for the clarity of presentation). In fact, consider for simplicity the two-stage case of Fig. 14.32: the Analysis and Synthesis of each of the second stage (collected in a dashed box in the figure) is equivalent, by assumption, to the identity on $\mathbb{Z}(2T_0)$, and therefore it can be conceptually removed. In such a way, the Analysis and the Synthesis of the first stage are directly connected and therefore give the identity on $\mathbb{Z}(T_0)$.

14.15.2 Octave-Band Subdivision

Another filter bank tree is shown in Fig. 14.33, where the second iteration is applied only to the previous low-pass channel, so that the Analysis part has only three outputs: $c_{0,1}(t)$, $c_{0,0}(t)$ on $\mathbb{Z}(4T_0)$ and $c_1(t)$ on $\mathbb{Z}(2T_0)$. Now, the fundamental band

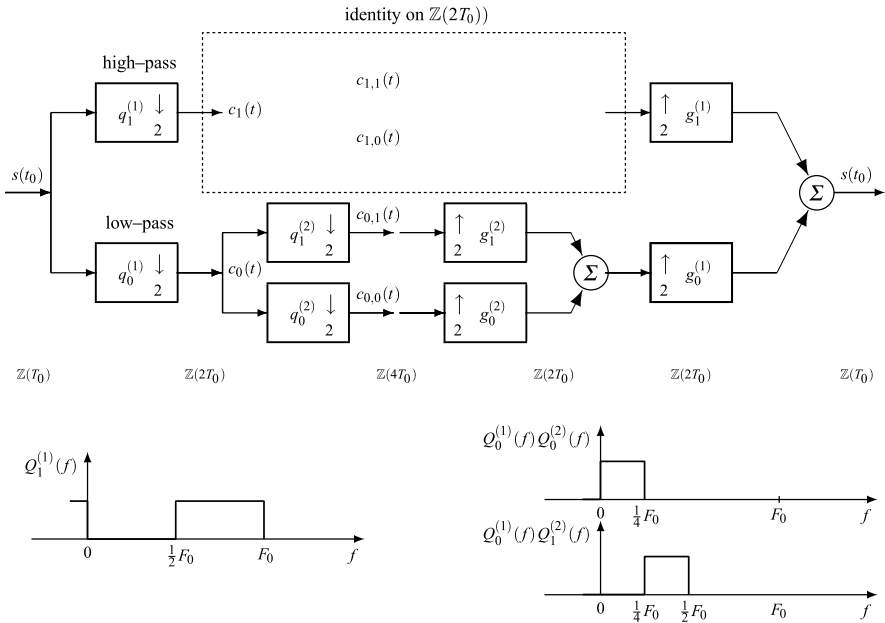


Fig. 14.33 Pruned tree filter bank of the second order

$[0, F_0)$ is subdivided into $[0, \frac{1}{4}F_0)$, $[\frac{1}{4}F_0, \frac{1}{2}F_0)$, and $[\frac{1}{2}F_0, F_0)$. In general, with J iterations to the previous low-pass channel, the final tree has $J + 1$ leaves, with bands

$$\left[0, \frac{1}{2^J}F_0\right), \left[\frac{1}{2^J}F_0, \frac{1}{2^{J-1}}F_0\right), \dots, \left[\frac{1}{2}F_0, F_0\right).$$

This tree is called *logarithmic filter bank* since the bandwidths are equal on a logarithmic scale. It is also called *octave-band tree* [14], since each successive high-pass output contains an “octave” of the original band.

Perfect Reconstruction The proof that the perfect reconstruction of the building blocks leads to the perfect reconstruction of the whole tree is less trivial, the reason being that the leaves of the tree have different rates. Reconsider for simplicity the two-stage case of Fig 14.33, where the target is to recover the input signal $s(t_0)$, $t_0 \in \mathbb{Z}$, from the output signals $c_1(t)$, $t \in \mathbb{Z}(2T_0)$, and $c_{0,1}(t)$, $c_{0,0}(t)$, $t \in \mathbb{Z}(4T_0)$. Then, (conceptually) expand the “medium-rate” signal $c_1(t)$ into two low-rate components $c_{1,1}(t)$, $c_{1,0}(t)$, $t \in \mathbb{Z}(4T_0)$. The expansion must be done in a reversible way, such that, in the synthesis side, $c_1(t)$ will be recovered from $c_{1,1}(t)$ and $c_{1,0}(t)$, e.g., by a $\mathbb{Z}(2T_0) \rightarrow \mathbb{Z}(4T_0)$ S/P converter, whose inverse is a $\mathbb{Z}(4T_0) \rightarrow \mathbb{Z}(2T_0)$ P/S converter. In this way, for the Analysis, we have (conceptually) obtained a full tree with 4 output signals $c_{i,j}(t)$, $t \in \mathbb{Z}(4)$, from which we can recover the signal $s(t_0)$ with a full tree Synthesis, exactly as done in the equal-band tree of Fig. 14.33. In fact, as before, the Analysis/Synthesis block of the second stages are equivalent to

the identity on $\mathbb{Z}(2T_0)$. Thus, a pruned version of a full tree can be studied as the full tree itself.

In conclusion, even through a pruned tree obtained with J steps has a number of leaves $< 2^J$ with different output rates, it behaves as a full tree channel filter bank with 2^J leaves working at the same rate.

14.15.3 Multiresolution Obtained with Tree Filter Banks

A tree filter bank provides a *multiresolution* analysis, called *discrete-time wavelet series* [14]. Assuming that the input signal $s(n)$ is defined on \mathbb{Z} and the signal on the subsequent branches on $\mathbb{Z}(2)$, $\mathbb{Z}(2^2)$, \dots , $\mathbb{Z}(2^J)$, the series over J octaves assumes the form

$$s(n) = w_1(n) + w_2(n) + \dots + w_J(n) + s_J(n), \quad (14.158)$$

where $w_i(n)$ is the high-pass contribution obtained in the i th octave, and $s_J(n)$ is a final low-pass contribution.

To see how a tree filter bank provides the wavelet series (14.158), consider a two-channel filter bank on $\mathbb{Z} \rightarrow \mathbb{Z}(2)$ with analysis filters $q_0^{(1)}$, $q_1^{(1)}$ and synthesis filters $g_0^{(1)}$, $g_1^{(1)}$. The analysis filters give the signals on $\mathbb{Z}(2)$

$$\begin{aligned} S_1(2k) &= \sum_{n \in \mathbb{Z}} q_0^{(1)}(2k - n)s(n), \\ D_1(2k) &= \sum_{n \in \mathbb{Z}} q_1^{(1)}(2k - n)s(n), \end{aligned} \quad (14.159)$$

and, assuming perfect reconstruction, the synthesis filters give back the original signal as $s(n) = s_1(n) + w_1(n)$, where

$$\begin{aligned} s_1(n) &= \sum_{2k \in \mathbb{Z}(2)} g_0^{(1)}(n - 2k)S_1(2k), \\ w_1(n) &= \sum_{2k \in \mathbb{Z}(2)} g_1^{(1)}(n - 2k)D_1(2k) \end{aligned} \quad (14.160)$$

are respectively the low-pass and the high-pass components of $s(n)$.

In (14.160) the signals $S_1(2k)$ and $D_1(2k)$ have the role of coefficients of the components $s_1(n)$ and $w_1(n)$, respectively.

In the second stage, working on $\mathbb{Z}(2) \rightarrow \mathbb{Z}(2^2)$, the high-pass component $w_1(n)$ remains unchanged, whereas the low-pass component $s_1(n)$ is further split by low-pass/high-pass filtering and down-sampling. Thus, one gets the decomposition $s_1(n) = s_2(n) + w_2(n)$. The coefficients $S_2(2^2k)$ and $D_2(2^2k)$ of the new components are signals defined on $\mathbb{Z}(2^2)$. The beautiful thing, which will be proved in the next chapter and known as *Mallat's algorithm*, is that the coefficients $S_2(2^2k)$ and $D_2(2^2k)$ can be obtained directly from the coefficients $S_1(2k)$ by the analysis side of a two-channel filter bank.

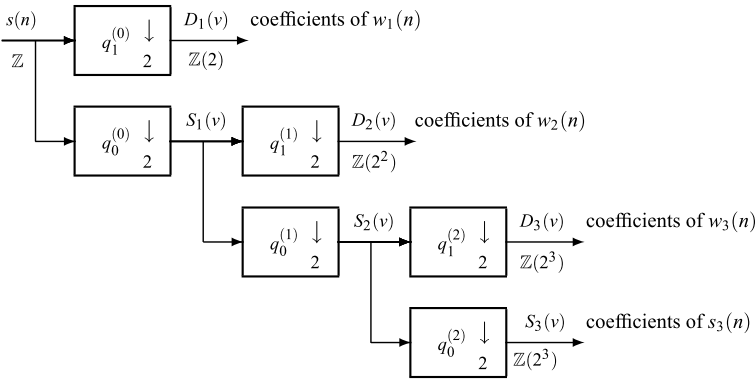


Fig. 14.34 Mallat’s algorithm for the evaluation of coefficients in the *discrete-time wavelet series*

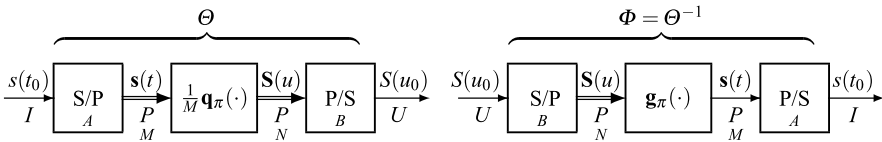


Fig. 14.35 Full polyphase decomposition of a generalized transform and of its inverse

This decomposition, in terms of coefficients, can proceed on the subsequent stages, where the coefficients $S_i(2^i k)$ and $D_1(2^i k)$ of the components $s_i(n)$ and $w_i(n)$ are directly obtained from $S_{i-1}(2^{i-1} k)$ by a two-channel filter bank on $\mathbb{Z}(2^{i-1} k) \rightarrow \mathbb{Z}(2^i k)$, as shown in Fig. 14.34.

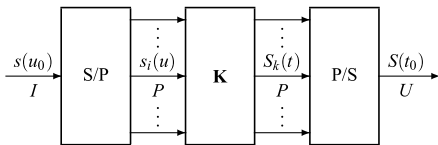
In conclusion, a tree structured filter bank with the architecture of Fig. 14.34) does not give directly the discrete-time wavelet series (14.158), but it provides the coefficients of each term of the series. The architecture has other important features, such as the orthogonality of the components and the property that the filters at the different stages can be obtained by a single prototype filter.

14.16 The Block Transform

In the study of subband decomposition we have considered the *partial* architecture of Fig. 14.16, where the inner P/S and S/P conversions of the *full* architecture of Fig. 14.15 are dropped. Here we are interested in restoring the inner P/S and S/P conversions and using polyphase decomposition for the partial architecture. In other words, we insert the inner P/S and S/P conversion in the architecture of Fig. 14.22 and obtain the scheme of Fig. 14.35.

In this scheme the forward transform Θ is implemented by 1) an S/P conversion with generator $A = [I/P]$, 2) the polyphase network $\mathbf{q}_\pi(t)/M$, and 3) a P/S conversion with generator $B = [U/P]$. The inverse transform is implemented analogously with the polyphase network $\mathbf{g}_\pi(t)$ at the central part.

Fig. 14.36 Implementation of the block transform



14.16.1 The Block and Lapped Transforms

The impulse responses in the previous architectures (subband, transmultiplexer, polyphase) may have an unlimited extension, but in the applications, the case of a limited extension, or FIR (finite impulse response), has a fundamental importance. Here we develop the case in which the extensions of the polyphase matrices (regarded as signals): $\mathbf{q}_\pi(t)$, $t \in P$, and $\mathbf{g}_\pi(t)$, $t \in P$, are limited to the origin and are given by an impulse on P . In particular,

$$\frac{1}{M} \mathbf{q}_\pi(t) = \mathbf{K} \delta_P(t), \tag{14.161}$$

where $\mathbf{K} = [k_{ba}]$ is an $N \times M$ complex matrix. The corresponding input–output relationship is

$$\mathbf{S}(t) = \int_P du \frac{1}{M} \mathbf{q}_\pi(t - u) \mathbf{s}(u) = \mathbf{K} \mathbf{s}(t), \quad t \in P, \tag{14.162}$$

where $\mathbf{s}(u)$ and $\mathbf{S}(t)$ collect the polyphase components of the signal $s(u_0)$ and of the transform $S(t_0)$, respectively.

The interpretation of (14.162) is the following (Fig. 14.36): the input signal $s(u_0)$ is fragmented into blocks of length M (by the S/P conversion) to form the vector signal $\mathbf{s}(t)$. At each time $t \in P$, the block $\mathbf{s}(t)$ is multiplied by the matrix \mathbf{K} to produce the block $\mathbf{S}(t)$. The blocks $\mathbf{S}(t)$ are finally P/S converted to the output signal $S(t_0)$. This is the idea of the *block transform*.

The block transform may be viewed as a modification of a given transform, say the DFT or the DCT, which is based on a relation of the form¹¹ [11, 12]

$$\mathbf{S} = \mathbf{K} \mathbf{s},$$

where \mathbf{s} is a signal vector, and \mathbf{S} is the corresponding transform. But this approach of processing a unique block \mathbf{s} becomes critical when the length is unbounded or, at least, far exceeds the length of the transform. A solution is that the signal can be processed in blocks of consecutive values, as stated by (14.162), by computing a block transform.

The use of the block transform has become popular in block coding and waveform quantization [6]. A disadvantage is the so-called *blocking effect*, caused by the discontinuous (or ungraceful) processing at the border of the blocks.

¹¹We recall from Sect. 7.5 that this relation implies that the signal to be processed is modeled as a periodic signal, so that its S/P conversion leads to a constant vector signal.

A technique to reduce the blocking effect was proposed by Cassereau [1] with the name of *lapped transform*. In the present context, the lapped transform may be obtained through an impulse response of the form

$$\frac{1}{M} \mathbf{q}_\pi(t) = \mathbf{K}_0 \delta_P(t) + \mathbf{K}_1 \delta_P(t - \tau),$$

where \mathbf{K}_0 and \mathbf{K}_1 are $N \times M$ complex matrices, and τ is a given point of P . With this form we have

$$\mathbf{S}(t) = \mathbf{K}_0 \mathbf{s}(t) + \mathbf{K}_1 \mathbf{s}(t - \tau).$$

For a detailed analysis and design (choice of the matrices \mathbf{K}_0 and \mathbf{K}_1) of the lapped transform, we suggest references [11, 12].

14.17 Problems

14.1 **★★** [Sect. 14.1] Given a generalized transform on $I \mapsto U$ with kernels $\theta(u, t)$ and $\varphi(t, u)$, prove that the kernels of the *dual* transform on $\hat{I} \mapsto \hat{U}$ are given by

$$\hat{\theta}(\lambda, f) = \Theta(\lambda, -f), \quad \hat{\varphi}(f, \lambda) = \Phi(f, -\lambda), \quad (14.163)$$

where $\Theta(\lambda, f)$ and $\Phi(f, \lambda)$ are respectively the FTs of $\theta(u, t)$ and $\varphi(t, u)$. Here *dual* is not intended in the sense of (14.13a), (14.13b) but as a frequency representation.

14.2 **★★** [Sect. 14.1] Prove that, if the kernels of a generalized transform $\theta(u, t)$ and $\varphi(t, u)$ are self-reciprocal, also the kernels of the dual transform $\hat{\theta}(\lambda, f)$ and $\hat{\varphi}(f, \lambda)$ are self-reciprocal.

14.3 **★** [Sect. 14.2] Check that the IDFT/DFT are a special case of (14.16a) and (14.16b).

14.4 **★★** [Sect. 14.2] Show that for the Fourier series expansion both forward and inverse reconstruction conditions (14.6) and (14.8) hold.

14.5 **★★** [Sect. 14.2] Apply the expansion/reconstruction (14.22) to the signal

$$s(t) = \text{sinc}^2(Ft), \quad t \in \mathbb{R},$$

and show that, if the sampling frequency $F_c = 1/T < 2F$, the imperfect reconstruction gives the projector of $s(t)$ onto the class $H(B)$. *Hint*: consider that the projector defined by (14.23) is given by the cascade sampling/interpolation of the Fundamental Sampling Theorem and proceed in the frequency domain.

14.6 **★★** [Sect. 14.3] Consider the Mercedes Benz frame defined in Example 14.3. Verify that it is a tight frame and find the redundancy.

14.7 **★★** [Sect. 14.3] Find a dual of the Mercedes Benz frame and discuss its multiplicity.

14.8 **★** [Sect. 14.6] Formulate Proposition 14.2 in the case $I = \mathbb{R}$ and $U = \mathbb{Z}$. Note that in this case the cell B degenerates.

14.9 **★★** [Sect. 14.6] Interpret the *Fundamental Sampling Theorem* (see Sect. 8.4) as a subband decomposition on $I = \mathbb{R}$ and $U = \mathbb{Z}(T)$, where the Analysis performs the $\mathbb{R} \rightarrow \mathbb{Z}(T)$ sampling, and the Synthesis gives the reconstruction of the signal from the samples.

14.10 **★★** [Sect. 14.6] Formulate Proposition 14.2 in the case $I = \mathbb{Z}^2$, $U = \mathbb{Z}^2$, and $P = \mathbb{Z}_2^1(2, 2)$, the quincunx lattice defined in Sect. 3.3.

14.11 **★★** [Sect. 14.6] Formulate Proposition 14.2 in the case $I = \mathbb{Z}(2, 2)$, $U = \mathbb{Z}^2$ and $P = \mathbb{Z}_2^1(2, 2)$. Which is the main difference with respect to the previous problem?

14.12 **★★** [Sect. 14.7] The direct connection of the transmultiplexer architecture consists of an N -input one-output $P \rightarrow U$ interpolator (transmitter side) and one-input N -output $U \rightarrow P$ decimator (receiver side). The $N \times N$ global impulse response is the matrix $[\tilde{q}_b * \tilde{g}_c(t)]$, $t \in P$, $b, c \in B$. Note that this is a convolution between the high-rate signals $\tilde{q}_b(t_0)$ and $\tilde{g}_c(t_0)$, $t_0 \in U$, subsequently evaluated at the low-rate argument $t \in P$ (after the evaluation on $t_0 \in U$, there is a $U \rightarrow P$ down-sampling). Evaluate the global frequency response (note that the connection transmitter–receiver is equivalent to a filter on P).

14.13 **★** [Sect. 14.9] Consider a subband decomposition with $I = \mathbb{Z}$, $U = \mathbb{Z}$, and $P = \mathbb{Z}(4)$. Explicitly write the distortion-free and the alias-free conditions.

14.14 **★★** [Sect. 14.9] Consider a subband decomposition with $I = \mathbb{Z}$, $U = \mathbb{Z}(2/3)$, and $P = \mathbb{Z}(4)$. Explicitly write the distortion-free and the alias-free conditions.

14.15 **★★** [Sect. 14.9] Consider a 2D subband decomposition with (see Problem 14.10) $I = \mathbb{Z}^2$, $U = \mathbb{Z}^2$, and $P = \mathbb{Z}_2^1(2, 2)$. Explicitly write the distortion-free and the alias-free conditions.

14.16 **★★** [Sect. 14.9] Write the IRC condition for the subband decomposition architecture obtained by imposing that the cascade of the $P \rightarrow I$ interpolator followed by the $I \rightarrow P$ decimator be equivalent to the N -input N -output identity on P (see Table 14.1).

14.17 **★★** [Sect. 14.9] Write the IRC condition of the previous problem in the frequency domain (see Table 14.1).

14.18 ★ [Sect. 14.10] Consider a subband decomposition with $I = \mathbb{Z}$, $U = \mathbb{Z}$, and $P = \mathbb{Z}(4)$. Explicitly write the polyphase matrix $\mathbf{g}_\pi(t)$.

14.19 ★★ [Sect. 14.10] Consider the subband decomposition of the previous problem. Explicitly write the polyphase matrix $\mathbf{G}_\pi(f)$ in the frequency domain in terms of the original frequency responses.

14.20 ★★ [Sect. 14.10] Consider a 2D subband decomposition with (see Problem 14.10) $I = \mathbb{Z}^2$, $U = \mathbb{Z}^2$, and $P = \mathbb{Z}_2^1(2, 2)$. Explicitly write the polyphase matrix $\mathbf{g}_\pi(t)$. *Hint*: use the lexicographical order (see Sect. 7.6).

14.21 ★ [Sect. 14.12] Prove that in (14.147) $D(f)$ verifies the condition $D(f - F) = -D(f)$, which implies that the impulse response $d(nT_0)$ is zero for n even.

14.22 ★ [Sect. 14.12] Prove relation (14.149) on the Synthesis filters of Choice II.

14.23 ★★ [Sect. 14.16] Prove that with the impulse response given by (14.161), the kernel $\theta(u_0, t_0)$ of the corresponding PI transformation is specified by $h(b, a) = K_{ba}$, where K_{ba} are the entries of \mathbf{K} . Prove also that the extension of h is given by $\theta(h) = \{B \times A + (t, t) | t \in P\}$.

Appendix A: Proof of Theorem 14.1 on Projections

We first prove that the operator \mathcal{P}_b , defined by the kernel (14.57), is idempotent, that is, $\mathcal{P}_b^2 = \mathcal{P}_b$. The kernel of \mathcal{P}_b^2 is given by

$$\begin{aligned} h_{12}(t_3, t_1) &= \int_I dt_2 h_b(t_3, t_2) h_b(t_2, t_1) \\ &= d(U)^2 \sum_{p, p' \in P} \int_I dt_2 \varphi_b(t_3 - p) \theta_b(t_2 - p) \varphi_b(t_2 - p') \theta_b(t_1 - p') \\ &= d(U) \sum_{p, p' \in P} \varphi_b(t_3 - p) \left\{ d(U) \int_I dt_2 \theta_b(t_2 - p) \varphi_b(t_2 - p') \right\} \theta_b(t_1 - p') \\ &= d(U) \sum_{p \in P} \varphi_b(t_3 - p) \theta_b(t_1 - p) = h_b(t_3, t_1), \end{aligned}$$

where in $\{\cdot\}$ we have used condition (14.50b) with $b = b'$. Hence, \mathcal{P}_b is a projector.

The sum of the kernels gives, after use of (14.21),

$$\sum_{b \in B} h_b(t_3, t_1) = d(U) \sum_{b \in B} \sum_{p \in P} \varphi_b(t_3 - p) \theta_b(t_1 - p) = h_H(t_3, t_1),$$

which states the second of (14.58).

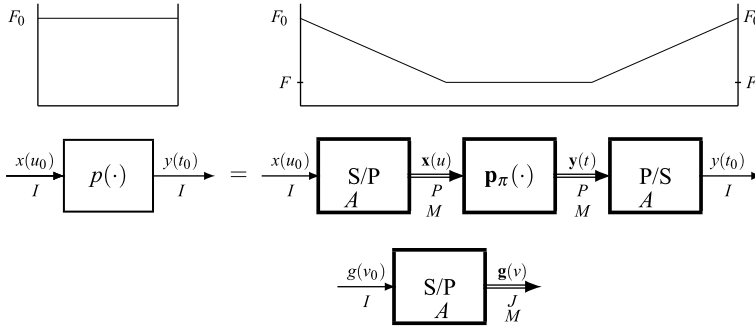


Fig. 14.37 Polyphase decomposition of a filter with impulse response $p(t_0)$, $t_0 \in P$

When the self-reciprocal condition holds, it is immediate to check that $h_b^*(t'_0, t_0) = h_b(t_0, t'_0)$, which states that the projectors \mathcal{P}_b are Hermitian.

Appendix B: Alias-Free Condition in Subband Decomposition

In Sect. 7.7 we have developed the polyphase architecture of a filter, given by an $I \rightarrow J$ S/P converter, a polyphase filter on J , and a P/S converter (Fig. 14.37). The $M \times M$ polyphase matrix $\mathbf{p}_\pi(t) = [p_{\pi ji}(t)]$ is obtained from the impulse response $p(t_0)$, $t_0 \in I$, of the filter as

$$p_{\pi ji}(t) = \frac{1}{L} p(t + \tau_j - \tau_i), \quad t \in J, \tau_i, \tau_j \in A, \quad (14.164)$$

where we suppose that the PD is obtained with the same generator $A = \{\tau_0, \dots, \tau_{M-1}\}$ both at the S/P side and at the P/S side. We see from (14.164) that the polyphase matrix is redundant, since its j, i element depends only on the difference $\tau_j - \tau_i$.

Now, we relate the polyphase matrix to the PD of the impulse response $p(t_0)$, given by

$$p_k(t) = \frac{1}{L} p(t + \tau_k), \quad t \in J, \tau_k \in A. \quad (14.165)$$

To this end, note that the differences $\tau_j - \tau_i$ are points of I and therefore have the unique decomposition

$$\tau_j - \tau_i = t_{ji} + \tau_k = t_{ji} + \tau_{\alpha_{ji}}, \quad t_{ji} \in J, \tau_{\alpha_{ji}} \in A, \quad (14.166)$$

where $\tau_{\alpha_{ji}}$ is a convenient point of the generator A . Hence, the j, i element of the polyphase matrix can be written in the form

$$p_{\pi, ji}(t) = \frac{1}{M} p(t + \tau_j - \tau_i) = \frac{1}{M} p(t + t_{ji} + \tau_{\alpha_{ji}}) = \frac{1}{M} p_{\alpha_{ji}}(t + t_{ji}), \quad (14.167)$$

where $p_{\alpha_{ji}}(t + t_{ji})$ is the polyphase component of $p(t_0)$ of index α_{ji} shifted by $-t_{ji}$. In conclusion:

Proposition 14.6 *For a filter with impulse response $p(t_0)$, $t_0 \in I$, the polyphase matrix $\mathbf{p}_\pi(t)$, $t \in J$, obtained with a cell $A = [I/P]$ of cardinality M , has M^2 elements defined by (14.164). Let $p^{(k)}(t) = p(t + \tau_k)$, $t \in J$, $\tau_k \in A$, be the PD of the impulse response $p(t_0)$, $t_0 \in I$. All the M^2 elements of $\mathbf{p}_\pi(t)$ can be obtained from the M elements of the PD $p^{(k)}(t)$ according to (14.167).*

As an example, consider a cell $A = \{0, \tau_1, \tau_2\} \subset I$ of cardinality $M = 3$. Then, the polyphase matrix is

$$\begin{aligned} \mathbf{p}_\pi(t) &= \begin{bmatrix} p_{\pi 00}(t) & p_{\pi 10}(t) & p_{\pi 20}(t) \\ p_{\pi 01}(t) & p_{\pi 11}(t) & p_{\pi 21}(t) \\ p_{\pi 02}(t) & p_{\pi 12}(t) & p_{\pi 22}(t) \end{bmatrix} \\ &= \frac{1}{3} \begin{bmatrix} p(t) & p(t + \tau_1) & p(t + \tau_2) \\ p(t - \tau_1) & p(t) & p(t + \tau_2 - \tau_1) \\ p(t - \tau_2) & p(t - \tau_2 + \tau_1) & p(t) \end{bmatrix}. \end{aligned}$$

The PD of the impulse response $p(t_0)$ has the 3 components $p_0(t) = p(t)$, $p_1(t) = p(t + \tau_1)$, $p_2(t) = p(t + \tau_2)$, and we can express the 9 elements of $\mathbf{p}_\pi(t)$ in terms of the 3 components $p_k(t)$, $k = 0, 1, 2$. In fact, $p(t) = p_0(t)$, $p(t + \tau_1) = p_1(t)$, $p(t + \tau_2) = p_2(t)$. For the other 6 elements, we note that $-\tau_1$, $-\tau_2$, $\tau_2 - \tau_1$, $-\tau_2 + \tau_1$ can be written in the form $t_{ij} + \tau_{\alpha_{ij}}$, then, e.g., $\tau_2 - \tau_1 = t_{21} + \tau_{\alpha_{21}}$, and then $p(t + \tau_2 - \tau_1) = p^{(\alpha_{21})}(t + t_{21})$. To be more specific, we continue the example in the 1D case, where $A = \{0, T_0, 2T_0\}$. Then $-\tau_1 = -T_0 = -3T_0 + 2T_0$, so that $p(t - \tau_1) = p^{(2)}(t - 3T_0)$, $\tau_2 - \tau_1 = T_0$, so that $p(t + \tau_2 - \tau_1) = p^{(1)}(t)$, etc. In conclusion,

$$\mathbf{p}_\pi(t) = \frac{1}{3} \begin{bmatrix} p_0(t) & p_1(t) & p_2(t) \\ p_2(t - T) & p_0(t) & p_1(t) \\ p_1(t - T) & p_2(t - T) & p_0(t) \end{bmatrix}, \quad T = 3T_0. \quad (14.168)$$

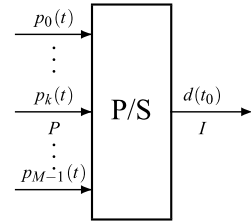
The symmetry of this matrix is referred to as *pseudo-circulant*. Evidently, $\mathbf{p}_\pi(t)$ is completely determined by the elements of its 0th row, which represent the PD of the impulse response of the filter.

In the general multidimensional case, the symmetry of the polyphase matrix is stated by (14.165) and (14.166), and we referred to it as *generalized pseudo-circulant*. Proposition 14.6 represents a generalization of a theorem by Vaidyanathan and Mitra [13].

The conclusion is the following:

Proposition 14.7 *The alias-free condition in a subband decomposition filter bank requires that the global polyphase matrix $\mathbf{p}_\pi(t) = (1/M)\mathbf{g}_\pi * \mathbf{q}_\pi(t)$ must be gener-*

Fig. 14.38 Interpretation of the impulse response of the equivalent filter $d(t_0)$, $t_0 \in I$, in subband coding when the global matrix $\mathbf{p}_\pi(t)$ is pseudo-circulant



alized pseudo-circulant. In this case the global Analysis–Synthesis is equivalent to a filter $d(t_0)$ whose polyphase components are given by the 0th row of $\mathbf{p}_\pi(t)$.

Hence, the filter $d(t_0)$ is obtained as the P/S conversion of the M elements of the 0th row of the matrix $\mathbf{p}_\pi(t)$ as (Fig. 14.38)

$$d(t + \tau_k) = p_k(t), \quad t \in J, k = 0, 1, \dots, M - 1, \quad (14.169)$$

and in the frequency domain, using (7.32)

$$D(f) = \frac{1}{M} \sum_{k=0}^{L-1} P_k(f) e^{-i2\pi f \tau_k}. \quad (14.170)$$

Once eliminated the aliasing according to the above statement, the perfect reconstruction imposes that $d(t_0) = \delta_I(t_0)$, which implies that $p_k(t) = d(t + \tau_k) = \delta_I(t + \tau_k)$. In words: the first row of $\mathbf{p}_\pi(t)$ must contain pure shifts.

B.1 Alias-Free Condition in 1D Case

The alias-free condition requires the pseudo-circulant symmetry of global polyphase matrix

$$p_\pi(t) = \mathbf{g}_\pi * \frac{1}{M} \mathbf{q}_\pi(t) \quad \xrightarrow{\mathcal{F}} \quad \mathbf{P}_\pi(f) = \mathbf{G}_\pi(f) \frac{1}{M} \mathbf{Q}_\pi(f).$$

This symmetry can be formulated more specifically in the 1D case, where decomposition (14.166) becomes

$$\tau_j - \tau_i = (j - i)T_0 = \begin{cases} (j - i)T_0, & j \geq 0, \\ [M + (j - i)]T_0 - MT_0, & j < i. \end{cases}$$

For instance, for $L = 4$, this gives

$$\mathbf{p}_\pi(t) = \frac{1}{4} \begin{bmatrix} p_0(t) & p_1(t) & p_2(t) & p_3(t) \\ p_3(t-T) & p_0(t) & p_1(t) & p_2(t) \\ p_2(t-T) & p_3(t-T) & p_0(t) & p_1(t) \\ p_1(t-T) & p_2(t-T) & p_3(t-T) & p_0(t) \end{bmatrix}, \quad T = 4T_0,$$

$$\mathbf{P}_\pi(f) = \frac{1}{4} \begin{bmatrix} P_0(f) & P_1(f) & P_2(f) & P_3(f) \\ z^{-1}P_3(f) & P_0(f) & P_1(f) & P_2(f) \\ z^{-1}P_2(f) & z^{-1}P_3(f) & P_0(f) & P_1(f) \\ z^{-1}P_1(f) & z^{-1}P_2(f) & z^{-1}P_3(f) & P_0(f) \end{bmatrix}, \quad z = e^{i2\pi fT}.$$
(14.171)

With this symmetry, the global subband system becomes a filter with frequency response (see (14.170))

$$D(f) = \frac{1}{4} [P_0(f) + z_0^{-1}P_1(f) + z_0^{-2}P_2(f) + z_0^{-3}P_3(f)], \quad z_0 = e^{i2\pi fT_0}.$$

To eliminate the distortion, the further condition is $D(f) = 1$. A solution may be obtained with $P_k(f) = z_0^k$.

Appendix C: z -Domain Analysis of 1D Subband Decomposition

The frequency-domain analysis developed in Sect. 14.13 can be transferred to the z -domain using the rules outlined in Chap. 11 for the fundamental discrete-time components, where, for the complex variable, we use symbols z for low-rate signals with spacing T and z_0 for high-rate signals with spacing T_0 . Since (in this chapter) $T = MT_0$, the variables are related as $z = z_0^M$. We also recall that we find it convenient to define the z -transform as a Haar integral over $\mathbb{Z}(T)$ or $\mathbb{Z}(T_0)$ and with the explicit presence of the time spacing, namely

$$X(z) = \sum_{n=-\infty}^{+\infty} Tx(nT)z^{-n}, \quad Y(z_0) = \sum_{n=-\infty}^{+\infty} T_0y(nT_0)z_0^{-n}$$

for low-rate and a high-rate signals, respectively. The frequency domain analysis is obtained as a particularization by¹²

$$z = e^{i2\pi fT}, \quad z_0 = e^{i2\pi fT_0}.$$

¹²With an abuse of notation, for simplicity, we denote by the same symbol the Fourier transform and the z -transform, e.g., $X(f)$ and $X(z)$ or $X(z_0)$. Also, we will not indicate the convergence region of each z -transform.

At this point we invite the reader to reconsider in detail the second part of Chap. 11 from Sect. 11.5 on, in particular, the rules concerning the passage from the frequency domain to the z -domain. Here, we simply recall the relations in a $\mathbb{Z}(T_0) \rightarrow \mathbb{Z}(T)$ decimator, with $T = MT_0$, given by

$$Y(f) = \sum_{k=0}^{M-1} X(f - kF), \quad Y(z_0^M) = \sum_{k=0}^{M-1} X(z_0 W_M^{-k}) \stackrel{\Delta}{=} \text{dec}_M X(z_0), \quad (14.172)$$

and the relations in a $\mathbb{Z}(T) \rightarrow \mathbb{Z}(T_0)$ interpolator, given by

$$Y(f) = G(f)X(f), \quad Y(z_0) = G(z_0)X(z_0^M). \quad (14.173)$$

So, caution must be paid with filters and interpolators, whose frequency relation is the same (but the difference comes from the context).

We also recall the relations of the P/S and S/P conversions, obtained with the cells (14.154). They are respectively (see (11.59) and (11.60))

$$\begin{aligned} X(z_0) &= \frac{1}{M} \sum_{i=0}^{M-1} z_0^{-i} X^{(i)}(z_0^M), \\ X^{(i)}(z_0^M) &= \sum_{k=0}^{M-1} z_0^i W_M^{ki} X(z_0 W_M^{-k}) = \text{dec}_M^i [z_0^i X(z_0)]. \end{aligned} \quad (14.174)$$

Using the above rules, we are now ready to obtain the relation in the z -domain from the Fourier analysis. The relationships in the Analysis/Synthesis scheme, given by (14.156), become (considering that the Analysis consists of a decimator and the Synthesis of an interpolator)

$$\mathbf{C}(z_0^M) = \text{dec}_M [\mathbf{Q}(z_0)S(z_0)], \quad \tilde{\mathbf{S}}(z_0) = \mathbf{G}(z_0)\mathbf{C}(z_0^M).$$

By combination we find

$$\begin{aligned} \tilde{\mathbf{S}}(z_0) &= \mathbf{G}(z_0) \text{dec}_M [\mathbf{Q}(z_0)V(z_0)] \\ &= \mathbf{G}(z_0) \sum_{k=0}^{M-1} \mathbf{Q}(z_0 W_M^{-k}) S(z_0 W_M^{-(M-1)}) \end{aligned}$$

and, more explicitly,

$$\begin{aligned} \tilde{\mathbf{S}}(z_0) &= \mathbf{G}(z_0)\mathbf{Q}(z_0)S(z_0) \\ &\quad + \mathbf{G}(z_0)\mathbf{Q}(z_0 W_M^{-1})V(z_0 W_M^{-1}) \\ &\quad \vdots \\ &\quad + \mathbf{G}(z_0)\mathbf{Q}(z_0 W_M^{-(M-1)})V(z_0 W_M^{-(M-1)}). \end{aligned}$$

The first line represents a filtered version of the original signal, and the rest represents aliasing. Hence, the perfect recovery condition is stated by

$$\mathbf{G}(z_0)\mathbf{Q}(z_0) = 1, \quad \mathbf{G}(z_0)\mathbf{Q}(z_0 W_M^{-k}) = 0, \quad k = 1, \dots, M - 1,$$

i.e.,

$$\boxed{\mathbf{G}(z_0)\mathbf{Q}(z_0 W_M^{-k}) = \delta_{k0}.} \quad (14.175)$$

C.1 Polyphase Analysis

The general frequency domain relation (14.129) can be directly rewritten in the z -domain, since they are concerned with ordinary low-rate filters (hence we use the variable z). Thus,

$$\mathbf{C}(z) = \frac{1}{M}\mathbf{Q}_\pi(z)\mathbf{S}(z), \quad \tilde{\mathbf{S}}(z) = \mathbf{G}_\pi(z)\mathbf{C}(z), \quad (14.176)$$

where $\mathbf{S}(z)$ is the PD of $S(z_0)$, and $\mathbf{Q}_\pi(z)$, $\mathbf{G}_\pi(z)$ are the polyphase matrices. Combination of (14.176) gives the global relation $\tilde{\mathbf{S}}(z) = \mathbf{P}_\pi(z)\mathbf{S}(z)$, where

$$\mathbf{P}_\pi(z) = \mathbf{G}_\pi(z) \frac{1}{M}\mathbf{Q}_\pi(z)$$

is the global polyphase matrix. Hence, the orthogonality condition becomes

$$\mathbf{P}_\pi(z) = \frac{1}{M}\mathbf{G}_\pi(z)\mathbf{Q}_\pi(z) = \mathbf{I}_M. \quad (14.177)$$

It remains to relate the polyphase vector $\mathbf{S}(z)$, with elements $S^{(j)}(z)$, to the z -transform $S(z_0)$ of the input signal $s(t_0)$. The extraction of the polyphase components (S/P conversion) in the z -domain is given by the second of (14.174). Then

$$S^{(j)}(z_0^M) = \text{dec}_M^j[z_0^j S(z_0)]$$

and, in matrix form,

$$\mathbf{S}(z_0^M) = \text{dec}_M \mathbf{Q}_{S/P}(z_0) S(z_0).$$

Analogously, we can relate the elements of the polyphase matrices $\mathbf{Q}_\pi(z)$ and $\mathbf{G}_\pi(z)$ to the original subband filters $Q(z_0)$ and $G(z_0)$. Following (14.157), we find

$$Q_n^{(j)}(z_0^M) = \text{dec}_M^j[z_0^j Q(z_0)], \quad G_m^{(j)}(z_0^M) = \text{dec}_M^j[z_0^j G(z_0)]. \quad (14.178)$$

As results from the above relationships, the approach in the z -domain may be viewed as a duplicate of the one carried out in the frequency domain (in the 1D

case). Now, the z -domain approach can continue with the investigation on the alias-free and distortion-free conditions. But, now it is a simple exercise to transfer results from the frequency domain to the z -domain.

References

1. P. Cassereau, A new class of orthogonal transforms for image processing, Dept. EECS, Mass. Inst. Technol., Cambridge, May 1985
2. A. Croisier, D. Esteban, C. Galand, Perfect channel splitting by use of interpolators, decimators/tree decomposition techniques, in *Int. Symp. on Info., Circuits and Systems*, Patras, Greece (1976)
3. I. Daubechies, *Ten Lectures on Wavelets* (SIAM, Philadelphia, 1992)
4. L.E. Franks, *Signal Theory* (Prentice Hall, Englewood Cliffs, 1969)
5. R.A. Horn, C.R. Johnson, *Matrix Analysis* (Cambridge University Press, London, 1985)
6. N.S. Jayant, P. Noll, *Digital Coding of Waveforms* (Prentice Hall, Englewood Cliffs, 1984)
7. J. Kovačević, A. Chebira, An introduction to frames. *Found. Trends Signal Process.* **2**(1), 1–94 (2008)
8. S. Mallat, A theory of multiresolution signal decomposition: the wavelet representation. *IEEE Trans. Pattern Anal. Mach. Intell.* **11**, 674–693 (1989)
9. S. Roman, *Advance Linear Algebra* (Springer, New York, 1992)
10. M.J. T Smith, T.P. Barnwell, A procedure for designing exact reconstruction filter banks for tree-structured subband coders. *Proc. Int. Conf. Acoust. Speech Signal Process.* **2**, 27.1.1–27.1.4 (1984)
11. D. Taubman, M.W. Marcellin, *JPEG2000, Image Compression Fundamentals and Practice* (Kluwer Academic, Boston, 2002)
12. P.P. Vaidyanathan, *Multirate Systems and Filter Banks* (Prentice Hall, Englewood Cliffs, 1993)
13. P.P. Vaidyanathan, S.K. Mitra, Polyphase network, block digital filtering, LPTV systems, and alias-free QMF banks: a unified approach based on pseudo circulants. *IEEE Trans. Acoust. Speech Signal Process.* **ASSP-36**, 81–94 (1988)
14. M. Vetterli, J. Kovačević, *Wavelets and Subband Coding* (Prentice Hall, Englewood Cliffs, 1995)

Chapter 15

Multiresolution and Wavelets

15.1 Introduction

Multiresolution analysis is a relatively new field of Signal Theory that has received tremendous interest in the last twenty years and has brought to the discovery of *wavelets*. The introduction to these topics, multiresolution and wavelets, can be done in several ways. A comprehensive way, followed, e.g., by Daubechies [4] and Vaidyanathan [13], is to start from the short-time Fourier transform (STFT) and consider its possible improvements and modifications, to arrive in such a way at the wavelet transform (WT). A second way, due to Mallat [7], starts from a few axioms and develops their consequences.

Both the STFT and the WT have *continuous* and *discrete* versions; so we have

- CSTFT (continuous STFT)
- DSTFT (discrete STFT)
- CWT (continuous WT)
- DWT (discrete WT)

There is another form of wavelet transform, called *wavelet series* or *wavelet series transform* (WST), where the input is continuous, and the output is discrete (in the DWT both the input and the output are discrete).

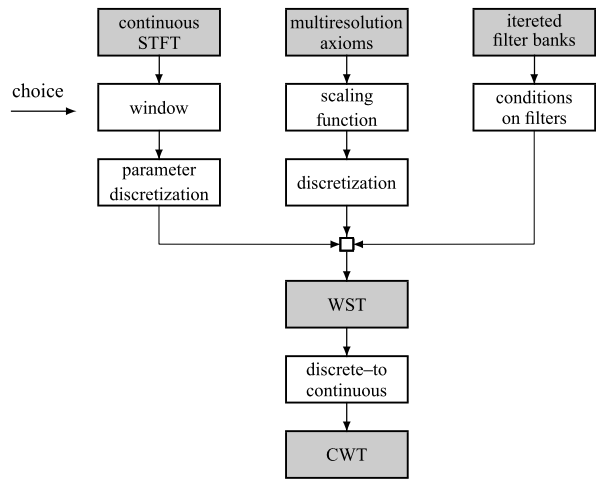
The heuristic deduction of the CWT from the CSTFT is usually done with an intermediate discretization of both transforms. This approach is also applied to the deduction of the CWT from the multiresolution axioms, as illustrated in the flow diagram of Fig. 15.1. This flow contains a third possibility, where the deduction of the CWT is made starting from a filter bank.

In all the approaches a choice is required to define the transformations therein, specifically a *window* in the STFT, a *scaling function* in the axiomatic approach, and a *mother wavelet* in the filter bank approach.

Note that the flow can be reversed, that is, one can start from the CWT and deduce the other transforms. In any case the importance of the diagram is in showing the “main players” in multiresolution analysis and their connections.

In this chapter we first develop the STFT approach, and then we will consider the axiomatic approach, which is comprehensive of the deduction from filter banks.

Fig. 15.1 Logical deductions of continuous wavelet transform (CWT)



15.2 The Short-Time Fourier Transform

The standard Fourier transform (FT)

$$S(f) = \int_I dt s(t)e^{-i2\pi ft}, \quad f \in \hat{I},$$

represents a signal as a linear combination of complex exponentials (and ultimately of sine and cosine terms), but it is not suitable to directly give *time localization*, that is, *where* the signal manifests its time behavior. Time localization can be achieved by the introduction of a window $w(t)$ in the form

$$S_{\text{CSTFT}}(f, \tau) = \int_I dt s(t)w^*(t - \tau)e^{-i2\pi ft}, \tag{15.1}$$

where the window is localized at time τ and cuts off a slice of the signal around τ . Usually, the window has a finite support and is chosen sufficiently smooth to avoid boundary effects. The duration of the window determines the time localization (and the frequency resolution): a narrow window gives a good time localization and a poor frequency resolution, while a wide window gives a poor time resolution and a good frequency resolution.

The frequency-time function defined by (15.1) is called *continuous short-time Fourier transform* (CSTFT), and also *windowed Fourier transform*, and is a very popular time-frequency representation of a signal. It is a compromise of the fact that some aspects of the signal are more conveniently represented in the time domain, and some others in the frequency domain. Clearly, the CSTFT is a redundant representation since it represents a 1D signal in terms of a 2D function and, in general, an mD signal by a $2mD$ function. It is evident that, owing to redundancy, the signal can be easily recovered from its STFT. In fact, the inverse FT of (15.1) gives

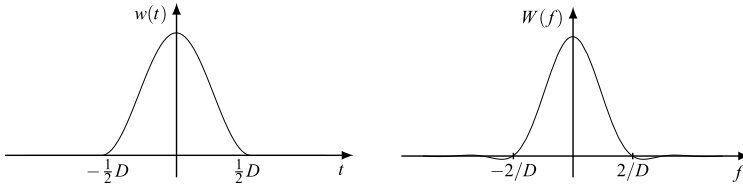


Fig. 15.2 The Hanning window and its Fourier transform

$s(t)w^*(t - \tau)$, and with $\tau = t$, we get $s(t)$, provided that $w(0) \neq 0$. Then

$$s(t) = \frac{1}{w(0)} \int_I df \, S_{\text{CSTFT}}(f, t) e^{i2\pi ft}, \quad t \in I. \tag{15.2}$$

The discrete STFT (DSTFT) is given by the samples of $S_{\text{CSTFT}}(f, \tau)$ on a uniform grid kF_0, nT_0 , with the signal $s(t)$ still continuous, that is,

$$S_{\text{DSTFT}}(kF_0, nT_0) = \int_I dt \, s(t) w^*(t - nT_0) e^{-i2\pi kF_0 t}. \tag{15.3}$$

15.2.1 Most Popular Windows

Historically, the STFT was first considered by Gabor in 1946 [5] with a complex Gaussian window, and for this reason, the STFT is often called the *Gabor transform*. But, usually, *real* valued windows with a finite duration D are chosen, where D is considered as a parameter. A gallery of well-shaped windows was illustrated at the end of Chap. 12 in the discrete case (but they can be easily rewritten for the continuous case). Here, in the illustrations we shall consider the *Hanning window* given by (Fig. 15.2)

$$w(t) = \frac{1}{2} [1 + \cos 2\pi t/D] \text{rect}(t/D),$$

whose FT is

$$W(f) = \frac{1}{2} D \text{sinc}(fD) + \frac{1}{4} D \text{sinc}(fD - 1) + \frac{1}{4} D \text{sinc}(fD + 1).$$

A test of the STFT can be made with the impulse $\delta_I(t - t_0)$ and with the complex exponential $e^{i2\pi f_0 t}$, that is, in frequency with the impulse $\delta_{\mathcal{F}}(f - f_0)$, which represent the maximum concentration in the time and in the frequency domain, respectively. The CSTFT of $\delta_I(t - t_0)$ is

$$S_{\text{CSTFT}}(f, \tau) = w^*(t_0 - \tau) e^{-i2\pi f t_0}. \tag{15.4}$$

The CSTFT of $e^{i2\pi f_0 t}$ is

$$S_{\text{CSTFT}}(f, \tau) = e^{-i2\pi(f-f_0)\tau} W^*(f - f_0), \tag{15.5}$$

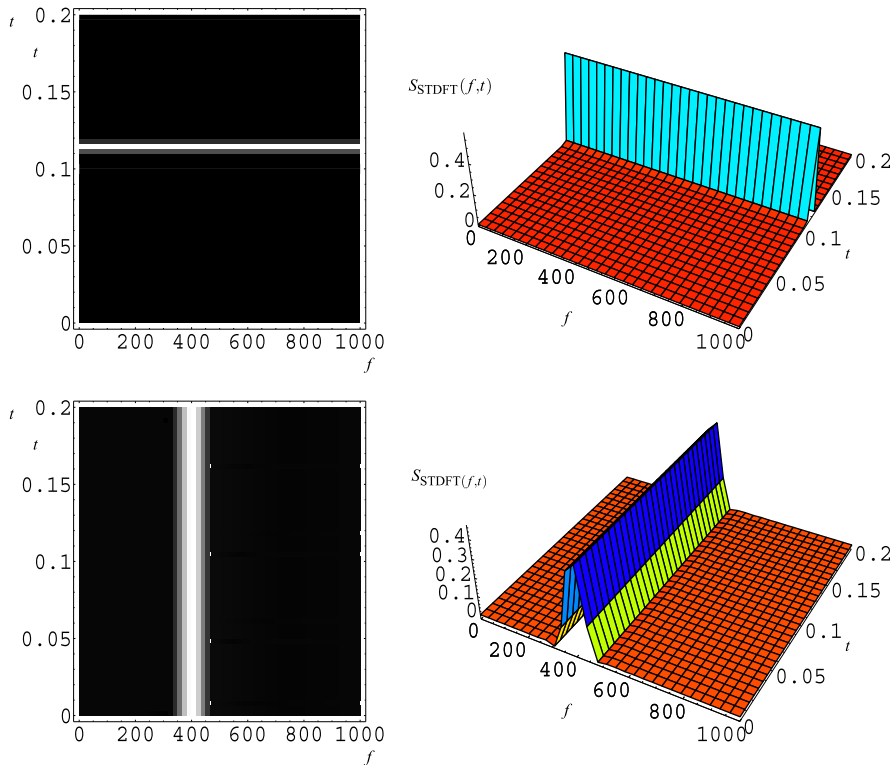


Fig. 15.3 Continuous short-time Fourier transform (CSTFT) with a Hanning window of duration is $D = 0.01$. Above with the signal $\delta(t - t_0)$ with $t_0 = 0.12$, and below with the signal $e^{i2\pi(f - f_0)}$ with $f_0 = 200$

where $W(f)$ is the FT of the window shape $w(t)$. These CSTFTs are shown in Fig. 15.3.

In the figures the gray levels indicate the values of the CSTFT with white standing for the highest value. As expected, in the (τ, f) plane, the CSTFT (15.4) is represented by a narrow vertical line (having chosen D small) displayed at $\tau = t_0$, and the CSTFT (15.5) by a narrow horizontal line at $f = f_0$.

The worst-case test for a time-frequency representation is the signal given by the sum of the two previous signals. The corresponding representation is shown in Fig. 15.4.

The CSTFT as a Linear Transform The CSTFT is a linear transformation of the type $I \rightarrow \hat{I} \times I$

$$S_{\text{CSTFT}}(f, \tau) = \int dt s(t)w_{f,\tau}^*(t) \quad \text{with } w_{f,\tau}^*(t) = w(t - \tau)e^{i2\pi ft}. \quad (15.6)$$

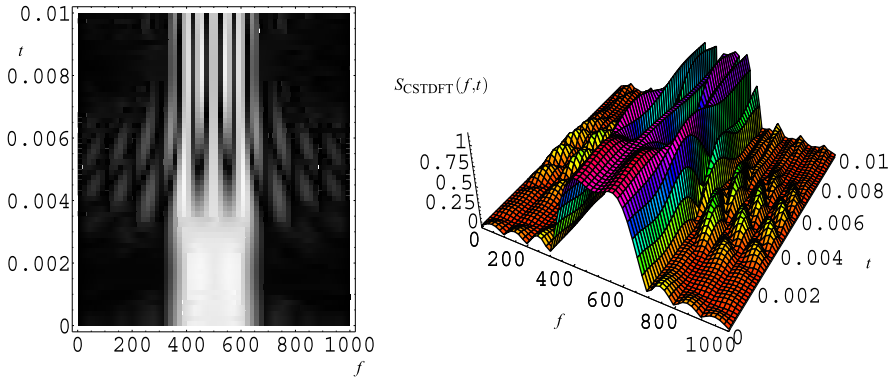


Fig. 15.4 Continuous short-time Fourier transform (CSTFT) with a Hanning window of duration $D = 0.01$. The signal is given by the sum of the impulse $\delta(t - t_0)$ with $t_0 = 0.12$, and the exponential $e^{i2\pi(f-f_0)t}$ with $f_0 = 400$

The inverse transform is given by (15.2). Note that the CSTFT can be expressed as an inner product $S_{\text{CSTFT}}(f, \tau) = \langle s, w_{f,\tau} \rangle$.

15.2.2 Interpretation and Properties of the STFT

In definition (15.1) we have considered a general signal domain I , and $S_{\text{CSTFT}}(f, \tau)$ is defined on $\hat{I} \times I$. However, in the illustrations and examples, we consider the 1D case $I = \mathbb{R}$, $\hat{I} \times I = \mathbb{R}^2$, and later the discrete 1D case.

An interpretation of the STFT is obtained by writing (15.1) in the form

$$\begin{aligned}
 S_{\text{CSTFT}}(f, \tau) &= e^{-i2\pi f \tau} \int_I dt s(t) w^*(t - \tau) e^{i2\pi f(\tau - t)} \\
 &= e^{-i2\pi f \tau} \int_I dt s(t) g_f(\tau - t),
 \end{aligned}
 \tag{15.7}$$

where the integral is a convolution of the signal $s(t)$ with the function

$$g_f(t) = w^*(-t) e^{i2\pi f t}.$$

Then (Fig. 15.5), for a fixed frequency $f = f_0$, the STFT is obtained from the signal $s(t)$ by the filter $g_{f_0}(t)$ followed by an exponential modulator with frequency $-f_0$. Note that the FT $W(f)$ is usually low-pass, and then $G_{f_0}(f) = W^*(f - f_0)$ is centered around the frequency f_0 . The filter takes the portion $S(f)G_{f_0}(f)$ of the FT, and the modulator with frequency $-f_0$ brings back this portion to the low-pass frequencies, giving $S(f - f_0)W^*(f)$.

In practice, a set of uniformly spaced frequencies $f_k = kF_0, k = 0, 1, \dots, M - 1$, is chosen, and then the M signals $y_k(\tau) = S_{\text{CSTFT}}(f_k, \tau)$ are obtained from a bank

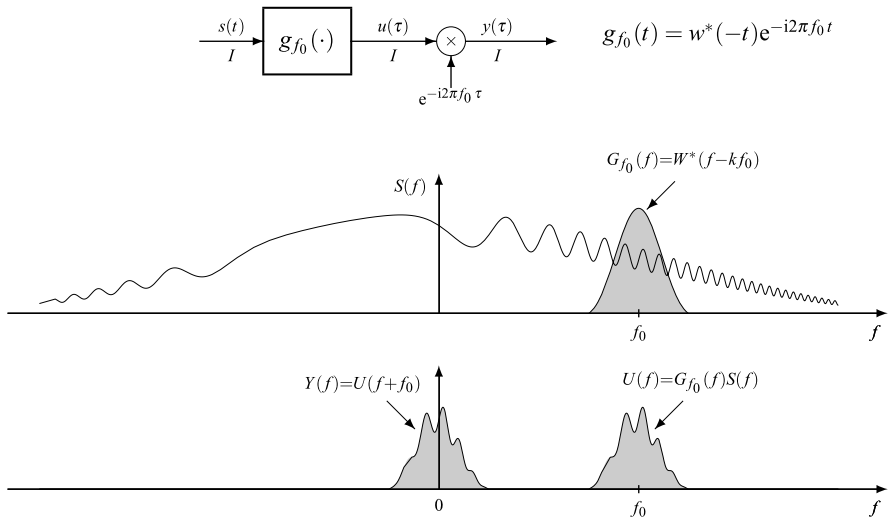


Fig. 15.5 Interpretation of the STFT for a fixed frequency $f = f_0$: the filter $g_{f_0}(t)$, followed by an exponential modulator with frequency f_0 , produces $y(\tau) = S_w(f_0, \tau)$

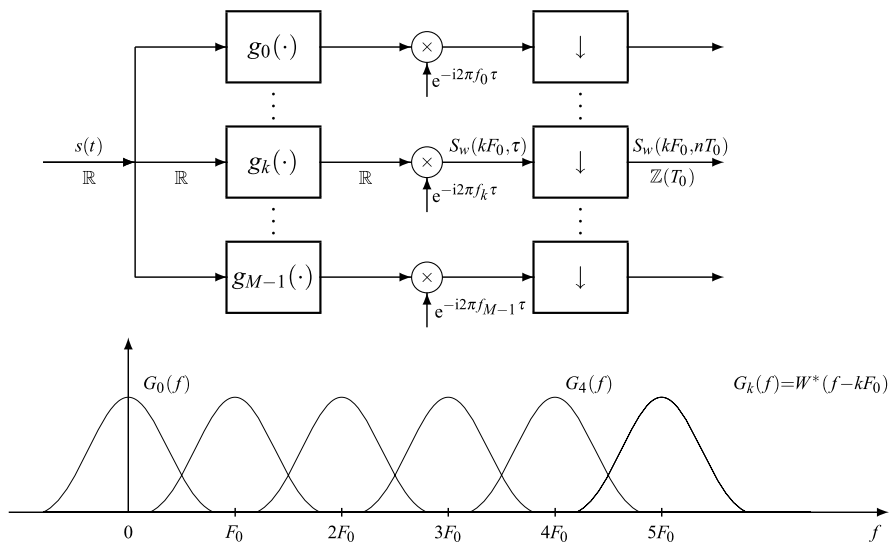


Fig. 15.6 Filter bank producing the STFT at the frequencies $f_k = k F_0$ and at the times $n T_0$: all the filters have the same frequency resolution, and the shifts τ are down-sampled with the same rates $1/T$

of filters and modulators, as shown in Fig. 15.6. These signals provide the signal components around the frequencies f_k . All the filters are obtained by *equally spaced frequency shifts* $f_k = k F_0$ of the same prototype filter $g_0(t)$, $G_0(f)$ accord-

ing to

$$g_k(t) = w^*(-t)e^{i2\pi k F_0 t} \xrightarrow{\mathcal{F}} G_k(f) = W^*(f - kF_0), \quad (15.8)$$

so that these filters have the *same frequency resolution*. In practice, also the time shifts are discretized as $\tau = nT_0$, which means that the windows are moved in uniform steps of T_0 . In other words, the continuous STFT $y_k(\tau) = S_k(kF_0, \tau)$ is $\mathbb{R} \rightarrow \mathbb{Z}(T_0)$ down-sampled in τ ; the sampling rate $1/T_0$ is the same for all the components $y_k(\tau)$, since they are the outputs of filters, which have the same bandwidth. With this down-sampling we get a *discrete* STFT.

The STFT gives a time-frequency representation of a signal, which can be illustrated on the (τ, f) plane. We have seen that, in practice, both τ and f are discretized as nT_0, kF_0 , and then the representation is limited to a lattice, commonly called *time-frequency grid*, where the STFT is evaluated. This is shown in Fig. 15.8.

15.3 From the CSTFT to Wavelets

Conceptually, the transition from the CSTFT to the wavelet transform may be obtained in two steps, which will provide the WST (wavelet series transform), and a third step is needed to arrive at the CWT.

The first step is replacing the filters in the CSTFT, which are obtained by equally spaced *frequency-shifts* of a unique prototype filter according to (15.8) by the filters

$$h_k(t) = a_0^{-k/2} h_0(a_0^{-k} t) \xrightarrow{\mathcal{F}} H_k(f) = a_0^{k/2} H_0(a_0^k f), \quad (15.9)$$

where $a_0 > 1$, k is an integer, and the factor $a_0^{-k/2}$ is introduced to ensure that the norm $\|h_k\|^2$ is independent of k . With this choice the CSTFT is modified into (see (15.7))

$$\tilde{S}(f_k, \tau) = a_0^{-k/2} e^{-i2\pi f_k \tau} \int_I dt s(t) h_0(a_0^{-k}(\tau - t)). \quad (15.10)$$

The filters (15.9) are also obtained from a single prototype filter $h_0(t)$, $H_0(f)$, but with an exponential *frequency scaling* instead of frequency shifts. Typically, in wavelets the prototype is pass-band, and the scaling with a_0^k allows one to explore *different frequency ranges with different resolution*. In fact, if the extension of $H_0(f)$ is (f_1, f_2) and the bandwidth is $B_0 = f_2 - f_1$, then the extension of $H_0(a_0^k f)$ becomes $(a_0^{-k} f_1, a_0^{-k} f_2)$, and the bandwidth becomes $B_k = a_0^{-k} B_0$. Thus, B_k decreases as k increases, as shown in Fig. 15.7.

The second step regards time localization. Considering that the extension of $h_k(t)$ becomes larger as k increases, we can move the window by a larger step size, by replacing the localization variable τ in the form $na_0^k T_0$, with n integer. Now, the kernel becomes $h_0(a_0^{-k}(\tau - t)) = h_0(nT_0 - a_0^{-k} t)$, and the final form is the wavelet

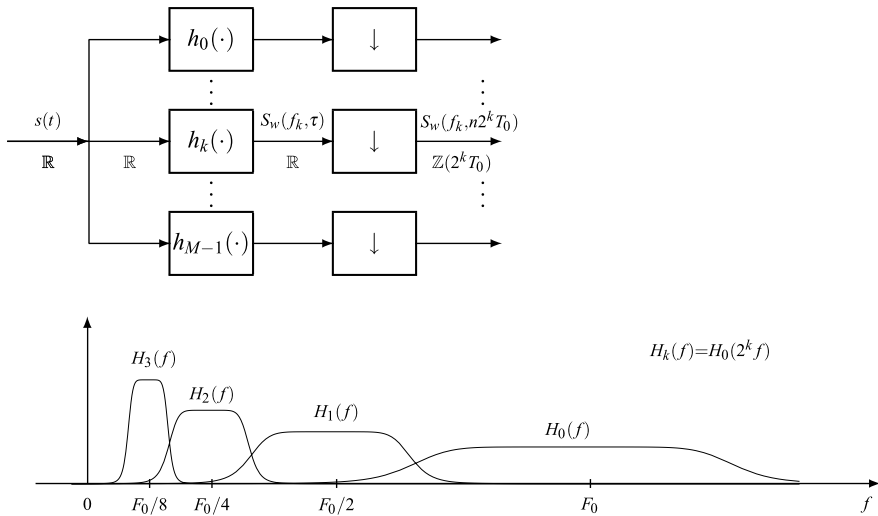


Fig. 15.7 Filter bank producing the WST at the frequencies $f_k = 2^k F_0$. The filters have smaller bandwidth at lower frequencies, and correspondingly the sampling rate is chosen as $1/(2^k T_0)$

series transform (WST)

$$\begin{aligned}
 S_{\text{WST}}(k, nT_0) &= a_0^{-k/2} \int_I dt s(t) h_0(nT_0 - a_0^{-k}t) \\
 &= \int_I dt s(t) h_k(na_0^k T_0 - t), \tag{15.11}
 \end{aligned}$$

where we have omitted the exponential term $e^{-i2\pi f_k \tau}$, which, after the discretization of τ , becomes an irrelevant phasor.

Note that the choice of the step $\tau = na_0^k T_0$ can be also explained as a choice of sampling rate. In fact, the filter $h_k(t)$ has bandwidth $B_k = a_0^{-k} B_0$, and then, according to the Sampling Theorem, if the output of $h_0(t)$ is sampled with spacing T_0 , the output of $h_k(t)$ must be sampled with spacing $a_0^k T_0$.

The Continuous Wavelet Transform We now write the expression of the standard form of the CWT and show that it gives the WST by discretization of the parameters. The CWT has the form

$$S_{\text{wav}}(a, b) = |a|^{-1/2} \int_{\mathbb{R}} dt s(t) \psi^* \left(\frac{t-b}{a} \right), \tag{15.12}$$

where the function $\psi(t)$, $t \in \mathbb{R}$, is called the *mother* wavelet. We can see that the DWT introduced above is obtained from the CWT (15.12) with

$$a = a_0^k, \quad b = na_0^k T_0, \quad \text{and} \quad \psi(t) = h_0^*(-t).$$

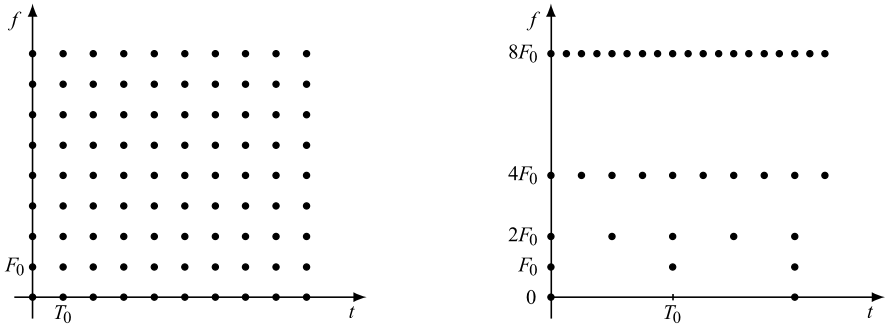


Fig. 15.8 Time-frequency *uniform* grid for the discretization of the STFT and *uniform/exponential* grid for the discretization of the CWT

Time-Frequency Grid Comparison The fundamental difference between STFT and WT may be investigated in the time-frequency grid. In the STFT the time spacing nT_0 and the frequency spacing kF_0 are *uniform*. In the WT, the frequency spacing is smaller at lower frequency according to the law $B_k = a_0^{-k} B_0$ (the bandwidth decreases as k increases), and the time spacing, that is, the sampling period used at the filters output, increases with k according to $a_0^k T_0$, but for a given k , the sampling is uniform according to $na_0^k T_0$. In conclusion, the time-frequency grid is represented by the points (nT_0, kF_0) for the STFT and by the points $(na_0^k T_0, a_0^{-k} F_0)$ for the wavelets, as shown in Fig. 15.8 with $a_0 = 2$.

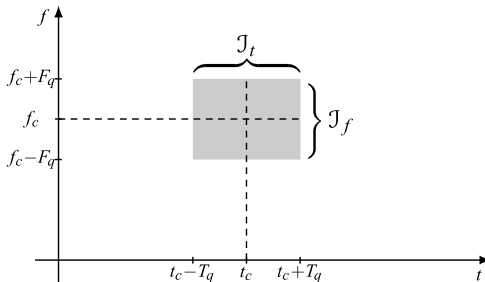
15.3.1 Time-Frequency Representation

In several signal representations, and particularly in multiresolution analysis, the “localization” in time and frequency is of primary importance. There are several ways to define the localization, but all are expressed in terms of the *spread* of the signal behavior in time and frequency, which can be expressed by appropriate definition of *duration* and *bandwidth*.

In particular, for continuous time signals, we have seen in Sect. 9.5 the incompatibility of strict band-limitation and finite durations. To get a quantitative indication, it may be useful to consider the rms duration D_q and the rms bandwidth B_q (see Sect. 9.5). This allows us to define a time interval $\mathcal{J}_t = (t_c - T_q, t_c + T_q)$ and a frequency interval $\mathcal{J}_f = (f_c - B_q, f_c + B_q)$, where t_c and f_c are centroid abscissas of $|s(t)|^2$ and $|S(f)|^2$, respectively. Then, an indication of the spread in the two domains is given by the rectangle $\mathcal{J}_t \times \mathcal{J}_f$ (Fig. 15.9), which is called a *tile* in the time-frequency domain. In Sect. 9.5, it is shown that $B_q D_q \leq 1/(4\pi)$ and that equality holds only for Gaussian pulses.

Another way to introduce a tile $\mathcal{J}_t \times \mathcal{J}_f$ is based on the amplitude or on the energy of $|s(t)|^2$ and $|S(f)|^2$ (see Sect. 13.11). In any case we can determine how the tile is modified by some basic signal operations. Clearly, a time shift of τ results in a

Fig. 15.9 Tile in the (t, f) plane indicating the time and frequency dispersion of a signal



shifting of the tile by τ , and a modulation by $e^{i2\pi f_0 t}$ shifts the tile by f_0 in frequency. As a consequence of a scaling by a , that is, when a signal $s(t)$ is modified as $s(at)$, $a > 0$, and its FT $S(f)$ becomes $(1/a)S(f/a)$, the size $|J_t|$ of the interval J_t becomes $(1/a)|J_t|$, and the size $|J_f|$ of J_f becomes $a|J_f|$. However, the area of the tile does not change, rather the resolution in frequency is traded for resolution in time.

The above considerations are referred to separate representations of the signal $s(t)$ and its FT $S(f)$. In a joint time-frequency representation of a signal, as provided by STFT and wavelet expansion, a signal is analyzed by a family of functions with different localization in the time-frequency domain. Each family of functions identifies a different tiling of the time-frequency domain corresponding to some discretization grid for the time and frequency parameters.

15.4 The Continuous Wavelet Transform (CWT)

Now we formalize the definition of the CWT, previously obtained from the CSTFT.

Let $\psi(t)$, $t \in \mathbb{R}$, be a square-summable function, $\psi \in L_2(\mathbb{R})$, which we assume as a *mother wavelet*. Then, the *wavelets* are obtained by shifting and scaling $\psi(t)$ according to

$$\psi_{a,b}(t) = \frac{1}{\sqrt{|a|}} \psi\left(\frac{t-b}{a}\right), \quad a, b \in \mathbb{R}, \quad a \neq 0. \tag{15.13}$$

In order to define the CWT, the mother wavelet must verify the *admissibility condition*

$$C_\psi = \int_{-\infty}^{+\infty} \frac{|\Psi(f)|^2}{|f|} df < \infty, \tag{15.14}$$

where $\Psi(f)$ is the Fourier transform of $\psi(t)$. We also assume that $\psi(t)$ has unit norm, that is, $\|\psi\| = \|\Psi\| = 1$, which implies that also all the wavelets are normalized: $\|\psi_{a,b}\| = 1$.

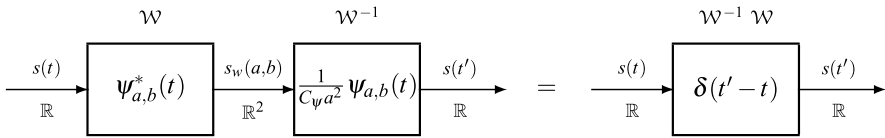


Fig. 15.10 For the proof of the correct recovery of the CWT: the cascade of the CWT and inverse CWT must give the identity

15.4.1 CWT Definition and Inversion Formula

For every signal $s(t) \in L_2(\mathbb{R})$, the CWT is defined as

$$\mathcal{W} \quad S_{\text{wav}}(a, b) = \int_{-\infty}^{+\infty} \psi_{a,b}^*(t) s(t) dt \tag{15.15}$$

and produces a 2D function of the shifting and scaling parameters a, b . Therefore, \mathcal{W} is a linear transformation of the type $\mathbb{R} \rightarrow \mathbb{R}^2$.

The inverse CWT is

$$\mathcal{W}^{-1} \quad s(t) = \frac{1}{C_\psi} \int_{-\infty}^{+\infty} \int_{-\infty}^{+\infty} \psi_{a,b}(t) S_{\text{wav}}(a, b) \frac{da db}{a^2}, \tag{15.16}$$

which defines a linear tf of the type $\mathbb{R}^2 \rightarrow \mathbb{R}$ (Fig. 15.10).

Proof We prove that the cascade on $\mathbb{R} \rightarrow \mathbb{R}^2 \rightarrow \mathbb{R}$ of \mathcal{W} and \mathcal{W}^{-1} gives the identity on $\mathbb{R} \rightarrow \mathbb{R}$. The kernels of \mathcal{W} and \mathcal{W}^{-1} are respectively

$$\begin{aligned} \mathcal{W} \quad h_1(a, b; t) &= \psi_{a,b}^*(t) = \frac{1}{\sqrt{|a|}} \psi^*\left(\frac{t-b}{a}\right), \\ \mathcal{W}^{-1} \quad h_2(t'; a, b) &= \frac{1}{C_\psi a^2} \psi_{a,b}(t) = \frac{1}{C_\psi} \frac{1}{\sqrt{|a|} a^2} \psi\left(\frac{t'-b}{a}\right), \end{aligned}$$

and the kernel of the cascade is

$$\begin{aligned} h_{12}(t', t) &= \int_{-\infty}^{+\infty} da \int_{-\infty}^{+\infty} db h_2(t'; a, b) h_1(a, b; t) \\ &= \frac{1}{C_\psi} \int_{-\infty}^{+\infty} da \frac{1}{|a| a^2} \int_{-\infty}^{+\infty} db \psi\left(\frac{t'-b}{a}\right) \psi^*\left(\frac{t-b}{a}\right) \\ &= \frac{1}{C_\psi} \int_{-\infty}^{+\infty} da \frac{1}{|a|^2} \int_{-\infty}^{+\infty} dc \psi\left(\frac{t'-t}{a} + c\right) \psi^*(c), \end{aligned}$$

where $c = (t - b)/a$, so that $db = -|a| dc$. Now, we introduce the correlation of the mother wavelet and its FT given by

$$k_\psi(\tau) = \int_{-\infty}^{+\infty} dc \psi(c + \tau) \psi^*(c) \xrightarrow{\mathcal{F}} K_\psi(f) = |\Psi(f)|^2,$$

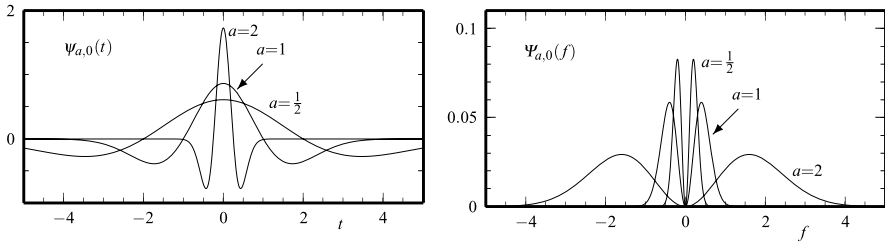


Fig. 15.11 The Mexican hat wavelets $\psi_{a,b}(t)$ and its Fourier transform $\Psi_{a,b}(f)$ for some values of the scale factor a and $b = 0$

and we see that the global kernel can be written in the form

$$h_{12}(t', t) = \frac{1}{C_\psi} \int_{-\infty}^{+\infty} da \frac{1}{|a|^2} k_\psi \left(\frac{t' - t}{a} \right).$$

Hence, we realize that the global cascade is shift-invariant (equivalent to a filter on \mathbb{R}) with impulse response

$$g_{12}(\tau) = \frac{1}{C_\psi} \int_{-\infty}^{+\infty} da \frac{1}{|a|^2} k_\psi \left(\frac{\tau}{a} \right). \tag{15.17}$$

Considering that the FT of $k_\psi(\tau/a)$ is $|a|K_\psi(af)$, the filter frequency response is

$$G_{12}(f) = \frac{1}{C_\psi} \int_{-\infty}^{+\infty} da \frac{1}{|a|} K_\psi(af) = \frac{1}{C_\psi} \int_{-\infty}^{+\infty} da \frac{1}{|a|} |\Psi(af)|^2. \tag{15.18}$$

Finally, with the change of variable $b = af$, we can see that the latter integral is independent of f and given by C_ψ . The conclusion is that $G_{12}(f) = 1$ and the global cascade is the identity. \square

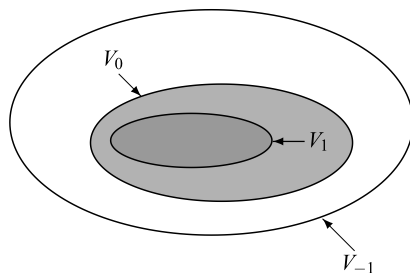
Example: the Mexican Hat Wavelet

An example of a mother wavelet is given by the second derivative of the Gaussian function

$$\psi(t) = A_0 e^{-t^2/2} (1 - t^2) \xrightarrow{\mathcal{F}} \Psi(f) = B_0 e^{-2\pi^2 f^2} f^2, \tag{15.19}$$

sometime called the *Mexican hat function* because it resembles a cross section of a Mexican hat. The constants in (15.19) are obtained by normalization and are given by $A_0 = 23^{1/2} \pi^{-1/4}$ and $B_0 = 8(2/3)^{1/2} \pi^{9/4}$. The Mexican hat wavelet verifies the admissibility condition (15.14) with $C_\psi = (8\sqrt{\pi})/3$. Note that the FT $\Psi(f)$ has two maxima at $f_0 \pm 1/\sqrt{2\pi}$, and in $\Psi_{a,0}(f)$ these maxima move to f_0/a . Figure 15.11 shows the wavelet functions $\psi_{a,b}(t)$ for some values of the scale factor a and $b = 0$.

Fig. 15.12 The nested resolution spaces of multiresolution axioms



15.4.2 Comparison with the CSTFT

We compare the CSTFT, written in the form (15.6), and the CWT given by (15.13). Both transforms represent a 1D signal with a 2D function, which is obtained by taking the *inner product* of the signal $s(t)$ with a family of functions indexed by two labels [4], respectively given by

$$w_{f,\tau}(t) = w(t - \tau)e^{i2\pi ft}, \quad \psi_{a,b}(t) = |a|^{-1/2}\psi\left(\frac{t-b}{a}\right).$$

In the CSTFT the $w_{f,\tau}(t)$ have the same envelope $|w_{f,\tau}(t)| = |w(t - \tau)|$ and the same duration, regardless of the frequency f , and are “filled in” with oscillations due to the exponential. In the CWT the scaling parameter a replaces the role of “inverse” frequency, while the shift b is a localization parameter, as is τ in the CSTFT. The $\psi_{a,b}(t)$ adapt their duration to the frequency: for small $|a|$, that is, for high frequencies, they are narrow; for large $|a|$, that is, for low frequencies, they are broad. This is the ability of wavelets in describing high-frequency behavior (such as transients and discontinuities) of a signal.

15.5 The Axioms of Multiresolution Analysis

The classical approach to multiresolution analysis, pioneered by Mallat [7] and Mayer [9], refers to the class $L_2(\mathbb{R})$ of continuous-time functions subdivided in a nested sequence of subspaces with increasing resolution (Fig. 15.12)

$$\cdots \subset V_2 \subset V_1 \subset V_0 \subset V_{-1} \subset V_{-2} \subset \cdots, \quad (15.20)$$

where V_m is called the *resolution space* at step m (note that resolution increases with decreasing m). In these spaces the bases are constructed starting from a function $\varphi(t) \in V_0$ of unit norm, called *scaling function*, and using two fundamentals operations, *dilation* and *shift*, which deserve a preliminary careful examination. The function $\varphi(t)$ may be in general complex, but it is often chosen to be real.

The *dilation operation* (or scale change, see Sect. 6.5) is obtained by writing $\varphi(at)$, $t \in \mathbb{R}$, $a > 0$, and gives a compression for $a > 1$ and an expansion (or dilation) for $a < 1$. The values of a are discretized in the exponential form $a = a_0^m$,

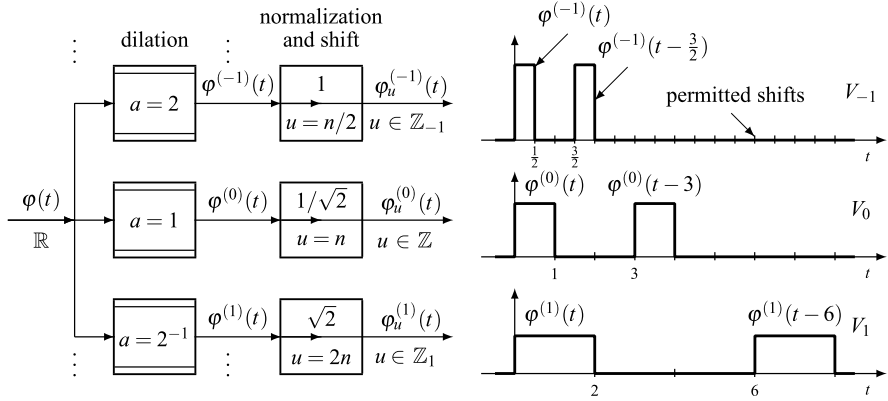


Fig. 15.13 Generation of dilated and shifted functions from a *scaling function* $\varphi(t)$ (in the block representation the scale factors $2^{-m/2}$ are neglected)

$m \in \mathbb{Z}$, where $a_0 > 1$. The typical value of a_0 is 2, and, for concreteness, we will refer to this value. Then, we obtain the functions

$$\varphi^{(m)}(t) \triangleq 2^{-m/2} \varphi(2^{-m}t), \quad t \in \mathbb{R}, \tag{15.21}$$

where the factor $2^{-m/2}$ is introduced to preserve the norm ($\|\varphi\| = 1 \rightarrow \|\varphi^{(m)}\| = 1$). The function $\varphi^{(m)}(t)$ may be regarded as the *scaling function at resolution* V_m .

The *shift operation* has the general form $\varphi(t - \tau)$ with $\tau \in \mathbb{R}$, but in the present context τ is also discretized in the form (see Sect. 15.1) $\tau = b_0 a_0^m = b_0 2^m$. We choose $b_0 = 1$, and thus in V_m the shift τ is limited to be a multiple of 2^m , that is, $\tau \in \mathbb{Z}(2^m)$. Hence, from the scaling function in V_m we obtain the shifted functions

$$\varphi_u^{(m)}(t) \triangleq \varphi^{(m)}(t - u) = 2^{-m/2} \varphi(2^{-m}(t - u)), \quad u \in \mathbb{Z}(2^m). \tag{15.22}$$

These functions are illustrated in Fig. 15.13 with $\varphi(t) = \text{rect}_+(t)$.

In conclusion, starting from a scaling function $\varphi(t) \in V_0$, we obtain the families¹

$$\Phi_m = \{ \varphi_u^{(m)}(t) | u \in \mathbb{Z}_m \} \quad \text{with } \mathbb{Z}_m \triangleq \mathbb{Z}(2^m) \tag{15.23}$$

that form the bases of the spaces V_m . Note that the group \mathbb{Z}_m contains the permitted shifts in V_m .

We are now ready to introduce the axioms. The axioms impose that the sequence of subspaces (15.20) satisfy the following conditions:

¹In the notation $\varphi_u^{(m)}(t)$ the subscript m gives the resolution, and u the shift amount with respect to $\varphi^{(m)}(t)$. In the literature the notation $\varphi_n^{(m)}(t)$, or $\varphi_{mn}(t)$, is used to denote a shifted version of $n2^m$ with respect $\varphi_0^{(m)}(t)$.

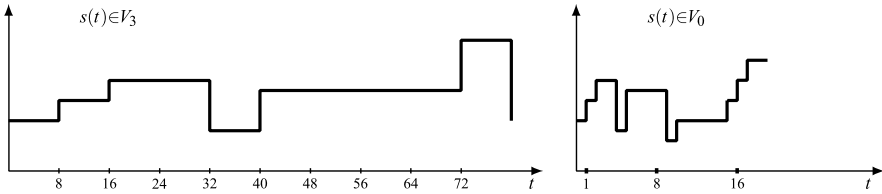


Fig. 15.14 Example of piecewise constant signals over interval of length 2^m for $m = 3$ (space V_3) and $m = 0$ (space V_0). In V_0 the permitted shifts are multiples of 1, and in V_3 they are multiples of $2^3 = 8$

A1 Upward completeness

$$\bigcup_{m \in \mathbb{Z}} V_m = L_2(\mathbb{R}), \tag{15.24}$$

which means that every signal $s(t) \in L_2(\mathbb{R})$ is the limit of its projections, $s_m(t) \in V_m$, onto successively higher-resolution spaces V_{m-1}, V_{m-2}, \dots

A2 Downward completeness

$$\bigcap_{m \in \mathbb{Z}} V_m = \{0\}, \tag{15.25}$$

which means that the projection $s_m(t)$ converges to zero as $m \rightarrow +\infty$.

A3 Scale invariance $s(t) \in V_m \iff s(2^m t) \in V_0$.

Thus, dilating a signal from the reference resolution space V_0 by $a = 2^m$ yields a signal in the resolution space V_m .

A4 Shift invariance $s(t) \in V_0 \implies s(t - n) \in V_0 \forall n \in \mathbb{Z}$.

Combining with A3, it states that in V_m the shift amount of multiples of 2^m does not alter the resolution.

A5 Existence of a basis There exists an orthonormal basis of V_0 of the form

$$\Phi_0 = \{\varphi(t - n) | n \in \mathbb{Z}\}, \tag{15.26}$$

where $\varphi(t)$ is called the *scaling function*.

The orthonormality of the integer shifts of the scaling function, $\varphi(t - n)$, is explicitly written as

$$\int_{-\infty}^{+\infty} \varphi(t - n) \varphi^*(t - n') dt = \delta_{nn'}, \tag{15.27}$$

where $\delta_{nn'}$ is the Kronecker symbol.

An example of spaces V_m is given by piecewise constant signals over the regularly spaced intervals $[i2^m, (i + 1)2^m)$, $i \in \mathbb{Z}$, of length 2^m and with scaling function $\varphi(t) = \text{rect}_+(t)$. Figure 15.14 shows two examples of signals of the resolution spaces V_3 and V_0 .

15.5.1 First Consequences of the Axioms

From the above axioms several properties can be established for the functions introduced in the axioms. Note that the FTs of the functions $\varphi^{(m)}(t)$ and $\varphi_u^{(m)}(t)$ are respectively

$$\Phi^{(m)}(f) = \Phi(2^m f), \quad \Phi_u^{(m)}(f) = \Phi(2^m f)e^{-i2\pi fu}, \quad f \in \mathbb{R}, \quad (15.28)$$

where $\Phi(f)$ is the FT of the scaling function $\varphi(t)$. For the moment, we note the following property, which can be easily proved by a variable change.

Proposition 15.1 *The existence of the basis Φ_0 of V_0 ensures the existence of a basis of V_m given by the family (15.23), that is,*

$$\Phi_m = \{ \varphi_u^{(m)}(t) = \varphi^{(m)}(t - u) | u \in \mathbb{Z}_m \}, \quad (15.29)$$

where $\varphi^{(m)}(t) = 2^{-m/2}\varphi(2^{-m}t)$ is the scaling function in V_m . Since $V_{m-1} \supset V_m$, the basis of V_{m-1} is also a basis of V_m . In particular, the basis Φ_{-1} of V_{-1} is also a basis of V_0 . The orthonormality of the bases Φ_m is obtained from the orthonormality given by (15.27) and can be written in the form

$$\int_{-\infty}^{+\infty} \varphi^{(m)}(t - u)\varphi^{(m)*}(t - u) dt = \delta_{uu'}, \quad u, u' \in \mathbb{Z}_m. \quad (15.30)$$

An important remark for the implementation is:

Proposition 15.2 *The bases Φ_m verify the property of periodic shift invariance (PI) with periodicity $P = \mathbb{Z}_m$.*

In fact, the bases have the structure (14.51) with $B = \{0\}$ and $P = \mathbb{Z}_m$ in agreement with the fact that they are constructed from a single function ($|B| = 1$).

The set $\mathbb{Z}_m = \mathbb{Z}(2^m)$ gives the *admissible shifts* in V_m in the sense that, if $s(t) \in V_m$, then also $s(t - u) \in V_m$ for all $u \in \mathbb{Z}_m$.

15.6 Axiom Interpretation with Symmetry Theory

The multiresolution axioms are conveniently interpreted and developed with the tools of Symmetry Theory introduced at the end of Chap. 4 (see also Sect. 14.5). We now indicate the targets of the wavelet expansion, and then we show how they can be achieved in the framework of Symmetry Theory. In this contest we use the following notation.

\mathcal{P}_m projector onto V_m , \mathcal{R}_m projector onto W_m
 $p_m(t, t')$, $r_m(t, t')$ kernels of \mathcal{P}_m and \mathcal{R}_m

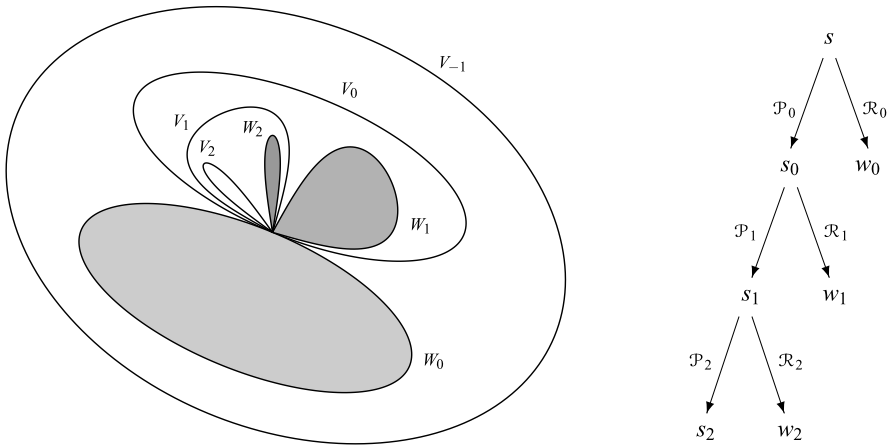


Fig. 15.15 Decomposition of resolution spaces by projectors \mathcal{P}_m and \mathcal{R}_m that give the components as $s_m = \mathcal{P}_m[s_{m-1}]$ and $w_m = \mathcal{R}_m[s_{m-1}]$, and the orthogonal subspaces as $V_m = \sigma(\mathcal{P}_m)$, $W_m = \sigma(\mathcal{R}_m)$

- $\mathcal{C}_m, \mathcal{E}_m$ compressor (decimator) and expander (interpolator) of \mathcal{P}_m
- c_m, e_m impulse responses of \mathcal{C}_m and \mathcal{E}_m
- $\mathcal{D}_m, \mathcal{F}_m$ compressor (decimator) and expander (interpolator) of \mathcal{R}_m
- d_m, f_m impulse responses of \mathcal{D}_m and \mathcal{F}_m

15.6.1 Target I: Decomposition into Symmetric Components

Consider as reference the resolution space V_{-1} and its subspace V_0 . The space V_{-1} can be written as the direct sum

$$V_{-1} = V_0 \oplus W_0, \tag{15.31}$$

where W_0 is the orthogonal complement of V_0 in V_{-1} . A signal $s(t) \in V_{-1}$ has the unique decomposition

$$s(t) = s_0(t) + w_0(t),$$

where $s_0 \in V_0$, $w_0 \in W_0$, and $s_0 \perp w_0$. This is step 0 (Fig. 15.15).

In step 1 the decomposition becomes

$$V_0 = V_1 \oplus W_1 \quad \longrightarrow \quad s_0(t) = s_1(t) + w_1(t),$$

where W_1 is the orthogonal complement of V_1 in V_0 and $s_1 \perp w_1$. In this step also the space W_0 could be decomposed, but the decomposition is conveniently limited to the subspaces V_m . Thus, in step 2 we get $V_1 = V_2 \oplus W_2$ and $s_1(t) = s_2(t) + w_2(t)$, and in the general step m

$$V_{m-1} = V_m \oplus W_m \quad \longrightarrow \quad s_{m-1}(t) = s_m(t) + w_m(t). \tag{15.32}$$

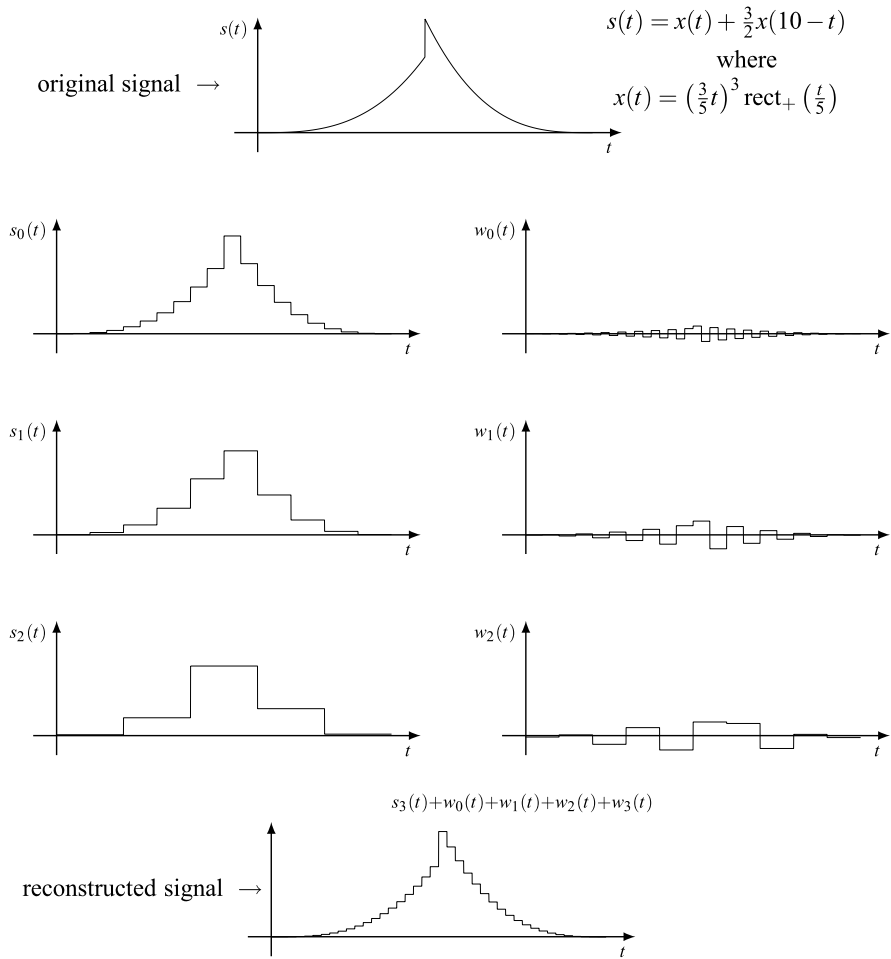


Fig. 15.16 Decomposition of a (discontinuous) signal with the Haar wavelet. After three steps of iteration the reconstructed signal is $s_2(t) + w_0(t) + w_1(t) + w_2(t)$

Hence, a signal $s(t)$ at resolution V_{-1} is decomposed into the form

$$\begin{aligned}
 s(t) &= w_0(t) + s_0(t) && \text{step 0} \\
 &= w_0(t) + w_1(t) + s_1(t) && \text{step 1} \\
 &= w_0(t) + w_1(t) + w_2(t) + s_2(t) && \text{step 2} \\
 &\vdots && \vdots
 \end{aligned}
 \tag{15.33}$$

Figure 15.16 illustrates the decomposition of a signal obtained with the Haar wavelets and the reconstruction after three steps of iterations.

If in the step m the contribution of $s_m(t)$ is negligible, we obtain the decomposition of $s(t)$ into m components

$$s(t) \approx w_0(t) + w_1(t) + \cdots + w_m(t). \quad (15.34)$$

By taking the limit as $m \rightarrow \infty$ and using axioms A1 and A2 on completeness, we can write the class of square-summable signals on \mathbb{R} as the *direct sum* of the spaces W_m , symbolized by

$$L_2(\mathbb{R}) = \bigoplus_{m \in \mathbb{Z}} W_m.$$

At this point we introduce the interpretation of the decomposition with the Symmetry Theory, where the subspaces V_m and W_m become *symmetries obtained by projectors*. Specifically, at step m we have a system of two *binary projectors* \mathcal{P}_m and \mathcal{R}_m that are operators with the properties

$$\mathcal{P}_m^2 = \mathcal{P}_m, \quad \mathcal{R}_m^2 = \mathcal{R}_m, \quad \mathcal{P}_m \mathcal{R}_m = 0. \quad (15.35)$$

The subspaces (symmetries) are given by the images of the projectors, symbolized in the forms

$$V_m = \text{im}(\mathcal{P}_m) = \sigma(\mathcal{P}_m), \quad W_m = \text{im}(\mathcal{R}_m) = \sigma(\mathcal{R}_m), \quad (15.36)$$

and the components are obtained from application of the projectors

$$s_m = \mathcal{P}_m[s_{m-1}], \quad w_m = \mathcal{R}_m[s_{m-1}]. \quad (15.37)$$

The recurrence (15.32) becomes for projectors

$$\mathcal{P}_m + \mathcal{R}_m = \mathcal{P}_{m-1}. \quad (15.38)$$

We shall see that the projectors are *Hermitian*, and this ensures that the components s_m and w_m are *orthogonal* and that W_m is the *orthogonal* complement of V_m in V_{m-1} (see Proposition 4.9).

In conclusion, the decomposition is interpreted as a *decomposition into symmetric components*,² and the tools to achieve the decomposition are provided by projectors. In the next sections we will obtain these specific projectors from multiresolution axioms.

²We recall that in our theory “symmetry” is a subspace consisting of “symmetric” signals. Hence, V_m and W_m are symmetries consisting of signals that have the properties $s_m = \mathcal{P}_m[s_m] \in V_m$ and $w_m = \mathcal{R}_m[s_m] \in W_m$, respectively.

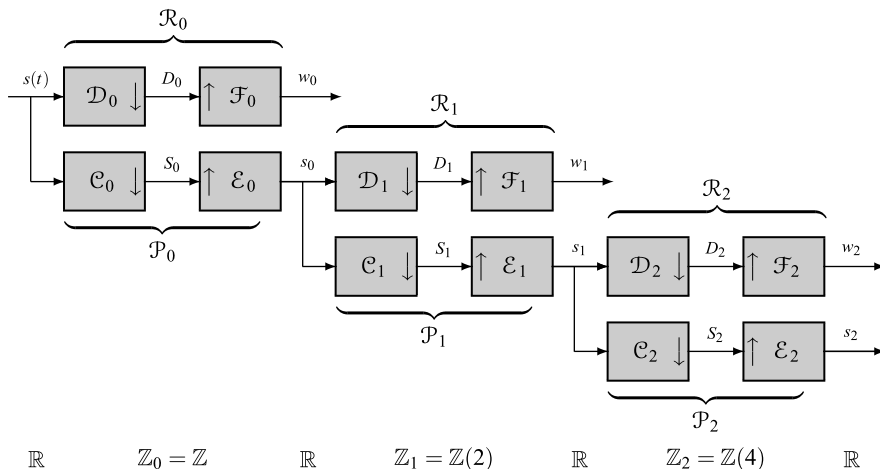


Fig. 15.17 Tree architecture for wavelet generation with intermediate discretizations

15.6.2 Target II: Intermediate Discretization

In the above decomposition the signals are continuous-time, but practical DSP cannot deal with continuous-time signals, and we have to search for an efficient discrete time solution, where signals are represented by their expansion coefficients.

To this end, we can use the *projector separability* discussed in Sect. 14.5, where relations (15.37) are split in the form

$$\begin{aligned}
 S_m &= \mathcal{C}_m[s_{m-1}], & s_m &= \mathcal{E}_m[S_m], \\
 D_m &= \mathcal{D}_m[s_{m-1}], & w_m &= \mathcal{F}_m[D_m],
 \end{aligned}
 \tag{15.39}$$

with $\mathcal{C}_m, \mathcal{D}_m$ compressors and $\mathcal{E}_m, \mathcal{F}_m$ expanders. In this specific case the separability leads to a very efficient solution, since the bases have the property of periodic invariance (PI). Then, according to Corollary 14.2, the compressors \mathcal{C}_m represent $\mathbb{R} \rightarrow \mathbb{Z}_m$ decimators, and the expanders \mathcal{E}_m represent $\mathbb{Z}_m \rightarrow \mathbb{R}$ interpolators. This allows us to reach the discrete domains \mathbb{Z}_m . In (15.39) the D_m are called the *detail* or the *wavelet coefficients*, and the S_m the *scaling coefficients*.

This idea is illustrated in Fig. 15.17, where the projector separability is applied to the tree of Fig. 15.15. Starting from the signal $s(t), t \in \mathbb{R}$, the compressor/decimator \mathcal{D}_0 gives the discrete signal $D_0(u), u \in \mathbb{Z}$, and then the expander/interpolator \mathcal{F}_0 produces the component $w_0(t), t \in \mathbb{R}$. Analogously, \mathcal{C}_0 gives $S_0(u), u \in \mathbb{Z}$, and \mathcal{E}_0 produces $s_1(t), t \in \mathbb{R}$. Then, $s_0(t)$ is processed in a similar way, and the iteration proceeds. Note that the signals $D_m(u)$ and $S_m(u)$ convey the coefficients of the corresponding components.

An intermediate discretization step is shown in Fig. 15.18 with the decomposition of Fig. 15.16, where the compressor \mathcal{D}_1 , with input the continuous component $s_0(t)$, gives the discrete signal $D_1(2n), 2n \in \mathbb{Z}(2)$, and then the expander \mathcal{F}_1 gives the continuous component $w_1(t)$.

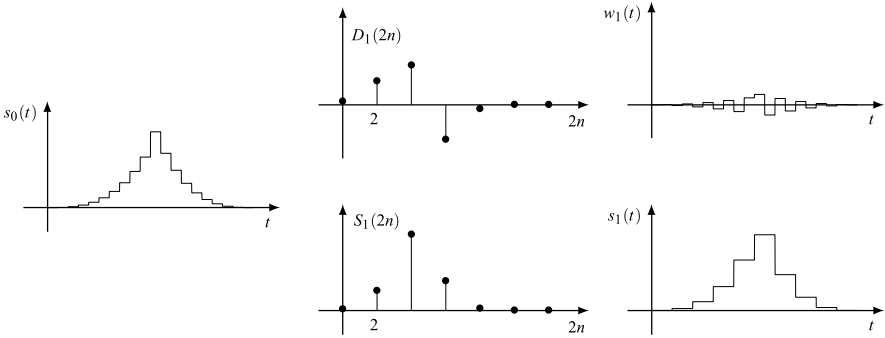


Fig. 15.18 Intermediate *discretization* in wavelet decomposition: from the component $s_1(t)$ the coefficients $D_1(2n)$ and $S_1(2n)$ are obtained and then the new components $w_2(t)$ and $s_2(t)$ are obtained from the coefficients

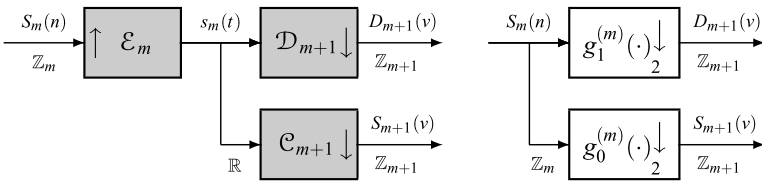


Fig. 15.19 Architectures for evaluation of wavelet coefficients combining step m and step $m + 1$

Inspection of Fig. 15.17 shows that the decomposition is still performed on continuous time, although the intermediate domains are discrete. In fact, both $\mathbb{R} \rightarrow \mathbb{Z}_m$ decimators and $\mathbb{Z}_m \rightarrow \mathbb{R}$ interpolators make the signal processing on continuous time, as we can see considering that the inner filters of these components work on \mathbb{R} (in Fig. 15.17 and in the following figures, the blocks working on continuous time are filled with gray).

15.6.3 Target III: Complete Discretization

The final target is a complete discretization of the decomposition, and this is achieved by considering the direct relation between the wavelet coefficients at adjacent levels. We will find a surprising and fortunate relationship, which was discovered by Mallat [7] and Daubechies [4]. The link between the coefficients at adjacent levels is given by an interpolator followed by two decimators and is equivalent to two discrete decimators, as shown in Fig. 15.19 (see Proposition 15.6 for the details). More specifically, in steps m and $m + 1$, both the cascade $\mathcal{E}_m, \mathcal{D}_{m+1}$ and the cascade $\mathcal{E}_m, \mathcal{C}_{m+1}$ are equivalent to $\mathbb{Z}_m \rightarrow \mathbb{Z}_{m+1}$ decimators, say $g_1^{(m)}$ and $g_0^{(m)}$. In other words, this part of the scheme can be implemented by the Analysis side of a two-channel subband decomposition (see Sect. 14.12). This allows a full discretiza-

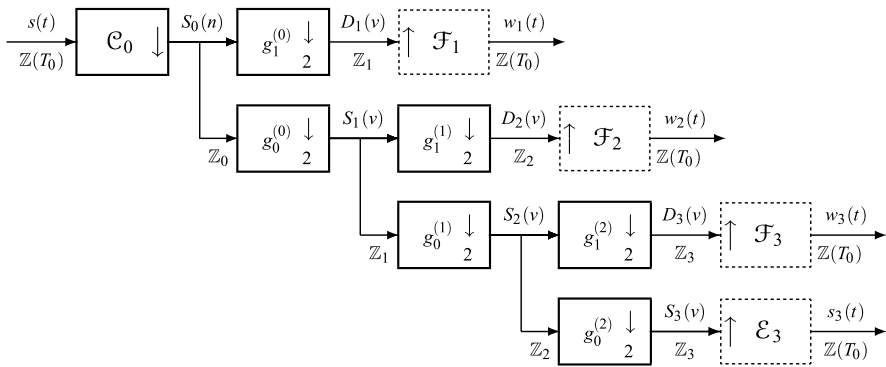


Fig. 15.20 Discrete version of Mallat’s algorithm for evaluation of wavelet coefficients. The first continuous-time block is replaced by a discrete-time block

tion of the tree *as far as the expansion coefficients are concerned*, but in practice the interest is just confined to the coefficients.

For instance, the coefficients $D_1(u)$ and $S_1(u)$ in the decomposition of Fig. 15.16 can be obtained from the coefficients $S_0(n)$ by a filter bank without the intermediate evaluation of the continuous signal $s_0(t)$.

Considering that the coefficients at adjacent steps are evaluated through two-channel filter banks, the original iteration procedure of Fig. 15.17 can be implemented with the tree architecture of Fig. 15.20, where the coefficients $D_m(u)$ of the projection onto W_m are obtained by filtering and down-sampling by 2 the coefficients $S_{m-1}(u)$ of the projection onto V_{m-1} . Thus, starting from the coefficients $S_0(n)$, the implementation is based on a *purely discrete-time* algorithm. In principle, at each step, the continuous-time wavelets $w_m(u)$ could be evaluated from the coefficients $D_m(u)$, but in practice this operation is only conceptual (represented with a dashed box in the block diagram of Fig. 15.20).

In this scheme the only processing over continuous time is in the initial step, where the coefficients $S_0(n) = \langle s, \varphi_n \rangle$ are given by the inner products of the input signal $s(t)$ with the functions $\varphi(t - n)$, that is, by the compressor \mathcal{C}_0 . However, if the reference space V_0 corresponds to a sufficiently fine resolution compared to the resolution of the input signal $s(t)$, then sampling in the form

$$S_0(n) = \langle s, \varphi_n \rangle \simeq s(n)$$

will be sufficient. The reason is that $\varphi(t)$ is a low-pass signal with unit area (see [14] and examples). If V_0 is not fine enough, we can start with an higher-resolution space V_{-m_0} , with m_0 sufficiently large to meet the required accuracy.

15.7 Projectors from the Axioms

For the application of the above procedure to a specific case, one has to know the projectors \mathcal{P}_m and \mathcal{R}_m at each step. In fact, from \mathcal{P}_m and \mathcal{R}_m one gets

- (1) the compressors (decimators) and the expanders (interpolators) that will be specified by impulse responses;
- (2) the decimators of the final discrete implementation, whose impulse responses are obtained as a combination of the previous ones.

In this section we identify the projectors from the axioms, whereas the detailed expression of decimators and interpolators will be seen in the next sections.

15.7.1 The Projectors in the Resolution Spaces V_m

We recall that a projector on a space V_m can be identified by an orthogonal basis (see Theorem 14.1 and Corollary 14.1). Now, the axioms ensure the existence of an orthonormal basis Φ_0 of $V_0 = \sigma(\mathcal{P}_0)$, which is identified by the scaling function $\varphi(t)$. Then, once a scaling function $\varphi(t)$ is chosen, we can evaluate the projector \mathcal{P}_0 . But $\varphi(t)$ identifies also the bases Φ_m of the subspaces $V_m = \sigma(\mathcal{P}_m)$ (see Proposition 15.1). In such a way we identify all the projectors \mathcal{P}_m from the scaling function $\varphi(t)$.

To obtain the expression of kernels $p_m(t, u)$ of the projectors \mathcal{P}_m from the bases

$$\Phi_m = \{ \varphi^{(m)}(t - u) = 2^{-m/2} \varphi(2^{-m}(t - u)) \mid u \in \mathbb{Z}_m \}, \tag{15.40}$$

we have to recall that: (1) the Φ_m verify the PI property with periodicity $P = \mathbb{Z}_m$ (see Proposition 15.2), and (2) they are orthonormal. Then the application of Corollary 14.1 gives the following expression:

$$\mathcal{P}_m \quad h_m(t, t') = \sum_{p \in \mathbb{Z}_m} \varphi^{(m)}(t - p) \varphi^{(m)*}(t' - p). \tag{15.41}$$

In conclusion, the projector \mathcal{P}_m are directly identified from the axioms, and their explicit formula is available as soon as a scaling function has been chosen.

15.7.2 The Projectors \mathcal{R}_m in the Orthogonal Subspaces W_m

In principle, to identify the projectors \mathcal{R}_m , we can use the recurrence (15.38), that is,

$$\mathcal{P}_{m-1} = \mathcal{P}_m + \mathcal{R}_m, \tag{15.42}$$

which gives \mathcal{R}_m from \mathcal{P}_m and \mathcal{P}_{m-1} . More explicitly, one can use the recurrence for the corresponding kernels, $p_{m-1}(t, t') = p_m(t, t') + r_m(t, t')$, where $r_m(t, t')$ is the kernel of \mathcal{R}_m . But, for the next developments, we need to identify the bases Ψ_m (a basis identifies a projector, but not the converse).

On the other hand, the Ψ_m should have the scaling properties established by the axioms. This is a crucial (and not easy) problem of wavelet theory: one has to find

a function $\psi(t)$, which will be called *mother wavelet*, such that its integer translates $\psi(t - n)$ form a basis Ψ_0 of W_0 . Then, from the mother wavelet $\psi(t)$ we form the families of *wavelets*

$$\Psi_m = \{ \psi^{(m)}(t - u) = 2^{-m/2} \psi(2^{-m}(t - u)) \mid u \in \mathbb{Z}_m \}$$

exactly as we have seen in the construction of the bases Φ_m from the scaling function $\varphi(t)$ (see (15.21) and (15.23)). The families Ψ_m represent the bases of the subspaces W_m and have the same properties (orthonormality and PI) as the bases Φ_m . Then the expression of the kernels are given by

$$\mathcal{R}_m \quad r_m(t, t') = \sum_{p \in \mathbb{Z}_m} \psi^{(m)}(t - p) \psi^{(m)*}(t' - p). \quad (15.43)$$

15.7.3 Concluding Remarks

We refine the above results noting that, by construction, the bases Φ_m and Ψ_m are also orthogonal to each other, that is, $\varphi_u^{(m)} \perp \varphi_v^{(m)}$ for $u \neq v$ (see Proposition 15.5). This leads to the orthogonality of the projectors, which means $\mathcal{P}_m \mathcal{R}_m = 0$ (see Sect. 4.13, in particular (4.108) and (4.109)).

Proposition 15.3 *The bases Φ_m and Ψ_m identify a system of binary projectors $\{\mathcal{P}_m, \mathcal{R}_m\}$ with the properties (15.35). The two projectors are Hermitian; this ensures the orthogonality of the projections $s_m = \mathcal{P}_m[s]$ and $w_m = \mathcal{R}_m[s]$.*

In conclusion, we start from a scaling function, and we evaluate the mother wavelet. Then, we can obtain all the projectors and operators necessary for the implementation of the wavelet decomposition. This will be seen in detail in the next sections.

Organization of the Following Sections

In the next section we consider the problem of the identification of the mother wavelet $\psi(t)$ from a given scaling function $\varphi(t)$. Then, we have the bases Φ_m and Ψ_m of the subspaces V_m and W_m . We shall see the fundamental role played by the Fourier coefficients of the functions $\varphi(t)$ and $\psi(t)$, which identify a *two-channel filter bank*. In Sect. 15.9 from the bases we obtain the expressions of the projectors in terms of their kernels, and of the decimators and interpolators in terms of their impulse responses. In Sect. 15.10 we consider the complete discretization of the decomposition obtained by combining the interpolators and decimators at adjacent steps, and we will discover that this combination is just given by the two-channel filter bank mentioned above. In Sect. 15.11 we transfer the study in the frequency domain, where we can find scaling functions and mother wavelets with interesting properties.

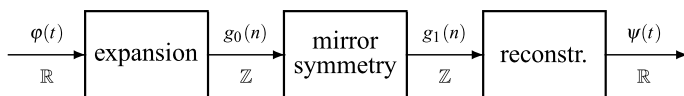


Fig. 15.21 How the mother wavelet $\psi(t)$ is obtained from the scaling function $\varphi(t)$

15.8 Evaluation of Wavelets from Scaling Function

For a given scaling function $\varphi(t)$, following the axioms, it is possible to identify a *mother* wavelet $\psi(t)$, which generates a wavelet family Ψ_0 by the operations of dilation and shifting, exactly in the same way as $\varphi(t)$ generates Φ_0 . The identification³ can be carried out in three steps, as shown in Fig. 15.21:

- (1) We expand the scaling function $\varphi(t) \in V_0$ using the basis Φ_{-1} of V_{-1} . The expansion coefficients $g_0(n)$, $n \in \mathbb{Z}$, identify a filter on \mathbb{Z} .
- (2) We use the mirror symmetry QMF (see Sect. 14.12) to define a companion filter, namely

$$g_1(n) = (-1)^n g_0^*(-(n - 1)) \xrightarrow{\mathcal{F}} G_1(f) = -e^{-i2\pi f} G_0^*\left(f + \frac{1}{2}\right). \tag{15.44}$$

- (3) The filter coefficients $g_1(n)$, $n \in \mathbb{Z}$, interpreted as expansion coefficients of the basis Ψ_{-1} , identify the mother wavelet $\psi(t)$.

We now develop step (1) and step (3). By Proposition 15.1, the scaling function $\varphi(t) \in V_0$ can be expanded by the basis Φ_{-1} of V_{-1} , whose functions are

$$\varphi_{n/2}^{(-1)}(t) = \varphi^{(-1)}(t - n/2) = \sqrt{2}\varphi(2t - n), \quad n \in \mathbb{Z}. \tag{15.45}$$

The explicit expansion is

$$\varphi(t) = \sum_{n=-\infty}^{+\infty} g_0(n)\varphi_{n/2}^{(-1)}(t) = \sum_{n=-\infty}^{+\infty} \sqrt{2}\varphi(2t - n)g_0(n), \tag{15.46a}$$

where the expansion coefficients $g_0(n)$, $n \in \mathbb{Z}$, are given by

$$g_0(n) = \langle \varphi, \varphi_{n/2}^{(-1)} \rangle = \int_{-\infty}^{+\infty} \sqrt{2}\varphi(t)\varphi^*(2t - n) dt. \tag{15.46b}$$

Relation (15.46a) links the scaling function at two scales and is called the *two-scale relation*.

³The line followed here for the identification of the mother wavelet $\psi(t)$ starting from the scaling function $\varphi(t)$ is due to Taubman and Marcellin [12]. Other authors, e.g., Daubechies [4] and Vetterli and Kovačević [14] identify $\psi(t)$ by imposing the desired cross properties with $\varphi(t)$.

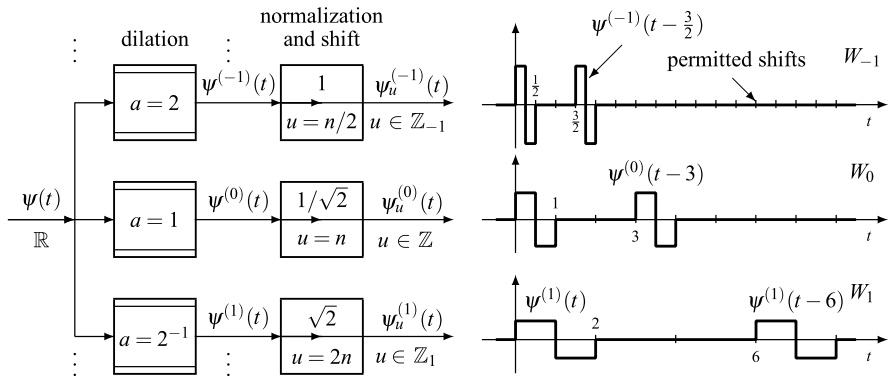


Fig. 15.22 Generation of dilated and shifted functions from the mother wavelet $\psi(t)$ (in the block generation the scale factors $2^{-m/2}$ are neglected)

Now, according to step (3), the mother wavelet $\psi(t)$ is given by the series expansion with the basis Φ_{-1} obtained with the coefficients $g_1(n)$,

$$\psi(t) = \sum_{n=-\infty}^{+\infty} g_1(n)\varphi_{n/2}^{(-1)}(t) = \sum_{n=-\infty}^{+\infty} \sqrt{2}\varphi(2t - n)g_1(n). \tag{15.47}$$

Starting from the mother wavelet $\psi(t)$, we can construct by dilation and shift the functions (wavelets) (Fig. 15.22):

$$\psi^{(m)}(t) = 2^{-m/2}\psi(2^{-m}t), \quad \psi_u^{(m)}(t) = \psi^{(m)}(t - u), \quad u \in \mathbb{Z}_m. \tag{15.48}$$

Hence, at each resolution m , one has the family

$$\Psi_m = \{ \psi^{(m)}(t - u) \mid u \in \mathbb{Z}_m \} \tag{15.49}$$

exactly in the same way we have seen in (15.21) and (15.22) for the scaling function $\varphi(t)$. Figure 15.22 gives examples of the functions $\psi_u^{(m)}(t)$ obtained with the mother wavelet $\psi(t) = \text{rect}_+(2t) - \text{rect}_+(2t - 1)$ of the Haar decomposition.

Example 15.1 (Haar wavelets) We have seen that the scaling function

$$\varphi(t) = \text{rect}_+(t), \quad t \in \mathbb{R},$$

generates, by dilation and shifts, the bases Φ_m of the piecewise constant signals over the intervals $[i2^m, (i + 1)2^m]$, $i \in \mathbb{Z}$ (see Figs. 15.13 and 15.14). In particular, the basis Φ_{-1} is given by $\{\varphi_u^{(-1)}(t) = \varphi^{(-1)}(t - u) = 2^{-1/2} \text{rect}_+(2t - n) \mid u \in \mathbb{Z}_{-1}\}$. The expansion coefficients of $\varphi(t)$ with respect to Φ_{-1} are (see (15.46b))

$$g_0(n) = \int_{-\infty}^{+\infty} \sqrt{2} \text{rect}_+(t) \text{rect}_+(2t - n) dt = \begin{cases} 1/\sqrt{2}, & n = 0, 1, \\ 0 & \text{otherwise.} \end{cases}$$

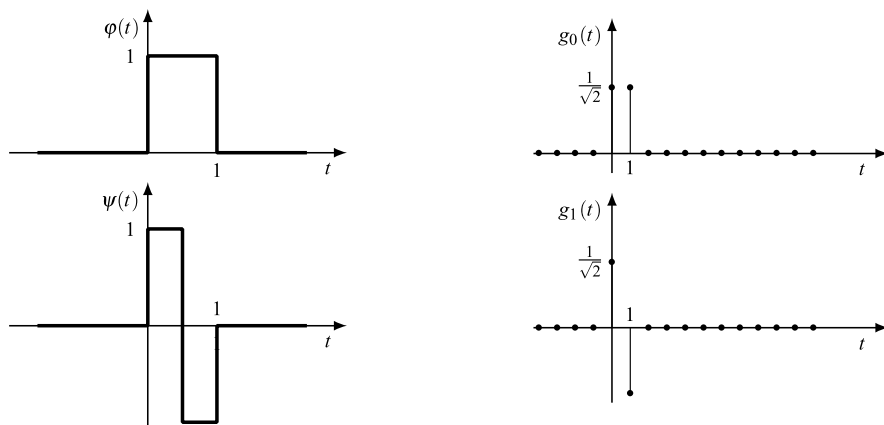


Fig. 15.23 Haar scaling function and mother wavelet and corresponding expansion coefficients

The coefficients of the companion filter, given by (15.44), result in

$$g_1(n) = (-1)^n g_0(-(n - 1)) = \begin{cases} 1/\sqrt{2}, & n = 0, \\ -1/\sqrt{2}, & n = 1, \\ 0 & \text{otherwise.} \end{cases}$$

Hence, from (15.47) we obtain the mother wavelet

$$\psi(t) = \varphi(2t) - \varphi(2t - 1) = \text{rect}_+(2t) - \text{rect}_+(2t - 1). \tag{15.50}$$

The functions $\varphi(t)$ and $\psi(t)$ and the corresponding expansion coefficients are illustrated in Fig. 15.23.

15.8.1 Properties of Coefficients $g_0(n)$ and $g_1(n)$

The pair $g_0(n), g_1(n)$ identifies the Synthesis of a two-channel filter bank with the properties established in Sect. 14.12. These properties guarantee that the wavelet family will have the desired properties. Remarkable is the fact that, again, the wavelets generation turns out to be well anchored to the theory of filter banks.

From the coefficients we introduce the families of functions of $L_2(\mathbb{Z})$

$$\mathbf{G}_0 = \{g_0(n - 2k) \mid k \in \mathbb{Z}\}, \quad \mathbf{G}_1 = \{g_1(n - 2k) \mid k \in \mathbb{Z}\}. \tag{15.51}$$

Proposition 15.4 *The families \mathbf{G}_0 and \mathbf{G}_1 consist of orthonormal functions, that is,*

$$\sum_{n \in \mathbb{Z}} g_0(n) g_0^*(n - 2k) = \delta_{k0}, \quad \sum_{n \in \mathbb{Z}} g_1(n) g_1^*(n - 2k) = \delta_{k0}. \tag{15.52}$$

Moreover, the families are orthogonal, $\mathbf{G}_0 \perp \mathbf{G}_1$, that is,

$$\sum_n g_0(n - 2h)g_1^*(n - 2k) = 0, \quad h, k \in \mathbb{Z}. \tag{15.53}$$

Proof We use the two-scale relation of $\varphi(t)$ given by (15.46a) in (15.27). Then,

$$\begin{aligned} \delta(k) &= \int_{-\infty}^{+\infty} \varphi(t)\varphi^*(t - k) dt \\ &= \sum_n \sum_{n'} g_0^*(n)g_0(n') \int_{-\infty}^{+\infty} \varphi_{n/2}^{(-1)}(t)\varphi_{n'/2}^{(-1)*}(t - k) dt, \end{aligned}$$

where $\varphi_{n'/2}^{(-1)}(t - k) = \varphi^{(-1)}(t - n'/2 - k) = \varphi_{n'/2-k}(t)$. Hence, by the orthonormality of the functions of $\varphi_{n/2}^{(-1)}(t)$, $n \in \mathbb{Z}$, the integral is 1 for $n = n' - 2k$ and zero otherwise, and the first of (15.52) follows. The second of (15.52) and (15.53) follow from the QMF definition (15.44). \square

As discussed in Sect. 14.12, Proposition 15.4 and (15.44) state exactly the conditions required to define a two-channel orthonormal subband transform.

15.8.2 Properties of the Wavelets

The properties of the families \mathbf{G}_0 and \mathbf{G}_1 , obtained by 2-translates of the coefficients $g_0(n)$ and $g_1(n)$, allow us to establish several properties for the wavelet family Ψ_0 and cross properties with Φ_0 .

Proposition 15.5 *The family $\Psi_0 = \{\psi_n(t) = \psi(t - n) | n \in \mathbb{Z}\}$ consists of orthonormal functions of V_{-1} , and $\text{span}(\Psi_0) = W_0$. Moreover, Ψ_0 is an orthonormal basis for W_0 , and Φ_0 is an orthonormal basis for V_0 .*

Moreover, the two families are orthogonal, $\Phi_0 \perp \Psi_0$.

Proof We want to prove that $\langle \psi_0, \psi_k \rangle = \delta(k)$. Using (15.47), we have

$$\begin{aligned} \langle \psi_0, \psi_k \rangle &= \int_{-\infty}^{+\infty} \sum_n g_1(n)\varphi_{n/2}^{(-1)}(t) \sum_{n'} g_1^*(n')\varphi_{n'/2}^{(-1)*}(t - k) dt \\ &= \sum_n \sum_{n'} g_1(n)g_1^*(n') \int_{-\infty}^{+\infty} \varphi_{n/2}^{(-1)}(t)\varphi_{n'/2}^{(-1)*}(t - k) dt, \end{aligned}$$

where $\varphi_{n'/2}^{(-1)}(t - k) = \varphi^{(-1)}(t - n'/2 - k) = \varphi_{n'/2-k}^{(-1)}(t)$, and the integral yields $\delta(n - n' - 2k)$. Hence, using (15.53),

$$\langle \psi_0, \psi_k \rangle = \sum_n g_1(n)g_1^*(n - 2k) = \delta_{k0}.$$

To prove that $\text{span}(\Psi_0) = W_0$, one has to prove that any function $w(t) \in W_0$ can be written as a linear combination of the functions of Ψ_0 . This proof is omitted here and can be found in [4, pp. 134–135] (see also [14, p. 219]).

The orthogonality $\Phi_0 \perp \Psi_0$ is a consequence of the orthogonality $\mathbf{G}_0 \perp \mathbf{G}_1$ (see Problem 15.2). □

Now, from the axioms we have $\text{span}(\Phi_0) = V_0$, and from the above proposition we have $\text{span}(\Psi_0) = W_0$ and $\Phi_0 \perp \Psi_0$. The consequence is that the subspaces V_0 and W_0 are orthogonal, $V_0 \perp W_0$. It can be also proved that the bases Φ_0 and Ψ_0 together span V_{-1} , that is, every $s(t) \in V_{-1}$ can be written as a linear combination of $\varphi_n(t)$ and $\psi_n(t)$ [14]. This permits to conclude that

$$V_0 \oplus W_0 = V_{-1}, \tag{15.54}$$

that is, W_0 is the *orthogonal complement of V_0 in V_{-1}* .

The conclusion seen for the reference subspaces V_0 and W_0 holds for all degrees of resolution. In fact, using the axioms, we can prove that [14]:

- (1) the family $\Psi_m = \{\psi_u^{(m)}(t) | u \in \mathbb{Z}_m\}$ is a basis,
- (2) $V_m \perp W_m$, and W_m is the orthogonal complement of V_m in V_{m-1} , and
- (3) the bases Ψ_m and $\Phi_{m'}$ are orthogonal, that is,

$$\langle \psi_u^{(m)}, \varphi_{u'}^{(m')} \rangle = \delta_{m'm} \delta_{u'u}, \quad m, m' \in \mathbb{Z}, \quad u, u' \in \mathbb{Z}_m \tag{15.55}$$

(orthogonality across scales and with respect to shifts).

15.9 Evaluation of Decimators and Interpolators

From the orthonormal bases Φ_m and Ψ_m we obtain the projectors \mathcal{P}_m and \mathcal{R}_m , and now we consider their synthesis. To this end, we could use the general results of the previous chapter (see Corollaries 14.1 and 14.2), but here the synthesis is obtained directly. The essential property is that the bases verify the condition of PI, as stated by Proposition 15.2 for the bases Φ_m and could be established for the bases Ψ_m .

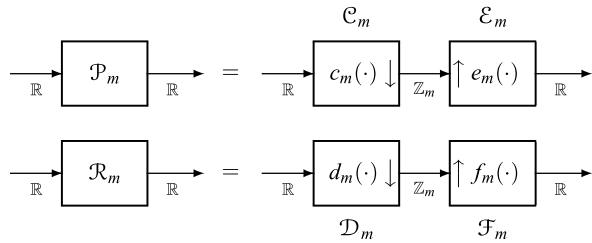
15.9.1 Impulse Responses

We show that the projectors are equivalent to the cascade of a decimator followed by an interpolator, considering explicitly the expansion and the reconstruction in (15.39), namely

$$S_m(u) = \langle s_{m-1}(\cdot), \varphi^{(m)}(\cdot - u) \rangle = \int_{\mathbb{R}} dt s_{m-1}(t) \varphi^{(m)*}(t - u), \quad u \in \mathbb{Z}_m, \tag{15.56}$$

$$s_m(t) = \sum_{u \in \mathbb{Z}_m} S_m(u) \varphi^{(m)}(t - u), \quad t \in \mathbb{R}.$$

Fig. 15.24 Synthesis of the projectors \mathcal{P}_m and \mathcal{R}_m at step m



Now, to identify the nature of these transformations, we write the relations of an $\mathbb{R} \rightarrow \mathbb{Z}_m$ decimator and of a $\mathbb{Z}_m \rightarrow \mathbb{R}$ interpolator with the same inputs and outputs as in (15.56), namely

$$\begin{aligned}
 S_m(u) &= \int_{\mathbb{R}} dt c_m(u-t) s_{m-1}(t), \quad u \in \mathbb{Z}_m, \\
 s_m(t) &= \int_{\mathbb{Z}_m} du e_m(t-u) S_m(u) = \sum_{u \in \mathbb{Z}_m} d(\mathbb{Z}_m) e_m(t-u) S_m(u), \quad t \in \mathbb{R},
 \end{aligned}
 \tag{15.57}$$

where $d(\mathbb{Z}_m) = 2^m$. Then, comparison of (15.57) with (15.56) allows the complete identification. An analogous identification is obtained using the relations of the second line of (15.39).

Proposition 15.6 *The projector \mathcal{P}_m is separable in the form $\mathcal{P}_m = \mathcal{E}_m \mathcal{C}_m$, where \mathcal{C}_m is an $\mathbb{R} \rightarrow \mathbb{Z}_m$ decimator, and \mathcal{E}_m is a $\mathbb{Z}_m \rightarrow \mathbb{R}$ interpolator with impulse responses respectively*

$$c_m(t) = \varphi^{(m)*}(-t), \quad t \in \mathbb{R}, \quad e_m(t) = 2^{-m} \varphi^{(m)}(t), \quad t \in \mathbb{R}.
 \tag{15.58}$$

The projector \mathcal{R}_m is separable in the form $\mathcal{P}_m = \mathcal{F}_m \mathcal{D}_m$, where \mathcal{D}_m is an $\mathbb{R} \rightarrow \mathbb{Z}_m$ decimator, and \mathcal{F}_m is a $\mathbb{Z}_m \rightarrow \mathbb{R}$ interpolator with impulse responses respectively

$$d_m(t) = \psi^{(m)*}(-t), \quad t \in \mathbb{R}, \quad f_m(t) = 2^{-m} \psi^{(m)}(t), \quad t \in \mathbb{R}.
 \tag{15.59}$$

The syntheses of the projectors are shown in Fig. 15.24.

15.10 Combination of Interpolators and Decimators

In this section we establish the relation between the coefficients at adjacent levels, thus obtaining the full discretization of the decomposition, as anticipated in Sect. 15.6 and in Fig. 15.19.

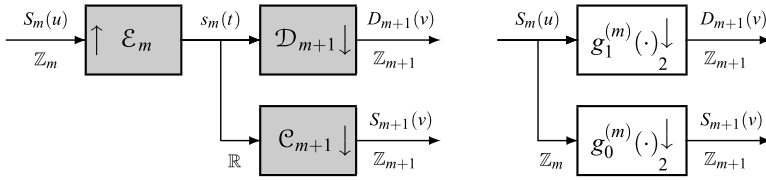


Fig. 15.25 Architectures for evaluation of wavelet coefficients combining step m and step $m + 1$

15.10.1 Links Between Coefficients at Step m and Step $m + 1$

Figure 15.25 shows the links relating the coefficients $S_m(u)$, $u \in \mathbb{Z}_m = \mathbb{Z}(2^m)$, to the coefficients $S_{m+1}(v)$, $D_{m+1}(v)$, $v \in \mathbb{Z}_{m+1}$. In Appendix A we first show that these links are given by a two-channel filter bank operating on $\mathbb{Z}_m \rightarrow \mathbb{Z}_{m+1}$. Then, we evaluate the impulse responses of the two $\mathbb{Z}_m \rightarrow \mathbb{Z}_{m+1}$ decimators by combination of the impulse responses of \mathcal{E}_m and of \mathcal{D}_{m+1} , \mathcal{C}_{m+1} , given by Proposition 15.6. In this combination, we use the *two-scale relations* (15.46a) and (15.47).

We finally obtain:

Proposition 15.7 *The links between the coefficients at adjacent levels, $S_m(u) \rightarrow S_{m+1}(v)$ and $S_m(u) \rightarrow D_{m+1}(v)$, can be implemented by the Analysis side of a two-channel filter bank on $\mathbb{Z}_m \rightarrow \mathbb{Z}_{m+1}$ with impulse responses*

$$g_0^{(m)}(n2^m) = 2^{-m} g_0^*(-n), \quad g_1^{(m)}(n2^m) = 2^{-m} g_1^*(-n), \quad (15.60)$$

where $g_0(n)$ and $g_1(n)$ are respectively the expansion coefficients, with respect to the basis Φ_{-1} , of the scaling function $\varphi(t)$ and of the mother wavelet $\psi(t)$.

Note from (15.60) that the frequency response are related as (see Problem 15.4)

$$G_0^{(m)}(f) = G_0^*(2^m f), \quad G_1^{(m)}(f) = G_1^*(2^m f), \quad (15.61)$$

where $G_i(f)$, $f \in \mathbb{R}/\mathbb{Z}$, and $G_i^{(m)}(f)$, $f \in \mathbb{R}/\mathbb{Z}_{-m}$. In words, we find a band compression at the increase of m . The laws (15.60) and (15.61) are illustrated in Fig. 15.26 for a *real* filter.

In fact, the law (15.60) establishes a simple dilation (and reflection) of the impulse response that leads to the domain $\mathbb{Z}_m = \mathbb{Z}(2^m)$ starting from the domain $\mathbb{Z} = \mathbb{Z}_0$ of $g(n)$, but the coefficients of the filters are simply scaled, and their number does not change, as shown in Fig. 15.26. Note that if the $g_i(n)$ are *causal*, the $g_i^{(m)}(n)$ are *anticipatory* (in the figure, $g_i^{(m)}(-n)$ instead of $g_i^{(m)}(n)$ are represented). In particular, if the $g_i(-n)$ are causal FIR with extension $e(g_i) = \{0, 1, \dots, N_g\}$, the extensions of $g_i^{(m)}(-n)$ are reversed and dilated as $e(g_i^{(m)}) = \{-2^m N_g, -2^m(N_g - 1), \dots, -2^m, 0\}$, but the number of nonzero coefficients does not change. Note that, at step m , at the output of the filters the coefficients $D_m(u)$ and $S_m(u)$ are defined on the group $\mathbb{Z}_m = \mathbb{Z}(2^m)$, which also gives the admissible shifts at this

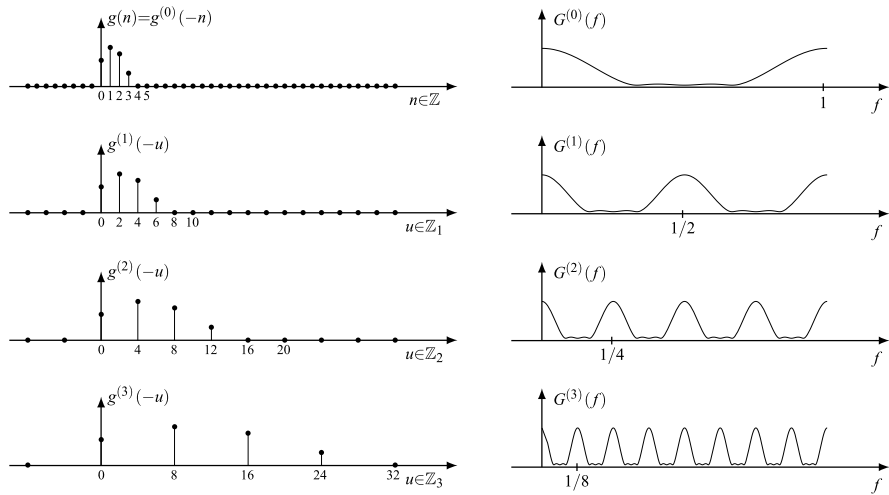


Fig. 15.26 The filters in the subsequent steps of Mallat's algorithm

level of resolution (spaces V_m and W_m). The frequency response follows the law $G^{(m)}(f) = G^*(2^m f)$ with a restriction of the band at the increase of m . The period of $G^{(m)}(f)$ becomes 2^{-m} , 1 being the period of $G(f)$.

The important conclusion is that all the filters in the tree structured architecture are obtained from the prototype filters $g_0(n)$ and $g_1(n)$; moreover, $g_1(n)$ is obtained from $g_0(n)$ by the QMF symmetry, and this is a relevant advantage for the implementation: *all filters are obtained from a unique prototype filter!*

15.10.2 Global Behavior

Now, we examine in detail the global behavior of the filters in each branch of Fig. 15.20, starting from the radix $S_0(n)$ and ending at leaves $w_m(t)$, $m = 1, 2, \dots, m_{\max}$, and $s_{m_{\max}}(t)$ ($m_{\max} = 3$ in the figure). In this analysis we use the following statement, which deals with the cascade of two decimators in the various domains. For generality, we consider two consecutive down-samplers on an arbitrary lattice sequence $J_0 \rightarrow J_1 \rightarrow J_2$ and use the Noble Identity NI3 of Theorem 7.5.

Proposition 15.8 *The cascade of two decimators on $J_0 \rightarrow J_1 \rightarrow J_2$ with impulse responses $g_1(t), t \in J_0$, and $g_2(t), t \in J_1$, shown in Fig. 15.27, is equivalent to a $J_0 \rightarrow J_2$ down-sampler with impulse response $g_{12}(t) = g_1 * \tilde{g}_2(t), t \in J_1$, where $\tilde{g}_2(t), t \in J_1$, is the $J_1 \rightarrow J_0$ up-sampled version of $g_2(t), t \in J_1$.*

The frequency response is simply given by $G_{12}(f) = G_1(f)G_2(f), f \in \mathbb{R}/J_1^$, and, in terms of z-transform, $G_{12}(z_0) = G_1(z_0)G_0(z_0^N)$, where $N = (J_1 : J_2)$.*

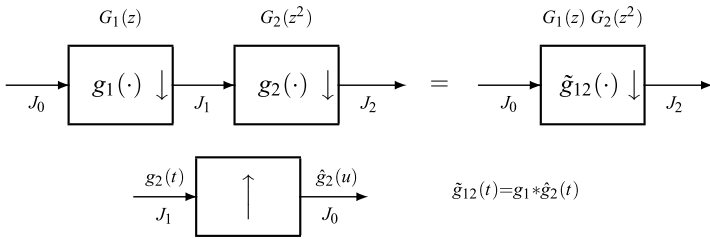


Fig. 15.27 Interpretation of Proposition 15.8: the impulse response $\tilde{g}_{12}(u)$ of the equivalent $J_0 \rightarrow J_2$ decimator is the convolution $g_1 * \hat{g}_2(t)$, $t \in J_0$, where $\hat{g}_2(t)$ is the up-sampled version of $g_2(t)$

In branch 0 of Fig. 15.20, the $\mathbb{Z}_0 \rightarrow \mathbb{Z}_1$ decimator has impulse response $g^{(0)}(n) = g_1(n)$. In branch 1, the decimator $g^{(0)}(n) = g_0(n)$ on $\mathbb{Z}_0 \rightarrow \mathbb{Z}_1$ is followed by the decimator $g_1^{(1)}(u)$ on $\mathbb{Z}_1 \rightarrow \mathbb{Z}_2$, where $g_1^{(1)}(u)$ is defined on \mathbb{Z}_1 ; this cascade is equivalent to a $\mathbb{Z}_0 \rightarrow \mathbb{Z}_2$ decimator with impulse response

$$h_{01}(n) = g_0^{(0)} * \tilde{g}_1^{(1)}(n), \quad n \in \mathbb{Z}_0 = \mathbb{Z}, \tag{15.62}$$

where $\tilde{g}_1^{(1)}(n)$ is the up-sampled version of $g_1^{(1)}(n)$. Analogously, we find that branch 2 is equivalent to a $\mathbb{Z}_0 \rightarrow \mathbb{Z}_3$ decimator with impulse response

$$h_{001}(n) = g_0^{(0)} * \tilde{g}_0^{(1)} * \tilde{g}_1^{(2)}(n),$$

where the tilde denotes that the impulse responses are appropriately up-sampled. In particular, if the basic filters are FIR, with extension $\sigma(g_0) = \sigma(g_1) = \{0, 1, \dots, N_g\}$, all the equivalent impulse responses are FIR with extensions

$$\sigma(h_{01}) = -\{0, 1, \dots, 2N_g + 1\}, \quad \sigma(h_{001}) = -\{0, 1, \dots, 3N_g + 1\}, \quad \dots$$

This is illustrated in Fig. 15.28, where the basic filters are the Haar filters with $\sigma(g_0) = \sigma(g_1) = \{0, 1\}$.

A clearer specification of the equivalent filters is obtained in the z -domain, where the global transfer functions become

$$\begin{aligned} H_{01}(z^{-1}) &= G_0(z)G_1(z^2), \\ H_{001}(z^{-1}) &= G_0(z)G_0(z^2)G_1(z^4), \\ H_{0001}(z^{-1}) &= G_0(z)G_0(z^2)G_0(z^4)G_1(z^8), \\ H_{0000}(z^{-1}) &= G_0(z)G_0(z^2)G_0(z^4)G_0(z^8) \end{aligned}$$

(z^{-1} corresponds to an axis inversion).

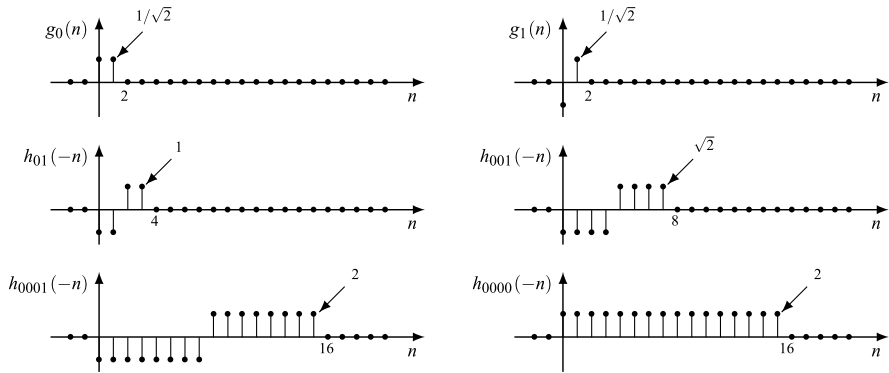


Fig. 15.28 Equivalent filters in three-order tree with basic Haar filter

15.11 Fourier Analysis in the Wavelet Decomposition

We establish further properties on the functions $\varphi(t)$, $\psi(t)$ and on the associated filters $g_0(n)$, $g_1(n)$, arriving at the evaluation of the mother wavelet using the Fourier analysis.

15.11.1 Frequency Relation Between $\varphi(t)$ and $\psi(t)$ and Their Coefficients

We relate the FT of the scaling function to the FT of the associated filters that are given by

$$\Phi(f) = \int_{\mathbb{R}} dt \varphi(t) e^{-i2\pi ft}, \quad f \in \mathbb{R}, \quad G_0(f) = \sum_{n \in \mathbb{Z}} g_0(n) e^{-i2\pi fn}, \quad f \in \mathbb{R}/\mathbb{Z},$$

and the FT $\Psi(f)$ of the mother wavelet $\psi(t)$ and the FT $G_1(f)$ of the associated filter $g_1(n)$ have similar expressions. Note that $\Phi(f)$ and $\Psi(f)$ are aperiodic, whereas $G_0(f)$ and $G_1(f)$ have period 1.

Using the expansion and reconstruction of $\varphi(t)$ and $\psi(t)$ with the basis Φ_{-1} , in Appendix B we obtain the following:

Proposition 15.9 *The FT of the scaling function $\varphi(t)$ and the FT of the associated filter $g_0(n)$ are related by*

$$\Phi(f) = \frac{1}{\sqrt{2}} \Phi\left(\frac{1}{2}f\right) G_0\left(\frac{1}{2}f\right), \quad G_0(f) = \sqrt{2} \text{rep}_1[\Phi^*(f)\Phi(2f)], \quad (15.63)$$

where rep_1 is the periodic repetition with period 1. Perfectly similar relations link the FT of $\psi(t)$ and the FT of the associated filter $g_1(n)$:

$$\begin{aligned} \Psi(f) &= \frac{1}{\sqrt{2}} \Phi\left(\frac{1}{2}f\right) G_1\left(\frac{1}{2}f\right), \\ G_1(f) &= \sqrt{2} \text{rep}_1[\Phi^*(f)\Psi(2f)]. \end{aligned} \tag{15.63b}$$

Note that (15.21) may be viewed as *two-scale relations* in the frequency domain.

15.11.2 Orthonormality Conditions in the Frequency Domain

The orthonormality with respect to the integer shifts of the scaling function is explicitly given by (15.27) and can be conveniently expressed in terms of the autocorrelation of $\varphi(t)$, given by (see Sect. 5.7)

$$c_\varphi(\tau) = \int_{-\infty}^{+\infty} \varphi(t + \tau)\varphi^*(t) dt \xrightarrow{\mathcal{F}} C_\varphi(f) = |\Phi(f)|^2. \tag{15.64}$$

Then, orthonormality (15.27) states that the $\mathbb{R} \rightarrow \mathbb{Z}$ down-sampled version of $c_\varphi(\tau)$, $\tau \in \mathbb{R}$, is the impulse $\delta_{\mathbb{Z}}(k)$. Correspondingly, in the frequency domain we have that the $\mathbb{R} \rightarrow \mathbb{R}/\mathbb{Z}$ up-periodization of $C_\varphi(f) = |\Phi(f)|^2$ gives a constant FT with value 1 (see Sect. 8.1). Then:

Proposition 15.10 (Nyquist criterion) *The orthonormality of the integer shifts $\varphi(t - n)$ of the scaling function, expressed in terms of the autocorrelation $c_\varphi(\tau)$, $\tau \in \mathbb{R}$, is*

$$c_\varphi(\tau) = \delta_{\mathbb{Z}}(n). \tag{15.65}$$

In the frequency domain this condition becomes

$$\boxed{\text{rep}_1 |\Phi(f)|^2 = \sum_{k=-\infty}^{+\infty} |\Phi(f - k)|^2 = 1.} \tag{15.66}$$

Identical conditions hold for the correlation $c_\psi(\tau)$, $\tau \in \mathbb{R}$, of the mother wavelet and its FT $|\Psi(f)|^2$.

Using Proposition 15.10 in Appendix B we also prove the following:

Proposition 15.11 *The FT $G_0(f)$, $f \in \mathbb{R}/\mathbb{Z}$, of the coefficients $g_0(n)$ verifies the condition*

$$\boxed{|G_0(f)|^2 + \left|G_0\left(f + \frac{1}{2}\right)\right|^2 = 2,} \tag{15.67}$$

which is called the *power complementary property* (see (14.150)).

15.11.3 Evaluation of the Mother Wavelet in the Frequency Domain

The evaluation of the filters and of the mother wavelet can be carried out in the frequency domain and is simplified when the scaling function is band-limited. The procedure leads to the class of *Mayer's wavelets*.

Given the FT $\Phi(f)$, the steps to follow are:

- (1) evaluation of the frequency response $G_0(f) = \sqrt{2}\text{rep}_1[\Phi(f)\Phi(2f)]$;
- (2) evaluation of $G_1(f)$ using the QMF property $G_1(f) = -e^{-i2\pi f}G_0(f - 1/2)$;
- (3) evaluation of $\Psi(f)$ from (15.63b), that is, $\Psi(f) = (1/\sqrt{2})\Phi(f/2)G_1(f/2)$;
- (4) evaluation of $\psi(t)$ as the inverse FT of $\Psi(f)$.

If the FT $\Phi(f)$ is band-limited in the interval $(-B, B)$ with $B \leq 1$, as shown in Fig. 15.29, where $B = 4/5$, we have several simplifications due to the fact that the terms of the periodic repetition do not overlap, and often we can arrive at closed form results. We let

$$P(f) = \Phi(f)\Phi(2f)$$

which has extension $(-\frac{1}{2}B, \frac{1}{2}B)$. Then,

$$G_0(f) = \sqrt{2}\text{rep}_1 P(f) = \sqrt{2} \sum_{k \in \mathbb{Z}} P(f - k),$$

where the terms of the periodic repetition have disjoint extensions. In particular, the inverse FT is

$$g_0(n) = \int_{\mathbb{R}/\mathbb{Z}} df G_0(f) e^{i2\pi fn} = \sqrt{2} \int_{-\frac{1}{2}B}^{\frac{1}{2}B} P(f) e^{i2\pi fn} df. \quad (15.68)$$

The frequency response $G_1(f)$ is given by

$$G_1(f) = -e^{-i2\pi f} G_0\left(f - \frac{1}{2}\right) = -e^{-i2\pi f} \sqrt{2} \sum_{k \in \mathbb{Z}} P\left(f - \frac{1}{2} - k\right),$$

where the extension of the k th term is $(k + \frac{1}{2} - B, k + \frac{1}{2} + B)$.

The FT of the mother wavelet is evaluated as

$$\Psi(f) = \frac{1}{\sqrt{2}} \Phi\left(\frac{1}{2}f\right) G_1\left(\frac{1}{2}f\right) = -\Phi\left(\frac{1}{2}f\right) e^{-i\pi f} \sum_{k \in \mathbb{Z}} P\left(\frac{1}{2}f - \frac{1}{2} - k\right),$$

where $\Phi(\frac{1}{2}f)$ has extension $(-2B, 2B)$, and $P(\frac{1}{2}f - \frac{1}{2} - k)$ has extension $(-B + 2k + 1, B + 2k + 1)$. Thus, in the extension $(-2B, 2B)$, we find only two terms of the repetition: the terms $k = 0$ and $k = 1$. If we limit the evaluation of $\Psi(f)$ to $f > 0$, only the term $k = 1$ gives a contribution, and we find

$$\Psi_+(f) = -\Phi\left(\frac{1}{2}f\right) e^{-i\pi f} P\left(\frac{1}{2}(f - 1)\right), \quad f > 0, \quad (15.69)$$

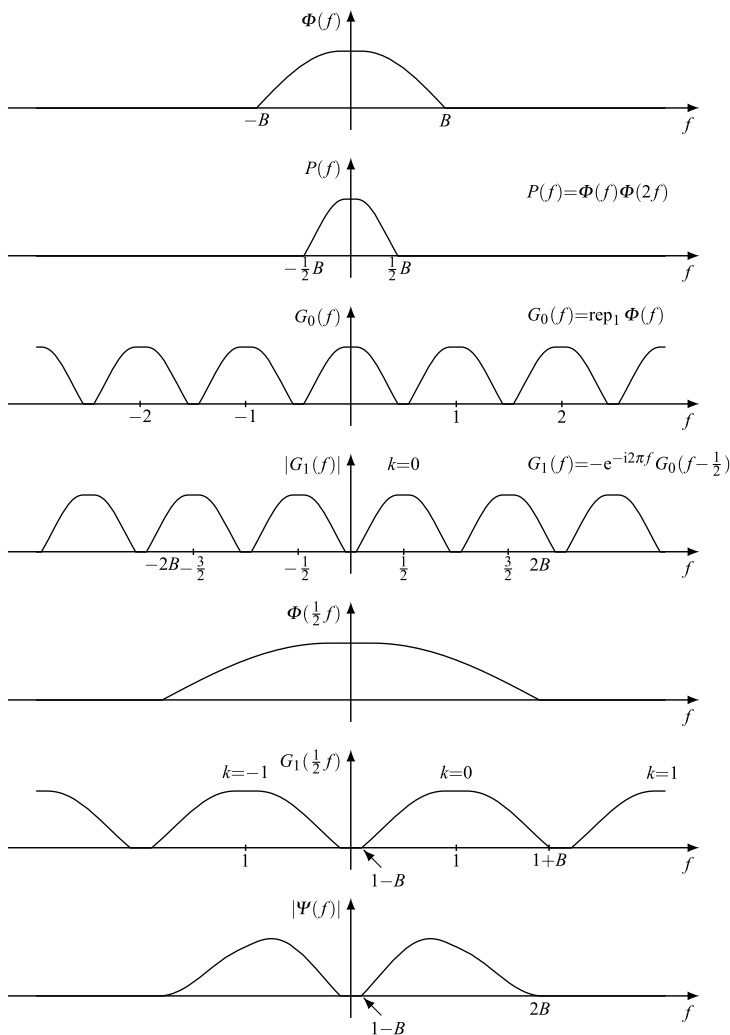


Fig. 15.29 Evaluation of the mother wavelet in the frequency domain when the Fourier transform $\Phi(f)$ of the scaling function is bandlimited to the interval $(-B, B)$ with $B \leq 1$

whose extension is $(1 - B, 2B)$. The inverse FT of $\Psi_+(f)$, the component of $\Psi(f)$ with positive frequencies, is

$$\begin{aligned} \psi_+(t) &= \int_0^\infty \Psi_+(f) e^{i2\pi ft} \, df \\ &= - \int_{1-B}^{2B} \Phi\left(\frac{1}{2}f\right) P\left(\frac{1}{2}(f-1)\right) e^{i2\pi f(t-\frac{1}{2})} \, df. \end{aligned}$$

Considering that $\Psi(f) = \Psi_+(f) + \Psi_+(-f)$ if $\Phi(f)$ is real, we find

$$\psi(t) = -2 \int_{1-B}^{2B} \Phi\left(\frac{1}{2}f\right) P\left(\frac{1}{2}(f-1)\right) \cos\left[2\pi f\left(t - \frac{1}{2}\right)\right] df. \tag{15.70}$$

Example 15.2 We illustrate the evaluation of the filters and of the mother wavelet when $\Phi(f)$ is the square root of a raised cosine function, given by (see (9.23))

$$\Phi(f) = \text{rrcos}(f, \alpha) = \begin{cases} 1, & 0 < f < f_1, \\ \cos \frac{\pi}{2} \left(\frac{f-f_1}{\alpha}\right), & f_1 < f < f_2, \\ 0, & f > f_2, \end{cases}$$

where $\Phi(-f) = \Phi(f)$, $f_{1,2} = \frac{1}{2}(1 \pm \alpha)$, and α is the roll-off factor. By construction, $|\Phi(f)|^2$ verifies the Nyquist criterion (15.66). The band is $B = f_2 = \frac{1}{2}(1 + \alpha) < 1$. The inverse FT of $\Phi(f)$ is (see (9.25a), (9.25b))

$$\varphi(t) = \frac{\sin \pi(t-1/4)}{4t} \text{sinc}\left(\alpha t + \frac{1}{4}\right) + \frac{\sin \pi(t+1/4)}{\pi t} \text{sinc}\left(\alpha t - \frac{1}{4}\right).$$

The coefficients $g_0(n)$ can be calculated from (15.68). Note that, for $\alpha \leq 1/3$, it results in $\Phi(f) = 1$ in the extension of $\Phi(2f)$, then $P(f) = \Phi(2f)$, and

$$g_0(n) = \sqrt{2} \int_{-\frac{1}{2}B}^{\frac{1}{2}B} \Phi(2f) e^{i2\pi f n} df = 2\sqrt{2}\varphi\left(\frac{1}{2}n\right).$$

(For the general case of α , see Problem 15.7.) Once $g_0(n)$ is evaluated, the coefficients $g_1(n)$ are obtained as $(-1)^n g_0(-(n-1))$.

Considering the extensions, (15.70) becomes

$$\psi(t) = -2 \int_{1/3}^{4/3} \Phi\left(\frac{1}{2}f\right) \Phi(f-1) \cos\left[2\pi f\left(t - \frac{1}{2}\right)\right] df,$$

where

$$\Phi\left(\frac{1}{2}f\right) \Phi(f-1) = \begin{cases} \Phi(f-1) = \cos\left[\frac{\pi}{2}(-3f+2)\right], & 1/3 < f/2/3, \\ \Phi\left(\frac{1}{2}f\right) = \cos\left[\frac{\pi}{2}\left(-\frac{3}{2}f-2\right)\right], & 1/3 < f/2/3. \end{cases}$$

The result of the integration is

$$\psi(t) = \frac{4[3\sqrt{2} \cos[\frac{2\pi u}{3}] - 6\sqrt{2} \cos(2\pi u) + 6 \cos[\frac{8\pi u}{3}] - 8\sqrt{2}u \sin[\frac{2\pi u}{3}]]}{\pi[64u^2 - 9]},$$

where $u = 2\pi(t - \frac{1}{2})$. The coefficients $g_0(n)$ and $g_1(n)$ and the functions $\varphi(t)$ and $\psi(t)$ are illustrated in Fig. 15.30.

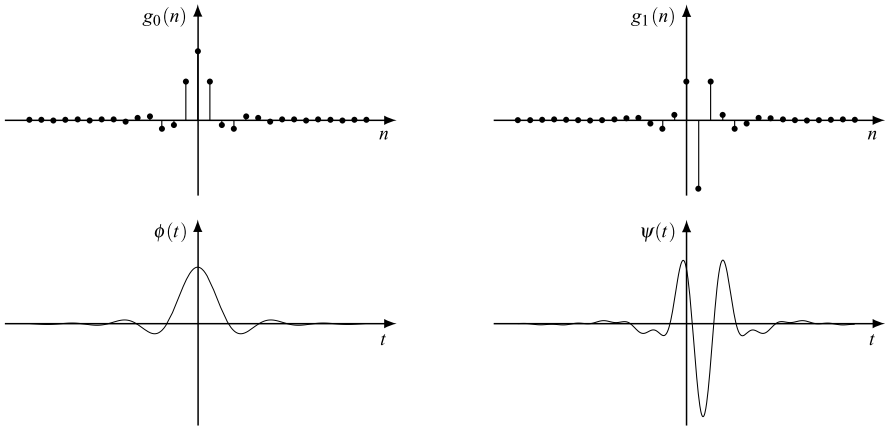


Fig. 15.30 The coefficients $g_0[n]$, $g_1[n]$, the scaling function $\phi(t)$, and the mother wavelet $\psi(t)$ with $\Phi(f) = \text{rrcos}(f, 1/3)$

15.12 Wavelets from Iterated Filter Banks

In the previous sections we have obtained the wavelets (mother wavelet and related families) starting from the multiresolution axioms. In this section, we follow a different approach, which is based on iterated applications of filter banks. Then, instead of continuous construction, we proceed on discrete time domains, but under certain convergence conditions, we will finally obtain continuous-time wavelet. The approach, due to Daubechies [4], leads to very interesting decomposition schemes which are implementable by FIR filters.

15.12.1 Basic Relations

There are several ways to introduce the constructions of wavelets from filter banks. Here we start from Proposition 15.9 and in particular from the two-scale equations in the frequency domain. We rewrite these equations in the form

$$\begin{aligned} \Phi(f) &= \Phi\left(\frac{1}{2}f\right)M_0\left(\frac{1}{2}f\right), & M_0(f) &= G_0(f)/\sqrt{2}, \\ \Psi(f) &= \Psi\left(\frac{1}{2}f\right)M_1\left(\frac{1}{2}f\right), & M_1(f) &= G_1(f)/\sqrt{2}, \end{aligned} \tag{15.71}$$

which clearly exhibit an iterative nature. In fact, using the first relation, we can express $\Phi(\frac{1}{2}f)$ as $\Phi(\frac{1}{4}f)M_0(\frac{1}{4}f)$ and $\Phi(\frac{1}{4}f)$ as $\Phi(\frac{1}{8}f)M_0(\frac{1}{8}f)$, and iterating the procedure L times, we obtain

$$\Phi(f) = \Phi(f2^{-L})A_L(f), \quad \Psi(f) = \Psi(f2^{-L})B_L(f), \tag{15.72}$$

where

$$A_L(f) = M_0\left(\frac{1}{2}f\right) \prod_{i=2}^L M_0(2^{-i}f), \quad (15.73)$$

$$B_L(f) = M_1\left(\frac{1}{2}f\right) \prod_{i=2}^L M_0(2^{-i}f).$$

These relations hold for any $L \geq 2$ and can be studied as L increases. Considering that $\Phi(2^{-L}f) \rightarrow \Phi(0)$ and that $\Phi(0)$ can be assumed as unitary, the limits of $A_L(f)$ and $B_L(f)$ give respectively

$$\Phi(f) = \lim_{L \rightarrow \infty} A_L(f), \quad \Psi(f) = \lim_{L \rightarrow \infty} B_L(f). \quad (15.74)$$

The problem of convergence will be discussed below.

15.12.2 Interpretation of the Product $A_L(f)$ and $B_L(f)$

The functions $M_0(f)$ and $M_1(f)$ are normalized frequency responses of the given filters $g_0(n)$ and $g_1(n)$, as indicated in (15.71). Define the filters

$$m_0(n) = (1/\sqrt{2})g_0(n), \quad m_1(n) = (1/\sqrt{2})g_1(n), \quad n \in \mathbb{Z}.$$

For the interpretation of the factors of the products in (15.73), we search for interpolators with up-sampling ratio 2. We begin with the frequency response $M_0(f)$, which has period 1. In this case the right interpolator is on $\mathbb{Z}(2) \rightarrow \mathbb{Z}$, where the input-output relation has the form

$$y(t) = \int_{\mathbb{Z}(2)} du h(t-u)x(u) = \sum_{n \in \mathbb{Z}} 2h(t-2n)x(2n)$$

with impulse response $h(t)$, $t \in \mathbb{Z}$, and frequency response $H(f)$, $f \in \mathbb{R}/\mathbb{Z}$. Then, $M_0(f)$, $f \in \mathbb{R}/\mathbb{Z}$, is interpreted as the frequency response of a $\mathbb{Z}(2) \rightarrow \mathbb{Z}$ interpolator with impulse response $m_0(n)$, $n \in \mathbb{Z}$.

Next, consider the factor $M_0(\frac{1}{2}f)$, which has period 2 and can be interpreted as the frequency response of a $\mathbb{Z} \rightarrow \mathbb{Z}(1/2)$ interpolator with impulse response $h(t) = 2m_0(2t)$, $t \in \mathbb{Z}(1/2)$. In general, we find that the factor $M_0(2^{-i}f)$, $f \in \mathbb{R}/\mathbb{Z}(2^L)$, can be interpreted as the frequency response $M_0^{(i)}(f)$ of a $\mathbb{Z}(2^{-i+1}) \rightarrow \mathbb{Z}(2^{-i})$ interpolator with impulse response

$$m_0^{(i)}(t) = 2^i m_0(2^i t), \quad t \in \mathbb{Z}(2^{-i}). \quad (15.75)$$

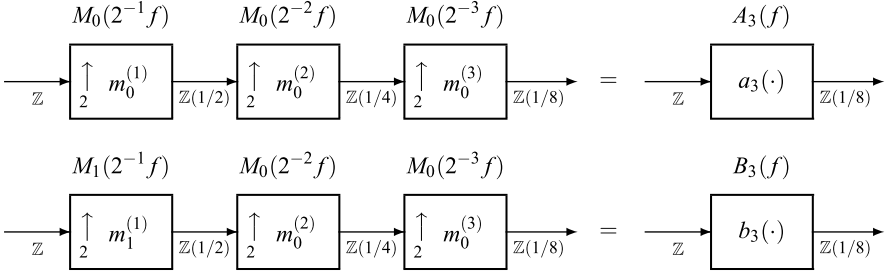


Fig. 15.31 System interpretation of the products $A_L(f)$ and $B_L(f)$ for $L = 3$ as frequency responses of a cascade of interpolators on $\mathbb{Z} \rightarrow \mathbb{Z}(1/2) \rightarrow \mathbb{Z}(1/4) \rightarrow \mathbb{Z}(1/8)$

Finally, considering that the frequency response of the cascade of interpolators is given by the product of the component frequency responses, we arrive at the scheme of Fig. 15.31, which shows the interpretation of the products $A_L(f)$ and $B_L(f)$ for $L = 3$.

Considering that $M_0(f)$ is low-pass and $M_1(f)$ is high-pass, the product $A_L(f)$ is low-pass, while $B_L(f)$ is band-pass, as shown in the example of Fig. 15.32.

Note that $A_L(f)$ and $B_L(f)$ have period 2^L and then, in the limit, become aperiodic, and consequently their inverse FTs $\varphi(t)$ and $\psi(t)$ become continuous-time ones.

Example 15.3 Consider the Haar filters that have frequency response $G_0(f) = (1 + z^{-1})/\sqrt{2}$ and $G_1(f) = (1 - z^{-1})/\sqrt{2}$ with $z = e^{i2\pi f}$. Then

$$M_0(f) = \frac{1}{2}(1 + z^{-1}) = e^{-i\pi f} \cos(\pi f),$$

$$M_1(f) = \frac{1}{2}(1 - z^{-1}) = ie^{-i\pi f} \sin(\pi f),$$

and

$$\Phi(f) = \lim_{L \rightarrow \infty} A_L(f) = \prod_{k=1}^{\infty} e^{-i\pi f 2^{-k}} \prod_{i=1}^{\infty} \cos(\pi f 2^{-k}).$$

This first product gives

$$\prod_{k=1}^{\infty} e^{-i\pi f 2^{-k}} = e^{-i\pi f \sum_{k=1}^{\infty} 2^{-k}} = e^{-i\pi f},$$

while for the second product, we use the identity [13]

$$\prod_{k=1}^{\infty} \cos(\pi f 2^{-k}) = \text{sinc}(f).$$

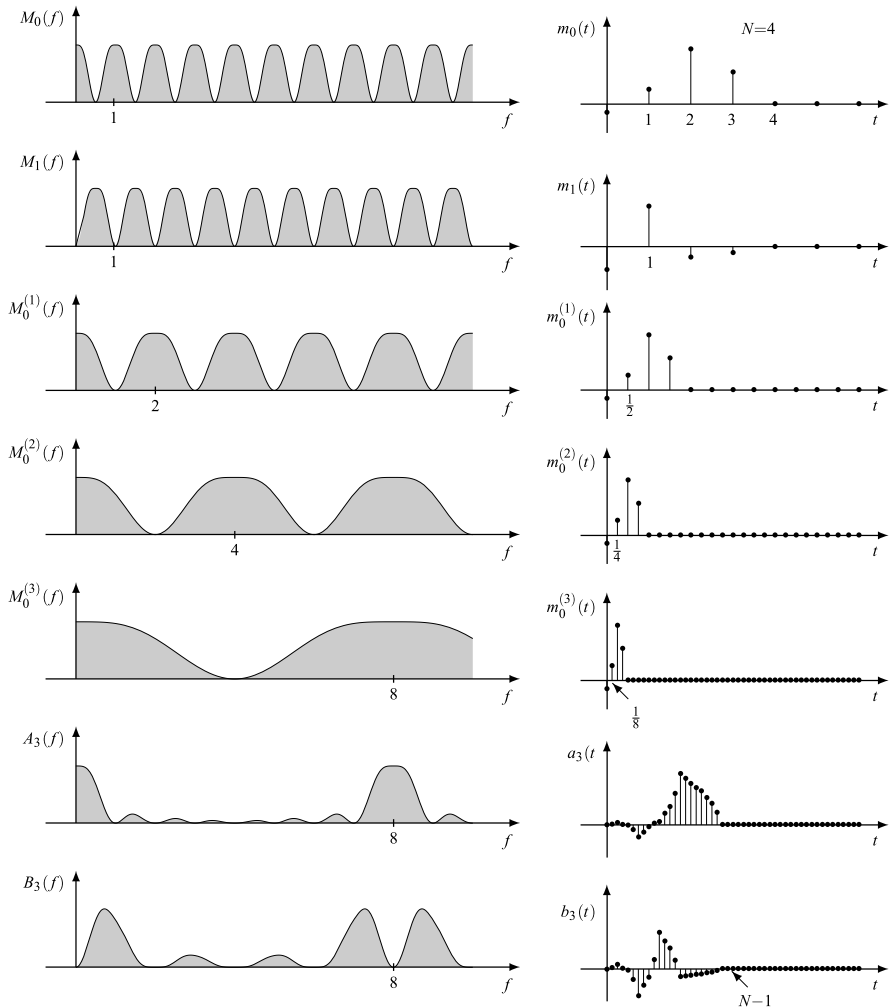


Fig. 15.32 On the *left*, the factors in the iterative procedure and the products $A_L(f)$ and $B_L(f)$ for $L = 3$. On the *right*, the corresponding signals (impulse responses)

Hence,

$$\Phi(f) = e^{-i\pi f} \operatorname{sinc}(f) \xrightarrow{\mathcal{F}^{-1}} \operatorname{rect}_+(t).$$

Analogously, we find

$$\Psi(f) = i\frac{1}{2} \operatorname{sinc}(2f)[1 - e^{-i\pi f}] \xrightarrow{\mathcal{F}^{-1}} \operatorname{rect}_+\left(\frac{1}{2}t\right) - \operatorname{rect}_+\left(\frac{1}{2}t - \frac{1}{2}\right)$$

that correspond to the functions illustrated in Fig. 15.23 and obtained directly from the axioms.

15.12.3 FIR Property of the Iterated Construction

A fundamental property of the iterated procedure is that, if the starting filters $g_0(n)$ and $g_1(n)$ are FIR, that is, with a finite extension, then the wavelets also have a finite extension.

Consider the product $A_L(f)$ for $L = 2$, that is, $A_2(f) = M_0(\frac{1}{2}f)M_1(\frac{1}{4}f) = M_0^{(1)}(f)M_0^{(2)}(f)$, which gives the frequency response of a $\mathbb{Z} \rightarrow \mathbb{Z}(1/2)$ interpolator followed by a $\mathbb{Z}(1/2) \rightarrow \mathbb{Z}(1/4)$ interpolator. Suppose that the original filter $g_0(n)$ is a FIR of length N with extension $e(g_0) = e(m_0) = \{0, 1, \dots, N - 1\} = [0, N - 1] \cap \mathbb{Z}$. Considering (15.75), the extension of the impulse responses $m_0^{(1)}$ and $m_0^{(2)}$ are respectively $e(m_0^{(1)}) = [0, (N - 1)/2] \cap \mathbb{Z}(1/2)$ and $e(m_0^{(2)}) = [0, (N - 1)/4] \cap \mathbb{Z}(1/4)$. Now, the product $M_0^{(1)}(f)M_0^{(2)}(f)$ does not correspond to a convolution in the time domain because the impulse responses are defined on different domains. But, for the first interpolator, we can use the Noble Identity NI2 of Sect. 7.3. This identity allows us to replace the standard decomposition of an interpolator (up-sampler followed by filtering) by filtering followed by up-sampler, provided that the impulse response $m_0^{(1)}(t)$ is replaced by its up-sampled version $\tilde{m}_0^{(1)}(t)$. In this way we find that the product $A_2(f)$ in the time domain becomes the convolution $\tilde{m}_0^{(1)} * m_0^{(2)}$ on $\mathbb{Z}(1/4)$. Then, we can apply the rule on the extension of convolution

$$\begin{aligned} e(a_2) &= e(\tilde{m}_0^{(1)}) + e(m_0^{(2)}) = \{[0, (N - 1)/2] + [0, (N - 1)/4]\} \cap \mathbb{Z}(1/4) \\ &= [0, (N - 1)/2 + (N - 1)/4] \cap \mathbb{Z}(1/4). \end{aligned}$$

In a similar way it can be shown that the extension of $a_3(t) \xrightarrow{\mathcal{F}^{-1}} A_3(f)$ is given by

$$e(a_3) = [0, (N - 1)/2 + (N - 1)/4 + (N - 1)/8] \cap \mathbb{Z}(1/8).$$

In the limit as $L \rightarrow \infty$, we find that $e(a_L)$ is contained in the interval $[0, N - 1]$.

Proposition 15.12 *If the original filters $g_0(n)$ and $g_1(n)$ are FIR with extension $\{0, 1, \dots, N - 1\}$, the scaling function $\varphi(t)$ and the mother wavelet $\psi(t)$ are causal with finite extension given by the interval $[0, N - 1]$.*

15.12.4 The Problem of Regularity

In the construction of wavelets from the multiresolution axioms we have seen that the properties of wavelets are strongly related to the properties of the filters $g_0(n)$ and $g_1(n)$. In particular, the orthogonality of wavelets implies and are implied by the orthogonality of these filters.

Here, the procedure has been reversed: the functions $\varphi(t)$ and $\psi(t)$ are obtained as limits of discrete-time iterated filters, and, in principle, it must be shown that

they are actually a scaling function and a mother wavelet. Of course, a necessary condition to impose is that the filters must have the properties found in the axiomatic approach, which are essentially that they must be linked by the mirror symmetry (see Fig. 15.21), and, moreover, they must have the complementary power property. Assuming that the limits converge in $L_2(\mathbb{R})$ norm to the functions $\varphi(t)$ and $\psi(t)$, it can be shown that the limiting functions have all the required properties and are valid scaling and wavelet functions.

It remains to investigate the existence of the limits of the infinite products in (15.74). A variety of mathematical studies can be found in the literature, in particular in [3, 4], where explicit conditions on the filters are formulated for the existence of the limits. These studies have an important mathematical interest, but they may have a scarce practical importance because those conditions may lead to discontinuous and highly irregular scaling functions and wavelets [12].

More useful may be the investigations concerning the *regularity* (continuity, differentiability, etc.). A necessary condition to ensure that $\varphi(t)$, the inverse FT of the infinite product in (15.74), is square summable is that the frequency response $M_0(f)$ has a zero at $f = 1/2$. Then, to increase the regularity of $\varphi(t)$, $M_0(f)$ must have multiple zeros at $f = 1/2$, and adding more zeros, the regularity increases. For a complete and a concise formulation of this topic, we suggest reference [12].

15.13 The Wavelet Series Expansion

We now define wavelet expansions, both continuous and discrete, and their efficient implementation. In particular, we will show that, with an appropriate interpretation of the continuous wavelet expansion, one can obtain the continuous wavelet transform (CWT) introduced in Sect. 15.4. In this way the CWT turns out to be linked to the multiresolution axioms, whereas in Sect. 15.4 it was related to the CSTFT. We remark that *continuous* expansions and transforms are usually considered for theoretic developments, but in practice only *fully discrete* (discrete input, discrete output) expansions and transforms are used, that is, the DWT.⁴

15.13.1 Wavelet Expansion of Continuous Signals (WST)

In resolution steps (15.33) we assumed V_0 as the reference resolution space. If V_0 is replaced by another reference space V_{m_0} and the iteration procedure terminates at resolution V_{m_1} with $m_0 < m_1$, we find

$$s_{m_0}(t) = w_{m_0+1}(t) + w_{m_0+2}(t) + \cdots + w_{m_1}(t) + s_{m_1}(t), \quad (15.76)$$

⁴For the terms and acronyms (nonstandard) we use, see the introduction to this chapter.

where $s_{m_1}(t)$ is the orthogonal projection of the given signal $s(t) \in L_2(\mathbb{R})$ onto V_{m_1} . Then, considering (15.56) and (15.57), we can write

$$s_{m_0}(t) = s_{m_1}(t) + \sum_{m=m_0+1}^{m_1} w_m(t), \tag{15.77}$$

where

$$s_{m_1}(t) = \sum_{u \in \mathbb{Z}_{m_1}} \varphi^{(m_1)}(t-u) S_{m_1}(u), \quad w_m(t) = \sum_{u \in \mathbb{Z}_m} \psi^{(m)}(t-u) D_m(u)$$

with

$$S_{m_1}(u) = \int_{\mathbb{R}} dt \varphi^{(m_1)}(t-n) s(t), \quad D_m(u) = \int_{\mathbb{R}} dt \psi^{(m)}(t-u) s(t).$$

The $S_{m_1}(u)$ are the *approximation* or *scaling coefficients*, and the $D_m(u)$ are the *detail* or *wavelet coefficients*.

Now, as $m_1 \rightarrow \infty$, the projection $s_{m_1}(t) \rightarrow s(t)$, and we get a first form of continuous wavelet expansion

$$s_{m_0}(t) = \sum_{m=m_0+1}^{\infty} \sum_{u \in \mathbb{Z}} S_{\psi}(m, u) \psi^{(m)}(t-u), \tag{15.78}$$

where $D_m(u)$ has been relabeled by

$$S_{\psi}(m, u) = \int_{\mathbb{R}} dt \psi^{(m)}(t-u) s(t), \quad u \in \mathbb{Z}_m. \tag{15.79}$$

In this formulation, the orthogonal projection $s_{m_0}(t)$ with finite m_0 approximates the signal $s(t)$, and the approximation becomes a more precise representation as m_0 decreases, in the limit $\lim_{m_0 \rightarrow -\infty} s_{m_0}(t) = s(t)$. Hence, a second form of wavelet series expansion is given by

$$s(t) = \sum_{m \in \mathbb{Z}} \sum_{u \in \mathbb{Z}_m} S_{\psi}(m, u) \psi^{(m)}(t-u). \tag{15.80}$$

Connection with the CWT We rewrite for convenience the discrete wavelet series (15.79) and the inverse DWT (15.80), using the definition $\psi^{(m)}(t) = 2^{-m/2} \psi(2^{-m}t)$,

$$S_{\text{DWT}}(m, u) = \frac{1}{2^{m/2}} \int_{\mathbb{R}} dt \psi\left(\frac{t-u}{2^m}\right) s(t), \quad m \in \mathbb{Z}, \quad u \in \mathbb{Z}_m, \tag{15.81}$$

$$s(t) = \sum_m \sum_{u \in \mathbb{Z}_m} \frac{1}{2^{m/2}} \psi\left(\frac{t-u}{2^m}\right) S_{\text{DWT}}(m, u), \quad t \in \mathbb{R}.$$

Next, considering that in these formulas we have used the discretization $a = a_0^m = 2^m$, $b = a_0^m n = 2^m n = u$, we can write

$$S_{\text{CWT}}(a, b) = \frac{1}{|a|^{1/2}} \int_{\mathbb{R}} dt \psi\left(\frac{t-b}{a}\right) s(t), \quad (15.82a)$$

$$s(t) = \sum_a \sum_{b \in \mathbb{Z}_m} \frac{1}{|a|^{1/2}} \psi\left(\frac{t-b}{a}\right) S_{\text{CWT}}(a, b). \quad (15.82b)$$

In particular, (15.82a) is identical to the CWT (see below), with the difference that here the parameters a and b are discrete, while in the CWT they are continuous. The inversion formula (15.82b) is not identical to the corresponding inverse CWT, but this is due to the replacement of a summation with an integral.

This is the conceptual link of the CWT to the multiresolution axioms (recall that the discrete wavelet expansion was obtained from the axioms).

15.13.2 Wavelet Expansion of Discrete Signals (DWT)

In order to introduce the DWT, we consider the continuous expansion (15.77) with a few but important modifications. We let $m_0 = 0$ and $m_1 = M - 1$, and we restrict the continuous time t from \mathbb{R} to $\mathbb{Z}(T_0)$, with T_0 to be chosen conveniently. Then

$$s(t) = s_{M-1}(t) + \sum_{m=1}^{M-1} w_m(t), \quad t \in \mathbb{Z}(T_0), \quad (15.83)$$

where

$$\begin{aligned} s_{M-1}(t) &= \sum_{u \in \mathbb{Z}_{M-1}} \varphi^{(M-1)}(t-u) S_{M-1}(u), \\ w_m(t) &= \sum_{u \in \mathbb{Z}_M} \psi^{(m)}(t-u) D_m(u), \end{aligned} \quad t \in \mathbb{Z}(T_0), \quad (15.84)$$

with

$$\begin{aligned} S_{M-1}(u) &= \int_{\mathbb{Z}(T_0)} dt s(t) \varphi^{(M-1)}(t-u), \\ D_m(u) &= \int_{\mathbb{Z}(T_0)} dt s(t) \psi^{(m)}(t-u), \end{aligned} \quad u \in \mathbb{Z}_m. \quad (15.85)$$

The problem consists in finding the conditions that ensure that expansion (15.83) represents correctly every signal of the class $L_2(\mathbb{Z}(T_0))$.

The discretization introduced above has severe constraints on shifting and dilation operations in the discrete domain, whereas in the continuous domain \mathbb{R} they have no constraints. For instance, if $s(t)$ is defined on \mathbb{R} , the dilation of the form

$s(2^{-1}t)$ brings back the signal to \mathbb{R} , but if $s(t)$ is defined on \mathbb{Z} , the form $s(t/2)$ defines a signal on $\mathbb{Z}(2)$ but cannot be forced to \mathbb{Z} because, at $t = \pm 1, \pm 3, \dots$, the values of $s(t/2)$ do not exist.

Such problems are overcome in the implementation of the Mallat algorithm, with the discretization of the unique block operating at continuous time, as was anticipated in Fig. 15.20.

15.14 Generalizations on Wavelets

This section consists of an overview of generalizations on the topic of wavelets, articulated in four items.

(1) The formulation of multiresolution axioms, in particular, Axiom A5, implies orthogonal wavelets and correspondingly orthogonal filter banks, but a generalization to *biorthogonal wavelets* is possible and convenient. (2) The dilation factor in the axioms is $D = 2$, but it may be an arbitrary integer $D \geq 2$. (3) In the N -dimensional space $L_2(\mathbb{R}^N)$ the construction of *multidimensional wavelets* is possible, where the dilation factor D becomes an $N \times N$ matrix. Finally, (4) a further generalization of wavelets, called *curvelets*, is currently developed by the digital signal processing community.

15.14.1 Biorthogonal Wavelets

The multiresolution axioms lead to an orthonormal wavelet basis and a related implementation by orthonormal two-channel filter banks. On the other hand, in Sect. 14.12 we have seen that there are no useful two-channel orthogonal filter banks with linear phase and finite impulse response (FIR). These requirements are mandatory for several applications and find a solution in biorthogonality. Then Axiom A5 on orthogonality is relaxed to allow biorthogonality. In this way, the wavelet families $\tilde{\Psi}_m$ used for the Analysis become different from the wavelet families Ψ_m used for the Synthesis. Consequently, the orthogonality of the families Ψ_m , that is, $\Psi_{m'} \perp \Psi_m, m' \neq m$, is replaced by the biorthogonality condition, namely $\tilde{\Psi}_{m'} \perp \Psi_m, m' \neq m$.

The biorthogonality leads to two distinct nested sequences of subspaces V_m and \tilde{V}_m and to two distinct sequences of complementary spaces W_m and \tilde{W}_m , where W_m is a *nonorthogonal* complement of V_m in V_{m-1} , and \tilde{W}_m is a *nonorthogonal* complement of \tilde{V}_m in \tilde{V}_{m-1} . However, the biorthogonality ensures that $\tilde{W}_m \perp V_m$ and $W_m \perp \tilde{V}_m$. The symmetry interpretation seen for the orthogonal case and, in particular, Proposition 15.3 must be slightly modified: the binary projectors \mathcal{P}_m and \mathcal{R}_m are no more Hermitian, and the projections $s_m = \mathcal{P}_m[s]$ and $w_m = \mathcal{R}_m[s]$ are no more orthogonal.

In the construction of the biorthogonal bases Φ_m and Ψ_m , the requirement of linear independence is still maintained, so that they actually form *bases*. A further

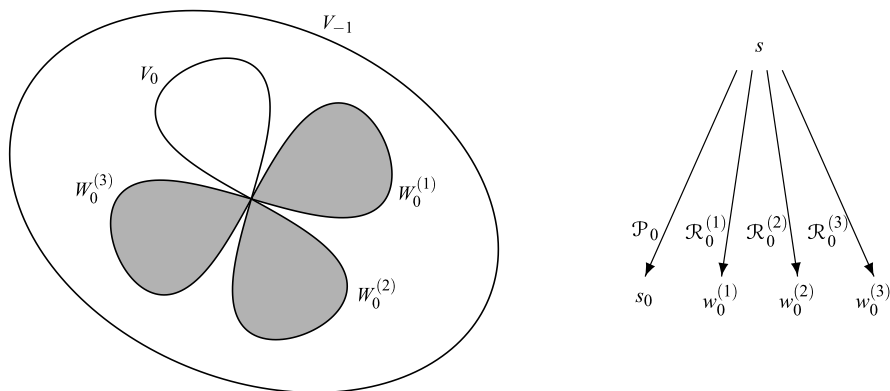


Fig. 15.33 Decomposition of the resolution space V_{-1} with a *quaternary* symmetry obtained with a dilation factor $D = 4$. In a signal decomposition the projector \mathcal{P}_0 gives the projection s_0 onto V_0 , and the projectors $\mathcal{R}_0^{(i)}$ give the projections $w_0^{(i)}(t)$ onto $W_0^{(i)}$, $i = 1, 2, 3$

generalization is obtained by removing the linear independence. In such a way, with linear dependent sets of functions, one can obtain *frames of wavelets* [4, 14].

15.14.2 One-Dimensional Wavelets with Dilation Factor $D > 2$

In the standard multiresolution axioms, the *dilation factor* is $D = 2$, but an axiom reformulation is possible with $D > 2$. Then, in the nested sequence of subspaces $\dots \subset V_{-1} \subset V_0 \subset V_1 \subset \dots$ each subspace V_{m-1} will be written as the direct sum of D orthogonal subspaces, namely

$$V_{m-1} = V_m \oplus W_m^{(1)} \oplus \dots \oplus W_m^{(D-1)}, \tag{15.86}$$

and correspondingly we will find one scaling function and $D - 1$ mother wavelets. In other words, Symmetry Theory interpretation gives a *D-ary symmetry* instead of a binary symmetry, as shown in Fig. 15.33 for $D = 4$.

There are several ways to see this generalization. Here we use the periodic invariance (PI) of the bases involved, where a fundamental role is played by the *admissible shifts* in each subspace.

When the multiresolution axioms are generalized to a dilation factor D , Axiom A3 on *scale invariance* must be modified as

$$s(t) \in V_m \iff s(D^m t) \in V_0.$$

Then the scaling function of V_m becomes $\varphi^{(m)}(t) = D^{-m/2}\varphi(D^{-m}t)$, and the shifted versions forming the basis are given by

$$\varphi_u^{(m)}(t) = \varphi^{(m)}(t - u) = D^{-m/2}\varphi(D^{-m}t), \quad u \in \mathbb{Z}(D^m), \tag{15.87}$$

where the shifts belong to the lattice $\mathbb{Z}_m = \mathbb{Z}(D^m)$. Relation (15.87) generalizes relation (15.22) seen for the case $D = 2$, and we see that the set of admissible shifts in V_m becomes $\mathbb{Z}_m = \mathbb{Z}(D^m)$. The function (15.87), defined from the scaling function $\varphi(t)$, forms the orthogonal basis Φ_m of the subspace V_m .

After this generalization, the theory of wavelets can be developed as in the case $D = 2$ (two-scale equations, coefficients of the related filter bank, evaluation of the mother wavelets, and so on). Here, we limit ourselves to justifying the multiplicity of mother wavelets. To this end, we find it useful to formulate a general statement on the PI of the bases of resolution spaces.

Proposition 15.13 *Let V_{-1} and V_0 be the two adjacent resolution spaces, and let \mathbb{Z}_{-1} and \mathbb{Z}_0 be the corresponding sets of admissible shifts. Then there exists an orthogonal basis $\Gamma = \{\gamma_u(t) \mid u \in \mathbb{Z}_{-1}\}$ of V_{-1} that verifies the PI condition with periodicity \mathbb{Z}_0 .*

The proposition is formulated in the context of multidimensional wavelets [2] and holds in particular in the one-dimensional case. Note that Γ is a basis of V_{-1} , alternative to the basis Φ_{-1} . We have seen that, with a dilation factor D , the sets of admissible shifts are $\mathbb{Z}_{-1} = \mathbb{Z}(D^{-1})$ and $\mathbb{Z}_0 = \mathbb{Z}$. These lattices identify the cell

$$B = [\mathbb{Z}_{-1}/\mathbb{Z}_0] = \{0, 1/D, \dots, (D - 1)/D\} \triangleq \{0, b_1, \dots, b_{D-1}\}$$

of cardinality L given by the dilation factor D . Then the PI property allows us to decompose the basis Γ into the L subfamilies (see Sects. 14.4 and 14.5)

$$\Gamma_b = \{\gamma_u(t - p) \mid p \in \mathbb{Z}_0\}, \quad b \in B. \tag{15.88}$$

These subfamilies are pairwise orthogonal, $\Gamma_b \perp \Gamma_{b'}$, $b' \neq b$, and define an L -ary symmetry $\sigma_b = \text{span}(\Gamma_b)$, $b \in B$, where $\sigma_0 = V_0$ and $\sigma_b = W_0^{(b)}$, $b \neq 0$, are the orthogonal subspaces that appear in (15.86). Moreover, $\gamma_0(t) = \varphi(t)$ defines the scaling function, and $\psi_b(t) = \gamma_b(t)$ with $b \neq 0$ define the $L - 1$ mother wavelets.

We can check that the above statement holds in the standard case $D = 2$ developed in the previous sections, where in V_{-1} the shifts are given by $\mathbb{Z}_{-1} = \mathbb{Z}(1/2)$ and in V_0 by $\mathbb{Z}_0 = \mathbb{Z}$. Then, $B = [\mathbb{Z}(1/2)/\mathbb{Z}] = \{0, 1\}$, and we have a binary symmetry. The orthogonal basis is given by

$$\Gamma = \Phi_0 \cup \Psi_0 \tag{15.89}$$

and can be split into $\Gamma_0 = \Phi_0$ and $\Gamma_{1/2} = \Psi_0$, the bases of V_0 and W_0 , respectively.

The generalization with $D > 2$ can be completed, as seen for the binary case, and instead of a two-channel filter bank, we will find a D -channel filter bank. Moreover, starting from this filter bank, under appropriated assumptions on filters, one can construct by iterations the scaling function and the $D - 1$ mother wavelets [4].

15.14.3 Multidimensional Wavelets

The multiresolution axioms have been introduced in the one-dimensional class $L_2(\mathbb{R})$ but can be generalized to the N -dimensional class $L_2(\mathbb{R}^N)$ by handling dilations and shifts in an appropriate form. In particular, Axiom A3 becomes

$$s(\mathbf{t}) \in V_m \iff s(\mathbf{D}^m \mathbf{t}) \in V_0,$$

where \mathbf{D} is a nonsingular $N \times N$ integer matrix, called *dilation matrix*, and the shift invariance of Axiom A4 is expressed by N -dimensional shifts, namely

$$s(\mathbf{t}) \in V_0 \implies s(\mathbf{t} - \mathbf{n}) \in V_0 \quad \forall \mathbf{n} \in \mathbb{Z}^N.$$

Note that the matrix \mathbf{D} identifies a sublattice of \mathbb{Z}^N given by $D = \{\mathbf{D}\mathbf{n} \mid \mathbf{n} \in \mathbb{Z}^N\} = \mathbf{D}\mathbb{Z}^N$ (see Sect. 3.3).

Given a scaling function $\varphi(\mathbf{t}) \in V_0$, the functions of the bases Φ_m of the different resolution spaces V_m are obtained as a generalization of (15.87). The scaling function of V_m is given by $\varphi^{(m)}(\mathbf{t}) = L^{-m/2} \varphi(\mathbf{D}^{-m} \mathbf{t})$, where $L = |\det \mathbf{D}|$, and the shifted versions are given by

$$\varphi_{\mathbf{u}}^{(m)}(\mathbf{t}) = \varphi^{(m)}(\mathbf{t} - \mathbf{u}) = L^{-m/2} \varphi(\mathbf{D}^{-m}(\mathbf{t} - \mathbf{u})), \quad \mathbf{u} \in D_m,$$

where the shifts belong to the lattice $D_m = \mathbf{D}^m \mathbb{Z}^N$.

In the applications the dilation matrix \mathbf{D} must have the eigenvalues λ with $|\lambda| > 1$ in order to ensure dilation in each direction [4]. In Chap. 3, Sect. 3.3, we have seen that the basis of a given lattice D is not unique. For instance, the three different matrices

$$\mathbf{D}_1 = \begin{bmatrix} 1 & 1 \\ 1 & -1 \end{bmatrix}, \quad \mathbf{D}_2 = \begin{bmatrix} 1 & -1 \\ 1 & 1 \end{bmatrix}, \quad \mathbf{D}_3 = \begin{bmatrix} 2 & 1 \\ 0 & 1 \end{bmatrix} \quad (15.90)$$

determine the quincunx lattice $\mathbb{Z}_2^1(1, 1)$ and have the eigenvalues $\{-\sqrt{2}, \sqrt{2}\}$, $\{1 - i, 1 + i\}$, and $\{2, 1\}$, respectively. Thus, only \mathbf{D}_1 and \mathbf{D}_2 are correct as dilation matrices. Incidentally, note that although both represent the same lattice, they have a different behavior in the construction of wavelets [14].

When the dilation matrix is diagonal, e.g.,

$$\mathbf{D} = \begin{bmatrix} 2 & 0 \\ 0 & 2 \end{bmatrix}, \quad (15.91)$$

the multidimensional wavelets are obtained as the *tensor product* of 1D wavelets, and the underlying filter bank becomes separable (see the application described in the next section).

To get further insight on multidimensional wavelets, we can start from Proposition 15.13. Considering that the set of admissible shifts in V_m is given by the N -dimensional lattice $D_m = \mathbf{D}^m \mathbb{Z}^N$, it remains to evaluate the cardinality of the cell

$B = [D_{-1}/D_0]$. We recall that the cardinality of a discrete cell is given by (3.45); in this case

$$|B| = d(D_0)/d(D_{-1}) = |\det(\mathbf{D}^0)|/|\det(\mathbf{D}^{-1})| = |\det(\mathbf{D})| = L.$$

The conclusion is that in general the number of mother wavelets is given by $L - 1 = |\det(\mathbf{D})| - 1$, where \mathbf{D} is the dilation matrix.

In the 2D separable case (15.91) the cardinality is $L = 4$, and, using Proposition 15.13, we can prove that (see Problem 15.9), given a 1D scaling function $\varphi(t)$ and a mother wavelet $\psi(t)$, the 2D scaling function is given by $\varphi_1(t_1)\varphi_2(t_2)$ and the three 2D mother wavelets by $\varphi(t_1)\psi(t_2)$, $\psi(t_1)\varphi(t_2)$, $\psi(t_1)\psi(t_2)$.

15.14.4 The Curvelet Transform

Wavelets, implemented mainly by the DWT, are widely used in several applications (mathematical analysis and signal processing) but have the disadvantage of a poor directionality, which reduces their usage. In recent years a significant progress in the development of directional wavelets has been made, mainly with the introduction of the *complex* wavelet transform. The 2D complex wavelets are constructed as a tensor product of 1D wavelets and achieve a certain improvement in directionality with respect to the classical DWT (six directions instead of three directions). However, also the complex wavelet transform supplies a poor directionality.

To overcome this drawback, a multiresolution geometric analysis, named *curvelet transform*, was recently proposed [1]. The idea of the curvelet transform is to contract from a “mother” curvelet a set of curvelets, adding to the shift-dilation invariance of wavelets, the rotation invariance. The main mathematical tool to achieve the rotation invariance is provided by polar coordinates in the frequency domain, as we shall see for the Radon transform in Chap. 16.

For a review on the theory and recent applications of curvelets, see [8].

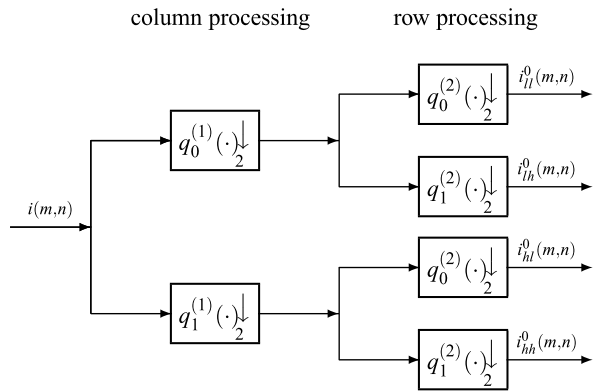
15.15 An Example of the Application of Wavelets

This example will consider the application of wavelets to image multiresolution analysis, which is the first step in many image processing applications, including compression and noise removal.⁵ As a matter of fact, the recent image compression standard JPEG2000 [12] operates in the wavelet transform domain, as opposed to the old JPEG standard [15], which adopts the DCT as the image transform.

As seen before, the Discrete Wavelet Transform (DWT) of a discrete one-dimensional signal can be computed using a tree-structured filter bank, which is

⁵The author wants to thank Roberto Rinaldo for his contribution to this section.

Fig. 15.34 Separable 2D filter bank for image expansion



obtained by iterating on the low-pass signal a perfect reconstruction, and orthogonal two-channel filter bank. As seen in the previous section, the theory of the wavelet transform, and in particular Mallat’s axiomatic definition of multiresolution analysis, can be extended to the multidimensional case, and in particular to the two-dimensional (2D) domain where images are defined. Even if other constructions are possible, the most common and widespread solution adopted in applications is to extend the one-dimensional concepts to 2D by using a *separable* approach, which consists in defining a two-dimensional wavelet $\psi_2(x, y)$ via the *tensor product* of one dimensional wavelets, i.e.,

$$\psi_2(x, y) = \psi(x)\psi(y), \tag{15.92}$$

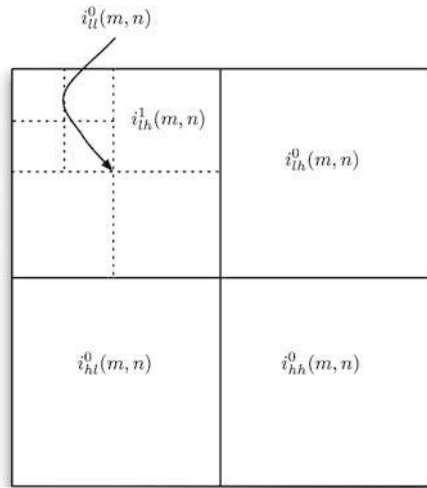
where $\psi(\cdot)$ is a wavelet associated to a one-dimensional multiresolution analysis. One can easily show that the family of functions obtained by dilation and translation of $\psi_2(x, y)$, both in the x and y directions, actually constitute an orthonormal basis of functions for $L_2(\mathbb{R}^2)$.

For 2D discrete signals, one obtains a tree-structured 2D separable filter bank, where a two-channel decomposition is first computed in the vertical direction and, then, in the horizontal direction. If the 2D signal is the discrete domain image $i(m, n)$, this corresponds to filtering and subsampling the columns and then the rows of the image, as shown in Fig. 15.34.⁶

In case $i(m, n)$ is an $N_r \times N_c$ pixel image, it is usually extended periodically before filtering, both in the row and column directions. This is done in order not to increase the dimension of the filtered signals that would result because of the convolution with the filter kernels. As a matter of fact, the filter output corresponding to a periodic input signal is indeed periodic, and one can retain the values in one period without any loss of information. Because of the decimators in Fig. 15.34, one obtains therefore four $N_r/2 \times N_c/2$ subbands, each with dimension one-fourth of that of the original image.

⁶Note that, since we are dealing with separable 2D filters $h_{ij}(m, n) = h_i(m)h_j(n)$, one can first process the rows and then the columns of the image, without changing the result.

Fig. 15.35 Multiresolution image decomposition using the wavelet transform



The image obtained by processing both the rows and columns with the low-pass filter $q_0(\cdot)$ is denoted as $i_{ll}^0(m, n)$. Similarly, $i_{lh}^0(m, n)$ is obtained by processing the columns with the low-pass filter $q_0(\cdot)$ and the rows with the high-pass filter $q_1(\cdot)$. As a result, subband $i_{lh}^0(m, n)$ has large magnitude coefficients in correspondence with the vertical edges of the image. Along the same lines, $i_{hl}^0(m, n)$ and $i_{hh}^0(m, n)$ reveal the horizontal and diagonal image details, respectively.

In a multiresolution wavelet decomposition, the 2D separable filter bank is iterated on the low-pass image $i_{ll}^0(m, n)$, thus obtaining a pyramidal decomposition at different scales. Subband signals can be arranged as in Fig. 15.35, which shows the structure of the subbands in a two-level wavelet decomposition, and where the superscript k denotes the subbands at level $k + 1$ of the multiresolution decomposition.

In this first application we use the analysis and synthesis FIR filter coefficients of the Daubechies two-channel length-4 orthogonal filter bank corresponding to wavelets with compact support [4]. The coefficients of these filters were listed in Table 14.2, and the frequency responses were illustrated in Fig. 14.29. It is easy to verify that the filters satisfy, within numerical precision, the perfect reconstruction property and the orthogonality conditions. The use of FIR filters is particularly convenient in image processing applications because of the easier implementation compared to IIR filter banks.

Figure 15.36 shows an image of the wavelet coefficients of the standard image *Lenna*, organized according to the structure of Fig. 15.35. It can be seen that $i_{ll}^1(m, n)$ is indeed a low-pass decimated version of the original image. The other subband coefficients are represented as gray levels, with gray corresponding to the zero value. It can be seen that the subbands generally have small value coefficients, due to the low-pass characteristics of most natural images, and that the largest ones are located near the edges. This can be exploited efficiently in image compression schemes, since the image can be represented by a relatively small number of significant coefficients. In particular, as mentioned before, $i_{lh}^k(m, n)$ reveals most of

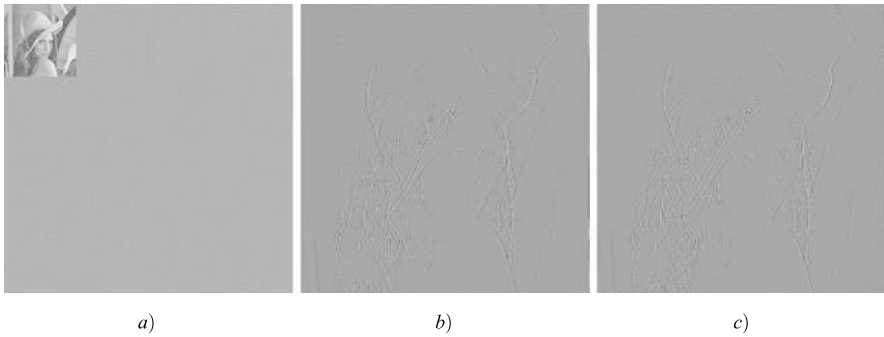


Fig. 15.36 Lenna wavelet decomposition using Daubechies length-4 orthogonal filter bank: (a) wavelet coefficients, (b) subband $i_{lh}^0(m, n)$, (c) subband $i_{lh}^1(m, n)$

the vertical details at different scales. Figures 15.36(b) and (c) show rescaled and enlarged versions of subbands $i_{lh}^0(m, n)$ and $i_{lh}^1(m, n)$, respectively. Note that the regions corresponding to nearly zero coefficients are colocated across scales in different subbands. This property can also be exploited in coding applications, where a single symbol can represent an entire tree of quantized zero coefficients [10, 11].

In image processing applications, the use of FIR orthogonal filter banks, like those resulting from wavelets with compact support, has some drawbacks. In particular, it restricts the possibility to have linear phase symmetric filters. As a matter of fact, it is possible to show that, apart from the trivial Haar filters, there are no two-channel orthogonal filter banks, with linear phase and with real coefficients, ensuring perfect reconstruction [14]. Linear phase is a desirable property in image processing applications, since the edge structure in filtered subbands is preserved, due to the fact that all the edge frequency components are translated coherently, thus resulting in a symmetric shape of the filtered edge. In lossy image coding applications, where the image is reconstructed from quantized coefficients, the use of nonlinear phase filters may cause particularly visible, asymmetric ringing artifacts around the edges, due to the lack of perfect reconstruction resulting from coefficient quantization.

Moreover, linear phase symmetric filters allow one to use a symmetric rather than periodic extension of the image before filtering, still not increasing the support of the filtered subbands. The possibility of using a symmetric extension is particularly useful in coding applications, because the periodic extension can give rise to discontinuities around the image borders, which in turn require many large wavelet coefficients for representation. The effect of the periodic extension can be seen at the right border of Fig. 15.36(c), where a few columns of large magnitude coefficients are visible.

FIR linear phase filters can be designed instead within the general case of perfect reconstruction biorthogonal filter banks. Figure 15.37 shows an image of the wavelet coefficients of *Lenna*, where we used the analysis and synthesis filters of the Cohen–Daubechies–Feauveau 9–7 symmetric *biorthogonal* filter bank, corresponding to a set of compactly supported biorthogonal wavelets [4]. The coefficients of these

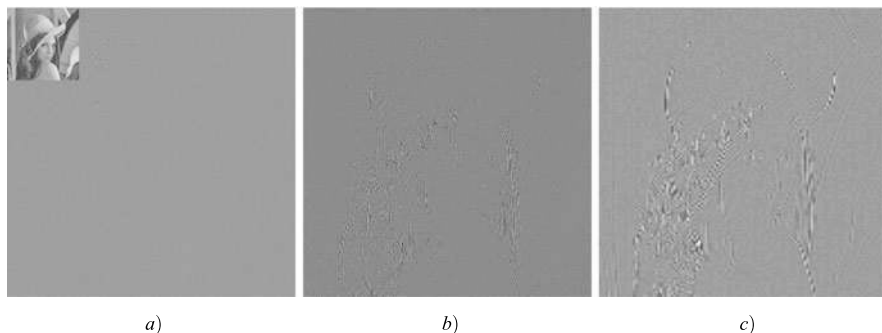


Fig. 15.37 Lenna wavelet decomposition using Cohen-Daubechies-Feauveau 9–7 filter bank: (a) wavelet coefficients, (b) subband $i_{lh}^0(m, n)$, (c) subband $i_{lh}^1(m, n)$

filters were listed in Table 14.3, and the frequency responses were illustrated in Fig. 14.30. The image was symmetrically extended before filtering, and it can be seen from the figures that this reduces the coefficient magnitude at the image borders [6]. Note that the JPEG2000 compression standard uses the Cohen–Daubechies–Feauveau 9–7 filter bank for lossy compression.

15.16 Problems

15.1 ★ [Sect. 15.8] Prove the mirror symmetry in the frequency domain, as stated by (15.44).

15.2 ★ [Sect. 15.9] Using the orthogonality $\mathbf{G}_0 \perp \mathbf{G}_1$ in Proposition 15.4, prove the orthogonality $\Phi_0 \perp \Psi_0$ claimed in Proposition 15.5. In other words, prove that $\psi(t - k)$ and $\varphi(t - k')$, $k, k' \in \mathbb{Z}$, are orthogonal using (15.53).

15.3 ★★ [Sect. 15.9] Prove the recurrence

$$p_m(t, t') + r_m(t, t') = p_{m-1}(t, t')$$

of the projector kernels. *Hint*: prove the equivalent relation $\mathcal{P}_m + \mathcal{R}_m = \mathcal{P}_{m-1}$ and use the property $s = \mathcal{P}_{m-1}[s]$ for every $s \in V_{m-1}$.

15.4 ★ [Sect. 15.10] Prove the relations of Mallat filters in the frequency domain

$$G_0^{(m)}(f) = G_0^*(2^m f), \quad G_1^{(m)}(f) = G_1^*(2^m f),$$

that is, prove (15.61) starting from (15.60).

15.5 ★ [Sect. 15.10] Evaluate Mallat filters in the case of the discrete sinc basis defined in Example 14.5.

15.6 ★ [Sect. 15.10] Prove Proposition 15.14 of Appendix A. *Hint*: write the global kernel of g_1 followed by g_2 and realize that it is a sampled version with convolution.

15.7 ★★★ [Sect. 15.11] Evaluate the mother wavelet $\psi(t)$ in the case of Example 15.2 with a roll-off $\alpha = 1$.

15.8 ★★ [Sect. 15.14] Find the set of *admissible shifts* $D_m = \mathbf{D}^m \mathbb{Z}^N$, where the dilation matrix \mathbf{D} is the first matrix in (15.90), that is,

$$\mathbf{D} = \begin{bmatrix} 1 & 1 \\ 1 & -1 \end{bmatrix}.$$

15.9 ★★ [Sect. 15.14] Consider the dilation matrix given by (15.91). Prove that, if $\varphi(t)$ and $\psi(t)$ are 1D, then the scaling function is $\varphi(t_1)\varphi(t_2)$, and the 2D mother wavelets are given by $\varphi(t_1)\psi(t_2)$, $\psi(t_1)\varphi(t_2)$, and $\psi(t_1)\psi(t_2)$.

Appendix A: Proof of Proposition 15.7 on Coefficients at Steps m and $m + 1$

We first establish the following statement:

Proposition 15.14 *A $\mathbb{Z}_m \rightarrow \mathbb{R}$ interpolator followed by an $\mathbb{R} \rightarrow \mathbb{Z}_{m+1}$ decimator is equivalent to a $\mathbb{Z}_m \rightarrow \mathbb{Z}_{m+1}$ decimator. To calculate the global impulse response $\tilde{g}_{12}(t)$, first calculate the convolution of the component impulse response $g_{12}(t) = g_2(t) * g_1(t)$, $t \in \mathbb{R}$, and then apply the $\mathbb{R} \rightarrow \mathbb{Z}_m$ down-sampling, that is,*

$$\tilde{g}_{12}(v) = \int_{\mathbb{R}} d\tau g_1(v - \tau)g_2(\tau), \quad v \in \mathbb{Z}.$$

The statement, illustrated in Fig. 15.38, is a consequence of the general result on the cascade of QIL tf, developed in Chap. 7, as soon as we note that $\mathbb{Z}_m \supset \mathbb{Z}_{m+1}$ (see Problem 15.6). The conclusion is that the combination of the two blocks, each one operating on continuous times, gives a block operating on discrete times, which is the crucial point for the full discretization.

We now prove Proposition 15.7. The link $S_m(u) \rightarrow S_{m+1}(v)$ is given by $\mathbb{Z}_m \rightarrow \mathbb{R}$ interpolator followed by a decimator with impulse response respectively

$$c_{m+1}(t) = \varphi^{(m+1)*}(-t), \quad e_m(t) = 2^{-m} \varphi^{(m)}(t). \quad (15.93)$$

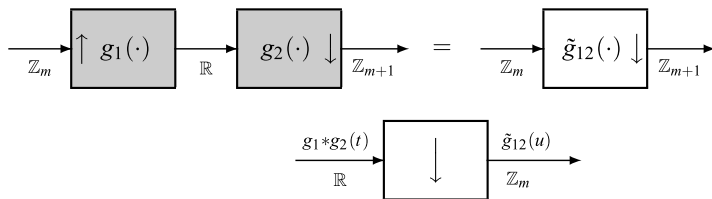


Fig. 15.38 Interpretation of Proposition 15.14: the impulse response $\tilde{g}_{12}(u)$ of the $\mathbb{Z}_m \rightarrow \mathbb{Z}_{m+1}$ decimator is the sampled version of the convolution $g_1 * g_2(t)$, $t \in \mathbb{R}$

Then, we apply Proposition 15.14 with $g_1 = c_{m+1}$ and $g_1 = e_m$ and evaluate the continuous convolution

$$g_{12}(t) = 2^{-m} \int_{\mathbb{R}} d\tau \varphi^{(m+1)*}(\tau - t) \varphi^{(m)}(\tau), \tag{15.94}$$

where, by (15.22),

$$\begin{aligned} \varphi^{(m+1)}(t) &= 2^{-(m+1)} \varphi(2^{-(m+1)}t) = 2^{-m} 2^{-1/2} \varphi(2^{-m}(t/2)), \\ \varphi^{(m)}(t) &= 2^{-m} \varphi(2^{-m}t). \end{aligned}$$

Hence,

$$\begin{aligned} g_{12}(t) &= 2^{-m} 2^{-m} 2^{-1/2} \int_{\mathbb{R}} d\tau \varphi^* \left(\frac{2^{-m}\tau - 2^{-m}t}{2} \right) \varphi(2^{-m}\tau) \\ &= 2^{-m} 2^{-1/2} \int_{\mathbb{R}} d\tau \varphi^* \left(\frac{\tau - 2^{-m}t}{2} \right) \varphi(\tau), \end{aligned}$$

where we have made the variable change $\tau \rightarrow 2^{-m}\tau$. Next, we use the two-scale relation (15.46a) with $t \rightarrow (\tau - 2^{-m}t)/2$ and obtain

$$g_{12}(t) = 2^{-m} \sum_n g_0^*(n) \int_{\mathbb{R}} d\tau \varphi^*(\tau - n - 2^{-m}t) \varphi(\tau),$$

where in general we cannot use the orthogonality condition. But, restricting t to \mathbb{Z}_m , that is, $t = 2^m k$, the integral gives δ_{n-k} . Hence,

$$\tilde{g}_{12}(2^m k) = g_{12}(2^m k) = 2^{-m} g_0^*(-k).$$

To get the impulse response of the link $S_m(u) \rightarrow D_{m+1}(v)$, it is sufficient to replace c_{m+1} with d_{m+1} in (15.93) and the two-scale equation (15.46a) with (15.47). The result is $\tilde{g}_{12}(2^m k) = 2^{-m} g_1^*(-k)$.

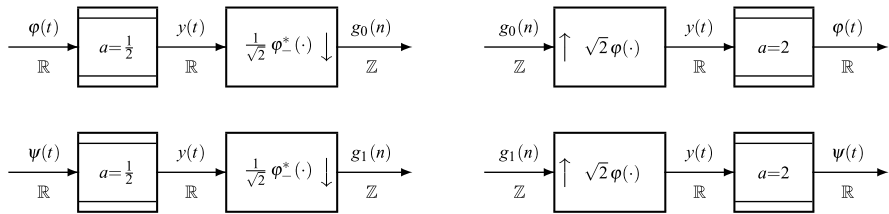


Fig. 15.39 Above: generation of expansion coefficients $g_0(n)$ from the scaling function $\varphi(t)$ and recovery of $\varphi(t)$ from $g_0(n)$. Below: generation of $g_1(n)$ from the mother wavelet $\psi(t)$ and recovery of $\psi(t)$ from $g_1(n)$

Appendix B: Interpretation of the Expansion of $\varphi(t)$ and $\psi(t)$

We consider the expansion of the functions $\varphi(t)$ and $\psi(t)$ obtained with the bases $\Phi_{-1} = \{\sqrt{2}\varphi(2t - n) \mid n \in \mathbb{Z}\}$

$$\begin{aligned}
 g_0(n) &= \sqrt{2} \int_{\mathbb{R}} dt \varphi(t) \varphi^*(2t - n), & \varphi(t) &= \sqrt{2} \sum_{n=-\infty}^{+\infty} g_0(n) \varphi(2t - n), \\
 g_1(n) &= \sqrt{2} \int_{\mathbb{R}} dt \psi(t) \varphi^*(2t - n), & \psi(t) &= \sqrt{2} \sum_{n=-\infty}^{+\infty} g_1(n) \varphi(2t - n),
 \end{aligned}
 \tag{15.95}$$

where the right-hand sides represent the two-scale equations.

The system interpretation of these relations shown in Fig. 15.39. With the introduction of the auxiliary signals

$$y(t) = \varphi(t/2), \quad g(t) = (1/\sqrt{2})\varphi^*(-t) \triangleq (1/\sqrt{2})\varphi_-^*(t),$$

the first of (15.95) can be written as

$$g_0(n) = \int_{-\infty}^{+\infty} (1/\sqrt{2})\varphi(u/2)\varphi(u - n) du = \int_{-\infty}^{+\infty} q(u - n)y(u) du.$$

Then, starting from $\varphi(t)$, $g_0(n)$ is obtained with scale change of $a = \frac{1}{2}$ followed by an $\mathbb{R} \rightarrow \mathbb{Z}$ decimator with impulse response $q(t)$, $t \in \mathbb{R}$. In the inverse relation (15.46a), (15.46b) the coefficients $g_0(n)$, $n \in \mathbb{Z}$, are $\mathbb{Z} \rightarrow \mathbb{R}$ interpolated with impulse response $\sqrt{2}\varphi(t)$ and give the intermediate signal $y(t)$; then, $y(t)$ is dilated by $a = \frac{1}{2}$ to give the scaling function $\varphi(t)$, $t \in \mathbb{R}$.

A similar interpretation, shown in Fig. 15.39, holds for the generation of the coefficients $g_1(n)$ from the mother wavelet $\psi(t)$ and the reconstruction of $\psi(t)$ from $g_1(n)$.

Using the rules of the Fourier analysis of interpolators and decimators, we find

$$Y(f) = \sqrt{2}\Phi(f)G_0(f), \quad \Phi(f) = \frac{1}{2}Y\left(\frac{1}{2}f\right) = \frac{\sqrt{2}}{2}\Phi\left(\frac{1}{2}f\right)G_0\left(\frac{1}{2}f\right),$$

$$Y(f) = 2\Phi(2f),$$

$$G_0(f) = \text{rep}_1[(1/\sqrt{2})\Phi^*(f)Y(f)] = \sqrt{2}\text{rep}_1[\Phi^*(f)\Phi(2f)],$$

which give (15.21).

We now prove Proposition 15.11. Combination of (15.63) and (15.66) gives

$$\begin{aligned} 2 &= \sum_{k=-\infty}^{+\infty} \left| \Phi\left(\frac{1}{2}f - \frac{1}{2}k\right) \right|^2 \left| G_0\left(\frac{1}{2}f - \frac{1}{2}k\right) \right|^2 \\ &= \sum_{h=-\infty}^{+\infty} \left| \Phi\left(\frac{1}{2}f - h\right) \right|^2 \left| G_0\left(\frac{1}{2}f - h\right) \right|^2 \\ &\quad + \sum_{h=-\infty}^{+\infty} \left| \Phi\left(\frac{1}{2}f - h - \frac{1}{2}\right) \right|^2 \left| G_0\left(\frac{1}{2}f - h - \frac{1}{2}\right) \right|^2. \end{aligned}$$

Next, considering that $G_0(f)$ has period 1 and using again (15.66), we have

$$\begin{aligned} 2 &= \left| G_0\left(\frac{1}{2}f\right) \right|^2 \sum_{h=-\infty}^{+\infty} \left| \Phi\left(\frac{1}{2}f - h\right) \right|^2 \left| G_0\left(\frac{1}{2}f - \frac{1}{2}\right) \right|^2 \sum_{h=-\infty}^{+\infty} \left| \Phi\left(\frac{1}{2}f - h - \frac{1}{2}\right) \right|^2 \\ &= \left| G_0\left(\frac{1}{2}f\right) \right|^2 + \left| G_0\left(\frac{1}{2}f - \frac{1}{2}\right) \right|^2, \end{aligned}$$

which is equivalent to (15.67). In fact, from (15.21) we obtain $2|\Phi(f)|^2 = |\Phi(\frac{1}{2}f)|^2 |G_0(\frac{1}{2}f)|^2$. Taking the periodic repetition and using (15.66), we get (15.67).

References

1. E. Candés, L. Demanet, D. Donoho, L. Ying, Fast discrete curvelet transforms. *Multiscale Model. Simul.* **5**, 861–899 (2006)
2. T. Colthurst, Multidimensional wavelets. Ph.D. Thesis, Massachusetts Institute of Technology, Dept. of Mathematics, June 1997
3. I. Daubechies, Orthonormal bases of compactly supported wavelets. *Commun. Pure Appl. Math.* **41**, 909–996 (1988)
4. I. Daubechies, *Ten Lecture on Wavelets* (SIAM, Philadelphia, 1992)
5. D. Gabor, Theory of communications. *J. Inst. Electr. Eng.* **93**, 429–457 (1946)
6. G. Karlsson, M. Vetterli, Extension of finite length signals for sub-band coding. *Signal Process.* **17**, 161–168 (1989)
7. S. Mallat, A theory of multiresolution signal decomposition: the wavelet representation. *IEEE Trans. Pattern Anal. Mach. Intell.* **11**, 674–693 (1989)
8. J. Ma, G. Plonka, The curvelet transform: a review of recent applications. *IEEE Signal Process. Mag.* **27**, 118–132 (2010)
9. R.A. Mayer, C.S. Burrus, A unified analysis of multirate and periodically time varying digital filters. *IEEE Trans. Circuits Syst.* **CAS-29**, 327–331 (1982)

10. A. Said, W.A. Pearlman, A new fast and efficient image codec based on set partitioning in hierarchical trees. *IEEE Trans. Circuits Syst. Video Technol.* **6**, 243–250 (1996)
11. J. Shapiro, Embedded image coding using zerotrees of wavelet coefficients. *IEEE Trans. Signal Process.* **41**, 3445–3462 (1993)
12. D. Taubman, M.W. Marcellin, *JPEG2000, Image Compression Fundamentals and Practice* (Kluwer Academic, Boston, 2002)
13. P.P. Vaidyanathan, *Multirate Systems and Filter Banks* (Prentice Hall, Englewood Cliffs, 1993)
14. M. Vetterli, J. Kovačević, *Wavelets and Subband Coding* (Prentice Hall, Englewood Cliffs, 1995)
15. G.K. Wallace, The JPEG still picture compression standard. *IEEE Trans. Consum. Electron.* **38**, 18–34 (1993)

Chapter 16

Advanced Topics on Multidimensional Signals

Comment on the Level of Interest Most of the topics of this chapter are very advanced and original or, at least, originally formulated. Their study is recommended only to the reader that, at an advanced research level, wants to have a deep knowledge on groups (gratings and lattices) and on cells. Otherwise, the development of the previous chapters is largely sufficient and this chapter can be simply regarded as a reference list of useful statements.

Computer Evaluation with Mathematica[®] Most of the topics of the chapter are concerned with the theory of integer matrices and their manipulation to find triangular and diagonal forms, the greatest common divisor, the least common multiple, and so on. All these *operations* are based on *elementary operations* on the columns and sometimes on the rows of the given integer matrices. Of course, this can be done by hand but becomes soon stressful, and the help of the computer is mandatory.

The author¹ has developed a package with Mathematica[®], which covers all the operations with integer matrices introduced in this chapter and is available on the Internet [2].

UT 16.1 Set and Group Transformations

A set mapping (or transformation) introduced in Sect. 3.3 is very useful to handle group operations and decompositions and will be used systematically in this chapter.

We recall Definition 3.2. Let \mathbf{A} be an $n \times m$ real matrix. Then the relation $\mathbf{t} = \mathbf{A}\mathbf{h}$ maps a point \mathbf{h} of \mathbb{R}^m into a point \mathbf{t} of \mathbb{R}^n . If H is a nonempty subset of \mathbb{R}^m , then

$$\mathbf{A}H \triangleq \{\mathbf{A}\mathbf{h} \mid \mathbf{h} \in H\} \quad (16.1)$$

¹The program has been thoroughly tested and adequately documented. However, the author wants to emphasize that he is not a professional programmer.

is the subset of \mathbb{R}^n obtained by mapping all the points of H . The set $\mathbf{A}H$ represents a *linear transformation* of the set H with matrix \mathbf{A} . In particular, if $n = m$ and the $m \times m$ matrix \mathbf{A} is nonsingular, the linear transformation becomes one-to-one, and the original set H can be recovered from the transformed set according to the graph

$$H \xrightarrow{\mathbf{A}} \mathbf{A}H \xrightarrow{\mathbf{A}^{-1}} H.$$

In connection with the standard operations, we find the rules

$$\mathbf{A}(P \cup Q) = \mathbf{A}P \cup \mathbf{A}Q, \quad (16.2a)$$

$$\mathbf{A}(P \cap Q) = \mathbf{A}P \cap \mathbf{A}Q, \quad (16.2b)$$

$$\mathbf{A}(P + Q) = \mathbf{A}P + \mathbf{A}Q. \quad (16.2c)$$

In particular, the linear transformation can be used to generate LCA group G of \mathbb{R}^m from a primitive group H in the synthetic form

$$G = \{\mathbf{G}\mathbf{h} \mid \mathbf{h} \in H\} = \mathbf{G}H, \quad (16.3)$$

where \mathbf{G} is the basis of the group, and H the signature (see (3.10)).

Now, a linear transformation with an $m \times m$ nonsingular matrix can be applied to m D group G and generates a new m D group, namely

$$J = \mathbf{A}G = \mathbf{A}\mathbf{G}H, \quad (16.4)$$

where the basis of the new group J is $\mathbf{J} = \mathbf{A}\mathbf{G}$, and the signature is the original one. Note that the notation $\mathbf{A}\mathbf{G}H$ in (16.4) has no ambiguity since $\mathbf{A}(\mathbf{G}H) = (\mathbf{A}\mathbf{G})H$. The generation of the group $J = \mathbf{A}\mathbf{G}H$ is done in two steps according to the graph

$$H \xrightarrow{\mathbf{G}} G \xrightarrow{\mathbf{A}} J, \quad (16.5)$$

where G is obtained from the signature H by the linear transformation $\mathbf{t} = \mathbf{G}\mathbf{h}$, and then J is obtained from G by the linear transformation $\mathbf{u} = \mathbf{A}\mathbf{t}$.

16.1.1 Group Decomposition into Reduced-Dimensional Subgroups

We begin by noting that a pair of points of \mathbb{R}^2 can be uniquely decomposed into the form

$$(r, s) = (r, 0) + (0, s), \quad r, s \in \mathbb{R}. \quad (16.6)$$

If A and B are nonempty subsets of \mathbb{R} , then for the Cartesian product $A \times B$, the above decomposition gives

$$A \times B = \{(a, b) \mid a \in A, b \in B\} = \{(a, 0) + (0, b) \mid a \in A, b \in B\}$$

$$\begin{aligned} &= \{(a, 0) \mid a \in A\} + \{(0, b) \mid b \in B\} \\ &= A \times \{0\} + \{0\} \times B = A \times \mathbb{O} + \mathbb{O} \times B, \end{aligned}$$

where $\mathbb{O} = \{0\}$ is the trivial subgroup of \mathbb{R} .

Then, in particular, if A and B are the *primitive* 1D groups \mathbb{R} and \mathbb{Z} (see Chap. 4), we can decompose 2D primitive groups into the form

$$\begin{aligned} \mathbb{R} \times \mathbb{R} &= \mathbb{R} \times \mathbb{O} + \mathbb{O} \times \mathbb{R}, \\ \mathbb{R} \times \mathbb{Z} &= \mathbb{R} \times \mathbb{O} + \mathbb{O} \times \mathbb{Z}, \quad \mathbb{Z} \times \mathbb{Z} = \mathbb{Z} \times \mathbb{O} + \mathbb{O} \times \mathbb{Z}. \end{aligned}$$

These decompositions can be easily extended. For instance,

$$\mathbb{R}^2 \times \mathbb{Z} = \mathbb{R}^2 \times \mathbb{O} + \mathbb{O}^2 \times \mathbb{Z} = \mathbb{R} \times \mathbb{O}^2 + \mathbb{O} \times \mathbb{R} \times \mathbb{O} + \mathbb{O}^2 \times \mathbb{Z},$$

and for a 3D group with signature $\mathbb{R}^2 \times \mathbb{Z}$,

$$G = \mathbf{G}\mathbb{R}^2 \times \mathbb{Z} = \underbrace{\mathbf{G}\mathbb{R}^2 \times \mathbb{O}}_{G_c} + \underbrace{\mathbf{G}\mathbb{O}^2 \times \mathbb{Z}}_{G_d},$$

where G_c is a 2D continuous group in \mathbb{R}^3 , and G_d is a 1D lattice in \mathbb{R}^3 . In general:

Proposition 16.1 *An m D group $G = \mathbf{G}\mathbb{R}^p \times \mathbb{Z}^q$ can be decomposed into the sum*

$$G = \mathbf{G}\mathbb{R}^p \times \mathbb{Z}^q = \underbrace{\mathbf{G}\mathbb{R}^p \times \mathbb{O}^q}_{G_c} + \underbrace{\mathbf{G}\mathbb{O}^p \times \mathbb{Z}^q}_{G_d}, \quad p + q = m, \quad (16.7)$$

where G_c is a p D continuous group in \mathbb{R}^m , and G_d is a q D lattice in \mathbb{R}^m . Both G_c and G_d are subgroups of G .

A more detailed decomposition is obtained in terms of 1D groups. Let \mathbf{g} be a vector of \mathbb{R}^m , that is, a $1 \times m$ matrix. Then the sets

$$\mathbf{g}\mathbb{R} = \{r\mathbf{g} \mid r \in \mathbb{R}\}, \quad \mathbf{g}\mathbb{Z} = \{n\mathbf{g} \mid n \in \mathbb{Z}\}$$

represent 1D groups in \mathbb{R}^m (this notation is consistent with (16.1)). Then, for instance, a 3D group G with basis $\mathbf{G} = [\mathbf{g}_1 \mathbf{g}_2 \mathbf{g}_3]$ and signature $\mathbb{R}^2 \times \mathbb{Z}$, whose generic point is given by $\mathbf{t} = r_1 \mathbf{g}_1 + r_2 \mathbf{g}_2 + n \mathbf{g}_3$, $r_1, r_2 \in \mathbb{R}$, $n \in \mathbb{Z}$, can be written in the form $G = \mathbf{g}_1 \mathbb{R} + \mathbf{g}_2 \mathbb{R} + \mathbf{g}_3 \mathbb{Z}$. In general:

Proposition 16.2 *An m D group G with basis $\mathbf{G} = [\mathbf{g}_1, \dots, \mathbf{g}_m]$ and signature $H = H_1 \times \dots \times H_m$ can be decomposed into the sum of m 1D groups in \mathbb{R}^m in the form*

$$G = \mathbf{g}_1 H_1 + \dots + \mathbf{g}_m H_m. \quad (16.8)$$

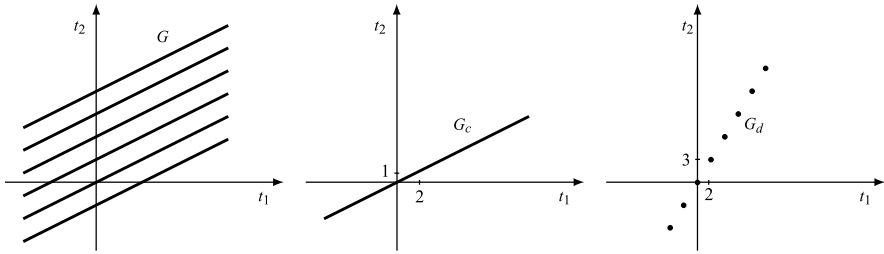


Fig. 16.1 Decomposition of a 2D grating G into 1D continuous group G_c and 1D lattice G_d

Example 16.1 A 2D grating G with basis and signature

$$\mathbf{G} = [\mathbf{g}_1 \quad \mathbf{g}_2] = \begin{bmatrix} 2 & 2 \\ 1 & 3 \end{bmatrix}, \quad H = \mathbb{R} \times \mathbb{Z},$$

is decomposed into the sum

$$G = \mathbf{g}_1\mathbb{R} + \mathbf{g}_2\mathbb{Z} = \begin{bmatrix} 2 \\ 1 \end{bmatrix}\mathbb{R} + \begin{bmatrix} 2 \\ 3 \end{bmatrix}\mathbb{Z},$$

where $\mathbf{g}_1\mathbb{R}$ and $\mathbf{g}_2\mathbb{Z}$ are 1D groups of \mathbb{R}^2 . The decomposition is shown in Fig. 16.1.

16.1.2 Interpretation of Continuous Subgroups

The additive group \mathbb{R}^m is also a *vector space* (with respect to the *field* of real numbers), where the multiplication by a scalar $\alpha\mathbf{t}$ is defined as $(\alpha t_1, \dots, \alpha t_m)$ for every $\mathbf{t} = (t_1, \dots, t_m) \in \mathbb{R}^m$ and every $\alpha \in \mathbb{R}$. A basis $\mathbf{G} = [\mathbf{g}_1, \dots, \mathbf{g}_m]$ of a group G is also a basis of the vector space \mathbb{R}^m since it allows the representation of every point \mathbf{t} of \mathbb{R}^m in the form $\mathbf{t} = (r_1\mathbf{g}_1 + \dots + r_m\mathbf{g}_m)$ for convenient $r_i \in \mathbb{R}$. A *pD subspace* of \mathbb{R}^m can be generated using p vectors of the basis \mathbf{G} , e.g., the first p vectors generate the subspace

$$V(\mathbf{g}_1 \cdots \mathbf{g}_p) = \{r_1\mathbf{g}_1 + \dots + r_p\mathbf{g}_p \mid r_1, \dots, r_p \in \mathbb{R}\}. \quad (16.9)$$

Also a *subspace* of \mathbb{R}^m turns out to be an Abelian group, and, in fact, we find by comparison that

$$V(\mathbf{g}_1 \cdots \mathbf{g}_p) = \mathbf{G}\mathbb{R}^p \times \mathbb{O}^{m-p}$$

is a continuous p D group in \mathbb{R}^m . For instance, in \mathbb{R}^3 the subspace/subgroup $V(\mathbf{g}_1) = \mathbf{G}\mathbb{R} \times \mathbb{O}^2$ is a line through the origin, $V(\mathbf{g}_1\mathbf{g}_2) = \mathbf{G}\mathbb{R}^2 \times \mathbb{O}$ is a plane through the origin, and $V(\mathbf{g}_1\mathbf{g}_2\mathbf{g}_3)$ is \mathbb{R}^3 itself.

UT 16.2 Representation of Gratings

In this section we study in detail *gratings*, that is, the LCA of \mathbb{R}^m with signature $\mathbb{R}^p \times \mathbb{Z}^q$ with $p, q > 0$ and $p + q = m$. While lattices are extensively considered in the framework of multidimensional signals, gratings have received a scarce attention, although they are encountered in several fields, particularly in image scanning (see Chap. 17).

In a general representation ($\mathbf{G}, \mathbb{R}^p \times \mathbb{Z}^q$) the grating depends on several parameters, most of which are redundant, but a very efficient representation (*reduced representation*) can be easily found.

16.2.1 Reduced Representation

Let $G = \mathbf{G}\mathbb{R}^p \times \mathbb{Z}^q$ be an m D grating. In the relation $\mathbf{t} = \mathbf{G}\mathbf{h}$ mapping the signature $H = \mathbb{R}^p \times \mathbb{Z}^q$ onto the grating G , we introduce the partitions

$$\mathbf{G} = \begin{bmatrix} \mathbf{A} & \mathbf{B} \\ \mathbf{C} & \mathbf{D} \end{bmatrix}, \quad \mathbf{h} = \begin{bmatrix} \mathbf{h}_r \\ \mathbf{n} \end{bmatrix}, \quad \mathbf{t} = \begin{bmatrix} \mathbf{t}_r \\ \mathbf{t}_d \end{bmatrix}, \quad (16.10)$$

where \mathbf{A} is $p \times p$, \mathbf{B} is $p \times q$, \mathbf{C} is $q \times p$, \mathbf{D} is $q \times q$, $\mathbf{h}_r \in \mathbb{R}^p$, and $\mathbf{n} \in \mathbb{Z}^q$. In such a way $\mathbf{t} = \mathbf{G}\mathbf{h}$ is split into the pair of relations

$$\mathbf{t}_r = \mathbf{A}\mathbf{h}_r + \mathbf{B}\mathbf{n}, \quad \mathbf{t}_d = \mathbf{C}\mathbf{h}_r + \mathbf{D}\mathbf{n}. \quad (16.11)$$

Now, suppose that \mathbf{A} is nonsingular, so that we can solve the first of (16.11) with respect to \mathbf{h}_r , namely $\mathbf{h}_r = \mathbf{A}^{-1}\mathbf{t}_r - \mathbf{A}^{-1}\mathbf{B}\mathbf{n}$. Then, substituting into the second, we find

$$\mathbf{t}_d = \mathbf{E}\mathbf{t}_r + \mathbf{F}\mathbf{n}, \quad (16.12)$$

where

$$\mathbf{E} = \mathbf{C}\mathbf{A}^{-1}, \quad \mathbf{F} = \mathbf{D} - \mathbf{C}\mathbf{A}^{-1}\mathbf{B}. \quad (16.13)$$

Since \mathbf{A} is nonsingular, it is easy to see that \mathbf{t}_r spans \mathbb{R}^p as well as \mathbf{h}_r . So, we can replace relations (16.11) by the new pair

$$\boxed{\mathbf{t}_r = \mathbf{r}, \quad \mathbf{t}_d = \mathbf{E}\mathbf{r} + \mathbf{F}\mathbf{n}, \quad \mathbf{r} \in \mathbb{R}^p, \quad \mathbf{n} \in \mathbb{Z}^q}, \quad (16.14)$$

which provides the *reduced representation* of the grating G . The new basis is given by the matrix

$$\mathbf{G}_r = \begin{bmatrix} \mathbf{I} & \mathbf{0} \\ \mathbf{E} & \mathbf{F} \end{bmatrix}, \quad (16.14a)$$

where \mathbf{I} is the $p \times p$ identity matrix, and $\mathbf{0}$ is the $p \times q$ zero matrix.

In conclusion, starting from an arbitrary representation ($\mathbf{G}, \mathbb{R}^p \times \mathbb{Z}^q$), where the first p rows and the first p columns of \mathbf{G} form a nonsingular matrix \mathbf{A} , we can find

the reduced representation $(\mathbf{G}_r, \mathbb{R}^p \times \mathbb{Z}^q)$, where \mathbf{E} and \mathbf{F} are defined by (16.13). If \mathbf{A} is singular, we can arrive at a reduced representation by an appropriate permutation of the coordinates.

16.2.2 Interpretation and Factorization

In the space \mathbb{R}^m with coordinates \mathbf{t}_r and \mathbf{t}_d , the grating G consists of *parallel p D hyperplanes* of (16.12), where each hyperplane is generated by the integer coordinates $\mathbf{n} \in \mathbb{Z}^q$; in particular, for $\mathbf{n} = \mathbf{0}$, the equation $\mathbf{t}_d = \mathbf{E}\mathbf{t}_r$ gives the hyperplanes through the origin. We call the hyperplanes the *rows* of the grating G . For $p = 1$, the rows are lines, for $p = 2$, they are planes, and for $p \geq 3$, the rows are hyperplanes.

Now, to investigate the meaning of the matrices \mathbf{E} and \mathbf{F} of the reduced representation, we introduce the coordinate change

$$\mathbf{t}_r = \mathbf{v}_r, \quad \mathbf{t}_d = \mathbf{E}\mathbf{v}_r + \mathbf{v}_d \quad (16.15)$$

to get from (16.14)

$$\mathbf{v}_r = \mathbf{r}, \quad \mathbf{v}_d = \mathbf{F}\mathbf{n}. \quad (16.16)$$

This relation pair defines the m D grating

$$G_0 = \mathbb{R}^p \times F \quad \text{with } F = \{\mathbf{F}\mathbf{n} \mid \mathbf{n} \in \mathbb{Z}^q\}, \quad (16.17)$$

where F is a q D lattice. Note that (16.15) defines a linear transformation (or coordinate change) $\mathbf{t} = \mathbf{a}_E \mathbf{v}$ with matrix

$$\mathbf{a}_E = \begin{bmatrix} \mathbf{I} & \mathbf{0} \\ \mathbf{E} & \mathbf{I} \end{bmatrix}, \quad (16.18)$$

which performs a coordinate *inclination*. Hence, every m D grating with signature $\mathbb{R}^p \times \mathbb{Z}^q$ can be obtained from the separable grating $G_0 = \mathbb{R}^p \times F$ by a coordinate change, which “tilts” \mathbb{R}^p with respect to F . This factorization is very useful in signal representation.

Essential Parameters We have seen that the general representation of a grating is somewhat redundant and one can always refer to the reduced representation, which is identified by two matrices, \mathbf{E} and \mathbf{F} . From the interpretation of a grating as a collection of rows, an alternative identification is provided by the zeroth row \mathbf{r}_0 , determined by \mathbf{E} , and the q D lattice $F = \mathbf{F}\mathbb{Z}^q$. Note that, for a given grating G , the matrix \mathbf{E} is unique, whereas the matrix \mathbf{F} is not, but unique is the *projection* lattice $F = \mathbf{F}\mathbb{Z}^q$.

The determinant of the reduced basis (16.14a) is given by

$$d(\mathbf{G}_r) = d(\mathbf{I})d(\mathbf{F}) = d(F), \quad (16.19)$$

where $d(F)$ is the lattice determinant, which is a quantity depending only on the lattice F . Hence, $d(\mathbf{G}_r)$ becomes independent of the representation.

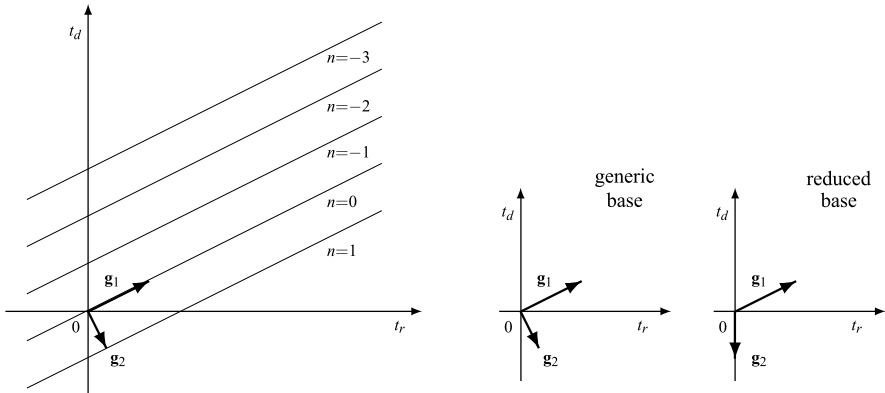


Fig. 16.2 Example of 2D grating with a generic basis and a reduced basis

16.2.3 2D and 3D Examples

Example 16.2 Consider the 2D grating with representation

$$\mathbf{G} = \begin{bmatrix} 2 & \frac{1}{2} \\ 1 & -1 \end{bmatrix}, \quad H = \mathbb{R} \times \mathbb{Z}.$$

Then, (16.11) becomes

$$t_r = 2h_r + \frac{1}{2}n, \quad t_d = h_r - n, \quad h_r \in \mathbb{R}, \quad n \in \mathbb{Z},$$

which can be written in the form (16.12), namely

$$t_r = r, \quad t_d = \frac{1}{2}r - \frac{5}{4}n, \quad r \in \mathbb{R}, \quad n \in \mathbb{Z}.$$

Hence, the grating consists of equally spaced parallel lines, as shown in Fig. 16.2. The reduced representation is given by

$$\mathbf{G}_r = \begin{bmatrix} 1 & 0 \\ \frac{1}{2} & -\frac{5}{4} \end{bmatrix}, \quad H = \mathbb{R} \times \mathbb{Z}.$$

The grating G can be obtained by the linear transformation with matrix

$$\mathbf{a}_E = \begin{bmatrix} 1 & 0 \\ \frac{1}{2} & 1 \end{bmatrix}$$

from the separable grating $G_0 = \mathbb{R} \times \mathbb{Z}(5/4)$.

Example 16.3 Consider the 3D gratings (Fig. 16.3)

$$G_1 = \mathbb{R}^2 \times \mathbb{Z}(d_3), \quad G_2 = \mathbb{R} \times \mathbb{Z}(d_2) \times \mathbb{Z}(d_3),$$

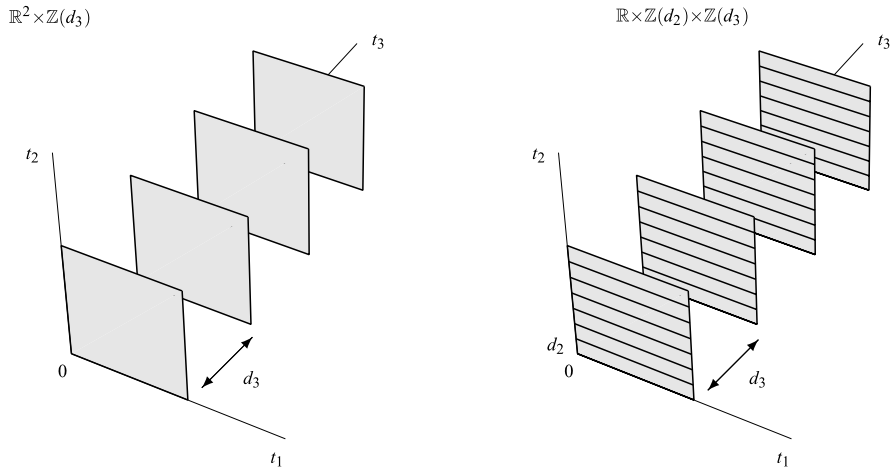


Fig. 16.3 Separable 3D gratings

which are separable and therefore do not require a representation for their specification. Anyway, their representations are respectively (in a reduced form)

$$\mathbf{G}_1 = \begin{bmatrix} 1 & 0 & 0 \\ 0 & 1 & 0 \\ 0 & 0 & d_3 \end{bmatrix}, \quad H_1 = \mathbb{R}^2 \times \mathbb{Z}, \quad \text{and}$$

$$\mathbf{G}_2 = \begin{bmatrix} 1 & 0 & 0 \\ 0 & d_2 & 0 \\ 0 & 0 & d_3 \end{bmatrix}, \quad H_2 = \mathbb{R} \times \mathbb{Z}^2.$$

The grating G_1 consists of *planes*, parallel to the t_1, t_2 plane and equally spaced by d_3 along the t_3 axis; its subspace is given by the t_1, t_2 plane. The grating G_2 consists of equally spaced *lines* parallel to the t_1 axis; its subspace is given by the t_1 axis. Note that G_2 is a subgroup of G_1 .

Example 16.4 Consider the 3D nonseparable gratings with reduced representations (Fig. 16.4)

$$\mathbf{G}_1 = \begin{bmatrix} 1 & 0 & 0 \\ 0 & 1 & 0 \\ 0 & a & d_3 \end{bmatrix}, \quad H_1 = \mathbb{R}^2 \times \mathbb{Z},$$

$$\mathbf{G}_2 = \begin{bmatrix} 1 & 0 & 0 \\ a & d_2 & 0 \\ b & 0 & d_3 \end{bmatrix}, \quad H_2 = \mathbb{R} \times \mathbb{Z}^2.$$

The grating G_1 consists of *parallel planes*, equally spaced of d_3 along the t_3 axis, but the planes are tilted with respect to the t_1, t_2 plane in dependence of the parameter a (for $a = 0$, we obtain the grating G_1 of the previous example). This grating can be

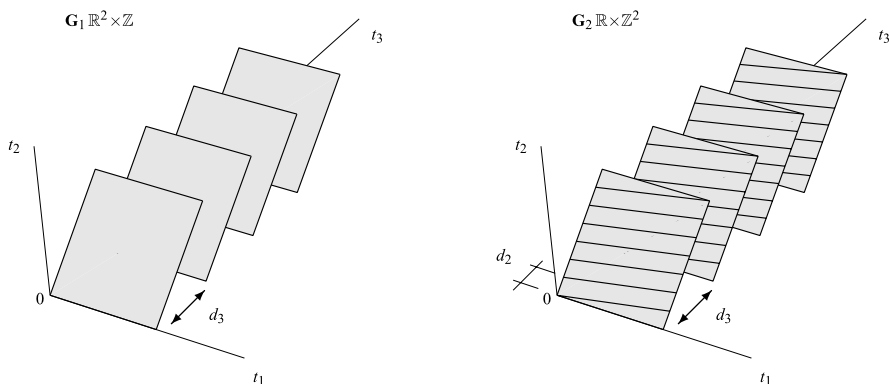


Fig. 16.4 Nonseparable 3D gratings

obtained from the separable grating $G_0 = \mathbb{R}^2 \times \mathbb{Z}(d_3)$ with the coordinate change

$$\mathbf{a}_E = \begin{bmatrix} 1 & 0 & 0 \\ 0 & 1 & 0 \\ 0 & a & 1 \end{bmatrix}, \quad \mathbf{E} = [0, \quad a], \quad v_1 = t_1, \quad v_2 = t_2 + at_3, \quad v_3 = t_3.$$

The grating G_2 consists of *parallel lines*, which are tilted with respect to all coordinate axes. The inclination is given by the parameters a and b , whereas d_2 and d_3 give the spacings between the lines. This grating can be obtained from the separable grating $G_0 = \mathbb{R}^2 \times \mathbb{Z}(d_3)$ with the coordinate change

$$\mathbf{a}_E = \begin{bmatrix} 1 & 0 & 0 \\ a & 1 & 0 \\ b & 0 & 1 \end{bmatrix}, \quad \mathbf{E} = \begin{bmatrix} a \\ b \end{bmatrix}.$$

UT 16.3 Signals on a Grating

A signal defined on a grating G is not a simple object, but it becomes amenable as soon as the reduced representation and the factorization of the grating are considered.

16.3.1 Signals and Fourier Transforms on a Separable Grating

We begin with this case, which will be the reference for the general case. Let $G_0 = \mathbb{R}^p \times F$ be the separable grating, where $F = \mathbf{F}\mathbb{Z}^q$ is a q D lattice. Then, a signal on G_0 has the structure

$$s_0(\mathbf{r}, \mathbf{u}), \quad \mathbf{r} \in \mathbb{R}^p, \quad \mathbf{u} \in F. \tag{16.20}$$

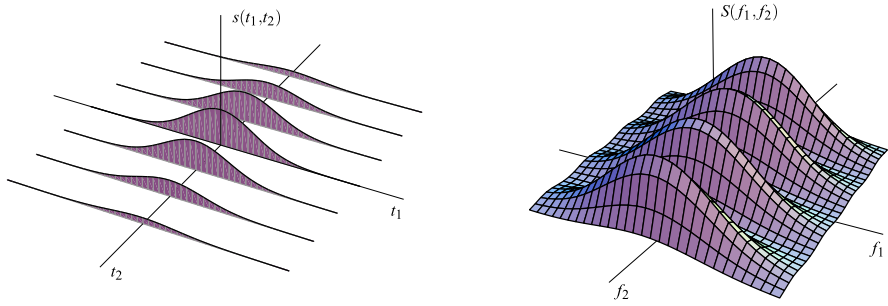


Fig. 16.5 Signal on the grating $\mathbb{R} \times \mathbb{Z}(d)$ and its Fourier transform

An example of 2D signal with $G = \mathbb{R} \times \mathbb{Z}(d)$ is shown in Fig. 16.5.

The Haar integral of signal (16.20) is easily written considering the separability

$$\int_{G_0} d\mathbf{v} s_0(\mathbf{v}) = \int_{\mathbb{R}^p} d\mathbf{r} \sum_{\mathbf{u} \in F} d(F) s_0(\mathbf{r}, \mathbf{u}) \tag{16.21}$$

and is the combination of a p D Lebesgue integral and a q D series.

The frequency domain is given by

$$\widehat{G}_0 = \mathbb{O}^p \times \mathbb{R}^q / F^*, \tag{16.22}$$

where F^* is the reciprocal lattice. Then, the FT $S_0(\lambda_r, \mu)$ is aperiodic with respect to the first p coordinate and periodic with respect to the last q coordinates with periodicity F^* . The expressions of the FT and inverse FT are

$$\begin{aligned} S_0(\lambda_r, \mu) &= \int_{\mathbb{R}^p} d\mathbf{r} \sum_{\mathbf{u} \in F} d(F) s_0(\mathbf{r}, \mathbf{u}) e^{-i2\pi(\lambda'_r \mathbf{r} + (\mu')' \mathbf{u})}, \\ s_0(\mathbf{r}, \mathbf{u}) &= \int_{\mathbb{R}^p} d\lambda_r \int_{\mathbb{R}^q / F^*} d\mu S_0(\lambda_r, \mathbf{u}) e^{i2\pi(\lambda'_r \mathbf{r} + \mu' \mathbf{u})}. \end{aligned} \tag{16.23}$$

16.3.2 Signals and Fourier Transforms on a Nonseparable Grating

When the grating is nonseparable, it is convenient to adopt the reduced representation (16.14), which expresses the signal in the form $s(\mathbf{t})$, $\mathbf{t} \in \mathbf{G}_r \mathbb{R}^p \times \mathbb{Z}^q$, and more explicitly

$$s(\mathbf{r}, E\mathbf{r} + \mathbf{F}\mathbf{n}), \quad \mathbf{r} \in \mathbb{R}^p, \mathbf{n} \in \mathbb{Z}^q. \tag{16.24}$$

Considering that the determinant is given by (16.19), the Haar integral of signal (16.24) is given by

$$\int_G d\mathbf{t} s(\mathbf{t}) = \int_{\mathbb{R}^p} d\mathbf{r} \sum_{\mathbf{n} \in \mathbb{Z}^q} d(F) s(\mathbf{r}, E\mathbf{r} + \mathbf{F}\mathbf{n})$$

$$= \int_{\mathbb{R}^p} d\mathbf{r} \sum_{\mathbf{u} \in F} d(F) s(\mathbf{r}, \mathbf{E}\mathbf{r} + \mathbf{u}), \quad (16.25)$$

where the last summation is extended to the projection lattice $F = \mathbf{F}\mathbb{Z}^q$.

The frequency domain is given by

$$\widehat{G} = \mathbb{R}^m / G^* \quad \text{with } G^* = \mathbf{G}_r^* \otimes \mathbb{O}^p \times \mathbb{Z}^q. \quad (16.26)$$

Considering the simple expression (16.14a) of the reduced basis, the *reciprocal* matrix (the inverse of the transpose) is easily found. In fact,

$$\mathbf{G}'_r = \begin{bmatrix} \mathbf{I} & \mathbf{E}' \\ \mathbf{0} & \mathbf{F}' \end{bmatrix}, \quad \mathbf{G}_r^* = (\mathbf{G}'_r)^{-1} = \begin{bmatrix} \mathbf{I} & -\mathbf{E}'\mathbf{F}^* \\ \mathbf{0} & \mathbf{F}^* \end{bmatrix}.$$

Then, from (16.26) we find that the FT $S(\mathbf{f})$ has a continuous m D domain and a partial periodicity, only with respect to q coordinates.

Now, the FT can be written in terms of the Haar integral expression (16.25), but we consider it more convenient to introduce a coordinate change that removes the inclination and the nonseparability of the frequency-domain periodicity. The needed transformation is given by the matrix \mathbf{a}_E defined by (16.18). Then, we introduce the auxiliary signal

$$s_0(\mathbf{v}) = s(\mathbf{a}_E\mathbf{v}), \quad \mathbf{v} \in G_0 = \mathbb{R}^p \times F, \quad (16.27)$$

which is defined on the separable grating G_0 , and we follow the graph

$$\begin{array}{ccccccc} s(\mathbf{t}) & \xrightarrow{\mathbf{a}_E} & s_0(\mathbf{v}) & \xrightarrow{\mathcal{F}} & S_0(\boldsymbol{\lambda}) & \xrightarrow{\mathbf{a}'_E} & S(f) \\ G & & G_0 & & \widehat{G}_0 & & \widehat{G} \end{array} \quad (16.28)$$

Here, the FT $S_0(\boldsymbol{\lambda})$ of the auxiliary signal is calculated according to (16.23), and $S(\mathbf{f})$ is obtained by a linear transformation with matrix \mathbf{a}'_E (the transpose of \mathbf{a}_E). In fact, in the frequency domain (16.27) becomes (see (5.93) and note that $d(\mathbf{a}_E) = 1$)

$$S_0(\boldsymbol{\lambda}) = S(\mathbf{a}_E^* \boldsymbol{\lambda}), \quad \boldsymbol{\lambda} \in \widehat{G}_0, \quad (16.29)$$

where $\mathbf{a}_E^* = (\mathbf{a}'_E)^{-1}$ is the reciprocal matrix. Then, the inverse of this relation is expressed with the inverse of \mathbf{a}_E^* , that is, \mathbf{a}'_E .

We summarize for convenience the matrices

$$\begin{array}{ll} \mathbf{a}_E = \begin{bmatrix} \mathbf{I} & \mathbf{0} \\ \mathbf{E} & \mathbf{I} \end{bmatrix}, & \mathbf{a}_E^{-1} = \begin{bmatrix} \mathbf{I} & \mathbf{0} \\ -\mathbf{E} & \mathbf{I} \end{bmatrix}, \\ \mathbf{a}'_E = \begin{bmatrix} \mathbf{I} & \mathbf{E}' \\ \mathbf{0} & \mathbf{I} \end{bmatrix}, & \mathbf{a}_E^* = \begin{bmatrix} \mathbf{I} & -\mathbf{E}' \\ \mathbf{0} & \mathbf{I} \end{bmatrix} \end{array} \quad (16.30)$$

and the coordinate changes

$$\begin{aligned}
 s_0(\mathbf{v}) = s(\mathbf{a}_E \mathbf{v}) &\longrightarrow s_0(\mathbf{r}, \mathbf{u}) = s(\mathbf{r}, \mathbf{E}\mathbf{r} + \mathbf{u}), \\
 s(\mathbf{t}) = s(\mathbf{a}_E^{-1} \mathbf{v}) &\longrightarrow s(\mathbf{t}_r, \mathbf{t}_d) = s_0(\mathbf{t}_r, -\mathbf{E}\mathbf{t}_r + \mathbf{t}_d), \\
 S(\mathbf{f}) = S_0(\mathbf{a}'_E \mathbf{v}) &\longrightarrow S(\mathbf{f}_r, \mathbf{f}_d) = S_0(\mathbf{f}_r + \mathbf{E}'\mathbf{f}_d, \mathbf{f}_d), \\
 S_0(\boldsymbol{\lambda}) = S(\mathbf{a}_E^* \boldsymbol{\lambda}) &\longrightarrow S_0(\boldsymbol{\lambda}_r, \boldsymbol{\mu}) = S(\boldsymbol{\lambda}_r - \mathbf{E}'\boldsymbol{\mu}, \boldsymbol{\mu}).
 \end{aligned} \tag{16.31}$$

UT 16.4 Generation of Subgroups

In this section we investigate the generation of the subgroups of a given group $G \in \mathcal{G}(\mathbb{R}^m)$, that is, the groups of the class $\mathcal{G}(G)$. As an application, we may refer to down-sampling, where, starting from a signal defined on G , we want to obtain a signal defined on a subgroup of G . Another application is in the operation of image scanning where the original image is often defined on a grating, and we want to transform the image to pixels.

We suppose that the reference group G is full-dimensional:

$$G = \mathbf{G}H \quad \text{with } H = \mathbb{R}^p \times \mathbb{Z}^q, \quad p + q = m.$$

Then, the dimensionality of a subgroup J of G is at most m , and the signature of J is always a subgroup of H (apart from a permutation).

There are two natural ways to get subgroups. A first way is a *restriction of the signature* from $H = \mathbb{R}^p \times \mathbb{Z}^q$ to $\mathbb{R}^{p-1} \times \mathbb{Z}^{q+1}$ or $\mathbb{R}^{p-2} \times \mathbb{Z}^{q+2}$, etc. In such a way, some of the real coefficients of the linear combination generating G become integer. If we allow the presence of the factor \mathbb{O} in the signature, we obtain subgroups with a reduced dimensionality. For instance, starting from the 3D signature $\mathbb{R} \times \mathbb{Z}^2$, the restrictions with the factor \mathbb{O} may be $\mathbb{R} \times \mathbb{Z} \times \mathbb{O}$, $\mathbb{R} \times \mathbb{O}^2$, etc.

The second way is a *basis enhancement*. To explain the idea, consider the 2D case in which the basis $\mathbf{G} = [\mathbf{g}_1 \mathbf{g}_2]$ consists of two vectors, \mathbf{g}_1 and \mathbf{g}_2 . Then an enhanced basis is obtained by multiplying the vectors by integers, e.g., by 2 and 5, to get the enhanced basis $\mathbf{J} = [\mathbf{j}_1, \mathbf{j}_2] = [2\mathbf{g}_1, 5\mathbf{g}_2]$, which provides a subgroup as $J = \mathbf{J}H$.

Signature restriction and basis enhancement can be combined for subgroup generation. As we shall see, the topic is not trivial, and so we proceed by steps.

16.4.1 Subgroup Generated from Points of the Group

A basis of an m D group is an arbitrary $m \times m$ nonsingular real matrix. In the context of subgroup generation, it is “convenient” to form bases by picking up m independent points of the group G .

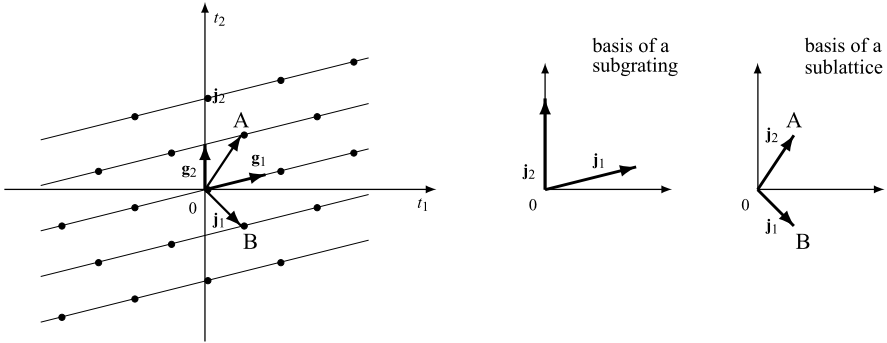


Fig. 16.6 2D grating and bases for its subgroups

We begin by noting that a point \mathbf{j} of $G = \mathbf{G}H$, written in compact form, is $\mathbf{j} = \mathbf{G}\mathbf{k}$, $\mathbf{k} \in H$, and a couple of points $\mathbf{j}_1 = \mathbf{G}\mathbf{k}_1$, $\mathbf{j}_2 = \mathbf{G}\mathbf{k}_2$ can be written in the form $[\mathbf{j}_1 \mathbf{j}_2] = \mathbf{G}[\mathbf{k}_1 \mathbf{k}_2]$, $\mathbf{k}_1, \mathbf{k}_2 \in H$. With m points $\mathbf{j}_1, \dots, \mathbf{j}_m$ of G , we obtain an $m \times m$ matrix, namely

$$\underbrace{[\mathbf{j}_1 \cdots \mathbf{j}_m]}_{\mathbf{J}} = \mathbf{G} \underbrace{[\mathbf{k}_1 \cdots \mathbf{k}_m]}_{\mathbf{K}}, \quad \mathbf{k}_i \in H. \tag{16.32}$$

Hence, a “convenient” basis \mathbf{J} for generating a subgroup J of a group $G = \mathbf{G}H$ is formed by m independent points $\mathbf{j}_1 = \mathbf{G}\mathbf{k}_1, \dots, \mathbf{j}_m = \mathbf{G}\mathbf{k}_m$ of G . The basis can be written in the form

$$\mathbf{J} = \mathbf{G}\mathbf{K}, \quad \mathbf{K} = \left[\begin{array}{l} \mathbf{K}_1 \\ \mathbf{K}_2 \end{array} \right] \left. \begin{array}{l} \} p \text{ real,} \\ \} q \text{ integer,} \end{array} \right. \tag{16.33}$$

where, if the group signature is $H = \mathbb{R}^p \times \mathbb{Z}^q$, the first p rows of \mathbf{K} are real, and the last q rows are integer. For instance, if G is a 2D grating $G = [\mathbf{g}_1 \mathbf{g}_2]$ ($\mathbb{R} \times \mathbb{Z}$), the points of J are explicitly

$$\mathbf{j}_1 = r_1 \mathbf{g}_1 + n_1 \mathbf{g}_2, \quad \mathbf{j}_2 = r_2 \mathbf{g}_1 + n_2 \mathbf{g}_2, \tag{16.34}$$

where $r_1, r_2 \in \mathbb{R}$ and $n_1, n_2 \in \mathbb{Z}$. Then, the “convenient” basis can be written in the form

$$\mathbf{J} = \underbrace{[\mathbf{g}_1 \quad \mathbf{g}_2]}_{\mathbf{G}} \underbrace{\left[\begin{array}{cc} r_1 & r_2 \\ n_1 & n_2 \end{array} \right]}_{\mathbf{K}} \left. \begin{array}{l} \text{real,} \\ \text{integer.} \end{array} \right. \tag{16.35}$$

Now, we investigate when a “convenient” basis \mathbf{J} , equipped with a signature $K = K_1 \times \dots \times K_m$, really generates a subgroup $J = \mathbf{J}\mathbf{K}$ of G . We begin with the case of 2D grating $G = [\mathbf{g}_1 \mathbf{g}_2]$ ($\mathbb{R} \times \mathbb{Z}$), which consists of equally distant parallel lines (Fig. 16.6), and its subgroups may be gratings with signature $K = \mathbb{R} \times \mathbb{Z}$ and lattices (with signature $K = \mathbb{Z}^2$), and also reduced-dimensional groups (here not considered). A subgrating J is formed by a subset of equally spaced lines of G , and

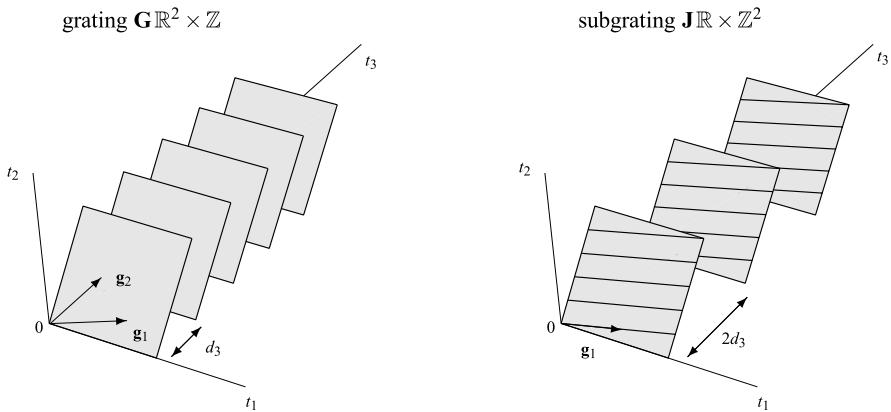


Fig. 16.7 3D grating with signature $\mathbb{R}^2 \times \mathbb{Z}$ and subgrating with signature $\mathbb{R} \times \mathbb{Z}^2$

it is evident that its basis $\mathbf{J} = [\mathbf{j}_1, \mathbf{j}_2]$ has the constraint that \mathbf{j}_1 must be aligned with \mathbf{g}_1 , otherwise \mathbf{j}_1 would produce lines not contained in G . On the other hand, for a sublattice, there is no constraint, and, in fact, if we take two arbitrary nonparallel vectors \mathbf{j}_1 and \mathbf{j}_2 connecting the origin to two points A and B of the grating, we obtain a basis for a sublattice. These constraints can be expressed in terms of the matrix \mathbf{K} in relation (16.35), where \mathbf{J} forms a basis for the candidate subgroup $J = \mathbf{J}\mathbf{K}$, and the vectors of \mathbf{J} are explicitly given by (16.34). Now, if $K = \mathbb{Z}^2$, that is, if we consider a sublattice, we have no constraint. But, if $K = \mathbb{R} \times \mathbb{Z}$, we have the constraint that \mathbf{j}_1 must be parallel to \mathbf{g}_1 , which implies, and is implied by, the condition that in (16.34) $n_1 = 0$. If the signature K becomes $\mathbb{Z} \times \mathbb{R}$, the constraint is that \mathbf{j}_2 must be parallel to \mathbf{g}_2 and therefore $n_2 = 0$. In conclusion, the possible matrices \mathbf{K} are

$$\mathbf{K} = \begin{bmatrix} r_1 & r_2 \\ n_1 & n_2 \end{bmatrix}, \quad \mathbf{K} = \begin{bmatrix} r_1 & r_2 \\ 0 & n_2 \end{bmatrix}, \quad \mathbf{K} = \begin{bmatrix} r_1 & r_2 \\ n_1 & 0 \end{bmatrix} \begin{matrix} \text{real,} \\ \text{integer.} \end{matrix} \tag{16.36}$$

$$K = \mathbb{Z} \times \mathbb{Z} \qquad K = \mathbb{R} \times \mathbb{Z} \qquad K = \mathbb{Z} \times \mathbb{R}$$

Next, consider the subgroups of the 3D grating $G = \mathbf{G}\mathbb{R}^2 \times \mathbb{Z}$, which consists of equidistant parallel planes (Fig. 16.7). The vectors of the subgroup basis

$$\mathbf{J} = [\mathbf{j}_1 \quad \mathbf{j}_2 \quad \mathbf{j}_3] = \mathbf{G}\mathbf{H} = [\mathbf{g}_1 \quad \mathbf{g}_2 \quad \mathbf{g}_3] \begin{bmatrix} r_1 & r_2 & r_3 \\ s_1 & s_2 & s_3 \\ n_1 & n_2 & n_3 \end{bmatrix} \begin{matrix} \text{real,} \\ \text{real,} \\ \text{integer} \end{matrix}$$

are explicitly

$$\mathbf{j}_k = r_k \mathbf{g}_1 + s_k \mathbf{g}_2 + n_k \mathbf{g}_3, \quad r_k, s_k \in \mathbb{R}, \quad n_k \in \mathbb{Z}, \quad k = 1, 2, 3,$$

and their choice is constrained by the signature K of the candidate subgroup $J = \mathbf{J}\mathbf{K}$. Again, if $K = \mathbb{Z}^3$, we have no constraint. If $K = \mathbb{R}^2 \times \mathbb{Z}$, the subgroup

J is formed by a subset of the planes of G , and to generate such planes, the first two vectors \mathbf{j}_1 and \mathbf{j}_2 must lie on the plane determined by \mathbf{g}_1 and \mathbf{g}_2 . This is assured if \mathbf{j}_1 and \mathbf{j}_2 do not receive a contribution from \mathbf{g}_3 , that is, if $n_1 = n_2 = 0$. If $K = \mathbb{R} \times \mathbb{Z}^2$, the subgroup J is formed by parallel lines belonging to the planes of G (Fig. 16.7, right). Since the lines are parallel to the vector $\mathbf{j}_1 = r_1\mathbf{g}_1 + s_1\mathbf{g}_2 + n_1\mathbf{g}_3$, the condition is that \mathbf{j}_1 lie on the plane determined by \mathbf{g}_1 and \mathbf{g}_2 , that is, $n_1 = 0$ (which ensures that \mathbf{j}_1 has no contribution from \mathbf{g}_3). The conclusion is summarized by

$$\begin{aligned} \mathbf{K} &= \begin{bmatrix} r_1 & r_2 & r_3 \\ s_1 & s_2 & s_3 \\ n_1 & n_2 & n_3 \end{bmatrix}, & \mathbf{K} &= \begin{bmatrix} r_1 & r_2 & r_3 \\ s_1 & s_2 & s_3 \\ 0 & n_2 & n_3 \end{bmatrix}, \\ K &= \mathbb{Z} \times \mathbb{Z} \times \mathbb{Z} & K &= \mathbb{R} \times \mathbb{Z} \times \mathbb{Z} \end{aligned} \tag{16.37}$$

$$\begin{aligned} \mathbf{K} &= \begin{bmatrix} r_1 & r_2 & r_3 \\ s_1 & s_2 & s_3 \\ 0 & 0 & n_3 \end{bmatrix}. \\ K &= \mathbb{R} \times \mathbb{R} \times \mathbb{Z} \end{aligned}$$

16.4.2 Fundamental Theorem on Subgroups

We have seen how to generate a basis $\mathbf{J} = [\mathbf{j}_1 \cdots \mathbf{j}_m] = \mathbf{G}\mathbf{K}$ from m independent points of a group $G = \mathbf{G}\mathbb{R}^p \times \mathbb{Z}^q$ and the construction of a subgroup $J = \mathbf{J}\mathbf{K}$. We have also seen, in the 2D and 3D cases, that the subgroup condition $J \subset G$ requires that some entries of the matrix \mathbf{K} must be zero, in dependence on the subgroup signature K (see (16.36) and (16.37)). In general, with a signature $K = \mathbb{R}^{p-a} \times \mathbb{Z}^{q+a}$, the condition is essentially that the first $p - a$ vectors $\mathbf{j}_1, \mathbf{j}_2, \dots, \mathbf{j}_{p-a}$ must not receive a contribution from the vectors $\mathbf{g}_{p-a+1}, \dots, \mathbf{g}_m$. This general condition is developed in Appendix, with an alternative approach with respect to the preliminary considerations done for the 2D and 3D cases. The final statement is the following:

Theorem 16.1 *Let $G = \mathbf{G}\mathbb{R}^p \times \mathbb{Z}^q$ be an m D group of \mathbb{R}^m , and let $\mathbf{j}_s = \mathbf{G}\mathbf{k}_s$ be m independent points of G , written in the form*

$$\mathbf{J} = [\mathbf{j}_1 \cdots \mathbf{j}_m] = \mathbf{G}\mathbf{K}, \quad \mathbf{K} = [\mathbf{k}_1 \cdots \mathbf{k}_m], \tag{16.38}$$

where the first p rows of \mathbf{K} are real, and the last q rows are integer. Then

- (1) the group

$$J = \mathbf{J}\mathbb{R}^{p-a} \times \mathbb{Z}^{q+a}, \quad 0 \leq a \leq p, \tag{16.39}$$

is a subgroup of G if and only if the last q elements of the first $p - a$ columns of \mathbf{K} are zero,

- (2) all subgroups of G are generated in the form (1), apart from a signature permutation.

16.4.3 Corollaries on Subgroups: Degenerate Subgroups

The fundamental theorem has several corollaries. For $a = p$, it provides the way to generate *all the sublattices* of a given group:

Corollary 16.1 *Let $G = \mathbf{G}\mathbb{R}^p \times \mathbb{Z}^q$ be an mD group with $m = p + q$. Then, all the mD sublattices are generated by the bases of the form*

$$\mathbf{J} = \mathbf{G}\mathbf{K}, \tag{16.40}$$

where \mathbf{K} are nonsingular matrices with the first p rows real and the last q rows integer.

With $a = p = 0$ and $q = m$, Theorem 16.1 gives all sublattices of a given lattice, as we shall see in detail in the next section, and with $a = 0$ it gives all subgratings of a given grating.

The fundamental theorem can be easily extended to include subgroups with a reduced dimensionality. The simplest way to generate such subgroups is the *signature restriction* of a full-dimensional subgroup. Thus, if the signature of the subgroup is, e.g., $K = \mathbb{R} \times \mathbb{Z}^2$, by replacing one or two of the factors $\mathbb{R}, \mathbb{Z}, \mathbb{Z}$ by \mathbb{O} we obtain respectively 2D or 1D subgroups.

UT 16.5 Lattices and Sublattices

In this and the following sections we examine in great detail the mD lattices of \mathbb{R}^m , that is, the groups with signature $H = \mathbb{Z}^m$ generated according to

$$G = \{ \mathbf{G}\mathbf{n} \mid \mathbf{n} \in \mathbb{Z}^m \} = \mathbf{G}\mathbb{Z}^m. \tag{16.41}$$

As we shall see, lattice theory is strongly related to the theory of *integer matrices*. The class of the nonsingular $m \times m$ integer matrices will be denoted by \mathcal{J}_m , and the subclass of *unimodular matrices* by \mathcal{U}_m . A unimodular matrix \mathbf{E} is an integer matrix, $\mathbf{E} \in \mathcal{J}_m$ having $d(\mathbf{E}) = 1$, that is, $\det \mathbf{E} = \pm 1$, and has the property that its inverse also is unimodular, $\mathbf{E}^{-1} \in \mathcal{U}_m$.

16.5.1 The Possible Bases of a Lattice

The basis \mathbf{G} of a group G is not unique, but for lattices, the variety of bases is limited according to the following:

Theorem 16.2 *If \mathbf{G} is a basis of a lattice G , all the possible bases have the form $\mathbf{G}\mathbf{E}$, where \mathbf{E} is a unimodular matrix, $\mathbf{E} \in \mathcal{U}_m$.*

This represents one of the most relevant results of lattice theory [3]. As a consequence, the *determinant* is given by

$$d(\mathbf{GE}) = d(\mathbf{G})d(\mathbf{E}) = d(\mathbf{G}), \quad \mathbf{E} \in \mathcal{U}_m, \quad (16.42)$$

and therefore it is independent of the basis and denoted by $d(G)$ instead of $d(\mathbf{G})$.

Proof By the fundamental theorem, if \mathbf{G} is a basis of the lattice G , the basis $\mathbf{J} = \mathbf{GE}$, $\mathbf{E} \in \mathcal{U}_m \subset \mathcal{J}_m$, generates a sublattice J of G . But, if $\mathbf{E} \in \mathcal{U}_m$ is unimodular, so is \mathbf{E}^{-1} . Then, we also have $\mathbf{G} = \mathbf{JE}^{-1}$, $\mathbf{E}^{-1} \in \mathcal{J}_m$, which states that G is a sublattice of J . Hence, $J \subset G$ and $G \subset J$, and therefore $J = G$. \square

Related to a lattice $G = \mathbf{G}\mathbb{Z}^m$ is the *fundamental parallelepiped*

$$P = \mathbf{G}[0, 1)^m = \{\alpha_1 \mathbf{g}_1 + \cdots + \alpha_m \mathbf{g}_m \mid \alpha_1, \dots, \alpha_m \in [0, 1)\}, \quad (16.43)$$

which represents a cell of \mathbb{R}^m modulo G (see Sect. 3.5). Its volume is given by the determinant of G (as is for any other cell of type $[\mathbb{R}^m/G)$).

Also related to a lattice $G = \mathbf{G}\mathbb{Z}^m$ is its reciprocal G^* . By Theorem 5.2, the reciprocal is a lattice given by

$$G^* = \mathbf{G}^*\mathbb{Z}^m, \quad \mathbf{G}^* = (\mathbf{G}')^{-1}. \quad (16.44)$$

16.5.2 Sublattices

According to Theorem 16.1 (or Corollary 16.1), the class $\mathcal{L}_m(G)$ of the sublattices of a given lattice can be generated as follows:

Corollary 16.2 *Let G be a lattice, and let \mathbf{G} be a basis of G . Then, all sublattices J of G are generated by the bases*

$$\mathbf{J} = \mathbf{G}\mathbf{K}, \quad \mathbf{K} \in \mathcal{J}_m. \quad (16.45)$$

Since \mathbf{K} is a nonsingular integer matrix, it follows that $d(\mathbf{K})$ is a natural with $d(\mathbf{K}) \geq 1$. If $d(\mathbf{K}) = 1$, \mathbf{K} is unimodular, and, by Theorem 16.2, $J = G$. Then, $d(\mathbf{K}) \geq 2$ is the condition for J to be a proper sublattice of G .

For a given pair G, J , where G is a lattice and J a sublattice, the ratio

$$(G : J) \stackrel{\Delta}{=} d(J)/d(G) \in \mathbb{N}$$

is a natural called the *index of J in G* (see Sect. 3.3). It represents the reduction of the density of J with respect to the density of G .

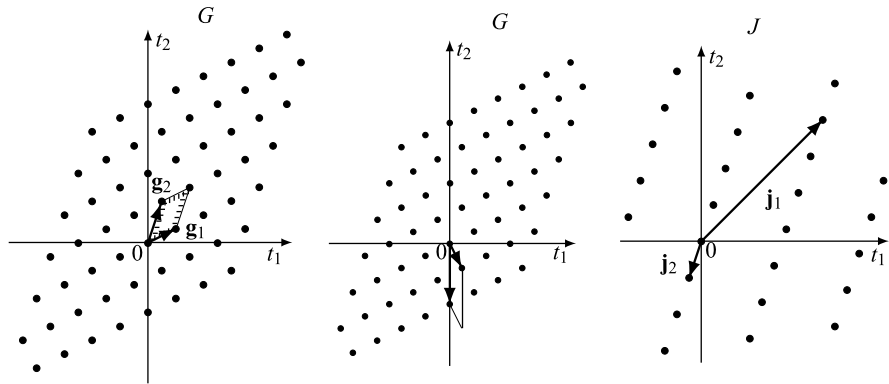


Fig. 16.8 2D lattice G with illustration of the fundamental parallelepiped, with two different bases. On the *right*, a sublattice J of G

16.5.3 Illustrations for 2D Lattices

The above statements are now detailed for 2D lattices. A 2D lattice $G = \mathbf{G}\mathbb{Z}^2$ with basis

$$\mathbf{G} = \begin{bmatrix} g_{11} & g_{12} \\ g_{21} & g_{22} \end{bmatrix}, \quad d(\mathbf{G}) = |g_{11}g_{22} - g_{21}g_{12}| > 0,$$

is given by the points (t_1, t_2) of \mathbb{R}^2 generated by the relations

$$t_1 = g_{11}n_1 + g_{12}n_2, \quad t_2 = g_{21}n_1 + g_{22}n_2, \quad n_1, n_2 \in \mathbb{Z}.$$

Figure 16.8 shows a lattice with basis

$$\mathbf{G} = \begin{bmatrix} 2 & 1 \\ 1 & 3 \end{bmatrix}, \quad d(G) = 5. \tag{16.46}$$

By right multiplying the basis \mathbf{G} by a unimodular matrix \mathbf{A} , we obtain a new basis \mathbf{GA} ; for instance,

$$\mathbf{GA} = \begin{bmatrix} 2 & 1 \\ 1 & 3 \end{bmatrix} \begin{bmatrix} 1 & 1 \\ -1 & -2 \end{bmatrix} = \begin{bmatrix} 1 & 0 \\ -2 & -5 \end{bmatrix}$$

is a new basis, as shown in Fig. 16.8. The fundamental parallelepiped changes, but not its area, given by $d(G) = 5$.

By right multiplying \mathbf{G} by an integer matrix \mathbf{A} with $d(\mathbf{A}) \geq 2$ we obtain a basis \mathbf{J} of a sublattice J of I . For instance,

$$\mathbf{J} = \begin{bmatrix} 2 & 1 \\ 1 & 3 \end{bmatrix} \begin{bmatrix} 4 & 0 \\ 2 & -1 \end{bmatrix} = \begin{bmatrix} 10 & -1 \\ 10 & -3 \end{bmatrix}, \quad d(J) = 5 \cdot 4 = 20, \tag{16.47}$$

gives the sublattice J of Fig. 16.8.

The reciprocal of G is obtained by calculating the reciprocal basis, namely

$$\mathbf{G} = \begin{bmatrix} 2 & 1 \\ 1 & 3 \end{bmatrix}, \quad \mathbf{G}' = \begin{bmatrix} 2 & 1 \\ 1 & 3 \end{bmatrix}, \quad (\mathbf{G}')^{-1} = \begin{bmatrix} \frac{3}{5} & -\frac{1}{5} \\ -\frac{1}{5} & \frac{2}{5} \end{bmatrix} = \mathbf{G}^*.$$

UT 16.6 Triangularization and Diagonalization of Integer Matrices

In this section we develop some topics on integer matrices, which are fundamental for lattice theory. For a survey on integer matrices, see reference [4].

16.6.1 Elementary Operations

Elementary operations provide the rearrangement of an integer matrix to obtain canonical forms. Given an $m \times n$ integer matrix \mathbf{A} , the *elementary operations on the columns* are:

- (1) permutation of two columns,
- (2) multiplication of a column by -1 ,
- (3) replacement of a column by the sum of itself and an integer k multiple of any other column.

For instance, if $\mathbf{A} = [\mathbf{a}_1 \mathbf{a}_2 \mathbf{a}_3]$ is an $m \times 3$ matrix, examples of (1), (2), and (3) are respectively

$$[\mathbf{a}_3 \mathbf{a}_2 \mathbf{a}_1], \quad [\mathbf{a}_1 - \mathbf{a}_2 \mathbf{a}_3], \quad [\mathbf{a}_1 \mathbf{a}_2 \mathbf{a}_3 + k \mathbf{a}_1].$$

We can check that the modified matrices can be obtained from \mathbf{A} by a *right multiplication by a unimodular matrix*. In fact,

$$\begin{aligned} [\mathbf{a}_3 \mathbf{a}_2 \mathbf{a}_1] &= [\mathbf{a}_1 \mathbf{a}_2 \mathbf{a}_3] \begin{bmatrix} 0 & 0 & 1 \\ 0 & 1 & 0 \\ 1 & 0 & 0 \end{bmatrix}, \\ [\mathbf{a}_1 - \mathbf{a}_2 \mathbf{a}_3] &= [\mathbf{a}_1 \mathbf{a}_2 \mathbf{a}_3] \begin{bmatrix} 1 & 0 & 0 \\ 0 & -1 & 0 \\ 0 & 0 & 1 \end{bmatrix}, \\ [\mathbf{a}_1 \mathbf{a}_2 \mathbf{a}_3 + m \mathbf{a}_1] &= [\mathbf{a}_1 \mathbf{a}_2 \mathbf{a}_3] \begin{bmatrix} 1 & 0 & k \\ 0 & 1 & 0 \\ 0 & 0 & 1 \end{bmatrix}. \end{aligned}$$

In a similar way we introduce the *elementary operations on the rows* of a matrix \mathbf{A} , which correspond to a *left multiplication by a unimodular matrix*.

An immediate application of elementary operations is for modifying the basis of a lattice.

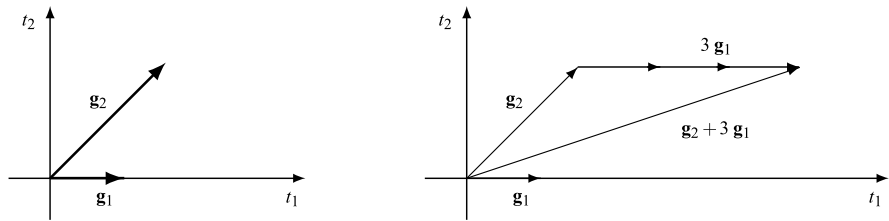


Fig. 16.9 The vectors $\mathbf{g}_1, \mathbf{g}_2$, and $\mathbf{g}_1, \mathbf{g}_2 + 3\mathbf{g}_1$ generate the same lattice

Proposition 16.3 *Let \mathbf{G} be a basis of a lattice G . Then, elementary operations on the columns of \mathbf{G} provides new bases of G .*

In fact, k elementary operations applied to the columns of \mathbf{G} are equivalent to a right multiplication

$$\mathbf{G} \rightarrow \mathbf{G}\mathbf{E}_1 \cdots \mathbf{E}_k,$$

where $\mathbf{E}_1, \dots, \mathbf{E}_k \in \mathcal{U}_m$ and also their product $\mathbf{E}_1 \cdots \mathbf{E}_k \in \mathcal{U}_m$, and the conclusion follows from Theorem 16.2.

We illustrate the meaning of elementary operations on the basis $\mathbf{G} = [\mathbf{g}_1 \mathbf{g}_2]$ of a 2D lattice. The permutation $[\mathbf{g}_1 \mathbf{g}_2] \rightarrow [\mathbf{g}_2 \mathbf{g}_1]$ does not change the lattice since the points of G are $m\mathbf{g}_1 + n\mathbf{g}_2$ and become $n\mathbf{g}_2 + m\mathbf{g}_1$. Also $[\mathbf{g}_1 \mathbf{g}_2] \rightarrow [-\mathbf{g}_1 \mathbf{g}_2]$ does not change the lattice. Finally, if we add to \mathbf{g}_2 the first column multiplied by 3, that is, $[\mathbf{g}_1 \mathbf{g}_2] \rightarrow [\mathbf{g}_1, \mathbf{g}_2 + 3\mathbf{g}_1]$, the new matrix generates the same lattice, as shown in Fig. 16.9. As a check, note that the parallelograms determined by $\mathbf{g}_1, \mathbf{g}_2$ and by $\mathbf{g}_1, \mathbf{g}_2 + 3\mathbf{g}_1$ have the same area.

16.6.2 Definition of Canonical Forms

A matrix $\mathbf{A} = \|a_{ij}\|_{m \times n}$ is:

- upper-triangular (type **U**) if $a_{ij} = 0$ for $i > j$,
- lower-triangular (type **L**) if $a_{ij} = 0$ for $i < j$, and
- diagonal (type **Δ**) if $a_{ij} = 0$ for $i \neq j$.

Examples are:

$$\begin{bmatrix} 3 & 2 & 1 \\ 0 & 2 & -1 \end{bmatrix} \quad \begin{bmatrix} 3 & -1 \\ 0 & 2 \\ 0 & 0 \end{bmatrix} \quad \begin{bmatrix} 3 & -1 & 2 \\ 0 & 2 & 1 \\ 0 & 0 & 3 \end{bmatrix} \quad \text{type U}$$

$$\begin{bmatrix} 3 & 0 & 0 \\ -1 & 2 & 0 \end{bmatrix} \quad \begin{bmatrix} 3 & 0 \\ 4 & 2 \\ 1 & -1 \end{bmatrix} \quad \begin{bmatrix} 3 & 0 & 0 \\ 2 & 1 & 0 \\ 1 & 1 & 2 \end{bmatrix} \quad \text{type L}$$

$$\begin{bmatrix} 3 & 0 & 0 \\ 0 & 2 & 0 \end{bmatrix} \quad \begin{bmatrix} 3 & 0 \\ 0 & 1 \\ 0 & 0 \end{bmatrix} \quad \begin{bmatrix} 3 & 0 & 0 \\ 0 & 1 & 0 \\ 0 & 0 & 1 \end{bmatrix} \quad \text{type } \mathbf{A}.$$

Normally, these definitions are applied to square matrices, but sometimes also to rectangular matrices.

16.6.3 Hermite Triangularization

Theorem 16.3 *An integer matrix \mathbf{H} can be decomposed into the form*

$$\mathbf{H} = \mathbf{U} \mathbf{E}_1 = \mathbf{L} \mathbf{E}_2,$$

$m \times n \quad m \times n \quad n \times n \quad m \times n \quad n \times n$

where \mathbf{U} is upper-triangular, \mathbf{L} is lower-triangular, and $\mathbf{E}_1, \mathbf{E}_2$ are unimodular.

For a proof, see [7, 8].

These decompositions are obtained by repeated applications of column elementary operations. As we shall see, Hermite triangularization is not unique.

The case of main interest is the decomposition of a square matrix \mathbf{A} . Then, \mathbf{U} and \mathbf{L} assume the forms

$$\mathbf{U} = \begin{bmatrix} a_{11} & a_{12} & \cdots & a_{1m} \\ 0 & a_{22} & \cdots & a_{2m} \\ \vdots & \vdots & \ddots & \vdots \\ 0 & 0 & \cdots & a_{mm} \end{bmatrix}, \quad \mathbf{L} = \begin{bmatrix} b_{11} & 0 & \cdots & 0 \\ b_{21} & b_{22} & & 0 \\ \vdots & \vdots & \ddots & \vdots \\ b_{m1} & b_{m2} & \cdots & b_{mm} \end{bmatrix}, \quad (16.48)$$

and we can choose for \mathbf{U} and \mathbf{L} the *canonical* form, having the following constraints (when \mathbf{A} is non singular):

$$\begin{aligned} a_{ii} > 0, & \quad 0 \leq a_{ij} < a_{ii} \quad (j > i) \quad \text{with } a_{ii} \text{ and } a_{ij} \text{ coprime.} \\ b_{ii} > 0, & \quad 0 \leq b_{ij} < b_{ii} \quad (j < i) \quad \text{with } b_{ii} \text{ and } b_{ij} \text{ coprime.} \end{aligned} \quad (16.49)$$

Example 16.5 We develop the \mathbf{U} decomposition for the matrix

$$\mathbf{H} = \begin{bmatrix} 3 & -1 & 4 \\ 2 & 1 & -3 \\ 0 & 2 & -1 \end{bmatrix}.$$

Then:

- summing to the second column the third multiplied by 2,
- summing to the second column the first multiplied by 3,
- summing to the first column the second multiplied by -2 ,
- summing to the third column the second multiplied by 3,

- multiplying by -1 the first and the third columns,
- summing to the third column the first multiplied by 2,

we obtain

$$\begin{aligned} \mathbf{H} &\rightarrow \begin{bmatrix} 3 & 7 & 4 \\ 2 & -5 & -3 \\ 0 & 0 & -1 \end{bmatrix} \rightarrow \begin{bmatrix} 3 & 16 & 4 \\ 2 & 1 & -3 \\ 0 & 0 & -1 \end{bmatrix} \rightarrow \begin{bmatrix} -29 & 16 & 4 \\ 0 & 1 & -3 \\ 0 & 0 & -1 \end{bmatrix} \\ &\rightarrow \begin{bmatrix} -29 & 16 & 52 \\ 0 & 1 & 0 \\ 0 & 0 & -1 \end{bmatrix} \rightarrow \begin{bmatrix} 29 & 16 & -52 \\ 0 & 1 & 0 \\ 0 & 0 & 1 \end{bmatrix} \rightarrow \begin{bmatrix} 29 & 16 & 6 \\ 0 & 1 & 0 \\ 0 & 0 & 1 \end{bmatrix} = \mathbf{U}, \end{aligned}$$

where \mathbf{U} has the *canonical* form defined by (16.49). The unimodular matrix \mathbf{E}_1 can be obtained as the product of the unimodular matrices of each elementary operation or, globally, as $\mathbf{E}_1 = \mathbf{U}^{-1}\mathbf{H}$. Analogously, we obtain the \mathbf{L} decomposition, which is given by

$$\mathbf{H} \rightarrow \begin{bmatrix} 1 & 0 & 0 \\ 0 & 1 & 0 \\ 5 & 7 & 29 \end{bmatrix} = \mathbf{L}.$$

16.6.4 Smith Diagonalization

Theorem 16.4 *An integer matrix \mathbf{H} can be decomposed into the form*

$$\mathbf{H} = \mathbf{E}_1 \mathbf{\Delta} \mathbf{E}_2,$$

$m \times n \quad m \times m \quad m \times n \quad n \times n$

where $\mathbf{\Delta}$ is diagonal, and $\mathbf{E}_1, \mathbf{E}_2$ are unimodular.

For a proof, see [6, 8].

To obtain this diagonal form, the elementary operations must be applied to both columns and rows. A canonical form is possible also for the diagonal decomposition, where the diagonal matrix $\mathbf{\Delta}$ has nonnegative entries. In particular, when \mathbf{H} is square and nonsingular, in the canonical form the diagonal matrix ($\mathbf{\Delta}$) = $\text{diag}(\delta_1, \dots, \delta_m)$ has positive diagonal entries.

Example 16.6 We reconsider the previous example, where with the \mathbf{L} decomposition we have obtained

$$\mathbf{H} = \mathbf{L}\mathbf{E}_2 \Rightarrow \begin{bmatrix} 3 & -1 & 4 \\ 2 & 1 & -3 \\ 0 & 2 & -1 \end{bmatrix} = \begin{bmatrix} 1 & 0 & 0 \\ 0 & 1 & 0 \\ 5 & 7 & 29 \end{bmatrix} \begin{bmatrix} 3 & -1 & 4 \\ 2 & 1 & -3 \\ -1 & 0 & 0 \end{bmatrix}.$$

Now, we apply elementary operations on the rows of the lower triangular matrix \mathbf{L} . Specifically:

- summing to the third row the second multiplied by -7 ,
- summing to the third row the first multiplied by -5 ,

we obtain

$$\mathbf{L} = \begin{bmatrix} 1 & 0 & 0 \\ 0 & 1 & 0 \\ 5 & 7 & 29 \end{bmatrix} \rightarrow \begin{bmatrix} 1 & 0 & 0 \\ 0 & 1 & 0 \\ 5 & 0 & 29 \end{bmatrix} \rightarrow \begin{bmatrix} 1 & 0 & 0 \\ 0 & 1 & 0 \\ 0 & 0 & 29 \end{bmatrix} = \mathbf{\Delta}.$$

Finally, the unimodular matrix \mathbf{E}_1 is obtained as $\mathbf{L}\mathbf{\Delta}^{-1}$.

16.6.5 Triangular Basis of Lattices

Let J be an arbitrary lattice of class $\mathcal{L}_m(G_0)$, and let $\mathbf{J} = \mathbf{G}_0\mathbf{H}$, with $\mathbf{H} \in \mathcal{J}_m$, be a basis of J . Then, the basis can be modified into the forms

$$\mathbf{J}_u = \mathbf{G}_0\mathbf{U}, \quad \mathbf{J}_l = \mathbf{G}_0\mathbf{L}, \tag{16.50}$$

where \mathbf{U} and \mathbf{L} are respectively upper-triangular and lower-triangular and, possibly, having canonical forms.

To obtain (16.50), it is sufficient to find the Hermite decompositions of \mathbf{H} , that is, $\mathbf{H} = \mathbf{U}\mathbf{E}_1$ and $\mathbf{H} = \mathbf{L}\mathbf{E}_2$, where \mathbf{E}_1 and \mathbf{E}_2 are unimodular. Then, the original basis becomes $\mathbf{J} = \mathbf{G}_0\mathbf{U}\mathbf{E}_1 = \mathbf{G}_0\mathbf{L}\mathbf{E}_1$. Hence, we find that $\mathbf{G}_0\mathbf{U}$ and $\mathbf{G}_0\mathbf{L}$ are bases for J .

The basis triangularization will be discussed in detail for the class $\mathcal{L}_m(\mathbb{Z}(\mathbf{d}))$, where $\mathbb{Z}(\mathbf{d}) = \mathbb{Z}(d_1, \dots, d_m)$.

16.6.6 Basis Alignment of a Lattice and a Sublattice

Let G be a lattice, and J a sublattice. The corresponding bases $\mathbf{G}_0 = [\mathbf{g}_1 \cdots \mathbf{g}_m]$ and $\mathbf{J}_0 = [\mathbf{j}_1, \dots, \mathbf{j}_m]$ are *aligned* if they verify the condition

$$\mathbf{J}_0 = \mathbf{G}_0\mathbf{\Delta}, \quad \mathbf{\Delta} = \text{diag}(\delta_1, \dots, \delta_m), \tag{16.51}$$

where δ_k are naturals. For the basis vectors, the alignment condition becomes

$$\mathbf{j}_1 = \delta_1\mathbf{g}_1, \dots, \mathbf{j}_m = \delta_m\mathbf{g}_m. \tag{16.51a}$$

The basis alignment is always possible. In fact:

Theorem 16.5 *Let $G = \mathbf{G}\mathbb{Z}^m$ and $J = \mathbf{J}\mathbb{Z}^m$ with J sublattice of G . Let $\mathbf{J} = \mathbf{G}\mathbf{H}$ with $\mathbf{H} \in \mathcal{J}_m$. Then, the Smith decomposition $\mathbf{H} = \mathbf{E}_1\mathbf{\Delta}\mathbf{E}_2$ allows one to define the alignment bases as*

$$\mathbf{G}_0 = \mathbf{G}\mathbf{E}_1, \quad \mathbf{J}_0 = \mathbf{J}\mathbf{E}_2^{-1}. \tag{16.52}$$

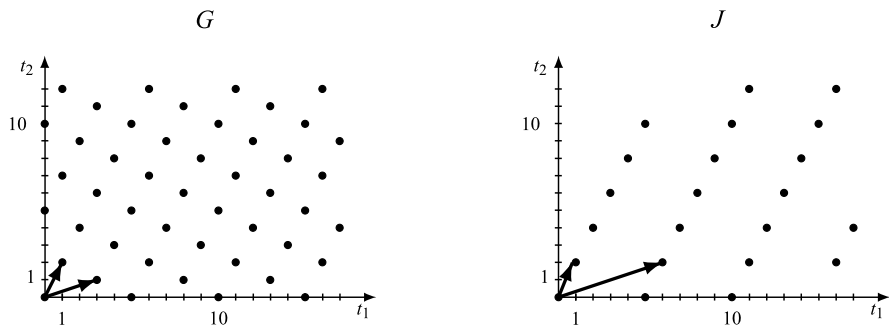


Fig. 16.10 Aligned bases of two 2D lattices

The basis alignment gives a detailed information about the *density reduction* in passing from a lattice to its sublattice. From the generic basis relation $\mathbf{J} = \mathbf{G}\mathbf{H}$ we can compute the global reduction as $d(\mathbf{H}) = (G : H)$, while from the alignment relation $\mathbf{J}_0 = \mathbf{G}_0\mathbf{\Delta}$ we can evaluate the reduction with respect to each vector. For instance, if $d(\mathbf{H}) = 24$, the global reduction is of 24 times, but knowing that $\mathbf{\Delta}$ is, e.g., $\text{diag}(3, 2, 4)$, we find that the reduction is 3 times along \mathbf{g}_1 , 2 times along \mathbf{g}_2 , and 4 times along \mathbf{g}_3 . This knowledge may find applications in down-sampling and up-periodization.

Example 16.7 Consider the 2D bases

$$\mathbf{G} = \begin{bmatrix} 3 & 1 \\ 0 & 1 \end{bmatrix}, \quad \mathbf{J} = \begin{bmatrix} 14 & 2 \\ 2 & 2 \end{bmatrix} \rightarrow \mathbf{H} = \mathbf{G}^{-1}\mathbf{J} = \begin{bmatrix} 4 & 0 \\ 2 & 2 \end{bmatrix}.$$

Since $d(\mathbf{H}) = 8$, we find that the sublattice J is 8 times sparser than G . The Smith decomposition gives

$$\mathbf{H} = \begin{bmatrix} 4 & 0 \\ 2 & 2 \end{bmatrix} = \begin{bmatrix} 2 & 1 \\ 1 & 0 \end{bmatrix} \begin{bmatrix} 2 & 0 \\ 0 & 4 \end{bmatrix} \begin{bmatrix} 1 & 1 \\ 0 & -1 \end{bmatrix} = \mathbf{E}_1 \mathbf{\Delta} \mathbf{E}_2.$$

Hence, the aligned bases are

$$\mathbf{G}_0 = \mathbf{G}\mathbf{E}_1 = \begin{bmatrix} 7 & 3 \\ 1 & 0 \end{bmatrix}, \quad \mathbf{J}_0 = \mathbf{J}\mathbf{E}_2^{-1} = \begin{bmatrix} 14 & 12 \\ 2 & 0 \end{bmatrix}, \quad \mathbf{J}_0 = \mathbf{G}_0 \text{diag}[2, 4].$$

Consequently, $\mathbf{j}_1 = 2\mathbf{g}_1$ and $\mathbf{j}_2 = 4\mathbf{g}_2$, as shown in Fig. 16.10.

16.6.7 Primitive Points of a Lattice

Definition 16.1 A point of a lattice G is *primitive* if the segment connecting the point to the origin does not contain other lattice points, origin excepted.

Fig. 16.11 Primitive points of the lattice $\mathbb{Z}_4^3(d_1, d_2)$

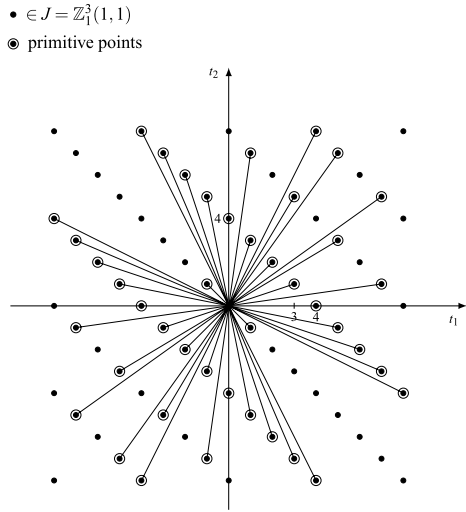


Figure 16.11 shows the primitive points of the 2D lattice $\mathbb{Z}_4^3(d_1, d_2)$.

Proposition 16.4 A point $\mathbf{t} = \mathbf{G}\mathbf{h}$ of a lattice $G = \mathbf{G}\mathbb{Z}^m$ is primitive if $\text{GCD}(\mathbf{h}) = 1$, where $\text{GCD}(\mathbf{h})$ is the greatest common divisor of the integers $\mathbf{h} = (h_1, \dots, h_m)$.

Proof Consider, for brevity, the case $m = 3$, where $\mathbf{h} = (h_1, h_2, h_3)$, and let $n = \text{GCD}(h_1, h_2, h_3)$. Then, $\mathbf{h} = n(k_1, k_2, k_3) = n\mathbf{k}$, where $\text{GCD}(\mathbf{k}) = 1$. The point $\mathbf{t}_0 = \mathbf{G}\mathbf{k}$ is a lattice point, as well as $\mathbf{t} = \mathbf{G}\mathbf{h} = n\mathbf{k}$. If $n \neq 1$, the point \mathbf{t} is not primitive since the segment $(\mathbf{0}, \mathbf{t})$ contains \mathbf{t}_0 . Hence, \mathbf{t} is primitive if $n = 1$.

It remains to consider the case in which some $h_i = 0$. For instance, the point with $\mathbf{h} = (6, 0, 2) = 2(3, 0, 1)$ is not primitive, but with $\mathbf{h} = (3, 0, 1)$, it is primitive. The conclusion is that we have to ignore zeros in $\text{GCD}(\mathbf{h})$, unless $\mathbf{h} = (0, 0, 0)$, which gives a zero GCD. □

The primitive points will be used to identify Voronoi cells (see Sect. 16.9). In the class $\mathcal{L}_m(\mathbb{Z}(\mathbf{d}))$ a particular interest is given by the *primitive axis points*, that is, the primitive points falling on the coordinate axes (see Sect. 16.7).

UT 16.7 Classes of Lattices

16.7.1 Standard Lattices and Tilted Lattices

The previous theory is developed for general lattices of \mathbb{R}^m , but the applications are almost completely confined to the sublattices of

$$\mathbb{Z}(\mathbf{d}) = \mathbb{Z}(d_1, \dots, d_m) \stackrel{\Delta}{=} \mathbb{Z}(d_1) \times \dots \times \mathbb{Z}(d_m)$$

and often to the sublattices of \mathbb{Z}^m . In this regard, in the literature, the general reference is to the class $\mathcal{L}_m(\mathbb{Z}^m)$, but we prefer to refer to the class $\mathcal{L}_m(\mathbb{Z}(\mathbf{d}))$, where the spacings d_i account for the physical dimensions of the specific application. This more general reference includes almost all lattices of interest and has also an advantage in the frequency domain, where the reciprocal lattices become more “readable” and anchored to the frequency context.

The reference to the subclass $\mathcal{L}_m(\mathbb{Z}(\mathbf{d}))$ substantially means that we consider *lattices that are sublattices of a separable lattice*; for convenience, we call them *standard* lattices and the other ones *tilted* lattices. Tilted lattices are conveniently transformed to lattices of the class $\mathcal{L}_m(\mathbb{Z}(\mathbf{d}))$ or $\mathcal{L}_m(\mathbb{Z}^m)$ by an appropriate linear transformation. In fact, for a general class $\mathcal{L}_m(G_0)$, with $G_0 = \mathbf{G}_0\mathbb{Z}^m$ the reference “tilted” lattice, the linear transformation with matrix $\mathbf{A} = \mathbf{G}_0^{-1}$ gives (see (16.4))

$$\mathbf{G}_0^{-1}G_0 = \mathbf{G}_0^{-1}\mathbf{G}_0\mathbb{Z}^m = \mathbb{Z}^m.$$

In such a way, every lattice $J \in \mathcal{L}_m(G_0)$, as a sublattice of G_0 , can be written in the form (see Corollary 16.2) $J = \mathbf{G}_0\mathbf{K}\mathbb{Z}^m$ with $\mathbf{K} \in \mathcal{J}_m$, and, after the transformation becomes $\mathbf{G}_0^{-1}J = \mathbf{K}\mathbb{Z}^m$, that is, a lattice K of $\mathcal{L}_m(\mathbb{Z}^m)$ with basis $\mathbf{K} \in \mathcal{J}_m$.

16.7.2 Properties of the Lattices of $\mathcal{L}_m(\mathbb{Z}(\mathbf{d}))$

The canonical basis of $\mathbb{Z}(\mathbf{d})$ is the diagonal matrix

$$\mathbf{D} = \text{diag}[d_1, \dots, d_m],$$

and therefore the bases of a lattice $G \in \mathcal{L}_m(\mathbb{Z}(\mathbf{d}))$ have the general form

$$\mathbf{G} = \mathbf{D}\mathbf{H}, \quad \mathbf{H} \in \mathcal{J}_m,$$

where \mathbf{H} is an integer matrix. The canonical bases of G are

$$\mathbf{D}\mathbf{U} = \mathbf{D} \begin{bmatrix} a_{11} & a_{12} & \dots & a_{1m} \\ 0 & a_{22} & \dots & a_{2m} \\ \vdots & & \ddots & \\ 0 & 0 & \dots & a_{mm} \end{bmatrix}, \quad \mathbf{D}\mathbf{L} = \mathbf{D} \begin{bmatrix} b_{11} & 0 & \dots & 0 \\ b_{21} & b_{22} & \dots & \vdots \\ \vdots & \vdots & \ddots & 0 \\ b_{m1} & b_{m2} & \dots & b_{mm} \end{bmatrix} \quad (16.53)$$

with the constraints (16.49).

The main property of the lattices of $\mathcal{L}_m(\mathbb{Z}(\mathbf{d}))$ is that they are “anchored” to the coordinate axes in the sense that lattice points fall on each of the axes. The precise statement is made in terms of *primitive axis points*, that is, the primitive points falling on the coordinate axes.

Proposition 16.5 *Every lattice G of $\mathcal{L}_m(\mathbb{Z}(\mathbf{d}))$ has two primitive points for each coordinate axis.*

For instance, for the lattices $\mathbb{Z}_i^b(d_1, d_2)$, with i and b coprime, the primitive axis points are $(\pm id_1, 0)$ and $(0, \pm id_2)$. A general procedure to find the primitive axis point is based on the Hermite triangularization of the basis, say \mathbf{DU} . In fact, considering the structure of this basis (see (16.53)), we find that $(a_{11}d_1, 0, \dots, 0)$ is a primitive point on the axis t_1 , and then, by the group property, $(-a_{11}d_1, 0, \dots, 0)$ also is a primitive point on t_1 . Similarly, considering the lower-triangular basis \mathbf{DL} , we find that $(0, \dots, 0, b_{mm}d_m)$ is a primitive point on the axis t_m . To find the other axis primitive points, we introduce a coordinate permutation and then evaluate a triangular form.

Example 16.8 Consider a 3D lattice with canonical basis

$$\mathbf{U} = \begin{bmatrix} 3 & 1 & 2 \\ 0 & 2 & 1 \\ 0 & 0 & 4 \end{bmatrix} \quad \longrightarrow \quad \mathbf{L} = \begin{bmatrix} 24 & 0 & 0 \\ 15 & 1 & 0 \\ 8 & 0 & 1 \end{bmatrix}. \tag{16.54}$$

Then, from the first of \mathbf{U} we have that $(3, 0, 0)$ is a primitive point on t_1 , and from the third column of L that $(0, 0, 1)$ is the primitive point on t_3 . Now, with the permutation of coordinates $(t_1, t_2, t_3) \rightarrow (t_2, t_1, t_3)$ we obtain the alternative triangular forms

$$\mathbf{U}_1 = \begin{bmatrix} 1 & 3 & 2 \\ 0 & 6 & 3 \\ 0 & 0 & 4 \end{bmatrix}, \quad \mathbf{L}_1 = \begin{bmatrix} 8 & 0 & 0 \\ 5 & 3 & 0 \\ 2 & 0 & 1 \end{bmatrix}.$$

Hence, the first column of \mathbf{U}_1 , with the reverse permutation, that is, $(0, 1, 0)$, gives the primitive point on t_2 . From \mathbf{L}_1 , as a check, we have that $(0, 0, 1)$ is the primitive point on t_3 .

The primitive axis points are used in the following statement (and also in the identification of Voronoi cells):

Proposition 16.6 *The largest separable lattice $\mathbb{Z}(u_1d_1, \dots, u_md_m)$ contained in a lattice $G \in \mathcal{L}(\mathbf{D})$ is determined by the primitive axis points of G .*

Proposition 16.7 *The largest separable lattice $\mathbb{Z}(u_1d_1, \dots, u_md_m)$ contained in a lattice $G \in \mathcal{L}(\mathbf{D})$ is determined by the GCD of the rows of a basis \mathbf{G} of G .*

For instance, with

$$\mathbf{G} = \begin{bmatrix} 6 & 2 & 2 \\ 0 & 4 & 2 \\ 6 & 0 & 9 \end{bmatrix} \quad \begin{array}{l} \text{GCD}(6, 2, 2) = 2 \\ \text{GCD}(0, 4, 2) = 2 \\ \text{GCD}(6, 0, 9) = 3 \end{array}$$

the smallest separable lattice is $\mathbb{Z}(2, 2, 3)$. The two lattices are illustrated in Fig. 16.12.

For the 3D lattice G with basis (16.54), we have found that the primitive axis points are $(3, 0, 0)$, $(0, 1, 0)$, $(0, 0, 1)$. Then, the largest separable sublattice of G is $\mathbb{Z}(3, 1, 1)$.

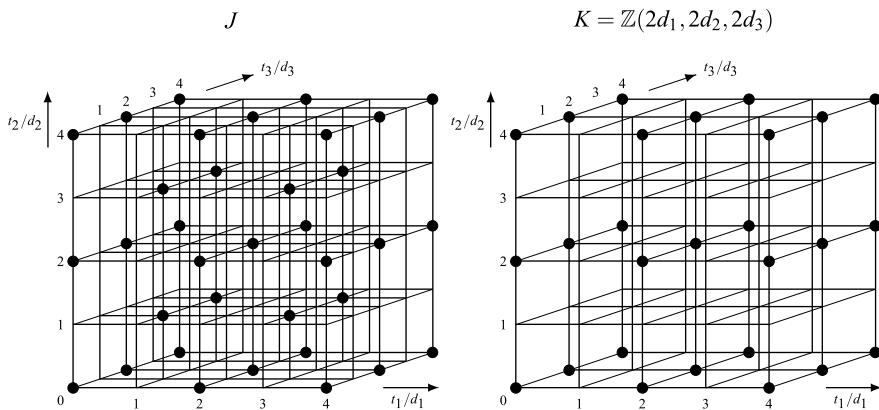


Fig. 16.12 3D nonseparable lattice J and largest separable sublattice K contained in J

16.7.3 2D Standard Lattices

The sublattices of $\mathbb{Z}(d_1, d_2)$ are obtained with the bases

$$\mathbf{J} = \begin{bmatrix} d_1 & 0 \\ 0 & d_2 \end{bmatrix} \begin{bmatrix} h_{11} & h_{12} \\ h_{21} & h_{22} \end{bmatrix} \triangleq \mathbf{D}\mathbf{H}, \tag{16.55}$$

where the diagonal matrix \mathbf{D} is the basis of $\mathbb{Z}(d_1, d_2)$, and \mathbf{H} is an integer matrix with $d(\mathbf{H}) > 0$, that is, $\mathbf{H} \in \mathcal{J}_2$. The canonical bases are

$$\begin{bmatrix} d_1 & 0 \\ 0 & d_2 \end{bmatrix} \begin{bmatrix} a_{11} & a_{12} \\ 0 & a_{22} \end{bmatrix}, \quad \begin{bmatrix} d_1 & 0 \\ 0 & d_2 \end{bmatrix} \begin{bmatrix} b_{11} & 0 \\ b_{21} & b_{22} \end{bmatrix} \tag{16.56}$$

with $0 \leq a_{12} < a_{22}$ and $0 \leq b_{21} < b_{22}$ with a_{12}, a_{11} and b_{21}, b_{22} coprime. Moreover, for the equality of the determinants, we have

$$a_{11}a_{22} = b_{11}b_{22}. \tag{16.56a}$$

In particular, if $a_{22} = b_{22} = 1$, the canonical bases assume the forms

$$\begin{bmatrix} d_1 & 0 \\ 0 & d_2 \end{bmatrix} \begin{bmatrix} i & b \\ 0 & 1 \end{bmatrix}, \quad \begin{bmatrix} d_1 & 0 \\ 0 & d_2 \end{bmatrix} \begin{bmatrix} 1 & 0 \\ \tilde{b} & i \end{bmatrix}, \tag{16.57}$$

as anticipated in Sect. 3.3, where the corresponding lattice was denoted by

$$\mathbb{Z}_i^b(d_1, d_2) \tag{16.57a}$$

(see the gallery of Fig. 3.11) for the illustrations).

As seen in Problem 3.7, the integers b and \tilde{b} are given by the solution of the integer equation (for $b \neq 0$)

$$mi + b\tilde{b} = 1.$$

For the first orders i , we have

	$i = 2$	$i = 3$	$i = 4$	$i = 5$	$i = 6$	$i = 7$	$i = 8$
$b \rightarrow$	1	1 2	1 3	1 2 3 4	1 5	1 2 3 4 5 6	1 3 5 7
$\tilde{b} \rightarrow$	1	1 2	1 3	1 3 2 4	1 5	1 4 5 2 3 6	1 3 5 7

It is easy to show that the symbol (16.57a) can be used to express every sublattice of $\mathbb{Z}(d_1, d_2)$. For instance, the lattice generated by the basis

$$J_1 = \begin{bmatrix} d_1 & 0 \\ 0 & d_2 \end{bmatrix} \begin{bmatrix} 10 & 8 \\ 0 & 3 \end{bmatrix} = \begin{bmatrix} 2d_1 & 0 \\ 0 & 3d_2 \end{bmatrix} \begin{bmatrix} 5 & 4 \\ 0 & 1 \end{bmatrix} \tag{16.58}$$

can be denoted by $\mathbb{Z}_3^4(2d_1, 3d_2)$.

The simplest nonseparable 2D lattice is called the *quincunx lattice* $\mathbb{Z}_2^1(d_1, d_2)$, which was introduced in Sect. 3.3.

Primitive Axis Points From the canonical representation (16.56) we find that the positive primitive axis points of the lattice are

$$(\pm a_{11}d_1, 0), \quad (0, \pm b_{22}d_2) \tag{16.59a}$$

and in particular, for the lattices with basis (16.57),

$$(\pm id_1, 0), \quad (0, \pm id_2). \tag{16.59b}$$

Reciprocal The reciprocal of the lattices $J = \mathbb{Z}_i^b(d_1, d_2)$ were evaluated in Chap. 5 and have the form

$$J^* = \mathbb{Z}_i^c(F_1, F_2), \quad F_1 = 1/(id_1), \quad F_2 = 1/(id_2),$$

where the integer c (coprime with respect to i) is determined as the solution of the integer equation

$$mi + cb = 1.$$

More generally, referring to the lattice $J = \mathbb{Z}_i^b(ed_1, a_{22}d_2)$, the reciprocal is

$$J^* = \mathbb{Z}_i^c(F_1, F_2), \quad F_1/(ied_1), \quad F_2 = 1/(ia_{22}d_2).$$

16.7.4 Standard 3D Lattices

The canonical representations of the sublattices of $\mathbb{Z}(d_1, d_2, d_3)$ are

$$\begin{bmatrix} d_1 & 0 & 0 \\ 0 & d_2 & 0 \\ 0 & 0 & d_3 \end{bmatrix} \begin{bmatrix} a_{11} & a_{12} & a_{13} \\ 0 & a_{22} & a_{23} \\ 0 & 0 & a_{33} \end{bmatrix}, \quad \begin{bmatrix} d_1 & 0 & 0 \\ 0 & d_2 & 0 \\ 0 & 0 & d_3 \end{bmatrix} \begin{bmatrix} b_{11} & 0 & 0 \\ b_{21} & b_{22} & 0 \\ b_{31} & b_{32} & b_{33} \end{bmatrix},$$

where the diagonal matrix is a basis of $\mathbb{Z}(d_1, d_2, d_3)$, the diagonal entries a_{ii} and b_{ii} are positive, and $a_{12}, a_{13} < a_{11}$, $a_{23} < a_{22}$, $b_{21} < b_{22}$.

UT 16.8 Sum and Intersection of Lattices

The topic was considered in a preliminary form in Sect. 3.9, where we have seen that the sum $J + K$ and the intersection $J \cap K$ of two lattices may be neither a lattice nor a regular group. The following equivalent conditions assure that $J + K$ and $J \cap K$ are lattices:

- (1) J and K are sublattices of a same lattice G_0 , that is, $J, K \in \mathcal{L}_m(G_0)$,
- (2) the bases \mathbf{J} and \mathbf{K} of the lattices are such that \mathbf{JK}^{-1} is a rational matrix.

We recall that condition (2) has been used in Chap. 3 to define *rationally comparable* lattices.

By the first proposition, the bases of $J, K \in \mathcal{L}_m(G_0)$ can be written in the form

$$\mathbf{J} = \mathbf{G}_0\mathbf{M}, \quad \mathbf{K} = \mathbf{G}_0\mathbf{N}, \quad \mathbf{M}, \mathbf{N} \in \mathcal{J}_m, \quad (16.60)$$

where \mathbf{M} and \mathbf{N} are integer matrices. Then, we can restrict our attention to the lattice class $\mathcal{L}_m(\mathbb{Z}^m)$, which is linked to the class $\mathcal{L}_m(G_0)$ by a one-to-one correspondence. In this correspondence the lattices J and K of $\mathcal{L}_m(G_0)$ are represented respectively by $M = \mathbf{M}\mathbb{Z}^m$ and $N = \mathbf{N}\mathbb{Z}^m$ of $\mathcal{L}_m(\mathbb{Z}^m)$. Now, if we evaluate their sum $M + N$ and their intersection $M \cap N$, we transfer the result to the class $\mathcal{L}_m(G_0)$ according to

$$J + K = \mathbf{G}_0(M + N), \quad J \cap K = \mathbf{G}_0(M \cap N). \quad (16.61)$$

In conclusion, the evaluation of the sum and intersection can be limited to the sublattices of \mathbb{Z}^m , whose bases are given by the class \mathcal{J}_n of nonsingular integer matrices.

In the 1D case the sublattices of $\mathcal{L}_1(\mathbb{Z})$ have the form $\mathbb{Z}(N) = \{mN \mid m \in \mathbb{Z}\}$, where N is a natural, and the sum and intersection can be handled by the *greatest common divisor* (GCD) and *least common multiple* (lcm). In fact (see Sect. 3.9),

$$\begin{aligned} \mathbb{Z}(M) + \mathbb{Z}(N) &= \mathbb{Z}(L), & \text{where } L &= \text{GCD}(M, N), \\ \mathbb{Z}(M) \cap \mathbb{Z}(N) &= \mathbb{Z}(R), & \text{where } R &= \text{lcm}(M, N). \end{aligned} \quad (16.62)$$

To handle the sum and intersection in $\mathcal{L}_m(\mathbb{Z}^m)$, we have to extend the concepts of GCD and lcm to integer matrices. This requires a long journey on the algebra of integer matrices with several definitions and statements. The interested reader can see the details in the very exhaustive paper by Chen and Vaidyanathan [4]. Here, we give directly the final statement to calculate the sum and the intersection of two lattices of $\mathcal{L}(\mathbb{Z}^m)$.

Theorem 16.6 *Let M and N be two lattices of $\mathcal{L}_m(\mathbb{Z}^m)$ with bases \mathbf{M} and \mathbf{N} , respectively.*

- (1) Compose the $m \times 2m$ matrix $[\mathbf{M}|\mathbf{N}]$.
- (2) Evaluate the Hermite lower triangular form of $[\mathbf{M}|\mathbf{N}]$. This form has the structure $[\mathbf{L}_0|\mathbf{0}]$ and is obtained by a right multiplication of $[\mathbf{M}|\mathbf{N}]$ by a $2m \times 2m$ unimodular matrix \mathbf{E} :

$$[\mathbf{M}|\mathbf{N}]\mathbf{E} = [\mathbf{L}_0|\mathbf{0}], \quad \mathbf{E} = \begin{bmatrix} \mathbf{E}_{11} & \mathbf{E}_{12} \\ \mathbf{E}_{21} & \mathbf{E}_{22} \end{bmatrix}, \quad (16.63)$$

where \mathbf{E}_{ij} are $m \times m$ matrices.

Then, \mathbf{L}_0 is a basis of $M + N$, and $\mathbf{R}_0 = \mathbf{N}\mathbf{E}_{22}$ is a basis of $M \cap N$. At the end of the calculation, we can check the determinant identity

$$d(M + N) d(M \cap N) = d(M) d(N). \quad (16.64)$$

Example 16.9 Consider the 2D lattices $M = \mathbb{Z}_4^3(1, 2)$ and $N = \mathbb{Z}_3^2(1, 1)$ whose canonical bases are respectively the integer matrices

$$\mathbf{M} = \begin{bmatrix} 4 & 3 \\ 0 & 2 \end{bmatrix}, \quad \mathbf{N} = \begin{bmatrix} 3 & 2 \\ 0 & 1 \end{bmatrix}. \quad (16.65)$$

We compose the 2×4 matrix

$$[\mathbf{M}|\mathbf{N}] = \begin{bmatrix} 4 & 3 & 3 & 2 \\ 0 & 2 & 0 & 1 \end{bmatrix}.$$

Then, we apply elementary operations to obtain the Hermite triangularization which provides relation (16.63). We find

$$[\mathbf{M}|\mathbf{N}]\mathbf{E} = \begin{bmatrix} 4 & 3 & 3 & 2 \\ 0 & 2 & 0 & 1 \end{bmatrix} \begin{bmatrix} 1 & -2 & -3 & 4 \\ -1 & 0 & 0 & 1 \\ 0 & 2 & 4 & -5 \\ 0 & 1 & 0 & -2 \end{bmatrix} = \begin{bmatrix} 1 & 0 & 0 & 0 \\ -2 & 1 & 0 & 0 \end{bmatrix}.$$

Then

$$\begin{aligned} \mathbf{L}_0 &= \begin{bmatrix} 1 & 0 \\ -2 & 1 \end{bmatrix} \rightarrow \begin{bmatrix} 1 & 0 \\ 0 & 1 \end{bmatrix}, & \mathbf{E}_{22} &= \begin{bmatrix} 4 & -5 \\ 0 & -2 \end{bmatrix}, \\ \mathbf{R}_0 &= \mathbf{M}\mathbf{E}_{22} = \begin{bmatrix} 4 & 3 \\ 0 & 2 \end{bmatrix} \begin{bmatrix} 4 & -5 \\ 0 & -2 \end{bmatrix} = \begin{bmatrix} 12 & -19 \\ 0 & -2 \end{bmatrix} \rightarrow \begin{bmatrix} 12 & 7 \\ 0 & 2 \end{bmatrix}. \end{aligned}$$

The basis \mathbf{L}_0 defined the lattice $\mathbb{Z}(1, 1) = \mathbb{Z}^2$ and the basis \mathbf{R}_0 the lattice $\mathbb{Z}_{12}^7(1, 2)$. Hence,

$$\mathbb{Z}_4^3(1, 2) + \mathbb{Z}_3^2(1, 1) = \mathbb{Z}(1, 1), \quad \mathbb{Z}_4^3(1, 2) \cap \mathbb{Z}_3^2(1, 1) = \mathbb{Z}_{12}^7(1, 2).$$

These lattices are shown in Fig. 16.13. Note that

$$d(M) = 8, \quad d(N) = 3, \quad d(M + N) = 1, \quad d(M \cap N) = 24,$$

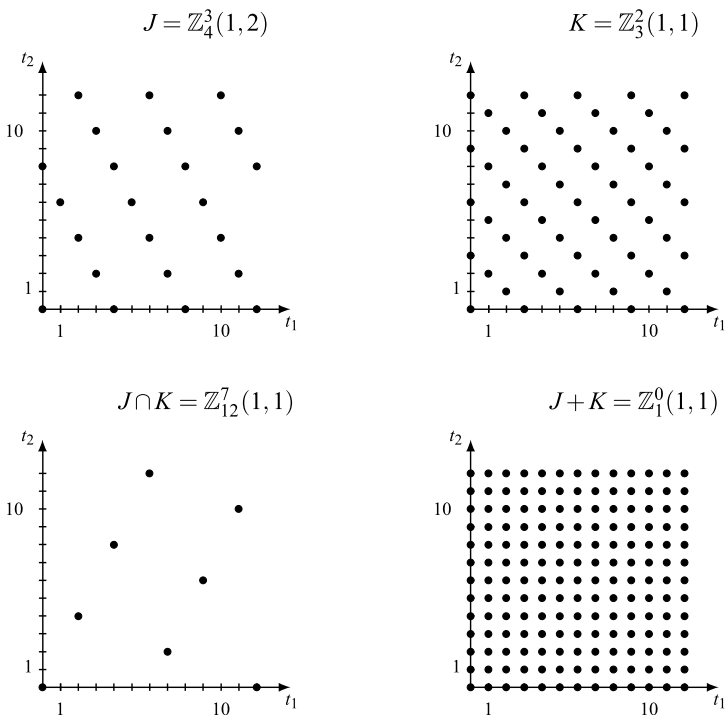


Fig. 16.13 Examples of sum and intersection of 2D lattices

and the determinant identity is verified.

UT 16.9 Aperiodic Cells

Cells were introduced in Chap. 3 and are now developed in great detail.

16.9.1 Cell Identification

We have seen a few examples of cells, aperiodic and periodic, but not a general procedure to find cells. Since periodic cells can be obtained from aperiodic cells, we can limit the identification to aperiodic cells.

A general identification procedure may be the following: (1) we consider some reference groups, may be primitive groups, where cells are easily evaluated, and then (2) we transfer these cells to other groups using *isomorphism* (in practice, a set linear transform). In this way we finally provide cells on every group of interest. The specific rules are:

Proposition 16.8 (Cartesian product) *If $C_1 = [G_1/P_1]$ and $C_2 = [G_2/P_2]$ are two cells of the groups G_1 and G_2 , then the Cartesian product $C_1 \times C_2$ is a cell of $G_1 \times G_2$ modulo $P_1 \times P_2$*

$$[G_1/P_1] \times [G_2/P_2] = [G_1 \times G_2/P_1 \times P_2].$$

Proposition 16.9 (Intersection) *Let G be a subgroup of G_0 , and let $C_0 = [G_0/P]$, where P is a subset of G . Then, the intersection*

$$C = G \cap C_0 = [G/P]$$

is a cell of G modulo P .

Proposition 16.10 (Isomorphism) *If $[H/P]$ is a cell of H , modulo P and G is isomorphic to H , with isomorphism map $\alpha : H \rightarrow G$, then $[G/\alpha(P)]$ is a cell of G modulo $\alpha(P) = \{\alpha(t) \mid t \in P\}$.*

Proposition 16.11 (Cut and paste) *Let $C = [G/P]$, and let C_1, \dots, C_k be a partition of C . Then, the set*

$$(C_1 + p_1) \cup (C_2 + p_2) \cup \dots \cup (C_k + p_k) \quad (16.66)$$

with $p_1, \dots, p_k \in P$ arbitrary repetition centers, is a new cell of G modulo P .

The first proposition is evident. For the second, it is sufficient to use the set identity $(A \cup B) \cap C = (A \cap C) \cup (B \cap C)$ in (16.66). The proof of the other propositions are left to the reader.

16.9.2 Relationship Between Cells

Given a group G and a set P of repetition centers, we may find several different cells $[G/P]$. Their relation is stated by the following:

Theorem 16.7 *Let C_0 be a reference cell of G modulo P . Then any other cell C of G modulo P is related to C_0 by*

$$C = \bigcup_{p \in P_0} [A(p) + p], \quad (16.67)$$

where

$$A(p) = (C - p) \cap C_0, \quad p \in P_0, \quad (16.68)$$

is a partition of C_0 , and P_0 is a subset of P .

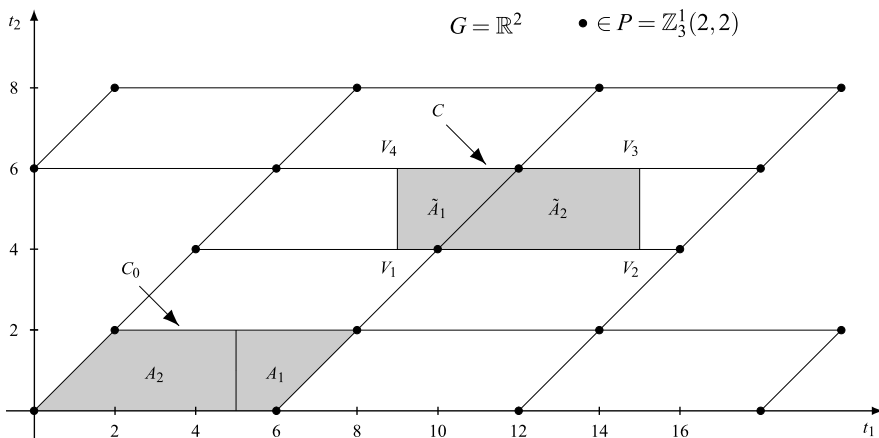


Fig. 16.14 Relation between two cells C and C_0 of the form $[\mathbb{R}^2/P)$ with $P = \mathbb{Z}_3^1(2, 2)$. The subsets \tilde{A}_i of C are shifted version of the subsets A_i of C_0 with shifts $\in P$

Proof The partition of the group G , given by $C_0 + p, p \in P$, induces the following partition of the cell C :

$$\tilde{A}(p) = C \cap (C_0 + p), \quad p \in P.$$

Each of these sets (as subsets of $C_0 + p$) can be written in the form

$$\tilde{A}(p) = A(p) + p,$$

where $A(p)$ is given by (16.68). Then, (16.67) follows, as soon as we remove empty contributions (so P is restricted to some subset P_0). However, we claim that (16.68) is a partition of C_0 . In fact, considering that C is a cell of G , we find

$$\bigcup_p A(p) = \bigcup_p [(C - p) \cap C_0] = C_0 \cap \left[\bigcup_p (C - p) \right] = C_0 \cap G = C_0,$$

$$A(p) \cap A(q) = [(C - p) \cap (C - q)] \cap C_0 = \emptyset \cap C_0 \quad \text{if } q \neq p. \quad \square$$

Example 16.10 Let $G = \mathbb{R}^2$ and $P = \mathbb{Z}_3^1(2, 2)$ and take as a reference cell C_0 the fundamental parallelogram shown in Fig. 16.14. Another cell C is the rectangle with vertices $V_1 = (9, 4), V_2 = (15, 4), V_3 = (15, 6), V_4 = (9, 6)$. The partition $C_0 + p, p \in P$, has two nonempty intersections \tilde{A}_1 and \tilde{A}_2 with the rectangle C , which are shown in the figure. Now, we can check that each \tilde{A}_i is a shifted version $A_i + p_i$ of a piece A_i of C_0 , with $p_1 = 2s_2$ and $p_2 = s_1 + 2s_2$ (s_1 and s_2 are the basis vectors of P), which form the subset P_0 of the repetition centers P .

In conclusion, the rectangle C can be expressed in the form (16.67) with $A(p) = A_p$ and $P_0 = \{p_1, p_2\}$.

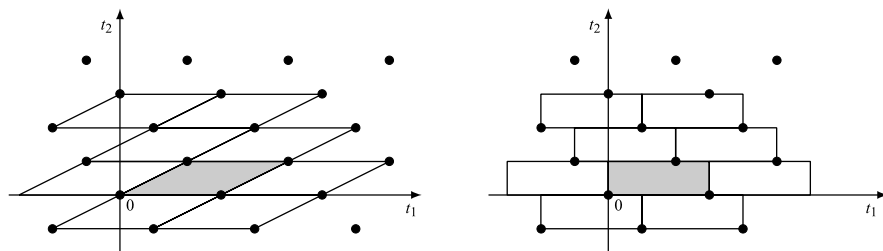


Fig. 16.15 Covering of fundamental parallelepipeds and of rectangular cells

16.9.3 Orthogonal Cells

Orthogonal cells are natural shapes with separable lattices. For instance, a cell $[\mathbb{R}^2/\mathbb{Z}(d_1, d_2)]$ is the rectangle $[0, d_1) \times [0, d_2)$, a cell $[\mathbb{R}^3/\mathbb{Z}(d_1, d_2, d_3)]$ is the orthogonal parallelepiped $[0, d_1) \times [0, d_2) \times [0, d_3)$, etc. It may be surprising, and indeed in the literature it was not realized, that orthogonal cells can be found with nonseparable lattices, as shown in Fig. 16.15.

We begin to show this possibility in the 2D case for the lattices $\mathbb{Z}_i^b(1, 1)$ whose canonical bases are

$$\begin{bmatrix} a_{11} & a_{12} \\ 0 & a_{22} \end{bmatrix}, \quad \begin{bmatrix} b_{11} & 0 \\ b_{21} & b_{22} \end{bmatrix}.$$

The two fundamental parallelepipeds obtained with these bases are shown in Fig. 16.16, left. To get rectangular cells, we apply the cut-and-paste procedure. Specifically, we partition the parallelepipeds C into the two polygons C' and C'' , where C'' is a triangle. Then, in the first case (related to the upper triangular basis) we apply a shift of $p = (-a_{11}, 0)$ to C'' , and we see that the union $C' \cup (C'' + p)$ gives the rectangle $[0, a_{11}) \times [0, a_{22})$. In the second case we apply a shift of $p = [0, -b_{11})$ to obtain the rectangle $[0, b_{11}) \times [0, b_{22})$. Note that in both cases the shift p belongs to the lattice, as required for the correct application of the procedure.

The general statement is:

Theorem 16.8 *Let L be a lattice of $\mathcal{L}_m(G_0)$, and let $\mathbf{G}_0\mathbf{U}$ be a triangular basis of L . Then*

$$\mathbf{G}_0[0, u_{11}) \times \cdots \times [0, u_{mm}) = [\mathbb{R}^m/P), \tag{16.69}$$

where u_{ii} are the diagonal entries of \mathbf{U} , is a cell of \mathbb{R}^m modulo P .

In this statement \mathbf{U} may be any Hermite triangular form, upper or lower triangular, and also obtained after a coordinate permutation. So, in general we may have $2(m!)$ triangular forms and so many orthogonal cells.

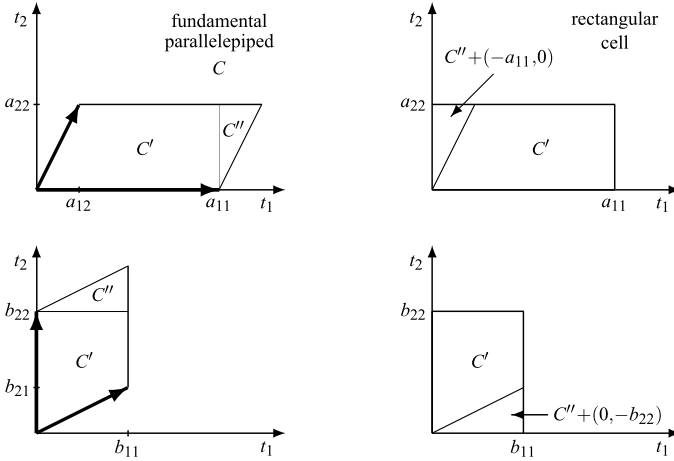


Fig. 16.16 Application of cut-and-paste procedure to obtain a rectangular cell

Example 16.11 Consider the 3D sublattice L of \mathbb{Z}^3 with canonical upper and lower triangular bases

$$\mathbf{U} = \begin{bmatrix} 3 & 1 & 2 \\ 0 & 2 & 1 \\ 0 & 0 & 4 \end{bmatrix}, \quad \mathbf{L} = \begin{bmatrix} 24 & 0 & 0 \\ 15 & 1 & 0 \\ 8 & 0 & 1 \end{bmatrix}.$$

Then, 2 orthogonal cells (\mathbb{R}^3/L) are given by

$$C_1 = [0, 3) \times [0, 2) \times [0, 4), \quad C_2 = [0, 24) \times [0, 1) \times [0, 1)$$

and illustrated in Fig. 16.17.

With the permutation of coordinates $(t_1, t_2, t_3) \rightarrow (t_2, t_1, t_3)$ we obtain the alternative triangular forms

$$\mathbf{U}_1 = \begin{bmatrix} 1 & 3 & 2 \\ 0 & 6 & 3 \\ 0 & 0 & 4 \end{bmatrix}, \quad \mathbf{L}_1 = \begin{bmatrix} 8 & 0 & 0 \\ 5 & 3 & 0 \\ 2 & 0 & 1 \end{bmatrix}$$

and then the further orthogonal cells

$$C_3 = [0, 6) \times [0, 1) \times [0, 4), \quad C_4 = [0, 3) \times [0, 8) \times [0, 1).$$

The cut-and-paste procedure becomes cumbersome for $m \geq 3$, so we give an alternative proof of the existence of orthogonal cells. The proof is based on the following:

Proposition 16.12 *The sets*

$$C + p, \quad p \in P, \tag{16.70}$$

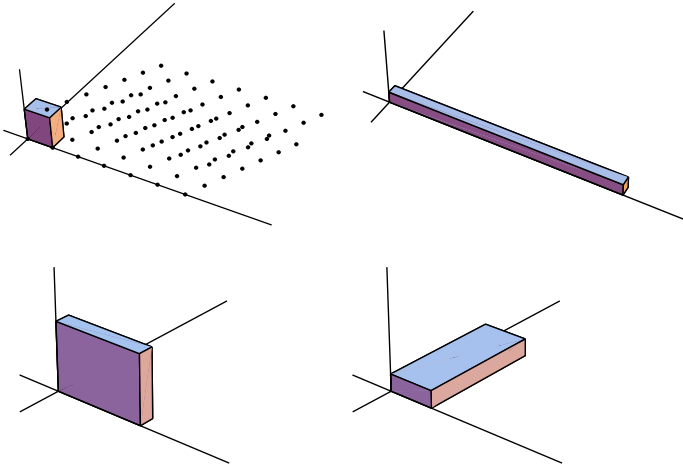


Fig. 16.17 Example of orthogonal cells of a same 3D lattice

represent a partition of \mathbb{R}^m (and then C is a cell of the type $[\mathbb{R}^m/P)$) if

- (1) $I(p) \triangleq C \cap [C + p) = \emptyset$ for $p \neq 0$,
- (2) $\text{meas } C = d(P)$.

Proposition 16.13 Let C in (16.70) be orthogonal, and let $I_i(p)$ be the projection of the intersection $I(p)$ onto the i th coordinate t_i of the space \mathbb{R}^m . Then, $I_i(p) = \emptyset$.

In Proposition 16.12, condition (1) is standard and assures that the cells do not overlap, while condition (2) replaces the standard condition on the covering of \mathbb{R}^m . Here, the covering is guaranteed by the cell measure that is the right one (the same as the fundamental parallelepiped). Proposition 16.13 is strictly related to the assumption of orthogonality for C . In fact, the intersection is given by $I(p) = I_1(p) \times \dots \times I_m(p)$.

We are now ready to prove Theorem 16.8. The orthogonal cell (16.69) has measure

$$d(G_0)u_{11} \cdots u_{mm} = d(G_0) d(\mathbf{U}) = d(P),$$

that is, the right measure of the cells $[\mathbb{R}^m/P)$. It remains to prove that C verifies condition (1) of Proposition 16.12. Without loss of generality we continue the proof in a specific 3D case, namely with

$$\mathbf{U} = \begin{bmatrix} 3 & 1 & 2 \\ 0 & 2 & 1 \\ 0 & 0 & 4 \end{bmatrix}, \quad p = (3m + n + 2k, 2n + k, 4k), \quad m, n, k \in \mathbb{Z}.$$

Then

$$C = [0, 3) \times [0, 2) \times [0, 4), \quad C + p = C + (3m + n + 2k, 2n, 4k),$$

and the three projections of $I(p) = C \cap [C + p]$ are

$$\begin{aligned} I_1(p) &= [0, 3) \cap \{[0, 3) + 3m + n + 2k\}, \\ I_2(p) &= [0, 2) \cap \{[0, 2) + 2n + k\}, \\ I_3(p) &= [0, 4) \cap \{[0, 4) + 4k\}. \end{aligned}$$

We find that $I_3(p) = \emptyset$ for $k \neq 0, \forall m, n$. Then, it is sufficient to check the disjointness of $I_2(p)$ for $k = 0$. We have $I_2(p) = [0, 2) \cap \{[0, 2) + 2n\} = \emptyset$ for $n \neq 0$. So, we continue the check for $k = 0$ and $n = 0$, and we find $I_1(p) = [0, 3) \cap \{[0, 3) + 3m\} = \emptyset$ for $m \neq 0$. The conclusion is that for $(m, n, k) \neq (0, 0, 0)$ at least one projection is empty. Hence, $I(p) = \emptyset$ for $p \neq \mathbf{0}$.

16.9.4 Voronoi Cells

The Voronoi cell (also called *Dirichlet region*, *Brillouin zone*, and *Wigner–Seitz region*) [5] is a cell $[\mathbb{R}^m/L]$ that is conceptually different from the previous cells, which are mainly related to the fundamental parallelepiped. Also its identification is very different and not easy.

Definition 16.2 Given a lattice L of \mathbb{R}^m , the Voronoi cell $\mathcal{V}_m(L)$ is the subset of \mathbb{R}^m given by the points that are *nearer to the origin* than any other lattice point.

The definition has an ambiguity concerning the border points, which must be solved by deciding which of them belong to the cell. For instance, the definition for the 1D cell of type $[\mathbb{R}/\mathbb{Z}(d)]$ gives the closed interval $[-\frac{1}{2}d, \frac{1}{2}d]$, but to have a partition of \mathbb{R} with repetition centers $\mathbb{Z}(d)$, one of the two border points $-\frac{1}{2}d$ or $\frac{1}{2}d$ must be removed to get $(-\frac{1}{2}d, \frac{1}{2}d]$ or $[-\frac{1}{2}d, \frac{1}{2}d)$. In conclusion, Definition 16.2 provides a true cell of type $[\mathbb{R}^m/L]$ apart from a set of zero measure. Hereafter we neglect the problem of the borders.

Another remark is that a Voronoi cell implies the notion of Euclidean distance $\sqrt{t_1^2 + \dots + t_m^2}$; this is not a problem in a dimensionless environment, but when the coordinates t_1, \dots, t_m represent physical quantities, an appropriate normalization is necessary.

Ideas for the Identification

Since the definition is strongly related to the Euclidean distance, the identification of a Voronoi cell becomes essentially a geometric problem. To get some ideas, we begin with two simple 2D examples. If L is the separable lattice $\mathbb{Z}(4, 3)$, we realize immediately that the Voronoi cell is given by the rectangle $[-2, 2] \times [-\frac{3}{2}, \frac{3}{2}]$, as illustrated in Fig. 16.18. If L is the nonseparable lattice $\mathbb{Z}_3^2(1, 1)$, with a simple graphical procedure we find that the Voronoi cell is given by a hexagon, shown

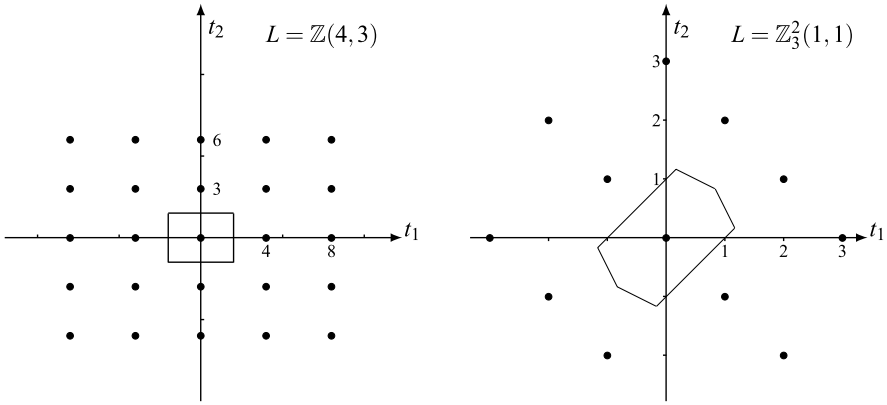


Fig. 16.18 Voronoi cells of lattices $\mathbb{Z}(4, 3)$ and $\mathbb{Z}_3^2(1, 1)$

on the right of Fig. 16.18. This hexagon is not regular, but its opposite edges are parallel.

With these two examples we learn a few rules useful for the identification: (1) a Voronoi cell has always the *even* symmetry, that is, if a point $\mathbf{t} \in \mathbb{R}^m$ belongs to the cell \mathcal{V}_m , then also $-\mathbf{t} \in \mathcal{V}_m$; (2) the cell \mathcal{V}_m is always a *convex* polyhedron in \mathbb{R}^m ; (3) considering the convexity, the identification is done by its borders; (4) the number of edges is not the same for a given dimension, e.g., in \mathbb{R}^2 the Voronoi cells may have $N = 4$ or $N = 6$ edges.

A strategy for the identification is based on the *primitive points* of the lattice L , introduced in Definition 16.1. We recall that a point P of L is primitive if the segment PO , connecting P to the origin O , does not contain any other point of the lattice L (Fig. 16.19). Now, the middle point Q of PO is a *candidate* to be a point of the cell, in the sense that it really belongs to the border unless it is “shadowed” by other points nearer to the origin O . This consideration can be extended to the plane $\pi(P)$ that is orthogonal to the segment PO and contains the middle point Q of PO . This plane contains a part of the border, unless it is not shadowed by other planes of the same type (generated by other primitive points). A first statement is that the border of the Voronoi cell will belong to planes $\pi(P)$ *identified by some primitive points* that we call for convention *generating points*. Then the problem is to establish whether a primitive point is a generating point or not.

These ideas can be refined by considering the *primitive axis* points, which can be easily identified working on the basis \mathbf{L} of the lattice L (see Proposition 16.5). In the subclass $\mathcal{L}(\mathbb{Z}^m)$ we find $2m$ primitive axis points given by the coordinates of the form $(\pm p, \mathbf{0})$ and the permutation of $(\pm p, \mathbf{0})$. Now, these primitive points P_i identify a parallelepiped \mathcal{R} , as shown in Fig. 16.19, and the corresponding “middle” points Q_i identify a smaller parallelepiped \mathcal{P} . We claim that

- (1) in the identification procedure the test can be limited to the primitive points inside the region \mathcal{R} ,
- (2) the cell \mathcal{V}_m is contained in the region \mathcal{P} .

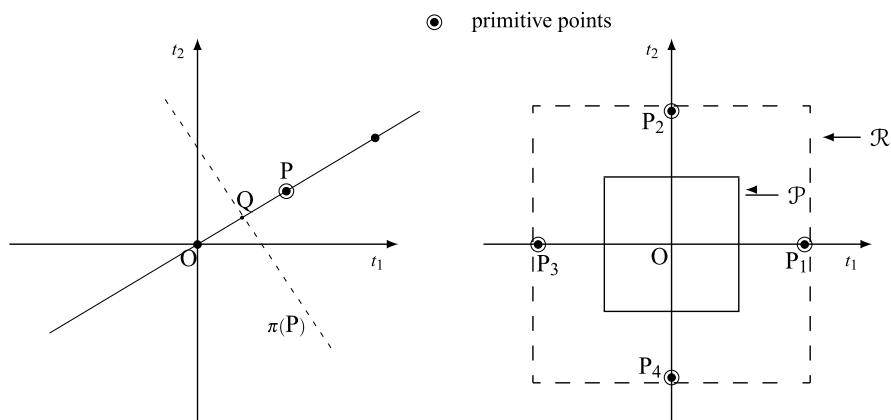


Fig. 16.19 For the identification of a Voronoi cell $\mathcal{V}_m(L)$. At the *left*: P is a primitive point of the lattice L , Q is the *middle* point between P and the origin O , and $\pi(P)$ is the plane orthogonal to OP and containing Q . At the *right*: P_i are the *primitive axis points* that determine the parallelepipeds \mathcal{R} and \mathcal{P} . The cell is inside \mathcal{P}

16.9.5 Identification of 2D Voronoi Cells

We now outline the identification procedure of a Voronoi cell $\mathcal{V}_2(L)$ in a specific case.

Example 16.12 We consider the lattice $\mathbb{Z}_3^2 = \mathbb{Z}_3^2(1, 1)$ with basis

$$\mathbf{L} = \begin{bmatrix} 3 & 2 \\ 0 & 1 \end{bmatrix}.$$

This lattice is illustrated in Fig. 16.20, where the primitive points (inside \mathcal{R}) are enhanced with respect to the other points of the lattice. The primitive axis points are $(0, \pm 3)$ and $(\pm 3, 0)$ and determine the rectangle $\mathcal{R} = [-3, 3] \times [-3, 3]$, which contains 12 primitive points; the points outside \mathcal{R} are not useful. The cell will be contained in the rectangle $\mathcal{P} = [-3/2, 3/2] \times [-3/2, 3/2]$ determined by the middle points of the segments OP_i , where P_i are the 4 *primitive axis points* $(3, 0), (-3, 0), (0, 3), (-3, 0)$. The rectangle \mathcal{R} contains the generating points, and the problem is to disregard the primitive points of \mathcal{R} that are not generating points. This can be done by inspection in the 2D case, but for the general case a procedure is needed. It can be shown that a general procedure is the following. Let P_1, \dots, P_M be the primitive points in \mathcal{R} (Fig. 16.21). Then, a point P_i is a generating point if and only if

$$(P_j - P_i) \cdot (P_j - O) > 0, \quad j = 1, \dots, M, \quad j \neq i, \tag{16.71}$$

where O is the origin, and \cdot denotes the inner product (inner product criterion).

For instance, in the specific case two primitive points of \mathcal{R} are $P_1 = (3, 3)$ and $P_2 = (2, 1)$. We see that P_1 is not a generating point because $(P_2 - P_1) \cdot (P_2 - O) =$

Fig. 16.20 Identification of Voronoi cell $\mathcal{V}_2(\mathbb{Z}_3^2)$. The region \mathcal{R} is identified by the four primitive axis points $(0, \pm 3)$ and $(\pm 3, 0)$. The region \mathcal{P} is determined by “middle” points and will contain the Voronoi cell

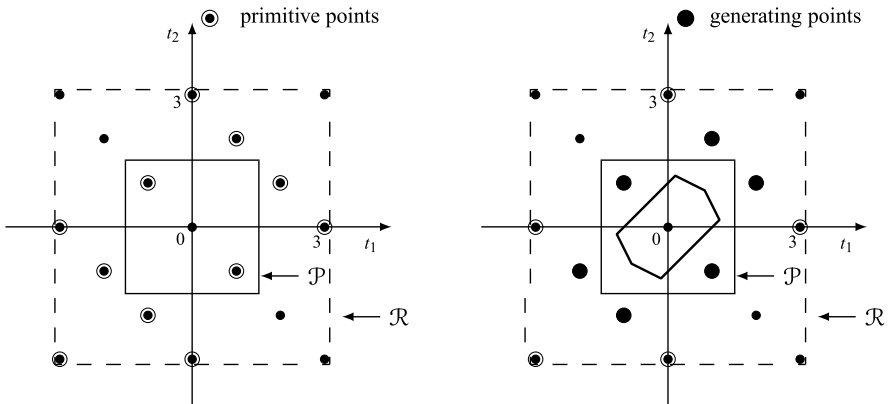
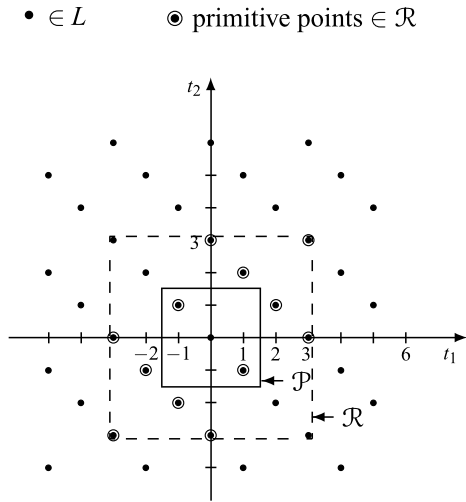


Fig. 16.21 Identification of Voronoi cell $\mathcal{V}(\mathbb{Z}_3^2)$: the region \mathcal{R} contains 11 primitive points, but only 6 of them are generating points

$(-1, -2) \cdot (2, 1) = -4 < 0$. On the other hand, $P_3 = (1, 1)$ verifies all conditions (16.71) and therefore is a generating point. In such a way we find the six generating points G_k marked by a dark disk in Fig. 16.21.

Now, the generating points G_k determine so many planes $\pi(G_k)$ (straight lines in the 2D case), which contain the border of the cell. The final step is to cut out the piece of borders from these planes. We continue the procedure in the 2D case, where we have to determine the segments $A_k B_k$ (with center Q_k) of the lines $\pi(G_k)$ representing the k th edge of the cell. To this end, for every fixed $\pi(G_k)$, consider the points of intersection with the other lines $\pi(G_h)$, $h = 1, \dots, N$, $h \neq k$. The points A_k and B_k are given by the two points of intersection that are the nearest to the point Q_k . Applying this procedure to the specific case we find the six consecutive segments giving the border of the cell.

Outline of the General Procedure

From the previous considerations we can state the following procedure to find a Voronoi cell $\mathcal{V}_m(L)$:

- (1) Find the *primitive axis points* of L , using repeated application of upper-triangularization and lower-triangularization of the basis \mathbf{L} (see Proposition 16.5).
- (2) The primitive axis points determine the parallelepiped \mathcal{R} , and their middle points determine the parallelepiped \mathcal{P} containing the cell.
- (3) Find the primitive points P_1, \dots, P_M belonging to \mathcal{R} .
- (4) From the points P_1, \dots, P_M select the generating points G_1, \dots, G_N , using the inner product criterion (16.71). These N points determine so many planes $\pi(G_k)$, which contain the border \mathcal{B} of the cell.
- (5) The cell is in general a polyhedron of \mathbb{R}^m whose *faces* are determined by the intersections of the planes $\pi(G_k)$.

Results on 3D Voronoi Cells

We have seen in the 2D case how cumbersome is the find step of the above procedure. We were able to implement the procedure in the 3D case, where the intersections of the planes $\pi(G_k)$ are given by 2D polygons (faces), and the cell itself is a polyhedron.

We have found that the 3D Voronoi cell may be a parallelepiped or an octahedron. The faces may be rectangles or hexagons. An example is shown in Fig. 16.22, where the 3D lattices have the basis

$$\mathbf{L} = \begin{bmatrix} 6 & 0 & 2 \\ 0 & 4 & 0 \\ 0 & 0 & 7 \end{bmatrix}, \quad (16.72)$$

and the Voronoi cell $\mathcal{V}_3(L)$ is given by an octahedron.

We want to underline that these results found for 3D Voronoi cells are not a mathematical statement, rather a consolidated conjecture.

UT 16.10 Change of Signal Dimensionality

In several applications we encounter the operation of *change of signal dimensionality*, where an m D signal is converted to an n D signal, and the change may be both a *reduction* ($n < m$) and an *increase* ($n > m$). For instance, the operation performed by a video camera is the acquisition of a *time varying image*, which is represented by a 3D signal, with a final production of the *video signal*, which is a 1D signal. Hence, it performs a $3\text{D} \rightarrow 1\text{D}$ reduction of the signal dimensionality. In the reproduction, where the image is restored from the video signal, we find a $1\text{D} \rightarrow 3\text{D}$ increase.

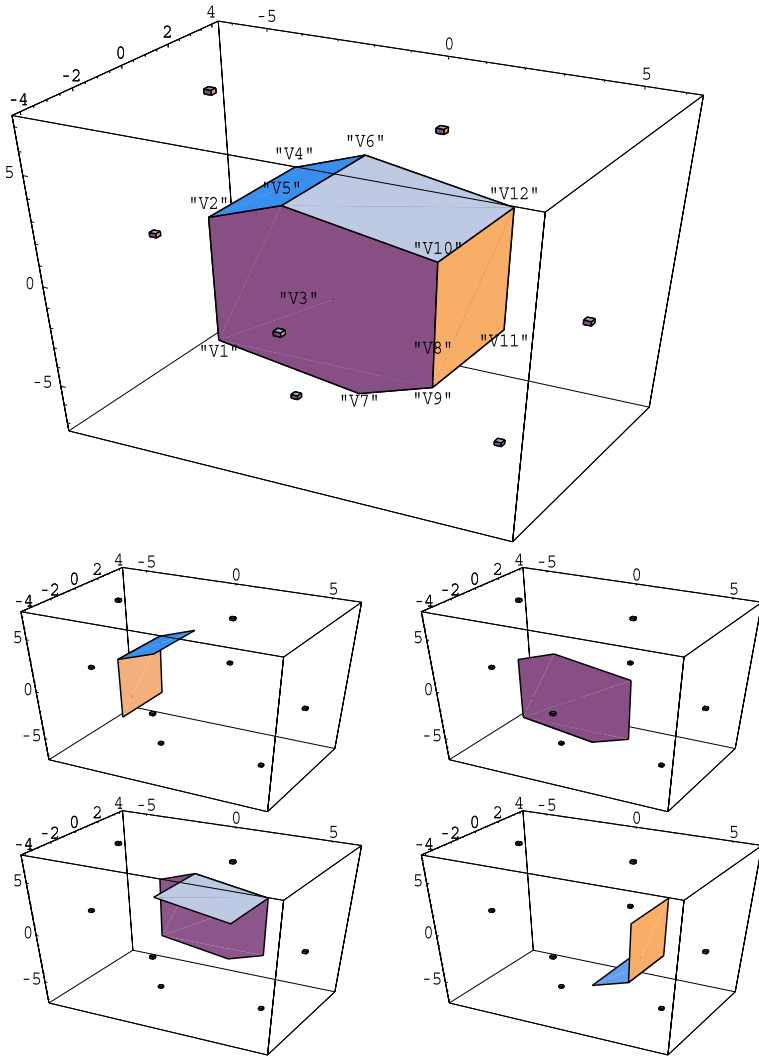


Fig. 16.22 3D Voronoi cell identified by the lattice L with basis (16.72). The region \mathcal{R} and the generating points are also shown. Below, the pairs of adjacent faces

In this section we consider in general the problem of dimensionality *changes*. This topic has not received much attention in the literature, apart from very few contributions [1, 9] and a few specific formulations in the framework of television scanning [5, 10, 11]. Sometimes dimensionality reduction is considered as a degenerate form of sampling [5]. However, sampling and dimensionality reduction are different in nature, as will be evident from the comparison of the corresponding fundamental theorems. In fact, the assumption for dimensionality reduction is

Table 16.1 Terminology and graphic symbols of elementary changes of dimensionality

Elementary change	Dual change
<p>Zero reduction</p>	<p>Integral reduction</p>
<p>Integral reduction</p>	<p>Zero reduction</p>
<p>Sum reduction</p>	<p>Zero reduction</p>
<p>Hold increase</p>	<p>Delta increase</p>
<p>Delta increase</p>	<p>Hold increase</p>

on the signal extension, whereas in sampling it is on the Fourier transform extension.

Dimensionality reduction shows some similarity with the *lexicographical order*, where a matrix, or more generally an array, is converted to a vector (see Sect. 7.6). Also in this conversion, the assumption is based on size limitation (finite matrix or finite array).

In the study of dimensionality change the approach is to consider first *elementary* changes and then *composite* changes, following the same approach used for transformations in Chap. 6.

16.10.1 Elementary Changes of Dimensionality

The linear transformations of Table 16.1 provide a *reduction* or an *increase* of signal dimensionality. They are akin to impulse transformations in that dimensionality changes are achieved in the “simplest possible way.” Their kernels are appropriate impulses, and, in fact, these new tfs may be regarded as a generalization of *impulse* tfs seen in Chap. 6.

Dimensionality *reductions* take the form $U \times V \rightarrow U$, where U is p -dimensional, and V is q -dimensional. In *zero reduction* the last q coordinates of a $(p + q)$ -dimensional signal are set to zero

$$y(\mathbf{u}) = x(\mathbf{u}, \mathbf{0}), \quad \mathbf{u} \in U.$$

In *integral reduction* the signal is integrated with respect to the last q coordinates

$$y(\mathbf{u}) = \int_V d\mathbf{v} x(\mathbf{u}, \mathbf{v}), \quad \mathbf{u} \in U. \quad (16.73)$$

In the frequency domain, zero reduction becomes integral reduction, and vice versa.

Dimensionality *increases* take the form $U \rightarrow U \times V$. In *hold increase* the relationship is

$$y(\mathbf{u}, \mathbf{v}) = x(\mathbf{u}), \quad (\mathbf{u}, \mathbf{v}) \in U \times V, \quad (16.74)$$

which states that the p -dimensional signal $x(\mathbf{u})$ is spread to the $(p + q)$ -dimensional domain by a hold operation. In *delta increase* the relationship is

$$y(\mathbf{u}, \mathbf{v}) = x(\mathbf{u})\delta_V(\mathbf{v}), \quad (\mathbf{u}, \mathbf{v}) \in U \times V, \quad (16.75)$$

that is, an impulse is attached as a factor to the original signal. In the frequency domain, hold increase becomes delta increase, and vice versa.

Table 16.1 lists a third kind of dimensionality reduction, *sum reduction*, with the relationship

$$y(\mathbf{u}) = \sum_{\mathbf{v} \in V} x(\mathbf{u}, \mathbf{v}) = (1/d(V)) \int_V d\mathbf{v} x(\mathbf{u}, \mathbf{v}), \quad (16.76)$$

where V is a lattice. The dual of a sum reduction is a zero reduction followed by a multiplication by $1/d(V)$.²

Elementary Changes as Linear Transformations

The elementary changes are linear tfs, and, more specifically, reductions and increases are respectively $U \times V \rightarrow U$ and $U \rightarrow U \times V$ linear tfs. Their kernels are expressed by appropriate impulses. For instance, the kernel of the integral reduction is $h(\mathbf{u}; \mathbf{u}_0, \mathbf{v}_0) = \delta_U(\mathbf{u} - \mathbf{u}_0)$ (see Problem 16.5 for the other kernels).

The duality claimed in Table 16.1 can be proved by inspection by writing signals as inverse FTs. For instance, for the zero reduction $y(\mathbf{u}) = x(\mathbf{u}, \mathbf{0})$, we have

$$x(\mathbf{u}, \mathbf{0}) = \int_{\hat{U}} d\mathbf{f} \int_{\hat{V}} d\boldsymbol{\lambda} X(\mathbf{f}, \boldsymbol{\lambda}) e^{i2\pi\mathbf{f}\mathbf{u}}, \quad y(\mathbf{u}) = \int_{\hat{U}} d\mathbf{f} Y(\mathbf{f}) e^{i2\pi\mathbf{f}\mathbf{u}}. \quad (16.77)$$

²In Table 16.1 multiplication factors are indicated below the corresponding block.

Hence, by comparison we find $Y(\mathbf{f}) = \int_{\hat{V}} d\lambda X(\mathbf{f}, \lambda)$, which represents an integral reduction. Incidentally, note that the first of (16.77) extends the FT rule $x(0) = \text{area}(X)$.

16.10.2 Dimensionality Reduction Theorem

The possibility of recovering the signal after a dimensionality reduction is linked to *the limitation of the signal extension* and to the nature of the signal domains.

Let U be a p -D group, and V a q -D lattice. In a $U \times V \rightarrow U$ zero reduction the condition for the signal extension is $e(x_0) \subset U \times \mathbb{O}^q$. For instance, in a $2\text{D} \rightarrow 1\text{D}$ reduction of the form $\mathbb{R} \times \mathbb{Z}(d) \rightarrow \mathbb{R}$, the 2D signal extension must be confined to the \mathbb{R} line.

In a *sum reduction* the condition is less trivial and is stated in terms of lines and projections. The $U \times V$ lines are the subsets $(U \times V)_{\mathbf{v}} = \{(\mathbf{u}, \mathbf{v}) \mid \mathbf{u} \in U\}$, $\mathbf{v} \in V$, which form a partition in cells of $U \times V$ modulo $U \times \mathbb{O}^q$. For a signal $x_0(\mathbf{u}, \mathbf{v})$, $(\mathbf{u}, \mathbf{v}) \in U \times V$, the *extension lines* are

$$e(x_0)_{\mathbf{v}} = e(x_0) \cap (U \times V)_{\mathbf{v}}, \quad \mathbf{v} \in V,$$

and their *projections* are the subsets of U

$$\pi(x_0)_{\mathbf{v}} = \{\mathbf{u} \mid (\mathbf{u}, \mathbf{v}) \in e(x_0)_{\mathbf{v}}, \mathbf{u} \in U\}, \quad \mathbf{v} \in V.$$

Such lines are illustrated in Fig. 16.23 for $U \times V = \mathbb{R} \times \mathbb{Z}(d)$. After a sum reduction, i.e.,

$$y_0(\mathbf{u}) = \sum_{\mathbf{v} \in V} x_0(\mathbf{u}, \mathbf{v}), \quad \mathbf{u} \in U,$$

the y_0 extension is given by the union of the x_0 projections $\pi(x_0)_{\mathbf{v}}$. If $\pi(x_0)_{\mathbf{v}}$ do not overlap as in Fig. 16.23(c), the original signal can be recovered by a *hold increase* $U \rightarrow U \times V$, which spreads the $y_0(\mathbf{u})$ values to the whole domain $U \times V$, followed by a window $\eta_0(\mathbf{u}, \mathbf{v})$ that confines the signal values to the original support, as illustrated in Fig. 16.23(d).

Theorem 16.9 (Dimensionality Reduction Theorem) *Let U be a p -dimensional group, and V a q -dimensional lattice. A signal $x_0(\mathbf{u}, \mathbf{v})$, $(\mathbf{u}, \mathbf{v}) \in U \times V$, that satisfies the disjoint projection condition*

$$\pi(x_0)_{\mathbf{v}_1} \cap \pi(x_0)_{\mathbf{v}_2} = \emptyset, \quad \mathbf{v}_1 \neq \mathbf{v}_2,$$

can be perfectly recovered after a $U \times V \rightarrow V$ sum reduction by a $U \rightarrow U \times V$ hold increase, followed by a window with the shape $\eta_e(x_0)(\mathbf{u}, \mathbf{v})$.

As anticipated in the previous considerations, the theorem is similar to the Sampling Theorem, but here the assumption is concerned with the *extension limitation of the signal* instead of the *extension limitation of the FT* (band limitation).

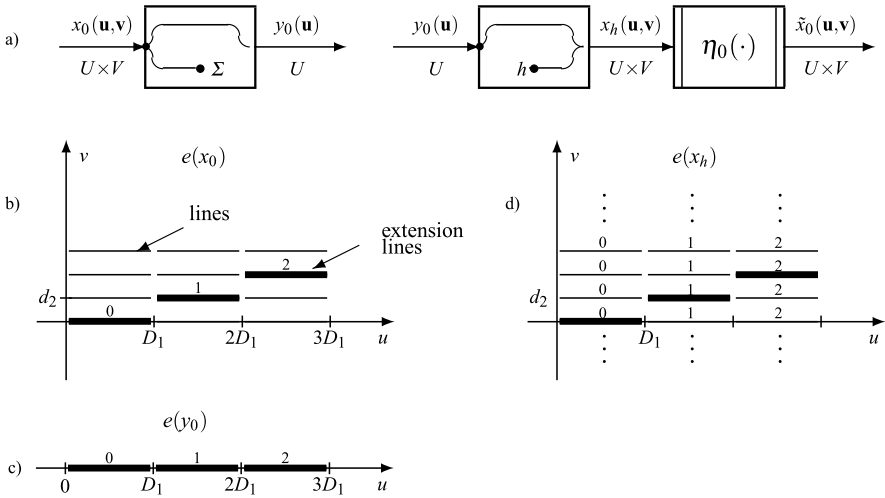


Fig. 16.23 Dimensionality Reduction Theorem. (a) $U \times V \rightarrow U$ elementary dimensionality reduction followed by an $U \rightarrow U \times V$ elementary increase; the final window $\eta_0(\cdot)$ provides the line limitation to the original format. (b) Shows the extension of a 2D signal $x_0(u, v)$, $(u, v) \in \mathbb{R} \times \mathbb{Z}(d_2)$, that meets the *disjoint projection condition*. (c) Support of the 1D signal $y_0(u)$ obtained by a sum-reduction, (d) lines obtained after an $\mathbb{R} \rightarrow \mathbb{R} \times \mathbb{Z}(d_2)$ hold increase

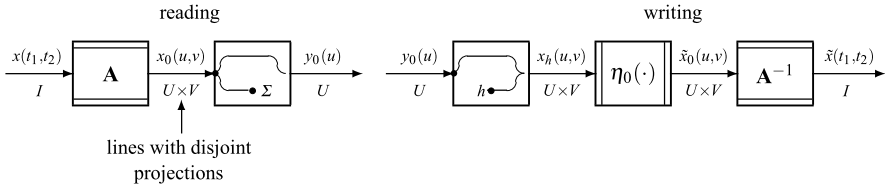


Fig. 16.24 Reading $mD \rightarrow nD$ and writing $nD \rightarrow mD$ decomposed into “simple” operations

UT 16.11 Composite Dimensionality Changes: Reading and Writing

The *disjoint projection condition* is unlikely for a signal extension since a signal, e.g., an image, rarely meets this requirement. However, this condition can be obtained from signals with a more interesting extension limitation.

In general we can start from a $(p + q)$ -dimensional signal $x(\mathbf{t})$, $\mathbf{t} \in I$, with a limited extension $e(x)$. If an $I \rightarrow U \times V$ tf exists, typically a coordinate change, such that the signal $x_0(\mathbf{u}, \mathbf{v})$ has disjoint projections after the tf, then the original signal $x(\mathbf{t})$, $\mathbf{t} \in I$, can be perfectly recovered, provided that the $I \rightarrow U \times V$ tf possesses an inverse $U \times V \rightarrow I$ tf. Then, we have a “composite” dimensionality reduction (*reading*) with a consequent “composite” dimensionality increase (*writing*) (Fig. 16.24).

A reading reduction consists of an $I \rightarrow U \times V$ coordinate change (with matrix \mathbf{A}) tf followed by an elementary $U \times V \rightarrow U$ reduction.

A writing increase consists of an elementary $U \rightarrow U \times V$ increase, followed by a window, and then by the inverse $U \times V \rightarrow I$ coordinate change (with matrix \mathbf{A}^{-1}).

The purpose of the window $\eta_0(\mathbf{u}, \mathbf{v})$ is to confine the values to the extension of the signal $x_0(\mathbf{u}, \mathbf{v})$.

In a *reading reduction* we have two explicit conditions:

- (1) The original group I and the matrix \mathbf{A} must be such that, after the coordinate change, the *reading* group has the separable form $U \times V$ with V a lattice, that is,

$$U \times V = \mathbf{A}^{-1}I \quad (V \text{ lattice}). \quad (16.78)$$

- (2) The original signal extension $e(x)$ and the matrix \mathbf{A} must be such that the extension after the coordinate change, that is,

$$e(x_0) = \mathbf{A}^{-1}e(x), \quad (16.79)$$

have disjoint projections.

We now develop the *continuous reading* operation, which produces a continuous signal, and then the *discrete reading*, which produces a discrete signal.

16.11.1 A Preliminary Example: 2D \rightarrow 1D Reading

We begin with 2D \rightarrow 1D continuous reading, where the 1D signal is defined on \mathbb{R} .

Example 16.13 Figure 16.25 illustrates a reading of a 2D signal $x(t_1, t_2)$ defined on a tilted grating I to give a 1D signal $y_0(u)$, $u \in \mathbb{R}$. The 2D signal $x(t_1, t_2)$ is first converted to a signal $x_0(u, v)$, $(u, v) \in \mathbb{R} \times \mathbb{Z}(d_2)$, by means of a coordinate change with a matrix of the form

$$\mathbf{A} = \begin{bmatrix} 1 & -D_1/d_2 \\ \alpha & 1 - \alpha D_1/d_2 \end{bmatrix} \rightarrow \mathbf{A}^{-1} = \begin{bmatrix} 1 - \alpha D_1/d_2 & D_1/d_2 \\ -\alpha & 1 \end{bmatrix}. \quad (16.80)$$

The extension of $x(t_1, t_2)$ is such that, after the coordinate change, the signal $x_0(u, v)$ meets the disjoint projection condition. Then, according to Theorem 16.9, $x_0(u, v)$ can be perfectly recovered from $y_0(u)$, and $x(t_1, t_2)$ is finally restored by the inverse coordinate change.

We check that conditions (1) and (2) really hold in this case. The tilted grating has generic point $(t_1, t_2) = (r, \alpha r + nd_2)$, $r \in \mathbb{R}$, $n \in \mathbb{Z}$, where α gives the inclination, and d_2 is the vertical spacing. After the coordinate change the point becomes

$$(u, v) = \mathbf{A}^{-1}(t_1, t_2) = \mathbf{A}^{-1}(r, \alpha r + nd_2) = (r + nD_1, nd_2) = (r', nd_y),$$

where $r' \in \mathbb{R}$ and $nd_2 \in \mathbb{Z}(d_2)$. Hence, (u, v) describes the separable grating $U \times V = \mathbb{R} \times \mathbb{Z}(d_2)$.

The extension $e(x)$ of the original signal is horizontally limited, and its lines have the common projection $[0, D_1)$, and therefore they are not disjoint projections, but the coordinate change provides appropriate shifts for each line, and the new projections are $[nD_1, (n+1)D_1)$, which are disjoint.

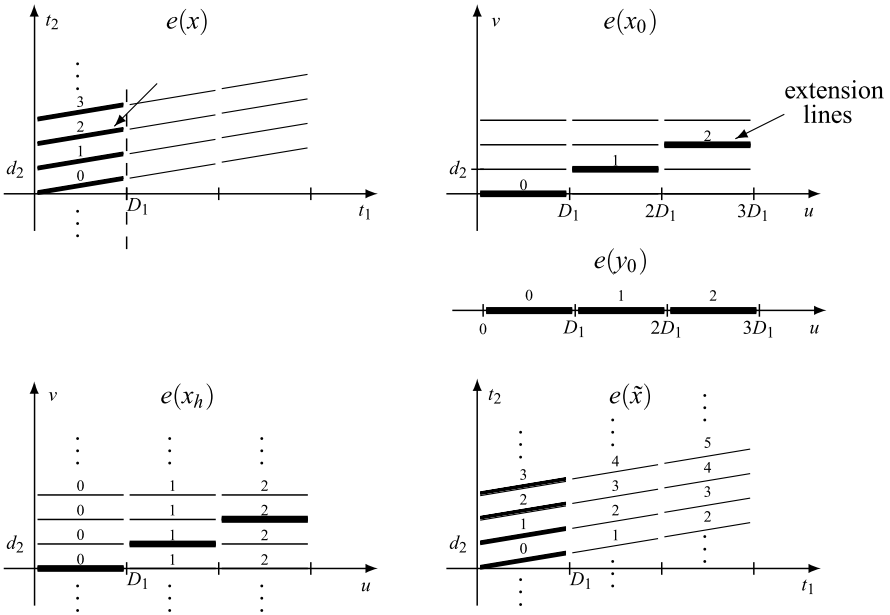


Fig. 16.25 Continuous Reading 2D \rightarrow 1D and Writing 1D \rightarrow 2D illustrated by the signal extensions: $e(x)$ extension of the original signal, $e(x_0)$ extension after coordinate change (here, the disjoint projection condition are verified), $e(y_0)$ extension of 1D signal, $e(x_h)$ extension after hold operation on the 1D signal, and $e(\tilde{x})$ extension of the reconstructed 2D signal

In the above example the coordinate change has the twofold task: to remove the inclination to obtain a separable group $U \times V$, and to provide appropriate shifts for each line. When the inclination removal is not required, the matrix has the simple form

$$\mathbf{A} = \begin{bmatrix} 1 & -D_1/d_2 \\ 0 & 1 \end{bmatrix}, \quad \mathbf{A}^{-1} = \begin{bmatrix} 1 & D_1/d_2 \\ 0 & 1 \end{bmatrix}. \tag{16.81}$$

16.11.2 The Composite Shift Matrix

Hereafter we concentrate our attention on the shifts, neglecting the inclination, which can be removed by a preliminary coordinate change. In other words, we consider a reading of the form $U \times V \rightarrow V$. Then, the matrix \mathbf{A} that provides the shift has the form

$$\mathbf{A} = \begin{bmatrix} \mathbf{I}_p & -\mathbf{M} \\ \mathbf{0} & \mathbf{I}_q \end{bmatrix} \rightarrow \mathbf{A}^{-1} = \begin{bmatrix} \mathbf{I}_p & \mathbf{M} \\ \mathbf{0} & \mathbf{I}_q \end{bmatrix}, \tag{16.82}$$

where \mathbf{I}_p and \mathbf{I}_q are identity matrices, and the matrix \mathbf{M} (of dimension $p \times q$) provides the shifts. The corresponding coordinate change has the form

$$x_0(\mathbf{u}, \mathbf{v}) = x(\mathbf{u} - \mathbf{M}\mathbf{v}, \mathbf{v}).$$

Now, if $c_{\mathbf{v}}$ is a line of $e(x)$, the coordinate change yields the line $q_{\mathbf{v}}$ of $e(x_0)$ in the form

$$q_{\mathbf{v}} = c_{\mathbf{v}} + (\mathbf{M}, \mathbf{0})\mathbf{v}, \quad (16.83)$$

which is not a rigid shift of equal amount for all the lines, but a specific shift for each line, that is, $(\mathbf{M}, \mathbf{0})\mathbf{v}$ for the line \mathbf{v} . This is a surprising and lucky peculiarity of a coordinate change in the presence of a limited signal extension: it gives appropriate and differentiated shifts for the line extensions, obtaining in such a way an interesting dimensionality reduction in a very simple form.

We call \mathbf{A} of the form (16.82) a *composite shift matrix*, of which (16.81) is an elementary example.

16.11.3 Continuous Reading

We develop the reading of the form $U \times V \rightarrow U$, where $U = \mathbb{R}$ and $V = \mathbb{Z}(d_2, \dots, d_m)$, with the target to find the matrix \mathbf{M} in (16.83) such that the shifted lines have disjoint projections.

The case $m = 2$, that is, $\mathbb{R} \times \mathbb{Z}(d_2) \rightarrow \mathbb{R}$, has been developed above, where we have seen that the composite shift matrix is given by (16.81). We now develop the case $m = 3$, which is sufficient to understand how to handle the case of general m .

Example 16.14 We consider the 3D \rightarrow 1D dimensionality reduction of the form

$$U \times V \rightarrow U \quad \text{with } U = \mathbb{R}, V = \mathbb{Z}(d_2, d_3),$$

where the 3D signals $x(t_1, t_2, t_3)$ has extension given by the cell

$$C = [0, D_1) \times \mathbb{Z}_N(d_2) \times \mathbb{Z}(d_3) \quad (D_2 = Nd_2),$$

which is limited along t_1 and t_2 and unlimited along t_3 , as shown in Fig. 16.26. The lines of C are

$$c_{nk} = [0, D_1) \times \{nd_2\} \times \{kd_3\}, \quad n \in \mathbb{Z}_{N_2}, k \in \mathbb{Z},$$

and have $[0, D_1)$ as a common projection on \mathbb{R} . The application of the shifts

$$(nD_1 + kND_1, 0, 0), \quad n \in \mathbb{Z}_{N_2}, k \in \mathbb{Z}, \quad (16.84)$$

give the shifted lines

$$\begin{aligned} q_{nk} &= c_{nk} + (nD_1 + kND_1, 0, 0) \\ &= [nD_1 + kND_1, D_1 + nD_1 + kND_1) \times \{nd_2\} \times \{kd_3\}, \end{aligned}$$

which have disjoint projections. For the identification of the matrix \mathbf{M} , it is sufficient to observe that the shifts (16.84) can be written in the form $(\mathbf{M}, \mathbf{0})\mathbf{v}$ (see (16.83)) with

$$\mathbf{M} = [D_1/d_2, ND_1/d_3], \quad \mathbf{v} = \begin{bmatrix} nd_2 \\ kd_3 \end{bmatrix}.$$

In conclusion, the composite shift matrix which allows the correct $\mathbb{R} \times \mathbb{Z}(d_2, d_3) \rightarrow \mathbb{R}$ reduction is given by

$$\mathbf{A} = \begin{bmatrix} 1 & -D_1/d_2 & -ND_1/d_3 \\ 0 & 1 & 0 \\ 0 & 0 & 1 \end{bmatrix}. \tag{16.85}$$

The composite shifts are illustrated in Fig. 16.26, where for clarity we have applied the shifts (nD_1, kND_1) in two steps: first, the shifts nD_1 in figure b), and then the shifts kND_1 in figure c).

Incidentally, note that if we would stop at figure b), we would have the disjoint conditions for the $\mathbb{R} \times \mathbb{Z}(d_2) \times \mathbb{Z}(d_3) \rightarrow \mathbb{R} \times \mathbb{Z}(d_3)$ reduction, that is, a 3D \rightarrow 2D reduction.

16.12 Discrete Reading

Discrete reading can be handled as continuous reading, at least in the separable case $U \times V \rightarrow U$, but for generality, we also consider the case $J \rightarrow U$, where J is not separable into the form $U \times V$. Considering that J is a lattice, we can use the upper-triangular representation to handle the effect of composite shifts. We write the upper-triangular basis of J in the partitioned block form

$$\mathbf{J} = \begin{bmatrix} \mathbf{J}_{11} & \mathbf{J}_{12} \\ \mathbf{0} & \mathbf{J}_{22} \end{bmatrix},$$

where \mathbf{J}_{11} is $p \times p$, \mathbf{J}_{22} is $q \times q$, etc. Then, the application of the composite shift matrix modifies the basis in the form

$$\mathbf{K} = \mathbf{A}^{-1}\mathbf{J} = \begin{bmatrix} \mathbf{I}_p & \mathbf{M} \\ \mathbf{0} & \mathbf{I}_q \end{bmatrix} \begin{bmatrix} \mathbf{J}_{11} & \mathbf{J}_{12} \\ \mathbf{0} & \mathbf{J}_{22} \end{bmatrix} = \begin{bmatrix} \mathbf{J}_{11} & \mathbf{J}_{12} + \mathbf{M}\mathbf{J}_{22} \\ \mathbf{0} & \mathbf{J}_{22} \end{bmatrix}. \tag{16.86}$$

The crucial point is that, if the J is not separable ($\mathbf{J}_{12} \neq \mathbf{0}$), we have to provide a shift matrix \mathbf{M} such that the lattice K with basis \mathbf{K} becomes separable in the form $K = J_{11} \times J_{22}$.

We now develop the discrete readings 2D \rightarrow 1D and 3D \rightarrow 1D.

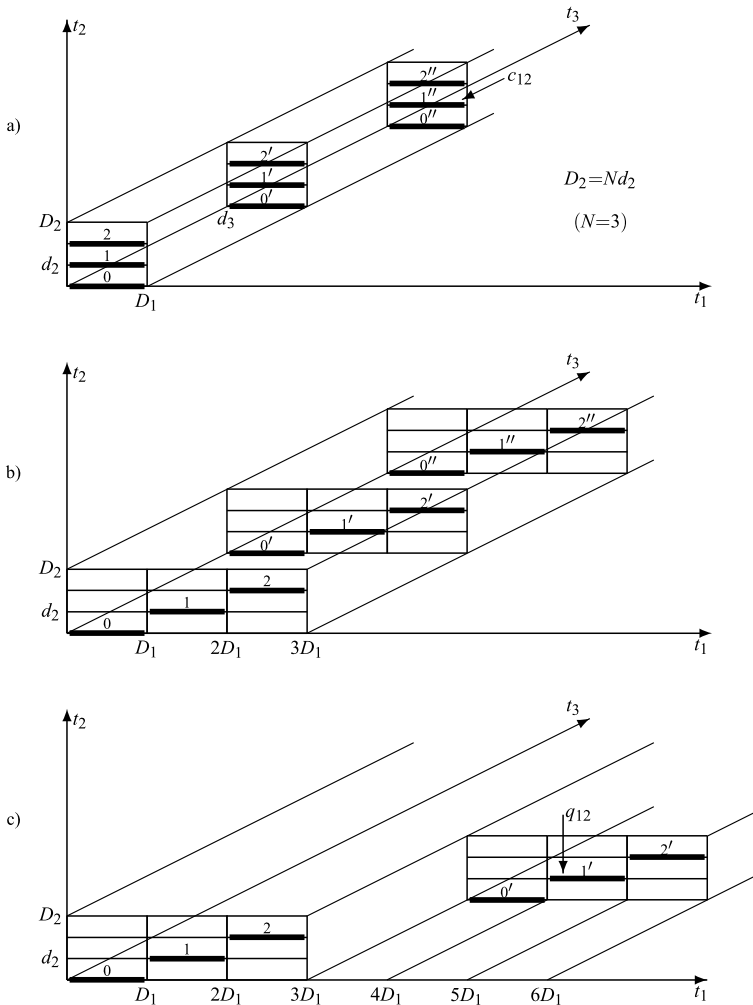


Fig. 16.26 Extensions in the reading $\mathbb{R} \times \mathbb{Z}(d_2, d_3) \rightarrow \mathbb{R}$ of a signal $x(t_1, t_2, t_3)$ with a limited extension along t_1 and t_2 : (a) original extension, (b) extension after the first shift, and (c) extension after the second shift

16.12.1 2D→1D Discrete Reading: Preliminary Examples

We first consider a separable case and then a nonseparable case to understand the problems arising in the second case.

Example 16.15 Consider the $\mathbb{Z}(d_1, d_2) \rightarrow \mathbb{Z}(d_1)$ reading, where a 2D discrete signal is converted to a 1D discrete signal on $\mathbb{Z}(d_1)$. The assumption is that the extension of the 2D signal $x(t_1, t_2)$ is contained in the cell of the form $C = \mathbb{Z}_M(d_1) \times \mathbb{Z}(d_2)$, as shown in Fig. 16.27. This cell is a subset of the cell $[0, D_1) \times \mathbb{Z}(d_2)$, with $D_1 =$

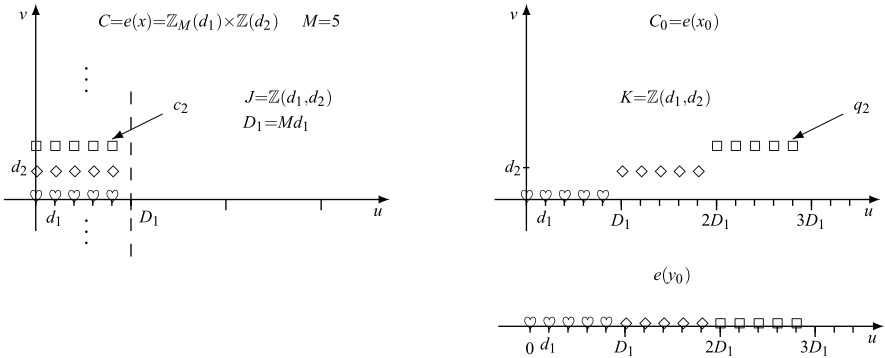


Fig. 16.27 Extensions in the $\mathbb{Z}(d_1, d_2) \rightarrow \mathbb{Z}(d_1)$ reading: on the left the original extension, on the right after the composite shift, and below after the projection on the u axis. After the shifts the lattice $K = J$ is still separable, and the 1D signal is correctly defined on $\mathbb{Z}(d_1)$

Md_1 , considered in $\mathbb{R} \times \mathbb{Z}(d_2) \rightarrow \mathbb{R}$ reduction and has the same structure with the continuous interval $[0, D_1]$ replaced by the “discrete” interval $\mathbb{Z}_M(d_1)$, consisting of M equally spaced points, or *pixels*, thinking of images. The lines of the cell are $c_n = \mathbb{Z}_M(d_1) \times \{nd_2\}$, each one consisting of M pixels. The matrix

$$\mathbf{A} = \begin{bmatrix} 1 & -Md_1/d_2 \\ 0 & 1 \end{bmatrix}, \quad \mathbf{A}^{-1} = \begin{bmatrix} 1 & Md_1/d_2 \\ 0 & 1 \end{bmatrix}, \quad (16.87)$$

provides the appropriated shifts of nM to get the disjoint projections, as shown in Fig. 16.27. Finally, a 1D signal on $\mathbb{Z}(d_1)$ is obtained.

We can see that after the application of the composite shifts, the lattice $J = \mathbb{Z}(d_1, d_2)$ does not change and therefore is still separable.

The above procedure can be easily extended to the reading $\mathbb{Z}(d_1, d_2, d_3) \rightarrow \mathbb{Z}(d_1)$, where, reconsidering Fig. 16.26, the continuous lines of size $[0, D_1]$ must be replaced by discrete lines of M pixels. Also in this case we finally obtain a correct signal on $\mathbb{Z}(d_1)$.

Example 16.16 We now consider a 2D→1D reading, where the original 2D signal is defined on a *nonseparable* lattice. Specifically, we consider the case where the original 2D signal is defined on a quincunx lattice $\mathbb{Z}_2^1(d_1, d_2)$ and investigate the conversion to a signal defined on $\mathbb{Z}(2d_1)$. This reading is illustrated in Fig. 16.28. The assumption is the same as in the separable case of Fig. 16.27, where the cell is contained in the vertical string $[0, D_1] \times \mathbb{R}$ of the (u, v) plane with $D_1 = Md_1$. With the previous format $\mathbb{Z}(d_1, d_2)$, M represents the number of pixels per lines, but, with the quincunx format the effective number of pixel per line is reduced and may be different from line to line. In any case we call M the *nominal* number of pixels per line. Figure 16.28 shows two cases, $M = 5$ and $M = 6$.

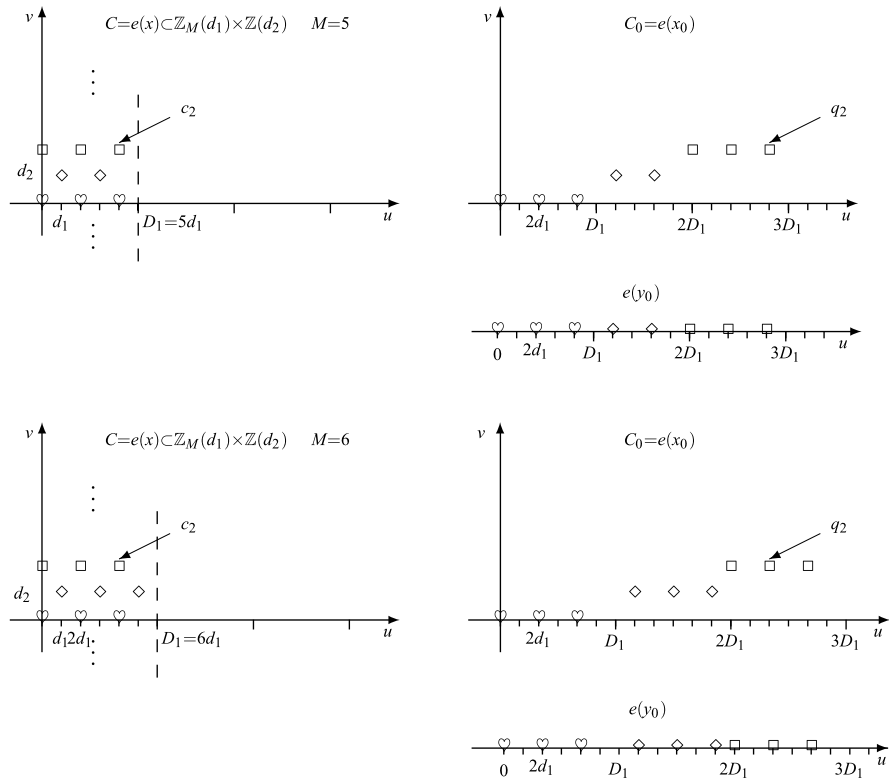


Fig. 16.28 Extensions in the $\mathbb{Z}_2^1(d_1, d_2) \rightarrow \mathbb{Z}(d_1)$ reading: *above* with $N = 5$ gives a 1D signal correctly defined on $\mathbb{Z}(2d_1)$, *below* with $N = 6$ does not give a correct 1D signal

With $M = 5$ we find 3 pixels in the even lines and 2 pixels in the odd lines, but with the composite shifts given by the matrix (16.87) the projections of all the pixels fall exactly $2d_1$ separated along the u axis, and a correct 1D signal on $\mathbb{Z}(2d_1)$ is obtained by the reading operation.

With $M = 6$ we find 3 pixels in all the lines, but the shifts provided by matrix (16.87) do not produce a correct 1D signal. In the projected extension $e(y_0)$ we find contributions in the points

$$0, 2d_1, 4d_1, 7d_1, 9d_1, 11d_1, 12d_1, 14d_1, \dots,$$

which are not $2d_1$ equally spaced. The conclusion is that with $M = 6$, and in general with M even, the reading operation does not produce a *correct* 1D signal. For “correct,” we mean a signal defined on a group, according to the main rule of the Unified Theory.

16.12.2 2D \rightarrow 1D Discrete Reading: General Case

We have just seen that the reading $\mathbb{Z}_2^1(d_1, d_2) \rightarrow \mathbb{Z}(2d_1)$ imposes a constraint on the parameter M of the extension $e(x)$. We consider the problem for a general 2D lattice $J = \mathbb{Z}_a^p(d_1, d_2)$, whose basis is given by

$$\mathbf{J} = \begin{bmatrix} d_1 & 0 \\ 0 & d_2 \end{bmatrix} \begin{bmatrix} a & p \\ 0 & 1 \end{bmatrix}, \quad 0 \leq p < a, \quad (16.88)$$

and, without loss of generality, we suppose that a and p are *relatively prime* (otherwise, if a and p had a common factor n_0 , we would replace d_1 with n_0d_1). We assume that the extension of the original 2D signal is given by the vertical strip

$$C = \{\mathbb{Z}_M(d_1) \times \mathbb{Z}(d_2)\} \cap J. \quad (16.89)$$

The points of J are given by $(u, v) = ((ma + pn)d_1, nd_2)$, $m, n \in \mathbb{Z}$, and within the extension C , they are constrained as follows:

$$0 \leq ma + pn < M, \quad n \in \mathbb{Z}. \quad (16.90)$$

After the composite shifts the basis of the lattice becomes

$$\mathbf{K} = \mathbf{A}^{-1}\mathbf{J} = \begin{bmatrix} 1 & Md_1/d_2 \\ 0 & 1 \end{bmatrix} \mathbf{J} = \begin{bmatrix} d_1 & 0 \\ 0 & d_2 \end{bmatrix} \begin{bmatrix} a & p + M \\ 0 & 1 \end{bmatrix} \quad (16.91)$$

and can be reduced to the diagonal form (with elementary operations on the basis) as soon as $p + M$ is multiple of a . Then, the lattice K with basis \mathbf{K} becomes separable.

Proposition 16.14 Consider the reading $J = \mathbb{Z}_a^p(d_1, d_2) \rightarrow \mathbb{Z}(ad_1)$, where J is an arbitrary sublattice of $\mathbb{Z}(d_1, d_2)$ and the extension of the 2D signal is given by the cell (16.89). If the nominal number of pixels per line M verifies the condition

$$p + M \in \mathbb{Z}(a) \implies p + M = M_0a, \quad (16.92)$$

then the reading produces a correct 1D signal on $\mathbb{Z}(ad_1)$.

Proof The key consequence of assumption (16.92) is that the lattice K becomes separable as $\mathbb{Z}(ad_1, d_2)$. This ensures that the points of projections fall in the right places, equally spaced by ad_1 . But to complete the proof for a correct signal on $\mathbb{Z}(ad_1)$, it remains to show that the projections do not exhibit “holes.” This is achieved by the balance of the numbers of pixels and requires to examine in detail the structure of the cell C . We can easily see that C has a vertical period ad_2 , as shown in Fig. 16.29 with $a = 5$, $p = 2$, and $M = 13$. It can also be shown that the number of pixels per period is given by M (see Problem 16.7). In a period of the room for the pixels is given by the intervals $[0, D_1)$, with $D_1 = ad_1$, which globally have a length aD_1 . After the shifts of kD_1 , these intervals becomes the consecutive intervals $[0, D_1), [D_1, 2D_1), \dots, [(a - 1)D_1, aD_1)$, preserving inside the original

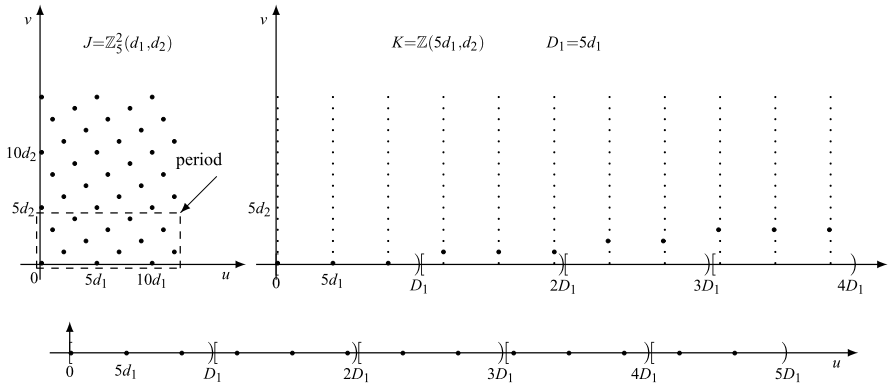


Fig. 16.29 Vertical strip of the lattice $\mathbb{Z}^2_5(d_1, d_2)$ of $M = 13$ nominal pixels per line. After the shifts, the lines of pixels fall on the separable lattice $\mathbb{Z}(5d_1, d_2)$, and their projections fall equally spaced on the 1D lattice $\mathbb{Z}(5d_1)$ without “holes”

number of pixels. Finally, considering that the pixels fall equally spaced by ad_1 and in $[0, aD_1)$, we have room for exactly M pixels, we conclude that the projections have no hole. □

16.12.3 3D→1D Discrete Reading

We consider the reading $J \rightarrow \mathbb{Z}(ad_1)$, where J is an arbitrary sublattice of $\mathbb{Z}(d_1, d_2, d_3)$ with upper triangular basis

$$\mathbf{J} = \begin{bmatrix} d_1 & 0 & 0 \\ 0 & d_2 & 0 \\ 0 & 0 & d_3 \end{bmatrix} \begin{bmatrix} a & p & q \\ 0 & i & b \\ 0 & 0 & 1 \end{bmatrix}, \quad 0 \leq p, q < a, 0 \leq b < i, \quad (16.93)$$

where, without restriction, we assume that both a, p, q and i, b have *no common factors*, otherwise we can redefine d_1 and d_2 including such factors. We suppose that the extension C of the 3D signal $x(t_1, t_2, t_3)$ is limited along t_1 and t_2 as

$$C = \{[0, Md_1] \times [0, Nd_2] \times \mathbb{Z}(d_3)\} \cap J. \quad (16.94)$$

We want to investigate the conditions on the lattice J and on the cell C that allow the 3D→1D reduction to a correct signal on $\mathbb{Z}(ad_1)$. The appropriate 3×3 composite shift matrix \mathbf{A} is given by (16.81) with

$$\mathbf{M} = [Md_1/id_2, MNd_1/id_3].$$

The application of \mathbf{A} changes the basis of the lattice as follows:

$$\mathbf{K} = \mathbf{A}^{-1}\mathbf{J} = \begin{bmatrix} d_1 & 0 & 0 \\ 0 & d_2 & 0 \\ 0 & 0 & d_3 \end{bmatrix} \begin{bmatrix} a & p + M & q + bM/i + MN/i \\ 0 & i & b \\ 0 & 0 & 1 \end{bmatrix},$$

and we have to search conditions under which the corresponding lattice K becomes separable in the form $K = \mathbb{Z}(ad_1) \times \mathbb{Z}_i^b(d_2, d_3)$ (see (16.86) and related comments).

Proposition 16.15 *The reading $J \rightarrow \mathbb{Z}(ad_1)$, with J defined by (16.93) and an extension of the 3D signal limited on the cell (16.94), gives a correct 1D signal on $\mathbb{Z}(ad_1)$ if there exist naturals M_0, N_0, L_0 such that*

$$p + M = aM_0, \quad b + N = iN_0, \quad q + MN_0 = aL_0. \quad (16.95)$$

For instance, with

$$a = 2, \quad p = q = 1, \quad i = 5, \quad b = 2, \quad M = 9, \quad N = 13, \quad (16.96)$$

we have

$$p + M = 1 + 9 = 2M_0, \quad b + N = 2 + 13 = 5N_0, \quad q + MN_0 = 1 + 27 = 2L_0,$$

so that the naturals $M_0 = 5$, $N_0 = 3$, and $L_0 = 14$ exist, and the final signal is correctly formed on $\mathbb{Z}(2d_1)$.

Proof We first prove that if the lattice parameters verify condition (16.95), the lattice K becomes separable in the desired form. In fact, the elements 1, 2 and 1, 3 of the matrix \mathbf{K} become multiples of ad_1 and can be replaced by 0 with the usual elementary operations on the lattice basis (see Sect. 16.6). This ensures that the projections fall in the $\mathbb{Z}(ad_1)$ lattice.

We sketch the ideas for the proof that projections are formed without holes (for a detailed proof, see [1]). The points of the lattice J are given by

$$x = (ma + np + kq)d_1, \quad y = (ni + kb)d_2, \quad z = kd_3, \quad m, n, k \in \mathbb{Z}, \quad (16.97)$$

and, within the cell C , they are constrained by

$$0 \leq ma + np + kq < M, \quad 0 \leq ni + kb < N, \quad k \in \mathbb{Z}. \quad (16.98)$$

Now, in place of lines it is convenient to consider the *fields* Q_k which are 2D sets obtained with the above coordinates (x, y) for k fixed and m, n constrained as in (16.98). The fields obtained with the values (16.96) are shown in Fig. 16.30. Now, we note that (see problems)

- (1) the fields Q_k are periodic with period ai , that is, $Q_{k+ai} = Q_k$,
- (2) in a period the number of lines is Na , and the number of pixels is MN .

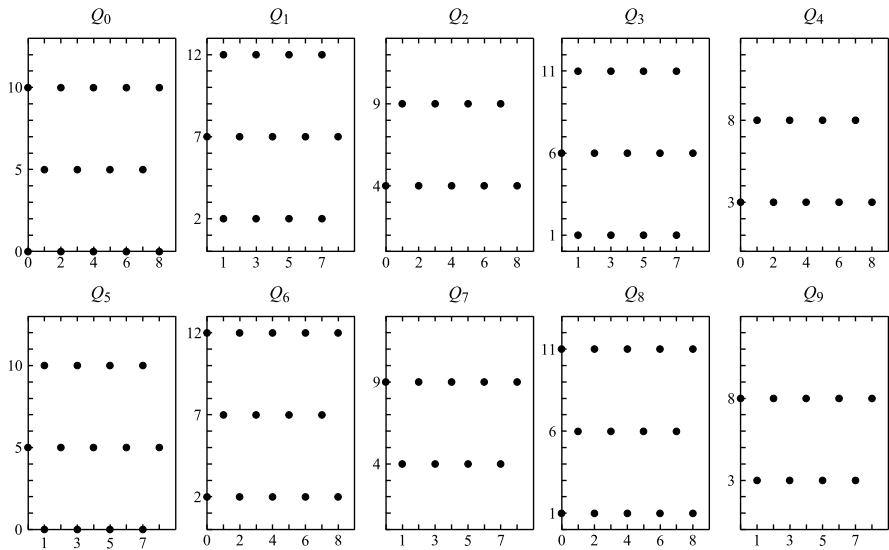


Fig. 16.30 The fields Q_k in the discrete scanning with $a = 2$, $p = 1$, $q = 1$, $M = 9$, $N = 13$. The field C_0 is $\mathbb{Z}_2^1(2d_1, 5d_2)$, and the fields are periodic with period 10

The lines in the fields are vertically separated by id_2 , and the shift they receive is given by $(Md_1/id_2)id_2 = Md_1 \stackrel{\Delta}{=} D_1$. Globally, the aN lines receive a shift of $aND_1 = aNMd_1$, which is the right room necessary to display the NM pixels, equally spaced of ad_1 without holes. □

Concluding Remarks on Discrete Reading

The topic here presented is original and was carried out in the framework of the European project of high-definition television (HD-MAC project) in the eighties of the last century.

We have seen in the 2D→1D and 3D→1D discrete reading how to construct a correct 1D signal by a reading operation, under some constraints on the original lattice and on the parameters of the signal extension. We remark that the reading operation is essentially based on an appropriate coordinate change provided by the composite shift matrix. This allows us to obtain the dimensionality reduction in an extremely simple form with a remarkable simplification from the Signal Theory viewpoint, as we shall see in the Fourier analysis of the next section.

We finally note that other forms of dimensionality reductions are possible, without the constraints on the lattice and on the extension, but at the expense of a cumbersome Signal Theory formulation [1]. In other words, the theory here presented seems to be more natural and efficient.

16.13 Fourier Analysis of Reading

The reading operation discussed in detail in the previous section is based on the combination of two “simple” operations which allow a very simple Fourier analysis. Remarkable is the fact that this analysis has a complete generality, which holds both for continuous and discrete reading.

The decomposition of the reading into two “simple” tfs is shown in Fig. 16.24, where we find:

- (1) A coordinate change with matrix \mathbf{A} from $I \rightarrow U \times V$. The dual tf is a coordinate change with matrix \mathbf{A}^* from $\widehat{I} \rightarrow \widehat{U} \times \widehat{V}$ and a multiplication by the constant $\mu(\mathbf{A}) = d(\mathbf{A}^*)$ (see Sect. 5.9). Then, the relation is

$$X_0(\mathbf{f}, \boldsymbol{\lambda}) = \mu(\mathbf{A})X(\mathbf{A}^*(\mathbf{f}, \boldsymbol{\lambda})), \quad \mathbf{f} \in \widehat{U}, \boldsymbol{\lambda} \in \widehat{V}. \quad (16.99)$$

- (2) A sum reduction from $U \times V \rightarrow U$. The dual tf is a zero reduction from $\widehat{U} \times \widehat{V} \rightarrow \widehat{U}$ (see Table 16.1). The corresponding relation is

$$Y_0(\mathbf{f}) = \mu(\mathbf{A})\mu(V)X_0(\mathbf{f}, \mathbf{0}). \quad (16.100)$$

Combining the two relations, one gets

$$\boxed{Y_0(\mathbf{f}) = \mu(\mathbf{A})\mu(V)X(\mathbf{A}^*(\mathbf{f}, \mathbf{0})), \quad \mathbf{f} \in \widehat{U}}, \quad (16.101)$$

which gives the FT of the mD signal $y_0(\mathbf{u})$, $\mathbf{u} \in U$, in terms of the FT of the $(m+n)D$ signal $x(\mathbf{t})$, $\mathbf{t} \in I$.

When the matrix \mathbf{A} has the form (16.82), where \mathbf{M} is real, we have $\mu(\mathbf{A}) = 1$ and

$$\mathbf{A}^* = \begin{bmatrix} \mathbf{I}_p & \mathbf{0} \\ \mathbf{M}' & \mathbf{I}_q \end{bmatrix},$$

and (16.101) becomes

$$\boxed{Y_0(\mathbf{f}) = \mu(V)X(\mathbf{f}, \mathbf{M}'\mathbf{f}), \quad \mathbf{f} \in \widehat{U}}. \quad (16.102)$$

Then, $Y_0(\mathbf{f})$ is obtained by reading the Fourier transform $X(\mathbf{f})$ of the original signal $x(\mathbf{t})$ along the hyperplane of equation

$$\{\mathbf{f}, \mathbf{M}\mathbf{f}\}, \quad \mathbf{f} \in \widehat{U}. \quad (16.103)$$

An application of (16.102) will be done in the following chapter in the scanning of 2D and 3D images.

The decomposition of Fig. 16.24 also simplifies the Fourier analysis of the reproduction process (see [1]).

16.14 Problems

16.1 ★ [Sect. 16.3] Explicitly write (16.30) and (16.31) for the grating G_2 of Example 16.4.

16.2 ★★ [Sect. 16.4] Write a reduced basis \mathbf{G}_r of a grating G with signature $\mathbb{R}^2 \times \mathbb{Z}^2$. Then, find all subgroups of G with signature $\mathbb{R} \times \mathbb{Z}^3$.

16.3 ★★ [Sect. 16.4] Find all 1D subgroups of the grating $\mathbb{R}\mathbb{Z}(2, 1)$.

16.4 [Sect. 16.6] Find the aligned bases of the 2D lattices defined by the bases

$$\mathbf{G} = \begin{bmatrix} 3 & 1 \\ 1 & 2 \end{bmatrix}, \quad \mathbf{J} = \begin{bmatrix} 6 & 13 \\ 2 & 6 \end{bmatrix}.$$

16.5 ★ [Sect. 16.10] Check that the kernels of *zero* and *integral-reductions* are respectively

$$h(\mathbf{u}; \mathbf{u}_0, \mathbf{v}_0) = \delta_V(\mathbf{v}_0)\delta_U(\mathbf{u} - \mathbf{u}_0), \quad h(\mathbf{u}; \mathbf{u}_0, \mathbf{v}_0) = \delta_U(\mathbf{u} - \mathbf{u}_0).$$

16.6 ★ [Sect. 16.10] Check that the kernels of the *hold* and *delta-increases* are respectively

$$h(\mathbf{u}, \mathbf{v}; \mathbf{u}_0) = \delta_U(\mathbf{u} - \mathbf{u}_0), \quad h(\mathbf{u}, \mathbf{v}; \mathbf{u}_0) = \delta_U(\mathbf{u} - \mathbf{u}_0)\delta_V(\mathbf{u}).$$

16.7 ★★★ [Sect. 16.12] Consider the $\mathbb{Z}_a^p(d_1, d_2) \rightarrow \mathbb{Z}(ad_1)$ reading of Proposition 16.14. Prove the following statements (recall that a and p are relatively prime):

- (1) the abscissa of the first pixel of line n is given by $m_n d_1$, where $m_n = \mu_a(nb)$, with $\mu_a(x)$ the remainder of the integer division of x by a ;
- (2) the number of pixels of line n is given by

$$M_n = \rho_a(M - 1 - m_n) + 1,$$

where $\rho_a(x)$ denotes the integer part of x ;

- (3) m_n and M_n have period a ;
- (4) the number of pixels in a period is M .

For instance, with $a = 5$, $b = 2$, and $M = 13$, we find $m_0 = 0$, $m_1 = 2$, $m_2 = 4$, $m_3 = 1$, $m_4 = 3$ and $M_0 = 3$, $M_1 = 3$, $M_2 = 2$, $M_3 = 3$, $M_4 = 2$, and the sum of M_N is $M = 13$.

16.8 ★★ [Sect. 16.12] Show that in the 3D \rightarrow 1D reading with lattice (16.93) and extension (16.94), the period of the fields Q_k is given by $L = ai$ (recall that a , p , q and i , b have no common factor). *Hint*: the period is given by the smallest integer $k > 0$ such that the lattice coordinates result $(x, y) = (0, 0)$, which represents the position of the first pixel of the field Q_0 .

16.9 *** [Sect. 16.12] Continuing the previous problem, show that the number of lines in a period is Na and the number of pixels is MN .

16.10 * [Sect. 16.13] Find the Fourier analysis of the $\mathbb{R} \times \mathbb{Z}(d_2, d_3) \rightarrow \mathbb{R}$ reading, where the composite shift matrix \mathbf{A} is given by (16.85).

16.11 ** [Sect. 16.13] Find the Fourier analysis of the $\mathbb{Z}_2^1(d_1, d_2) \rightarrow \mathbb{Z}(2d_2)$ reading, where the composite shift matrix is given by (16.87) with M odd.

16.12 ** [Sect. 16.13] Find the Fourier analysis of the writing operation of Fig. 16.24.

Appendix: Condition for Getting a Subgroup (Theorem 16.1)

We investigate when the “convenient” basis given by (16.38) generates a subgroup $J = \mathbf{J}K$ of G . To this end, we decompose the candidate subgroup J into its 1D components (see (16.8))

$$J = \mathbf{j}_1 K_1 + \mathbf{j}_2 K_2 + \cdots + \mathbf{j}_m K_m, \tag{16.104}$$

where K_i are the factors of the signature $K = K_1 \times \cdots \times K_m$. Now, a necessary and sufficient condition for J be a subgroup of G is that all the 1D components $\mathbf{j}_r K_r$ be subgroups of G , that is,

$$\mathbf{j}_1 K_1, \dots, \mathbf{j}_m K_m \subset G \iff J \subset G. \tag{16.105}$$

Lemma 16.1 *Let $\mathbf{j} = \mathbf{G}\mathbf{k}$, $\mathbf{k} \in \mathbb{R}^p \times \mathbb{Z}^q$ be a point of a group $G = \mathbf{G}\mathbb{R}^p \times \mathbb{Z}^q$, and let $\mathbf{j}\mathbb{Z}$ or $\mathbf{j}\mathbb{R}$ be the 1D group generated by \mathbf{j} . Then:*

- (1) $\mathbf{j}\mathbb{Z}$ is always a subgroup of G ,
- (2) $\mathbf{j}\mathbb{R}$ is a subgroup of G if and only if it belongs to the subspace $V(G)$ of G , that is,

$$\mathbf{j} \in \mathbf{G}\mathbb{R}^p \times \mathbb{O}^q = V(G) \iff \mathbf{h} \in \mathbb{R}^p \times \mathbb{O}^q. \tag{16.106}$$

Proof (1) We have to prove that $n\mathbf{j} \in G$ for $\forall n \in \mathbb{Z}$. This is easily done by induction, using the group properties: $\mathbf{j} \in G$, then $2\mathbf{j} = \mathbf{j} + \mathbf{j} \in G$, $3\mathbf{j} = 2\mathbf{j} + \mathbf{j} \in G$, etc. and also $-\mathbf{j}\mathbb{Z} \in G$, $-2\mathbf{j}\mathbb{Z} \in G$, etc.

(2) We have to prove condition (16.106) that $r\mathbf{j} \in G$ for all $r \in \mathbb{R}$ if and only if the point \mathbf{j} belongs to the subspace $V(G)$. The reason of this condition is due to the fact that $\mathbf{j}\mathbb{R}$ is a line *through the origin*, specifically

$$\mathbf{j}\mathbb{R} = \{r(h_1 \mathbf{g}_1 + \cdots + h_p \mathbf{g}_p + h_{p+1} \mathbf{g}_{p+1} + \cdots + h_m \mathbf{g}_m) \mid r \in \mathbb{R}\},$$

and G consists of hyperplanes, and only one of them crosses the origin, namely

$$\mathbf{g}_1\mathbb{R} + \cdots + \mathbf{g}_p\mathbb{R} = V(G).$$

Now, in order that $\mathbf{j}\mathbb{R} \subset G$, the continuum $\mathbf{j}\mathbb{R}$ must lie in the continuum $V(G)$, and this implies, and is implied by, the condition that $\mathbf{j}\mathbb{R}$ does not receive contributions from the vectors $\mathbf{g}_{p+1}, \dots, \mathbf{g}_m$. This happens when

$$h_{p+1} = 0, \dots, h_m = 0. \quad (16.107)$$

□

We illustrate this condition in the 2D and 3D case. In the 2D case, consider the grating $G = \mathbf{G}\mathbb{R} \times \mathbb{Z}$, which is formed by equally distant parallel lines, and $\mathbf{g}_1\mathbb{R}$ is the line passing through the origin and containing \mathbf{g}_1 (see Fig. 16.2). But, also $\mathbf{j}\mathbb{R} = \{r(h_1\mathbf{g}_1 + h_2\mathbf{g}_2) \mid r \in \mathbb{R}\}$ is a line passing through the origin, which belongs to the grating G if and only if $h_2 = 0$. If this is the case, we have $\mathbf{j}\mathbb{R} = \{rh_1\mathbf{g}_1 \mid r \in \mathbb{R}\} = \mathbf{g}_1\mathbb{R}$, provided that $h_1 \neq 0$.

Next, suppose that G is a 3D grating $G = \mathbf{G}\mathbb{R}^2 \times \mathbb{Z}$, which consists of equidistant parallel planes, and $V(G) = \mathbf{g}_1\mathbb{R} + \mathbf{g}_2\mathbb{R}$ is the plane passing through the origin determined by \mathbf{g}_1 and \mathbf{g}_2 . Now

$$\mathbf{j}\mathbb{R} = \{r(h_1\mathbf{g}_1 + h_2\mathbf{g}_2 + h_3\mathbf{g}_3) \mid r \in \mathbb{R}\}$$

is a line through the origin, and it belongs to the grating G if it lies on the plane $V(G)$. This implies that $h_3 = 0$. In other words, $\mathbf{j}\mathbb{R}$ must not receive a contribution from the vector \mathbf{g}_3 . If G is the grating $G = \mathbf{G}\mathbb{R} \times \mathbb{Z}^2$, the space $V(G)$ becomes $V(G) = \mathbf{G}\mathbb{R} \times \mathbb{O}^2 = \mathbf{g}_1\mathbb{R}$, that is, a line through the origin, and the line $\mathbf{j}\mathbb{R}$ must coincide with the line $V(G)$. This implies that $h_2 = h_3 = 0$.

We have seen how to generate a basis $\mathbf{J} = [\mathbf{j}_1 \cdots \mathbf{j}_m]$ from m independent points $\mathbf{j}_s = \mathbf{G}\mathbf{h}_s$ of a group G and the construction of a subgroup in the form $J = \mathbf{j}_1 K_1 + \cdots + \mathbf{j}_m K_m$. The subgroup condition $\mathbf{j}_s K_s \subset G$ is that the last q entries of \mathbf{h}_s be zero when $K_s = \mathbb{R}$ (see (16.107)). When the basis is written in the form $\mathbf{J} = \mathbf{G}\mathbf{K}$, the above condition requires that some entries of the matrix \mathbf{K} be zero.

We illustrate this in the 3D case; starting from the grating $G = \mathbf{G}\mathbb{R}^2 \times \mathbb{Z}$, we suppose to generate three subgroups with the signatures (1) $\mathbb{K} = \mathbb{Z}^3$, (2) $\mathbb{K} = \mathbb{R} \times \mathbb{Z}^2$, and (3) $\mathbb{R}^2 \times \mathbb{Z}$. In the matrix \mathbf{K} we have the constraints

$$\mathbf{K} = [\mathbf{k}_1 \mathbf{k}_2 \mathbf{k}_3] = \begin{bmatrix} r_1 & r_2 & r_3 \\ s_1 & s_2 & s_3 \\ n_1 & n_2 & n_3 \end{bmatrix} \begin{array}{l} \text{real,} \\ \text{real,} \\ \text{integer.} \end{array}$$

In case (1), $J = \mathbf{j}_1\mathbb{Z} + \mathbf{j}_2\mathbb{Z} + \mathbf{j}_3\mathbb{Z}$, and we have no further constraints. In case (2), $J = \mathbf{j}_1\mathbb{R} + \mathbf{j}_2\mathbb{Z} + \mathbf{j}_3\mathbb{Z}$, and the constraints is on $\mathbf{j}_1 = \mathbf{G}\mathbf{k}_1$, where the last entry of \mathbf{k}_1 must be zero, that is, $n_1 = 0$. In case (3), $J = \mathbf{j}_1\mathbb{R} + \mathbf{j}_2\mathbb{R} + \mathbf{j}_3\mathbb{Z}$, and the constraint is on both $\mathbf{j}_1 = \mathbf{G}\mathbf{k}_1$ and $\mathbf{j}_3 = \mathbf{G}\mathbf{k}_3$, specifically, $n_1 = n_2 = 0$. In conclusion, for the matrix \mathbf{K} , we find in the three cases the constraints indicated in (16.37).

References

1. G. Cariolaro, Scanning theory with application to HDTV. Available at www.springer.com/978-0-85729-463-0
2. G. Cariolaro, E. Ruffa, Lattice operations with Mathematica. Available at www.springer.com/978-0-85729-463-0
3. J.W.S. Cassels, *An Introduction to the Geometry of Numbers* (Springer, Berlin, 1959)
4. T. Chen, P.P. Vaidyanathan, The role of integer matrices in multidimensional multirate systems. *IEEE Trans. Signal Process.* **SP-41**, 1035–1047 (1993)
5. E. Dubois, The sampling and reconstruction of time-varying imagery with application in video systems. *Proc. IEEE* **73**, 502–523 (1985)
6. F.R. Gantmacher, *The Theory of Matrices*, vol. 1 (Chelsea, New York, 1977)
7. T. Kailath, *Linear Systems* (Prentice Hall, Englewood Cliffs, 1980)
8. C.C. MacDuffee, *The Theory of Matrices* (Chelsea, New York, 1946)
9. R.M. Mersereau, D.E. Dudgeon, The representation of two-dimensional sequences as one-dimensional sequence. *IEEE Trans. Acoust. Speech Signal Process.* **ASSP-22**, 320–325 (1974)
10. P. Mertz, F. Gray, A theory of scanning and its relation to the characteristics of the transmitted signal in telephotography and television. *Bell Syst. Tech. J.* **13**, 464–515 (1934)
11. G.J. Tonge, The television scanning process. *SMPTE J.* **93**, 657–666 (1984)

Chapter 17

Study of Images

Organization of the Chapter The first topic is a preamble on still images with the introduction of some fundamental concepts as framing, aspect ratio, and the special units of measure used in image processing, as “width,” cycle per width (cpw), and so on. Then we consider the operations of scanning and reproduction, both for still images and for time-varying images. In this part the theory *dimensionality changes* of a signal developed in the previous chapter is applied, specifically, the dimensionality reduction in scanning and the dimensionality increase in reproduction.

In the final part of the chapter the reconstruction of an image from its projections is developed. The main goal is the correct formulation of signals and transforms involved in this topic, but also a few examples of applications are considered.

17.1 Introduction to Still Images

17.1.1 Image Framing

If a still image is considered as the projection of a 3D image on a plane, i.e., a spatially unbounded domain, the source image $\ell(x, y)$ results in a 2D signal redefined on \mathbb{R}^2 . However, a photograph or a document is typically limited to a rectangle or *field* (Fig. 17.1)

$$Q = [0, D_x] \times [0, D_y]. \tag{17.1}$$

Therefore it is appropriate to consider the 2D signal

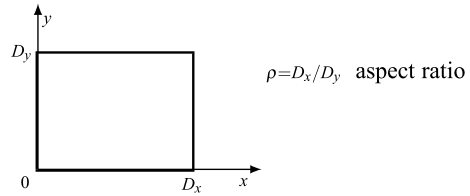
$$\ell_Q(x, y) = \ell(x, y), \quad (x, y) \in Q, \tag{17.2}$$

extending over Q . Operation (17.2) will be called *framing*.

The width-to-height ratio of a field Q

$$\rho = D_x/D_y \tag{17.3}$$

Fig. 17.1 Natural domain of a still image



is called *aspect ratio* and is typically greater than one. Customarily, at least in the study of images, the absolute dimensions of coordinates x and y (to be expressed in meters) of an image point are not as much as interesting as its *relative dimensions* with respect to the height and width of Q . The unit measurements therefore are

“height” (h) and “width” (w).

For instance, $0.25 h$ corresponds to a vertical dimension of one fourth the field’s height, and $0.5 w$ to a horizontal dimension of half the field’s width. Absolute and relative units can be converted by means of aspect ratio ρ and either D_x or D_y .

17.1.2 Concept of Spatial Frequencies

The customary interpretation of *frequency* is related to a time-varying signal, and, in fact, its amount is commonly expressed in “hertz” or “cycles per second” (cps). For a still image, which is a spatially varying signal, *spatial frequencies* are considered.

In order to get acquainted with these concepts, consider a luminance signal of sinusoidal type in both spatial dimensions

$$\ell(x, y) = L \sin(2\pi f_x x + 2\pi f_y y) + L, \quad (17.4)$$

where the term L is added because luminance signals cannot be negative. The range of (17.4) therefore goes from 0 (black) to $2L$ (white). If the vertical coordinate y was in meters, the frequency f_y ought to be in cycles per meter. Instead, if y is expressed as a fraction of height, f_y is expressed in cycles per height (cph). Similarly f_x is expressed in cycles per width (cpw). Figure 17.2 shows schematically the 2D signal (17.4) for different values of spatial frequencies f_x and f_y (for the sake of simplicity, the values greater than L are represented as white, and those smaller than L as black). At $f_x = 0$ one obtains horizontal white and black bars alternating, and their number depends on f_y : at $f_y = 1$, cpw one has exactly a pair of bars, at $f_y = 3$, cpw three pairs of bars, and so on. Similarly, at $f_y = 0$, one obtains pairs of vertical bars, as shown in Fig 17.2. Finally, f_x and f_y both positive give tilted bars.

It is worth noting that (17.4) cannot give a checkerboard image, which instead can be obtained from a factorizable signal

$$\ell(x, y) = L \sin(2\pi f_x x) \sin(2\pi f_y y) + L, \quad (17.5)$$

Fig. 17.2 Luminance bars produced by a 2d sinusoidal signal

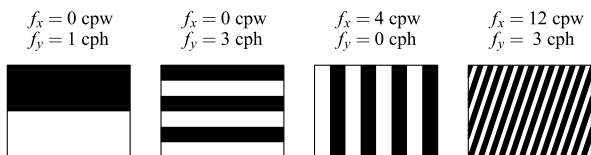


Fig. 17.3 Checkerboard luminance produced by a factorable sinusoidal signal

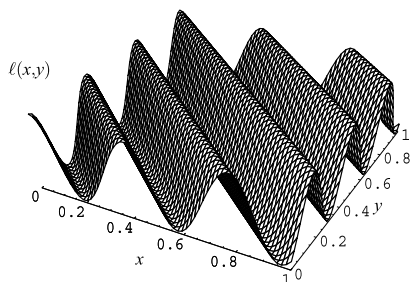
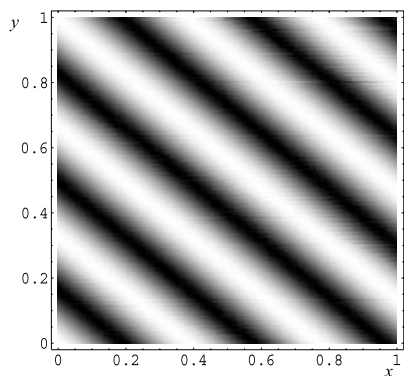
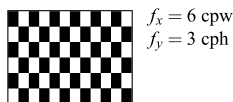


Fig. 17.4 Sinusoidal greyscale luminance with corresponding signal obtained with $f_x = 2.6$ cpw and $f_y = 3$ cph

as Fig. 17.3 shows.

In the above figure, for simplicity, the gray levels are limited to black and white (which corresponds to a square wave signal instead of a sinusoid). Figure 17.4 shows a true sinusoidal luminance and the corresponding signal $\ell(x, y)$.

17.1.3 Choice of the Domain

The rectangle $Q = [0, D_x) \times [0, D_y)$, naturally considered as a domain for still images, is a subset of \mathbb{R}^2 which is not a group. In order to correctly comply with Signal Theory, the definition of $\ell(x, y)$ must be extended on a group. Note that in order to define $\ell(x, y)$ on the smallest group of \mathbb{R}^2 including Q , one has to define the value of $\ell(x, y)$ outside Q . This operation can be accomplished in infinitely many ways. This issue is typically neglected, and many authors, without explicitly stating it, complete the definition of the image signal by setting it *equal to 0 outside Q* . By

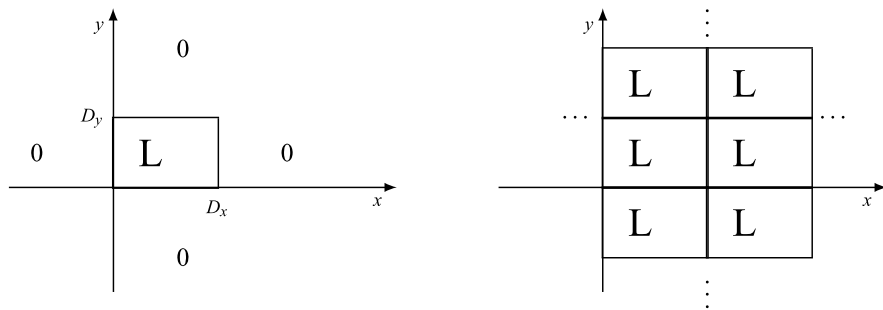


Fig. 17.5 Ordinary domain (\mathbb{R}^2) and quotient domain ($\mathbb{R}^2/\mathbb{Z}(D_x, D_y)$) of a still image

referring to the source signal, a still image can therefore be defined as (Fig. 17.5)

$$\ell_Q(x, y) = w_Q(x, y)\ell(x, y) = \begin{cases} \ell(x, y), & (x, y) \in Q, \\ 0 & \text{elsewhere,} \end{cases} \quad (17.6)$$

where w_Q is the field's indicator function.

An alternative choice is the *extension by periodicity* of $\ell(x, y)$ outside Q (Fig. 17.5), which gives the signal

$$\ell_p(x, y) = \sum_{m=-\infty}^{+\infty} \sum_{n=-\infty}^{+\infty} \ell_Q(x - mD_x, y - nD_y), \quad (17.7)$$

with periodicity $\mathbb{Z}(D_x, D_y)$, which can therefore be defined on the quotient group $\mathbb{R}^2/\mathbb{Z}(D_x, D_y)$. In this way the original field Q is a cell of \mathbb{R}^2 modulo $\mathbb{Z}(D_x, D_y)$. The periodic extension, even though it is less straightforward, comes at some advantages in frequency domain analysis.

17.2 Scanning of Still Images

The transmission or the storage of a framed image $\ell_Q(x, y)$ requires its conversion to a 1D signal $u(t)$, which we call hereafter the *video signal*. This is accomplished by going through the image along an appropriate path and by taking from every path point a signal proportional to the luminance. This process is called *scanning*.

17.2.1 Continuous Scanning

The simplest way of scanning consists in partitioning the field into a sufficient number of *lines* N (so that the desired resolution may be kept) and then subsequently

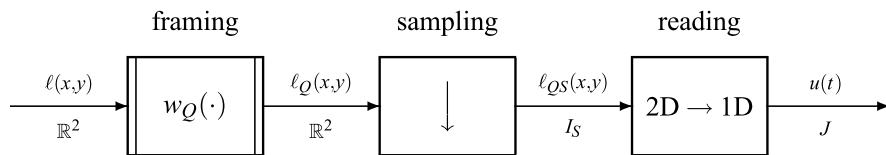


Fig. 17.6 Operations in 2D image scanning

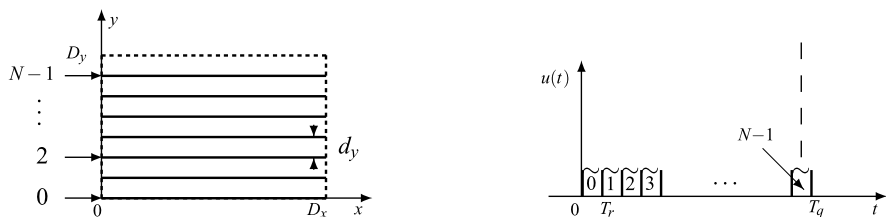


Fig. 17.7 Subdivision of the field into lines and resulting signal from reading

“reading” these lines, for instance, from left to right and from bottom up, in order to explore the whole field.

The scanning task may be conceptually subdivided into the following operations, modeled as in Fig. 17.6:

- (1) *framing* of the source image $\ell(x, y)$ into a *framed image*

$$\ell_Q(x, y) = w_Q(x, y)\ell(x, y), \quad (x, y) \in \mathbb{R}^2.$$

- (2) *grating operation*, i.e., the subdivision of the field into N equally spaced lines, which, therefore, have a distance $d_y = D_y/N$ from each other (Fig. 17.7). This operation may be seen as a vertical sampling by which the image domain is reduced from \mathbb{R}^2 to the grating $\mathbb{R} \times \mathbb{Z}(d_y)$ according to

$$\ell_{QS}(x, nd_y) = \ell_Q(x, nd_y), \quad (x, nd_y) \in \mathbb{R} \times \mathbb{Z}(d_y). \quad (17.8)$$

- (3) *Reading* of the lines at a constant velocity $v_x = D_x/T_r$ (w/s), where T_r is the line period. If the scanning process begins at $t = 0$, the x coordinate is given by $x = v_x t$ with $0 \leq t < T_r$ for line 0, $x = v_x(t - T_r)$, with $T_r \leq t < 2T_r$ for line 1, and in general for the n th line, by

$$x = v_x(t - nT_r), \quad nT_r \leq t < (n + 1)T_r. \quad (17.9)$$

In this way the n th line gives the contribution

$$\ell_{QS}(v_x(t - nT_r), nd_y), \quad nT_r \leq t < (n + 1)T_r, \quad (17.9b)$$

and the 1D signal, obtained from the line by line contribution, can be written as

$$u(t) = \sum_{n=0}^{N-1} \ell_{QS}(v_x(t - nT_r), nd_y). \quad (17.10)$$

The duration of this signal is one field period $T_q = NT_r$. For instance, if one wants to transmit an image in one minute ($T_q = 60$ s) with $N = 1000$ scanning lines, the line period is $T_r = 60$ ms, and $v_x = 1000/60 = 16.67$ w/s is the reading velocity, corresponding to 16.67 width per second. The sampling frequency is

$$F_y = 1/d_y = N/D_y$$

and corresponds to the *number of lines per height*. It is interesting to observe the meaning of this frequency with respect to the signal examples previously considered. Spatial frequencies f_x and f_y do not have any intrinsic limitation on \mathbb{R}^2 , and one may consider an infinite number of bars, both horizontally and vertically. After the vertical sampling with $F_y = N$ lines per height, evidently the number of bars, given by $2f_y$, cannot be greater than the number of lines. Therefore one has to fulfill the condition $2f_y \leq F_y$, which may be seen as the correct sampling condition. Indeed, as will be clearer in the following, the alias-free condition guaranteeing that one can correctly reproduce the image from its grating version is $F_y \geq 2B_y$, where B_y is the vertical bandwidth of the image (in cph).

17.2.2 Discrete Scanning on a Separable Lattice

The discrete scanning is similar to the continuous scanning with grating operation replaced by a *latticed operation*

$$\ell_{SQ}(md_x, nd_y) = \ell_Q(md_x, nd_y), \quad (md_x, nd_y) \in \mathbb{Z}(d_x, d_y). \quad (17.11)$$

The “latticed operation” is both horizontal and vertical, which leads to a finite number of image elements (pixels). Therefore, it is a sampling procedure along both spatial coordinates, with sampling periods

$$d_y = D_y/N, \quad d_x = D_x/M, \quad (17.12)$$

where N is the *number of lines per field*, and M the number of columns, or better, the *number of pixels per line* (Fig. 17.8).

The sampling frequencies are

$$F_y = 1/d_y = N/D_y, \quad F_x = 1/d_x = M/D_x,$$

and their product $N_Q = F_y F_x = NM/D_x D_y$ is the *number of points per field*. Note that N_Q is the reciprocal of the determinant of lattice $\mathbb{Z}(d_x, d_y)$, that is, the *density* of the lattice (see Sect. 3.3).

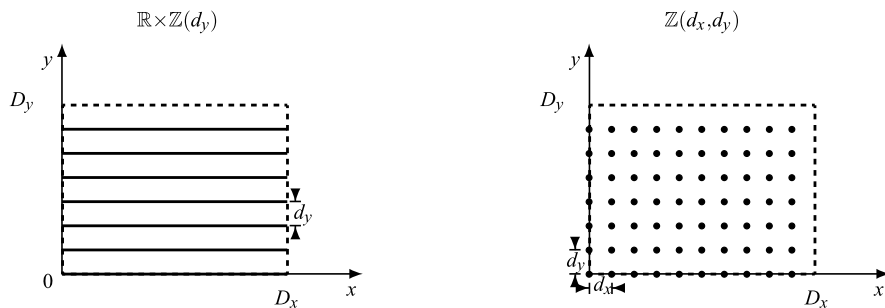


Fig. 17.8 Domains for an image: grating domain and latticed domain

The latticed image reading can be expressed as in the continuous case, with the only difference that now time is discrete. Therefore, (17.10) may be replaced by

$$u(mT_0) = \sum_{n=0}^{N-1} \ell_{QS}(v_x(mT_0 - nT_r), nd_y) \tag{17.13}$$

with T_0 the *pixel time* defined by $T_0 = d_x/v_x = T_r/M$.

Remark A discrete scanning can be obtained, in alternative, by sampling the 1D signal produced by continuous scanning. In both cases the same discrete-time video signal $u_e(t)$, $t \in \mathbb{Z}(T_e)$, is produced. Both interpretations, the one with a 2D latticed sampling and the one with a final 1D sampling, have practical significance and theoretical interest. The first interpretation, however, is the most interesting one because the sampling operation is directly related to the image.

17.2.3 Discrete Scanning on an Arbitrary Lattice

In the above discrete scanning the scanning lattice has the simple separable form $I_S = \mathbb{Z}(d_x, d_y)$. In general, the scanning lattice may be an arbitrary sublattice of $\mathbb{Z}(d_x, d_y)$, that is, with the form

$$I_S = \mathbb{Z}_a^p(d_x, d_y), \tag{17.14}$$

where a and p are naturals with $1 \leq p < a$ (Fig. 17.9). This opportunity can be used to reduce the number of pixels by a factor a ; in fact, a has the meaning of the density reduction of lattice (17.14) with respect to the “full” lattice $\mathbb{Z}(d_x, d_y)$. The choice of the sublattice must be done in dependence of the spectral extension of the image, as discussed in the next section.

For the formulation of this general scanning, it is convenient to introduce a *sub-sampling* of the video signal obtained with the full discrete scanning and going back

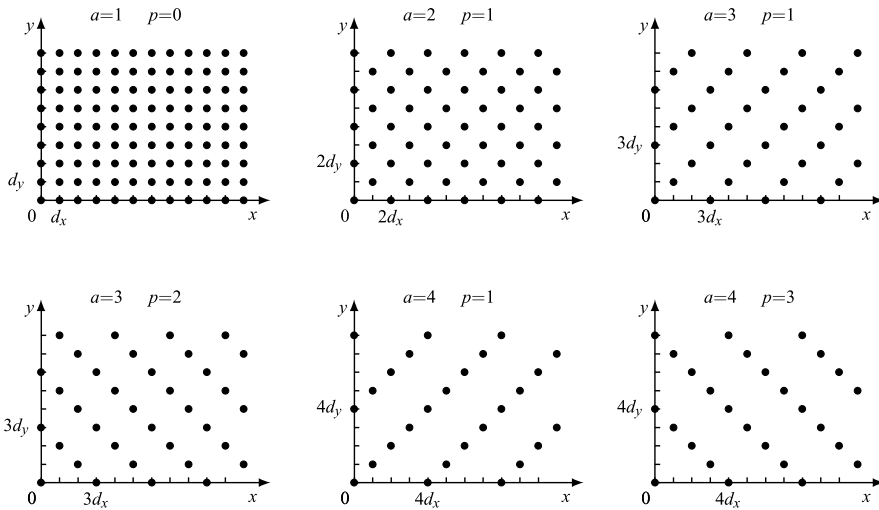


Fig. 17.9 Examples of sublattices $\mathbb{Z}_a^p(d_x, d_y)$ of $\mathbb{Z}(d_x, d_y)$ for discrete scanning

to see the corresponding subsampling of the image. Specifically, in place of $u(mT_0)$ we consider $u(maT_0)$. Then expression (17.13) of the video signal becomes

$$u(maT_0) = \sum_{n=0}^{N-1} \ell_{QS}(v_x(maT_0 - nT_r), nd_y). \tag{17.15}$$

Now, considering that $v_x T_0 = d_x$ and $v_x T_r = M d_x$, we see that the image is picked up at the points $(x, y) = (mad_x - nM d_x, nd_y)$, which belong to the lattice I_S with basis

$$\mathbf{I}_S = \begin{bmatrix} d_x & 0 \\ 0 & d_y \end{bmatrix} \begin{bmatrix} a & -M \\ 0 & 1 \end{bmatrix}.$$

In order to get the canonical upper-triangular basis of this lattice, it is sufficient to replace $-M$ with the remainder of the integer division $-M/a$, symbolized $\mu_a(-M)$. Thus, we recognize that the lattice has the form (17.14) with

$$p = \mu_a(-M) = \text{remainder of } -M/a. \tag{17.16}$$

Hence, the scanning lattice turns out to be determined by the reduction factor a and the “nominal” number of pixels per line (“nominal” refers to full scanning). For instance, if we choose $a = 4$ and M around 800, we find

$$\begin{aligned} M = 800, & \quad p = 0, & \quad I_S = \mathbb{Z}_4^0(d_x, d_y) = \mathbb{Z}(4d_x, d_y): \text{ separable}; \\ M = 801, & \quad p = 3, & \quad I_S = \mathbb{Z}_4^3(d_x, d_y); \\ M = 802, & \quad p = 2, & \quad I_S = \mathbb{Z}_4^2(d_x, d_y) = \mathbb{Z}_2^1(2d_x, 2d_y): \text{ quincunx}; \\ M = 803, & \quad p = 1, & \quad I_S = \mathbb{Z}_4^1(d_x, d_y). \end{aligned}$$

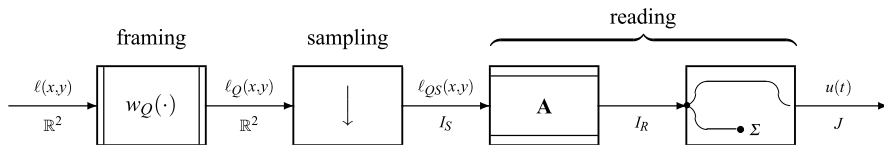


Fig. 17.10 Model of 2D image scanning with 2D→1D conversion expanded according to the theory of dimensionality reduction

17.2.4 General Expression of a Video Signal

We obtained the video signal for the continuous scanning, (17.10), for the “full” discrete scanning, (17.13), and for the general discrete scanning, (17.15). To get a unique expression, it is sufficient to denote by $t \in J$ the video signal argument in all cases, with $J = \mathbb{R}$, $J = \mathbb{Z}(T_0)$, or $J = \mathbb{Z}(aT_0)$ in dependence of the scanning format. Moreover, in all cases the finite summation can be replaced by an infinite summation, since, after frame limitation, this replacement does not add new contributions. Hence,

$$u(t) = \sum_{n=-\infty}^{+\infty} \ell_{QS}(v_x(t - nT_r), nd_y), \quad t \in J. \tag{17.17}$$

17.2.5 Application of the Theory of Dimensionality Reduction

In the previous subsection we have obtained the 2D→1D conversion of a still image to a 1D video signal. We now reformulate this conversion using the theory of dimensionality change developed in Sect. 16.10 of the previous chapter. To this end, we refine the scanning model of Fig. 17.6 as in Fig. 17.10, where the *reading operation* is decomposed into a coordinate change with matrix **A** (called *composite shift matrix*) and a 2D→1D sum reduction.

Now, we show that the unified expression of the video signal given by (17.17) can be obtained as a *reading* with matrix

$$\mathbf{A} = \begin{bmatrix} v_x & -v_x/v_y \\ 0 & 1 \end{bmatrix} \xrightarrow{\star} \mathbf{A}^\star = \begin{bmatrix} 1/v_x & 0 \\ 1/v_y & 1 \end{bmatrix}, \tag{17.18}$$

where $v_y = d_y/T_r$ is the *average vertical scanning velocity* (the *reciprocal matrix* \mathbf{A}^\star , given by the transpose inverse of **A**, will be used later on). To show this, we apply the general theory of Sect. 16.10 with $p + q = 2$, $p = 1$, and with the following domain correspondence:

$$I \rightarrow I_S = \begin{cases} \mathbb{R} \times \mathbb{Z}(d_y) & \text{for continuous scanning,} \\ \mathbb{Z}_i^b(d_x, d_y) & \text{for discrete scanning,} \end{cases}$$

$$U \rightarrow J = \begin{cases} \mathbb{R} & \text{for continuous scanning,} \\ \mathbb{Z}(T_0) & \text{for discrete scanning,} \end{cases}$$

$$V \rightarrow \mathbb{Z}(d_y),$$

and with the following signal correspondence:

$$x(\mathbf{u}, \mathbf{v}) \rightarrow \ell_{QS}(x, y), \quad x_0(\mathbf{u}, \mathbf{v}) \rightarrow \ell_{QSR}(x, y), \quad y(\mathbf{u}) \rightarrow u(t).$$

Now, the coordinate change applied to the framed-sampled image $\ell_{QS}(\cdot)$ gives the shifted image

$$\begin{aligned} \ell_{QSR}(t, nd_y) &= \ell_{QS}(\mathbf{A}(t, nd_y)) = \ell_{QS}(v_x t - (v_x/v_y)nd_y, nd_y) \\ &= \ell_{QS}(v_x(t - nT_r), nd_y), \quad (t, nd_y) \in J \times \mathbb{Z}(d_y). \end{aligned} \quad (17.19)$$

Next, the sum reduction gives the video signal $u(t)$,

$$u(t) = \sum_{n=-\infty}^{+\infty} \ell_{QSR}(t, nd_y) = \sum_{n=-\infty}^{+\infty} \ell_{QS}(v_x(t - nT_r), nd_y),$$

which is exactly as in (17.17).

For the invertibility of the scanning process with the possibility of the image recovery from the video signal (by a reproduction process), we have to check the *disjoint projection* condition (see Theorem 16.9). Here we limit ourselves to checking that the reading group I_R is separable, as required by the scanning model (where it is given by $U \times V$). In the continuous scanning, $I_R = I_S = \mathbb{R} \times \mathbb{Z}(d_y)$ is separable and then no condition is required. In the discrete scanning I_R is given by

$$I_R = \mathbf{A}^{-1} \mathbb{Z}_a^p(d_x, d_y),$$

where (see (17.18))

$$\mathbf{A}^{-1} = \begin{bmatrix} 1/v_x & 1/v_y \\ 0 & 1 \end{bmatrix} = \begin{bmatrix} T_0/d_x & MT_0/d_y \\ 0 & 1 \end{bmatrix}.$$

Then, the basis of I_R is

$$\mathbf{I}_R = \mathbf{A}^{-1} \mathbf{I}_S = \mathbf{A}^{-1} \begin{bmatrix} d_x & 0 \\ 0 & d_y \end{bmatrix} \begin{bmatrix} a & p \\ 0 & 1 \end{bmatrix} = \begin{bmatrix} T_0 & 0 \\ 0 & d_y \end{bmatrix} \begin{bmatrix} a & p + M \\ 0 & 1 \end{bmatrix},$$

and the separability condition is $p + M$ multiple of a , so that the lattice I_R becomes separable as $\mathbb{Z}(aT_0) \times \mathbb{Z}(d_y)$.

This condition is equivalent to the condition $p = \mu_a(-M)$ given by (17.16) and obtained with other considerations and is in agreement with the general theory of the discrete $2D \rightarrow 1D$ reading developed in Sect. 16.11 (see Proposition 16.14).

17.2.6 Fourier Analysis of 2D Scanning

We now evaluate the Fourier transforms of the signals involved in still image scanning. To this end, we follow the scanning model of Fig. 17.10, which consists of “simple operations,” and therefore its analysis will be immediate.

The FT of source image $\ell(x, y)$, $(x, y) \in \mathbb{R}^2$, is a 2D complex function $L(f_x, f_y)$, $(f_x, f_y) \in \mathbb{R}^2$, where the frequencies have dimensions of cycles per width (cpw) and cycles per height (cph), respectively. The relationships are

$$L(f_x, f_y) = \int_{\mathbb{R}^2} dx dy \ell(x, y) e^{-i2\pi(f_x x + f_y y)}, \quad (f_x, f_y) \in \mathbb{R}^2, \quad (17.20a)$$

$$\ell(x, y) = \int_{\mathbb{R}^2} df_x df_y L(f_x, f_y) e^{i2\pi(f_x x + f_y y)}, \quad (x, y) \in \mathbb{R}^2. \quad (17.20b)$$

Framing and Sampling The framing is expressed as $\ell_Q(x, y) = w_Q(x, y)\ell(x, y)$, $(x, y) \in \mathbb{R}^2$, which becomes a 2D convolution in the frequency domain (see Problem 17.1).

The sampling of the framed image $\ell_Q(x, y)$ can be written in the form

$$\ell_{QS}(x, y) = \ell_Q(x, y), \quad (x, y) \in I_S, \quad (17.21)$$

where I_S is the *scanning group*. Thus, we have an $\mathbb{R}^2 \rightarrow I_S$ down-sampling, which becomes an $\mathbb{R}^2 \rightarrow \mathbb{R}^2/I_S^*$ periodic repetition in the frequency domain with relation

$$L_{QS}(f_x, f_y) = \sum_{(p_x, p_y) \in I_S^*} L_Q(f_x - p_x, f_y - p_y), \quad (f_x, f_y) \in \mathbb{R}^2/I_S^*, \quad (17.22)$$

where I_S^* is the reciprocal group, and (p_x, p_y) are the repetition centers. The above relations hold for all types of scanning. In order to get more explicit results, the specific forms of I_S and I_S^* must be introduced.

Coordinate Change and Sum Reduction In the frequency domain the coordinate change (17.19) becomes a coordinate change with matrix \mathbf{A}^* (see (17.18)) and a multiplication by $\mu(\mathbf{A}) = 1/v_x$:

$$L_{QSR}(f_x, f_y) = (1/v_x)L_{QS}(\mathbf{A}^*(f_x, f_y)) = (1/v_x)L_{QS}(f_x/v_x, f_x/v_x + f_y).$$

The sum reduction becomes a zero reduction followed by a multiplication by $\mu(\mathbb{Z}(d_y)) = 1/d_y$ and we finally obtain the FT of the video signal, namely

$$\boxed{U(f) = \frac{1}{v_x d_y} L_{QS}\left(\frac{f}{v_x}, \frac{f}{v_y}\right), \quad f \in \mathbb{R}/J^*,} \quad (17.23)$$

where $v_x = d_x/T_r$ is the horizontal velocity and $v_y = d_y/T_r$ is the *average* vertical velocity.

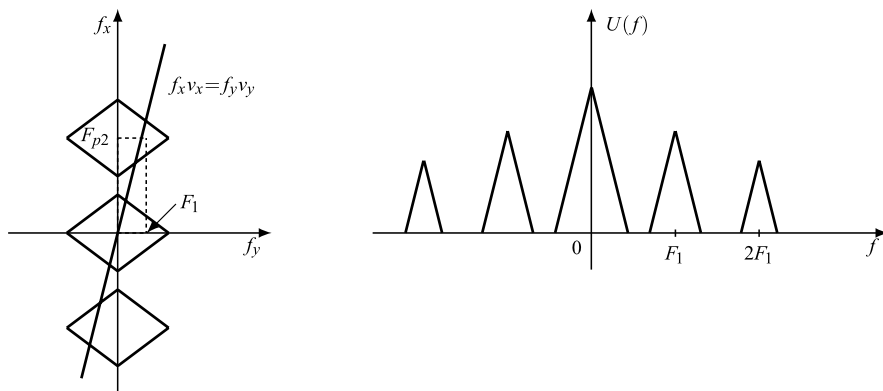


Fig. 17.11 Interpretation of Fourier analysis of reading operation (in the continuous scanning). On the *left*, the extension of $L_{QS}(f)$ and the line along which $L_{QS}(f)$ gives the values of $U(f)$. On the *right*, $U(f)$ (for convenience, we suppose that $L_{QS}(f_x, f_y)$ has a pyramidal shape)

Table 17.1 Parameters \bar{p} giving the reciprocal

a	2	3	3	4	5	5	5	5
p	1	1	2	2	1	2	3	4
\bar{p}	1	2	1	2	4	3	2	1

Note that relation (17.23) holds for the continuous scanning, where $U(f)$ is aperiodic ($J^* = \mathbb{O}$), and for discrete scanning, where $U(f)$ is periodic ($J^* = \mathbb{Z}(F_0)$, $F_0 = 1/T_0$), and also for the general discrete scanning, where $J^* = \mathbb{Z}(F_0/a)$.

The interpretation of (17.23) is shown in Fig. 17.11. Apart from a scale factor, the FT $U(f)$ of the video signal is obtained by “reading” the values of $L(f_x, f_y)$ along the line of the (f_x, f_y) plane with parametric equations $f_x = f/v_x$, $f_y = f/v_y$.

Particular Cases The above relationships on Fourier analysis hold for every type of 2D scanning, and now we give some details for the specific types of scanning. In the continuous scanning, I_S is the separable grating $I_S = \mathbb{R} \times \mathbb{Z}(d_y)$, and its reciprocal is therefore $I_S^* = \mathbb{O} \times \mathbb{Z}(dF_y)$, $F_y = 1/d_x$. Hence, in practice, (17.22) becomes a 1D periodic repetition along the vertical coordinate, and $L_{QS}(f_x, f_y)$ becomes periodic only with respect to vertical frequency f_y .

In the scanning on a general lattice $\mathbb{Z}_a^p(d_x, d_y)$ we have to evaluate the reciprocal lattice, as done in Sect. 5.9. In particular, if a and p are coprime, one finds

$$I_S = \mathbb{Z}_a^p(d_x, d_y) \xrightarrow{*} I_S^* = \mathbb{Z}_a^{\bar{p}}(F_x/a, F_y/a), \tag{17.24}$$

where for the first orders, \bar{p} takes the values listed in Table 17.1.

UT 17.3 Sampling and Reproduction of 2D Images

17.3.1 Sampling Theorem for Still Images

We discuss in detail the sampling of a still image with the possibility of reconstruction from its sample values. The Unified Sampling Theorem (see Sect. 8.5) gives the following:

Theorem 17.1 *A band-limited image $\ell_Q(x, y)$, $(x, y) \in \mathbb{R}^2$, can be $\mathbb{R}^2 \rightarrow I_S$ down-sampled and reconstructed from its sample values $\ell_{QS}(x, y)$, $(x, y) \in I_S$. The band-limitation condition is*

$$e(L_Q) \subset C_0, \quad (17.25)$$

where $e(L_Q)$ is the spectral extension of $\ell_Q(x, y)$, and C_0 is a cell of \mathbb{R}^2 modulo I_S^* . The reconstruction is provided by an $I_S \rightarrow \mathbb{R}^2$ interpolator with frequency response $G(f_x, f_y) = \eta_{C_0}(f_x, f_y)$, given by the indicator function of C_0 .

We limit the discussion to the sampling on a lattice.

17.3.2 Sampling on the Separable Lattice $\mathbb{Z}(d_x, d_y)$

The reference is the sampling on the separable lattice $I_S = \mathbb{Z}(d_x, d_y)$, which leads to the field subdivision into MN pixels, where

$$M = D_x/d_x, \quad N = D_y/d_y \quad (17.26)$$

are respectively the number of pixels per line and the number of lines per field. The reciprocal is $I_S^* = \mathbb{Z}(F_x, F_y)$ with $F_x = 1/d_x$, $F_y = 1/d_y$.

Since one assumes that D_x and D_y have unit values, i.e., that $D_x = 1$ w and $D_y = 1$ h, from (17.26) it follows that $F_x = M$, $F_y = N$, and the product $F_x F_y = MN = N_Q$ gives the number of pixels per field.

Now, if the luminance spectral extension is rectangular (Fig. 17.12), $e(L_Q) = [-B_x, B_x] \times [-B_y, B_y]$, assuming a rectangular cell $C_0 = [-\frac{1}{2}F_x, \frac{1}{2}F_x] \times [-\frac{1}{2}F_y, \frac{1}{2}F_y]$, the alias-free condition (17.25) imposes that

$$F_x \geq 2B_x, \quad F_y \geq 2B_y. \quad (17.27)$$

For instance, for $B_x = 500$ cpw and $B_y = 500$ cph, which corresponds to an excellent photographic resolution, it must be $F_x \geq 1000$ cpw and $F_y \geq 1000$ cph, leading to $N_Q = 1\,000\,000$ pixel/field.

However, if the spectral extension is not rectangular, but, for instance, rhomboidal (which is more likely with “real” images), condition (17.27) still guarantees alias-free if B_x and B_y are the highest vertical and horizontal frequencies of the

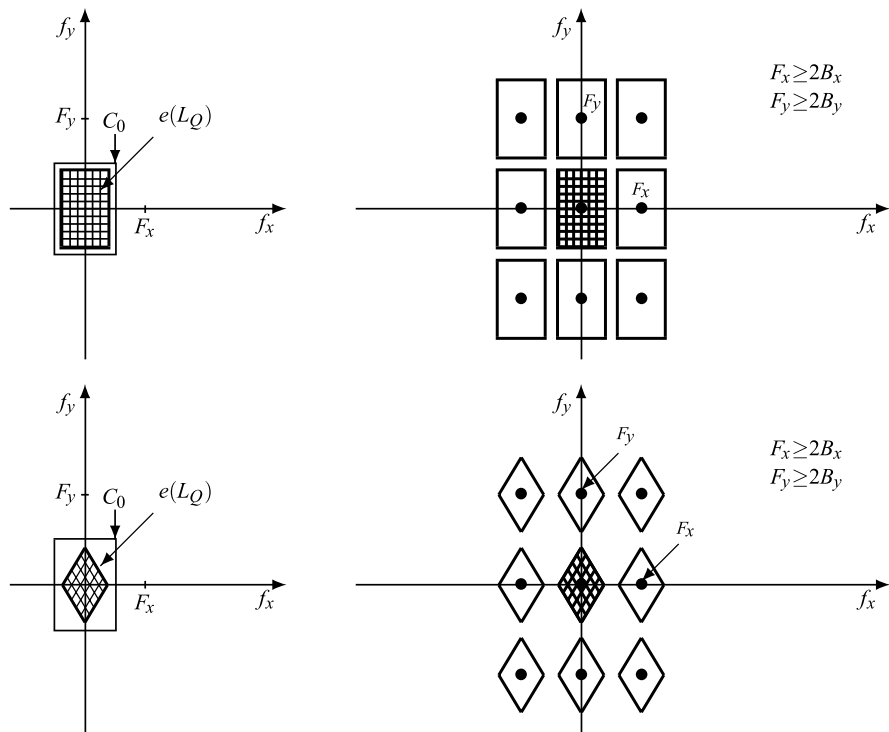


Fig. 17.12 Nonaliasing condition for an $\mathbb{R}^2 \rightarrow \mathbb{Z}(d_x, d_y)$ sampling with rectangular and rhomboidal spectral extensions

image. In this case sampling on a separable lattice is rather inefficient. Indeed, by considering sampling efficiency (see Sect. 8.6), $\eta = \text{meas } e(L_Q) / \text{meas } C_0$, separable sampling with a rhomboidal spectral extension can give at most a 50% sampling efficiency.

17.3.3 Sampling on Nonseparable Lattices

A separable lattice is only one possibility, and one can find more convenient lattices and appropriate reference cells. For instance, consider as scanning group the quincunx lattice $I_S = \mathbb{Z}_2^1(d_x, d_y)$, where d_x and d_y denote the same quantities as above, but the number of pixels per field N_Q is halved, since in this case it is $N_Q = \frac{1}{2}F_x F_y = \frac{1}{2}MN$. Considering that the reciprocal of a quincunx lattice is still a quincunx lattice and more precisely $I_S^* = \mathbb{Z}_2^1(\frac{1}{2}F_x, \frac{1}{2}F_y)$ with $F_x = 1/d_x$, $F_y = 1/d_y$, one can choose a better tailored cell C_0 for the alias-free condition in order to increase the sampling efficiency.

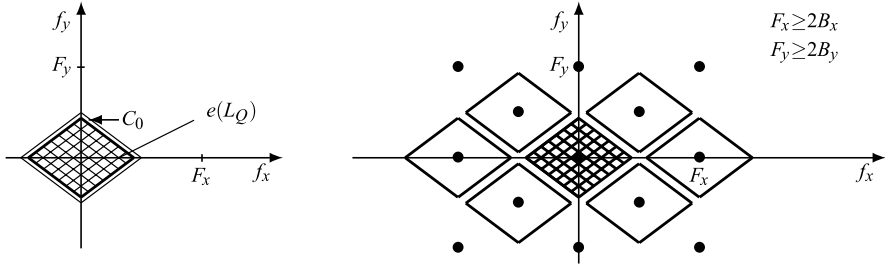


Fig. 17.13 Nonaliasing condition for an $\mathbb{R}^2 \rightarrow \mathbb{Z}_2^1(d_x, d_y)$ sampling with rhomboidal spectral extension and a rhomboidal cell

Figure 17.13 shows the alias-free condition with spectral supports of rhomboidal type. Now, a rhomboidal cell is feasible, and the alias-free condition is $F_x \geq 2B_x$, $F_y \geq 2B_y$, as with the separable lattice. In the case of the previous example, where $M = F_x = 1000$ cpw and $N = F_y = 1000$ cph, one finds that with a quincunx lattice operation one may still obtain resolutions $B_x = 500$ cpw and $B_y = 500$ cph with half the number of pixels per field.

This result applies to rhomboidal extensions, because in the case of rectangular extensions there is nothing to gain with a quincunx lattice. The important fact is that “real” spectral supports, in a first approximation, can be assumed to be rhomboidal, rather than rectangular. Therefore the quincunx lattice operation is certainly more efficient.

17.3.4 On the Variety of Cells

In general, starting from the reciprocal lattice I_S^* , one may find several centered parallelepipeds as alternative basis, and one may therefore generate in this way a series of cells. There are also other ways of obtaining the other types of cells relative to the same lattice as discussed in Sect. 16.9. Here we confine ourselves to a few examples showing the wide variety of possible cells.

Figure 17.14 shows (a) examples of cells relative to the lattice $I_S^* = \mathbb{Z}(F_x, F_y)$ and (b) relative to the lattice $I_S^* = \mathbb{Z}_2^1(\frac{1}{2}F_x, \frac{1}{2}F_y)$.

Note that the alias-free condition $B_x \leq \frac{1}{2}F_x$, $B_y \leq \frac{1}{2}F_y$ is not intrinsic to the lattice $\mathbb{Z}(F_x, F_y)$, because it implicitly refers to a rectangular cell. For instance, with parallelogram cell, the second of Fig. 17.14, the vertical resolution can also be greater than F_y , and with the third cell the horizontal resolution can also be greater than F_x .

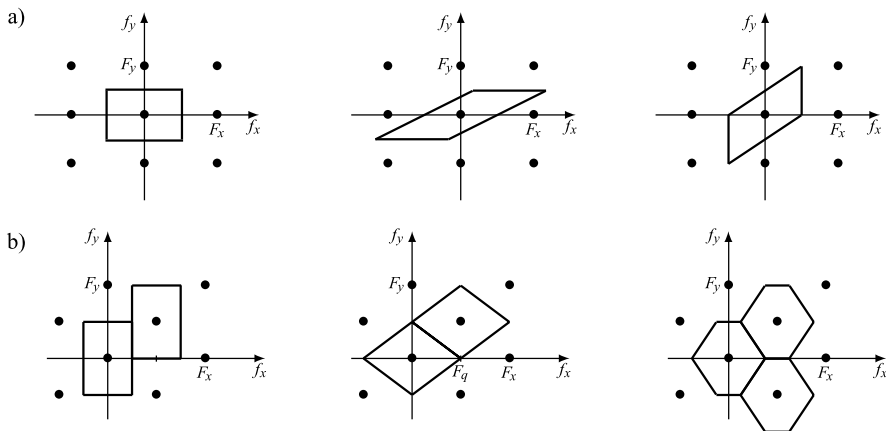


Fig. 17.14 Examples of symmetrical cells of \mathbb{R}^2 : (a) modulus $\mathbb{Z}(F_x, F_y)$ and (b) modulus $\mathbb{Z}_2^1(F_x, F_y)$

17.3.5 Image Reproduction

The decomposition of scanning into the two operations of “sampling” and “reading” leads to an obvious reconstruction procedure. Starting from the video signal $u(t)$, one needs to perform:

- (1) reconstruction of the “framed-sampled” image $\ell_{QS}(x, y)$,
- (2) interpolation of the sampled image.

We consider the reproduction in continuous scanning (in discrete scanning the reproduction can be obtained similarly). Since the contributions of the N lines forming $u(t)$ do not overlap, one obtains (from (17.10)) $\ell_{QS}(v_x(t - nT_r), nd_y) = u(t)$, where $nT_r \leq t < (n + 1)T_r$. Then, letting $x = v_x(t - nT_r)$, we get

$$\ell_{QS}(x, nd_y) = u(x/v_x + nT_r)w_r(x), \quad x \in \mathbb{R}, \tag{17.28}$$

where $w_r(x)$ is the indicator function of a line, $w_r(x) = \eta_{[0, D_x)}(x)$.

Since $u(t)$ is zero outside the field period, expression (17.28) holds everywhere on the grating image and may be written as

$$\ell_{QS}(x, y) = u(x/v_x + y/v_y)w_r(x), \quad (x, y) \in \mathbb{R} \times \mathbb{Z}(d_y), \tag{17.29}$$

where the parameter $v_y \triangleq d_y/T_r$ may be interpreted as the (perceived) vertical reading velocity.

From the “grating” image $\ell_{QS}(x, nd_y)$ one may obtain a continuous image by vertical interpolation. In the case of ideal interpolation, from the Sampling Theorem

one has

$$\ell_i(x, y) = \sum_{n=0}^{N-1} \ell_{QS}(x, nd_y) \operatorname{sinc}[(y - nd_y)/d_y], \quad (x, y) \in \mathbb{R}^2. \quad (17.30)$$

If the sampling frequency¹ satisfies $F_y \geq 2B_y$, there is the perfect image reproduction, i.e., $\ell_i(x, y) = \ell(x, y)$, $(x, y) \in \mathbb{R}^2$.

17.4 Scanning of Time-Varying Images

A time-varying image is a 3D signal, which we write in the form

$$\ell(x, y, t), \quad (x, y, t) \in \mathbb{R}^3, \quad (17.31)$$

where x , y , and t are the horizontal, vertical, and temporal coordinates, respectively. All three coordinates are continuous and unlimited, so that each takes a value from the set \mathbb{R} of real numbers. This signal may represent the luminance of the point (x, y) at time t , but is also suitable to represent the color or any other information of the image. In the frequency domain the image is represented by its FT $L(f_x, f_y, f_t)$, where the spatial frequencies f_x and f_y are expressed respectively in cpw and cph, as for still images, and the temporal frequency f_t in cycles per second (cps) or hertz.

One of the problems is the image conversion into a 1D signal for transmission or storage or, more generally, processing. Here we develop the conversion (scanning) with reference to television, which represents the most typical application. The topic is similar to the scanning of a still image, but more complex because the time variation of the image requires that the scanning operation be performed *in real time*.

As done for the still images, we introduce progressively the basic ideas with the usual tool of the Unified Theory, paying particular attention to the domains of signals, and finally we apply the theory of dimensionality changes (in this context $3D \rightarrow 1D$ and $1D \rightarrow 3D$). At first, it is convenient to summarize the symbolism of the (many) parameters introduced in the scanning formulation

Main Symbols Related to Scanning Process

- D_x : horizontal frame dimensionality
- D_y : vertical frame dimensionality
- N : number of lines per frame
- M : number of pixels per line (in full format)
- $d_y = D_y/N$: line separation (in full format)

¹Since framing is actually a source-image truncation, also in the vertical direction, the band cannot be limited in strict sense. Therefore, the parameter B_y can only correspond to a *conventional* band.

- id_y : line separation (in interlace format)
- $d_x = D_x/M$: pixel separation on a line (in the full format)
- ad_x : pixel separation in the general discrete scanning
- T_q : frame period
- i : interlace factor
- $T_f = T_q/i$: field period
- $T_r = T_q/N$: line period
- $T_0 = T_r/N$: pixel period (in full format)
- aT_0 : pixel period (in general discrete scanning)
- $v_x = D_x/T_r$: horizontal scanning velocity
- $v_y = id_y/T_r$: vertical scanning velocity
- $\mathbb{Z}_i^b(d_y, T_f)$: vertical-temporal lattice
- I_S : scanning group

17.4.1 Progressive Continuous Scanning

To begin, let us consider the simplest form of scanning process, according to the *progressive 1:1 format*, with the aim of illustrating the nature and variety of the operations involved. The source image is spatially unlimited, so that the first operation is to limit the image to the *frame* (Fig. 17.15), a rectangle $Q = [0, D_x) \times [0, D_y)$. The limited image is temporally sampled to capture pictures (or *fields*) every T_q seconds, and each field is divided into N equally spaced *lines* (vertical sampling). Finally, the lines of each field are sequentially read to pick up a signal proportional to the image luminance (or chrominance). Thus, the video signal consists of replicas of the image signal portions limited by the line-field format.

The relations are as follows. From the source image (17.31), the framing² is simply expressed as

$$\ell_Q(x, y, t) = w_Q(x, y)\ell(x, y, t), \quad (x, y, t) \in \mathbb{R}^3, \quad (17.32)$$

where $w_Q(x, y)$ is the indicator function of the frame Q . Hence, $\ell_Q(x, y, t)$ is set to zero outside the frame. The image domain after sampling, i.e., the subset of \mathbb{R}^3 consisting of the field-line format, is the 3D grating

$$I_S = \mathbb{R} \times \mathbb{Z}(d_y) \times \mathbb{Z}(T_q), \quad (17.33)$$

where $d_y = D_y/N$ is the vertical line spacing, and T_q is the frame period.

Hence, the down-sampling operation is given by

$$\boxed{\ell_{QS}(x, nd_y, kT_q) = \ell_Q(x, nd_y, kT_q), \quad (x, nd_y, kT_q) \in I_S,} \quad (17.34)$$

²The frame limitation is usually neglected in literature. Its introduction, however, is essential for a correct formulation of the scanning process.

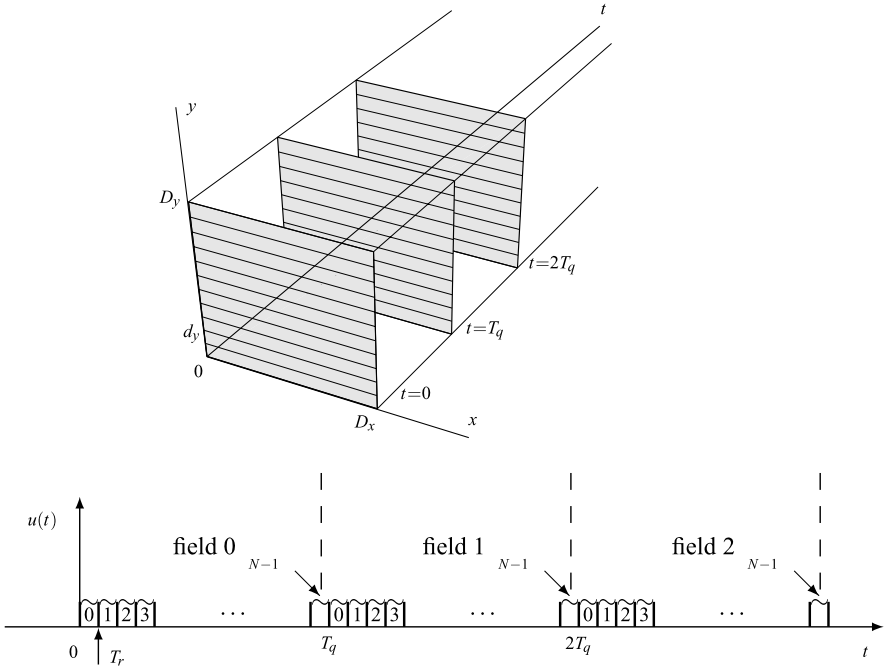


Fig. 17.15 The grating of progressive scanning (with memory) of a time-varying image and the corresponding video signal $u(t)$

and restricts the domain from \mathbb{R}^3 to I_S .

For the $3D \rightarrow 1D$ conversion we note that the framed image at a fixed frame instant kT_q may be regarded as a still image, given by $\ell_Q(x, y, kT_q)$. Then, we can apply the scanning process seen for the still image, and correspondingly we obtain a video signal contribution $u_k(t)$. The constraint is that the scanning must begin at kT_q and be completed before the next instant $(k + 1)T_q$. Hence, the extension of $u_k(t)$ must be limited to the interval $\mathcal{J}_k = [kT_q, (k + 1)T_q)$. In other words, the $3D \rightarrow 1D$ conversion is a *time-division* procedure, where a duration T_q is assigned to each frame.

Let us examine the scanning process in detail (Fig. 17.16). Let N be the number of lines per frame; then the line period and the reading velocity are respectively

$$T_r = T_q/N, \quad v_x = D_x/T_r. \tag{17.35}$$

For frame 0, the lines are read according to

$$x = v_x(t - nT_r), \quad nT_r < t < (n + 1)T_r.$$

For the subsequent frame, the reading is carried out in the same way but with a delay of T_q , and in general, for the frame k , the delay is kT_q . Therefore, the reading of line n of frame k starts at the time $t_{nk} \triangleq nT_r + kT_q, 0 \leq n \leq N, k \in \mathbb{Z}$; the *motion*

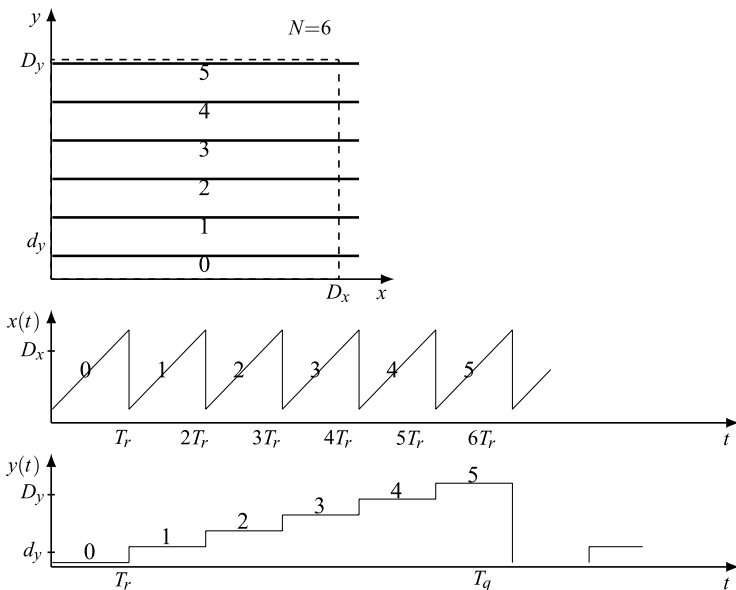


Fig. 17.16 Motion law in progressive scanning

law for such line is (see Fig 17.16)

$$\begin{cases} x(t) = v_x(t - t_{nk}), \\ y(t) = nd_y, \end{cases} \quad t \in [t_{nk}, t_{nk} + T_r) \triangleq \mathcal{J}_{nk}, \quad (17.36)$$

and yields the signal

$$u_{nk}(t) = \ell(v_x(t - t_{nk}), nd_y, kT_q), \quad t \in \mathcal{J}_{nk}. \quad (17.37)$$

This expression holds only in the interval \mathcal{J}_{nk} since, for $t \notin \mathcal{J}_{nk}$, the expression (17.37) picks up values outside the frame. To obtain a correct expression for every $t \in \mathbb{R}$, it is sufficient to replace the unlimited image $\ell(\cdot)$ with the framed image $\ell_{QS}(\cdot)$, that is,

$$u_{nk}(t) = \ell_{QS}(v_x(t - t_{nk}), nd_y, kT_q), \quad t \in \mathbb{R}. \quad (17.38)$$

This replacement ensures that the extension of $u_{nk}(t)$ is exactly \mathcal{J}_{nk} .

The complete video signal is given by the sum of all contributions $u_{nk}(t)$, that is,

$$u(t) = \sum_{n=0}^{N-1} \sum_{k=-\infty}^{+\infty} \ell_{QS}(v_x(t - t_{nk}), nd_y, kT_q), \quad t \in \mathbb{R}, \quad (17.39)$$

where t_{nk} are defined by (17.36).

From the above formulation we can make the following observations. The scanning operation involves different kinds of signals: the source image is a 3D signal

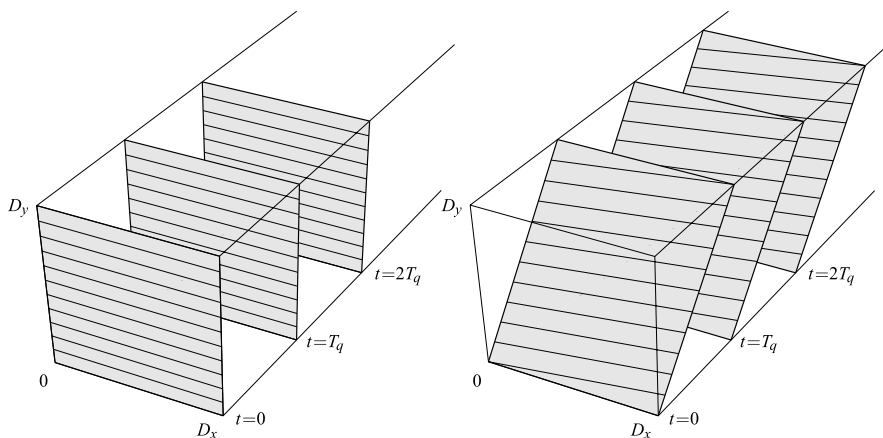


Fig. 17.17 Memory progressive scanning and *instantaneous* progressive scanning

defined on \mathbb{R}^3 and remains so after frame limitation, the sampled image is defined on the 3D *grating* I_S , given by (17.33), and the video signal is a continuous-time 1D signal defined on \mathbb{R} .

Finally, we note that the scanning model outlined above may be an approximation to the real scanning process performed by conventional cameras, since we have tacitly assumed that the image fields are taken at instants kT_q , $k \in \mathbb{Z}$, like film frames, and that the line scanning is performed on these fixed-time frames (Fig. 17.17). This model (*memory model*) implies image storage at field level. In conventional cameras, lines are not taken from a fixed-time frame since the image signal evolves during line scanning operations, so that we have to write $\ell(\cdot, \cdot, t)$ instead of $\ell(\cdot, \cdot, kT_q)$. Thus, we arrive at the *instantaneous model* (Fig. 17.17), where fields and lines are tilted with respect to the (x, y) plane, and the grating must be modified as

$$I_S = \{v_x(t - nT_r - kT_q), v_y(t - nT_r - kT_q) + nd_y, t \mid n, k \in \mathbb{Z}, t \in \mathbb{R}\}, \quad (17.40)$$

where v_x and v_y are the horizontal and vertical velocities, respectively.

Note, for comparison with (17.40), that the grating $I_S = \mathbb{R} \times \mathbb{Z}(d_x, d_y)$ of the memory model can be written in the form

$$I_S = \{v_x(t - nT_r - kT_q), nd_y, kT_q \mid n, k \in \mathbb{Z}, t \in \mathbb{R}\}. \quad (17.40a)$$

Modern cameras based on CCD devices operate according to the memory model, and for this reason, and also for simplicity, hereafter we will refer to the memory model, where the scanning group is

$$I_S = \mathbb{R} \times \mathbb{Z}(d_y) \times \mathbb{Z}(T_q)$$

or a subgroup of this. For the development of the instantaneous model, compared to the memory model, see [5].

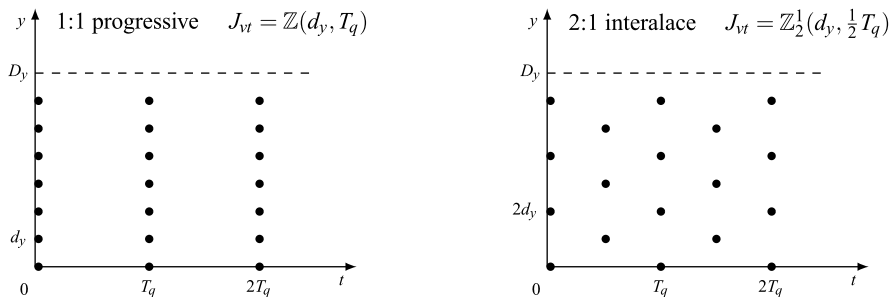


Fig. 17.18 Comparison of progressive and interlace scanning on the (y, t) plane, showing the corresponding vertico-temporal lattices

17.4.2 Interlace Scanning

In the progressive 1:1 format all the lines of each frame are picked up. An alternative is the *interlace 2:1 format* in which only *even* lines of *even* frames and *odd* lines of *odd* frames are picked up. The comparison of the two formats is illustrated in Fig. 17.18, where the line projections on the (y, t) plane are shown. In progressive format these projections give the separable lattice $\mathbb{Z}(d_y, T_q)$, whereas in interlace 2:1 format they give the quincunx lattice $\mathbb{Z}_2^1(d_y, \frac{1}{2}T_q)$, and consequently the scanning group becomes the nonseparable grating

$$I_S = \mathbb{R} \times \mathbb{Z}_2^1\left(d_y, \frac{1}{2}T_q\right).$$

The use of interlace scanning is mainly due to the fact that the corresponding sampling may be more efficient, as seen for still images in Sect. 17.3. However, it has also a historical reason due to technological limits at the beginning of the TV era. In fact, most common standards use the interlace 2:1 format. Table 17.2 collects the scanning parameters of the numerical conversion of NTSC and PAL analog systems and also the standards proposed for the high-definition television (HDTV) and for the ultra high-definition television (UHDTV). Note in UHDTV the progressive format, which nowadays is preferred to the interlace format.

17.4.3 Higher Order Interlace. Frames and Fields

It is possible to perform the scanning with a higher-order interlace in which the nominal number of lines per frames is shared by three or more consecutive fields. The vertico-temporal lattice, which gives the line projections onto the (y, t) plane, is given in general by $\mathbb{Z}_i^b(d_y, T_q)$. Then, the scanning grating becomes

$$I_S = \mathbb{R} \times \mathbb{Z}_i^b(d_y, T_f), \tag{17.41a}$$

Table 17.2 Scanning parameters of two historical TV standards and of two new standards

Standard	PAL	NTSC	HDTV	UHDTV
Number of lines N	625 (576)	525 (486)	1080	7680
Aspect ratio ρ	$\frac{4}{3}$	$\frac{4}{3}$	$\frac{16}{9}$	$\frac{16}{9}$
Interlace	2:1	2:1	2:1	1:1
Frame frequency F_q	25	30	25	60
Line frequency F_r	15 625	15 750	27 000	460 800
Pixel frequency F_e	12.0×10^6	10.2×10^6	51.8×10^6	1990×10^6
Pixel period T_e [ns]	83.43	97.98	19.29	0.50
Number of pixels per line	766.67	648.00	1 920	4 320
Number of pixels per frame	441 602	340 200	2 073 600	33 177 600
Number of bits per pixel	16	16	24	30
Nominal rate R_n [Mb/s]	176.41	163.30	1 244.16	59 719.68

and the corresponding basis can be written in the form

$$\mathbf{I}_S = \begin{bmatrix} D_x & 0 & 0 \\ 0 & d_y & 0 \\ 0 & 0 & T_f \end{bmatrix} \begin{bmatrix} 1 & 0 & 0 \\ 0 & i & b \\ 0 & 0 & 1 \end{bmatrix}, \quad H_S = \mathbb{R} \times \mathbb{Z}^2. \quad (17.41b)$$

The index i is the interlace order and represents the reduction of the line density with respect to the full format $\mathbf{M}(1:1)$. For instance, with $i = 4$, the nominal number of lines $N = 14$ is subdivided into 4 fields, with $N/4$ lines per fields in the average, as shown in Fig. 17.19 below (we choose a small value of N for illustrations). We denote by $\mathbf{M}(1:1)$, $\mathbf{M}(2:1)$, and in general by $\mathbf{M}(i:1/b)$ the scanning format determined by the scanning group (17.41a), (17.41b), where \mathbf{M} stands for *memory* model.

To find the field format, we write the generic point of the scanning grating, given by (see (17.41b))

$$x = r, \quad y = nid_y, \quad t = kT_f, \quad r \in \mathbb{R}, n, k \in \mathbb{Z}.$$

Then, the k th field, that is, the projection of I_S onto the (x, y) plane obtained with k fixed, is given by

$$C_k = \{(r, nid_y + kbd_y) \mid r \in \mathbb{R}, n \in \mathbb{Z}\}.$$

In particular, the *zereth* field is $C_0 = \{(r, nid_y) \mid r \in \mathbb{R}, n \in \mathbb{Z}\} = \mathbb{R} \times \mathbb{Z}(id_y)$, and one easily sees that the k th field is a shifted replica of C_0 , namely

$$C_k = C_0 + k(0, bd_y).$$

The sequence of fields C_k is periodic with period i , so that the distinct fields are C_0, C_1, \dots, C_{i-1} . Figure 17.19 shows examples of fields (frame-limited) for $i = 1$,

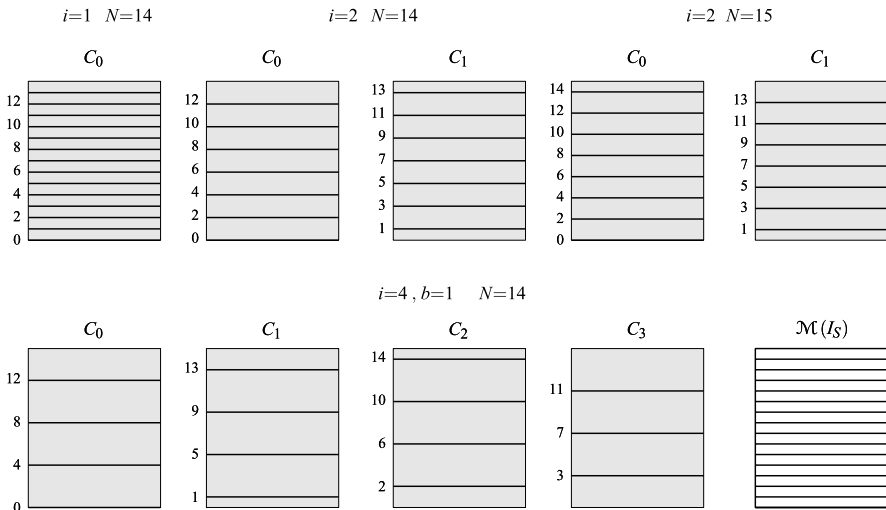
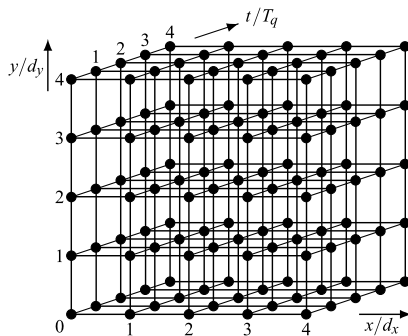


Fig. 17.19 Framed fields in continuous scanning with different interlace orders i . $\mathcal{M}(I_S)$ is the “mosaic,” given by the union of the fields

Fig. 17.20 The fundamental example of scanning group: the separable lattice $I_{S1:1}$



$i = 2$, and $i = 4$. Note that the number of lines may be different in the frame limited fields. For instance, with $N = 14$, $i = 4$, and $b = 1$, the fields C_0 , C_1 , C_2 , and C_3 have respectively 4, 4, 3, 3 lines.

17.4.4 Discrete Scanning

In *discrete* scanning even the horizontal coordinate becomes discrete, and the reference scanning group becomes a 3D *lattice* of the form (Fig. 17.20)

$$I_{S1:1} = \mathbb{Z}(d_x) \times \mathbb{Z}(d_y) \times \mathbb{Z}(T_q), \tag{17.42}$$

where $d_x = D_x/M$ is the horizontal spacing with M the number of pixels per line. Then, the final video signal becomes discrete-time with domain $\mathbb{Z}(T_0)$, where T_0 is the *pixel period* given by

$$T_0 = T_r/M = T_q/(MN). \quad (17.43)$$

In the general case, the scanning lattice I_S becomes an arbitrary sublattice of $I_{S1:1}$, whose basis can be written in the upper-triangular form

$$\mathbf{I}_S = \begin{bmatrix} d_x & 0 & 0 \\ 0 & d_y & 0 \\ 0 & 0 & T_f \end{bmatrix} \begin{bmatrix} a & p & q \\ 0 & i & b \\ 0 & 0 & 1 \end{bmatrix}, \quad H_S = \mathbb{Z}^3, \quad (17.44)$$

where the diagonal matrix is a basis for the full lattice $I_{S1:1}$.

As in continuous scanning, the integers i and b describe the vertico-temporal interlace. The values a , p , and q are integers, with $0 \leq p$ and $q < a$, where a specifies the horizontal pixel spacing as ad_x , and p and q complete the interlace specification of the lattice. The reduction of pixel density with respect to the reference case (*reduction factor*) is given by

$$r(I_S) \triangleq \mu(I_S)/\mu(I_{S1:1}) = ai,$$

where a and i represent the horizontal and vertical reductions, respectively. In the video signal the time spacing becomes aT_0 , where T_0 is given by (17.43).

From (17.44) we find that the generic point (x, y, z) of I_S is given by

$$x = (ma + np + kq)d_x, \quad y = (ni + kb)d_y, \quad t = kT_f, \quad m, n, k \in \mathbb{Z}.$$

Then, the k th field, given by pixel projections on (x, y) plane for $t = kT_f$, is the discrete set

$$C_k = \{((ma + np + kq)d_x, (ni + kb)d_y) \mid m, n \in \mathbb{Z}\}.$$

In particular, the *zeroth* field is $C_0 = \{((ma + np)d_x, nid_y) \mid m, n \in \mathbb{Z}\}$ and is recognized to be the 2D lattice with basis

$$\mathbf{C}_0 = \begin{bmatrix} d_x & 0 \\ 0 & d_y \end{bmatrix} \begin{bmatrix} a & p \\ 0 & i \end{bmatrix} \rightarrow C_0 = \mathbb{Z}_i^p(ad_x, d_y).$$

Then, also in this case the fields are shifted replicas of C_0 , specifically

$$C_k = C_0 + k(qd_x, bd_y),$$

and their *sequence is periodic with finite period L* . The evaluation of the period L is not immediate: it is given by the smallest L such that $L(qd_x, bd_y) \in C_0$; this condition assures that $C_L = C_0$.

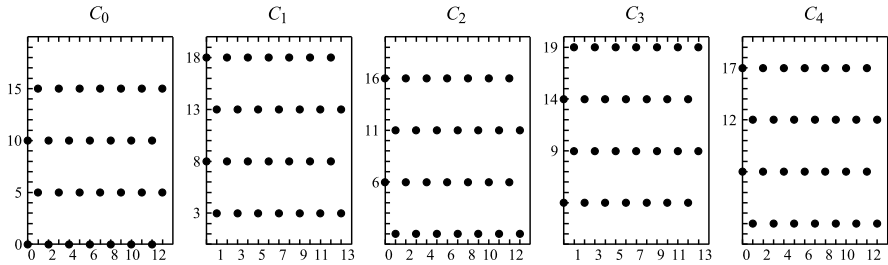


Fig. 17.21 Framed fields of a scanning lattice I_S with field period $L = 5$

As an example, consider the scanning lattice I_S with basis

$$I_S = \begin{bmatrix} d_x & 0 & 0 \\ 0 & d_y & 0 \\ 0 & 0 & T_f \end{bmatrix} \begin{bmatrix} 2 & 1 & 1 \\ 0 & 5 & 3 \\ 0 & 0 & 1 \end{bmatrix}.$$

The reduction factor is $r(I_S) = ai = 2 \times 5 = 10$. The fields are $C_k = C_0 + k(d_x, 3d_y)$ with $C_0 = \mathbb{Z}_2^1(d_x, 5d_y)$. The period is $L = 5$, and, in fact, $5(d_x, 3d_y) \in C_0$. The five distinct framed fields are illustrated in Fig. 17.21 with $N = 20$ and $M = 14$.

17.4.5 General Expression of a Video Signal

We have obtained the video signal for the continuous scanning, given by (17.10). To find the expression in the general case, we note that the first summation in (17.39) can be extended from $-\infty$ to $+\infty$, since, after frame limitation, the infinite summation does not add new contributions. Then

$$\begin{aligned} u(t) &= \sum_{n=-\infty}^{+\infty} \sum_{k=-\infty}^{+\infty} \ell_{QS}(v_x(t - nT_r - kT_q), nd_y, kT_q), \quad t \in \mathbb{R}, \\ &= \sum_{(n,k) \in \mathbb{Z}^2} \ell_{QS}(v_x(t - nT_r - kT_q), nd_y, kT_q). \end{aligned} \tag{17.45}$$

Note that $(n, k) \in \mathbb{Z}^2$ yields $(nd_y, kT_q) \in \mathbb{Z}(d_y, T_q)$, where the latter is the vertico-temporal lattice of the progressive format $\mathbf{M}(1:1)$. In the general case of multiple interlace, the vertico-temporal lattice becomes $\mathbb{Z}_i^b(d_x, T_f)$, and, in order to obtain the video signal from (17.45), it is sufficient to replace \mathbb{Z}^2 with $\mathbb{Z}_i^b = \mathbb{Z}_i^b(1, 1)$ and T_q with T_f . Hence, we find

$$\boxed{u(t) = \sum_{(n,k) \in \mathbb{Z}_i^b} \ell_{QS}(v_x(t - nT_r - kT_f), nd_y, kT_q), \quad t \in J,} \tag{17.46}$$

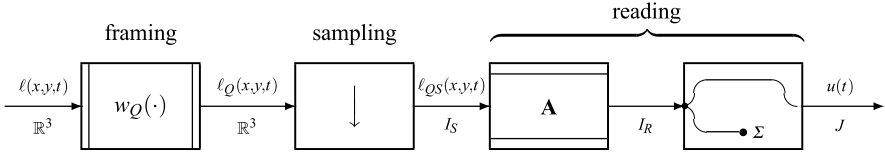


Fig. 17.22 Model of 3D image scanning with 3D→1D conversion expanded according to the theory of dimensionality reduction

which represents the general expression for continuous scanning, with time $t \in \mathbb{R}$. But, if t is confined to the spacing aT_0 of the video signal, that is, $t \in \mathbb{Z}(aT_0)$, the above expression holds also for discrete scanning with an arbitrary scanning lattice.

Historical Note The television scanning theory began with television itself, with the fundamental work of Mertz and Gray [14], who introduced the *periodic model* of scanning. Later on, fundamental contributions were made by Robinson [18], Drewery [7], Tonge [21–23], and Dubois [8]. However, to the author’s knowledge, a systematic approach with an appropriated “Signal Theory formulation” has never been developed. As will be evident, such a formulation based on dimensionality change is essential in scanning and reproduction.

17.5 Scanning of Time-Varying Images Revisited

As done for still images, we now reconsider the scanning of time-varying images (television scanning) with the theory of dimensionality changes. The scanning model is illustrated in Fig. 17.22, where the reading operation is subdivided into a coordinate change and a sum reduction. This model allows us to establish the correct formats for the reproduction (disjoint projection condition) and also an easy Fourier analysis.

17.5.1 Reading of Time-Varying Images

In the previous section we derived the general expression of the video signal for television scanning, given by (17.46). We now show that such an expression can be obtained as a reading with matrix

$$\mathbf{A} = \begin{bmatrix} v_x & -v_x/v_y & -v_x \\ 0 & 1 & 0 \\ 0 & 0 & 1 \end{bmatrix} \rightarrow \mathbf{A}^* = \begin{bmatrix} 1/v_x & 0 & 0 \\ 1/v_y & 1 & 0 \\ 1 & 0 & 1 \end{bmatrix}.$$

To this end, we apply the general theory of dimensionality reduction seen in Sect. 16.10 and Sect. 16.11 with $p + q = 3$, $p = 1$, and with the following cor-

response:

$$I \rightarrow I_S = \begin{cases} \mathbb{R} \times \mathbb{Z}_i^b(d_y, T_f) & \text{for continuous scanning,} \\ \text{sublattice of } \mathbb{Z}(d_x, d_y, T_f) & \text{for discrete scanning,} \end{cases}$$

$$U \rightarrow J = \begin{cases} \mathbb{R} & \text{for continuous scanning,} \\ \mathbb{Z}(T_0) & \text{for discrete scanning,} \end{cases}$$

$$V \rightarrow \mathbb{Z}_i^b(d_y, T_f) \triangleq J_{vt},$$

and with the following signal correspondence:

$$x(\mathbf{u}, \mathbf{v}) \rightarrow \ell_{QS}(x, y, t), \quad x_0(\mathbf{u}, \mathbf{v}) \rightarrow \ell_{QSR}(x, y, t), \quad y(\mathbf{u}) \rightarrow u(t).$$

The coordinate change applied to the framed-sampled image $\ell_{QS}(\cdot)$ gives

$$\begin{aligned} \ell_{QSR}(t, nd_y, kT_f) &= \ell_{QS}(\mathbf{A}(t, nd_y, kT_f)) \\ &= \ell_{QS}(v_x t - (v_x/v_y)nd_y - v_x kT_f, nd_y, kT_f) \\ &= \ell_{QS}(v_x(t - nT_r - kT_f), nd_y, kT_f). \end{aligned}$$

Then, the sum reduction gives the video signal

$$u(t) = \sum_{(n,k) \in \mathbb{Z}_i^b} \ell_{QSR}(t, nd_y, kT_f), \quad t \in J,$$

in agreement with (17.46).

17.5.2 Disjoint Projection Condition for Television Scanning

To find the disjoint projection condition or, equivalently, the production of a “correct” video signal, we apply the theory developed in Sect. 16.11. We limit ourselves to discrete scanning, and therefore we apply Proposition 16.15.

Given an arbitrary scanning lattice I_S , defined by (17.44) and specified by the naturals a, p, q, i, b , and given the nominal number of pixels per line M and the nominal number of lines per frame N (M and N refer to the full format), the conditions are

$$p + M = aM_0, \quad b + N = iN_0, \quad q + MN_0 = aL_0$$

with naturals M_0, N_0 , and L_0 .

We see that in the *full format* $\mathbf{M}(1 : 1)$ ($a = i = 1, p, q, b = 0$) the conditions are always verified. In the *interlace format* $\mathbf{M}(2 : 1)$, where $i = 2$ and $b = 0$, the number of lines must be odd (and this was recognized in the history of television for the fact that N even creates some problems). For higher-order interlaces, M and N must be chosen appropriately in dependence of the lattice parameters, or given M and N , we have to use convenient values of the lattice parameters.

17.6 Fourier Analysis of Television Scanning

We follow the model of Fig. 17.22, which consists of “simple” tfs, whose Fourier analysis is well established. Before proceeding, we evaluate the reciprocal of the scanning group, which plays a fundamental role in this analysis.

17.6.1 Reciprocal of Scanning Group

In the *full format* of discrete scanning we have

$$I_{S1:1} = \mathbb{Z}(d_x, d_y, T_f) \xrightarrow{\star} I_{S1:1}^{\star} = \mathbb{Z}(F_x, F_y, F_f),$$

where

$$F_x = \frac{1}{d_x} = \frac{M}{D_x}, \quad F_y = \frac{1}{d_y} = \frac{N}{D_y}, \quad F_f = \frac{1}{T_f}.$$

Analogously, in the full format of continuous scanning

$$I_{S1:1} = \mathbb{R} \times \mathbb{Z}(d_y, T_f) \xrightarrow{\star} I_{S1:1}^{\star} = \mathbb{O} \times \mathbb{Z}(F_y, F_f).$$

In general, the scanning group I_S is a subgroup of the corresponding full-format group $I_{S1:1}$. Hence, $I_S^{\star} \supset I_{S1:1}^{\star}$, and we can write

$$I_S^{\star} = I_{S1:1}^{\star} + P, \quad P = [I_S^{\star}/I_{S1:1}^{\star}], \quad (17.47)$$

where the cell P is a finite set with a number of points given by the *reduction factor* $r = r(I_S)$ ($r = i$ in continuous scanning, and $r = ai$ in discrete scanning).

Now, we proceed separately for continuous and discrete scanning.

Continuous Scanning In the general case the grating I_S is separable as in (17.41a), (17.41b), that is, $I_S = \mathbb{R} \times J_{vt}$, where J_{vt} is the vertico-temporal lattice given by $J_{vt} = \mathbb{Z}_i^b(d_y, T_f)$. Hence, the reciprocal is (see Sect. 5.9)

$$I_S^{\star} = \mathbb{O} \times J_{vt}^{\star} = \mathbb{O} \times \mathbb{Z}_i^c(F_y/i, F_f), \quad c = i - \tilde{b}. \quad (17.48)$$

Since the points of I_S^{\star} lie in the (f_y, f_t) plane, we use decomposition (17.47) in the 2D form

$$J_{vt}^{\star} = J_{vt1:1}^{\star} + P, \quad P = [J_{vt}^{\star}/J_{vt1:1}^{\star}],$$

where $J_{vt1:1}^{\star} = \mathbb{Z}(F_y, F_f)$ is the reciprocal of the vertico-temporal lattice of progressive 1:1 scanning. The cell P contains i points that can be written in the form (see (17.24))

$$(kcF_y/i, kF_f/i), \quad k = 0, 1, \dots, i - 1.$$

These points can be chosen within the rectangle $[0, F_y) \times [0, F_f)$ by replacing kc with $\rho_i(kc)$, as illustrated in Fig. 17.23 for the first interlace orders.

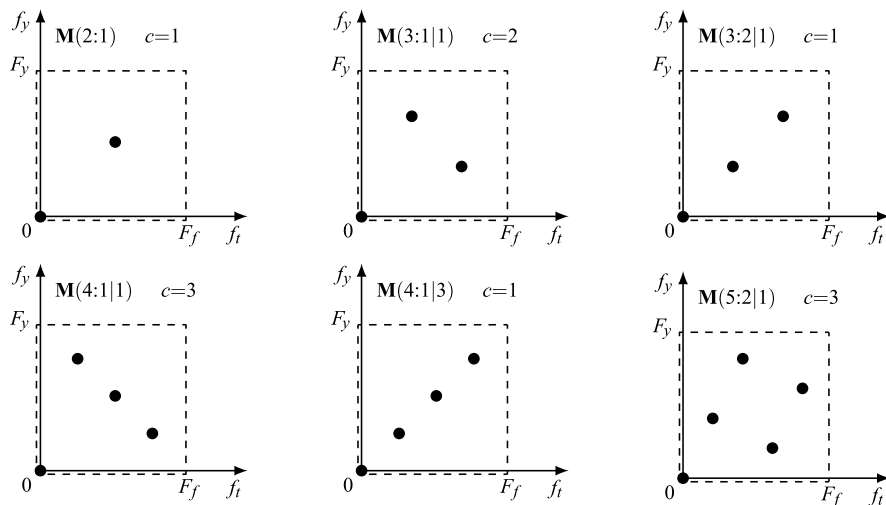


Fig. 17.23 Illustration of the cell of *additional centers* of I_S^* with respect to $I_{S_{1:1}}^*$ in $M(i : 1|b)$ scanning

Discrete Scanning In general, the lattice I_S is not separable (see (17.44)), and to find the reciprocal I_S^* , we have to calculate the reciprocal (transpose inverse) of the basis \mathbf{I}_S , where it will be convenient to refer to triangular forms.

Example 17.1 Consider a scanning lattice I_S with Hermitian bases

$$\mathbf{I}_S = \begin{bmatrix} d_x & 0 & 0 \\ 0 & d_y & 0 \\ 0 & 0 & T_f \end{bmatrix} \begin{bmatrix} 2 & 1 & 1 \\ 0 & 2 & 1 \\ 0 & 0 & 1 \end{bmatrix} \rightarrow \begin{bmatrix} d_x & 0 & 0 \\ 0 & d_y & 0 \\ 0 & 0 & T_f \end{bmatrix} \begin{bmatrix} 1 & 0 & 0 \\ 0 & 1 & 0 \\ 2 & 3 & 4 \end{bmatrix}, \quad (17.49)$$

where \rightarrow means the application of elementary operations (see Sect. 16.6). Evaluating the reciprocal basis and using the triangularization techniques, we obtain the following Hermitian bases for the reciprocal group I_S^* (Fig. 17.24):

$$\mathbf{I}_S^* = \begin{bmatrix} \frac{1}{4}F_x & 0 & 0 \\ 0 & \frac{1}{4}F_y & 0 \\ 0 & 0 & \frac{1}{4}F_f \end{bmatrix} \begin{bmatrix} 4 & 0 & 2 \\ 0 & 4 & 1 \\ 0 & 0 & 1 \end{bmatrix} \rightarrow \begin{bmatrix} \frac{1}{4}F_x & 0 & 0 \\ 0 & \frac{1}{4}F_y & 0 \\ 0 & 0 & \frac{1}{4}F_f \end{bmatrix} \begin{bmatrix} 2 & 0 & 0 \\ 1 & 2 & 0 \\ 1 & 2 & 4 \end{bmatrix}. \quad (17.50)$$

The reduction factor is $r(I_S) = 4$, and the cell P of the additional repetition centers has 4 points, specifically

$$P = \left\{ k \left(\frac{1}{2}F_x, \frac{1}{4}F_y, \frac{1}{4}F_f \right) \mid k = 0, 1, 2, 3 \right\}.$$

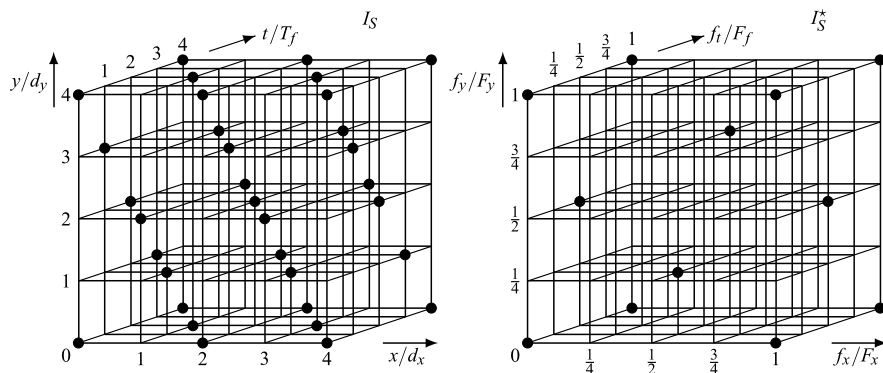


Fig. 17.24 Example of a scanning lattice I_S and its reciprocal I_S^*

17.6.2 Analysis of the Four “Simple Operations”

We start from the FT of the source image $\ell(x, y, t)$, which is a complex 3D function $L(f_x, f_y, f_t)$, where the frequencies have dimensions of cycles per width (cpw), cycles per height (cph), and cycles per second (cps or Hz), respectively.

Framing The dual of frame limitation (17.32) is a 2D convolution in \mathbb{R}^3 given by

$$L_Q(\mathbf{f}) = \int_{\mathbb{R}^2} d\lambda_x d\lambda_y W_Q(\lambda_x, \lambda_y) L(f_x - \lambda_x, f_y - \lambda_y, f_t), \tag{17.51}$$

where $\mathbf{f} = (f_x, f_y, f_t)$ is the 3D frequency, and $W_Q(f_x, f_y)$ is given by

$$W_Q(f_x, f_y) = W_1(f_x)W_2(f_y), \tag{17.52}$$

with

$$W_1(f_x) = D_x \text{sinc}(f_x D_x) \exp(-i\pi f_x D_x), \tag{17.52a}$$

$$W_2(f_y) = D_y \text{sinc}(f_y D_y) \exp(-i\pi f_y D_y). \tag{17.52b}$$

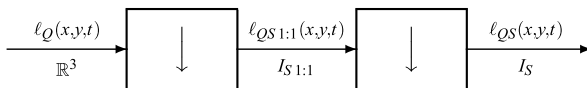
Sampling The dual of the $\mathbb{R}^3 \rightarrow I_S$ sampling is a periodic repetition with *repetition centers* given by the reciprocal group I_S^* ,

$$L_{QS}(\mathbf{f}) = \sum_{\mathbf{p} \in I_S^*} L_Q(\mathbf{f} - \mathbf{p}), \quad \mathbf{f} \in \mathbb{R}^3 / I_S^*, \tag{17.53}$$

where $\mathbf{p} = (p_x, p_y, p_z)$ are the repetition centers.

In continuous scanning the sampling has the form $\mathbb{R}^3 \rightarrow \mathbb{R} \times \mathbb{Z}_i^b(d_y, T_f)$, which is a 2D sampling limited to the (y, t) coordinates. Correspondingly, the periodic repetition is 2D with repetition centers in the (f_x, f_t) plane (see (17.48)). In discrete

Fig. 17.25 Decomposition of $\mathbb{R}^3 \rightarrow I_S$ sampling



scanning the sampling has a full format, that is, with respect to the three coordinates (x, y, t) , and correspondingly the periodic repetition becomes 3D. In any case it is convenient to decompose the $\mathbb{R}^3 \rightarrow I_S$ sampling into the cascade of two samplings: $\mathbb{R}^3 \rightarrow I_{S1:1}$ and $I_{S1:1} \rightarrow I_S$, where $I_{S1:1}$ is the full-format scanning group (Fig. 17.25). Then, periodic repetition (17.53) is decomposed into the two periodic repetitions $\mathbb{R}^3 \rightarrow \mathbb{R}^3/I_{S1:1}^*$ and $\mathbb{R}^3/I_{S1:1}^* \rightarrow \mathbb{R}^3/I_S^*$ with relations

$$L_{QS1:1}(\mathbf{f}) = \sum_{\mathbf{p1} \in I_{S1:1}^*} L_Q(\mathbf{f} - \mathbf{p1}), \quad L_{QS}(\mathbf{f}) = \sum_{\mathbf{p2} \in P} L_{QS1:1}(\mathbf{f} - \mathbf{p2}), \quad (17.54)$$

where $P = [I_S^*/I_{S1:1}^*]$ gives the extra repetition centers due to the density reduction with respect to full scanning. This decomposition is useful to understand the penalty to pay for the density reduction, because the extra repetition centers require a reduction of the reference cell of Sampling Theorem, or, put in another way, the image bandwidth must be smaller than in the case of progressive scanning.

Coordinate Change and Sum Reduction In the frequency domain the coordinate change with matrix \mathbf{A} becomes a coordinate change with matrix \mathbf{A}^* , specifically

$$L_{QSR}(f_x, f_y, f_t) = \mu(\mathbf{A})L_{QS}(\mathbf{A}^*(f_x, f_y, f_t)). \quad (17.55)$$

The sum reduction becomes a zero reduction, specifically

$$U(f) = \mu(J_{vt})L_{QSR}(f, 0, 0) = \mu_0L_{QS}(f/v_x, f/v_y, f), \quad (17.56)$$

where $\mu_0 = \mu(J_{vt})/v_x$. Since $\mu(J_{vt}) = 1/(id_y T_f)$, $v_x = D_x/T_r$, $iT_f = T_q = NT_r$, and $Nd_y = D_y$, it turns out that $\mu_0 = 1/(D_x D_y) = 1$ for all types of scanning. Hence,

$$U(f) = L_{QS}\left(\frac{f}{v_x}, \frac{f}{v_y}, f\right), \quad f \in \mathbb{R}/J^*, \quad (17.57)$$

where $v_x = D_x/T_r$ is the horizontal velocity, and $v_y = d_y/T_r$ is the average vertical velocity. This result holds for both continuous scanning, where $U(f)$ is aperiodic ($J^* = \mathbb{O}$), and discrete scanning, where $U(f)$ is periodic with period given by the pixel frequency ($J^* = \mathbb{Z}(F_0/a)$, $F_0 = 1/T_0$). The continuous scanning may have an arbitrary interlace, and discrete scanning an arbitrary scanning lattice.

Relationship (17.57) states that the FT $U(f)$ of the video signal is obtained by “reading” the 3D function $L_{QS}(f_x, f_y, f_t)$ along the line with equation

$$(f_x, f_y, f_t) = (f/v_x, f/v_y, f), \quad f \in \mathbb{R}, \quad (17.58)$$

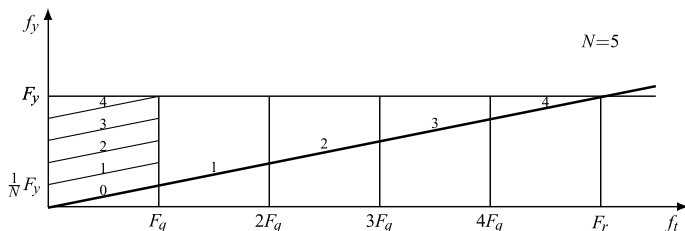


Fig. 17.26 Illustrations of “reading” operations giving the Fourier transforms of video signals for progressive continuous scanning

and therefore it is determined by the scanning velocities. This “reading” operation is illustrated in Fig. 17.26 for the progressive continuous scanning, where the repetition centers are $(0, rF_y, sF_q)$, $r, s \in \mathbb{Z}$, so that they lie on the f_y, f_t plane. The reading line is *tilted* with respect to this plane and a reference point being $(1/D_x, F_y, NF_q)$. The FT $U(f)$ depends on how the reading line intersects the periodic repetitions of $L_{QS}(\mathbf{f})$. Note that in the absence of the *tilt*, $U(f)$ would be periodic.

Effect of Framing An evaluation of the convolution (17.51) can be avoided in most cases, since $Q(f_x, f_y)$ can be replaced by an impulse $\delta(f_x)\delta(f_y)$. However, framing cannot be neglected in several steps of the analysis and in particular in a correct settlement of dimensionality reduction.

17.7 The Three-Dimensional Television

17.7.1 The Fundamentals

A 3D time-varying image is represented by a 4D signal

$$\ell(x, y, z, t), \quad (x, y, z, t) \in \mathbb{R}^4, \tag{17.59}$$

where the depth-coordinate z is added with respect to the 2D time-varying image of the standard television (see (17.31)). In principle, the scanning and reproduction of image (17.59) is a simple extension of theory developed in Sect. 17.4 with the introduction of the parameters related to the depth-coordinate z .

The *framing* is obtained by limiting the source image (17.59) within the parallelepiped $Q = [0, D_x) \times [0, D_y) \times [0, D_z)$ of the spatial coordinates x, y, z according to the relation

$$\ell_Q(x, y, z, t) = w_Q(x, y, z)\ell(x, y, z, t), \tag{17.60}$$

where $w_Q(x, y, z)$ is the indicator function of Q . This limitation is necessary to ensure the reproduction of the image from the 1D video signal, as established in Chap. 16 by the theory on dimensionality reduction.

Considering directly the discrete scanning, the sampling operation has the form $\mathbb{R}^4 \rightarrow I_S$, where I_S is the lattice

$$I_S = \mathbb{Z}(d_x) \times \mathbb{Z}(d_y) \times \mathbb{Z}(d_z) \times \mathbb{Z}(T_q) \quad (17.61)$$

in the case of full-progressive format, but an interlaced lattice is possible (in principle). The spacings d_x, d_y are given as in Sect. 17.4, that is, $d_x = D_x/M$, $d_y = D_y/M$, and $d_z = D_z/L$ is chosen to subdivide the depth length D_x in L spacings of size d_z . Then, from the frame Q we collect MLN pixels, and the pixel period is given by $T_q/(MNL)$, where T_q is the frame period.

The scanning model is the same as in Fig. 17.22, where now the composite shift matrix \mathbf{A} becomes 4×4 , and the disjoint projection conditions, for correct reproduction, can be easily established.

17.7.2 The Technological Viewpoint

Current television evolution focuses on human implications of stereoscopic visualization. The perception of depth (“stereos” in ancient Greek), besides other cues, is due to the position of the human eyes about six centimeters apart. Because of this, the two eyes perceive the scene from slightly different viewpoints. Electronic stereoscopic systems mimic this fact at every point of the processing chain going from capture to visualization.

The capture of a stereoscopic video signal can be simply obtained by a camera featuring two optics placed at human eye distance, e.g., about six centimeters apart. The left and right stereo video signals could be alternately obtained by rendering 3D models (or simply textured depth-maps) from viewpoints at mutual eye distance. This is the necessary way to go for the production of text and graphics material for stereo cinema and television.

The compression of stereo video pairs can take great advantage from the redundancy due to the degree of spatial superposition between the two viewpoints as current standard feature. This is an element without any counterpart in monoscopic television compression [11, 15, 19].

Stereoscopic visualization must ensure that each eye is reached each one by the appropriate video flux. Many current television commercial displays use special glasses to be worn by viewers. This can be obtained in many ways. For instance, as in popular products, one may use a monitor alternately displaying the left and right video flux and equip viewers with glasses mounting LCD lenses. The LCD glass lenses alternately block light entering the left or right eye at video-rate and synchronously with the monitor. There are other types of active stereo glass technology (called “active” because it assumes hardware interacting with the display), and there also are “passive” glass stereo visualization systems based on light polarization (linear or circular). The reader is sent to [11, 15, 19] for detailed accounts.

Autostereoscopic displays overcome the need of wearing glasses. Such devices produce a number of video-fluxes, usually no less than eight, corresponding to different viewpoint directions and have front-end mechanisms blocking the fluxes corresponding to directions different from the viewer's one. There exist various types of autostereoscopic displays; the most popular today are the ones based on parallax barrier and lenticular lens technology. In general, the greater the number of generated video fluxes, the more effective the results are. Autostereoscopic devices technology is rapidly evolving.

It is finally worth mentioning that "3D video," the term currently used in the market to denote stereoscopic visualization, was originally, and not until too long ago, used instead to denote what today is typically called *free-viewpoint video* in order to avoid misunderstanding. The motivation of free-viewpoint video is to allow viewers to freely choose the scene observation viewpoint. Differently than in traditional television (either monoscopic or stereoscopic), where the viewer is forced to see the scene from the viewpoint which was decided by the operator at taking time, in free-viewpoint video the viewer can arbitrarily decide viewing position, distance, and angle at any time. This fruition modality clearly poses great technological challenges.

The capture of free-viewpoint video data requires systems suitable to reconstruct at photorealistic quality dynamic 3D scenes of any type under any illumination, and is a major open issue in computer vision since several decades. The transmission requires suitable compression methods way beyond current practical solutions, let alone standardization. Visualization requires suitable display devices and interfaces way from being available in spite of the very interesting prototypes so far developed in the computer graphics community. The interested reader is addressed to the literature [11, 15, 19] for further information.

17.8 Numerical Conversion of Images

Pixel subdivision is a preliminary step for the numerical representation of an image. We consider separately still images and time-varying images.

17.8.1 Numerical Conversion of a Still Image

In the simplest coding system, called PCM (Pulse Code Modulation), each pixel is quantized obtaining $\ell_q(md_x, nd_y) = \mu[\ell(md_x, nd_y)]$, where the quantizer characteristic $\mu[\cdot]$ is typically uniform with $L = 2^{B_\ell}$ levels. In this way each pixel is represented with B_ℓ bits, and the whole image is represented by

$$H_0 = B_\ell MN = B_\ell \rho N^2 \quad \text{bits/image,}$$

where ρ is the aspect ratio. A typical value is $B_\ell = 8$ bits/pixel, which guarantees a signal-to-noise ratio $\approx 6B_\ell = 48$ dB for the reconstructed image.

For color images, besides the luminance signal, one must numerically convert the chrominance signal with a given number B_c of bit/pixel. In this way the image is represented with

$$H_0 = BMN \quad \text{bits/image} \quad (B = B_\ell + B_c),$$

where typically $B_c = B_\ell$.

The values associated to H_0 are very large; for instance, the representation of a color image with a good resolution, e.g., $N = 800$ lines, $M = 800$ pixel/line, and $B = 16$ bit/pixel, requires more than 10 Mbit/image. This has a considerable impact, not only in the transmission, but also in the storage. In transmission, assuming that the available channel has a nominal rate of R bit/s, the time required for transmitting an image with nominal information H_0 is

$$T_q = H_0/R = B_\ell \rho N^2/R.$$

Let us consider a few examples. With an old telephone line modem with rate $R = 2400$ bit/s, the time needed for the transmission of an image with $H_0 = 1024000$ bit/image was approximately $T_q = 400$ s, i.e., beyond six minutes. The transmission time for the same image with rate 2 Mbit/s would be just $T_q = 0.5$ s.

This evaluation refers to the full scanning format on the lattice $I_S = \mathbb{Z}(d_x, d_y)$. If an interlace format as the lattice $I_S = \mathbb{Z}_a^p(d_x, d_y)$ is adopted, we have a reduction of a times. In any case the value of H_0 is large for adequately representing still images and *redundancy compression coding* is customarily adopted. Let us recall that the above expression of H_0 gives the real information of the quantized image only when the pixels are statistically independent and uniformly distributed over the 2^B values. Actually, there is typically a considerable correlation among adjacent pixels, and the quantized image is consequently highly redundant. Redundancy compression methods are quite complex, and we will only mention a straightforward technique, namely DPCM (i.e., differential PCM). In this coding method the first pixel of each line is encoded as in PCM, whereas for the other pixels, the difference with respect to the first pixel is encoded with less bits, in force of the fact that, statistically, luminance and chrominance variations among adjacent pixels are small. For instance, 8 bits for the first pixel and 3 bits for the difference give image reconstruction of quality comparable to that of PCM.

As a concrete example, Table 17.3 reports the data relative to the numerical transmission of images from the NASA spacecraft Voyager 2 during the external planets exploration. The scanning parameters are the following: $N = 800$, $M = 800$, $MN = 640000$ pixel/image. The adopted redundancy compression method were PCM with 8 bit/pixel for transmission from Jupiter and Saturn and DPCM with 3 bit/pixel for transmission from Uranus and Neptune. Incidentally, in a more recent mission, as Galileo to Jupiter (1995) and Cassini to Saturn (2003), the DCT coding (see Sect. 12.5) was used with a further redundancy reduction.

Table 17.3 Images transmission from spacecraft Voyager 2

Planet (date of close encounter)	Distance ^a	Rate	Coding	T_q
Jupiter (July 9, 1979)	5 AU	115.2 kbit/s	PCM	44 s
Saturn (August 25, 1981)	10 AU	28 kbit/s	PCM	183 s
Uranus (January 24, 1986)	20 AU	22 kbit/s	DPCM	87 s
Neptune (August 24, 1989)	30 AU	22 kbit/s	DPCM	87 s

^aThe astronomical unit (AU) is the mean distance of the Earth from the Sun (150 Gm)

17.8.2 Numerical Conversion of a Time-Varying Image

We refer to the *digital* television, where the interest is mainly confined to the *rate* R (in number of bits/s) required for a reliable transmission. Considering that television is obtained with a sequence of still images, the rate is simply given as $R = H_0 F_f$, where H_0 is the number of bits required to represent a field, and F_f is the number of fields per second. In the full progressive format, $H_0 = BMN$ bits/field, and therefore the rate is

$$R_{1:1} = BMNF_f \quad \text{bits/s,}$$

which is the reference for the comparison with other formats. In general, with an interlace format given by the lattice (17.44), the rate is reduced by the factor ia , that is,

$$R = BMNF_f / (ia) = BMNF_q / a \quad \text{bits/s.}$$

We consider two examples. In the PAL standard (see Table 17.2), where $N = 625$ is the nominal number of lines, but the effective number is 576, $M = (4/3)576 \simeq 767$, $F_q = 25$ frames/s, $B = 16$ bits/pixel, $i = 2$, $a = 1$, we find $R = 176.41$ Mbits/s. In the HDTV standard, where $N = 1080$, $M = (16/9)N$, $F_q = 25$ frames/s, $B = 24$ bits/pixel, $i = 2$, $a = 1$, we find $R = 1244.16$ Mbits/s, seven times the rate needed for PAL.

These high rates do not represent any problem for the transmission with optical fiber channel, but with radio channel they are not acceptable, and the redundancy reduction is mandatory. In the last twenty years a considerable effort has been made to achieve this goal, in particular by Joint Photographic Expert Group (JPEG) [20], who reached very brilliant results, arriving at a rate reduction of more than forty times!

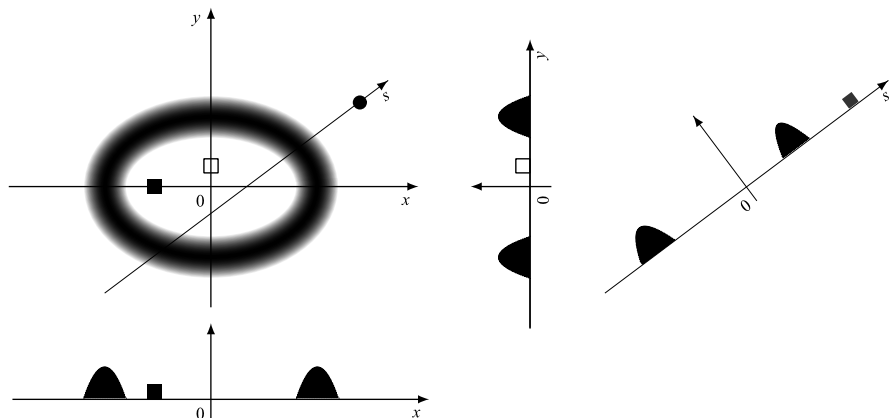


Fig. 17.27 Integration along x , along y , and along a tilted line

17.9 Projections (Radon Transform)

Consider a 2D image $\ell(x, y)$, represented in Fig. 17.27 by its density distribution (density plot). The integral of the image along the coordinate y

$$g_{or}(x) = \int_{\mathbb{R}} dy \ell(x, y) \tag{17.62}$$

gives a function of the coordinate x , where, for each x fixed to \bar{x} , the values of the 1D function $\ell(\bar{x}, y)$ are “compressed” into a single value $g_{or}(\bar{x})$. Technically speaking, this value is called *projection of the image at \bar{x}* . From this value one has not all the information on $\ell(\bar{x}, y)$ along y , but some information; for instance, if $\ell(\bar{x}, y)$ is zero for every y , then $g_{or}(\bar{x}) = 0$, if $\ell(\bar{x}, y)$ is high valued, then $g_{or}(\bar{x})$ also is a high value, and so on. In particular, if $\ell(\bar{x}, y)$ is concentrated at a given point $y = y_0$, say $\ell(\bar{x}, y) = A_0\delta(y - y_0)$, the integral gives $g_{or}(\bar{x}) = A_0$, and we realize that the information on the *localization* of the impulse at $y = y_0$ is lost in the projection.

If we free the point from the fixed value \bar{x} to an arbitrary value x , integral (17.62) defines a 1D function $g_{or}(x)$ and gives the projection at any x , which is called the *projection of the image onto the x -coordinate*. Analogously, the integral along x

$$g_{vert}(y) = \int_{\mathbb{R}} dx \ell(x, y) \tag{17.63}$$

gives the projection of the image onto the y -coordinate. The 1D function $g_{vert}(y)$ adds new information about the image, and in certain limit cases the pair $g_{or}(x)$, $g_{vert}(y)$ may also give an indication on the *location* of the values of the image. In particular, if $\ell(x, y) = A_0\delta(x - x_0)\delta(y - y_0)$, we get $g_{or}(x) = A_0\delta(x - x_0)$ and $g_{vert}(y) = A_0\delta(y - y_0)$, and clearly the localization of the 2D impulse is identified. But this is a very lucky and unique case, and in general the two projections give a very restricted information about the image.

To get more information about the image $\ell(x, y)$, an idea is to integrate $\ell(x, y)$ along an arbitrary line, say the equation

$$L(s, \theta): \quad x \cos \theta + y \sin \theta = s, \quad (17.64)$$

which gives another projection. This projection depends on the parameters s and θ that identify the line (17.64), and therefore the integral along $L(s, \theta)$, symbolized

$$g(s, \theta) = \int_{L(s, \theta)} dL \ell(x, y), \quad (17.65)$$

may be viewed as a *collection of projections* depending on the line parameters s and θ and define a 2D function. In particular, for $\theta = 0$, we have the line of equation $s = x$ and then $g(s, 0) = g_{\text{or}}(s)$, and for $\theta = \pi/2$, the line becomes $s = y$, and then $g(s, \pi/2) = g_{\text{vert}}(s)$. In conclusion, the collection of projections (17.65) defines a 2D function $g(s, \theta)$, which are briefly called *projections*. The question is: do the projections $g(s, \theta)$ allow the reconstruction of the image $\ell(x, y)$? The answer was found by Johann Radon in 1917 [17], who proved that the transform (17.65), which will be formalized below as the *Radon transform*, is invertible.

The discovery of the Radon transform opened a new field, called *tomography*, having several important applications. The best known examples of applications come from medicine in x-ray computed tomography and in magnetic resonance imaging, where the “image” to be reconstructed is given by the density of tissues. But reconstruction from projections finds application in several other disciplines, as astronomy and nondestructive testing of materials [2, 10]. At the end of this chapter we will give more details on the application of the Radon transform.

The 2D function $g(s, \theta)$ will be now formalized as the Radon transform \mathcal{R} of the image $\ell(x, y)$. This transform is invertible, as formalized by the inverse Radon transform \mathcal{R}^{-1} . Related to the Radon transform, we shall see several other transforms which try to overcome the difficulty in the inversion of the Radon transform, that is, the reconstruction of an image from its projections.

The main goal of this final part of the book is the formulation of all these transforms within the Unified Theory. The original contribution will be to recognize that all the functions involved in this topic are given by only three classes of 2D functions: *Cartesian*, *polar*, and *grating* functions, which will be defined in the next section.

17.9.1 The Radon Transform

The integration along the line of (17.64) can be written in the form

$$\mathcal{R}: \quad g(s, \theta) = \int_{\mathbb{R}^2} dx dy \ell(x, y) \delta_{\mathbb{R}}(x \cos \theta + y \sin \theta - s), \quad (17.66)$$

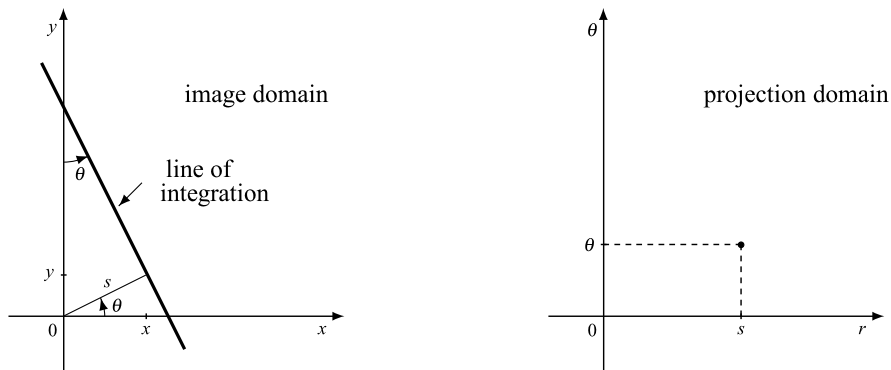


Fig. 17.28 Image space and projection space

where $g(s, \theta)$ is called the *projection* or the *Radon transform* of the image $\ell(x, y)$ and denoted by $g = \mathcal{R}\ell$. The Radon operator \mathcal{R} defined by (17.66) maps the *spatial domain* (x, y) onto the *projection domain* (s, θ) , where each point corresponds to a line in the spatial domain. In general, $\ell(x, y)$ may be a complex function, and, more commonly, it is real, and so are the projections $g(s, \theta)$.

Note that the line is at an angle θ from the y -axis and at a distance s from the origin; θ is also given as the angle between the x -axis and the perpendicular from the origin, s being the perpendicular length (Fig. 17.28).

It is possible to get a more explicit formula for the Radon transform (17.66) by expressing the Cartesian coordinates (x, y) in the form

$$x = s \cos \theta - u \sin \theta, \quad y = s \sin \theta + u \cos \theta.$$

Specifically (see Problem 17.6) one gets

$$\mathcal{R}: \quad g(s, \theta) = \int_{-\infty}^{+\infty} \ell(s \cos \theta - u \sin \theta, s \sin \theta + u \cos \theta) du. \tag{17.67}$$

The fundamental goal is the reconstruction of the image $\ell(x, y)$ from its projections $g(s, \theta)$. If we know all projections $g(s, \theta)$ for every $s \in \mathbb{R}$ and every $\theta \in [0, \pi)$, the perfect reconstruction is possible. Indeed, the Radon transform $g = \mathcal{R}\ell$ is an invertible linear transformation $\ell = \mathcal{R}^{-1}g$, where the inverse transformation is given by [10]

$$\mathcal{R}^{-1}: \quad \ell(x, y) = \frac{1}{2\pi^2} \int_0^\pi \int_{-\infty}^{+\infty} \frac{\partial g(s, \theta) / \partial s}{x \cos \theta + y \sin \theta - s} d\theta ds. \tag{17.68}$$

In practice, we can get the projections at a finite number of angles θ_m and at a countable set of distances s_n , and hence the goal becomes the reconstruction of the image from the sample values $g(s_n, \theta_m)$. Conceptually, the reconstruction can be carried out in two steps: first, we have to reconstruct $g(s, \theta)$ from $g(s_n, \theta_m)$; next,

we get $\ell(x, y)$ according to (17.68). This is a typical *Sampling Theorem*, which will be seen at the end.

As we shall see, the image reconstruction is not directly performed by inversion formula (17.68), but using “ancillary” functions in several ways. So, the theory of projections is characterized by a lot of functions and operators, and a preliminary task is the study of some function formats that are specific for projections.

17.9.2 Examples

We consider three simple examples of projections and then a more articulate example. In the first three the image has a circular symmetry, that is, with the form $\ell(x, y) = \ell_0(\sqrt{x^2 + y^2})$. Then it is easily shown, from the preliminary interpretation, that the Radon transform is independent of θ , namely

$$g_0(s) = \int_{\mathbb{R}^2} dx dy \ell_0(\sqrt{x^2 + y^2}) \delta_{\mathbb{R}}(x - s) = \int_{\mathbb{R}} dy \ell_0(\sqrt{s^2 + y^2}), \quad (17.69)$$

where we have used the sifting property with respect to x . Next, with the variable change $r = \sqrt{s^2 + y^2}$ we obtain

$$g_0(s) = 2 \int_s^{\infty} \frac{r}{\sqrt{r^2 - s^2}} \ell_0(r) dr, \quad (17.70)$$

which represents the *Abel transform* of $\ell_0(r)$ (see [2]).

Example 17.2 We evaluate the Radon transform of the unitary disk of radius R centered at the origin, whose image is

$$\ell(x, y) = \ell_0(\sqrt{x^2 + y^2}) = \text{rect}_+ \left(\frac{\sqrt{x^2 + y^2}}{R} \right).$$

From (17.69) we obtain, for $s < R$,

$$\begin{aligned} g_0(s) &= \int_{-\infty}^{+\infty} \text{rect}_+ \left(\frac{\sqrt{s^2 + y^2}}{R} \right) dy = \int_{s^2 + y^2 < R^2} dy \\ &= \int_{-\sqrt{R^2 - s^2}}^{\sqrt{R^2 - s^2}} dy = 2\sqrt{R^2 - s^2}, \end{aligned}$$

whereas $g_0(s) = 0$ for $s > R$ (see interpretation of Fig. 17.28). Hence,

$$\ell(x, y) = \text{rect}_+ \left(\frac{\sqrt{x^2 + y^2}}{2R} \right) \xrightarrow{\mathcal{R}} g(s, \theta) = 2\sqrt{R^2 - s^2} \text{rect} \left(\frac{s}{2R} \right).$$

Example 17.3 Consider the *ring impulse*

$$\ell(x, y) = \ell_0(\sqrt{x^2 + y^2}) = \delta(\sqrt{x^2 + y^2} - R),$$

which is zero on the whole (x, y) -plane, except the circle $x^2 + y^2 = R^2$, where the function has a concentrated area. In this case we apply (17.70), that is,

$$g_0(s) = 2 \int_s^\infty \frac{r}{\sqrt{r^2 - s^2}} \delta(r - R) dr.$$

For $s > R$, $\delta(r - R) = 0$, and the result is zero. For $s < R$, we use the sifting property. The result is

$$\ell(x, y) = \delta(\sqrt{x^2 + y^2} - R) \xrightarrow{\mathcal{R}} g(s, \theta) = \frac{2R}{\sqrt{R^2 - s^2}} \operatorname{rect}\left(\frac{s}{2R}\right).$$

Example 17.4 Consider the Gaussian image

$$\ell(x, y) = e^{-\pi(x^2 + y^2)}. \quad (17.71)$$

From (17.69) we have

$$g_0(s) = \int_{-\infty}^{+\infty} e^{-\pi(s^2 + y^2)} dy = e^{-\pi s^2} \int_{-\infty}^{+\infty} e^{-\pi y^2} dy = e^{-\pi s^2}.$$

Hence,

$$\ell(x, y) = e^{-\pi(x^2 + y^2)} \xrightarrow{\mathcal{R}} g(s, \theta) = e^{-\pi s^2}.$$

Note that image (17.71), written in polar coordinates, is an eigenfunction of the Radon transform.

17.9.3 Reference Example

We throughout consider a real image defined by the expression (Fig. 17.29)

$$\ell(x, y) = 2^4 4! \frac{J_4(\sqrt{x^2 + y^2})}{(x^2 + y^2)^2} p(x, y), \quad (17.72)$$

where $J_4(r)$ is a Bessel function of the first kind, and $p(x, y)$ is the polynomial

$$p(x, y) = 1 + Ax + By + Cxy. \quad (17.72a)$$

The illustrations will be obtained with the following numerical values:

$$A = -\frac{1}{3}, \quad B = \frac{4}{15}, \quad C = \frac{1}{5}. \quad (17.72b)$$

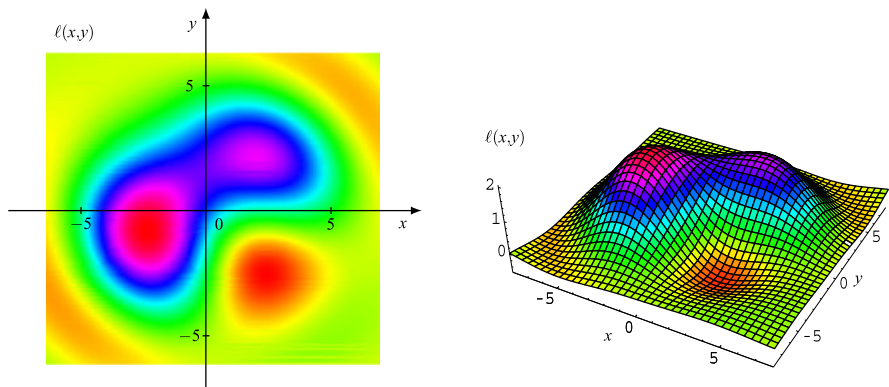


Fig. 17.29 Reference image and the corresponding signal $\ell(x, y)$

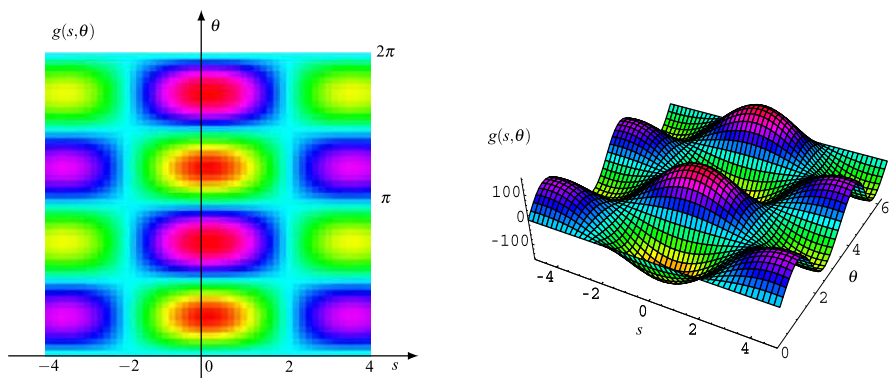


Fig. 17.30 Projections of the reference example shown with a density plot and a standard plot

This example will be useful to illustrate the many representations we shall introduce for a same image. The calculation details for each representation is available on line attached to the solutions of problems [4].

The Radon transform of the reference image, shown in Fig. 17.30, is given by

$$g(s, \theta) = \frac{\pi}{24} \sum_{n=0}^5 q_n(\theta) p^{(n)}(s), \tag{17.73}$$

where $p^{(n)}(s)$ are the derivatives of $p(s) = \sin s/s$, and

$$\begin{aligned} q_0(\theta) &= 1, & q_1(\theta) &= -6(A \cos \theta + B \sin \theta), \\ q_2(\theta) &= 192C\pi^4 \sin 2\theta, & q_3(\theta) &= -12(A \cos \theta + B \sin \theta), \\ q_4(\theta) &= 3 + 192C\pi^4 \sin 2\theta, & q_5(\theta) &= -6(A \cos \theta + B \sin \theta). \end{aligned}$$

The deduction of this expression will be done in several steps.

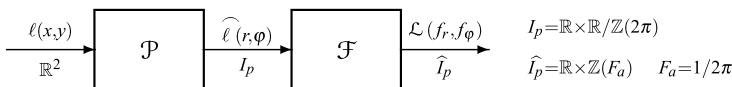


Fig. 17.31 Starting from a Cartesian function $\ell(x, y)$, the polar operator \mathcal{P} gives a polar function $\widehat{\ell}(r, \varphi)$, and the Fourier operator \mathcal{F} , applied to $\widehat{\ell}(r, \varphi)$, gives a grating function $\mathcal{L}(f_r, f_\varphi)$

UT 17.10 Cartesian, Polar, and Grating Functions

In the notation of the image $\ell(x, y)$, the pair (x, y) will be regarded as Cartesian coordinates, and $\ell(x, y)$ as *Cartesian representation* of the image. A function $\widehat{\ell}(r, \varphi)$, obtained expressing the Cartesian coordinates (x, y) in polar coordinates (r, φ) , will be called a *polar function*, as shown in Fig. 17.31, where \mathcal{P} is the *polar operator*. In particular, we will find that the projection function $g(s, \theta)$, where s is a distance, and θ an angle, is a polar function. If we apply the Fourier operator \mathcal{F} to a polar function, we obtain a new kind of function $\mathcal{L}(f_r, f_\varphi)$, which is defined on a grating and will be called a *grating function*.

These three types of functions will be now studied in detail.

17.10.1 Polar Functions

A Cartesian representation $\ell(x, y)$ can be expressed in polar coordinates (r, φ) using the transformations (at argument level)

$$x = r \cos \varphi, \quad y = r \sin \varphi, \tag{17.74a}$$

$$r = |x + iy|, \quad \varphi = \arg(x + iy), \tag{17.74b}$$

where (r, φ) are polar coordinates. Then, we get the relationships

$$\mathcal{P} \quad \widehat{\ell}(r, \varphi) = \ell(r \cos \varphi, r \sin \varphi), \tag{17.75a}$$

$$\mathcal{P}^{-1} \quad \ell(x, y) = \widehat{\ell}(|x + iy|, \arg(x + iy)), \tag{17.75b}$$

where \mathcal{P} is the polar operator, and $\widehat{\ell}(r, \varphi)$ is the *polar representation* of $\ell(x, y)$. In order to avoid ambiguities, in definition (17.74b) of the amplitude r and phase φ , we find it expedient to associate to the Cartesian coordinates (x, y) the complex variable $z = x + iy$.

The polar representation (17.75a) is defined in the semi-infinite strip of the (r, φ) plane, delimited by the conditions

$$r \geq 0, \quad 0 \leq \varphi < 2\pi. \tag{17.76}$$

It is however convenient to extend the definition to the whole (r, φ) plane. The reason is that the subset of \mathbb{R}^2 defined by (17.76) is not a group, and in connection

with the Fourier transform, we need to operate with functions defined on groups. The natural extension of the domain to \mathbb{R}^2 is provided by expression (17.75a) itself by removing the constraints (17.76). In fact, the right-hand side expression, $\ell(r \cos \varphi, r \sin \varphi)$, makes sense for every $r \in \mathbb{R}$ and every $\varphi \in \mathbb{R}$. The extended function $\widehat{\ell}(r, \varphi)$, $(r, \varphi) \in \mathbb{R}^2$, is not arbitrary but exhibits the intrinsic symmetries

$$\widehat{\ell}(r, \varphi + k2\pi) = \widehat{\ell}(r, \varphi), \quad \widehat{\ell}(-r, \varphi + \pi) = \widehat{\ell}(r, \varphi). \quad (17.77)$$

In general, we shall call *polar function* a 2D function with these two properties.

Conditions (17.77) state that a polar function assumes the same values on the sequence of points $(r, \varphi + 2k\pi + \pi)$, $(-r, \varphi + 2\pi)$ displayed in a zig-zag sequence on the (r, φ) -plane. For this reason, (17.77) will be called *zig-zag symmetry*. The function $\widehat{\ell}(r, \varphi)$ is periodic in the second argument with periodicity given by the 1D subgroup of \mathbb{R}^2

$$P = \mathbb{O} \times \mathbb{Z}(2\pi) \quad \text{with } \mathbb{O} = \{0\}. \quad (17.78)$$

Then a polar function $\widehat{\ell}(r, \varphi)$ must be specified on the quotient group

$$I_p \triangleq \mathbb{R}^2 / [\mathbb{O} \times \mathbb{Z}(2\pi)] = \mathbb{R} \times (\mathbb{R} / \mathbb{Z}(2\pi)), \quad (17.79)$$

which entails consideration of the 1D periodicity.

In conclusion, the polar representation $\widehat{\ell}(r, \varphi)$ of an image is originally defined on the semi-infinite strip (17.76). After its expansion on the whole (r, φ) -plane it becomes a *polar function*, i.e., a function of the form $\widehat{\ell}(r, \varphi)$, $(r, \varphi) \in I_p$, which exhibits the zig-zag symmetry.

Reference Example Figure 17.32 illustrates the polar representation $\widehat{\ell}(r, \varphi)$ of the reference image (17.72): on the left, the function is represented in the strip (17.76), on the right, it is extended to \mathbb{R}^2 .

17.10.2 Grating Functions

The domain I_p of a polar function $\widehat{\ell}(r, \varphi)$ is given by (17.79), and the dual domain is the grating

$$\widehat{I}_p = \mathbb{R} \times \mathbb{Z}(F_a), \quad F_a = 1/(2\pi). \quad (17.80)$$

Then, the (full) Fourier transform $\mathcal{L}(f_r, f_\varphi)$ of a polar function is given by

$$\begin{aligned} \mathcal{F}_{ra}: \quad \mathcal{L}(f_r, f_\varphi) &= \int_{\mathbb{R}^2/P} dr d\varphi \widehat{\ell}(r, \varphi) e^{-i2\pi(f_r r + f_\varphi \varphi)} \\ &= \int_{-\infty}^{\infty} \int_0^{2\pi} \widehat{\ell}(r, \varphi) e^{-i2\pi(f_r r + f_\varphi \varphi)} dr d\varphi. \end{aligned} \quad (17.81)$$

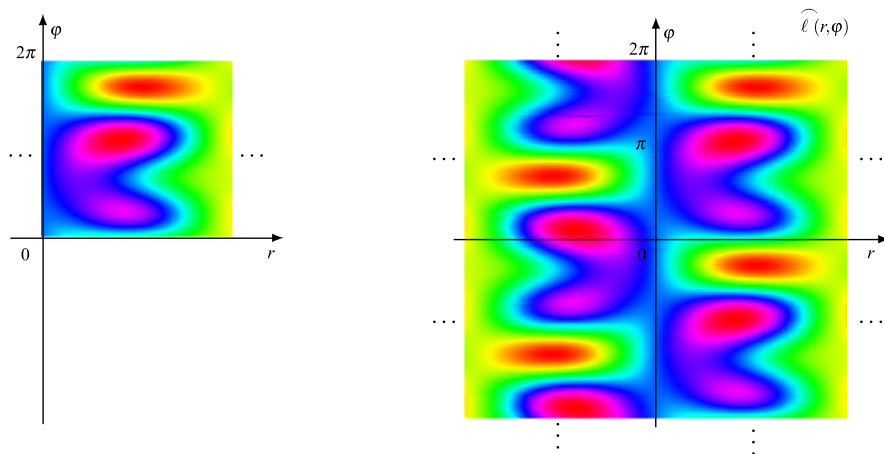


Fig. 17.32 Polar representation $\widehat{\ell}(r, \varphi)$ of the reference image in the minimum strip $0 \leq r \leq +\infty, 0 \leq \varphi \leq 2\pi$, and extension to the whole (r, φ) -plane

Hence, $\mathcal{L}(f_r, f_\varphi)$ is continuous-frequency in f_r and discrete-frequency in f_φ .

Since the original function $\widehat{\ell}(r, \varphi)$ is not arbitrary, $\mathcal{L}(f_r, f_\varphi)$ also is not arbitrary. The angular periodicity of $\widehat{\ell}(r, \varphi)$ has already been used with the consequence that $\mathcal{L}(f_r, f_\varphi)$ is defined on the grating $\mathbb{R} \times \mathbb{Z}(F_a)$. To use the zig-zag symmetry, $\widehat{\ell}(-r, \varphi) = \widehat{\ell}(r, \varphi + \pi)$, we apply the familiar rules on axis inversion and translation to get $\mathcal{L}(-f_r, f_\varphi) = \mathcal{L}(f_r, f_\varphi)e^{i2\pi f_\varphi \pi}$. Since $f_\varphi \in \mathbb{Z}(F_a)$ and $f_\varphi \pi \in \mathbb{Z}(1/2)$, we find explicitly

$$\boxed{\mathcal{L}(-f_r, nF_a) = (-1)^n \mathcal{L}(f_r, nF_a).} \tag{17.82}$$

Hence, for even n , $\mathcal{L}(f_r, nF_a)$ is even in f_r , and, for odd n , it is odd, as shown in Fig. 17.33 for the reference example. This property will be called *even-odd symmetry*. A function defined on $\mathbb{R} \times \mathbb{Z}(F_a)$ and with even-odd symmetry (17.82) will be called a *grating function*.

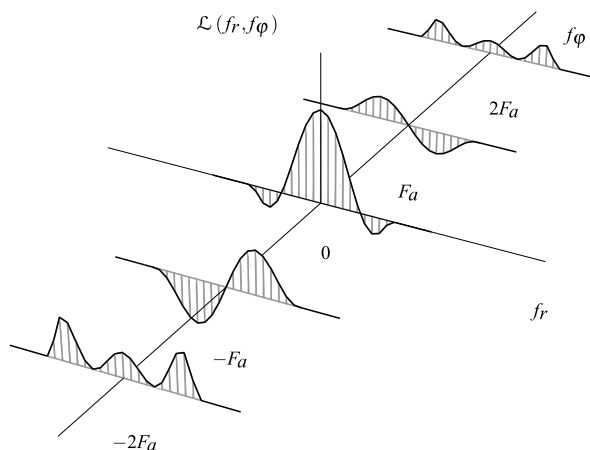
17.10.3 Fourier Transforms of Polar Functions

A polar function, $\widehat{\ell}(r, \varphi), (r, \varphi) \in I_p$, offers the choice of three Fourier transforms:

- 1D *radial* FT, $\mathcal{L}_r(f_r, \varphi)$, obtained by taking the FT with respect to r , for φ fixed,
- 1D *angular* FT, $\mathcal{L}_a(r, f_\varphi)$, obtained by taking the FT with respect to φ , for r fixed,
- 2D *full* FT, $\mathcal{L}(f_r, f_\varphi)$, obtained by taking the FT with respect to both φ and r .

The full FT has been considered above, where we have seen that $\mathcal{L}(f_r, f_\varphi)$ is a grating function. We now see the other two FTs.

Fig. 17.33 Fourier transform of polar representation $\widehat{\ell}(r, \varphi)$, as an example of grating function



Radial Fourier Transform It is given by

$$\mathcal{F}_r: \mathcal{L}_r(f_r, \varphi) = \int_{\mathbb{R}} dr \widehat{\ell}(r, \varphi) e^{-i2\pi f_r r}, \quad (f_r, \varphi) \in I_p, \quad (17.83)$$

where $\widehat{\ell}(r, \varphi)$ and $\mathcal{L}_r(f_r, \varphi)$ have the same domain \mathbb{R}^2 and the same periodicity $P = \mathbb{O} \times \mathbb{Z}(2\pi)$. Moreover, the zig-zag symmetry of $\widehat{\ell}(r, \varphi)$ is preserved in the radial FT, $\mathcal{L}_r(-f_r, \varphi) = \mathcal{L}_r(f_r, \varphi + \pi)$. In conclusion, the radial FT of a polar function is itself a *polar function*.

Angular Fourier Transform This 1D FT is given by

$$\begin{aligned} \mathcal{F}_a: \mathcal{L}_a(r, f_\varphi) &= \int_{\mathbb{R}/\mathbb{Z}(2\pi)} d\varphi \widehat{\ell}(r, \varphi) e^{-i2\pi f_\varphi \varphi} \\ &= \int_0^{2\pi} \widehat{\ell}(r, \varphi) e^{-i2\pi f_\varphi \varphi} d\varphi, \quad (r, f_\varphi) \in \mathbb{R} \times \mathbb{Z}(F_a). \end{aligned} \quad (17.84)$$

We can easily see that the angular FT $\mathcal{L}_a(f_r, f_\varphi)$ is a grating function.

The operators introduced above are summarized in Table 17.4, where we have added the Fourier operator \mathcal{F} directly applied to a Cartesian function, which produces a Cartesian function.

Table 17.4 Linear operators related to projections (I)

Operator	Kernel	Relationship
Polar $\frac{\ell(x,y)}{C} \rightarrow \boxed{\mathcal{P}} \xrightarrow{P} \widehat{\ell}(r,\varphi)$	$\delta_{\mathbb{R}^2}(r \cos \varphi - x, r \sin \varphi - y)$	$\widehat{\ell}(r, \varphi) = \ell(r \cos \varphi - x, r \sin \varphi - y)$
Fourier transform $\frac{\ell(x,y)}{C} \rightarrow \boxed{\mathcal{F}} \xrightarrow{C} L(f_x, f_y)$	$e^{-i2\pi(f_x x + f_y y)}$	$L(f_x, f_y) = \int_{-\infty}^{+\infty} \int_{-\infty}^{+\infty} \ell(x, y) e^{-i2\pi(f_x x + f_y y)} dx dy$
Radial Fourier transform $\frac{\widehat{\ell}(r,\varphi)}{P} \rightarrow \boxed{\mathcal{F}_r} \xrightarrow{P} \mathcal{L}_r(f_r, \theta)$	$e^{-i2\pi f_r r} \delta_{\mathbb{R}/\mathbb{Z}(2\pi)}(\theta - \varphi)$	$\mathcal{L}_r(f_r, \varphi) = \int_{-\infty}^{+\infty} \widehat{\ell}(r, \varphi) e^{-i2\pi f_r r} dr$
Angular Fourier transform $\frac{\widehat{\ell}(r,\varphi)}{P} \rightarrow \boxed{\mathcal{F}_a} \xrightarrow{G} \mathcal{L}_a(s, nF_a)$	$\delta_{\mathbb{R}}(r - s) e^{-in\varphi}$	$\mathcal{L}_a(r, nF_a) = \int_0^{2\pi} \widehat{\ell}(r, \varphi) e^{-in\varphi} d\varphi$
Radial-angular Fourier tr. $\frac{\widehat{\ell}(r,\varphi)}{P} \rightarrow \boxed{\mathcal{F}_{ra}} \xrightarrow{G} \mathcal{L}(f_r, nF_a)$	$e^{-i2\pi f_r r - in\varphi}$	$\mathcal{L}(f_r, nF_a) = \int_{-\infty}^{+\infty} \int_0^{2\pi} \widehat{\ell}(r, \varphi) e^{-i2\pi f_r r - in\varphi} dr d\varphi$

Note: P: polar format; C: Cartesian format; G: grating format

17.10.4 Harmonic Expansion of a Polar Functions

The angular periodicity of a polar function $\widehat{\ell}(r, \varphi)$ allows for the Fourier series expansion with respect to φ , namely

$$\mathcal{F}_a^{-1}: \widehat{\ell}(r, \varphi) = \sum_{n=-\infty}^{n=+\infty} \widehat{\ell}_n(r) e^{in\varphi}, \tag{17.85a}$$

where the Fourier coefficients are given by

$$\mathcal{F}_a: \widehat{\ell}_n(r) = \frac{1}{2\pi} \int_0^{2\pi} \widehat{\ell}(r, \varphi) e^{-in\varphi} d\varphi. \tag{17.85b}$$

We call (17.85a), (17.85b) the *harmonic expansion* of the polar function $\widehat{\ell}(r, \varphi)$ and the n th harmonic $\widehat{\ell}_n(r) e^{in\varphi}$ a function with *harmonic symmetry of order n* , briefly HS(n) (see Sect. 17.13). Now, we recognize that this expansion is essentially an inverse angular FT and that the *harmonics* are provided by an angular FT. In fact, comparing (17.85b) with (17.84), where $f_\varphi = nF_a$, we find

$$\mathcal{L}(r, nF_a) = 2\pi \widehat{\ell}_n(r). \tag{17.86}$$

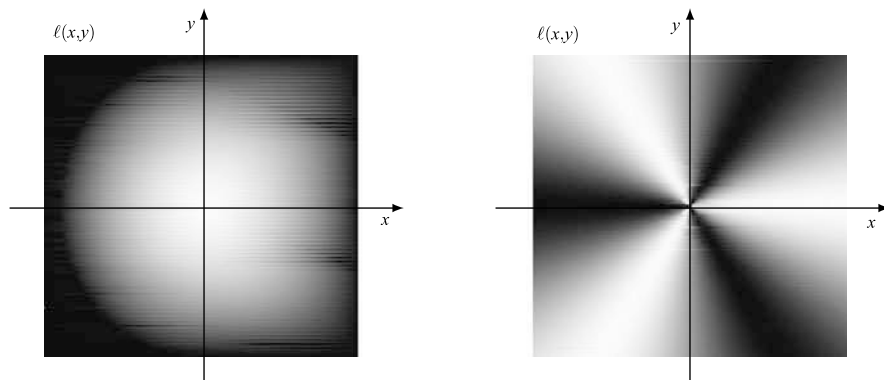


Fig. 17.34 Examples of image with circular symmetry and image with radial symmetry

The only difference lies in the format: $\mathcal{L}_a(r, nF_a)$ is a 2D function defined on the grating $\mathbb{R} \times \mathbb{Z}(F_a)$, whereas $\widehat{\ell}_n(r)$ may be viewed as a sequence of 1D functions on \mathbb{R} . In the representation of a grating function, as in Fig. 17.33, the n th slice gives the n th harmonic. The even-odd symmetry of $\mathcal{L}_a(r, nF_a)$ for the harmonics becomes

$$\widehat{\ell}_n(-r) = (-1)^n \widehat{\ell}_n(r). \tag{17.87}$$

The harmonic expansion holds for every polar functions like $\widehat{\ell}(r, \varphi)$, $\mathcal{L}_r(f_r, \varphi)$ and, as we shall see, the projection signal $g(s, \theta)$.

17.10.5 Circular, Radial and Harmonic Symmetries

An image with *circular symmetry* has the form

$$\ell(x, y) = c(|x + iy|) \xrightarrow{\mathcal{P}} \widehat{\ell}(r, \varphi) = c(r), \tag{17.88}$$

where $c(r)$ is a 1D function. An image with *radial symmetry* (RS) has the form

$$\ell(x, y) = e(\arg(x + iy)) \xrightarrow{\mathcal{P}} \widehat{\ell}(r, \varphi) = e(\varphi), \tag{17.89}$$

where $e(\varphi)$ is a 1D function of period 2π . Image (17.88) takes the constant value $c(r)$ on the circle of radius r , $|x + iy|^2 = x^2 + y^2 = r^2$. Image (17.89) takes the constant value $e(\varphi)$ on the radius tilted by the angle $\arg(x + iy) = \varphi$. Figure 17.34 illustrates an image with circular symmetry with $c(r) = (1 - r^2) \text{rect}_+(r)$ and an image with radial symmetry with $e(\varphi) = \cos 3\varphi$.

Circular and radial symmetries are in some sense orthogonal. Their combination appears in harmonic expansions. We say that an image $\ell(x, y)$ has *harmonic symmetry* of order n , briefly HS(n), when its polar representation has the form

$$\widehat{\ell}(r, \varphi) = \widehat{\ell}_n(r) e^{in\varphi}, \tag{17.90}$$

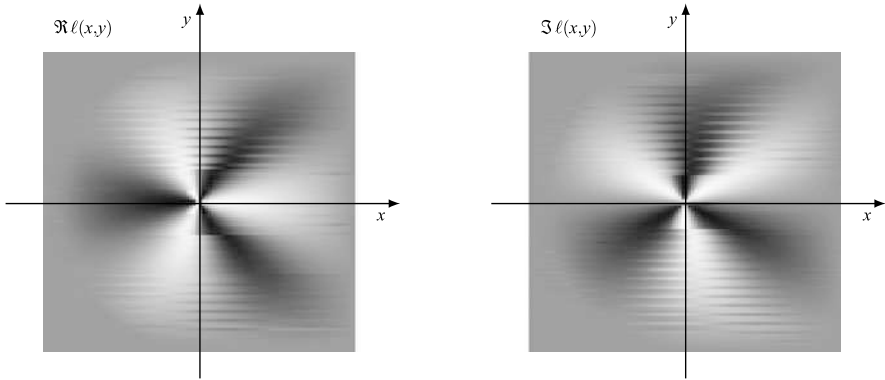


Fig. 17.35 Example of image with HS(3) symmetry and $\widehat{\ell}_n(r) = (1 - r^2) \text{rect}_+(r)$

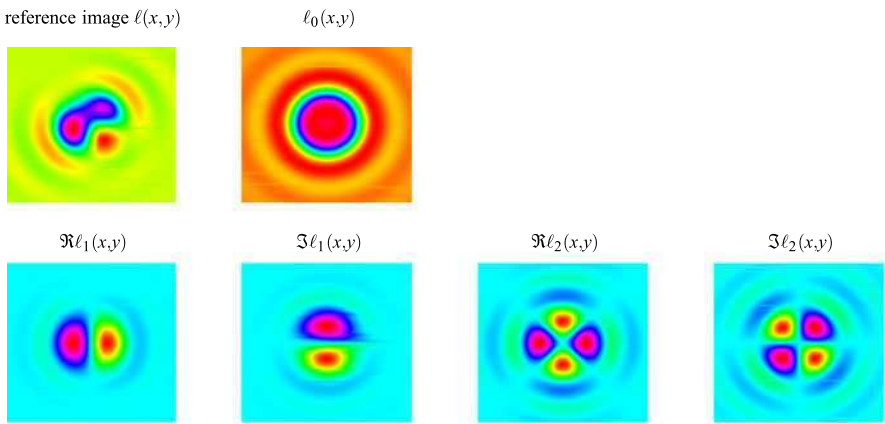


Fig. 17.36 HS components $\ell_n(x, y) = \widehat{\ell}_n(r)e^{in\varphi}$ of reference image

that is, when its harmonic expansion has only the n th harmonic.

Figure 17.35 shows an example of HS(3) symmetry.

Example 17.5 The reference image is real and its harmonics (or HS components) are (Fig. 17.36)

$$\begin{aligned} \widehat{\ell}_0(r) &= c(r), \\ \widehat{\ell}_1(r)e^{i\varphi} &= \frac{1}{2}(A - iB)rc(r)e^{i\varphi}, \\ \widehat{\ell}_2(r)e^{i2\varphi} &= -\frac{1}{2}iCr^2c(r)e^{i2\varphi}, \quad \widehat{\ell}_n(r)e^{in\varphi} = 0, \quad |n| > 2. \end{aligned}$$

Since the image is real, $\ell_{-n}(r) = \ell_n^*(r)$.

17.11 Properties of the Radon Transform

The preliminaries of the previous section allow the right formulation of the Radon operator in the framework of Signal Theory.

From definition (17.66) it is immediate to recognize that the Radon operator \mathcal{R} is an $\mathbb{R}^2 \rightarrow I_p$ linear tf with kernel

$$h(s, \theta; x, y) = \delta_{\mathbb{R}}(x \cos \theta + y \sin \theta - s), \quad (x, y) \in \mathbb{R}^2, (s, \theta) \in I_p. \quad (17.91)$$

We have seen that this linear tf is invertible, according to relation (17.68), which defines the inverse Radon operator \mathcal{R}^{-1} . We now see other fundamental properties.

17.11.1 The Radon Transform as a Polar Function

The Radon transform is a polar function according to:

Theorem 17.2 Let $q(a, b)$, $(a, b) \in \mathbb{R}^2$, be the following linear transformation of the given image $\ell(x, y)$:

$$\mathcal{R}_0: \quad q(a, b) = |a + ib| \int_{-\infty}^{+\infty} \ell(a - vb, b + va) dv. \quad (17.92)$$

Then, the Radon transform is the polar representation of $q(a, b)$, namely

$$g(s, \theta) = \widehat{q}(s, \theta) = q(s \cos \theta, s \sin \theta).$$

In fact, if we let $a = s \cos \theta$, $b = s \sin \theta$ in (17.92), we find

$$\begin{aligned} q(s \cos \theta, s \sin \theta) &= |s| \int_{-\infty}^{+\infty} \ell(s \cos \theta - vs \sin \theta, s \sin \theta + vs \cos \theta) dv \\ &= g(s, \theta). \end{aligned}$$

The function $q(a, b)$ can be interpreted as the Cartesian representation of the projections. This function is illustrated in Fig. 17.37 for the reference example.

By the above result we can apply to the Radon transform all the considerations and properties of polar functions, namely:

- the minimum range of the definition of $g(s, \theta)$ is the string $s \geq 0, 0 \leq \theta < 2\pi$,
- the extension of $g(s, \theta)$ to the whole (s, θ) plane leads to a polar function,
- the radial FT $G_r(f_s, \theta)$ is a polar function, while the angular FT, $G_a(s, f_\theta)$, and the full FT, $G(f_s, f_\theta)$, are grating functions.
- the polar functions $g(s, \theta)$ and $G_r(f_s, \theta)$ have the *harmonic expansion*.

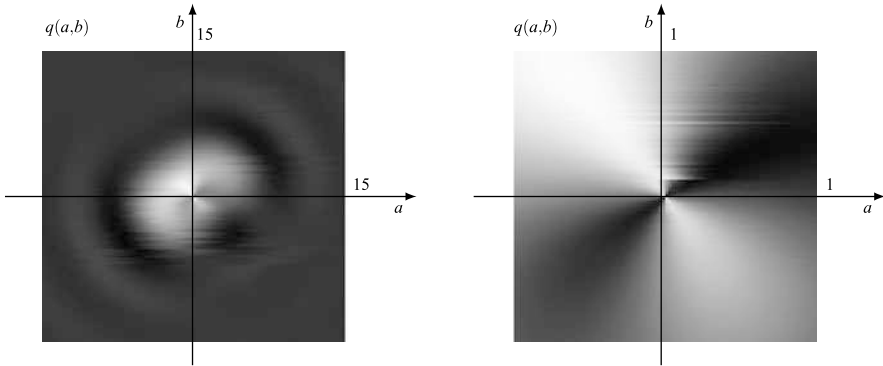


Fig. 17.37 Cartesian coordinate representation $q(a, b)$ of the projections of the reference image with different ranges for a and b

17.11.2 Radon Operator in Polar Coordinates

The original Radon operator \mathcal{R} , defined by (17.66), maps a Cartesian function $\ell(x, y)$ to a polar function $g(s, \theta)$. The Radon operator in polar coordinates \mathcal{R}_p is obtained starting from polar representation $\widehat{\ell}(r, \varphi)$ instead of the Cartesian representation $\ell(x, y)$.

Letting $x = r \cos \varphi$, $y = r \sin \varphi$ in (17.66), we obtain

$$\mathcal{R}_p: g(s, \theta) = \int_0^\infty dr r \int_0^{2\pi} d\varphi \widehat{\ell}(r, \varphi) \delta_{\mathbb{R}}(r \cos(\theta - \varphi) - s) \quad (17.93a)$$

and more explicitly from (17.67)

$$\mathcal{R}_p: g(s, \theta) = \int_{\mathbb{R}} \widehat{\ell}(|s + iu|, \theta + \arg(s + iu)) du. \quad (17.93b)$$

17.11.3 Other Properties

We have seen the linearity of the Radon transform. Other few properties are collected in Table 17.5.

17.12 Image Reconstruction from Projections

In this section we investigate the possibility of decomposing the Radon operator \mathcal{R} into a few, possibly simple, linear operators. The final target is to simplify the management of the inverse operator \mathcal{R}^{-1} , that is, the reconstruction of the image from its projections.

Table 17.5 Radon transform properties

Property	Image $\ell(x, y)$ or $\widehat{\ell}(r, \varphi)$	Radon transform $g(s, \theta)$
1. shift	$\ell(x - x_0, y - y_0)$	$g(s - x_0 \cos \theta - y_0 \sin \theta, \theta)$
2. rotation	$\widehat{\ell}(r, \varphi + \varphi_0)$	$g(s, \theta + \varphi_0)$
3. extension limitation	$\widehat{\ell}(r, \varphi) = 0, r > R$ $\ell(x, y) = 0, x , y > R$	$g(s, \theta) = 0, s > R$ $ s > R\sqrt{2}$
4. scaling	$\ell(ax, ay)$	$\frac{1}{ a }g(as, \theta)$
5. area	$\text{area}(\ell) = \int_{\mathbb{R}^2} dx dy \ell(x, y)$	$\int_{-\infty}^{+\infty} g(s, \theta) ds = \text{area}(\ell)$

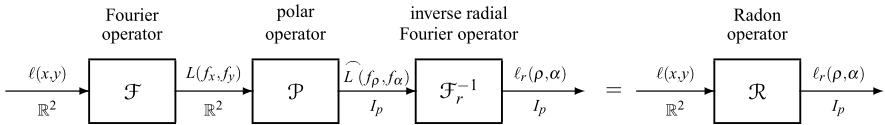


Fig. 17.38 A decomposition of the Radon operator

17.12.1 A Fundamental Decomposition (Fourier Connection)

Consider the sequence of operators of Fig. 17.38 applied to the image $\ell(x, y)$. The first is the Fourier operator \mathcal{F} , which gives the FT $L_x(f_x, f_y)$ of the image, that is

$$\mathcal{F}: L(f_x, f_y) = \int_{\mathbb{R}^2} dx dy \ell(x, y) e^{-i2\pi(f_x x + f_y y)}, \quad (f_x, f_y) \in \mathbb{R}^2. \quad (17.94)$$

The second one is the polar operator \mathcal{P} applied to $L(f_x, f_y)$, where the spatial frequencies f_x, f_y are expressed in terms of a radial frequency f_ρ and an angle α , according to $f_x = f_\rho \cos \alpha, f_y = f_\rho \sin \alpha$. Then

$$\mathcal{P}: \widehat{L}(f_\rho, \alpha) = L(f_\rho \cos \alpha, f_\rho \sin \alpha), \quad (f_\rho, \alpha) \in I_\rho. \quad (17.95)$$

The final operator is the 1D inverse radial FT, applied to the function $\widehat{L}(f_\rho, \alpha)$ with respect to f_ρ with α fixed, that is,

$$\mathcal{F}_r^{-1}: \ell_r(\rho, \alpha) = \int_{\mathbb{R}} df_\rho \widehat{L}(f_\rho, \alpha) e^{i2\pi f_\rho \rho}, \quad (\rho, \alpha) \in I_\rho. \quad (17.96)$$

Note that both $\widehat{L}(f_\rho, \alpha)$ and $\ell_r(\rho, \alpha)$ are polar functions, whereas $L(f_x, f_y)$ is a Cartesian function.

Theorem 17.3 *The cascade of the operators \mathcal{F}, \mathcal{P} , and \mathcal{F}_r^{-1} is equivalent to the Radon operator, that is,*

$$\boxed{\mathcal{F}_r^{-1} \mathcal{P} \mathcal{F} = \mathcal{R}.} \quad (17.97)$$

Proof Substitution of (17.94) into (17.95) yields

$$\widehat{L}(f_\theta, \alpha) = \int_{\mathbb{R}^2} dx dy \ell(x, y) e^{-i2\pi f_\rho(x \cos \alpha + y \sin \alpha)}.$$

Hence, from (17.96) we obtain

$$\begin{aligned} \ell_r(\rho, \alpha) &= \int_{\mathbb{R}^2} dx dy \ell(x, y) \left\{ \int_{\mathbb{R}} df_\rho e^{i2\pi f_\rho(\rho - x \cos \alpha - y \sin \alpha)} \right\} \\ &= \int_{\mathbb{R}^2} dx dy \ell(x, y) \delta_{\mathbb{R}}(\rho - x \cos \alpha - y \sin \alpha) = g(\rho, \alpha), \end{aligned}$$

where, inside $\{\cdot\}$ we have used the orthogonality condition $\int_{\mathbb{R}} df_\rho e^{i2\pi f_\rho X} = \delta_{\mathbb{R}}(X)$, and then we have compared the result with expression (17.66). \square

The consequence of (17.97) is that the inverse Radon operator can be decomposed into the form

$$\boxed{\mathcal{R}^{-1} = \mathcal{F}^{-1} \mathcal{P}^{-1} \mathcal{F}_r.} \quad (17.98)$$

Hence, to recover the image from projections $g(s, \theta)$, we can apply

- the radial FT of $g(s, \theta)$

$$\mathcal{F}_r: \quad G_r(f_s, \theta) = \int_{\mathbb{R}} ds g(s, \theta) e^{-i2\pi f_s s},$$

- the polar to Cartesian coordinates conversion

$$\mathcal{P}^{-1}: \quad L(f_x, f_y) = G_r(|f_x + i f_y|, \arg(f_x + i f_y)),$$

- the inverse FT

$$\mathcal{F}^{-1}: \quad \ell(x, y) = \int_{\mathbb{R}^2} df_x df_y L(f_x, f_y) e^{i2\pi(f_x x + f_y y)}.$$

17.12.2 The Projection Theorem

From decomposition (17.97) or (17.98) one obtains the operator relation

$$\mathcal{F}_r = \mathcal{P} \mathcal{F} \mathcal{R}^{-1}, \quad (17.99)$$

which provides the basis for several reconstruction algorithms. Its explicit formulation is known as the *projection theorem* or *projection-slice theorem*.

Theorem 17.4 (Projection Theorem) *The radial Fourier transform $G_r(f_s, \theta)$ of the projections $g(s, \theta)$ is equal to the central slice, at angle θ , of the Fourier transform $L(f_x, f_y)$ of the image, that is,*

$$G_r(f_s, \theta) = L(f_s \cos \theta, f_s \sin \theta) = \widehat{L}(f_s, \theta). \quad (17.100)$$

Proof By definition the application of \mathcal{F}_r to $g(s, \theta)$ gives $G_r = \mathcal{F}_r g$. On the other hand,

$$\mathcal{P}\mathcal{F}\mathcal{R}^{-1}g = \mathcal{P}\mathcal{F}\ell = \mathcal{P}L = \widehat{L},$$

where \widehat{L} is the polar representation of L . □

17.12.3 The Convolution-Projection Theorem

We establish the relation between the *convolution* of two images $\ell_1(x, y)$ and $\ell_2(x, y)$, given by

$$\ell_1 * \ell_2(x, y) = \int_{\mathbb{R}^2} du dv \ell_1(x - u, y - v) \ell_2(u, v), \quad (17.101)$$

and the 1D *radial* convolution of the corresponding projections $g_1(s, \theta)$ and $g_2(s, \theta)$, which is defined by

$$g_1 \overset{\text{rad}}{*} g_2(s, \theta) = \int_{\mathbb{R}} dz g_1(s - z, \theta) g_2(z, \theta). \quad (17.102)$$

The explicit relation is given by the *convolution-projection theorem*, which is the basis of filtering in the context of projections.

Theorem 17.5 *The Radon transform of the convolution of two images ℓ_1 and ℓ_2 are equal to the radial convolution of the corresponding projections*

$$\mathcal{R}[\ell_1 * \ell_2] = g_1 \overset{\text{rad}}{*} g_2 = \mathcal{R}[\ell_1] \overset{\text{rad}}{*} \mathcal{R}[\ell_2]. \quad (17.103)$$

In other words, the theorem states that *the projections of convolution are equal to the radial convolution of the projections.*

Proof Reconsider the fundamental relation (17.97), $\mathcal{R} = \mathcal{F}_r^{-1} \mathcal{P}\mathcal{F}$. When applied to an image $\ell(x, y)$, it gives

$$\mathcal{R}\ell = \mathcal{F}^{-1} \mathcal{P}\mathcal{F}\ell = \mathcal{F}^{-1} \mathcal{P}L = \mathcal{F}^{-1} \widehat{L}, \quad (17.104)$$

where \widehat{L} is the polar representation of the image FT $L(f_x, f_y)$. When the image is given by a convolution $\ell = \ell_1 * \ell_2$, in the frequency domain one gets a product

$L = L_1 L_2$. The latter relation holds also in polar coordinates, that is, $\widehat{L} = \widehat{L}_1 \widehat{L}_2$. Hence, $\mathcal{R}[\ell_1 * \ell_2] = \mathcal{F}_r^{-1}[\widehat{L}_1 \widehat{L}_2]$. But the inverse radial FT of a product is the radial convolution, where “radial” refers to the radial coordinate at a fixed angle (see (17.102)). Hence,

$$\mathcal{F}_r^{-1}(\widehat{L}_1 \widehat{L}_2) = \mathcal{F}_r^{-1}(\widehat{L}_1) \overset{\text{rad}}{*} \mathcal{F}_r^{-1}(\widehat{L}_2) = \mathcal{R}(\ell_1) \overset{\text{rad}}{*} \mathcal{R}(\ell_2),$$

where in the last equality we have applied (17.104) to images ℓ_1 and ℓ_2 . \square

17.12.4 Back Projection

The back-projection operator \mathcal{B} maps a polar function, typically given by the projections $g(s, \theta)$, onto a Cartesian function according to

$$\mathcal{B}: b(x, y) = \int_0^\pi g(x \cos \theta + y \sin \theta, \theta) d\theta,$$

where $b(x, y)$ is called the *back projections* of $g(s, \theta)$.

The back projections are used for the image reconstruction. In fact, it can be shown [10] that, if the projections are prefiltered with a radial filter with impulse response

$$h_r(s) = |s|,$$

then, the back projections of the resulting function give the image $\ell(x, y)$. However, the implementation of such prefilter, apparently simple, is not straightforward.

We do not insist further on back projections and related techniques. We prefer to save room for an original method based on the *Hankel transform*, which not only provides alternatives for the image reconstruction, but also gives more insight on the nature of projections.

17.13 The Hankel Connection to Projections

The standard methods of image reconstruction from projections are essentially based on the Radon operator decomposition $\mathcal{R} = \mathcal{F}_r^{-1} \mathcal{P} \mathcal{F}$, which clearly shows the fundamental role of the Fourier transform. In this section we develop an alternative method in which the central role is played by the Hankel transform.

17.13.1 Fourier Transform in Polar Coordinates

The sequence of operators

$$\widehat{\mathcal{F}} \triangleq \mathcal{P} \mathcal{F} \mathcal{P}^{-1}$$

links the polar representation $\widehat{\ell}(r, \varphi)$ of an image $\ell(x, y)$ to the polar representation $\widehat{L}(f_\varphi, \alpha)$ of the FT $L(f_x, f_y)$. To find explicitly the operator $\widehat{\mathcal{F}}$, consider the ordinary FT

$$\mathcal{F}: L(f_x, f_y) = \int_{\mathbb{R}^2} dx dy \ell(x, y) e^{-i2\pi(f_x x + f_y y)}$$

and express the Cartesian coordinate (x, y) in polar form, that is,

$$\mathcal{F}\mathcal{P}^{-1}: L(f_x, f_y) = \int_0^\infty dr r \int_0^{2\pi} d\varphi \widehat{\ell}(r, \varphi) e^{-i2\pi(f_x r \cos \varphi + f_y r \sin \varphi)}.$$

Hence, we introduce the polar representation of $L(f_x, f_y)$, namely

$$\widehat{\mathcal{F}}: \widehat{L}(f_\rho, \alpha) = \int_0^\infty dr r \int_0^{2\pi} d\varphi \widehat{\ell}(r, \varphi) e^{-i2\pi f_\rho r \cos(\varphi - \alpha)}, \quad (17.105a)$$

which relates the two polar representations.

Analogously, the inverse relation reads

$$\widehat{\mathcal{F}}^{-1}: \widehat{\ell}(r, \varphi) = \int_0^\infty df_\rho f_\rho \int_0^{2\pi} d\alpha \widehat{L}(f_\rho, \alpha) e^{i2\pi f_\rho r \cos(\varphi - \alpha)}. \quad (17.105b)$$

17.13.2 The Generalized Hankel Transform

The Hankel transform $\bar{g}(w)$ of a 1D function $g(r)$ was introduced in Sect. 5.9 to handle the FT of a 2D signal having a circular symmetry. The *generalized Hankel transform* is obtained by replacing $J_0(x)$ with the n th-order Bessel function [16]

$$J_n(x) = \frac{1}{2\pi} \int_0^{2\pi} e^{i(n\alpha - x \sin \alpha)} d\alpha, \quad (17.106)$$

that is,

$$\boxed{\mathcal{H}_n: \bar{g}_n(w) = 2\pi i^{-n} \int_0^\infty r g(r) J_n(2\pi wr) dr,} \quad (17.107a)$$

which represents the n th-order Hankel transform of $g(r)$. The inverse transform is symmetric, namely

$$\mathcal{H}_n^{-1}: g(r) = 2\pi i^n \int_0^\infty w \bar{g}_n(w) J_n(2\pi wr) dw. \quad (17.107b)$$

Now, consider the harmonic expansions of the polar functions $\widehat{\ell}(r, \varphi)$ and $\widehat{L}(\lambda, \alpha)$,

$$\widehat{\ell}(r, \varphi) = \sum_{n=-\infty}^{+\infty} \widehat{\ell}_n(r) e^{in\varphi}, \quad \widehat{L}(\lambda, \alpha) = \sum_{n=-\infty}^{+\infty} \widehat{L}_n(\lambda) e^{in\alpha}.$$

We claim:

Theorem 17.6 *The harmonics $\widehat{\ell}_n(r)$ of $\widehat{\ell}(r, \varphi)$ and $\widehat{L}_n(\lambda)$ of $\widehat{L}(\lambda, \alpha)$ are related by the n th-order Hankel transform*

$$\widehat{L}_n(\lambda) = \mathcal{H}_n[\widehat{\ell}_n(\cdot)|\lambda], \quad \widehat{\ell}_n(r) = \mathcal{H}_n^{-1}[\widehat{L}_n(\cdot)|r]. \tag{17.108}$$

Proof Use of the harmonic expansion of $\ell(r, \varphi)$ in (17.105a) yields

$$\begin{aligned} \widehat{L}(\lambda, \alpha) &= \sum_{n=-\infty}^{+\infty} \int_0^\infty dr r \widehat{\ell}_n(r) \int_0^{2\pi} d\varphi e^{i[n\varphi - 2\pi\lambda r \cos(\varphi - \alpha)]} \\ &= \sum_{n=-\infty}^{+\infty} e^{in\alpha} \int_0^\infty dr r \widehat{\ell}_n(r) \int_0^{2\pi} d\beta e^{i[n\beta - 2\pi\lambda r \cos \beta]}. \end{aligned}$$

Now, introduce the Bessel function (17.106) written in the form

$$2\pi J_n(x) = \int_0^{2\pi} d\alpha e^{in(\alpha - x \cos(\alpha - \pi/2))} = i^n \int_0^{2\pi} d\beta e^{in(\beta - x \cos \beta)}.$$

This yields

$$\widehat{L}(\lambda, \alpha) = \sum_{n=-\infty}^{+\infty} e^{in\alpha} 2\pi i^{-n} \int_0^\infty dr r \widehat{\ell}_n(r) J_n(2\pi\lambda r) = \sum_{n=-\infty}^{+\infty} e^{in\alpha} \widehat{L}_n(\lambda),$$

which gives the first of (17.108). The proof of the second is similar, starting from (17.105b). □

For n fixed, the n th-order Hankel operator \mathcal{H}_n is 1D since it acts on a 1D function and produces a 1D function, but considering \mathcal{H}_n for every $n \in \mathbb{Z}$, we obtain a 2D operator \mathcal{H} that acts on a grating function and produces a grating function. In fact, recall that harmonics are essentially angular FTs of polar functions (see (17.85a) and (17.85b))

$$\begin{aligned} 2\pi \widehat{\ell}_n(r) &= \mathcal{L}_a(r, nF_a) = \mathcal{F}_a[\widehat{\ell}], \\ 2\pi \widehat{L}_n(\lambda) &= \ell_a(\lambda, nF_a) = \mathcal{F}_a[\widehat{L}] = \mathcal{F}_a \widehat{\mathcal{F}}[\widehat{\ell}], \end{aligned} \tag{17.109}$$

where \mathcal{L}_a and ℓ_a are the angular FTs of $\widehat{\ell}$ and \widehat{L} , respectively. Now, by Theorem 17.6 $\widehat{L}_n = \mathcal{H}_n[\widehat{\ell}_n]$, and this defines the 2D Hankel operator \mathcal{H} , which gives $\ell_a = \mathcal{H}[\mathcal{L}_a]$.

From (17.109) we obtain the relation

$$\mathcal{H} = \mathcal{F}_a \widehat{\mathcal{F}} \mathcal{F}_a^{-1} \tag{17.110}$$

and, in explicit form,

$$\boxed{\mathcal{H}: \ell_a(\lambda, nF_a) = 2\pi i^{-n} \int_0^\infty dr r J_n(2\pi r \lambda) \mathcal{L}_a(r, nF_a).} \tag{17.111}$$

The inverse operator is

$$\mathcal{H}^{-1}: \mathcal{L}_a(r, nF_a) = 2\pi i^n \int_0^\infty d\lambda \lambda J_n(2\pi r \lambda) \widehat{\ell}_a(\lambda, nF_a). \tag{17.112}$$

17.13.3 Relation Between Hankel and Radon Transforms

The relation is provided by decompositions (17.110) of \mathcal{H} and the fundamental decomposition of the Radon operator $\mathcal{R} = \mathcal{F}_r^{-1} \mathcal{P} \mathcal{F}$. Their combination gives

$$\mathcal{H} = \mathcal{F}_a \mathcal{F}_r \mathcal{R} \mathcal{P}^{-1} \mathcal{F}_a^{-1}.$$

Hence, introducing the Radon operator in polar coordinates $\mathcal{R}_p = \mathcal{R} \mathcal{P}^{-1}$ and letting $\mathcal{F}_a \mathcal{F}_r = \mathcal{F}_{ar}$, we obtain

$$\boxed{\mathcal{H} = \mathcal{F}_{ra} \mathcal{R}_p \mathcal{F}_a^{-1}.} \tag{17.113}$$

Relation (17.113) can be used in several ways: in the direct form for the evaluation of the Hankel transform via the Radon transform and in the form

$$\mathcal{R}_p = \mathcal{F}_{ra}^{-1} \mathcal{H} \mathcal{F}_a$$

to evaluate the Radon transform via the Hankel transform. The image reconstruction from projections is provided by the form

$$\mathcal{R}_p^{-1} = \mathcal{F}_a^{-1} \mathcal{H}^{-1} \mathcal{F}_{ra}. \tag{17.114}$$

Hence, we have found an alternative reconstruction method based on the Hankel transform. A similar method was proposed in the literature [9], where the central role is played by the *circular harmonic transform*.³

Now, we formulate the Hankel approach in terms of harmonic expansions.

³The operator \mathcal{C} of this transform is related to the Hankel operator by

$$\mathcal{C} = \mathcal{F}_r^{-1} \mathcal{H} = \mathcal{F}_a \mathcal{R}_p^{-1} \mathcal{F}_a^{-1}.$$

17.13.4 Image Reconstruction via Hankel Transform

The projections, as polar functions, have the harmonic expansion

$$\mathcal{F}_a^{-1}: g(s, \theta) = \sum_{n=-\infty}^{+\infty} g_n(s) e^{in\theta}, \tag{17.115}$$

where

$$\mathcal{F}_a: g_n(s) = \frac{1}{2\pi} \int_0^{2\pi} g(s, \theta) e^{-in\theta} d\theta. \tag{17.116}$$

The radial FT in (17.115) gives

$$\mathcal{F}_r: G(f_s, \theta) = \sum_{n=-\infty}^{+\infty} G_n(f_s) e^{in\theta}, \tag{17.117}$$

which must be compared with the harmonic expansion

$$\widehat{L}(\lambda, \alpha) = \sum_n \widehat{L}_n(\lambda) e^{in\alpha}.$$

In fact, by the projection theorem we have $\widehat{L}(f_s, \theta) = G_r(f_s, \theta)$. Hence,

$$\widehat{L}_n(\lambda) = G_n(\lambda).$$

On the other hand, by Theorem 17.6, the harmonic $\widehat{L}_n(\lambda)$ is related to the image harmonic $\widehat{\ell}_n(r)$ by

$$\widehat{\ell}_n(r) = \mathcal{H}_n^{-1}[L_n(\cdot)]r]. \tag{17.118}$$

Hence, the image reconstruction from projections can be formulated in the steps:

- (1) evaluate the projection harmonics $g_n(s)$,
- (2) evaluate the radial FT $G_n(f_s)$ of $g_n(s)$,
- (3) evaluate the inverse Hankel transform $\widehat{\ell}_n(r)$ of $\widehat{L}_n(\lambda) = G_n(\lambda)$,
- (4) evaluate the image $\widehat{\ell}(r, \varphi)$ from its harmonics

$$\widehat{\ell}(r, \varphi) = \sum_{n=-\infty}^{+\infty} \ell_n(r) e^{in\varphi}.$$

The peculiarity of this approach is that, at each step, the harmonic of the same order n is involved, and it is particularly efficient where the projections (and then the image) have a finite number of harmonics. Note that for a real image, the evaluation can be limited to nonnegative n .

UT 17.14 Gallery of Operators Related to Projections

In the previous sections we have introduced several “representations” of the same image $\ell(x, y)$ and several operators that are illustrated in the flow-chart diagram of Fig. 17.39. The left part of the diagram is concerned with the image and the right part with the projections.

The starting point is the image to be represented, given as a Cartesian function $\ell(x, y), (x, y) \in \mathbb{R}^2$. Following the upper-left part of the diagram, we find the polar operator \mathcal{P} which produces the polar representation $\widehat{\ell}(r, \varphi)$. Then, the 2D operator \mathcal{F}_{ra} yields the radial-angular FT $\mathcal{L}_{ra}(f_r, f_\varphi)$, which is a grating function, whereas the 1D operators \mathcal{F}_r and \mathcal{F}_a yield the radial FT $\mathcal{L}_r(f_r, \varphi)$ and the angular FT $\mathcal{L}_a(r, f_\varphi)$, respectively.

Starting again from the image $\ell(x, y)$ and following the bottom-left part, we find the Fourier operator \mathcal{F} which gives the FT $L(f_x, f_y)$ and, going down, the polar operator \mathcal{P} which gives the polar representation $\widehat{L}(f_\rho, \alpha)$. The remaining part is symmetric to the upper part. In fact, $L(f_x, f_y)$, like $\ell(x, y)$, is a Cartesian function, and therefore to $L(f_x, f_y)$ we can apply the same sequence of operators applied to $\ell(x, y)$ at the top of the diagram. Hence, once arrived at $\widehat{L}(f_\rho, \alpha)$, we have the three choices $\mathcal{F}_{ra}, \mathcal{F}_r$, and \mathcal{F}_a , etc. In the bottom part of the diagram we have replaced \mathcal{F}_r by \mathcal{F}_r^{-1} and so $\mathcal{F}_{ra} = \mathcal{F}_r \mathcal{F}_a$ by $\widetilde{\mathcal{F}}_{ra} = \mathcal{F}_r^{-1} \mathcal{F}_a$ to be ready for the Hankel connection (see below), but this has no relevance to the function formats.

The transition from the “image world” (left) to the “projection world” (right) is provided by the Radon operator \mathcal{R} , which gives the projections $g(s, \theta)$. The projections are not represented at the same level as the image $\ell(x, y)$, but at the level of the polar representation $\widehat{\ell}(r, \alpha)$; the reason is that $g(s, \theta)$ is a polar function. The connection at the same level is provided by the Radon operator in Cartesian coordinates \mathcal{R}_0 , which produces a Cartesian function $q(a, b)$ (see Theorem 17.2). Now, $q(a, b)$ for the “projection world” has the same role as $\ell(x, y)$ for the “image world,” and, in fact, we can apply to the former the same sequence of operators applied to the latter. Thus, the right part of the flow diagram is achieved.

In the diagram some external “connections” are also shown. An identity connection (operator \mathcal{J}) links the functions $\widehat{L}(f_\rho, \alpha)$ and $G_r(f_s, \theta)$; this is stated by the *projection theorem*. A Radon connection (operator \mathcal{R}) links the function $\ell(x, y)$ and $\ell_r(\rho, \alpha)$, and this is stated by the identity $\mathcal{R} = \mathcal{F}_r^{-1} \mathcal{P} \mathcal{F}$ proved in Sect. 17.12. However, the same sequence of operations links $L(f_x, f_y)$ to $\mathcal{L}_r(f_r, \varphi)$, and also $\ell(x, y)$ to $\ell_r(\rho, \alpha)$; this explains the other Radon connection on the left. The connections with the operator \mathcal{R}_ρ are justified in a similar way.

The Hankel connections (provided by the operator \mathcal{H}) are a consequence of relation (17.110), that is, $\mathcal{H} = \mathcal{F}_a \widehat{\mathcal{F}} \mathcal{F}_a^{-1}$, where $\widehat{\mathcal{F}} = \mathcal{P} \mathcal{F} \mathcal{P}^{-1}$. The connections in the “projection world” are identical since the two worlds are identical.

Table 17.6 completes the collection of operators related to projections, which was initiated with Table 17.4.

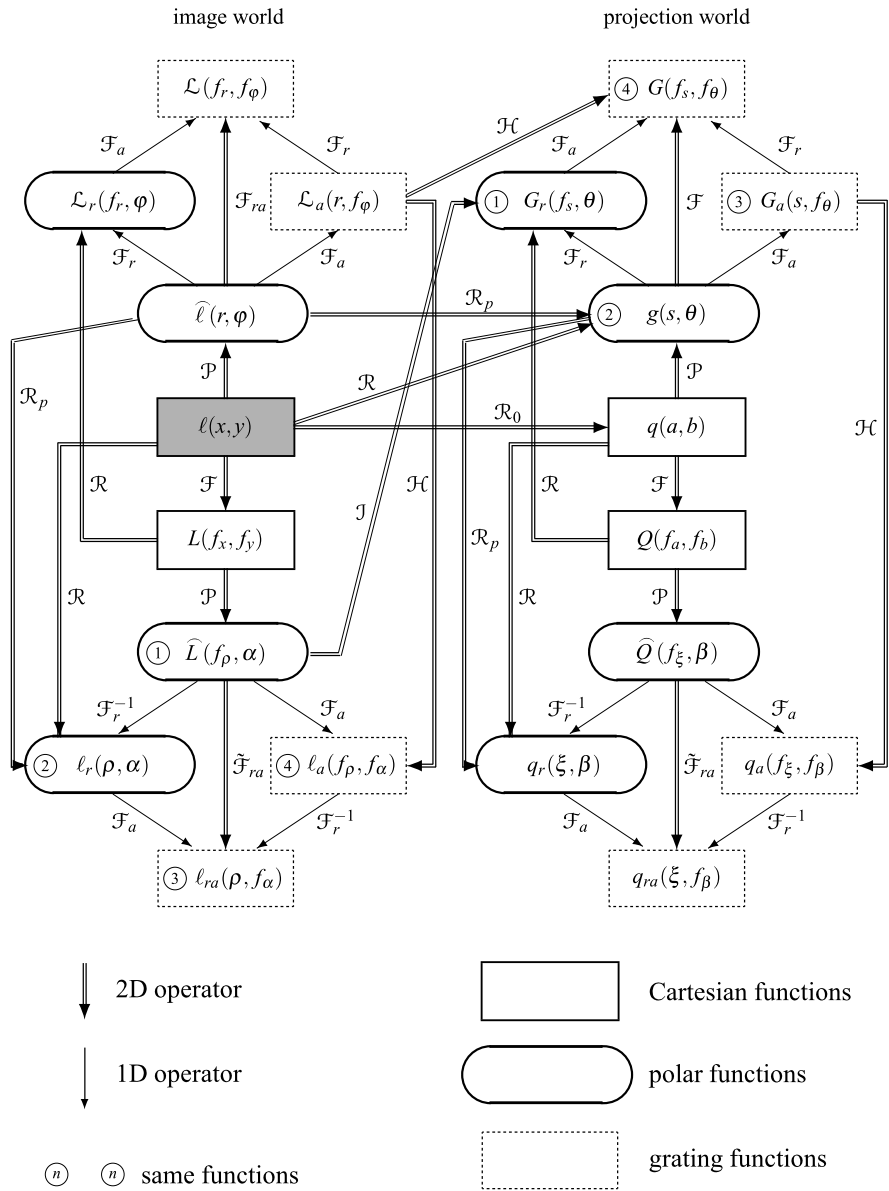


Fig. 17.39 Operators' relationships in images and projections

UT 17.15 Sampling and Interpolation of Projections

In practice the image is reconstructed from a sampled version of the projections, whereas the inverse Radon transform requires the whole continuous-domain projec-

Table 17.6 Linear operators related to projection (II)

Operator	Kernel	Relationship
Radon transf. in polar coord.		
$\frac{\widehat{\ell}(r, \varphi)}{P} \rightarrow \mathcal{R}_p \xrightarrow{P} g(s, \theta)$	$\frac{1}{2} r \delta_{\mathbb{R}}(r \cos(\theta - \varphi) - s)$	$g(s, \theta) = \int_{-\infty}^{+\infty} \widehat{\ell}(s + iu , \theta + \arg(s + iu)) du$
Radon transf. in Cart. coord.		
$\frac{\ell(x, y)}{C} \rightarrow \mathcal{R}_0 \xrightarrow{C} q(a, b)$	$ a + ib \delta_{\mathbb{R}}(a^2 + b^2 - ax - by)$	$q(a, b) = a + ib \int_{-\infty}^{+\infty} \ell(a - vb, b + va) dv$
Back projection		
$\frac{g(s, \theta)}{P} \rightarrow \mathcal{B} \xrightarrow{C} b(x, y)$	$\frac{1}{2} \delta_{\mathbb{R}}(x \cos \theta + y \sin \theta - s)$	$b(x, y) = \frac{1}{2} \int_0^{2\pi} g(x \cos \theta, y \sin \theta) d\theta$
Hankel transform		
$\frac{g(r, nF_a)}{G} \rightarrow \mathcal{H} \xrightarrow{G} q(f, nF_a)$	$(-i)^n \pi r J_n(2\pi fr) \delta_{mn}$	$q(f, nF_a) = (-i)^n \pi \int_{-\infty}^{+\infty} g(r, nF_a) r J_n(2\pi fr) dr$

Note: *P*: polar format; *C*: Cartesian format; *G*: grating format

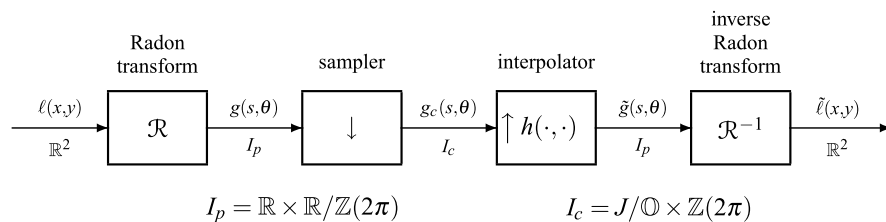


Fig. 17.40 Reference scheme for reconstruction of an image from its projections after a down-sampling

tions. The problem may be formulated according to the following conceptual steps (Fig. 17.40). The image $\ell(x, y)$ is first projected according to the Radon operator \mathcal{R} to get the projections $g(s, \theta)$. The projections are sampled on a lattice J of the (s, θ) -plane and then interpolated. Finally, the reconstructed image $\tilde{\ell}(x, y)$ is obtained by the inverse Radon transform.

The down-sampling and interpolation of the inner part of the scheme can be handled by the Unified Sampling Theorem of Chap. 8. As we shall see, the presence of periodicity and symmetry leads to constraints on sampling/interpolation parameters.

17.15.1 Sampling Theorem for Projections

The projection down-sampling has the format

$$I_p = \mathbb{R}^2/P = \mathbb{R} \times [\mathbb{R}/\mathbb{Z}(2\pi)] \quad \rightarrow \quad I_c = J/P = J/[\mathbb{O} \times \mathbb{Z}(2\pi)],$$

where J is a 2D lattice that contains the periodicity $P = \mathbb{O} \times \mathbb{Z}(2\pi)$. In the frequency domain the format becomes

$$\widehat{I}_p = \mathbb{R} \times \mathbb{Z}(F_a) \quad \rightarrow \quad \widehat{I}_c = \mathbb{R} \times \mathbb{Z}(F_a)/J^*,$$

where $F_a = 1/(2\pi)$, and J^* is the reciprocal lattice. Then, application of the Unified Sampling Theorem (Theorem 8.2) gives:

Theorem 17.7 *Let $g(s, \theta)$, $(s, \theta) \in \mathbb{R}^2/P$, be the projections of an image, and let $g_c(s, \theta) = g(s, \theta)$, $(s, \theta) \in J/P$, be its sampled version with J a lattice of \mathbb{R}^2 that contains the periodicity $P = \mathbb{O} \times \mathbb{Z}(2\pi)$. If the frequency extension of the projections is limited according to*

$$e(G) \subseteq C \quad (\text{alias-free condition}), \tag{17.119}$$

where C is a cell of $\mathbb{R} \times \mathbb{Z}(F_a)$ modulo J^* , then the projections $g(s, \theta)$ can be perfectly recovered from their samples by an interpolator with frequency response $H(f_s, f_\theta)$ given by the indicator function of the cell C , namely

$$H(f_s, f_\theta) = \eta_C(f_s, f_\theta), \quad (f_s, f_\theta) \in \mathbb{R} \times \mathbb{Z}(F_a). \tag{17.120}$$

The interpolation formula is given by

$$g(s, \theta) = \sum_{(s', \theta') \in [J/S]} d(J) h(s - s', \theta - \theta') g(s', \theta'), \tag{17.121}$$

where $h(s, \theta)$ is the inverse FT of $H(f_s, f_\theta)$.

The Sampling Theorem is characterized by the presence of a *partial* periodicity in the signal (the projections) and by a grating $\mathbb{R} \times \mathbb{Z}(F_a)$ as frequency domain. We shall see that sampling and interpolation parameters (lattice J and cell C) have some constraints because the projection signal is not arbitrary but a polar function.

17.15.2 Sampling Patterns

The projections $g(s, \theta)$, $(s, \theta) \in \mathbb{R}^2/P$, are defined on \mathbb{R}^2 and have the 1D periodicity $P = \mathbb{O} \times \mathbb{Z}(2\pi)$. The $\mathbb{R}^2/P \rightarrow J/P$ down-sampling

$$g_c(s, \theta) = g(s, \theta), \quad (s, \theta) \in J/P, \tag{17.122}$$

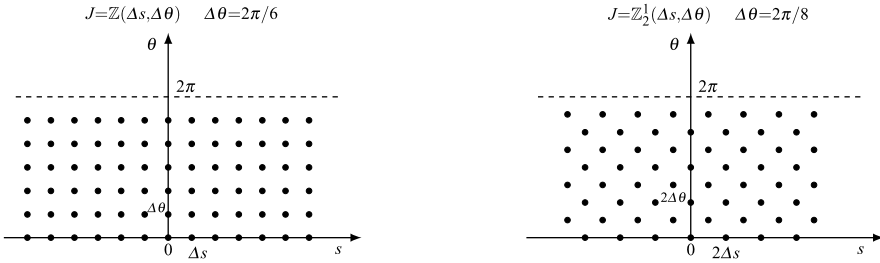


Fig. 17.41 Sampling lattices for projections (representation limited to cell (17.123))

is a *restriction* of the 2D function $g(s, \theta)$ from \mathbb{R}^2 down to the subgroup J , whereas the original periodicity P is preserved. Considering the periodicity, the acquisition of the sample values can be limited to a cell $[J/P]$, which is given by the horizontal strip of the sampling lattice

$$[J/P] = \mathbb{R} \times [0, 2\pi) \cap J, \tag{17.123}$$

and, in fact, in the interpolation formula (17.121) the summation is limited to this cell. However, $g(s, \theta)$ is a polar function, and, by the sampling relation (17.122), also the sample values form a discrete-domain polar function, i.e., a function with the properties

$$g_c(s, \theta + 2\pi) = g_c(s, \theta), \quad g_c(-s, \theta) = g_c(s, \theta + \pi), \tag{17.124}$$

for every $(s, \theta) \in J$.

Now we consider which of the 2D lattices are compatible for the projection sampling. For an arbitrary signal, all the 2D lattices would be compatible, but the projection signal $g(s, \theta)$ is a polar function, and this sets severe constraints on the choice. From (17.124) we find that the lattice J must verify the conditions:

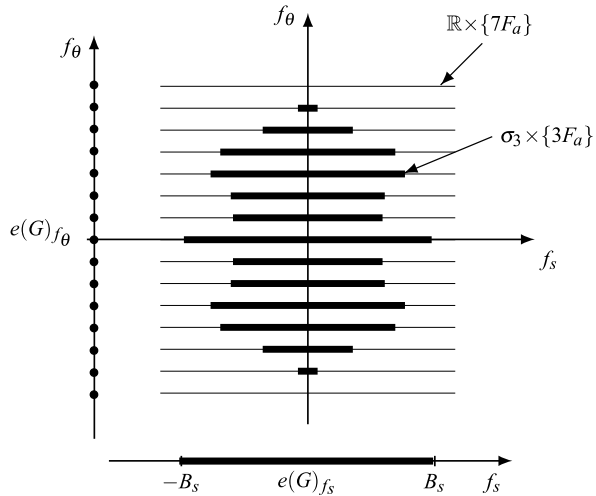
- (1) J must contain the periodicity $P = \mathbb{O} \times \mathbb{Z}(2\pi)$.
- (2) J must be symmetric with respect to the vertical axis of the (s, θ) -plane, i.e., if $(s, \theta) \in J$, then $(-s, \theta) \in J$.

In the class of the lattices $\mathbb{Z}_i^b(\Delta s, \Delta \theta)$ (see the gallery of Fig. 3.11), we find that condition (2) limits the choice to the lattices (Fig. 17.41):

- the separable lattice $J = \mathbb{Z}(\Delta s, \Delta \theta)$,
- the quincunx lattice $J = \mathbb{Z}_2^1(\Delta s, \Delta \theta)$.

Moreover, the zig-zag symmetry for the separable lattice sets the constraint that the angular subdivision must be done *in a even number of parts* and, for the quincunx lattice, *in a number multiple of 4*. Figure 17.41 shows the separable lattice with $\Delta \theta = 2\pi/6$ and the quincunx lattice with $\Delta \theta = 2\pi/8$.

Fig. 17.42 Example of extension $e(G)$ of band-limited projections



17.15.3 Projection Band Limitation and Alias-Free Condition

For their exact reconstruction, the projections must be band-limited, that is the FT $G(f_s, f_\theta)$, $(f_s, f_\theta) \in \widehat{I}_p$, must have a finite extension $e(G)$, according to condition (17.119). The frequency domain is the grating $\widehat{I}_p = \mathbb{R} \times \mathbb{Z}(F_a)$, which consists of the “lines” $\mathbb{R} \times \{nF_a\}$, $n \in \mathbb{Z}$, and, for the band limitation, $e(G)$ must consist of a finite number of segments $\sigma_n \times \{nF_a\}$, as shown in Fig. 17.42. Consider the “geometric” projections of the 2D extension $e(G)$ on the axes of the (f_s, f_θ) -plane, say $e(G)_{f_s}$ and $e(G)_{f_\theta}$. Then, we have that the projections are *radially band-limited* if $e(G)_{f_s}$ is a finite subset of \mathbb{R} and *angularly band-limited* if $e(G)_{f_\theta}$ is a finite subset of $\mathbb{Z}(F_a)$. Note in particular that the angular band-limitation has the consequence that the projections have a finite number of harmonics (see (17.115)). Typically, for *real* projections, we have

$$e(G)_{f_s} = (-B_s, B_s), \quad e(G)_{f_\theta} = \{-N_a F_a, \dots, -F_a, 0, F_a, \dots, N_a F_a\}, \tag{17.125}$$

where B_s is the *radial band*, and $B_a = N_a F_a$ is the *angular band*.

Example 17.6 For the image (17.72) of the Reference Example, the Fourier transform of the projections is

$$G(f_s, nF_a) = \begin{cases} P_n(f_s) \text{rect}(\pi f_s), & |n| \leq 2, \\ 0, & |n| > 3, \end{cases}$$

where $P_n(f_s)$ are polynomial in f_s (see [4]). Hence, the projections are band-limited according to (17.125) with $B_s = 1/(2\pi)$ and $N_a = 2$.

17.15.4 Interpolator Design

We now discuss the alias-free condition $e(G) \subseteq C$, that is, the choice of the cell C . The $I_p \rightarrow I_c$ down-sampling, stated by (17.122), becomes the $\widehat{I}_p \rightarrow \widehat{I}_c$ periodic repetition in the frequency domain. Considering that $\widehat{I}_p = P^* = \mathbb{R} \times \mathbb{Z}(F_a)$ and $\widehat{I}_c = P^*/J^*$, the periodic repetition has the form $P^* \rightarrow P^*/J^*$ with relation

$$G_c(f_s, f_\theta) = \sum_{(p_s, p_\theta) \in J^*} G(f_s - p_s, f_\theta - p_\theta), \quad (f_s, f_\theta) \in [P^*/J^*]. \quad (17.126)$$

In the two possible cases the reciprocal lattices are

$$\begin{aligned} J &= \mathbb{Z}(\Delta s, \Delta \theta) \quad \rightarrow \quad J^* = \mathbb{Z}(F_s, F_\theta), \quad F_s = 1/\Delta s, \quad F_\theta = 1/\Delta \theta, \\ J &= \mathbb{Z}_2^1(\Delta s, \Delta \theta) \quad \rightarrow \quad J^* = \mathbb{Z}_2^1\left(\frac{1}{2}F_s, \frac{1}{2}F_\theta\right), \quad F_s = 1/\Delta s, \quad F_\theta = 1/\Delta \theta. \end{aligned} \quad (17.127)$$

In particular, in the first case the periodic repetition (17.126) becomes

$$G_c(f_s, kF_a) = \sum_{i=-\infty}^{+\infty} \sum_{j=-\infty}^{+\infty} G(f_s - iF_s, kF_a - j2N_0F_a) \quad (17.128)$$

and is illustrated in Fig. 17.43.

The cell C is chosen in dependence of the reciprocal lattice J^* . In fact, the replicas of C over the repetition centers given by J^* must cover the frequency domain $P^* = \mathbb{R} \times \mathbb{Z}(F_a)$ without superposition. Figure 17.44 shows examples of cells for the two types of sampling, where $e(G)$ has a rhomboidal shape.

In the separable sampling, where $J^* = \mathbb{Z}(F_s, F_\theta)$, the cell C has a rectangular shape of dimensions $F_s \times F_\theta$. With the notation of (17.125), the alias-free conditions are

$$F_s \geq 2B_s, \quad F_\theta = MF_a \geq 2N_a F_a = 2B_a. \quad (17.129)$$

The quantity $F_s F_\theta$ represents the *sampling density*, given by the density of the lattice $\mathbb{Z}(\Delta s, \Delta \theta)$. The minimal choice for $F_s F_\theta$ is⁴

$$\mu_{\text{orth}} = (2B_s)(2B_a) = 4B_s N_a F_a.$$

In the quincunx sampling, where $J^* = \mathbb{Z}_2^1(\frac{1}{2}F_s, \frac{1}{2}F_\theta)$, the cell has a rhomboidal shape of dimensions $F_s \times F_\theta$. The alias-free conditions are still given by (17.129), but the sampling density of $\mathbb{Z}_2^1(\Delta s, \Delta \theta)$ is $\frac{1}{2}F_s F_\theta$, and the minimal choice is

$$\mu_{\text{quincunx}} = \frac{1}{2}(2B_s)(2B_a) = 2B_s N_a F_a.$$

⁴With the constraints discussed below.

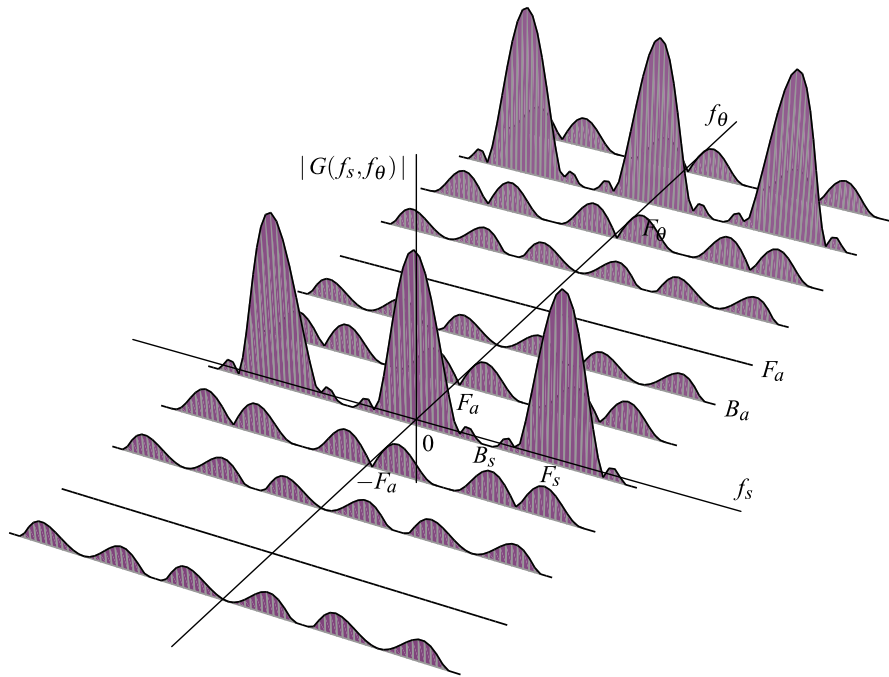


Fig. 17.43 Periodic repetition of the Fourier transform $G(f_s, f_\theta)$ in the reference example

In conclusion, the quincunx sampling is twice as efficient as the separable sampling (with a “realistic” spectral extension).

Constraints A first constraint is on the number M of subdivisions of the angle 2π : M must be even in the separable sampling and multiple of 4 in the quincunx sampling. Hence, from (17.129) the minimal choice is (see Fig. 17.44): in the first case $M = 2N_a + 2$, and in the second case $M = 2(N_a + 1)$ for N_a even and $M = 2(N_a + 2)$ for N_a odd. Now, in the separable sampling the constraint $M = 2N_0 + 2$ imposes that the minimal cell is $C = (-B_s, B_s) \times \{-N_a F_a, \dots, -F_a, 0, F_a, \dots, (N_a + 1)F\}$, which is not angularly symmetric. The consequence is that the interpolator is complex and, in fact, the impulse response is (see Problem 17.11) $h(s, \theta) = h_r(s)h_a(\theta)$ with

$$\begin{aligned}
 h_r(s) &= 2B_s \operatorname{sinc}(B_s s), \\
 h_a(\theta) &= F_a \frac{1 - e^{i2(N_a+1)\theta}}{(1 - e^{i\theta}) e^{iN_a\theta}},
 \end{aligned}
 \tag{17.130}$$

where $h_a(\theta)$ is a complex function of θ . However, considering the interpolation formula (17.121), where both $g(s, \theta)$ and $g(s', \theta')$ are real, we find that $h_a(\theta)$ can be replaced by its real part. Then, the angular frequency response becomes

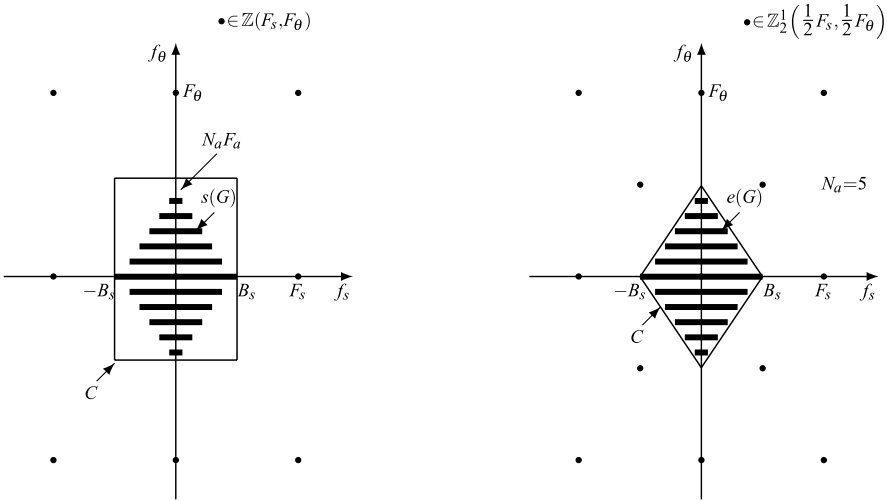


Fig. 17.44 Cells and repetition centers with orthogonal and quincunx samplings

$$\frac{1}{2}H_a(nF_a) + \frac{1}{2}H_a^*(-nF_a) = \begin{cases} 1, & |n| \leq N_a, \\ \frac{1}{2}, & |n| = N_a + 1, \\ 0, & |n| \geq N_a + 1, \end{cases} \quad (17.131)$$

as shown in Fig. 17.45. This problem is not present with the quincunx sampling, where the cell C is also angularly symmetric (see Fig. 17.44).

Another constraint for the interpolator is due to the polar nature of the signal. In the frequency domain the interpolator relation (in the ideal case of reconstruction) is

$$G(f_s, nF_a) = H(f_s, nF_a)G_c(f_s, nF_a), \quad (17.132)$$

but both sampled and reconstructed projections are polar functions, and therefore, in the frequency domain, they have the even-odd symmetry, namely $G_c(f_s, nF_a) = (-1)^n G_c(-f_s, nF_a)$ and $G(f_s, nF_a) = (-1)^n G(-f_s, nF_a)$.

Therefore, from (17.132) we find the condition on the frequency response

$$\boxed{H(f_s, nF_a) = H(-f_s, nF_a)}, \quad (17.133)$$

i.e., it must be an even function of f_s for every n . However, this condition is verified with the cells of Fig. 17.45, which are radially symmetric.

17.16 Applications of Radon Transform

Among applications that have been developed for the reconstruction of images from projections, only a few can be mentioned such as industrial application of the x-ray

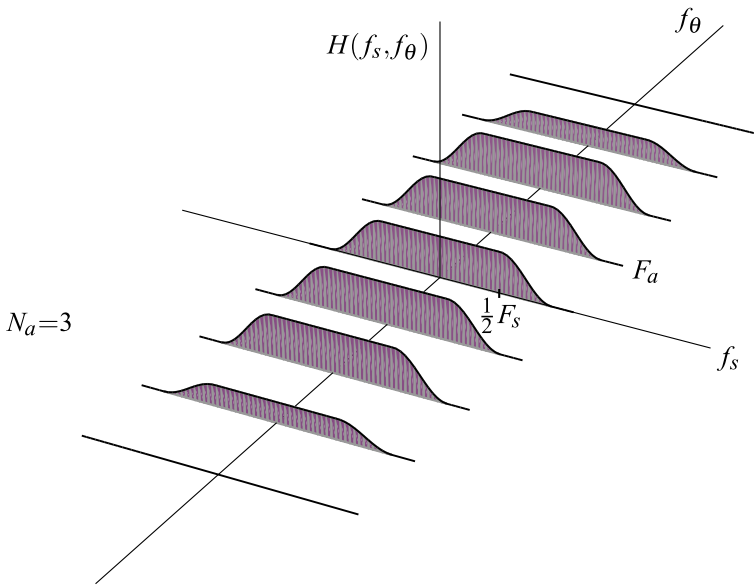


Fig. 17.45 Frequency response of the interpolator with a rhombic cell C (radially it is assumed a raised-cosine shape)

and gamma-ray scanning. One of the most important application is given by the development of magnetic-resonance imaging. The nucleus of a hydrogen atom has a magnetic moment which tends to align itself in a magnetic field H and to recover if disaligned. It also has angular moment (spin), and then the tendency to recover has the nature of gyroscopic precession with angular frequency, also known as Larmor frequency, directly proportional to magnetic field. Thus, nuclear resonance is excitable by Herizian waves and detectable by radio receivers: the strength of the received signal is proportional to the number of atoms engaged. One can count these atoms plane by plane, which is analogous to integrating along a line with x-rays, but in a higher dimensionality. Various geometries and time schedules are available, from which not only the density distribution can be reconstructed. Injections of elements such as gadolinium allow further richness in imaging methods. 3D reconstruction was pioneered experimentally by [1, 12, 13].

In geophysical exploration efforts have been made to map a vertical plane between two boreholes by lowering a source down one hole to a succession of stations, while, for each station, a receiver is scanned from top to bottom of the second hole. A feature of this technique is that there will be sectors missing from the coverage in θ [3].

A fascinating oceanographic development is the demonstration that underwater sound generated in the oceans can be detected as far away as remote coasts. Transit time is a curvilinear line integral of the reciprocal of sound velocity, which is dependent on water temperature. Hence, it will be possible to make global maps of ocean temperatures.

We remark that x-rays are not refracted, so line integrals are appropriate to the discussion of computed x-ray tomography, but in other applications the measurable integrals may pertain to curved rays. For example, this is the case where the medium is not an isotropic scatterer and the rays are curved, as in the proposal, to map ocean temperatures by timing the arrival of underwater sound. A variety of other applications, including astronomical, seismic, and positron emission, are described by [6].

17.17 Problems

17.1 ★ [Sect. 17.2] Starting from the Fourier transform $L(f_x, f_y)$ of a 2D source image, explicitly write the Fourier transform $L_Q(f_x, f_y)$ of the framed image.

17.2 ★ [Sect. 17.2] Consider the 2D continuous scanning where the framed image $\ell_Q(x, y)$, $(x, y) \in \mathbb{R}^2$, is down-sampled in the form $\mathbb{R}^2 \rightarrow \mathbb{R} \times \mathbb{Z}(d_y)$ to give $\ell_{QS}(x, y)$. Explicitly write the relationship between the Fourier transforms. In addition, write the expression of the Fourier transform of $\ell_{QS}(x, y)$ and its inverse.

17.3 ★★ [Sect. 17.2] Consider the 2D discrete scanning where the framed image $\ell_Q(x, y)$, $(x, y) \in \mathbb{R}^2$, is down-sampled in the form $\mathbb{R}^2 \rightarrow \mathbb{Z}(d_x, d_y)$ to give $\ell_{QS}(x, y)$. Explicitly write the relationship between the Fourier transforms. In addition, write the expression of the Fourier transform of $\ell_{QS}(x, y)$ and its inverse.

17.4 ★★ [Sect. 17.2] Consider a general discrete scanning of a still image obtained with a general lattice $I_S = \mathbb{Z}_a^p(d_x, d_y)$. Explicitly write the Fourier transform of $\ell_{QS}(x, y)$ and its inverse.

17.5 ★ [Sect. 17.2] Consider the discrete scanning of a still image. Write the reconstruction of the image starting from the video signal $u(mT_0)$.

17.6 ★★ [Sect. 17.10] Consider the expression of the Radon transform given by (17.66). Prove that it can be written in the form (17.67).

17.7 ★★ [Sect. 17.10] Show that the image of Fig. 17.35 with polar representation

$$\widehat{\ell}(r, \varphi) = \text{rect}_+(1 - r^2) \cos 3\varphi$$

has Cartesian representation

$$\ell(x, y) = [(x^3 - 3xy^2)/|x + iy|^3] \text{rect}_+(1 - x^2 - y^2).$$

Hint: Use identity $e^{in \arg(x+iy)} = (x + iy)^n / |x + iy|^n$.

17.8 ★ [Sect. 17.10] Write the polar representation $\widehat{\ell}(r, \varphi)$ of the reference image (17.72).

17.9 ** [Sect. 17.10] The reference image has the structure $\ell(x, y) = \ell_0(x, y) \times p(x, y)$, where

$$\ell_0(x, y) = J_4(\sqrt{x^2 + y^2}) / (x^2 + y^2)$$

has circular symmetry, and its FT $L_0(f_x, f_y)$ can be calculated via Hankel transform (see Sect. 5.9). Considering that the Hankel transform of $J_4(r)/r^2$ is $\frac{\pi}{24}(1 - (2\pi\lambda)^2)^3 \text{rect}(\pi\lambda)$, find the FT of $\ell(x, y)$. *Hint:* $p(x, y)$ is a polynomial, and using the differentiation rule of the FT

$$(-i2\pi x)^m (-i2\pi y)^n \ell_0(x, y) \xrightarrow{\mathcal{F}} \frac{\partial^{m+n} L_0(f_x, f_y)}{\partial f_x^m \partial f_y^n},$$

one can obtain the terms as $(-i2\pi x)(-i2\pi y)\ell_0(x, y) \xrightarrow{\mathcal{F}} \frac{\partial L_0(f_x, f_y)}{\partial f_x \partial f_y}$.

17.10 ** [Sect. 17.15] Explain why the lattice $\mathbb{Z}_3^1(\Delta s, \Delta\theta)$ cannot be used in the projection sampling.

17.11 ** [Sect. 17.15] Show that with the cell

$$C = (-B_s, B_s) \times (-N_a F_a, \dots, -F_a, 0, F_a, \dots, (N_a + 1)F_a)$$

the interpolator impulse response is given by (17.130).

17.12 *** [Sect. 17.15] Explicitly write the frequency response of the rhomboidal cell of Fig. 17.44 and prove that the corresponding impulse response is given by

$$h(s, \theta) = 2F_a B_s \text{sinc}(2B_s s) + \sum_{n=1}^{N_a} 4F_a B_n \text{sinc}(2B_n s) \cos n\theta,$$

where $B_n = B_s(1 - n/(N_a + 1))$.

References

1. E.R. Andrew, Nuclear magnetic resonance imaging: the multiple sensitive point method. IEEE Trans. Nucl. Sci. **NS-27**, 1232–1238 (1980)
2. R.N. Bracewell, *Two-Dimensional Imaging* (Prentice Hall, Englewood Cliffs, 1995)
3. R.N. Bracewell, S.J. Wernecke, Image reconstruction over a finite field of view. J. Opt. Soc. Am. **65**, 1342–1346 (1975)
4. G. Cariolaro, Exact evaluation of projections and of related representations of the reference example, in *Solutions of Problems of Unified Signal Theory*. Available at <http://springer.com/CariolaroUST>
5. G. Cariolaro, Scanning theory with application to HDTV. Available at <http://dei.unipd.it/~cariolar/USTdocuments>
6. S.R. Deans, *The Radon Transform and Some of Its Applications* (Wiley, New York, 1983)

7. J.O. Drewery, The filtering of luminance and chrominance signals to avoid cross-colour in a PAL colour system. *BBC Eng.*, 8–39 (1976)
8. E. Dubois, The sampling and reconstruction of time-varying imagery with application in video systems. *Proc. IEEE* **73**, 502–523 (1985)
9. E.P. Hansen, Theory of circular harmonic image reconstruction. *J. Opt. Soc. Am.* **71**, 304–308 (1981)
10. A.K. Jain, *Fundamentals of Digital Image Processing* (Prentice Hall, Englewood Cliffs, 1999)
11. B. Javidi, F. Okano (eds.), *Three-Dimensional Television, Video, and Display Technologies* (Springer, New York, 2003)
12. P.C. Lauterbur, Image formation by induced local interaction: examples employing nuclear magnetic resonance. *Nature* **242**, 190–191 (1973)
13. P.C. Lauterbur, C.-M. Lai, Zeugmatography by reconstruction from projections. *IEEE Trans. Nucl. Sci.* **NS-27**, 1227–1231 (1980)
14. P. Mertz, F. Gray, A theory of scanning and its relation to the characteristics of the transmitted signal in telephotography and television. *Bell Syst. Tech. J.* **13**, 464–515 (1934)
15. H.M. Ozaktas, L. Onural (eds.), *Three-Dimensional Television: Capture, Transmission, Display (Signals and Communication Technology)* (Springer, New York, 2008)
16. A. Papoulis, *Systems and Transforms with Applications in Optics* (McGraw–Hill, New York, 1968)
17. J. Radon, Über die Bestimmung von Funktionen durch ihre Integralwerte längs gewisser Mannigfaltigkeiten, in *Berichte über die Verhandlungen der Königlich Sächsischen Gesellschaft der Wissenschaften zu Leipzig (Reports on the proceedings of the Saxony Academy of Science)*, vol. 69 (Mathematisch-Physikalische Klasse, 1917), pp. 262–277
18. A.H. Robinson, Multidimensional Fourier transform and image processing with finite scanning apertures. *Appl. Opt.* **12**, 2344–2352 (1973)
19. O. Schreer, P. Kauff, T. Sikora (eds.), *3D Videocommunication: Algorithms, Concepts and Real-Time Systems in Human Centred Communication* (Wiley, New York, 2005)
20. D. Taubman, M.W. Marcellin, *JPEG2000, Image Compression Fundamentals and Practice* (Kluwer Academic, Boston, 2002)
21. G.J. Tonge, The sampling of television images, Independent Broadcasting Authority, Experimental and Development Rep. 112/81, May 1981
22. G.J. Tonge, Three-dimensional filters for television sampling, Independent Broadcasting Authority, Experimental and Development Rep. 117/82, June 1982
23. G.J. Tonge, The television scanning process. *SMPTE J.* **93**, 657–666 (1984)

Glossary

\Downarrow	marks a section that can be jumped at first reading
∇	marks an argument that requires knowledge of a topic developed later
UT	marks a section of the UST fundamentals
UST	Unified Signal Theory
FT	Fourier transform
SI	strictly shift-invariant
PI	periodically shift-invariant
QIL	quasi-shift-invariant linear
PIL	periodically shift-invariant linear
tf	transformation
$I \rightarrow U$ tf	transformation with input domain I and output domain U
\mathbb{N}	set of natural numbers (zero excluded)
\mathbb{N}_0	set of natural numbers (zero included)
\mathbb{Z}	set of integer numbers
\mathbb{Q}	set of rational numbers
\mathbb{R}	set of real numbers
\mathbb{C}	set of complex numbers
\mathbb{O}	set consisting of the identity element of a group, i.e., $\mathbb{O} = \{0\}$
$\mathbb{Z}(\infty)$	alternative notation of \mathbb{O}
$\mathbb{Z}(a)$	set of the multiples of a
\oplus	direct sum, see Chap. 4
$\int_a^b f(x) dx$	ordinary integral
$\int_G dx f(x)$	Haar integral
δ_{ij}	Kronecker symbol $\delta_{ij} = 1$ for $i = j$, $\delta_{ij} = 0$ for $i \neq j$
$\delta(x)$	delta function, see Sect. 2.3–E
$\delta_I(x)$	impulse on I , see Sect. 4.9–F
$\mathcal{G}(G_0)$	class of regular subgroups of G_0 , see Sect. 3.3
$\mathcal{Q}(G_0)$	class of regular quotient groups of G_0 , see Sect. 3.2
$\mathcal{S}(I)$	class of signals defined on I
$L_2(I)$	class of square integrable functions on I
$A + B$	sum of sets A and B , see Sect. 3.2

$A + b$	shift of A by b , i.e., $A + b = A + \{b\}$, see Sect. 3.2
$-A$	reverse of set A , see Sect. 3.2
$e(s)$	extension of s , see Sect. 4.8
$e_0(s)$	minimal extension of s , see Sect. 4.8
$\mathcal{E}(s)$	spectral extension of s , see Sect. 5.4
$\mathcal{E}_0(s)$	minimal spectral extension of s , see Sect. 5.4
I_0/P	quotient group, see Sect. 3.2
I^*	reciprocal group, see Sect. 5.3
\widehat{I}	dual group, see Sect. 5.3
$[C/P]$	cell of C modulo P , see Sect. 3.5
$\sum_{t \in C/P}$	summation extended over the cell $[C/P]$
$\sum_{t \in [C/P]}$	summation extended over the cell $[C/P]$
$\psi(f, t)$	Fourier transform kernel, see Sect. 5.3
$[a_{ij}]$	matrix with elements a_{ij}
$\ s\ $	norm of s , (see (4.37))
$\langle x, y \rangle$	inner product of x and y , see (4.39)
$x * y$	convolution of x with y , see (4.68)
$x * y(t)$	convolution of x with y evaluated at t
rep_{T_p}	periodic repetition with period T_p , see (2.16)
$\text{meas}(A)$	measure of the set A , see Sect. 4.1
$\text{rect}(x)$	rectangular function over $(-\frac{1}{2}, \frac{1}{2})$, see (2.25)
$\text{rect}_+(x)$	rectangular function over $(0, 1)$, see (2.28)
$\text{triang}(x)$	triangular function
$\text{sinc}(x)$	sinc function, see (2.35)
$\text{sinc}_N(x)$	periodic sinc, see (2.37)
$\text{sgn}(x)$	signum function,
$1(x)$	step function, see (2.22)
$I_0(x)$	discrete step function, see (2.80)
$\text{rcos}(x)$	raised cosine, see Sect. 9.6
$\text{rrcos}(x)$	square-root raised cosine, see Sect. 9.6
$\text{ircos}(x)$	inverse Fourier transform of $\text{rcos}(x)$, see Sect. 9.6
$\text{irrcos}(x)$	inverse Fourier transform of $\text{rrcos}(x)$, see Sect. 9.6

Index¹

- A**
- Abel transform, 883
 - Abelian group, 86
 - Adjoint operator, 156
 - Admissible shifts, 734, 750, 767
 - Algebra of convolution, 172
 - Alias-free condition, 411, 681, 692, 712, 906
 - All-pass filter, 175, 400, 550
 - Ambiguity of a frequency, 529
 - Analysis, 674
 - Analytic function, 472, 536
 - Analytic signal, 495, 630
 - Anti-Hermitian symmetry, 165, 225
 - Anticausal exponential, 482
 - Anticipatory, 472, 749
 - Aperiodic signals
 - continuous, 8, 451
 - discrete, 8, 521
 - Area, 19, 136, 220
 - over a period, 22
 - Aspect ratio, 843
 - Asymptotic behavior, 474, 502
 - of Fourier transforms, 479
 - * Axis primitive points, 817
- B**
- Back projection, 898
 - Band, 217, 514, 526
 - Band-limitation, 47, 411, 412, 908
 - Bandwidth, 216, 217, 471
 - conventional, 633
 - of an image, 848
 - rms, 472
- Basis**
- alignment, 801
 - canonical, 98, 798
 - of a group, 91
 - of a vector space, 149
 - triangular, 801
 - * Basis/signature of a group, 96, 214
 - Bessel functions, 470, 518, 884, 899
 - Bilateral exponential, 482
 - Biorthogonality condition, 654, 679
 - Block functions, 159
 - Block transform, 593, 707
- C**
- Canonical representation, 95
 - Cardinal functions, 158, 651
 - Carrierless modulation, 362
 - Cartesian functions, 885
 - Cartesian product, 87
 - Cascade of linear transformations, 283
 - Cascade of QIL transformations, 349–353
 - Cauchy principal value, 497
 - Cauchy–Schwartz inequality, 151
 - Causal exponential, 459, 471, 531
 - discrete, 531
 - Causal signal, 18, 749
 - Causal version, 25
 - Causality condition, 51, 333, 491, 547
 - * Cells, 101, 810–820, 857
 - aperiodic, 102, 810
 - in FFT computation, 612
 - in sampling, 417, 418
 - multiplicity, 811

¹* terms introduced by the author.

- * Cells (*cont.*)
 - of \mathbb{R} , 106
 - of $\mathbb{Z}(T)$, 107
 - orthogonal, 813
 - periodic, 102, 810
 - Centroid abscissas, 473
 - Change of dimensionality, 820–824
 - composite, 825–836
 - Characters, 206, 268
 - as eigenfunctions, 209
 - Chebyshev polynomials, 471
 - Chirp signal, 460, 470
 - Circular symmetry, 242, 891
 - Class of integrable signals, 150
 - Class of signals, 148
 - Coefficients, 157, 649
 - detail, 763
 - scaling, 738
 - wavelet, 738, 763
 - * Comparable lattices, 125
 - Compatibility condition (of a quotient group), 112
 - Complex signals, 7, 135
 - Composite shift matrix, 827
 - Composition principle, 350
 - Compressor, 665, 734
 - Conditional identity, 401
 - Continuous-time signals, 4, 17
 - Conventional bandwidth, 633–637
 - Conventional duration, 633–637
 - Convergence region
 - of bilateral Laplace transform, 480
 - of bilateral z -transform, 536
 - of unilateral Laplace transform, 486
 - of unilateral z -transform, 541
 - Convolution, 84, 168–171
 - 1D, 175
 - computation via FFT, 629
 - extension, 170
 - multidimensional, 178
 - of aperiodic signals, 31
 - of periodic signals, 36
 - on \mathbb{R} , 451
 - on $\mathbb{R}/\mathbb{Z}(T_p)$, 509
 - on $\mathbb{Z}(T)$, 521
 - properties, 33, 170
 - Convolution-projection theorem, 897
 - Coordinate change, 197, 853, 874
 - for Fourier transform, 245
 - with Haar integral, 145
 - Correct interpolation condition, 406
 - Correlation, 219, 228, 229, 729
 - Cosets, 103, 104, 362, 559
 - Critical sampling, 676, 700, 702
 - Cross-energy, 151, 227
 - Crossings, 454
 - Curvelet transform, 769
 - Cycles per height (cph), 844, 859
 - Cycles per second (cps), 859
 - Cycles per width (cpw), 844, 859
 - Cyclic convolution, 37, 63, 176, 569, 629
- D**
- Damping, 474–479, 514
 - theorem, 476
 - Dc component, 20, 455, 524
 - DCT, 583–590, 878
 - computation via FFT, 631
 - Decimator, 318, 552, 554, 556, 668, 673, 747
 - Decomposition
 - into sinusoidal components, 238
 - of QIL tf, 315, 319, 320
 - Delay, 19, 285
 - Delta function, 27, 453
 - * Delta increase, 822
 - Density of a group, 95
 - Determinant of a group, 95, 137
 - Deterministic signal, 2, 9
 - DFT, 232, 391, 574
 - computational complexity, 597, 598
 - cosine, 581
 - fractional, 593
 - multidimensional, 244, 610
 - Differentiation, 453, 522
 - of periodic signals, 510
 - rule, 456
 - Digital signals, 4
 - Dilation, 731
 - Dilation factor, 766
 - Dimensionality, 118
 - increase, 824
 - of a group, 92
 - of a vector space, 149
 - reduction, 824, 851
 - Dirac delta function, 27
 - Direct sum, 187, 190, 766
 - Discontinuous signals, 21, 452
 - decomposition, 452
 - Discrete
 - exponential, 528, 537, 546
 - filter, 546
 - impulse, 60
 - signals, 4
 - sinusoids, 528, 571
 - Discrete Fourier transform, *see* DFT
 - Discrete wavelet expansion (DWT), 762–765
 - Disjoint projection condition, 824, 870

- Distortion-free condition, 681, 692
- Domain complexity, 302
- Domain/periodicity, 167
- * Down-periodization, 305, 313, 324
- Down-sampling, 305, 306, 324, 348
 - z -transform, 553
- Down-sampling factor, 668
- Down-sampling ratio, 308, 669, 676
- Dual
 - of a decimator, 327
 - of a filter, 322
 - of a window, 322
 - of an interpolator, 327
 - of down-periodization, 326
 - of down-sampling, 324
 - of up-periodization, 325
 - of up-sampling, 325
- Dual group, 212, 269
- Duality theorem, 324
- Duration, 165–167, 471
 - conventional, 633
 - minimal, 165
 - of a discrete signal, 56
 - of convolution, 32
 - of periodic signals, 514
 - on $\mathbb{Z}(T)$, 526
 - rms, 472
- Duration–bandwidth relation, 239
- Duration-limited signal, 20

- E**
- Efficiency of sampling interpolation, 422
- Eigenfunctions
 - of filters, 210
 - of Fourier transform, 258, 460
- Eigenvalue, 210
- Elementary operations, 779, 797–803
- * Elementary transformations, 305
- Energy
 - of a discrete signal, 56
 - of samples, 420
 - over a period, 23, 57
 - specific, 20
 - spectral density, 228
- Equalization, 399–405
 - perfect, 400
- Error in sampling, 435–444
- Error (or distortion), 399
- Even signals, 17, 54
- Even symmetry, 184, 229
- Expander, 665, 735
- Expansion
 - as generalized transform, 649–662

- Exponential
 - as eigenfunctions of filters, 210
 - discrete signal, 60
 - form of Fourier series, 38
 - mode, 490
 - modulators, 348
 - signals, 24
- * Extension, 165–167
 - limitation, 824
 - minimal, 165
 - of a discrete signal, 56
 - spectral, 216, 471

- F**
- Fast Fourier transform, *see* FFT
- FDM, 384, 394
- FFT, 12, 597–640
 - as parallel computation, 602–610
 - computational complexity, 600, 604, 609–614
 - convolution calculus, 630
 - implementation, 600
 - multidimensional, 610–621
 - on nonseparable lattices, 617–620
 - on separable lattices, 614–617
- Field, 843, 864
- Filter bank
 - multichannel, 699
 - tree structured, 703–706
 - two-channel, 691, 742, 749
- Filters, 329, 348
 - concentrate constants, 492
 - continuous-time, 489
 - discrete-time, 546
 - distributed constants, 492
 - for periodic signals, 519
 - ideal, 493
- Finite-energy signal, 20
- Finite-power signal, 20
- FIR filters, 547, 697, 749, 772
- Fourier coefficients, 38, 157, 664, 665
- Fourier kernel, 268
- Fourier series, 37, 230, 511
 - properties, 39
- Fourier transform, 12, 42, 84
 - calculation, 535
 - causal version, 458
 - computation via FFT, 622–629
 - explicit 1D forms, 229–233
 - explicit mD forms, 240–244
 - general rules, 217–222
 - in polar coordinates, 898
 - interpretation, 209
 - inverse, 42, 206

- Fourier transform (*cont.*)
 invertibility, 269
 kernel, 85, 205
*m*D examples, 246–253
 of continuous signals, 230
 of discrete impulse, 66
 of discrete signals, 63, 231
 of discrete sinusoidal signal, 67
 of periodic continuous signals, 230
 of periodic discrete signals, 232
 of singular signals, 208, 531
 on \mathbb{R} and $\mathbb{R}/\mathbb{Z}(T_p)$, relation, 222
 on \mathbb{R} and $\mathbb{Z}(T)$, relation, 221
 on multiplicative groups, 254, 255
 on \mathbb{R} , 455
 on $\mathbb{R}/\mathbb{Z}(T_p)$, 510
 on $\mathbb{Z}(T)$, 523
 on $\mathbb{Z}(T)/\mathbb{Z}(T_p)$, 570
 orthogonality condition, 207
 properties, 44
 regularity, 475
 specific rules on \mathbb{R} , 456
 specific rules on $\mathbb{R}/\mathbb{Z}(T_p)$, 512
 specific rules on $\mathbb{Z}(T)$, 525
 symmetries, 223
 unified, 205–210
- Fractional DFT and DCT, 593
 Fractional Fourier transform, 255–263
 Fractional interpolators, 557
 Frames, 650, 656, 864
 Framing, 843, 873
 Frequency decimation (in FFT), 604
 Frequency response, 51, 330
 FT, *see* Fourier transform
 Fundamental bands, 522
 Fundamental parallelepiped, 107, 795
- G**
- Gaussian pulse, 460, 470, 473
 GCD (greatest common divisor), 126, 808
 Generalized transform, 277, 643–649
 * Generating points, 817
 Generator of a class, 90
 Generator (of P/S conversion), 365, 707
 Generator (of S/P conversion), 365, 707
 * Grating functions, 887
 * Grating, 92
 2D, 100
 of still images, 847
 reduced representation, 784
 signal on, 787–790
- Group
 1D LCA groups, 91
 2D LCA, 100
 comparable, 125
 continuous, 92
 decomposition, 780
 full-dimensional, 93
 LCA, 89–100
 multiplicative, 119–124
 nonseparable, 94, 96
 partition, 101
 rationally comparable, 125
 reduced-dimensional, 93
 separable, 94, 96
 zero dimensional, 93
- H**
- Haar basis, 660, 671
 Haar integral, 11, 84, 135
 integration rules, 138
 on a grating, 143
 on the groups of \mathbb{R} , 140
 on the groups of \mathbb{R}^m , 141
 over a subset, 136
 over multiplicative groups, 146, 147
 properties, 137
 uniqueness, 136
 with coordinate change, 145
- Haar measure, 139
 Half-band, 522
 Hankel transform, 243
 generalized, 899
 relation with Radon transform, 901
- Harmonic expansion, 889
 Harmonic frequency, 514
 Harmonic symmetry, 890
 Heaviside's condition, 399, 401
 Hermite polynomials, 460
 Hermite triangularization, 799
 Hermite–Gauss functions, 159, 259
 Hermitian operator, 156
 Hermitian symmetry, 43, 165, 225, 511
 Hilbert filter, 496, 550
 Hilbert transform, 458
 computation via FFT, 630
 continuous, 496
 discrete, 550
 inverse, 497
 properties, 498
- * Hold increase, 822
 Hold interpolation, 55
- I**
- Ideal filters, 53, 331, 550
 Idempotent, 156
 Identity, 86, 175, 285, 647
 conditional, 276

- IIR filters, 547, 697, 771
 - Image
 - of a transformation, 646
 - of an operator, 156
 - Image element (pixel), 848
 - Image framity, 843
 - Image reconstruction
 - from projections, 894
 - via Hankel transform, 902
 - Impulse response
 - of a filter, 281
 - of a QIL tf, 299
 - * Impulse transformations, 304
 - * Impulse, 171–174
 - 1D, 176
 - discrete, 27
 - multidimensional, 181
 - noble identity, 174
 - on \mathbb{R} , 452
 - Incompatibility between bandwidth and duration limitations, 472
 - Increment, 525
 - of a discrete signal, 521
 - Index for lattices, 95
 - Indicator function, 136
 - Inner product, 151, 647
 - Inner product vector space, 150
 - Input–output relation of a tf, 273
 - Integral
 - on $\mathbb{R}/\mathbb{Z}(T_p)$, 509
 - on $\mathbb{Z}(T)$, 521
 - * Integral reduction, 822
 - Integration, 453
 - of periodic signals, 510
 - on $\mathbb{R}/\mathbb{Z}(T_p)$, rule, 512
 - rule, 456
 - Interlace
 - higher order, 864
 - scanning, 863
 - Interpolating function, 405, 416, 420
 - Interpolation, 405–409
 - of a still image, 859
 - of projection, 904
 - Interpolator, 318, 552, 555, 558, 668, 673, 747
 - parallel architecture, 563
 - Interpolator/decimator filters, 319
 - Intersection
 - of groups, 124–129
 - of lattices, 810
 - of quotient groups, 129, 130
 - Ircos, 463
 - Irrcos, 463
 - Isomorphism, 90, 100, 196, 810
- K**
- Kernel, 155, 280
- L**
- $L_p(I)$, class of integrable signals, 150
 - $L_2(I)$, class of square integrable signals, 151
 - Laplace transform, 12, 479–487
 - bilateral, 480
 - general rules, 487
 - inverse, 480
 - properties, 487
 - relationship with the Fourier transform, 484
 - unilateral, 486
 - unitary step, 482
 - Lapped transform, 707
 - Lattice, 92, 794–797
 - 2D, 795
 - largest separable, 805
 - of $\mathcal{L}_m(\mathbb{Z}(\mathbf{d}))$, 804
 - possible bases, 794
 - reciprocal, 270, 854
 - LCA, *see* groups
 - LCA quotient groups, 114
 - LCA subgroups of \mathbb{R} , 92
 - Lcm (least common multiple), 126, 808
 - Least-squares approximation, 161
 - Lebesgue integral, 11, 140
 - Lexicographical order, 701
 - Linear independence, 149
 - Linear tf, 12
 - definition, 279
 - dual kernel, 280
 - input–output relation, 280
 - kernel, 280
 - of a set, 90, 780
 - Lines (of a group), 828
 - Lower-triangularization, 798
 - Luminance, 2, 844
- M**
- Matrix viewpoint, 652
 - Mean power in a period, 23
 - Mean value, 20, 55
 - in a period, 23
 - Minimum period, 21
 - Modulated signals, 458, 517, 519
 - Modulus of a cell, 101
 - Mother wavelet, 754, 766
 - Multidimensional groups, 87
 - Multidimensional signals, 6, 135
 - Multiplexing, 427, 558
 - of signals with different rates, 560
 - Multiplication by constant, 285

- Multirate identity, 138, 371
- Multirate transformation, 345
- Multiresolution analysis, 706, 719–728, 731–734
- Mutual energy, 227
- N**
- Negative delay, 19, 560
- Noble identities, 353–358
- Noble identities with modulators, 358–362
- Nonlinear transformations, 294
- Norm (in a vector space), 150
- Number of lines, 848
- Numerical conversion of a still image, 877
- Numerical conversion of a time-varying image, 879
- Nyquist
 - criterion, 402, 753
 - frequency, 65, 414, 478
- O**
- Odd signals, 18, 54
- Odd symmetry, 184, 226
- OFDM, 384, 674
- Operations on the subsets of a group, 87
- Operator, 155, 279
- Orthogonal
 - complement, 152
 - operators, 156, 187
 - projection, 161
 - projector, 162
 - signals, 152
- Orthogonality condition, 69, 152, 654
 - forward (FRC), 646, 688
 - inverse (IRC), 646, 688
 - of Fourier transform, 207
- Orthonormal basis, 157, 734
- Orthonormal functions, 157
- Orthonormality conditions, 753
- Oversampling, 676, 700, 702
- P**
- P/S conversion, 362–369, 559, 605, 668, 708
- Parallel architectures, 370–383
 - of a decimator, 376
 - of a filter, 375
 - of a PIL tf, 381
 - of a QIL tf, 374
 - of an interpolator, 375
 - of PIL transformations, 377
 - with modulators, 380
- Parallel computation
 - multidimensional, 610
 - one-dimensional, 602
- Parseval's theorem, 220, 227, 572, 587, 647
 - generalized, 648
- Pass-band, 331, 494
- PCM, 877
- Perfect reconstruction, 679, 686, 703
- Periodic repetition, *see* periodization
- Periodic shift-invariance (PI), 278, 345, 657, 734
- Periodic signals, 17, 57
 - continuous, 8, 509
 - discrete, 8, 569
- Periodic sinc, 30
- Periodicity, 21
 - maximal, 111
 - of a set, 104
 - of a signal, 110
 - of a transformation, 296, 350, 657
 - partial, 93
- * Periodization, 310
- Phase-shifters
 - discrete, 550
 - ideal, 493, 550
- Physic signals, 1
- * PI (periodic invariance), 298
- * PIL (periodically-invariant linear), 296
- Pixel, 848, 855, 877
- Poisson summation formula, 220, 270
- Polar functions, 886
 - Fourier transform, 888
- Poles, 487
- Polyphase decomposition, 362–370, 695
 - in subband decomposition, 683
 - in the frequency domain, 686
 - in z-domain, 562
- Polyphase network, 393
- Power complementary property, 694, 754
- Power (specific), 20, 56
- Pre-filtering in sampling, 439
- * Primitive cells, 106, 107
- * Primitive groups, 90, 92, 95
- * Primitive points, 804, 816
- Progressive scanning, 860
- Projection, 162, 711, 879–894
 - theorem, 896
- Projector, 156, 226, 663, 734
 - Hermitian, 664
 - synthesis, 665
- Pseudo-circulant, 713
- Pulse, 26
 - rectangular, 26, 531
 - triangular, 26, 531

- Q**
- * QIL (quasi-invariant linear), 299, 349
 - Quadrature mirror filters, 693
 - Quantized signals, 4
 - * Quasi shift-invariance (QI), 298, 345
 - Quincunx lattice, 97, 768
 - Quotient groups, 110
- R**
- Radial symmetry, 891
 - Radon transform, 879–894
 - Raised cosine, 461, 478, 505, 756
 - square root, 462
 - Random signals, 5
 - Rate, 95
 - * Rate diagram, 275
 - Rate ratio, 675, 676
 - Rate variation, 527
 - * Rationally comparable, 125, 300, 808
 - RC filter, 52, 490
 - Rcos, *see* raised cosine
 - * Reading, 825–836
 - continuous, 828
 - discrete, 829
 - Fourier analysis, 837
 - of a still image, 847
 - of time-varying images, 869
 - speed, 847
 - Real numbers additive group, 451
 - Real transformations, 276
 - linear, 281
 - Reciprocal group, 211
 - 1D, 212
 - multidimensional, 213
 - Reconstruction condition
 - forward (FRC), 646
 - inverse (IRC), 646
 - Rectangular pulse, 47
 - Reflector, 156, 188, 226
 - Regularity degree, 527
 - Repetition centers, 104, 417, 811
 - Representation
 - of a group, 91, 214
 - of the dual group, 270
 - Reproduction, 857
 - Residues, 487, 544
 - Reverse, 87
 - Riemann integral, 140
 - Roll-off, 478
 - Root mean square value, 23
 - Rrcos, 462
 - Running sum, 521, 525
- S**
- S/P conversion, 362–369, 559, 605, 668, 708
 - Sampling, 58
 - multidimensional, 431–435
 - natural, 442
 - of bimodal signals, 424
 - of continuous periodic signals, 575
 - of non band-limited signals, 439
 - of projection, 904
 - of unimodal signals, 423
 - $\mathbb{R}/\mathbb{Z}(T_p) \rightarrow \mathbb{Z}(T)/\mathbb{Z}(T_p)$, 431
 - $\mathbb{R} \rightarrow \mathbb{Z}(T)$, 423–427
 - sample and hold, 440
 - $\mathbb{Z}(T_0) \rightarrow \mathbb{Z}(T)$, 427
 - Sampling frequency, 411
 - Sampling period, 410
 - Sampling theorem, 70
 - for projection, 905
 - fundamental, 409–415
 - unified, 415–419
 - Scale change, 510
 - on \mathbb{R} , 453
 - on $\mathbb{R}/\mathbb{Z}(T_p)$, 510
 - on $\mathbb{Z}(T)$, 522
 - Scale invariance, 733
 - Scaling function, 732, 733, 742, 766
 - Scanning
 - continuous, 846, 871
 - discrete, 848, 866
 - Fourier analysis, 852, 870
 - group, 871
 - instantaneous model, 863
 - memory model, 863
 - of still images, 846, 854
 - of time-varying images, 859–870
 - Schwartz inequality, 151
 - Schwartz–Gabor inequality, 152, 473
 - Self-dual groups, 257
 - Self-energy, 227
 - Self-reciprocal, 653, 664
 - filters, 680
 - kernels, 669
 - Semi-value, 21, 452
 - Set of representative, 103, 104
 - Shape of a window, 286
 - Shift, 87, 731
 - Shift invariance, 733
 - Shift-variant, 278
 - Short-time Fourier transform (STFT), 719–725
 - SI (strict invariant), 299
 - Sifting property, 27, 60, 172
 - Signal
 - band, 46
 - bandwidth, 46

- Signal (*cont.*)
 - definition, 83, 135
 - duration, 21
 - expansion, 157–163
 - extension, 21
- * Signature, 92
- Signum function, 18, 25
- Sinc, 30, 47
 - basis, 660, 671
- Singular signal, 470
- Sinusoidal mode, 490
- Sinusoidal signals, 23, 61, 528
- Smith diagonalization, 800
- Span, 149
- Spatial frequencies, 844
- Specification of a signal, 113
- Spectral
 - extension, 46, 216, 471
 - lines, 457, 526
- Standard lattice, 805
- Step signal, 25, 50, 470
 - discrete, 58, 529
- Still image, 1
 - reading, 848
- Stop band, 331
- Strict shift-invariance (SI), 278, 297
- Subband decomposition, 674–691
 - one dimensional, 699
- Subgroup, 86, 793
 - generation, 790–794
 - trivial, 86
- Sublattice, 795
- Subspaces, 149
- Sum
 - as set operation, 87
 - of groups, 124–129
 - of lattices, 810
 - of quotient groups, 129, 130
- * Sum reduction, 822, 853, 874
- Superposition principle, 279
- Support, *see* extension
- Symmetry
 - anti-Hermitian, 164
 - between signals and Fourier transforms, 215
 - binary, 189
 - even, 163
 - fundamental, 163
 - Hermitian, 164
 - M -ary, 189
 - odd, 163
 - on $\mathbb{Z}(T)$, 525
 - on $\mathbb{Z}(T)/\mathbb{Z}(T_p)$, 579
 - rule, 216
 - Symmetry rule, 46, 535, 572
 - applications, 236
 - Symmetry theory, 183–193, 225, 663–667, 734–742
 - Synthesis, 674
- T**
- TDM, 559
- Tensor product, 137, 287, 702, 770
- Three-dimensional television, 875
- Tilted lattice, 803
- Time compression, 291
- Time decimation(in FFT), 603
- Time expansion, 291
- Time localization, 720
- Time size, 54
- Time-frequency grid, 727
- Time-frequency representation, 727
- Time-shift, 19
- Transfer function, 489, 558
 - of a discrete filter, 546
- Transform
 - dual, 648
 - forward, 643
 - Gabor, 721
 - generalized, 667
 - inverse, 643
 - periodic invariant (PI), 670
- Transformation (tf)
 - definition, 273
- Translation, 285
- Transmission
 - of still images, 846
 - speed, 878
- Transmultiplexer, 384–395
 - architecture, 671
- Two-scale relation, 745, 749, 753
- U**
- Uncertainty principle, 503
- Unimodal matrix, 794
- Unit step response, 490
- Unitary operator, 156
- * Up-periodization, 305, 324
- Up-sampling, 305, 308, 348, 526
 - z -transform, 552
- Up-sampling factor, 668
- Up-sampling ratio, 310, 669, 676
- Up/down-sampling commutativity, 354
- Upper-triangularization, 798
- V**
- Value at origin, 220
- Vector space, 148–155, 782

- Velocity
 - of a discrete signal, 54
 - variation of a signal, 474
- Vertical bandwidth of an image, 848
- Video signal, 851, 868
- Volterra transformations, 294
- Voronoi cell, 103, 816–820
- W**
- Walsh functions, 159
- Wavelet transform
 - continuous, 726, 728
 - discrete, 719, 725, 762
- Wavelets, 728, 742
 - Mayer, 754
- Window, 285, 637, 721
 - Bartlett, 637
 - Blackman, 637
 - Hanning, 637, 721
- * Writing, 825–836
- X**
- X-UT21, 339
- Z**
- z -transform, 535–541, 715
 - ambiguity of the inverse transform, 538
 - bilateral, 535
 - convergence region, 535
 - general rules, 542
 - inverse, 536
 - of step signal, 538
 - properties, 543
 - relation with Fourier transform, 539
 - relation with Laplace transform, 544
 - unilateral, 541
- Zero counting, 453
- * Zero reduction, 822
- * Zig-zag symmetry, 887, 907